Acta Chemica Scandinavica A 37 (1983) 1–4

Acid Catalyzed Decomposition of Ethyl Vinyl Ether in 2,2,2-Trifluoroethanol

ROBERT ELIASON *

Chemistry Department, University of Bergen, N-5014 Bergen-Univ., Norway

The acid catalyzed solvolysis of ethyl vinyl ether has been studied in 90% v/v 2,2,2-trifluoroethanol – methanol. A series of carboxylic and methanesulfonic acids were used as catalysts. The dissociation constants, K_{HA}, and the catalytic coefficients, k_{HA}, for these acids have been determined. A Brønsted plot was constructed, and the results were analyzed in terms of the Marcus' theory for proton transfer reactions. The results support the notion that part of the free energy of activation is required to desolvate the proton prior to the actual transfer.

The hydrolysis of vinyl ethers has been extensively studied in aqueous media [1,2] and the reation has been shown to proceed *via* rate determining proton transfer to carbon. We have reported that the hydrolysis of ethyl vinyl ether in 80% DMSO – 20% H_2O by weight also occurs by the same AS_E2 mechanism as in water.[3] In that study, a Brønsted plot, as defined by a series of carboxylic acids, appeared to be curved. However, the pK_{HA} range covered was insufficient to allow this to be unambiguously established and, therefore, the data could not serve as a test for the Marcus' theory of proton transfer. The number of carboxylic acids used in the study was limited by a combination of factors. Firstly, there are no carboxylic acids stronger than trifluoroacetic acid by at least a pK_a unit. Secondly, carboxylic acids weaker than formic acid produce inconveniently slow rates. It was felt that a change in solvent may alleviate some of these problems.

It has been shown [4] previously that for rate determining proton transfer to carbon the reaction rate increases upon changing the solvent from hydrogen bond accepting (DMSO) to hydrogen bond donating (methanol – trimethoxyborane). Thus, 2,2,2-trifluoroethanol was chosen for this study as it was expected to be a good hydrogen bond donating solvent.

EXPERIMENTAL

Methanol (Merck "*zur Analyse*") was distilled prior to use. 2,2,2-trifluoroethanol (Fluka "*puriss*" grade) was purified by distillation from phosphorous pentoxide and then stored over 4 Å molecular sieves. Prior to use, it was distilled again from phosphorous pentoxide. All the acids were purified by distillation. Ethyl vinyl ether was purified as described before.[1]

The solvent mixed prior to use was 90% 2,2,2-trifluoroethanol and 10% methanol by volume (TFE-M). Stock solutions of the acids were prepared and standardized by the usual potentiometric techniques. A dilution series for each acid was prepared, and all subsequent measurements were made on these solutions. Conductance measurements on each solution were made using a Philips PW 9512 101 conductance cell with platinized electrodes and a Wayne Kerr B 642 Autobalance Universal Bridge. A Radiometer GK 2301 C combination electrode, which was preconditioned by soaking in 0.1 M hydrochloric acid, was used for all potentiometric measurements. The electrode could be used directly in the solvent.

Kinetic measurements were made by the usual spectrophotometric techniques in thermojacketed cell holders. The reaction was monitored by following the decrease in absorption of ethyl vinyl ether at 225 nm. The kinetic runs were initiated by injecting 5 – 10 μl of 50% ethyl vinyl ether – 50 %

* Present address: Chemistry Department, Southwest State University, Marshall, Minnesota 56258, U.S.A.

0302-4377/83 $2.50

methanol by volume into approximately 3 ml catalyst solution.

The viscosity of TFE-M was determined using an Ostwald viscosimeter with both 2,2,2-trifluoroethanol and methanol as standards.

All solutions were allowed to come to thermal equilibrium by standing for at least 15 min. Physicochemical measurements were made at 25.0 ± 1 °C as maintained by a constant temperature bath.

RESULTS

The acid dissociation constants (K_a) for the acids used in this study (except the two weakest) were determined from a combination of conductance and potentiometric measurements. The dilution range used for each acid in both types of measurements was one thousandfold. From the conductance data, the iterative computational method of Fuoss and Kraus was used to evaluate K_a. These calculations require a value for the solvent viscosity coefficient (μ) which was determined to be 1.58×10^{-3} N s m^{-2} from five separate measurements. All the calculations were performed using a computer. The limiting conductance, Λ_o, was calculated by choosing a large value and then going through several iterations. After each iteration, the calculated K_{HA} value was used with the potentiometric data to construct a *mV vs.* p*H* curve. The constants A and B of the equation $mV = A \cdot \mathrm{p}H + B$ were then evaluated. Iterations with both sets of data were continued until the best straight line was produced for both sets. The values of K_{HA} that were finally arrived at are shown in Table 1. It is felt that K_{HA} values determined in this way probably are in error within 20%. A final standard *mV vs.* p*H* curve was constructed, and a least squares analysis gave a slope of -61.2 ± 2.3 *mV*/p*H* and an intercept of 600 ± 8 mV. This *mV* per p*H* response is in reasonable agreement with the theoretical response of -59.2 *mV*/p*H*. For the two weakest acids, chloroacetic and acetic acids, the p*H* at each acid concentration was determined from the *mV* reading, and the acid dissociation constant was calculated. The dissociation constants for each acid were averaged, and the values are listed in Table 1. The standard deviation for both K_{HA} values is about 50%. This is rather large, but considering the weakness of the acids and the possible errors in dilution, it probably is not that bad.

Table 1. Catalytic coefficients and acid dissociation constants in 90% 2,2,2-trifluoroethanol – 10% methanol (v/v).

Acid	k_{HA}/M^{-1}s^{-1} [a]	K_{HA}/M [b]
CF_3SO_3H	$(5.58 \pm 0.63) \times 10^2$	2.56×10^{-2}
CH_3SO_3H	$(6.68 \pm 0.43) \times 10^2$	4.26×10^{-2}
CF_3COOH	$(2.36 \pm 0.13) \times 10^1$	1.06×10^{-4}
CCl_3COOH	$(6.02 \pm 0.27) \times 10^1$	3.68×10^{-5}
CCl_2HCOOH	6.75 ± 0.39	4.24×10^{-6}
$CClH_2COOH$	$(6.97 \pm 0.22) \times 10^{-1}$	5.99×10^{-8}
CH_3COOH	$(5.19 \pm 0.32) \times 10^{-2}$	1.46×10^{-9}
H^+	$(4.40 \pm 1.10) \times 10^2$ [c]	
Solvent	$(5.71 \pm 0.10) \times 10^{-5}$ [d]	

[a] The reported uncertainties are standard deviations. [b] Determined as described in the Result section and the error is estimated to be no worse than 20%. [c] This value is the mean of two determinations and the uncertainty is the average deviation of the mean. [d] This value is the average of four determinations and the uncertainty is the average deviation of the mean.

The rates of acid catalyzed decomposition of ethyl vinyl ether were measured spectrophotometrically by monitoring the decrease in vinyl ether absorption at 225 nm. The pseudo-first-order rate constants, k_1, were evaluated graphically and could be replicated with discrepancies of about 5%. The acid solutions were unbuffered resulting in a changing solvated proton concentration throughout an acid concentration series. The expression for general acid catalysis is given by eqn. 1, where k_o is the rate constant for spontaneous decomposition, k_{solv} is the decomposition rate constant caused by the solvent, and k_{H^+} and k_{HA} have their usual meanings.

$$k_1 = k_o + k_{solv} + k_{H^+}[H^+] + k_{HA}[HA] \quad (1)$$

It was assumed that k_o was negligible, but k_{solv} was measured directly. This left k_{H^+} and k_{HA} as the variables to be calculated. The $[H^+]$ values were calculated from the quadratic equation solution to the normal acid dissociation expression assuming that the $[H^+]$ is not negligible compared to [HA]. A regression analysis on the two independent variables, k_{H^+} and k_{HA}, was done for the trifluoromethane and methanesulfonic acid data using the MINITAB II computer program package.[5] The k_{H^+} calculated in this way is a second order rate constant; the concentration of H^+ was that calculated from the dissociation expression and does not include the solvent concentration. Taking the average of the k_{H^+} values and then using this value for k_{H^+}, a regression analysis on the

independent variable k_{HA} using MINITAB II was done on the data for the carboxylic acids. All these results are given in Table 1.

DISCUSSION

The acid dissociation constants, K_{HA}, listed in Table 1 are "formal" dissociation constants. They were calculated using the mass action law assuming that the equilibrium involved only free ions and the unionized molecule. Since rather dilute solutions were used, it was felt that this may be a valid assumption. For the carboxylic acids plotting either $\log K_a$ *vs.* σ^* or pK_a in the present solvent *vs.* pK_a in water yielded linear correlations. The latter linear plot was anticipated.[7] These observations indicate an internal consistency of the present data.

From an inspection of Table 1, it appears that methanesulfonic acid is stronger by a factor of two than trifluoromethanesulfonic acid. It is possible that part of this difference in K_{HA}'s is due to a fortunate combination of errors operating in opposite directions. A more likely explanation, however, may be that the trifluoromethanesulfonic acid is completely ionized to ion pairs in this solvent.[6] Dissociation would then occur from the ion pair, and the "normal" dissociation constant, K_{HA}, would most certainly be some function of the ion pair dissociation. Also, it seems unlikely that the acid dissociation constants for dissociation from the unionized and ionized molecule would be equivalent. Previous evidence[4] indicated that methansulfonic acid may also form an ion pair. The extent to which this occurs was thought to be less than that for the trifluoro analog.[4]

It appears (Table 1) that the catalytic coefficients for the sulfonic acids and the solvated proton may be different. I do not think that this is the case, however. The k_{H+} value was not determined by experiment but is rather a calculated value, and there is no statistical evidence that it is different from the other two strong acids. The difference in k_{HA}'s for the two sulfonic acids may or may not be statistically true but, if it is, an explanation is available. If trifluoromethanesulfonic acid does indeed exist primarily as an ion pair, then it seems reasonable that this ion pair would be strongly solvated. Part of the solvation could consist of a hydrogen-bond between the acidic proton and the solvent oxygen. For proton transfer to take place, the hydrogen-bonded solvent must be removed. The accompanying net energy input over that required for a similar process for methanesulfonic acid could be responsible for the lower catalytic power.

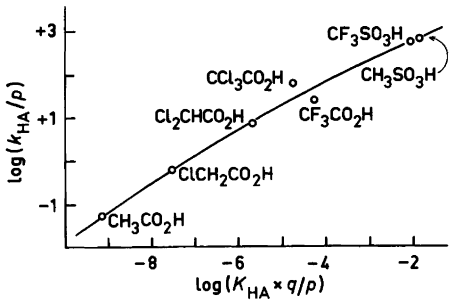

Fig. 1. Brønsted plot for acid decomposition of diphenyl diazomethane. The solid line represents the treatment of data according to Marcus' theory.

Fig. 1 shows a Brønsted plot of all the acids in Table 1 except the solvated proton. The data were fitted by a least-squares analysis to a quadratic expression in $\log(q \cdot K_{HA}/p)$. The line obtained is shown, and the data give a respectably curved plot. The coefficients of the quadratic expression can be related through Marcus' rate theory to the fundamental parameters by which proton transfer reactions can be characterized. This treatment gives an intrinsic barrier $\Delta G_o^{\ddagger} = 79.9$ kJ mol^{-1} and a work term $w^r = 41.8$ kJ mol^{-1}. ($\Delta G_o^{\ddagger}$ is the purely kinetic component of the activation free energy for the hypothetical proton transfer reaction step whose $\Delta G_o = 0$, and w^r is the free energy required to bring the reactants together and to form them into a reaction complex.) There are two obvious difficulties with this analysis. Firstly, two different acid types have been used to construct a curve, and there is no assurance that they may not each describe their own independent curves.[7b] Secondly, even with the sulfonic acids, the data do not show unequivocal curvature.

A similar analysis can be made with the data obtained in water[1] and in 80% DMSO – 20% water[3] for the same reaction as here. In the former case $\Delta G_o^{\ddagger} = 8.8$ kJ mol^{-1} and $w^r = 68.2$ kJ mol^{-1}, and in the latter case $\Delta G_o^{\ddagger} = 7.9$ kJ mol^{-1} and $w^r = 82.4$ kJ mol^{-1}. Unfortunately, the data from which these Marcus' parameters are derived, do not show unequivocal curvature either. But, the trends are interesting, w^r increases on going from water to the better hydrogen bond acceptor[8] solvent 80% DMSO. Changing the solvent to TFE, which is

considered a good hydrogen bond donating species,[9] causes a decrease in w^r. This is exactly in the direction predicted assuming that part of the contribution to w^r involves the breaking of the acid – solvent hydrogen bond.[4] It should take more energy to break the acid-DMSO hydrogen bond than a similar bond with TFE.

Acknowledgements. I thank the Royal Norwegian Council for Scientific and Industrial Research (NTNF) for a post-doctoral fellowship. The help of Knut Maartmann-Moe to solve computer programming problems is much appreciated. I am grateful to Jon Songstad for his generous hospitality.

REFERENCES

1. Kreevoy, M. M. and Eliason, R. *J. Phys. Chem. 72* (1968) 1313.
2. Kresge, A. J., Chen, H. L., Chiang, Y., Murrill, E., Payne, M. A. and Sagatys, D. S. *J. Am. Chem. Soc. 93* (1971) 413.
3. Eliason, R. and Kreevoy, M. M. *J. Phys. Chem. 78* (1974) 2658.
4. Eliason, R. *Acta Chem. Scand. A 33* (1979) 343.
5. This is an interactive statistical computing package written in FORTRAN IV. Information concerning MINITAB II can be obtained from D. T. A. Ryan, Jr., Statistics Dept., 215 Pond Laboratory, The Pennsylvania State University, University Park, PA 16802 USA.
6. Hine, J. *Structural Effects on Equilibria in Organic Chemistry*, Wiley, New York 1975, p. 136.
7. Bell, R. P. *The Proton in Chemistry*, 2nd Ed., Cornell Univ. Press, Ithaca, New York 1973, a. Chapter IV; b. Chapter X.
8. Gramstad, T. *Spectrochim. Acta 19* (1963) 829.
9. Evans, P. F., Nadas, J. A. and Matesiah, M. A. *J. Phys. Chem. 75* (1971) 1708.

Received April 19, 1982.

Acta Chemica Scandinavica A 37 (1983) 5–13

The Crystal Structure of Bis [aqua-μ-(2-chloropropionato-O,O')-di(2-chloropropionato)-μ_3-(2-diethylaminoethanolato-N,μ_3-O)-μ-(2-diethylaminoethanolato-N,μ-O)-μ_3-hydroxo-tricopper(II)]

KIMMO SMOLANDER

Department of Chemistry, University of Joensuu, PL 111, SF-80101 Joensuu 10, Finland

$[Cu_3(C_6H_{14}NO)_2(ClC_3H_4O_2)_3(OH)(H_2O)]_2$ is triclinic, space group $P\bar{1}$, with $a=10.712(7)$, $b=12.914(4)$, $c=13.295(7)$ Å, $\alpha=73.74(4)$, $\beta=67.57(4)$ $\gamma=85.35(4)°$ and $Z=1$. The structure was solved by direct and Fourier methods and refined to $R=0.075$ for 2834 reflections.

The crystal structure is composed of centrosymmetric hexanuclear complexes where the copper(II) ions are linked by triply bridging ethanolato oxygen atoms and OH^- ions, and by carboxylato and ethanolato oxygen bridges. The three independent copper(II) ions have a square-pyramidal coordination. Carboxylato, aqua and ethanolato oxygens are in apical positions at distances 2.349(9), 2.469(11) and 2.301(8) Å from Cu1, Cu2 and Cu3, respectively. In the basal planes the distances vary between 1.920 and 2.013 Å for Cu–O and between 2.054 and 2.062 Å for Cu–N.

Two of the three independent 2-chloropropionato groups are unidentate. The third carboxylato group bridges a basal coordination site of Cu2 with the apical site of Cu1 in an asymmetric *syn-syn* configuration.

Many carboxylato complexes of copper(II) with N,N-dialkylaminoethanol ($R_2NCH_2CH_2OH = R_2LOH$) as the second ligand have been reported.[1,2] The structures of $[Cu(Bu_2LO)(acetato)]_2$[3] and $[Cu(Et_2LO)(benzoato)]_2$[4] complexes are dimeric. The $[Cu_3(Bu_2LO)_2(benzoato)_4(ethanol)_2]$[5] forms a linear trinuclear structure. Haloacetato complexes[6,7] of the general formula $[Cu(R_2LO)-(R'COO)]_4$ have tetrameric cubane-type structures. The $[Cu_3(Et_2LO)_2(acetato)_3(OH)]_2 \cdot H_2O$[8] complex has a centrosymmetric, hexanuclear structure with a triply bridging hydroxo ion. A μ_3-bridging OH^- group is not very common. A Cu_3OH group in copper(II) complexes is found in $[Cu_3(3\text{-(phenylimino)-butanone 2-oximato})_3(OH)(ClO_4)] \cdot ClO_4$,[9] $[Cu_2(quinoline)_2(F_3CCOO)_3(OH)]_2$,[10] $[Cu_3(pyridine\text{-}2\text{-}carbaldehyde\ oximato)_3(OH)(SO_4)] \cdot 16.3H_2O$[11] and in $[Cu_3(2\text{-propylamino-2-methyl-3-butane oximato})_3(OH_3)(H_2O)_3] \cdot (ClO_4)_{3/2}(H_2O)_4$.[12] To obtain further information on aminoalcohol copper(II) complexes, we have prepared bis[aqua-μ-(2-chloropropionato-O,O')-di(2-chloropropionato)-μ_3-(2-diethylaminoethanolato-N,μ_3-O)-μ-(2-diethylaminoethanolato-N,μ-O)-μ_3-hydroxo-tricopper(II)] which is a new compound in the Et_2LOH series.

EXPERIMENTAL

Copper(II) 2-chloropropionate was synthesized from basic copper(II) carbonate (Merck) and 2-chloropropionic acid (Merck) by the method of Bateman and Conrad.[13] 1.5 g of the starting material was dissolved in 60 ml methanol and the solution was heated. To this boiling solution 1.35 ml of 2-diethylaminoethanol (Fluka AG) in 20 ml methanol was added with stirring. The solution was filtered and propanol was added so that the final methanol–propanol ratio was 3:1. After some weeks at about 5 °C dark blue crystals had formed. A single crystal, $0.81 \times 0.80 \times 0.78$ mm was used for the measurements of crystal and intensity data.

The unit cell parameters and the orientation matrix were determined by a least-square refinement based on 19 centered reflections measured at 24–25 °C on a Syntex $P2_1$ diffractometer. Intensity data were collected ($5 < 2\theta < 45°$) in the ω-scan mode, using graphite-monochromatized Mo$K\alpha$

0302-4377/83 $2.50

radiation. The scan range was $\pm 0.5°$ and the scan speed varied from 3.0 to 29.3° min^{-1}, depending on the number of counts accumulated in a preliminary scan. Background measurements were taken at both ends of the scan with a displacement of 1.0° from the Mo$K\alpha$-peak. Each background was measured for half the scan time. Two selected reflections were monitored as standard after every 100 measurements. Their intensities showed no significant change with time. The intensities were corrected for Lorentz and polarization effects and for absorption from empirical ψ-scan data from six reflections. Of the 3852 reflections collected, 2834 had $|F_o| > 5\sigma(F_o)$ and were used in subsequent calculations.

CRYSTAL DATA

$[Cu_3(C_6H_{14}NO)_2(ClC_3H_4O_2)_3(OH)(H_2O)]_2$,
$FW = 1561.25$;
Crystal system: Triclinic;
Space group: $P\bar{1}$ (No. 2);
$a = 10.712(7)$, $b = 12.914(4)$, $c = 13.295(7)$ Å;
$\alpha = 73.74(4)$, $\beta = 67.57(4)$, $\gamma = 85.35(4)°$;
$V = 1631.2$ Å^3, $Z = 1$, $F(000) = 802$;
μ(Mo$K\alpha$) = 23.1 cm^{-1}, λ(Mo$K\alpha$) = 0.71069 Å;
$D_m = 1.58$ g cm^{-3} (by flotation);
$D_x = 1.59$ g cm^{-3}.

STRUCTURE DETERMINATION

Direct methods (MULTAN 78)[14] gave the positional parameters of the three copper atoms. The remaining non-hydrogen atoms of the structure were found from successive Fourier syntheses. The discrepancy factor R was 0.168 with isotropic temperature factors and 0.136 after the copper atoms were made anisotropic.

Some of the carbon and chlorine atoms (C4*a*, C3*c*, C2*d*, C3*d*, Cl*d* and Cl*e*) had unusually large thermal motions and a difference Fourier map indicated that the structure might be disordered. First they were all given a site occupation factors 0.5, which were subsequently refined. The two disordered positions of atoms C3*c* and Cl*e* refined well and the corresponding bond length pairs were fixed together and refined as such. The disordered positions of C4*a* gave site occupation factors about one and zero, and thus C4*a* was considered ordered in subsequent calculations.

Considerable residual electron density was observed near the C2*d*, C3*d* and Cl*d* atoms, indicating rotational disorder or librational motion of the chloroethyl group of the carboxylato ligand. Attemps to account for rotational disorder in the chloroethyl group failed.

Experiments for the refinement in the non-centrosymmetric space group $P1$ were also made, but the positional parameters were nearly the same as before. Since there was no improvement in the disorder resolution the subsequent calculations were performed in the space group $P\bar{1}$. Atoms C3*c* and C3*e* were refined isotropically because anisotropic refinements did not give positive definite temperature factors.

The hydrogen atoms bonded to carbon were included at calculated positions with fixed bond lengths (C–H = 0.96 Å) and constrained angles. The isotropic thermal parameters for the hydrogen atoms were set 1.2 times the equivalent isotropic thermal parameters for the corresponding carbon atom. The hydrogen atom positions of the aqua and hydroxo ligands could not be found from a regular difference Fourier map.

Consequently, a second difference Fourier map was calculated using approximately two-thirds of the data (1781 reflections; $(\sin\theta)/\lambda \leq 0.31$ Å^{-1}). This map showed peaks of density about 0.3 e/Å^3 near the aqua and hydroxo oxygen atoms. The same peaks appeared in a third map using 1436 reflections ($(\sin\theta)/\lambda \leq 0.40$ Å^{-1}) and the hydrogen atoms were fixed at these positions.

The refinement converged to an R value of 0.075 and a weighted discrepancy factor $R_w = \Sigma \| F_o | - | F_c \| \sqrt{w}$ of 0.074 with the weighting scheme $w^{-1} = \sigma^2(F_o) + 0.0005 |F_o|^2$. The largest peaks in a final difference Fourier map had a maximum density of 1.1 e/Å^3 and were in the region of the atoms C3*e* and Cl*d* belonging to the disordered chloroethyl groups.

The structure was refined by the blocked-cascade full-matrix least-squares method.[15] The neutral atom scattering factors have been taken from *International Tables for X-Ray Crystallography*.[16] The preliminary refinements were performed with a Univac 1108 computer using programs from XRAY 76.[17] The final calculations were performed on a Nicolet R3m diffractometer system with SHELXTL[15] software for minicomputer (Nova 3). The figures were drawn with SHELXTL[15] programs on a Zeta-plotter. The final atomic positional and thermal parameters with their e.s.d. for non-hydrogen atoms and including the hydrogen atoms H*h*, H1*w* and H2*w* are given in Table 1. Bond distances and angles are given in Table 2 and intermolecular contact less than 3.6 Å in Table 3.

Table 1. Fractional atomic coordinates ($\times 10^4$) and thermal parameters ($\times 10^3$) with e.s.d.'s in parentheses.

Atom	x	y	z	U[a]	U_{22}	U_{33}	U_{23}	U_{13}	U_{12}
Cu1	1736(1)	1720(1)	-2316(1)	47(1)	44(1)	53(1)	-11(1)	-9(1)	-12(1)
Cu2	2936(1)	-246(1)	-891(1)	30(1)	44(1)	68(1)	-19(1)	-8(1)	-5(1)
Cu3	528(1)	415(1)	704(1)	34(1)	41(1)	53(1)	-15(1)	-10(1)	-9(1)
O*h*	1930(6)	1108(5)	-824(6)	28(4)	40(4)	56(5)	-13(4)	-1(4)	-10(3)
H*h*[b]	2525	1803	-738	54					
O*w*	3276(8)	-148(7)	815(7)	56(6)	70(6)	99(7)	-17(5)	-39(5)	-7(5)
H1*w*[b]	2881	410	1236	94					
H2*w*[b]	4287	-141	681	94					
O*a*	1136(6)	-825(5)	30(6)	33(4)	39(4)	60(5)	-17(4)	-15(4)	-9(3)
N*a*	3496(9)	-1802(8)	-908(9)	39(6)	60(7)	89(8)	-37(6)	-9(5)	-8(5)
C1*a*	1210(11)	-1954(9)	540(10)	39(7)	38(8)	69(9)	-7(6)	-16(6)	-16(6)
C2*a*	2196(11)	-2417(9)	-392(11)	50(8)	45(7)	103(11)	-30(7)	-27(8)	-3(6)
C3*a*	4366(14)	-2134(10)	-238(14)	65(10)	66(9)	162(15)	-41(10)	-70(10)	15(7)
C4*a*	4799(23)	-3336(13)	-70(25)	213(23)	80(13)	396(36)	-101(19)	-230(26)	65(14)
C5*a*	4301(15)	-1897(12)	-2078(12)	81(11)	84(11)	118(13)	-60(10)	3(10)	-7(9)
C6*a*	3657(18)	-1433(13)	-2911(13)	135(16)	104(13)	80(11)	-37(10)	-21(11)	-33(11)
O*b*	742(7)	443(6)	-2099(6)	46(5)	49(5)	54(5)	-9(4)	-2(4)	-23(4)
N*b*	1499(10)	2217(8)	-3847(8)	66(7)	69(7)	59(7)	-12(6)	-15(6)	-15(6)
C1*b*	636(14)	342(11)	-3106(10)	77(10)	81(10)	58(9)	-24(8)	-18(7)	-25(8)
C2*b*	1610(14)	1197(10)	-4121(11)	83(10)	68(10)	55(9)	-5(8)	-15(8)	-14(8)
C3*b*	2666(14)	2965(12)	-4750(11)	71(10)	79(11)	71(10)	-2(8)	-7(8)	-19(8)
C4*b*	2614(18)	3234(15)	-5922(11)	116(14)	152(17)	47(10)	25(10)	-15(10)	-56(12)
C5*b*	186(14)	2702(11)	-3759(12)	81(11)	76(10)	76(10)	11(8)	-29(9)	-5(8)
C6*b*	-7(18)	3793(12)	-3509(15)	110(14)	95(13)	106(14)	3(11)	-27(11)	32(11)
O1*c*	336(7)	1724(6)	1188(7)	39(5)	56(5)	62(5)	-30(4)	-8(4)	-7(4)
O2*c*	2130(10)	1516(8)	1648(9)	61(7)	93(8)	117(9)	-45(7)	-40(6)	1(6)
C1*c*	1150(12)	2014(10)	1529(10)	51(8)	66(8)	52(8)	-23(7)	-5(6)	-21(6)
C2*c*	866(13)	3122(13)	1799(12)	57(9)	109(12)	73(10)	-60(9)	3(7)	-18(8)
C3*c*[c]	469(21)	3992(15)	950(16)	69(7)					
C3*c**[c]	1999(25)	3914(22)	1511(26)	48(10)					
Cl*c*	-367(6)	2818(4)	3225(4)	143(5)	159(5)	109(4)	-78(4)	21(3)	-44(4)
O1*d*	2231(10)	3169(7)	-2458(8)	96(8)	37(5)	83(7)	-4(5)	-20(6)	-28(5)
O2*d*	3295(11)	2914(8)	-1261(9)	129(9)	66(6)	108(8)	-14(6)	-45(7)	-50(6)
C1*d*	2892(15)	3464(9)	-2006(12)	104(12)	36(7)	85(10)	4(7)	-19(9)	-34(7)
C2*d*	3302(35)	4713(17)	-2500(17)	476(46)	132(18)	120(16)	20(13)	-147(24)	-188(24)
C3*d*	3714(27)	5170(14)	-3616(16)	378(37)	98(15)	125(17)	78(13)	-100(21)	-172(20)
Cl*d*	3626(21)	5225(8)	-1713(10)	960(37)	164(8)	279(12)	9(8)	-258(17)	-228(14)
O1*e*	3995(9)	1309(7)	-3222(7)	68(6)	89(6)	69(6)	-26(5)	-4(5)	-7(5)
O2*e*	4703(7)	411(7)	-1835(8)	33(5)	62(6)	82(7)	-13(5)	-8(5)	-17(4)
C1*e*	4870(12)	1050(11)	-2775(12)	40(8)	66(9)	61(9)	-23(8)	-4(7)	-8(7)
C2*e*	6348(13)	1464(10)	-3496(13)	79(12)	83(12)	135(15)	2(11)	-15(11)	-45(9)
C3*e*	7286(18)	686(10)	-4040(15)	51(3)					
Cl*e*[c]	6476(11)	2688(8)	-4300(15)	136(9)	136(9)	212(18)	18(8)	33(9)	-31(6)
Cl*e**[c]	6683(20)	2461(23)	-3111(27)	127(15)	273(28)	169(28)	-76(22)	-18(14)	-56(16)

[a] U_{11} or U_{iso}. [b] Fixed atom. [c] The site occupation factors are 0.65 for atoms C3*c* and Cl*e* and 0.35 for atoms C3*c** and Cl*e**.

Table 2. Interatomic distances (Å) and angles (°) with estimated standard deviations in parentheses.[a]

The copper(II) environments

Cu1 – Oh	2.004(8)	Cu2 – Oh	1.984(7)	Cu3 – Oh	2.013(6)
Cu1 – Ob	1.929(8)	Cu2 – Oa	1.922(6)	Cu3 – Oa	1.995(8)
Cu1 – Nb	2.062(12)	Cu2 – Na	2.054(10)	Cu3 – O1c	1.941(9)
Cu1 – O1d	1.925(10)	Cu2 – O1e	1.931(7)	Cu3 – Ob^i	1.920(9)
Cu1 – O2e	2.349(9)	Cu2 – Ow	2.469(11)	Cu3 – Oa^i	2.301(8)
Oh – Cu1 – Ob	91.0(3)	Oh – Cu2 – Oa	79.7(3)	Oh – Cu3 – Oa	77.3(3)
Oh – Cu1 – Nb	175.1(4)	Oh – Cu2 – Na	164.9(4)	Oh – Cu3 – Ob^i	171.5(3)
Oh – Cu1 – O1d	94.1(4)	Oh – Cu2 – O1e	97.3(3)	Oh – Cu3 – O1c	92.7(3)
Nb – Cu1 – Ob	84.3(4)	Na – Cu2 – Oa	87.0(3)	Ob^i – Cu3 – Oa	94.2(3)
Nb – Cu1 – O1d	90.8(5)	Na – Cu2 – O1e	95.9(4)	Ob^i – Cu3 – O1c	95.7(3)
Ob – Cu1 – O1d	163.8(4)	Oa – Cu2 – O1e	176.9(3)	Oa – Cu3 – O1c	167.8(3)
O2e – Cu1 – Oh	89.0(3)	Ow – Cu2 – Oh	86.9(3)	Oa^i – Cu3 – Oh	90.1(3)
O2e – Cu1 – Ob	103.5(3)	Ow – Cu2 – Oa	89.9(3)	Oa^i – Cu3 – Oa	92.5(3)
O2e – Cu1 – Nb	90.5(4)	Ow – Cu2 – Na	100.2(4)	Oa^i – Cu3 – Ob^i	90.6(3)
O2e – Cu1 – O1d	92.0(4)	Ow – Cu2 – O1e	90.5(3)	Oa^i – Cu3 – O1c	94.5(3)
Cu1 – Oh – Cu2	107.4(4)	Cu1···Cu2	3.213	Oa···Oh	2.503
Cu1 – Oh – Cu3	129.8(4)	Cu1···Cu3	3.638	Oa···Ob	3.013
Cu2 – Oh – Cu3	92.7(3)	Cu1···$Cu1^i$	6.433	Oa···Oa^i	3.111
		Cu1···$Cu2^i$	5.250	Oa···Ob^i	2.869
Cu1···Oa	3.745	Cu1···$Cu3^i$	3.448	Oa···Oh^i	3.060
Cu1···Oa^i	3.392	Cu2···Cu3	2.891	Ob···Ob^i	4.994
Cu2···Ob	3.261	Cu2···$Cu2^i$	5.865	Ob···Oh	2.805
Cu2···Oa^i	4.283	Cu2···$Cu3^i$	3.643		
Cu3···Oh^i	3.342	Cu3···$Cu3^i$	2.978		
Cu3···Ob	3.635				
Cu3···Ow	3.024				

The 2-diethylaminoethanolato ligands *a* and *b*

	a	*b*		*a*	*b*
O – C1	1.44(1)	1.43(2)	C1 – O – Cu3	131.4(7)	
C1 – C2	1.52(2)	1.55(2)	C1 – O – $Cu3^i$	114.2(7)	115.9(7)
N – C2	1.48(2)	1.45(2)	Cu – O – $Cu3^i$		127.2(5)
N – C3	1.49(2)	1.53(2)	Cu2 – O – Cu3	95.1(3)	
N – C5	1.50(2)	1.47(2)	Cu2 – O – $Cu3^i$	118.9(3)	
C3 – C4	1.56(2)	1.52(2)	Cu3 – O – $Cu3^i$	87.5(3)	
C5 – C6	1.49(3)	1.52(2)			
	n = 2	*n* = 1			
Cu*n* – N – C2	103.7(7)	100.2(8)			
Cu*n* – N – C3	107.7(9)	111.8(10)			
Cu*n* – N – C5	112.2(7)	112.9(8)			
C2 – N – C3	113.3(9)	108.3(9)			
C2 – N – C5	112.2(12)	111.7(12)			
C3 – N – C5	107.6(10)	111.4(9)			
N – C2 – C1	109.5(11)	109.8(10)			
N – C3 – C4	115.1(18)	113.0(14)			
N – C5 – C6	114.5(12)	115.4(15)			
O – C1 – C2	106.3(8)	108.0(12)			
C1 – O – Cu*n*	108.7(6)	113.9(6)			

Table 2. Continued.

The 2-chloropropionato ligands *c*, *d* and *e*

	c	*d*	*e*
O1 – C1	1.25(2)	1.23(2)	1.25(2)
O2 – C1	1.23(2)	1.25(2)	1.27(2)
C1 – C2	1.55(2)	1.59(3)	1.55(2)
C2 – C3	1.52(3)	1.34(3)	1.49(2)
C2 – C3*	1.52(3)		
C2 – C1	1.80(1)	1.54(4)	1.62(2)
C2 – C1*			1.62(2)
O1 – C1 – O2	126.1(13)	128.7(12)	126.8(11)
O1 – C1 – C2	114.8(11)	113.0(17)	114.8(13)
O2 – C1 – C2	119.0(14)	118.3(19)	118.2(11)
C1 – C2 – C3	114.9(15)	119.9(21)	116.1(8)
C1 – C2 – C3*	121.7(14)		
C1 – C2 – Cl	104.4(8)	115.2(16)	113.8(10)
C1 – C2 – Cl*			109.9(13)
Cl – C2 – C3	114.8(11)	122.0(22)	115.0(7)
Cl – C2 – C3*	116.6(17)		
C3 – C2 – C3*	84.1(16)		
C3 – C2 – Cl*			129.3(8)
Cl – C2 – Cl*			59.9(14)
Cu1 – O1 – C1		128.3(8)	126.4(8)
Cu2 – O1 – C1			119.2(9)
Cu3 – O1 – C1	123.1(9)		

Symmetry code: (i) $-x, -y, -z$.

[a] E.s.d.'s were not calculated for distances >2.5 Å.

DISCUSSION

The crystal structure of bis[aqua-μ-(2-chloropropionato-*O*,*O'*)-di(2-chloropropionato)-μ_3-(2-diethylaminoethanolato-*N*,μ_3-*O*)-μ-(2-diethylaminoethanolato-*N*,μ-*O*)-μ_3-hydroxo-tricopper(II)],$[Cu_3(Et_2LO)_2(ClC_3H_4O_2)_3(OH)(H_2O)]_2$, is composed of centrosymmetrical hexanuclear molecules located at the inversion center (0,0,0), Fig. 1. The closest intermolecular contact is 2.916 Å between the oxygen atoms of the 2-chloropropionato, (O2*e*), and aqua (1-*x*, -*y*, -*z*) ligands, which might be considered as weak hydrogen bonds. Other short contacts lie in the range 3.3 – 3.6 Å and correspond to van der Waals contact distances,[18] see Table 3.

The bridging oxygen and copper atoms form a centrosymmetric Cu_6O_6 core which is built up of two distorted and fused cubes with the common face Cu3-O*a*-Cu3^{i}-O*a*^{i}. These cubes have two long non-bonding Cu – O distances (Cu2-O*b* = 3.261 and Cu1-O*a*^{i} = 3.392 Å) perpendicular to each other and two parallel bonding Cu – O distances (Cu3-O*a*^{i} = 2.301 Å). The short Cu – O distances completing a cube vary between 1.922 and 2.013 Å, see Fig. 2.

Table 3. Intermolecular contacts <3.6 Å.

O2*e*···O*w*^{ii}	2.916	O*w*···O*w*^{ii}	3.483
O2*d*···C4*a*^{ii}	3.327	Cl*e**···C5*b*^{v}	3.534
C3*a*···C4*a*^{ii}	3.371	O2*c*···C3*a*^{ii}	3.537
Cl*e*···C3*d*^{iii}	3.379	C3*b*···C4*b*^{vi}	3.576
C3*a*···C3*a*^{iv}	3.365		

Symmetry codes

ii: $1-x, -y, -z$	iv: $-x, 1-y, -z$
iii: $1-x, 1-y, -1-z$	v: $1+x, y, z$
	vi: $x, y, 1+z$

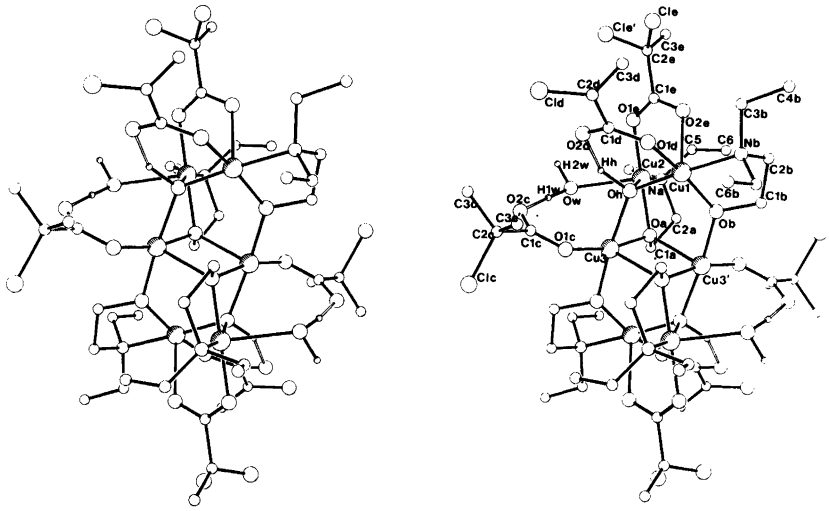

Fig. 1. Stereoview of $[Cu_3(C_6H_{14}NO)_2(ClC_3H_4O_2)_3(OH)\,(H_2O)]_2$.

The $[Cu_3(Et_2LO)_2(H_3CCOO)_3(OH)]_2 \cdot H_2O$ [8] complex has a similar Cu_6O_6 core, where the long perpendicular Cu–O distances of the cubane skeleton are 3.063 and 3.404 Å and the two parallel ones both are 2.369 Å. The short distances vary from 1.919 to 2.048 Å.

These cubes can be compared to those of the $[Cu(R_2LO)\,(R'COO)]_4$ tetramers with respect to the arrangement of the long and short Cu–O distances. In the tetramers there are two pairs of long Cu–O distances perpendicular to each other giving the cubane skeleton a boat-like conformation. The long Cu–O distances vary from 2.52 to 3.01 Å and the short Cu–O distances from 1.85 to 2.02 Å.[6,7]

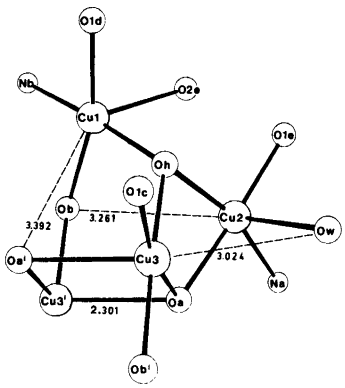

Fig. 2. The central cubane fragment.

In the present investigation all the three copper(II) ions have a square-pyramidal coordination in contrast to $[Cu_3(Et_2LO)_2(H_3CCOO)_3(OH)]_2 \cdot H_2O$,[8] where the coordination number varies from four to six depending on the site population parameter of water. The basal atoms of the Cu1 environment have the largest deviations from their least-squares plane. The *Ob* and *O1d* atoms lie 0.14 and 0.13 Å below and Nb and Oh atoms 0.14 and 0.13 Å above the plane. The dihedral angle between Cu1,-*Oh*,O1*d* and Cu1,*Ob*,Nb is 15.5° indicating some distortion. Cu2 and Cu3 are 0.69 and 0.68 Å above their least-squares basal planes towards the apical oxygen atoms as compared to 0.121 Å for Cu1. All these planes have the triply bridging oxygen atom of the hydroxo ion in common. In addition the Cu2 and Cu3 atoms are bridged by the oxygen atom O*a*. The angles between the least-squares basal planes of Cu1–Cu2 (*a-b*), Cu1–Cu3 (*a-c*) and Cu2–Cu3 (*b-c*) are 91.8, 53.1 and 38.7°, respectively, (Table 4).

The short Cu-ligand distances 1.920–2.013 Å for Cu–O, 2.054 and 2.062 Å for Cu–N are in the range normally observed for Cu(II) complexes.[1,2,4–12] In the apical site of Cu1 there is the second oxygen atom O2*e* of the 2-chloropropionato group coordinated to Cu2, the Cu1–O2*e* distance being 2.349(9) Å. Similar distances in other carboxylato complexes have been reported.[8,19]

The water molecule occupies the apical position of the tetragonal pyramid in the Cu2 coordination

Table 4. Least-squares planes (unit weights) and deviations from the planes (Å).

a. Plane defined by O*h*, O*b*, N*b*, O1*d*:
$8.263x-4.860y-2.985z=1.168$

O*h*	0.134	O1*d*	−0.132
O*b*	−0.144	Cu1	0.121
N*b*	0.142	O2*e*	2.459

b. Plane defined by O*h*, O*a*, N*a*, O1*e*:
$5.831x+2.743y+13.045z=0.413$

O*h*	−0.058	O1*e*	0.049
O*a*	0.063	Cu2	0.069
N*a*	−0.053	O*w*	2.520

c. Plane defined by O*h*, O*a*, O1*c*, O*b*^{i}:
$9.839x-0.838y+8.573z=1.156$

O*h*	−0.057	O*b*^{i}	−0.049
O*a*	0.056	Cu3	−0.068
O1*c*	0.049	O*a*^{i}	−2.368

d. Plane defined by O1*c*, O2*c*, C1*c*, C2*c*:
$2.700x+2.987y-9.191z=-0.488$

O1*c*	0.002	Cu3	0.108
O2*c*	0.002	O*w*	0.580
C1*c*	−0.005		
C2*c*	0.001		

e. Plane defined by O1*d*, O2*d*, C1*d*, C2*d*:
$6.331x-4.580y-6.605z=1.580$

O1*d*	0.004	Cu1	0.260
O2*d*	0.004	O*h*	−0.322
C1*d*	−0.011		
C2*d*	0.003		

f. Plane defined by O1*e*, O2*e*, Cl*e*, C2*e*:
$0.123x+11.905y+7.650z=-0.845$

O1*e*	−0.012	Cu1	1.143
O2*e*	−0.012	Cu2	−0.093
C1*e*	0.032		
C2*e*	−0.009		

sphere. The Cu−O*w* distances of 2.469(11) Å to Cu2 and 3.024 Å to Cu3 differ considerably from the corresponding distances, 2.60(2) and 2.75(3) Å, found in the $[Cu_3(Et_2LO)_2(H_3CCOO)_3(OH)]_2 \cdot H_2O$[8] complex. Thus in the acetato complex the O*w* oxygen forms two weak bonds with the copper(II) ions, while in the 2-chloropropionato complex it forms a somewhat elongated bond and a weak interaction. One reason for the difference coordination of water is the difference in packing between the acetato and 2-chloropropionato complexes. In the acetato complex the water only occupies half of the available positions, whereas in the 2-chloropropionato complex all the positions are occupied. The triply bridging 2-diethylaminoethanolato oxygen completes the coordination sphere of Cu3 (Cu3-O*a*^{i} = 2.301(8) Å). In the sixth site the water oxygen is situated, at a distance of 3.024 Å and with a 19.7° deviation from the *z*-axis, which allows the coordination of Cu3 to be described as 4+1 or 4+1+1*.[20-22]

With the triply bridging oxygen atom of the hydroxo group the three copper(II) ions form a trigonal pyramid, where the oxygen is on the top. The final evidence of this structure was provided by the location of a hydrogen atom at the expected position to complete a distorted tetrahedral environment around the oxygen atom. The Cu-Oh-Cu angles and the location of Oh 0.62 Å above the Cu1-Cu2-Cu3 plane agree well with the data of other Cu_3OH fragments,[8-12,25,26] Table 5. The hydrogen atom of the OH^- group forms a hydrogen bond to the unbonded carboxylato oxygen atom O2*d* (O-H = 1.12, H···O = 1.55, O···O = 2.66 Å and O-H···O = 149.7°).

Two of the three independent 2-chloropropionato ligands are unidentate. The carboxylato group, *c*, bonded to Cu3 is planar and forms a hydrogen bond with the axial water molecule (O−H = 1.00,

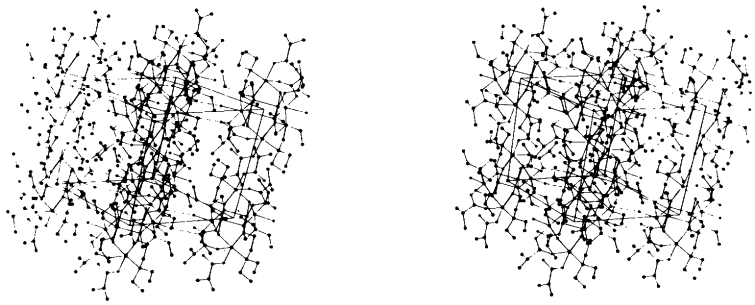

Fig. 3. Stereoview of the packing.

Table 5. The space groups, the interatomic distances (Å) and angles (°) and the deviation from the Cu–Cu–Cu planes in Cu_3OH fragments.

Complex[a]	Space group	Cu1–O	Cu2–O	Cu3–O	Cu1–O–Cu2	Cu2–O–Cu3	Cu1–O–Cu3	Dev.	O···O	Ref.
$[Cu_3(Et_2LO)_2(H_3CCOO)_3(OH)]_2 \cdot H_2O$	$P\bar{1}$	1.934	1.999	2.048	104.1	130.4	94.5	0.63	2.64	8
$[Cu_3(Et_2LO)_2(ClC_3H_4O_2)_3(OH)(H_2O)]_2$	$P\bar{1}$	1.984	2.004	2.013	107.4	129.8	92.7	0.62	2.657	*b*
$[Cu_2(C_9H_7N)_2(F_3CCOO)_3(OH)]_2$	$P\bar{1}$	1.964	1.963	1.990	116.9	124.8	98.6	0.51	2.550	10
$Ag[Cu_2(C_8H_4O_4)_2(OH)] \cdot 5H_2O$	$P\bar{1}$	1.955	1.911	1.949	109.9	117.3	96.8		2.535	25
$[Cu_4(C_6H_5NO_3)_4(OH)_2(SO_4)(H_2O)_4]$	$C2$	1.99	1.97	1.95		117.9	92.1	0.53	2.51	26
$[Cu_3(C_{10}H_{11}N_2O)_3(ClO_4)(OH)] \cdot ClO_4$	$P2_1/n$	1.946	1.969	1.978	107.1	110.0	109.3	0.70		9
$[Cu_3(C_6H_5N_2O)_3(SO_4)(OH)] \cdot 16.3H_2O$	$P\bar{3}$	1.98	1.98	1.98	108.2	108.2	108.2	0.70	2.36	11
$[Cu_3(C_8H_{17}N_2O)_3(H_2O)_3(OH_{\frac{1}{2}})]$-$\cdot 1.5ClO_4 \cdot 4H_2O$	$R\bar{3}$	1.97	1.97	1.97	110.9	110.9	110.9	0.7	2.75	12

[a] Abbreviations: Et_2LO = 2-diethylaminoethanolato, $ClC_3H_4O_2$ = 2-chloropropionato, C_9H_7N = quinoline, $C_8H_4O_4$ = *o*-phthalato, $C_{10}H_{11}N_2O$ = 3-(phenylimino)-butane 2-oximato, $C_6H_5N_2O$ = pyridine-2-carbaldehyde oximato, $C_6H_5NO_3$ = isonicotinato *N*-oxide, $C_8H_{17}N_2O$ = 2-propylamino-2-methyl-3-butane oximato. [b] This work.

H···O = 1.70, O···O = 2.69 Å and O–H···O = 165.3°). The carboxylato group, *d*, is coordinated to the Cu1 and forms a hydrogen bond with the triply bridging hydroxo ion as mentioned before. The third carboxylato group, *e*, is bidentate bridging from the basal coordination site of Cu2 to the apical position of Cu1 in a *syn-syn* configuration. This coordination type is quite common in carboxylato complexes.[6–8,10,19]

The bond distances and angles of the 2-chloropropionato ligands are normal except for the C–Cl bond lengths. In the *c* ligand the C2-Cl 1.80(1) Å is in the range normally reported[23,24] but the other two C–Cl bonds are much shorter, 1.54(4) and 1.62(2) Å for the ligands *d* and *e*, respectively. One reason for this is the structural disorder. Since the 2-chloropropionato ligand is optically active and the complex has an inversion centre, the symmetry related molecules must have different enantiomorphs in the crystal structure. In this structure the enantiomorphs are probably mixed. This is also supported by the peaks observed close to the carboxylato groups in the difference Fourier maps.

The bond distances and angles of the two 2-diethylaminoethanolato ligands are as expected.[1–8] In the five-membered ethanolato-copper rings the dihedral angles O,Cl,C2,N are 55.1 and −43.8° for the ligands *a* and *b*. In the chelate ring of ligand *a*, C1 lies 0.48 Å above and C2 0.23 Å below the plane defined by O*a*-Cu2-N*a*. In the other chelate ring C1 and C2 lie on the same side and 0.32 and 0.84 Å from the plane defined by O*b*-Cu1-N*b*. The ethanolato O*a* is tetracoordinated, while O*b* is tricoordinated. The angles around O*a* are approximately tetrahedral (mean value 109.3°) as in the $[Cu_3(Et_2LO)_2(H_3CCOO)_3(OH)]_2 \cdot H_2O$[8] complex and in $[Cu(R_2LO)(R'COO)]_4$ tetramers.[6,7]

The bond angles around O*b* vary from 113.9 to 127.2° (mean 119.0°). The atom O*b* deviates 0.18 Å from the plane defined by Cu1–Cu3^i–C1*b*. The oxygen environment can be considered as a deformed tetrahedron.

REFERENCES

1. Smolander, K. *Acta Chem. Scand. A 35* (1981) 815 and references therein.
2. Mergehenn, H. and Haase, W. *J. Chem. Soc. Dalton Trans.* (1980) 1703.
3. Estes, E. D. and Hodgson, D. J. *Inorg. Chem. 14* (1975) 334.
4. Smolander, K. *Acta Chem. Scand. A 36* (1982) 589.

5. Muhonen, H., Pajunen, A. and Hämäläinen, R. *Acta Crystallogr. B 36* (1980) 2790.
6. Smolander, K. *Acta Chem. Scand. A 36* (1982) 189 and references therein.
7. Ahlgrén, M., Turpeinen, U. and Hämäläinen, R. *Acta Crystallogr. B 38* (1982) 429.
8. Ahlgrén, M., Turpeinen, U. and Smolander, K. *Acta Crystallogr. B 36* (1980) 1091.
9. Butcher, R. J., O'Connor, C. J. and Sinn, E. *Inorg. Chem. 20* (1981) 537.
10. Little, R. G., Moreland, J. A., Yawney, D. B. W. and Doedens, R. J. *J. Am. Chem. Soc. 96* (1974) 3834.
11. Beckett, R. and Hoskins, B. F. *J. Chem. Soc. Dalton Trans.* (1972) 291.
12. Ross, P. F., Murmann, R. K. and Schlemper, E. O. *Acta Crystallogr. B 30* (1974) 1120.
13. Bateman, W. G. and Conrad, D. B. *J. Am. Chem. Soc. 37* (1915) 2553.
14. Main, P., Hull, S. E., Lessinger, L., Germain, G., Declerq, J. P. and Woolfson, M. M. *MULTAN 78*. Universities of York, England and Louvain, Belgium 1978.
15. Sheldrick, G. M. *The SHELXTL 1981 (Revision 3) Computer Programs*, Nicolet XRD Corporation, Cupertino, USA 1981.
16. *International Tables for X-Ray Crystallography*, Kynoch Press, Birmingham 1974, Vol. 4.
17. Stewart, J. M., Ed., *The X-Ray System, Version of 1976*, Technical Report TR-446, Computer Science Center, Univarsity of Maryland, College Park 1976.
18. Bondi, A. *J. Phys. Chem. 68* (1964) 441.
19. Cingi, M. B. *Acta Crystallogr. B 35* (1979) 312.
20. Hathaway, B. J. and Hodgson, P. G. *J. Inorg. Nucl. Chem. 35* (1973) 4071.
21. Hathaway, B. J. *Struct. Bonding (Berlin) 14* (1973) 49.
22. Gažo, J., Bersuker, I. B., Garaj, J., Kabešová, M., Kohout, J., Langfelderová, H., Melník, M., Serátor, M. and Valach, F. *Coord. Chem. Rev. 19* (1976) 253.
23. Turpeinen, U. *Ann. Acad. Sci. Fenn. Ser. A 2, 182* (1977).
24. *International Tables for X-Ray Crystallography*, Kynoch Press, Birmingham 1976, Vol. 3, Table 4.2.1.
25. Cingi, M. B., Lanfredi, A. M. M., Tiripicchio, A. and Camellini, T. *Acta Crystallogr. B 35* (1979) 312.
26. Knuutila, P. *Inorg. Chim. Acta 58* (1982) 201.

Received April 8, 1982.

Acta Chemica Scandinavica A 37 (1983) 15–23

Chloromethyl-cyclopropane. Molecular Structure and Conformation in the Gas Phase as Determined by Electron Diffraction and Compared to Molecular Mechanics Calculation

S. H. SCHEI

Department of Chemistry, University of Trondheim, NLHT Rosenborg, N-7000 Trondheim, Norway

A gas phase electron diffraction study of chloromethyl-cyclopropane indicates that at 45 °C there is predominantly *gauche* conformer. The structure results in terms of r_a distances and $\angle_\alpha$ angles are as follows: $r(\langle C-C\rangle)=1.519(3)$ Å ($\langle\ \rangle$ denoting average), $r(C-Cl)=1.798(5)$ Å, $r(\langle C-H\rangle)=1.087(9)$ Å, $\angle C-C-C(\text{exocyclic})=117.2(.9)^\circ$, $\angle C-C-Cl=112.6(.7)^\circ$, $\angle C-C-H(\text{ring})=116.0(1.5)^\circ$, $\angle C-C-H(CH_2Cl)=110.3(3.2)^\circ$, τ_g (*gauche* torsional angle relative to 0° for C–Cl bond eclipsing cyclopropane ring)=116.0(3.8)°. Uncertainties are given as 2σ, where σ includes uncertainties due to correlation among observations, electron wavelength and other parameters used in the data reduction. A molecular mechanics calculation agrees to the conformational result of the electron diffraction study. A normal coordinate analysis based on a valence force field was made, and some frequencies were suggested reassigned.

Conformational behaviour when a cyclopropane ring has a vinyl or another double bond containing substituent, has to some extent been investigated in gas phase by electron diffraction (ED).[1-4] However, studies of such molecules with saturated substitution seem to be fewer.[5] The simplest example of rotational conformation of a saturated group connected to a cyclopropane ring is a CH_2X group. Both bromomethyl- and chloromethyl-cyclopropane have been studied in the gas phase by microwave (MW) spectroscopy[6-8] and by infrared and Raman spectroscopy.[9-11] From one of the MW studies of chloromethyl-cyclopropane,[7] it was concluded that two conformers coexisted. The other MW investigation[8] and the infrared and Raman data of Ref. 9 were interpreted as showing practically only *gauche* conformer. In a more recent work[10] it was concluded that the amount of *gauche* conformer was 95 % in the liquid phase.

Methyl-cyclopropane has been studied by ED.[13] It was not expected as possible to obtain relaible information, neither about deviations between the skeletal structure of methyl-cyclopropane and chloromethyl-cyclopropane, nor about differences within the ring bond lengths.[14] Therefore, the main objective of this investigation is to study the conformation of the molecule.

EXPERIMENTAL AND DATA REDUCTION

A commercial sample of chloromethyl-cyclopropane (>98 %) was obtained from Aldrich Chemical Company. Data were recorded with the Balzer Eldigraph KDG-2 apparatus[15,16] at a nozzle temperature of 45 °C. Nozzle-to-plate distances of 50.0 and 25.0 cm were used. The electron wavelength was calibrated against benzene.[17] Electron diffraction photographs were recorded on Kodak Electron Image plates. Optical densities were measures by a single-beam densitometer. For the 50 and 25 cm data, 4 and 3 plates, respectively, were selected for analysis. The data were reduced using standard data reduction programs for the Norwegian ED group.[18]

A calculated background[19] was subtracted from the experimental data. This was done for each plate to yield data I_m (s) corresponding to the formula

$$I_m(s)=k\sum_{i\neq j} n_{ij}|f'_j(s)|f'_j(s)|cos[\eta_i(s)-\eta_j(s)]$$
$$\exp(-\tfrac{1}{2}l_{ij}^2s^2)\sin(r_{ij}s)(r_{ij}s)^{-1}$$

f's are modified electron scattering amplitudes, η's the phases of the scattered waves r_{ij} and l_{ij} the interatomic distances r_a and the root-mean-square

0302-4377/83 $2.50

amplitudes of vibration, and n_{ij} the multiplicity of these distances.

Data for each camera distance were combined to one average curve.[18] The least square refinements were based on curves in the form $sI_m(s)$. Least square calculations were made by a modified version of a program originally written by L. Hedberg, who also wrote the original versions of the programs used to calculate backgrounds and radial distribution (RD) curves. Calculation of vibrational quantities used in the analysis were made by a program written by R. L. Hilderbrandt. The electron scattering amplitudes and phase shifts[18] were calculated analytically by a program originally written by A. C. Yates. For these calculations Hartree-Fock potentials were used[20] for C and Cl while molecular bonded potentials were used for H.[21] The molecular mechanics calculations were made by a program written by S. Rustad, R. Stølevik and H. M. Seip.

Table 1. Chloromethyl-cyclopropane. Results from the normal coordinate analysis. Observed frequencies are taken from Ref. 9.

Frequency Obs.	Calc.	Approx. description	Potential energy distribution
gauche conformer			
3085	3105	asym. str. CH_2 (ring)	$C-H_{ring}$ (100)
–	3103	asym. str. CH_2 (ring)	$C-H_{ring}$ (100)
3077	3077	str. CH	$C-H_3$ (87)
3031	3039	sym. str. CH_2 (ring)	$C-H_{ring}$ (86)
3009	3019	sym. str. CH_2 (ring)	$C-H_{ring}$ (99)
2996	2984	asym. str. CH_2 (Cl)	$C-H_{Cl}$ (100)
2956	2962	sym. str. CH_2(Cl)	$C-H_{Cl}$ (98)
1460	1483	sci. CH_2 (ring)	$H-C-H_{ring}$ (48) $C-C-H_{ring}$ (46) $C-C_{ring}$ (26)
1447	1449	sci. CH_2 (Cl)	$H-C-H_{Cl}$ (63) $C-C-H_{Cl}$ (15)
1433	1433	sci. CH_2 (ring)	$H-C-H_{ring}$ (65) $C-C-H_{ring}$ (15)
1375	1366	bend CH	$C-C-H_3$ (34) $C-C-H_{ring}$ (22) $C-C-H_2Cl$ (20)
1293	1233	str. $C-CH_2Cl$	$C-CH_2Cl$ (25) $C-C-H_{Cl}$ (19)
1281	1296	wag CH_2 (Cl)	$C-C-H_{Cl}$ (54) $Cl-C-H$ (42)
1268	1262	tw. CH_2(Cl)	$C-C-H_{Cl}$ (40) $C-CH_2Cl$ (28)
1197	1144	def. ring	$C-C_{ring}$ (29) $C-C-H_{ring}$ (17) $C-CH_2Cl$ (17)
1168	1189	asym. rock CH_2 (ring)	$C-C-H_{ring}$ (99)
1117	915	asym. tw. CH_2 (ring)	$C-C-H_{ring}$ (52)
1051	1038	asym. wag CH_2 (ring)	$C-C-H_{ring}$ (72)
1022	1005	sym. wag CH_2 (ring)	$C-C-H_{ring}$ (69)
973	970	sym. rock CH_2 (ring)	$C-C_{ring}$ (35) $C-C-H_{ring}$ (43) $Cl-C-H$ (23)
918	924	def. ring	$C-C_{ring}$ (75) $C-C-H_{ring}$ (17)
882	882	rock CH_2 (Cl)	$C-C-H_{ring}$ (60) $Cl-C-H$ (28)
834	805	def. ring	$C-C_{ring}$ (44) $C-C-H_{ring}$ (17)
796	796	bend CH	$C-C-H_3$ (54) tors. ring (14) $C-C-H_{ring}$ (16)
773	736	sym. tw. CH_2 (ring)	$C-C-H_{ring}$ (103) tors. ring (24)
700	700	str. C – Cl	C – Cl (62)
399	412	bend C – C – C	C – C – C (70)
343	328	bend C – C – C	C – C – C (43) C – Cl (23)
213	215	bend C – C – Cl	C – C – Cl (42) C – C – C (31)
100	99	tors. $C-CH_2Cl$	tors. $C-CH_2Cl$ (82)
syn conformer			
–	689	str. C – Cl	C – Cl (43) $C-C_{ring}$ (39)
462	457	bend C – C – C	C – C – C (34) C – Cl (37)
–	331	bend C – C – C	C – C – C (71) tors. ring (23)
–	164	bend C – C – Cl	C – C – Cl (53) C – C – C (33)
–	108	tors. $C-CH_2Cl$	$C-CH_2Cl$ (71) tors. ring (24)

NORMAL COORDINATE ANALYSIS

The present conformational study was expected to be sensitive to the values of the vibrational quantities, which therefore should be calculated as accurately as possible. A valence force field was used. The force field was combined from two sources. For the cyclopropane ring, the force field in Ref. 22 was used. For the CH_2Cl group part of a force field for 3-chloro-propene was used. This force field has shown good transferability,[23] partly because great care was taken to devlope the force field with as few and as local interaction force constants as possible.

As a start it was decided to use $C-C_2-H_3$ bend and interaction force constants equal to those of the ring CH_2 groups. The force constants for exocyclic $C-C-C$ bends and $C-C-C/C-C-C$ interaction was first taken from Ref. 24. The torsional force constants were fitted to the observed *gauche* torsional frequency,[9,10] 100 cm^{-1}. By using this force field, the normal coordinate calculation for *gauche* conformer gave most frequencies in good agreement with observed ones.[9,10] However, the approximate description according to the present calculation is partly different from earlier interpretations.[9,10] In Table 1 are given calculated frequencies and the description suggested from the present calculation. The calculated frequencies in Table 1 are the result of a force field with slight modifications for $C-C-C$, $C-C-C/C-C-C$ and $C-C_2-H_3$ force constants. The force constants associated with the $CH-CH_2Cl$ part of the molecule are given in Table 2.

Table 2. Chloromethyl-cyclopropane. Valence force constants used for the $CH-CH_2Cl$ part of the molecule.

Type of force constant	Value[a]
C_2-C_3	4.96
$C-Cl$	2.66
C_3-H	4.82
C_2-H_3	5.13
$C-C-Cl$	1.01
C_2-C_3-H	0.77
$Cl-C-H$	0.64
$H-C_3-H$	0.52
$C-C_2-H_3$[b]	0.51
$C-C-C$[b]	0.95
$\tau(C-CH_2Cl)$[b]	0.11
C_3-H/C_3-H	0.07
C_2-C_3/C_2-C_3-H	0.43
C_2-C_3-H/C_2-C_3-H	−0.04
$Cl-C-H/C_2-C_3-H$	0.08
$C-C-C/C-C-C$[b]	0.20

[a] In mdyn $Å^{-1}$ and mdyn Å rad^{-2}. [b] Force constants fitted to observations.

The frequencies observed at 1293, 1168, 973 and 796 are described differently from the interpretations of Refs. 9 and 10. The present interpretation is strengthened by the fact that ring CH_2 twist and rock and CH bend frequencies are now quite close to the corresponding frequencies in bromocyclopropane[25] and cyclopropane.[22] It should be pointed out that, by varying the force constants within resonable limits, the present calculation can definitely not give as low a $C-CH_2Cl$ frequency as 970 cm^{-1}.

The present calculation shows good transferability of the force field used for the CH_2Cl group. However, there is an interesting similarity to 3-chloro-1-propene not associated with the CH_2Cl part of the molecule. The value obtained for $C-C_2-H_3$ bend force constants is very close to the value of the $=C\overset{C}{\underset{H}{<}}$ force constant in 3-chloro-1-propene, 0.52 mdyn Å rad^{-2}. If the double bond in 3-chlor-1-propene is regarded as a bent bond, the low $C-C_2-H_3$ bend in chloromethyl-cyclopropane corresponds to the out-of-plane $=C-H$ bend in 3-chloro-1-propene, observed at 590 cm^{-1}.[26] By giving double masses to the terminal $=CH_2$ group in 3-chloro-1-propene, the $CH_2=CH$ group is made equally heavy as the C_3H_5 group in chloromethyl-cyclopropane. Such a calculation gives a $=C-H$ out-of-plane frequency of 870 cm^{-1}, while the in-plane $=C-H$ bend is still close to 1300 cm^{-1}. This corresponds quite well to 796 and 1375 cm^{-1} for similar bend frequencies in chloromethyl-cyclopropane.

As to the present interpretation, the calculated frequencies of the *gauche* conformer deviates by 19 cm^{-1} as an average from the ones observed in Ref. 9. It is likely that the *gauche* vibrational quantities are calculated as good approximations to the actual values. However, for the *syn* conformer ($C-Cl$ bond eclipsing the ring) there is more uncertainty associated with the vibrational quantities, especially since there is no observed torsional frequency. All force constants used for *syn* conformer were directly transferred from the *gauche* conformer. However, the effect of variation in *syn* torsional force constants was estimated by a calculation according to the method of partial force constants

Table 3. Chloromethyl-cyclopropane. Vibrational amplitudes, calculated and refined, at temperature 45 °C.

Type of distance	$r^{a,b,c}$	l^a		
		Calc.[b]	Refined[d]	Parameter No.
C–H	1.09	0.77	0.071(5)	12
$C-C_{ring}$	1.59	0.049	0.052 } (3)	13
$C-CH_2Cl$	1.59	0.051	0.054 }	
C–Cl	1.80	0.052	0.043(3)	14
$C_1\cdots C_3$	2.59	0.079		
$C_2\cdots Cl$	2.76	0.079	0.079(7)	15
$C_1\cdots Cl$	3.50(3.00)	0.172(0.156)	0.179(33)	16
$C_4\cdots Cl$	4.09(3.16)	0.094(0.156)	0.096(10)	17

[a] In Å. [b] Values in parentheses for *syn* conformer. [c] r_a distances correspond to independent parameters in Table 6. [d] Error estimates as described in text.

developed for acyclic halopropanes[27] and by comparison to 3-chloro-1-propene.[23] Thus, apart from the *gauche* value of 0.11; 0.05 and 0.20 mdyn Å rad^{-2} were used for calculating *syn* vibrational quantities. However, the influence on the vibrational quantities associated with the conformational dependent distances $C_1\cdots Cl$ and $C_4\cdots Cl$ (see Fig. 2) is small; Calculated root-mean-square amplitudes of vibration are given in Table 3.

In Table 1 are included the lower frequencies calculated for *syn* conformer.

In liquid phase there was observed a band at 462 cm^{-1} which was assigned as belonging to the *syn* conformer.[9] The present normal coordinate calculation supports this by a calculated *syn* frequency of 457 cm^{-1}. Contrary to the calculation in Ref. 9, the present potential energy distribution shows considerable contribution from C–Cl stretch to the corresponding normal coordinate. This frequency may be expected to be one of the strongest in the *syn* conformer spectrum. Therefore, even at low concentration of *syn* conformer this frequency may show up as a weak band.

MOLECULAR MECHANICS CALCULATION

The molecular mechanics (MM) calculations were based on use of non-bonded potential functions described as Morse curves.[28] The intrisic torsional barrier was determined by a similar MM calculation for methyl-cyclopropane, where the energy barrier was fitted to an observed value of 2.90 k cal mol^{-1}.[29,30] Other parameters were identical to those used for MM calculations of a series of haloalkanes.[31,32]

The MM calculations were made with complete geometry relaxation. Two well-defined minima were found. The energetically most stable conformer was found to be *gauche*. The ED observable quantities, *gauche* torsional angle τ_g and *syn* torsional amplitude $\langle\tau_s^2\rangle^{\frac{1}{2}}$, and other results from the MM calculations are given in Table 4.

The MM calculated energies do not include zero-point vibrational energy. This was included in the calculation of conformational composition (α_g, α_s, g and s denoting *gauche* and *syn* respectively) by calculating the vibrational partition functions, Q^{vib}, with respect to the potential energy minima. The conformational composition in the gas phase is described by

$$\frac{\alpha_g}{\alpha_s} = 2\left(\frac{Q_g}{Q_s}\right)^{rot}\left(\frac{Q_g}{Q_s}\right)^{vib} \times \exp(-\Delta E/RT) = 2q\exp(-\Delta E/RT)$$

Table 4. Chloromethyl-cyclopropane. Results obtained from molecular mechanics calculation.[a]

Conformer	*gauche*	*syn*
$-\Delta E$ (k J mol^{-1})[b]	0.0	6.9(6.6)[c]
Barriere towards *gauche*[b]	15.9	17.1
Torsional angle in energy minimum	117.1	0.0
τ and $\langle\tau_s^2\rangle^{\frac{1}{2}}$	117.5	11.0
Torsional force constant (mdyn Å rad^{-2})	0.11	0.13
∠C–C–Cl	109.2	113.9
∠C–C–C	118.0	119.9

[a] For meaning of symbols, see text. [b] Used following charges: C_{ring} −0.016, C_3 0.005, H_{ring} 0.018, $H_{4,5}$ 0.041, Cl −0.141. [c] Calculated by using zero charge on all atoms.

where ΔE is the difference between minima of *gauche* and *syn* conformer. The rotational partition functions were calculated from the MM obtained geometries. The value of $(Q_g/Q_s)^{vib}$ is somewhat dependent on the unknown *syn* torsional frequency. By using the same limits for force constants as described for calculation of vibrational quantities, the value of q varied from 0.7 to 1.0. If this variation is used as the only error estimate, the MM calculations give a contribution of 94 ± 3 % *gauche* conformer.

The torsional force constants were also calculated directly from the MM results. As can be seen from Tables 2 and 4, the MM calculated *gauche* torsional force constant is in excellent agreement with the value obtained from observations.

STRUCTURE AND CONFORMATION

In Fig. 2 is shown the RD curve calculated from the experimental intensity curve in Fig. 1 as

$$D(r)=\frac{2}{\pi}\Delta s\sum_{s_{min}}^{s_{max}}(|f'_{Cl}||f'_{C}|)^{-1}sI_m(s)\exp(-Bs)\sin rs$$

The main interatomic distances (for atomic numbering see Fig. 2) for the *gauche* conformer are indicated on the figure. The torsion dependent C···Cl distance of a possible *syn* conformer will be located at 3.1 Å. It is obvious from the experimental RD curve that the amount of *syn* conformer is very small, if any at all.

For the least square refinements a unit weight matrix was used. The molecular geometry was calculated using the geometry consistent r_α parameters,[32] $r_a=r_\alpha-\frac{l^2}{r}+K$. After a preliminary test only *gauche* and *syn* conformers were considered. Some restrictions had to be made on the molecular geometry. Experience from 1-butene[34] and 3-chloro-1-propene[12] indicates that MM calculations will give quite reliable angle differences between conformers. Except for the torsion angle, the most pronounced parameter difference between *gauche* and *syn* conformers are the C–C–Cl angle and the exocyclic C–C–C angles. The *syn* C–C–Cl and C–C–C angles are MM calculated to be respectively 4.7 and 1.9° larger than the *gauche* ones. The differences were kept constant at these values during the least square refinements. However, as the refinements showed a quite large *gauche* C–C–

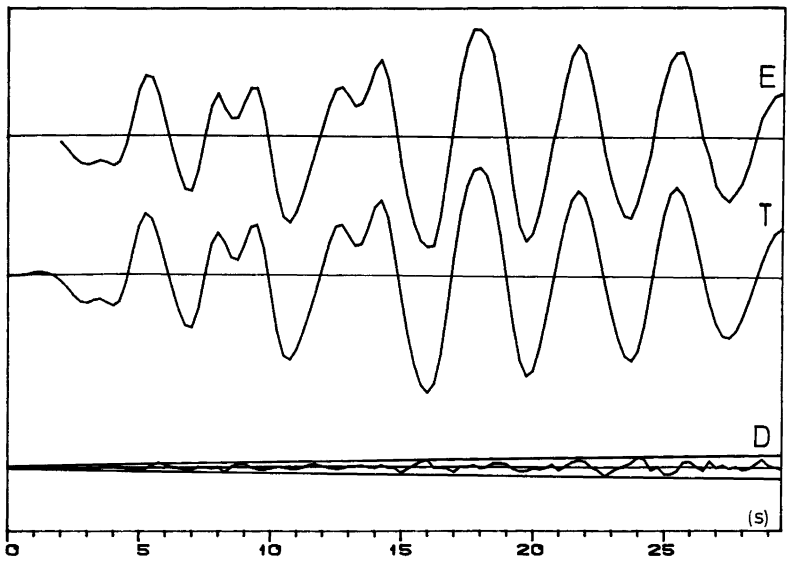

Fig. 1. Chloromethyl-cyclopropane. Intensity curves in the form $sI_m(s)$. Experimental curve (E) is the composite curve for all plates and camera distances. Theoretical curve (T) was calculated from parameters in Tables 3 and 6. Difference curve (D) is $E-T$. All curves are on the same scale. $\Delta s=0.25$. The straight lines give the experimental uncertainties as three times the standard deviation.

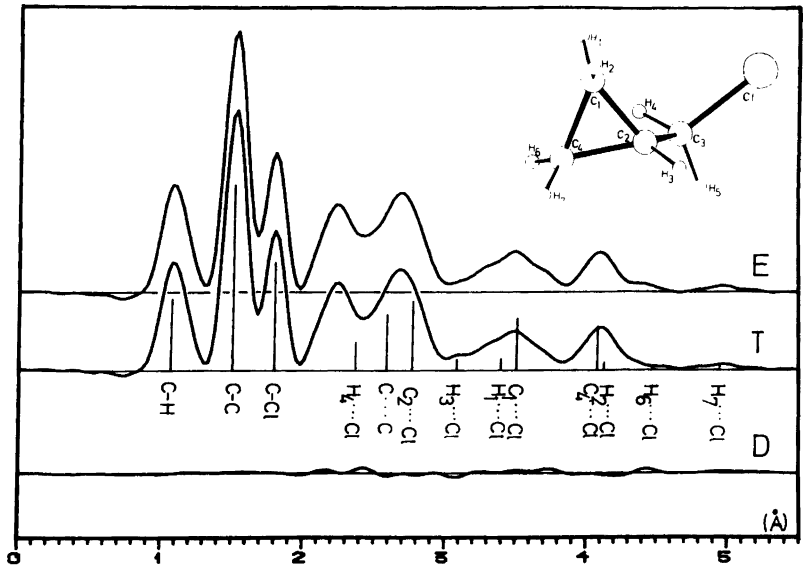

Fig. 2. Chloromethyl-cyclopropane. Radial distribution curves as fourier transforms of the intensity curves in Fig. 1, using $B=0.0015$ Å^2 and theoretical data for unobserved area $0<s<2.0$. The vertical lines show the most important distances, height being proportional to weight of distance. All curves are on the same scale.

Cl angle, the difference was reduced to 2.0°. In addition only the torsion angle was different for the two conformers.

All C–C bond lengths within the ring were assumed to be equal. Also all ring C–C–H angles were refined to an average value C_s symmetry was assumed for the CH_2Cl group. These assumptions seemed to be justified by the MM calculations, since the variation within the parameters refined as averages were very small. In addition all C–H distances were assumed to have the same length.

The difference $\Delta C-C=r(C-CH_2Cl)-r(C-C_{ring})$ could not be determined directly from the ED data. A refinement where all the vibrational amplitudes were kept at their calculated values gave an unreasonably large value $\Delta C-C=0.05\pm0.02$ Å. Though $\Delta C-C$ was systematically varied, it was not possible to judge from *R*-factors or RD curves whether the actual difference was positive or negative. However, when the MW results for rotational constants, B_0, for $C_3H_5CH_2{}^{35}Cl$ were taken into consideration,[8] the best fit to B_0 was obtained for $\Delta C-C=0.00$ Å. The r_α parameters were converted to a r_z structure[33] according to the formula

$$r_z=r_\alpha(0)=r_\alpha(T)-\tfrac{3}{2}a(\langle l(T)^2\rangle-\langle l(0)^2\rangle)+K(T)-K(0),$$

where 0 and T denote parameter value at 0 K and actual temperature, *a* is the Morse anharmonicity parameters whose values were taken from diatomic molecules.[35] Corrections for vibration–rotation interaction were made[33] and resulting B_0 values can be compared to MW observations from Table 5.

$\Delta C-C$ strongly correlated to other geometry parameters, (correlation coefficients $\rho(1/2)=-.9$, $\rho(2/8)=-.5$ and $\rho(2/9)=-.4$). A variation of $\Delta C-C=0.02$ changes the exocyclic C–C–C and the C–C–Cl angles by 0.5 and 0.8°, respectively. However, a larger absolute value than 0.02 Å for $\Delta C-C$ seems unreasonable. Thus, the influence on other parameters from keeping $\Delta C-C=0.00$ for further refinements, was not very large. After

Table 5. Chloromethyl-cyclopropane. Calculated rotational constants (in MHz) and values obtained from microwave experiment of Ref. 8.

	$C_3H_5CH_2{}^{35}Cl$		$C_3H_5CH_2{}^{37}Cl$	
Constant	ED	MW	ED	MW
A	11747	11746	11731	11692
B	2018	2047	1968	1998
C	1867	1887	1823	1843

Table 6. Chloromethyl-cyclopropane. Final structural results from analysis of electron diffraction data at 45 °C.

No.	Parameter type	Parameter value (r_a, $\angle_\alpha$)[a]
1	$\langle C-C_{ring}\rangle$	1.519(3)
2	$\Delta C-C$[b]	0.00[e]
3	C–Cl	1.798(5)
4	$\langle C-H\rangle$	1.087(9)
5	C_2-C_3-H	110.3(3.2)
6	$pCl-C-H$[c]	120.[d]
7	$C-C-H_{ring}$	116.0(1.5)
8	C–C–Cl	112.6(.7)
9	C–C–C	117.2(.9)
10	τ_g	116.0(3.8)
11	α_g	96(9)
	R	7.9

[a] In Å and deg. [b] Defined in text. [c] Angle between projections of C_3-Cl and C_3-H on plane perpendicular to the $C-CH_2Cl$ bond. [d] Assumed. [e] For choice of value, see text.

introducing a constant value for ΔC–C, root-mean-square amplitudes associated with bonded distances and C···Cl distances of the *gauche* conformer were allowed to refine.

The value of syn torsional amplitude influences the obtained composition quite strongly. Allowing $\langle\tau_s^2\rangle^{\frac{1}{2}}$ to take the value 40°, gave as result 85 % *gauche* conformer. However, such a model did not improve the fit to the experimental data. Because of the quite strong influence of the value of $\langle\tau_s^2\rangle^{\frac{1}{2}}$ on the conformational composition, it was decided to introduce pseudo-conformers in *syn* position. Instead of one *syn* conformer, whose ED observable position is determined by $\langle\tau_s^2\rangle^{\frac{1}{2}}$, several pseudo-conformers at equally distributed torsional angles were used. Vibrational amplitudes were calculated without contribution from the torsional movement. A *gauche* contribution as low as 85 % could not be obtained for this model. In the final model were used 4 *syn* pseudo-conformers distributed according to the potential energy function resulting from the MM calculations. The torsional angles and distribution within the *syn* pseudo-conformers thus obtained were: 5.° (56 %), 15.° (32 %), 25.° (9 %) and 35.° (3 %).

RESULTS

The molecular structure of the *gauche* conformer, which is essentially the only conformer present, is given in Table 6. The error estimates are obtained

Table 7. Chloromethyl-cyclopropane. Parameter value comparison to some related molecules.[b]

Molecule	Method	$\langle C-C_{ring}\rangle$	ΔC–C	$\langle C-C\rangle$[c]	∠C–C–C	∠C–C–Cl	C–Cl	τ_g	Ref.
Methyl cyclopropane	*ab initio*	1.518	−.018	1.513	115.6	–	–	–	14
	MW	(1.514)[a]	.008	1.516	118.9	–	–	–	30
	ED	1.509(2)	.008	1.511	118.4	–	–	–	13
Bromomethyl-cyclopropane	MW	(1.514)[a]	.008	1.516	117.7	–	–	–	6
Chloromethyl cyclopropane	MW	(1.514)[a]	(.008)[a]	–	(115.8)[a]	(109.5)[a]	1.791(2)	120.2(.5)	8
	ED	–	–	1.519(3)	117.2(.9)	112.6(.7)	1.798(5)	116.0(3.8)	this work
3-chloro-1-propene	ED	–	–	1.494(2)	–	110.7(.4)	1.791(1)	–	12
3-chloro-2-methyl-1-propene	ED	–	–	1.499(1)	–	113.0(.2)	1.790(1)	–	23
1-chloro-propane	ED	–	–	1.53(2)	–	111.(2.)	1.77(2)	–	41
Ethylchloride	ED	–	–	1.526(4)	–	110.7(.3)	1.802(3)	–	42
1,3-dichloro-propane	ED	–	–	1.529(4)	–	111.6(.1)	1.796(3)	–	39

[a] Assumed value. [b] Error estimates are not directly comparable throughout the table. [c] For acyclic molecules this is the $C-CH_2Cl$ bond length.

from least square standard deviation, σ_0, as $2\sigma = 2[(c_1\sigma_0)^2 + c_2 r^2]^{\frac{1}{2}}$, where c_1 includes correction for correlation among observations;[36] $c_1 = 2$ when $r < 2$ Å, $= 1.5$ when $2 < r < 3$ Å and $= 1$ when $r > 3$ Å. c_2 includes corrections for uncertainty in the electron wavelength and other parameters used in data reduction; $c_2 = 0.001$ for distances and amplitudes of vibration. For angles and conformational composition $c_1 = 1.5$ and $c_2 = 0$.[36] The correlation coefficients for which $|\rho| > 5$ are: $\rho(4/10) = .6$, $\rho(5/8) = .-5$, $\rho(8/9) = .5$, $\rho(8/10) = .6$, $\rho(9/10) = .7$, $\rho(11/16) = .7$ and $\rho(11/17) = .6$.

Based on the parameters described in Table 3 (refined *l*'s) and 6, and use of the *syn* pseudo-conformer model, the amount of *gauche* conformer was found to be 96 ± 9 %. The RD curve obtained from this model is shown in Fig. 2.

DISCUSSION

The ED data support the conclusions from the MW[8] and the infrared and Raman[9] studies that gaseous phase chloromethyl-cyclopropane exists predominantly as *gauche* conformer. The result is also very close to the conclusion from liquid data in Ref. 10, 95 % *gauche*. 96 % *gauche* conformer is in excellent agreement with the MM calculation, where non-bonded potential values corresponding to sp^3 hybridized carbon atoms where used. Since the cyclopropane ring may be regarded as having pseudo π-orbitals,[37] a comparison to 3-chloro-1-propene, which is found to exist as *ca.* 80 % *gauche* conformer, is of interest.[12,26,38] It was found that MM calculations for 3-chloro-1-propene, using the same non-bonded potentials, gave as result only *gauche* conformer. Also the observed *gauche* torsional angle is close to the MM calculated one.

In Table 7 some of the geometrical parameters of chloromethyl-cyclopropane are listed together with those of related molecules. The present study did not give any additional information about the relative length of the C–C bonds. However, there is an indication that the C–C distances are longer than in methyl-cyclopropane. If the ring bonds were fixed at the same length as found in the ED study of methyl-cyclopropane, the exocyclic C–C bond refined to an unreasonably large value. Although distances found by MW and ED studies are not directly comparable, it can be said that there is good agreement between the partial r_0 structure of bromomethyl-cyclopropane (where the C–CH_2Br distance was fitted to observed data) and the result of this study. The C–Cl bond length is close to what have been found for other molecules having terminal CH_2Cl groups.

Due to large uncertainties, it is difficult to establish definite conclusions about the effect of the cyclopropane ring on conformation and bond lengths. The conformational composition seems to be as expected for a saturated system. However, although not observed, it may be that the pseudo π-system of the ring slightly affects the exocyclic bond lengths, while at the same time the apparent *syn* stabilizing effect observed in 3-chloro-1-propene is not provided by this system. Theoretical calculations[40] have shown that both vinyl-like and non-vinyl-like properties of the cyclopropane ring may be explained by the Walsh orbital model.[37]

The refined non-bonded vibrational amplitudes (Table 3) did not show much deviation from calculated ones. Thus, it is probable that also the other calculated amplitudes were good approximations to the experimental ones. The deviations in bonded vibrational amplitudes had no observable effect on other parameters.

With the small amount of *syn* conformer present, it was not considered worthwhile to study the conformational composition at a higher temperature. Using the MM results, only 10 % *syn* conformer would be expected at 200 °C.

Acknowledgements. Thanks are due to Mrs. S. Gundersen for technical assistance. Financial support from *Norges Almenvitenskapelige Forskningsråd* is acknowledged.

REFERENCES

1. Bartell, L. S. and Guillory, J. P. *J. Chem. Phys. 43* (1965) 647.
2. Bartell, L. S., Guillory, J. P. and Parks, A. T. *J. Phys. Chem. 69* (1965) 3043.
3. de Meijere, A. and Lüttke, W. *Tetrahedron 25* (1969) 2047.
4. Trætteberg, M. *To be published.*
5. Hagen, K., Hagen, G. and Trætteberg, M. *Acta Chem. Scand. 26* (1972) 3649.
6. Mohammade, M. A. and Brooks, W. V. F. *J. Mol. Spectrosc. 77* (1979) 42.
7. Fujiwara, F. G., Chang, J. C. and Kim, H. *J. Mol. Struct. 41* (1977) 177.
8. Mohammade, M. A. and Brooks, W. V. F. *J. Mol. Spectrosc. 73* (1978) 347.
9. Hirokawa, T. and Murata, H. *J. Sci. Hiroshima Univ., Ser. A Phys. Chem. 38* (1974) 271.

10. Kalasinsky, V. F. and Wurrey, C. J. *J. Raman Spectrosc. 9* (1980) 315.
11. Wurrey, C. J., Krishnamoorthi, R., Pechsiri, S. and Kalasinski, V. F. *J. Raman Spectrosc. 12* (1982) 95.
12. Schei, S. H., Shen, Q. and Hilderbrandt, R. L. *To be published.*
13. Klein, A. W. and Schrumpf, G. *Acta Chem. Scand. A 35* (1981) 425.
14. Scancke, A. and Boggs, J. B. *J. Mol. Struct. 50* (1978) 173.
15. Zeil, W., Haase, J. and Wegman, L. *Z. Instrumentenkd. 74* (1966) 84.
16. Bastiansen, O., Graber, R. and Wegman, L. *Balzer's High Vacuum Rep. 24* (1969) 1.
17. Tamagawa, K., Iijima, T. and Kimura, M. *J. Mol. Struct. 30* (1976) 243.
18. Andersen, B., Seip, H. M., Strand, T. G. and Stølevik, R. *Acta Chem. Scand. 23* (1969) 3224.
19. Hedberg, L. *Abstracts. 5th Austin Symposium on Gas Phase Molecular Structure*, Austin, Texas 1974, p. 37.
20. Strand, T. G. and Bonham, R. A. *J. Chem. Phys. 40* (1964) 1686.
21. Stewart. R. F., Davidson, E. R. and Simpson, W. T. *J. Chem. Phys. 42* (1965) 3175.
22. Spiekerman, M., Bougeard, D. and Schrader, B. *J. Mol. Struct. 60* (1980) 55.
23. Schei, S. H. *To be published.*
24. Snyder, R. G. and Schachtschneider, J. H. *Spectrochim. Acta 21* (1965) 169.
25. Maillols, J. and Tabacik, V. *Spectrochim. Acta 35* (1979) 125.
26. Sourisseau, C. and Pasquier, B. *J. Mol. Struct. 12* (1972) 1.
27. Stølevik, R. *Acta Chem. Scand. A 31* (1977) 359.
28. Abraham, R. J. and Stølevik, R. *Chem. Phys. Lett. 58* (1978) 622.
29. During, J. R., Lopata, A. D. and Wurrey, C. J. *J. Raman Spectrosc. 3* (1975) 345.
30. Ford, R. G. and Beaudet, R. A. *J. Chem. Phys. 48* (1968) 4671.
31. Rydland, T. *Thesis*, University of Trondheim, Trondheim 1981.
32. Abraham, R. J. and Stølevik, R. *Chem. Phys. Lett. 77* (1981) 181.
33. Kuchitsu, K. and Cyvin, S. J. In Cyvin, S. J., Ed., *Molecular Structures and Vibrations*, Elsevier, Amsterdam 1972, Chapter 12.
34. Van Hemelrijk, D., Van den Enden, L., Geise, H. J., Sellers, H. L. and Schäfer, L. *J. Am. Chem. Soc. 102* (1980) 2189.
35. Kuchitsu, K. and Morino, Y. *Bull. Chem. Soc. Jpn. 38* (1965) 805.
36. Seip H. M. and Stølevik, R. In Cyvin, S. J., Ed., *Molecular Structures and Vibrations*, Elsevier, Amsterdam 1972, Chapter 11.
37. Walsh, A. D. *Trans. Faraday Soc. 45* (1949) 179.
38. Rondeau, R. E. and Harrah, L. A. *J. Mol. Spectrosc. 21* (1966) 332.
39. Grindheim, S. and Stølevik, R. *Acta Chem. Scand. 30* (1976) 625.
40. Wilcox, C. F., Loew, L. M. and Hoffman, R. *J. Am. Chem. Soc. 95* (1973) 8192.
41. Morino, Y. and Kuchitsu, K. *J. Chem. Phys. 28* (1958) 175.
42. Hirota, M., Iijima, T. and Kimura, M. *Bull. Chem. Soc. Jpn. 51* (1978) 1594.

Received April 7, 1982.

Acta Chemica Scandinavica A 37 (1983) 25–29

Calcium Phosphate Crystallization. IV. Kinetics of Heterogeneous Nucleation of Tetracalcium Monohydrogen Phosphate on Brushite Crystals

H. E. LUNDAGER MADSEN

Chemistry Department, Royal Veterinary and Agricultural University, Thorvaldsensvej 40, DK-1871 Copenhagen V, Denmark

The kinetics of heterogeneous nucleation of OCP ($Ca_4H(PO_4)_3 \cdot 2.5H_2O$) on brushite ($CaHPO_4 \cdot 2H_2O$) at 37 °C has been studied, partly by pH-static titration with calcium hydroxide. Nucleation is strongly favoured by crystal defects of the substrate. At constant supersaturation the rate of crystallization of OCP is initially very low, thereafter being in accordance with the rate expression $M(t) = k(t - t_i)^4$, where $M(t)$ is the amount of OCP formed at time t, and t_i is the induction time. The stationary nucleation rate calculated from k follows the classical (Becker-Döring-Volmer) expression, but the critical nucleus contains only 1–2 formula units. t_i increases in steps with decreasing supersaturation. This is most easily understood if it is assumed that t_i is not the induction time for nucleation, but rather a relaxation time of the critical nucleus.

In a previous paper [1] we reported the pH-static titration of a mixed suspension of brushite ($CaHPO_4 \cdot 2H_2O$) and OCP ($Ca_4H(PO_4)_3 \cdot 2.5H_2O$) with calcium hydroxide as a useful means of determining the overall growth kinetics of OCP. The essential points were that (1) the rate of dissolution of brushite is so high that the solution is always saturated with respect to the latter, and (2) calcium hydroxide is one of the components of the system. The consequence of these two facts is that the whole process takes place at constant supersaturation. Clearly, the method should also be useful in studying the heterogeneous nucleation of OCP on brushite. The present paper reports the results of such a study.

0302-4377/83 $2.50

EXPERIMENTAL

The pH-static titrations were carried out as previously described [1] with the exception that 0.5 g of brushite and no OCP was added to the dilute phosphoric acid solution. In addition, some experiments were carried out in which pH was allowed to vary freely, following the procedure described in the first paper in this series.[2]

The brushite used for all the experiments was separated into a number of fractions according to crystal size, using sieves with 90, 105, 125, 149, 180 and 250 μm mesh size.

All experiments were carried out at 37 °C. This temperature was chosen for its physiological importance and because it yielded a suitable reaction rate.

RESULTS

Fig. 1 shows an example of unusually well-developed OCP spherulites on a brushite crystal. It is evident that OCP is indeed formed by heterogeneous nucleation. Preliminary experiments with freely varying pH were carried out to determine the effect of crystal size on the induction time t_i. It was found that t_i decreased with increasing crystal size for constant total mass of brushite; Fig. 2 shows some of the results. A sample of crystals <90 μm which had been compressed in a steel cylinder to about 60 MPa for a couple of seconds showed a significantly reduced induction time (Fig. 2).

All pH- static titrations were carried out with the 149–180 μm fraction. A series of experiments with the 90–105 μm fraction was abandoned after a few

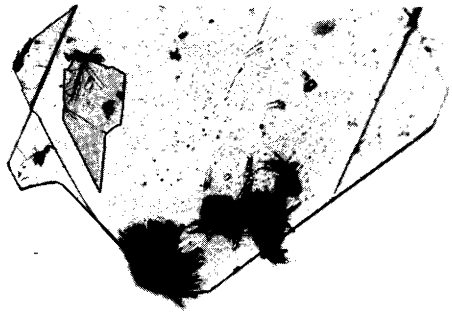

Fig. 1. Brushite crystal with OCP spherulites. The brushite crystal is about 0.5 mm across.

trials, because crystallization of OCP took place on all surfaces in the cell, not only on the brushite crystals. With the former fraction, a typical plot of the amount of OCP formed (equal to the amount of $Ca(OH)_2$ consumed) *versus* time had the appearance as shown in Fig. 3. Experiments were carried out at mean pH intervals of 0.05 units. The comments in Ref. 1 concerning the limits of precision apply to the present study as well.

DISCUSSION

From the form of Fig. 2 it is concluded that nucleation of OCP is strongly favoured by crystal defects, which are more abundant in large than in small crystals. If nucleation were equally probable

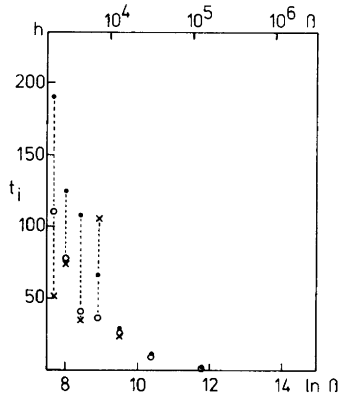

Fig. 2. Induction time by variable pH as a function of initial supersaturation. Crystal size of brushite 180 −250 μm. ○; crystal size of brushite <90 μm, ●; same after compression to 60 MPa, ×.

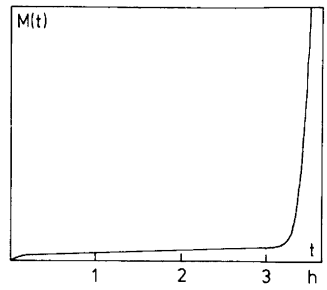

Fig. 3. Amount of OCP formed (in arbitrary units) as a function of time for ln $\beta = 8.27$.

all over the surface, we should expect the induction time to increase with increasing crystal size (equivalent with decreasing specific surface), contrary to our observation.

Curves similar to Fig. 3 have been observed by Dugua and Simon [3,4] for the crystallization of sodium perborate at constant supersaturation. As shown by Gindt and Kern [5] the total mass $M(t)$ crystallized at time t is given by the convolution integral (1), where $J(t_o)$ is the nucleation frequency at

$$M(t) = \int_0^t J(t_o) m(t - t_o) \mathrm{d}t_o \qquad (1)$$

time t_o and $m(t-t_o)$ is the mass of a single crystal formed at time t_o. Eqn. (1) is valid only for constant supersaturation, and it is assumed that the evolution of a single crystal is independent of t_o. If the individual crystal faces advance with constant linear velocity, we have eqn. (2), where A is a function of

$$m(t - t_o) = A(t - t_o)^3 \qquad (2)$$

supersaturation. If J were constant, we should simply have eqn. (3). As Fig. 4 shows, $M(t)^{1/4}$ is partly

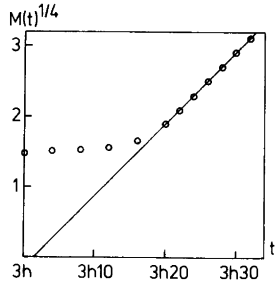

Fig. 4. Fourth root of the ordinate in Fig. 2 as a function of time.

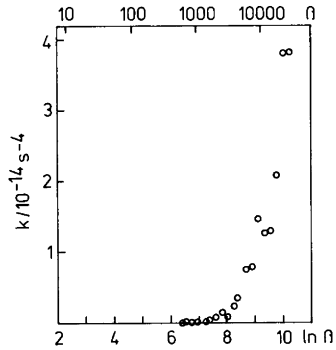

Fig. 5. k from eqn. (4) as a function of supersaturation.

$$M(t) = \tfrac{1}{4} J A t^4 \tag{3}$$

a linear function of t, but the part of the curve for which this is valid is given by eqn. (4). For $t < t_i$ the

$$M(t) = k(t - t_i)^4 \tag{4}$$

rate of crystallization is very low and difficult to analyze.

Taking the fourth derivative of $M(t)$ according to eqn. (1) and (2) yields eqn. (5) and similarly, from eqn.

$$M^{(4)}(t) = 6AJ(t) \tag{5}$$

$$M^{(4)}(t) = 6k \tag{6}$$

(4), eqn. (6), whence $k = AJ_s$, where J_s is the steady-state rate of nucleation. The shape of our curves shows that $J(t)$ is very low initially and then, in a rather short time interval around t_i, increases to the limiting value J_s. This means that the frequently quoted expression,[5] eqn. (7), does not apply to the present case.

$$J(t) = J_s \exp(-t_i/t) \tag{7}$$

Fig. 5 shows k as a function of ln β, where β is the ratio between the ionic product and the solubility product of OCP. A in eqn. (2) is proportional to R^3, where R is the average rate of growth of a crystal face on OCP, known as a function of β from our previous investigation.[1] According to eqn. (5) and (6) $k/R^3 = k'$ is proportional to the steady-state nucleation rate J_s.

The heteronuclei are either two-dimensional, cap-shaped (rounded), or polyhedral, like an ordinary crystal. As OCP crystallizes in spherulites, the latter case is not very likely, because such a nucleus would be expected to develop into a single crystal. The Gibbs function of formation of a two-dimensional heteronucleus containing N formula units is given by eqn. (8), where $\bar{s}$ is the surface area of one formula

$$\Delta G(N) = N[-kT \ln \beta + (\gamma_{nl} - \gamma_{sl} + \gamma_{ns})\bar{s}] + 4\lambda\sqrt{\bar{s}N} \tag{8}$$

unit in the nucleus, γ_{nl}, γ_{sl}, and γ_{ns} are the nucleus-liquid, substrate-liquid, and nucleus-substrate interfacial tensions, respectively, and λ is the edge free energy per unit length of the nucleus, assumed to be quadratic in shape. Eqn. (8) leads to the expression (9) for J_s,[6,7]

$$J_s = f\{c_i\} \exp\left(-\frac{4\lambda^2\bar{s}}{kT[kT \ln \beta - (\gamma_{nl} - \gamma_{sl} + \gamma_{ns})\bar{s}]}\right) \tag{9}$$

where $f\{c_i\}$ is a function of the concentrations of the different ionic species present. As the system is always in equilibrium with respect to brushite, the surface concentrations will not change much, whence we shall treat $f\{c_i\}$ as a constant. When $\gamma_{nl} - \gamma_{sl} + \gamma_{ns} > 0$, which corresponds to imperfect wetting in the case of a liquid drop on a solid surface, eqn. (9) predicts the existence of a critical supersaturation, eqn. (10), below which two-

$$\beta_{crit} = \exp\left(\frac{(\gamma_{nl} - \gamma_{sl} + \gamma_{ns})\bar{s}}{kT}\right) \tag{10}$$

dimensional nucleation can no longer take place (but the two other possibilities still exist). The slope of a plot of ln J_s against $1/\ln \beta$ should tend to $-4\lambda^2\bar{s}/k^2T^2$ for high β and to $-\infty$ as $\beta \to \beta_{crit}$.

If the nucleus is cap-shaped (we assume a spherical cap), we may introduce the contact angle α with the aid of Young's equation, eqn. (11).

$$\gamma_{sl} = \gamma_{ns} + \gamma_{nl} \cos \alpha \tag{11}$$

The area of the nucleus-liquid interface is then given by eqn. (12), whereas the area of the nucleus-

$$A_{nl} = 2\pi r^2 (1 - \cos \alpha) \tag{12}$$

substrate interface is as eqn. (13), where r is the radius of curvature of the cap. Instead of eqn. (8) we now find, using eqn. (11), eqn. (14).

$$A_{ns} = \pi r^2 \sin^2\alpha \tag{13}$$

$$\Delta G(N) = -NkT\ln\beta + \pi r^2\gamma_{nl}(1-\cos\alpha)(2-\cos\alpha-\cos^2\alpha) \tag{14}$$

The volume of the nucleus is given by eqn. (15), where $\bar{v}$ is the volume of one formula unit in the nucleus. We may now express ΔG as a function of r; eqn. (16)

$$V_n = \frac{\pi}{3}r^2(1-\cos\alpha)(2-\cos\alpha-\cos^2\alpha) = N\bar{v} \tag{15}$$

$$\Delta G(r) = \left(-\frac{\pi r^3}{3\,v}kT\ln\beta + \pi r^2\gamma_{nl}\right)(1-\cos\alpha)(2-\cos\alpha-\cos^2\alpha) \tag{16}$$

$$r^* = \frac{2\gamma_{nl}\bar{v}}{kT\ln\beta} \tag{17}$$

The radius of the critical nucleus is given, as usual, by the Gibbs-Kelvin equation, eqn. (17), and the nucleation rate will now be as eqn. (18), which, apart from geometrical factors, corresponds to the classical expression for three-dimensional nucleation.[6,7]

$$J_s = f\{c_i\}\exp\left[-\frac{4\pi}{3}\frac{\gamma_{nl}^3\bar{v}^2}{k^3T^3\ln^2\beta}(1-\cos\alpha)(2-\cos\alpha-\cos^2\alpha)\right] \tag{18}$$

As Figs. 6 and 7 show, both the two-dimensional and the spherical cap nucleus may explain the present data. From the slopes of the regression lines we find the following parameter values:

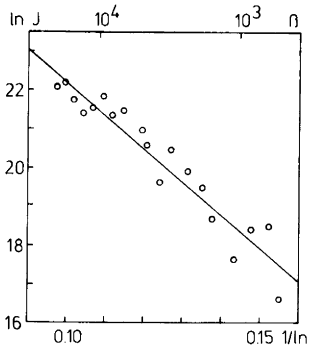

Fig. 6. Test of two-dimensional nucleation.

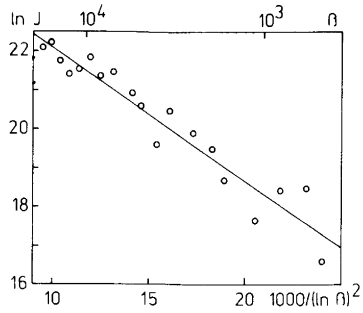

Fig. 7. Test of nucleation with cap-shaped nuclei.

$$\lambda\sqrt{\bar{s}} = 11.9 \text{ kJ/mol}$$

for the two-dimensional nucleus and

$$\gamma_{nl}\bar{v}^{2/3}[(1-\cos\alpha)(2-\cos^2\alpha)]^{1/3} = 11.2 \text{ kJ/mol}$$

for the spherical cap nucleus. The value of $\lambda\sqrt{\bar{s}}$ is not very far from that found for the surface-nucleation growth mechanism of OCP.[1] As we do not known α, we are unable to calculate γ_{nl}.

For $\beta \gg \beta_{crit}$, the number of formula units in the critical two-dimensional nucleus is given by eqn. (19).

$$N^* = \frac{4\lambda^2\bar{s}}{(kT\ln\beta)^2} \tag{19}$$

The corresponding value for the cap-shaped nucleus is found from eqns. (15) and (17); eqn. (20).

$$N^* = \frac{8\pi}{3}\frac{\gamma_{nl}^3\bar{v}^2}{(kT\ln\beta)^3}(1-\cos\alpha)(2-\cos\alpha-\cos^2\alpha) \tag{20}$$

In both cases we find that the critical nucleus contains from a little less than 1 to a little more than 2 formula units. The smallest electrically neutral nucleus is $Ca_3(PO_4)_2\cdot xH_2O$, and $N^*=2$ corresponds to the formula $Ca_8H_2(PO_4)_6\cdot 5H_2O$, *i.e.* it contains 19 particles. From this it is obvious that a distinction between the two shapes of a nucleus has no real significance. Furthermore, we should expect such a small nucleus to possess structural features not found in a macroscopic crystal,[8-10] which may explain why it develops into a spherulite instead of a single crystal.

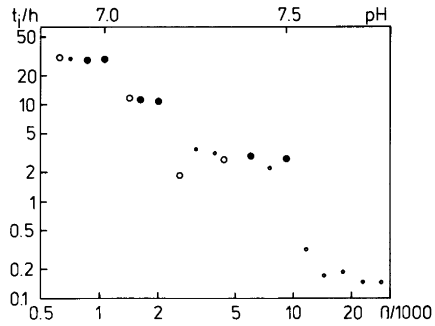

Fig. 8. Induction time as a function of supersaturation. Different symbols indicate results from different series of experiments.

The induction time t_i depends on β in a very peculiar way (Fig. 8). This is obviously a step function. The only possible explanation of this behaviour is that the size of the critical nucleus is not a continuous variable and that it solely determines the value of t_i, without any explicit influence from the composition of the surrounding solution. Thus is seems unlikely that t_i should be the induction time for nucleation in the usual sense; we believe it to represent some kind of relaxation time of the nucleus.

What probably takes place is the following: Critical clusters – not nuclei, because their structure is different from that of the OCP crystal – are formed on the furface of the brushite crystals with frequency J; their size is a step function of β, increasing with decreasing β. After the formation of a critical cluster, it undergoes a transformation, the nature of which we do not know at present. This transformation takes the time t_i, and then crystals start to grow in many different directions from the cluster. With this model, we have

$$m(t) = \begin{cases} 0 \text{ for } t \leq t_i \\ A(t-t_i)^3 \text{ for } t > t_i \end{cases}$$

We further assume that the induction time for nucleation is very short compared to t_i, so that we may put $J(t) = J_s$. A well-known theorem for convolution integrals, eqn. (21), gives eqn. (22). This

$$M(t) = \int_0^t J(t_o)m(t-t_o)dt_o = \int_0^t J(t-t_o)m(t_o)dt_o \qquad (21)$$

$$M(t) = J_s A \int_{t_i}^t (t_o - t_i)^3 dt_o = \frac{1}{4} J_s A (t-t_i)^4 \qquad (22)$$

expression agrees perfectly with our observation.

In the first study,[1] in which unsieved brushite was used and supersaturation was not constant, no discontinuities in t_i were found, but inverse proportionality between t_i and $[PO_4^{3-}]^2$ was observed. As a matter of fact, a plot of ln t_i against ln $[PO_4^{3-}]$ using the results of the present study will also yield a slope of exactly -2 if we neglect points with ln $\beta > 9.2$. Since there is no apparent way to explain the stepwise variation of t_i on the basis of the mechanism proposed in Ref. 2, this must be considered as purely accidental.

Some of the results reported in this paper were presented at the 2nd European Conference on Crystal Growth at Lancaster, U.K., September 1979, on the poster "Crystallization of some Constituents of Human Lithiasis" by F. Abbona, D. Aquilano, M. Franchini, C. Rinaudo, R. Boistelle, and H. E. Lundager Madsen.

Acknowledgements. This work was supported financially by NATO Research Grant No. 1438. The author wishes to thank Mrs. B. Søndergaard Sørensen for technical assistance.

REFERENCES

1. Madsen, H. E. *Acta Chem. Scand. A 36* (1982) 239.
2. Madsen, H. E. L. *Acta Chem. Scand. 24* (1970) 1677.
3. Dugua, J. *Influence des agents tensio-actifs sur la cristallisation du perborate de sodium*, Thesis, Université d'Aix-Marseille III, Marseille 1977.
4. Dugua, J. and Simon, B. *J. Cryst. Growth 44* (1978) 265.
5. Gindt, R. and Kern, R. *Ber. Bunsenges. Phys. Chem. 68* (1965) 124.
6. Becker, R. and Döring, W. *Ann. Phys. N.Y. 24* (1935) 719.
7. Volmer, M. *Kinetik der Phasenbildung*, Steinkopff, Leipzig and Dresden 1939.
8. Bonissent, A. and Mutaftschiev, B. *J. Chem. Phys. 59* (1973) 3727.
9. Hoare, M. R. and McInnes, J. *Faraday Discuss. Chem. Soc. 61* (1976) 12.
10. Briant, C. L. *Faraday Discuss. Chem. Soc. 61* (1976) 25.

Received April 19, 1982.

Acta Chemica Scandinavica A 37 (1983) 31 – 39

The Crystal and Molecular Structure of 2-Diisopropylamino-4,6-dimethyl-3,4,6-triaza-1,6a-dithiapentalenylium-5-olate, $C_{11}H_{20}N_4OS_2$

LARS K. HANSEN

Department of Chemistry, Institute of Mathematical and Physical Sciences, University of Tromsø, Box 953, N-9001 Tromsø, Norway

The structure of $C_{11}H_{20}N_4OS_2$ has been determined by X-ray crystallographic methods. 4091 independent reflections were measured on a diffractometer using the $\omega-2\theta$ scan technique and Mo$K\alpha$ radiation. The compound crystallizes in an orthorhombic space group $P2cb$ with unit cell dimensions, $a=7.000(1)$, $b=20.321(2)$ and $c=22.027(2)$ Å. There are two independent molecules per asymmetric unit, giving a total of 8 molecules in the unit cell. The structure was solved by Patterson synthesis and refined by full matrix least squares to an R of 0.040 for 2607 observed reflections. The central ring system is planar in both molecules with the planes normal to the a-axis. The two independent molecules are related by a rotation of approximately 90° about [100] and the thiadiazole parts of the two molecules overlap. Differences in the bond lengths for corresponding bonds in the two molecules are insignificant except for the S(1)–S(6a) bond distances which are found to be 2.522(1) Å in one of the molecules and 2.561(1) Å in the other. Other sulfur-containing bond lengths in the central part of molecule 1 are, S(6a1)–N(61)=1.791(2) Å, S(11)–C(21)=1.711(3) Å and S(6a1)–C(3a1)=1.758(3) Å. Corresponding bond lengths in molecule 2 are, S(6a2)–N(62)=1.780(2) Å, S(12)–C(22)=1.719(3) Å and S(6a2)–C(3a2)=1.758(3) Å. The lengths of the C–O bonds are 1.235(4) and 1.228(3) Å, respectively, in 1 and 2. The angles S(1)–S(6a)–N(6) are 169.3(1) and 169.0(1)°, respectively, in molecules 1 and 2. The bond lengths have been corrected for libration.

The results from CNDO/2 calculations show that the electron charge density distribution is different in the S–S–N sequences of the respective molecules. This difference, caused by the crystal packing, may explain why the S–S bond lengths are found to be different in the two molecules.

0302-4377/83 $2.50

Recent studies on three 1,6a-dithiapentalenylium-5-thiolates (I–III)[1-3] have shown that different substituents in the 6-position have a considerable influence on the S(1)–S(6a) bond length.

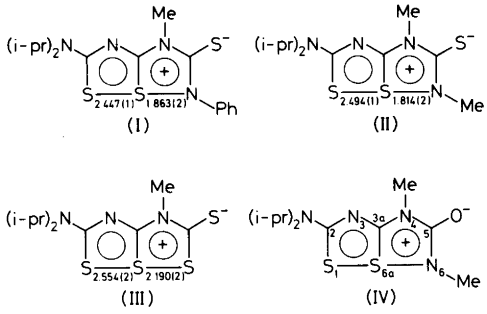

The value of the S(1)–S(6a) bond distances varies from 2.447(1) Å in I to 2.554(2) Å in III. Furthermore, since it is possible to exchange the sulfur substituent in 5-position of *e.g.* II with the more electronegative element oxygen (IV),[4] it was thought of interest to carry out an X-ray structure determination of IV in order to find out whether this change of 5-substituent causes a change in the S(1)–S(6a)–N(6) bonding.

STRUCTURE ANALYSIS

The crystals were supplied by Dr. J. Goerdeler, University of Bonn.[4] Recrystallization from acetone gave crystals suitable for single crystal X-ray work. The crystals are colourless prisms, and a crystal of dimensions $0.50\times0.30\times0.30$ mm was used for all X-ray measurements.

CRYSTAL DATA

$C_{11}H_{20}N_4OS_2$; M.W. = 288.44

Space group *P2cb* (No. 32) with $Z = 8$

$a = 7.0001(12)$ Å, $b = 20.3207(23)$ Å, $c = 22.0274(21)$ Å
$V = 3133(1)$ Å^3
$D_x = 1.223$ g/cm^3, D_m(flotation) = 1.21 g/cm^3
μ(Mo$K\alpha$) = 5.19 cm^{-1}, $F_{000} = 1232$

Unit cell dimensions and intensity data were collected on a CAD4 diffractometer using graphite monochromator and Mo$K\alpha$ radiation ($\lambda = 0.71069$ Å). The unit cell dimensions were determined from 25 reflections with $2\theta > 40°$. Three-dimensional intensity data for 4091 independent reflections within $2\theta < 56°$ were collected at room temperature (20 °C) by the $\omega - 2\theta$ scan technique and with scan width $\Delta\omega = 0.75° + 0.35°$ tan θ. Lp-corrections were carried out but absorption corrections were considered unnecessary. 2607 reflections with net intensity I greater than $2\sigma(I)$ were regarded as observed; $\sigma(I)$ based on counting statistics.

Precession photographs indicated that the $h00$ reflections are systematically absent for $h = 2n+1$ thus indicating a 2-fold screw axis. But this observation leads to a space group that could not be derived from International Tables.[5] A more careful examination of the profile of each reflection along the a-axis taken from the diffractometer output showed no systematic absences. The observed structure factors together with their standard deviations are listed in Table 1 for the $h00$ reflections. One notes that the reflections with odd h indices are very weak, although observed, as compared to the even h indices. It can therefore be concluded that the a-axis is not a 2-fold screw axis.

Program NORMSF[6] was used to try to establish whether the space group is centrosymmetric or not, *e.g. Pmcb* or *P2cb*. The statistics indicated a non-centrosymmetric space group. The space group *P2cb* was therefore chosen and further work confirmed this assumption. This means that there are two independent molecules in the asymmetric unit.

Table 1. Observed structure factors (F_o) and standard deviations (σF_o) for the $h00$ reflections.

h	F_o	σF_o	Status
1	10.24	0.05	Obs.
2	294.19	0.71	Obs.
3	2.19	0.44	Obs.
4	159.48	0.79	Obs.
5	3.91	0.14	Obs.
6	64.72	0.21	Obs.
7	1.60	0.48	Weak
8	23.04	0.12	Obs.
9	1.91	0.57	Weak

As mentioned above, the other possible space group was the centrosymmetric *Pmcb*. Refinement in this space group with the molecules in the mirror planes at $x = 0$ and $\frac{1}{2}$ leads to unrealistic bond lengths and temperature parameters, and it was concluded that the non-centrosymmetric space group was the correct one in agreement with the statistics.

The structure was solved by Patterson synthesis and from this map 4 sulfur atoms were located. Subsequent Fourier maps revealed the remaining non-hydrogen atoms and the hydrogen atoms were eventually found from difference maps. The hydrogen atoms were included in the further refinement with isotropic thermal parameters, and all of them refined to reasonable positions. The atomic parameters were refined by full matrix least squares to an R factor of 0.040. The weighted R_w was 0.031. The function minimized in the refinement was $\Sigma w(|F_o| - |(1/k)F_c|)^2$, where $w = 1/\sigma F^2$. Due to the large number of parameters, 483, only one of the molecules was refined at a time, but the final refinement was done on all atoms simultaneously, refining the parameters in 5 blocks. At the end of this refinement the average shift/error ratio was 0.18.

The scattering factors used in the structure factor calculations were those of Stewart *et al.*[7] for hydrogen and of Cromer and Mann[8] for the other atoms. Final atomic coordinates and temperature parameters for the non-hydrogen atoms are listed in Table 2; those of the hydrogen atoms are listed in Table 3. The final structure factor list is available from the author on request.

Rigid body analyses have been carried out on the central parts of the two independent molecules according to the method of Schomaker and Trueblood.[9] The corresponding librational tensors are given in Table 4.

All calculations were carried out on the CYBER 171 MP computer at the University of Tromsø. The programs used were mainly those of the X-RAY 76 program system.[6] The data reduction programs and the RBM-analysis program used were adopted for the CYBER 171 MP computer by the author.

DISCUSSION

ORTEP[10] drawings of the two independent molecules of the title compound are shown in Fig. 1 with the numbering of atoms. Least squares planes show that both molecules are planar within the error. The estimated errors are 0.03 and 0.04 Å, respectively, for molecules 1 and 2. The plane

Table 2. Atomic coordinates and temperature parameters U_{ij}(Å$^2 \times 10^3$) for the sulfur, oxygen, nitrogen and carbon atoms. The temperature factor is $\exp\{-2\pi^2(h^2a^{*2}U_{11} + \cdots 2\,hka^*b^*U_{12} + \cdots)\}$.

MOLECULE 1

ATOM	X	Y	Z	U11	U22	U33	U12	U13	U23
S(11)	.0016(6)	.42282(4)	.43478(3)	104(1)	51(1)	44(1)	-5(3)	8(2)	-1(1)
S(6A1)	0.0000	.36845(3)	.33223(3)	73(1)	63(1)	38(1)	-3(1)	2(1)	2(1)
C(21)	.0029(19)	.34794(13)	.44908(11)	51(2)	58(2)	39(1)	9(7)	1(7)	-4(1)
N(31)	-.0068(15)	.29208(10)	.43547(9)	56(2)	53(1)	36(1)	9(6)	-4(6)	-3(1)
C(3A1)	.0022(18)	.29725(12)	.37634(11)	41(2)	58(2)	43(1)	-7(8)	-1(7)	-3(1)
N(41)	.0025(17)	.24224(10)	.34131(9)	57(1)	56(1)	44(1)	2(7)	6(6)	-8(1)
C(51)	.0090(20)	.25216(17)	.27798(13)	50(3)	86(2)	42(2)	-6(8)	-10(5)	-15(2)
N(61)	-.0002(17)	.31616(12)	.26730(8)	85(2)	76(2)	35(1)	8(8)	-0(7)	-3(1)
C(71)	.0095(22)	.34522(17)	.20635(12)	143(5)	104(3)	39(2)	21(9)	-34(6)	-2(2)
O(81)	.0007(13)	.20631(10)	.24169(8)	101(2)	91(2)	53(1)	9(8)	-3(7)	-26(1)
C(91)	.0029(19)	.17598(14)	.36695(12)	84(3)	60(2)	61(2)	-24(7)	-13(7)	-10(2)
N(101)	-.0021(16)	.34089(10)	.52966(8)	81(2)	53(1)	37(1)	3(8)	6(8)	-1(1)
C(111)	-.0066(25)	.27529(15)	.55993(12)	109(3)	56(2)	36(1)	13(10)	-2(10)	-0(1)
C(121)	.1828(18)	.2369(5)	.5474(6)	122(9)	80(10)	56(7)	40(7)	-15(7)	2(6)
C(131)	-.1793(23)	.2379(6)	.5485(6)	169(12)	101(13)	70(9)	-47(10)	-14(9)	20(8)
C(141)	-.0109(29)	.39923(16)	.56888(15)	169(5)	59(2)	41(2)	-15(11)	-12(10)	-7(1)
C(151)	.1507(28)	.3987(6)	.6136(6)	316(14)	79(5)	92(5)	-59(7)	-94(7)	1(4)
C(161)	-.1979(29)	.4053(8)	.6004(7)	355(20)	125(8)	174(13)	70(11)	171(14)	21(7)

MOLECULE 2

ATOM	X	Y	Z	U11	U22	U33	U12	U13	U23
S(12)	.4961(5)	.14164(3)	.43899(3)	83(1)	52(1)	40(1)	-1(2)	-5(2)	-1(1)
S(6A2)	.4983(5)	.25698(3)	.39284(3)	55(1)	47(1)	53(1)	4(2)	-0(2)	-4(1)
C(22)	.4914(17)	.10836(12)	.36779(11)	51(2)	49(1)	45(1)	9(6)	-3(6)	3(1)
N(32)	.4983(14)	.14790(9)	.31809(8)	67(2)	43(1)	42(1)	-3(7)	-11(6)	2(1)
C(3A2)	.4943(16)	.21143(12)	.32556(11)	45(2)	52(2)	47(1)	18(6)	-2(6)	2(1)
N(42)	.5012(14)	.25170(10)	.27626(9)	70(2)	48(1)	47(1)	-8(7)	-3(7)	7(1)
C(52)	.5030(18)	.31997(13)	.28759(13)	60(2)	49(2)	76(2)	14(7)	-11(8)	11(2)
N(62)	.4987(15)	.32897(9)	.34726(10)	74(2)	42(1)	70(2)	6(7)	-0(8)	-0(1)
C(72)	.4879(19)	.39381(14)	.37589(15)	82(3)	49(2)	97(2)	-12(6)	-18(7)	-5(2)
O(82)	.4965(13)	.36116(9)	.24710(9)	107(2)	57(1)	88(1)	6(6)	0(8)	26(1)
C(92)	.5041(20)	.22629(14)	.21440(12)	104(3)	64(2)	52(2)	11(8)	-11(8)	13(1)
N(102)	.5060(15)	.04396(10)	.35739(9)	81(2)	42(1)	41(1)	-0(6)	2(5)	2(1)
C(112)	.4815(21)	.01570(15)	.29472(14)	129(5)	41(2)	48(2)	-14(6)	22(6)	-3(1)
C(122)	.3122(15)	.0324(5)	.2619(5)	139(9)	67(7)	62(6)	-20(6)	-49(7)	7(5)
C(132)	.6743(17)	.0294(6)	.2597(5)	207(13)	79(8)	86(9)	-0(8)	47(9)	-27(6)
C(142)	.4926(20)	-.00351(14)	.40826(12)	112(3)	49(2)	47(2)	30(7)	6(8)	5(1)
C(152)	.3157(13)	-.0423(4)	.4122(4)	122(7)	94(5)	86(6)	-53(6)	-27(5)	47(5)
C(162)	.6854(22)	-.0422(7)	.4077(5)	339(17)	253(12)	99(9)	194(13)	5(9)	35(8)

Table 3. Atomic coordinates and isotropic temperature parameters U(Å$^2 \times 10^3$) for the hydrogen atoms. The temperature factor is $\exp\{-8\pi^2 U(\sin^2\theta/\lambda^2)\}$.

MOLECULE 1					MOLECULE 2				
ATOM	X	Y	Z	U	ATOM	X	Y	Z	U
H(711)	-.058(6)	.3150(16)	.1818(14)	82(13)	H(721)	.552(4)	.4308(12)	.3472(11)	53(9)
H(712)	-.057(9)	.3912(27)	.2053(24)	182(29)	H(722)	.561(3)	.3890(11)	.4152(9)	64(8)
H(713)	.155(5)	.3503(15)	.1913(14)	84(12)	H(723)	.341(6)	.4071(18)	.3849(17)	107(15)
H(911)	-.038(6)	.1483(11)	.3356(10)	58(9)	H(921)	.438(4)	.2624(12)	.1883(11)	56(9)
H(912)	-.095(4)	.1733(14)	.4048(13)	77(9)	H(922)	.641(6)	.2131(20)	.2091(18)	99(15)
H(913)	.145(7)	.1628(23)	.3813(18)	133(20)	H(923)	.422(5)	.1899(13)	.2109(15)	76(15)
H(111)	.027(7)	.2890(11)	.6023(10)	66(9)	H(112)	.541(4)	-.0305(9)	.2992(9)	37(7)
H(1211)	.228(5)	.2069(15)	.5770(13)	47(10)	H(1221)	.358(5)	.0071(17)	.2184(15)	73(12)
H(1212)	.307(6)	.2647(20)	.5533(20)	70(13)	H(1222)	.182(4)	.0153(18)	.2883(17)	86(14)
H(1213)	.170(4)	.2121(14)	.5061(13)	52(9)	H(1223)	.302(4)	.0756(15)	.2506(14)	79(8)
H(1311)	-.283(11)	.2810(25)	.5712(28)	215(29)	H(1321)	.741(4)	.0007(14)	.2354(13)	45(9)
H(1312)	-.252(5)	.2439(18)	.5139(16)	71(11)	H(1322)	.644(10)	.0714(28)	.2311(28)	242(28)
H(1313)	-.138(5)	.1914(16)	.5693(14)	59(11)	H(1323)	.775(7)	.0439(24)	.2947(21)	116(18)
H(141)	-.042(5)	.4371(10)	.5397(9)	42(8)	H(142)	.463(5)	.0229(9)	.4452(8)	40(8)
H(1511)	.244(5)	.3667(16)	.6185(14)	78(11)	H(1521)	.338(4)	-.0714(14)	.4485(12)	42(8)
H(1512)	.241(3)	.4154(10)	.5865(8)	78(5)	H(1522)	.323(7)	-.0734(20)	.3736(18)	112(16)
H(1513)	.161(5)	.4439(14)	.6296(12)	66(9)	H(1523)	.198(7)	-.0075(24)	.4277(22)	162(20)
H(1611)	-.228(11)	.3571(16)	.6185(18)	176(21)	H(1621)	.263(11)	-.0227(26)	.4460(29)	218(29)
H(1612)	-.175(5)	.4396(16)	.6370(13)	79(11)	H(1622)	.643(4)	-.0922(14)	.4172(13)	40(8)
H(1613)	-.308(9)	.4185(24)	.5812(20)	219(24)	H(1623)	.266(5)	-.0457(17)	.3812(16)	67(10)

calculations comprise all atoms except the methyl groups.

Bond lengths and angles for the non-hydrogen atoms as calculated from the atomic coordinates in Table 2, are listed in Tables 5 and 6. It is realized that the temperature factors for carbon atoms in the isopropyl groups show unusually high values, *e.g.* atoms C(151), C(161) and C(162). However,

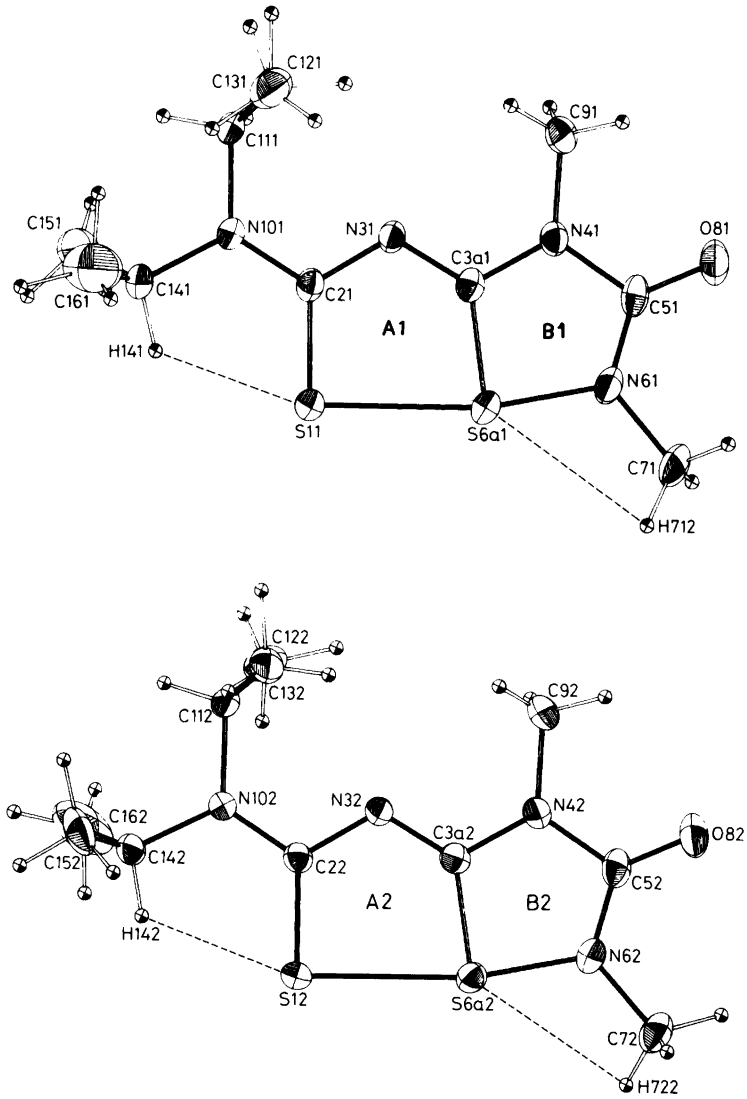

Fig. 1. ORTEP[10] drawings of the two molecules in the title compound with the numbering of the atoms in the molecules. Thermal ellipsoides for the non-hydrogen atoms are drawn at the 20 % probability level.

values of such magnitude are often found for carbon atoms in isopropyl substituent groups, see *e.g.* Ref. 11. The bond lengths between the atoms that were included in the least squares plane calculation have been corrected for libration, *cf.* Table 5. The *l'* values are corrected according to the librational tensors L_1 and L_2 given in Table 4 using Cruickshank's[12] method. The corrections range from 0.004 to 0.012 Å. The r.m.s. differences between observed U_{ij}'s and those calculated from the derived T,L,S molecular tensors are 0.0100 and 0.0096 Å^2, respectively, for molecules 1 and 2.

The bonds in the 'linear' S–S–N sequences are S(11)–S(6a1) = 2.522(1) Å and S(6a1–N)61 = 1.791(2) Å for molecule 1, and S(12)–S(6a2) = 2.561(1) Å and S(6a2)–N(62) = 1.780(2) Å for molecule 2. The S(1)–S(6a)–N(6) angles are 169.3(1) and 169.0(1)°, respectively, for molecules

Table 4. Rigid body libration tensors L_1 and L_2 of of the 2-diisopropylamino-4,6-dimethyl-3,4,6-triaza-1,6a-dithiapentalenylium-5-olate molecules.

	Eigenvalues	Eigenvectors Direction cosines × 10^4 relative to *a*, *b*, and *c*, respectively.		
L_1	41.6(°)^2	− 534	2658	9626
	15.7	−1182	9555	−2704
	6.0	−9916	−1281	− 197
L_2	35.5(°)^2	− 526	−9600	2751
	10.5	−4348	2700	8591
	5.8	−8990	− 744	−4316

1 and 2. Except for the S−S bonds, the other non-hydrogen bond lengths in the two molecules are equal within the error (3σ). According to Hamilton and Abrahams[13] a more realistic estimate of the deviations would probably be obtained by multiplying those by a factor of 2. This means that the C(111)−C(131), C(112)−C(122) and C(142)−C(152) bond lengths, *cf.* Table 5, are not significantly different from the accepted value for a C(sp^3)−C(sp^3) bond length of 1.536 Å.[14] A comparison with the analogous compound II shows that the S−S and S−N bonds in IV are significantly different from the corresponding values in II. In II S(1)−S(6a) = 2.492(1) Å and S(6a)−N(6) = 1.814(2) Å. The differences can be explained by the fact that when the sulfur substituent in 5-position in II is replaced by the more electronegative oxygen substituent in IV, there will be a redistribution of charge on the neighbouring atoms. The nitrogen atom in 6-position in IV will have a more positive charge relative to the same atom in II. It has been shown[15,16] that the more positive the charge on the 6-position atom is, the shorter becomes the 6a−6 bond length. A comparison of other equivalent bonds in II and IV shows only minor or insignificant differences.

A projection on the *yz*-plane of the two molecules in the asymmetric unit is given in Fig. 2 and a stereoscopic view of the arrangements of molecules is shown in Fig. 3.[10] The molecules are stacked upon each other almost perpendicular to the *a*-axis, and the spacing between two molecules are about *a*/2, *i.e.* 3.50 Å. It can further be seen from Fig. 2 that the two molecules overlap each other partly; the overlapping parts being rings B1 and B2, *cf.* Fig. 1.

Table 5. Bond lengths *l* in 2-diisopropylamino-4,6-dimethyl-3,4,6-triaza-1,6a-dithiapentalenylium-5-olate. Standard deviations in parentheses. The *l'* values have been corrected for libration according to the librational tensors L_1 and L_2.

Bond	*l*(Å)	*l'*(Å)
Molecule 1		
S(11)−S(6a1)	2.513(1)	2.522
S(11)−C(21)	1.699(3)	1.711
S(6a1)−C(3a1)	1.746(3)	1.758
S(6a1)−N(61)	1.784(2)	1.791
C(21)−N(31)	1.357(3)	1.364
C(21)−N(101)	1.343(3)	1.348
N(31)−C(3a1))	1.308(3)	1.313
C(3a1)−N(41)	1.358(3)	1.365
N(41)−C(51)	1.410(4)	1.416
N(41)−C(91)	1.460(3)	1.470
C(51)−N(61)	1.323(4)	1.333
C(51)−O(81)	1.229(4)	1.236
N(61)−C(71)	1.468(3)	1.475
N(101)−C(111)	1.491(4)	1.501
N(101)−C(141)	1.468(4)	1.475
C(111)−C(121)	1.563(19)	
C(111)−C(131)	1.450(21)	
C(141−C(151)	1.500(24)	
C(141)−C(161)	1.486(27)	
Molecule 2		
S(12)−S(6a2)	2.555(1)	2.561
S(12)−C(22)	1.708(3)	1.719
S(6a2)−C(3a2)	1.748(3)	1.758
S(6a2)−N(62)	1.774(2)	1.780
C(22)−N(32)	1.359(3)	1.365
C(22)−N(102)	1.332(3)	1.337
N(32)−C(3a2)	1.302(3)	1.306
C(3a2)−N(42)	1.361(3)	1.366
N(42)−C(52)	1.410(3)	1.415
N(42)−C(92)	1.457(3)	1.467
C(52)−N(62)	1.327(4)	1.336
C(52)−O(82)	1.224(3)	1.228
N(62)−C(72)	1.463(4)	1.470
N(102)−C(112)	1.505(4)	1.515
N(102)−C(142)	1.482(4)	1.487
C(112)−C(122)	1.429(16)	
C(112)−C(132)	1.580(17)	
C(142)−C(152)	1.470(15)	
C(142)−C(162)	1.562(19)	

The overlap is such that the most electronegative atoms, oxygen and nitrogen, come close to the more electropositive atoms, carbon and sulfur. Furthermore, the methyl group C(91) is positioned below

Table 6. Bond angles in 2-diisopropylamino-4,6-dimethyl-3,4,6-triaza-1,6a-dithiapentalenylium-5-olate. Standard deviations in parentheses.

Bond angle	(°)
Molecule 1	
S(6a1)–S(11)–C(21)	90.4(1)
S(11)–S(6a1)–C(3a1)	82.2(1)
S(11)–S(6a1)–N(61)	169.3(1)
S(11)–C(21)–N(31)	120.4(2)
S(11)–C(21)–N(101)	122.5(2)
C(3a1)–S(6a1)–N(61)	87.1(2)
S(6a1)–C(3a1)–N(31)	128.3(3)
S(6a1)–C(3a1)–N(41)	111.6(2)
S(6a1)–N(61)–C(51)	116.4(2)
S(6a1)–N(61)–C(71)	119.5(3)
N(31)–C(21)–N(101)	116.9(3)
C(21)–N(31)–C(3a1)	118.3(3)
C(21)–N(101)–C(111)	122.7(3)
C(21)–N(101)–C(141)	120.0(3)
N(31)–C(3a1)–N(41)	120.0(3)
C(3a1)–N(41)–C(51)	116.4(3)
C(3a1)–N(41)–C(91)	122.6(3)
C(51)–N(41)–C(91)	121.0(3)
N(41)–C(51)–N(61)	108.3(3)
N(41)–C(51)–O(81)	122.2(4)
N(61)–C(51)–O(81)	128.8(4)
C(51)–N(61)–C(71)	123.8(3)
C(111)–N(101)–C(141)	117.3(3)
N(101)–C(111)–C(121)	110.5(11)
N(101)–C(111)–C(131)	114.1(11)
N(101)–C(141)–C(151)	110.5(12)
N(101)–C(141)–C(161)	112.3(13)
C(121)–C(111)–C(131)	114.5(8)
C(151)–C(141)–C(161)	111.0(10)
Molecule 2	
S(6a2)–S(12)–C(22)	89.9(1)
S(12)–S(6a2)–C(3a2)	81.5(1)
S(12)–S(6a2)–N(62)	169.0(1)
S(12)–C(22)–N(32)	120.3(2)
S(12)–C(22)–N(102)	123.0(3)
C(3a2)–S(6a2)–N(62)	87.5(2)
S(6a2)–C(3a2)–N(32)	129.2(2)
S(6a2)–C(3a2)–N(42)	111.0(2)
S(6a2)–N(62)–C(52)	116.5(2)
S(6a2)–N(62)–C(72)	119.9(2)
N(32)–C(22)–N(102)	116.1(3)
C(22)–N(32)–C(3a2)	118.9(3)
C(22)–N(102)–C(112)	121.6(3)
C(22)–N(102)–C(142)	120.3(3)
N(32)–C(3a2)–N(42)	119.7(3)
C(3a2)–N(42)–C(52)	116.8(3)
C(3a2)–N(42)–C(92)	122.3(3)
C(52)–N(42)–C(92)	120.9(3)

Table 6. Continued.

N(42)–C(52)–N(62)	108.1(3)
N(42)–C(52)–O(82)	122.9(3)
N(62)–C(52)–O(82)	128.8(3)
C(52)–N(62)–C(72)	123.5(3)
C(112)–N(102)–C(142)	116.0(3)
N(102)–C(112)–C(122)	117.9(9)
N(102)–C(112)–C(132)	106.5(10)
N(102)–C(142)–C(152)	116.6(9)
N(102)–C(142)–C(162)	105.5(9)
C(122)–C(112)–C(132)	114.8(7)
C(152)–C(142)–C(162)	117.3(7)

the center of A2 and methyl group C(72) above the S(11)–S(6a1) bond. A *ca.* 90° rotation of one of the molecules in the *yz*-plane makes the two molecules overlap almost exactly. Thus, it can be concluded that the molecules are packed in the *a*-axis direction by stacking-forces consisting of both electrostatic and van der Waals' interactions.

The stacking of the molecules also explains the variation in intensity of the *h*00 reflections (see Table 1).

The only significant differences in the two molecules are between the S–S bonds. An explanation for this may be that the two S–S–N sequences have different surroundings. N(61) of molecule 1 may exchange π-electron charge with atom C(52) of molecule 2, and N(62) may interact with the central sulfur atom S(6a1) of molecule 1. The methyl group C(91) has a distance of 3.45 Å to the least squares plane of molecule 2. There may, therefore, be a transfer of π-electron charge from S(12) to the methyl group, thus increasing the σ-electron density on S(12), which implies a longer S(12)–S(6a2) bond relative to the same bond in an isolated molecule.[16]

The methyl group C(72) is situated so that π-electron charge may be transferred from both sulfur atoms S(11) and S(6a1), thus giving rise to a redistribution of charge on the two sulfur atoms.

There are a few more intermolecular contacts shorter than the corresponding van der Waals' distances[17–19] between symmetry related molecules, S(11)$[x,y,z]\cdots$H(141)$[x,\bar{y},\bar{z}]$ = 2.92(2) Å and O(82)$[x,y,z]\cdots$H(112)$[x,\frac{1}{2}+y,\frac{1}{2}-z]$ = 2.45(2) Å.

A few intramolecular contacts in the two molecules are indicated in Fig. 1. These interactions seem to fix the conformation of both the methyl groups

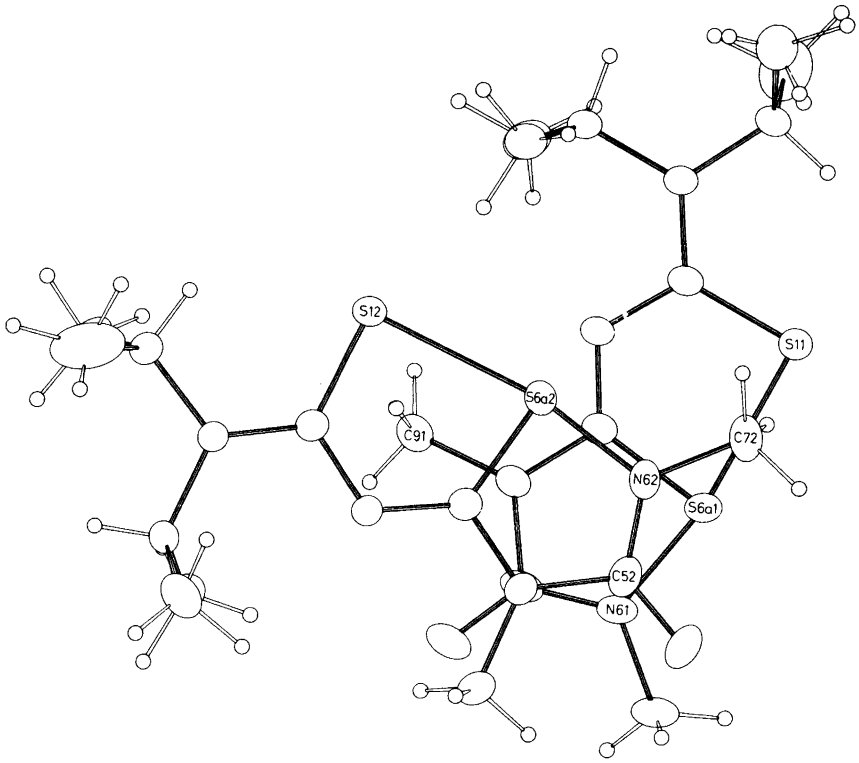

Fig. 2. A projection on the *yz*-plane of the stacking of the molecules in the unit cell.

and the isopropyl groups relative to the central ring systems, thus making the orientation of the substituent groups almost identical in the two independent molecules. In molecule 1 we have S(11)···H(141) = 2.35(2) Å and S(6a1)···H(712) = 2.86(2) Å. In molecule 2 we have contacts between the same atoms S(12)···H(142) = 2.43(2) and S(6a2)···H(722) = 2.76(2) Å.

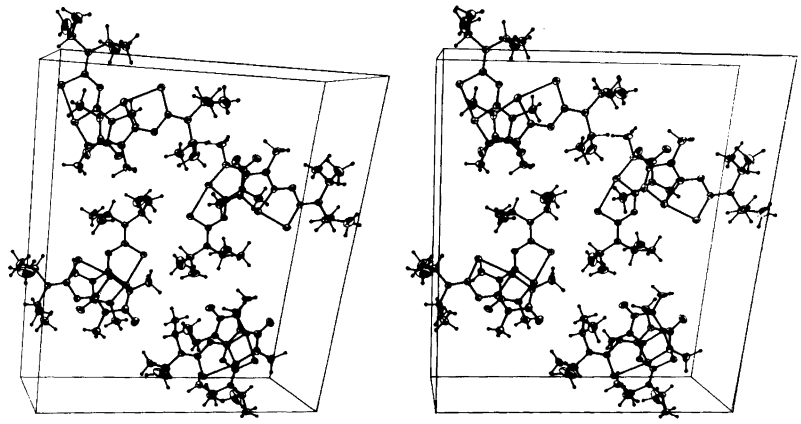

Fig. 3. A stereoscopic view of the arrangement of the molecules in the unit cell.

Table 7. Net charges (q) on the atoms in the S–S–N sequence from the CNDO/2 calculations on the two models of IV. The values given are for the σ-, π- and $(\sigma+\pi)$- net charges.[a] Models (i) and (ii) comprise a non-interacting molecule and two interacting molecules, respectively.

Atom	q_σ(e)	q_π(e)	$q_{(\sigma+\pi)}$(e)	S–S–N bond lengths (Å)
Model (i)				
S(1)	−0.408	0.147	−0.261	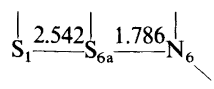
S(6a)	−0.049	−0.011	−0.060	
N(6)	−0.545	0.333	−0.212	
Model (ii)				
S(11)	−0.401	0.148	−0.253	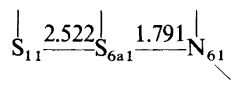
S(6a1)	−0.056	−0.004	−0.060	
N(61)	−0.550	0.338	−0.212	
S(12)	−0.422	0.141	−0.281	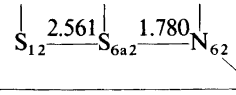
S(6a2)	−0.048	−0.019	−0.067	
N(62)	−0.540	0.330	−0.210	

[a] 2 π-electrons assumed in the valence shell for sulfur and nitrogen.

CNDO/2 calculations. The only significant difference in bond length between the two molecules is found for the S–S bonds of the respective S–S–N sequences. Since the surroundings of the sequences are different, it was thought worthwhile to calculate the charge distribution by semiempirical CNDO/2 calculations.[20] The calculations were performed with two different models: (i) a non-interacting molecule with bond lengths and angles being the average values of molecules 1 and 2; (ii) the two molecules together with values as found in the present X-ray work. In both models the molecules were assumed exactly planar and the two isopropyl groups were replaced by H-atoms. The N–H and C–H bond lengths were chosen to be 1.04 Å and 1.09 Å, respectively.[21]

It has been shown earlier through CNDO/2 calculations on 1,6,6a-trithiapentalenes[16] that changes in the S–S bond lengths are related to variations in the net charges on the sulfur atoms. If the S–S bond length in the 1,6,6a-trithiapentalene molecule is varied from 2.35 to 2.60 Å the difference in net charge between atom S(1) and S(6a) varies from −0.082 to −0.189 in total $(\sigma+\pi)$ net charge $\Delta q_{\sigma+\pi}$; from −0.049 to −0.357 in σ net charge Δq_σ and from −0.033 to +0.168 in π net charge Δq_π. This means that a change in bond length of 0.25 Å gives a variation in $(\sigma+\pi)$, σ and π net charge differences of −0.107, −0.308 and +0.201 electrons, respectively, and it shows that the variation in the σ and π net charge differences are 3 and 2 times, respectively, more sensitive to changes in the

Table 8. Net charge differences Δq between S(1)–S(6a) and N(6)–S(6a) in the two models. Differences are given for σ, π and $(\sigma+\pi)$.

Bond	l(Å)	Net charge difference Δq_σ(e)	Δq_π(e)	$\Delta q_{(\sigma+\pi)}$(e)	
S(1)–S(6a)	2.542	−0.359	0.158	−0.201	Model (i)
S(11)–S(6a1)	2.522	−0.345	0.152	−0.193	Model (ii)
S(12)–S(6a2)	2.561	−0.374	0.160	−0.214	
N(6)–S(6a)	1.786	−0.496	0.344	−0.152	Model (i)
N(61)–S(6a1)	1.791	−0.494	0.342	−0.152	Model (ii)
N(62)–S(6a2)	1.780	−0.492	0.349	−0.143	

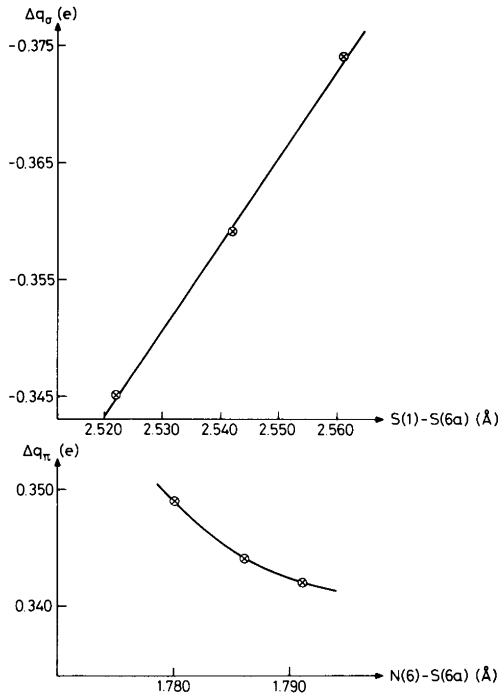

Fig. 4. Net charge differences Δq_σ and Δq_π in models (i) and (ii) as functions of the S(1)–S(6a) and N(6)–S(6a) bond lengths.

S–S bond lengths than the $(\sigma+\pi)$ net charge differences.

The results from the CNDO/2 calculations on the atoms in the S–S–N sequence in the present work are given in Table 7. It shows that atom N(61) has an increase in σ-electron charges and N(62) a decrease in σ-electron charges relative to a non-interacting molecule. Atom S(12) has also increased its σ-electron charge while atoms S(11) and S(6a1) have had a decrease and an increase, respectively, in the σ-electron charge density. The net charge differences between the terminal atoms S(1) and N(6) and the central atom S(6a) are given in Table 8. The results for the variations in the σ net charge difference with the S(1)–S(6a) bond length and the π net charge difference with the N(6)–S(6a) bond length are plotted on Fig. 4. The plots show that for the Δq_σ charge difference the relationship with bond length is almost linear and that the largest difference implies the longest S(1)–S(6a) bond length. For the Δq_π charge difference the relationship is non-linear and the smallest difference gives the largest S(6a)–N(6) bond length.

These observations are in accordance with what has been found earlier for the 1.6,6a-trithiapentalene molecule.[16]

Acknowledgement. The author wishes to thank Dr. J. Goerdeler, University of Bonn, for supplying a crystalline sample of the title compound.

REFERENCES

1. Hansen, L. K. *Acta Chem. Scand. A 31* (1977) 855.
2. Hansen, L. K. *Acta Chem. Scand. A 35* (1981) 61.
3. Hansen, L. K. *Acta Chem. Scand. A 36* (1982) 445.
4. Goerdeler, J., Büchler, R. and Sôlyom, S. *Chem. Ber. 110* (1977) 285.
5. *International Tables for X-Ray Crystallography*, Kynoch Press, Birmingham 1969, Vol. 1.
6. Stewart, J. M., Ed., *The X-Ray System, Version of 1976*, Technical Report TR-446, Computer Science Center, University of Maryland, College Park 1976.
7. Stewart, R. F., Davidson, E. R. and Simpson, W. T. *J. Chem. Phys. 42* (1965) 3175.
8. Cromer, D. and Mann, J. *Acta Crystallogr. A 24* (1968) 321.
9. Schomaker, V. and Trueblood, K. N. *Acta Crystallogr. B 24* (1968) 63.
10. Johnson, C. K. *ORTEP-II: A Fortran Thermal-Ellipsoid Plot Program For Crystal Structure Illustrations*, Report ORNL-3794, Oak Ridge National Laboratory, Oak Ridge 1971.
11. Sletten, J. *Acta Chem. Scand. A 29* (1975) 317.
12. Cruickshank, D. W. J. *Acta Crystallogr. 9* (1956) 757.
13. Hamilton, W. C. and Abrahams, S. C. *Acta Crystallogr. A 26* (1970) 18.
14. Bastiansen, O. and Trætteberg, M. *Tetrahedron 17* (1962) 147.
15. Hansen, L. K., Hordvik, A. and Sæthre, L. J. *Chem. Commun.* (1972) 222.
16. Hansen, L. K. *Cand. real. thesis*, University of Bergen, Bergen 1971.
17. Sletten, J. *Acta Chem. Scand. 25* (1971) 3577.
18. Sletten, J. *Thesis*, University of Bergen, Bergen 1976, p. 19.
19. Pauling, L. *The Nature of the Chemical Bond*, 3rd. Ed., Cornell University Press, Ithaca, New York 1960.
20. Details about the program are given in Ref. 2.
21. *CRC Handbook of Chemistry and Physics*, 52nd Ed., (1971–1972) F-175, F-173.

Received April 20, 1982.

Acta Chemica Scandinavica A 37 (1983) 41–45

Conformational Analysis. XVII. The Structure of 1,1-Dichloropropane Cl_2CH-CH_2-CH_3 as Determined by Electron Diffraction and Compared with Molecular-mechanics Calculations

TERJE RYDLAND,[a] RAGNHILD SEIP,[b] REIDAR STØLEVIK [a] and ØYVIND VORREN [a]

[a] Department of Chemistry, University of Trondheim, NLHT, Rosenborg, N-7000 Trondheim, Norway and [b] Department of Chemistry, University of Oslo, P.O. Box 1033, Blindern, Oslo 3, Norway

Gaseous 1,1-dichloropropane was studied at a nozzle temperature of 25 °C. Two conformers, *AG* and *GG*, were detected with 66±3% of *AG*. The following values for bond lengths (r_g) and bond angles (∠) are conformational averages: r(C–C) = 1.522(6) Å, r(C–Cl) = 1.781(6) Å, ∠CCC = 113.3(14)°, ∠CCCl = 110.7(4)°, ∠ClCCl = 109.3(4)°. The results have been presented with error limits (2σ). A normal-coordinate calculation gave the value 130 cm^{-1} for the $C-CHCl_2$ torsional mode within both conformers. The ED results agree with those from molecular-mechanics calculations.

This work is part of a conformational study of halogenated alkanes by gas-phase electron diffraction and molecular-mechanics calculations. The two 1:2 staggered conformers are *AG* and *GG* as indicated in Table 1. The multiplicity of *AG* is two corresponding to enantiomeric forms.

CALCULATIONS

Calculations of conformational energies and torsional barriers. Molecular-mechanics calculations were carried out using non-bonded potential functions in the Morse formulation.[1] The potential parameters are found in Ref. 2. The electrostatic terms of the potential have been calculated with the following charges (q) on the atoms: q(Cl) = −0.12, $q(C_1)$ = 0.039, $q(H_1)$ = 0.050, $q(C_2)$ = −0.009, $q(H_2)$ = 0.029, $q(C_3)$ = −0.011 and $q(H_3)$ = 0.028 in e-units. The charges were derived as suggested by Sanderson,[3] but reduced by a factor of 1.6.[4] The diagonal force constants of Ref. 4 were used for bond lengths and bond angles. An intrinsic torsional potential with threefold symmetry and a barrier height of 11.1 kJ/mol was included.

Calculated results are given in Table 1. Each energy value has been obtained by adjusting bond lengths and bond angles. At the energy minima the torsional angles were also adjusted. Energy minima are represented by the numbers 0 and 1.7 for *GG* and *AG*, respectively. Thus *GG* is energetically the most stable form. The energy minima, represented by the central number in each block of Table 1, are surrounded by torsional barriers, represented by the remaining eight numbers in each block, corresponding to forms with one or both terminal groups eclipsing the central CH_2 group. *AG* has approximately a staggered conformation while *GG* is exactly staggered. Each conformer corresponds to well-defined minima of the potential energy function.

The CH_3-torsional barriers are 12.1 and 12.9 kJ/mol for *GG* and *AG*, respectively. The lowest barrier for a conformational transition is 14.2 for the transition between enantiomeric forms of *AG*. For the transition *GG*→*AG* the lowest barrier is 23.4 kJ/mol.

Conformational differences between parameter values of bond angles are small. The largest value was 1.8° for ∠CCC. All conformational differences between bond lengths were negligible.

If the charges on the atoms are neglected the difference in energy $\Delta E = E(AG) - E(GG)$ is reduced to 0.8 kJ/mol.

MM calculations were also carried out on 1-

0302-4377/83 $2.50

Table 1. Conformational energies and structural parameters, for 1,1-dichloropropane obtained by molecular-mechanics calculations.

X=Cl	*AG*	*GG*
Conformer	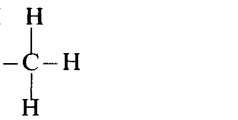	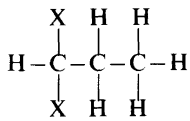
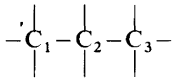		
Symmetry	C_1	C_s
Energies[a] in kJ/mol	46.9 14.6 32.2 23.4 1.7 16.3 46.9 14.6 32.2	46.9 12.1 46.9 23.4 0[b] 23.4 36.9 12.1 46.9
Torsional angle deviations from staggered form		
$\Delta\phi(1-2)$ in deg.	+6.2	0
$\Delta\phi(2-3)$ in deg.	−2.9	0
Valence angles in deg.		
∠CCC	113.4	115.2
∠CCX	110.2	110.8

[a] Horisontal variation corresponds to 60° change in $\phi(1-2)$. Vertical variation corresponds to 60° change in $\phi(2-3)$. [b] All energy values are relative to this value.

Table 2. Calculated mean amplitudes of vibration (u). The range of u values and the corresponding internuclear distances (r) are given. $T=298$ K.

Type of distance (X=Cl)	r(Å)	u(Å) × 10^3
C−H	1.108	78−79
C−X	1.781	52
C−C	1.522	51−52
X···X	2.87	68
X···H	2.35	107
C···H	2.16	107−108
X···C	2.72	67
H···H	1.78	127−128
C···C	2.55	70−71
C···H(g)	2.73−2.83	152−172
C···H(a)	3.48−3.51	105−106
H···H(g)	2.44−2.52	166−181
H···H(a)	3.05−3.06	130
X···C(g)	3.15−3.25	132−138
X···C(a)	4.09	70
X···H(g)	2.83−2.94	150−155
X···H(a)	3.67−3.68	102
H···H(aa)	4.31	144
H···H(ag)	3.82	174
H···H(ga)	3.72	177
H···H(gg″)	2.48	236
H···H(gg)	3.12	250
X···H(ga)	4.19−4.20	166−167
X···H(ag)	4.36−4.48	157−162
X···H(aa)	4.87	122
X···H(gg)	3.56−3.61	263−254
X···H(gg″)	2.81−2.92	231−242

chloropropane.[4] A conformational energy difference of 1.5 kJ/mol in favour of *gauche* was obtained, in agreement with the observed[5] value 1.3±0.8 kJ/mol. Also in this case the energy difference was reduced to about half when charges on the atoms were neglected.

Calculation of vibrational quantities. A normal-coordinate analysis[6] was carried out for each of the conformers, and mean amplitudes of vibration (u- and K-values) were computed.[7] Internuclear distances and their u-values are given in Table 2. The force constants, except for the torsional part, were taken from Ref. 8. The torsional force constants (F_ϕ) were computed from the formula given in Ref. 9. The values of $F_\phi(C_1-C_2)$ are 0.31 and 0.24 mdyn Å

Table 3. Calculated values of the torsional frequencies in cm^{-1}. Variation with the torsional force constant $F_\phi(C_1-C_2)$. The value of $F_\phi(C_2-C_3)$ was 0.086 m dyn Å(rad)$^{-2}$.

$F_\phi(C_1-C_2)$ m dyn Å(rad)$^{-2}$	0.22(*GG*) 0.17(*AG*)	0.31(*GG*) 0.24(*AG*)	0.40(*GG*) 0.31(*AG*)
GG	114	131	144
	204	205	205
AG	112	130	145
	202	202	202

(rad)$^{-2}$ for *GG* and *AG*, respectively. For $F_\phi(C_2-C_3)$ the value 0.086 mdyn Å(rad)$^{-2}$ was obtained for both conformers. The variation of the torsional frequencies with the value of $F_\phi(C_1-C_2)$ is shown in Table 3. Clearly the torsional modes are well separated with about 200–205 cm^{-1} corresponding to the methyl torsion and the lower mode corresponding to $C-CHX_2$ torsion at about 130 cm^{-1}.

Both of the torsional modes within the *GG* conformer belong to the species A″. In the low-frequency region below 300 cm^{-1} are found two additional modes corresponding to 214(A′) and 294(A′) for *GG*, but 243 and 286 cm^{-1} for *AG*.

EXPERIMENTAL

The compound was provided by K&K-laboratories and purified by gas chromatography. The sample used for ED had a purity in excess of 98%. ED-diagrams were recorded with the Balzers apparatus[10,11] at a nozzle temperature of 25 °C. Two sets of plates were obtained:

	Set 1	Set 2
Number of plates	6	6
Nozzle-to-plate distance (mm)	500.1	250.1
Electron wavelength (Å)	0.05859	0.05859

The electron wavelength was determined by calibration against benzene.[12] The data were treated in the usual way[13] to yield an intensity curve for each plate. Average curves for each set of distances were formed. A composite curve was then made by connecting the two average curves after scaling. The intensities have been calculated by the partial-wave method[14] using Hartree-Fock atomic potentials.[15]

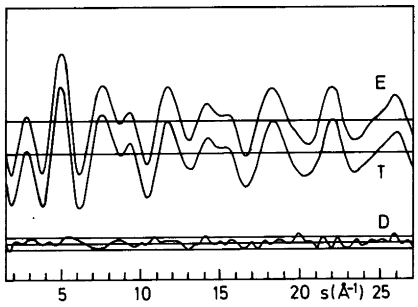

Fig. 1. Experimental (*E*) and theoretical (*T*) intensity curves for 1,1-dichloropropane and $D=E-T$ corresponding to the final least-square parameters. The straight lines show the experimental uncertainties (±3 times the experimental standard deviation).

RESULTS AND DISCUSSION

Final intensity curves and radial distribution curves (RD) are shown in Figs. 1 and 2. RD-curves for the individual conformers together with the experimental RD-curve are shown in Fig. 3. Clearly both of the conformers are present, *AG* being the most abudant conformer. The peak at 4.1 Å corresponds to the internuclear distance Cl···C(*anti*) only found in *AG*, while the peak at 3.2 Å corresponds to Cl···C (*gauche*) also found in *GG*. All distances are listed in Table 2.

It was assumed that the groups of atoms possess symmetry as follows: C_s for X_2HC-C, C_{2v} for $C-CH_2-C$, and C_{3v} for $C-CH_3$. All C–H bonds have equal lengths and the two C–C bonds also have equal lengths. Thus the conformers have identical structures except for the values of the torsional angles around the C_1-C_2 and C_2-C_3

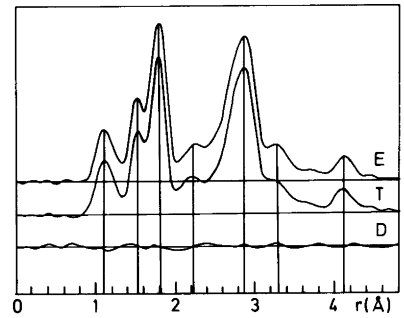

Fig. 2. Experimental (*E*) and theoretical (*T*) radial distribution curves for 1,1-dichloropropane and $D=E-T$. The damping constant was 0.002 Å^2.

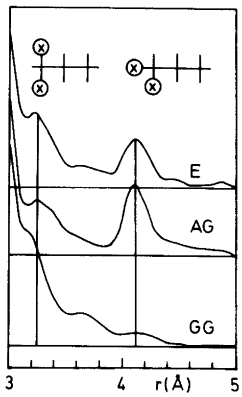

Fig. 3. Radial distribution curves for conformers of 1,1-dichloropropane are shown together with the final experimental curve. Only the conformational sensitive part is shown. Damping constant was 0.002 Å^2.

bonds. For *GG* the torsional angles were restricted at values corresponding to exactly staggered form. The torsional angles of *AG* were defined in the following way: $\phi(1-2)=126.2°+\phi_o$ and $\phi(2-3)=-(2.9°+\phi_o)$. If $\phi_o=0°$ the torsional angles have values corresponding to those in Table 1. The parameter ϕ_o was refined together with the parameters r(C−H), r(C−C), r(C−X), ∠CCX, ∠CCC, $\alpha(GG)$ and ∠(XCX)* which is the projection of the XCX angle on a plane perpendicular to the C_1-C_2 axis. Parameters from the final least-squares refinements and standard deviations(σ) corrected for correlation [16] are given in Table 4. The uncertainty in the *s*-scale (0.14 %) has been included in the σ values for bond lengths. Non-bonded distances were computed as dependent parameters restricted under the constrains of r_α parameters.[17,18]

Table 4. Structural parameters and conformational composition for 1,1-dichloropropane. Standard deviations (σ) apply to the last digit given (X=Cl).

Bond lengths (r_g) in Å and bond angles (∠$_\alpha$) in deg.			
C−H	1.108(5)	∠CCC	113.3(7)
C−C	1.522(3)		
C−X	1.781(3)	∠CCX	110.7(2)
∠XCX	109.3(2)	∠HCX	107.7(3)
∠HC_2H	107.6(−)[a]	∠C_2CH	109.9(−)[a]
∠HC_3H	108.9(4)	∠CC_2H	108.6(3)

Torsional angle deviations from staggered form	*AG*	*GG*
$\Delta\phi(1-2)$ in deg.	+10.0(12)[c]	0[b]
$\Delta\phi(2-3)$ in deg.	−6.7(12)[c]	0[b]
Composition(%)	66(3)	34(3)

[a] Assumed value from MM-calculations. [b] Exactly staggered form was assumed. [c] $\phi_o=3.8(12)°$ and ∠(XCX)* = 121.5(5)°, see text.

The following parameter-correlation coefficients(ρ) had absolute values greater than 0.4:$\rho(2,5)=-0.48$, $\rho(3,6)=-0.46$, $\rho(4,7)=-0.57$ and $\rho(5,6=+0.90$, with the parameters numbered as follows: 2,3,4,5,6,7 for r(C−C), r(C−X), ∠CCC, ∠CCX, ∠(XCX)*, ϕ_o, respectively.

Comparing the structural parameter values of Tables 1 and 4 shows that the predictions based on MM calculations are confirmed by the experimental findings.

Assuming equal vibrational and rotational partition functions for the conformers, the value of the energy difference $\Delta E=E(AG)-E(GG)$ is zero as computed from the composition in Table 4. If, however, the ratio $Q(GG)/Q(AG)=0.83$ between vibrational partition functions(Q) is included as determined by the calculated frequencies, then $\Delta E=0.5$ kJ/mol. The values of the rotational partition functions were very nearly equal. Including error limits ($\pm 2\sigma$) $\Delta E=0.4\pm0.8$ kJ/mol is presented as the final value. From the MM calculations (Table 1) $\Delta E=1.7$ was obtained. Both values indicate that *GG* is the energetically most stable conformer.

Acknowledgements. We are grateful to Hans Volden for measuring the intensities. Financial support from *Norges almenvitenskapelige forskningsråd* (NAVF) is acknowledged.

REFERENCES

1. Abraham, R. J. and Stølevik, R. *Chem. Phys. Lett. 58* (1978) 622.

2. Abraham, R. J. and Stølevik, R. *Chem. Phys. Lett.* 77 (1981) 181.
3. Sanderson, R. T. *Chemical Bonds and Bond Energy*, Academic, New York 1976.
4. Rydland, T. *Thesis*, University of Trondheim, Trondheim 1981.
5. Morino, Y. and Kuchitsu, K. *J. Chem. Phys. 28* (1958) 175.
6. Gwinn, W. D. *J. Chem. Phys. 55* (1971) 477.
7. Stølevik, R., Seip, H. M. and Cyvin, S. J. *Chem. Phys. Lett. 15* (1972) 263.
8. Schachtschneider, J. H. and Snyder, R. G. *Vibrational Analysis of Polyatomic Molecules. IV. Force constants for the haloparaffins*, Project No. 31450, Technical Report No. 122–63 of Shell Development Company.
9. Stølevik, R. *Acta Chem. Scand. A 31* (1977) 359.
10. Zeil, W., Haase, J. and Wegmann, L. *Z. Instrumentenkd. 74* (1969) 84.
11. Bastiansen, O., Graber, R. and Wegmann, L. *Balzers High Vacuum Rep. 25* (1969) 1.
12. Tamagawa, K., Iijima, T. and Kimura, M. *J. Mol. Struct. 30* (1976) 243.
13. Andersen, B., Seip, H. M., Strand, T. G. and Stølevik, R. *Acta Chem. Scand. 23* (1969) 3224.
14. Yates, A. C. *Comput. Phys. Commun. 2* (1971) 175.
15. Strand, T. G. and Bonham, R. A. *J. Chem. Phys. 40* (1964) 1686.
16. Seip, H. P. and Stølevik, R. In Cyvin, S. J., Ed., *Molecular Structures and Vibrations*, Elsevier, Amsterdam 1972.
17. Morino, Y., Kuchitsu, K. and Oka, T. *J. Chem. Phys. 36* (1962) 1108.
18. Kuchitsu, K. *J. Chem. Phys. 49* (1968) 4456.

Received April 27, 1982.

Acta Chemica Scandinavica A 37 (1983) 47–50

Studies of Stacking in AMP and Its Pd(II) Complexes by Ultrasonic Velocity Measurements

ARNE SKAUGE and PER IVAR VESTUES

Department of Chemistry, University of Bergen, N-5014 Bergen-U., Norway

The self-association of AMP and Pd(II) complexes of AMP was studied by ultrasonic velocity measurements. Using an isodesmic model, equiblibrium constants of the stacking process were obtained.

Two different Pd(II) complexes were used in the reactions with AMP, one in which two of the Pd^{2+} coordination sites were blocked by ethylenediamine (en), and one where three sites were blocked by diethylenetriamine (dien). In the first case two sites are available for coordination with AMP and in the other case one. We find that addition of the metal complexes induce stacking but the enhancement is much greater with $enPd^{2+}$ than with $dienPd^{2+}$.

The stacking constant for AMP^- was found to be, $K = 2.3 \pm 0.5$. Addition of $dienPd^{2+}$ and $enPd^{2+}$ increased the stacking constant with a factor of 3.5 and 14, respectively.

The self-association of nucleic bases, nucleosides and nucleotides has been the subject of intensive discussion in the literature. The field was reviewed, about a decade ago [1,2] and Sigel *et al.*[3] give a good review on later explorations in the field.

Different techniques have been employed to evaluate equilibrium constants for the aggregation of these compounds. Vapour pressure osmometry,[4–11] NMR-studies [2,3,12,13] and sedimentation equilibria [6,14,15] give information on the geometry and extent of the self-association. It is now generally accepted that the aggregation is due to stacking of the planar bases.

The interplay between metal ions and nucleic acid constituents has been subject of extensive research lately.[16–19] Especially since the antitumor action of *cis*-$[PtCl_2(NH_3)_2]$ was discovered in 1969,[20] has the effort in the field been steadily growing.

The strong ion–ion interactions make such methods as vapour pressure osmometry less useful. Only spectroscopic methods have been successfully applied to measure association of charged compounds (nucleotides).[21]

Quite recently, ultrasonic velocity measurements were utilized by Hemmes *et al.*[22] to evaluate equilibrium constants by stacking of nucleic bases. Hemmes *et al.* based their calculations on the isodesmic model of indefinite non-cooperative stacking. We applied their method to evaluate stacking constants of AMP and Pd(II) complexes of AMP.

THEORETICAL SECTION

The models for self-association have been reviewed by Magar.[23] We have applied the sequential equal constant-model (SEK), also referred to as the isodesmic model. The basic idea is that adding a monomer into an aggregate is characterized by the same equilibrium constant independent of the size of the aggregate. The various stages of association can be described as follows:

$$N_1 + N_1 \overset{K_1}{\rightleftharpoons} N_2 \quad K_1 = C_2/C_1$$

$$N_1 + N_2 \overset{K_2}{\rightleftharpoons} N_3 \quad K_2 = C_2/C_2C_1 \qquad (1)$$

$$N_1 + N_n \overset{K_n}{\rightleftharpoons} N_{n+1} \quad K_n = C_{n+1}/C_nC_1$$

where $K_1 = K_2 = K_3 = \ldots K$

The total concentration C can be expressed in terms of the concentrations of the aggregates.

0302-4377/83 $2.50

$$C = C_1 + 2C_2 + 3C_3 + \ldots \quad (2)$$

By introducing the equilibrium constant, the concentration is expressed as a function of the monomer concentration, C_1, and K.

$$C = \sum_{n=1}^{\infty} nK^{n-1}C_1^n \quad (3)$$

$$C = C_1/(1+KC_1)^2 \quad (4)$$

$$\Delta u/u = A_1C_1 + A_2C_2 + \ldots \quad (5)$$

$$A_n = nA_1 - 2n\Delta + 2\Delta \quad (6)$$

$$\Delta u/u = \sum_{i=1}^{\infty} n(A_1 - 2\Delta)K^{n-1}C_1^n + 2\Delta K^{n-1}C_1^n \quad (7)$$

$$\Delta u/uC = A_1 + 2\Delta KC_1 \quad (8)$$

$$\left(A_1 - \frac{\Delta u}{uC}\right) = 2\Delta KC_i \quad (9)$$

$$\left[\left(A_1 - \frac{\Delta u}{uC}\right)/C\right]^{1/2} = \left(\frac{K}{2\Delta}\right)^{1/2}\left[2\Delta - \left(A_1 - \frac{\Delta u}{uC}\right)\right] \quad (10)$$

$$\left[\left(A_1 - \frac{\Delta u}{uC}\right)/C\right]^{1/2} = \left(\frac{K}{2\Delta}\right)^{1/2}\left(A_1 - \frac{\Delta u}{uC}\right) + (2\Delta K)^{1/2} \quad (11)$$

$$A_1 = \lim_{c \to 0} \frac{\Delta u}{uC} \quad (12)$$

This series converges, when $KC_1 < 1$, giving eqn. (4). Rao[24] has shown that the contribution of non-interacting solutes to the ultrasonic velocity are additive. That is eqn. (5). Following the arguments of Hemmes *et al.*,[22] eqn. (6), where $n = 1, 2, 3, \ldots$ and Δ is the reduction in the A_n coefficients resulting from the association of two monomers. Combining eqn. (5) and eqn. (6), gives eqn. (7). This equation is simplified by dividing by C to eqn. (8); rearranging eqn. (8) gives eqn. (9), which still has three unknowns, C_1, Δ and K. Dividing by C, taking the square root and using eqn. (4) eliminates C_1, and gives eqn. (10); rearranging this equation gives us the linear eqn. (11) cited by Hemmes *et al.*, K and Δ are determined from the plot of $[(A_1 - \Delta u/uC)/C]^{1/2}$ *versus* $(A_1 - \Delta u/uC)$. A_1 is measured from the intercept of $\Delta u/uC$ *versus* C, eqn. (12).

MATERIALS AND METHODS

AMP of the best quality was purchased from Sigma Chemical Co., and used without further purification. Nitrates of dienPd$(H_2O)^{2+}$ and enPd$(H_2O)_2^{2+}$ were prepared as described earlier.[25,26] Solutions were prepared in the concentration range 0.16 to 0.01 M. The pH of the solutions corresponded to the nucleotide with a neutral adenine ring and monodeprotonated phosphate, (AMP^-).

The ultrasound velocity was measured at 25 °C ±0.01 by the resonant method, as described by Garnsey *et al.*[27] The method was improved by controlling the return signal by means of an oscilloscope. This made it possible to adjust the amplitude of the signal to a constant level. The resonance frequency of the x-cut crystals was 9 MHz. The ultrasonic cell was made from glass, with piezoceramic transducers in brass mountings. The cell had a volume of 5 ml, with an ultrasonic path of 5 cm. The accuracy of the ultrasonic velocity was ±1 cm/s, this makes the accuracy of the relativ velocity in the order of 10^{-3}%.

RESULTS AND DISCUSSION

Vapour pressure osmometry cannot give information on equilibrium constants of the charged nucleotides, without coarse approximation of the effect of the ionic interactions on the osmotic coefficients. In the ultrasonic method the effects of interacting forces are reflected in the limiting slope, A_1 (Fig. 1). Stacking constants can be obtained, because the solute–solvent interactions are eliminated as K is determined from the concentration dependence of the difference $(A_1 - \Delta u/uC_T)$. This difference is equal to the decrease in the slope of relative velocity *versus* concentration, resulting from the association of the nucleotides.

The application of the isodesmic model to the charged AMP-systems, can be justified from earlier investigations. The osmotic coefficients of 5'-AMP-methylester compared to NaH_2PO_4 verifies a strong association in water solutions.[8] Also ultracentrifuge studies by Rossetti *et al.*[14,15] show

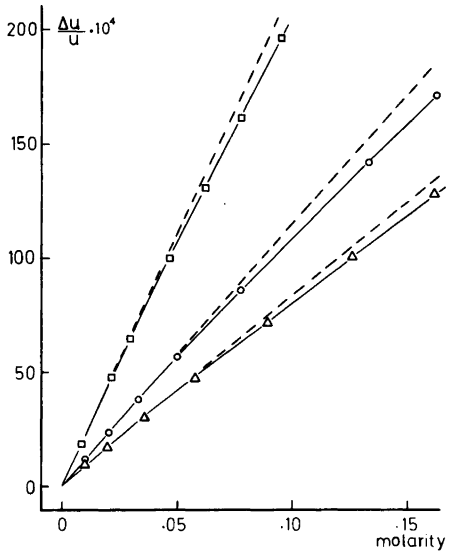

Fig. 1. Relative velocity *versus* concentration at 25 °C for ○ AMP^-, □ $dienPdAMP^+$ and △ $enPdAMP^+$. Dashed lines mark the limiting slopes.

that aggregation occurs beyond the dimer stage.

The results obtained are summarized in Table 1. Our value for AMP^-, $K=2.3\pm0.5$ is in good agreement with values published for AMP^{2-} by Sigel *et al.*[3] $K=2.1\pm0.4$ M^{-1} (27 °C), Neurohr and Mantsch,[12] $K=1.9$ M^{-1} (30 °C) and by Imoto,[28] $K=2.6$ M^{-1} (28 °C). Results for ATP show only a slight decrease in K upon deprotonation of the terminal phosphate.[29]

Comparison of the association constant for $dienPdAMP^+$ with the corresponding value for uncomplexed AMP^- shows an increase in the constant by a factor of 3.5 (*cf.* Table 1). In $Mg(ATP)^{2-}$, Sigel *et al.*[3] found a three-fold increase in going from the uncomplexed ATP^{4-}. In the magnesium complex there is no metal–purine coordination, and hence no intermolecular interaction induced by the metal ion. The behaviour

Table 1. Association parameters and stacking constants.

	$A_1[M^{-1}]$	$\Delta[M^{-1}]$	$K[M^{-1}]$
AMP^-	0.1175	0.0295	2.3 ± 0.5
$dienPdAMP^+$	0.2290	0.0398	8 ± 2
$enPdAMP^+$	0.0865	0.00605	33 ± 6

of dien Pd^{2+}, binding to AMP, has recently been described by Vestues and Martin.[30] The palladium coordinates to the purine ring in AMP, but since it already has three of its four available coordination sites blocked by dien, it is not able to form intermolecular crosslinks between different AMPs. The situation could be comparable to protonation of N(1) in the free nucleotide. Studies of ATP[29] show an almost threefold increase in the association constant upon protonation of N(1).

The ion–ion interactions in solution, and especially the few results reported, make a discussion of A_1, the limiting slope and the Δ quantity very difficult. The $A_1(AMP^-)=0.1175$ M^{-1} is much larger than the corresponding value for adenosine (0.0499 M^{-1}).[22] This is probably a result of the ionic interactions in the AMP solutions. $\Delta(AMP^-)=0.0295$ M^{-1} compared to Δ(adenosine) $=0.0355$ M^{-1}, indicates that the charge of the AMP has only a small effect on the actual association process.

A further treatment of the data for A_1 and Δ, in terms of compressibilities and solvation of the aggregates are of little value, regarding the ionic strength of the solutions.

A very interesting feature arises when comparing the association constant of $enPdAMP^+$, with $dienPdAMP^+$ and AMP^-. An increase in the self-stacking tendency by a factor of 4 and 14, respectively, indicates that there is a very strong additional effect operating, besides the effect of fixing a positive charge onto the adenine ring.

The reaction between $enPd^{2+}$ and AMP has been characterized by means of ^1H NMR.[31] Polymerization occurs within the actual pH-range, with relatively short stacks in the complex of +1 overall charge, and long stacks in the complex of net zero charge. Preliminary results from a single-crystal X-ray study, under progress in this laboratory, seem to confirm this polymerization. The two adjacent coordination sites in $enPd^{2+}$ form bridges between two nucleotides by coordination to N7. Another $enPd^{2+}$ ion bridges from N1 in these two AMPs to N1 in new nucleotides. The polymerization can be described as

$$(-\text{enPd}-\overset{\frown}{\text{N7}}\ \overset{\frown}{\text{N1}}-\text{enPd}-\overset{\frown}{\text{N1}}\ \overset{\frown}{\text{N7}}-\text{enPd}-)$$

It is to be expected that intermolecular interactions of this type would influence the association constant derived from an isodesmic

model. Sigel *et al.*[3] observed similar effects in the reactions between Zn^{2+} or Cd^{2+} and ATP^{4-}. The average association constants derived, with the assumption of the isodesmic model, were 11.1 and ~17, respectively. These values are explained with a high equilibrium constant for the dimerization of two metal $(ATP)^{2-}$ units. The metal ion coordinates to the phosphate of one ATP^{4-} and to N7 of the adenine in the next. The same arguments can be put forward in this case where the $enPd^{2+}$ binds to two adjacent adenine rings. This demonstrates limitations in applying the isodesmic model to get quantitative measurements of the stacking process, but the qualitative arguments still hold.

REFERENCES

1. Ts'o, P. O. P. In Fasman, G. D. and Timasheff, S. N., Eds., *Fine Structure of Proteins and Nucleic Acids*, Dekker, New York 1970, p. 49.
2. Ts'o, P. O. P. In *Basic Principles in Nucleic Acid Chemistry*, Academic, New York 1974, Vol. 1.
3. Scheller, K. H., Hofstetter, F. H., Mitchell, P., Prijs, B. and Sigel, H. *J. Am. Chem. Soc. 103* (1981) 247.
4. Ts'o, P. O. P., Melvin, I. S. and Olson, A. C. *J. Am. Chem. Soc. 85* (1963) 1289.
5. Broom, A. D., Schweizer, M. P. and Ts'o, P. O. P. *J. Am. Chem. Soc. 89* (1967) 3612.
6. Solie, T. N. and Schellman, J. A. *J. Mol. Biol. 33* (1968) 61.
7. Helmkamp, G. K. and Kondo, N. S. *Biochem. Biophys. Acta 159* (1968) 242.
8. Schweizer, M. P., Broom, A. D., Ts'o, P. O. P. and Hollis, D. P. *J. Am. Chem. Soc. 90* (1968) 1042.
9. Plesiewicz, E., Stepien, E., Bolewska, K. and Wierzhowski, K. L. *Biophys. Chem. 4* (1976) 131.
10. Sakurai, M., Morimoto, S. and Inoue, Y. *J. Am. Chem. Soc. 102* (1980) 5572.
11. Ts'o, P. O. P. and Chan, S. I. *J. Am. Chem. Soc. 86* (1964) 4176.
12. Neurohr, K. and Mantsch, H. H. *Can. J. Chem. 57* (1979) 1986.
13. Cheng, D. M., Kan, L. S., Ts'o, P. O. P., Giessner-Prettre, C. and Pullmann, B. *J. Am. Chem. Soc. 102* (1980) 525.
14. Rosetti, G. P. and Van Holde, K. E. *Biochem. Biophys. Res. Commun. 26* (1967) 717.
15. Van Holde, K. E. and Rosetti, G. P. *Biochemistry 6* (1967) 2189.
16. Marzilli, L. G. *Prog. Inorg. Chem. 23* (1977) 255.
17. Gellert, R. W. and Bau, R. *Met. Ions Biol. Syst. 8* (1979) 1.
18. Martin, R. B. and Mariam, Y. H. *Met. Ions Biol. Syst. 8* (1979) 57.
19. Eichhorn, G. L. *Met. Ions Biol. Syst. 10* (1980) 1.
20. Cleare, M. J. and Hydes, P. C. *Met. Ions Biol. Syst. 11* (1980) 1.
21. Heyn, M. P. and Bretz, R. *Biophys. Chem. 3* (1975) 35.
22. Hemmes, P., Mayevski, A. A., Buchin, V. A. and Sarvazyan, A. P. *J. Phys. Chem. 84* (1980) 699.
23. Magar, M. E. *Data Analysis in Biochemistry and Biophysics*, Academic, New York 1972.
24. Rao, M. R. *Curr. Sci. 9* (1940) 534.
25. Lim, M. C. and Martin, R. B. *J. Inorg. Nucl. Chem. 38* (1976) 1915.
26. Lim, M. C. and Martin, R. B. *J. Inorg. Nucl. Chem. 39* (1976) 1911.
27. Garnsey, R., Mahoney, R. and Litowitz, T. A. *J. Chem. Phys. 64* (1964) 2073.
28. Imoto, T. *Biochim. Biophys. Acta 475* (1977) 409.
29. Gilligan, T. J. and Schwarz, G. *Biophys. Chem. 4* (1976) 55.
30. Vestues, P. I. and Martin, R. B. *J. Am. Chem. Soc. 103* (1981) 806.
31. Sovago, I. and Martin, R. B. *Inorg. Chem. 19* (1980) 2868.

Received April 6, 1982.

Acta Chemica Scandinavica A 37 (1983) 51 – 55

The Crystal Structure of Aqua-bis(*N*-salicylidene-β-alaninato)dicopper(II) Monohydrate

PER-ERIK WERNER,[a] ALADÁR VALENT,[b] VOLRATH ADELSKÖLD[a] and OĽGA ŠVAJLENOVÁ[b]

[a] Department of Structural Chemistry, Arrhenius Laboratory, University of Stockholm, S-106 91 Stockholm, Sweden and [b] Department of Inorganic and Organic Chemistry, Faculty of Pharmacy, Komenský University, Kalinčiakova 8, 83232 Bratislava, Czechoslovakia

The crystal structure of aqua-bis(*N*-salicylidene-β-alaninato)dicopper(II) monohydrate, $[(C_{10}H_9NO_3Cu)H_2O)(C_{10}H_9NO_3Cu)]H_2O$, has been determined by X-ray diffraction methods. The structure has been determined and refined in the triclinic space group $P\bar{1}$ with the unit cell dimensions $a=12.581(4)$ Å, $b=10.339(4)$ Å, $c=8.156(3)$ Å, $\alpha=92.04(3)°$, $\beta=95.36(3)°$, $\gamma=77.44(3)°$. Intensity data were collected on a diffractometer with Cu$K\alpha$ radiation. The final R index for 1004 "observed" reflections is 0.060. The asymmetric unit contains two differently coordinated copper atoms in a dimeric molecule; the copper – copper distance being 3.028(3) Å. The copper atoms are bridged by two phenolic oxygens. One copper atom has a distorted square-pyramidal, and the other one a distorted square-planar coordination. The five-coordinated copper is bound to a water molecule in the apical direction at a distance of 2.295(11) Å. The dimeric structure proposed on the basis of magnetic behaviour has been confirmed by the results of the crystal structure determination.

The metal complexes of Schiff bases derived from salicylaldehyde and amino acids [1,2,3] have received comparatively little attention in spite of their apparent usefulness as models for the more complicated metal – pyridoxal – amino acid systems, which are intermediates in biologically important transamination reactions.[4] Earlier, some crystal structures of the copper(II) complexes derived from salicylaldehyde and amino acids have been solved.

Carlisle *et al.*[5] have prepared the *N*-salicylidene-L-valinatocopper(II) complex and on the basis of magnetic properties described the structure as tetrameric. They suggest that the magnetic state may be closely approximated by considering any in-plane spin-spin coupling. Švajlenová *et al.*[6] have prepared the aqua-*N*-salicylidene-β-alaninato-copper(II) complex, which has a subnormal value of its magnetic moment even at room temperature ($\mu_{eff}=0.91$ B.M.). This value of μ_{eff} eliminates the possibility of H_2O bonded "in-plane" together with donor atoms of the Schiff base. Molecular water could be coordinated only by a weak bond in an axial direction, without influence on the super-exchange mechanism in the basal square plane. In order to obtain more information about these aspects, we decided to determine the crystal structure of the title compound.

EXPERIMENTAL

Aqua-bis(*N*-salicylidene-β-alaninato)dicopper(II) monohydrate was prepared by reaction of β-alanine (5×10^{-2} mol), copper(II) acetate monohydrate (5×10^{-2} mol), and salicylaldehyde (5×10^{-2} mol) in boiling aqueous ethanol (50 ml ethanol + 60 ml H_2O). The mixture was stirred and heated for 90 min. The dark green crude product was obtained by cooling the solution. The compound was recrystallized from hot aqueous ethanol. Carbon, nitrogen and hydrogen were determined by micro-analytical methods. The results of the analysis were: C 44.3 %, N 5.0 % and H 4.0 %, which are in good agreement with the calculated values: C 44.04%, N 5.14% and H 4.07% for the formula $C_{20}H_{18}N_2O_6Cu_2(H_2O)_2$.

A crystal of approximate dimensions $0.05\times0.15\times0.6$ mm^3 was selected for X-ray analysis. Data were collected with a Philips PW1100 four-circle diffractometer, equipped with a graphite mono-

0302-4377/83 $2.50

Table 1. Crystal data.

Aqua-bis(*N*-salicylidene-β-alaninato)dicopper(II) monohydratemonohydrate $[(C_{10}H_9NO_3CuH_2O)\text{-}(C_{10}H_9NO_3Cu)]H_2O$; F. W. = 545.5
Space group $P\bar{1}$ (No. 2); $Z = 2$
$a = 12.581(4)$ Å $\alpha = 92.04(3)°$
$b = 10.339(4)$ $\beta = 95.36(3)$
$c = 8.156(3)$ $\gamma = 77.44(3)$
$D_x = 1.757$ g cm^{-1}
μ(Cu$K\alpha$) = 7.9 cm^{-1}

chromator to reflect Cu$K\alpha$ radiation. Lattice parameters were determined by least-squares refinement of the θ values for 25 centered reflections. Crystal data are given in Table 1.

Intensities were measured by the $\theta-2\theta$ scan mode ($\theta_{max} = 50°$) at a speed of 0.9° min^{-1} in θ and a scan width of 1.5°. The background was measured at each end of the interval for half the scan time. 1004 independent reflections were considered as observed according to the criterion $I \geq 3\sigma(I)$. Three reflections were monitored periodically during the data collection and showed no sign of crystal deterioration. The data were corrected for Lorentz and polarization effects, but not for absorption ($\mu = 7.9$ cm^{-1}).

Calculations were carried out with the SHELX program system.[7] The figures were drawn with the PLUTO 78 program.[8] Scattering factors were taken from *International Tables for X-Ray Crystallography*.[9] Anomalous dispersion was taken into account.

STRUCTURE DETERMINATION AND REFINEMENT

A Patterson synthesis favoured the centrosymmetric space group $P\bar{1}$ and yielded the Cu positions. Fourier syntheses revealed the positions of the other non-hydrogen atoms. Initially, the structure was least-squares refined isotropically. Next, all H atoms except for those of the crystal water molecules were introduced geometrically, and the structure was refined with Cu anisotropic and the rest of the non-hydrogen atoms isotropic. The H atoms were treated as riding on the corresponding C atoms, with fixed bond length (1.08 Å) and with the same thermal parameters as the C atoms. In the final cycles of refinement the weighting scheme $w = 1/[\sigma^2(F_o) + (0.023\ F_o)^2]$ was employed. There were no changes larger than 0.06σ in any of the 139 parameters varied in the final refinement cycle. The final unweighted R factor was 0.060, and $R_w = [\Sigma w(|F_o| - |F_c|)^2/\Sigma w F_o^2]^{1/2} = 0.059$. The attempt to locate hydrogen linked to the two water oxygen atoms from the difference Fourier map calculated after refinement was unsuccessful.

A list of observed and calculated structure factors are obtainable from the authors on request.

RESULTS AND DISCUSSION

The atomic coordinates and isotropic thermal parameters are given in Table 2. The numbering scheme of the asymmetric unit is shown in Fig. 1. The crystal water oxygen O8, not directly bound to copper, is omitted in the figure.

Table 2. Atomic coordinates ($\times 10^4$) and isotropic temperature factors (Å$^2 \times 10^3$). $T = \exp(-8\pi^2 U \sin^2\theta/\lambda^2)$.

	x	y	z	U (Å^2)
Cu1	3052(2)	2973(2)	2238(3)	38
Cu2	2684(2)	5724(2)	839(3)	38
C1	4879(13)	4342(15)	2654(19)	35(5)
C2	5470(13)	5196(16)	1975(20)	43(5)
C3	6518(13)	5210(16)	2627(19)	41(4)
C4	7049(15)	4351(17)	3867(22)	56(6)
C5	6461(14)	3520(17)	4482(21)	47(5)
C6	5408(14)	3469(16)	3882(20)	41(5)
C7	4852(13)	2670(16)	4722(20)	44(5)
C8	6568(16)	8324(18)	4554(22)	64(6)
C9	2951(15)	479(18)	4456(24)	67(7)
C10	1965(16)	1051(18)	3441(23)	57(6)
C11	1412(12)	3923(15)	−725(19)	30(5)
C12	1393(12)	2613(15)	−1248(19)	33(5)
C13	697(13)	2362(17)	−2523(20)	42(5)
C14	−52(13)	3388(16)	−3364(21)	48(5)
C15	−17(13)	4684(16)	−2854(19)	38(5)
C16	708(12)	4956(15)	−1607(18)	31(5)
C17	661(13)	6337(16)	−1257(19)	38(5)
C18	1260(13)	8237(16)	−35(22)	51(6)
C19	2264(14)	8709(18)	−415(22)	52(6)
C20	3250(15)	8253(18)	677(22)	53(6)
N1	3896(11)	2407(12)	4240(16)	41(4)
N2	1396(10)	6785(13)	−281(16)	41(4)
O1	3847(8)	4382(9)	2021(12)	35(3)
O2	2119(8)	4147(9)	501(12)	31(3)
O3	1916(9)	2045(11)	2494(13)	50(4)
O4	1200(10)	439(13)	3288(15)	72(4)
O5	3346(9)	7174(11)	1520(13)	49(4)
O6	3995(10)	8908(11)	927(14)	62(4)
O7	3977(9)	1505(11)	413(13)	52(4)
O8	9010(13)	1197(16)	4108(20)	126(6)

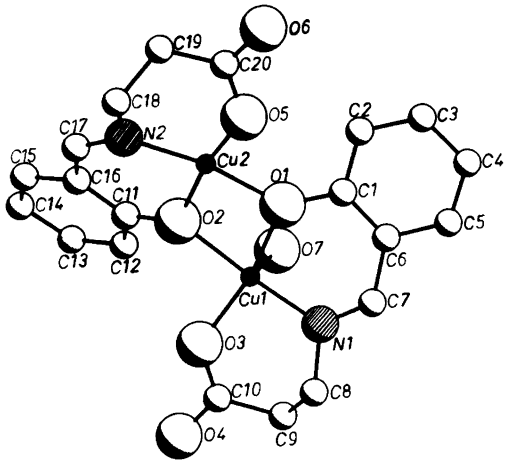

Fig. 1. The conformation of the title compound and the numbering of the atoms. Crystal water not bound to copper is omitted.

Two copper(II) ions and two tridentately coordinated *N*-salicylidene-*β*-alaninato (L^-) ions form a binuclear complex, where one of the copper(II) ions is also bound to a water molecule, ($CuLH_2O$) (CuL). Thus, one copper(II) ion (Cu1) exhibits a distorted square-pyramidal coordination, whereas the other (Cu2) is approximately square-coordinated. The copper atoms are bridged by two phenolic O atoms, with a copper–copper distance of 3.028(3) Å. The remaining two coordination sites in the square planes are occupied by a N atom and a carboxylate O atom. The fifth site in the coordination sphere around Cu1 is occupied by a water molecule at a distance of 2.295 Å in the apical direction. Thus, the dimeric structure that could be predicted from the magnetic measurement is confirmed by the structure determination. The coordination distances and angles around the Cu atoms are given in Table 3. As can be seen from the table, the bonds between the five-coordinated copper, Cu1, and the bridging oxygen atoms are somewhat longer than the corresponding bonds around Cu2.

The displacements of Cu from least-squares planes through the basal coordination planes are given in Table 4. The angle between the planes is 33°, *cf.* the stereo view in Fig. 2.

The displacement of Cu1 from its coordination plane is 0.25 Å, which is somewhat larger value than found in related complexes: 0.14 Å in the glycinato,[10] 0.17–0.18 Å in threoninato[11] and 0.18–0.20 Å in the phenylalaninato[12] complex. On the other hand, the square coordinated Cu2 is situated only 0.08 Å from its coordination plane.

In Cu(II) complexes formed with salicylaldehyde and amino acids, the bond between N and C atoms of the amino acid or the bond between the N and C atoms of the aldehyde part are sometimes shorter than a normal single or double bond, respectively. This finding was first discussed by Ueki *et al.*[10] They suggested that the bond distances around

Table 3. Bond distances (Å) and angles (°) around the Cu atoms.

Cu1–N1	1.900(14)	Cu2–N2	1.920(13)
Cu1–O1	1.960(10)	Cu2–O2	1.917(9)
Cu1–O2	2.013(10)	Cu2–O1	1.986(10)
Cu1–O3	1.917(11)	Cu2–O5	1.909(10)
Cu1–O7	2.295(11)		
N1–C7	1.312(21)	N2–C17	1.314(20)
N1–C8	1.494(23)	N2–C18	1.482(20)
Cu1–O1–Cu2	100.3(5)	Cu1–O2–Cu2	100.8(5)
O1–Cu1–O2	76.3(4)	O1–Cu2–O2	77.9(4)
O1–Cu1–N1	91.4(5)	O2–Cu2–N2	91.9(5)
N1–Cu1–O3	96.3(6)	N2–Cu2–O5	95.7(5)
O2–Cu1–O3	92.1(5)	O1–Cu2–O5	94.2(4)
O1–Cu1–O3	162.7(5)	O2–Cu2–O5	170.5(5)
N1–Cu1–O2	161.2(5)	N2–Cu2–O1	169.4(5)
O1–Cu1–O7	96.6(4)		
O2–Cu1–O7	95.3(4)		
O3–Cu1–O7	97.2(5)		
N1–Cu1–O7	100.3(5)		

Table 4. Displacements (Å) of the atoms from least-squares planes in $[(C_{10}H_9NO_3CuH_2O)$-$(C_{10}H_9NO_3Cu)]H_2O$ defined by:
Plane I: O1, O2, O3, N1
Plane II: O1, O2, O5, N2

Atom	Plane I	Atom	Plane II
O1	−0.014(10)	O1	0.016(10)
O2	0.013(10)	O2	−0.016(10)
O3	−0.012(10)	O5	−0.014(10)
N1	0.012(13)	N2	0.014(13)
Cu1	−0.252(3)	Cu2	0.075(3)
O7	−2.546(11)		

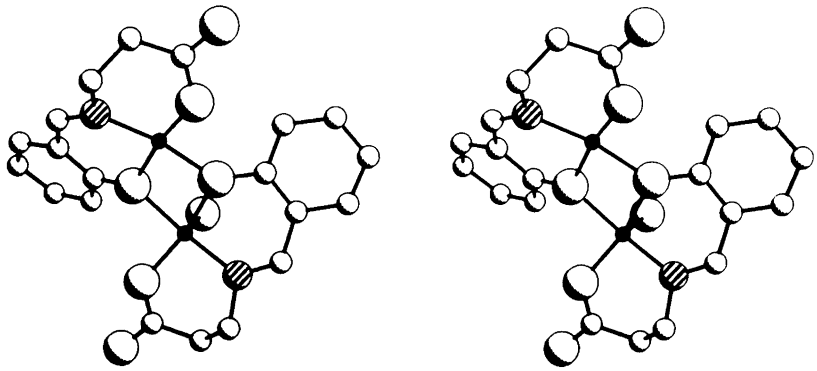

Fig. 2. Stereoscopic view of aqua-bis(*N*-salicylidene-β-alaninato)dicopper(II).

the nitrogen atom may give a clue to the reaction mechanism in the nonenzymatic transamination reactions. The reaction mechanism proposed by Metzler *et al.*[4] was concerned with the migration of the double bond around the nitrogen atom. However, in the present structure, as well as in the valinato [13] and the threoninato [11] complexes, no significant deviations from normal single and double bond distances are found (*cf.* Table 3).

The projection of the crystal structure along the *c* axis is shown in Fig. 3. The neighbouring molecules are connected by intermolecular hydrogen bonding between water and carboxylate oxygen. Thus, the binuclear xomplexes are connected by four hydrogen

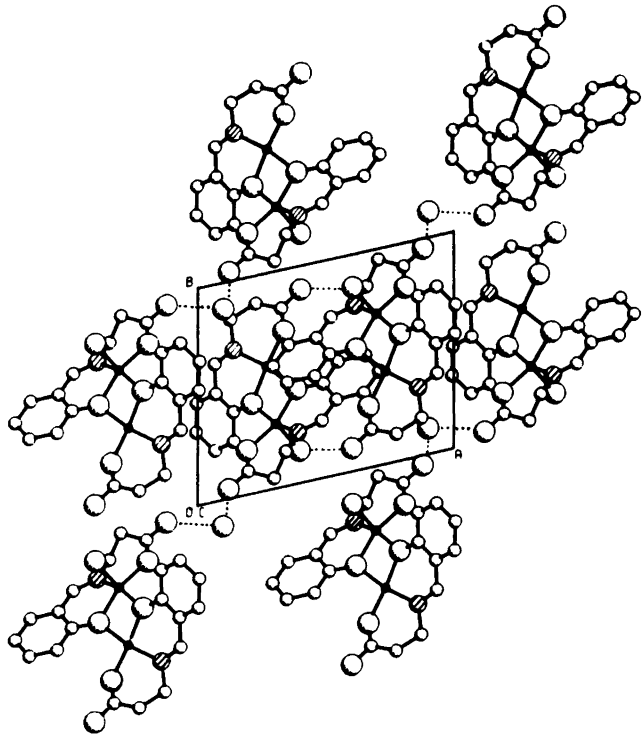

Fig. 3. Projection of the crystal structure along the *c* axis. Broken lines indicate hydrogen bonds.

Table 5. Hydrogen bond distances (Å).

$O7^{i}-H\cdots O6$	2.727(15)
$O7^{ii}-H\cdots O6$	2.811(15)
$O8^{iii}-H\cdots O4$	2.832(20)
$O8^{iv}-H\cdots O4$	2.827(21)

Symmetry code

(i) $x, 1+y, z$	(iii) $x-1, y, z$
(ii) $1-x, 1-y, -z$	(iv) $1-x, -y, 1-z$

bonds in a three-dimensional network. The hydrogen bond distances between the two non-equivalent water molecules and the carboxylate oxygen atoms are given in Table 5. It is unlikely that a direct electron exchange between the copper atoms operates in the present structure where the copper – copper distance is as long as 3.028(3) Å. The situation is similar to that discussed by Barclay and Hoskins [14] for acetylacetone-mono(*o*-hydroxyanil)-copper(II), where the coordination around the copper atoms in a dimeric unit is also square – pyramidal around one of the copper atoms and square-planar around the other one, just as in the present structure.

Acknowledgements. One of the authors, (Aladár Valent), would like to express his thanks to the Swedish Institute for a research fellowship grant which has made his stay at the Arrhenius Laboratory possible.

The authors wish to thank Prof. P. Kierkegaard for his kind interest in this work. Our heartfelt thanks are due to Mr. L. Göthe for his skilful technical assistance.

This work har received financial support from The Swedish Natural Research Council.

REFERENCES

1. Nakao, Y., Sakarai, K. and Nakahara, A. *Bull. Chem. Soc. Jpn. 40* (1967) 1536.
2. Gillard, R. D. and Wootton, R. *J. Chem. Soc. B* (1970) 364.
3. Švajlenová, O., Krätsmár-Šmogrovič, J. and Šeršeň, F. *Chem. Zvesti 32* (1978) 12.
4. Metzler, D. E., Ikawa, M. and Snell, E. E. *J. Am. Chem. Soc. 76* (1954) 648.
5. Carlisle, G. O., Ganguli, K. K. and Theriot, L. J. *Inorg. Nucl. Chem. Lett. 7* (1971) 527.
6. Švajlenová, O., Krätsmár-Šmogrovič, J. and Valent, A. *To be published.*
7. Sheldrick, G. M. *SHELX, Program for Crystal Structure Determination*, Univ. of Cambridge, England 1978.
8. Motherwell, W. D. S. *PLUTO. Program for Plotting Crystal and Molecular Structures*, Univ. of Cambridge, England 1976.
9. *International Tables for X-ray Crystallography*, Kynoch Press, Birmingham 1974, Vol. IV, p. 99.
10. Ueki, T., Ashida, T., Sasada, Y. and Kakudo, M. *Acta Crystallogr. B 25* (1969) 328.
11. Korhonen, K. and Hämäläinen, R. *Acta Crystallogr. B 37* (1981) 829.
12. Hämäläinen, R., Turpeinen, U., Ahlgrén, M. and Rantala, M. *Acta Chem. Scand. A 32* (1978) 549.
13. Korhonen, K. and Hämäläinen, R. *Acta Chem. Scand. A 33* (1979) 569.
14. Barclay, G. A. and Hoskins, B. F. *J. Chem. Soc. 2* (1965) 1979.

Received May 7, 1982.

Acta Chemica Scandinavica A 37 (1983) 57–62

Crystal Structures of Tetrabutylammonium Dichlorocuprate(I) and Tetrabutylammonium Dibromocuprate(I), $[N(C_4H_9)_4][CuCl_2]$ and $[N(C_4H_9)_4][CuBr_2]$

MILJA ASPLUND,[a] SUSAN JAGNER[a] and MARTIN NILSSON[b]

[a] Department of Inorganic Chemistry and [b] Department of Organic Chemistry, Chalmers University of Technology and University of Göteborg, S-412 96 Göteborg, Sweden

The crystal structures of the title compounds have been determined from single-crystal X-ray diffractometer data collected at 168 K. $[N(C_4H_9)_4][CuCl_2]$ and $[N(C_4H_9)_4][CuBr_2]$ are isostructural and crystallize in space group $C2/c$, with $a=13.055(1)$, $b=9.844(1)$, $c=15.776(2)$ Å, $\beta=92.39(1)°$, $Z=4$ and $a=13.059(8)$, $b=10.060(5)$, $c=15.920(7)$ Å, $\beta=92.56(4)°$, $Z=4$, respectively. Full-matrix least-squares refinement of the 147 structural parameters gave $R=0.038$ for tetrabutylammonium dichlorocuprate(I) [1094 observed independent reflections, $I>3.0\ \sigma\ (I)$] and $R=0.033$ for tetrabutylammonium dibromocuprate(I) [1291 observed independent reflections, $I>3.0\ \sigma\ (I)$]. The $[CuCl_2]^-$ and $[CuBr_2]^-$ ions are linear with Cu at a centre of symmetry; Cu–Cl = 2.107(1) Å and Cu–Br = 2.226(1) Å.

Whereas the dichlorocuprate(I) ion has been found as a linear monomer in a number of crystal structures,[1–6] there seems to be little evidence for the existence of discrete dibromocuprate(I) or diiodocuprate(I) ions in the solid state. Recently, tetrabutylammonium diiodocuprate(I) has been shown to contain discrete centrosymmetric $[Cu_2I_4]^{2-}$ dimers in which copper(I) has approximately trigonal planar coordination.[7] The structure of the analogous $[Cu_2Br_4]^{2-}$ has been determined in the cation radical salt of tetrathiotetracene with dibromocuprate(I); there are, however, additional Cu–S contacts to the tetrathiotetracene cation radicals such that the configuration of ligands about copper(I) is approximately trigonal bipyramidal.[8] There does not appear to be any crystallographic determination of a discrete linear $[CuBr_2]^-$ ion, though infrared and Raman spectra and nuclear quadrupole resonance frequencies suggest that tetrabutylammonium dichlorocuprate(I) and tetrabutylammonium dibromocuprate(I) both contain linear centrosymmetric anions.[9] In order to ascertain the nature of the copper(I) coordination in these compounds, their crystal structures have been investigated.

EXPERIMENTAL

Tetrabutylammonium dichlorocuprate(I) and tetrabutylammonium dibromocuprate(I) were prepared from the copper(I) halides as described previously.[10] The compounds crystallize as rhombic plates showing pronounced polysynthetic twinning. Single-crystal fragments of the approximate size indicated in Table 1 were used for the measurement of intensities at 168 K with a Syntex $P2_1$ diffractometer and graphite-monochromated Mo$K\alpha$ radiation. Crystal data and details concerning the data collection are given in Table 1.

Periodical measurement of the intensities of two reflections showed that the crystals were not subject to decay during the collection of data. A 96-step profile was recorded for each reflection and the Lehmann and Larsen profile-analysis method[11] was used to calculate the intensities.[12] Data were corrected[13] for Lorentz and polarization effects but not for absorption, owing to the irregular shapes of the crystals. The unit-cell parameters at 168 K were determined by least-squares from diffractometer setting angles for 14 reflections.

STRUCTURE DETERMINATION AND REFINEMENT

The structure of $[N(C_4H_9)_4][CuBr_2]$ was determined from Patterson and successive electron

0302-4377/83 $2.50

Table 1. Crystal data for tetrabutylammonium dichlorocuprate(I) and tetrabutylammonium dibromocuprate(I).

	$[N(C_4H_9)_4][CuCl_2]$	$[N(C_4H_9)_4][CuBr_2]$
M_r	376.9	465.8
Unit-cell dimensions	$a=13.055(1)$, $b=9.844(1)$, $c=15.776(2)$ Å $\beta=92.39(1)°$	$a=13.059(8)$, $b=10.060(5)$, $c=15.920(7)$ Å $\beta=92.56(4)°$
Space group [15a]	$C2/c$ (No. 15)	$C2/c$ (No. 15)
Z	4	4
D_c	1.24 g cm^{-3}	1.48 g cm^{-3}
μ(Mo$K\alpha$)	13.8 cm^{-1}	51.3 cm^{-1}
Habit	Colourless rhombic plates	Colourless rhombic plates
Crystal size	0.18 × 0.26 × 0.04 mm	0.11 × 0.20 × 0.08 mm
Temperature	168 K	168 K
$2\theta_{max}$	50°	50°
Scan mode; 2θ scan rate	$\omega-2\theta$; 2.5 – 12.0° min^{-1}	$\omega-2\theta$; 2.5 – 12.0° min^{-1}
No. of independent reflections measured	1771	1851
No. of observed independent reflections $[I>3\sigma(I)]$	1094	1291
No. of parameters refined	147	147
Weighting scheme [16]	$w=(30.0+F_o+0.010\,F_o^2)^{-1}$	$w=(36.0+F_o+0.007\,F_o^2)^{-1}$
Final R (observed reflections)	0.038	0.033
Final R (observed + unobserved reflections)	0.072	0.058

density maps [13] and the atomic coordinates were used as the starting point also for the refinement of $[N(C_4H_9)_4][CuCl_2]$. Block-diagonal least-squares refinement [13] of positional, isotropic and then anisotropic thermal parameters for the non-hydrogen atoms yielded $R=0.064$ for $[N(C_4H_9)_4][CuCl_2]$ and $R=0.049$ for $[N(C_4H_9)_4][CuBr_2]$. The hydrogen atoms were located from difference maps and included in the refinement with isotropic temperature factors set equal to the equivalent isotropic values [14] of the carrying carbon atoms. Full-matrix least-squares refinement of 147 parameters terminated in $R=0.038$ for $[N(C_4H_9)_4][CuCl_2]$ (1094 reflections) and $R=0.033$ for $[N(C_4H_9)_4][CuBr_2]$ (1291 reflections). Atomic scattering factors were taken from the *International Tables for X-Ray Crystallography* [15b] and F_o values were weighted [16] as indicated in Table 1. Final difference maps showed a maximum electron density of 0.26 e Å^{-3} for $[(C_4H_9)_4][CuCl_2]$ and 0.40 e Å^{-3} for $[N(C_4H_9)_4][CuBr_2]$. Atomic coordinates and thermal parameters are listed in Tables 2 and 3. Structure factors are available from the authors on request.

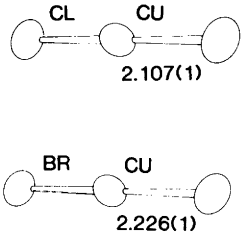

Fig. 1. The dichlorocuprate(I) and dibromocuprate(I) ions. [18]

DISCUSSION

In tetrabutylammonium dichlorocuprate(I) and tetrabutylammonium dibromocuprate(I) the anions are linear with copper(I) at a centre of symmetry. The Cu – Cl bond length (Fig. 1) appears to be

Table 2. Fractional coordinates and thermal parameters, $U_{ij} \times 10^3$ or B (Å^2), for $[N(C_4H_9)_4][CuCl_2]$. For the non-hydrogen atoms the anisotropic temperature factor has the form $\exp[-2\pi^2(U_{11}a^{*2}h^2 + \cdots + U_{23}b^*c^*kl)]$. For the hydrogen atoms $B = B_{eq}$ of the carrying carbon atom where B_{eq} is defined as $B_{eq} = (8\pi^2/3)(U_{11}a^{*2}a^2 + \cdots + U_{23}b^*c^*bc \cos\alpha)$. Estimated standard deviations are given in parentheses.

Atom	x	y	z	U_{11}	U_{22}	U_{33}	U_{12}	U_{13}	U_{23}
Cu	0.2500	0.2500	0.5000	46.5(4)	51.7(5)	37.4(4)	−18.5(9)	11.7(6)	−14.4(8)
Cl	0.2660(1)	0.0710(1)	0.5725(1)	75.8(9)	52.3(8)	51.0(7)	22.8(13)	8.3(12)	4.4(12)
N	0.0000	0.1524(4)	0.2500	27(2)	21(2)	29(2)	0	9(3)	0
C(1)	0.0930(3)	0.0592(4)	0.2653(3)	28(2)	29(2)	33(2)	6(3)	1(3)	−4(3)
C(2)	0.1959(3)	0.1318(4)	0.2702(2)	26(2)	35(2)	37(2)	6(3)	7(3)	−5(4)
C(3)	0.2792(3)	0.0386(5)	0.3071(3)	29(2)	39(3)	45(2)	6(4)	−9(4)	−4(4)
C(4)	0.3827(3)	0.1084(6)	0.3125(4)	31(2)	50(3)	65(3)	1(4)	0(4)	3(5)
C(5)	0.0139(3)	0.2451(4)	0.1738(2)	29(2)	23(2)	29(2)	0(4)	3(3)	5(4)
C(6)	0.0293(4)	0.1753(4)	0.0901(2)	38(2)	35(2)	33(2)	7(4)	4(3)	4(4)
C(7)	0.0637(4)	0.2802(5)	0.0255(3)	56(3)	43(3)	32(2)	−9(4)	22(4)	−1(4)
C(8)	0.0875(5)	0.2146(6)	−0.0590(3)	68(3)	64(4)	35(2)	19(6)	18(5)	7(4)

Atom	x	y	z	B	Atom	x	y	z	B
H(11)	0.084(4)	0.012(6)	0.320(3)	2.4	H(51)	−0.043(4)	0.309(5)	0.171(3)	2.1
H(12)	0.091(4)	−0.011(6)	0.223(3)	2.4	H(52)	0.071(4)	0.305(5)	0.191(3)	2.1
H(21)	0.220(4)	0.168(6)	0.210(3)	2.6	H(61)	0.077(4)	0.107(6)	0.097(3)	2.8
H(22)	0.196(4)	0.211(6)	0.305(3)	2.6	H(62)	−0.030(4)	0.133(6)	0.070(3)	2.8
H(31)	0.275(4)	−0.052(6)	0.279(3)	3.0	H(71)	0.013(4)	0.356(6)	0.013(3)	3.4
H(32)	0.267(4)	0.009(6)	0.368(4)	3.0	H(72)	0.123(5)	0.334(6)	0.051(3)	3.4
H(41)	0.380(5)	0.194(7)	0.336(4)	3.9	H(81)	0.031(5)	0.169(7)	−0.083(4)	4.4
H(42)	0.440(5)	0.045(6)	0.344(4)	3.9	H(82)	0.141(5)	0.144(7)	−0.051(4)	4.4
H(43)	0.391(5)	0.125(6)	0.254(4)	3.9	H(83)	0.109(5)	0.284(7)	−0.096(4)	4.4

Table 3. Fractional coordinates and thermal parameters, $U_{ij} \times 10^3$ or B (Å^2), for $[N(C_4H_9)_4][CuBr_2]$. For the non-hydrogen atoms the anisotropic temperature factor has the form $\exp[-2\pi^2(U_{11}a^{*2}h^2 + \cdots + U_{23}b^*c^*kl)]$. For the hydrogen atoms $B = B_{eq}$ of the carrying carbon atom where B_{eq} is defined as $B_{eq} = \frac{8\pi^2}{3}(U_{11}a^{*2}a^2 + \ldots + U_{23}b^*c^*bc \cos\alpha)$. Estimated standard deviations are given in parentheses.

Atom	x	y	z	U_{11}	U_{22}	U_{33}	U_{12}	U_{13}	U_{23}
Cu	0.2500	0.2500	0.5000	48.0(5)	50.9(5)	34.6(4)	−19.8(9)	6.2(7)	−8.5(8)
Br	0.27181(4)	0.06186(6)	0.57223(3)	66.5(4)	53.0(3)	46.5(3)	23.0(6)	4.4(5)	2.4(5)
N	0.0000	0.1477(5)	0.2500	26(2)	23(2)	27(2)	0	0(4)	0
C(1)	0.0923(3)	0.0586(4)	0.2653(3)	31(2)	29(2)	33(2)	2(4)	−6(4)	1(4)
C(2)	0.1956(3)	0.1271(5)	0.2722(3)	27(2)	43(3)	37(2)	7(4)	0(4)	−3(4)
C(3)	0.2778(4)	0.0347(5)	0.3095(3)	31(2)	44(3)	43(3)	5(4)	−6(4)	−11(4)
C(4)	0.3825(4)	0.1004(7)	0.3142(4)	29(2)	62(4)	75(4)	8(5)	−3(5)	−7(6)
C(5)	0.0147(3)	0.2400(4)	0.1750(2)	33(2)	25(2)	31(2)	0(4)	2(3)	8(3)
C(6)	0.0267(4)	0.1704(5)	0.0905(3)	41(3)	36(2)	31(2)	−9(4)	2(4)	6(4)
C(7)	0.0624(4)	0.2708(5)	0.0276(3)	53(3)	43(3)	36(3)	−6(5)	13(4)	7(4)
C(8)	0.0787(5)	0.2076(6)	−0.0571(3)	68(4)	55(3)	35(3)	13(6)	9(5)	7(5)

Atom	x	y	z	B	Atom	x	y	z	B
H11	0.081(4)	0.008(6)	0.313(4)	2.4	H(51)	−0.042(5)	0.302(6)	0.171(3)	2.3
H(12)	0.093(4)	−0.006(6)	0.218(4)	2.4	H(52)	0.072(5)	0.302(6)	0.189(3)	2.3
H(21)	0.218(5)	0.161(6)	0.215(4)	2.8	H(61)	0.070(5)	0.100(7)	0.099(4)	2.8
H(22)	0.189(5)	0.201(6)	0.307(4)	2.8	H(62)	−0.035(5)	0.124(6)	0.075(4)	2.8
H(31)	0.282(5)	−0.041(7)	0.282(4)	3.1	H(71)	0.023(5)	0.339(7)	0.020(4)	3.5
H(32)	0.263(5)	0.002(7)	0.362(4)	3.1	H(72)	0.115(5)	0.307(7)	0.047(4)	3.5
H(41)	0.380(6)	0.193(8)	0.340(5)	4.4	H(81)	0.020(6)	0.157(8)	−0.080(4)	4.2
H(42)	0.435(6)	0.036(7)	0.342(4)	4.4	H(82)	0.131(5)	0.135(8)	−0.048(4)	4.2
H(43)	0.391(6)	0.104(8)	0.266(5)	4.4	H(83)	0.099(5)	0.275(7)	−0.102(4)	4.2

Table 4. Bond lengths (Å) within the tetrabutylammonium ions in tetrabutylammonium dichlorocuprate(I) and tetrabutylammonium dibromocuprate(I). Estimated standard deviations in parentheses.

	$[N(C_4H_9)_4][CuCl_2]$	$[N(C_4H_9)_4][CuBr_2]$
N–C(1)	1.533(5)	1.514(5)
C(1)–C(2)	1.521(5)	1.514(6)
C(2)–C(3)	1.519(6)	1.521(7)
C(3)–C(4)	1.515(6)	1.517(7)
N–C(5)	1.526(4)	1.531(5)
C(5)–C(6)	1.510(5)	1.530(6)
C(6)–C(7)	1.531(6)	1.511(7)
C(7)–C(8)	1.526(7)	1.514(7)
C(1)–H(11)	0.99(5)	0.93(6)
C(1)–H(12)	0.96(5)	0.99(6)
C(2)–H(21)	1.08(5)	1.02(6)
C(2)–H(22)	0.95(6)	0.94(6)
C(3)–H(31)	1.00(6)	0.88(7)
C(3)–H(32)	1.03(6)	0.92(7)
C(4)–H(41)	0.92(7)	1.02(8)
C(4)–H(42)	1.08(6)	1.02(7)
C(4)–H(43)	0.96(6)	0.79(8)
C(5)–H(51)	0.98(5)	0.96(6)
C(5)–H(52)	0.98(5)	1.00(6)
C(6)–H(61)	0.92(6)	0.91(7)
C(6)–H(62)	0.92(6)	0.96(6)
C(7)–H(71)	1.02(6)	0.86(7)
C(7)–H(72)	1.01(6)	0.82(7)
C(8)–H(81)	0.93(7)	0.99(7)
C(8)–H(82)	0.99(7)	1.01(8)
C(8)–H(83)	0.95(7)	1.03(7)

slightly longer than values reported for $[CuCl_2]^-$ at room temperature[1-6] but is in close agreement with that in $[N_6P_6(N(CH_3)_2)_{12}CuCl][CuCl_2]$ after correction for thermal libration, *i.e.* 2.11(1) Å.[2]

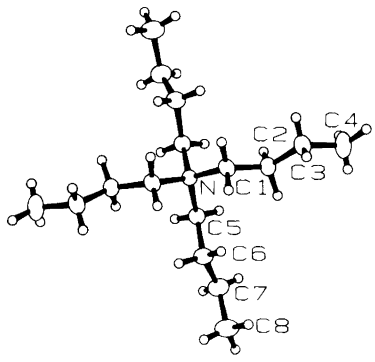

Fig. 2. The tetrabutylammonium ion in $[N(C_4H_9)_4][CuBr_2]$ showing the atomic numbering.[18] The thermal ellipsoids of the non-hydrogen atoms are drawn at the 50 % probability level and hydrogen atoms are represented as spheres of radius 0.1 Å.

We believe that this is the first determination of Cu–Br in a discrete $[CuBr_2]^-$ ion. As expected, the distance, 2.226(1) Å, is shorter than both $Cu-Br_{terminal}$ and $Cu-Br_{bridging}$ in $[Cu_2Br_4]^{2-}$, *i.e.* 2.328(2), and 2.490(2) and 2.472(3) Å, respectively, in which copper(I) is essentially three-coordinated with two longer Cu–S contacts completing a trigonal bipyramid.[8] In $[Cu(NH_3)_4][CuBr_2]_2$ which the anions form infinite chains of edge-sharing Cu(I)–Br tetrahedra the Cu–Br distance is 2.503(4) Å.[17]

Which factors are decisive for the attainment of discrete linear $[CuX_2]^-$ ions *contra* a dimeric or polymeric configuration seem as yet to be uncertain. It has been suggested[1b] that stabilization of monomeric $[CuCl_2]^-$ may be due to the presence of large bulky cations. The structures of the anions in the series $[N(C_4H_9)_4][CuX_2]$, X = Cl, Br, I, might thus suggest an increased tendency to polymerization from X=Cl to X=I counterbalanced by stabilization of a monomeric configuration by

Table 5. Interatomic angles (°) within the tetrabutylammonium ions in tetrabutylammonium dichlorocuprate(I) and tetrabutylammonium dibromocuprate(I). Estimated standard deviations in parentheses. Symmetry code: (i) $-x, y, \frac{1}{2}-z$.

	$[N(C_4H_9)_4][CuCl_2]$	$[N(C_4H_9)_4][CuBr_2]$
C(1)–N–C(1^i)	106.5(4)	107.3(4)
C(1)–N–C(5)	111.3(2)	111.0(2)
C(1)–N–C(5^i)	110.7(2)	111.1(2)
C(5)–N–C(5^i)	106.5(4)	105.4(4)
N–C(1)–C(2)	114.8(3)	116.2(4)
C(1)–C(2)–C(3)	110.6(3)	111.1(4)
C(2)–C(3)–C(4)	111.7(4)	111.8(4)
N–C(5)–C(6)	116.2(3)	115.4(4)
C(5)–C(6)–C(7)	109.2(4)	108.9(4)
C(6)–C(7)–C(8)	111.8(4)	111.6(4)

tetrabutylammonium ions. The far infrared spectrum of tetraethylammonium dibromocuprate(I) has been interpreted in terms of a polymeric structure for the anion,[9] which would also support the hypothesis that a cation the size of $[N(C_4H_9)_4]^+$ is a prequisite for suppression of polymerization.

Bond distances and angles within the tetrabutylammonium ion in the two compounds are given in Tables 4 and 5, the atomic numbering being in accordance with Fig. 2. A stereoscopic view[18] of the unit cell is shown in Fig. 3. The cation has the usual staggered conformation and there are no abnormal bond distances or angles. Nor do any of the carbon atoms have large thermal parameters as was the case in bis(tetrabutylammonium)di-μ-iodo-diiododicuprate(I).[7] The closest non-bonded approach distances between carbon and copper(I) are C(3)···Cu = 3.720(4) Å in $[N(C_4H_9)_4][CuCl_2]$ and C(3)···Cu = 3.757(5) Å in $[N(C_4H_9)_4][CuBr_2]$. The shortest distances between carbon and halogen are C(2)...Cl = 3.846(4) Å and C(2)···Br = 3.876(5) Å.

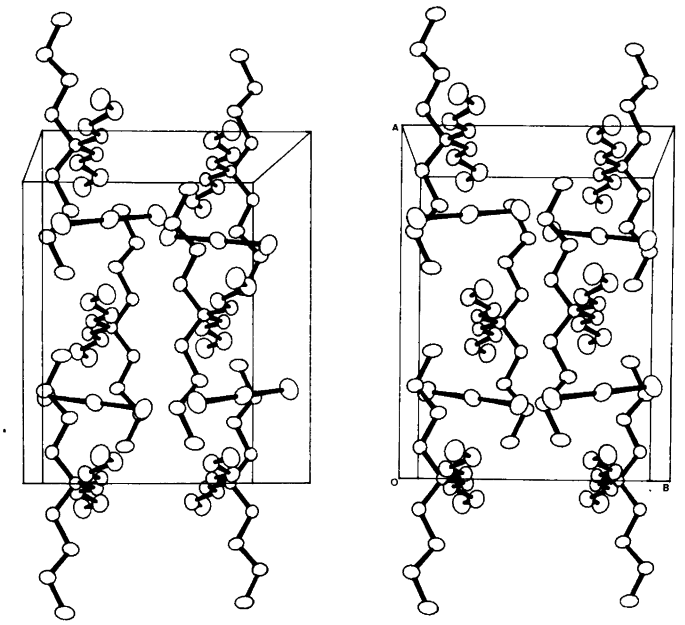

Fig. 3. Stereoscopic view of the unit cell of $[N(C_4H_9)_4][CuBr_2]$.

Acknowledgements. Financial support from the Swedish Natural Science Research Council (NFR) and the National Swedish Board for Technical Development (STU) is gratefully acknowledged.

REFERENCES

1. a. Newton, M. G., Caughman, H. D. and Taylor, R. C. *Chem. Commun.* (1970) 1227; b. *J. Chem. Soc. Dalton Trans.* (1974) 258.
2. Marsh, W. C. and Trotter, J. *J. Chem. Soc. A* (1971) 1482.
3. Kaiser, J., Brauer, G., Schröder, F. A., Taylor, I. F. and Rasmussen, S. E. *J. Chem. Soc. Dalton Trans.* (1974) 1490.
4. Siiman, O., Huber, C. P. and Post, M. L. *Inorg. Chim. Acta 25* (1977) L11.
5. Huber, C. P., Post, M. L. and Siiman, O. *Acta Crystallogr. B 34* (1978) 2629.
6. Francisco, R. H. P., de Almeida Santos, R. H., Lechat, J. R. and Massabni, A. C. *Acta Crystallogr. B 37* (1981) 232.
7. Asplund, M., Jagner, S. and Nilsson, M. *Acta Chem. Scand. A 36* (1982) 751.
8. Shibaeva, R. P. and Kaminskii, V. F. *Kristallografiya 26* (1981) 332.
9. Bowmaker, G. A., Brockliss, L. D. and Whiting, R. *Aust. J. Chem. 26* (1973) 29.
10. Nilsson, M. *Acta Chem. Scand. B 36* (1982) 125.
11. Lehmann, M. S. and Larsen, F. K. *Acta Crystallogr. A 30* (1974) 580.
12. Lindqvist, O. and Ljungström, E. *J. Appl. Crystallogr. 12* (1979) 134.
13. Lindgren, O. *An Integrated Set of Crystallographic Programs.* In *On the Oxygen Coordination of Cerium in Some Sulfates and Chromates*, Thesis, Department of Inorganic Chemistry, Chalmers University of Technology and University of Göteborg, Göteborg 1977.
14. Hamilton, W. C. *Acta Crystallogr. 12* (1959) 609.
15. a. *International Tables for X-Ray Crystallography*, Kynoch Press, Birmingham 1952, Vol. I, p. 101; b. *Ibid.* 1974, Vol. IV, p. 72.
16. Cruickshank, D. W. J. *Crystallographic Computing*, Munksgaard, Copenhagen 1970, p. 195.
17. Baglio, J. A. and Vaughan, P. A. *J. Inorg. Nucl. Chem. 32* (1970) 803.
18. Johnson, C. K. *ORTEP*, Report ORNL-3794. Oak Ridge National Laboratory, Oak Ridge 1965.

Received May 13, 1982.

Acta Chemica Scandinavica A 37 (1983) 63 – 69

Kinetics of Rust Formation. A Small Angle Neutron Scattering Investigation on Iron(III) Hydroxide

A. NØRLUND CHRISTENSEN,[a] M. S. LEHMANN[b] and A. WRIGHT[b]

[a] Department of Inorganic Chemistry, University of Aarhus, DK-8000 Aarhus C, Denmark and
[b] Institut Max von Laue – Paul Langevin, B. P. 156, F-38042 Grenoble Cedex, France

The aging of amorphous iron(III) hydroxide to α-Fe_2O_3 and α-FeOOH was studied by small angle neutron scattering techniques. The main parameters in determining the growth rate were pH of the solution, time and temperature of aging. The particles have a polydisperse size distribution which changes with time. The scattering density of the particles increases with time and each particle of the amorphous product produces a particle of α-Fe_2O_3 in acid solution. There is no indication of a process where the particles dissolve and reprecipitate.

The hydrolysis of iron(III) solutions with ammonia or sodium hydroxide solutions develops with the formation of the dimer complex $[(H_2O)_4Fe(OH)_2Fe(H_2O)_4]^{4+}$ followed by a series of polynuclear complexes.[1-5] When these complexes are sufficiently large in size, coagulation takes place and an amorphous gel-like precipitate of iron(III) hydroxide is formed. Aging of these precipitates at room temperature, at elevated temperatures, or under hydrothermal conditions results in the formation of crystalline products. In acid solutions hematite, α-Fe_2O_3, or possibly hydrohematite, is obtained from amorphous iron(III) hydroxide gels made from iron(III) nitrate solutions and ammonia or sodium hydroxide.[6,7] The rate of crystallization is increased by increasing temperature[6] or by the presence of oxalate in the gels.[7] However, the formation of the iron oxide hydroxides, α-FeOOH, γ-FeOOH and β-FeOOH has been reported from acid media containing nitrate, perchlorate and chloride ions, respectively.[7] Apparently, a number of factors including the presence and concentration of complex forming anions modifies the crystallization rate of amorphous iron(III) hydroxide gels and the structure and composition of the crystalline products obtained.

In alkaline media iron(III) hydroxide gels are aged to goethite, α-FeOOH,[8] and under hydrothermal conditions α-Fe_2O_3 and α-FeOOH may be formed.[6] The formation of hematite rather than goethite is observed in the presence of hydroxicarboxylic acids,[9] or small concentrations of Al^{3+} ions.[10] Traces of aluminium eliminate the formation of goethite and favour the formation of hydrohematite when amorphous iron(III) hydroxide is treated hydrothermally.[11,12]

In contrast to the hydrolysis of aluminium(III) solutions where a polynuclear complex $Al_{13}O_4(OH)_{24}(H_2O)_{12}^{7+}$ is formed,[13] little is known about the nature of the polynuclear complexes and the particles formed in the hydrolysis of iron(III) solutions with respect to the sizes of the complexes and particles, or the growth rate of these species at different temperatures. To study this, it was decided to investigate the aging of iron(III) hydroxide gels obtained by hydrolysis using small angle neutron scattering.

The rate of hydrothermal crystallization of amorphous iron(III) hydroxide recently studied by on-line neutron powder diffraction showed that crystallization was complete within a few hours.[6] An investigation of the growth rate of the particles in the early stages of the crystallization of amorphous iron(III) hydroxides by on-line small angle neutron scattering experiments would thus be possible within an acceptable time period. To our knowledge, this on-line technique for small angle neutron scattering has not been used previously.

0302-4377/83 $2.50

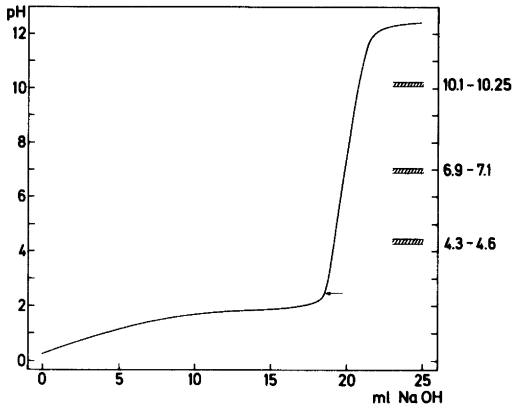

Fig. 1. Titration curve of a 20 ml 1.5185 M iron(III) nitrate solution with 4.45 M NaOH. The arrow indicates where the heavy precipitate of iron(III) hydroxide is formed.

EXPERIMENTAL

Hydrolysis of iron(III) nitrate solutions. Solutions of iron(III) nitrate were made from $Fe(NO_3)_3.9H_2O$ (Merck *p.a.*), and solutions of sodium hydroxide were made from NaOH (Merck *p.a.*). A preliminary investigation of the hydrolysis of a 1.518 M iron(III) nitrate solution was made by titration with a solution of 4.45 M sodium hydroxide. The titration was made with a Radiometer REA 160 Titrigraph unit and pH of the solution was measured with a Radiometer PHM 64 pH-meter. Fig. 1 shows the

Table 1. Suspensions of iron(III) hydroxide in mother liquid (H_2O) kept at 20 °C. 1.5 M iron(III) nitrate solution precipitated with 4.5 M sodium hydroxide.

pH of mother liquid precipitation	after diffraction exp.	Age of the precipitate in days
6.91	7.44	40
7.04	6.56	4
10.25	12.64	40
10.13	10.20	36
10.15	9.96	32
10.20	9.97	28
10.22	10.00	24
10.10	9.71	20
10.21	10.22	16
10.15	9.64	12
10.10	9.58	8
10.10	9.84	4

Table 2. Suspensions of iron(III) hydroxide in mother liquid (H_2O) heat treated. 1.5 M iron(III) nitrate solution precipitated with 4.5 M sodium hydroxide to pH = 4.31.[a]

Heat treatment of sample Temp. °C	Time, min	pH of mother liquid after heat treatment
113	20	3.14
	40	2.75
	60	2.46
	80	2.39
	100	2.30
	120	2.24
107	20	3.20
	40	2.88
	60	2.58
	80	2.43
	100	2.35
	120	2.28
102	80	2.50
	160	2.29
	240	2.16
	320	2.03
	400	1.96
	480	1.92
	Time, h	
90	4	2.51
	8	2.34
	12	2.22
	16	2.16
	20	2.08
	24	2.02
94	1	
	3	
	5	
	7	
	9	
	11	
	13	
	14	
	16	
	18	
	20	
	22	

[a] Sample for kinetic scattering experiment (Fig. 10): 1.5 M iron(III) nitrate solution precipitated with 4.5 M sodium hydroxide pH = 11.45. The sample was used in an on-line diffraction experiment with the sample kept at 50 °C.

titration curve. In the first part of the titration the pH of the solution changes slowly with the volume of NaOH. When approximately 2.7 mmol OH^- per 1 mmol Fe^{3+} has been added the solution becomes suddenly very thick by a coagulation of the polynuclear complexes formed during the titration and the characteristic rust brown precipitate of iron(III) hydroxide is observed. Further addition of NaOH yields a relatively fast increase of pH of the suspension.

Preparation of iron(III) hydroxide samples for small angle neutron scattering experiments. Iron(III) hydroxide was precipitated by adding the sodium hydroxide solution dropwise to the iron(III) nitrate solution. During the precipitation the solution was stirred and pH was measured with a Radiometer PHM 64 Research pH-meter. The precipitations were interrupted at the pH values indicated in Fig. 1. Samples (15 ml) of the suspensions of the precipitated iron(III) hydroxide in the mother liquid were transferred to pyrex ampouls. These were sealed with rubber stoppers and kept at room temperature for the periods of time listed in Table 1, or were kept at higher temperatures in a thermostated oven at the experimental conditions listed in Table 2. After the diffraction experiments the pH of some of the suspensions were measured again.

Suspension of iron(III) hydroxide in the mother liquid are aged when kept for long periods of time at room temperature. This process may be observed as a change in pH of the solution. Fig. 2 shows the variation of pH with time for two series of iron(III) hydroxide precipitated to pH 6.9 – 7.1 and to pH 10.1 – 10.25, respectively. Both series show a drop in pH with time and for the precipitate with the initial pH 10.1 – 10.25 a clear change in colour is observed after approximately 30 days due to the formation of α-FeOOH. For the other series no colour change was observed. Precipitates of iron(III)

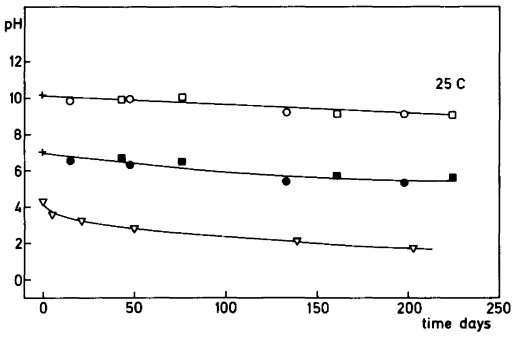

Fig. 2. Precipitate of iron(III) hydroxides aged at room temperature. pH of the solutions are decreasing with time.

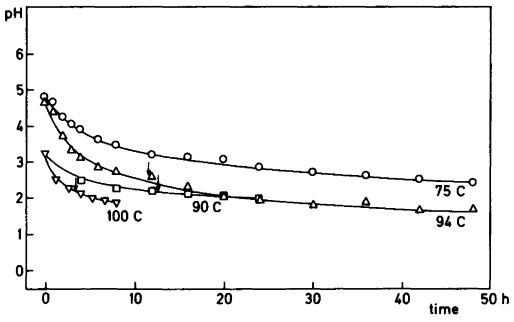

Fig. 3. Precipitates of iron(III) hydroxides aged by heat treatments. pH of the solutions are decreasing with time and with the temperature of the heat treatments. The arrows indicate where colour changes of the precipitates are observed.

hydroxide with an initial pH value of 4.3 show an even more drastic change in pH with time (Fig. 2). When precipitates of iron(III) hydroxide (pH = 3.3 and 4.8) are treated hydrothermally the aging is accelerated and crystalline products of hematite may be formed. The pH of the mother liquids measured after the hydrothermal treatments are displayed *vs.* time of treatment in Fig. 3 and show the same tendency as Fig. 2.

Small angle neutron scattering of iron(III) hydroxide specimens. The measurements were carried out on the neutron small angle diffractometer D11 of the Institut Max von Laue – Paul Langevin, Grenoble. The instrument is located at a neutron guide connected to the cold source, and the wave length was in the range from 10 to 16 Å. The detector consists of 64 × 64 elements of 1 cm^2, and was located either at 10 m or at 20 m from the sample. This gives typical maximum momentum transfer of $Q = 1.2 \times 10^{-2}$ to 1.5×10^{-2} $Å^{-1}$ ($Q = 4\pi \sin \theta/\lambda$). The samples were contained in quartz cuvettes of 1 mm path length and the cuvettes were mounted in a thermostated rack so that temperatures up to 100 °C could be obtained during the experiment. The size of the beam was between 0.5 and 1 cm^2.

The samples were either prepared beforehand for the long time treatment and measured at ambient temperature, or measured at reaction temperature for some of the fast reactions. In both cases the results are similar. The isotropic scattering curves were obtained by radial averaging over the detector surface, and in order to correct for background, a water spectrum was subtracted. Likewise, the detector response function was obtained using a water spectrum. This was done using standard ILL programs.[14]

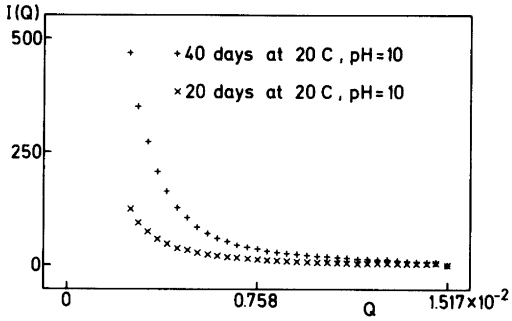

Fig. 4. $I(Q)$ *vs.* Q for two specimens of iron(III) hydroxide aged at room temperature in suspensions with pH = 10.

It was clear from the scattering curves that the particles belonged to a polydisperse size distribution (Fig. 4 and 5), and a simple model was therefore used. The basic equation for the calculation is

$$I(Q) \approx P(Q)S(Q)$$

where $I(Q)$ is the intensity scattered for momentum transfer Q, $P(Q)$ is the single particle form factor and $S(Q)$ is the inter-particle scattering function. Polydispersity is taken care of in $P(Q)$ which will be a sum, $\sum_i Pi(Q)$, of the form factors for the different particles. Polydispersity introduces a broadening in the interparticle correlation function and hence cross terms between $Pi(Q)$ and $S(Q)$, but these were neglected in the model. The particles are described as hard, uniform spheres with a size distribution according to a Gaussian distribution. The interaction between spheres were taken into account using the Percus-Yevick [15] approximation. A least-squares fit was done employing the program SMALL,[16] and the parameters varied were the mean radius of gyration of the particle, the standard deviation of the distribution (σ), the volume fraction occupied by the particles (evf), and the scale factors. This last value gives the forward scattering $I(Q_o)$ and is proportional to the square of the integrated scattering density of the mean particle in excess of the scattering density of the solution.[17] In the present case, the solution is water, for which the neutron scattering density is nearly zero. The particle itself, consisting of iron hydroxides and bound water, has scattering density above zero, consisting of Fe and O with positive scattering lengths and H with negative scattering lengths. Moreover, as H (and H_2O) are ejected from the particle its scattering density will increase corresponding to an increase of $I(Q)$ which is discussed below.

The fits were good for the start and end products, i.e. for samples which are generally rather stable in time. One example of the quality of the fitting is given in Fig. 6. However, the agreement was less good, although acceptable, in the medium range, indicating some breakdown in the model. It was moreover found that the mean particle size was sensitive to the cutoff at low Q, so that the lower the cutoff the larger the particle. This is what would be expected where some of the particles are too large to give scattering within the geometry of the experimental set up. Typical particle sizes were in the range from 700 to 1000 Å, so in the analysis this limits the range of the particles that were seen.

A series of measurements was also done to study the kinetics of particle formation using hydrolysis of urea for pH control. Mixtures of Fe(III) nitrate and urea were heated to temperatures between 90 and 100 °C, and the scattering curves were recorded for constant intervals of time, typically 15 min. At these temperatures urea disintegrates into ammonia and carbon dioxide, and one can thus follow the formation of the polynuclear units from the dimer complex. No information could be obtained about

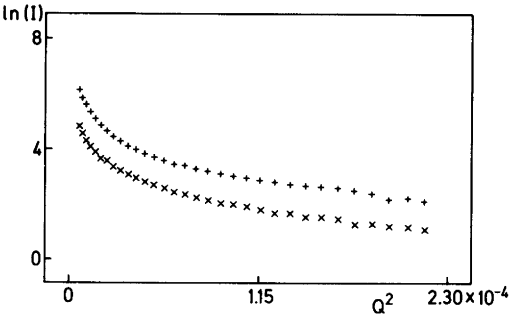

Fig. 5. $\ln(I)$ *vs.* Q^2 (Guinier plot) for the same specimens as shown in Fig. 4.

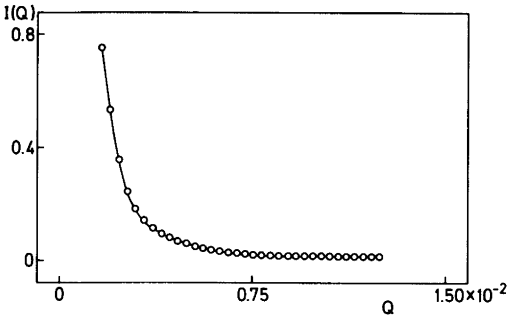

Fig. 6. Least-squares fit of data $I(Q)$ *vs.* Q to the model of a specimen (94 °C, 3 h, Table 2), showing a good fit of the scattering data to the model.

the size of the intermediate particles as the change from the dimer to the large particle was too rapid for the time scale of the measurement.

RESULTS AND DISCUSSIONS

The specimens listed in Table 1 were measured with a sample-detector distance of 10 m. For the two specimens where pH of the mother liquid was approximately 7 the two scattering profiles I(Q) *vs.* Q were identical. The composition and size of the particles in these two specimens have thus not changed with time, and suspensions of amorphous iron(III) hydroxide in solutions with pH = 7 show no great tendency to produce crystalline products when kept at room temperature. In contrast to this, crystalline α-Fe-OOH is obtained from amorphous iron(III) hydroxide when kept at room temperature in solutions with pH = 10. At the time of the diffraction experiment a substantial fraction of the 40 days old specimen (Table 1) was converted to α-FeOOH, which was observed as a change in colour of the specimen. For this series of samples the scattering profiles $I(Q)$ *vs.* Q changes with the age of the samples. Fig. 4 displays $I(Q)$ *vs.* Q for two samples aged for 20 and 40 days, respectively. An interesting feature of the curves is the large increase of $I(Q)$ with time.

$I(Q)$ at zero angle of scattering $I(Q_o)$ is dependent on the number of particles in the specimen, on their size and atomic composition. The most likely process in the early stages of the aging is an expulsion of hydrogen ions from the particles, and as hydrogen has a scattering length of $b = -0.37\ 10^{-12}$ cm, $I(Q_o)$ will increase. Fig. 5 displays a Guinier plot, ln(I) *vs.* Q^2 for the same two specimens. It clearly shows the polydispersity of the specimens as the plots exhibit no linearity for low value of Q^2, and a single radius of gyration can thus not be found from the curves. However, the measurements (Fig. 6) may be fitted a curve describing a model for a polydisperse system from which the parameters $I(Q_o)$, effective volume fraction of the particles (evf), and a parameter (σ) for the particle distribution function may be found.[16] Fig. 7 displays the results obtained for the samples listed in Table 1. As mentioned previously, $I(Q_o)$ increases with time. The effective volume fraction decreases with time and σ goes through a minimum indicating that the particle size distribution changes with time. When the fraction of α-FeOOH in the specimen starts to be of significant magnitude, the values of σ increase gain.

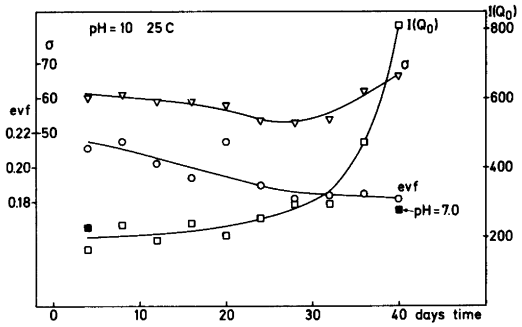

Fig. 7. $I(Q_o)$ effective volume fraction (evf) and σ for specimens with pH = 10 listed in Table 1.

The heat treatment of the iron(III) hydroxide specimens has an accelerating effect on the aging for the specimens precipitated to pH = 4.31 and heated to 90, 102, 107, and 113 °C, respectively (Table 2). This is observed as drop in pH which appears earlier for specimens treated at higher temperatures than for specimens heated at lower temperatures. The scattering profiles for all these specimens were recorded, and the values for $I(Q_o)$, evf, and σ were determined as described above. Fig. 8 displays the values obtained for the specimens which were heated to 90 and 102 °C, respectively. The characteristic feature is again an increase of $I(Q_o)$ with time, and that this increase comes much faster for the specimens treated at 102 °C than for those treated at 90 °C. In contrast to the results displayed in Fig. 7 where σ goes through a minimum and where the crystalline product obtained is α-FeOOH, the results displayed in Fig. 8 show only a decrease in σ for the two series of specimens. In this case the crystalline product is α-Fe_2O_3. It is also interesting to note that the effective volume fraction goes through a maximum in Fig. 8 and that this maximum appears when $I(Q_o)$ starts to increase significantly, and that a corresponding feature is not observed in Fig. 7.

The model used for describing the data is indeed very simple, giving as main information the scattering at zero angle $I(Q_o)$ with a simple interpretation. The explanation of the behaviour of the evf is less obvious. It is, however, to be expected that at the stage of aging when α-Fe_2O_3 is crystallized, water is expelled and the volume fraction decreases. This is observed when $I(Q_o)$ increases which coincides with the moment where a significant change in

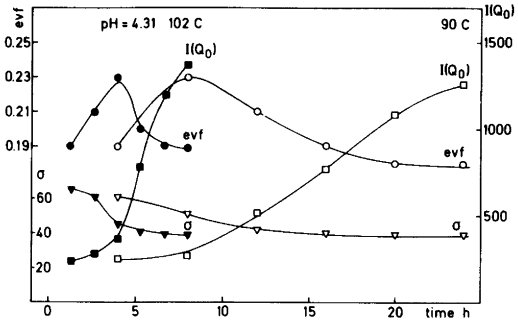

Fig. 8. $I(Q_o)$, evf, and σ for specimens aged at 90 °C (open symbols) and at 102 °C (filled symbols).

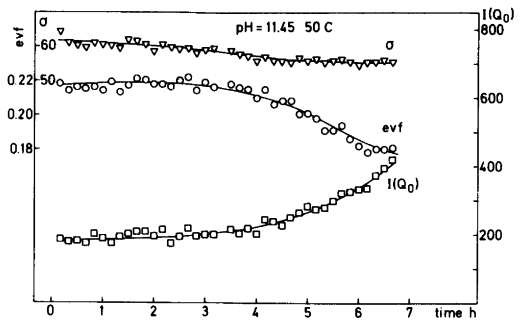

Fig. 10. $I(Q_o)$ evf and σ for on-line diffraction experiment with iron(III) hydroxide specimens at pH = 11.45 kept at 50 °C.

colour of the specimens is observed, indicating the formation of α-Fe_2O_3. The mechanism in the convertion of the polynuclear complexes to crystalline α-Fe_2O_3 must be that each particle of the polynuclear complex produces a particle of α-Fe_2O_3. There is no indication of a process where the particles dissolve and reprecipitate. In this time interval where the convertion of the polynuclear complex to α-Fe_2O_3 is dominant, the greatest drop in the value of σ is observed. It is also in this interval that the model calculation gives the poorest fit with the data. The model may be improved by introducing a σ-value for the polynuclear complex and a σ-value for the product, α-Fe_2O_3.

Fig. 9 displays the values of $I(Q_o)$, evf, and σ for the specimens of iron(III) hydroxide precipitated to pH = 4.60 and heat treated as listed in Table 2. (These data were measured with a 20 m distance betwéen sample and detector.) The results agree well with those displayed in Fig. 8. The specimens used in this series of experiments were precipitated to a pH-value of 4.60. Due to this higher value of pH,

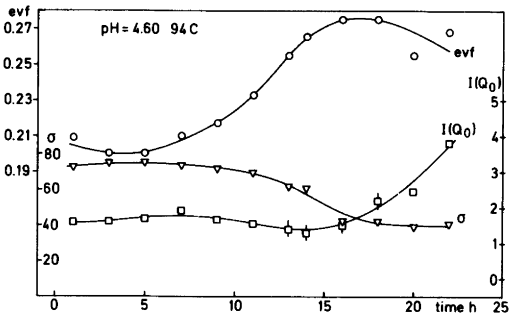

Fig. 9. $I(Q_o)$, evf and σ for specimens of iron(III) hydroxide with pH = 4.60 heated to 94 °C.

the crystallization starts at a much later time in this series of specimens heated to 94 °C than for the specimens with pH = 4.31 heated to 90 °C (Fig. 8). In addition to the temperature, pH of the gels thus plays an important role in the speed with which the aging of the iron(III) hydroxide gels proceeds.

In the on-line diffraction experiment, an iron(III) hydroxide sample with pH = 11.45 was housed in a cuvette kept at 50 °C and the neutron counts were collected every 10 min. For each measurement the $I(Q)$ *vs.* Q plots were fitted to the model described above and the results for $I(Q_o)$, evf and σ are are displayed in Fig. 10. As this experiment was made with a specimen of iron(III) hydroxide in an alcaline liquid the results of Fig. 10 may be compared with the results displayed in Fig. 7. The development in time of the three parameters show the same trend in the two sets of experiments. The on-line experiment was interrupted after 7 h. At that time the aging of the gel had advanced to a stage that roughly corresponds to that of a gel aged for 30 days at room temperature (Fig. 7).

In conclusion, it can be said that the speed of aging of amorphous iron(III) hydroxide gels may be studied by small angle neutron scattering and that it increases with temperature. For specimens in acid liquids the speed of aging increases with decreasing values of pH. For specimens with pH = 7, the speed of aging at room temperature is very low.

Acknowledgements. Mr. N. J. Hansen and Mr. O. Lillelund are acknowledged for valuable assistance in the preparation of the specimens. Dr. Haesslin and Dr. Oberthür are thanked for the loan of the sample heater. The Danish Natural Science Research Council is acknowledged for financial support.

REFERENCES

1. Biedermann, G. and Schindler, P. *Acta Chem. Scand 11* (1957) 731.
2. Vértes, A., Ranogajec-Komor, M. and Gelenczér, P. *Acta Chim. Acad. Sci. Hung. 77* (1973) 55.
3. Knight, R. J. and Sylva, R. N. *J. Inorg. Nucl. Chem. 36* (1974) 591.
4. Baes, C. F. and Mesmer, R. F. *The Hydrolysis of Cations*, Wiley, New York 1976.
5. Knudsen, J. M., Larsen, E., Moreira, J. E. and Nielsen, O. F. *Acta Chem. Scand. A 29* (1975) 833.
6. Christensen, A. N., Convert, P. and Lehmann, M. S. *Acta Chem. Scand. A 34* (1980) 771.
7. Fischer, W. R. and Schwetmann, U. *Clays Clay Miner. 23* (1975) 33.
8. Lahann, R. W. *Clays Clay Miner. 24* (1976) 320.
9. Cornell, R. M. and Schwetmann, U. *Clays Clay Miner. 27* (1979) 402.
10. Wolska, E. *Monatsh. Chem.* (1975) 905.
11. Wolska, E. *Monatsh. Chem.* (1977) 819.
12. Wolska, E. *Monatsh. Chem.* (1980) 889.
13. Johansson, G. *Acta Chem. Scand. 14* (1960) 771.
14. Ghosh, R. *A Computer Guide for Small-Angle Scattering Experiments*, ILL Report 78GH247T.
15. Egelstoff, P. A. *An Introduction to the Liquid State*, Academic, New York 1967, p. 56.
16. Harris, N. M. *Thesis*, ILL and St. John's College, Oxford 1980.
17. Jacrot, B. *Rep. Prog. Phys. 39* (1976) 911.

Received April 16, 1982.

Acta Chemica Scandinavica A 37 (1983) 71–77

Short Communications

The Crystal Structure of the (2:1) Complex between 1,4,7,10-Tetra-(2-hydroxyethyl)-1,4,7,10-tetraazacyclododecane and Lithium Chloride Dihydrate at −150 °C

P. GROTH

Department of Chemistry, University of Oslo, Oslo 3, Norway

The complexation properties of 1,4,7,10-tetra-(2-hydroxyethyl)-1,4,7,10-tetraazacyclododecane have been studied in various solvents by titration with dry salt, monitored by ^{13}C NMR spectroscopy.[1] The ^{13}C signal for the ring carbons was found to move only moderately upfield on complexation, suggesting a similar ring conformation in the hydrate and in the three cation complexes with Li^+, Na^+ and K^+. The signals for the side-chain NCH_2 carbons on the other hand, indicated conformational differences for the side-chains. In order to clarify these conformational differences, the hydrate and some cation complexes have been studied by single crystal X-ray diffraction methods. The results for the dihydrated (2:1) complex with lithium chloride are now presented.

The crystals are monoclinic with space group $P1_1/n$ and cell dimensions $a = 10.388(6)$, $b = 19.719(5)$, $c = 11.778(12)$ Å, $\beta = 91.00(5)°$. There are four formula units, $(C_{16}H_{36}O_4N_4)\cdot(LiCl)_2\cdot(H_2O)_2$, in the cell ($D_x = 1.29$ g cm^{-3}, $D_m = 1.22$ g cm^{-3}). 2387 observed reflections were recorded on an automatic four-circle diffractometer at *ca.* −150 °C ($2\theta_{max} = 50°$, Mo$K\alpha$-radiation, ω-scan). The crystal size was $0.3 \times 0.3 \times 0.1$ mm, and no corrections for absorption on secondary extinction were made.

The structure was solved by direct methods [2] and refined by full-matrix least-squares technique.[3,*] Weights in least squares were obtained from the

*All programs used (except those for phase determination) are included in this reference.

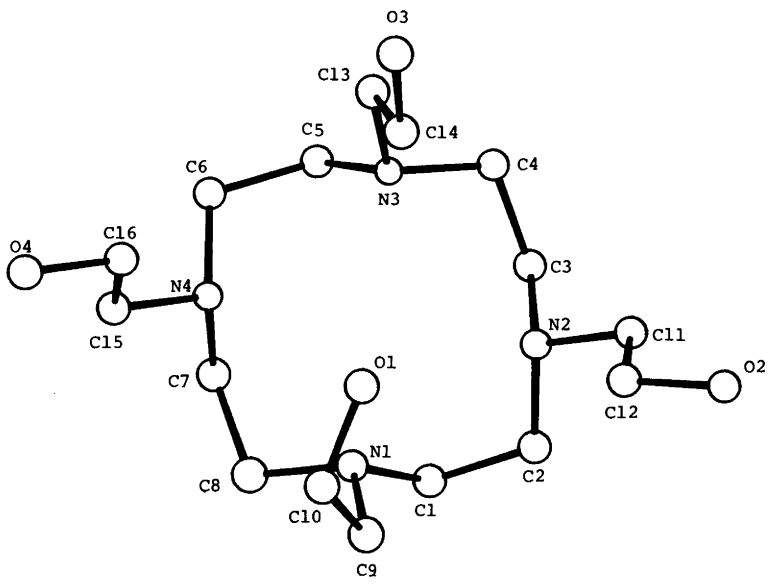

Fig. 1. Schematic drawing of the ligand showing the numbering of atoms.

0302-4377/83 $2.50

Table 1. Final fractional coordinates with estimated standard deviations. Hmn is bonded to Cm, HOm, to Om, and HWmn to OWm.

ATOM	X	Y	Z
CL1	.65790(11)	.38664(6)	.43090(9)
CL2	.74612(11)	.39245(6)	.03965(9)
LI1+	.7372(7)	.1339(3)	-.2249(6)
LI2+	.9312(7)	.0764(3)	-.7332(6)
OW1	.7726(3)	.2865(2)	.2427(4)
OW2	.8228(3)	-.0028(1)	-.7579(4)
O1	.9161(3)	.1616(1)	-.2036(3)
O2	.8510(3)	.1555(1)	.1971(2)
O3	.9202(3)	-.0649(1)	-.1710(3)
O4	.9822(3)	.0881(1)	-.5768(2)
N1	.6996(3)	.2364(1)	-.2501(3)
N2	.6309(3)	.1543(1)	-.0542(3)
N3	.6299(3)	.0418(1)	-.2247(2)
N4	.6850(3)	.1269(1)	-.4192(2)
C1	.5885(5)	.2548(2)	-.1806(4)
C2	.5963(5)	.2272(2)	-.0603(4)
C3	.5172(4)	.1121(2)	-.0821(3)
C4	.5556(4)	.0411(2)	-.1187(3)
C5	.5398(4)	.0460(2)	-.3225(3)
C6	.6060(4)	.0653(2)	-.4325(3)
C7	.6024(4)	.1880(2)	-.4251(4)
C8	.6696(5)	.2482(2)	-.3719(4)
C9	.8186(4)	.2709(2)	-.2128(4)
C10	.9347(4)	.2291(2)	-.2437(4)
C11	.6789(4)	.1389(2)	.0612(4)
C12	.8178(4)	.1578(2)	.0782(4)
C13	.7125(4)	-.0194(2)	-.2301(4)
C14	.8415(4)	-.0052(2)	-.1749(4)
C15	.7814(4)	.1288(2)	-.5093(4)
C16	.8970(4)	.0851(2)	-.4819(4)
H11	.512(3)	.237(2)	-.217(3)
H12	.580(3)	.304(2)	-.185(3)
H21	.514(4)	.238(2)	-.023(3)
H22	.663(3)	.252(2)	-.018(3)
H31	.468(3)	.134(2)	-.150(3)
H32	.460(3)	.111(2)	-.016(3)
H41	.476(3)	.014(2)	-.132(3)
H42	.610(3)	.022(1)	-.064(3)
H51	.469(3)	.078(1)	-.308(3)
H52	.493(3)	.000(2)	-.329(3)
H61	.583(3)	.069(1)	-.493(3)
H62	.658(3)	.030(2)	-.455(3)
H71	.514(4)	.178(2)	-.387(3)
H72	.581(4)	.195(2)	-.507(3)
H81	.617(3)	.287(2)	-.379(3)
H82	.760(4)	.260(2)	-.410(3)
H91	.815(3)	.278(2)	-.128(3)
H92	.822(3)	.317(1)	-.246(3)
H101	1.015(4)	.250(2)	-.211(3)
H102	.947(4)	.229(2)	-.325(3)
H111	.663(3)	.089(2)	.077(3)
H112	.620(3)	.159(1)	.119(3)
H121	.836(4)	.203(2)	.054(3)
H122	.878(4)	.127(2)	.032(3)
H131	.725(3)	-.034(2)	-.308(3)
H132	.669(4)	-.055(2)	-.193(3)
H141	.830(4)	.012(2)	-.094(3)
H142	.885(3)	.030(2)	-.219(3)
H151	.813(4)	.175(2)	-.515(3)
H152	.738(4)	.112(2)	-.584(3)
H161	.882(4)	.037(2)	-.468(4)
H162	.943(3)	.106(2)	-.412(3)
HO1	.975(5)	.150(2)	-.173(5)
HO2	.858(5)	.186(3)	.230(5)
HO3	.904(4)	-.085(2)	-.118(4)
HO4	1.048(4)	.092(2)	-.566(4)
HW11	.763(5)	.310(2)	.188(4)
HW12	.748(5)	.304(2)	.295(4)
HW21	.829(4)	-.028(2)	-.795(4)
HW22	.815(6)	-.022(3)	-.682(5)

standard deviations in intensities, $\sigma(I)$, taken as $\sigma(I) = [C_T + (0.02C_N)^2]^{\frac{1}{2}}$, where C_T is the total number of counts, and C_N the net count. Methylene hydrogen atom positions were calculated while those of the hydroxyl groups and the water molecules were localized in a difference Fourier map. The form factors were those of Hanson *et al.*,[4] except for hydrogen.[5] Anisotropic temperature factors were introduced for O, N and C atoms. Standard deviations in bond distances and angles were calculated from the correlation matrix of the final least-squares refinement cycle. The final *R*-value was 5.4% (R_w = 3.8%) for 2387 observed reflections.

Final fractional coordinates with estimated standard deviations are given in Table 1. Bond distances and angles and torsional angles may be found in Table 2. In Table 3 coordination bonds and hydrogen bonds are listed. The dihedral angles of Table 2 show that the ring conformation is [3 3 3 3].[6]* There are one *gauche* and three *anti*

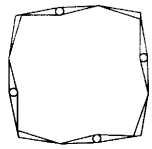

[3 3 3 3]

N–C–C–O torsional angles. This is illustrated in Fig. 1 which also shows the numbering of atoms. It may be seen that the N–C–C planes of all four side-chains are tilted towards the "corner" atoms of the ring.

Fig. 2 is a stereoscopic view showing the complex with the hydrogen bonding system. One of the lithium cations is coordinated to four nitrogen atoms and to the oxygen of the *gauche* side-chain. The other is coordinated to three different *anti* side-chain oxygen atoms of three different symmetry related ligands, and to one of the water molecules. Cl 1 and Cl 2 receive four and three hydrogen bonds, respectively, donated by the water molecules and the side-arm hydroxyl groups. Finally, the third *anti* side-chain hydroxyl group donates its hydrogen to one of the water molecules. Bond distances and angles have normal values within estimated limits of error.

Maximum root mean squares anisotropic thermal vibration amplitudes range from 0.15 to

* A shorthand notation for conformational type, consisting of a series of numbers within brackets, each giving the number of bonds in one "side", starting with the shortest. The direction around the ring is so chosen that the following number is smallest possible.

Table 2. Bond distances and angles and torsional angles with estimated standard deviations.

DISTANCE	(Å)	DISTANCE	(Å)
O1 – C10	1.428(6)	O2 – C12	1.438(5)
O3 – C14	1.434(6)	O4 – C16	1.439(6)
N1 – C1	1.472(6)	N1 – C8	1.481(6)
N1 – C9	1.472(6)	N2 – C2	1.483(6)
N2 – C3	1.478(6)	N2 – C11	1.471(6)
N3 – C4	1.479(6)	N3 – C5	1.474(6)
N3 – C13	1.482(6)	N4 – C6	1.475(6)
N4 – C7	1.481(6)	N4 – C15	1.472(6)
C1 – C2	1.519(7)	C3 – C4	1.520(6)
C5 – C6	1.525(6)	C7 – C8	1.508(7)
C9 – C10	1.510(7)	C11 – C12	1.500(6)
C13 – C14	1.506(7)	C15 – C16	1.509(7)

ANGLE	(°)	ANGLE	(°)
C1 – N1 – C8	110.2(4)	C1 – N1 – C9	112.5(4)
C8 – N1 – C9	112.2(4)	C2 – N2 – C3	110.1(4)
C2 – N2 – C11	108.9(4)	C3 – N2 – C11	110.2(3)
C4 – N3 – C5	109.1(3)	C4 – N3 – C13	109.9(4)
C5 – N3 – C13	111.8(4)	C6 – N4 – C7	110.2(4)
C6 – N4 – C15	109.2(4)	C7 – N4 – C15	110.3(4)
N1 – C1 – C2	113.6(4)	N2 – C2 – C1	113.7(4)
N2 – C3 – C4	111.6(4)	N3 – C4 – C3	112.0(4)
N3 – C5 – C6	112.9(4)	N4 – C6 – C5	112.0(4)
N4 – C7 – C8	111.0(4)	N1 – C8 – C7	111.5(4)
N1 – C9 – C10	110.2(4)	O1 – C10 – C9	108.5(4)
N2 – C11 – C12	112.4(4)	O2 – C12 – C11	109.7(4)
N3 – C13 – C14	110.0(4)	O3 – C14 – C13	111.3(4)
N4 – C15 – C16	112.3(4)	O4 – C16 – C15	108.0(4)

DIHEDRAL ANGLE	(°)
C1 – N1 – C8 – C7	-85.8(5)
C8 – N1 – C1 – C2	164.5(4)
C1 – N1 – C9 – C10	155.1(4)
C9 – N1 – C1 – C2	-69.4(5)
C8 – N1 – C9 – C10	-81.9(5)
C9 – N1 – C8 – C7	148.0(4)
C2 – N2 – C3 – C4	159.3(4)
C3 – N2 – C2 – C1	-78.4(5)
C2 – N2 – C11 – C12	-81.7(5)
C11 – N2 – C2 – C1	160.7(4)
C3 – N2 – C11 – C12	157.5(4)
C11 – N2 – C3 – C4	-80.6(5)
C4 – N3 – C5 – C6	165.1(4)
C5 – N3 – C4 – C3	-82.2(5)
C4 – N3 – C13 – C14	-89.7(5)
C13 – N3 – C4 – C3	154.9(4)
C5 – N3 – C13 – C14	149.0(4)
C13 – N3 – C5 – C6	-73.1(5)
C6 – N4 – C7 – C8	159.9(4)
C7 – N4 – C6 – C5	-79.7(5)
C6 – N4 – C15 – C16	-81.2(5)
C15 – N4 – C6 – C5	159.0(4)
C7 – N4 – C15 – C16	157.5(4)
C15 – N4 – C7 – C8	-79.4(5)
N1 – C1 – C2 – N2	-47.7(6)
N2 – C3 – C4 – N3	-63.7(5)
N3 – C5 – C6 – N4	-51.9(5)
N4 – C7 – C8 – N1	-61.4(5)
N1 – C9 – C10 – O1	-51.0(5)
N2 – C11 – C12 – O2	167.5(4)
N3 – C13 – C14 – O3	175.5(4)
N4 – C15 – C16 – O4	177.5(4)

Table 3. Coordination bond distances and hydrogen bond distances with estimated standard deviations.

DISTANCE	(Å)	DISTANCE	(Å)
CL1 - OW1	3.213(4)	CL1 - OW2'	3.159(5)
CL1 - O1'	3.096(4)	CL1 - O3'	3.106(4)
CL2 - OW1	3.184(5)	CL2 - OW2'	3.207(5)
CL2 - O4'	3.068(4)	LI1+ - O1	1.948(8)
LI1+ - N1	2.079(8)	LI1+ - N2	2.346(8)
LI1+ - N3	2.151(8)	LI1+ - N4	2.347(8)
LI2+ - OW2	1.927(9)	LI2+ - O2'	1.943(8)
LI2+ - O3'	1.941(8)	LI2+ - O4	1.922(8)
OW1 - O2	2.764(5)		

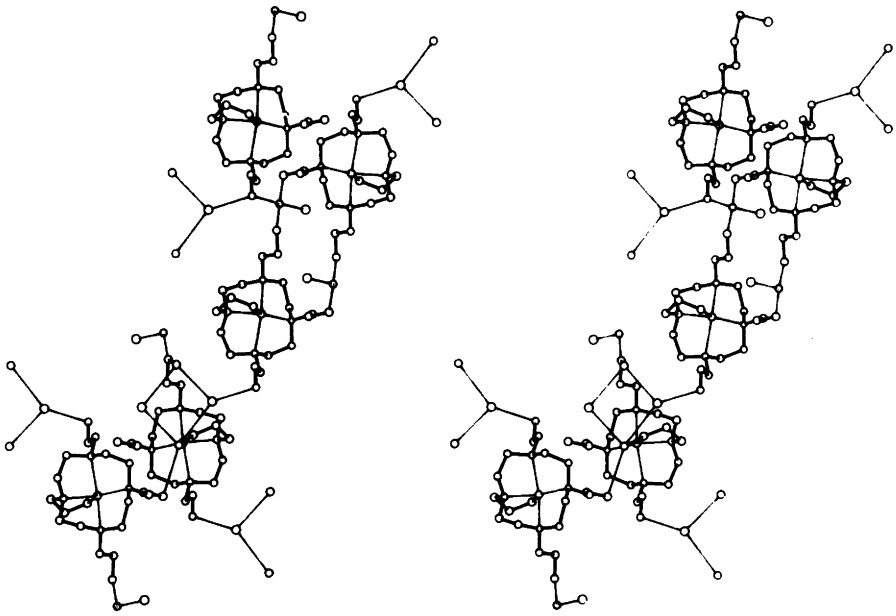

Fig. 2. Stereoscopic view of the complex illustrating the type of coordination and the hydrogen bonding system.

0.22 Å. C–H bond distances lay between 0.93 and 1.04 Å while O–H range from 0.70 to 0.81 Å.

Like for the Li-complexes of the 6-crown-18-ether,[7] the conformational problem for the ligand in a (1:1) water-free complex with Li^+ is not settled. In fact, considerable effort has been put into attempts to solve the structure of the (1:1) complex with LiSCN. It is, however, highly disordered, and no definite conclusions about the ligand conformation could be drawn.

Lists of thermal parameters and observed and calculated structure factors are available from the author.

Acknowledgement. The author thanks S. Buøen for preparing the compound.

1. Buøen, S., Dale, J., Groth, P. and Krane, J. *Chem. Commun. 20* (1982) 1172.
2. Germain, G., Main, P. and Woolfson, M. M. *Acta Crystallogr. A 27* (1971) 368.
3. Groth, P. *Acta Chem. Scand. 27* (1973) 3131.
4. Hanson, H. P., Herman, F., Lea, J. D. and Skillman, S. *Acta Crystallogr. 17* (1965) 1040.
5. Stewart, R. F., Davidson, E. R. and Simpson, W. T. *J. Chem. Phys. 42* (1965) 3175.
6. Dale, J. *Acta Chem. Scand. 27* (1973) 1115.
7. Groth, P. *Acta Chem. Scand. A 36* (1982) 109.

Received September 3, 1982.

Crystal Structure Analysis of 1,4,7,10-Tetra-(2-hydroxyethyl)-1,4,7,10-tetraazacyclododecane Hydrate at −150 °C

P. GROTH

Department of Chemistry, University of Oslo, Oslo 3, Norway

^{13}C NMR spectroscopy [1] indicates conformational differences of 1,4,7,10-tetra-(2-hydroxyethyl)-1,4,-7,10-tetraazacyclododecane as a hydrate and in its complexes with Li^+, Na^+ and K^+. Some single crystal X-ray analyses have been carried out in order to seek more precise information about these differences. The results for the hydrate are now reported.

The crystals of $(C_{16}H_{36}O_4N_4)\cdot H_2O$ are triclinic with space group $P\bar{1}$ and cell dimensions (for Dirichlet's reduced cell) $a = 7.022(2)$, $b = 9.680(3)$, $c = 14.709(5)$ Å, $\alpha = 97.38(2)$, $\beta = 92.10(3)$, $\gamma = 96.99(2)°$. There are two formula units in the cell ($D_x = 1.24$ g cm^{-3}, $D_m = 1.22$ g cm^{-3}), 2221 observed reflections were recorded on an automatic four-circle diffractometer at *ca.* −150 °C ($2\theta_{max} = 50°$, Mo$K\alpha$-radiation, ω-scan). No corrections for absorption or secondary extinction were applied (crystal size 0.2 × 0.3 × 0.3 mm).

The structure was solved by direct methods [2] and refined by full-matrix least-squares technique.[3,*]

Methylene hydrogen atom positions were calculated, the others were localized in a difference Fourier map. Anisotropic temperature factors were introduced for O, N and C atoms. Weights in least squares were calculated from the standard deviations in intensities, $\sigma(I)$, taken as $\sigma(I) = [C_T + (0.02C_N)^2]^{\frac{1}{2}}$, where C_T is the total number of counts and C_N the net count. The form factors used were those of Hanson *et al.*[4] except for hydrogen.[5] The final R-value was 5.6% (weighted value 4.2%) for 2221 observed reflections.

Final fractional coordinates with estimated standard deviations may be found in Table 1. Bond distances and angles and diheral angles with standard deviations (calculated from the correlation matrix of the final least squares refinement cycle) are listed in Table 2. Fig. 1 is a schematic drawing of the ring showing the numbering of atoms. Bond distances and angles have normal values within estimated limits of error. The torsional angles of Table 2 show that the 12-membered ring has the

*All programs used (except those for phase determination) are included in this references.

0302-4377/83 $2.50

Table 1. Final fractional coordinates with estimated standard deviations. Hmn is bonded to Cm, HOm to Om, and HWm to OW.

ATOM	X	Y	Z
OW	.9175(3)	.7650(2)	.7198(1)
O1	.9469(3)	.2979(2)	.6176(1)
O2	.9180(3)	.7988(2)	.5414(1)
O3	1.1405(3)	1.2567(2)	.7786(1)
O4	1.1733(3)	.7504(2)	.8612(1)
N1	.6148(3)	.5413(2)	.7145(1)
N2	.5400(3)	.8120(2)	.6326(1)
N3	.7182(3)	.9747(2)	.8126(1)
N4	.7636(3)	.7026(2)	.9029(1)
C1	.4742(4)	.5534(3)	.6391(2)
C2	.3947(4)	.6946(3)	.6452(2)
C3	.4870(4)	.9466(3)	.6747(2)
C4	.5154(4)	.9720(3)	.7790(2)
C5	.7280(4)	.9570(3)	.9110(2)
C6	.6458(4)	.8129(3)	.9339(2)
C7	.6523(4)	.5627(3)	.8871(2)
C8	.5170(4)	.5363(3)	.8018(2)
C9	.7061(4)	.4126(3)	.6921(2)
C10	.8594(4)	.4240(3)	.6225(2)
C11	.5745(4)	.8157(3)	.5352(2)
C12	.7735(4)	.8841(3)	.5201(2)
C13	.8304(4)	1.1093(3)	.8000(2)
C14	1.0428(4)	1.1023(3)	.7897(2)
C15	.9275(4)	.7029(3)	.9681(2)
C16	1.0991(4)	.6546(3)	.9205(2)
H11	.360(4)	.474(3)	.638(2)
H12	.548(4)	.540(3)	.579(2)
H21	.340(4)	.715(3)	.706(2)
H22	.277(4)	.681(3)	.597(2)
H31	.343(4)	.956(3)	.661(2)
H32	.566(4)	1.023(3)	.646(2)
H41	.434(4)	.894(3)	.806(2)
H42	.474(4)	1.067(3)	.800(2)
H51	.657(4)	1.026(3)	.946(2)
H52	.858(4)	.978(3)	.934(2)
H61	.507(4)	.781(3)	.906(2)
H62	.632(4)	.820(3)	1.001(2)
H71	.577(4)	.546(3)	.943(2)
H72	.743(4)	.492(3)	.885(2)
H81	.426(4)	.610(3)	.807(2)
H82	.441(4)	.442(3)	.800(2)
H91	.604(4)	.528(3)	.670(2)
H92	.771(4)	.392(3)	.748(2)
H101	.957(4)	.505(3)	.641(2)
H102	.810(4)	.439(3)	.562(2)
H111	.464(4)	.857(3)	.506(2)
H112	.561(4)	.718(3)	.501(2)
H121	.797(4)	.900(3)	.451(2)
H122	.801(4)	.989(3)	.553(2)
H131	.809(4)	1.189(3)	.849(2)
H132	.783(4)	1.142(3)	.747(2)
H141	1.061(4)	1.054(3)	.736(2)
H142	1.103(4)	1.070(3)	.846(2)
H151	.896(4)	.648(3)	1.022(2)
H152	.968(4)	.799(3)	.996(2)
H161	1.071(4)	.555(3)	.888(2)
H162	1.198(4)	.650(3)	.967(2)
HO1	.978(4)	.270(3)	.562(2)
HO2	.916(4)	.796(3)	.600(2)
HO3	1.087(4)	1.257(3)	.732(2)
HO4	1.089(4)	.752(3)	.815(2)
HW1	.850(4)	.700(3)	.722(2)
HW2	.847(4)	.827(3)	.745(2)

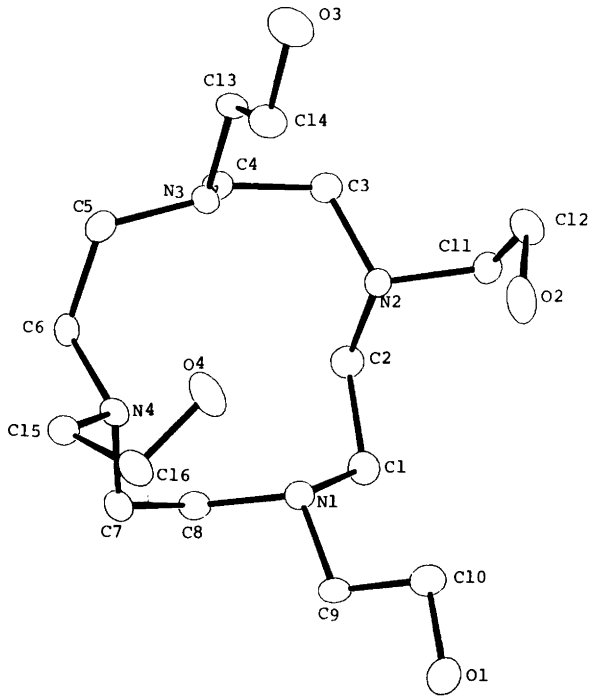

Fig. 1. Schematic drawing of the 12-membered ring showing the numbering of atoms.

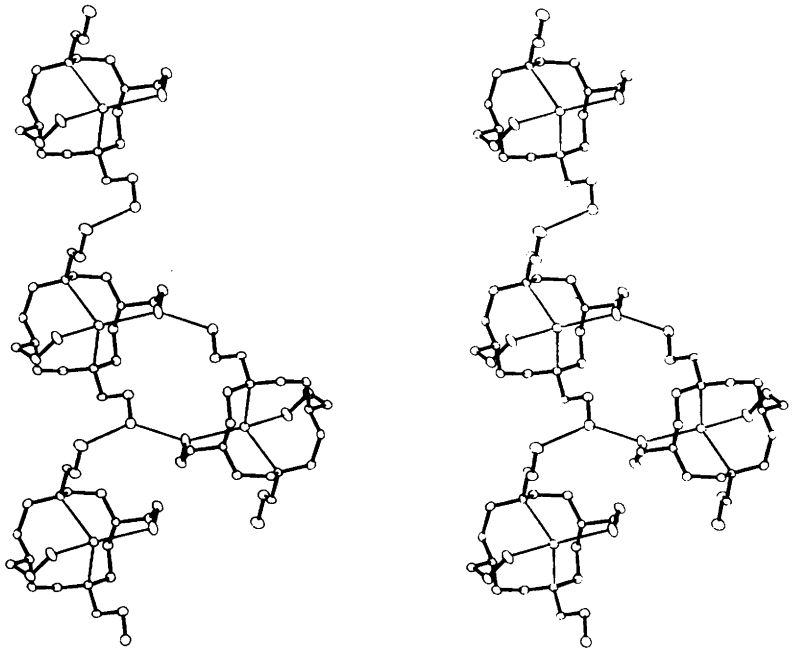

Fig. 2. Stereoscopic view showing the hydrogen bonding system.

Table 2. Bond distances and angles and torsional angles with estimated standard deviations.

DISTANCE	(Å)	DISTANCE	(Å)
OW - O2	2.685(3)	OW - O4	2.727(3)
OW - N1	2.835(3)	OW - N3	2.839(3)
O1 - O3"	2.852(3)	O1 - O2	2.658(3)
O1 - C10	1.426(4)	O2 - C12	1.435(4)
O3 - C14	1.426(4)	O4 - C16	1.419(4)
N1 - C1	1.483(4)	N1 - C8	1.482(4)
N1 - C9	1.475(4)	N2 - C2	1.467(4)
N2 - C3	1.466(4)	N2 - C11	1.466(4)
N3 - C4	1.487(4)	N3 - C5	1.479(4)
N3 - C13	1.476(4)	N4 - C6	1.466(4)
N4 - C7	1.465(4)	N4 - C15	1.470(4)
C1 - C2	1.532(4)	C3 - C4	1.523(4)
C5 - C6	1.527(4)	C7 - C8	1.521(4)
C9 - C10	1.516(4)	C11 - C12	1.509(4)
C13 - C14	1.513(4)	C15 - C16	1.509(4)

ANGLE	(°)	ANGLE	(°)
O1 - C10 - C9	106.7(2)	O2 - C12 - C11	111.7(3)
O3 - C14 - C13	110.8(3)	O4 - C16 - C15	111.4(2)
N1 - C1 - C2	114.9(2)	C1 - N1 - C8	110.1(2)
C1 - N1 - C9	109.5(2)	N1 - C8 - C7	114.3(2)
C8 - N1 - C9	109.7(2)	N1 - C9 - C10	114.3(2)
N2 - C2 - C1	113.2(2)	C2 - N2 - C3	111.6(2)
C2 - N2 - C11	111.3(2)	N2 - C3 - C4	114.2(2)
C3 - N2 - C11	110.6(2)	N2 - C11 - C12	112.7(2)
N3 - C4 - C3	113.5(2)	C4 - N3 - C5	110.5(2)
C4 - N3 - C13	109.9(2)	N3 - C5 - C6	115.8(2)
C5 - N3 - C13	109.3(2)	N3 - C13 - C14	114.4(2)
N4 - C6 - C5	112.9(2)	C6 - N4 - C7	112.5(2)
C6 - N4 - C15	111.3(2)	N4 - C7 - C8	114.6(2)
C7 - N4 - C15	109.9(2)	N4 - C15 - C16	111.8(2)

DIHEDRAL ANGLE	(°)
O1 - C10 - C9 - N1	173.2(2)
O2 - C12 - C11 - N2	69.9(3)
O3 - C14 - C13 - N3	-179.5(2)
O4 - C16 - C15 - N4	65.7(3)
C8 - N1 - C1 - C2	69.5(3)
C7 - C8 - N1 - C1	-164.7(2)
C9 - N1 - C1 - C2	-169.8(3)
C10 - C9 - N1 - C1	77.1(3)
C9 - N1 - C8 - C7	74.7(3)
C10 - C9 - N1 - C8	-161.9(2)
C3 - N2 - C2 - C1	-156.6(2)
C4 - C3 - N2 - C2	75.5(3)
C11 - N2 - C2 - C1	79.4(3)
C12 - C11 - N2 - C2	-153.3(2)
N2 - C2 - C1 - N1	67.0(3)
C11 - N2 - C3 - C4	-159.9(2)
C12 - C11 - N2 - C3	82.1(3)
C5 - N3 - C4 - C3	-163.1(2)
C6 - C5 - N3 - C4	68.2(3)
C13 - N3 - C4 - C3	76.2(3)
C14 - C13 - N3 - C4	-153.5(2)
N3 - C4 - C3 - N2	61.1(3)
C13 - N3 - C5 - C6	-170.8(2)
C14 - C13 - N3 - C5	85.2(3)
C7 - N4 - C6 - C5	-154.8(2)
C8 - C7 - N4 - C6	72.6(3)
C15 - N4 - C6 - C5	81.6(3)
C16 - C15 - N4 - C6	-148.9(2)
N4 - C6 - C5 - N3	70.0(3)
C15 - N4 - C7 - C8	-162.8(2)
C16 - C15 - N4 - C7	85.8(3)
N4 - C7 - C8 - N1	63.2(3)

[3333] conformation[6] with two *anti* and two *gauche* N–C–C–O torsional angles.

As to be expected from the NMR studies,[1] the ring conformation corresponds to that of the dihydrated (2:1) complex with LiCl.[6] The dissimilarity in conformation stems from the various number of *anti* and *gauche* side-chains (only one *gauche* chain in the Li-complex). It may be noted that all side-arms bend off towards the corner atoms. The same pattern was observed in the Li-complex.

Fig. 2 is a stereoscopic view which illustrates the hydrogen bonding system. The water molecule donates its two hydrogen atoms to N1 and N3, and accepts hydrogen bonds from the two *gauche* side-arms. It is thus completely encapsulated tetrahedrally. The hydroxyl groups of the *anti* chains are involved in two inter-molecular hydrogen bonds.

The principal thermal vibration ellipsoids for non-hydrogen atoms correspond to maximum r.m.s. amplitudes between 0.13 and 0.25 Å. The C–H and O–H bond distance ranges are 0.93–1.06 and 0.83–0.88 Å, respectively.

Lists of thermal parameters and observed and calculated structure factors are available from the author.

Acknowledgement. The author thanks S. Buøen for preparing the crystals.

1. Buøen, S., Dale, J., Groth, P. and Krane, J. *Chem. Commun. 20* (1982) 1172.
2. Germain, G., Main, P. and Woolfson, M. M. *Acta Crystallogr. A 27* (1971) 368.
3. Groth, P. *Acta Chem. Scand. 27* (1973) 3131.
4. Hanson, H. P., Herman, F., Lea, J. D. and Skillman, S. *Acta Crystallogr. 17* (1964) 1040.
5. Stewart, R. F., Davidson, E. R. and Simpson, W. T. *J. Chem. Phys. 42* (1965) 3175.
6. Groth, P. *Acta Chem. Scand. A 37* (1983) 71.

Received September 7, 1982.

Acta Chemica Scandinavica A 37 (1983) 79–91

Conformational Analysis of 1,2-Ethanediamine and 1,3-Propanediamine by CFF, PCILO and *ab initio* Methods

KJELD RASMUSSEN[a] and CAMILLO TOSI[b]

[a]Chemistry Department A, The Technical University of Denmark, DK-2800 Lyngby, Denmark and [b]Istituto Donegani, Via Fauser 4, I-28100 Novara, Italy

Ten equilibrium conformations of 1,2-ethanediamine (en) and twenty-five of 1,3-propanediamine (tn) were calculated using convergent energy minimisation, both with a potential energy function (PEF) which has proven its value for coordinated amines, and with the semirigorous quantum mechanical method PCILO. All conformers of en and four selected conformers of tn, in the geometries produced by PEF computations, were also analysed with *ab initio* molecular orbital theory (extended 6 −31 G basis set). Conformational predictions of molecular geometries made with PEF are in better agreement with available experimental data than those made by PCILO. There are noticeable differences in the Boltzmann populations, not only as regards the single conformers, but also the "gross" conformations defined by the central torsions only: At this level, the agreement between PEF and *ab initio* is closer than between either and PCILO. This leads to the prediction that tn exists in an AG "gross" conformation or as a mixture of AG and GG'.

As a preliminary to the development of a potential energy function (PEF) for amines by the Consistent Force Field (CFF),[1] we have calculated the equilibrium conformations (conformers) of 1,2-ethanediamine (en) and 1,3-propanediamine (tn), using convergent energy minimisation in a well-tried PEF, and with PCILO. In addition, all en conformers and selected conformers of tn are studied by *ab initio* calculations using GAUSSIAN-70.

Our ultimate goal is a CFF for linear and cyclic saturated polyamines. Such work requires a good initial parameter set for the PEF, and experience has shown that proper modelling of non-bonded interactions is crucial, and that *ab initio* calculations may be of help in this particular problem. We have previously made such studies for several molecules; in a rather conventional way using the total SCF energy for each of a number of conformations[2] and, in a more economical way[3,4] using Bond Energy Analysis (BEA).[5,6] The present work provides a comparison between CFF and PCILO for calculation of conformer geometry and relative energy, with *ab initio* as a check on the latter. At the same time this study gives data for a subsequent development of a better PEF.

The two primary diamines en and tn (using the spectrochemical abbreviations accepted in coordination chemistry) were chosen as model substances in this initial study for a number of reasons. (1) They represent systems with large though manageable numbers of conformers; (2) they show intramolecular hydrogen bonding; (3) they are of prime importance in coordination chemistry; (4) we already have a reasonable PEF which has proven its worth in many calculations on tris-(diamine) coordination complexes.[7]

The presence of hydrogen bonding means that we should include Coulomb interactions in the modelling of non-bonded interactions.[8] We intend to do so in the monopole approximation which has worked well in many cases.[9]

The scope of the present work is thus to test the existing PEF towards PCILO results, with geometry optimisation, and to use *ab initio* results to check the PEF and PCILO results for selected conformers; to estimate fractional atomic charges for later use as PEF parameters; and to obtain data for analytic functions for non-bonded interactions.

0302-4377/83 $2.50

PREVIOUS WORK

Theoretical conformational analysis on en has been performed before. Jhon *et al.* made an extended Hückel study;[10] using fixed bond lengths and valence angles they calculated the energies of all ten conformers and all saddle points with respect to torsion around the C–C bond. The C–C torsional angle was varied in steps of 60°, and no geometry optimisation was attempted.

Concurrent with this work, Hadjiliadis *et al.* also made an extended Hückel study on one *anti* and one *gauche* conformer,[11] using a fixed valence geometry, and varying the C–C torsion in steps of 20° and, near the minima, in steps of 2°. To some extent, the C–N torsions were also varied. Thus a certain amount of geometry optimisation was done.

Shortly after, Graffeuil *et al.* published a CNDO/2 study,[12] in which they mapped the entire torsional space of three torsions in steps of 60°, still with fixed valence geometry. They calculated further the equilibrium distribution over the six conformers of lowest energy, neglecting statistical weights and all degrees of freedom except the three torsions. Based on this, they got an average dipole moment in good agreement with the experimental.

Recently, Zahradnik *et al.* reported another CNDO/2 study,[13] in which they used geometry optimisation on bond lengths and angles for a number of conformers. They list energies and some bond angles of twelve conformations, some of them eclipsed.

Radom *et al.* undertook the first *ab initio* study,[14] using GAUSSIAN-70 with the 4-31G extended basis set. They calculated the energies of all ten conformers using standard geometry and found two G conformers to be well below the others on the energy scale.

The next attempt at an extensive conformational analysis was made by Cetina *et al.* who used PCILO to study eight of the ten conformers of en plus a large number of other conformations.[15] In this way they were able to plot sections of the Born-Oppenheimer (BO) surface in conformational space. They give the total energies and the conformational energy differences, and the C–C torsional angles of some conformers, but no further data. Unfortunately, there are inconsistencies between energy values in figures and in the table.

Finally, a preliminary *ab initio* study was made with MOLECULE by Johansen and Hald.[16] They studied only one *gauche* conformer, with fixed geometry, except for using three values of the C–C torsion near the experimental value. Unfortunately, they chose, for reasons of economy, a structure with C_2 symmetry, which has a rather high energy

Table 1. Experimentally determined conformers of 1,2-ethanediamine.[a]

Ref.	19		20		21
Method	ED, r_g, r_α		MV, r_o		X
Temp. (°C)	−118		−30		−60
Conformer	−G−	GGG′		AGG′	AAA
CC	1.545(8)		1.546[b]		1.51(2)
CN	1.469(4)		1.469[b]		1.47(1)
CH	1.109(10)		1.093[b]		1.015[c] (135)
NH	1.0302[b]		1.017[b]		0.865[c] (135)
CCN	110.2(7)	109.0(10)		111.5(10)	114.5(10)
CNH	112.1[b]		109.48[b]		106.5(40)
NCH	–		–		110[c] (4)
CCH	111.9(46)		109.48[b]		107[c] (4)
HNH	105.9[b]		109.48[b]		102 (6)
HCH	112.7(85)		109.48[b]		108 (6)
NCCN	64.0(45)	63(2)		63(2)	180 (0)
lpNCC[b]	81, −160 or −52(9)	60,[b] −60[b]		180,[b] −60[b]	
μ		1.770(33)		2.203(6)	
Population		0.64(5)		0.36(5)	

[a] Bond lengths in Ångström, angles in degree, dipole moments in Debye. [b] Assumed and fixed. [c] Average. [d] A torsional angle involving a lone pair, such as C–C–N–lp, is defined as the supplement to the angle halving the two C–C–N–H torsional angles around the same N–C bond.

relative to the conformers found by previous workers using simpler programs. They used GTO, (7*s* 3*p*) contracted to ⟨4*s* 2*p*⟩ for N and C, taken from Roos and Siegbahn,[17] and (4*s*) contracted to ⟨2*s*⟩ for H, taken from Huzinaga.[18]

No theoretical study seems to have appeared on the conformations of tn.

EXPERIMENTAL BACKGROUND

The conformation of en is well-known in both gaseous and crystalline phases.

Yokozeki and Kuchitsu derived the r_g structure from gas phase electron diffraction.[19] They found a *gauche* conformer with a C−C torsional angle of 64°, any other conformer being present to less than 5%. Their results are reproduced in Table 1.

Marstokk and Møllendal made a penetrating study of the microwave spectrum.[20] In spite of having only one isotopomer they managed to derive such crucial conformational details as the CCN angle and the CC torsion for two very similar *gauche* conformers. Their dipole moments were also determined. From intensity measurements, relative populations and thence K and ΔG were derived. Those data important to the present study are reproduced in Table 1.

In the crystal, en takes the *anti* conformation, as found by Jamet-Delcroix.[21] Her results are also cited in Table 1.

CFF CALCULATIONS

The ten conformers of en were constructed with the CFF program and minimised in a PEF

Table 2. Energies and populations of 1,2-ethanediamine conformers. Energy in kJ mol^{-1}.

No.	Conformer	Stat. wt.	CFF ΔE	CFF ΔE + st.wt.	CFF ΔG	PCILO ΔE	PCILO ΔE + st.wt.	PCILO[15] ΔE	4-31G[14] ΔE	4-31G[14] ΔE + st.wt.
1	AAA	1	0.064	3.470	5.428	15.431	18.868	18.368	9.205	12.642
2	AAG	4	0.031	0.000	0.000	11.125	11.125	10.753	6.862	6.862
3	GAG	2	0.000	1.688	3.174	2.770	4.489	3.013	5.439	7.157
4	GAG′	2	0.052	1.740	1.530	3.013	4.732	2.552	4.770	6.488
5	AGA	2	1.839	3.527	5.876	13.740	15.459	0.753	16.443	18.161
6	AGG	4	2.241	2.210	2.492	9.188	9.188	–	13.012	13.012
7	AGG′	4	0.042	0.011	0.340	8.611	8.611	6.736	0.000	0.000
8	GGG	2	2.429	4.117	5.886	1.130	2.849	0.000	8.452	10.170
9	GGG′	4	0.127	0.096	0.196	0.000	0.000	15.565	1.088	1.088
10	G′GG′	2	0.017	1.705	3.313	0.916	2.521	–	24.560	26.278
	ΣXAX									
	ΣXGX									

No.	6-31G ΔE	6-31G ΔE + st.wt.	CFF $n(\Delta E$ + st.wt.)	CFF $n(\Delta G)$	PCILO $n(\Delta E)$	PCILO $n(\Delta E$ + st.wt)	4-31G[14] $n(\Delta E$ + st.wt.)	6-31G $n(\Delta E$ + st.wt.)	Exp.[20] n
1	6.602	10.039	0.04	0.03	0.00	0.00	0.00	0.01	
2	5.611	5.611	0.18	0.22	0.00	0.01	0.03	0.06	
3	5.763	7.482	0.09	0.06	0.11	0.08	0.03	0.02	
4	5.167	6.886	0.09	0.12	0.10	0.07	0.04	0.03	
5	5.891	7.610	0.04	0.02	0.00	0.00	0.00	0.02	
6	5.550	5.550	0.07	0.08	0.01	0.01	0.00	0.06	
7	0.000	0.000	0.18	0.19	0.01	0.01	0.54	0.53	0.36
8	4.945	6.664	0.03	0.02	0.21	0.15	0.01	0.04	
9	2.106	2.106	0.17	0.20	0.33	0.49	0.35	0.23	0.64
10	25.006	26.725	0.09	0.06	0.23	0.18	0.00	0.00	
			0.40	0.43	0.21	0.16	0.10	0.12	0.00
			0.58	0.57	0.79	0.84	0.90	0.88	1.00

Table 3. Conformers of 1,2-ethanediamine from CFF calculations.

No.	Conformer	N–H	C–H	C–C	N–C	N–C–C	C–N–H	N–C–H	C–C–H	H–N–H	H–C–H	lp–N–C–C	N–C–C–N	C–C–N–lp	σ
1	AAA	1.012	1.094	1.548	1.475	110.6	110.6	109.2	109.6	109.7	108.6	−178.5	180.0	178.5	2
2	AAG	1.012	1.094	1.547	1.475	110.3	110.5	109.3	109.5	109.6	108.7	−178.4	−179.1	62.7	1
3	GAG	1.012	1.095	1.546	1.474	110.0	110.4	109.5	109.5	109.3	108.9	62.1	−178.3	63.7	2
4	GAG′	1.012	1.095	1.546	1.474	110.0	110.3	109.5	109.5	109.2	108.9	62.1	180.0	−62.1	1
5	AGA	1.011	1.094	1.550	1.475	111.7	111.1	109.1	109.3	110.2	108.2	173.3	62.9	167.8	2
6	AGG	1.011	1.094	1.549	1.475	111.5	110.8	109.2	109.2	109.6	108.4	173.1	64.9	167.8	1
7	AGG′	1.012	1.094	1.548	1.475	110.6	110.5	109.0	109.4	109.4	108.5	180.0	60.8	−61.9	1
8	GGG	1.011	1.094	1.548	1.475	111.2	110.5	109.4	109.1	108.8	108.6	71.8	66.1	72.5	2
9	GGG′	1.012	1.094	1.547	1.475	110.4	110.3	109.5	109.4	109.1	108.7	63.1	61.9	−61.9	1
10	G′GG′	1.012	1.094	1.546	1.475	110.1	110.4	109.5	109.4	109.4	108.7	−63.3	58.8	−61.6	2

Table 4. Conformers of 1,2-ethanediamine from PCILO calculations.

No.	Conformer	N–H	C–H	C–C	N–C	N–C–C	C–N–H	N–C–H	C–C–H	lp–N–C–C	N–C–C–N	C–C–N–lp	μ	μ(6–31G)
1	AAA	1.083	1.139	1.485	1.424	115.9	110.3	108.1	110.8	179.5	180.0	180.0	0.079	0.000
2	AAG	1.083	1.139	1.486	1.423	113.7	110.2	108.5	110.2	−179.1	179.9	60.3	3.048	2.833
3	GAG	1.082	1.140	1.484	1.421	111.8	110.4	110.3	110.8	58.9	−178.7	59.6	3.021	2.742
4	GAG′	1.083	1.140	1.484	1.422	111.7	110.4	110.3	110.8	58.9	−179.4	−58.4	0.098	0.000
5	AGA	1.083	1.139	1.486	1.425	115.8	110.4	107.9	110.5	176.1	57.2	−177.5	0.752	0.214
6	AGG	1.083	1.139	1.484	1.423	113.7	110.3	108.4	110.4	175.5	59.0	60.9	2.976	2.837
7	AGG′	1.082	1.139	1.485	1.424	113.1	110.2	108.5	110.7	179.6	54.6	−60.7	2.775	2.868
8	GGG	1.083	1.139	1.484	1.423	111.7	110.4	110.1	110.9	54.8	58.4	58.2	0.300	0.088
9	GGG′	1.083	1.139	1.483	1.422	110.9	110.4	110.3	111.1	59.1	54.7	−58.6	2.888	2.731
10	G′GG′	1.083	1.139	1.483	1.422	111.0	110.4	110.3	111.0	−58.4	54.0	−59.2	2.542	2.761

Table 5. Energies and populations of 1,3-propanediamine conformers. Energy in kJ mol^{-1}.

No.	Conformer	Stat. wt.	CFF ΔE	CFF ΔE + st.wt.	CFF ΔG	PCILO ΔE	PCILO ΔE + st.wt.	6−31G ΔE	6−31G ΔE + st.wt.	CFF $n(\Delta E$ + st.wt.)	CFF $n(\Delta G)$	PCILO $n(\Delta E$ + st.wt.)	6−31G $n(\Delta E$ + st.wt.)
1	AAAA	1	0.108	3.483	3.697	21.690	25.127			0.03	0.03	0.00	
2	AAAG	4	0.092	0.058	0.000	17.640	17.640	1.790	1.790	0.10	0.12	0.00	0.25
3	GAAG	1	0.072	3.495	4.892	9.661	13.098			0.03	0.02	0.00	
4	GAAG′	2	0.078	1.763	1.464	9.623	11.342			0.05	0.07	0.01	
5	AG′AA	4	2.095	2.061	2.723	20.184	20.184			0.04	0.04	0.00	
6	G′G′AA	4	2.570	2.536	2.844	14.949	14.949			0.04	0.04	0.00	
7	GG′AA	4	0.071	0.037	0.308	15.042	15.042			0.10	0.11	0.00	
8	AG′AG′	4	2.129	2.095	2.410	16.096	16.096			0.04	0.04	0.00	
9	G′G′AG′	4	2.601	2.567	2.627	7.874	7.874			0.04	0.04	0.03	
10	GG′AG′	4	0.076	0.042	0.073	7.699	7.699			0.10	0.12	0.03	
11	AG′AG	4	1.995	1.961	2.388	16.138	16.138			0.05	0.05	0.00	
12	G′G′AG	4	2.465	2.431	2.508	7.828	7.828			0.04	0.04	0.03	
13	GG′AG	4	0.034	0.000	0.027	7.958	7.958	0.000	0.000	0.10	0.12	0.03	0.50
14	AG′G′A	2	3.941	5.626	9.452	18.163	19.882			0.01	0.00	0.00	
15	AG′G′G′	4	4.184	4.150	5.850	14.117	14.117			0.02	0.01	0.00	
16	AG′G′G	4	1.797	1.763	2.631	13.715	13.715			0.05	0.04	0.00	
17	G′G′G′G′	2	4.750	6.435	9.511	6.180	7.899			0.01	0.00	0.03	
18	G′G′G′G	4	2.277	1.803	2.749	5.690	5.690			0.05	0.04	0.07	
19	GG′G′G	2	0.000	1.685	3.785	5.782	7.501	1.931	3.650	0.05	0.03	0.03	0.12
20	AG′GA	2	12.873	14.558	16.711	24.870	26.589			0.00	0.00	0.00	
21	AG′GG′	4	4.183	4.149	5.427	8.000	8.000			0.02	0.01	0.03	
22	AG′GG	4	12.991	12.957	14.371	20.179	20.179			0.00	0.00	0.00	
23	G′G′GG′	4	4.791	8.194	5.252	0.000	0.000	3.442	3.442	0.00	0.01	0.68	0.13
24	G′G′GG	2	12.874	14.499	15.644	11.715	13.434			0.00	0.00	0.00	
25	GG′GG′	2	0.883	2.568	3.287	6.226	7.945			0.04	0.03	0.03	
	Σ XAAX									0.20	0.23	0.01	0.25
	Σ XAGX									0.55	0.59	0.12	0.50
	Σ XGGX									0.19	0.12	0.13	0.12
	Σ XGG′X									0.06	0.06	0.74	0.13

Table 6. Conformers of 1,3-propanediamine from CFF calculations.

No.	Conformer	N–H	C–H	C–C	N–C	N–C–C	C–C–C	C–N–H	N–C–H
1	AAAA	1.012	1.094	1.548	1.475	110.6	110.3	110.7	109.1
2	AAAG	1.012	1.094	1.547	1.475	110.2	110.3	110.6	109.3
3	GAAG	1.012	1.094	1.546	1.474	109.9	110.4	110.4	109.4
4	GAAG′	1.012	1.094	1.546	1.474	109.9	110.4	110.4	109.4
5	AG′AA	1.012	1.094	1.549	1.475	111.1	111.6	111.0	109.0
6	G′G′AA	1.012	1.094	1.549	1.475	110.8	111.7	110.7	109.1
7	GG′AA	1.012	1.094	1.548	1.475	110.5	110.6	110.5	109.3
8	AG′AG′	1.012	1.094	1.549	1.475	110.8	111.6	110.9	109.1
9	G′G′AG′	1.012	1.094	1.548	1.475	110.6	111.7	110.8	109.3
10	GG′AG′	1.012	1.094	1.547	1.475	110.2	110.7	110.4	109.4
11	AG′AG	1.012	1.094	1.549	1.475	110.8	111.6	110.9	109.1
12	G′G′AG	1.012	1.094	1.548	1.475	110.5	111.7	110.6	109.1
13	GG′AG	1.012	1.094	1.547	1.475	110.2	110.7	110.4	109.4
14	AG′G′A	1.011	1.094	1.551	1.475	111.9	113.1	111.2	109.1
15	AG′G′G	1.011	1.094	1.551	1.475	111.6	113.1	111.1	109.2
16	AG′G′G	1.012	1.094	1.549	1.475	111.1	112.0	110.9	109.3
17	G′G′G′G′	1.011	1.094	1.550	1.475	111.4	113.3	110.5	109.4
18	G′G′G′G	1.012	1.094	1.549	1.475	110.9	112.1	110.6	109.4
19	GG′G′G	1.012	1.094	1.548	1.475	110.4	111.0	110.4	109.5
20	AG′GA	1.011	1.094	1.552	1.476	112.4	112.9	111.2	109.4
21	AG′GG′	1.012	1.094	1.550	1.475	111.9	112.5	110.6	109.1
22	AG′GG	1.011	1.094	1.551	1.476	111.9	112.9	111.0	109.1
23	G′G′GG′	1.012	1.094	1.550	1.475	111.5	112.6	110.5	109.3
24	G′G′GG	1.011	1.094	1.551	1.475	111.6	112.9	110.8	109.2
25	GG′GG′	1.012	1.094	1.549	1.475	110.9	111.4	110.3	109.4

developed for use with coordination complexes of diamines.[7]

The 25 conformers of tn were constructed by removal of a hydrogen atom from each methyl group of the four conformers of n-pentane, which were available from a previous study.[9] They were then minimised in the same PEF.

The nomenclature of the conformers may be exemplified by tn conformer No. 4 GAAG′: lone-pair1 *gauche* to C2, N1 *anti* to C3, C1 *anti* to N2, C2 minus- *gauche* to lone-pair2. For tn conformers No. 5–25 the names in Table 6 of Niketić and Rasmussen[7] represent the mirror images of the actual conformers.

Detailed results on energy terms for these two series are given by Niketić and Rasmussen,[7] and relative energies, free enthalpies and conformer populations are reproduced in Tables 2 and 5. Geometric details are given in Tables 3 and 6.

QUANTUM MECHANICAL CALCULATIONS

(a) Preliminary comments. Before exposing our quantum mechanical computations, a brief discussion on their interplay with CFF appears in order. As remarked by Gund *et al.*[22] *ab initio* is a deductive method which describes the average disposition of electrons about an assemblage of fixed nuclei, according to the Schrödinger equation: it therefore aims at the *electronic* level of the BO approximation. CFF is an inductive method, which finds the positions of atomic nuclei, through a common analytical representation of their motion in a field of fast-moving electrons: it therefore aims at the *nuclear* level of the BO approximation. PCILO, like all other semirigorous quantum methods containing empirical parameters, is partly inductive. This distinction should be borne in mind when comparing results on a class of molecules obtained with all of these approaches.

A second point which deserves careful attention is that such a comparison is hampered by the fact that

C–C–H	H–N–H	H–C–H	lp–N–C–C	N–C–C–C	C–C–C–N	C–C–N–lp	σ
109.5	109.7	108.7	−178.5	−180.0	180.0	178.5	2
109.5	109.6	108.8	−178.4	−179.9	−179.2	58.1	1
109.5	109.5	108.9	58.2	−179.2	−179.2	58.2	2
109.5	109.5	108.9	58.1	−179.2	179.2	−58.1	1
109.4	110.2	108.5	−173.5	−63.4	−175.9	179.7	1
109.4	109.5	108.5	−53.4	−65.5	−175.7	179.7	1
109.5	109.6	108.6	58.3	−61.0	−179.5	179.3	1
109.4	110.1	108.6	−173.4	−63.4	−176.6	−58.0	1
109.3	109.4	108.6	−53.4	−65.5	−176.4	−57.9	1
109.4	109.5	108.6	58.3	−61.1	179.8	−58.1	1
109.4	110.1	108.6	−173.5	−63.2	−174.0	58.2	1
109.3	109.4	108.7	−53.5	−65.3	−174.8	58.2	1
109.4	109.5	108.7	58.3	−61.0	−178.6	58.2	1
109.2	109.5	108.7	−173.1	−58.8	−59.7	−175.6	2
109.2	110.1	107.9	−172.9	−58.7	−66.7	−53.2	1
108.2	110.2	108.1	−173.4	−61.7	−56.6	58.3	1
109.1	109.4	108.0	−52.9	−60.1	−60.1	−52.9	2
109.3	109.4	108.2	−53.3	−63.6	−56.4	58.3	1
109.4	109.5	108.5	58.2	−60.2	−60.2	58.2	2
109.2	110.0	107.9	178.0	−93.6	60.9	173.2	1
109.1	109.5	108.1	−172.9	−63.3	71.9	−58.1	1
109.1	109.6	108.0	176.8	−92.4	59.3	48.1	1
109.1	109.3	108.3	−50.1	−64.7	71.8	−59.0	1
109.1	109.4	108.1	−59.3	−93.0	59.2	48.3	1
109.3	109.2	108.4	59.0	−64.1	64.1	−59.0	1

each method has its own equilibrium values for any kind of intramolecular force, which in general do not coincide with those of the others. For example, in the CFF case, equilibrium values are calculated through a parameter set chosen and fitted in such a way as to reproduce values derived from experimental measurements of conformational quantities with the best possible accuracy. For this reason, CFF predictions of molecular geometries are highly reliable. This is not the case with the PCILO method in CNDO Hamiltonian approximation, which tends to grossly overestimate bond lengths between heavy ($Z>1$) and hydrogen atoms, and to underestimate bond lengths between heavy atoms. Moreover, for a given displacement of a bond length from its equilibrium value, the PCILO restoring force is consistently stronger than with usual PEF's used in the CFF context.[23] In consequence, the narrow scatter of final bond lengths and angles observed in conformers minimised in a PEF, which gives very small contributions to stretching and bending energies, would give rise to fairly large contributions, should we analyse these geometries with PCILO, thus obscuring the order of stability due to torsion. Hence the need for a particular strategy in the PCILO computations, which will be discussed later. This phenomenon should be present in *ab initio* computations to a negligible extent only, since, in general, equilibrium values resulting from all-electron computations are in nice agreement with experiments. A direct computation on geometries produced by CFF minimisation is therefore meaningful.

The results are clearly subject to the errors inherent in this approximation. Complete *ab initio* energy minimisation with respect to all internal degrees of freedom should give the most accurate results, but this is at present too expensive. In addition, the use of the flexible rotor approach, instead of the rigid rotor, has in general a marked effect on the relative energies of maxima and minima of internal rotation curves, but affects little the energy differences between the various minima.

(b) PCILO calculations. There are three main

Table 7. Conformers of 1,3-propanediamine from PCILO calculations.

No.	Conformer	N–H	C–H	C–C	N–C	N–C–C	C–C–C	C–N–H
1	AAA	1.083	1.139	1.486	1.426	116.5	113.4	110.4
2	AAAG	1.083	1.140	1.485	1.424	114.5	114.0	110.3
3	GAAG	1.082	1.140	1.486	1.422	112.2	113.7	110.5
4	GAAG′	1.082	1.140	1.485	1.423	112.0	113.9	110.4
5	AG′AA	1.083	1.140	1.486	1.424	116.6	113.9	110.4
6	G′G′AA	1.083	1.140	1.486	1.424	114.4	114.0	110.5
7	GG′AA	1.084	1.139	1.486	1.424	114.4	113.9	110.5
8	AG′AG′	1.083	1.140	1.486	1.424	114.4	113.9	110.4
9	G′G′AG′	1.083	1.140	1.486	1.423	112.0	113.8	110.5
10	GG′AG′	1.083	1.140	1.486	1.423	111.9	113.5	110.6
11	AG′AG	1.084	1.140	1.485	1.424	114.4	114.1	110.4
12	G′G′AG	1.083	1.140	1.486	1.423	112.0	113.8	110.6
13	GG′AG	1.083	1.140	1.486	1.422	112.0	113.5	110.7
14	AG′G′A	1.084	1.139	1.487	1.424	116.9	114.2	110.6
15	AG′G′G′	1.085	1.139	1.486	1.424	114.7	114.4	110.4
16	AG′G′G	1.083	1.139	1.486	1.425	114.4	113.6	110.2
17	G′G′G′G′	1.083	1.140	1.487	1.423	112.5	114.1	110.6
18	G′G′G′G	1.083	1.139	1.486	1.423	112.1	113.5	110.4
19	GG′G′G	1.083	1.139	1.485	1.423	111.8	113.2	110.5
20	AG′GA	1.084	1.139	1.487	1.425	116.8	113.7	110.5
21	AG′GG′	1.085	1.139	1.486	1.426	114.3	113.3	110.0
22	AG′GG	1.083	1.139	1.486	1.426	114.5	113.8	110.4
23	G′G′GG′	1.085	1.139	1.488	1.424	112.0	113.3	110.2
24	G′G′GG	1.083	1.139	1.487	1.422	112.1	114.0	110.5
25	GG′GG′	1.083	1.139	1.486	1.424	112.0	113.0	110.5

reasons for the preference we give to PCILO over other quantum–mechanical techniques.

(1) This method, although semirigorous, was claimed to be extremely reliable for angular conformational analysis,[24] especially due to the fact that, thanks to a limited configuration interaction, it takes account, to some extent, of correlation effects.

(2) We have available a version[25] which is a special implementation of the standard QCPE version,[26] in that a minimisation routine, based on the Powell algorithm,[27] was inserted into the program, thus enabling it to compute directly not only the energy of a molecule in a certain geometry, but also the whole set of energies along the descent pathway towards the nearest minimum on the conformational energy hypersurface.

(3) Because it avoids the time-consuming SCF step, PCILO is much faster than any other quantum–mechanical program with comparable performances.

By now, our version of PCILO is dimensioned to treat a maximum of 9 different internal degrees of freedom simultaneously, whether bond lengths or valence angles or internal rotation angles. Since the number of variables both in en and in tn exceeds 9, a complete minimisation cannot be performed in a single run. We therefore devised a minimisation strategy based on a three–step procedure. Taking as starting geometries the coordinates produced by CFF minimisation, we first optimised all bond lengths (C–C, C–N, C–H, N–H) and four bond angles (N–C–C, N–C–H, C–N–H, C–C–H for en, and C–C–C, C–C–N, C–N–H, C–C–H for tn), with torsions kept fixed; then we optimised, on the conformations yielded by the first step, internal rotation angles at fixed valence geometry; finally a re-optimisation of bond lengths and angles was made. Results are given in Tables 4 and 7. The gain in energy is large in the first step (on average, 150 kJ mol^{-1} for en and 180 kJ mol^{-1} for tn) and small both in the second (2 kJ mol^{-1}) and in the third (0.1 kJ mol^{-1}). This is explained by the fact already mentioned, and illustrated quantitatively by Tables 3 and 4, and 6 and 7, that PCILO equilibrium values of bond lengths and, to a much smaller extent, of bond angles are different from those resulting

C–C–H	lp–N–C–C	N–C–C–C	C–C–C–N	C–C–N–lp	μ	μ(6–31G)
110.5	−179.5	−180.0	180.0	180.0	2.844	
110.4	180.0	−179.9	−179.2	60.0	2.149	2.028
110.6	60.0	−177.0	−178.7	60.0	1.611	
110.7	60.1	−177.0	−179.1	−60.1	3.485	
110.5	176.9	−63.1	−179.1	−179.5	2.444	
110.6	−61.7	−67.4	−179.3	−179.7	1.721	
110.5	61.5	−58.7	179.4	180.0	3.754	
110.6	178.8	−63.4	179.6	−60.5	2.058	
110.8	−60.1	−67.7	−176.8	−59.0	3.440	
110.7	60.5	−58.8	178.3	−59.6	1.798	
110.7	179.5	−63.0	−179.1	62.0	2.533	
110.8	−60.0	−67.4	−178.9	60.3	2.139	
110.8	59.5	−58.6	−178.5	60.3	2.236	2.014
110.5	−179.8	−57.7	−56.8	179.9	1.697	
110.6	−179.5	−57.9	−56.1	−59.3	2.435	
110.6	−179.7	−61.4	−53.2	60.6	3.627	
110.6	−58.9	−61.5	−59.4	−59.4	2.252	
110.7	−59.3	−65.6	−56.3	60.2	2.136	
110.8	58.9	−57.7	−56.5	60.0	2.032	1.703
110.7	179.8	−92.6	57.9	180.0	2.141	
110.7	163.4	−62.2	58.9	−55.2	4.013	
110.8	179.1	−91.5	55.6	57.5	1.945	
110.7	−68.3	−66.7	60.3	−55.5	2.570	2.006
110.9	−61.5	−94.6	55.8	55.5	3.259	
110.5	−61.0	−61.7	55.3	−59.9	2.190	

from CFF computations (N–H and C–H lengths are higher by *ca.* 7 and 4%, and C–C and C–N lengths are lower by *ca.* 4%).

(c) Ab initio *calculations. Ab initio* calculations were carried out using GAUSSIAN-70 with the extended 6–31 G basis set.[28] In addition to the ten conformers of en, four selected conformers of tn (Nos. 2, 13, 19 and 23), chosen in such a way as to be representative of all possible pairs of central rotations (AA, AG, GG, GG'), were analysed. The results are shown in Tables 2 and 5. The absolute energy of the most stable conformer of en (AGG') is −189.184101 hartree (0.2 hartree closer to the Hartree-Fock limit than the energy reached with the 4–31 G basis set[14]), and of tn (GG'AG) is −228.200043 hartree.

DISCUSSION

Energy and population. In Tables 2 and 5 we list also the relative energies ΔE corrected for statistical weight, and conformer populations based on these. In this way, statistical summation over internal degrees of freedom is left out, which introduces some error. This is not too serious, because the differences between conformers are modest, as judged from CFF calculations of populations based on ΔE and ΔG, and certainly much lower than the rather large energy differences emerging from the quantum mechanical calculations. Inclusion of statistical weights is imperative in the CFF context, less so in the PCILO and the *ab initio* because of the much higher energy differences.

One important difference between the CFF and the quantum mechanical calculations is the complete neglect of hydrogen bonding in the PEF of Niketić and Rasmussen,[7] leading to too high populations of C–C *anti* conformers. This is of no consequence in calculations on coordinated amines but unacceptable for free amines. The populations calculated from the PCILO results should be more reliable, though showing unrealistic predominance of some *G* conformations, a phenomenon already observed in n-butane.[29]

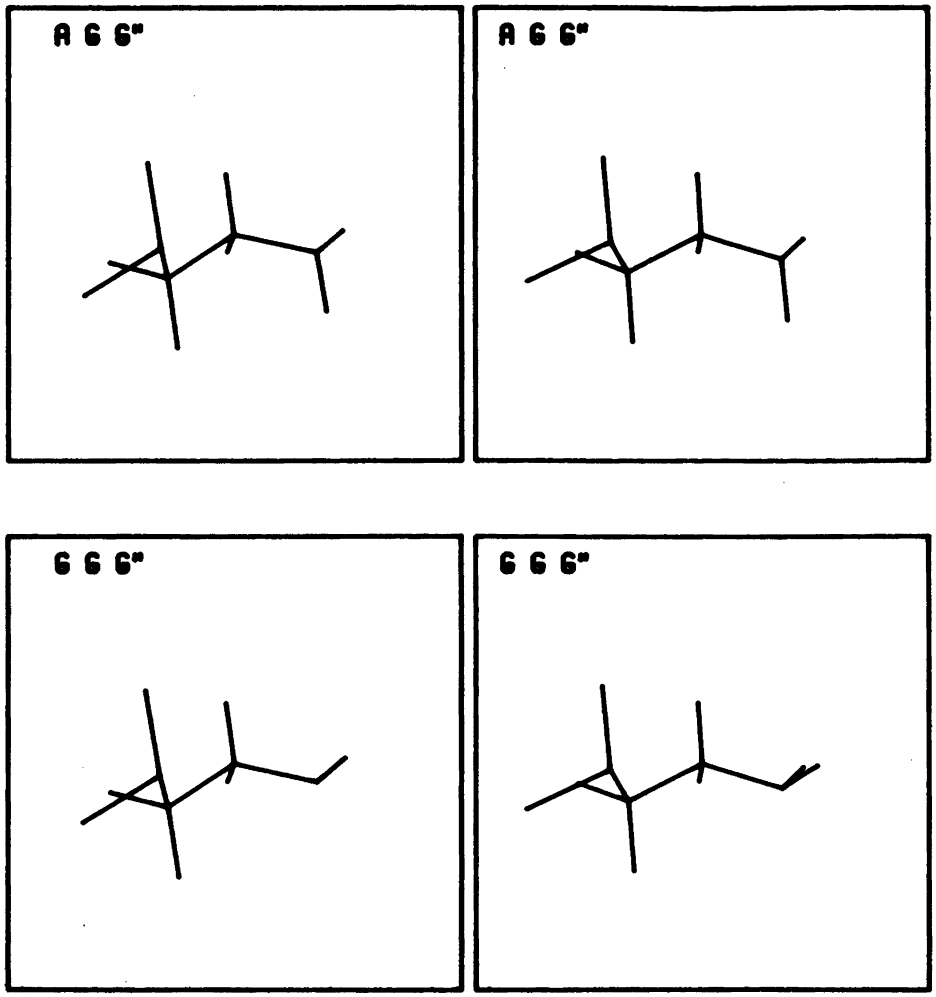

Fig. 1. The two most populated conformers of 1,2-ethanediamine.

For en we find that one conformer, No. 9 GGG′, contributes with almost half of the total to the equilibrium distribution. The overall C–C *gauche* : *anti* ratio is 0.84:0.16, in fair agreement with experimental data.

The distribution on *gauche* conformers is not quite correct in the PCILO results; only the predominance of No. 9 GGG′ is supported by experiment. In the CFF results there is a better balance between the two conformers actually found.

For tn, the pronounced population of one particular conformer is even more striking: No. 23 G′G′GG′ (or GGG′G) contributes two-thirds of the total.

For en, our CFF results on the low-energy conformers are at variance with the *ab initio* results, which are in fair agreement, except for the two conformers AGA and AGG, with those of Radom *et al.*[14] The discrepancy cannot be attributed to the use of different geometries.

Dipole moment and atomic charges. The PCILO dipole moments for the two conformers of en known from microwave measurements are 2.775 and 2.888 D, and the *ab initio* values are similar, 2.868 and 2.731 D, against the measured values 2.203 and 1.770 D. The population weighted dipole moment of en is 2.24 D (PCILO) and 2.55 D (*ab initio*); the experimental value is 1.90 D at 298 K in solution

extrapolated to zero concentration [30] and 1.96 D in the gas phase at 355 K.[31]

The population weighted PCILO dipole moment of tn is 2.52 D.

The gross atomic charges derived from the PCILO results are numerically much lower than from *ab initio* results; the averages for en are N −0.1422, C +0.1103, H(N) +0.0485, H(C) −0.0323 (PCILO) against N −0.809, C −0.118, H(N) +0.308, H(C) +0.156 (*ab initio*). Johansen and Hald[16] found N −0.7609, C −0.1400, H(N) +0.2645, H(C) +0.1859.

In tn, the charge distribution is almost the same as in en, except for the central carbon atom, +0.011 (PCILO), −0.295 (*ab initio*), and its hydrogens, −0.013 (PCILO), +0.151 (*ab initio*).

Geometry. When comparing calculated with measured geometry we see first of all that PCILO underestimates C−C and N−C bond lengths grossly, and that C−H and maybe N−H are similarly overestimated. In this respect, CFF is of course far more reliable, as it is based on empiry. For the N−C−C angle, CFF makes all conformers almost equal, whereas PCILO differentiates between the known GGG′, AGG′ and AAA in the correct sence, though giving too large values. If bond lengths could just be made proper, angles might be expected to fit perfectly.

The central torsional angle N−C−C−N is much too small in the PCILO results, but fitted to within the standard deviation by the CFF. Torsional angles in general show the same pattern in the CFF and PCILO series. The *gauche* angles are, without exception, numerically somewhat smaller in the PCILO than in the CFF results.

Stereo drawings of the two *gauche* conformers, Nos. 7 and 9, are shown in Fig. 1.

Just the same picture of the relative merits of CFF and PCILO emerges from the tn calculations. Stereo drawings of conformers Nos. 2 and 13 are shown in Fig. 2.

An observation concerning molecular symmetry may be of interest. Where the conformer name implies the presence of a symmetry element, here a twofold axis, this is, for en, not observed in any case. Nos. 1, 3, 5, 8 and 10 display lower symmetry than the theoretical C_2, and this applies to CFF as well as to PCILO calculations. Had it been the case only for CFF, we might have ascribed it to inadequacies in the PEF; as matters now stand, the effect may be real.

For tn, the picture is different. In the CFF results, Nos. 1 and 14 do not attain the theoretical C_2 symmetry, whereas Nos. 3, 17 and 19 do. In the PCILO results, no conformer has C_2 symmetry.

The deviation from C_2 symmetry is so small that it has not been taken into account in the summations over rotational degrees of freedom when calculating ΔG in the CFF context.

A comment of a general nature may be added here. It has been postulated by Ermer[32] that Newton minimisation always keeps a symmetry element present at the beginning of the minimisation. This property is certainly undesirable in a minimisation algorithm intended for general use. Therefore it is gratifying that the fault is absent from our algorithm, as has also been noted before.[7,9] Ermer's remark is of course not an error; it must pertain to a simpler algorithm which does not modify the Hessian matrix when it is not positive definite.

CONCLUSION

It would seem that CFF calculations give much better geometries than PCILO. This depends of course on the availability of an adequate PEF. In the absence of this, PCILO can give reasonable though crude estimates. If we take *ab initio* results as reference, CFF gives better relative energies than PCILO, whether we look at single conformers or at the "gross" conformations defined by chain atoms such as A and G for en. It is likely that introduction into the PEF used here[7] of an explicit term accounting for hydrogen bonding would lead to a decrease in the population of *anti* conformers and would thereby improve the agreement with *ab initio*. On this basis we predict that tn exists as an AG 'gross' conformer or as a mixture of AG and GG′.

Similar conclusions on the relative merits of CFF and PCILO were reached in work on two disaccharides.[33,34]

Acknowledgements. CFF calculations were performed at the Technical University Computer Centre and were paid with a grant from the Danish Natural Science Research Council. PCILO and GAUSSIAN-70 calculations were made at Dipartimento di Calcolo Chimico, Istituto Donegani; we wish to acknowledge the skilful assistance of Dr. Raimondo Scordamaglia. Drawings were made with MONSTER, property of Mr. Per Jacobi, Brede 50, DK-2800 Lyngby.

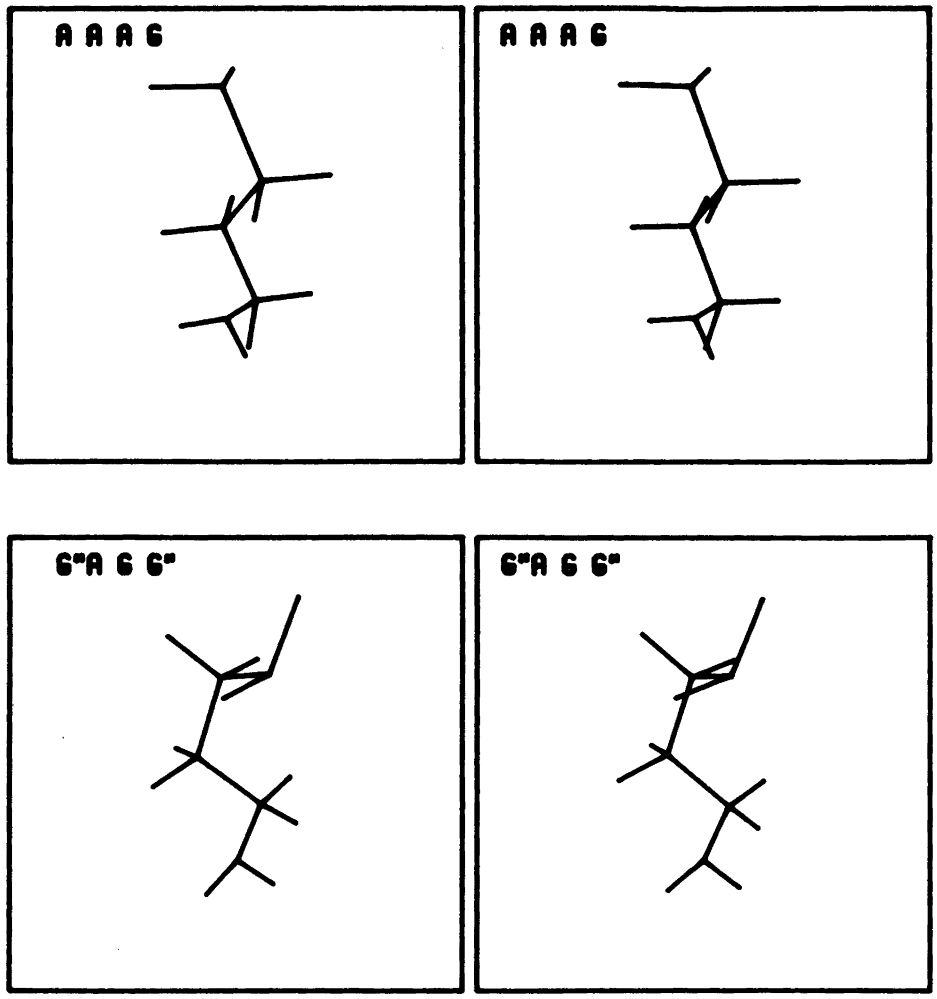

Fig. 2. Two of the most populated conformers of 1,3-propanediamine.

REFERENCES

1. Niketić, S. R. and Rasmussen, K. *The Consistent Force Field: A Documentation, Lecture Notes in Chemistry*, Vol. 3, Springer, Heidelberg 1977.
2. Tosi, C., Clementi, E. and Matsuoka, O. *Biopolymers 17* (1978) 51.
3. Melberg, S., Rasmussen, K., Scordamaglia, R. and Tosi, C. *Carbohydr. Res. 76* (1979) 23.
4. Tosi, C. and Lipari, G. *Theor. Chim. Acta 60* (1981) 41.
5. Clementi, E. *Determination of Liquid Water Structure. Coordination Numbers for Ions and Solvation for Biological Molecules, Lecture Notes in Chemistry*, Vol. 2, Springer, Heidelberg 1976, pp. 28–38.
6. Corongiu, G. and Clementi, E. *Gazz. Chim. Ital. 109* (1978) 273.
7. Niketić, S. R. and Rasmussen, K. *Acta Chem. Scand. A 35* (1981) 623 and references therein.
8. Hagler, A. T., Huler, E. and Lifson, S. *J. Am. Chem. Soc. 86* (1974) 5319.
9. Melberg, S. and Rasmussen, K. *J. Mol. Struct. 57* (1979) 215.
10. Jhon, M. S., Cho, U.-L., Kier, L. B. and Eyring, H. *Proc. Natl. Acad. Sci. U.S.A. 68* (1972) 121.
11. Hadjiliadis, N., Diot, A. and Theophanides, T. *Can. J. Chem. 50* (1972) 1005.
12. Graffeuil, M., Labarre, J.-F., Leibovici, C. and Theophanides, T. *J. Chim. Phys. 70* (1973) 1295.

13. Zahradnik, P., Masler, J. and Leska, J. *Chem. Zvesti 34* (1980) 291.
14. Radom, L., Lathan, W. A., Hehre, W. J. and Pople, J. A. *J. Am. Chem. Soc. 85* (1973) 693.
15. Cetina, R., Rubio, M. and Morea, M. A. *Rev. Latinoam. Quim. 9* (1977) 26.
16. Johansen, H. and Hald, N. C. P. *Private communication.*
17. Roos, B. and Siegbahn, P. *Theor. Chim. Acta 17* (1970) 209.
18. Huzinaga, S. *J. Chem. Phys. 42* (1965) 1293.
19. Yokozeki, A. and Kuchitsu, K. *Bull. Chem. Soc. Jpn. 44* (1971) 2926.
20. Marstokk, K.-M. and Møllendal, H. *J. Mol. Struct. 48* (1978) 221.
21. Jamet-Delcroix, S. *Acta Crystallogr. B 29* (1973) 977.
22. Gund, P., Andose, J. D., Rhodes, J. B. and Smith, G. M. *Science 209* (1980) 1425.
23. Tosi, C. and Saenger, W. *Chem. Phys. Lett. 90* (1982) 277.
24. Pullman, B. and Courrière, P. In Bergmann, E. D. and Pullman, B., Eds., *Proc. Jerusalem Symposia Quantum Chem. Biochem.*, Jerusalem Academic Press, Jerusalem 1972, Vol. V, p. 547.
25. Fantucci, P. C. and Tosi, C. *XVI National Congress of the Italian Association of Chemical Physics*, Abano Terme, Padua 1981, abstracts of papers, p. 33.
26. Claverie, P., Daudey, J. P., Diner, S., Giessner-Prettre, C., Gilbert, M., Langlet, J., Malrieu, J. P., Pincelli, U. and Pullman, B. *QCPE 10* (1972) 220.
27. Powell, M. J. D. *Comput. J. 7* (1964) 155.
28. Hehre, W. J., Lathan, W. A., Ditchfield, R., Newton, M. D. and Pople, J. A. *QCPE 10* (1974) 236.
29. Tosi, C. and Hilgenfeld, R. *Theor. Chim. Acta. In press.*
30. Trunel, P. *C. R. Acad. Sci. 203* (1936) 563; *Ann. Chim. 12* (1939) 93.
31. Zahn, C. T. *Phys. Z. 33* (1932) 525.
32. Ermer, O. *Tetrahedron 31* (1975) 1849.
33. Melberg, S. and Rasmussen, K. *Carbohydr. Res. 68* (1979) 27.
34. Melberg, S. and Rasmussen, K. *Carbohydr. Res. 71* (1979) 25.

Received April 20, 1982.

Acta Chemica Scandinavica A 37 (1983) 93–98

The Crystal Structure of $TiCu_2P$ and Its Relationship to the Structure of Mn_3As

WILDER CARRILLO-CABRERA

Institute of Chemistry, University of Uppsala, Box 531, S-751 21 Uppsala, Sweden

The crystal structure of $TiCu_2P$ has been determined from single-crystal X-ray diffractometer data. The structure has been refined to an $R(F^2)$ value of 0.077 without excluding any reflections. The space group is $I4_1/amd$ (No. 141). The tetragonal unit cell, of dimensions $a=3.5164(2)$ Å and $c=33.574(3)$ Å, contains eight formula units. $TiCu_2P$ contains structural units which are found in other transition-metal phosphides and arsenides. The $TiCu_2P$ structure type, which can be derived from the Mn_3As structure by a glide operation, belongs to the Cu_2Sb structure family. It is shown that $NdTe_3$ and Mn_3As, whose crystal structures have been described in different space groups, are geometrically equivalent (*i.e.* $NdTe_3$ is an antitype to Mn_3As).

In the course of a study of the Ti–Cu–P alloy system, a ternary phase with the approximate composition $TiCu_2P$ was found.[1] This paper presents a complete single-crystal X-ray determination of the structure of $TiCu_2P$, showing that the composition and the space group assignment given in Ref. 1 are correct. However, the structure is closely related to the Cu_2Sb family rather than $TiAl_3$, as suggested earlier.[1]

EXPERIMENTAL

Preparation. Titanium (Koch-Light Laboratories, Colnbrook, England, claimed purity 99.999 %) was arc-melted together with material of the composition $CuP_{0.15}$ (prepared by the sealed silica tube method[1] at 800 °C), in an atmosphere of purified argon. The solidified melt (approx. 2.5 g, nominal composition $Ti_{0.10}Cu_{0.78}P_{0.12}$) thus prepared was found to contain the TiP,[2] Cu_3P (low temperature form[3]) and Cu phases. Subsequently the ternary sample was heat-treated at 800 °C for 84 h and plate-like crystals and aggregates of $TiCu_2P$ were then formed (TiP was also present in the copper matrix). After dissolving the matrix in nitric acid, a very thin plate-like crystal was selected for collecting the X-ray intensity data. It was limited by the {100} and {001} faces and its dimensions were approximately $56 \times 48 \times 3$ μm (its smallest extension being along the *c*-axis). Larger crystals were obtained by longer heating periods at temperatures between 800 and 950 °C, but the quality of the crystals was poorer.

Significant variations of the unit cell dimensions of $TiCu_2P$ were observed, indicating a range of homogeneity. The unit cell volume varied from 414.64(2) Å^3 (Ref. 1), for a specimen in an alloy ($Ti_{0.07}Cu_{0.78}P_{0.15}$; 900 °C, 11d) with nominal Ti/P = 0.47, to 414.89(4) Å^3 for a specimen in an alloy ($Ti_{0.33}Cu_{0.33}P_{0.33}$; 900 °C, 14d) with nominal Ti/P = 1.00. The latter volume value is slightly smaller than that in Table 1 (415.14(6) Å^3), which was measured on a specimen in a more copper rich alloy with nominal Ti/P = 0.83, that was however, heat-treated at 800 °C.

X-Ray diffraction measurements and data reduction. The cell dimensions were determined using a Guinier-Hägg focusing camera with $CuK\alpha_1$ radiation ($\lambda=1.540598$ Å) and semiconductor grade silicon ($a=5.431065$ Å)[4] as calibration standard, and least-squares refined using the local program CELNE.[5] The equipment and single-crystal X-ray data collection procedure have been described previously.[6] Intensities of all the reflections were measured up to $2\theta=25°$ to check the space group conditions and absorption (as well as possible extinction) correction. For $25° < 2\theta < 100°$ only reflections with h, k, and l positive and $h+k+l=2n$ were recorded. The instrumental stability and crystal setting were checked by remeasuring three test reflections. Totally 1766 reflections were measured. After checking the conditions of the space group, reflections that should be systematically absent were

0302-4377/83 $2.50

deleted [all of them had $I < 3\sigma(I)$]. In order to correct for absorption and extinction effects only the reflections having identical indices (*e.g.* test reflections) were averaged. The X-ray data were thus reduced to 1082 reflections. The intensities were corrected for Lorentz and polarization effects.

After applying absorption and extinction corrections, equivalent reflections were averaged, which reduced the material to 538 non-equivalent reflections. Correction for absorption was applied using the Gaussian grid method and a linear absorption coefficient of 252 cm^{-1} (calculated with the mass absorption coefficients given in Ref. 7). The minimum and maximum transmission factors obtained were 0.373 and 0.907. Extinction effects were taken care of by a method devised by Coppens and Hamilton.[8]

The numerical calculations were performed using IBM 1800 and NORD 100 computers. Crystallographic programs used for the structure analysis are described in Ref. 5.

STRUCTURE DETERMINATION AND REFINEMENT

Inspection of Weissenberg films, taken with crystals rotating about the *a* and *c* axes, indicated and *I*-centred tetragonal cell. Furthermore, they showed systematic absences for *hk*0 and *hhl* reflections corresponding to the $I4_1/amd$ (No. 141) space group. A closer look at the diffractometer data revealed additional conditions for the *hkl* reflections: $2h+l=2n+1$ or $4n$, which indicates 8(*e*), 4(*b*) and 4(*a*) as possible atom sites. These special conditions are also valid for the non-centrosymmetric space group $I4_1md$ with the atoms at the 4(*a*) site. The centrosymmetric alternative was chosen and finally confirmed in the refinement.

The very strong (0 0 16) reflection and the long *c*-axis indicated that the atoms must be essentially confined to planes $\sim c/16$ apart. Moreover, the very weak (0 0 8) reflection indicated that the sets of atomic layers which are $\sim c/8$ apart scatter almost equally. The unit cell volume and the approximate composition $TiCu_2P$ suggested a unit cell content of 32 atoms (16 copper, 8 titanium and 8 phosphorus). These facts, coupled with interatomic distance considerations and the possible similarity to other known structures were utilized to construct trial models of the structure.

A reasonable model of the structure could be constructed with all the atoms at 8(*e*) sites. A series of refinements on F and F^2 was then started. A full-matrix least-squares program[5] and complex neutral-atoms scattering factors were used.[7] Extinction effects were discernible and an isotropic correction was applied.[8] The following 10 parameters were initially refined: one scale factor, one isotropic extinction parameter, four positional parameters and four isotropic temperature factors. The refinement, based on F^2 converged to an $R(F^2)$ value of 0.094 [$R_w(F^2)=0.093$].

Incorporation of anisotropic temperature factors for three atoms (three further parameters were refined) resulted in a significant drop in the *R*-values: the refinement on F^2 with anisotropic temperature factors for Cu(1), Cu(2) and P (atoms in Ti site were found to vibrate isotropically) converged to $R(F^2)=0.088$ and $R_w(F^2)=0.088$ for the whole material (1082 reflections). The standard deviation of an observation of unit weight[9] was $S=1.08$. A ΔR plot[10] gave a least-squares line with a slope of 1.04 and an intercept of -0.05 (on the expected ΔR axis) in the interval $|R|<4.0$. The largest extinction correction was 32%. An internal consistency factor (defined in Ref. 6) for symmetry related reflections (126 reflections, of which 20 were non-equivalent) with $2\theta < 25°$ decreased from 3.90 % (after absorption correction only) to 3.06 %, after extinction correction. The agreement indices used in the text have been defined elsewhere.[11] The function minimized in the refinement on F^2 was $\Sigma w(F_o^2 - F_c^2)^2$. Weights were assigned to the reflections according to the formula $w^{-1} = \sigma_c^2(F_o^2) + (pF_o^2)^2$, where $\sigma_c(F_o^2)$ is based on counting statistics and the empirical factor p, which modifies w to obtain a satisfactory weight analysis, was set to 0.020.

When occupancies were allowed to vary, no significant deviations from full occupancy were found. The composition of the crystal investigated, selected from a copper-rich alloy, is thus $TiCu_2P$.

A final refinement on F^2 using averaged extinction-corrected data (538 reflections) gave $R(F^2)=0.077$ and $R_w(F^2)=0.059$. At this stage a final Fourier difference synthesis was calculated. It exhibited no positive or negative peaks exceeding 6 % of a phosphorus maximum in the corresponding F_o synthesis.

A list of observed and calculated structure factors can be obtained on request from the Institute of Chemistry, University of Uppsala, Uppsala, Sweden. Final structure data are presented in Table 1. Corresponding interatomic distances are given in Table 2.

Table 1. Final structural data[a] for $TiCu_2P$ (from refinement based on F^2), including anisotropic thermal parameters[b] $U_{ij}(\times 10^4)$ Å^2. Standard deviations are given in parantheses.

Space group: $I4_1/amd$ (No. 141)
Unit cell dimensions: $a = 3.5164(2)$ Å, $c = 33.574(3)$ Å;
$V = 415.14(6)$ Å^3; $Z = 8$.
Calculated density: 6.59 g/cm^3

Atom	z	U_{11}	U_{33}
Cu(1)	0.09753(3)	63(3)	94(4)
Cu(2)	0.40468(3)	66(3)	85(3)
P	0.29612(5)	36(5)	60(6)
Ti	0.22198(3)	[c]	

[a] All the atoms lie in the special position 8(*e*) and the origin at 4*m*2. [b] The anisotropic temperature factor is of the form: $\exp[-2\pi^2 U_{11}(h^2+k^2)a^{*2} - 2\pi^2 U_{33} l^2 c^{*2}]$; $U_{22} = U_{11}$, $U_{12} = U_{13} = U_{23} = 0$. [c] $U_{iso} = 58(2) \times 10^{-4}$ Å^2.

Table 2. Interatomic distances in $TiCu_2P$. The table shows all M – P and P – P distances less than 3.65 Å and M – M distances less than 4.20 Å. Standard deviations within parentheses.

Cu(1) – 2P	2.464(1)	Cu(2) – 2P	2.412(1)
– 4Cu(2)	2.488(0)	– 4Cu(1)	2.488(0)
– 2Cu(1)	2.548(1)	– 2Cu(1)	2.602(1)
– 2Cu(2)	2.602(1)	– 2Cu(2)	2.658(1)
– 2Ti	2.922(1)	– 2Ti	2.863(1)
– 4Cu(1)	3.516(0)	– 4Cu(2)	3.516(0)
– Ti	4.178(1)	– P	3.645(2)
P – 2Cu(2)	2.412(1)	Ti – P	2.489(2)
– 2Cu(1)	2.464(1)	– 4P	2.560(1)
– Ti	2.489(2)	– 2Cu(2)	2.863(1)
– 4Ti	2.560(1)	– 2Cu(1)	2.922(1)
		– 4Ti	3.118(1)
– P	3.516(0)	– 4Ti	3.516(0)
– Cu(2)	3.645(2)		
		– Cu(1)	4.178(1)

DESCRIPTION AND DISCUSSION OF THE $TiCu_2P$ STRUCTURE

A projection of the structure along the *a*-axis is illustrated in Fig. 1. The projection of the atomic environment of Cu(1) [being identical to that of Cu(2)] and the corresponding one for Ti are outlined in Fig. 1. It should be mentioned that neighbours which are situated at distances 22 % larger than the corresponding atomic radius sum are not considered to belong to the near environment of the central atom. The Goldschmidt metal radius (12 C.N.) and the tetrahedral covalent radius of phosphorus have been used to calculated the radius sums.[12,13] In Table 2, a gap in the list of interatomic distances indicates this borderline. The copper and titanium atoms have thus 12 and 17 nearest neighbours. High coordination numbers (= number of nearest neighbours) for the larger atoms (Ti) as in this metal-rich compound (with radius ratios $r_P/r_{Ti} = 0.76$, $r_P/r_{Cu} = 0.86$, $r_{Cu}/r_{Ti} = 0.88$) occur in other transition-metal silicides, phosphides and arsenides as well (*e.g.* Ti_7P_4 (Nb_7P_4) and related compounds[14]). It should be emphasized that the coordination of copper in the structure of pure copper metal (face-centred cubic, A1 type) is a

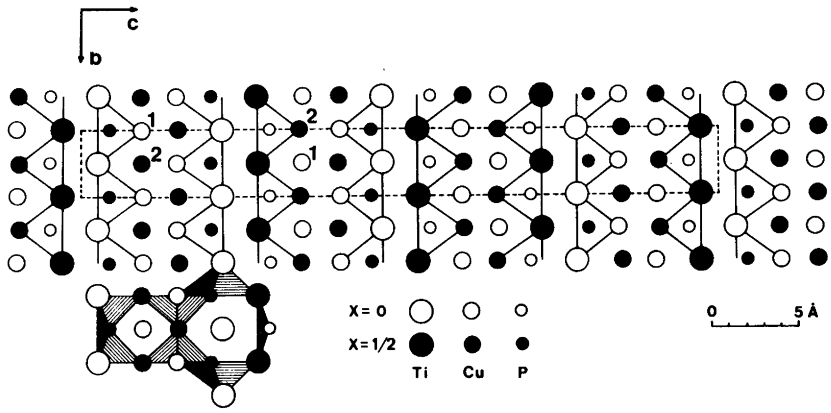

Fig. 1. Projection of the structure of $TiCu_2P$ as viewed along the *a*-axis.

regular cubo-octahedron, which is distorted in $TiCu_2P$ due to the replacement of four copper atoms by two titaniums and two phosphorus atoms.

Each phosphorus atom has nine metal neighbours. Eight of them are located at the corners of a somewhat distorted Archimedean or square-antiprism (the square formed by the four copper atoms has a side $1/\sqrt{2}$ shorter than that formed by the four titaniums) and the remaining titanium atom is situated outside the larger square face of the antiprism. The atomic environment of phosphorus can also be described as a tricapped trigonal prism with three atoms (2Cu+1Ti) outside the quadrilateral faces of the prism (this environment occurs frequently for *p*-elements in compounds with transition metals [15]). Only the triangular faces of the prism or square-antiprism are indicated in the projection of $TiCu_2P$ in Fig. 1.

From Table 2 it is evident that only the Ti–P distances along the c-axis and the Cu–Cu distances along [110] direction are shorter than the radius sum of 2.55 and 2.56 Å, respectively. All the Cu–P, Cu–Ti and Ti–Ti distances are larger than the corresponding radius sum (2.38, 2.73 and 2.90 Å, respectively.

The structure of $TiCu_2P$ can also be described as a stacking of 16 atomic layers. Eight of these are practically planar and formed by copper atoms only (Cu layers) and the other eight are puckered, with

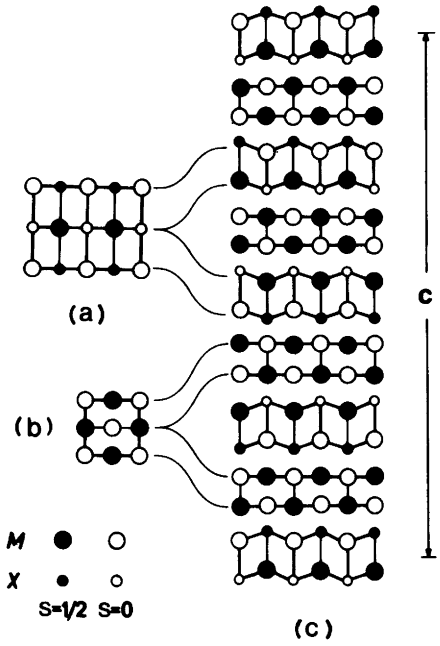

Fig. 2. Comparison of the projection of the structures of (a) NaCl (B1 type) along the [110] direction and (b) Cu (face-centred cubic, A1 type) along the *a*-axis with that of (c) $TiCu_2P$ along the *a*-axis. M = metal, X = non-metal and *s* is the fractional height along the direction of projection.

Table 3. Crystallographic data for Mn_3As.

Space group *Pmmn* (Ref. 18)					Space group *Bmmb* (this work)				
Atom	Position	*x*	*y*	*z*	Atom	Position	*x*	*y*	*z*
Mn(1)	2*a*	0	0	0.1935	Mn(1,4)	4*c*	0	1/4	0.0565
Mn(4)	2*b*	0	1/2	0.3065					
Mn(2)	2*a*	0	0	−0.1935	Mn(2,5)	4*c*	0	1/4	0.4435
Mn(5)	2*b*	0	1/2	−0.3065					
Mn(3)	2*a*	0	0	−0.4345	Mn(3,6)	4*c*	0	1/4	0.6845
Mn(6)	2*b*	0	1/2	−0.0655					
As(1)	2*a*	0	0	0.409	As(1,2)	4*c*	0	1/4	0.841
As(2)	2*b*	0	1/2	0.091					

an equal number of titanium and phosphorus atoms (Ti–P layers). By examination of the form of packing of the layers, fragments of the face-centred cubic (Cu, A1 type) and NaCl (B1 type, ZrP phase[16] also adopts this type) structures can be identified. The width of the Cu-like slices is half the unit cell length of the Cu structure and the NaCl-like fragments are layers of distorted half-cells of the NaCl type as demonstrated in Fig. 2. The two types of fragments are packed together, alternating along the *c*-axis of $TiCu_2P$.

The $TiCu_2P$ structure constitutes a new structure type. Considering the composition and the metallic lustre of its crystals, the compound is likely to be metallic.

The main features of the structure of $TiCu_2P$ presented in Figs. 1 and 2c, reveal a striking resemblance to Fe_2As[17] (C38, Cu_2Sb type[17]) and related structures: Mn_3As,[18] $NdTe_3$,[19] Nd_2Te_5[20] and La_2Sb[21] (Ti_2Bi type[22]). Since the relationship of the latter structures to the C38 type has been established in the earlier descriptions of the structures, we restrict this part of the discussion to describe the relationship between $TiCu_2P$ and Mn_3As structures only. It may first be mentioned that the structure of Mn_3As is in fact the antitype to that of $NdTe_3$, although they have been described in different space groups. In the structure of Mn_3As (*Pmmn*, Ref. 18) the atoms are either at 2(*a*) or 2(*b*) (see left part of Table 3). By first adding 3/4 to all *y*-coordinates and then subtracting 1/4 from all *z*-coordinates (*i.e.* shifting the origin to $0,-3/4,1/4$), it appears that two positions [one 2(*a*) and one 2(*b*)] in *Pmmn* correspond to only one position, 4(*c*), in *Bmmb* (identical with *Cmcm*, No. 63). Thus it seems more appropriate to describe the Mn_3As structure in the space group *Bmmb* (see right part of Table 3).

The structures of Mn_3As (anti-$NdTe_3$) and $TiCu_2P$ are compared in Fig. 3, as viewed along the *a*-axis. The figure shows how the position of six common subunits (denoted by C_1) changes in the two structures. This subunit consists of one unit cell of the Fe_2As structure. In Fig. 3, it can also be distinguished that $TiCu_2P$ and Mn_3As contain another common subunit (denoted by C_2) which coincides with one unit cell of the Mn_3As structure. Each cell represents one *slab* (formed by interconnected Fe_2As or Mn_3As cells). The $TiCu_2P$ structure can thus be derived from the Mn_3As structure through a glide operation. In this manner, these structures can be regarded as different stackings of *slabs* of Fe_2As (C_1 type) or Mn_3As (C_2 type)

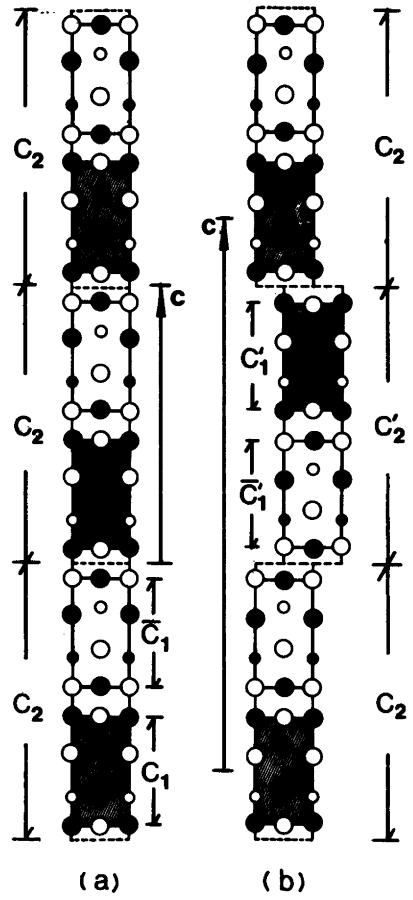

Fig. 3. Structural relationships between (a) Mn_3As (anti $NdTe_3$, *Bmmb* setting) and (b) $TiCu_2P$ structures, as viewed along the *a*-axis. The notations are consistent with those given for Fig. 2.

unit cells. In Table 4, the respective stacking sequence and the slip between adjacent *slabs* (C_1 or C_2) in the structures of Fe_2As, Mn_3As and $TiCu_2P$ are given.

There are other structures, for instance Mo_8P_5 and Cr_3C_2,[23,24] which contain other kinds of structural fragments common to Fe_2As (C38) structure type. The structural fragments in common are built up of atomic layers, which are perpendicular to the *a* (or *b*) directions in Fe_2As.

Acknowledgements. The author is indebted to Professor S. Rundqvist and Docent T. Lundström for valuable discussions and for their criticism of

Table 4. Stacking sequence of C_1-slabs (or C_2-slabs) of Fe_2As (or Mn_3As) unit cells in the Fe_2As, Mn_3As and $TiCu_2P$ structures.

Structure	Stacking sequence[a]	Glide between slabs		
		Slab pairs	Slip magnit.	Slip direct.
Fe_2As	$\underline{C_1C_1}\ldots$	C_1C_1	0	–
Mn_3As	$\underline{C_1\bar{C}_1C_1\bar{C}_1}\ldots$	$C_1\bar{C}_1$	$a/2$	[100]
	or $\underline{C_2C_2}\ldots$	C_2C_2	0	–
$TiCu_2P$	$\underline{C_1\bar{C}_1C_1'\bar{C}_1'}C_1\bar{C}_1C_1'\bar{C}_1'\ldots$	$C_1\bar{C}_1$ or $C_1'\bar{C}_1'$	$a/2$	[100]
		$\bar{C}_1C_1'$ or $\bar{C}_1'C_1$	$b/2$	[010]
	or $\underline{C_2C_2'}C_2C_2'\ldots$	C_2C_2'	$(a+b)/2$	[110]

[a] C_1 = *slab* perpendicular to the c-axis of Fe_2As with a width equal to c_{Fe_2As}. $\bar{C}_1$, C_1' or $\bar{C}_1'$ = *slabs* displaced relative to C_1 perpendicular to the stacking (c) direction. C_2 = *slab* perpendicular to the c-axis of Mn_3As with a width equal to c_{Mn_3As}. C_2' = *slab* displaced relative to C_2 perpendicular to the stacking (c) direction.

the manuscript. The financial support of the Swedish Natural Science Research Council is gratefully acknowledged.

REFERENCES

1. Carrillo-Cabrera, W. and Lundström, T. *Acta Chem. Scand. A 33* (1979) 401.
2. Snell, P.-O. *Acta Chem. Scand. 21* (1967) 1773.
3. Olofsson, O. *Acta Chem. Scand. 26* (1972) 2777.
4. Deslettes, R. D. and Henis, A. *Phys. Rev. Lett. 31* (1973) 972.
5. Lundgren, J.-O., Ed., *Crystallographic Computer Programs*, Institute of Chemistry, University of Uppsala, Uppsala 1975. UUIC-B13-04-02.
6. Carrillo-Cabrera, W. and Lundström, T. *Acta Chem. Scand. A 34* (1980) 415.
7. *International Tables for X-Ray Crystallography*, Kynoch Press, Birmingham 1974, Vol. 4.
8. Coppens, P. and Hamilton, W. C. *Acta Crystallogr. A 26* (1970) 71.
9. Abrahams, S. C. *Acta Crystallogr. A 25* (1969) 165.
10. Abrahams, S. C. and Keve, E. T. *Acta Crystallogr. 27* (1971) 157.
11. Carrillo-Cabrera, W. and Lundström, T. *Acta Chem. Scand. A 35* (1981) 545.
12. Laves, F. *Theory of Alloy Phases*, Am. Soc. Metals, Cleveland, Ohio 1956.
13. Pauling, L. *Nature of the Chemical Bond*, 3rd Ed., University Press, Ithaca, New York 1960.
14. Carrillo-Cabrera, W. *Acta Chem. Scand. A 36* (1982) 563.
15. Aronsson, B., Lundström, T. and Rundqvist, S. *Borides, Silicides and Phosphides*, Methuen, London 1965.
16. Irani, K. S. and Gingerich, K. A. *J. Phys. Chem. Solids 24* (1963 1153.
17. Elander, M., Hägg, G. and Westgren, A. *Ark. Kemi Mineral. Geol.* B 12 (1936) 1.
18. Nowotny, H., Funk, R. and Pesl, J. *Monatsh. Chem. 82* (1951) 513.
19. Nordling, B. K. and Steinfink, H. *Inorg. Chem. 5* (1966) 1488.
20. Pardo, M.-P. and Flahaut, J. *Bull. Soc. Chim. Fr.* (1967) 3658.
21. Stassen, W. N., Sato, M. and Calvert, L. D. *Acta Crystallogr. B 26* (1970) 1534.
22. Auer-Welsbach, H., Nowotny, H. and Kohl, A. *Monatsh. Chem. 89* (1958) 154.
23. Johnsson, T. *Acta Chem. Scand.* 26 (1972) 365.
24. Rundqvist, S. and Runnsjö, G. *Acta Chem. Scand. 23* (1969) 1191.

Received April 27, 1982.

Acta Chemica Scandinavica A 37 (1983) 99 – 103

The Solubility of Hydrocarbons in Water

AASE HVIDT

Department of Chemistry, H. C. Ørsted Institute, Universitetsparken 5, DK-2100 Copenhagen Ø, Denmark

The dissolution of a hydrocarbon, R, in water is tentatively considered as a two-step process: (1) The transfer to water, and (2) the solvation. The solvation is regarded as a relaxation to the equilibrium $R + n\ H_2O \rightleftharpoons R(H_2O)_n$ and as such it enhances the solubility. The low solubility of hydrocarbons in water is ascribed to the strong attractive forces between water molecules in the liquid state. The increase of the solubility with decreasing temperature, characteristic of hydrocarbons in water, is explained by displacements of the solvation equilibrium with changes in the temperature ($\Delta H^{\ominus}_{solv} < 0$). Estimated values of thermodynamic parameters which, according to the considered model, determine the solubility are given for methane and ethane.

Hydrocarbons are sparingly soluble in water and, below some given temperature, the solubility of a hydrocarbon decreases with increasing temperature as illustrated in Fig. 1 for methane and ethane. The negative enthalpy change of solution (calculated from the temperature dependence of the solubility), compared with the positive change in standard Gibbs energy (the low solubility) indicates that entropy-low water structures are introduced by the nonpolar solute species. This striking feature of water as a solvent was first pointed out by Frank and Evans,[1] and it has led to the currently accepted view that the solubility of hydrocarbons in water is low *because* the solute particles introduce entropy-low structures in the water.[2-5]

An alternative approach to the thermodynamics of aqueous solutions of hydrocarbons[6] has, however, led to the conclusion that the solubility of nonpolar molecules in water is low due to the positive 'normal' enthalpy of mixing components of different nature, and that the formation of entropy-low (and energy-low, 'icelike'[1]) structures in the solvent *promotes* the solubility.[6-8] This latter point of view is shared by the present author and is elaborated on in this paper.

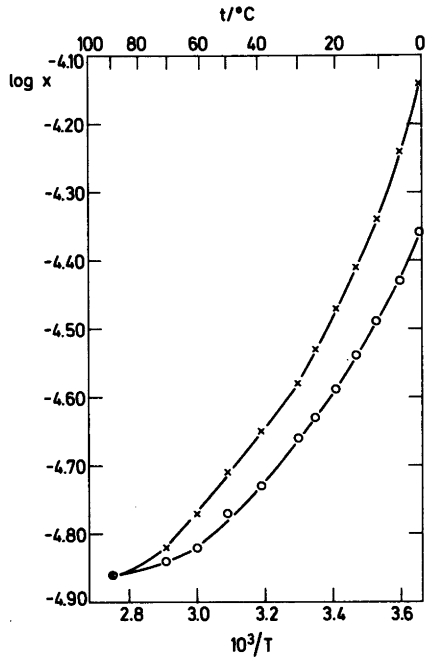

Fig. 1. The temperature dependence of the solubility of methane (○), or ethane (×) in water. x is the mol fraction of the hydrocarbon in an aqueous solution in equilibrium with the hydrocarbon gas at atmospheric pressure. The data is from Ref. 14.

In the following an aqueous solution of a hydrocarbon, R, in water is regarded as a binary mixture, and the interaction of the components in the mixture is considered as a "chemical" equilibrium

0302-4377/83 $2.50

$$R + n\,H_2O \rightleftharpoons R(H_2O)_n \qquad (1)$$

for which $\Delta H^{\ominus} < 0$, $\Delta S^{\ominus} < 0$, and $\Delta V^{\ominus} > 0$. $R(H_2O)_n$ denotes an R molecule surrounded by a solvation sphere of n water molecules with a structure more 'icelike' than the (average) structure of bulk water.

An outstanding discussion of the role of solvent structure in solution theory in terms of radial and angular dependence of the molecular correlation function is presented in Ref. 9. However, this discussion is beyond the scope of the primitive, thermodynamic model of aqueous hydrocarbon solutions considered here. The aim of the present paper is to illustrate that the temperature dependence of the solubility of hydrocarbons in water is in accordance with the existence of solute – solvent interactions of the type described in eqn. (1). Such equilibria enhance the solubility of hydrocarbons in water, while the low solubility is ascribed to strong attractive forces between water molecules in the liquid state.[4,10]

THE MODEL

The dissolution of a hydrocarbon, R, in water is regarded as a two-step process: (1) The mixing of the components (R and H_2O), and (2) the structural relaxation to the equilibrium state (1), *i.e.* the hydrophobic solvation. Thus the change in Gibbs energy of the dissolution is expressed as a sum of two terms; eqn. (2)

$$\Delta G = \Delta G_{mix} + \Delta G_{solv} \qquad (2)$$

The first step in the dissolution process – before solvation occurs – is considered as the formation of a simple ('regular'), binary mixture;[11] ΔG_{solv} (< 0) is the change in Gibbs energy of the relaxation of this mixture to the equilibrium state (1). The main difference between the model here discussed and the two-step model proposed by Ben-Naim,[13] and discussed in Ref. 9, is the consideration of the change in Gibbs energy of the solvation process.

'Regular' solutions. The molar Gibbs energy of a binary mixture in which molecules of the same size are (nearly) randomly distributed – a so-called 'regular' solution[11] – may be expressed as eqn. (3).

$$G = x_1(\mu_1^* + RT\ln x_1) + x_o(\mu_o^* + RT\ln x_o) + (\Delta\varepsilon L)x_1x_o \qquad (3)$$

In eqn. (3) x denotes mol fraction, and the subscripts 1 and o refer to the components. The superscript * indicates the pure, liquid state. ε is the intermolecular energy, $\Delta\varepsilon = \varepsilon_{o1} - 1/2(\varepsilon_{11} + \varepsilon_o)$, and L is the Avogadro constant.

The chemical potential of the components of the mixture, obtained from eqn. (3), is as eqn. (4).

$$\mu_i = \mu_i^* + RT\ln x_i + (\Delta\varepsilon L)(1 - x_i)^2,\ i = 0,\ 1 \qquad (4)$$

The expression (4) has been generalized to include mixtures of molecules of different sizes.[13] The molar Gibbs energy of a solution of a polymer (an r-mer) in a monomer solvent (the component o) is expressed as eqn. (5)

$$G = x_r(\mu_r^* + RT\ln\phi_r) + x_o(\mu_o^* + RT\ln\phi_o) + (\Delta\varepsilon L)x_o\phi_r \qquad (5)$$

In eqn. (5) ϕ denotes volume fraction, $\phi_r = rx_r/(rx_r + x_o)$. It is assumed that the polymer molecules behave as random chains, and $\Delta\varepsilon$ is defined for solvent molecules and polymer segments. For $r = 1$, eqn. (5) is identical with eqn. (3).

In (polymer) solutions in which the component o is present in large excess the chemical potential of a monomer is given by eqn. (6).

$$\mu_1 \cong \mu_1^{\ominus} + RT\ln\phi_1;\ \mu_1^{\ominus} = \mu_1^* + (\Delta\varepsilon L) \qquad (6)$$

In the following, the $R(H_2O)_n$ complex in eqn. (1) is considered as a polymer. The volume of the complex is assumed to be equal to the sum of the volumes of the $(n+1)$ constituent monomers.

The hydrophobic solvation. Let us now assume that subscript 1 in eqn. (3) refers to a hydrocarbon, and o to water, so that eqn. (3) is the molar Gibbs energy of a 'regular' mixture of the nonsolvated hydrocarbon and water. If the components interact according to eqn. (1), a relaxation of the mixture to the equilibrium state (the solvation) takes place.

If p is the extent of the solvation

$$p = \frac{[R(H_2O)_n]}{[R] + [R(H_2O)_n]}, \qquad (7)$$

the mol fraction, x, and the volume fraction, ϕ, of the species R, H_2O and $R(H_2O)_n$ at equilibrium are

$$x_R = x'_1 = \frac{(1-p)x_1}{1-pnx_1}; \quad \phi_R = \phi'_1 = (1-p)x_1$$

$$x_{H_2O} = x'_o = 1 - \frac{x_1}{1-pnx_1}$$
$$\phi_{H_2O} = \phi'_o = 1-(1+pn)x_1 \qquad (8)$$

$$x_{R(H_2O)_n} = \frac{px_1}{1-pnx_1}; \quad \phi_{R(H_2O)_n} = p(n+1)x_1$$

In eqn. (8) x_1 is the stoichiometric mol fraction of the hydrocarbon.

The change in Gibbs energy of the relaxation, ΔG_{solv}, obtained from eqn. (6) is

$$\Delta G_{solv} = RT[x_1 \ln(\phi'_1/x_1) + x_o \ln(\phi'_o/x_o)]. \qquad (9)$$

The Gibbs energy of an aqueous solution of a hydrocarbon. The molar Gibbs energy of a solution of a hydrocarbon in water, obtained from eqns. (3) and (9), is

$$G = x_1[\mu_1^* + RT\ln\phi'_1] + x_o[\mu_o^* + RT\ln\phi'_o] + x_1x_o\Delta H^\ominus_{trf} \qquad (10)$$

ϕ'_1 and ϕ'_o are given in eqn. (8), and $\Delta H^\ominus_{trf} = \Delta\varepsilon L$ is the enthalpy change of the transfer of one mol of the hydrocarbon from the pure liquid state to the unsolvated state at infinite dilution in water. Due to the exceptionally strong attraction between the water molecules in liquid water ($\varepsilon_{oo} < \varepsilon_{o1}, \varepsilon_{11}$ (<0)), $\Delta\varepsilon = \varepsilon_{o1} - 1/2(\varepsilon_{oo} + \varepsilon_{11}) > 0$, so $\Delta H^\ominus_{trf}$ is positive.

The molar excess Gibbs energy of the solution, G^E, is

$$G^E = RT[x_1 \ln(\phi'_1/x_1) + x_o \ln(\phi'_o/x_o)] + x_1x_o\Delta H^\ominus_{trf}$$
$$<0 \qquad <0 \qquad >0 \qquad (11)$$

The sign of the terms in eqn. (11) is indicated below the equation in order to illustrate – in accordance with Refs. 6 and 7 – that the immiscibility of hydrocarbons and water (the positive value of G^E) is due to energy effects. The contribution to the Gibbs energy of the solutions from the hydrophobic solvation is negative.

If $pnx_1 \ll x_o$ – a condition presumably met in aqueous solutions of hydrocarbons – the chemical potential of the hydrocarbon is

$$\mu_1 \cong \mu_1^* + RT\ln\phi'_1 + \Delta H^\ominus_{trf}$$
$$= \mu_1^* + RT\ln(1-p)x_1 + \Delta_{trf}^\ominus \qquad (12)$$

p varies with the concentration and the temperature. If K is the equilibrium constant of the equilibrium (1) in terms of mol fractions

$$K = \frac{p}{1-p\,x^n_{H_2O}}; \quad p = \frac{K\,x^n_{H_2O}}{1+K\,x^n_{H_2O}}, \qquad (13)$$

we have

$$\left(\frac{\partial p}{\partial \ln x_{H_2O}}\right)_T = np(1-p) \quad (>0) \qquad (14)$$

and

$$\left(\frac{\partial p}{\partial T^{-1}}\right)_{x_{H_2O}} = \left(\frac{\partial p}{\partial \ln K}\right)_{x_{H_2O}} \frac{d\ln K}{dT^{-1}} =$$
$$-p(1-p)\frac{\Delta H^\ominus_{solv}}{R} (>0). \qquad (15)$$

$\Delta H^\ominus_{solv}$ is $\Delta H^\ominus$ of the solvation equilibrium (1).

The enthalpy of an aqueous solution of a hydrocarbon. In accordance with eqn. (2) the molar enthalpy of an aqueous solution of a hydrocarbon is expressed as

$$H = x_1H_1^* + x_oH_o^* + \Delta H_{mix} + \Delta H_{solv}, \qquad (16)$$

where

$$\Delta H_{mix} = x_1(1-x_1)\Delta H^\ominus_{trf}$$

and

$$\Delta H_{solv} = px_1\,\Delta H^\ominus_{solv}$$

For $x_1 \ll 1$, the apparent molar enthalpy of the hydrocarbon is

$$H_1 \cong H_1^* + \Delta H^\ominus_{trf} + p\Delta H^\ominus_{solv} \qquad (17)$$

COMPARISON BETWEEN THE MODEL AND EXPERIMENTAL DATA

The decrease with increasing temperature of the solubility of hydrocarbons in water,[1,4,5,14] as well as

direct calorimetric measurements of the heat of solution of liquid hydrocarbons in water,[15] show that below room temperature the enthalpy of solution of hydrocarbons in water is negative. For the model described in the preceding paragraphs it means that in eqn. (17) $\Delta H^{\ominus}_{trf} + \Delta H^{\ominus}_{solv} < 0$. Hydrogen bonds between water molecules are broken in the transfer process in the creation of a cavity in water holding a hydrocarbon molecule ($\Delta H^{\ominus}_{trf} > 0$), but more bonds, or stronger bonds, seem to be formed in a solvation sphere.

The heat capacity of the aqueous hydrocarbon solutions studied is, however, so large[4,5,14] that a minimum in the solubility is to be expected at higher temperatures. The existence of such a minimum is demonstrated in calculations of the solubility of hypothetical liquid hydrocarbons.[6] The calculations in Ref. 6 are based on available data on the solubility

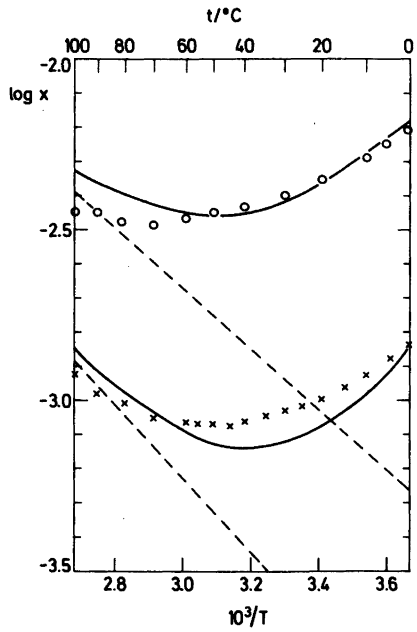

Fig. 2. The temperature dependence of the solubility in water of hypothetical liquid hydrocarbons, methane (○) or ethane (×). x is the mol fraction of the hydrocarbon in an aqueous solution in equilibrium with the pure liquid hydrocarbon. The points are replotted from Fig. 1 in Ref. 6.

The curves are calculated according to eqn. (18) for the values of the thermodynamic parameters given in Table 1. The dashed lines represent the estimated solubility of the nonsolvated hydrocarbons.

of the hydrocarbons at atmospheric pressure, and results obtained for methane and ethane are shown in Fig. 2.

In Ref. 6 and in Fig. 2 the solubility of a hydrocarbon in water is defined as the mol fraction, $x_{1,sat}$, of the hydrocarbon in an aqueous solution in equilibrium with the pure liquid hydrocarbon. From eqn. (12) one obtains

$$\log x_{1,sat} = -\log(1-p_{sat}) - \Delta H^{\ominus}_{trf}/RT\ln 10 \qquad (18)$$

In order to estimate approximate values of thermodynamic parameters of the two-step model considered here eqn. (18) has tentatively been fitted to the data from Ref. 6. Considering the low solubility of hydrocarbons in water, the concentration dependence of p [eqn. (14)] is ignored so that in the calculations p_{sat} is calculated for $x_{H_2O}=1$, *i.e.* $(1-p_{sat})=(1+K)^{-1}$, where $K = \exp(-\Delta H^{\ominus}_{solv}/RT + \Delta S^{\ominus}_{solv}/R)$. The values obtained of the model parameters are reported in Table 1, and the accordance between the model and the available data is illustrated in Fig. 2. In this figure the full curves are calculated according to eqn. (18) for the values of the parameters given in Table 1. The dashed lines represent the solubility of the nonsolvated hydrocarbons,

$$\log x = -\Delta H^{A}_{trf}/RT\ln 10.$$

Fig. 2 illustrates the extent to which the simple model described here is able to account for the observed temperature dependence of the solubility of hydrocarbons in water. The large values reported in Table 1 of enthalpy and entropy changes following the dissolution of hydrocarbons in water are in accordance with the notion that enthalpy −entropy compensation phenomena are a ubiquitous property of water.[16] $\Delta G^{\ominus}_{solv}$, *i.e.* the change in Gibbs energy when n mol of water are transferred from pure water to the solvation spheres of 1 mol of a hydrocarbon in water, calculated from the values in Table 1, is, at room temperature

Table 1. Values of thermodynamic parameters used in calculations from eqn. (18) of the curves in Fig. 2.

	Methane	Ethane
$\Delta H^{\ominus}_{trf}$/kJ mol^{-1}	17	20.5
$\Delta H^{\ominus}_{solv}$/kJ mol^{-1}	−35	−42
$(\Delta H^{\ominus}_{solv}/\Delta S^{\ominus}_{solv})$/K	323	313

$$\Delta G^{\ominus,298K}_{solv} = \begin{cases} -2.7\ \text{kJ mol}^{-1} & (CH_4) \\ -2.0\ \text{kJ mol}^{-1} & (C_2H_6) \end{cases}$$

The corresponding values of the extent of the solvation at infinite dilution is

$$p(x_{H_2O} = 1;\ 298\ \text{K}) = \begin{cases} 0.75\ (CH_4) \\ 0.69\ (C_2H_6) \end{cases}$$

The p values (<1) indicate that the nonpolar molecules fluctuate between solvated and non-solvated states. This interpretation of the experimental data is in accordance with the conception[3] that solvation spheres around nonpolar molecules appear as 'flickering clusters'. Consideration of the concentration dependence of the volume and the heat capacity of aqueous solutions has led to a similar conception of the solvation of nonpolar groups of amphiphilic molecules dissolved in water.[17,18] The probability of finding a nonpolar group in the solvated state decreases with increasing solute concentration and with increasing temperature; the solvation can be observed experimentally only in very dilute aqueous solutions.

The most important point of the present discussion of the solubility of hydrocarbons in water is the support of the conclusion[6-8] that the formation of 'icelike' water structures around nonpolar solute particles, just as any other type of solvation of solute molecules, enhances the solubility.

REFERENCES

1. Frank, H. S. and Evans, M. W. *J. Chem. Phys. 13* (1945) 507.
2. Kauzmann, W. *Adv. Protein Chem. 14* (1959) 1.
3. Némethy, G. and Scheraga, H. A. *J. Phys. Chem. 66* (1962) 1773.
4. Tanford, C. *The Hydrophobic Effect*, 2nd Ed., Wiley, New York 1980.
5. Franks, F. In Jones, M. N., Ed., *Biochemical Thermodynamics*, Elsevier, Amsterdam 1979 p. 15.
6. Shinoda, K. and Fujihira, M. *Bull. Chem. Soc. Jpn. 41* (1968) 2612.
7. Patterson, D. and Barbe, M. *J. Phys. Chem. 80* (1976) 2435.
8. Klotz, I. M. In *Protein Structure and Function (Brookhaven Symposia in Biology)* 1960 (No. 13) 25.
9. Marcelja, S., Mitchell, D. J., Ninham, B. W. and Sculley, M. M. *J. Chem. Soc. Faraday Trans. 2, 73* (1977) 630.
10. Hartley, G. S. *Aqueous Solutions of Paraffin-Chain Salts*, Hermann, Paris 1936, p. 44.
11. McGlashan, M. L. *Chemical Thermodynamics*, Academic, New York 1979, Chapter 16.
12. Ben-Naim, A. *Hydrophobic Interactions*, Plenum, New York 1980.
13. Flory, P. J. *Principles of Polymer Chemistry*, Cornell University Press, Ithaca 1953, Chapter 12.
14. Lax, E. *Taschenbuch für Chemiker und Physiker, 3. Aufl. Band I*, Springer, Berlin 1967, p. 1205.
15. Gill, S. J., Nichols, N. F. and Wadsö, I. *J. Chem. Thermodyn. 8* (1976) 445.
16. Lumry, R. and Rajender, S. *Biopolymers 9* (1970) 1125.
17. Hvidt, Aa. *Biochim. Biophys. Acta 537* (1978) 374.
18. Hvidt, Aa. *Pol. J. Chem. 54* (1980) 1967.

Received May 5, 1982.

Acta Chemica Scandinavica A 37 (1983) 105—115

A Stopped-flow Polarimetric Study of the Hydroxide Ion Catalyzed Mutarotation of a Series of Glucopyranoses in Water

H. NIELSEN * and P. E. SØRENSEN

Chemistry Department A, Building 207, The Technical University of Denmark, DK-2800 Lyngby, Denmark

The construction and use of a polarimeter unit for a Durrum stopped-flow spectrophotometer is described. It is demonstrated that the apparatus is a good tool for investigating kinetic details of fast optical rotatory phenomena such as the hydroxide ion catalyzed mutarotation of sugars. In a series of glucopyranoses, glucose differs remarkably from its substituted analogues, probably due to the dissociation of two hydroxyl groups as the hydroxide ion concentration is increased. Acidity constants for the sugars are determined conductometrically, but the changes in pK with substituents are too small to justify any quantitative conclusions from Brønsted plots. However, the experimental data do suggest coupled proton transfer in water catalysis, whereas for the hydroxide ion a stepwise mechanism, involving formation of the sugar anion – and for glucose also to some extent the dianion – as an intermediate, is more likely. First order rate constants for the mutarotation of some of the sugar anions and apparent catalytic constants for the hydroxide ion are presented. For glucose, k_{G^-} (25 °C)=2.2 s^{-1} and k_{HO^-} (25 °C)=90±10 dm^3 mol^{-1} s^{-1}. Our kinetic data were best explained by assuming the second dissociation constants of glucose to be no larger than $10^{-14.6}$ and those for the substituted compounds to be considerably smaller.

The mutarotation of monosaccharides such as glucose and its various analogues is no doubt one of the most studied types of reaction in all physical organic chemistry. Change in optical rotation with time for freshly prepared solutions of glucose in water was reported for the first time by Dubrunfaut in 1846,[1] and the mutarotation reaction has played a major role in chemical kinetics ever since, in particular with respect to studies of mechanism in acid-base catalysis. The strong development in this area is obvious from a number of monographs and review articles from the early part of the century and from more recent contributions by Isbell and Pigman.[2] However, it is interesting to note that although an enormous amount of experimental work has indeed been done, kinetic investigations are almost totally limited by the rate capacity of relatively slow techniques such as conventional polarimetry, dilatometry, *etc.*, and the behaviour of relatively strong basic catalysts in mutarotation – requiring faster techniques – has not yet been subject to direct systematic studies. This may seem surprising because stopped-flow polarimeters have now been available for quite some time and have been relatively widely applied in chemical kinetics, though mainly to biological systems. The proper function of a stopped-flow polarimeter is often checked by measuring the rate of glucose mutarotation in *e.g.* 0.5 M aqueous sodium hydroxide, but usually no further attention is paid to the kinetics of the reaction itself. Thus, in testing their stopped-flow polarimeter, Goodall and Cross[3] correctly report a decreasing catalytic constant for the hydroxide ion with increasing concentration of this catalyst, but, as we shall see later, interpret this effect in an ambiguous way as being due to gradual conversion of glucose to its *less* reactive anionic form.

* Present address: H. Lundbeck & Co. A/S, Department of Biochemistry, Ottiliavej 7–9, DK-2500 Valby, Denmark.

0302-4377/83 $2.50

Extended kinetic studies of sugar mutarotation in strong basic media are of interest for several reasons: (1) Catalytic constants for hydroxide ions and similar species are predominantly known from conventional studies and exhibit large scatter. More direct determinations using a stopped-flow technique are likely to produce more precise values for this constant. (2) Catalytic constants for hydroxide seem to vary with hydroxide ion concentration at high pH.[3] This effect may be reasonably explained by the conversion of the sugar to its anion. (3) In strong alkaline solution several sugar hydroxyl groups are likely to dissociate and thereby affect kinetics. The qualitative and quantitative extent of this behaviour is practically unknown. (4) Considerable extensions of the existing Brønsted plots for base-catalyzed mutarotation of glucose[4] and other sugars are possible if catalytic constants for stronger bases are determined. Brønsted plots covering large ΔpK-ranges often exhibit curvature and thereby reveal important information about reaction mechanisms such as changes in coupling between relevant degrees of freedom or shifts in rate-determining steps. (5) The diagnostic importance of kinetic deuterium isotope effects as a function of ΔpK in studies of mechanisms in acid-base catalysis is well-known, and no reliable data have so far been reported for mutarotation catalyzed by relatively strong bases.

In the present paper we report kinetic data primarily concerning the hydroxide ion catalyzed mutarotation of various glucoses (1–3 in the previous paragraph). A paper dealing with base catalysis in general of these reactions and corresponding kinetic deuterium isotope effects (4–5 in the previous paragraph) will be published shortly.[5]

EXPERIMENTAL

Materials. The following glucopyranoses were used without further purification: α-D-(+)-glucopyranose (α-glucose)(BDH Chemicals, Analar); 2-amino-2-deoxy-α-glucose·HCl (α-glucosamine·HCl)(BDH Biochemicals); 2-acetamino-2-deoxy-α-glucose (*N*-acetyl-α-glucosamine)(BDH Biochemicals); 2-benzamido-2-deoxy-α-glucose (*N*-benzoyl-α-glucosamine) (Sigma Chemical Company); 4,6-*O*-ethylidene-α-glucose (EGA-CHEMIE); 2-*O*-methyl-β- and 3-*O*-methyl-α-glucose were synthesized at the Institute of Organic Chemistry, Technical University of Denmark, and kindly supplied by Professor Chr. Pedersen (the compounds had m.p. 152–153 and 161–162 °C, respectively, and were identified by NMR spectroscopy); 2,3,4,6-tetra-*O*-methyl-α-glucose (TMG) was prepared and tested as described earlier.[6] Other chemicals were of Analar grade, and millipore water from a Milli-Q2 system was used throughout.

Acidity constants. The pK_a values of the anomeric hydroxyl group of the various sugars apart from α-glucosamine·HCl, were determined by a conductivity method described by Bell and Onwood.[7] The electrode unit (CDC104) of a

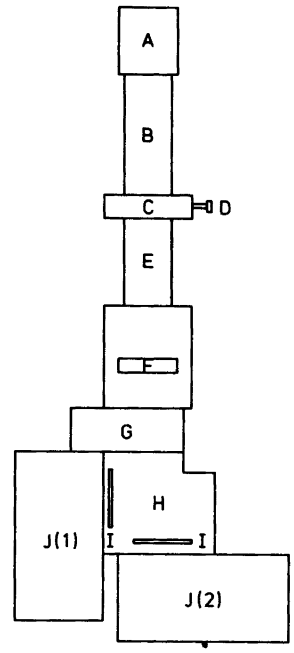

Fig. 1. Schematic drawing of the polarimeter unit fitted on a Durrum stopped-flow apparatus. A. Lamp house with mercury lamp (Hanau, st. 48). B+E. Light-tubes with lenses (Spindler and Hoyer, type 311115 biconvex, 50 mm focal length). C + I. Polarizers (B. Halle, type Glan-Thomsen-II, 7.5 mm aperture). D+I. Polarizer adjustment. F. Interchangable mercury line interference filter (Oriel Corp., type G-522-4358 (435.8 nm) or G-522-5461 (548.1 nm)). G. Reaction cell housing of the Durrum stopped-flow spectrophotometer (20 mm light path). H. Beam splitter (Spindler and Hoyer, type 344161). J. Photodetector houses provided with lenses (Spindler and Hoyer, type 314811, 40 mm focal length) and detectors (EMI, type 9660B).

Radiometer CDM201 conductivity meter was placed in a thermostated solution of the sugar (in excess) in sodium hydroxide, and the conductivity was measured. The solution was carefully protected from atmospheric carbon dioxide by a stream of nitrogen.

Kinetic measurements. Mutarotation rates in pure water were measured by a Perkin-Elmer 141 polarimeter fitted with a 10 cm thermostated reaction cell and data acquisition system. The typical concentration of sugar was 0.01 M, and the 365 nm filter was used in most cases for the polarized light, resulting in relatively large changes in optical rotations.

Mutarotation rates of sugars in alkaline media (pH > *ca.* 10) could conveniently be measured by mixing freshly prepared solutions of the sugar in water (usually 0.08 M) with aqueous sodium hydroxide in a Durrum stopped-flow apparatus equipped with a polarimeter unit built in our laboratory. This unit is shown schematically in Fig. 1, where G denotes the original reaction cell housing of the Durrum instrument. Several stopped-flow polarimeters have been reported in the literature[3,8,9] and may now be regarded as a standard type of apparatus. The application of a dual detector system (Fig. 1) yields enhanced signals when the ratio of the two detector outputs is analyzed. With the polarizers adjusted according to well-defined rules[10] the output voltage from each detector (v_1 and v_2) is closely proportional to the angle of the optical rotation of the solution in the reaction cell. The performance of the apparatus is demonstrated in Fig. 2, where *ca.* two hundred measurements of $(v_1-v_2)/v_1$ – recorded by a data acquisition system – are plotted against time for a reacting solution of glucose. The solid line (hardly visible) is a computer-fitted (least squares) exponential.

A Radiometer pH-meter 28 equipped with calomel electrode K401 and glass electrode G202 B was used for pH-measurements. Standard borate buffer and saturated aqueous calcium hydroxide (25 °C)[11] were used for calibration and pH-values were corrected for errors due to sodium ion where necessary.

All experiments were carried out at 25.0± 0.2 °C and ionic strengths were adjusted to 0.2 by sodium chloride where possible in kinetic runs.

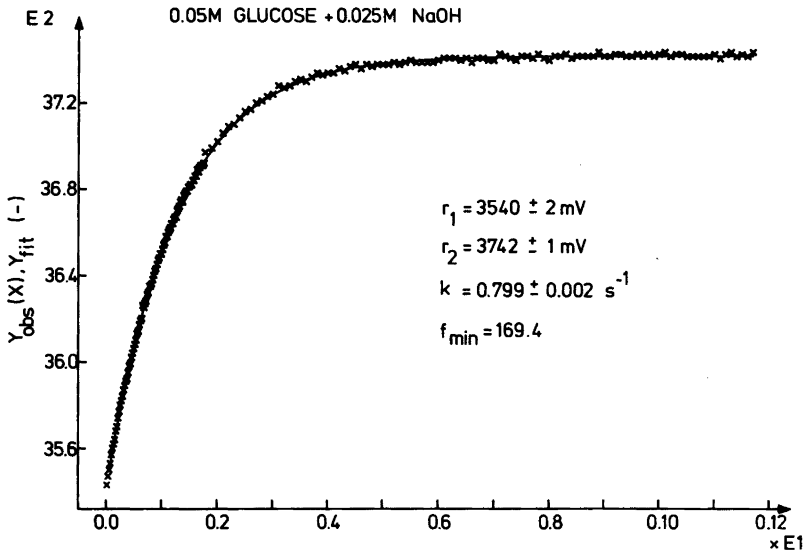

Fig. 2. Plot of output signal ($(v_1-v_2)/v_1$ from J(1) and J(2) in Fig. 1) against time, obtained by mixing 0.05 M glucose with 0.025 M NaOH (0.4 M in NaCl) in the stopped-flow polarimeter at 25 °C and λ=435.8 nm. The observed total change in voltage (~200 mV) correspond to a change of approximately .04 degrees in optical rotation of the sugar solution in the cell. The solid curve represents a computed function (exponential) $r'_t=(r_1-r_2)\exp(-kt)+r_2$ where r_1 (initial voltage), r_2 (final voltage) and k (first order rate constant) are determined by an iterative procedure to give the best fit with the observed points (r_t, t), which means minimization of $f=\Sigma(r_t'-r_t)^2$. The calculated values of r_1, r_2, k and f_{min} in the present case are given in the plot.

Table 1. Dependence of conductivity on sugar concentration in a 2–3×10^{-3} M solution of sodium hydroxide at 25.0 °C. I. Glucose. II. 3-*O*-Methylglucose. III. 2-*O*-Methylglucose. IV. *N*-Acetylglucosamine. V. *N*-Benzoylglucosamine. VI. 4,6-*O*-Ethylideneglucose. VII. TMG.

[Sugar]/ mol dm^{-3}	$10^6 \times \kappa$/ohm^{-1}cm^{-1} I	II	III	IV	V	VI	VII
0.0000	607.6	637.0	646.8	612.5	597.8	399.8	612.5
0.0110	448.8	459.6	461.1	395.9	383.2	242.9	431.2
0.0125	434.4	441.0	450.8	381.2	370.4	232.6	406.7
0.0143	419.4	424.3	433.2	363.6	352.8	221.2	395.9
0.0167	400.8	409.6	411.6	347.9	335.2	210.6	374.4
0.0200	377.3	385.1	392.0	328.3	318.5	198.9	354.8
0.0250	354.8	360.6	364.6	304.8	299.9	185.6	330.3
0.0333	332.2	333.2	342.0	284.2	277.3	170.5	305.8
0.0500	297.9	302.8	307.7	254.8	254.8	157.4	273.4
0.1000	250.9	254.8	259.7	220.5	205.8	135.7	227.4
K_1/K_w [a]	50(5)	60(5)	60(5)	88(5)	93(5)	109(5)	63(5)
pK_1	12.30(4)	12.22(3)	12.22(3)	12.06(3)	12.03(2)	11.96(2)	12.20(3)

[a] Negative intercept in eqn. (1) (Fig. 3).

Table 2. Observed first-order rate constants for mutarotation of some of the sugars in Table 1 in sodium hydroxide solution [Sugar]=4×10^{-2} M, *I* adjusted to 0.20 (NaCl) where [HO^-] <0.20 M, temp.=25.0±0.2 °C, λ=435.8 nm. Each constant is an average from at least 3 single runs (7 for glucose). Numbering of the sugars refer to Table 1.

$10^2 \times$[HO^-]/[a] mol dm^{-3}	$10^2 \times k_{obs}$/ s^{-1}	$10^2 \times$[HO^-]/[a] mol dm^{-2}	$10^2 \times k_{obs}$/ s^{-1}
Glucose (I)			
0.038	3.61(9)	20	420(5)
0.067	6.63(6)	22	475(6)
0.098	9.90(6)	24	510(8)
0.600	35.0(4)	25	500(7)
1.01	70.1(4)	27	500(10)
2.01	120(4)	29	595(11)
3.0	150(3)	30	550(5)
4.0	200(8)	32	605(6)
6.2	215(7)	34	645(5)
8.0	240(6)	35	600(7)
8.4	250(5)	37	650(5)
9.6	300(6)	39	700(6)
11.0	315(4)	40	700(5)
13.2	360(8)	42	725(9)
13.8	362(8)	44	875(15)
15	375(9)	45	750(9)
17	395(4)	48	770(12)
18	400(6)	50	850(9)

Table 2. Continued.

N-Acetylglucosamine (IV)			
0.172	26.5(5)	36	119(1)
0.600	56(1)	46	122(3)
1.78	84.7(4)	56	121(2)
5.12	108(2)	66	125(1)
6.0	106(1)	76	128(6)
16	114(1)	86	114(2)
26	116(1)	96	116(2)
2-*O*-Methylglucose (III) [b]			
0.229	14(2)	26	138(10)
0.389	27(4)	36	148(15)
0.954	54(3)	46	198(34)
2.24	74(3)	56	152(32)
5.3	116(5)		
11.7	138(11)		
3-*O*-Methylglucose (II)			
0.229	26(1)	12.6	229(8)
0.407	45(1)	26	240(2)
0.976	89(1)	36	247(3)
2.09	135(3)	46	265(3)
5.12	196(1)	56	277(1)
4,6-*O*-Ethylideneglucose (VI)			
0.051	950(30)	0.544	6900(400)
0.105	1500(100)	1.74	10700(500)
0.166	3700(700)	4.49	17700(1600)

[a] Below 0.2 M, hydroxide ion concentrations were obtained from the pH of the reacting solutions and an activity coefficient (f_{HO^-}) calculated according to Kielland.[16] The higher values are derived by subtracting 0.04 M, due to neutralization by the sugar, from the actual hydroxide ion concentration. There was good agreement between calculations from either method in the transition area and the uncertainties are in all cases believed to be less than 5–10 %. [b] At low hydroxide ion concentrations this compound behaves "normally" but the relatively large errors associated with k_{obs} at higher [HO^-] reflect a substantial decrease in total change of optical rotation under these conditions, the reason for which is not understood.

RESULTS AND DISCUSSION

Acidity constants. It has been shown that the acidity constant of a weak acid such as formaldehyde hydrate can be determined fairly accurately by measuring the conductivity of solutions where the acid is partly neutralized by sodium hydroxide.[7] Under circumstances where less than a few percent neutralization has taken place the following expression holds:

$$1/a = \frac{K_1 K_w^{-1}(l_{HO^-} - l_{A^-})}{l_{Na^+} + l_{HO^-}} \cdot \frac{\kappa_{NaOH}}{\kappa_{NaOH} - \kappa} - K_1 K_w^{-1} \quad (1)$$

where a denotes the total concentration of acid; l_{OH^-}, l_{A^-} and l_{Na^+} are specific conductivities (mobilities) of the various ions in solution (A^- is the acid anion); κ_{NaOH} and κ are conductivities of the aqueous sodium hydroxide before and after addition of acid, and K_1 the acidity constant for HA. Eqn. (1) predicts linearity between $1/a$ and $\kappa_{NaOH}/(\kappa_{NaOH} - \kappa)$ where $K_1 K_w^{-1}$ is given by the intercept. Bell and Onwood [7] found the pK_1 of formaldehyde hydrate to be 13.27 at 25 °C. By repetition of their experiment we obtained a value of 13.26 and, furthermore, found that the method is also readily applicable to sugars such as the glucoses investigated in this paper. Table 1 contains conductivity measurements for these compounds.

Fig. 3 shows plots * according to eqn. (1) for these measurements and the resulting pK_1 values are given in Table 1. Because of the relatively alkaline conditions under which the pK_a values are determined – leading to equilibrated solutions in all cases – these are weighted means of pK_1 (α-form) and pK_1 (β-form) in each case.

The acidity constant K_1 for glucose was determined as early as 1900 by Osaka,[12] who found pK_1=11.89 at 25 °C. Our value of 12.30 for glucose is in excellent agreement with pK_1=12.28 found as a weighted average of pK_1 (α-form)=12.47 and pK_1 (β-form)=12.17 by Los and Simpson [13] as the result of reliable potentiometric studies. For TMG Wit *et al.*[14] have recently reported a pK_1 of 12.2 determined by ^{13}C NMR ([TMG]=0.53 M, temp. 3–5 °C) compared with our value of 12.20 at 25 °C for this compound.

For the remaining sugars in Table 3, only the pK_1 of glucosamine is available in the literature (12.66 and 12.34 for α- and β-forms, respectively, at 5 °C).[15] We were not able to investigate this species by the conductivity method, due to the presence of HCl, but a pK_1 value of approximately 12.0 (mean) is obtained at 25 °C from the data at 5 °C by the van't Hoff equation if ΔH for the acid dissociation is taken as 42 kJ mol^{-1}, which is the experimental value found for glucose.[13] This result seems reasonable compared to $pK \sim 12.05$ for the two substituted glucosamines.

Kinetics. Kinetic results from measurements of the spontaneous (water catalyzed) mutarotation of the sugars by conventional polarimetry are shown in Table 4 and those for hydroxide solutions by stopped-flow technique in Table 2.

All data from Table 2 are plotted in Fig. 4, from which the non-linearity of each plot is

* For some of the sugars considerable curvature of the plots were observed – especially at higher sugar concentrations – and we discovered this to be caused by small amounts of conducting impurities in the sugar, which could be corrected.

Table 3. Statistical fitting of data for glucose in Table 2 to expression (3). Values and standard deviations of k'_β and k''_β determined for varying K_2. Sum of squares refers to deviations along the k_{obs}-axis.

pK_2	k'_β/s^{-1}	k''_β/s^{-1}	Sum of squares/s^{-2}
13.7	0.3(2)	3.4(4)	4.93
14.0	0.4(2)	4.2(5)	3.74
14.2	0.4(1)	6.6(8)	2.90
14.3	0.5(1)	7.8(9)	2.76
14.6	0.5(1)	14(2)	2.54
14.9	0.5(1)	25(3)	2.47
15.2	0.5(1)	48(6)	2.44
15.5	0.5(1)	94(12)	2.43
15.8	0.5(1)	187(24)	2.43
16.5	0.5(1)	925(121)	2.43

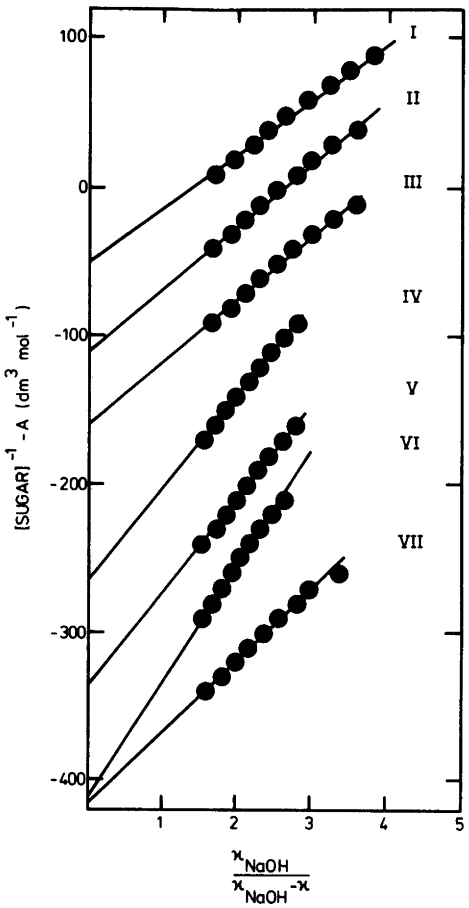

Fig. 3. Plots according to Table 1 and eqn. (1) and from which pK_1 of the various sugars can be evaluated. I. Glucose (A=0). II. 3-*O*-Methylglucose (A=50). III. 2-*O*-Methylglucose (A=100). IV. *N*-Acetylglucosamine (A=180). V. *N*-Benzoylglucosamine (A=50). VI. 4,6-*O*-Ethylideneglucose (A=300). VII. TMG (A=350).

Table 4. Collected thermodynamic and kinetic data for the various sugars investigated. I=0.20 (NaCl), temp.=25.0±0.2°C. Numbering of the sugars refer to Table 1.

Sugar	pK_1[a]	$10^4 \times k_G$/[b] s^{-1}	$k_{G^-} = k'_\alpha + k'_\beta$/[c] s^{-1}	$k_{G^-} = k'_\alpha + k'_\beta$/[d] s^{-1}	k_{HO^-}/[e] $dm^3\ mol^{-1}\ s^{-1}$
Glucose (I)	12.30(4)	4.00(3)	2.2[f]	2.2[f]	91[g]
2-*O*-Methyl-glucose (III)	12.22(3)	5.02(2)	1.7	1.2	72
3-*O*-Methyl-glucose (II)	12.22(3)	3.53(3)	2.8	2.1	127
TMG (VII)	12.20(3)	3.68(8)	–	0.5[h]	31[i]
N-Acetyl-glucosamine (IV)	12.06(3)	5.17(3)	1.2	2.3	200
N-Benzoyl-glucosamine (V)	12.03(2)	5.08(5)	–	–	–
4,6-*O*-Ethyl-ideneglucose (VI)	11.96(2)	6.4(1)	215	172	19000

[a] From Table 1. [b] Rate constants for mutarotation in pure water, averages from at least four runs. [c] From intercepts in Fig. 5. [d] From slopes of Fig. 5 and pK_1 values in Table 1 (see expression (5)). [e] Calculated from expression (7). [f] From $k'_\alpha + k'_\beta = 3.42\ k'_\beta + k'_\beta = 4.42\ k'_\beta$, where $k'_\beta = 0.5$ according to Table 3. [g] Calculated from expression (6). [h] Calculated from k_{HO^-} and pK_1 according to expression (7). [i] Taken from Ref. 6.

obvious as well as certain differences in individual shapes of these. Previously obtained stopped-flow data for glucose [3] are also indicated for comparison.

The first order mutarotation rate constants in Table 2 were all obtained at a constant and relatively low sugar concentration (0.04 M) to suppress catalysis by the sugar anion. As shown as early as 1925 by v. Euler and Ölander [17] the catalytic properties of this species must also be taken into account in alkaline solution, although the effect is strongly masked by the hydroxide ion. As catalysis of mutarotation by bases in general is dealt with in another paper [5,18] this subject will not be treated further here.

Rate expressions. The fact that the plots of observed rate constants in Table 2 (Fig. 4) do not exhibit a linear increase with hydroxide ion concentration but level off at more or less the same value of $[HO^-]$ – corresponding to 50 % "titration" of the anomeric hydroxyl group – may suggest a preequilibrium mechanism in alkaline solution *i.e.* rapid formation of the glucose anion, which then mutarotates in a second rate-determining step. In the case of glucose the deprotonation of more than one hydroxyl group, leading to

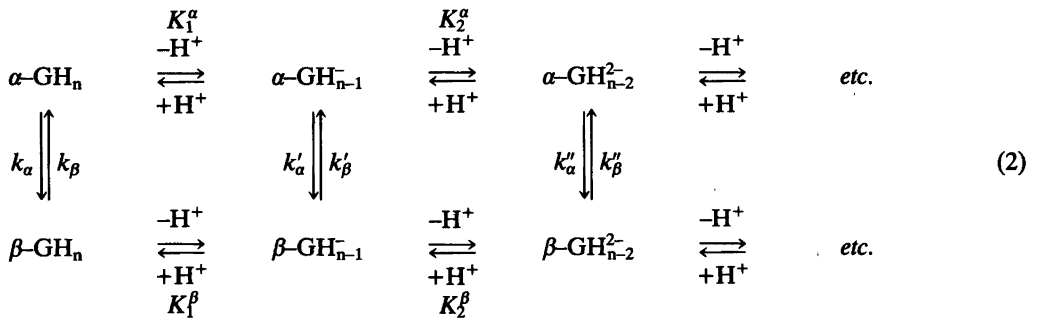

(2)

Scheme 1.

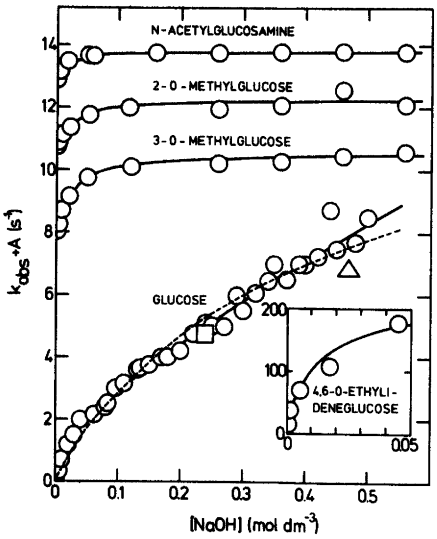

Fig. 4. Dependence of observed first order rate constants for the mutarotation of some glucoses on hydroxide ion concentration. The plots contain all data from Table 2 except a few which are omitted for clarity. The solid curves are drawn according to Eqns. (4) and (5) and figures from Table 4 for the substituted glucoses, whereas eqn. (3) is employed in the case of glucose as described in the text. For glucose pK_2 was chosen as 14.6, and higher values (Table 3) do not change the position or shape of the fitted curve substantially. However, when lower pK_2 values are taken bad fits are obtained as seen from the broken curve which represents pK_2=13.7. *N*-Acetylglucosamine (A=12.6), 3-*O*-methylglucose (A=7.8), 2-*O*-methylglucose (A=10.6), Glucose (A=0), 4,6-*O*-Ethylideneglucose (A=0). △,□ Ref. 3.

anions more reactive than the monoanion, can readily explain the steady increase of the curve for this compound with hydroxide ion concentration.

This mechanism now results in a general scheme for the mutarotation process (Scheme 1),* where mutarotation rate constants for the various protolytic forms of the sugar are indicated. K_1 and K_2 are acid dissociation constants and, as we shall see later, the experimental data can only justify the consideration of two successive dissociative steps, *i.e.* in the case of glucose.

If it is assumed that the protolytic reactions in eqn. (2) are always at equilibrium it can be shown that the observed first order rate constant from the rate expression for mutarotation, $v=|d\alpha/dt|=k_{obs}([\alpha_\alpha]_\lambda^{25}[\alpha\text{-G}]+[\alpha_\beta]_\lambda^{25}[\beta\text{-G}])\cdot l$ $[\alpha_\alpha]_\lambda^{25}$ and $[\alpha_\beta]_\lambda^{25}$ being specific optical rotations and l the light path, is given by expression (3):

$$k_{obs}=\frac{k_\alpha K_w^2+k'_\alpha K_1^\alpha K_w[HO^-]+k''_\alpha K_1^\alpha K_2^\alpha[HO^-]^2}{K_w^2+K_1^\alpha K_w[HO^-]+K_1^\alpha K_2{}^\alpha[HO^-]^2} + \frac{k_\beta K_w^2+k'_\beta K_1^\beta K_w[HO^-]+k''_\beta K_1^\beta K_2^\beta[HO^-]^2}{K_w^2+K_1^\beta K_w[HO^-]+K_1^\beta K_2^\beta[HO^-]^2} \quad (3)$$

It is now appropriate to divide further treatment of the experimental data in Table 2 (Fig. 4) into two groups: (1) glucose and (2) other sugars.

Glucose. The behaviour of this substance clearly deviates from the other sugars and it is necessary to apply eqn. (3) in full. In this expression the constants k_α, k_β, K_w, K_1^α and K_1^β are known already* for glucose and can be inserted. The remaining parameters k'_α, k'_β,k''_α, $k''_\beta K_2^\alpha$ and K_2^β may now be determined by a statistical analysis where the data in Table 2 (Fig. 4) are fitted to expression (3). However, although the data set for glucose in Table 2 are rather extensive – at least compared to the other sugars – it is clearly not sufficiently detailed and accurate for an unambiguous determination of all these constants, not even when further limitations are introduced, *e.g.* that

$k'_\alpha=k'_\beta\times k_\alpha K_1^\beta/k_\beta K_1^\alpha=3.42k'_\beta$, $k''_\alpha=3.42k''_\beta$ (assumed) and $K_2^\alpha\approx K_2^\beta\approx K_2$ (mean value). We have tried to vary K_2 systematically over a range of realistic values (pK_2=13.7–16.5) and then see how the calculated values and accuracies of the fitted k'_β and k''_β 's are affected. The results are given in Table 3 and it is clear from these that k'_β stabilizes at a value of $k'_\beta=0.5\pm0.1$ s^{-1} for pK_2 values higher than 14.2.

The second rate constant k''_β is, however, very uncertain and no clear minimum is reached in the

* The excellent first order behaviour always observed experimentally suggests that the consideration of a more complicated kinetic scheme, involving a consecutive reaction with the chain form of the sugar as an intermediate,[2b] is unnecessary under the present conditions.

* $k_G=k_\alpha+k_\beta$ = 4.00×10^{-4} s^{-1} (Table 4) and k_α/k_β = 1.71 [2] leading to $k_\alpha=2.52\times10^{-4}$ s^{-1} and k_β = 1.48×10^{-4} s^{-1}. K_w is taken as $10^{-14.00}$ while K_1^α and K_1^β are equal to $10^{-12.47}$ and $10^{-12.17}$, respectively.[13]

sum of squares even when an unreasonably high pK_2 value is employed. The only way to overcome this problem is to choose a likely value for pK_2 of glucose – apparently higher than 14.2 – and then accept the fitted value for k''_β. Two estimates of pK_2 for glucose have been reported in the literature: 13.8 [19a] and 13.9 [19b] both at 25 °C and determined by combined measurements of conductivities and hydrogen ion concentrations of alkaline glucose solutions. These rather qualitative values are lower than suggested by our results, but the discrepancy seems to be systematic, since the same authors also found pK_1=12.11 and 12.09, respectively, *vs.* our pK_1=12.30. We think that a pK_2 similar to pK_1 for ethylene glycol (14.77) [20] or rather glycerol (14.40) [20] is not unreasonable, although more specific experimental work is needed to verify this (see also next paragraph).

Other sugars. There is a pronounced difference in kinetic behaviour of glucose and its substituted analogues. Apart from 4,6-*O*-ethylideneglucose, the mutarotation of which is too fast to be followed at high hydroxide concentrations, all the substituted glucoses clearly exhibit almost completely $[HO^-]$-independent k_{obs} values at high $[HO^-]$. This situation can be accounted for by omitting the third terms of the numerators in eqn. (3) and probably also of the denominators as this would otherwise ultimately lead to decreasing k_{obs} for increasing $[HO^-]$ which is not observed. We see no immediate reason why k''_α and k''_β should be considerably smaller for substituted glucose than for unsubstituted with no distinction between different substituent sites and we therefore tend to believe that the explanation is to be sought in a gradually decreasing K_2 as glucose is successively converted into mono-, di-, *etc.*, substituted derivatives, qualitatively like the trend of K_1 in the series glycerol, ethylene glycol and propanol. If this is the case expression (3) reduces to eqn. (4):

$$k_{obs} = \frac{k_\alpha K_w + k'_\alpha K_1^\alpha [HO^-]}{K_w + K_1^\alpha [HO^-]} + \frac{k_\beta K_w + k'_\beta K_1^\beta [HO^-]}{K_w + K_1^\beta [HO^-]} \quad (4)$$

The hydroxide ion concentrations applied in the stopped-flow measurements are always high enough to justify neglect of $k_\alpha K_w$ and $k_\beta K_w$ (deriving from water catalysis) in eqn. (4), and if K_1^α and K_1^β are both replaced by K_1, which is the usual weighted average value that has been found experimentally, expression (4) can be further reduced to a double reciprocal linear equation as follows:

$$1/k_{obs} = \frac{K_w}{(k'_\alpha + k'_\beta)K_1} \times 1/[OH^-] + 1/(k'_\alpha + k'_\beta) \quad (5)$$

from which a plot of $1/k_{obs}$ *vs.* $1/[HO^-]$ should give $k'_\alpha + k'_\beta$ as well as K_1.* Such plots are shown for the various sugars in Fig. 5 ** and the respective values of $k'_\alpha + k'_\beta$ calculated from the intercepts and from the slopes – using experimentally determined K_1 values from Table 1 – are given in Table 4 together with other relevant data. This sum, which is actually the observed rate constant for mutarotation of purely monoanionic sugars, seems to be somewhat dependent on the method of calculation, although obviously not in a uniform way. We believe that the values deduced from the *slopes* of eqn. (5) are the most reliable and these are therefore used in subsequent calculations of k_{HO^-} (next paragraph).

Apparent catalytic constants for the hydroxide ion (k_{HO^-}) can be deduced from eqn. (3) by considering conditions under which $[HO^-]$ is low, *i.e.* eqn. (3) reduces to eqn. (6):

$$k_{obs} = (k'_\alpha K_1^\alpha + k'_\beta K_1^\beta) \times [HO^-] = k_{HO^-}[HO^-] \quad (6)$$

where again terms referring to water catalysis are omitted. If K_1 is only known as an averaged value, eqn. (6) becomes eqn. (7):

$$k_{obs} = (k'_\alpha + k'_\beta) K_1 K_w^{-1} \times [HO^-] = k_{HO^-}[HO^-] \quad (7)$$

A value for k_{HO^-} of glucose equal to 91 dm^3 mol^{-1} s^{-1} is determined from eqn. (6), and should be preferred to k_{HO^-}=110 dm^3 mol^{-1} s^{-1} according to eqn. (7). As mentioned earlier in this paper

* As expected the deviation from linearity for glucose at high hydroxide ion concentrations is pronounced.

** In principle, K_1 can be calculated from the kinetic results as K_1=intercept×K_w/slope according to eqn. (5). The following values are obtained for pK_1: II(12.34), III(12.38), IV(11.78) and VI(12.05) (for numbering see Table 1). Qualitatively these figures are of the right order of magnitude although presumably much more inaccurate than the constants derived more directly from conductivity measurements.

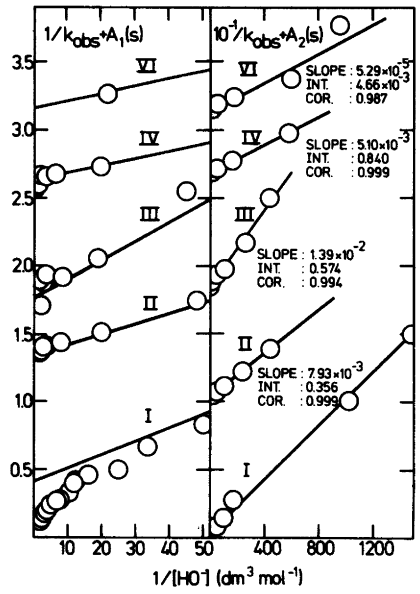

Fig. 5. Plots according to eqn. (5) for the sugars in Table 2 (a few points are omitted for clarity). I. Glucose. II. 3-*O*-Methylglucose (A_1=1.0, A_2=1.0). III. 2-*O*-Methylglucose (A_1=1.2, A_2=1.8). IV. *N*-Acetylglucosamine (A_1=1.8, A_2=2.6). VI. 4,6-*O*-Ethylideneglucose (A_1=2.7, A_2=3.1, 10^{-2} k_{obs} on Y-axis) (notations follow Table 1). Results from linear regression treatments are given in the plots. It is clear that glucose fails to obey eqn. (5) as expected (deviation from linearity at large hydroxide ion concentrations). The plot is divided into two parts to allow different scalings. A_1 and A_2 are constants chosen arbitrarily so as to arrange the plots conveniently in the diagram.

a number of different values of k_{HO^-} have been presented in the literature throughout the years: $k_{HO^-}^{25°C}$ (dm^3 mol^{-1} s^{-1})=374,[21] 359,[22] 165,[23] 83,[13] 91,[24] 80,[25] 148,[26] 230,[27] demonstrates this. Taking into account the uncertainties due to neglect of possible catalytic effects by the sugar anion we think that a value of k_{HO^-} for glucose at 25 °C in the range 80–100 dm^3 mol^{-1} s^{-1} ($k_{HO^-}^{25°C}$=90±10 dm^3 mol^{-1} s^{-1}) has now been rendered most probable.

The data in Table 4 represent a case not often met with in general acid-base catalysis, namely a situation where the catalyst (H_2O or HO^-) is kept constant in a series of reactions where the acid-base strength of the *substrate* is changed systematically by substitution. However, the change in p*K*-value of the sugars is far too small to permit any quantitative conclusions to be drawn from Brønsted plots. Nevertheless, an interesting qualitative difference between water and hydroxide ion catalysis may be noticed, *i.e.* for water catalysis the data seem to obey a usual Brønsted relationship with $0<\alpha<1$, indicating at least partly rate-determining proton transfer possibly in a coupled or concerted mechanism, while the situation is quite different for hydroxide ion catalysis, where the large increase in k_{HO^-} as glucose is converted into the 4,6-*O*-ethylidene derivative is incompatible with rate-determining proton transfer and rather suggests, as pointed out earlier, a stepwise mechanism with diffusion controlled proton transfer and rate-determining ring opening of the glucose anion. The fast mutarotation of 4,6-*O*-ethylideneglucose compared to glucose is presumably due to a weakening of the hemiacetal C–O bond in the ring imposed by the strain creating ethylidene bridge.

Acknowledgements. We thank Carl E. Foverskov and Tage Frederiksen for constructing the stopped-flow polarimeter unit and Birthe Johnsen and Pernille B. Petersen for carrying out some of the experiments. Furthermore, we appreciate valuable comments from Ronald P. Bell and Martin G. Ettlinger and their kind interest in this work.

REFERENCES

1. Dubrunfaut, A. P. *Compt. Rend. 23* (1846) 38.
2. a. Pigman, W. and Isbell, H. S. *Adv. Carbohydr. Chem. 23* (1968) 11; b. Isbell, H. S. and Pigman, W. *Ibid. 24* (1969) 14.
3. Goodall, D. M. and Cross, M. T. *Rev. Sci. Instrum. 46* (1975) 391
4. Bell, R. P. *Acid-Base Catalysis,* The Clarendon Press, Oxford 1941.
5. Preliminary results are presented in *Proc. RSC Fast Reactions in Solution Disc. Group Meeting,* University College, Cardiff, Sept. 1981.
6. Johnsen, B. and Sørensen, P. E. *Acta Chem. Scand. A 33* (1979) 241.
7. Bell, R. P. and Onwood, D. P. *Trans. Faraday Soc. 58* (1962) 1557.
8. a. Hiromi, K., Ono, S., Itah, S. and Nagamura, T. *J. Biochem. 64* (1968) 897; b. Watanabe, F. and Nagamura, T. *Chem. Lett.* (1974) 1373.

9. Tsuda, M. *Rev. Sci. Instrum. 46* (1975) 1419.
10. Poulsen, K. G. *Anal. Chem. 32* (1960) 410.
11. Robertson, R. A. and Stokes, R. H. *Electrolyte Solutions,* 2nd Ed., Butterworths, London 1959.
12. Osaka, Y. *Z. Physik. Chem. 35* (1900) 661.
13. Los, J. M. and Simpson, L. B. *Rec. Trav. Chim. 75* (1956) 267.
14. Wit, G. de, Kieboom, A. P. G. and Bekkum, H. v. *Rec. Trav. Chim. Pays-Bas 98* (1979) 355.
15. Neuberger, A. and Fletcher, A. P. *Carbohydr. Res. 17* (1971) 79.
16. Kielland, J. *J. Am. Chem. Soc. 59* (1937) 1675.
17. a. v. Euler, H. and Ölander, A. *Z. Anorg. Allg. Chem. 146* (1925) 45; b. *Ibid. 152* (1926) 113.
18. Nielsen, H. and Sørensen, P. E. *To be published.*
19. a. Hirsch, P. and Schlags, R. *Z. Physik. Chem. 141* (1929) 387; b. Urban, F. and Schaffer, P. A. *J. Biol. Chem. 94* (1932) 697.
20. Ballinger, P. and Long, F. A. *J. Am. Chem. Soc. 82* (1960) 795.
21. Hudson , C. S. *J. Am. Chem. Soc. 29* (1907) 1571.
22. Kuhn, R. and Jacob, P. *Z. Physik. Chem. A 113* (1924) 339.
23. Bell, R. P. and Prue, J. E. *Trans. Faraday Soc. 46* (1950) 14.
24. Schmid, H. and Bauer, G. *Monatsh. Chem. 96* (1965) 1503.
25. Capon, B. and Walker, R. B. *J. Chem. Soc. Perkin Trans. 2* (1974) 1600.
26. Kilde, G. and Wynne-Jones, W. F. K. *Trans. Faraday Soc. 49* (1953) 243.
27. Brønsted, J. N. and Guggenheim, E. A. *J. Am. Chem. Soc. 49* (1927) 2554.

Received May 31, 1982.

Acta Chemica Scandinavica A 37 (1983) 117—123

Phase Analysis Studies in the System Cu_2O–CuO–Ta_2O_5

PIERRE NDALAMBA WA ILUNGA

Department of Inorganic Chemistry, Arrhenius Laboratory, University of Stockholm, S-106 91 Stockholm, Sweden

The ternary system Cu_2O–CuO–Ta_2O_5 has been studied by X-ray powder diffraction methods after heat treatment of the samples at 1120 and 1440 K. In addition to the phases $Cu_3Ta_7O_{19}$ and $Cu_5Ta_{11}O_{30}$ on the Cu_2O–Ta_2O_5 line, two ternary phases exist: $Cu_{1.05+x}Ta_{1.98}O_6$ ($0 \leq x \leq 0.12$) has a cubic perovskite-type structure with $a \approx 7.5$ Å, and $Cu_xTa_3O_8$ ($0.77 \leq x \leq 0.85$) is orthorhombic with a structure of $LiNb_6O_{15}F$-type. The variation of the unit cell parameters with composition has been studied for these two phases. Magnetic measurements between 70 and 350 K showed Curie-Weiss behaviour.

Although there have been several studies over the past 20 years on the phases occurring in the Cu–Ta–O and Cu–Nb–O systems, some of the results have been contradictory, and our knowledge is still rather incomplete.

A series of investigations of complex systems involving Ta_2O_5 or Nb_2O_5 in combination with Cu_2O, CuO and/or NbO_2F has therefore been undertaken at this laboratory to provide more information on these systems.

In the earlier publications on the Cu–Ta–O system, a perovskite-type phase of the composition $CuTaO_3$ was reported as a valence isomer.[1,2] A high pressure non-perovskite modification of that stoichiometry has also been reported.[3] No further communication confirming the existence of an ABO_3-type compound has appeared since.

Two independent groups reported[4,5] the preparation of a compound with divalent copper, $CuTa_2O_6$, having cubic symmetry with the perovskite unit cell parameter doubled (a=7.52 Å). This compound could be obtained at 1200 °C. In a subsequent report on $CuTa_2O_6$ the space group $Pm3$ was suggested on the basis of spectral data and X-ray powder diffraction results. The crystal structure of $CuTa_2O_6$ was first refined by Hong.[7] This perovskite-type structure was described as built of strongly distorted TaO_6 octahedra creating a square coplanar configuration at the A-sites, suitable for accommodation of Cu^{II} atoms. $CuTa_2O_6$ has also been reported to show a slight distortion from cubic to tetragonal symmetry in an olive green sample prepared at 1000 °C.[8]

In a recent study[9] the structure of a crystal obtained from a 10 CuO/Ta_2O_5 flux was refined. The intensity distribution in the single crystal pattern indicated orthorhombic symmetry, but no deviation from cubic symmetry was observed in the powder patterns. A wide homogeneity range, $Cu_{1+x}Ta_2O_6$ with $0 \leq x \leq 0.30$, was suggested without further details. The refinement indicated a composition of $Cu_{1.03}Ta_2O_6$ of the single crystal studied.

In a previous study at this laboratory[10] a compound $Cu_{0.80}Ta_3O_8$ was obtained at 1445 K with a structure representing a version of the $LiNb_6O_{15}F$-type.[11] Two phases with monovalent copper have recently been reported by Jahnberg,[12] *viz.* $Cu_5Ta_{11}O_{30}$ and $Cu_3Ta_7O_{19}$, having structures based on stacking of α-U_3O_8-type layers.[12,13] The first compound was obtained at both 800 °C and 1100 °C, while the second could be prepared only at the lower temperature.[14]

In this paper a phase analysis of the Cu_2O–CuO–Ta_2O_5 system is reported.

EXPERIMENTAL

The starting materials were Cu_2O (Matheson, Coleman and Bell min 96.0 %), CuO (Baker Analysed, min 99.9 %) and Ta_2O_5 (Fuka, Buch

0302-4377/83 $2.50

SG, min 99.9 %). To reduce weighing errors when the variation of properties within homogeneity ranges were to be studied, two stock mixtures having compositions near the extreme ends of the range were first prepared, and the intermediate samples were made by mixing appropriate amounts of these. Special precautions had to be taken to avoid unintentional oxidation of Cu_2O. Therefore, the silica tubes containing appropriate amounts of the compounds, thoroughly mixed, were dried, carefully evacuated to 0.1 Pa and sealed off. samples representing compositions on the CuO–Ta_2O_5 line were also prepared in nonevacuated but sealed platinum tubes.

In general, samples were prepared by preheating, and then gradually increasing the temperature, keeping them for 3–5 days at the temperature of preparation and finally quenching the tubes in cold water. The low-temperature samples were pre-heated at about 870 K for a few days followed by annealing at 1120 K, while the high-temperature samples were pre-heated at about 1020 K and then held at 1440 K.

All samples were examined in an optical microscope and by X-ray diffraction using a Guinier-Hägg focusing camera with strictly monochromatic $CuK\alpha_1$ radiation (λ=1.540598 Å).[15] Potassium chloride (a_{KCl}=6.2930 Å)[16] was used as an internal standard. The 2θ values were calculated from powder photographs followed by indexing and refinements of cell parameters by means of a least squares procedure.[17] An automatic single beam microdensitometer designed for X-ray powder photographs was used.[18] The magnetic susceptibility was measured using an automatized apparatus applying the Faraday method and using $HgCo(SCN)_4$ as a standard.[19] The measurement covered the temperature range 70 to 350 K. The density was determined from the apparent loss of weight in hexane, using an apparatus designed for density determination on small powder samples.[20]

RESULTS AND DISCUSSION

The results of the phase analysis are summarized in Fig. 1, illustrating the isothermal diagram. For the sake of clarity only a representative selection of the compositions investigated have been indicated and listed in Table 1. The intermediate phases observed at 1120 K are marked *A*, *C* and *D*. *A* is a perovskite-type phase ~$CuTa_2O_6$, *C* is $Cu_5Ta_{11}O_{30}$ and *D* is $Cu_3Ta_7O_{19}$.[12] Another phase *B*, $Cu_{\sim 0.8}Ta_3O_8$, reported previously,[10] was observed only in the high-temperature experiments.

The perovskite-type and $Cu_{\sim 0.8}Ta_3O_8$ phases have appreciable homogeneity ranges.

All samples with gross compositions CuO·-$nTaO_{2.5}$ (n>9) gave complex X-ray powder patterns which were similar to that of Ta_2O_5. These phases will be objects of further studies, which will include also high resolution electron microscopy.

A. The perovskite-type phase. A single phase was obtained at 1120 K for samples with compositions along the line $Cu_{1.05+x}Ta_{1.98}O_6$. The X-ray diffraction patterns indicated a cubic perovskite-type structure with $a\approx$7.5 Å, as reported in Refs. 4 and 5 for $CuTa_2O_6$. However, samples prepared at this composition ($CuTa_2O_6$), invariably showed weak extra lines of a Ta_2O_5-like phase, and this composition thus does not seem to represent a single phase.

The unit cell parameter of the specimens on the line $Cu_{1.05+x}Ta_{1.98}O_6$ are observed to vary with composition within the range $0\leq x\leq 0.12$, as seen from Fig. 2. The single phase sample with x=0 (on the line CuO–$TaO_{2.5}$) has a unit cell parameter a=7.516(1) Å (Table 2). The same parameter is obtained for this phase in two-phase samples obtained at the composition $CuTa_2O_6$. It seems reasonable to assume that the composition

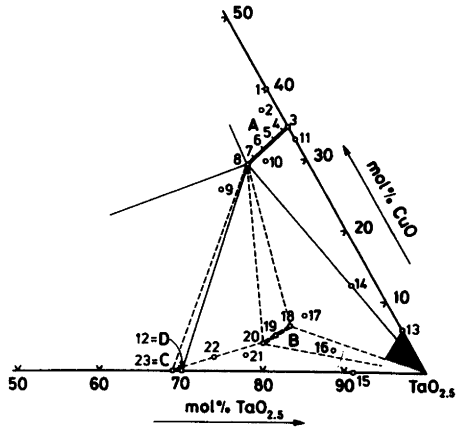

Fig. 1. Part of the phase diagram for the system Cu_2O–CuO–Ta_2O_5 at 1120 K and 1440 K. Broken lines refer to phase *B*, which could be prepared only at the higher temperature. The dashed area close to Ta_2O_5 is not yet explored and may contain several Ta_2O_5-like phases.

Table 1. The results of the phase analysis for some representative samples with reference to Fig. 1.
A = perovskite-type phase ~$CuTa_2O_6$ C = $Cu_5Ta_{11}O_{30}$
B = $Cu_{\sim 0.8}Ta_3O_8$ D = $Cu_3Ta_7O_{19}$

No.	Gross composition $pCuO_{0.5}$	$+qCuO$	$+rTaO_{2.5}$	Observed X-ray powder patterns
	p	q	r	
Temperature: 1120 K				
1	0	0.397	0.603	A+CuO
2	0.019	0.371	0.610	A+CuO
3	0	0.347	0.653	
4	0.007	0.342	0.651	
5	0.026	0.329	0.645	
6	0.045	0.316	0.639	A
7	0.064	0.304	0.632	
8	0.076	0.295	0.0629	
9	0.120	0.260	0.620	A+Cu_2O+D
10	0.050	0.300	0.650	A+Ta_2O_5-type phase
11	0	0.330	0.670	"$CuTa_2O_6$"=A+Ta_2O_5-type phase
12	0.300	0	0.700	D+Ta_2O_5-type phase+C
13	0	0.060	0.940	Ta_2O_5 type phase
14	0.030	0.125	0.845	Ta_2O_5 type phase+A
15	0.090	0	0.910	Ta_2O_5 type phase+D
Temperature: 1440 K				
16	0.100	0.030	0.870	B+Ta_2O_5-type phase
17	0.108	0.081	0.811	B+A
18	0.133	0.067	0.800	
19	0.158	0.053	0.789	B
20	0.180	0.040	0.780	
21	0.210	0.021	0.769	B+C
22	0.250	0.020	0.730	B+C
23	0.310	0	0.630	C

$x=0$ is the lower bound of the homogeneity range. The upper limit of the homogeneity range is close to $x=0.12$, as is evident from Fig. 2 and Table 1. At this point 21 % of the Cu atoms are monovalent.

Specimens of $Cu_{1.05+x}Ta_{1.98}O_6$ ($0 \leq x \leq 0.12$) synthesized in the way mentioned above are brown. Fully oxidized samples with $x=0$ are green. The diffraction lines were sharp, and no splitting that would indicate a symmetry lower than cubic could be observed.

When specimens are prepared at high temperature (1440 K) their colour becomes black. Samples with starting composition corresponding to point 1 in Fig. 1, for example, were green when prepared at low temperature and gave the value $a=7.516$ Å for the cell parameter of the perovskite phase. Prepared at 1440 K they are black, and the a value is 7.527 Å, which corresponds to $x \approx 0.10$ according to Fig. 2. There is thus strong evidence that there is a loss of oxygen and an increase in the Cu^{I}/Cu^{II} ratio at the higher temperatures. Hong,[7] Longo *et al.*[8] and Vincent *et al.*[9] also obtained a black phase using a flux method at high temperatures.

The density was measured for two single phase samples with $x=0$ and $x=0.10$ prepared at 1120 K. The calculated densities assuming four formula units of $Cu_{1.05+x}Ta_{1.98}O_6$ per unit cell, agree well with the observed values. The sample with

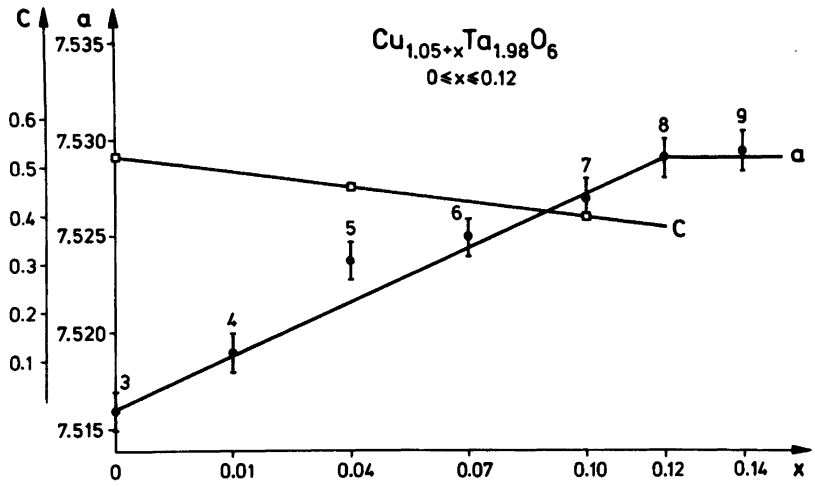

Fig. 2. Unit cell parameter a (in Å) and Curie constant C (m^3 K mol^{-1}) as functions of copper content x for the perovskite-type phase $Cu_{1.05+x}Ta_{1.98}O_6$. The numbers of the samples refer to Fig. 1 and Table 1.

x=0 gave the values ρ_{obs}=8.14 g cm^{-3} and ρ_{calc}=8.15 g cm^{-3}, while the sample with x=0.10 gave ρ_{obs}=8.20 g cm^{-3} and ρ_{calc}=8.21 g cm^{-3}.

The magnetic susceptibility measurements, covering the temperature range 70–350 K, showed paramagnetic behaviour of all samples investigated. The thermal variation of the magnetic susceptibility obeyed the Curie -Weiss law. The variation of C (the Curie constant) with x, shown in Fig. 2, is in concord with a decrease in

Table 2. X-Ray powder diffraction pattern of $Cu_{1.03}(Cu_{0.02}Ta_{1.98})O_6$. Figures of merits (26,27) M(20)=32, F(20)=15. Symmetry: Cubic. a=7.516(1) Å; ρ_{obs}=8.14 g cm^{-3}; ρ_{calc}=8.15 g cm^{-3}.

$2\theta_{obs}$ (°)	$2\theta_{obs}-2\theta_{calc}$ (°)	d_{obs} (Å)	$I_{obs} \cdot 1000/I_{max}$	h	k	l
11.621	-0.144	7.609	3	1	0	0
16.657	-0.011	5.318	60	1	1	0
23.540	-0.116	3.776	907	2	0	0
26.566	0.070	3.353	4	2	1	0
29.087	0.009	3.068	36	2	1	1
33.594	-0.107	2.666	1000	2	2	0
37.835	0.014	2.376	45	3	1	0
41.593	0.003	2.170	338	2	2	2
45.103	0.005	2.009	29	3	2	1
48.390	-0.014	1.880	602	4	0	0
51.548	0.000	1.772	16	3	3	0
54.531	-0.029	1.682	760	4	2	0
57.456	-0.008	1.603	11	3	3	2
60.215	-0.061	1.536	975	4	2	2
63.014	0.002	1.474	8	5	1	0
68.303	0.005	1.372	9	5	2	1
70.855	-0.012	1.329	538	4	4	0
73.392	-0.005	1.289	16	5	3	0
75.881	-0.002	1.253	547	6	0	0
78.381	0.018	1.219	8	6	1	1

the amount of Cu^{II} when x is increased. The observed μ_{eff}/Cu^{II} in this compound ranges from 1.84–2.02 B.M., which is in agreement with previously observed values for Cu^{II} compounds. For example, a value of 2.04 B.M. has been reported for $CuNbO_3F$,[21] while 1.91 and 2.06 B.M. are the values previously obtained for '$CuTa_2O_6$'.[8,22]

The copper atom distribution in this phase is not obvious, especially as copper exists in two valence states for $x>0$. The following points can be made, however:

(*a*) The copper atoms should mainly occupy the *A*-site of the ideal perovskite structure, as is also suggested by Hong[7] and by Vincent *et al.*[9]

(*b*) It seems reasonable to assume that there is a substitution of divalent copper for a small amount of tantalum, since vacancies at the *B*-sites are not likely. The radius of Cu^{II} in 6-coordination is 0.73 Å compared to 0.64 Å for Ta^{V}.[22] The most probable cation distribution for $x=0$ can then be written as $Cu^{II}_{1.03}(Cu^{II}_{0.02}Ta^{V}_{1.98})O_6$. At the upper composition limit, $x=0.12$, the corresponding formula is $Cu^{I}_{0.24}Cu^{II}_{0.91}(Cu^{II}_{0.02}Ta^{V}_{1.98})O_6$. The magnetic measurements and densities are in reasonable agreement with this model.

(*c*) The observed expansion of the lattice when the value of x is increased may be caused mainly by two things: (i) the increased number of metal atoms in the unit cell and (ii) the replacement of divalent copper atoms by larger monovalent atoms at the same crystallographic site.

B. $Cu_{\sim 0.8}Ta_3O_8$. The phase $Cu_xTa_3O_8$ is orthorhombic.[10] It was difficult to prepare as a single phase when using Cu_2O as one of the starting materials. However, by replacing copper(I) oxide by an equivalent amount of Cu metal powder and CuO, single phase samples could be obtained at 1440 K. Attempts to obtain this phase at about 1220 K failed, therefore it seems reasonable to assume that it is a high temperature phase.

A variation in the length of the axes with x was observed, as seen in Fig. 3. The data suggested a homogeneity range $0.77 \leq x \leq 0.85$. No extra lines that would indicate a second phase could be seen in the powder patterns of samples with $x=0.75$, 0.80 (Table 3) and 0.85. The point $x=0.75$ is probably outside the single phase range, but the amount of additional phase is then too small to be detected in the powder patterns. The colour of the single phase samples is reddish-brown.

The copper distribution in this phase has been reported previously.[10] When x goes from 0.77 to 0.85 it changes from 0.54 Cu^{I}+0.23 Cu^{II} to 0.70 Cu^{I}+0.15 Cu^{II}. The unit cell parameters thereby decrease, as seen in Fig. 3. The total number of copper atoms increases, but there is also a replacement of Cu^{II} by Cu^{I}. These atoms occupy different crystallographic positions: Cu^{I} is located in interstitial holes which are considerably larger than the interstices where Cu^{II} is located. This replacement may therefore explain the shrinkage of the unit cell when x is increased. A comparison can be made with $Li_{1-x}Ta_3O_{8-x}F_x$,[24] which is isostructural with $Cu_xTa_3O_8$.[10] The Li^{I} atoms in the former structure are suggested to

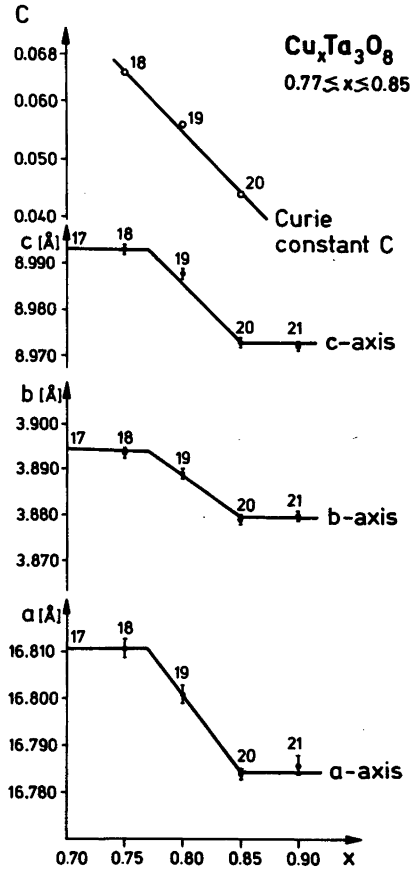

Fig. 3. Unit cell parameters and Curie constant *C* (m^3 K mol^{-1} as functions of copper content x for the phase $Cu_xTa_3O_8$. The numbers of the samples refer to Fig. 1 and Table 1.

Table 3. X-Ray powder diffraction pattern of $Cu_{0.80}Ta_3O_8$. Figures of merits (26,27) M(20)=20, F(20)=25. Symmetry: orthorhombic. a=16.80(1) Å, b=3.889(1) Å, c=8.988(1) Å.

$2\theta_{obs}$ (°)	$2\theta_{obs}-2\theta_{calc}$ (°)	d_{obs} (Å)	$I_{obs} \cdot 1000/I_{max}$	h	k	l
9.883	0.051	8.943	16	0	0	1
10.580	0.057	8.355	24	2	0	0
11.204	0.049	7.891	30	1	0	1
19.766	0.028	4.488	16	0	0	2
20.473	0.033	4.335	25	1	0	2
22.449	0.031	3.957	53	2	0	2
22.868	0.018	3.886	1000	0	1	0
23.382	0.024	3.802	318	4	0	1
25.402	0.012	3.504	886	3	0	2
30.290	0.013	2.948	385	1 0	0 1	3 2
30.856	0.012	2.896	26	1	1	2
31.690	0.009	2.821	228	2	0	3
31.949	0.014	2.799	79	6	0	0
32.236	0.010	2.775	106	2	1	2
32.917	-0.043	2.719	250	4	1	1
33.278	0.012	2.690	70	5	0	2
33.509	0.016	2.672	56	6	0	1
33.930	0.015	2.641	16	3	0	3
34.416	-0.003	2.604	556	3	1	2
36.705	0.000	2.445	417	5	1	1

occur at nearly the same crystallographic sites as the Cu^I atoms in $Cu_xTa_3O_8$. With increasing lithium content in the structure the lattice contracts;[24] the two structures thus behave similarly in this respect.

The magnetic susceptibility was found to be temperature dependent in the range investigated: 70–350 K, with the Curie–Weiss law nicely obeyed. The variation of the Curie constant C with x is indicated in Fig. 3. The values of μ_{eff}/Cu^{II} fall in the range 1.45–1.53 B.M. This is considerably lower than for the perovskite-type phase. An even lower value has, however, been reported for the corresponding niobium phase with $LiNb_3O_8$-type structure.[25]

Acknowledgements. I wish to express my gratitude to Professor Arne Magnéli who introduced me to the field, Professor Lars Kihlborg and Dr. Monica Lundberg for their constant interest in this investigation and for all their valuable comments and criticism. Thanks are also due to Mr. Bo Blom for his enthusiastic help with the magnetic measurements.

This project has been sponsored by the Swedish Natural Science Research Council.

REFERENCES

1. Krylov, E. I., Samarina, V. A. and Shtolts, A. K. *Dokl. Akad. Nauk SSSR 130* (1960) 556.
2. Shick, L. and Vorres, K. S. *AEC Accession* No. 4244, Report TID-2220 D, 1965.
3. Sleight, A. W. and Prewitt, C. T. *Mater. Res. Bull. 5* (1970) 207.
4. Felten, E. J. *J. Inorg. Nucl. Chem. 29* (1967) 1168.
5. Kasper, H. *Rev. Chim. Miner. 4* (1967) 759.
6. Reinen, D. and Propach, V. *Inorg. Nucl. Chem. Lett. 7* (1971) 569.
7. Hong, H. Y. P. *Lincoln Laboratory, M. I. T., Solid State Research Report 2* (1972) 33.
8. Longo, J. M. and Sleight, A. W. *Mater. Res. Bull. 10* (1975) 1273.
9. Vincent, H., Bochu, B., Aubert, J. J., Jaubert, J. C. and Marezio, M. *J. Solid State Chem. 24* (1978) 245.
10. Wa Ilunga, N. P., Marinder, B. O. and Lundberg, M. *Chem. Scr. 18* (1981) 217.
11. Lundberg, M. *Acta Chem. Scand. 19* (1965) 2274.
12. Jahnberg, L. *Mat. Res. Bull. 16* (1981) 513.
13. Jahnberg, L. *J. Solid State Chem. 41* (1982) 286.
14. Jahnberg, L. *Private communication.*

15. Deslattes, R. D. and Hening, A. *Phys. Rev. Lett. 31* (1973) 972.
16. Hambling, P. G. *Acta Crystallogr. 6* (1953) 98.
17. Werner, P.-E. *Ark. Kemi 31* (1969) 513.
18. Johansson, K. E., Palm, T. and Werner, P. E. *J. Phys. E. 13* (1980) 1289.
19. Blom, B. and Hörlin, T. *Chem. Commun. Univ. Stockholm* (1977) No. 5.
20. Niklewski, T., Nygren, M., Kihlborg, L. and Sävborg, Ö. *Chem. Commun. Univ. Stockholm* (1975) No. 12.
21. Lundberg, M. and Sävborg, Ö. *Chem. Scr. 13* (1978–79) 197.
22. Krylov, E. I., Bazeuv, G. V. and Khan, V. P. *Izv. Akad. Nauk SSSR, Neorg. Mater 5* (1969) 239.
23. Shannon, R. D. and Prewitt, C. T. *Acta Crystallogr. B 25* (1969) 925.
24. Werner, P.-E., Marinder, B.-O. and Magnéli, A. *Mater Res. Bull. 13* (1978) 1371.
25. Marinder, B.-O., Werner, P.-E., Wahlström, E. and Malmros, G. *Acta Chem. Scand. A 34* (1980) 51.
26. De Wolff, P. M. *J. Appl. Crystallogr. 1* (1968) 108.
27. Smith, G. S. and Snyder, R. L. *J. Appl. Crystallogr. 12* (1979) 60.

Received June 4, 1982.

Acta Chemica Scandinavica A 37 (1983) 125—130

Structural Characterization of the Triiron Undecacarbonyl Anion $[HFe_3(CO)_{11}]^-$ in the $[N(PPh_3)_2]^+$ Salt and Locating the Site of the Bridging Hydrogen

EERO IIŠKOLA, TAPANI A. PAKKANEN, TUULA T. PAKKANEN and TAPANI VENÄLÄINEN

Department of Chemistry, University of Joensuu, P.O. Box 111, SF-80101 Joensuu 10, Finland

$[N(PPh_3)_2](\mu\text{-H})Fe_3(CO)_{10}(\mu\text{-CO})$, $FW=1015.3$, crystallizes in space group $P2_1/c$ with $Z=4$, $a=18.158(13)$, $b=16.512(10)$, $c=15.492(13)$ Å, $\beta=99.62(7)°$, $V=4579.4(60)$ Å^3, $D_c=1.47$ g cm^{-3}, $F(000)=2064$. The hydrogen atom in the metal cluster was located with low-angle reflection data. The positional and anisotropic thermal parameters of the atoms were refined by the least-squares methods. The final residual R is 0.053 for 2817 reflections ($I>2\sigma(I)$).

The molecular structure of $[HFe_3(CO)_{11}]^-$ anion consists of a triangular array of iron atoms with one edge bridged by a carbonyl group and a hydrogen atom. The result is supported by earlier neutron and preliminary X-ray diffraction studies.

The unsubstituted trinuclear iron carbonyl series, *e.g.* $Fe_3(CO)_{12}$,[1] $[HFe_3(CO)_{11}]^-$,[2,3] and $[Fe_3(CO)_{11}]^{2-}$,[4] have been of particular interest due to their unique geometry and fluxional behaviour in solution.[5] The $[Fe_3(CO)_{11}]^{2-}$ dianion, for example, possesses an $M_3(CO)_9(\mu\text{-CO})(\mu_3\text{-CO})$ configuration, with an unsymmetrically triply bridging carbonyl.

Prior to this work only a preliminary X-ray study by Dahl and Blount[2] on the $[HFe_3(CO)_{11}]^-$ monoanion has been published with no detailed structural information. The $[HFe_3(CO)_{11}]^-$ anion was determined as a $[(C_2H_5)_3NH]^+$ salt and found to contain a triangular array of iron atoms with one edge bridged by a CO. The presence of a hydrogen atom was not directly established for $[HFe_3(CO)_{11}]^-$ by the X-ray work but was inferred both from stereochemical and bonding considerations to bridge the same edge as the only bridging carbonyl.

Teller and Bau tabulate in their review article[3] structural parameters of some metal hydride clusters. $[HFe_3(CO)_{11}]^-$ is also included, but the details of this neutron diffraction study are unpublished. During the course of our studies on mixed-metal cluster syntheses we prepared and characterized the PPN salt of $[HFe_3(CO)_{11}]^-$. Since no detailed structural information is available of this commonly encountered iron cluster anion, we are reporting our results.

EXPERIMENTAL

The $[PPN][HFe_3(CO)_{11}]$ salt was formed as a by-product in a synthesis of $[PPN][Fe_3Co(CO)_{13}]$.[6] The sources of the hydride are presumably the impurities in the starting materials and solvents.

A dark brown irregularly shaped crystal of size 0.3×0.2×0.4 mm was mounted on a glass fiber. After optical alignment of the crystal on a Nicolet R3m diffractometer preliminary unit cell parameters were determined with 10 centered diffraction maxima and with axial photographs. Graphite monochromatized Mo$K\alpha$ radiation ($\lambda=0.71069$ Å) was used.

The measured lattice constants for the monoclinic unit cell based on 24 centered reflections are $a=18.158(13)$, $b=16.512(10)$, $c=15.492(13)$ Å and $\beta=99.62(7)°$. The unit cell volume of 4579.4 (60)Å^3 and FW of 1015.3 g mol^{-1} give rise to a calculated density of 1.47 g cm^{-3} based upon $Z=4$. Intensity data were collected in ω-scan

0302-4377/83 $2.50

Table 1. Final atomic parameters for $[PPN]^+[HFe_3(CO)_{11}]^-$.

	x	*y*	*z*	U_{eq} ($Å^2 \times 10^3$)[a]
Fe1	-1975(1)	2859(1)	1849(1)	52(1)
Fe2	-3333(1)	2357(1)	1660(1)	57(1)
Fe3	-2388(1)	1886(1)	3084(1)	62(1)
P1	1664(1)	3007(1)	3160(2)	39(1)
P2	3293(1)	3015(1)	3965(1)	38(1)
N	2538(4)	3055(4)	3301(4)	41(3)
O1	-3063(4)	4015(4)	2329(5)	69(3)
O2	-1870(4)	4150(4)	588(4)	84(3)
O3	-860(5)	1850(6)	1183(7)	129(5)
O4	-1044(5)	3645(5)	3343(5)	113(4)
O5	-3347(5)	704(5)	3749(6)	110(5)
O6	-2820(6)	3216(6)	4163(6)	123(5)
O7	-964(5)	1660(7)	4214(6)	118(5)
O8	-2039(6)	675(5)	1841(5)	114(4)
O9	-4188(6)	3204(6)	210(8)	176(6)
O10	-3750(5)	784(5)	836(7)	130(5)
O11	-4466(5)	2341(6)	2751(7)	135(5)
C1	-2867(6)	3362(7)	2108(6)	57(4)
C2	-1921(5)	3641(6)	1068(6)	54(4)
C3	-1309(6)	2195(7)	1471(7)	71(5)
C4	-1428(6)	3319(7)	2763(7)	71(5)
C5	-2987(7)	1188(8)	3490(9)	87(6)
C6	-2657(7)	2720(7)	3711(8)	79(5)
C7	-1534(7)	1736(8)	3751(7)	79(5)
C8	-2193(7)	1201(7)	2270(7)	83(5)
C9	-3844(7)	2860(7)	777(9)	104(6)
C10	-3543(6)	1374(7)	1198(8)	84(5)
C11	-4008(6)	2362(7)	2340(8)	85(5)
C12	1320(5)	1976(5)	3057(5)	41(3)
C13	618(5)	1771(6)	3200(6)	58(4)
C14	369(6)	968(7)	3080(7)	70(5)
C15	834(7)	397(6)	2834(7)	65(5)
C16	1535(6)	596(6)	2701(6)	62(4)
C17	1775(5)	1371(5)	2809(6)	52(4)
C18	1272(5)	3481(5)	4003(5)	40(3)
C19	1079(5)	4294(6)	3935(6)	52(4)
C20	882(6)	4702(6)	4650(7)	71(5)
C21	852(7)	4300(9)	5397(7)	91(6)
C22	1005(7)	3491(8)	5459(7)	79(5)
C23	1227(5)	3080(6)	4775(6)	53(4)
C24	1309(5)	3521(5)	2142(5)	36(3)
C25	591(5)	3435(6)	1760(7)	63(4)
C26	320(6)	3816(7)	964(7)	75(5)
C27	807(6)	4280(7)	597(6)	69(4)
C28	1515(6)	4383(7)	966(7)	76(5)
C29	1771(5)	4006(6)	1760(6)	60(4)
C30	3599(5)	1996(5)	4168(5)	40(3)
C31	4253(6)	1712(5)	3952(6)	53(4)
C32	4456(6)	916(7)	4051(7)	65(5)
C33	4004(7)	399(6)	4390(8)	88(5)
C34	3343(7)	635(6)	4613(7)	80(5)
C35	3154(5)	1448(6)	4515(7)	66(4)

Table 1. Continued.

C36	3273(5)	3473(5)	5018(6)	42(3)
C37	2942(6)	4209(6)	5060(6)	64(4)
C38	2959(6)	4598(6)	5850(8)	73(5)
C39	3309(6)	4225(7)	6602(7)	74(5)
C40	3648(8)	3520(7)	6579(7)	93(6)
C41	3647(7)	3131(6)	5772(6)	73(5)
C42	3989(4)	3551(5)	3475(5)	40(3)
C43	3910(5)	3624(5)	2585(6)	49(4)
C44	4454(7)	4029(7)	2235(7)	73(5)
C45	5068(7)	4337(8)	2749(10)	95(7)
C46	5141(7)	4252(8)	3619(9)	93(6)
C47	4605(5)	3877(6)	3995(6)	59(4)
H1	-2607(37)	2332(42)	1012(42)	79(29)

[a] $U_{eq}=1/3$ trace $|\tilde{U}$.

mode with a scan speed of 3 °/min. The intensities of two standard reflections were periodically measured at intervals of every 98 reflections in order to monitor the crystal's alignment and decay. No significant decay was found.

Intensities were measured at ambient temperature between 2θ limits of 3 and 40° for 4436 reflections. Lorentz and polarization corrections, as well as an empirical absorption correction based on ψ-scan data, were applied to the intensity data; the minimum transmission factor was 86 % from the maximum value, $\mu=11.0$ cm^{-1}. A data reduction gave 2817 independent reflections with $I \geq 2\sigma(I)$. The space group, $P2_1/c$, was deduced from the systematic absences.

The iron, phosphorus and nitrogen atoms were located by direct methods of the SHELXTL program package.[7] The other nonhydrogen atoms were found in successive Fourier syntheses. The asymmetric unit contains one $[HFe_3(CO)_{11}]^-$ anion and one $[PPN]^+$ cation. Isotropic and anisotropic refinements were made for the nonhydrogen atoms. The scattering factors for neutral atoms were taken from International Tables.[8] The phenyl hydrogens were placed in idealized positions with isotropic temperature factors. The final anisotropic refinement converged to an $R=0.056$.

In order to locate the hydrogen atom in the metal cluster, a difference Fourier map was calculated. Three peaks were found in the edges of the Fe_3 triangle. The hydrogen atom peak was assigned by the method of La Placa and Ibers.[9] A series of difference Fourier maps based on low angle reflection data were calculated with sin θ/λ limits (0.30, 0.25, 0.20 $Å^{-1}$). One of the peaks enhanced relative to the others, and was assigned to the hydrogen atom. The positional parameters and the isotropic temperature factor of the hydrogen were refined with the low angle data (sin $\theta/\lambda<0.30$ $Å^{-1}$) keeping the rest of the structure fixed. Finally the hydrogen parameters were fixed and all the other atoms were refined with all the reflection data. The final agreement factor is $R=0.053$ (701 parameters refined). The refinement was based on F_o with unit weights. The final atomic parameters are given in Table 1. Interatomic distances and bond angles are listed in Table 2. The listings of the structure factors and anisotropic thermal parameters are available from the authors upon request.

DISCUSSION

The unit cell contains four $[PPN]^+$ and $[HFe_3(CO)_{11}]^-$ ions. In the $[PPN]^+$ ion there is a slight structural distortion in the orientation of the phenyl rings (Fig. 1). The P–N bond lengths are equal (1.568(7) and 1.573(6) Å). The bonding angle P–N–P seems to be sensitive to the nature of the anion. A bond angle of 147.2(5)° was observed in the present structure, while smaller angles of 140.0(2)° and 139.7(6)° are found in the $[PPN]^+$ salts of $[CoRu_3(CO)_{13}]^-$ [6] and $[HRu_3(CO)_{11}]^-$,[10] respectively. All the other dimensions of the cation are similar to those found in other cluster complexes containing the $[PPN]^+$ ion.[10]

The structure of the $[HFe_3(CO)_{11}]^-$ anion (Fig. 2) consists of a triangular array of iron atoms containing an $Fe(CO)_4$ group which is symmetrically linked to two iron atoms in the $Fe_2(CO)_6(\mu\text{-}CO)(\mu\text{-}H)$ fragment by Fe–Fe

Table 2. Selected interatomic distances (Å) and bond angles (°) for $[PPN]^+[HFe_3(CO)_{11}]^-$.

Fe1–C1	1.922(11)	Fe2–C10	1.790(11)
Fe1–C2	1.783(10)	Fe2–C11	1.744(13)
Fe1–C3	1.801(12)	Fe3–C5	1.770(14)
Fe1–C4	1.761(10)	Fe3–C6	1.798(13)
Fe2–C1	1.938(11)	Fe3–C7	1.732(12)
Fe2–C9	1.731(12)	Fe3–C8	1.774(12)
Fe1–Fe2	2.572(2)	Fe1–H1	1.80(7)
Fe1–Fe3	2.699(2)	Fe2–H1	1.79(7)
Fe2–Fe3	2.674(2)		
C1–O1	1.202(13)	C7–O7	1.163(15)
C2–O2	1.137(12)	C8–O8	1.155(14)
C3–O3	1.145(16)	C9–O9	1.141(16)
C4–O4	1.172(13)	C10–O10	1.155(14)
C5–O5	1.147(15)	C11–O11	1.129(16)
C6–O6	1.149(16)		
P1–N	1.568(7)	P1–C24	1.812(8)
P2–N	1.573(6)	P2–C30	1.783(8)
P1–C12	1.811(9)	P2–C36	1.804(9)
P1–C18	1.772(9)	P2–C42	1.810(9)
Fe1–Fe2–Fe3	61.9(1)	Fe2–Fe3–Fe1	57.2(1)
Fe3–Fe1–Fe2	60.9(1)		
Fe1–H1–Fe2	92(3)	Fe1–C1–Fe2	83.5(4)
Fe1–Fe2–H1	45(2)	Fe3–Fe1–H1	90(2)
Fe2–Fe1–H1	44(2)	Fe3–Fe2–H1	91(2)
Fe2–Fe1–C1	48.5(3)		
Fe1–Fe2–C1	48.0(3)	Fe1–Fe3–C6	93.5(4)
Fe3–Fe1–C1	76.4(3)	Fe2–Fe3–C6	91.6(4)
Fe3–Fe2–C1	76.8(3)	Fe1–Fe3–C7	100.4(4)
Fe2–Fe1–C2	108.4(3)	Fe2–Fe3–C7	157.1(4)
Fe3–Fe1–C2	164.8(3)	Fe1–Fe3–C8	76.3(4)
Fe2–Fe1–C3	116.8(4)	Fe2–Fe3–C8	77.0(4)
Fe3–Fe1–C3	98.6(4)	Fe1–Fe2–C9	108.2(4)
Fe2–Fe1–C4	129.2(4)	Fe3–Fe2–C9	167.6(4)
Fe3–Fe1–C4	82.7(4)	Fe1–Fe2–C10	118.3(4)
Fe1–Fe3–C5	154.1(4)	Fe3–Fe2–C10	97.5(4)
Fe2–Fe3–C5	97.8(4)	Fe1–Fe2–C11	133.4(4)
		Fe3–Fe2–C11	85.5(4)
Fe1–C1–O1	138.3(8)	Fe2–C10–O10	171.7(10)
Fe1–C2–O2	177.9(9)	Fe2–C11–O11	176.7(10)
Fe1–C3–O3	172.1(11)	Fe3–C5–O5	176.3(11)
Fe1–C4–O4	176.6(11)	Fe3–C6–O6	175.1(11)
Fe2–C1–O1	137.5(8)	Fe3–C7–O7	177.6(12)
Fe2–C9–O9	178.3(13)	Fe3–C8–O8	169.8(10)
C1–Fe1–C2	88.4(5)	C9–Fe2–C10	94.0(5)
C1–Fe1–C3	165.1(5)	C9–Fe2–C11	97.9(6)
C1–Fe1–C4	91.5(5)	C10–Fe2–C11	97.0(6)
C1–Fe2–C9	91.0(5)	C5–Fe3–C6	93.9(6)

Table 2. Continued.

C1–Fe2–C10	166.2(5)	C5–Fe3–C7	103.7(6)
C1–Fe2–C11	95.1(5)	C5–Fe3–C8	92.5(6)
C2–Fe1–C3	96.0(5)	C6–Fe3–C7	94.8(6)
C2–Fe1–C4	98.4(5)	C6–Fe3–C8	167.6(5)
C3–Fe1–C4	101.8(5)	C7–Fe3–C8	93.9(6)
P1–N–P2	147.2(5)		

bonds. The two unbridged edges Fe1–Fe3 and Fe2–Fe3 are essentially equivalent 2.699(2) and 2.674(2) Å, while the third, bridged Fe1–Fe2 bond is considerably shorter, 2.572(2) Å. In the terminal carbonyl ligands the small variations in the Fe–C bond lengths, 1.731(12)–1.801(12) Å, and in the C–O bond lengths, 1.129(16)–1.172(13) Å, are similar to the variations observed in related structures.[10]

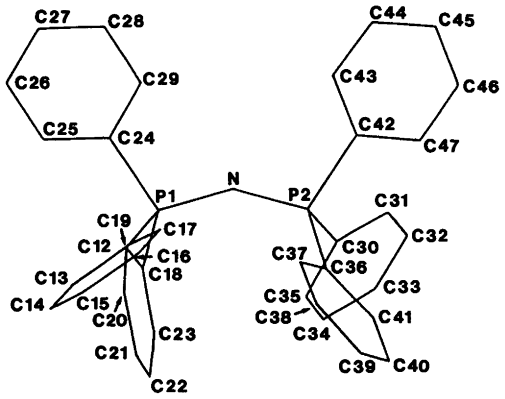

Fig. 1. The numbering scheme of the $[PPN]^+$ cation. Hydrogen atoms have been omitted for clarity.

The bridging carbonyl ligand is symmetrically coordinated to two iron atoms Fe1 and Fe2 with almost identical Fe1–C1 and Fe2–C1 distances of 1.922(11) and 1.938(11) Å. The C1–O1 bond length of 1.202(13) Å and Fe1–C1–Fe2 bond angle of 83.5(4)° are within the normal ranges for doubly bridged carbonyl ligands.[4] The bridging hydrogen atom lies above the plane of the iron triangle. The iron—hydrogen bond distances are essentially equal [1.80(7) and 1.79(7) Å]. The symmetric coordination of the bridging CO and hydrogen gives the $[HFe_3(CO)_{11}]^-$ ion an approximate C_s point group symmetry.

Comparision of the results from the present structure determination with earlier determinations on two related triangular iron clusters with a structural formula of $Fe_3(CO)_{10}(\mu\text{-H})(\mu\text{-Y})$, where $Y=CNMe_2$[11] or COMe,[12] reveals almost isosceles triangles of iron atoms. The two unbridged Fe–Fe bonds are longer than the bridged Fe–Fe bond in the $[Fe_3(CO)_{10}(\mu\text{-H})(\mu\text{-CO})]^-$ monoanion [2.687(2), 2.572(2) Å], in $Fe_3(CO)_{10}(\mu\text{-H})(\mu\text{-COMe})$ [2.667(2), 2.596(2) Å] and in $Fe_3(CO)_{10}(\mu\text{-H})(\mu\text{-C=NMe}_2)$ [2.696(2),

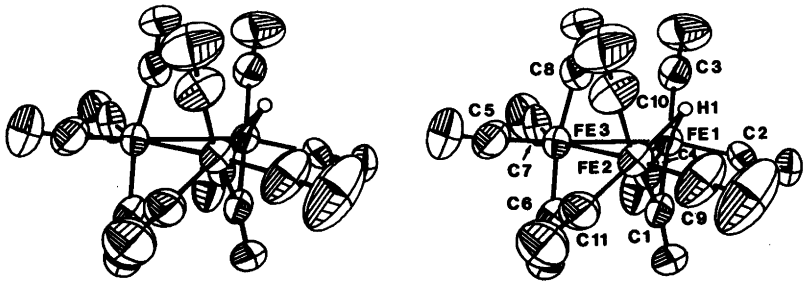

Fig. 2. Stereoscopic view of the structure of the $[HFe_3(CO)_{11}]^-$ anion. The thermal ellipsoids enclose 50 % electron probability.

Table 3. Comparision of bridged metal–metal and metal–hydrogen distances and metal–hydrogen–metal bond angles in hydrogen bridged triangulo-tri-iron complexes.

Molecule	Fe–Fe (Å)[a]	Fe–H (Å)[a]	Fe–H–Fe (°)[a]	Type[b]	Ref.
$[Et_3NH]^+[HFe_3(CO)_{11}]^-$	2.577(3)	–	–	X	2
$[N(PPh_3)_2]^+[HFe_3(CO)_{11}]^-$	2.589(2)	1.693(4)	99.7(2)	N	3
$[N(PPh_3)_2]^+[HFe_3(CO)_{11}]^-$	2.572(2)	1.80(7)	92(3)	X	c
$HFe_3(CO)_{10}(C{=}NMe_3)$	2.565(2)	1.61(9)	106(5)	X	11
$HFe_3(CO)_{10}(COMe)$	2.596(2)	–	–	X	12
$HFe_3(CO)_9(SPr^i)$	2.678(2)	1.80(13)	96(6)	X	13
$HFe_3(CO)_9(N{=}CHMe)$	2.588(1)	1.65(6)	103(3)	X	14
$HFe_3(CO)_9(NH{=}CMe)$	2.754(1)	1.71(3)	107(2)	X	14
$H_2Fe_3(CO)_8(PMe_2)_2$	2.645(1)	1.57(5)	116(3)	X	15
$H_3Fe_3(CO)_9(CMe)$	2.618	–	104	X	16

[a] Whenever appropriate, averages are reported. [b] N=neutron, X=X-ray. [c] Present paper.

2.565(2) Å]. This shortening is ascribed mainly to double bridging since a single bridging hydride ligand normally causes a lengthening of the distance between metal atoms.[17] Ligands such as μ–CO, μ–COMe and μ–$CNMe_2$ have a similar bond-shortening effect which more than counterbalances the lengthening effect of the μ–hydride.

Although the bridged Fe–Fe bonds in the hydrogen bridged triangulo-tri-iron complexes listed in Table 3 are single bonds on the basis of the 18-electron rule, the bond lengths range from 2.565 to 2.754 Å. The longest Fe–Fe distance of 2.754 Å observed in $HFe(CO)_9(NH{=}CMe)$[14] is attributed mainly to the steric requirements of the bridging iminyl group. A rather large variation in the observed Fe–H distances and Fe–H–Fe bond angles reflects the low accuracy of the metal–hydrogen bond length determinations by X-ray methods.

Acknowledgement. Financial support from the Neste OY Foundation is gratefully acknowledged.

REFERENCES

1. a. Wei, C.H. and Dahl, L.F. *J. Am. Chem. Soc. 88* (1966) 1821; *91* (1969) 1351; b. Cotton, F.A. and Troup, J.M. *J. Am. Chem. Soc. 96* (1974) 4155.
2. Dahl, L.F. and Blount, J.F. *Inorg. Chem. 4* (1965) 1373.
3. Takusagawa, F., Fumagalli, A. and Koetzle, T.F. *Unpublished results; cf.* Teller, R.G. and Bau, R. *Struct. Bonding (Berlin) 44* (1981) 69.
4. Lo, F.Y., Longoni, G., Chini, P., Lower, L.D. and Dahl, L.F. *J. Am. Chem. Soc. 102* (1980) 7691.
5. Wilkinson, J.R. and Todd, L.J. *J. Organomet. Chem. 118* (1976) 199.
6. Steinhardt, P.C., Gladfelter, W.L., Harley, A.D., Fox, J.R. and Geoffroy, G.L. *Inorg. Chem. 19* (1980) 1332.
7. Sheldrick, G.M. *The SHELXTL System,* Rev. 2.5, Nicolet Co., 1980.
8. *International Tables for X-Ray Crystallography,* Kynoch Press, Birmingham 1974, Vol. 4.
9. a. La Placa, S.J. and Ibers, J.A. *J. Am. Chem. Soc. 85* (1963) 3501; b. La Placa, S.J. and Ibers, J.A. *Acta Crystallogr. 18* (1965) 511.
10. Johnson, B.F.G., Lewis, J., Raithby, P.R. and Süss, G. *J. Chem. Soc. Dalton Trans.* (1979) 1356.
11. Herbstein, F.H. *Acta Crystallogr. B 37* (1981) 339.
12. Shriver, D.F., Lehman, D. and Strope, D. *J. Am. Chem. Soc. 97* (1975) 1594.
13. Bau, R., Don, B., Greatrex, R., Haines, R.J., Love, R.A. and Wilson, R.D. *Inorg. Chem. 14* (1975) 3021.
14. Andrews, M.A., van Buskirk, G., Knobler, C.B. and Kaesz, H.D. *J. Am. Chem. Soc. 101* (1979) 7245.
15. Keller, E. and Vahrenkamp, H. *Chem. Ber. 114* (1981) 1124.
16. Wong, K.S. and Fehlner, T.P. *J. Am. Chem. Soc. 103* (1981) 966.
17. Teller, R.G. and Bau, R. *Struct. Bonding (Berlin) 44* (1981) 1.

Received May 25, 1982.

Acta Chemica Scandinavica A 37 (1983) 131—140

The Molecular Structures of 1,1′-Dimethylgermanocene and 1,1′-Dimethylstannocene, $(C_5H_4Me)_2M$; M=Ge and Sn, Determined by Gas Electron Diffraction. Self-consistent Field Molecular Orbital Calculations on Germanocene, $(C_5H_5)_2Ge$

JAN ALMLÖF, LIV FERNHOLT, KNUT FÆGRI, JR., ARNE HAALAND, BIRGITTE E. R. SCHILLING, RAGNHILD SEIP and KJELL TAUGBØL

Department of Chemistry, University of Oslo, Blindern, Oslo 3, Norway

The gas electron diffraction patterns of 1,1′-dimethylgermanocene and 1,1′-dimethylstannocene have been recorded with nozzle temperatures of about 100 °C. The diffraction patterns are consistent with "bent sandwich" structures of C_2 symmetry and perpendicular metal-to-ring distances of 2.221(8) Å (Ge) and 2.400(6) Å (Sn), respectively, corresponding to average bond distances Ge–C=2.531(7) Å and Sn–C =2.689(6) Å. The angle between the ring planes is 34(7)° in the Ge- and 50(6)° in the Sn-compound. *Ab initio* molecular orbital calculations on $(C_5H_5)_2Ge$ indicate that metal-to-ring bonding is due primarily to interaction between the e_1 π-orbitals of the rings and the $4p_x$ and $4p_y$ orbitals on Ge. The totally symmetric "lone pair" orbital is predominantly a Ge 4*s* orbital. The 3*d* electrons of Ge are of secondary importance for the bonding. The potential energy curves obtained by the MO calculations and the vibrational amplitudes obtained in the GED study of $(C_5H_4Me)_2Ge$ and $(C_5H_4Me)_2Sn$ indicate that the molecules undergo large amplitude ring-metal-ring bending and deformation vibrations.

The synthesis of the first stable organic derivatives of divalent tin and lead, dicyclopentadienyltin and -lead, stannocene and plumbocene, was reported by Fischer and Grubert in 1956.[1] Gas electron diffraction (GED) studies carried out ten years later[2] confirmed earlier suggestions[3,4] that both molecules possess "bent sandwich" structures: The two $(C_5H_5)M$ fragments have at least approximate C_{5v} symmetry, but the ligand rings are not parallel. In $(C_5H_5)_2Pb$ the angle between the planes defined by the two rings is 45(5)°. The angular structures have, like the angular structures of the gaseous dihalides, been rationalized as due to the presence of a stereochemically active lone pair on the metal.

An early X-ray diffraction investigation of one of the two crystalline modifications of $(C_5H_5)_2Pb$ revealed a polymeric structure where each lead atom is surrounded by one terminal *pentahapto* and two bridging cyclopentadienyl rings.[5] Though this study brought out the main features, a reinvestigation would be desirable in order to determine the position of the bridging ligand rings more accurately and to provide clues to the direction of the electron lone pair.

More recently, the structures of the monomeric compounds $(C_5H_5)_2Sn$,[6] bis(pentamethylcyclopentadienyl)tin,[7] $(C_5Me_5)_2Sn$ and $(C_5Me_5)_2Pb$[6] have been determined by X-ray crystallography. In general, these studies confirm the results of the early GED investigations, but due to the low molecular symmetry of these species, the X-ray studies provide more exact information. In particular the angle between the ring planes is determined to the nearest degree.

The X-ray studies also show that in all these molecules the metal atom is displaced by 0.2 or 0.3 Å from the intersection of the fivefold symmetry axes of the rings, approximately in the

0302-4377/83 $2.50

direction of the intersection of the two ring planes. We shall return to these points in our discussion.

The synthesis of germanocene, $(C_5H_5)_2Ge$, was reported by Scibelli and Curtis in 1973.[8] The compound is, however, rather unstable: After only three hours at room temperature it is completely polymerized to give a solid which is nonvolatile and insoluble in common organic solvents.[8] Since 1,1'-dimethylgermanocene, $(C_5H_4Me)_2Ge$, was reported to be more stable,[9] we decided to attempt a structure determination of this and the analogous tin compound by GED. Since the results of an earlier GED study of $(C_5Me_5)_2Ge$[10] have been withdrawn,[11] $(C_5H_4Me)_2Ge$ is the first germanocene to be structurally characterized.

At the same time, we report the results of a series of SCF MO calculations on $(C_5H_5)_2Ge$ which elucidate the nature of the metal to carbon bonds and the potential energy surface of the molecule.

EXPERIMENTAL

$(C_5H_4Me)_2Ge$ and $(C_5H_4Me)_2Sn$ were synthesized from $(C_5H_4Me)K$ and GeI_2 and $SnCl_2$, respectively, as described by Stobart and coworkers.[9]

The scattering patterns of both compounds were recorded on Balzers Eldigraph KDG-2. In order to keep the temperature as low as possible, the data for the Ge compound were recorded with a convergent electron beam and a nozzle with a wide opening.[12] The nozzle temperature was about 100 °C. After the sample had evaporated, the ampoules were found to contain small amounts of yellow solid which we initially assumed to be a polymerization product. Subsequent analysis by neutron activation showed, however, that the sample as prepared contained significant amounts of iodine, possibly in the form of $(C_5H_4Me)GeI$. Consequently a new sample was prepared which by neutron activation analysis was free from iodine. When the electron diffraction experiment was repeated with the new sample, no residue was found and the scattering data were in agreement with those obtained with the impure sample.

The data for the tin compound were recorded with a narrow parallel electron beam and a new nozzle system: The inlet system ends in a torus (hollow doughnut) surrounding the electron beam. The gas emerges from a narrow horizontal slit extending over 360°. Trial runs with benzene show that this nozzle permits the recording of electron diffraction data with a gas pressure of about 1 torr and a conventional beam geometry. Structure refinements of benzene based on several plate sets, show no systematic errors due to broadening of the molecular beam. The diffraction data of $(C_5H_4Me)_2Sn$ were recorded with a temperature of about 100 °C.

Exposures were made with nozzle-to-plate distances of 50 and 25 cm. The number of plates used were five 50 cm and four 25 cm plates for M=Ge, and six 50 cm and six 25 cm plates for M=Sn.

The data were processed by standard methods. The complex atomic scattering factors, $f'(s)$, of Ge, C and bonded H were calculated from an analytical representation of the atomic potential[13] using a program written by Yates.[14] The scattering factor of Sn was obtained by interpolation of numerical tables.[15] The molecular intensities were modified through multiplication with $s/|f_C(s)|\ |f_M(s)|$. The average modified molecular intensities from the 50 cm plates ranged from s=2.00 to 15.00 Å^{-1} with s=0.125 Å^{-1}, and the molecular intensities from the 25 cm plates ranged from s=4.00 to 28.50 Å^{-1} with s=0.25 Å^{-1}.

STRUCTURE ANALYSIS

A molecular model for $(C_5H_4Me)_2M$, M=Ge or Sn is shown in Fig. 1. It was assumed that an

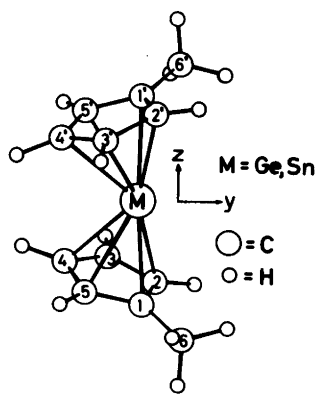

Fig. 1. Molecular model of $(C_5H_4Me)_2M$, M=Ge or Sn. The molecular symmetry is C_2 with the symmetry axis coinciding with the y-axis. In this model the position of the metal atom is such that all M–C bond distances are equal. Displacement of the metal atom from this position along the y-axis is denoted by δy and defined as positive when the metal atom is moved to the right.

adequate model for the C_5H_4Me ligand in either compound could be constructed from a C_5H_5 ring with D_{5h} symmetry by removing one H atom and replacing it by an Me group. The methyl groups were assumed to have C_{3v} symmetry with the symmetry axis along the C–C bonds and with one C–H bond in a plane perpendicular to the C_5 ring as indicated in Fig. 1. All C–H bonds were assumed equal. The structure of the ligand in each compound is then determined by the following independent parameters: The C–H, C(1)–C(2) and C(1)–C(6) bond distances, the methyl ∠CCH bond angle, and the angle between the C(1)–C(6) bond and the ring plane which we denote by $\angle C_5$,C–C and define as positive when the Me group is bent *away* from the metal atom.

The metal atom was assumed to lie on the fivefold symmetry axis of each ring at a perpendicular distance h from each. The ten M–C bond distances are then equal. (We shall return to the validity of this assumption below.)

Finally the molecular symmetry was assumed to be C_2 with the symmetry axis coinciding with the y-axis in Fig. 1. The molecular structure is then determined by eight independent parameters; the five parameters describing the ligands plus the M–C bond distance, the angle between the two ring planes which we denote by $\angle C_5,C_5$ and a dihedral angle, ϕ, determining the orientation of the ligand rings. We define ϕ as the angle between the yz plane and a plane through M and the C(1)–C(6) bond. When $\phi=0$, the C(1)–C(6) and C(1′)–C(6′) bonds are pointing along the positive y axis. It should here be pointed out that ϕ is determined primarily by the five distances C(1,2,3,4 or 5) to C(6′), rather than by the distance C(6) to C(6′). Subsequent least-squares refinement gave $\phi=55(25)°$ when M=Ge and $\phi=62(15)°$ when M=Sn. We do not feel that any significance can be attached to these values.

The independent structure parameters were refined by least-square calculations on the intensity data with diagonal weight matrices and under the constraints of geometrically consistent r_a structures.[16] For $(C_5H_4Me)_2Ge$ five r.m.s. vibrational amplitudes were included in the refinement, in the case of $(C_5H_4Me)_2Sn$ seven amplitudes could be refined. The refinements converged to give the structure parameters listed in Table 1. The estimated standard deviations have been multiplied by a factor of three to include uncertainty due to correlation in the experimental data and errors introduced by the assumptions made regarding the molecular model.

Experimental radial distribution curves calculated by Fourier inversion of experimental modified molecular intensity curves are shown in

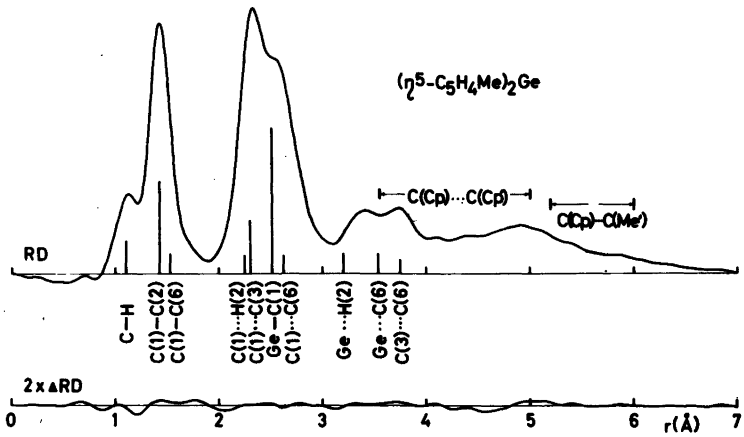

Fig. 2. Above: Experimental radial distribution (RD) curve for $(C_5H_4Me)_2Ge$. Artificial damping constant $k=0.002$ Å^2. Major interatomic distances are indicated by bars of height approximately proportional to the area under the corresponding peak. C(Cp)---C(Cp′) indicates the range of distances between carbon atoms in different C_5 rings. C(Cp)---C(Me′) indicates the range of distances from carbon atoms in one C_5 ring to the methyl C atom on the other. *Below:* Difference between the experimental curve and the theoretical curve calculated for the best model.

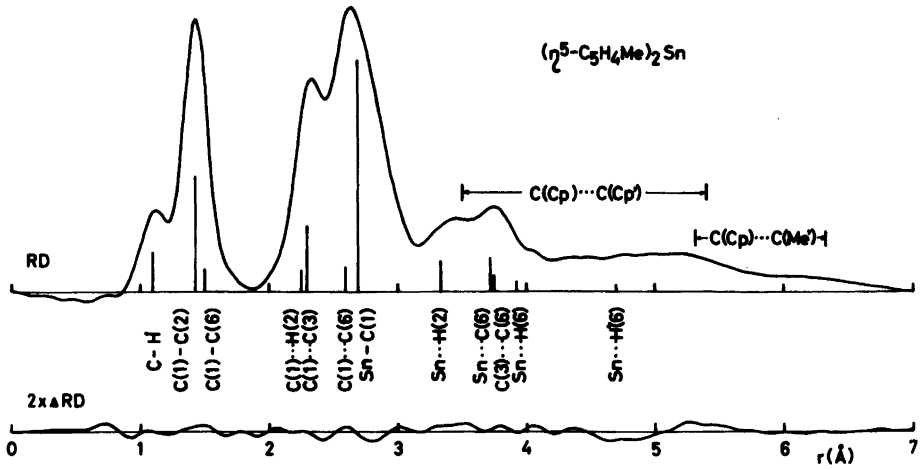

Fig. 3. Experimental RD curve and difference curve for $(C_5H_4Me)_2Sn$. For further comments consult text below Fig. 2.

Figs. 2 and 3 along with the difference between these curves and their theoretical counterparts calculated for the best model. We consider the agreement satisfactory.

MOLECULAR ORBITAL CALCULATIONS

As a measure of economy, we chose to carry out MO calculations on the unsubstituted germanocene, $(C_5H_5)_2Ge$, rather than on the dimethyl derivative. Comparison of the results with those obtained for decamethylgermanocene shows that full methyl substitution has little effect on metal-to-ligand bonding.[11]

Ab initio MO calculations were carried out with better than double zeta basis. For Ge we used a (14,11,5) Gaussian type basis contracted to ⟨8,7,3⟩,[17] for C a (7,3) basis contracted to ⟨4,2⟩,[18] and for H a (4) basis contracted to ⟨2⟩.[19] The calculations were carried out with the program DISCO.[20]

In all calculations the (C_5H_5) rings were assumed to have D_{5h} symmetry with C–C and C–H bond distances equal to 1.411 Å and 1.120 Å, respectively.

In Table 3 we first list the SCF energies obtained with molecular models of D_{5d} symmetry (*i.e.* with parallel and staggered ligand rings) and different perpendicular metal-to-ring distances h. For three different values of h the calculations were repeated on models of D_{5h} symmetry (*i.e.* with eclipsed rings).

Calculations on "bent sandwich" models were first carried out with retention of the C_{5v} symmetry of each $(C_5H_5)Ge$ cone. The molecular symmetry was assumed to be C_{2v} (eclipsed rings) and the angle between the ring planes, $\angle C_5,C_5$, changed in steps of 20°.

Finally a model reasonably close to the GED structure of $(C_5H_4Me)_2Ge$ (h=2.216 Å and $\angle C_5,C_5$=20°) was selected for investigation of the variation of energy when the metal atom is displaced along the C_2 axis (the y axis in Fig. 1). When y=0, each $(C_5H_5)Ge$ cone has C_{5v} symmetry, further calculations were carried out with y= –0.2, –0.1 and +0.1 Å. The resulting energies are listed in Table 3.

RESULTS AND DISCUSSION

The molecular structures of $(C_5H_4Me)_2Ge$ and $(C_5H_4Me)_2Sn$ by GED. The best values for the structure parameters of dimethylgermanocene and dimethylstannocene are listed in Table 1. In Table 2 we compare the perpendicular metal-to-ring distances (h), the average M–C bond distances, and the angle between the planes of the ligand rings in Group IVB metallocenes studied by electron or X-ray diffraction. The values obtained for metal-to-ring distances or for aver-

Table 1. Interatomic distances, valence angles and vibrational amplitudes (l) of $(C_5H_4Me)_2Ge$ and $(C_5H_4Me)_2Sn$. Estimated standard deviations in parentheses in units of the last digit. The angles have not been corrected for shrinkage.

	r_a/Å	l/Å	r_a/Å	l/Å
$(C_5H_4Me)_2Ge$			$(C_5H_4Me)_2Sn$	
M–C	2.531(7)	2.689(6)	0.164(4)	
C(1)–C(2)	1.426(3)	0.051(5)[a]	1.427(3)	0.049(3)[a]
C(1)–C(6)	1.517(16)	0.058(5)[a]	1.499(12)	0.045(3)[a]
C–H	1.112(10)	0.080(10)	1.105(7)	0.076(7)
M···C(6)	3.57(5)	0.20(5)	3.73(3)	0.17(4)
C(1)···C(3)	2.307(4)	0.057(6)	2.308(4)	0.060(4)
C(2)···C(6)	2.622(14)	0.070(ass)	2.603(12)	0.070(ass)
C(3)···C(6)	3.778(15)	0.082(ass)	3.755(15)	0.082(ass)
C···C′	3.61 to 6.04	0.035(9)[b]	3.54 to 6.34	0.033(9)[b]
h[c]	2.221(8)		2.400(6)	
	(°)		(°)	
<(1)C(6)H	112(ass)		112(ass)	
<C_5,C–C[d]	3(3)		7(3)	
<C_5,C–H[e]	0(ass)		0(ass)	
<C_5,C_5[f]	34(7)		50(6)	

[a] l(C(1)–C(2)) and l(C(1)–C(6)) were refined with constant difference. [b] All inter-ligand C···C′ vibrational amplitudes were assumed equal. [c] Perpendicular distance from metal atom to the C_5-ring plane. [d] Angle between C(1)–C(6) bond and C_5 plane. [e] Angle between C(2,3,4 or 5)–H bond and ring plane. [f] Angle between the two C_5 ring planes.

Table 2. Structure parameters of germanocenes, stannocenes and plumbocenes obtained by gas electron diffraction (GED) and X-ray crystallography (x).

		h/Å	R(M–C)[a]/Å		δ_1, δ_2 [b]/Å	$\angle C_5,C_5$/(°)	Ref.
$(C_5H_4Me)_2Ge$	GED	2.22	2.53		0 (ass)	34(7)	
$(C_5H_5)_2Sn$	GED	2.42	2.71		0 (ass)	~55	2
$(C_5H_5)_2Sn$	X[c]	2.40	2.67	(2.58 to 2.75)	0.21, 0.21[e]	48.4[e]	6
$(C_5H_5)_2Sn$	X[d]	2.42	2.68	(2.56 to 2.85)	0.36, 0.31[e]	45.9[e]	6
$(C_5H_4Me)_2Sn$	GED	2.40	2.69		0 (ass)	50(6)	
$(C_5Me_5)_2Sn$	X[c]	2.39	2.68	(2.57 to 2.78)	0.21, 0.26[e]	36.4	7
$(C_5Me_5)_2Sn$	X[d]	2.38	2.68	(2.59 to 2.77)	0.20, 0.24[e]	35.4	7
$(C_5H_5)_2Pb$	GED	2.50	2.78		0 (ass)	45(5)	2
$(C_5Me_5)_2Pb$	X	2.48	2.79	(2.60 to 2.90)	0.33, 0.24[e]	6	

[a] Mean value and range. [b] Distance from center of mass of each C_5 ring to projection of M onto the ring plane. [c] Molecule 1. [d] Molecule 2. [e] Calculated by us from the atomic coordinates.

age M–C bond distances in the different studies are in good agreement, and there is no indication that these parameters are changed when H-atoms are substituted by Me groups. The decrease of average M–C bond distances on going from Pb to Sn, about 0.10 Å, and from Sn to Ge, about 0.17 Å, is similar to the decrease of the M–Cl bond distances found in the dichlorides, MCl_2, Pb–Cl=2.443(1) Å,[21] Sn–Cl=2.347(7) Å,[22] and Ge–Cl=2.186(4) Å.[23] We assume, therefore, that these variations reflect the different bonding radii of Pb(II), Sn(II) and Ge(II).

The angle between the planes determined by the two ligand rings, $\angle C_5,C_5$, cannot be deter-

mined with accuracy by electron diffraction. Partly, this may be because this parameter is poorly defined by nature, *i.e.* because the molecules undergo large amplitude ring-metal-ring bending vibrations. On the other hand the GED and X-ray results leave no doubt that the equilibrium structures are bent, at least when M=Sn and Pb.

Comparison of the values for $\angle C_5,C_5$ in the complexes in Table 2, shows that full methyl substitution forces the two rings into a more parallel conformation, as indeed one would expect from steric effects. (The authors of Ref. 6 reached the opposite conclusion after confusing the angle between the ring normals with the ring-centroid metal ring-centroid angle.) One might also expect the angle between the ring planes to increase with the size of the metal atom, but no such effect is apparent from the data in Table 2.

Crystalline $(C_5H_5)_2Sn$ contains two crystallographically independent molecules, one of which is eclipsed (by space group symmetry), the other staggered, suggesting that the barrier to ring rotation is low. In the solid decamethyl compounds, $(C_5Me_5)_2Sn$ and $(C_5Me_5)_2Pb$, the ligand rings are approximately staggered.

As the maximum symmetry of a bent metallocene is C_{2v}, the ten M–C bond distances are no longer equal by symmetry: The metal atom needs no longer reside at the intersection of the C_5 symmetry axes of the rings, or more precisely the projection of the metal atom onto each ring needs not coincide with the center of mass of the ring. Indeed, the X-ray studies quoted in Table 2 show unequivocally that the individual M–C distances in one molecule may differ by as much as 0.30 Å. In each case the metal atom has moved away from the (approximate) fivefold symmetry axes of the rings towards the corner formed by the intersection of the two ring planes, *i.e.* roughly along the negative y axis in Fig. 1. In Table 2 we list the distance, δ, between the projection of the metal atom and the center of mass for each of the two rings. The different values obtained for δ in the two crystallographically independent molecules of $(C_5H_5)_2Sn$ and for the two rings in the same molecule of $(C_5Me_5)_2Pb$, show that the energy of the molecule varies slowly with δ. In other words the ring-metal-ring deformation (metal atom displacement) mode must be very soft.

Starting with a molecular model of D_{5h} symmetry, an idealized (C_{2v}) model of a bent metallocene may be obtained in two steps: A ring-metal-ring bending motion with retention of C_{5v} symmetry of the $(C_5H_5)M$ fragments, followed by displacement of the metal atom along the twofold symmetry axis y. In our structure refinements of $(C_5H_4Me)_2M$, we have explicitly assumed that the C_5M cones retain C_{5v} symmetry, *i.e.* that $\delta=0$. The large values obtained for the root-mean-square M–C vibrational amplitudes show that either this assumption is invalid for the equilibrium structure or that the metal displacement mode is very soft (or both). Indeed the M–C vibrational amplitudes obtained in the present study l(Ge–C)=0.201(7) Å and l(Sn–C)=0.164(4) Å, indicate that the equilibrium displacement is larger – or more softer – in the Ge than in the Sn compound.

There is, of course, no difficulty in principle in modifying our model to include a metal atom displacement coordinate along the y axis. The difficulty is that when $\delta = 0$, not only are the M–C bond distances unequal, but so are their vibrational amplitudes. Our experience in a GED study of $(C_5Me_5)GeCl$ shows that the value obtained for δ depends critically on the values of these amplitudes.[24] We have therefore preferred to study the lateral displacement of the metal atom in connection with self-consistent field molecular orbital calculations on $(C_5H_5)_2Ge$.

Molecular orbital calculations on $(C_5H_5)_2Ge$. No *ab initio* MO studies on germanocene or the other Group IVB metallocenes have been published. Stannocene has, however, been studied by Extended Hückel calculations: Jutzi, Hofmann and their coworkers[7] carried out calculations on models with different values for the angle $\angle C_5,C_5$, and suggested that the driving force responsible for the bending is the two "lone pair" electrons occupying the highest molecular orbital: The energy of this orbital was found to fall rapidly when the molecule is bent. This suggestion is in agreement with earlier rationalizations in terms of a stereochemically active lone pair.

The SCF energies obtained by *ab initio* calculations on various geometrical models of $(C_5H_5)_2Ge$ are listed in Table 3. The lowest energy was obtained with a model of D_{5h} symmetry and a metal-to-ring distance of h=2.34 Å, about 0.12 Å greater than the experimental

value for $(C_5H_4Me)_2Ge$. We do not regard this discrepancy as serious, though it does indicate that our calculations fail to account for the full strength of the metal-to-ligand bond. The failure of the Hartree-Fock approximation to give metal-to-ring distances in agreement with experiments for sandwich compounds of the transition elements has recently been the subject of extensive discussions.[25,26]

The barrier to internal rotation of the cyclopentadienyl rings is very small. At the experimental metal-to-ring distance the calculated energy difference between eclipsed (D_{5h}) and staggered (D_{5d}) models corresponds to a barrier of only 0.2 kJ mol^{-1}. At the optimal metal-to-ring distance the calculated barrier is even smaller.

Gross atomic populations and overlap populations obtained for three different geometries of $Ge(C_5H_5)_2$ are listed in Table 4. The gross population on Ge corresponds to a formal charge of +1.0. If two neutral (C_5H_5) rings and a Ge atom with electron configuration Ar $(3d)^{10}$ $(4s)^2$ $(4p_x)^1$ $(4p_y)^1$ are taken as point of departure, the orbital populations suggest that the major change introduced by bond formation is the transfer of

Table 3. Total energies (in atomic units) obtained by SCF MO calculations on different models of $(C_5H_5)_2Ge$.

Model	$-E-2458.0$ (a.u.)
D_{5d}	
h=1.987 Å	0.47500
h=2.087 Å	0.51742
h=2.216 Å[a]	0.54567
h=2.287 Å	0.55136
h=2.337 Å[b]	0.55196
h=2.387 Å	0.55101
h=2.487 Å	0.54083
C_{2v}, h=1.987 Å	
$\angle C_5,C_5$=0° (D_{5h})	0.47493
$\angle C_5,C_5$=20°	0.47646
$\angle C_5,C_5$=50°	0.47161
C_{2v}, h=2.216 Å[a]	
$\angle C_5,C_5$=0° (D_{5h})	0.54567
$\angle C_5,C_5$=20°	0.54543
$\angle C_5,C_5$=40°	0.54101
C_{2v}, h=2.337 Å[a]	
$\angle C_5,C_5$=0° (D_{5h})	0.55196
$\angle C_5,C_5$=20°	0.55159
$\angle C_5,C_5$=40°	0.54730
C_{2v}, h=2.216 Å,[a]	
$\angle C_5,C_5$=20°	
δy= 0[c]	0.54543
δy=+0.10 Å	0.54415
δy=−0.10 Å	0.54518
δy=−0.20 Å	0.54330

[a] Experimental value (for $(C_5H_4Me)_2Ge$). [b] Optimal value. [c] Displacement of metal atom along the y-axis in Fig. 1. See text for details.

Table 4. Orbital populations, gross atomic populations and overlap populations in $(C_5H_5)_2Ge$.

h / $\angle C_5,C_5$	2.337 Å[a] 0°	2.216 Å[b] 0°	2.216 Å[b] 20°
Orbital populations			
Ge s	8.21	8.24	8.22
p_x	4.48	4.47	4.45
p_y	4.48	4.47	4.46
p_z	4.11	4.06	4.12
d	9.79	9.76	9.76
Gross atomic populations			
Ge	31.07	30.99	31.01
C	6.34	6.35	6.36[c]
H	0.76	0.75	0.75[c]
(C_5H_5)	35.47	35.51	35.50
Overlap populations			
Ge–C	−0.01	−0.03	−0.03[c]
Ge–(C_5H_5)	−0.05	−0.19	−0.17

[a] Optimal value. [b] Experimental value. [c] Average values.

Table 5. Ionization potentials (in ev) calculated from Koopmans' theorem (IE= $-\varepsilon$) and from SCF energies of cation and neutral molecule [IE=ΔE_{SCF} = E_{SCF}(ion$^+$) − E_{SCF} (molecule)].

h (Å)	2.287	2.487
$-\varepsilon(9a_{1g})$	9.61	10.89
$E_{SCF}(^2A_{1g})-E_{SCF}(^1A_{1g})$	8.78	10.14
$-\varepsilon(5e_{1g})$	8.04	7.85
$E_{SCF}(^2E_{1g})-E_{SCF}(^1A_{1g})$	7.60	7.43
$-\varepsilon(6e_{1u})$	9.51	9.12
$E_{SCF}(^2E_{1u})-E_{SCF}(^1A_{1g})$	9.08	8.72

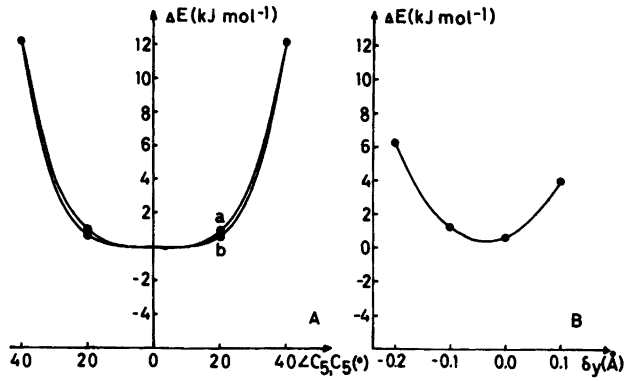

Fig. 4. A. Variation of SCF energy of $(C_5H_5)_2Ge$ with ring-metal-ring bending. $\angle C_5,C_5$ is the angle between the planes defined by the C_5 ligand rings. *a*: h=2.337 Å (optimal metal-to-ring distance) and *b*: h=2.216 Å (experimental distance). B. Variation of SCF energy with displacement of the metal atom along the C_2 symmetry axis of the molecule, *i.e.* the *y*-axis in Fig. 1. h=2.216 Å and $\angle C_5,C_5$=20°.

about 0.5 electron from each of the two *4p* orbitals into e_{1u} π-orbitals on the rings. The orbital population of the $4p_z$ orbital is insignificant, indicating that this orbital does not interact significantly with ligand orbitals. The orbital occupation of the Ge *d*-orbitals is 9.8 electrons, indicating a metal-to-ring donation of only 0.2 electrons, the involvement of *3d* electrons in bonding is thus clearly of secondary importance.

The energies of the three highest occupied molecular orbitals are listed in Table 5, the variation of orbital energies with the metal-to-ring distance is shown in Fig. 4. The $9a_{1g}$ orbital is predominantly a *4s* "lone pair" orbital on Ge, but it also contains a significant antibonding contribution from the ring a_{1g} π-orbitals. The total metal-ring overlap population in the a_{1g} representation is consequently negative (about –0.3), and the $9a_{1g}$ orbital energy falls rapidly with increasing metal-to-ring distance. The $5e_{1g}$ orbital is formed by combination of e_1 π-orbitals of the rings, as a good first approximation it may be regarded as nonbonding between metal and rings. The third high-lying orbital is $6e_{1u}$ which is a bonding combination of e_1 ring π-orbitals and $4p_x$ and $4p_y$ on Ge. The total metal-ring overlap population in the e_{1u} representation is about +0.2, and the energy of the $6e_{1u}$ orbital increases markedly with h. Because of the large negative overlap population in the a_{1g} representation, the total metal-ring overlap population becomes negative.

In Fig. 4A we show the change in SCF energies with ring-metal-ring bending. The potential energy curves obtained with optimal and experimental metal-to-ring distances are very similar with a minimum at – or close to – $\angle C_5,C_5$=0°, corresponding to a D_{5d} equilibrium structure. Both potential wells are very wide, $\angle C_5,C_5$ may reach nearly 30° before the potential energy becomes equal to the average thermal energy available at the temperature of the GED experiment, RT=3 kJ mol^{-1}. At small (~20°) values of $\angle C_5,C_5$ the energy curve obtained with the experimental value of h, falls below that obtained with the optimum value, and if the metal-to-ring distance is further decreased, the potential energy curve develops a maximum at $\angle C_5,C_5$=0°.

It may at first glance seem surprising that a bent form is calculated to be relatively more stable at short metal-to-ring distances when steric ring-ring repulsion would increasingly favor a parallel conformation. However, as suggested by Jutzi *et al.*, the driving force appears to be the two electrons in the $9a_{1g}$ lone pair orbital[7] and the energy of this orbital falls off more rapidly at short metal-to-ring distances when the orbital energy is higher.

Extended Hückel calculations[27] on $(C_5H_5)_2Ge$ with h fixed at the experimental value gave results similar to those obtained for $(C_5H_5)_2Sn$: The equilibrium structure was found to be bent with $\angle C_5,C_5$=50°. The energy of this conformation was 110 kJ mol^{-1} below that of a parallel

conformation. The reason for the large angle and high barrier appears to be that the EH calculations yield a $9a_{1g}$ orbital energy which is considerably higher than the $6e_{1u}$ orbital energy.

The value obtained for the angle between the two ligand rings in $(C_5H_4Me)_2Ge$ by means of GED, $<C_5,C_6=34(7)°$, is a *thermal average* and is expected to be greater than the *equilibrium value*. As already pointed out, the large estimated standard deviation of $\angle C_5,C_5$ may be regarded as an indication that the gas at a given instant contains molecules with very different bending angles, *i.e.* that the molecules undergo large amplitude bending motions.

The results obtained by GED and by SCF-MO calculations are therefore in reasonable – though not perfect – agreement. Taken together they indicate that *molecules in the gas phase are significantly bent with an average value at* $\angle C_5,C_5$ *between 20 and 40°, and that the molecules undergo large amplitude bending vibrations.* The *equilibrium* value of $\angle C_5,C_5$ remains uncertain, we estimate that it is between 10 and 30°.

Finally we carried out a series of calculations with h fixed at the experimental value $\angle C_5,C_5=20°$ and the metal atom displaced along the C_2 symmetry axis of the molecule, (the y-axis in Fig. 1). The displacement δy was defined as zero when all Ge–C bond distances are equal. The resulting potential energy curve is shown in Fig. 4B. The minimum appears to occur when the metal atom displaced two or three hundredths of an Å unit to the left in Fig. 1. Again the potential energy curve is very soft and the metal atom may move about 0.15 Å to either side of the minimum before the potential energy exceeds RT. This is in agreement with the large vibrational amplitude of the Ge–C bonds in $(C_5H_4Me)_2Ge$ obtained by least-squares refinement on a symmetrical ($\delta y=0$) model, $l=0.201(7)$ Å.

It is well known that the sequence of ionization potentials for transition metal complexes like ferrocene may differ from that obtained from the orbital energies using Koopmans' theorem.[28] In order to investigate whether similar discrepancies are to be expected for derivatives of germanocene, we have performed separate SCF calculations on some of the lower electronic states of $(C_5H_5)_2Ge^+$ and calculated the ionization energies from $IE=E_{SCF}(ion)-E_{SCF}(molecule)$. Inspection of Table 5 and Fig. 5 shows that the IE's obtained in this manner are somewhat smaller due to electronic relaxation. But the sequence of ionization potentials remains as predicted by Koopmans' theorem except near those values of h where orbital energy curves cross.

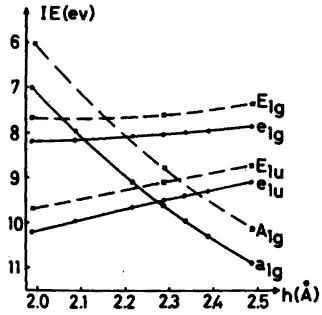

Fig. 5. Ionization energies of electrons in the three highest occupied molecular orbitals of $(C_5H_5)_2Ge$. ● and full line: calculated by Koopmans' theorem ($IE=-\varepsilon$). ■ and stippled line: calculated from SCF energies of cation and neutral molecule [$IE=\Delta E_{SCF}=E_{SCF}(ion)-E_{SCF}(molecule)$].

Acknowledgements. We are grateful to Dr. E. Kvåle for carrying out neutron activation analysis, to Dr. Chr. Rømming for calculating some of the parameters quoted in Table 2 from atomic coordinates, and to The Norwegian Research Council for Science and the Humanities and the Norwegian Research Council for Science and Technology for financial support.

REFERENCES

1. Fischer, E. O. and Grubert, H. *Z. Anorg, Chem. 286* (1956) 237.
2. Almenningen, A., Haaland, A, and Motzfeldt, T. *J. Organomet. Chem. 7* (1967) 97.
3. Dave, L. D., Evans, D. F. and Wilkinson, G. *J. Chem. Soc.* (1959) 3684.
4. Fritz, H. P. and Fischer, E. O. *J. Chem. Soc.* (1961) 3684.
5. Panattoni, C., Bambieri, G. and Croatto, U. *Acta Crystallogr. 21* (1966) 823.
6. Atwood, J. L., Hunter, W. E., Cowley, A. H., Jones, R. A. and Stewart, C. A. *J. Chem. Soc. Chem. Commun.* (1981) 925.
7. Jutzi, P., Kohl, F., Hofmann, P., Krüger, C. and Tsay, Y.-H. *Chem. Ber. 113* (1980) 757.
8. Scibelli, J. V. and Curtis, M. D. *J. Am. Chem. Soc. 95* (1973) 924.

9. Bonny, A., McMaster, A. D. and Stobart, S. R. *Inorg. Chem. 17* (1978) 935.
10. Fernholt, L., Haaland, A., Jutzi, P. and Seip, R. *Acta Chem. Scand. A 34* (1980) 585.
11. Fernholt, L., Haaland, A., Jutzi, P., Seip, R., Almlöf, J., Fægri, K., Kvåle, E., Lüthi, H. P., Schilling, B.E.R. and Taugböl, K. *Acta Chem. Scand. A 36* (1982) 93.
12. Ashby, E. C., Fernholt, L., Haaland, A., Seip, R. and Smith, R. S. *Acta Chem. Scand. A 34* (1980) 213.
13. Strand, T. G. and Bonham, R. A. *J. Chem. Phys. 40* (1964) 1686.
14. Yates, A. C. *Comput. Phys. Commun. 2* (1971) 175.
15. Bonham, R. A. and Schäfer, L. *International Tables for X-Ray Crystallography,* Kynoch Press, Birmingham 1974, Vol. 4.
16. Gundersen, G. *Annual Reports of the Norwegian Electron Diffraction Group,* Oslo 1980.
17. Huzinaga, S. *Personal communication.*
18. Roos, B. and Siegbahn, P. *Theor. Chim. Acta 17* (1970) 209.
19. Dunning, T. H. *J. Chem. Phys. 53* (1970) 2823.
20. Almlöf, J., Fægri, K., Jr. and Korsell, K. *J. Comp. Chem. 3* (1982) 385.
21. Hargittai, I., Tremmel, J., Vadja, E., Ischenko, A. A., Ivanov, A. A., Ivashkevich, L. S. and Spiridonov, V. P. *J. Mol. Struct. 42* (1977) 147.
22. Ischenko, A. A., Ivashkevich, L. S., Zasorin, E. Z., Spiridonov, U. P. and Ivanov, A. A. *Sixth Austin Symposium on Gas Phase Molecular Structure,* Austin, Texas 1976.
23. Schultz, Gy., Tremmel, J., Hargittai, I., Berecz, I., Bohátka, S., Kagramanov, N. D., Moltsev, A. K. and Nefedov, O. M. *J. Mol. Struct. 55* (1979) 207.
24. Fernholt, L., Haaland, A., Jutzi, P. and Seip, R. *Unpublished results.*
25. Lüthi, H. P., Ammeter, J., Almlöf, J. and Korsell, K. *Chem. Phys. Lett. 69* (1980) 540.
26. Lüthi, H. P., Ammeter, J., Almlöf, J. and Fægri, K., Jr. *J. Chem. Phys. 77*(1982) 2002.
27. Hoffmann, R., *J. Chem. Phys. 39* (1963) 1397; Hoffmann, R. and Lipscomb, W. N. *Ibid. 36* (1962) 2179; *37* (1962) 2872. A weighted H_{ii} formula was used: Ammeter, J. H., Bürgi, H.-B., Thibault, J.C. and Hoffmann, R. *J. Am. Chem. Soc. 100* (1978) 3686. The H_{ii}'s were taken from Hinze, J. and Jaffé, H. H. *J. Chem. Phys. 67* (1963) 1501 and orbital exponents from Burns, G. *J. Chem. Phys. 41* (1964) 1521.
28. Green, J. C. *Struct. Bonding (Berlin) 43* (1981) 37.

Received July 1, 1982.

Acta Chemica Scandinavica A 37 (1983) 141—152

Binuclear Chromium(III) Complexes with *N,N'*-Bis(2-pyridylmethyl)-1,2-propanediamine. Circular Dichroism and Stereochemical and Magnetic Properties

KIRSTEN MICHELSEN and ERIK PEDERSEN

Chemistry Department I (Inorganic Chemistry), University of Copenhagen, H.C. Ørsted Institute, Universitetsparken 5, DK-2100 Copenhagen Ø, Denmark

The synthesis, stereochemical and magnetic properties of binuclear di-μ-hydroxo complexes of the type $[(C_{15}H_{20}N_4)Cr(OH)_2Cr(C_{15}H_{20}N_4)]^{4+}$ with the racemic and optically active tetradentate ligand *N,N'*-bis(2-pyridylmethyl)-1,2-propanediamine are reported. Where the title complex is prepared from racemic ligand, three racemic pairs of complexes are obtained, each resolvable into catoptric forms, two of which are identical with the complexes prepared from *N,N'*-bis(2-pyridylmethyl)-1,2(*R*)-propanediamine. The structures of the complexes are deduced from the decompositions to parentage mononuclear *cis*-α-dichloro complexes of established structures.

The circular dichroism spectra of the optically active di-μ-hydroxo complexes as well as the μ-hydroxo-μ-oxo and di-μ-oxo complexes are reported. Only the first ones (vis. region) can be used in assigning the absolute configurations unambiguously. The magnetic susceptibilities of four of the di-μ-hydroxo complexes indicate antiferromagnetic exchange coupling giving rise to singlet–triplet separations between 44 and 50 cm^{-1}. A fit of the data to a model assuming independent triplet, quintet and septet energies is almost consistent with the Heisenberg model corrected for biquadratic exchange.

Binuclear chromium(III) complexes with one or two bridging hydroxo groups, the so-called monools and diols, have recently received much attention because of their spectroscopic, structural and magnetic properties.[1–31]

In previous works from this laboratory we have reported the synthesis, resolution and properties of diols of chromium(III) with pyridyl substituted bidentate ligands such as (2-pyridyl)methylamine (abbrev. pic),[14] 1-(2-pyridyl)ethylamine (mepic)[21] and the tetradentate ligand *N,N'*-bis(2-pyridylmethyl)-1,2-ethanediamine (bispicen).[17] This work deals with the corresponding compounds of the related ligand *N,N'*-bis(2-pyridylmethyl)-1,2-propanediamine (bispicpn), Fig. 1.

While the structure of our dimeric compound with mepic has been shown by X-ray analysis to be a diol,[25] we have not yet proved that the dimeric complexes with bispicen and bispicpn are diols of the formula $[ACr(OH)_2CrA](ClO_4)_4.4H_2O$ and not aquahydroxo monools of the formula $[(H_2O)ACr(OH)CrA(OH)](ClO_4)_4.3H_2O$. The latter possibility cannot be entirely excluded after the discovery of a relatively fast equilibrium in solution between a corresponding diol and monool with 1,2-ethanediamine.[32–35] Thus, for example, thermogravimetry showed that our compounds were totally dehydrated below 140 °C. It was not possible, however, to distinguish between crystal and complex-bound water. No other physical measurements gave a final answer to this problem although our magnetic and spectroscopic measurements strongly indicate the presence of diols in the solid state and in the solutions, respectively.

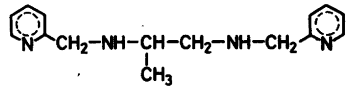

Fig. 1. *N,N'*-Bis(2-pyridylmethyl)-1,2-propanediamine, bispicpn, $C_{15}H_{20}N_4$.

0302-4377/83 $2.50

EXPERIMENTAL

Reagents. Pyridine-2-carboxaldehyde was purchased from Merk-Schuchardt. 1,2-Propanediamine was resolved following the method of Dwyer *et al.*[36] SP-Sephadex C-25 was purchased from Pharmacia, Uppsala, Sweden. All other compounds were of reagent grade and were used without further purifications.

Analyses. The chromium analyses were performed on a Perkin Elmer 403 Atomic Absorption Spectrophotometer. The microanalytical laboratory of this institute carried out the carbon, nitrogen, hydrogen and halogen analyses by standard methods.

Physical measurements. Absorption spectra were recorded on a Cary Model 14 and a Cary Model 118 spectrophotometer. The spectra are characterized by their maxima and minima (ε, λ), where the molar extinction coefficient ε is in units of 1 mol^{-1} cm^{-1} and λ is in nm. Circular dichroism was measured on Roussel-Jouan Dichrographe III in the region 650–200 nm. The extrema are given below as ($\Delta\varepsilon$, λ)=[(ε_l–ε_r),λ]. $[Coen_3]Cl_3 \cdot 1/2NaCl \cdot 3H_2O$ was used as a standard with ($\Delta\varepsilon$, λ)=(1.92, 489). The compounds were dissolved in 0.1 M hydrochloric acid, 0.01 M sodium hydroxide + 1 M sodium chloride, 4 M sodium hydroxide and a solution of lithium methoxide in ethanol (vis. region only). The different media were chosen in order to obtain spectra of the di-μ-hydroxo ion, the μ-hydroxo-μ-oxo ion and the di-μ-oxo ion. The acid dissociation constant K_{a1} of the di-μ-hydroxo ion with *N,N'*-bis(2-pyridylmethyl)-1,2-ethanediamine (bispicen) was roughly determined by Ole Mønsted. A more detailed description of the potentiometric method and of the equipment is published elsewhere.[37] The preliminary result is pK_{a1}=9.3, μ=1 M, 25 °C. Judging from spectral measurements the acid dissociation constants for the corresponding diols with *N,N'*-bis(2-pyridylmethyl)-1,2(*R*)-propanediamine {bispic(–pn)} have values of the same magnitude. Optical rotation was measured on a Perkin Elmer Model 141 polarimeter. The magnetic susceptibilities of powdered samples were measured by the Faraday method in the temperature range 4–270 K at a field strength of 12.000 Oe. The magnetic field was calibrated with $Hg[Co(NCS)_4]$.[38] A more detailed description of the equipment is published elsewhere.[7,20] Thermogravimetry was performed on an instrument, which has been described previously.[39]

Preparations. 1. *N,N'*-Bis(2-pyridylmethyl)-1,2-propanediamine, $C_{15}H_{20}N_4$ (abbrev. bispicpn) and *N,N'*-bis(2-pyridylmethyl)-1,2(*R*)-propanediamine, $(-)_D$-$C_{15}H_{20}N_4$ (abbrev. bispic(–pn)). The ligands were prepared from pyridine-2-carboxaldehyde and 1,2-propanediamine or $(-)_D$-1,2(*R*)-propanediamine following mainly the principles of Goodwin and Lions.[40] The crude amines were purified *via* the hydrochlorides as described for *N,N'*-bis(2-pyridylmethyl)-1,2-ethanediamine.[17] The pure hydrochlorides normally crystallized with 2 mol of crystal water.

2. Di-μ-hydroxobis[{*N,N'*-bis(2-pyridylmethyl)-1,2(*R*)-propanediamine}chromium(III)] perchlorate, $(+)_D$-[{bispic(–pn)}$Cr(OH)_2$Cr{bispic(–pn)}]$(ClO_4)_4 \cdot 3H_2O$ and $(-)_D$-[{bispic(–pn)}$Cr(OH)_2$Cr{bispic(–pn)}]$(ClO_4)_4 \cdot 3H_2O$. A crude product from which we isolated two different red compounds was prepared using in principle the general method developed in our laboratory for the preparation of diols with pyridyl-substituted amine ligands.[14,17,21] $[CrBr_2(H_2O)_4]Br \cdot 2H_2O$ (1.00 g, 2.50 mmol) was dissolved in water (1 ml). 2-Methoxyethanol (2 ml), a spatula of zinc dust and bispic(–pn) (0.8 ml 2.50 mmol) were stirred in. Filtering from zinc dust after 10 min was followed by precipitation with ethanol and ether. The red precipitate was dissolved in water (400 ml) and transferred to a column of SP-Sephadex C 25 (l~22 cm, diam.~4 cm). The compounds were eluted with a phosphate solution (0.1 M NaH_2PO_4 – 0.1 M Na_2HPO_4). Two red bands presumed to contain binuclear complexes were recognized. The first band, called 1, was very weak. The second band, called 2, was very distinct and large. The eluates were both diluted four times with water and adsorbed to short columns, where sodium and phosphate ions were eluted with 0.1 M hydrochloric acid, and the complexes afterwards with 4 M hydrochloric acid. The chlorides were precipitated with ethanol and ether from the ice-cooled solutions. Afterwards they were converted to the corresponding perchlorates by the addition of saturated solutions of sodium perchlorate to hot water solutions of the compounds in question. Cooling on ice, filtering and washing with ethanol followed. Recrystallizations from boiling water normally gave losses of about 25 %.

Band 1. The yields were very small (<1 %). Therefore the eluates from several syntheses were collected and treated at one time.

Anal. $(+)_D$-$[Cr\{(R)\text{-}C_{15}H_{20}N_4\}(OH)]_2(ClO_4)_4 \cdot 3H_2O$: Cr, C, N, H, Cl.
$(\varepsilon, \lambda)_{max}$: (220, 533), (148, 384),
$(\varepsilon, \lambda)_{min}$: (36.8, 437), (82.6, 350.5).
$(\Delta\varepsilon, \lambda)_{ex}$: (+4.47, 521), (−0.73, 377).

When the perchlorate was left for a week with conc. hydrochloric acid in a stoppered flask, red-violet crystals appeared. They were identified by their absorption and circular dichroism spectra as

$(+)_D$-*cis*-α-[Cr{bispic(–pn)}Cl_2]ClO_4.[41]
$(\varepsilon, \lambda)_{max}$: (103, 542.5), (101, 406).
$(\varepsilon, \lambda)_{min}$: (25.8, 462), (10.4, 353).
$(\Delta\varepsilon, \lambda)_{ex}$: (−1.05, 576), (+1.14, 508).

Band 2. The yields varied from 680 mg to 1030 mg (49 %–75 %) and were most frequently 840 mg (61 %).
Anal. $(-)_D$-[Cr{(*R*)-$C_{15}H_{20}N_4$}(OH)]$_2(ClO_4)_4$·$3H_2O$: Cr, C, N, H, Cl.

In other cases the compound crystallized with 4 mol of crystal water.
$(\varepsilon, \lambda)_{max}$: (173, 529), 147, 386)
$(\varepsilon, \lambda)_{min}$: (34.6, 439), (74.0, 350)
$(\Delta\varepsilon, \lambda)_{ex}$: (−5.86, 522), (+1.48, 381).

When the perchlorate was left for one week with conc. hydrochloric acid in a stoppered flask, blue-violet crystals appeared. They were identified by their absorption and circular dichroism spectra as
$(-)_D$-*cis*-α-[Cr{bispic(–pn)}Cl_2]ClO_4.[41]
$(\varepsilon, \lambda)_{max}$: (96.5, 553), (90.9, 410).
$(\varepsilon, \lambda)_{min}$: (22.4, 468), (5.3, 355).
$(\Delta\varepsilon, \lambda)_{ex}$: (+1.23, 595), (−1.65, 522).

Two violet bands were left on the original column. They were later isolated and investigated.

3. Di-μ-hydroxobis[{*N*,*N*′-bis(2-pyridylmethyl)-1,2-propanediamine}chromium(III)] perchlorate, [{bispicpn}Cr$(OH)_2$Cr{bispicpn}]$(ClO_4)_4$·$4H_2O$, three isomers. When the optically active amine was replaced by racemic amine, bispicpn, in the synthesis described above, we obtained three different red bands on the Sephadex column. The first band, called 11, was very weak. The next band, called 12, was of considerable size, and the last band, called 22, was the largest. From the bands three red compounds were isolated as perchlorates as described above.

Band 11: The yield of this compound was normally less than 1 %. Therefore the elutates from several syntheses were collected and treated at one time.
Anal. [Cr$(C_{15}H_{20}N_4)(OH)]_2(ClO_4)_4$·$4H_2O$: Cr
$(\varepsilon, \lambda)_{max}$: (222, 533), (147, 384).
$(\varepsilon, \lambda)_{min}$: (35.2, 436.5), (81.1, 350.5).

As the absorption spectrum of the compound is identical with that of the compound from band 1, this compound must be the corresponding racemate.

Band 12: The yield was normally about 290 mg (21 %). In a single experiment it was 30 %.
Anal. [Cr$(C_{15}H_{20}N_4)(OH)]_2(ClO_4)_4$·$4H_2O$: Cr, C, N, H, Cl.

Sometimes the compound crystallized with 3 mol of crystal water.
$(\varepsilon, \lambda)_{max}$: (198, 532), (149, 384).
$(\varepsilon, \lambda)_{min}$: (34.1, 431), (77.8, 350).

When the chloride salt was left for 14 days in a stoppered flask with conc. hydrochloric acid, large blue-violet crystals separated. They were identified by their absorption spectrum as one of the two possible *cis*-α-dichloro complexes, *cis*-α_2-[Cr{bispicpn}Cl_2]Cl·$3H_2O$.[41]
$(\varepsilon, \lambda)_{max}$: (95.6, 553), (91.1, 409).
$(\varepsilon, \lambda)_{min}$: (22.3, 468), (7.1, 356).

To the filtrate from these crystals were added ethanol and ether. The precipitated chloride salt was converted to an iodide by redissolution in water and precipitation by the addition of sodium iodide. The lavender-coloured compound was identified by its absorption spectrum as the second of the two possible *cis*-α-dichloro complexes, *cis*-α_1-[Cr{bispicpn}Cl_2]I.[41]
$(\varepsilon, \lambda)_{max}$: (102, 543), (101, 407).
$(\varepsilon, \lambda)_{min}$: (27.4, 463), (23.9, 353).

The resolution of this racemic dinuclear compound into its catoptromers was performed and will be published later.

Band 22. The yields varied from 490 mg to 602 mg (35 %–43 %). Anal. [Cr$(C_{15}H_{20}N_4)$-$(OH)]_2(ClO_4)_4$·$4H_2O$: Cr, C, N, H, Cl. Sometimes the compound crystallized with 3 mol of crystal water.
$(\varepsilon, \lambda)_{max}$: (172, 529), (147, 386).
$(\varepsilon, \lambda)_{min}$: (33.7, 439), (74.0, 350).

The absorption spectrum of the compound is identical with that of the compound isolated from band 2. Add to this that a resolution of the iodide salt following the same method as described for the resolution of [{bispicen}Cr$(OH)_2$Cr{bispicen}]I_4 [17] gave $(-)_D$-[{bispicpn}Cr$(OH)_2$Cr{bispicpn}]$I_2$2$(SbOtart)_2$·$9H_2O$ with the following data:
$(\varepsilon, \lambda)_{max}$: (172, 529), (150, 386).
$(\varepsilon, \lambda)_{min}$: (36.2, 440), (79.2, 350).
$(\Delta\varepsilon, \lambda)_{ex}$: (−5.84, 521), (+1.45, 380).
Therefore the compound must be the racemate corresponding to the compound from band 2. When the perchlorate was left for one week in a stoppered flask with conc. hydrochloric acid, blue-violet crystals appeared. They were identified by the absorption spectrum as one of the *cis*-α-dichloro complexes,
cis-α_2-[Cr{bispicpn}Cl_2]ClO_4.[41]
$(\varepsilon, \lambda)_{max}$: (95.5, 553), (89.7, 409).
$(\varepsilon, \lambda)_{min}$: (24.7, 468), (9.8, 356).

Two violet bands were left on the original column. They were later isolated and investigated.

RESULTS AND DISCUSSION

Synthesis and resolution. We have earlier discovered,[14,17,21] that binuclear hydroxobridged chromium(III) complexes with pyridyl substituted ligands could be obtained by the reaction of

chromium(III) bromide hexahydrate and the amine in question in the presence of zinc dust or chromium(II). In the present case the method worked equally well, and we got two optically active diols with bispic(–pn), the corresponding two *racemic* diols with bispicpn and an extra *racemic* diol with bispicpn. The separation of the isomers was accomplished by column chromatography. Two of the *racemic* compounds (bands 12 and 22) were resolved with sodium antimonyl $(+)_D$-tartrate as a resolving agent. In both cases the $(-)_D$-isomer formed the less soluble diastereoisomer. The yields of the third *racemic* compound (band 11) were too small to allow a resolution.

The compounds mentioned above all had the same red colour. We could also isolate blue-violet compounds. The results from their investigation will be published later.

While heating at 140 °C for 1 h of solid aquahydroxo monool and solid *racemic* diol with 1,2-ethanediamine resulted in conversion to *meso* diol of 95 and 20 % respectively,[35] similar reactions did not seem to take place in our case, as absorption as well as circular dichroism spectra remained unchanged after the compounds had undergone the same treatment.

Stereochemistry of the compounds. In a previous work on *cis*-dichloro complexes of chromium(III) with *N,N'*-bis(2-pyridylmethyl)-1,2-propanediamine, bispic(–pn),[41] we have isolated and investigated the two possible *cis*-α-isomers, *Δ-cis*-α-$[Cr\{bispic(-pn)\}Cl_2]^+$, $\{\Delta(\alpha)(R)\}$ and *Λ-cis*-α-$[Cr\{bispic(-pn)\}Cl_2]^+$, $\{\Lambda(\alpha)(R)\}$, Figs. 2a and 2b. (R=bispic(–pn)). The structure of one of the compounds has later been confirmed by an

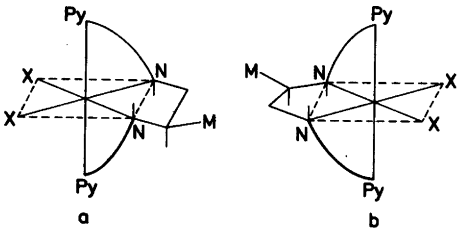

Fig. 2.
a, *Δ-cis*-α-$[Cr\{bispic((-pn)\}Cl_2]^+$, $\{\Delta(\alpha)(R)\}$.
b, *Λ-cis*-α-$[Cr\{bispic(-pn)\}Cl_2]^+$, $\{\Lambda(\alpha)(R)\}$.
Bispic(–pn)=*N,N'*-bis(2-pyridylmethyl)-1,2(R)-propanediamine. Py symbolizes the pyridine nitrogen, M the methyl group and X the chloride.

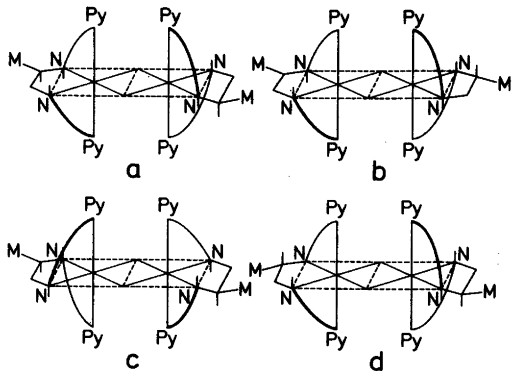

Fig. 3. Some of the different isomers of $[\{bispic(-pn)\}Cr(OH)_2Cr\{bispic(-pn)\}]^{4+}$
a, $\{\Lambda(\alpha)(R)\Lambda(\alpha)(R)\}$. b, $\{\Lambda(\alpha)(R)\Lambda(\alpha)(R)\}$.
c, $\{\Delta(\alpha)(R)\Delta(\alpha)(R)\}$. d, $\{\Lambda(\alpha)(R)\Lambda(\alpha)(S)\}$.

X-ray structure analysis carried out by Hata *et al.*[42]

When the diol prepared from bispic(–pn) and isolated from band 1 was decomposed by conc. hydrochloric acid, *Λ-cis*-α-$[Cr\{bispic(-pn)\}Cl_2]^+$ was formed. On the assumption that the acid cleavage reaction proceeds with the retention of configuration, the diol in question, $(+)_D$-$[\{bispic(-pn)\}Cr(OH)_2Cr\{bispic(-pn)\}]^{4+}$, therefore has one of the structures $\{\Lambda(\alpha)(R)\Lambda(\alpha)(R)\}$ that are illustrated in Figs. 3a and 3b (methyl group isomers). The diol isolated from band 11 constituted the corresponding *racemic* compound, $\{\Lambda(\alpha)(R)\Lambda(\alpha)(R), \Delta(\alpha)(S)\Delta(\alpha)(S)\}$.

Similarly the optically active diol isolated from band 2, $(-)_D$-$[\{bispic(-pn)\}Cr(OH)_2Cr\{bispic(-pn)\}]^{4+}$, was decomposed to *Δ-cis*-α-$[Cr\{bispic(-pn)\}Cl_2]^+$. One of the methyl group isomers of the structure $\{\Delta(\alpha)(R)\Delta(\alpha)(R)\}$ is pictured in Fig. 3 c. From band 22 the corresponding *racemic* compound $\{\Delta(\alpha)(R)\Delta(\alpha)(R), \Lambda(\alpha)(S)\Lambda(\alpha)(S)\}$ was isolated.

The diol that was isolated from band 12 decomposed when treated with conc. hydrochloric acid to both possible *racemic cis*-α-dichloro complexes, $\{\Lambda(\alpha)(R), \Delta(\alpha)(S)\}$ and $\{\Lambda(\alpha)(S), \Delta(\alpha)(R)\}$. These *cis*-α-skeletons may be combined to form two different types of resolvable diols, namely $\{\Lambda(\alpha)(R)\Lambda(\alpha)(S), \Delta(\alpha)(R)\Delta(\alpha)(S)\}$ and $\{\Lambda(\alpha)(R)\Delta(\alpha)(R), \Lambda(\alpha)(S)\Delta(\alpha)(S)\}$. Among these possibilities, the first one, Fig. 3d (the methyl group is omitted) is

the most probable because the above-mentioned diol had many properties in common with the two other diols of the similar structure, and because we did not get a third red compound (of the structure {$\Lambda(\alpha)$(R)$\Delta(\alpha)$(R)}) from the synthesis with bispic(–pn).

Electronic spectra. The absorption spectra of the three different racemic compounds dissolved in different media are presented in Figs. 4–8 and in Tables 1–3.

We presume that the spectra of the compounds dissolved in 0.1 M hydrochloric acid represent the spectra of di-μ-hydroxobis[{*N*,*N*′-bis-(2-pyridylmethyl)-1,2-propanediamine}chromium-(III) ions (diols). The absorption spectra in the vis. region, Figs. 4–6, Table 1, are slightly different from the corresponding spectra of the diols with 2-pyridyl-methylamine[14] and 1-(2-pyridyl)ethylamine,[17] the intensities of the second bands being 16–17 % higher, and the positions of both bands being shifted 6–10 nm. The spectra of the compounds dissolved in water and in 0.1 M hydrochloric acid are identical. When 4 M hydrochloric acid is used as a solvent, the only noticable change is a shifting of the first

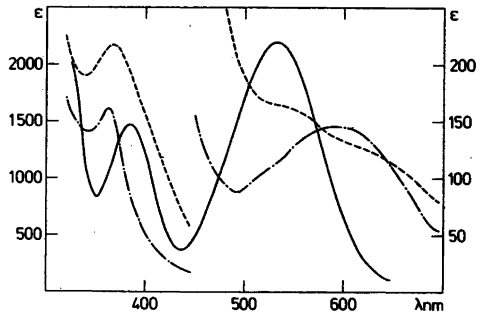

Fig. 4. The absorption spectra of [{bispicpn}Cr(OH)$_2$Cr{bispicpn}]$^{4+}$, bands 1 and 11 in 0.1 M HCl (di-μ-hydroxo), (———), in 0.01 M NaOH+1 M NaCl (μ-hydroxo-μ-oxo), (— · —) and in 4 M NaOH (di-μ-oxo), (– – –). Vis. region.

Table 1. Electronic spectral parameters for di-μ-hydroxocomplexes of chromium(III) with *N*,*N*′-bis(2-pyridylmethyl)-1,2-propanediamine (bispicpn) and *N*,*N*′-bis(2-pyridylmethyl)-1,2(*R*)-propanediamine (bispic(–pn) in 0.1 M HCl. Region 700–300 nm.

Ligand A	Ion, presumed to be dominant: $[ACr(OH)_2CrA]^{4+}$	$(\varepsilon, \lambda)_{max}$
bispicpn bispic(–pn)	band 11. $\Delta S\Delta S,\Lambda R\Lambda R$ band 1. $\Lambda R\Lambda R$	(222, 533), (147, 384)
bispicpn	band 12. $\Delta S\Delta R,\Lambda R\Lambda S$	(198, 532), (149, 384)
bispicpn bispic(–pn)	band 22. $\Delta R\Delta R,\Lambda S\Lambda S$ band 2. $\Delta R\Delta R$	(172, 529), (147, 386)

Table 2. Electronic spectral parameters for di-μ-hydroxocomplexes of chromium(III) with *N*,*N*′-bis(2-pyridylmethyl)-1,2-propanediamine (bispicpn) and *N*,*N*′-bis(2-pyridylmethyl)-1,2(*R*)-(propanediamine (bispic(–pn) in 0.01 M NaOH, 1 M NaCl. Region 700–300 nm.

Ligand A	Ion, presumed to be dominant: $[ACr(OH)(O)CrA]^{3+}$	$(\varepsilon, \lambda)_{max}$
bispicpn bispic(–pn)	band 11. $\Delta S\Delta S,\Lambda R\Lambda R$ band 1. $\Lambda R\Lambda R$	(145, 590), (1618, 363)
bispicpn	band 12. $\Delta S\Delta R,\Lambda R\Lambda S$	(130, 590), (1553, 365)
bispicpn bispic(–pn)	band 22. $\Delta R\Delta R,\Lambda S\Lambda S$ band 2. $\Delta R\Delta R$	(113, 585), (1397, 365)

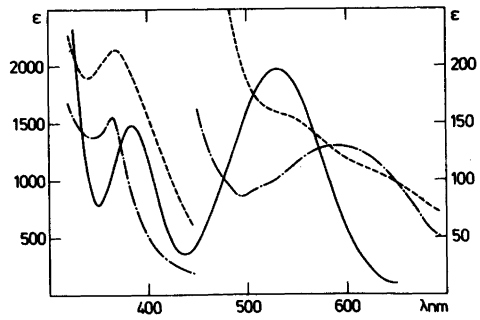

Fig. 5. The absorption spectra of $[\{bispicpn\}Cr(OH)_2Cr\{bispicpn\}]^{4+}$, band 12 in 0.1 M HCl (di-μ-hydroxo), (———), in 0.01 M NaOH+1 M NaCl (μ-hydroxo-μ-oxo), (— - —) and in 4 M NaOH (di-μ-oxo), (– – –). Vis. region.

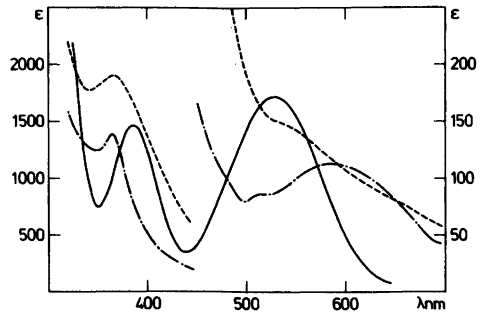

Fig. 6. The absorption spectra of $[\{bispicpn\}Cr(OH)_2Cr\{bispicpn\}]^{4+}$, bands 2 and 22 in 0.1 M HCl (di-μ-hydroxo), (———), in 0.01 M NaOH+1 M NaCl (μ-hydroxo-μ-oxo), (— - —) and in 4 M NaOH (di-μ-oxo), (– – –). Vis. region.

band on 1.5 nm. If the compounds therefore, contrary to all expectations, should be aquahydroxo monools, then the corresponding diaqua monools must be remarkably strong acids. In the case of diols of 1,2-ethanediamine the spectrum changed with time due to the rapid equilibrium between the diol and the aquahydroxo monool.[35] We did not recognize similar changes of the spectra within reasonable time (8 h).

Based on rough and preliminary determinations of the acidity constants for the diols, we also presume, that each of the bluish solutions of the diols in 0.01 M sodium hydroxide +1 M sodium chloride contains one species only, namely a μ-hydroxo-μ-oxobis[{*N*,*N*′-bis(2-pyridylmethyl)-1,2-propanediamine}chromium(III)] ion. The spectra, Figs. 4–6 and Table 2, did not change within 8 h, and they are utterly different from the spectrum of the dihydroxo monool of chromium(III) with 1,2-ethanediamine[35] but resemble the spectrum of the μ-hydroxo-μ-oxo bis[bis{1-(2-pyridyl)ethylamine}chromium(III)] ion.[30]

To obtain the spectra of the di-μ-oxobis[{*N*,*N*′-bis(2-pyridylmethyl)-1,2-propanediamine}chromium(III)] ions we dissolved the complexes in 4 M sodium hydroxide. These solutions are yellow, just as the compounds of the formula $[Cr\{bispicpn\}O]_2(ClO_4)_2 \cdot nH_2O$ which we can isolate from them. The first absorption bands, Figs. 4–6 and Table 3, show a splitting appearing as two shoulders. The bands at approx. 365 nm have the same high intensities as we observed in the case of the corresponding μ-hydroxo-μ-oxo complexes.

In Fig. 7 the spectra of the three different complexes are united to illustrate the systematic variation that manifested already in the different rates of migration on the column.

Table 3. Electronic spectral parameters for di-μ-hydroxocomplexes of chromium(III) with *N*,*N*′-bis(2-pyridylmethyl)-1,2-propanediamine (bispicpn) and *N*,*N*′-bis(2-pyridylmethyl)-1,2(R)-propanediamine (bispic(–pn) in 4 M NaOH. Region 700–300 nm.

Ligand A	Ion, presumed to be dominant: $[ACr(O)_2CrA]^{2+}$	$(\varepsilon, \lambda)_{max}$
bispicpn bispic(–pn)	band 11. ΔSΔS,ΔRΔR band 1. ΛRΛR	$(129, 610)_{sh}$, $(164, 535)_{sh}$, (2164, 365)
bispicpn	band 12. ΔSΔR,ΛRΛS	$(114, 610)_{sh}$, $(158, 535)_{sh}$, (2154, 367)
bispicpn bispic(–pn)	band 22. ΔRΔR,ΛSΛS band 2. ΔRΔR	$(96, 615)_{sh}$, $(149, 535)_{sh}$, (1906, 365)

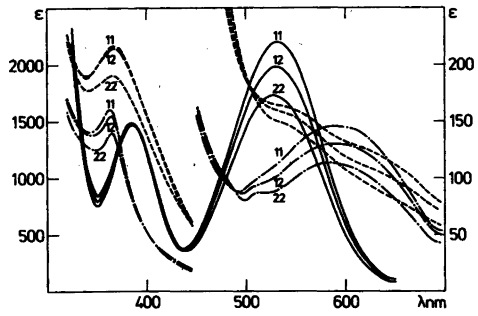

Fig. 7. The united spectra of the compounds isolated from bands 11, 12 and 22 illustrate the systematic variation in the spectroscopic properties.

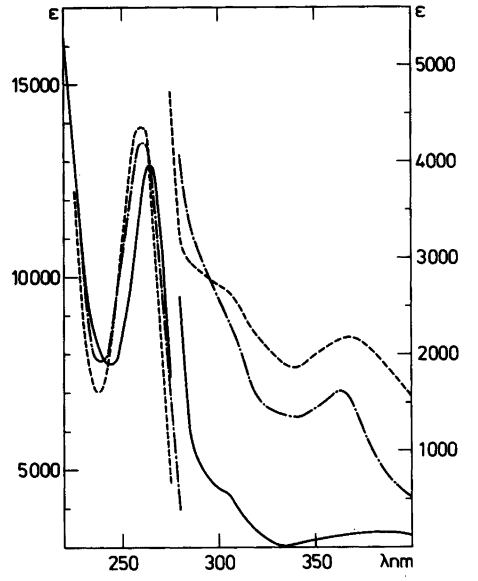

Fig. 8. The absoprtion spectra of $[\{bispicpn\}Cr(OH)_2Cr\{bispicpn\}]^{4+}$, band 1 in 0.1 M HCl (di-μ-hydroxo), (———), in 0.01 M NaOH+1 M NaCl (μ-hydroxo-μ-oxo), (— - —) and in 4 M NaOH (di-μ-oxo), (– – –). UV region.

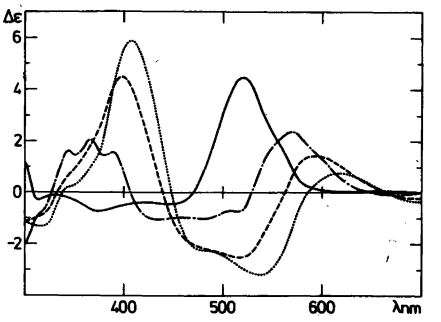

Fig. 9. The circular dichroism spectra of $\Lambda\Lambda$-$(+)_D$-$[\{bispic(-pn)\}Cr(OH)_2Cr\{bispic(-pn)\}]^{4+}$, band 1, in 0.1 M HCl (di-μ-hydroxo), (——), in 0.01 M NaOH+1 M NaCl (μ-hydroxo-μ-oxo), (— - —), in 4 M NaOH (di-μ-oxo), (– – –) and in LiOMe-ethanol (di-μ-oxo), (. . .). Vis. region.

The spectra in the UV region are presented by the spectra of one of the complexes, Fig. 8, as they are very similar with a relatively sharp ligand band at 260 nm and a shoulder at about 300 nm.

Circular dichroism spectra. The interesting circular dichroism spectra of the two different optically active compounds dissolved in the same different media as used for the absorption spectra are presented in Figs. 9–12 and in Tables 4–7.

The spectra in 0.1 M hydrochloric acid in the vis. region, Figs. 9–10 and Table 4, resemble those of the corresponding diols with 2-pyridylmethylamine[14] and 1-(2-pyridyl)ethylamine,[17] although some small differences can be noticed, for instance regarding the position of the first dominant band and the shape of the second. As mentioned above, the diol isolated from band 1, Fig. 9, has the structure $\{\Lambda(\alpha)(R)\Lambda(\alpha)(R)\}$ and the diol isolated from band 2, Fig. 10, the structure $\{\Delta(\alpha)(R)\Delta(\alpha)(R)\}$. This agrees with the empirical rule that relates the sign of the dominant CD-band in the region of the $^4A_{2g} \rightarrow {}^4T_{2g}$ d–d absorption of the chromium(III) ion to the

Table 4. CD-spectral parameters for di-μ-hydroxocomplexes of chromium(III) with *N,N'*-bis(2-pyridylmethyl)-1,2(R)-propanediamine (bispic(–pn)) in 0.1 M HCl. Region 700–300 nm.

Ligand A	Ion, presumed to be dominant: $[ACr(OH)_2CrA]^{4+}$	$(\Delta\varepsilon, \lambda)_{ex}$
bispic(–pn)	band 1 $(+)_D$-$\Lambda R\Lambda R$	(+4.47, 521), (−0.73, 377)
bispic(–pn)	band 2 $(-)_D$-$\Delta R\Delta R$	(−5.86, 522), (+1.48, 381)

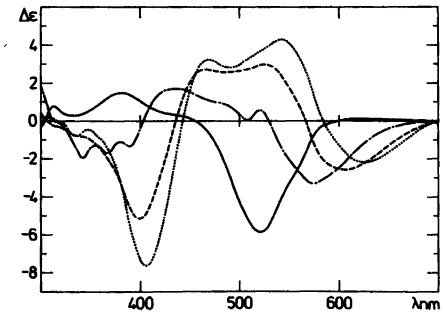

Fig. 10. The circular dichroism spectra of $\Delta\Delta$-$(-)_D$-[{bispic(–pn)}$Cr(OH)_2$Cr-{bispic(–pn)}]$^{4+}$, band 2, in 0.1 M HCl (di-μ-hydroxo), (———), in 0.01 M NaOH+1 M NaCl (μ-hydroxo-μ-oxo), (— - —), in 4 M NaOH (– – –) and in LiOMe-ethanol (di-μ-oxo), (. . .). Vis. region.

configuration around the metal atom.[43] The application of this rule, however, becomes more dubious regarding the spectra of the strongly basic solutions.

The spectra of the μ-hydroxo-μ-oxo complexes in the vis. region, Figs. 9–10 and Table 5, are specially interesting because of their fine structure. Unfortunately we are still not able to utilize all the information they offer because of their complexity. They are characterized by a lot of common features which we recognize from the μ-oxo-μ-hydroxo complex with 1-(2-pyridyl)ethylamine.[30]

The same resemblance is found between the spectra of the di-μ-oxo complexes, in the vis. region. Figs. 9–10 and Table 6, and the corresponding complex with 1-(2-pyridyl)ethylamine.[30] They are nearly identical in shape with the spectra of the compounds dissolved in lithium methoxide in ethanol, Figs. 9–10 and Table 7.

The less interesting circular dichroism spectra in the UV region are presented in Figs. 11 and 12.

Magnetic Properties. The average magnetic susceptibilities and effective moments as functions of temperature were determined for the two optically active compounds, band 1 and band 2,

Table 5. CD-spectral parameters for di-μ-hydroxocomplexes of chromium(III) with *N,N'*-bis(2-pyridylmethyl)-1,2(R)-propanediamine (bispic(–pn)) in 0.01 M NaOH, 1 M NaCl. Region 700–300 nm.

Ligand A	Ion, presumed to be dominant: $[ACr(OH)(O)CrA]^{3+}$	$(\Delta\varepsilon, \lambda)_{ex}$
bispic(–pn)	band 1. $(+)_D$-$\Lambda R\Lambda R$	(−0.10, 681), (+2.36, 569), (−0.75, 517), (−1.06, 480) (−1.06, 432), (+1.55, 390), (+2.05, 368), (+1.61, 344).
bispic(–pn)	band 2. $(-)_D$-$\Delta R\Delta R$	(−3.22, 574), (+0.56, 520), (+1.05, 472) (+1.69, 439), (−1.33, 389), (−1.68, 367), (−1.95, 343).

Table 6. CD-spectral parameters for di-μ-hydroxocomplexes of chromium(III) with *N,N'*-bis(2-pyridylmethyl)-1,2(*R*)-propanediamine (bispic(–pn)) in 4 M NaOH. Region 700–300 nm.

Ligand A	Ion, presumed to be dominant: $[ACr(O)_2CrA]^{2+}$	$(\Delta\varepsilon, \lambda)_{ex}$
bispic(–pn)	band 1 $(+)_D$-$\Lambda R\Lambda R$	(+1.42, 594), (−2.52, 519), (−2.24, 488), (+4.50, 399), (−0.92, 317)
bispic(–pn)	band 2 $(-)_D$-$\Delta R\Delta R$	(−2.61, 606), (+2.97, 524), (+2.69, 466), (−5.14, 399), (−0.80, 336).

Table 7. CD-spectral parameters for di-μ-hydroxocomplexes of chromium(III) with *N,N'*-bis(2-pyridylmethyl)-1,2(*R*)-propanediamine (bispic(–pn)) in $LiOCH_3$, C_2H_5OH. Region 700–300 nm.

Ligand A	Ion, presumed to be dominant: $[ACr(O)_2CrA]^{2+}$	$(\Delta\varepsilon, \lambda)_{ex}$
bispic(–pn)	band 1 $(+)_D$-$\Lambda R\Lambda R$	(+0.77, 619), (−3.19, 539), (−2.26, 487), (+5.88, 407), (+0.25, 345), (−1.32, 315).
bispic(–pn)	band 2 $(-)_D$-$\Delta R\Delta R$	(−2.16, 630), (+4.32, 542), (+3.23, 470), (−7.64, 407), (−0.79, 335), (+0.24, 309).

and for the two abundant racemic compounds, band 12 and band 22. As an example, the results for band 12 are shown in Fig. 13. The susceptibility data were fitted to the expression

$$\chi_A' = -(N/H)\frac{\sum_i \left(\frac{\partial E_i}{\partial H}\right) e^{-E_i/kT}}{\sum_i e^{-E_i/kT}} \quad (1)$$

where E_i are the energies of the 16 components of the ground state manifold by minimization of

$$\sum_i (\chi_i^{obs} - \chi_A')^2 \Big/ \left\{ \sigma^2(\chi) + \left(\frac{\partial \chi}{\delta T}\right)^2 \sigma^2(T) \right\} \quad (2)$$

The estimated standard deviations $\sigma(\chi)$ and $\sigma(T)$ are reported elsewhere.[22] The fitting was accomplished by application of three different models for the exchange Hamiltonian. Model 1 assumed the simple Heisenberg Hamiltonian

$$\mathcal{H} = J\vec{S}_1 \cdot \vec{S}_2 \quad (3)$$

Model 2 included a biquadratic exchange term according to

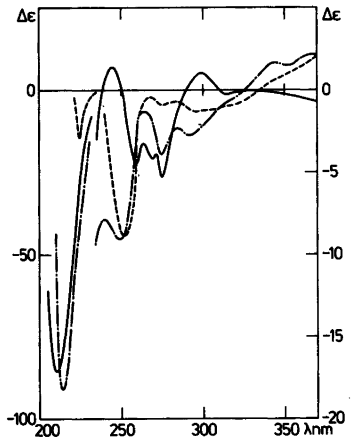

Fig. 11. The circular dichroism spectra of $\Lambda\Lambda$-$(+)_D$-[{bispic(–pn)}$Cr(OH)_2$-Cr{bispic(–pn)}]$^{4+}$, band 1, in 0.1 M HCl (di-μ-hydroxo), (——), in 0.01 M NaOH+1 M NaCl (μ-hydroxo-μ-oxo), (— - —) and in 4 M NaOH (di-μ-oxo), (– – –). UV region.

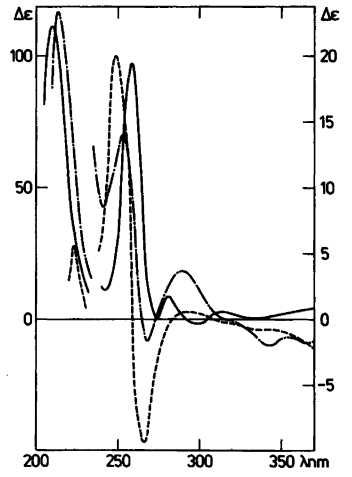

Fig. 12. The circular dichroism spectra of $\Lambda\Lambda$-$(-)_D$-[{bispic(–pn)}$Cr(OH)_2$-Cr{bispic(–pn)}]$^{4+}$, band 2, in 0.1 M HCl (di-μ-hydroxo), (——), in 0.01 M NaOH+1 M NaCl (μ-hydroxo-μ-oxo), (— - —) and in 4 M NaOH (di-μ-oxo), (– – –). UV region.

Table 8. Parameters derived from magnetic susceptibility data for di-μ-hydroxocomplexes of chromium(III) with *N,N'*-bis(2-pyridylmethyl)-1,2-propanediamine (bands 12 and 22) and *N,N'*-bis(2-pyridylmethyl)-1,2(*R*)-propanediamine (bands 1 and 2).

	Band 1 ΔRΔR		Band 12 ΔSΔR,ΔRΔS		Band 2 ΔRΔR		Band 22 ΔRΔR,ΔSΔS	
	Model 1[a]	Model 3	Model 1	Model 3	Model 1	Model 3	Model 1	Model 3
J (cm^{-1})	49.81(7)	–	44.44(6)	–	47.88(5)	–	44.79(7)	–
$E(1)$(cm^{-1})	49.81(7)[b]	49.20(3)	44.44(6)[b]	43.75(2)	47.88(5)[b]	47.50(2)	44.79(7)[b]	43.92(5)
$E(2)$(cm^{-1})	149.4(2)[b]	137.7(1)	133.3(2)[b]	126.7(1)	143.6(2)[b]	136.2(1)	134.4(2)[b]	125.0(3)
$E(3)$(cm^{-1})	298.9(4)[b]	263.4(4)	266.6(4)[b]	237.4(4)	287.3(4)[b]	261.6(2)	268.7(4)[b]	234.5(8)
g	2.002(5)	1.979(3)	2.008(5)	1.981(3)	2.021(3)	1.983(1)	2.009(6)	1.981(5)
% monomer	0.033(1)	0.005(6)	0.030(1)	0.007(6)	0.015(1)	0.006(1)	0.029(1)	–0.0009(9)[c]
var/f[d]	19.1	0.83	14.0	1.04	17.5	0.47	16.8	1.86
f	426	424	395	393	453	451	366	364

[a] See text for description of the models. [b] Calculated from the derived J values. [c] A negative value of this parameter is, of course, a pure artifact of our fitting procedure. Note that the value is only one standard deviation away from zero. [d] Variance per degree of freedom.

$$\mathcal{H}=J\vec{S}_1\cdot\vec{S}_2 + j(\vec{S}_1\cdot\vec{S}_2)^2 \quad (4)$$

Finally, model 3 assumed independent energies of the triplet, quintet and septet states; and it merely assumed, as do the earlier models, absence of any zero-field splitting within these levels and an isotropic Zeeman effect. Further details of the fitting procedure can be found elsewhere.[21]

Some of the results of the data fittings are displayed in Table 8 and an example of one set of measurements is shown in Fig. 13. It is obvious that within the estimated experimental uncertainties the data are not sufficiently well described by the simple Heisenberg Hamiltonian (model 1). Inclusion of the biquadratic exchange term (model 2) markedly improves the fits, lowering the variance per degree of freedom (var/f) from approx. 20 to approx. 3. Moreover, inclusion of the additional variable in model 3 in most cases leads to a further small but significant improvement, var/f being reduced to approx 1. In no case, however, did the calculated triplet energy change by more than 0.6 cm^{-1} by going from model 1 to model 2 and no more than 0.1 cm^{-1} by going from model 2 to model 3. As a common feature, it was found that within models 2 and 3 the septet energy was estimated to be approx. 30 cm^{-1} lower in energy than within model 1.

It is apparent from all these models that all four of these five isomers described herein have singlet ground states with triplet states lying approx. 45 cm^{-1} higher in energy. These results should be compared with the singlet-triplet separations ranging from 32 to 37 cm^{-1} as found in a related series of di-μ-hydroxo complexes of 1-(2-pyridyl)-ethylamine[21] one of which has been structurally characterized,[25] namely di-μ-hydroxobis[bis{(*S*)-1-(2-pyridyl)ethylamine}-chromium(III)] dithionate dihydrate. Since this compound has the hydrogens of the μ-hydroxo groups in the bridging plane, maximum exchange coupling for the given geometry of the bridging system is expected. The present series of complexes show even slightly larger coupling constants. It is, therefore, very unlikely that they should be aquahydroxo monools where only one superexchange path is possible which is expected to lead to smaller coupling constants. These arguments are based on the Glerup-Hodgson-Pedersen GHP model[44] for magnetic exchange in such systems. This model also predicts only small

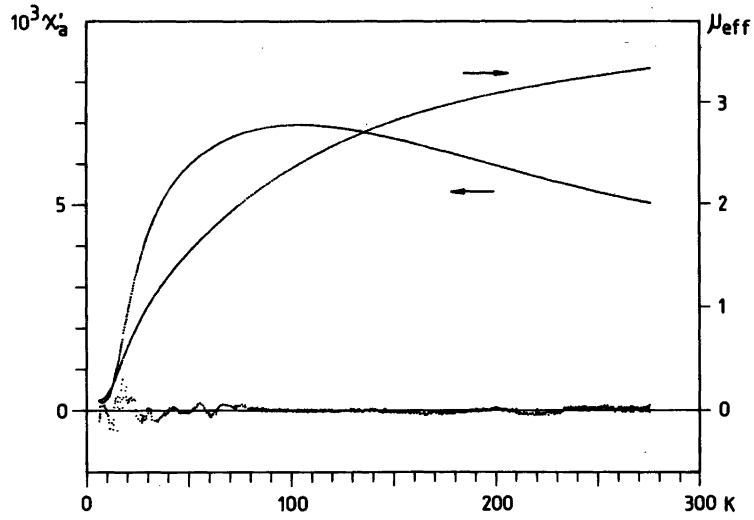

Fig. 13. Magnetic susceptibility (left scale in c.g.s. units) and effective magnetic moment (right scale in Bohrs magnetons) of $\Delta\Delta(-)_D$-[{bispic(-pn)}Cr(OH)$_2$Cr{bispic(-pn)}]$(ClO_4)_4$.4 H_2O. The lower set of points indicates $50\times(\chi_{obs}-\chi_{calc})$, as obtained from fitting of the results to model 3, *cf.* Table 8.

differences between the geometries of the bridging systems in the aforementioned complex dithionate[25] and the present series. The verification of this conclusion must, however, await the results of ongoing X-ray structural investigations.

Acknowledgements. We are grateful to Karen Margrethe Nielsen for the preparation of the amines and to Solveig Kallesøe for the measurements of the magnetic properties. Acknowledgement is further made to the Danish National Science Research Council through grants Nos. 511–742, 511–3993, and 511–10516 (to EP).

REFERENCES

1. Inskeep, R. G. and Benson, M. *J. Inorg. Nucl. Chem. 20* (1961) 290.
2. Earnshaw, A. and Lewis, J. *J. Chem. Soc.* (1961) 396.
3. Morishita, T., Hori, K., Kyono, E. and Tsuchiga, R. *Bull. Chem. Soc. Jpn. 38* (1965) 1276.
4. Ferraro, J. R., Driver, R., Walker, W. R. and Wosniak, W. *Inorg. Chem. 6* (1967) 1586.
5. Mason, S. F. and Wood, J. W. *Chem. Commun.* (1968) 1512.
6. Josephsen, J. and Schäffer, C. E. *Acta Chem. Scand. 24* (1970) 2929.
7. Pedersen, E. *Acta Chem. Scand. 26* (1972) 333.
8. Glerup, J. *Acta Chem. Scand. 26* (1972) 3775.
9. Veal, J. T., Hatfield, W. E. and Hodgson, D. J. *Acta Crystallogr. B 29* (1973) 12.
10. Veal, J. T., Hatfield, W. E., Jeter, D. Y., Hempel, J. C. and Hodgson, D. J. *Inorg. Chem. 12* (1973) 342.
11. Hodgson, D. J. In Interrante, L. V., Ed., *Extended Interactions between Metal Ions,* American Chemical Society, Washington D.C. 1974.
12. Scaringe, R. P., Singh, P., Eckberg, R. P., Hatfield, W. E. and Hodgson, D. J. *Inorg. Chem. 14* (1975) 1127.
13. Hodgson, D. J. *Prog. Inorg. Chem. 19* (1975) 173 and references therein.
14. Michelsen, K. *Acta Chem. Scand. A 30* (1976) 521.
15. Hancock, M. P., Josephsen, J. and Schäffer, C. E. *Acta Chem. Scand. A 30* (1976) 79.
16. Estes, E. D., Scaringe, R. P., Hatfield, W. E. and Hodgson, D. J. *Inorg. Chem. 15* (1976) 1179.
17. Michelsen, K. *Acta Chem. Scand. A 31* (1977) 429.
18. Scaringe, R. P., Hatfield, W. E. and Hodgson, D. J. *Inorg. Chim. Acta 22* (1977) 175.
19. Cline, S. J., Scaringe, R. P., Hatfield, W. E. and Hodgson, D. J. *J. Chem. Soc. Dalton Trans.* (1977) 1662.

20. Josephsen, J. and Pedersen, E. *Inorg. Chem. 16* (1977) 2534.
21. Michelsen, K. and Pedersen, E. *Acta Chem. Scand. A 32* (1978) 847.
22. Cline, S. J., Kallelsøe, S., Hodgson, D. J. and Pedersen, E. *Inorg. Chem. 18* (1979) 796.
23. Hodgson, D. J. and Pedersen, E. *Inorg. Chem. 19* (1980) 3116.
24. Güdel, H. U. and Hauser, U. *J. Solid State Chem. 35* (1980) 230.
25. Larsen, S. and Sørensen, B. *Acta Chem. Scand. A 35* (1981) 105.
26. Cline, S. J., Glerup, J., Hodgson, D. J., Jensen, G. S. and Pedersen, E. *Inorg. Chem. 20* (1981) 2229.
27. Srdanov, G., Radanovic, D. J. and Veselinivic, D. S. *Inorg. Chim. Acta 38* (1980) 37.
28. Oki, H. and Yoneda, H. *Inorg. Chem. 20* (1981) 3875.
29. Decurtins, S., Güdel, H. U. and Pfeuti, A. *Inorg. Chem. 21* (1982) 1101.
30. Michelsen, K., Pedersen, E., Wilson, S. R. and Hodgson, D. J. *Inorg. Chim. Acta 63* (1982) 141.
31. Cline, S. J., Hodgson, D. J., Kallesøe, S., Larsen, S. and Pedersen, E. *Inorg. Chem. 22* (1983). *To be published.*
32. Springborg, J. and Toftlund, H. *J. Chem. Soc. Chem. Commun.* (1975) 422.
33. Springborg, J. and Toftlund, H. *Acta Chem. Scand. A 30* (1976) 171.
34. Kaas, K. *Acta Crystallogr. B 35* (1979) 596, 1603.
35. Christensson, F., Springborg, J. and Toftlund, H. *Acta Chem. Scand. A 34* (1980) 317.
36. Dwyer, F. R., Garvan, F. L. and Shulman, A. *J. Am. Chem. Soc. 81* (1959) 290.
37. Mønsted, L. and Mønsted, O. *Acta Chem. Scand. A 30* (1976) 203.
38. Figgis, B. N. and Nyholm, R. S. *J. Chem. Soc.* (1958) 4190.
39. Pedersen, E. *J. Phys. E. Ser. 2 1* (1968) 1013.
40. Goodwin, H. A. and Lions, F. *J. Am. Chem. Soc. 82* (1960) 5021.
41. Michelsen, K. and Nielsen, K. M. *Acta Chem. Scand. A 34* (1980) 755.
42. Hata, Y., Yamamoto, Y. and Shimura, Y. *Bull. Chem. Soc. Jpn. 54* (1981) 1255.
43. Mason, S. F. *Q. Rev. Chem. Soc. 17* (1963) 20.
44. Glerup, J., Hodgson, D. J. and Pedersen, E. *Acta Chem. Scand. A 37* (1983) 161.

Received May 27, 1982.

Acta Chemica Scandinavica A 37 (1983) 153—158

2-Methoxypropene. Gas Phase Molecular Structure and Conformation as Determined by Electron Diffraction

S. H. SCHEI

Department of Chemistry, University of Trondheim, NLHT Rosenborg, N-7000 Trondheim, Norway

At room temperature gaseous 2-methoxypropene exists essentially as one conformer, the form where the O–CH_3 bond eclipses the carbon–carbon double bond. However, amounts of *ca.* 10 % of a second conformer cannot be excluded. The structural results in terms of r_a distances and $\angle_\alpha$ angles are as follows: r(C=C) = 1.330(7)Å, r(C–C) = 1.501(8)Å, r(=C–O) = 1.353(5)Å, r(O–CH_3) = 1.416(5)Å, ∠C=C–C = 123.9(8)°, ∠C=C–O = 125.8(7)°, ∠C–O–C = 116.0(1.1)°, ∠C=C–H = 121.4(3.9)°, ∠C–C–H = 112.1(2.7)°, ∠O–C–H = 109.7(1.7)°, *syn* torsional amplitude is 11.9(2.6)°. Error estimates are given as 2σ, where σ includes uncertainties due to correlation among observations, electron, wavelength and other parameters used in the data reduction.

Methyl vinyl ether, which is closely related to 2-methoxypropene, has been thoroughly investigated during the last decade. It is well established, both by theoretical [1–4] and experimental [5–12] methods, that the predominant conformer is the one with the O–CH_3 bond eclipsing the carbon–carbon double bond(τ=0°). The nature of the second conformer has been more questionable. However, the latest investigations point toward a second conformer with a planar skeleton.[1–3,6,11,12]

According to the observations made for methyl vinyl ether, 2-methoxypropene was expected to exist mainly as a *syn* conformer, τ=0°. For sterical reasons a possible planar second conformer may seem less likely in this case. An infrared vibrational spectroscopic study of 2-methoxypropene [13] concluded that two conformers coexisted both in liquid and vapour phases, the most abundant one being *syn*. The energy difference in liquid phase was estimated to 3.5 kJ mol^{-1}. However, it could not be determined whether the second conformer was one with a planar skeleton or not. The conformational energy difference as obtained from the infrared spectra [13] indicates a contribution of 15–20 % of the less abundant conformer, which was expected to be detectable from an ED study. No structural study of 2-methoxypropene seems to exist.

EXPERIMENTAL AND DATA REDUCTION

The sample of 2-methoxypropene used for ED recordings was synthesized by A. O. Diallo as described in Ref. 13. It was distilled just before use and the purity was found to be 99 % from a gas chromatography test. Data were recorded with the Balzers Eldigraph KDG-2 apparatus [14,15] at a nozzle temperature of 20 °C. Nozzle-to-plate distances of 50 and 25 cm were used. The electron wavelength was calibrated against benzene. [16]. The electron diffraction photographs were recorded on Kodak Electron Image plates. Optical densities were measured with a Joyce Loebl densitomer. For the 50 and 25 cm data, 4 and 3 plates, respectively, were selected for analysis.

The data were reduced in the standard way, [17–18] giving two average experimental intensity curves in the form $sI_m(s)$, one for each camera distance. For calculation of electron scattering amplitudes and phase shifts, Hartree-Fock potentials [19] for C and O were used, while molecular bonded potentials were used for H.[20]

0302-4377/83 $2.50

NORMAL COORDINATE CALCULATION

The present structural study involves a molecule of low symmetry and a possibility for more than one conformer. Therefore, it was important to calculate the vibrational quantities as accurately as possible. A valence force field was used. This force field consists of a combination of force constants from valence force field of methyl vinyl ether[21] and isobutene. A similar transference of force constants have been made for compounds of the type $CH_2=C(CH_3)-CH_2X$, X=Cl, Br, CN.[22] Those calculations reproduced the observed frequencies satisfactorily. A similar calculation for 2-methoxy-propene was expected to reproduce observed frequencies[13] quite accurately. Unfortunately, torsional frequencies, which will be the most uncertain part of such a calculation, are not observed. Therefore, vibrational quantities were calculated for a wide range of torsional force constants, varying from 0.12 (as in 1-butene) to 0.38 mdyn Å $(rad)^{-2}$ (as in methyl vinyl ether). The valence force constants of the *syn* conformer are listed in Table 1. In Table 2, root mean square amplitudes of vibration (*l*) are given, corresponding to a torsional force constant 0.20 mdyn Å $(rad)^{-2}$.

The frequencies thus calculated deviate from the observed ones[13] by an average of 12 cm^{-1}. The calculation agrees well with the interpretation given in Ref. 13, with one important exception. The symmetric C–O–C stretch frequency was calculated to 828 cm^{-1}. This suggested that the band observed at 830 cm^{-1} may not solely be due to a second conformer. If so should be the case, the relative conformational energy difference may be considerably different from 3.5 kJ mol^{-1}, which was estimated from temperature effects on the 830 and 800 cm^{-1} bands in the vibrational spectra.[13]

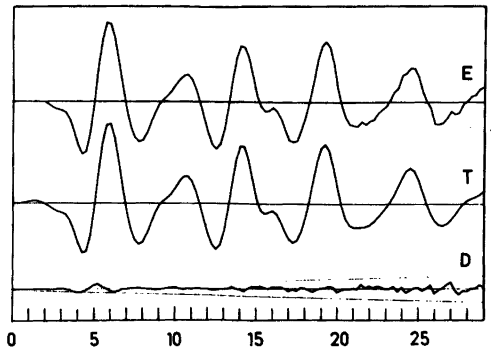

Fig. 1. 2-Methoxy-propene; intensity curves in the form $sI_m(s)$. Experimental curve (E) is the composite curve for all plates and camera distances. Theoretical curve (T) was calculated from parameters in Tables 2 and 3. Difference curve (D) is E–T. The straight lines show the experimental uncertainties as three times standard deviation. All curves are on the same scale. Δs=0.25 $Å^{-1}$.

STRUCTURAL ANALYSIS

The least squares refinements were based on intensity curves in the form $sI_m(s)$. The compo-

Table 1. 2-Methoxypropene; valence force constants in units of mdyn $Å^{-1}$ and mdyn Å $(rad)^{-2}$.

	Involved coordinate	Value	Involved coordinate(s)	Value	Involved coordinate(s)	Value
str.	C=C	9.14	$H-C_1-H$	0.35	$=C-O/O-CH_3$	0.28
	C–C	4.25	C–C–H	0.64	C_3-H/C_3-H	0.05
	=C–O	5.10	$H-C_3-H$	0.54	C_4-H/C_4-H	0.05
	$O-CH_3$	5.11	O–C–H	0.89	str/bend C=C/C=C–H	0.41
	=C–H	5.15	$H-C_4-H$	0.53	C=C/O–C–C	−0.43
	C_3-H	4.71	tors. C=C	0.49	C–C/O–C–C	0.32
	C_4-H	4.71	C–C	0.08	=C–O/O–C–C	0.32
bend	C=C–C	0.98	=C–O	0.20	C–C/C–C–H	0.38
	C=C–O	1.27	$O-CH_3$	0.08	$O-CH_3/O-C-H$	0.43
	O–C–C	0.73	o.o.p. CH_2	0.16	bend/bend C=C–O/C–O–C	0.46
	C–O–C	1.68	CC_2	0.35	C–C–H/C–C–H	−0.02
	C=C–H	0.52	str/str. =C–O/C–C	0.78	O–C–H/O–C–H	−0.04

Table 2. 2-Methoxy-propene; r_a distances and calculated root mean square amplitudes of vibration in Å.

Distance	r_a	l
=C–H	1.09	0.077
–C–H	1.10	0.079
C=C	1.33	0.042
=C–O	1.35	0.047
O–C_4	1.42	0.048
C–C	1.50	0.052
O···C_1	2.38	0.060
O···C_3	2.34	0.066
C_2···C_4	2.34	0.068
C_1···C_3	2.50	0.066
C_1···C_4	2.76	0.092
C_3···C_4	3.64	0.071

site experimental $sI_m(s)$ curve is shown in Fig. 1. A unit weight matrix was used. The molecular geometry was calculated using geometry consistent r_a parameters.[23]

Because of the low molecular symmetry, some constraints had to be made on the geometry parameters. Thus, both C=C–H angles were assumed to be equal. Both CH_3 groups were restricted to C_{3v} symmetry, with symmetry axis coinciding with the C–C and O–CH_3 bonds; one C–H bond in each methyl group was positioned *anti* to the =C–O bond. The difference Δr(C–H) = r(–C–H)–r(=C–H) was given an assumed value. Most of these geometrical parameters involving C–H, were difficult to refine together with the skeletal parameters. Therefore, their values were obtained from least squares refinements including fewer skeletal parameters than the final calculations (Table 3). For the calculations involving a second conformer, only the torsional angle τ (torsion around the =C–O bond) differed from the *syn* conformer value.

Along with the *syn* conformer, possible second conformers having different values for τ were included in refinements. In no case was the result more than 3±6 % contribution from the second conformer. Using vibrational quantity values calculated by the use of different torsional force constants had hardly any influence on the conformational composition.

Table 3. 2-Methoxy-propene; final structural results obtained from analysis of electron diffraction data at 20 °C (in Å and degrees, R in %).

Parameter No.	Parameter type	Parameter value (r_a, $\angle_a$)
1	r(C=C)	1.330(7)[a]
2	r(C–C)	1.501(8)
3	r(=C–O)	1.353(5)
4	r(O–CH_3)	1.416(5)
5	r(=C–H)	1.087(5)[b]
6	Δr(C–H)	0.015[c]
7	∠C=C–C	123.9(.8)
8	∠C=C–O	125.8(.7)
9	∠C–O–C	116.0(1.1)
10	∠C=C–H	121.4(3.9)[b]
11	∠C–C–H	112.1(2.7)[b]
12	∠O–C–H	109.7(1.7)
13	$\langle \tau_s^2 \rangle^{1/2}$	11.9(2.6)
	R	6.7

[a] Systematically varied, uncertainty estimated. [b] Value not obtained from final refinement, see text. [c] Assumed value.

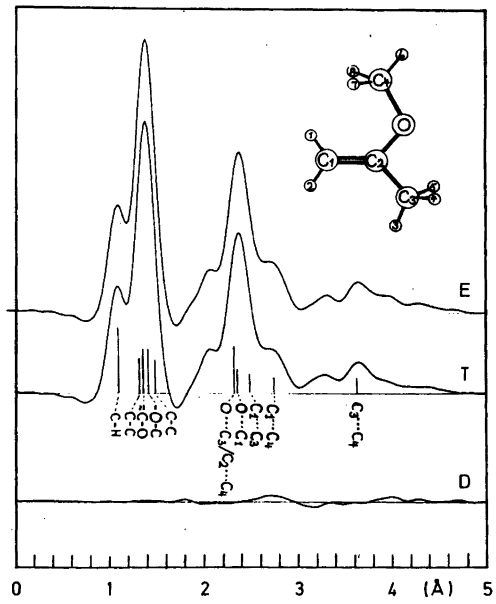

Fig. 2. 2-Methoxy-propene; radial distribution curves as Fourier transforms of the intensity curves in Fig. 1, using B=0.0020 Å, and theoretical data for unobserved area $0<s<2.25$. The vertical lines show the most important distances, height being proportional to weight of distance. All curves are on the same scale. In the atomic numbering figure, hydrogens are denoted by numbers only.

Table 4. 2-Methoxypropene; correlation matrix corresponding to the final refinement. Numbering of parameters is given in Table 3. σ_o is standard deviation obtained from least squares calculation.

No.	2	3	4	7	8	9	12	13
3	.36							
4	.12	−.36						
7	.10	.29	−.06					
8	.23	−.10	.23	−.61				
9	−.24	−.11	−.17	−.75	−.55			
12	−.20	.03	−.25	−.03	−.15	.18		
13	.03	−.11	.15	−.28	.08	−.39	−.36	
1	−.56	−.98	.88	−.88	−.06	−.21	−.39	.09
σ_o	.002	.001	.001	.3	.3	.4	.6	.9

In the final refinement, only one conformer was considered. All vibrational quantities were kept at their calculated values given in Table 2. All four bonded skeletal distances are located in the same peak in the radial distribution (RD) curve, separated by only 0.17 Å. Likewise, the four C···X (X=C,O) distances over one angle are closely positioned in the RD curve, differing by only 0.16 Å. Thus, there were large correlations among several of the parameters (Table 4). Therefore, the C=C distance was determined by a systematic variation, while all other skeletal geometrical parameters were refined.

RESULTS AND DISCUSSION

The geometry parameters as obtained from the final refinements are given in Table 3. The error estimates are 2σ, where σ includes correction for correlation among observations and uncertainties in wavelength and other parameters used in the data reduction.[18] The correlation matrix is given in Table 4. The corresponding theoretical intensity curve can be found in Fig. 1, while the RD curves are shown in Fig. 2.

It was found that gasous 2-methoxypropene consists of practically only one conformer. No significant evidence of a second form was found but amounts of up to 10 % of a second form could not be excluded. The essentially one-conformer result does not agree well with the conformational result from vibrational spectroscopy.[13] However, a reinterpretation of the observed frequencies as suggested from the normal coordinate analysis, would change the result anyway.

In Table 5 some of the geometrical parameters of 2-methoxypropene are compared with those of related molecules. Relative to methyl vinyl ether, the C=C–O angle is smaller. This was expected, since the neighbouring C=C–C angle is more resistant to decrease than a C=C–H angle. A similar trend is observed when comparing 1-butene[24] with 2-methyl-1-butene.[25] Then the =C–C–C angle increases as the C=C–C angle decreases. That the corresponding C–O–C angle in 2-methoxypropene decreases compared to the observed value in methyl vinyl ether,[6] may be due to the interaction between the lone pairs of oxygen and the 2-methyl group. Compared to the aliphatic ethers,[26–28] the C–O–C angle in 2-methoxypropene is still considerably larger.

The slight misfits observed at a few locations in the RD curve could have been smoothed out by refining some vibrational amplitudes. However, as so many carbon–carbon and carbon–oxygen distances are located closely together, it was considered better to use calculated values for vibrational quantities throughout the analysis.

Acknowledgements. The author is grateful to Dr. A. O. Diallo for providing the sample of 2-methoxypropene. Thanks are also due to Mrs. S. Gundersen for technical assistance. Financial support from *Norges Almenvitenskapelige Forskningsråd* is acknowledged.

Table 5. Comparison of geometrical parameters for molecules related to 2-methoxypropene.

Molecule	r(C–O)	r(O–CH_3)	r(C–C)	r(C=C)	C=C–O	C–O–C	Ref.
CH_2=C(CH_3)–O–CH_3(ED)	1.353(5)[a]	1.416(5)	1.501(8)	1.330(7)	125.8(.7)	116.0(1.1)	This work
CH_2=CH–O–CH_3(ED)	1.360(3)	1.428(3)	–	1.341	127.7(1.4)	118.3(1.1)	6
CH_2=C=CH–O–CH_3(ED)	1.375(7)	1.427(8)	–	–	125.3(1.2)	115.0(1.2)	30
CH_3–O–CH_3(ED)	–	1.416(3)	–	–	–	111.5(1.5)	27
CH_3–O–CH_2–CH_3(ED+MW)	–	1.413(9)	–	–	–	111.9(.5)	26
CH_3–O–CH_2–O–CH_3(ED)	–	1.432(4)	–	–	–	114.6(.5)	28
Ph–O–CH_3(ED)	1.361(15)	1.423(15)	–	–	–	120(2.0)	29
CH_2=C(CH_3)–CH_2CH_3(ED)	–	–	1.515	1.334	[125.2][b]	[116.0][b]	25
CH_2=CH–CH_2–CH_3(ED+MW)	–	–	1.502(2)	1.340(4)	[127.2(3)][b]	[114.9(.3)][b]	24

[a] Uncertainties are not comparable throughout the table. [b] C=C–C and C–C–C angles.

REFERENCES

1. Cadioli, B. and Pincelli, U. *J. Chem. Soc. Faraday Trans. 2, 68* (1972) 991.
2. Bernardi, F., Epiotis, N. D., Yates, R. L. and Schlegel, H. B. *J. Am. Chem. Soc. 98* (1976) 2885.
3. John, I. G. and Radom, L. *J. Mol. Struct. 36* (1977) 133.
4. Lister, D. G. and Palmieri, P. *J. Mol. Struct. 32* (1976) 355.
5. Owen, N. L. and Seip, H. M. *Chem. Phys. Lett. 5* (1970) 162.
6. Samdal, S. and Seip, H. M. *J. Mol. Struct. 28* (1975) 193.
7. Cahill, P., Gold, L. P. and Owen, N. L. *J. Chem. Phys. 48* (1968) 1620.
8. Sakakibara, M., Inagaki, F., Harada, I. and Shimanouchi, T. *Bull. Chem. Soc. Jpn. 49* (1976) 46.
9. Owen, N. L. and Sheppard, N. *Trans. Faraday Soc. 60* (1964) 634.
10. During, J. R. and Compton, D. A. C. *J. Chem. Phys. 69* (1978) 2028.
11. Ignatyev, I. S., Lazarev, A. N., Smirnov, M. B., Alpert, M. L. and Trofimov, B. A. *J. Mol.Struct. 72* (1981) 193.
12. Cadioli, B., Gallinella, E. and Pincello, U. *J. Mol. Struct. 78* (1982) 215.
13. Diallo, A. O. *Spectrochim. Acta A 37* (1981) 529.
14. Zeil, W., Haase, J. and Wegman, L. *Z. Instrumentenkd. 74* (1966) 84.
15. Bastiansen, O., Graber, R. and Wegman, L. *Balzer's High Vacuum Rep. 24* (1969) 1.
16. Tamagawa, K., Iijima, T. and Kimura, M. *J. Mol. Struct. 30* (1976) 243.
17. Andersen, B., Seip, H. M., Strand, T. G. and Stølevik, R. *Acta Chem. Scand. 23* (1969) 3224.
18. Schei, S. H. *Acta Chem. Scand. A 37* (1983) 15.
19. Strand, T. G. and Bonham, R. A. *J. Chem. Phys. 40* (1965) 3175.
20. Stewart, R. F., Davidson, E. R. and Simpson, W. T. *J. Chem. Phys. 42* (1965) 3175.
21. Schei, S. H. *Theochem. 9* (1983) 203.
22. Schei, S. H. *Spectrochim. Acta. In press.*
23. Kuchitsu, K. and Cyvin, S. J. In Cyvin, S. J., Ed., *Molecular Structures and Vibrations,* Elsevier, Amsterdam 1972, Chapter 12.
24. Van Hemelrijk, D., Van den Enden, L., Geise, H. J., Sellers, H. L. and Schäfer, L. *J. Am. Chem. Soc. 102* (1980) 2189.
25. Shimanouchi, T., Abe, Y. and Kuchitsu, K. *J. Mol. Struct. 2* (1968) 82.
26. Oyanagi, K. and Kuchitsu, K. *Bull. Chem. Soc. Jpn. 5* (1978) 2237.

27. Kimura, K. and Kubo, M. *J. Chem. Phys. 30* (1959) 151.
28. Astrup, E. E. *Acta Chem. Scand. 27* (1973) 3271.
29. Seip, H. M. and Seip, R. *Acta Chem. Scand. 27* (1973) 4024.
30. Bijen, J. M. J. M. and Derissen, J. L. *J. Mol. Struct. 14* (1972) 229.

Received June 16, 1982.

Acta Chemica Scandinavica A 37 (1983) 159—171

Short Communications

The Crystal Structure of Lead Carbonate Fluoride, $Pb_2F_2CO_3$

BENGT AURIVILLIUS

Division of Inorganic Chemistry 2,
The Lund Institute of Technology,
P.O. Box 740, S-220 07 Lund, Sweden

The crystal structure of phosgenite, $Pb_2Cl_2CO_3$, was determined by Sillén and Pettersson[1] and has later been refined by Giuseppetti and Tadini.[2] $Pb_2Br_2CO_3$ was found to be isotypic with $Pb_2Cl_2CO_3$.[1] In the course of a study of the system $PbF_2-Pb(SCN)_2$ by hydrothermal syntheses at 180 °C, the present author obtained a single crystal of $Pb_2F_2CO_3$ by chance. Since its crystal structure has quite another architecture than that of $Pb_2Cl_2CO_3$, the results are now reported. According to powder photographs the $Pb_2F_2CO_3$ sample is orthorhombic, $Z=4$, $a=8.0836(9)$, $b=8.309(2)$, $c=6.841(1)$ Å. Weissenberg photographs indicated space group *P bcn*. $Pb_2F_2CO_3$ can be synthetized in the following way. Aqueous solutions of $Pb(NO_3)_2$, NaF and K_2CO_3 are mixed to give the Pb:F:CO_3 ratios 2:2:1 and the slurry is boiled for one hour and filtered. Slightly larger crystals are obtained on treating the slurry hydrothermally at 180 °C but even these were not large enough for single crystal work. The single crystal used for the structure determination was obtained together with decomposition products, among them PbS, when a $5PbF_2 \cdot Pb(SCN)_2$ mixture was heated hydrothermally for 3 days at 180 °C. Because of the partial decomposition of $Pb(SCN)_2$ there was an overpressure in the tube when cooled down to room temperature.

Weissenberg photographs, Cu$K\alpha$ radiation, around [001], zero and first layer indicated the Laue symmetry *mmm* and the following conditions limited possible reflections: 0*kl*: $k=2n$, *h*0*l*: $l=2n$, *hk*0: $h+k=2n$, which uniquely lead to the space group *P bcn*. There is, however, a very weak extra reflection, 201. The single crystal had the form of a tetragonal prism with $A=B=0.082$ mm and $C=0.108$ mm. The *a*- and *b*-axes of the unit cell fall along the diagonals of the basal plane of the prism and the *c*-axis along the *C*-direction. The crystal was mounted on a Nicolet *P3m* diffractometer and 684 independent reflections were registered by means of Mo$K\alpha$ radiation in the range $5°<2\theta<70°$. 638 of the reflections had $I>3\sigma(I)$ and were corrected for LP^{-1} and for absorption. Out of these, nine violated the systematic extinctions given above. The four strongest of them had the following *hkl* and $|F/\sigma(F)|$-values: 100(19), 016(12), 014(12) and 011(6). The rest of the reflections 013, 051, 205, 401 and 405 had $|F/\sigma(F)|$ less than 5. The reflections 100, 011, 051 and 401 are not visible in the moderately exposed Weissenberg photographs and the reflection 201 visible in these photographs was not observed in the diffractometer data. The fact that different extra reflections occur in the Weissenberg photographs (Cu$K\alpha$ radiation) and diffractometer data (Mo$K\alpha$ radiation) is at least an indication that double reflections are present and the space group is therefore assumed to be *P bcn*. A three-dimensional Patterson function could be interpreted assuming 8 Pb atoms to be situated at the general point position of *P bcn*. Difference Fourier maps revealed the presence of light atoms and their positions could be rationalized as AB_3 groups with *A*–*B* distances ~1.2 Å and *B*–*B* distances ~2.2 Å and separate *B* atoms. No chemical analyses were performed on the single crystals, but with these distances possible formulae for the compound would be $Pb_2F_2CO_3$ or $Pb_2(OH)_2CO_3$. A compound $Pb_2(OH)_2CO_3$ has been described by Pannetier, Davignon and Feinstein[3] but their published *d*-values showed no resemblance to the ones obtained from the diffractometer data. Moreover, a synthesis of $Pb_2F_2CO_3$ as described above gave powder photographs that could be completely indexed by means of the cell edges found from the diffractometer measurements. Assuming the light atoms to be F, O and C, the positions of all atoms were refined using isotropic temperature factors. Because of the nine extra reflections the restriction $0.1<F_o/F_c<10$ was made. The *R*-factor was 0.047 for 627 reflections and 0.074 for all 638 reflec-

0302-4377/83 $2.50

Table 1. Final positional parameters and isotropic temperature factors for $Pb_2F_2CO_3$. Standard deviations are given within parentheses.

Atom	*x*	*y*	*z*	*B* (Å^2)
Pb	0.18322(6)	0.15907(6)	0.04948(7)	(1.14)
F	0.6098(12)	0.6143(13)	0.1000(15)	1.53(15)
O(1)	1/2	0.1754(22)	1/4	1.76(27)
O(2)	0.1296(15)	0.4404(15)	0.1929(18)	1.56(18)
C	1/2	0.0195(28)	1/4	1.30(30)

tions. The *B*-value of Pb was 1.14 Å^2. Anisotropic temperature factors were introduced for the lead atoms and the final *R*-factors were 0.041 (628) and 0.045 (638). Positional and isotropic thermal parameters are given in Table 1. Lists of F_o and F_c and the anisotropic temperature factors of Pb are available on request. Selected distances are summarized in Table 2.

The crystal structure so arrived at is isotypic with that of the mineral Brenkite, $Ca_2F_2CO_3$, determined by Leufer and Tillmanns.[4] Their structural description may be used also for $Pb_2F_2CO_3$. The building elements of the crystal structure are endless spiral chains of edge-sharing FPb_4 tetrahedra extending in the *c*-direction. These chains are joined by corner-sharing to a three-dimensional network of formula $(PbF)_n^{n+}$. The CO_3^{2-} groups are situated in the tunnels formed by this network. The Pb atoms are nine-coordinated by 4F and 5O, *cf.* Table 2. The PbO_5F_4 polyhedron may be described as a very distorted three-capped trigonal prism.

The difference between the structure of $Pb_2F_2CO_3$ and $Pb_2Cl_2CO_3$ is perhaps most clearly seen when considering the F(Cl)–Pb arrangement. In $Pb_2Cl_2CO_3$ there are [Pb,Cl(1)–Cl(2)–Cl(1)Pb] layers parallel to (001) and these layers are connected by CO_3^{2-} groups. In the present structure a three-dimensional network is formed by the Pb and F atoms and the CO_3^{2-} groups are situated within the tunnels so formed.

Table 2. Selected distances within the structure of $Pb_2F_2CO_3$. Standard deviations are given within parentheses.

Pb–F	2.42(1)	C–O(1)	1.30(3)
Pb–F	2.50(1)	C–2O(2)	1.30(2)
Pb–O(2)	2.56(1)	O(1)–2O(2)	2.26(2)
Pb–F	2.56(1)	O(2)–O(2)	2.24(3)
Pb–O(2)	2.57(1)		
Pb–F	2.72(1)		
Pb–O(1)	2.88(1)		
Pb–O(1)	2.91(0)		
Pb–O(2)	2.99(1)		

Acknowledgements. Dr. Lars Fälth is thanked for valuable discussions and Mr. Christer Jönsson for skilful assistance. This investigation is part of a research project financially supported by the Swedish Natural Science Research Council.

1. Sillén, L. G. and Pettersson, R. *Ark. Kemi Mineral. Geol. A 21* (1945) No. 13.
2. Giuseppetti, G. and Tadini, C. *Mineral. Petrogr. Mitt. 21* (1974) 101.
3. Pannetier, G., Davignon, L. and Feinstein, S. *Bull. Soc. Chim. Fr.* (1966) 319.
4. Leufer, U. and Tillmanns, E. *Mineral. Petrogr. Mitt. 27* (1980) 261.

Received November 1, 1982.

A Novel Correlation between Magnetism and Structural Parameters in Superexchange Coupled Chromium(III) Dimers

JØRGEN GLERUP,[a] DEREK J. HODGSON[b] and ERIK PEDERSEN[a,*]

[a] Chemistry Department I (Inorganic Chemistry), University of Copenhagen, H. C. Ørsted Institute, Universitetsparken 5, DK-2100 Copenhagen Ø, Denmark and [b] Department of Chemistry, University of North Carolina, Chapel Hill, North Carolina 27514, U.S.A.

There has been intense recent research activity in the magnetochemistry of dimeric transition metal complexes. While for the electronically simple copper(II) $[d^9,d^9]$ complexes of the type $[CuL_m(OH)]_2^{n+}$ an empirical relationship between structural and magnetic properties has been demonstrated,[1,2] for the electronically more complex chromium(III) $[d^3,d^3]$ systems this is not the case. For dimers of the type $[CrL_m(OR)]_2^{n+}$ where L is mono- or bidentate, and R is a hydrogen atom or an alkyl group,[3-16] the magnetic interaction has been shown to vary with the Cr–O–Cr bridging angle, ϕ,[6,16,20-22] the Cr–O bond length, r,[20,22] and recently particular emphasis has been placed on the dihedral angle between the bridging plane and the OR vector of the bridging group, θ.[11,16,20,23,24] Apart from our own preliminary reports[25,26] quantification of these dependencies has not been given.

In this paper we propose a model which correlates the magnitude of the magnetic interaction with r, ϕ and θ. The model is consistent with widely varying magnetic and structural data for all fifteen dimeric chromium(III) complexes of the aforementioned type being well characterized at present. The model is an extension of our own calculations,[27] based on Anderson's superexchange model,[28,29] allowing the concepts of the angular overlap model to account for the influences of ϕ and θ on competing ferro- and antiferromagnetic contributions. Further theoretical details are the subject of a forthcoming publication.[30]

Theory. The ground state manifold in chromium(III) dimers with $S=0$, 1, 2 and 3 consists of two coupled $^4A_2$ states derived from the $|t_2^3(a), t_2^3(b)\rangle$ configuration where $^4A_2$ and t_2^3 refer to their octahedral parentage functions and a and b to the two centers. The lowest energy metal–metal charge transfer states with $S=0$, 1 and 2 belong to the configuration $1/\sqrt{2}\ \{|t_2^4(a)\ t_2^2(b)\rangle + |t_2^2(a)\ t_2^4(b)\rangle\}$. It has been shown for a linear μ-oxo complex[27] that these symmetry adapted configurations interact *via* a one-electron ligand field matrix element. This can be generalized,[30] and in the present cases this matrix element is mainly of the type $\langle d_{zx}(a)|V_L|d_{yz}(b)\rangle$ with the coordinate systems defined in Fig. 1. In the angular overlap model these matrix elements are proportional to the product of the corresponding overlap integrals of the types $\langle d_{zx}(a)|p_z\rangle$ *and* $\langle d_{yz}(b)|p_z\rangle$ involving a p_z-orbital on the bridging oxygen atom. This configuration interaction gives rise to an antiferromagnetic coupling in the ground states of the chromium dimers according to the Heisenberg Hamiltonian $\mathcal{H}=JS_a \cdot S_b$ with

$$J_{af} \propto \frac{|\langle d_{zx}(a)|V_L|d_{yz}(b)\rangle|^2}{E_{C.T.}} \qquad (1)$$

where $E_{C.T.}$ is the energy of the charge transfer configuration. The energy of this configuration and the radial part of the overlap integrals have been estimated earlier.[27]

As part of our model, we assume that the orbitals on the bridging oxygen atoms are $2s$–$2p$ hybrids pointing towards the two metal atoms and the R group. They participate in three σ-bonds. This leaves a lone pair in an orthogonal sp-hybrid orbital. If the OR-vector is in the bridging plane this lone pair is in a pure p_z-orbital which gives maximum values of the π-overlap integrals.

For other geometries of the bridging system it can be shown[30] that

$$\langle d_{zx}(a)|V_L|d_{yz}(b)\rangle \propto \cos^2\theta/\{1-\sin^2\theta/\tan^2(\phi/2)\} \qquad (2)$$

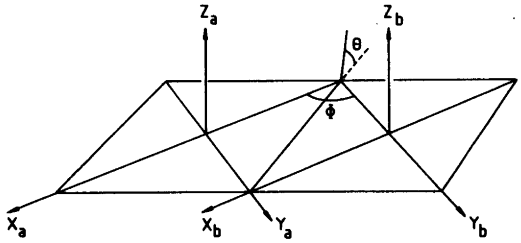

Fig. 1. Choice of coordinate systems for di-μ-hydroxochromium(III) complexes.

* To whom correspondence should be addressed.

0302-4377/83 $2.50

Through the application of eqn. 1 this leads to an angular dependence of the antiferromagnetic contribution according to

$$J_{af} \propto \cos^4\theta/\{1-\sin^2\theta/\tan^2(\phi/2)\}^2 \quad (3)$$

The next nearest charge transfer configuration is $1/\sqrt{2}\ \{|t_2^3e(a)t_2^2(b)\rangle + |t_2^2(a)\ t_2^3e(b)\rangle\}$ with energy $E_{C.T.}+\Delta+E_{rep}$ where $\Delta=10$ Dq, and E_{rep} is an interelectronic repulsion term. It interacts with the ground state configuration mainly *via* a matrix element of the type $\langle d_{z^2}(a)|V_L|d_{xy}(b)\rangle$ which is non-vanishing because there is a hybrid orbital having a σ-overlap with Cr(a) and a π-overlap with Cr(b) and *vice versa*. The angular dependence of these matrix elements can be shown to be

$$\langle d_{z^2}(a)|V_L|d_{xy}(b)\rangle \propto \sin\phi/\{1-\cos\phi\} \quad (4)$$

Transfer of an electron to the $e(a)$ orbital leads to $S=2$ or 1 on Cr(a) and similarly for Cr(b). This gives rise to two sets of charge transfer configurations. One set having states with $S=S_s+S_b=1$, 2 and 3 is derived from $S_a=2$ and $S_b=1$ and *vice versa*. The states with $S=3$ are
$1/\sqrt{2}\ \{|t_2^3e(a)(S_a=2)t_2^2(b)(S_b=1)\rangle +$
$|t_2^2(a)(S_a=1)t_2^3e(b)(S_b=2)\rangle\}$.
The other set having states with $S=0$, 1 and 2 is derived from $S_a=S_b=1$. The states with $S=2$ are
$1/\sqrt{2}\ \{|t_2^2e(a)(S_a=1)t_2^2(b)(S_b=1)\rangle -$
$|t_2^2(a)(S_a=1)t_2^3e(b)(S_b=1)\rangle\}$.

These sets give competing ferro- and antiferromagnetic contributions, respectively, to the magnetic interactions of the ground states, both according to the Heisenberg Hamiltonian. The states derived from the first configuration are lower in energy due to interelectronic repulsions. The ferromagnetic term will, therefore, be dominating. The net result is a ferro-magnetic term according to

$$J_f \propto \sin^2\phi/\{1-\cos\phi\}^2 \quad (5)$$

Hence, the observable exchange parameter is $J=J_{af}-J_f$.

Since the π-overlap integrals involved are expected to be small, J_{af} and J_f are expected to show an exponential decay with increasing Cr–O distances. Hence the total expression for J in the Heisenberg Hamiltonian is

$$J=J_{af}-J_f=e^{-a(r-1.8)}[b\cos^4\theta/ \{1-\sin^2\theta/\tan^2(\phi/2)\}^2-c\sin^2\phi/\{1-\cos\phi\}^2] \quad (6)$$

Here $r=1.8$ Å was arbitrarily chosen as zero-point for distance to reduce the correlation coefficients between the parameter sets a,b and a,c. b and c are, of course, dependent on $E_{C.T.}$, Δ and the interelectronic repulsion parameters; but the available dimers contain only oxygen and nitrogen ligators and the variations are, therefore, expected to be small.

Table 1. Observed and calculated coupling constants.

Compound	r/Å [a]	ϕ/deg [a]	θ/deg [a]	J_{exp}/cm^{-1} [b]	J_{calc}/cm^{-1} [c]
$[Cr(NH_3)_4OH]_2Cl_4\cdot aq$ [3]	1.975(2)	99.9(1)	41(3)	5.23(1)	9(3)
$[Cr(NH_3)_4OH]_2(S_2O_6)_2\cdot aq$ [3]	1.965(2)	101.5(1)	24(3)	9.12(1)	17(4)
$[Cr\,en_2\,OH]_2(S_2O_6)_2$ [4]	1.979(10)	100.0(4)	57(3)	3.40(10)	3(2)
$[Cr\,en_2\,OH]_2Cl_2(ClO_4)_2$ [5]	1.949(4)	103.4(2)	2(3)	26.8(5)	27(3)
$[Cr\,en_2\,OH]_2Cl_4\cdot aq$ [6]	1.944(6)	102.4(1)	5(3)	29.4(5)	30(7)
$[Cr\,acac_2\,OMe]_2$ [7]	1.962(10)	101.0(5)	29.8(5)	9.6(4)	16(5)
$[Cr(Cl\text{-}acac)_2OMe]_2$ [8]	1.959(4)	101.1(2)	24.4(10)	9.82(10)	18(5)
$[Cr(Br\text{-}acac)_2OMe]_2$ [9]	1.962(8)	101.5(4)	25.7(10)	8.53(50)	16(5)
$[Cr(Br\text{-}acac)_2OEt]_2$ [9]	1.951(12)	101.8(6)	18.3(10)	17.90(20)	23(7)
$[Cr(2\text{-}picetam)_2OH]_2(S_2O_6)_2$ [10,11]	1.945(8)	101.8(2)	0(5)	32.9(1)	29(9)
$[Cr(2\text{-}picetam)_2O]_2Cl_2\cdot aq$ [12]	1.890(10)	95.5(5)	–	83(2)	80(21)
$[Cr\,phen_2\,OH]_2Cl_4$ [13]	1.927(14)	103.1(6)	0(10)	43.0(5)	42(13)
$[Cr\,mal_2\,OH]_2Na_4\cdot aq$ [15]	1.988(4)	99.3(2)	54(6)	–2.16(4)	3(2)
$[Cr(Cl\text{-}dipic)aq\,OH]_2$ [16]	1.947(10)	100.7(4)	41(8)	10.24(6)	15(5)
$[Cr(NH_3)_5O_{1/2}]_2Cl_4\cdot aq$ [d]	1.815(10)	180(0)	–	450(2)	456(91)

[a] r,θ and ϕ are the structural parameters of the bridging system (see text). [b] Coupling constants obtained from magnetic susceptibility data. [c] Coupling constant calculated from eqn. (6). [d] The value of r was calculated from the atomic coordinates in Ref. 17 using unit cell constants determined by us (Ref. 18). The result is close to the average of the values reported in Refs. 17 and 19.

Discussion. The results of fitting the available data to eqn. (6) by a least squares technique are shown in Table 1. As standard deviations of r, ϕ and θ we have used the crystallographer's values multiplied by two. According to the resulting value of variance per degree of freedom *var*/f=0.09 the model describes all the data within the experimental standard deviations. The following parameters were obtained: a=19(1) Å^{-1}, b=611(39) cm^{-1}, c=172(56) cm^{-1}. The complex cation $[(NH_3)_5CrOCr(NH_3)_5]^{4+}$ is included in the data set since, although structurally different, it also has two Cr–O π-overlaps. The data for the di-μ-oxo complex has a large influence on the parameter c. A later publication[30] will include data for a μ-hydroxo-μ-oxo complex[12] and a better estimate of the ferromagnetic term is thus expected.

An analysis of the standard deviations of J_{calc} showed that the main contributions came from the standard deviations of the crystallographic parameters r and θ. The need for more sophisticated models for isotropic exchange interactions in chromium(III) dimers of the present type seems to be limited, therefore, by the accuracy of the X-ray methods.

Earlier work[27] showed that within certain approximations J_{af} can be expressed as

$$J_{af}=\tfrac{8}{9}\{\Delta(t_2)\}^2/E_{C.T.} \qquad (7)$$

where $\Delta(t_2)$ is the one-electron splitting of the t_2 level caused by the tetragonal distorsion. (The holohedrized symmetry of each center in the dimers is approximately tetragonal.) In cases where the angular part of eqn. (6) corresponds to maximum overlap, θ=0° and ϕ=90°, for example, a very simple correlation emerges from eqn. (7).

$$\tfrac{8}{9}\{\Delta(t_2)\}^2/E_{C.T.}=439\,e^{-19(r-1.8)} \qquad (8)$$

This does indeed make sense because $\Delta(t_2)$ is expected to decrease and $E_{C.T.}$ to increase with increasing bonding distance. The earlier estimate of $E_{C.T.}$ of 36.000 cm^{-1} in the μ-oxo complex[27] is, therefore, considered to be the lowest possible in the present series of dimers with two π-overlaps. In dimers with weak exchange and r-values near 2 Å, $E_{C.T.}$ is estimated to be in the range 60–100 kK in agreement with earlier estimates.[28]

Acknowledgements. We are very grateful to Mrs. Solveig Kallesøe whose preparations and measurements have contributed much to the data available. This research was supported by the Scientific Affairs Division, North Atlantic Treaty Organization (NATO) through grant No. 1318, by the Petroleum Research Fund, administered by the American Chemical Society, through grant No. 12128-AC 3.6 (to D.J.H.) and by the Danish Natural Science Research Council through grants (to E.P.) Nos. 511–742, 511–3993 and 511–10516.

1. Hodgson, D. J. *Prog. Inorg. Chem. 19* (1974) 173.
2. Crawford, V. H., Richardson, H. W., Wasson, J. R., Hodgson, D. J. and Hatfield, W. E. *Inorg. Chem. 15* (1976) 2107.
3. Cline, S. J., Hodgson, D. J., Kallesøe, S., Larsen, S. and Pedersen, E. *Inorg. Chem. 22* (1983). *In press.*
4. Cline, S. J., Scaringe, R. P., Hatfield, W. E. and Hodgson, D. J. *J. Chem. Soc. Dalton Trans.* (1977) 1662.
5. Kaas, K. *Acta Crystallogr. B 32* (1976) 2021.
6. Beutler, A., Güdel, H. U. and Snellgrove, T. R. *J. Chem. Soc. Dalton Trans.* (1979) 983.
7. Fischer, H. R., Glerup, J., Hodgson, D. J. and Pedersen, E. *Inorg. Chem. 21* (1982) 3063.
8. Estes, E. D., Scaringe, R. P., Hatfield, W. E. and Hodgson, D. J. *Inorg. Chem. 15* (1976) 1179.
9. Estes, E. D., Scaringe, R. P., Hatfield, W. E. and Hodgson, D. J. *Inorg. Chem. 16* (1977) 1605.
10. Larsen, S. and Hansen, B. *Acta Chem. Scand. A 35* (1981) 105.
11. Michelsen, K. and Pedersen, E. *Acta Chem. Scand. A 32* (1978) 847.
12. Michelsen, K., Pedersen, E., Wilson, S. R. and Hodgson, D. J. *Inorg. Chim. Acta 63* (1982) 141. The X-ray data were kindly provided by Dr. S. Larsen.
13. Veal, J. T., Hatfield, W. E. and Hodgson, D. J. *Acta Crystallogr. B 29* (1973) 12.
14. Scaringe, R. P., Hatfield, W. E. and Hodgson, D. J. *Inorg. Chim. Acta 22* (1977) 175. The oxalato complex was not included in our datafitting since the two hydrogen atoms have widely different θ-values.
15. Scaringe, R. P., Hatfield, W. E. and Hodgson, D. J. *Inorg. Chem. 16* (1977) 1600.
16. Cline, S. J., Kallesøe, S., Pedersen, E. and Hodgson, D. J. *Inorg. Chem. 18* (1979) 796.
17. Urushiyama, A. *Bull. Chem. Soc. Jpn. 45* (1972) 2406.
18. Pedersen, E. *Acta Chem. Scand. A 26* (1972) 333.
19. Yevitz, M. and Stanko, J. A. *J. Am. Chem. Soc. 93* (1971) 1512.

20. Josephsen, J. and Pedersen, E. *Inorg. Chem. 16* (1977) 2534.
21. Hodgson, D. J. and Pedersen, E. *Inorg. Chem. 19* (1980) 3116.
22. Scaringe, R. P., Hodgson, D. J. and Hatfield, W. E. *Transition Met. Chem. 6* (1981) 340.
23. Cline, S. J., Glerup, J., Hodgson, D. J., Jensen, G. S. and Pedersen, E. *Inorg. Chem. 20* (1981) 2229.
24. Güdel, H. U. and Hauser, U. *J. Solid State Chem. 35* (1980) 230.
25. Pedersen, E. *Int. Conf. Coord. Chem. XXI,* Toulouse 1980.
26. Pedersen, E. *Int. Conf. Electron Spin Res.,* Lancaster 1982.
27. Glerup, J. *Acta Chem. Scand. 26* (1972) 3775.
28. Anderson, P. W. *Phys. Rev. 115* (1959) 2.
29. Anderson, P. W. *Theory of Exchange in Isolators.* In *Solid State Phys. 14* (1963) 99.
30. Glerup, J., Hodgson, D. J. and Pedersen, E. *To be published.*

Reveived October 27, 1982.

Crystal Structure of Tetrabutylammonium Dicyanocuprate(I), $[N(C_4H_9)_4][Cu(CN)_2]$

MILJA ASPLUND,[a] SUSAN JAGNER [a] and MARTIN NILSSON [b]

[a] Department of Inorganic Chemistry and [b] Department of Organic Chemistry, Chalmers University of Technology and University of Göteborg, S-412 96 Göteborg, Sweden

Tetrabutylammonium dicyanocuprate(I) is of potential interest for preparative purposes.[1] Higher order mixed organocuprates(I) like $(C_4H_9)_2Cu(CN)Li_2$ have been found[2] to be useful reagents in organic synthesis, butyl but not cyanide being transferred in reactions with organic halides.

The dicyanocuprate(I) ion has a polymeric structure in both the potassium[3] and the sodium[4] compounds. Since the tetrabutylammonium dihalocuprates(I), X=Cl, Br, I, contain discrete monomeric[5] or dimeric[6] anions it was conceivable that tetrabutylammonium dicyanocuprate(I) might also crystallize with discrete anions.

Crystals of $[N(C_4H_9)_4][Cu(CN)_2]$, M_r=358.1, are triclinic, $P\bar{1}$, with a=13.731(13), b=14.680(10), c=12.659(8)Å, α=113.88(5), β=92.52(6), γ=65.04(6)° at 168 K, Z=4, D_c=1.14 g cm^{-3}, μ(Mo$K\alpha$)=10.9 cm^{-1}. The compound was prepared as described previously[1] and recrystallized from acetone yielding colourless prisms. As mentioned previously,[1] tetrabutylammonium dicyanocuprate(I) decomposes readily to give a compound with a higher melting point. Despite the low temperature (168 K) used in the investigation and a protective covering of epoxy resin, the crystals disintegrated within a few days. Several attempts were therefore made to collect a reasonably complete set of intensities.

Intensities from a crystal, 0.16×0.08×0.29 mm, were measured at 168 K for $2\theta \leq 45°$ with a Syntex $P2_1$ diffractometer using graphite-monochromated Mo$K\alpha$ radiation and the ω-scan mode with a scan rate of 1.0–8.0° min^{-1}. A 19-step profile was recorded for each reflection and the Lehmann and Larsen profile-analysis method[7] was used to calculate the intensities.[8] Of the 5472 independent reflections measured, 2635 had $I>3.0\ \sigma(I)$ and were considered to be observed. Correction was made for Lorentz and polarization effects but not for absorption. The unit-cell parameters at 168 K were determined by least squares from diffractometer setting angles for 13 reflections.

The structure was determined from Patterson and successive electron density maps.[9] Solution in $P\bar{1}$ necessitated statistical distribution of the carbon and nitrogen atoms of two of the bridging cyanide groups [CN(1) and CN(2)] over centres of symmetry. Moreover, the butyl chains of one of the two cations in the asymmetric unit [C(17)–C(32)]were poorly defined. Attempts were therefore made to remove the centre of symmetry but these did not reduce R. Intensity statistics[10] were, moreover, consistent with the presence of a centre of symmetry. It thus seemed unlikely that it would be possible to distinguish between alternative ordered models in $P1$ and the disordered model in $P\bar{1}$. Refinement was therefore continued on the basis of the disordered model in $P\bar{1}$, mean scattering factors $(f_C+f_N)/2$ being used for the atoms of all three cyanide bridges, *i.e.* CN(1)–CN(4), since trends in distances favouring designation of CN(3) as carbon and CN(4) as nitrogen were not substantiated by an improved fit to the data. It was not, however, possible to resolve the carbon atoms of the second cation into partially occupied sites. Block-diagonal least-squares refinement of positional and isotropic thermal parameters yielded R=0.130. Inclusion of anisotropic thermal parameters for all atoms (397 parameters; 2635 reflections) led to R=0.081 but also to unrealistically high thermal parameters for some of the carbon atoms of the second cation, indicating compensation for unresolved disorder. Refinement based on partial data sets obtained from other crystals gave essentially the same model. Atomic scattering factors were taken from the *International Tables for X-Ray Crystallography*[11] and F_o values were weighted[12] according to $w=(31.0+F_o+0.009F_o^2)^{-1}$. A final difference map showed a maximum electron density of 1.2 e Å^{-3}. No attempt was made to include hydrogen atoms in the calculations.

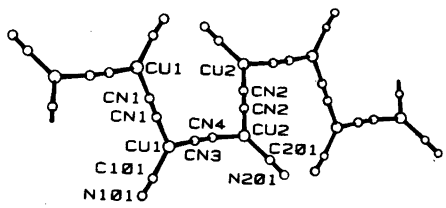

Fig. 1. Part of the $[Cu(CN)_2]^-$ chain showing the atomic numbering. The atoms have been drawn[14] as arbitrary spheres of radius 0.2 Å for copper(I) and 0.15 Å for all other atoms.

0302-4377/83 $2.50

Table 1. Fractional coordinates and equivalent isotropic thermal parameters (Å^2) with estimated standard deviations in parentheses. $B_{eq} = (8\pi^2/3)(U_{11}a^{*2}a^2 + \cdots + U_{23}b^*c^*bc\cos\alpha)$, the anisotropic temperature factor being defined as $\exp[-2\pi^2(U_{11}a^{*2}h^2 + \cdots + U_{23}b^*c^*kl)]$.

Atom	x	y	z	B_{eq}
Cu(1)	0.1749(1)	0.0112(1)	0.0563(2)	4.09(4)
Cu(2)	0.1491(1)	0.3091(1)	0.4485(1)	3.95(4)
C(101)	0.3047(10)	–0.1164(11)	–0.0449(12)	4.6(4)
N(101)	0.3732(10)	–0.1930(11)	–0.1100(12)	6.6(4)
C(201)	0.2532(10)	0.2626(9)	0.5460(10)	3.5(3)
N(201)	0.3158(9)	0.2308(8)	0.5981(11)	5.2(3)
CN(1)	0.0414(8)	0.0031(10)	0.0121(12)	5.0(4)
CN(2)	0.0371(10)	0.4569(9)	0.4891(10)	4.9(4)
CN(3)	0.1584(10)	0.1374(10)	0.1983(12)	5.0(4)
CN(4)	0.1500(9)	0.2064(9)	0.2892(11)	4.5(3)
N(1)	0.4699(9)	0.0593(8)	0.7809(9)	4.3(3)
C(1)	0.5307(10)	0.0439(9)	0.6720(10)	3.5(3)
C(2)	0.6428(11)	0.0377(13)	0.6860(15)	6.1(5)
C(3)	0.6880(11)	0.0346(11)	0.5741(14)	5.3(4)
C(4)	0.8098(17)	0.0050(19)	0.5695(19)	9.8(8)
C(5)	0.5317(11)	–0.0325(9)	0.8197(12)	4.4(4)
C(6)	0.5558(11)	–0.1519(9)	0.7245(12)	4.3(4)
C(7)	0.6182(11)	–0.2330(9)	0.7783(12)	4.3(4)
C(8)	0.6490(14)	–0.3542(11)	0.6864(17)	6.9(5)
C(9)	0.4548(13)	0.1649(10)	0.8893(12)	5.8(4)
C(10)	0.3883(18)	0.2714(12)	0.8683(14)	8.7(6)
C(11)	0.3803(18)	0.3725(13)	0.9813(18)	10.0(7)
C(12)	0.4726(16)	0.3860(14)	1.0004(30)	14.1(10)
C(13)	0.3589(11)	0.0649(12)	0.7473(13)	5.0(4)
C(14)	0.2788(14)	0.0861(14)	0.8482(17)	7.6(6)
C(15)	0.1751(14)	0.0755(14)	0.7943(21)	9.1(7)
C(16)	0.1085(16)	0.1766(17)	0.7668(22)	10.1(8)
N(2)	0.8084(8)	0.3799(8)	0.2147(9)	3.8(3)
C(17)	0.7086(20)	0.4790(20)	0.2850(24)	17.9(10)
C(18)	0.6199(14)	0.4982(13)	0.3323(22)	9.5(7)
C(19)	0.5158(18)	0.6024(23)	0.3751(19)	12.1(10)
C(20)	0.4258(21)	0.6351(26)	0.4275(33)	17.1(14)
C(21)	0.7954(15)	0.3298(31)	0.0922(15)	17.2(12)
C(22)	0.8479(18)	0.2782(22)	–0.0026(16)	13.2(9)
C(23)	0.8251(12)	0.2184(12)	–0.1210(12)	5.5(5)
C(24)	0.7739(18)	0.2927(17)	–0.1834(21)	10.1(8)
C(25)	0.8407(16)	0.3015(13)	0.2658(19)	9.7(6)
C(26)	0.8504(18)	0.2993(22)	0.3580(24)	17.2(11)
C(27)	0.8921(14)	0.2030(14)	0.3931(16)	7.8(6)
C(28)	0.9087(17)	0.2449(20)	0.5179(21)	10.4(9)
C(29)	0.8899(14)	0.4217(21)	0.2174(16)	13.3(9)
C(30)	0.9279(14)	0.4597(24)	0.1769(17)	13.5(9)
C(31)	0.9951(16)	0.5087(17)	0.1909(20)	9.4(7)
C(32)	1.0894(21)	0.4728(34)	0.1506(32)	18.5(16)

Atomic coordinates and equivalent isotropic thermal parameters are listed in Table 1 and interatomic distances and angles within the anion in Table 2. Structure factors, anisotropic thermal parameters and distances and angles within the tetrabutylammonium ions may be obtained from the authors.

As in the potassium [3] and sodium [4] compounds, the dicyanocuprate(I) ion forms a polymeric chain in which each copper(I) atom is coordi-

Table 2. Interatomic distances (Å) and angles (°) within the $[Cu(CN)_2]^-$ ion. Estimated standard deviations are given in parentheses.

Cu(1)–C(101)	1.94(1)	Cu(2)–C(201)	1.93(1)
C(101)–N(101)	1.12(2)	C(201)–N(201)	1.12(2)
Cu(1)–CN(1)	1.93(1)	Cu(2)–CN(2)	1.92(1)
CN(1)–CN(1)	1.20(2)	CN(2)–CN(2)	1.17(2)
Cu(1)–CN(3)	1.92(1)	Cu(2)–CN(4)	1.96(1)
CN(3)–CN(4)	1.16(2)		
C(101)–Cu(1)–CN(1)	113.8(5)	C(201)–Cu(2)–CN(2)	126.0(5)
C(101)–Cu(1)–CN(3)	130.7(5)	C(201)–Cu(2)–CN(4)	122.4(5)
CN(1)–Cu(1)–CN(3)	115.3(5)	CN(2)–Cu(2)–CN(4)	111.6(5)
Cu(1)–C(101)–N(101)	173(1)	Cu(2)–C(201)–N(201)	177(1)
Cu(1)–CN(1)–CN(1)	178(2)	Cu(2)–CN(2)–CN(2)	174(1)
Cu(1)–CN(3)–CN(4)	173(1)	Cu(2)–CN(4)–CN(3)	173(1)

nated by a terminal cyanide group and bridged to neighbouring copper(I) atoms by two other cyanide ligands (Fig. 1). Both copper atoms are surrounded by an approximately trigonal–planar arrangement of ligands, Cu(1) and Cu(2) lying 0.05(1) and 0.02(1) Å, respectively, from the planes defined by the three ligand atoms. These two planes are inclined at an angle of 43° so that in this respect the polymeric $[Cu(CN)_2]^-$ chain in $[N(C_4H_9)_4][Cu(CN)_2]$ is intermediate between the approximately planar chain in $Na[Cu(CN)_2]\cdot 2H_2O$[4] and that spiralling along a two-fold screw axis in $K[Cu(CN)_2]$.[3]

By analogy with $Na[Cu(CN)_2]\cdot 2H_2O$[4] and $K[Cu(CN)_2]$[3] it would seem likely that Cu(1) and Cu(2) are each coordinated by one nitrogen and two carbon atoms. Bond distances and angles are in good general agreement with those in the potassium and sodium compounds,[3,4] but a detailed comparison of the coordination geometry with those of the ordered dicyanocuprates(I) is not pertinent. The Cu(I)–CN distances in $[N(C_4H_9)_4][Cu(CN)_2]$ are, however, in good agreement with those in $Cu_3(NH_3)_3(CN)_4$[13] which crystallizes with disordered cyanide bridges.

The packing of tetrabutylammonium ions and $[Cu(CN)_2]^-$ chains is illustrated[14] in Fig. 2. Whereas bond distances and angles within cation (1) show no unusual features, there are some abnormally short C–C distances (≈1.2 Å) and large C–C–C angles (≈140°) within cation (2). These are undoubtedly artefacts of the inability to resolve this cation into proper sites. The closest distances of approach between cations and the $[Cu(CN)_2]^-$ chains are C(10)···N(201)=3.40(2) Å for cation (1) and C(22)···CN(1)=3.70(3) Å, C(21)···N(101)=

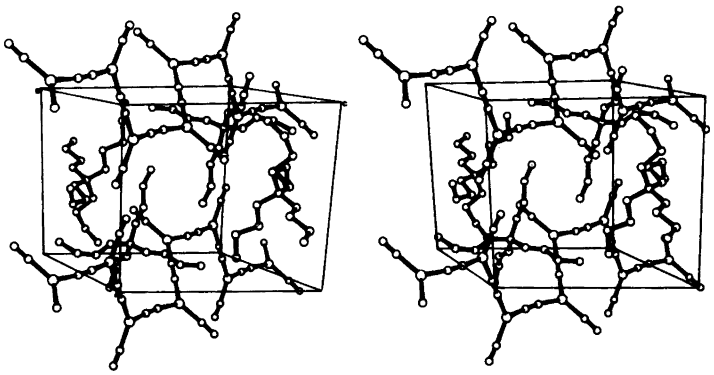

Fig. 2. Stereoscopic view of the unit cell of $[N(C_4H_9)_4][Cu(CN)_2]$. The atoms are depicted as spheres of radius 0.2 Å for copper(I) and 0.15 Å for all other atoms.

3.71(3) Å and C(29)···CN(2)=3.70(2) Å for cation (2).

It would thus seem that whereas the tetrabutylammonium cation stabilizes monomeric or dimeric configurations in the solid state for the dihalocuprates(I), *i.e.* $[CuCl_2]^-$, $[CuBr_2]^-$ and $[Cu_2I_4]^{2-}$, it is not sufficient to prevent the polymerization of $[Cu(CN)_2]^-$.

Acknowledgements. Financial support from the Swedish Natural Science Research Council (NFR) and the National Swedish Board for Technical Development (STU) is gratefully acknowledged.

1. Nilsson, M. *Acta Chem. Scand. B 36* (1982) 125.
2. Lipshutz, B. H., Wilhelm, R. S. and Floyd, D. M. *J. Am. Chem. Soc. 103* (1981) 7672.
3. Cromer, D. T. *J. Phys. Chem. 61* (1957) 1388.
4. Kappenstein, C. and Hugel, R. P. *Inorg. Chem. 16* (1977) 250.
5. Asplund, M., Jagner, S. and Nilsson, M. *Acta Chem. Scand. A 37* (1983) 57.
6. Asplund, M., Jagner, S. and Nilsson, M. *Acta Chem. Scand. A 36* (1982) 751.
7. Lehmann, M. S. and Larsen, F. K. *Acta Crystallogr. A 30* (1974) 580.
8. Lindqvist, O. and Ljungström, E. *J. Appl. Crystallogr. 12* (1979) 134.
9. Lindgren, O. *An Integrated Set of Crystallographic Programs.* In *On the Oxygen Coordination of Cerium in Some Sulfates and Chromates,* Thesis, Department of Inorganic Chemistry, Chalmers University of Technology and University of Göteborg, Göteborg 1977.
10. Main, P., Woolfson, M. M., Germain, G. and Declercq, J.-P. *MULTAN 77. A System of Computer Programs for the Automatic Solution of Crystal Structures from X-Ray Diffraction Data,* Univs. of York, England and Louvain, Belgium 1977.
11. *International Tables for X-Ray Crystallography,* Kynoch Press, Birmingham 1974, Vol. IV, p. 72.
12. Cruickshank, D. W. J. *Crystallographic Computing,* Munksgaard, Copenhagen 1970, p. 195.
13. Williams, R. J., Cromer, D. T. and Larson, A. C. *Acta Crystallogr. B 27* (1971) 1701.
14. Johnson, C. K. *ORTEP,* Report ORNL-3794, Oak Ridge National Laboratory, Oak Ridge 1965.

Received November 9, 1982.

Extraction of Amorphous Iron Oxides by EDTA from a Mixture of Akaganéite (β-FeOOH) and Amorphous Iron Oxides

O. K. BORGGAARD

Royal Veterinary and Agricultural University, Chemistry Department, Thorvaldsensvej 40, DK-1871 Copenhagen V, Denmark

Iron oxides are important constituents of catalysts and soils. Their effect depends on their surface area or crystallinity,[1-3] making the amorphous and poorly crystalline iron oxides the relatively most important. Prolonged extraction (>~3 months at 20 °C) with EDTA (ethylenediamine-*N,N,N',N'*-tetraacetic acid) can selectively remove these amorphous and poorly crystalline iron oxides from soil[4,5] and mixtures of amorphous and crystalline iron oxides.[6,7] These crystalline iron oxides did not include akaganéite (β-FeOOH). However, the short-term interaction between akaganéite and EDTA, investigated recently,[8] showed that negligible amounts of iron were dissolved in the pH range 2.5 to 7.5 but above pH 7.5 considerable dissolution of iron was found, *i.e.* up to nearly 1 % Fe dissolved after 11 days at 22 °C. Longer times are, however, required to reach equilibrium.[8] Therefore, prolonged extractions of a mixture of amorphous iron oxides and akaganéite with various EDTA solutions were carried out. The results of this investigation are reported in this paper.

Akaganéite was prepared by heating a solution made to contain 0.2 M $FeCl_3$ in 0.01 M HCl for 24 h at 90–100 °C. After centrifugation the precipitate was washed once with water, twice with ethanol and once with acetone and dried at 65 °C. Chloride was determined by potentiometric titration after dissolution in 20 % H_2SO_4 in a closed vessel at 100 °C.[9] The iron content was 57.7 %, determined by permanganate titration. The zero point of charge was 7.2, determined by the salt-addition technique.[10] The specific surface was 31 $m^2\ g^{-1}$, determined by applying the BET equation to N_2 adsorption after outgassing 20 h at 60 °C and 1 mPa and 44 $m^2\ g^{-1}$, determined by water adsorption at 19 % relative humidity.[11]

Amorphous iron oxides were prepared as described elsewhere[7] by mixing $Fe(NO_3)_3$ and NaOH solutions (OH/Fe 3.0, pH ~7). The product contained 53.1 % Fe. A 1+1 mixture of akaganéite and amorphous iron oxides was prepared for the extraction experiments.

EDTA solutions were prepared as described previously[4] by dissolving Titriplex II (Merck) and ammonium acetate in NH_3 and adding more NH_3 until the desired pH was obtained. The amounts of ammonium acetate were adjusted to give an ionic strength of 1.0 in the extractants.

The iron oxide mixture was weighed into PE bottles and the desired volume of EDTA was added. The bottles were closed by screw caps and shaken at room temperature (20 °C) in an end-over-end shaker for periods of from a few days to several months. The pHs of the 0.1 M or 0.2 M EDTA solutions were 4.0 to 9.9 and the solid–solution ratios were 1:2000 or 1:1000. Dissolved iron was measured by atomic absorption spectrophotometry.

Samples of akaganéite, before and after extraction for 180 days with 0.1 M EDTA at pH 9.9, were examined by X-ray diffraction using Fe-filtered Co-Kα radiation.

X-Ray diffraction showed the presence of 5–10 % of poorly crystalline hematite in the akaganéite. The X-ray spectra before and after extraction of the akaganéite for 180 days with 0.1 M EDTA at pH 9.9 showed no appreciable difference in the number and positions of lines, *i.e.* the hematite impurity was not dissolved.

Fig. 1 gives the amounts of iron dissolved from the mixture of akaganéite and amorphous iron

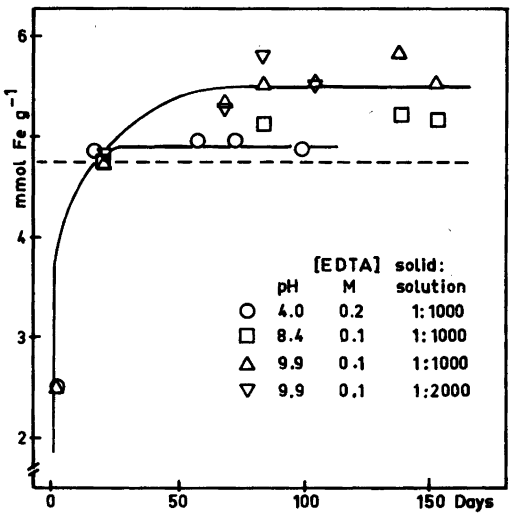

Fig. 1. Amount of iron extracted from a 1+1 mixture of akaganéite and amorphous iron oxides by various EDTA solutions plotted against extraction time at 20 °C. The dashed line corresponds to the amount of extractable iron assuming only added amorphous iron oxides are dissolved.

0302-4377/83 $2.50

oxides as a function of extraction time at various pH values, EDTA concentrations and solid–solution ratios. After 20 days, an amount of iron corresponding to that in amorphous iron oxides was dissolved by all extractants. During the dissolution of the amorphous fraction the pH of the extractant seemed of minor importance but the further developments were pH dependent. At pH 4 only negligible amounts of iron were extracted between 20 days and 101 days. A difference may, however, be seen between the amount of iron extracted after 20–101 days at pH 4 and the iron content of added amorphous iron oxides. This difference, corresponding to 0.32 (mmol Fe) g^{-1} akaganéite, is undoubtedly due to a small content of amorphous iron oxides in the akaganéite, because this fraction was extracted along with the added amorphous iron oxides. At pH 8.4–9.9 extracted iron continued to increase up to approximately 80 days. Between 80 days and 155 days no further iron was released. This surplus amounted to 1.18 (mmol Fe) g^{-1} akaganéite and corresponds to the dissolution of approximately 11 % akaganéite.

The results of this long-term interaction between akaganéite and EDTA are consistent with those of the short-term investigation,[8] showing that only weakly alkaline EDTA solutions but not weakly acidic or neutral EDTA solutions affect akaganéite. The results reported previously[6,7] for a number of other iron oxides, showing only negligible attack on the crystalline iron oxides when mixtures of amorphous and crystalline iron oxides were treated with EDTA, agree with the results for the interaction between akaganéite and EDTA at pH 4. The further increase in extracted iron between 20 days and 80 days with weakly alkaline EDTA solutions resembles that obtained when soils or selected minerals were extracted with EDTA[4,5,7] and was attributed to the dissolution of poorly crystalline iron oxides. This explanation does not apply to akaganéite, because no increase was observed between 20 days and 101 days at pH 4.

The resistance towards dissolution of akaganéite at pH $\lesssim$7.5 was considered[8] due to adsorption of EDTA onto the oxide, which inhibits dissolution. Even though this explanation may apply to akaganéite, it does not hold for amorphous iron oxides, which are shown (Fig. 1) to be dissolved with similar rates at pH 4 and pH 9.9. Furthermore, adsorption of anions by ligand exchange onto crystalline iron oxides does not necessarily inhibit their dissolution, *e.g.* it was shown[6,7,12] that several crystalline iron oxides dissolved in oxalate solution at pH 3, although oxalate is specifically adsorbed at least by goethite.[13]

Alternatively, the special structure of akaganéite may be responsible for the discrepancy between the akaganéite results and those of the other iron oxides, including the different susceptibility of akaganéite below and above pH ~7.5. The micro-structure of this oxide is based on the hollandite unit cell, which has a small central tunnel. These units are considered packed into bundles forming large square tunnels, approximately 3 by 3 nm wide,[14] although the existence of these large tunnels has been doubted.[15,16] The small tunnels are occupied – at least during formation – by chloride ions and the large tunnels by water.[14] Chloride ions seem essential for the structure and stability of akaganéite.[9,16] Thus, the stability was claimed to be markedly reduced when the chloride content was reduced.[9] In the present investigation, the chloride content of akaganéite was 4.3 %, close to the 4.6 % expected for one chloride ion per unit cell.[16] The chloride content was reduced to 1.7 % after extraction with 0.1 M EDTA for 180 days at pH 9.9, whereas extraction with 0.2 M EDTA for 80 days at pH 4.0 only reduced the content to 3.8 %. The greater reduction at pH 9.9 may be attributed to the higher hydroxyl concentration if it is assumed that the chloride ions are exchanged by hydroxyl ions. The reduction of the chloride content by extraction in alkaline solution may then increase the susceptibility of the oxide towards EDTA resulting in the observed surplus of 1.18 (mmol Fe) g^{-1} akaganéite being extracted between 20 days and 80 days.

Acknowledgements. My thanks are due to Charlotte Bak for carrying out most of the chemical analyses and to the Danish Agricultural and Veterinary Research Council for financial support.

1. Greenland, D. J. and Mot, C. J. B. In Greenland, D. J. and Hayes, M. H. B., Eds., *The Chemistry of Soil Constituents*, Wiley, Chichester 1978.
2. Schwertmann, U. *Proc. VI Int. Clay Conf. 1978*, Oxford 1979, p. 491.
3. Iizuka, T., Tatsumi, H. and Tanabe, K. *Aust. J. Chem. 35* (1982) 919.
4. Borggaard, O. K. *J. Soil Sci. 30* (1979) 727.
5. Borggaard, O. K. *J. Soil Sci. 32* (1981) 427.
6. Borggaard, O. K. *J. Soil Sci. 27* (1976) 478.
7. Borggaard, O. K. *Clay Miner. 17* (1982) 365.
8. Rubio, J. and Matijević, E. *J. Colloid Interface Sci. 68* (1979) 408.
9. Ellis, J., Giovanoli, R. and Stumm, W. *Chimia 30* (1976) 194.

10. Pyman, M. A. F., Bowden, J. W. and Posner, A. M. *Aust. J. Soil Res. 17* (1979) 191.
11. Quirk, J. P. *Soil Sci. 80* (1955) 423.
12. Kauffman, K. and Hazel, F. *J. Inorg. Nucl. Chem. 37* (1975) 1139.
13. Parfitt, R. L., Farmer, V. C. and Russell, J. D. *J. Soil Sci. 28* (1977) 29.
14. Howe, A. T. and Gallagher, K. J. *J. Chem. Soc. Faraday Trans. 1* (1975) 22.
15. Paterson, E. and Tait, J. M. *Clay Miner. 12* (1977) 345.
16. Childs, C. W., Goodman, B. A., Paterson, E. and Woodhams, F. W. D. *Aust. J. Chem. 33* (1980) 15.

Received November 19, 1982.

Acta Chemica Scandinavica A 37 (1983) 173–177

Determination of Solubility Curves by the Schlieren Method. Computer Control of Growth and Dissolution

J. DANIELSEN

Department of Inorganic Chemistry, Aarhus University, DK-8000 Aarhus C, Denmark

A system for computer control of growth and dissolution processes is described. The main components of the system are: An He–Ne laser as light source, a tv camera as monitor, a microprocessor as controller of temperature and concentration, and a medium size computer which controls the state of growth or dissolution on time sharing basis. By application of the schlieren technique the system has been used to determine solubility curves for K_2SO_4, $KBrO_3$, and $KAl(SO_4)_2.12H_2O$.

Application of a digital computer makes it possible to survey and to control growth and dissolution processes dynamically. The control signal can be produced by a TV camera if the solution is transparent. Quantitative measures can then be obtained for the size and for the convexity of the boundary of a crystal. Determination of solubility curves [1] using the schlieren technique can be made automatically and in a detailed way. This is illustrated by three examples in the present paper. Work on the experimental determination of the concentration variation near the surface of a growing crystal, using the schlieren technique, is in progress.

SCHLIEREN APPARATUS

The schlieren method [2] has been applied in studies of solid phase – solution processes.[3] A general comparison of schlieren technique with interferometric techniques is given by Brown,[4] and a review of the schlieren method by Shardin.[5]

The photo, Fig. 1, shows the construction used in the present work. All parts are mounted on an optical bench of length 1.5 m. The arrangement is classical, however, the following two remarks may be worth mentioning. Two vertical knife edges, Fig. 1 F, are applied, one after the other, to generate in principle symmetrical schlieren effects. This allows elimination of a possible optical skewness by the later data treatment.

The sample container, Fig. 1 D, is made of stainless steel plate and is formed as a thermostated cylindrical mantle of volume 1400 cm.[3] The sample is made of glass filter (mesh 10–20 μm) cut as an orthogonal prism with dimensions $2\times4\times4$ mm^3 and filled with the solid under investigation.

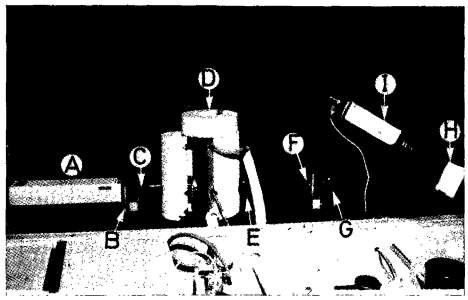

Fig. 1. Schlieren apparatus. A: He–Ne laser, output 0.5 mW, wavelength 632.8 nm (Spectra Physics, 155). B: Shutter, activated by a suction magnet. C: Beam expander (Melles Griot LBX 005). D: Sample container. E,G: Biconvex lenses, f=250 mm, diameter=75 mm (Melles Griot LDX 229). F: Knife edges, shifted vertically by a suction magnet. H: Screen of white, matt paper. I: TV camera (ITC IKEGAMI, model CTC-4500 M).

0302-4377/83 $2.50

TEMPERATURE CONTROL

A pump supplies the mantle of the sample container with water from a thermostat bath. The temperature of the bath is PID-controlled by a microprocessor, MC6800,[6] coupled to a transducer (Analog Devices 590 series) and a modified commercial thermostat (Heto 02 T 923). The microprocessor also monitors the temperature in the container. Calibration of the measured temperature is performed in ice water/(0.000 °C) and in $Na_2SO_4/Na_2SO_4.10H_2O$ (32.384 °C). The measured values are assumed to depend linearly on the temperature in the range 0–64 °C. 12 hours tests show that for constant setpoint the variance of the temperature measured in the container is less than 9×10^{-6} °C.[2]

PICTURE ANALYSIS

384 condensators (3×SAM 64) convert the video signal from the TV camera 1 line at a time. The grey tone of each point is digitized to values between 0 and 16. Each point represents an area of 0.003 mm^2 at the sample position. The picture is analyzed by a medium size computer, RC4000.[7]

Using the schlieren method, the maximum light intensity near the vertical sides of the picture of the sample is measured to decide whether the sample is growing, dissolving or in equilibrium with the solution. As discriminator is chosen:

$$I_d = I_r^1 - I_l^1 - (I_r^2 - I_l^2) \quad (1)$$

where the superscripts refer to the intensities obtained with each of the two knife edges in position, and the subscripts refer to the intensities at the right and left boundary of the sample.

The sign of I_d indicates whether the sample is growing or dissolving. The magnitude of I_d measures approximately the deviation from equilibrium.

12 hours tests show that for a steel rod in air, the average value of I_d is 0.0 grey tone and the sample variance is 0.01 (grey tone).[2] A deviation of more than ±0.2 grey tone is thus considered significant. For a solid sample of $KBrO_3$ in equilibrium with saturated solution either a temperature change of the solution of 0.01 °C or a relative change in concentration of the solution of 0.5 % is sufficient to produce a significant change in I_d.

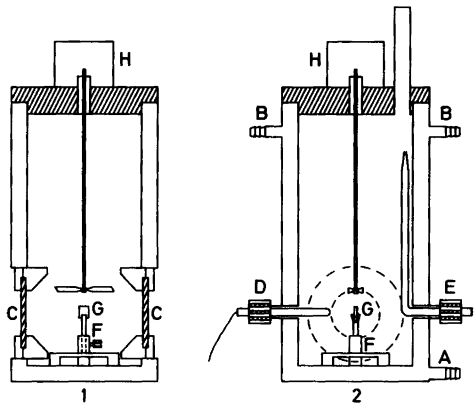

Fig. 2. Vertical sections of the sample container parallel (1) and perpendicular (2) to the optic axis. A, inlet; B, outlet for thermostat water; C, optic glass windows, 3 mm thick; D, temperature probe; E, inlet for solvent; F, sample holder; G, sample; H, step motor.

DETERMINATION OF SOLUBILITY CURVES

The solid sample, and a solution saturated at the temperature in the range 25–50 °C where the solubility is highest, are placed in the sample container. The temperature is adjusted until I_d is 0. The MC6800 is instructed to keep a specified temperature gradient, and the RC4000 takes over the solubility determination. With specified time intervals a set of pictures is taken and analyzed, and I_d is calculated. If I_d indicates that the sample is growing, RC4000 instructs MC6800 to add a volume of solvent proportional to the magnitude of I_d. The values of the temperature, the volume of water added, and I_d are recorded by the computer. After the next time interval the procedure is repeated. In this way the actual concentration oscillates around the decreasing equilibrium concentration until the final wanted temperature is reached. A chemical analysis of the saturated solution at the beginning of the experiment combined with the results recorded by the computer makes it possible to calculate the equilibrium concentration as a function of temperature on an absolute scale.

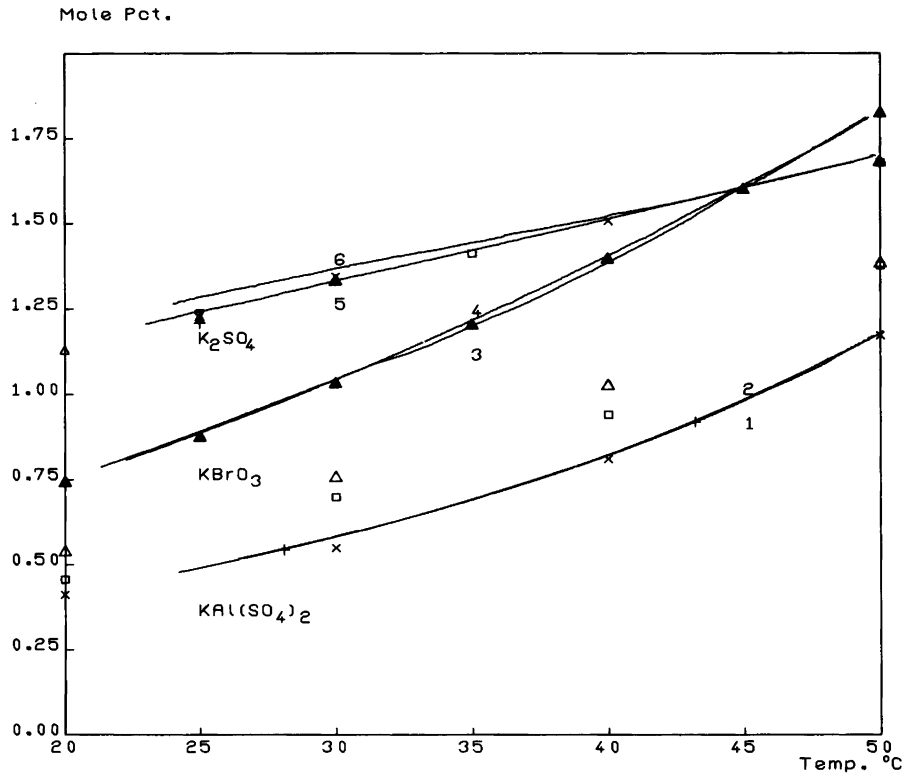

Fig. 3. Experimental solubility curves for K_2SO_4, $KBrO_3$ and $KAl(SO_4)_2 \cdot 12H_2O$. The mol percent in the solution is for water free salt. Values from the literature: $KAl(SO_4)_2 \cdot 12H_2O$: + × □ △.[8] $KBrO_3$: ▲.[9] K_2SO_4: + × □ ▲ △ ▽.[10]

The method was tested using three salts, K_2SO_4, $KBrO_3$, and $KAl(SO_4)_2 \cdot 12H_2O$. Fig. 3 shows the experimental results. The ordinate is given in mol % (=mol fraction × 100) of water free salt. Each curve is composed of more than 1000 points and represents running times of approximately 48 h. In all cases, the temperature gradient was –0.01 °C/min. Comparisons of the final concentration on each curve with the concentration obtained from a chemical analysis at the end of experiment show relative deviations between 0.2 and 1.3 %. These are probably due to an inherent weakness in the method: The many (up to 700) small additions of solvent with the risk of accumulating errors.

The curves were fitted by the eigenvalue method to functions of the type

$$x = A \exp [B/(RT)] \qquad (2)$$

where T is the Kelvin temperature in the container and R is the gas constant. Table 1 gives the values of A and B together with root mean square deviations of T and x. All experimental points on the curves were used despite that they all must deviate a little from the equilibrium values because of the oscillatory character of the method.

A calculation where T was replaced by $T+k_d \times I_d$, and k_d varied between 0.0 and 0.2 did not change neither the A or the B values nor the root mean square deviations significantly.

A calculation where x was replaced by

$$x+(c_2x^2+c_1x+c_o) \qquad (3)$$

and c_i found by the least squares method did not change the A and B values but diminished the root mean square deviations significantly in

Table 1. Values of A and B with root mean square deviations for the expression $x=A \exp(B/(RT))$. T is the Kelvin temperature.

$$rms_T = \left(\sum_{i=1}^{n} (T_{obs}-T_{calc})^2/n \right)^{1/2} \qquad rms_x = \left(\sum_{i=1}^{n} (x_{obs}-x_{calc})^2/n \right)^{1/2}$$

$$T_{calc}=B/\{R/[\ln(x_{obs})-\ln(A)]\} \qquad x_{calc}=A \exp[B/(RT_{obs})]$$

Compound	Curve	A	B(kJ/mol)	rms_T(°C)	rms_x (x 10^5)
$KAl(SO_4)_2$	1	444	-28.3	0.22	6.4
$KAl(SO_4)_2$	2	356	-27.8	0.27	7.9
$KBrO_3$	3	102	-23.2	0.14	4.9
$KBrO_3$	4	116	-23.5	0.17	7.1
K_2SO_4	5	0.742	-10.1	0.12	2.2
K_2SO_4	6	0.445	-8.8	0.19	3.2

Table 2. Values of c_2, c_1 and c_o with root mean square deviations corresponding to rms_T and rms_x of Table 1.

Compound	Curve	c_2	c_1 (x 10^2)	c_o (x 10^3)	rms_T (°C)	rms_x (x 10^5)
$KAl(SO_4)_2$	1	-18.84	30.08	-1.135	0.04	1.0
$KAl(SO_4)_2$	2	-19.24	29.08	-1.016	0.02	0.7
$KBrO_3$	3	-2.52	6.279	-0.3697	0.14	4.6
$KBrO_3$	4	8.789	-22.04	1.308	0.04	1.7
K_2SO_4	5	11.91	-34.14	2.423	0.05	0.8
K_2SO_4	6	-4.554	13.04	-0.9786	0.19	3.1

several cases. The results are given in Table 2. The use of a second degree polynomial is purely empirical. Its physical meaning is not obvious. It may be an expression for experimental error.

The B values are related to the heats of solution, but as the solutions are far from ideal, the exact relationship is difficult to evaluate. Values of x calculated from (2) and with A and B from Table 1 were compared with values of x calculated from the expression [13]

$$\log x = Q1 + Q2/T + Q3 \times \log T \qquad (4)$$

with $Q1$, $Q2$, and $Q3$ as given in the reference. The relative deviations for a given T in the range 298 to 323 K were in all cases less than 4.5 % and in most cases less than 2 %.

In the experiments on $KAl(SO_4)_2 \cdot 12H_2O$ (curves 1 and 2), the chemical analysis was made on sulfate.[11] Among the three salts the method worked best for $KAl(SO_4)_2 \cdot 12H_2O$ which is illustrated by the similarity of the two curves and of the corresponding c_i values.

In the experiments on $KBrO_3$ (curves 3 and 4), the chemical analysis was made on bromate.[12] The two curves deviate significantly from each other. The reason may be that $KBrO_3$ has a very limited metastable region of supersaturation, so that during one of the experiments some $KBrO_3$ has precipitated in the container for a while. At the end of the experiment corresponding to curve 3 a small crystal was observed on the stirrer. The introduction of the second degree polynomial reduces the root mean square deviations very little for curve 3.

In the experiments on K_2SO_4 (curves 5 and 6), the chemical analysis was the same as used for $KAl(SO_4)_2 \cdot 12H_2O$. K_2SO_4 represents the most

difficult of the three cases. Several experiments were done on that salt. The two curves show the two sets of results which deviated most from each other. As for curve 3, the root mean square deviations for curve 6 are not reduced significantly by introduction of a second degree polynomium.

A report with a more detailed description of the schlieren equipment and the control system can be obtained from the author on request.

Acknowledgements. The author wishes to thank Professor S. E. Rasmussen for many helpful and encouraging discussions, and Eng. H. J. Skov for skilled construction of the electronic hardware.

REFERENCES

1. Mýl, J. and Kvapil, J. *Coll. Czech. Chem. Commun. 25* (1960) 194.
2. Töpler, A. *Pogg. Ann. Phys. Chem. 127* (1866) 556
3. Chen, P. S., Shlichta, P. J., Wilcox, W. R. and Lefever, R. A. *J. Cryst. Growth 47* (1979) 43.
4. Brown, E. B. *Modern Optics,* Reinhold, New York 1965.
5. Shardin, H. *VDI Forschungsh. 367,5* (1934).
6. *MC6800 Application Manual,* Motorola Semiconductor Products Inc., Switzerland 1975.
7. Hansen, P. B. *RC4000 Reference Manual,* RCSL 55-D1, A/S Regnecentralen, Copenhagen 1969.
8. *Gmelins Handbuch der Anorganischen Chemie, 8. Aufl., B 35* (1934) 455.
9. Ricci, J. E. *J. Am. Chem. Soc. 56* (1934) 299.
10. *Gmelins Handbuch der Anorganischen Chemie, 8. Aufl., 22* (1938) 721.
11. Furman, N. H. *Scott's Standard Methods of Chemical Analysis,* 6th Ed., Van Nostrand-Reinhold, Princeton 1962, Vol. 1, p. 1008.
12. Blaedel, W. J. and Meloche, V. W. *Elementary Quantitative Analysis, Theory and Practice,* Harper & Row, New York 1963, p. 853.
13. Broul, M., Nývlt, J. and Söhnel, *Solubility in Inorganic Two-component Systems,* Elsevier, Amsterdam 1981.

Received June 24, 1982.

Acta Chemica Scandinavica A 37 (1983) 179–186

Stability of the Nickel(II) Complexes of N^1-Isopropyl-2-methyl-1,2-propanediamine in Aqueous Sodium Perchlorate Solutions and the Crystal Structure of Bis(N^1-isopropyl-2-methyl-1,2-propanediamine)nickel(II) Perchlorate

MARKKU AHLGRÉN and PIRKKO TILUS

Department of Inorganic Chemistry, University of Helsinki, SF-00100 Helsinki 10, Finland

The nickel(II) complex formation of N^1-isopropyl-2-methyl-1,2-propanediamine (=L) has been studied by emf titrations at 25 °C and at total ionic strengths of about 0.04, 0.05, 0.09, 0.5, 1.0 and 2.0. The complex species found were NiL^{2+} and NiL_2^{2+}. The absorption maximum at 450 nm suggested the latter to be a planar yellow complex, which was verified by X-ray crystal structure analysis.

$[Ni(C_7H_{18}N_2)_2](ClO_4)_2$ is monoclinic, space group $P2_1/c$, with a=20.399(12), b=15.026(4), c=16.670(10) Å, β=111.79(4)°, Z=8. Final R=0.061 for 3650 unique reflections. The coordination sphere of the two independent nickel(II) ions is distorted square-planar with Ni–N distances of 1.900(7)–1.959(7) Å. Complex cations and perchlorate ions form through hydrogen bonding two nonequivalent chains parallel to the b axis.

The nickel(II) complex formation of *N*-alkylated ethylenediamines has been widely studied in our laboratory.[1,2] The main species formed were NiX^{2+}, NiX_2^{2+} and NiX_3^{2+}, with X denoting the bidentate neutral diamine ligand. We have also found that *C*-alkyl-substituted ethylenediamines, with increased sodium perchlorate concentration and temperature, favour the formation of square-planar nickel(II) biscomplexes, where only species NiX^{2+} and NiX_2^{2+} appear.[3–6] In this work the tendency of N^1-isopropyl-2-methyl-1,2-propanediamine to form nickel(II) complexes has been studied with the aid of potentiometric titrations and a crystal structure determination of the yellow nickel(II) complex precipitated at a pH of about 8.5.

EXPERIMENTAL

Reagents. N^1-Isopropyl-2-methyl-1,2-propanediamine from Aldrich Chemical Co., Inc. was neutralized with 1 M $HClO_4$. An 0.1 M solution was prepared and was analyzed potentiometrically. The other chemicals, $Ni(ClO_4)_2.6H_2O$, $NaClO_4$ and NaOH, and their analysis were the same as before.[7]

Solution measurements and calculations. Radiometer digital pHM52 and pHM64 potentiometers were used for the emf measurements. An electrode system consisting of a Beckman glass electrode of type E and calomel electrode with J-shape liquid junction was tested using two buffers and by means of E_o-titrations. In ionic strengths 0.04, 0.05 and 0.09 the measured pH values were converted to values of $-\log h$ by means of apparent pf_{H^+} values.[8,9] These two methods proved to be in good agreement with each other.

The equilibrium study involved a series of titrations carried out in aqueous solutions at 25 °C and total ionic strengths about 0.04, 0.05, 0.09, 0.5, 1.0 and 2.0 ($NaClO_4$ as background electrolyte). In the solutions with 0.5 M $NaClO_4$ as background electrolyte, the establishment of equilibria (6–15 min) was followed with a sensitive REC 61 servograph recorder from Radiometer. The spectra of the complexes were recorded with a Perkin-Elmer model 402 spectrophotometer.

0302-4377/83 $2.50

Table 1. Initial concentrations of ligand (L) and metal (M) with ionic strengths (I), $-\log h$ and $\bar{n}$ ranges and titration points used in the final calculations.

I average	$M:L$	L mmol dm^{-3}	M mmol dm^{-3}	$-\log h$ range	$\bar{n}$ range	Number of points
0.040	1:6	14.3	2.4	6.5–8.8	0.1–1.95	67
	1:4	14.3	3.6			
	1:3	14.3	4.8			
	1:2	14.3	7.2			
0.051	1:2	16.6	8.2	6.6–8.1	0.1–1.4	22
0.088	1:4	33.1	8.2	5.3–8.0	0.01–1.8	56
0.533	1:2	5.5	2.7	5.6–8.5	0.02–1.91	121
	1:4	10.9	2.7			
	1:2	10.9	5.5			
	1:4	16.4	4.1			
1.032	1:4	10.0	2.6	6.2–8.1	0.03–1.5	91
	1:3	10.1	3.4			
	1:2	10.1	5.0			
2.030	1:4	17.5	4.4	6.7–7.5	0.1–1.0	52
	1:4	8.7	2.2			

The initial concentrations of metal and ligand, M and L, with the ranges of $-\log h$ and apparent $\bar{n}$ values can be seen in Table 1. The calculation procedure was the same as described in Ref. 7. The overall stability constant for the reaction

$$pH^+ + qNi^{2+} + rL = H_pNi_qL_r^{2q+p}$$

is here defined as

$$\beta_{pqr} = [H_pNi_qL_r]h^{-p}m^{-q}l^{-r}$$

where h, m, l denote the free concentrations of proton, metal and ligand, respectively.

The program MINIQUAD 75 [10] was adapted for calculations. The values for the protonation constants β_{101} and β_{201} were obtained from the results in Ref. 11.

Crystal preparation and data collection. The reddish-yellow crystals used for structure determination were obtained by slow evaporation of ethanol solution containing nickel(II) perchlorate and N^1-isopropyl-2-methyl-1,2-propanediamine in molar ratio 1:2. Weissenberg photographs showed the crystals to be identical with the poor quality ones separated from titrated solutions.

Lattice parameters were obtained from least-squares refinement of 23 well-centered reflections measured on a Syntex $P2_1$ diffractometer using graphite monochromatized Mo$K\alpha$ radiation (λ=0.71069 Å). Crystal data: a=20.399(12), b=15.026(4), c=16.670(10) Å, β=111.79(4)°, V=4744(4) Å^3, Z=8, space group $P2_1/c$, D_m=1.45(1), D_c=1.45 g cm^{-3}, μ(Mo$K\alpha$)=10.9 cm^{-1}, F(000)=2192, crystal dimensions 0.30×0.35×0.50 mm.

Intensity data were collected ($5<2\theta<45°$) at room temperature using the ω-scan technique and a scan rate varying from 2.5 to 30.0° min^{-1} depending upon the peak intensity. The intensity of one check reflection, recorded after every 99 measurements, remained essentially constant throughout the data collection. Out of 6197 independent reflections measured, 3650 had $I>3\sigma(I)$ and were used in the structure determination. The data were corrected for Lorentz and polarization factors.

Structure determination and refinement. The structure was solved by a combination of direct and Fourier methods using programs MULTAN 78 [12] and XRAY 76.[13] The function minimized in least-squares refinement was $\Sigma w(|F_o|-|F_c|)^2$ with $w=1/\sigma^2(F_o)$. Scattering factors for the non-hydrogen atoms were from Cromer and Mann [14] and for H atoms from Stewart, Davidson and Simpson.[15] Anomalous dispersion corrections were included for Ni and Cl.[16] Isotropic refinement of the model led to an R value of 0.108 ($R=\Sigma||F_o|-|F_c||/\Sigma|F_o|$). Refinement with anisotropic temperature factors for non-hydrogen atoms and fixed isotropic ones for geometrically positioned H atoms (U_{iso}=0.07 Å^2 and X–H=1.0 Å) gave the R value 0.061. The average shift/error ratio in the last cycle was 0.04. The largest peak on the final difference map had a density of 0.65 eÅ^{-3} near by O24 (B).

It is apparent that perchlorate groups are undergoing considerable thermal motion and

Table 2. Fractional atomic coordinates ($\times 10^4$) and the equivalent isotropic temperature factors[a] with e.s.d.'s in parentheses.

	x	y	z	B_{eq}(Å^2)		x	y	z	B_{eq}(Å^2)
Unit *A*					Unit *B*				
Ni (A)	4320(1)	1796(1)	2317(1)	3.29(5)	Ni (B)	9276(1)	2482(1)	2070(1)	3.49(5)
N11	3364(3)	2200(4)	1637(4)	4.2(3)	N11	8319(3)	2263(4)	2036(4)	5.0(4)
N12	3975(3)	1570(4)	3219(4)	4.2(3)	N12	8941(3)	1992(5)	938(4)	5.2(4)
C11	2910(4)	2062(6)	2147(5)	4.5(4)	C11	7876(4)	1907(6)	1187(5)	5.3(4)
C12	3207(4)	1328(5)	2788(5)	3.7(4)	C12	8350(4)	1373(5)	820(5)	4.2(4)
C13	3155(4)	415(6)	2340(5)	5.3(5)	C13	8634(4)	541(6)	1332(6)	6.1(5)
C14	2858(4)	1261(6)	3444(5)	5.4(5)	C14	7934(5)	1157(6)	−118(6)	6.7(6)
C15	3310(4)	3127(6)	1255(5)	4.3(4)	C15	7982(4)	3082(6)	2245(6)	5.3(5)
C16	3614(5)	3818(6)	1918(7)	7.6(6)	C16	7990(5)	3866(7)	1723(7)	7.0(6)
C17	2581(5)	3340(6)	673(6)	6.7(5)	C17	7274(5)	2863(7)	2287(6)	7.3(6)
N21	5275(3)	1398(4)	2978(3)	3.6(3)	N21	10226(3)	2685(4)	2124(4)	4.5(4)
N22	4609(3)	1831(4)	1350(4)	3.8(3)	N22	9634(4)	2802(4)	3266(4)	5.4(4)
C21	5686(4)	1395(6)	2401(5)	4.7(4)	C21	10680(4)	2984(5)	2993(5)	4.6(4)
C22	5198(4)	1203(5)	1486(4)	3.8(4)	C22	10402(4)	2598(6)	3670(5)	4.2(4)
C23	4915(4)	257(6)	1371(5)	5.6(5)	C23	10502(4)	1613(6)	3782(6)	5.9(5)
C24	5557(4)	1394(6)	842(5)	5.1(4)	C24	10758(5)	3096(6)	4516(5)	5.9(5)
C25	5653(4)	1863(7)	3824(5)	4.8(5)	C25	10292(4)	3278(6)	1440(5)	4.9(5)
C26	5658(5)	2856(7)	3708(6)	6.6(6)	C26	9973(5)	4186(6)	1431(6)	6.1(5)
C27	6371(4)	1488(8)	4292(5)	7.1(6)	C27	11057(4)	3350(6)	1514(5)	5.6(5)
Cl1	3143(1)	3913(2)	4233(2)	5.2(1)	Cl1	8439(2)	1056(2)	4144(2)	6.1(2)
O11	3730(3)	3391(6)	4268(5)	10.1(5)	O11	8917(6)	1746(8)	4277(7)	16.3(8)
O12	3124(4)	3922(6)	5042(4)	12.1(6)	O12	8031(8)	942(7)	3324(5)	19.9(9)
O13	3226(4)	4797(5)	4037(6)	12.3(6)	O13	8721(7)	264(7)	4572(7)	18.1(9)
O14	2527(3)	3597(5)	3623(5)	10.1(4)	O14	8103(5)	1406(9)	4626(8)	16.9(9)
Cl2	4783(1)	−920(1)	4000(1)	4.7(1)	Cl2	9269(1)	5437(2)	3550(2)	5.1(1)
O21	4183(4)	−814(6)	4227(5)	11.4(6)	O21	9831(3)	5905(5)	4153(4)	8.0(4)
O22	4998(5)	−89(5)	3883(5)	11.7(6)	O22	8925(5)	6010(6)	2871(7)	15.1(7)
O23	4579(4)	−1413(5)	3241(4)	8.7(5)	O23	9539(5)	4768(6)	3215(7)	15.3(7)
O24	5319(3)	−1377(4)	4675(4)	6.5(4)	O24	8825(5)	5113(9)	3871(6)	18.3(8)

[a] $B_{eq}=8/3\ \pi^2\Sigma_i\Sigma_j U_{ij}a_i^*a_j^*a_i\cdot a_j$.

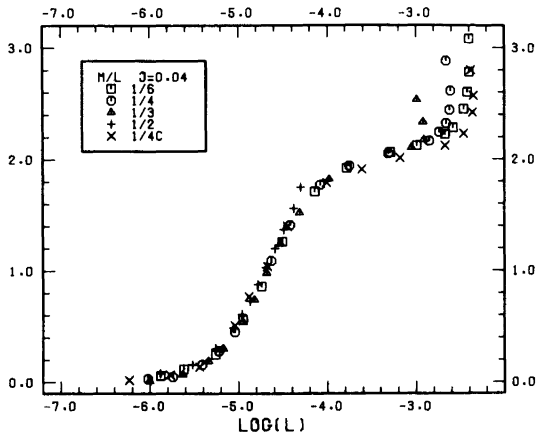

Fig. 1. Experimental data for Ni(II) plotted as curves $\bar{n}(\log l)$. The points $\bar{n}>2$ are probably affected by precipitation as in higher ionic strengths.

may indeed be disordered. Examination of Fourier maps throughout the course of the analysis did not reveal any meaningful disorder model, however. The best description of these atoms appears to be that of roughly tetrahedral groups undergoing considerable libration.

The atomic coordinates and isotropic temperature factors with standard deviations are given in Table 2. Lists of structure factors and anisotropic thermal parameters are obtainable on request from the authors.

RESULTS AND DISCUSSION

Fig. 1 illustrates the Bjerrum plot and Table 3 shows the log β values obtained with statistical observations at the ionic strength of 0.04. In the higher ionic strengths, precipitation began when the pH reached the value of about 8.5. Final results for all systems are therefore evaluated with $\bar{n} < 2$ and only NiL^{2+} and NiL_2^{2+} are included.

The formation curves are steep (Fig. 1), compared with the ethylenediamine nickel(II) system, for example, and it is difficult to determine the stability constant of NiL^{2+} with the same level of reproducibility and accuracy as for most diamines. Fig. 2 shows the distribution curves of the species calculated on the basis of the log β values in Table 4.

The nickel(II) complex formation of N^1-cyclohexyl-2-methyl-1,2-propanediamine described by Tomlinson *et al.*[17] seems to be very similar to that of N^1-isopropyl-2-methyl-1,2-propanediamine. The authors report values log β_{011} = 4.5 and log β_{012} = 9.8 or log β_{011} ~0, log β_{012} = 9.6 and log β_{013} = 13.5 at 20 °C and 0.1 M KCl. The negative log K_D values (Table 4) for the disproportion reaction

Table 3. The calculated log β_{pqr} values in the ionic strength 0.04 and at 25 °C, when different $\bar{n}$ ranges have been used.

Number of points	$\bar{n}$ range	$-\log h$ range	β_{011}	β_{012}	χ^2	R
105	0.01–1.95	5.2–8.8	4.51(1)	9.354(5)	67	0.0021
67	0.1 –1.95	6.5–8.8	4.52(1)	9.351(4)	11	0.0022

Table 4. Overall (β_{pqr}), stepwise (k_n) and disproportion (K_D) constants for Ni(II) complexes of N^1-isopropyl-2-methyl-1,2-propanediamine at 25 °C.

I	log β_{011}	log β_{012}	log k_2	log K_D
0.040	4.52(1)	9.351(4)	4.83(1)	–0.30(2)
0.051	4.61(1)	9.428(4)	4.82(1)	–0.21(2)
0.088	4.55(1)	9.419(5)	4.87(2)	–0.32(2)
0.533	4.67(1)	9.828(5)	5.16(2)	–0.49(3)
1.034	5.13(1)	10.367(5)	5.24(2)	–0.11(3)
2.030	5.53(2)	11.23(1)	5.70(3)	–0.17(5)

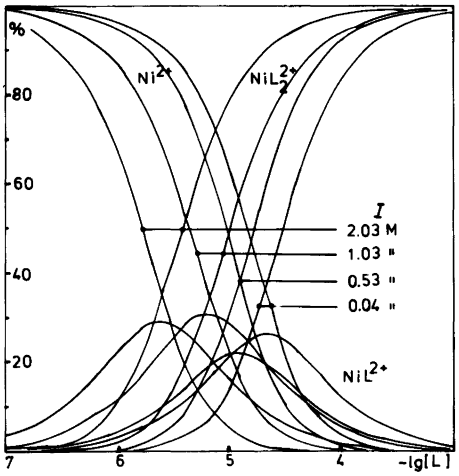

Fig. 2. The percentage distribution of various nickel(II) species as function of –log l at 25 °C.

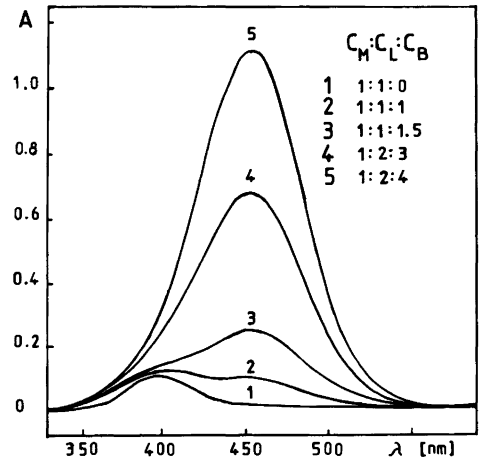

Fig. 3. Absorption spectra of Ni(II) complexes of N^1-isopropyl-2-methyl-1,2-propanediamine in different conditions at I=0.14.

$$2\ NiL^{2+} \rightleftharpoons Ni^{2+} + NiL_2^{2+}$$

of N^1-isopropyl-2-methyl-1,2-propanediamine suggest a change in the coordination geometry when NiL_2^{2+} is formed and more favoured formation of NiL_2^{2+} than NiL^{2+}, as found also for some *C*-alkyl substituted ethylenediamines.-[3-6] The spectrochemical studies support these conclusions. The absorption maximum at 450 nm, which is typical for square–planar nickel(II) complexes, becomes with base addition predominant over the octahedral maximum at 400 nm even in solutions where total metal and ligand concentrations are equal (Fig. 3).

The stabilities of Ni(II) complexes of N^1-isopropyl-2-methyl-1,2-propanediamine increases with increasing ionic strength more than those of octahedral Ni(II) diamine complexes. When ionic strength increases from 0.04 to 2.03 the changes in log β_{011} and log β_{012} are 1.0 and 1.9 log units for the studied complexes and 0.6 and 1.2 log units for the ethylenediamine Ni(II) complexes, respectively.[18]

The yellow nickel(II) compound precipitated from titrated solutions is composed of $[NiL_2]^{2+}$ complex cations and perchlorate ions loosely held together by hydrogen bonds and electrostatic forces (Fig. 4). The two crystallographically independent complexes exhibit a square–planar coordination geometry as shown in Fig. 5. Table 5 lists the bond lengths and angles characteristic of these species, while Table 6 summarizes the intermolecular distances below 3.4 Å.

The two nickel(II) complexes that form a part of the asymmetric unit are essentially the same. The four Ni–N distances of 1.900(7)–1.959(7) Å (av. 1.927 Å) in each complex are comparable to

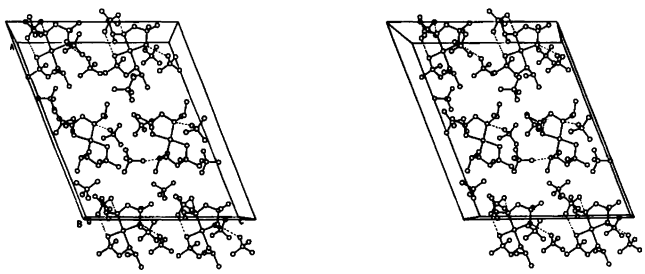

Fig. 4. A stereoview of the packing. Intermolecular distances below 3.1 Å are shown by dotted lines.

Table 5. Interatomic distances (Å) and angles (°) with estimated standard deviations in parentheses.

Unit	*A*	*B*		*A*	*B*		*A*	*B*
Ni–N11	1.952(5)	1.959(7)	N11–Ni–N12	86.1(3)	85.4(3)	N21–Ni–N22	85.9(2)	85.6(3)
Ni–N12	1.911(7)	1.900(7)	N11–Ni–N22	93.3(3)	93.6(3)	N21–Ni–N12	94.7(3)	95.3(3)
Ni–N21	1.943(5)	1.930(7)	N11–Ni–N21	179.1(3)	178.8(3)	N22–Ni–N12	170.6(3)	171.7(3)
Ni–N22	1.912(7)	1.912(7)						
C15–C17	1.479(10)	1.508(14)	C17–C15–C16	112.3(8)	115.1(7)	C27–C25–C26	112.9(8)	111.2(7)
C25–C27	1.491(11)	1.524(12)	C17–C15–N11	111.8(7)	111.0(7)	C27–C25–N21	112.2(8)	111.1(6)
C15–C16	1.475(12)	1.469(14)	C16–C15–N11	112.7(6)	114.2(9)	C26–C25–N21	111.4(6)	112.8(8)
C25–C26	1.506(14)	1.508(13)	C15–N11–C11	113.9(6)	110.4(6)	C25–N21–C21	112.9(6)	111.6(6)
C15–N11	1.519(10)	1.513(12)	C15–N11–Ni	115.5(4)	113.0(5)	C25–N21–Ni	116.5(5)	115.6(4)
C25–N21	1.504(9)	1.493(12)	C11–N11–Ni	108.9(4)	109.8(6)	C21–N21–Ni	108.7(4)	110.4(6)
N11–C11	1.487(12)	1.469(9)	N11–C11–C12	109.7(6)	108.6(6)	N21–C21–C22	109.5(6)	109.6(6)
N21–C21	1.492(11)	1.471(9)	C11–C12–C13	111.8(6)	111.9(8)	C21–C22–C23	112.6(6)	112.9(8)
C11–C12	1.498(11)	1.545(13)	C11–C12–C14	113.0(7)	109.2(6)	C21–C22–C24	111.3(6)	108.2(7)
C21–C22	1.509(9)	1.551(13)	C11–C12–N12	103.6(6)	102.7(6)	C21–C22–N22	103.1(6)	101.6(6)
C12–C13	1.546(12)	1.504(12)	C13–C12–C14	108.9(7)	111.0(7)	C23–C22–C24	110.1(7)	112.0(6)
C22–C23	1.519(12)	1.496(12)	C13–C12–N12	108.5(6)	108.9(6)	C23–C22–N22	109.3(6)	109.4(6)
C12–C14	1.513(14)	1.512(12)	C14–C12–N12	110.9(6)	112.9(8)	C24–C22–N22	110.2(6)	112.3(7)
C22–C24	1.536(13)	1.522(11)	C12–N12–Ni	106.8(4)	110.6(6)	C22–N22–Ni	110.0(4)	110.6(6)
C12–N12	1.507(9)	1.477(11)						
C22–N22	1.476(10)	1.488(10)						
Cl1–O11	1.415(8)	1.383(12)	O11–Cl1–O12	107.4(5)	113.5(7)	O21–Cl2–O22	106.8(6)	107.8(5)
Cl1–O12	1.363(9)	1.321(8)	O11–Cl1–O13	111.3(5)	115.1(7)	O21–Cl2–O23	107.9(5)	108.5(5)
Cl1–O13	1.392(9)	1.397(11)	O11–Cl1–O14	111.5(5)	95.5(8)	O21–Cl2–O24	109.2(4)	113.6(6)
Cl1–O14	1.376(6)	1.344(14)	O12–Cl1–O13	105.9(6)	113.6(6)	O22–Cl2–O23	111.3(5)	106.4(7)
Cl2–O21	1.418(9)	1.401(6)	O12–Cl1–O14	112.4(5)	113.8(8)	O22–Cl2–O24	111.3(4)	110.3(7)
Cl2–O22	1.361(8)	1.387(10)	O13–Cl1–O14	108.2(5)	103.5(8)	O23–Cl2–O24	110.2(4)	109.9(8)
Cl2–O23	1.389(7)	1.361(11)						
Cl2–O24	1.421(6)	1.305(13)						

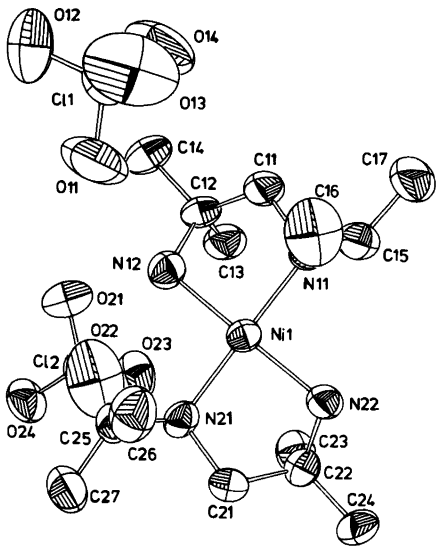

Fig. 5. A view of the *A* unit.

those found in square–planar nickel(II) complexes but considerably shorter than the Cu–N bond lengths of 1.973(4)–2.039(3) Å (av. 2.005 Å) in bis(N^1-isopropyl-2-methyl-1,2-propanediamine)copper(II) malonate,[19] which is the only known square–planar copper(II) biscomplex of N^1-isopropyl-2-methyl-1,2-propanediamine. This difference in the metal–nitrogen bond lengths is equal to the difference in the ionic radii of Ni^{II} and Cu^{II} in square–planar complexes and a direct consequence of the removal of the unpaired electron from the $d_{x^2-y^2}$ orbital of the d^9 configuration of Cu^{II} on going to the low-spin d^8 nickel(II) complexes. The Ni–N(secondary) bonds are somewhat longer (~0.04 Å) than the Ni–N(primary) bonds, as is common for copper(II) complexes.[20,21]

At both nickel(II) centres the coordination plane has a slight tetrahedral distortion and the metal ions are situated 0.08 Å from the coordination plane on the side of the isopropyl substituents. The *N*-isopropyl and *C*-methyl substituents together prevent the formation of 5- or 6-coordinated complexes. The diamine chelate rings are in *gauche* conformation. In each chelate the dimethyl-substituted C atom (C12 or C22) is located *ca.* 0.65 Å below the N–Ni–N plane, while the other ring C atom (C11 or C21) lies *ca.* 0.05 Å above the same plane. A similar asymmetric chelate ring is found in *L*-lactatobis(N^1-isopropyl-2-methyl-1,2-propanediamine)copper(II) and zinc(II) complexes[22,23] where in each case, however, one of the two chelate rings is much less asymmetric. Evidently the different intramolecular interactions and hydrogen bonding involving the amine nitrogen atoms cause this difference.

The perchlorate ions give evidence that their O atoms are undergoing marked thermal motion or have static disorder. It is clear from difference Fourier maps, however, that the observed disorder does not necessarily require the use of a number of fractionally weighted models for anions. Consequently, the calculated Cl–O bond lengths of 1.31(1)–1.42(1) Å, with an average of 1.38 Å, are shorter than normal.

The perchlorate ions are situated at hydrogen bond distances from complex cations (Table 6).

Table 6. Intermolecular contacts <3.4 Å.[a]

N11(A)···O12(A)^{ii}	3.030(10)	N11(B)···O12(B)	3.135(13)
N12(A)···O11(A)	3.384(11)	N12(B)···O11(B)^{ii}	3.342(14)
N12(A)···O22(A)	3.174(10)	N12(B)···O21(B)^{iii}	3.042(10)
N12(A)···O24(A)^{i}	3.277(8)	N12(B)···O14(B)^{ii}	3.276(13)
N21(A)···O22(A)	2.867(10)	N21(B)···O22(B)^{iii}	3.054(12)
N22(A)···O24(A)^{iv}	3.222(9)	N21(B)···O21(B)^{iii}	3.394(10)
N22(A)···O23(A)^{iv}	3.055(9)	N22(B)···O23(B)	2.960(11)
N22(A)···O11(A)^{ii}	3.279(9)	N22(B)···O11(B)	3.055(15)
N22(A)···O12(A)^{ii}	3.211(9)	O21(A)···O22(A)^{i}	3.263(10)
C25(A)···O22(A)	3.240(12)	C27(A)···O14(B)	3.367(14)
C26(A)···O23(A)^{iv}	3.290(12)	C24(B)···O21(B)^{v}	3.254(13)
C27(A)···O21(A)^{i}	3.237(13)	C26(B)···O13(B)^{ii}	3.307(13)

[a] Symmetry operations: i=1–*x*, –*y*, 1–*z*; ii=*x*, *1/2–y*, *z*–1/2; iii=2–*x*, *y*–1/2, 1/2–*z*; iv=1–*x*, *y*+1/2, 1/2–*z*; v=2–*x*, 1–*y*, 1–*z*.

The perchlorate ions Cl2(A) and Cl2(B) connect the complex cations *A* and *B*, respectively, into chains parallel to the *b* axis. The other perchlorate ions, Cl1(A) and Cl1(B), have a space-filling role, connecting chains weakly together in the direction of the *c* axis. The intermolecular distances between so built *A* and *B* layers are greater than 3.36 Å.

REFERENCES

1. Näsänen, R., Tilus, P. and Uro, T. *Suom. Kemistil. B 41* (1968) 314
2. Orama, M., Tilus, P., Lindell, E., Hakola, L. and Adler, L. *Finn. Chem. Lett.* (1975) 35.
3. Basolo, F., Chen, Y. T. and Murmann, R. K. *J. Am. Chem. Soc. 76* (1954) 956.
4. Sone, K. and Kato, M. *Z. Anorg. Allgem. Chem. 301* (1959) 277.
5. Leussing, D. L., Harris, J. and Wood, P. *J. Phys. Chem. 66* (1962) 1544.
6. Powell, H. K. J. and Curtis, N. F. *Aust. J. Chem. 26* (1973) 977.
7. Tilus, P. *Finn. Chem. Lett.* (1979) 76.
8. Näsänen, R., Koskinen, M., Tilus, P., Lindell, E., Lihavainen, J. and Pinomäki, M. *Suom. Kemistil. B 46* (1973) 61.
9. Saarinen, H., Orama, M. and Korvenranta, J. *Finn. Chem. Lett.* (1978) 74.
10. Gans, P., Vacca, A. and Sabatini, A. *Inorg. Chim. Acta 18* (1976) 237.
11. Näsänen, R., Tilus, P. and Eskolin, E. *Suom. Kemistil. B 45* (1972) 87.
12. Main, P., Hull, S. E., Lessinger, L., Germain, G., Declercq, J. P. and Woolfson, M. M. *MULTAN 78, A System of Computer Programs for the Automatic Solution of Crystal Structures from X-Ray Diffraction Data,* Universities of York, England and Louvain, Belgium 1978.
13. Stewart, J. M. *The X-RAY 76 SYSTEM,* Technichal Report TR-446, Computer Science Center, Univ. of Maryland, College Park 1976.
14. Cromer, D. T. and Mann, J. B. *Acta Crystallogr. A 24* (1968) 321.
15. Stewart, R. F., Davidson, E. R. and Simpson, W. T. *J. Chem. Phys. 42* (1965) 3171.
16. *International Tables for X-Ray Crystallography,* Kynoch Press, Birmingham 1974, Vol. 4.
17. Tomlinson, M. L., Sharp, M. L. R. and Irving, H. M. N. H. *J. Chem. Soc.* (1965) 603.
18. Näsänen, R., Koskinen, M. and Kajander, K. *Suom. Kemistil. B 38* (1965) 103.
19. Kansikas, J. *Private communication.*
20. Pajunen, A. and Näsäkkälä, E. *Finn. Chem. Lett.* (1977) 104.
21. Hämäläinen, R., Turpeinen, U. and Ahlgrén, M. *Acta Crystallogr. B 35* (1979) 2408.
22. Ahlgrén, M. and Hämäläinen, R. *Finn. Chem. Lett.* (1975) 211.
23. Ahlgrén, M., Turpeinen, U. and Hämäläinen, R. *Acta Chem. Scand. A. 36* (1982) 841.

Received June 18, 1982.

Acta Chemica Scandinavica A 37 (1983) 187–191

Thermodynamics of Swelling and Partition Equilibria in Gels

HANS VINK

Institute of Physical Chemistry, University of Uppsala, P.O. Box 532, S-751 21 Uppsala, Sweden

The thermodynamics of swelling and partition equilibria in gels is considered. The treatment is based on the integration of the Gibbs-Duhem equation for the gel system and relates the change of the chemical potential of the gel network to the partition coefficient of the solute and to pressure changes in the gel. Thermodynamic stability conditions for swelling equilibria in gels are also considered.

Gels of crosslinked macromolecules constitute an important class of substances, which have found use in many separation processes like ion exchange, gel permeation chronomatography, various membrane processes *etc.* It is therefore of importance to consider the thermodynamic aspects of the equilibrium properties of gels, in particular sorption and swelling equilibria. Although much work has been devoted to the subject in the past [1–9] many aspects have remained conceptually unclear and there is need for a rigorous thermodynamic treatment. The present work is purely thermodynamic (statistical thermodynamic aspects of the subject have recently been reviewed by Dušek and Prins [10]), and is based on the integration of the Gibbs-Duhem equations for a system consisting of the gel and an ambient solution.

Partition Equilibria. We consider an isothermal gel system consisting of a homogeneous gel phase (unprimed) and an ambient solution phase (primed). In the system three components are present: Gel matrix (1), solvent (2) and solute (3). The thermodynamic behaviour of the system is governed by the Gibbs-Duhem equation, applied to each homogeneous phase. For the gel phase we have

$$m_1 d\mu_1 + m_2 d\mu_2 + m_3 d\mu_3 - V dp = 0 \quad (1)$$

where m_i (i=1, 2, 3) is the mass of a component, μ_i its specific chemical potential, V the volume of the phase and p the pressure.

Dividing by V we obtain

$$c_1 d\mu_1 + c_2 d\mu_2 + c_3 d\mu_3 - dp = 0 \quad (2)$$

where c_i (i=1, 2, 3) is the concentration of a component. Concerning the choice of the composition variables it should be noted that molar concentrations/mol fractions are in general less suited for gel systems as the molecular weight of the matrix component is undefined. Also, it is more appropriate to use the weight concentration than the weight fraction, since the former is directly related to volume changes, and thus the swelling of the gel.

The concentrations in eqn. (2) are related through the equation

$$c_1 v_1 + c_2 v_2 + c_3 v_3 = 1 \quad (3)$$

where the partial specific volumes v_1, v_2 and v_3 are assumed to be constant.

Corresponding equations are valid for the surrounding solution phase. Taking the pressure of this phase (p') as fixed, we have the equations

$$c'_2 d\mu'_2 + c'_3 d\mu'_3 = 0 \quad (4)$$

$$c'_2 v'_2 + c'_3 v'_3 = 1 \quad (5)$$

For the sake of generality, we assume here that v'_2 and v'_3 may differ from v_2 and v_3, respectively.

The equilibrium conditions are

$$\mu_2 = \mu'_2 \quad (6)$$

$$\mu_3 = \mu'_3 \quad (7)$$

0302-4377/83 $2.50

As the chemical potential of solvent in the solution phase can be determined (by vapor pressure determination, osmometry *etc.*) μ'_2 is in principle a known quantity. Thus, with the aid of eqns. (3)–(7) an integration of eqn. (2) is possible.

Choosing the solute concentration as the independent variable we obtain the following expressions for the solvent concentrations: In the solution phase

$$c'_2 = (1-c'_3\nu'_3)/\nu'_2 \tag{8}$$

and in the gel phase

$$c_2 = (1-c_1\nu_1-c_3\nu_3)/\nu_2 \tag{9}$$

Using eqns. (4)–(9) we may write

$$c_2\mathrm{d}\mu_2+c_3\mathrm{d}\mu_3 = c_2\mathrm{d}\mu'_2+c_3\mathrm{d}\mu'_3 = \left(\frac{1-c_1\nu_1-c_3\nu_3}{\nu_2} - \frac{1-c'_3\nu'_3}{\nu'_2}\frac{c_3}{c'_3}\right)\mathrm{d}\mu'_2 \tag{10}$$

We now introduce the partition coefficient determining the solute distribution between the solution and gel phases:

$$c_3 = Kc'_3 = \gamma(1-c_1\nu_1)c'_3 \tag{11}$$

where K is the conventional partition coefficient and γ is the "reduced" partition coefficient corrected for the volume occupied by the gel matrix. Substituting eqn. (11) into eqn. (10) we obtain

$$c_2\mathrm{d}\mu_2+c_3\mathrm{d}\mu_3 = \left[\frac{\nu'_2}{\nu_2}-\gamma+\gamma\varepsilon c'_3\right]\frac{1-c_1\nu_1}{\nu'_2}\mathrm{d}\mu'_2 \tag{12}$$

where

$$\varepsilon = \nu'_3(1-\nu'_2\nu_3/\nu_2\nu'_3) \tag{13}$$

The partition coefficient is an experimentally determinable quantity, which in general depends on the concentration c'_3. Similarly, the volume V of the swelling gel is an experimentally determinable function of c'_3. As

$$c_1 = m_1/V \tag{14}$$

where m_1 is constant, also c_1 is a known function of c'_3. We may express these functions by the series expansions

$$\gamma = \gamma_0(1+\alpha_1c'_3+\ldots) \tag{15}$$

$$V = V_0(1+\beta_1c'_3+\ldots) \tag{16}$$

$$c_1 = c_1^{\circ}/(1+\beta_1c'_3+\ldots) \tag{17}$$

where α_1 and β_1 are experimentally determinable constants.

We also introduce an analytic expression for μ'_2. We may use the usual representation *via* the activity coefficient or, which is more convenient, the virial expansion of the osmotic pressure:

$$\mu'_2 = (\mu_2^{\circ})' - \nu_2'\pi' \tag{18}$$

where

$$\pi' = \frac{RT}{M_3}c'_3+A_2c'^2_3+\ldots \tag{19}$$

represents the osmotic pressure of the ambient solution, measured against pure solvent (M_3 is the molar mass of solute and A_2 the second virial coefficient).

Inserting eqn. (12), together with eqns. (15)–(19), into eqn. (2) and integrating between the limits $c'_3=0$ and $c'_3=c$, we obtain

$$\int_0^c \frac{\mathrm{d}\mu_1}{\mathrm{d}c'_3}\mathrm{d}c'_3 = \int_0^c \left(\frac{\nu'_2}{\nu_2}-\gamma+\gamma\varepsilon c'_3\right)\left(\frac{1}{c_1}-\nu_1\right)\times \frac{\mathrm{d}\pi'}{\mathrm{d}c'_3}\mathrm{d}c'_3 + \int_{p_0}^{p}\frac{\mathrm{d}p}{c_1} \tag{20}$$

where p_0 is the pressure in the gel phase for $c'_3=0$.

The second integral in eqn. (20) may be evaluated by term-by-term integration. Carrying out the integration to terms of second order, and evaluating the last integral by the mean value theorem for integrals, we obtain

$$\Delta\mu_1 = \left(\frac{\nu'_2}{\nu_2}-\gamma_o\right)\frac{(1-c_1^{\circ}\nu_1)\,RT}{c_1^{\circ}\quad M_3}c+B_2c^2+ \frac{\Delta p}{c_1^{\circ}}(1+\beta_1\theta c+) \tag{21}$$

where

$$B_2=\frac{RT\,(1-c_1^o v_1)}{2M_3\quad c_1^o}\left[\gamma_o(\varepsilon-\alpha_1)+\frac{2A_2M_3}{RT}\left(\frac{v_2'}{v_2}-\gamma_o\right)+\frac{\beta_1}{1-c_1^o v_1}\left(\frac{v_2'}{v_2}-\gamma_o\right)\right] \quad (22)$$

and

$\Delta p=p-p_0$ and $0\leq\theta\leq1$.

This equation relates the partition coefficient γ_o to changes in the chemical potential of the gel network and the hydrostatic pressure in the gel. The latter term is of particular interest, because partition of solutes induced by the "swelling pressure" of gels has been a controversial subject for a long time.[1-5] However, in freely swelling flexible gels the hydrostatic pressure in the gel phase must equal the ambient hydrostatic pressure. This may be concluded from general thermodynamic criteria for heterogeneous equilibria,[11] a more direct proof being given in the next section. Thus, for freely swelling gels

$$p=p_0=p' \quad (23)$$

and the pressure term vanishes in eqn. (21). In this case the partition coefficient is directly related to the change of the chemical potential of the gel matrix.

It is of some interest to consider a completely inert gel matrix, representing an "ideal" gel system. Then

$$\Delta\mu_1\equiv0 \quad (24)$$

and from (21) it follows

$$\gamma_o=\frac{v_2'}{v_2}=1 \quad (25)$$

the last equality indicating that for a non-interacting gel matrix the partial specific volumes in the two phases have to be equal. In this case the solution inside the gel is identical with the ambient solution (from eqns. (3), (5) and (11) we obtain $c_3/c_2=c_3'/c_2'$). More generally we have

$$\gamma_o>\frac{v_2'}{v_2} \text{ implies } \Delta\mu_1<0, \quad (26)$$

$$\gamma_o<\frac{v_2'}{v_2} \text{ implies } \Delta\mu_1>0 \quad (27)$$

As an example of the latter relation we may consider partition equilibria in charged gels (the present treatment is applicable to a polyelectrolyte gel–simple salt solution, where the constituents have one ion in common, since the system has three components in Gibbs sense). Because of the Donnan exclusion we always have $\gamma<1$. Thus $\Delta\mu_1>0$, the chemical potential of the gel network–fixed ion system increasing on addition of a simple salt.

For dilute solutions we may write

$$\Delta\mu_1=\left(\frac{\partial\mu_1}{\partial c_1}\right)_0\Delta c_1+\left(\frac{\partial\mu_1}{\partial c_3}\right)_0\Delta c_3+\left(\frac{\partial\mu_1}{\partial p}\right)_0\Delta p=-\left(\frac{\partial\mu_1}{\partial c_1}\right)_0\frac{c_1^o}{V_0}\Delta V+\left(\frac{\partial\mu_1}{\partial c_3}\right)_0\Delta c_3+v_1\Delta p \quad (28)$$

where we have used eqn. (14) to obtain the last equality.

If $\gamma\equiv0$, $\Delta c_3\equiv0$, and we obtain from (21), (23) and (28)

$$-\left(\frac{\partial\mu_1}{\partial c_1}\right)_0\frac{c_1^o}{V_0}\Delta V=\frac{v_2'\,(1-c_1^o v_1)\,RT}{v_2\quad c_1^o\quad M_3}c+B_2c^2 \quad (29)$$

This is the basic equation for gel-osmometry.[12-15] It shows that for impermeable gels the volume change of the gel is a direct measure of the osmotic pressure of the ambient solution. However, the method is not absolute, as the value of $\left(\frac{\partial\mu_1}{\partial c_1}\right)_0$ is unknown and has to be determined by calibration. Also, the second order coefficient B_2 differs from the second osmotic virial coefficient. With permeable gels interference from the solute term in eqn. (28) cannot in general be neglected and the volume change is no longer a measure of the osmotic pressure.

If in partition experiments the volume of the gel is kept constant ($c_1\equiv c_1^o$) pressure changes in the gel phase have to be considered. In this case the full eqn. (21) applies, with $\beta_1=0$. In particular, for an impermeable gel $\gamma\equiv0$, and $\Delta\mu_1=v_1\Delta p$

in eqn. (28). The exact integration of eqn. (20) then yields

$$\Delta p = -(v'_2/v_2)\pi' \tag{30}$$

Swelling equilibria in pure solvent. We will in this section consider swelling equilibria and pressure-volume relations for a gel immersed in a pure solvent. To derive the thermodynamic stability conditions for a gel, which has reached its equilibrium volume of swelling, we imagine that the gel is perturbed by changing its volume by a small amount δV. The work done *on* the gel, δw, equals the change of Gibbs free energy for the gel–solvent system:

$$\delta w = \delta G = -\int_0^{\delta V} (p-p')\mathrm{d}V = -(\bar{p}-p')\delta V \tag{31}$$

where, by the mean value theorem

$$\bar{p} = p_0 + \theta \frac{\mathrm{d}p}{\mathrm{d}V}\delta V, \quad 0 \le \theta \le 1 \tag{32}$$

From eqn. (2) we obtain (since the solvent is still in equilibrium with the strained gel, $\mathrm{d}\mu_2 \equiv 0$)

$$dp = c_1 d\mu_1 = c_1\left[\left(\frac{\partial \mu_1}{\partial c_1}\right)_p \mathrm{d}c_1 + v_1 \mathrm{d}p\right] \tag{33}$$

Or, with the aid of eqn. (14)

$$\frac{\mathrm{d}p}{\mathrm{d}V} = -\frac{c_1^2}{(1-c_1 v_1)V}\left(\frac{\partial \mu_1}{\partial c_1}\right)_p \tag{34}$$

Thus

$$\delta G = -(p_0-p')\delta V + \frac{\theta c_1^2}{(1-c_1 v_1)V}\left(\frac{\partial \mu_1}{\partial c_1}\right)_p (\delta V)^2 \tag{35}$$

At equilibrium G has a minimum, which implies

$$\delta G > 0 \tag{36}$$

for all variations δV. This is true only if

$$p_0 = p'; \left(\frac{\partial \mu_1}{\partial c_1}\right)_p > 0 \tag{37}$$

Thus, in a flexible gel at equilibrium the hydrostatic pressure is necessarily equal to the surrounding pressure. Furthermore, from eqns. (34) and (37) it follows that the pressure increases on compression and decreases on dilation. The straining of a gel thus induces pressure changes which may be designated the "swelling pressure" of a gel. In unstrained gels the term has no physical significance.

It should be noted that the above relations are valid for a gel where the components are truly integrated into a single homogeneous phase. This is a prerequisite for the Gibbs-Duhem equation to be valid. If all the straining forces are balanced by stresses set up in the gel matrix (like in a system of springs) the latter has to be considered as a separate phase. In this case the change in its chemical potential is not coupled to pressure changes, the hydrostatic pressure in the pore liquid in general being equal to the external pressure. Such a gel is, of course, heterogeneous.

Finally, it should be noted that from the thermodynamic point of view, a gel should always be considered in conjunction with its solution phase. This is an immediate consequence of the Gibbs phase rule:

$$f = r + 2 - g \tag{38}$$

where f is the number of degrees of freedom, r the number of components and g the number of phases. For a polymer solution, prior to crosslinking, $r=2$ and $g=1$. Thus $f=3$, representing an independent choice of temperature, pressure and concentration. After crosslinking one degree of freedom is lost, as the concentration of the gel can no longer be independently changed. Thus $f=2$ and $g=2$ in eqn. (38). This means that a gel should always be considered as being in contact with a solution phase (syneresis seems to be a manifestation of this tendency). Vapor phase equilibria with *homogeneous* gels therefore seem to be inadmissible thermodynamically, leading inevitably to the formation of heterogeneities in the gel.

REFERENCES

1. Gregor, H. P. *J. Am. Chem. Soc. 73* (1951) 643.
2. Glueckauf, E. *Proc. R. Soc. London A 214* (1952) 207.
3. Boyd, G. E. and Soldano, B. A. *Z. Electrochem. 57* (1953) 162.

4. Dickel, G. *Z. Phys. Chem. Neue Folge 25* (1960) 233.
5. Ginzburg, B. Z. and Cohen, D. *Trans. Faraday Soc. 60* (1964) 185.
6. Gary-Bobo, C. M. and Lindenberg, A. B. *J. Colloid Sci. 29* (1969) 702.
7. Hjertén, S. *J. Chromatogr. 50* (1970) 189.
8. De Ruvo, A. *J. Polym. Sci. 11* (1973) 3017.
9. Minton, A. P. *Biophys. Chem. 12* (1980) 271.
10. Dusēk, K. and Prins, W. *Adv. Polym. Sci. 6* (1969) 1.
11. Kirkwood, J. G. and Oppenheim, I. *Chemical Thermodynamics,* McGraw-Hill, New York 1961, p. 57.
12. Boyer, R. F. *J. Chem. Phys. 13* (1945) 363.
13. Edmond, E., Farquhar, S., Dunstone, J. R. and Ogston, A. G. *Biochem. J. 108* (1968) 775.
14. Ogston, A. G. and Wells, J. D. *Biochem. J. 119* (1970) 67.
15. Ogston, A. G. and Preston, B. N. *Biochem. J. 131* (1973) 843.

Received June 14, 1982.

Acta Chemica Scandinavica A 37 (1983) 193–201

Thermodynamics of the Copper(I) Halide and Thiocyanate Complex Formation in Acetonitrile

STEN AHRLAND, KARIN NILSSON and BERNT TAGESSON *

Inorganic Chemistry 1, Chemical Center, University of Lund, Box 740, S-220 07 Lund, Sweden

Potentiometric and calorimetric measurements have been performed to determine the stability constants and enthalpy changes of the copper(I) halide and thiocyanate complex formation in acetonitrile. As ionic media 0.1 M tetraethylammonium perchlorate and tetrafluoroborate have been used. Much the same results have been obtained in the two media. In the halide systems two mononuclear complexes are formed in endothermic reactions. For both steps the stabilities decrease in the order $Cl^- > Br^- > I^-$. In the thiocyanate system, three mononuclear complexes are formed. The enthalpy change is exothermic for the first and the third step and endothermic for the second one. For all the complexes formed, the entropy changes are large and positive.

The constant for the disproportionation $2Cu^+ \rightleftarrows Cu^{2+} + Cu(Hg)$ has been determined potentiometrically. The value found, $K_D = [Cu^{2+}]/[Cu^+]^2 = 10^{-21}$ M^{-1}, is very low which is ascribed to the strong solvation of Cu^+ relative to Cu^{2+} in acetonitrile.

The thermodynamics of copper(I) halide complex formation has previously been investigated in water,[1-3] dimethylsulfoxide[4] (DMSO) and, recently, in pyridine.[5] In aqueous solution, copper(I) disproportionates completely in copper(II) and metallic copper if ligands stabilizing the monovalent state are not present in sufficiently high concentrations. This makes the investigation of copper(I) in aqueous solution fairly difficult. In aprotic solvents, copper(I) is much more favoured. Dilute solutions in DMSO are only slightly disproportionated[4] and in pyridine the disproportionation is negligible at all concentrations.[5,6] This must be due to a stronger solvation of copper(I) relative to copper(II) in aprotic solvents.

In the aprotic solvent acetonitrile (AN), copper(I) is even more favoured relative to copper(II). The monovalent oxidation state is quite stable, with no tendency to disproportionation. Nor is the solution readily oxidized by air, in strong contrast to the conditions in DMSO.[4] The divalent oxidation state is, on the other hand, a powerful oxidizing agent in AN[7] where it has even been used as an analytical oxidant.[8] The easy reduction of copper(II) in AN has also been utilized for electrolytic regeneration of copper.[9,10]

The aim of this investigation has been to study the thermodynamics of the formation of the copper(I) halides and thiocyanate complexes in AN. The stability constants were determined potentiometrically and the enthalpy changes calorimetrically. The formation entropies were then calculated from these quantities. The extreme stability of the solvated copper(I) ion has, moreover, been quantitatively established by determination of the disproportionation constant for the reaction $2Cu^+ \rightleftarrows Cu^{2+} + Cu(Hg)$. The temperature in all experiments has been 25 °C.

Both tetraethylammonium perchlorate and tetrafluoroborate have been used as ionic media in the present investigation. Perchlorates have sometimes been found to react very violently in AN, causing dangerous explosions.[11,12] This seemingly does not happen to copper(I) solutions, nor to the solid solvate $Cu(AN)_4ClO_4$, but

* Present address: Alfa Laval AB, Thermal Division, P.O. Box 1008, S-221 03 Lund, Sweden.

0302-4377/83 $2.50

if the investigations are to be extended to other metals it seems safer to use a non-oxidizing medium anion. As such, the tetrafluoroborate ion has been chosen as it presumably interferes as little with the complex formation as does the perchlorate ion. The disadvantage hampering the use of the tetrafluoroborate ion in aqueous solutions, that it is readily hydrolyzed, is of course not felt in an aprotic solvent. The postulate that perchlorate and tetrafluoroborate media behave in much the same way must, however, be tested. This has been done by the present comparison.

The tetraethylammonium ion has been chosen as the medium cation because not only the perchlorate and tetrafluoroborate, but also the tetraethylammonium halides and thiocyanate are sufficiently soluble in AN to allow an ionic medium of reasonably high concentration. The perchlorate and tetrafluoroborate are most probably completely dissociated in AN.[13] This means a high conductivity which makes the emf measurements very accurate. Also in tetraethylammonium iodide and thiocyanate solutions, the dissociation is seemingly complete,[14,15] while a slight association is indicated for bromide[13] and, especially, chloride.[16] This is much the same behaviour as found for ammonium halides in DMSO.[17,18]

In the partly associated chloride and bromide systems, the activity of the halide ions, and hence the complex formation with other cations, should depend strongly on the concentration of the tetraethylammonium ion, more than would be expected from the change of the ionic strength alone. Such effects have previously been found just for DMSO solutions containing ammonium salts.[17,18] The concentration of ammonium ions exerts an abnormally large influence on the stabilities of the metal bromide and, especially, chloride complexes formed in the solution. In such cases, an approximately constant medium is best achieved if the total concentration of medium cation is kept at the same level. Under the circumstances, this is more adequate than to aim at constant ionic strength, or a constant anion concentration. Obviously, the "free" ligand concentrations formally denoted [L] which enter the expression for the formation of complexes, are in these media the sums of the concentrations of the solvated ligand L and its associate with the medium cation. The constants reported in this study all refer to the standard states thus defined. The total concentration of tetraethylammonium ions has been 0.1 M in all solutions.

Referred to a standard state where the chloride and bromide medium electrolytes are completely dissociated, the values of the constants K_j would be slightly higher than the present ones, presumably by about 0.1 or 0.2 log units.[18]

EXPERIMENTAL

Chemicals. Acetonitrile (Baker Analyzed) was purified by fractional distillation over calcium hydride and stored over 3 Å molecular sieves. The residual water content was about 0.01 %, as determined by Karl Fischer titration.

$Cu(CH_3CN)_4BF_4$ was prepared as described previously.[19] The salt was stored in a carbon dioxide atmosphere. When exposed to air a blue-green discolouration, indicating oxidation to copper(II), is noticed after ≈1 hr. For analysis, the salt was oxidized with nitric acid. After dilution, AN was removed by heating the solution to boiling point. After cooling, the copper content was determined by EDTA titration, with murexide as indicator (found 20.1 %, calc. 20.2 %).

$Cu(CH_3CN)_4ClO_4$ was prepared analogously and analyzed for copper by the same procedure (found 19.3 %, calc. 19.4 %).

$Cu(CH_3CN)_4(BF_4)_2$ was prepared by oxidation of copper with nitrosyl tetrafluoroborate, according to the method of Hathaway *et al.*[20] The solvate was analyzed by EDTA-titration (found 16.2 %, calc. 15.8 %). Elementary analysis was performed for carbon (found 22.3 %, calc. 24.0 %). Evidently, the solvate contains somewhat less than four AN molecules per copper atom.

Tetraethylammonium tetrafluoroborate and *perchlorate* were dried in vacuum at 80 °C.

Tetraethylammonium chloride, bromide, iodide (Merck) and *thiocyanate* (Fluka) were dried at 100 °C and the halide or thiocyanate content determined titrimetrically.

Copper amalgam, containing ≈3 % Cu, was prepared as previously described.[1]

Determination of the disproportionation constant K_D. The value of K_D has been found from the standard potentials E°_{01} and E°_{12} of the couples Cu(Hg)/Cu^+ and Cu^+/Cu^{2+}, respectively, according to the formula $\ln K_D=(E^\circ_{01}-E^\circ_{12})/RTF^{-1}$. The measurements have been carried out in 0.1 M tetrafluoroborate medium. The disproportionation is much too small to allow a check of

-Cu(Hg)	C_M $CuBF_4$ 0.1 M Et_4NBF_4	0.1 M Et_4NBF_4	0.1 M Et_4NClO_4	10 mM $AgClO_4$ 0.1 M Et_4NClO_4	Ag+

Scheme 1.

the value of K_D found by chemical analysis of the solutions, as was possible *e.g.* for the mercury(I) disproportionation in DMSO.[21]

The value of E°_{01} was established by measuring the emf's of the cell (Scheme 1) at varying concentrations of copper(I) tetrafluoroborate, C_M. For the silver reference electrode, the readily available anhydrous $AgClO_4$ was used as a source of Ag^+. As $AgBF_4$ is only slightly soluble in AN, a perchlorate medium was used in this half-cell. The value of E°_{01} determined thus includes the liquid junction potential perchlorate/tetrafluoroborate which, however, should be small. Simultaneously, E°_{12} was determined by varying the ratio C_N/C_M in the half cell

-Pt	C_M Cu(I) C_N Cu(II) 0.1 M Et_4NBF_4	0.1 M Et_4NBF_4

connected with the same reference half-cell. The variation of C_N/C_M could not be effected by the usual procedure of titration, as a solution of copper(II) in AN, prepared by dissolving $Cu(AN)_4(BF_4)_2$(s), is spontaneously reduced to copper(I). This has been observed spectrophotometrically, with 2,9-dimethyl-1,10-phenanthroline (neo-cuproine) as complexing agent.[22] In AN, the absorption maximum of the copper(I) neo-cuproine complex is at 457 nm, with an extinction coefficient of 7800 ± 100 M^{-1} cm^{-1}. At the same wavelength the extinction coefficient of the copper(II) neo-cuproine complex is only $\simeq100$ M^{-1} cm^{-1}. In an AN solution, originally containing only $Cu(AN)_4(BF_4)_2$, the absorption continuously increases due to increasing copper(I) concentration. The variation of the ratio C_N/C_M has instead been brought about by dissolving various portions of the copper(II) solvate in copper(I) solutions of known concentrations, the emf measured as soon as possible (after $\simeq3$ min), and then observed for about two hours. During this period, the drift was $\simeq3$ mV. By linear extrapolation to zero time, the emf for the known initial ratio C_N/C_M could thus be determined with good precision. The standard electrode potentials found for the two copper couples relative to the reference electrode actually used have been recalculated so as to refer to a standard silver electrode of unit silver ion activity.

From E°_{01} and E°_{12}, it is also possible to calculate E°_{02}, according to $E^\circ_{02}=(E^\circ_{01}+E^\circ_{12})/2$. The value of K_D is, of course, independent of the reference electrode chosen.

Potentiometric measurements. Data for the calculation of the stability constants were obtained by titrations of copper(I) solutions with solutions of the ligand concerned. All solutions contained the appropriate ionic medium. The emf's were measured with a copper amalgam electrode in the copper(I) solution within the concentration range $0.7<C_M<10$ mM. An amalgam electrode Cu(Hg)/10 mM Cu^+, or, in the later series a silver electrode Ag(s)/C_{Ag} Ag^+, with 3 mM$<C_{Ag}<$10 mM, were used as reference electrodes in the appropriate ionic medium. In this manner the liquid junction potentials were minimized. Aliquots of the ligand solution were added, concentration range $0.2<C_L<24$ mM. The emf's measured were generally reproducible within 2 mV for the halides and within 5 mV for the thiocyanate. In solutions containing no ligands the emf varied with the copper concentration according to Nernst's law.

To exclude moisture, the titrations were performed in a glove box, with silica gel as the main drying agent. The last traces of moisture were removed by phosphorus pentoxide. The solutions were kept free from moisture, and stirred, by a stream of oxygen-free nitrogen which had been dried by passing through concentrated sulfuric acid. The gas was saturated with AN of the proper vapour pressure by passing through a wash-bottle containing the ionic medium used. Each titration was completed in a day. During this time, no sign of oxidation of copper(I) could be discovered.

Calorimetric measurements. The calorimeter employed has been described previously.[23–25] The calibration constant, ε_v, depends upon the volume, V ml, according to $\varepsilon_v=a+b(V-80)$ J ohm^{-1} where $a=0.8\pm0.3$ J ohm^{-1} and $b=(0.98\pm0.08)\times10^{-2}$ J $ohm^{-1}ml^{-1}$. The calorimeter vessel initially contained 80 ml copper(I) solution, of a concentration $3<C_M<10$ mM. Aliquots of ligand solutions were added. The concentrations of the ligand solutions were $C_L=100$ mM for the halides, and 50 mM for the thiocyanate which is not soluble enough for the higher concentration.

Table 1. Standard electrode potentials (E°_{01}, E°_{12}, E°_{02}/mV) and disproportionation constant (K_D/M^{-1}), present and previous measurements in acetonitrile at 25 °C.

Method[a]	Ref.el.[a]	E°_{01}(Cu(Hg))	E°_{01}(Cu(s))	E°_{12}	E°_{02}	$-\log K_D$	Ref.
0.1 M Et_4NBF_4							
Pot	SSE,AN	−591±1		627±2	19±2	20.6	This
Pot	SSE,AN		−601±1	627±2	13±2	20.8	work
0.006 to 0.03 M Et_4NClO_4							
Pot	SSE,AN	−594.2±0.5	−604.4±0.5				30
Et_4NClO_4, ionic strength=0							
Pot	SSE,AN			679±1			35
0.1 M Et_4NClO_4							
Vol	Ag/AgCl,aq		450	1700		21.1	36
Vol	SSE,AN		−620	580		20.3	37
0.1 M $NaClO_4$							
Vol	SCE,aq		−260	1000		21.3	7
Medium unknown						20	9

[a] Methods: Pot=potentiometry, Vol=voltametry. SSE=standard silver electrode, SCE=saturated calomel electrode.

For Cu^+, the heat of dilution was negligible in the concentration range used. When ligand solutions were added to 80 ml of the pure perchlorate medium, small exothermic heats of dilution were found, *viz.* −0.08 J ml^{-1} for chloride, −0.03 J ml^{-1} for bromide and iodide, and −0.01 J ml^{-1} for thiocyanate. In the tetrafluoroborate medium the heats were even smaller, *viz.* −0.03 J ml^{-1} for chloride and quite negligible for the other ligands.

Calculations. The numerical calculations of the stability constants were performed by means of the computer program EMMA.[26] The stability constants found were used as fixed parameters

Table 2. Overall stability constants (β_j/M^{-j}) of the copper(I) halide and thiocyanate complexes in acetonitrile at 25 °C. The limits of error refer to three standard deviations; NP denotes the number of observations (emf's measured for each system).

Ligand	Cl^-	Br^-	I^-	SCN^-
Medium 0.1 M Et_4NClO_4				
β_1	$(1.05\pm0.07)10^4$	$(2.44\pm0.04)10^3$	$(1.34\pm0.02)10^3$	$(3.37\pm0.36)10^3$
β_2	$(3.57\pm0.05)10^9$	$(1.61\pm0.01)10^7$	$(0.93\pm0.02)10^6$	$(1.19\pm0.08)10^7$
β_3				$(1.34\pm0.19)10^9$
NP	122	119	119	183
Medium 0.1 M Et_4NBF_4				
β_1	$(2.23\pm0.10)10^4$	$(2.34\pm0.12)10^3$	$(1.34\pm0.04)10^3$	$(6.45\pm0.54)10^3$
β_2	$(4.95\pm0.09)10^9$	$(1.58\pm0.04)10^7$	$(1.05\pm0.02)10^6$	$(2.02\pm0.10)10^7$
β_3				$(0.87\pm0.17)10^9$
Np	106	141	141	235

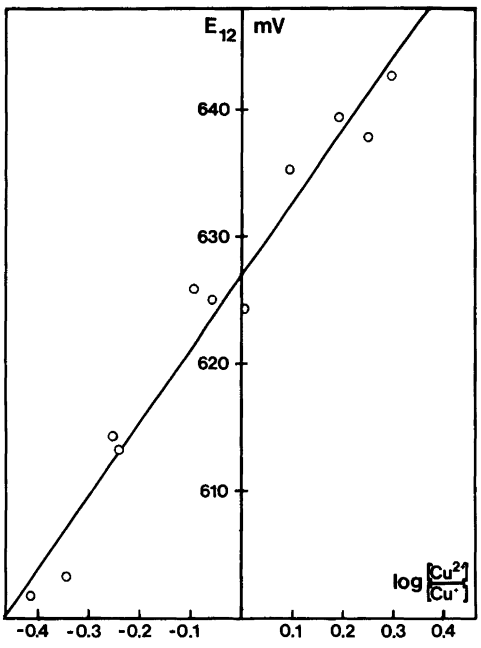

Fig. 1. The electrode potential of the couple Cu^+/Cu^{2+} referred to the standard silver electrode, as a function of the concentration ratio. Medium 0.1 M Et_4NBF_4; 25 °C.

for the calculation of the enthalpy changes by means of a modernized version of the program KALORI.[27]

RESULTS

The standard potential E°_{01} (Cu(Hg)) from the copper(I) titrations with Cu(Hg) electrode is listed in Table 1. The amalgamation makes the copper somewhat more noble. The emf E_{II} of the cell

$$-Cu(s)\,|\,Cu^{2+}(aq)\,|\,Cu(Hg)+$$

with the cell reaction $Cu(s) \rightarrow Cu(Hg)$ has been reported to be 5.1 mV.[28,30] This value is independent of the copper(II) concentration, and of the solvent used. From E_{II}, the free energy change of the cell reaction, $\Delta G = 2FE_{II} = -0.98$ kJ mol^{-1} is calculated, and also the activity of copper in the amalgam, $a(Cu(Hg)) = 0.67$. For the cell

$$-Cu(s)\,|\,Cu^{+}(sv)\,|\,Cu(Hg)+$$

involving the same cell reaction, the emf would thus be $E_I = -\Delta G/F = 10.2$ mV. The $E^\circ_{01}(Cu(s))$ in Table 1 has been calculated accordingly.

The values of E_{12} found for various ratios $[Cu^{2+}]/[Cu^+]$ have been plotted in Fig. 1. The intersection with the E_{12} axis gives the value of E°_{12} listed in Table 1. The values of K_D and E°_{02} hence calculated are reported in Table 1. The extremely low value of K_D means, of course, that no disproportionation whatever of Cu^+ occurs in AN solutions.

In several previous investigations voltammetric half-wave potentials, $E_{1/2}$, have been measured for the reductions $Cu^{2+} \rightarrow Cu^+$ and $Cu^+ \rightarrow Cu(s)$ in AN. From $E_{1/2}$, approximate values of E°_{01} and E°_{12}, referred to the reference electrode actually used, may be found. For the couples Cu^+/Cu^{2+}, $E^\circ_{12} \simeq E^\circ_{1/2}$; for $Cu(s)/Cu^+$, $E^\circ_{01} \simeq E^\circ_{1/2} - RTF^{-1} \ln C_M/2$ (the activity coefficient=1). The values of K_D calculated from the E°_{01} and E°_{12} thus obtained are not very different from that found presently, Table 1. Also another value of K_D quoted in the literature is of much the same order of magnitude.[9]

The overall stability constants, β_j, are listed in Table 2. The same values, within the limits of error, are found in the perchlorate and tetrafluoroborate media for the bromide and iodide systems. For chloride and thiocyanate, however, the constants are slightly different in the two media. Within the metal and ligand concentration ranges studied, all the halides form two mononuclear complexes, while for thiocyanate a third complex is also formed. The values found agree rather well with those of previous investigations.[29-31]

The overall enthalpy changes, ΔH_{β_j} (Table 3), are endothermic for all the halide complexes. For thiocyanate, ΔH_{β_1} is slightly exothermic, while $\Delta H_{\beta_2} \simeq 0$. Because of the difficulty to reach sufficiently high values of [L] in the calorimetric measurements, no accurate value of ΔH_{β_3} could be calculated for the thiocyanate system though a third complex is undoubtedly formed. Except for chloride, where considerably more endothermic values are found in the perchlorate medium, the values of ΔH_{β_j} are almost the same in the two media used.

Not unexpectedly, the thermodynamics of the reactions investigated are much the same in perchlorate and tetrafluoroborate media of the same concentration. Significant differences are

Table 3. **Overall enthalpy changes (ΔH_{β}/kJ mol^{-1}) for the formation of the copper(I) halide and thiocyanate complexes in acetonitrile, at 25 °C. The limits of error refer to three standard deviations; NP denotes the number of observations for each system.**

Ligand	Cl^-	Br^-	I^-	SCN^-
Medium 0.1 M Et_4NClO_4				
ΔH_{β_1}	16.8±1.4	10.5±0.7	8.5±0.4	–5.4±0.8
ΔH_{β_2}	21.2±0.3	27.2±0.4	21.3±0.4	0.6±0.7
NP	68	67	78	36
Medium 0.1 M Et_4NBF_4				
ΔH_{β_1}	11.7±0.9	11.9±0.5	8.3±0.5	–5.1±0.5
ΔH_{β_2}	18.4±0.3	27.4±0.3	19.9±0.5	–0.1±0.5
NP	57	64	56	53

Table 4. Equilibrium constants (K_j/M^{-1}) and thermodynamic functions (ΔG_j°, ΔH_j°/kJ mol^{-1}; ΔS_j°/J K^{-1} mol^{-1}) for the stepwise formation of copper(I) halide and thiocyanate complexes in acetonitrile (AN) and dimethylsulfoxide (DMSO) at 25 °C.

Ligand	Cl^-	Br^-	I^-	SCN^-	Cl^-	Br^-	I^-	SCN^-
AN, 0.1 M Et_4NClO_4[a]					AN, 0.1 M Et_4NBF_4[a]			
log K_1	4.02	3.39	3.13	3.53	4.35	3.37	3.13	3.81
log K_2	5.53	3.82	2.84	3.54	5.35	3.82	2.89	3.50
log K_3				2.05				1.63
K_1/K_2	0.031	0.37	1.9	0.95	0.010	0.35	1.7	2.1
K_2/K_3				31				73
$-\Delta G_1^\circ$	23.0	19.3	17.9	20.2	24.8	19.2	17.9	21.7
$-\Delta G_2^\circ$	31.6	21.8	16.2	20.3	30.5	21.5	16.5	20.0
$-\Delta G_3^\circ$				11.7				9.3
ΔH_1°	16.8	10.5	8.5	–5.4	11.7	11.9	8.3	–5.1
ΔH_2°	4.4	16.7	12.8	6.0	6.7	15.5	11.6	5.0
ΔS_1°	133	100	89	50	122	104	88	56
ΔS_2°	121	129	97	88	125	125	94	84
$-\Delta G_{\beta_2}^\circ$	54.5	41.1	34.1	40.4	55.3	41.1	34.4	441.7
$\Delta H_{\beta_2}^\circ$	21.2	27.2	21.3	0.6	18.4	27.4	19.9	–0.1
$\Delta S_{\beta_2}^\circ$	254	229	186	137	247	230	182	140
DMSO, 0.1 M Et_4NClO_4[b]					DMSO, 1 M NH_4ClO_4[c]			
log K_1	6.0	5.0	5.5		4.37	4.19	4.71	
log K_2	6.0	4.6	2.7		4.50	3.75	2.96	
log K_3					0.58			
K_1/K_2	1	3	600		0.7	2.8	56	
$-\Delta G_1^\circ$	34	29	31		24.9	23.9	26.9	
$-\Delta G_2^\circ$	34	26	16		25.7	21.7	16.9	
$-\Delta H_1^\circ$					6.4	9.3	13.6	
$-\Delta H_2^\circ$					7.8	–2.1	–3.1	
ΔS_1°					62	49	45	
ΔS_2°					60	78	67	

[a] This work. [b] Ref. 38. [c] Ref. 4.

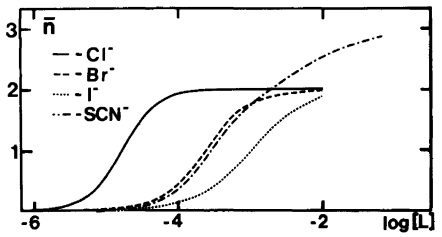

Fig. 2. The complex formation curves of the copper(I) halides and thiocyanate systems in acetonitrile. Medium 0.1 M Et_4NClO_4; 25 °C.

observed only for the chloride and thiocyanate systems, and even in these cases they are fairly small.

The stepwise stability constants, K_j, and enthalpy changes, ΔH_j, are listed in Table 4, with the values derived of the changes in free energy, ΔG_j°, and entropy, ΔS_j°.

The stabilities of the halide complexes follow an (a)-sequence $Cl^->Br^->I^-$. This is also illustrated by the complex formation curves of Fig. 2. The first two thiocyanate complexes are of much the same stability as the analogous bromide complexes. The formation of a third thiocyanate complex causes the formation curves of the two systems to deviate strongly at high ligand concentrations, however. The stability of the first complex relative to the second one increases from chloride to iodide, as seen from the increasing values of the ratio K_1/K_2. This change is also reflected in the decreasing steepness of the complex formation curves. Even more clearly, the increasing importance of the intermediate complex CuL is illustrated by the complex distribution curves of Fig. 3.

The values of ΔH_1° are endothermic for all the halides but less so in the order $Cl^->Br^->I^-$, Table 4. For SCN^-, ΔH_1°, is slightly exothermic. The values of ΔH_2° are endothermic for all the ligands. Remarkably enough, the most endothermic value is found for Br^-.

The endothermic values of ΔH_j° found for all the complexes except CuSCN counteract their formation. Only by large positive values of ΔS_j° do the complexes attain the fairly high stability which they, in fact, possess. Even in the case of CuSCN, formed in an exothermic reaction, the entropy term contributes by far most to the stability.

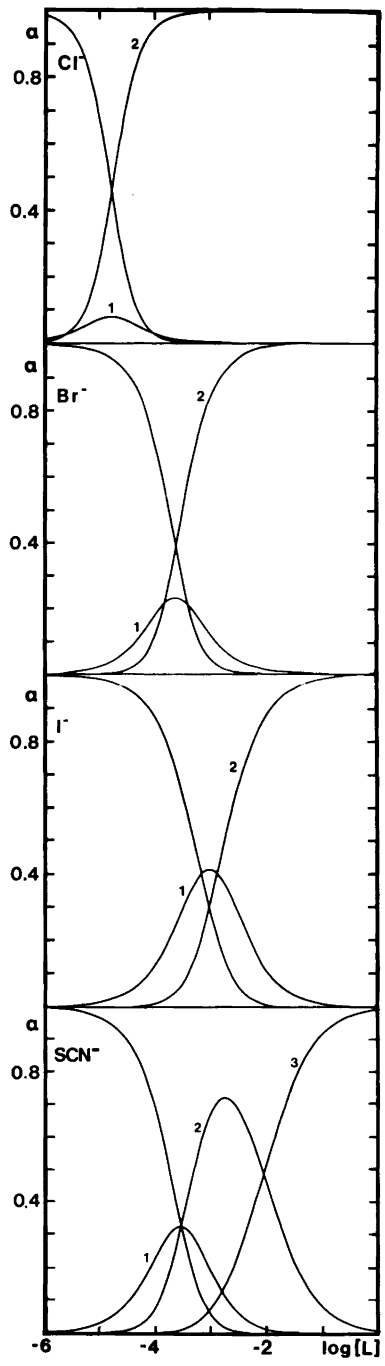

Fig. 3. The distribution of copper(I) between the species Cu^+, CuL (1), CuL_2^- (2) and CuL_3^{2-} (3) for the halide and thiocyanate systemms, as a function of the free ligand concentration. Medium 0.1 M Et_4NClO_4; 25 °C.

DISCUSSION

In protic solvents, the ability to form hydrogen bonds makes the chloride ion much more strongly solvated than the iodide ion. In aprotic solvents where no hydrogen bonds can be formed, this difference is smaller. Consequently, the chloride complexes are stronger relative to iodide ones in aprotic solvents than in protic solvents. This is reflected in the change of order for the stability of the complexes formed. In water the stabilities of the copper complexes formed follows a (b)-sequence, $Cl^- < Br^- < I^-$. In aprotic solvents the (b)-sequence tends to switch to an (a)-sequence, $Cl^- > Br^- > I^-$. In the aprotic DMSO, coordinating *via* oxygen, the first complex formation step displays a hybrid sequence $Cl^- > Br^- < I^-$, but for the second step an (a)-sequence is found.[4] In AN the (a)-sequence is quite marked, Table 4. Pyridine, another nitrogen-donating solvent, also gives an (a)-sequence.[5]

The stabilities of the complexes formed are, of course, also strongly influenced by the solvation of all the metal species involved. For obvious reasons, however, the solvation of the central ion is always much stronger than that of any of the complexes. A strongly solvating solvent will therefore mean a large net desolvation enthalpy, counterating the complex formation. In aprotic solvents, Cu^+ is strongly solvated; consequently the overall enthalpy changes are generally not favourable. They are, moreover, much more unfavourable in AN than in DMSO, Table 4. This reflects the strong increase of the solvation enthalpy of Cu^+ between DMSO and AN which is not at all counterbalanced by an equivalent increase for the complexes.[32] On the other hand, the breakup of the strong Cu^+ solvate formed in AN will bring about a large increase of entropy, which tends to make the overall entropy change of the complex formation very favourable. The actual increase of entropy due to this desolvation does not depend solely on the state of order of the solvate, however, but also on the degree of order prevailing in the bulk solvent. The larger the difference in order between the solvate and the bulk solvent, the larger the entropy gain.

The structural order of a solvent should be fairly well reflected in the ratio between the dielectric constant and the dipole moment, ε/μ. The higher the value of ε relative to that of μ, the more orderly the dipoles are lined up and, consequently, the more structured the solvent. By this criterion, AN is appreciably less ordered than DMSO.[33] Relative to DMSO, the desolvation in AN thus occurs from a more well-ordered solvate to a less well-ordered solvent. The considerably higher entropy gains found in AN are therefore just what to expect.

As is often found, even if the enthalpy and entropy changes of the formation of a certain complex differ widely between different solvents, these changes compensate each other extensively. Consequently, the free energy changes, and hence the stabilities, may not differ widely, in spite of the rather different characteristics of the reactions involved.

The difference in stability found for the chloride system between the two media used is essentially an enthalpy effect. For the thiocyanate system, on the other hand, the difference is mostly an entropy effect. Also for the bromide system, significant differences exist between the enthalpy and entropy changes in the two media, though these compensate each other completely. That the thermodynamics differ somewhat between different media is *per se* natural and also that various systems are influenced to various extents. At least presently, however, it does not seem fruitful to speculate about the details of the trends observed. The main conclusion is, however, that a change of perchlorate for tetrafluoroborate exerts only a marginal influence on the complex formation.

The very low value of K_D in AN reflects a strong stabilization of Cu^+ relative to Cu^{2+}, as compared with DMSO and, even more, with water. This stabilization is directly connected with the free energies of transfer ΔG°_{tr} which favour Cu^+ relative to Cu^{2+} especially between DMSO and AN.[34] The values of ΔG°_{tr} (DMSO→AN) are for Cu^+ −11.7 kJ mol^{-1} and for Cu^{2+} 98.3 kJ mol^{-1}. The relative contributions of the enthalpies and entropies of transfer are so far not known for these ions, however.

Acknowledgements. We wish to thank Mr. Mats Johnsson for experimental assistance. The financial support given by the Swedish Natural Science Research Council is gratefully acknowledged.

REFERENCES

1. Ahrland, S. and Rawsthorne, J. *Acta Chem. Scand. 24* (1970) 157.
2. Ahrland, S. and Tagesson, B. *Acta Chem. Scand. A 31* (1977) 615.
3. Ahrland, S., Tagesson, B. and Tuhtar, D. *Acta Chem. Scand. A 31* (1977) 625.
4. Ahrland, S., Bläuenstein, P., Tagesson, B. and Tuhtar, D. *Acta Chem. Scand. A 34* (1980) 265.
5. Ahrland, S., Ishiguro, S. and Persson, I. *To be published.*
6. Gupta, A. K. *J. Chem. Soc.* (1952) 3473.
7. Kolthoff, I. M. and Coetzee, J. F. *J. Am. Chem. Soc. 79* (1957) 1852.
8. Kratochvil, B. and Quirk, P. F. *Anal. Chem. 42* (1970) 535.
9. Parker, A. J. *Electrochim. Acta 21* (1976) 671.
10. Preston, J. S., Muir, D. M. and Parker, A. J. *Hydrometallurgy 5* (1980) 227.
11. Sax, I. *Dangerous Properties of Industrial Materials,* 4th Ed., Reinhold, New York 1976.
12. Persson, I. *Personal communication.*
13. Forcier, G. A. and Olver, J. W. *Electrochim. Acta 14* (1969) 135.
14. Harkness, A. C. and Daggett, H. M., Jr. *Can. J. Chem. 43* (1965) 1215.
15. Misumi, S., Aihara, M. and Kinoshita, S. *Bull. Chem. Soc. Jpn. 47* (1974) 127.
16. Davies, C. W. *Ion Association,* Butterworth, London 1962, p. 96.
17. Ahrland, S., Björk, N.-O. and Persson, I. *Acta Chem. Scand. A 35* (1981) 67.
18. Ahrland, S. and Persson, I. *Acta Chem. Scand. A 35* (1981) 185.
19. Hemmerich, P. and Sigwart, C. *Experientia 19* (1963) 488.
20. Hathaway, B. J., Holah, D. G. and Underhill, A. E. *J. Chem. Soc.* (1962) 2444.
21. Ahrland, S. and Persson, I. *Acta Chem. Scand. A 34* (1980) 645.
22. Smith, F. and McCurdy, W. H. *Anal. Chem. 24* (1952) 371.
23. Grenthe, I., Ots, H. and Ginstrup, O. *Acta Chem. Scand. 24* (1970) 1067.
24. Ots, H. *Acta Chem. Scand. 26* (1972) 3810.
25. Ahrland, S. and Björk, N.-O. *Acta Chem. Scand. 30* (1976) 257.
26. Sandell, A. *Personal communication.*
27. Karlsson, R. and Kullberg, L. *Chem. Scr. 9* (1976) 54.
28. Oku, M. *Science Rep. Tohoku Univ. Ser. 1, 22* (1933) 288.
29. Manahan, S. E. and Iwamoto, R. T. *Inorg. Chem. 4* (1965) 1409.
30. Senne, J. K. and Kratochvil, B. *Anal. Chem. 43* (1971) 79.
31. Heerman, L. F. and Rechnitz, G. A. *Anal. Chem. 44* (1972) 1655.
32. Ahrland, S. and Ishiguro, S. *To be published.*
33. Ahrland, S. In Lagowski, J. J., Ed., *The Chemistry of Nonaqueous Solvent,* Academic, New York–San Francisco–London 1978, Vol. V A, Chapter 1.
34. Ahrland, S. *Pure Appl. Chem. 54* (1982) 1451.
35. Senne, J. K. and Kratochvil, B. *Anal. Chem. 44* (1972) 585.
36. Duschek, O. and Gutmann, V. *Z. Anorg. Allg. Chem. 394* (1972) 243.
37. Sestili, L., Furlani, C., Ciana, A. and Garbassi, F. *Electrochim. Acta 15* (1970) 225.
38. Foll, A., Le Démézet, M. and Courtot-Coupez, J. *J. Electroanal. Chem. 35* (1972) 41.

Received June 30, 1982.

Acta Chemica Scandinavica A 37 (1983) 203–206

Structural Studies of Gadolinium Gallium Garnet

JUDIT SASVÁRI [a] and PER-ERIK WERNER [b]

[a] Magyar Tudományos Akadémia Központi Fizikai Intézete, Budapest XII, Konkoly Thege út 29–33, XXVI épület, Hungary and [b] Department of Structural Chemistry, Arrhenius Laboratory, University of Stockholm, S-106 91 Stockholm, Sweden

Structural parameters for $Gd_3Ga_5O_{12}$ garnets have been refined with single crystal diffractometer data. The occupancy parameters were strongly influenced by extinction errors. A simple semiempirical extinction correction procedure was shown to improve the result substantially. Topographic studies revealed that dislocations were present in non-calcium induced crystals whereas preparation of crystals in the presence of very small amounts of CaO gave crystals of high quality. From the diffraction data, however, no significant differences between calcium and non-calcium induced crystals were detectable.

The $Gd_3Ga_5O_{12}$ garnets crystallize in space group *Ia3d* with eight formula units per cell and are isomorphous with the naturally occurring garnets; that structure was first determined by Menzer.[1] The $Gd_3Ga_5O_{12}$ garnets, below termed GGG, have found application as substrates for magnetic bubble memories. At the Central Research Institute for Physics of the Hungarian Academy of Sciences, one of us (J.S.) attempted to differentiate between GGG single crystals prepared in the absence and the presence of very small amounts of CaO. Dislocations were then observed by X-ray topographic methods in the non-calcium induced crystals. The effect is illustrated in Fig. 1.

The GGG crystals were grown from a melt by weighing the following components into an iridium crucible: Gd_2O_3 53.7 wt % Ga_2O_3 46.3 wt %. The crucible was heated to 1800 °C and single crystals were prepared by a computer-controlled Czochralski method.[2] The crystals were rotated (10–30 r min^{-1}) around the [111] direction and pulled out at a speed of 6 mm h^{-1} from the melt.

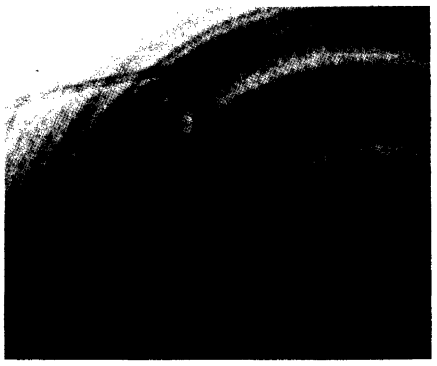

Fig. 1. Topographic study of a calcium-induced $Gd_3Ga_5O_{12}$ single crystal. The exposed surface of the crystal is a circular area, about 50 mm in diamater. Evidence for dislocations can be seen within the rectangular area on the figure.

According to the X-ray topographic studies, high quality single crystals, HQ, were obtained from melts containing 80 ppm of CaO, whereas crystals of lower quality, LQ, were obtained from melts without CaO (Fig. 1).

A large number of garnet structures have been investigated, and reviews of the field have been given by Euler and Bruce[3] and by Geller.[4] The cations are all in special positions in space group *Ia3d*, with no positional degrees of freedom, while the oxygen atoms all are in the general position (96*h*). (Nomenclature according to International Tables of Crystallography, 1974.[5]) The general character of the cation positions and their environments is shown in Fig. 2. In order to provide information about the oxygen and cation

0302-4377/83 $2.50

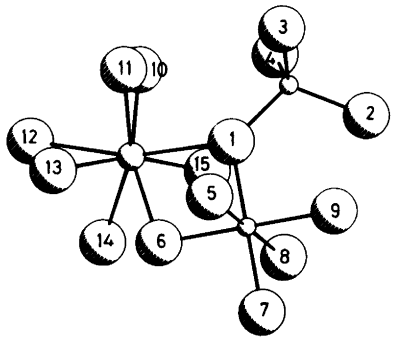

Fig. 2. The arrangement of gadolinium–oxygen dodecahedra gallium–oxygen octahedra and gallium–oxygen tetrahedra in $Gd_3Ga_5O_{12}$ garnet.

positions in GGG and, if possible, the differences between the HQ and LQ forms, an X-ray crystallographic study was performed.

EXPERIMENTAL

The data were collected on a Philips PW1100 diffractometer using pure Mo$K\alpha$ radiation (λ=0.71069 Å) obtained with a graphite monochromator. Colourless crystals of approximate dimensions 0.03×0.2×0.2 mm and 0.015×0.1×0.1 mm were cut from larger HQ and LQ crystals, respectively. The crystal data are listed in Table 1. The diffraction data were collected in the $\theta/2\theta$ scan mode with a scan rate of 1.2° min^{-1} and a scan width of $\Delta 2\theta$=1.8°. Background counts at the extremes of scan were taken with the total background time equalling the scan time. The intensities of three standard reflections, measured at intervals of 39 reflections throughout the data collection, showed no variation greater than 3 %. Reflections from one octant were collected to a 2θ limit of 60° (sin θ/λ=0.704 Å^{-1}). Lp and absorption corrections were made, and the data were averaged to give 233 and 229 unique reflections for HQ and LQ, respectively. The minimum and maximum absorption correction factors were 3.2 and 26.3 for HQ. The corresponding factors for the smaller LQ crystal were 1.9 and 4.3.

Table 1. Crystal data.

$Gd_3Ga_2Ge_3O_{12}$
Space group *Ia3d*
HQ a=12.3829(2) Å *
LQ a=12.3820(2) Å *
Cell content Z=8
M=1021.0
D_x=7.14 g cm^{-3}
μ=364.3 cm^{-1}

* Cell parameter determined by the Bond method.[6]

REFINEMENT

It was stated by Bonnet, Delapalme, Fuess and Thomas[7] that the crucial point in the refinement of garnet structures from single crystal X-ray diffraction data is an appropriate extinction correction. This conclusion is verified in the present study by the fact that the R-values were reduced by as much as 0.042 and 0.051 for the HQ and LQ refinements, respectively, when empirical extinction corrections were applied (Table 2). Furthermore, for HQ the cation occupancy parameters obtained without extinction corrections were all systematically too small. The latter effect is not found for the smaller LQ crystal, but the calculated standard deviations were very high. In the study by Bonnet *et al.*[7] several different models for extinction correc-

Table 2. Occupancy parameters and *R*-values.

Crystal	Extinction correction	Occupancy parameters (in assumed positions)			*R*	R_w
		k_{Gd} (24*c*)	k_{Ga} (16*a*)	k_{Ga} (24*d*)		
LQ	No	1.09(15)	0.98(20)	1.02(19)	0.128	0.212
HQ	No	0.86(5)	0.68(7)	0.65(6)	0.097	0.135
LQ	Yes	0.91(4)	0.85(6)	0.82(6)	0.077	0.098
HQ	Yes	0.94(5)	0.84(5)	0.82(5)	0.055	0.070

Table 3. Final positional and thermal parameters.

	x	*y*	*z*	*U* (Å^3)
a. Crystal HQ				
Gd (24*c*)	1/8	0	1/4	0.0047(7)
Ga(1) (16*a*)	0	0	0	0.0019(17)
Ga(2) (24*d*)	3/8	0	1/4	0.0036(17)
O (96*h*)	0.9720(6)	0.0539(7)	0.1502(6)	0.0044(23)
b. Crystal LQ				
Gd (24*c*)	1/8	0	1/4	0.0047(10)
Ga(1) (16*a*)	0	0	0	0.0029(24)
Ga(2) (24*d*)	3/8	0	1/4	0.0033(23)
O (96*h*)	0.9727(8)	0.0543(9)	0.1495(8)	0.0010(10)

tions were examined, but it was found that the positional and thermal parameters for the $Y_3Fe_5O_{12}$ garnet investigated were only slightly influenced by the choice of a particular extinction correction model. Therefore, we decided to use the simple empirical isotropic extinction correction procedure available in the SHELX program.[8] In the full-matrix least-squares refinement an extinction coefficient, g, was refined in the expression

$$F_{corr}=F_{calc}\ (1-g\cdot F_{calc}{}^2/\sin\theta)$$

The final values of g were $(2.6\pm0.3)\times10^{-8}$ and $(3.4\pm0.4)\times10^{-8}$ for HQ and LQ, respectively. The function minimized was

$$R_w=[\Sigma w\ (|F_o|-|F_c|)^2/\Sigma w\ |F_o|^2]^{1/2}$$

where the weight w was defined by

$$w=1/[\sigma^2(F)+bF^2]$$

In the final refinements, with extinction corrections included, the weight parameter b was 6.1×10^{-5} for HQ. The corresponding figure for LQ was 3.0×10^{-4}. Tables 2, 3 and 4 list structural parameters and cation–oxygen distances.

DISCUSSION

It was assumed that Gd^{3+} should fill the c site, although it was not considered impossible that some Gd^{3+} could also enter the a position.[4] From the present study, there are no indications for gadolinium at the a site. As can be seen from Table 2, the occupancy parameters for the cations are somewhat smaller than unity. This may be an effect of imperfect extinction corrections, although the empirical correction procedure used significantly reduces the *R*-values and improves the determination of the occupancy parameters.

No significant differences between the HQ and LQ crystals can be seen from Tables 2 and 3. This means only that the X-ray diffraction technique, as others, has a limit in its resolving power. The deviations in unit cell dimensions (*cf.* Table 1) and the differences found by X-ray topography (*cf.* Fig. 1) between the HQ and LQ crystals are too small to cause any significant changes in the single crystal diffraction data.

Table 4. Cation–oxygen distances (Å) in $Gd_3Ga_5O_{12}$ (HQ crystal). The average e.s.d. of cation–oxygen distances is 0.008 Å. The numbering of the atoms is shown in Fig. 2.

Ga tetrahedron	
Ga–O_i; i=1, 2, 3, 4	1.849
Ga octahedron	
Ga–O_i; i=1, 5, 6, 7, 8, 9	2.007
Gd dodecahedron	
Gd–O_i; i=1, 12, 13, 15	2.473
Gd–O_j j=6, 10, 11, 14	2.359

Acknowledgements. One of the authors, Judit Sasvári, would like to express her thanks to the Hungarian Academy of Science for a research fellowship grant which has made her stay at the Arrhenius Laboratory possible.

The interest shown and ecouragement given by Prof. P. Kierkegaard is highly appreciated. The authors are also indebted to Dr. J. Paitz for supplying the samples and for his continuous interest in this research.

This work has received financial support from The Swedish Natural Science Research Council.

REFERENCES

1. Menzer, G. *Centralbl. Min. A* (1925) 344.
2. Paitz, J. and Gosztonyi, L. *Acta Phys. Acad. Sci. Hung. 47* (1979) 233.
3. Euler, F. and Bruce, J. A. *Acta Crystallogr. 19* (1965) 971.
4. Geller, S. *Z. Kristallogr. 125* (1967) 1.
5. *International Tables for X-Ray Crystallography,* Kynoch Press, Birmingham 1974. Vol. 1.
6. Bond, W. L. *Acta Crystallogr. 13* (1960) 814.
7. Bonnet, M., Delapalme, A., Fuess, H. and Thomas, M. *Acta Crystallogr. B 31* (1975) 2233.
8. Sheldrick, G. M. *SHELX. Program for Crystal Structure Determination,* University of Cambridge, Cambridge 1978, England.

Received June 18, 1982.

Acta Chemica Scandinavica A 37 (1983) 207–217

Solutions of Chlorine in Molten Chlorides. 1. Solubility and Diffusivity of Chlorine in NaCl and CsCl Melts

OLE WÆRNES,[a] FRANCESCO PALMISANO[b] and TERJE ØSTVOLD[a]

[a] Institutt for uorganisk kjemi, Norges tekniske høgskole, N-7034 Trondheim-NTH, Norway and
[b] Istituto di Chimica Analitica, Universitá di Bari, Via Amendola 173, I-70126 Bari, Italy

The reduction of Cl_2 dissolved in molten NaCl, CsCl and NaCl–CsCl eutectic has been investigated by chronopotentiometry. The same value of the diffusion coefficient is obtained by using a plane or a cylindrical working electrode, both made of vitreous carbon.

In the temperature range 510–890 °C the diffusion coefficient of chlorine in alkali chloride melts is in the order of 10^{-4} cm^2s^{-1}, and does not seem to be sensitive to the size of the alkali metal cation.

The solubility of chlorine gas in molten NaCl and NaCl–CsCl eutectic has been determined by a manometric technique. This involves keeping the gas volume above the melt constant and to measure the pressure decrease as the gas dissolves in the liquid. The solubility, in the order of 10^{-6}–10^{-7} mol cm^{-3}, increases in the sequence NaCl to CsCl.

A positive enthalpy of dissolution was found for both NaCl and NaCl–CsCl melts.

The main purpose of the present work has been to obtain information on the diffusion coefficients of chlorine dissolved in chloride melts. This is part of a program aimed at an experimental determination of physicochemical parameters that are needed in the model for the back reaction in the magnesium electrolysis.[1,2] The diffusion coefficients together with the solubility of chlorine and magnesium in the melt will be used in a mass-transfer model for the back reaction mechanism.

In recent years there has been an increased interest in molten aluminium chloride–alkali chloride mixtures. One obvious reason for this is the development of a new aluminium process, which is based on electrolysis of aluminium chloride in alkali and alkaline earth metal chlorides at about 700 °C.

The solubility of chlorine and the kinetics of chlorine reduction in molten chloroaluminates are also important parameters with respect to high energy density batteries.

A paper which deals with solutions of chlorine in chloroaluminate melts will be published later.

Electrochemical methods for the determination of diffusion coefficients of dissolved chlorine in melts require a known chlorine solubility. Due to important improvements in our experimental solubility apparatus it was also of interest to compare our new solubilities with those obtained previously.[3–5]

PRINCIPLES

Chlorine solubility measurements. The following equilibrium is studied:

$$Cl_2(gas) \rightleftarrows Cl_2 \text{ (dissolved)} \quad (1)$$

The equilibrium constant is

$$K = a_{Cl_2(d)}/a_{Cl_2(g)} \quad (2)$$

where a denotes activity. Assuming that Henry's law is valid for the solute and that $Cl_2(g)$ is an ideal gas, with standard states of 1 mol cm^{-3} for dissolved chlorine and 1 atm for chlorine gas, respectively, the equilibrium constant becomes equal to the Henry's law constant.

$$K = c_{Cl_2(d)}/P_{Cl_2(g)} \quad (3)$$

0302-4377/83 $2.50

At 1 atm of chlorine pressure the Henry's law constant is equal to the solubility of chlorine. The standard enthalpy of dissolution is given by the equation

$$\Delta H_d^\circ = -R \, d \ln K_H / d (1/T) \quad (4)$$

The Henry's law constant for the dissolution reaction is determined by the relation [3,4]

$$K_H = \Delta P V_o \rho / RTw\Delta P_{eq} \quad (5)$$

ΔP is the pressure drop due to dissolution of chlorine, V_o is the volume of the gas reduced to the thermostated temperature, T, which normally was 25 °C.[3,4] ρ is the density of the melt, R is the universal gas constant (in cm^3 atm mol^{-1} deg^{-1}), w is the weight of the salt, and ΔP_{eq} is the change in equilibrium pressure. When initially $P_{Cl_2}=0$, ΔP_{eq} equals the final equilibrium pressure (P_{eq}^u).

Chronopotentiometric measurements. The fundamental equation for chronopotentiometry (semiinfinite linear diffusion to a plane electrode) is the Sand equation:[6]

$$\tau^{1/2} = \frac{\pi^{1/2} nFAcD^{1/2}}{2I} = \frac{\pi^{1/2} nFcD^{1/2}}{2i} \quad (6)$$

τ = transition time
n = number of electrons in the overall electrochemical reaction
F = Faraday's constant
A = electrode area
c = concentration (solubility of Cl_2 in the melt)
D = diffusion coefficient
I = applied current
i = current density (I/A)

It is seen from eqn. (6) that the square root of the transition time is proportional to the concentration of electrolyzed species and inversely proportional to the current. Hence the product $I\tau^{1/2}$ should be independent of the applied current for given conditions of electrolysis, and the diffusion coefficients may be determined.

Several empirical methods, and also least squares analysis of the chronopotentiogram have been suggested for determination of the transition time from experimental curves.[7–11] In the present study the method of Reinmuth [10] has been used.

Peters and Lingane [12] have derived the following equation for chronopotentiometry with cylindrical electrodes

$$I\tau^{1/2} = (\pi^{1/2} nFAcD^{1/2}/2) \times [1-(\pi^{1/2}/4)(D^{1/2}\tau^{1/2}/r) + (1/4)(D^{1/2}\tau^{1/2}/r)^2 - (3\pi^{1/2}/32)(D^{1/2}\tau^{1/2}/r)^3 + \ldots]^{-1} \quad (7)$$

where r is the working electrode radius, and A is the area of the cylindrical electrode. In the measurements with cylindrical electrodes, most of the transition times were less than 0.15 s (only very few longer than 0.25 s). Thus the maximum error introduced in $I\tau^{1/2}$ when the Sand equation is applied, is about 2 %. This gives diffusion coefficients which may be up to 4 % too large. As eqn. (7) is not strictly valid for the actual electrodes and the approximate correction is relatively small, eqn. (6) has been applied without correction for cylindrical diffusion.

Although the Sand equation is approximately valid when chronopotentiometry is performed with cylindrical electrodes, the accurate determination of the electrode area still remains. In the present study the vitreous carbon rod was immersed in the melt without any kind of shielding. Due to wetting of the rod, a meniscus may rise to a definite height, measured from the melt surface. An increase in the geometrical area, A_{geo}, determined from the immersion depth, l, will thus occur. The total area of the electrode in contact with the melt can thus be divided into two parts

$$A = A_{geo} + \Delta A = 2\pi r(l + r/2) + \Delta A \quad (8)$$

The area ΔA depends on wetting and may also include the influence of the "edge effect" at the end of the rod, and an error in A_{geo} due to incorrect determination of the surface level of the melt. This surface level, from which the immersion depth is measured, was determined by slowly lowering the electrode until electrical contact was achieved. A melt drop adhering to the end of the rod during measurements of the surface level will give a too high value for l and thus for A_{geo}. In that case ΔA should have a negative value.

From eqns. (6) and (8) at constant concentration it follows that

$$I\tau^{1/2} = kA = kA_{geo} + k\Delta A \quad (9)$$

$$k = (1/2)\pi^{1/2} FcD^{1/2} \quad (10)$$

A plot of $I\tau^{1/2}$ *versus* A_{geo} for different immersion depths should therefore yield a straight line. The area ΔA may be found from the slope and the intercept of that line. The diffusion coefficient may be determined directly from the slope, k, according to eqn. (10), or from eqns. (11) and (12) where i is the current density

$$k = \frac{I\tau^{1/2}}{A_{geo}+\Delta A} = i\tau^{1/2} \quad (11)$$

$$i\tau^{1/2} = \frac{\pi^{1/2}nFcD^{1/2}}{2} \quad (12)$$

EXPERIMENTAL

Chemicals. The purity of the salts is important for both electrochemical and solubility measurements. Sodium chloride (p.a.) and cesium chloride (p.a. and "Suprapur") from E. Merck AG were employed. Prior to use the salts had to be further purified.

Sodium chloride was dried under vacuum while heating at 400 °C for two hours. The salt was then slowly recrystallized from the melt under nitrogen atmosphere. Only clear crystals were used.

Cesium chloride was purified as follows: The salt was dehydrated with HCl gas up to 400 °C over a period of ten hours, transferred to a quartz glass tube and melted under chlorine atmosphere. The salt was then cooled to about 50 °C below the melting point and evacuated. The chlorine saturation and evacuation were repeated three times and a perfectly clear melt resulted. The salt was then recrystallized from the melt in a quartz glass crucible. The chlorine saturation procedure was important in order to obtain reproducible solubility measurements.

All handling of purified salts were performed in an N_2-atmosphere glovebox where the water vapour level was constantly monitored and kept below 2 ppm.

Chlorine (>99.8 %) and nitrogen (>99.6 %) from Norsk Hydro a.s., Norway, was used for the electrochemical studies. The gas was passed through concentrated H_2SO_4 and P_2O_5 before entering the electrochemical cell. The gas was also passed over graphite heated to 900 °C in order to remove impurities in the gas that could react with the electrodes. Chlorine (>99.6 % in "lecture bottles") from J. T. Baker Chemicals, Netherlands, was used for purification of salts and for solubility measurements.

HCl gas (>99.8 %), for the drying of salts from Gerling, Holz & Co., FRG and argon (>99.99 %) from Norsk Hydro a.s., Norway, were used without further purification.

Electrochemical measurements. The electrochemical experiments were performed with a potentiostat/galvanostat (Model 551) together with an analog function generator (Model 566) and a multifunction interface (Model 563) from AMEL, Milano, Italy. When operating in galvanostatic mode a pulse generator (made in our workshop) was connected to a mercury-wetted relay in Model 551. This generator was introduced to cut the current at a certain time to prevent metal reduction at the working electrode.

A Tektronix 564 storage oscilloscope (Tektronix, Inc., Beaverton, Oregon) with a Polaroid Land CR-9 camera (Polaroid Corp. Cambridge, Massachusetts) and a Linseis LY 822 X–Y recorder with time base (Linseis GmbH, FRG) were used for data collection and storage.

A Kanthal-wound laboratory tube furnace with three heating zones was used.

The temperature was regulated with a Eurotherm PID regulator and measured with a Pt/Pt10 %Rh thermocouple under the cell close to the outside cell wall. The actual melt temperature was found by a calibration curve correlating melt temperature and temperature outside the cell.

The electrochemical cell was made of a 50 mm diameter quartz glass tube attached to a Pyrex glass cover by a ground conical joint. Electrodes and a quartz glass gas inlet tube were inserted through S.V.L. screw joints (Sovirel, France) equipped with bored caps and Teflon sealing rings for sliding joints. The upper part of the cell had a side arm for gas outlet. The gas line to the cell was made of Teflon tubing and of the neoprene-like rubber "ISO-Versinic". Connections to the cell and the drying trap were made by "Rotulex" flexible joints and "Torion" valves (Sovirel, France).

A three-electrode system was used. The working electrode was always constructed of a vitreous carbon rod (approx. 3 mm diameter, grade V-25 from Le Carbone-Lorraine, France, or grade GC-30 from Tokai Electrode Mfg. Co. Ltd., Japan). In most of the experiments at temperatures below 550 °C, a plane vitreous carbon working electrode, vacuum sealed into a Pyrex tube was used. After sealing, the end of the Pyrex tube was cut with a diamond cutting wheel. Emery paper was used to polish the plane surface of the electrode. A mirror finish was obtained by lapping with 0.06 micron alumina. Electrical connection to the vitreous carbon rod was made by a thin Pt-wire coiled around the rod before vacuum sealing. The surface area of the electrode

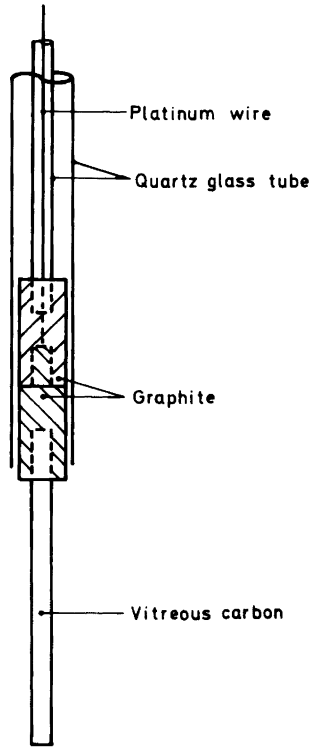

Fig. 1. Cylindrical working electrode.

was determined from the diameter of the vitrous carbon rod as measured by a micrometer screw.

For measurements at temperatures above the softening point of Pyrex glass this electrode could not be used.

A number of materials have been tried without success. Neither boron nitride nor ceramic adhesives gave proper seals with vitreous carbon.

Cylindrical working electrodes with the design shown in Fig. 1 have thus been adopted. The vitreous carbon rod, carefully polished, was press-fitted into a drilled hole at the end of a graphite rod. The electrode was held in place by a 3 mm diameter quartz glass tube through which a platinum wire made contact with the measuring instruments. A Tygon cap fastened the electrode support to a larger quartz glass tube. The working surface area of the electrode was determined from the depth of immersion (accuracy±0.01 mm) as measured by a calliper connected to the outer silica tube.

Both counter and reference electrodes were constructed from spectroscopic grade graphite rods (6 mm diameter, SPK, Union Carbide,

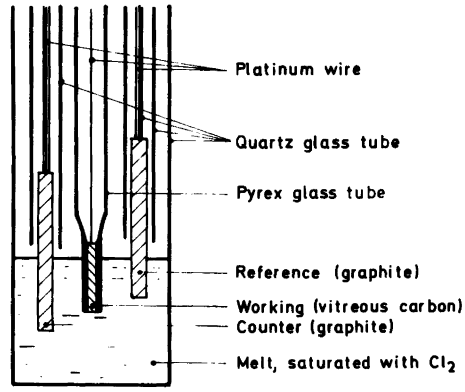

Fig. 2. Electrode assembly used in experiments where a plane working electrode was applied.

Chigaco, Illinois). The construction was similar to the cylindrical working electrode previously described (with the exception of the vitreous carbon rod). With Cl_2 in the melt, the reference electrode may act as a reversible chlorine electrode. The electrode assembly (plane working electrode) is shown schematically in Fig. 2.

Immediately before insertion into the cell the graphite electrodes were heated to a bright orange glow with a torch to remove impurities on the graphite surface. The electrodes were then inserted into the cell which was transferred to a glovebox. The cell was loaded and transferred to the furnace where the salt was melted under nitrogen atmosphere. Before introducing chlorine gas into the cell, cyclic voltammograms in the pure melt were recorded. These showed negligible background current (<50 μA cm^{-2}) within the actual potential range. Following this, the nitrogen was replaced by chlorine by bubbling the gas through the melt for at least three hours. After saturation a slow flow of Cl_2 was maintained above the melt surface. The same melt was used for electrochemical measurements up to two weeks.

Solubility measurements. The method used for measuring chlorine solubility is in principle the same as that used by Andresen,[3] Andresen *et al.*[4,5] and Carpio *et al.*[13] The apparatus which is shown schematically in Fig. 3 has, however, been modified since the previous studies.

Most of the apparatus is made of Pyrex glass, and the essential parts are the manometer (E), the reservoir or calibration bulb (C) and the container for molten salt (A).

The pressure is measured with a manometer (Model 145–01, Precision Pressure Gage, Texas

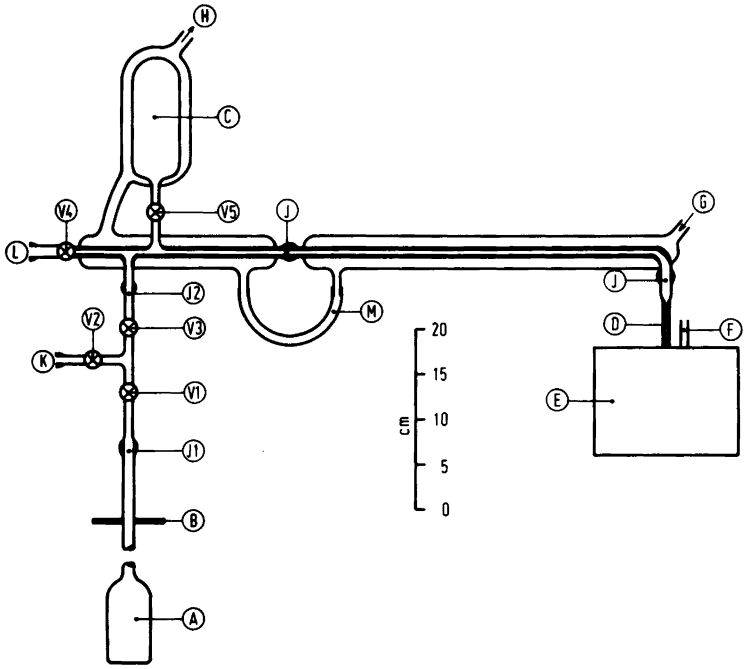

Fig. 3. Apparatus for chlorine solubility measurements. A – quarts glass cell, B – top plate of furnace, C – calibration volume bulb, D – capillary from the Bourdon tube, E – manometer, F – reference port (to vacuum pump), G and H – thermostated water inlet and outlet, respectively, K – vacuum line and gas (argon) inlet, L – chlorine gas inlet, M – plastic tube for thermostated water, v1, v2, v3 – "Interflon" valves, v4, v5 – "Torsion" valves, J – "Rotulex" flexible joints with Viton O-rings.

Instruments Inc., Houston, Texas) with a Bourdon Capsule (Type 800). The Bourdon Capsule assembly consists of a cylindrical case wherein a fused quartz Bourdon tube with attached mirror is mounted. The mirror rotates according to pressure changes within and outside the tube. The pressure gage measures the mirror rotation optically and displays the measurements as a direct pressure readout (in torr) on the digital counter. A data logger (Model 2242B, John Fluke Mfg. Co. Inc., Washington) together with a printer (Model 43, Teletype Corp., Skokie, Illinois) were connected to the external output of the manometer. A calibration curve correlated the output signals (mV) and the digital counter (torr). Pressure changes could also be followed with a strip chart recorder. The Bourdon capsule had no metal parts that could be attacked by chlorine. The solubility apparatus was connected to the pressure port of the Bourdon tube (D). The space surrounding the Bourdon tube was evacuated through the reference port (F) for absolute pressure measurements. A known pressure may also be applied to the reference port, permitting differential pressure measurements.

A Pyrex to quartz glass graded seal was fused to the pressure port capillary of the Bourdon tube (D). The different parts of the apparatus are connected by "Rotulex" flexible joints with Viton O-rings. The "Torion" and "Interflon" (G. Springham & Co. Ltd., Essex, England) valves are made with Teflon stems and keys, respectively. The arrangement of joints and valves allowed the cell to be loaded with salt in a glovebox, transferred to the furnace and connected to the apparatus without contact between atmospheric air and salt.

The container for molten salt (A) is made of quartz glass. A "Rotulex" flexible joint was welded to the end of the quartz glass stem by use of a Pyrex to quartz glass graded seal. A water-jacketed, thermostated (±0.02 °C) gas volume serves together with the volume above the melt as the known thermostated gas volume. The reservoir (C) was mainly used for volume calibration. As seen from Fig. 3, part of the gas volume was not thermostated (between B and J2). This part was insulated with styrofoam, and

the change in temperature in this part never exceeded ±0.5 °C during an experiment and a pressure correction could thus be neglected. A variable shunt for the upper zone of the furnace allowed adjustment of the temperature profile. The melt height in the container (A) was about 7 cm. A 6 °C temperature profile over this distance was established in order to impose convection in the melt during dissolution of chlorine.

After the cell had been loaded in the glovebox, valves v1, v2 and v3 (Fig. 3) were closed. The cell was then connected to the apparatus through joint J2, and evacuated. Valve v3 was closed and chlorine added to the rest of the apparatus, which was kept under chlorine pressure between measurements. The salts were then heated under vacuum and allowed to stand overnight for temperature equilibration (argon atmosphere).

By lowering the furnace, salt which had condensed in the neck could be drained back into the cell by melting it with a hand torch.

An experiment started by evacuating the cell (P^{l}_{eq}=0). Valve v1 was then closed, valve v3 opened and the chlorine pressure adjusted to 900–1000 Torr (valve v5 open). The pressure, P_i, was recorded on the teleprinter kept in the continuous scan mode. Valve v1 was opened allowing the gas to expand into the cell. The pressure was recorded each fourth second and appeared to be nearly constant within the 10–40 s period after the opening of valve v1. An average value of P_o for this period is used in the further calculations. The following pressure decrease was recorded on the strip chart recorder. The valve v5 was closed after the determination of P_o. The equilibrium pressure, P^{u}_{eq}, was assumed to be reached when no further change was observed in pressure (after 1–3 h). P^{u}_{eq} was determined as the average value of ten continuous recorded values on the teleprinter. A volume calibration procedure was performed with Cl_2 (g) to obtain the unknown volume of gas above the melt, V_o.[3]

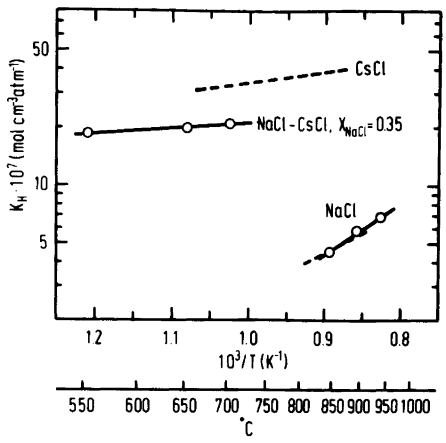

Fig. 4. Semilogarithmic plots of K_H *versus* inverse temperature. The dashed lines are results given by Andresen *et al.*[4]

The degassing procedure was as follows: The salt was cooled to about 20 °C above the freezing point, the cell evacuated (valve v3 closed) and the chlorine gas "boiled out" of the melt. The melt was then cooled to 10 °C below the freezing point and then slowly melted again while pumping. Two freeze-melt cycles were necessary to degas the melt. After the degassing procedure, the salt and apparatus were ready for a new solubility measurement.

RESULTS AND DISCUSSION

Chlorine solubilities. The solubilities of chlorine in a fused NaCl–CsCl mixture have been determined in order to calculate the diffusion coefficients of chlorine. For comparison with

Table 1. Solubility of chlorine in molten alkali chlorides.

System	Temperature (°C)	$(K_H \pm SD)10^7$ (mol cm^{-3}atm^{-1})
NaCl	846	4.54±0.19
	892	5.87±0.17
	937	6.86±0.50
NaCl–CsCl	554	18.5±0.7
	652	19.8±0.2
X_{NaCl} = 0.35	701	21.0±0.3

Table 2. Standard enthalpy for the dissolution of Cl_2 in molten alkali chlorides.

System	ΔH_d° (kJ mol^{-1})
NaCl	50.7±8.5
NaCl–CsCl (X_{NaCl}=0.35	5.6±1.3
CsCl (Andresen *et al.*[4])	11.1±1.9

literature data, solubility measurements in NaCl were also performed.

The Henry's law constants, K_H, are determined by eqn. (5). The mean values of K_H with standard deviation are given in Table 1.

According to eqn. (4) a linear relationship exists between the logarithm of the chlorine solubility and the inverse temperature. The enthalpy of dissolution can be determined from the slope of this curve while the intercept with the *Y*-axis defines the entropy of dissolution. Fig. 4 shows semilogarithmic plots of K_H (mean values) *versus* inverse temperature. Straight lines are obtained showing that the solubilities increase with increasing temperature. For comparison selected literature data[3,4] are included (dashed lines).

Linear regression analysis of the experimental data gives the following equations:

NaCl:

$$\log K_H = -3.973 - 2646/T \quad (13)$$

NaCl–CsCl(X_{NaCl}=0.35):

$$\log K_H = -5.384 - 290.4/T \quad (14)$$

CsCl (Andresen *et al.*[4]):

$$\log K_H = -4.882 - 581.3/T \quad (15)$$

The relative standard deviation in K_H calculated from eqns. (13) and (14) is 8 % and 2.8 %, respectively. From these equations and eqn. (4) the standard enthalpy of dissolution is calculated, and the values are presented in Table 2.

For NaCl ΔH_d° is about 40 % higher than reported by Andresen *et al.*[4] However, it is in close agreement with the value calculated by Andresen *et al.*[4] from data given by Ryabukhin and Bukun.[14]

The values of K_H in NaCl at low temperatures (801–850 °C) are in good agreement with previous work.[3,4] Due to the 40 % difference in the ΔH_d° value, the deviation in K_H becomes 12 % at 950 °C. Ryabukhin and Bukun,[14] using the stripping method, report about 40 % lower values of K_H compared with the present results. The low value for ΔH_d° in NaCl–CsCl eutectic is not surprising as the value in pure CsCl is as low as 11 kJ mol^{-1}.[3,4] In binary alkali chloride mixtures it has been observed that ΔH_d° is lower than in the respective pure chlorides.[15–17]

Diffusion coefficients of chlorine. Chronopotentiometric measurements have been performed in NaCl, CsCl and NaCl–CsCl melts saturated with chlorine. Representative cathodic chronopotentiometric curves are shown in Fig. 5.

Plots of $\tau^{1/2}$ *versus* inverse current were linear at all temperatures. Examples of such plots are shown in Fig. 6. As the curves also pass close to the origin, eqn. (6) is valid, *i.e.* a single diffusion controlled reaction is observed. For experiments using a plane working electrode, the diffusion coefficients of chlorine are thus determined from the mean values of $i\tau^{1/2}$ at each temperature (i is the current density). According to eqn. (9) a

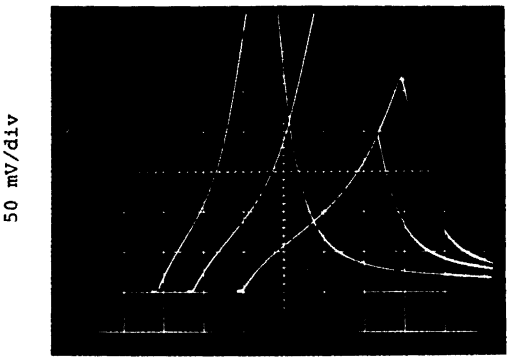

Fig. 5. Chronopotentiometric curves for the reduction of Cl_2 at a cylindrical electrode in molten CsCl at 677 °C. The starting point is shifted to the right for each curve. I=35, 30 and 25 mA.

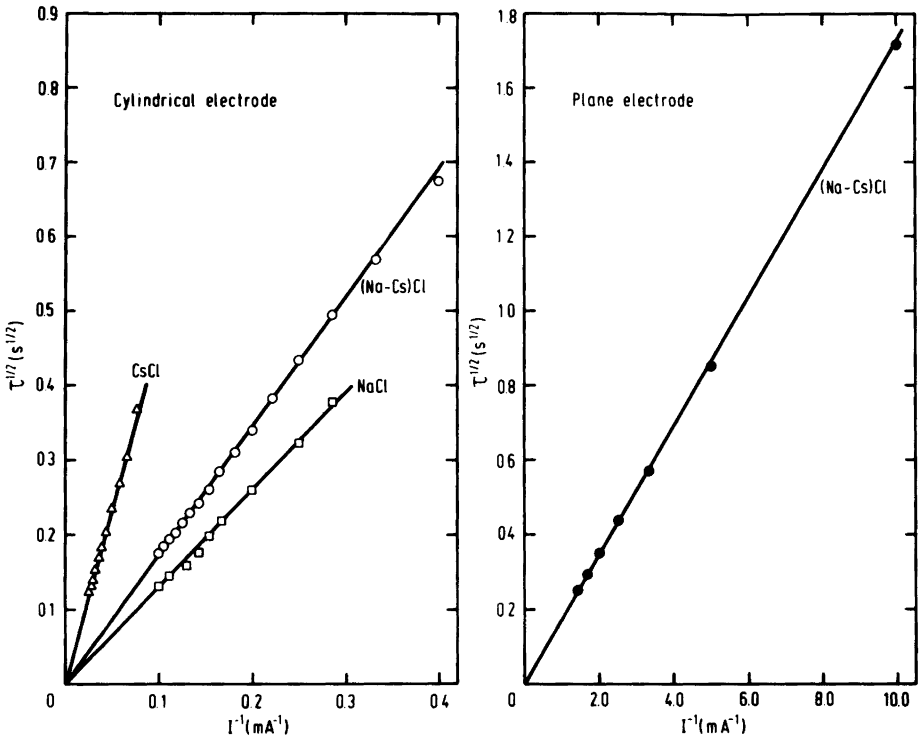

Fig. 6. Test of the Sand equation for the reduction of Cl_2 at vitreous carbon electrodes. Δ: 677 °C, A_{geo}=0.585 cm,^{2} ○: 512 °C, A_{geo}=0.523 cm^2, □: 827 °C, A_{geo}=1.013 cm^2, ●: 512 °C, A_{geo}=0.0535 cm^2.

linear relationship exists between $I\tau^{1/2}$ and A_{geo} when cylindrical working electrodes are used. A_{geo} is the surface area determined from the immersion depth of the working electrode. Typical plots are shown in Fig. 7 where the mean value of $I\tau^{1/2}$ at each immersion depth is plotted *versus* the corresponding electrode surface area. The chronopotentiometric constant, $i\tau^{1/2}$, is given by the slope of this curve [eqn. (11)]. The value of $i\tau^{1/2}$ at each temperature was determined by linear regression analysis of the data.

Calculated values of $i\tau^{1/2}$ and values of the diffusion coefficients of chlorine are presented in Table 3. The diffusion coefficients, D, are determined from the Sand equation [eqn. (6)] where the concentration c is the chlorine solubility given by eqns. (13) – (15). As the overall electrochemical reaction is

$$Cl_2+2e^-\rightarrow 2Cl^- \qquad (16)$$

n in eqn. (6) is equal to 2.

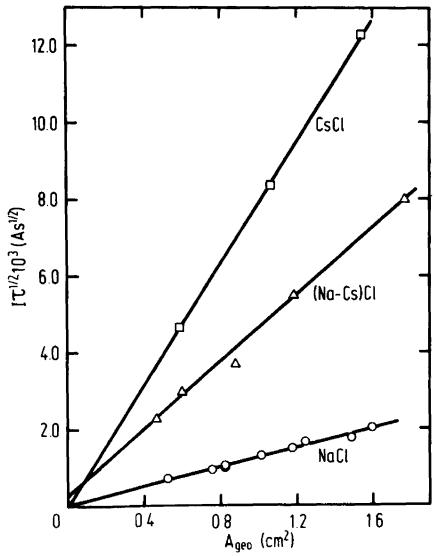

Fig. 7. Mean values of $I\tau^{1/2}$ *versus* corresponding cylindrical electrode area, A_{geo}. □: 677 °C, Δ: 647 °C, ○: 827 °C

Table 3. Diffusion coefficients of chlorine in molten alkali chlorides determined from chronopotentiometric measurements.

System	Temperature (°C)	Working electrode	Chronopot. constant $(i\tau^{1/2}\pm SD)10^3$ (A cm^{-2} s$^{1/2}$)	Number of curves	Diff. coeff. $(D\pm SD)10^5$ (cm^2 s^{-1})
NaCl	827	cylindrical	1.25±0.02	99	30.6±1.0
	887	cylindrical	1.55±0.01	62	26.5±0.3
CsCl	677	cylindrical	8.01±0.04	58	21.3±0.2
	777	cylindrical	9.91±0.07	45	24.9±0.4
	880	cylindrical	11.76±0.09	40	28.0±0.4
NaCl–CsCl	512	plane	3.23±0.02	27	11.5±0.1
X_{NaCl}=0.35	512	cylindrical	3.16±0.06	61	11.0±0.4
	647	cylindrical	4.38±0.05	73	16.4±0.4
	797	cylindrical	4.89±0.05	37	16.7±0.3

Both cylindrical and plane working electrodes have been applied for NaCl–CsCl eutectic mixture at 512 °C. The two electrodes gave the same result within the experimental uncertainty.

This confirms that corrections for the cylindricity of the diffusion field may be neglected for certain conditions of electrolysis.

The temperature dependence of the diffusion coefficient is well-described by the Arrhenius-type equation

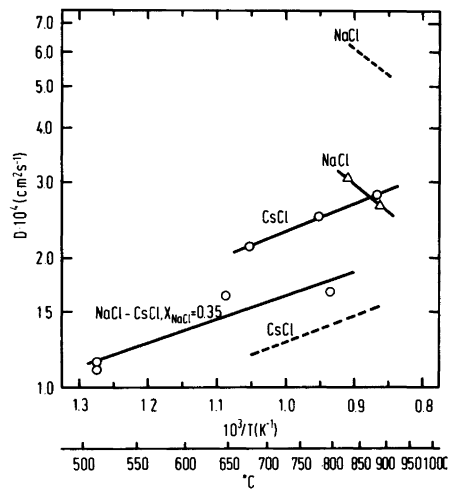

Fig. 8. Semilogarithmic plots of the diffusion coefficient of dissolved Cl_2 as function of inverse temperature. The dashed lines are calculated from data given by Leonova *et al.*[7]

$$D=D_0 \exp(-E_a^D/RT) \quad (17)$$

where D_0 is a pre-exponential factor, and E_a^D is the activation energy of the diffusion process. Fig. 8 shows semilogarithmic plots of D *versus* inverse temperature. For comparison, selected literature data[7] are included (dashed lines).

Linear regression analysis of the data given in Table 3 gives the following equations:

NaCl:

$$\log D = -4.722+1329/T \quad (18)$$

CsCl:

$$\log D = -2.995-642/T \quad (19)$$

NaCl–CsCl (X_{NaCl}=0.35):

$$\log D = -3.233-553/T \quad (20)$$

The relative standard deviation in D calculated by eqns. (19) and (20) is 1 and 9 %, respectively. For NaCl the diffusion coefficient is determined at two temperatures only, and no standard deviation is given. The activation energies of diffusion, E_a^D, are in fair agreement with literature data (Table 4).

For a diffusion-controlled process a positive energy of activation is expected. The observed negative value of E_a^D for NaCl, calculated from two temperatures only, does not necessarily have a real physical meaning. This will be discussed later.

Table 4. Activation energy of diffusion of chlorine in molten alkali chlorides.

System	E_a^D (kJ mol^{-1})	
	Present work	Leonova *et al.*[7]
NaCl	-25.4	-22.9
CsCl	12.3±0.4	11.8
NaCl–CsCl (X_{NaCl}=0.35)	10.6±2.9	

Diffusion coefficients of Cl_2 in pure NaCl and CsCl do not agree with literature data.[7] This discrepancy may be due to the fact that different solubility data are used in the calculations. When one set of solubility data is used to recalculate the diffusion coefficients of chlorine, improved agreement is obtained.

The relatively high diffusion coefficients of chlorine in molten alkali chlorides have been explained by a chain conduction of the Grotthus' type.[7,15–20] When chlorine is dissolved in the melts the equilibrium

$$Cl_2 + Cl^- \rightleftarrows Cl_3^- \quad (21)$$

is assumed to be established. The chain conduction is possible if a Cl_3^- ion transfers a Cl_2 molecule to an adjoining Cl^- ion which then becomes a Cl_3^- ion, *i.e.*

$$Cl_2 + Cl^- \rightarrow Cl_3^- \rightarrow Cl^- + Cl_2 \quad (22)$$

The net effect is transport of chlorine molecules. Kowalski and Harrington[21] and Baibakov *et al.*[22] found a rapid exchange between the chlorine gas and $^{36}Cl^-$ isotopes in molten $PbCl_2$–KCl and LiCl–NaCl.

Leonova *et al.*[7] and Ukshe *et al.*[20] claim that the diffusion process [eqn. (22)] is assumed to occur most readily in fused salts with small cations (Li^+, Na^+) where dense packing allows anion–anion contact. For larger cations, such contact becomes more difficult, *i.e.* lower diffusion coefficients. The negative value of E_a^D (NaCl) is thus explained as due to increased tendency to form molecular pairs of the type (Na^+Cl^-) when the temperature increases. This reduces the possibility for anion–anion contact, *i.e.* the diffusion coefficient of chlorine will decrease with increasing temperature. For salts with large cations (K^+, Cs^+), the possibility of anion–anion contact increases with increasing temperature due to increased vibrational movement and disturbance of the melt structure. A positive value of E_a^D is therefore found for these melts.

The postulated increased tendency to form molecular pairs of the type (Na^+Cl^-) at the actual temperature does not seem to be plausible. No anomality has been observed in the viscosity of the pure alkali chlorides[23] and approximately the same temperature dependence is found for the viscosities of both NaCl and CsCl. This implies that a positive energy of activation should be expected whatever the cation of the chloride melt and should indicate that the explanation given by Leonova *et al.*[7] to justify the negative value of E_a^D could be no longer valid. The apparent agreement of the activation energies for the Cl_2 diffusion in NaCl melts found in this work and in Ref. 7 is probably fortuitous and both data could be affected by uncertainties in solubility data and/or electrochemical measurements.

According to Ukshe *et al.*[20] the diffusion coefficients of chlorine in pure alkali chlorides exceed the self-diffusion coefficients of Cl^- by 1.5–2 orders of magnitude. The values of the self-diffusion coefficients used by Ukshe *et al.*[20] (taken from Bockris and Hooper[24]) are, however, a factor of ten too low. According to Bockris and Hooper, D_{Cl^-} in NaCl; increases from $0.7 \cdot 10^{-4}$ to $1.1 \cdot 10^{-4}$ cm^{2}s^{-1} in the temperature range 840–980 °C, while in CsCl D_{Cl^-} increases from $0.4 \cdot 10^{-4}$ to $0.6 \cdot 10^{-4}$ cm^{2}s^{-1} (670–790 °C). Grjotheim *et al.*[25] give slightly higher tracer diffusion coefficients of $^{36}Cl^-$ in NaCl; $9.7 \cdot 10^{-5}$ cm^{2}s^{-1} and $1.2 \cdot 10^{-4}$ cm^{2}s^{-1} at 810 and 912 °C, respectively. In KCl and $CaCl_2$ at 810 °C Tørklep[26] determined D_{Cl^-} to be $8.9 \cdot 10^{-5}$ cm^{2}s^{-1} and $3.8 \cdot 10^{-5}$ cm^{2}s^{-1}, respectively.

The present results (Fig. 8) indicate that the

diffusion coefficient of Cl_2 does not vary markedly from an NaCl to a CsCl melt, and the observed differences are within the experimental uncertainties. The values of D in these melts are *ca.* 3 times higher than the self-diffusion coefficients of Cl^-.

As slightly higher values of the chlorine diffusion coefficients are measured in alkali chlorides compared with the self-diffusion coefficients of Cl^-, the transport of molecular chlorine may occur by a chain conduction mechanism [eqn. (22)]. In any case, the transport does not seem to be sentitive to the size of the alkali cation. This is in agreement with data on the diffusion of iodine in fused alkali iodides where approximately the same value of D ($\sim 8 \cdot 10^{-5}$ cm^2s^{-1} at 700 °C)[27] was found in both NaI, KI and CsI.

Acknowledgements. Experimental assistance of Bente Faaness and Bjarte Haugsdal is gratefully acknowledged. This work has been supported financially by *Norsk Hydro a.s.* and *Norges Teknisk Naturvitenskapelige Forskningsråd* and also partly by a NATO Research Grant SA. 5-2-05B(808)372(74–77) for a cooperation program between the Institute of Inorganic Chemistry, the Norwegian Institute of Technology and the Institute of Analytical Chemistry, the University of Bari.

REFERENCES

1. Aarebrot, E., Andresen, R. E., Østvold, T. and Øye, H. A. *Light Metals 1977,* 106th AIME Annual Meeting, Atlanta 1977, Vol. 1, p. 491.
2. Østvold, T. and Øye, H. A. *Light Metals 1980,* 109th AIME Annual Meeting, Las Vegas 1980, p. 937.
3. Andresen, R. E. *Thesis,* Universitetet i Trondheim, Norges tekniske høgskole, Institutt for uorganisk kjemi, Trondheim 1976.
4. Andresen, R. E., Østvold, T. and Øye, H. A. In Pemsler, J. P., Braunstein, J., Morris, D. R., Nobe, K. and Richards, N. E., Eds., *Proc. Int. Symp. Molten Salts,* The Electrochem. Soc., Princeton, N.J. 1976, p. 111.
5. Andresen, R. E., Paniccia, F., Zambonin, P. G. and Øye, H. A. *Proc. 4th Nordic High Temp. Symp. – NORTEMPS – 75,* Vol. 1, p. 127.
6. Delahay, P. *New Instrumental Methods in Electrochemistry,* Interscience, New York 1954.
7. Leonova, L. S., Ryabukhin, Yu.M. and Ukshe, E. A. *Sov. Electrochem. 5* (1969) 190.
8. Delahay, P. and Berzins, T. *J. Am. Chem. Soc. 75* (1953) 2486.
9. Delahay, P. and Mamantov, G. *Anal. Chem. 27* (1955) 478.
10. Reinmuth, W. H. *Anal. Chem. 33* (1961) 485.
11. Russel, C. D. and Peterson, J. M. *J. Electroanal. Chem. 5* (1963) 467.
12. Peters, D. G. and Lingane, J. J. *J. Electroanal. Chem. 2* (1961) 1.
13. Carpio, R. A., King, L. A., Ratvik, A. P., Østvold, T. and Øye, H. A. *Light Metals 1981,* 110th AIME Annual Meeting, Chicago 1981, p. 325.
14. Ryabukhin, Yu.M. and Bukun, N. G. *Russ. J. Inorg. Chem. 13* (1968) 597.
15. Van Norman, J. D. and Tivers, R. J. In Mamantov, G., Ed., *Symp. on Characterization and Analysis of Molten Salts,* Dekker, New York 1969, p. 509.
16. Nekrasov, V. N., Biryukov, V. A., Ivanovskii, L. E. and Mironov, V. S. *Tr. Inst. Elektrokhim. Ural. Nauchn. Tsentr. Akad. Nauk. SSSR 27* (1978) 57.
17. Lenova, L. S., Ryabukhin, Yu.M. and Ukshe, E. A. *Sov. Electrochem. 5* (1969) 424.
18. Lenova, L. S. and Ukshe, E. A. *Sov. Electrochem. 6* (1970) 871.
19. Ukshe, E. A. and Leonova, L. S. *Sov. Electrochem. 6* (1970) 1376.
20. Ukshe, E. A., Leonova, L. S., Yavonova, G. N. and Bukun, N. G. *Sov. Electrochem. 7* (1971) 373.
21. Kowalski, M. and Harrington, G. W. *Inorg. Nucl. Chem. Lett. 3* (1967) 121.
22. Baibakov, D. P., Kukushkin, Yu.N. and Golosov, V. V. *Fiz. Khim. Elektrokhim. Rasplavl. Solei Tverd. Electrolitov. 1* (1973) 117.
23. Brockner, W., Tørklep, K. and Øye, H. A. *J. Chem. Eng. Data 26* (1981) 250.
24. Bockris, J.O'M. and Hooper, G. W. *Discuss. Faraday Soc. 32* (1961) 218.
25. Grjotheim, K., Naterstad, T., Tørklep, K. E. and Øye, H. A. *Electrochim. Acta 23* (1978) 451.
26. Tørklep, K. *Thesis,* Universitetet i Trondheim, Norges tekniske høyskole, Institutt for uorganisk kjemi, Trondheim 1972.
27. Ivanovskii, L. E., Nekrasov, V. I., Biryukov, V. A. and Mironov, V. S. *Sov. Electrochem. 11* (1975) 1285.

Received July 20, 1982.

Acta Chemica Scandinavica A 37 (1983) 219–225

A Planar, Four-coordinate Se(II) Compound. The Preparation and Crystal Structure of Bis(imidotetraphenyldithiodiphosphino-*S,S'*)selenium(II)

STEINAR HUSEBYE and KNUT MAARTMANN-MOE

Department of Chemistry, University of Bergen, N-5014 Bergen-Univ., Norway

Bis(imidotetraphenyldithiodiphosphino-*S,S'*)-selenium(II), $[Se\{N(Ph_2PS)_2\}_2]$ has been prepared from $NH_4^+N(Ph_2PS)_2^-$ and $[Se\{(EtO)_2PS_2\}_2]$ in methanol. Its crystal structure has been determined by X-ray crystallographic methods. Unit cell dimensions are a=10.703(1), b=13.760(2), c=17.499(3) Å, α=112.00(1), β=90.81(1), γ=91.31(1)°, Z=2.

Full matrix least squares refinement of 5064 observed reflections resulted in an R-value of 0.044. The triclinic crystals, space group $P\bar{1}$, are built up of four-coordinate Se(II) complexes. The SeS_4 coordination sphere is roughly trapezoid planar with selenium forming a long and a short bond to each bidentate ligand. Se–S bond lengths are Se–S1=2.264(1) Å, Se–S2=2.948(1) Å, Se–S3=2.270(1) Å and Se–S4=3.054(1) Å. For the intraligand S–Se–S angle, an average value of 84.0(2)° was found.

It has previously been shown that divalent selenium and tellurium have a great tendency to form trapezoid planar complexes with bidentate dithio ligands having small bites. In such compounds the ligands are anisobidentate, *i.e.* each ligand forms one strong and one weak bond to either the same central atom (class I), or two separate central atoms (weakly bonded polymers, class II).[1] Recent structural work on bis(imidotetraphenyldithiodiphosphino-*S,S'*)-tellurium(II) demonstrated that it was possible to form true square planar complexes of divalent tellurium with bidentate ligands with large bites (class V complexes).[2] The present investigation was undertaken to see if divalent selenium also could form square planar complexes with such ligands.

EXPERIMENTAL

Preparation of complex. The ammonium salt of the ligand, $L=N(Ph_2PS)_2^-$, was prepared by published procedures.[3,4] To 0.29 g (0.45 m mol) of bis(diethyldithiophosphato)selenium(II), $[Se\{(EtO)_2PS_2\}_2]$[5] dissolved in 40 ml methanol, was added 0.47 g (1.0 mmol) of ligand salt dissolved in 80 ml methanol. A yellow precipitate formed. It was filtered off and washed with cold ethanol and ether. Yield 90 % based on selenium compound added, m.p. 190–192 °C (decomp). Large, flat, light yellow prisms formed upon recrystallization from carbon disulfide.

Formation of Se_2S_6 upon decomposition of complex. The complex was very soluble in slightly polar solvents such as CH_2Cl_2 and $CHCl_3$. Attempts at recrystallization from such solvents resulted in orange crystals of poor quality. A preliminary X-ray investigation of the crystals from $CHCl_3$ showed that they corresponded to the Se_2S_6 phase with the disordered structure previously found by Laitinen, Niinistö and Steudel.[6]

X-Ray data. All data were measured on an Enraf-Nonius CAD-4 diffractometer. The crystal used for data collection had approximate dimensions 0.16×0.18×0.32 mm^3. Unit cell parameters were found from least squares refinement of the setting angles of 25 high-angle reflections. They are a=10.703(1), b=13.760(2), c=17.499(3) Å, α=112.00(1), β=90.81(1), γ=91.31(1)°, Z=2, D_m=1.34 gcm^{-3}, D_x=1.36 gcm^{-3}, μ(Mo$K\alpha$)=11.8 cm^{-1}. The space group is $P1$ (No. 1) or $P\bar{1}$ (No. 2).

Intensity data were collected using an ω-scan with scan width (1.00+0.35 tg θ)°, a graphite monochromator and Mo$K\alpha$ radiation. The scan

0302-4377/83 $2.50

Table 1. Atomic coordinates in fractions of cell edges with standard deviations.

Atom	*x*	*y*	*z*
Se	0.23853(4)	–0.00557(3)	0.24914(3)
S1	0.0568(1)	–0.06507(9)	0.28293(7)
S2	0.3304(1)	–0.21219(10)	0.23390(8)
S3	0.1682(1)	0.14549(9)	0.24251(7)
S4	0.4944(1)	0.08338(10)	0.22881(8)
P1	0.0035(1)	–0.17487(8)	0.16804(7)
P2	0.2476(1)	–0.27558(8	0.12428(7)
P3	0.2332(1)	0.24814(9	0.35698(7)
P4	0.4998(1)	0.18970(9)	0.34152(7)
N1	0.1036(3)	–0.2514(3)	0.1167(2)
N2	0.3726(3	0.2427(3)	0.3807(2)
C111	–0.0651(4)	–0.1066(3)	0.1090(2)
C112	–0.1394(5)	–0.0205(4)	0.1453(3)
C113	–0.1993(5)	0.0253(4)	0.0975(3)
C114	–0.1857(5)	–0.0148(4)	0.0144(3)
C115	–0.1117(6)	–0.0981(4)	–0.0221(3)
C116	–0.0502(5)	–0.1444(3)	0.0249(3)
C121	–0.1199(4)	–0.2474(3)	0.1948(3)
C122	–0.2412(5)	–0.2176(4)	0.2041(4)
C123	–0.3314(5)	–0.2786(5)	0.2243(4)
C124	–0.2979(6)	–0.3685(5)	0.2315(4)
C125	–0.1780(7)	–0.3984(4)	0.2223(4)
C126	–0.0879(6)	–0.3386(4)	0.2048(3)
C211	0.3297(4)	–0.2431(3)	0.0469(3)
C212	0.2901(5)	–0.2917(4)	–0.0349(3)
C213	0.3546(7)	–0.2692(5)	–0.0943(3)
C214	0.4518(7)	–0.2020(5)	–0.0747(4)
C215	0.4894(6)	–0.1534(4)	0.0050(4)
C216	0.4310(5)	–0.1736(4)	0.0677(3)
C221	0.2574(4)	–0.4162(3)	0.0877(3)
C222	0.3718(5)	–0.4619(4)	0.0858(3)
C223	0.3792(5)	–0.5695(4)	0.0580(4)
C224	0.2756(5)	–0.6325(4)	0.0313(4)
C225	0.1627(6)	–0.5884(4)	0.0316(4)
C226	0.1540(5)	–0.4808(4)	0.0590(3)
C311	0.1351(4)	0.2554(3)	0.4317(2)
C312	0.0086(4)	0.2041(4)	0.4156(3)
C313	–0.0649(5)	0.1805(4)	0.4708(3)
C314	–0.0127(5)	0.1783(4)	0.5415(3)
C315	0.1121(5)	0.2019(4)	0.5595(3)
C316	0.1873(5)	0.2249(4)	0.5042(3)
C321	0.2008(4)	0.3729(3)	0.3513(3)
C322	0.1399(5)	0.4494(4)	0.4118(3)
C323	0.1243(6)	0.5473(4)	0.4084(4)
C324	0.1674(6)	0.5672(4)	0.3436(4)
C325	0.2252(8)	0.4930(4)	0.2824(4)
C326	0.2427(7)	0.3958(4)	0.2862(3)
C411	0.6062(4)	0.2974(3)	0.3489(3)
C412	0.7239(5)	0.2789(4)	0.3178(3)
C413	0.8072(5)	0.3621(5)	0.3257(3)
C414	0.7705(6)	0.4619(4)	0.3634(4)
C415	0.6552(7)	0.4798(4)	0.3931(5)
C416	0.5724(6)	0.4001(4)	0.3872(4)
C421	0.5649(4)	0.1393(3)	0.4153(3)
C422	0.5760(5)	0.2042(4)	0.4967(3)
C423	0.6229(6)	0.1656(5)	0.5533(3)
C424	0.6607(6)	0.0654(5)	0.5299(4)

Table 2. Interatomic distances (Å) with standard deviations.

Se–S1	2.264(1)	P3–C311	1.799(4)
Se–S2	2.948(1)	P3–C321	1.798(4)
Se–S3	2.270(1)	P4–C411	1.813(5)
Se–S4	3.054(1)	P4–C421	1.816(5)
S1–P1	2.074(2)	S1–S2	3.529(2)
S2–P2	1.972(2)	S3–S4	3.604(2)
S3–P3	2.071(2)	S1–S3	3.423(2)
S4–P4	1.966(2)	S2–S4	4.425(2)
P1–N1	1.561(3)	P1–P2	2.960(1)
P2–N1	1.598(3)	P3–P4	2.971(2)
P3–N2	1.554(3)	S1–P2	3.831(2)
P4–N2	1.598(3)	S2–P1	3.775(2)
P1–C111	1.796(4)	S3–P4	3.862(2)
P1–C121	1.808(4)	S4–P3	3.827(2)
P2–C211	1.811(5)	Se–N1	3.564(3)
P2–C221	1.803(4)	Se–N2	3.581(3)

rate varied between 6.7 and 1.5° min^{-1}. Out of a total of 8392 unique reflections with $2\theta \leq 50°$, 5064 had $I \geq 2\sigma(I)$ and were treated as observed. The intensities were corrected for absorption (transmission factor range 0.81–0.87). More details about data collection and computer programs used in this investigtion can be found in a previous paper.[7]

IR spectrum. An IR spectrum of the crystals was obtained, using a Perkin-Elmer 683 instrument and the CsI disc technique.

Table 3. Bond angles (°) with standard deviations.

S1–Se–S2	84.14(4)	S3–P3–C311	106.30(14)
S1–Se–S3	98.06(5)	S3–P3–C321	101.53(15)
S1–Se–S4	172.01(4)	N2–P3–C311	109.35(20)
S2–Se–S3	172.47(4)	N2–P3–C321	111.24(20)
S2–Se–S4	94.99(4)	C311–P3–C321	110.09(20)
S3–Se–S4	83.83(5)	S4–P4–C411	110.53(16)
Se–S1–P1	99.16(5)	S4–P4–C421	111.93(17)
Se–S2–P2	89.75(5)	N2–P4–C411	105.60(20)
Se–S3–P3	98.50(5)	N2–P4–C421	105.14(20)
Se–S4–P4	93.52(5)	C411–P4–C421	103.71(20)
S1–P1–N1	118.22(13)	P1–C111–C112	121.5(4)
S2–P2–N1	117.59(14)	P1–C111–C116	119.2(3)
S3–P3–N2	117.93(14)	P1–C121–C122	123.6(4)
S4–P4–N2	118.69(14)	P1–C121–C126	117.1(4)
P1–N1–P2	139.13(22)	P2–C211–C212	118.4(4)
P3–N2–P4	140.98(23)	P2–C211–C216	121.2(4)
S1–P1–C111	108.10(14)	P2–C221–C222	120.3(4)
S1–P1–C121	101.38(14)	P2–C221–C226	121.6(3)
N1–P1–C111	110.27(19)	P3–C311–C312	120.5(3)
N1–P1–C121	110.10(20)	P3–C311–C316	119.9(3)
C111–P1–C121	108.09(19)	P3–C321–C322	122.6(4)
S2–P2–C211	112.07(18)	P3–C321–C326	119.7(4)
S2–P2–C221	109.41(15)	P4–C411–C412	120.8(4)
N1–P2–C211	107.11(20)	P4–C411–C416	121.2(4)
N1–P2–C221	106.55(19)	P4–C421–C422	119.2(4)
C211–P2–C221	102.98(20)	P4–C421–C426	120.7(4)

STRUCTURE DETERMINATION

The structure was solved by means of conventional heavy atom techniques and refined by least-squares full-matrix methods. The choice of $P\bar{1}$ as the proper space group was supported by the subsequent successful refinement. Anisotropic temperature factors were used for all atoms except hydrogen. The hydrogen positions were calculated and the hydrogen atoms included in the final refinement cycles with fixed positions and a constant temperature factor (B=8.0 Å^2); the value is the average found in the initial refinements with H included. The final R=0.044, while R_w with p=0.02 was 0.042. The error in an observation of unit weight was 1.235. A difference map showed no peaks above 0.4 e/Å^3. Tables of thermal parameters and observed and calculated structure factors are available from the authors upon request. Final atomic coordinates are shown in Table 1.

RESULTS

Interatomic distances and angles are listed in Tables 2 and 3. Molecular planes and interplanar angles are shown in Table 4. Fig. 1 shows the bis(imidotetraphenyldithiodiphosphino-*S,S'*)-selenium(II) molecule (SeL_2) seen roughly along the normal to the SeS_4 coordination plane (a), and also at approximately right angles to the above normal, (b). In Fig. 2, the SeS_4 coordination sphere is shown. For comparison, the TeS_4 group of the corresponding tellurium(II) complex and the SeS_4 groups of $[Se(CH_3OCS_2)_2]$[1] and $Se(Et_2NCS_2)_2$ is included in the figure. The packing of the molecules is indicated in Fig. 3. From the figures, it is seen that the structure is built up of separate SeL_2 molecules. Each selenium atom is coordinated to all four sulfur atoms of the molecule in a trapezoid planar configuration with greatly asymmetric Se–S bonds.

DISCUSSION

The SeS_4 group. The SeS_4 molecular core is roughly planar, with all atoms within 0.19 Å of its least squares plane. There are two short Se–S bonds, Se–S1=2.264(1) and Se–S3=2.270(1) Å. *Trans* to these, at an average angle of 172.24(33)° there are two long, weak bonds, Se–S2=2.948(1) and Se–S4=3.054(1) Å. The *intra*-ligand S–Se–S angles are both close to 84°, while the *inter*-ligand

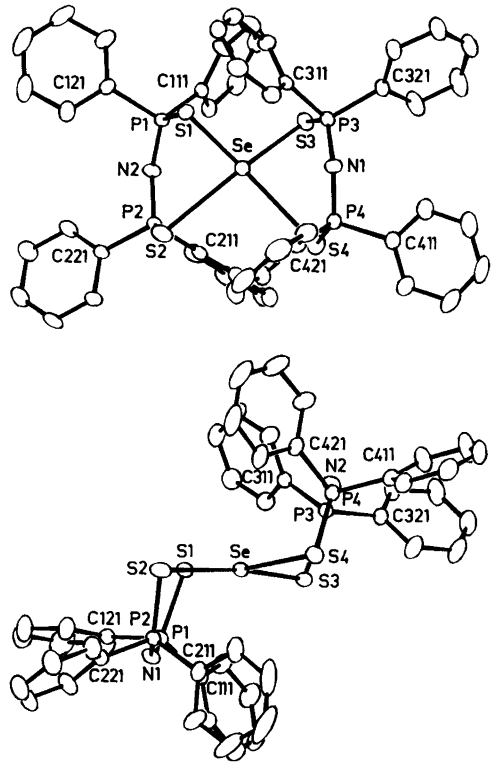

Fig. 1. a. The bis(imidotetraphenyldithiodiphosphino-*S,S'*)selenium(II) molecule as seen along the normal to the SeS1S2 plane. b. The complex molecule seen at right angles to the normal in 1a along a line approximately bisecting angle S1–Se–S3.

angles, S1–Se–S3 and S2–Se–S4 are close to 98 and 95°, respectively.

Since there are no intermolecular secondary bonds, this compound is best classified as a class I complex. From Fig. 2, it can clearly be seen that SeL_2 with respect to Se–S bond lengths is intermediate between a class I and a class II complex and that it is much closer to a class II complex with respect to Se–S bond angles. The average Se–S bond length is 2.634 Å as compared to 2.54 Å, the normal value for a class I complex[8] and 2.21 Å, the sum of Paulings covalent radii. From Fig. 2, the difference in the MS_4 groups (M=Te,Se) of SeL_2 and TeL_2 are clearly seen. While M–S bond angles are similar, there is only a slight asymmetry in the Te–S bonds ($\triangle$=0.02 Å) as compared to the great asymmetry in the Se–S bonds ($\triangle$=0.73 Å). In both complexes, the

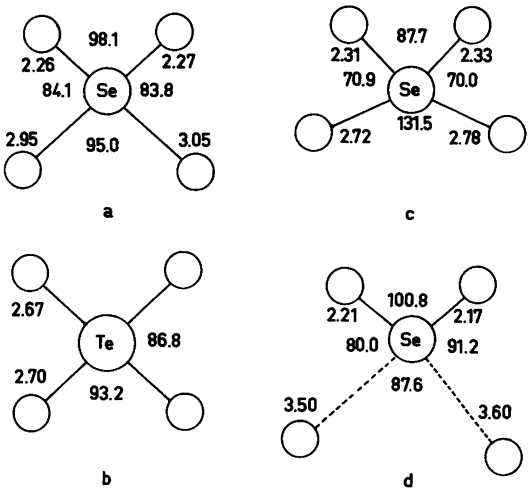

Fig. 2. Examples of planar four-coordinate selenium and tellurium complexes. a. $[SeL_2]$; b. $[TeL_2]$; $L=N(Ph_2PS)_2$; c. $[Se(Et_2NCS_2)_2]$[8] and d. $[Se(MeOCS_2)_2]$.[10] The MS_4 coordination spheres are seen along the normals to their least squares planes. Unlabelled spheres represent sulfur atoms. Bond lengths and angles (average values in b) are in ångstrøms and degrees. Intermolecular, secondary bonds are dashed.

bonding in the MS_4 group is probably essentially of the 3-center, 4-electron type.[9] Why then are their coordination spheres so different? It has been found earlier that Te(II) is a better acceptor of ligand electron density than Se(II) so that only with very strong donor ligands like dithiocarbamates do they both form complexes with relatively short average Te–S and Se–S bonds (2.68 and 2.54 Å, respectively).[1,9] Since the imidotetraphenyldithiodiphosphinate ion is a weaker donor, the overall Se–S bonding becomes weaker than the corresponding Te–S bonding. An even greater difference is found for ML'_2, where M=Se(II) and Te(II) and L'=methylxanthate.[1,10]

Ligand structure and molecular form. Average P–S and P–N bond lengths in the ligands are 2.021 and 1.578 Å, respectively, in good agreement with earlier investigations.[2] However, due to the asymmetry in the Se–S bond lengths, there is a pronounced tendency in the six-membered ligand-selenium rings of alternate short and long bonds. The short Se–S bond, average length 2.267(4) Å, is followed by a long S–P bond of average length 2.073(2) Å. This is joined to a short P–N bond, average length 1.558(5) Å which is connected to a long N–P bond, average length 1.598(0) Å. Completing the ring is a short P–S bond, average length 1.969(4) Å and a long S–Se

Table 4. Molecular planes.[a]

No. of plane	Atoms included	Interplanar angles (°)			
1	Se,S1,S2,S3,S4	1–2	74.7	6–7	7.2
2	S1,P1,S2,P2	1–3	71.6	6–8	8.0
3	S3,P3,S4,P4	1–6	6.0	6–9	11.4
4	P1N1P1	1–7	6.4	7–8	10.2
5	P3N2P4	1–8	3.8	7–9	7.8
6	S1SeS2	1–9	5.7	8–9	7.5
7	S1SeS3	2–3	9.8		
8	S2SeS4	2–4	6.8		
9	S3SeS4	2–10	95.1		
10	C111P1C121	2–11	91.2		
11	C211P2C221	3–5	7.9		
12	C311P3C321	3–12	91.4		
13	C411P4C421	3–13	88.8		

[a] Atomic displacement from planes 1–3 (Å).
1. Se,0.005(1); S1,–0.194(1); S2,0.147(1); S3,0.188(1); S4,–0.147(1);
2. S1,0.085(1); P1,–0.102(1); S2,–0.089(1); P2,0.106(1); Se,1.851(1); N1,–0.051(4); C111,1.132(4); C121,–1.727(5); C211,1.682(5); C221,–1.110(4)
3. S3,–0.011(1); P3,0.013(1); S4,0.011; P4,–0.014(1); Se,–1.837(1); N2,–0.072(4); C311,–1.361(4); C321,1.574(5); C411,1.446(5); C421,–1.406(5)

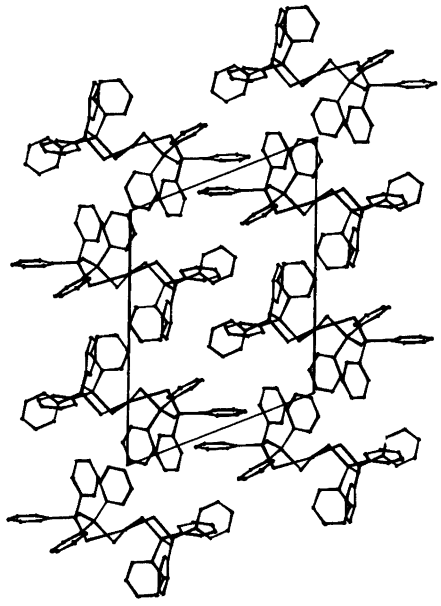

Fig. 3. The molecular packing as seen in the projection along *a*.

bond, average length 3.00(5) Å. Except for the Se–S bonds which are intermediate between a covalent bond and a van der Waals contact, the bond lengths are intermediate between single and double bonds, with the P–S bonds being close to both extremes. The average ring angles are similar to those in the tellurium analog.[2] As can be seen from Fig. 1b and Table 4, ligand ring 1 (S1,S2) has a tendency to chair form while ring 2 (S3,S4) has a tendency to boat form. The conformation of the whole molecule (minus the phenyl groups) approaches chair form, just like the tellurium analog. The average bond lengths and angles in the phenyl groups are 1.370(16) Å and 120.00(1.08)°, respectively.

Molecular packing. The packing of the molecules in the unit cell is shown in Fig. 3. There are no especially short contacts between the molecules, but there are more short van der Waals contacts than in the tellurium analog,[2] the shortest C–C contact being 3.48 Å.

Infrared spectra. The infrared spectrum of SeL_2 is very similar to that of TeL_2,[2] especially at frequencies above 650 cm^{-1} Tentative assignments based on spectra of metal complexes with the imidotetraphenyldithiodiphosphinate ligand and TeL_2[2] are (ν in cm^{-1}):ν_{as}(PNP), 1175 ms; ν(PC), 709 s and 690 vs. The absorptions occur at nearly the same frequencies in TeL_2. However ν_s(PS) is found at 600 cm^{-1} as compared to 580 cm^{-1} for TeL_2 while ν_{as}(PS) is found at 545 cm^{-1}, as compared to 559 cm^{-1} for TeL_2. These changes in the PS absorptions probably reflect the increased asymmetry in P–S bond strength in SeL_2 as compared to TeL_2. The PS absorptions may be compared to those found near 570–590 and near 450–470 cm^{-1} and assigned to ν(P=S) and ν(P–S) for selenium and tellurium diethyldithiophosphinates.[9,11] Similarly δ(PNP) found at 527 cm^{-1}(w) in TeL_2 has disappeared and may have merged with the absorption at 512–513 cm^{-1} found in both compounds. Finally δ(NPS) is found at 438 (w) as compared to 430 in the tellurium analog. The differences in δ(PNP) and δ(NPS) for the two compounds SeL_2 and TeL_2 are probably due to the greater asymmetry in P–N and P–S bonding in the selenium compound. A medium strong absorption at 318 cm^{-1} may be due to Se–S stretching. This is supported by the observation of Eysel *et al.* that a normal Se–S bond absorbs at 360 cm^{-1}.[12] The strong Se–S bonds observed in the present work are 0.06 Å longer than a covalent Se–S bond and should thus be expected to absorb at a lower frequency.

REFERENCES

1. Brøndmo, N. J., Esperås, S. and Husebye, S. *Acta Chem. Scand. A 29* (1975) 93.
2. Bjørnevåg, S., Husebye, S. and Maartmann-Moe, K. *Acta Chem. Scand. A 36* (1982) 195 and references therein.
3. Bereman, R. D., Wang, F. T., Najdzionek, J. and Braitsch, D. M. *J. Am. Chem. Soc. 98* (1976) 7266.
4. Schmidpeter, A. and Groeger, H. *Z. Anorg. Allg. Chem. 345* (1966) 106.
5. Husebye, S. *Acta Chem. Scand. 19* (1965) 1045.
6. Laitinen, R., Niinistö, L. and Steudel, R. *Acta Chem. Scand. A 33* (1979) 737.
7. Aaberg, A., Gramstad, T. and Husebye, S. *Acta Chem. Scand. A 34* (1980) 717.
8. Helland-Madsen, G. and Husebye, S. *Acta Chem. Scand. 24* (1970) 2273.
9. Husebye, S. *Compounds of Divalent Selenium and Tellurium with Bidentate Liagnds; Their Preparation, Structure and Bonding,* Diss., University of Bergen, Bergen 1969.

10. Brøndmo, N. J., Esperås, S., Graver, H. and Husebye, S. *Acta Chem. Scand. 27* (1973) 713.
11. Husebye, S. *Acta Chem. Scand. 19* (1965) 774 and *20* (1966) 2007.
12. Eysel,. H. H. and Sunder, S. *Inorg. Chem. 18* (1979) 2626.

Received June 30, 1982.

Acta Chemica Scandinavica A 37 (1983) 227–233

The Crystal and Molecular Structures of Two Isonicotinato *N*-Oxide Complexes of Cu(II)

HILKKA KNUUTTILA and PEKKA KNUUTTILA

Department of Chemistry, University of Jyväskylä, SF-40100 Jyväskylä 10, Finland

The crystal and molecular structures of diaquabis(isonicotinato *N*-oxide)copper(II), $[Cu(N\text{-inicO})_2(H_2O)_2]$ (*1*) and diaquabis-(isonicotinato *N*-oxide)bis(pyridine)copper(II), $[Cu(N\text{-inicO})_2(H_2O)_2(py)_2]$ (*2*) have been determined by X-ray diffraction and refined to final *R*-values of 0.047 and 0.040 for *1* and *2*, respectively. The crystals of *1* are monoclinic. The space group is *C*2/c, with $Z=4$ and a cell of dimensions $a=14.136(7)$, $b=9.791(3)$, $c=10.768(3)$ Å, and $\beta=110.91(3)°$. For *2* the space group is $P\bar{1}$, with $Z=1$ and a cell of dimensions $a=7.036(5)$, $b=9.640(3)$, $c=9.752(4)$ Å, $\alpha=110.05(3)$, $\beta=70.95(5)$ and $\gamma=104.28(5)°$.

Both molecules are centrosymmetric. The copper ion in *1* is surrounded by four oxygen atoms in a square-planar arrangement with Cu–O bond lengths of 1.934(4) Å from the carboxylato ligands and 1.930(2) Å from the aqua ligands, and by two out-of-plane carboxylato oxygen atoms with very long Cu–O distances of 2.691(4) Å. The coordination geometry around the copper

Table 1. Details of the data collection.

Compound	$[Cu(N\text{-inicO})_2(H_2O)_2]$	$[Cu(N\text{-inicO})_2(H_2O)_2(py)_2]$
Crystal data		
Space group	*C*2/*c*	$P\bar{1}$
Unit cell		
a (Å)	14.136(7)	7.036(5)
b	9.791(3)	9.640(3)
c	10.768(3)	9.752(4)
α(°)	90.0	110.05(3)
β	110.91(3)	70.95(5)
γ	90.00	104.28(5)
V(Å^3)	1392.3(9)	580.6(5)
Z	4	1
μMo*K*α (cm^{-1})	16.8	10.2
M.W.	375.78	533.98
Intensity measurements		
Collection	$\theta/2\theta$	$\theta/2\theta$
Radiation	Mo*K*α	Mo*K*α
Scan range	$4°<2\theta<65°$	$4°<2\theta<50°$
Scan rate ° min^{-1}	1.5 to 20.0	1.5 to 20.0
Refl. meas.	2924	2338
obs. ($I>3\sigma(I)$)	1477	1886
$R(=\Sigma\|\|F_o\|-\|F_c\|\|/\Sigma\|F_o\|)$	0.047	0.040

0302-4377/83 $2.50

ion in *2* can be described as an elongated octahedron with equatorial Cu–O and Cu–N bonds of 1.973(1) and 2.006(1) Å, respectively, and with axial Cu–O aqua bonds of 2.509(1) Å.

The isonicotinato *N*-oxide group coordinates to the copper ion through both carboxylato oxygen atoms in *1* and through one carboxylato oxygen atom for *2*. There is no coordination through the *N*-oxide oxygen atom.

Of 3*d* metal compounds containing isonicotinic acid *N*-oxide, the structures of Mn(II), Fe(II), Co(II) and Ni(II) compounds [1,2] and tetranuclear tetraaqua-μ_3-hydroxo-μ-sulfatotetrakis-μ-(isonicotinato *N*-oxide)tetracopper(II) [3] have been described earlier. The isonicotinato *N*-oxide group coordinates to the central metal ion through only one carboxylato oxygen atom in the Mn(II) complex [1] and through both carboxylato oxygen atoms to adjacent Cu atoms in the tetranuclear Cu(II) complex.[3] Coordination to the central metal ion does not occur through the *N*-oxide oxygen atom. The Fe(II), Co(II) and Ni(II) compounds of isonicotinic acid *N*-oxide are ionic and their crystals form an isomorphous series. Hexaaqua metal(II) cations and isonicotinate

Table 2. Final positional parameters for non-hydrogen atoms with e.s.d's in parentheses and U_{eq} (Å×10³).

Atom	*x*	*y*	*z*	U_{eq} [a]
[Cu(*N*-inicO)$_2$(H$_2$O)$_2$]				
Cu(1)	0.7500	0.2500	0.5000	25.9(3)
O(1)	0.5553(2)	0.3227(3)	0.1177(3)	40(2)
O(2)	0.6849(3)	0.0922(3)	–0.3420(3)	59(2)
O(3)	0.6923(2)	0.3166(3)	–0.3735(3)	39(2)
O(4)	0.6171(2)	0.2284(4)	0.3659(2)	48(2)
N(1)	0.5850(2)	0.2945(3)	0.0157(3)	27(1)
C(1)	0.5980(4)	0.1618(5)	–0.0156(4)	44(2)
C(2)	0.6260(4)	0.1337(4)	–0.1221(4)	42(2)
C(3)	0.6427(3)	0.2418(5)	–0.1967(3)	27(2)
C(4)	0.6305(4)	0.3770(5)	–0.1615(4)	39(2)
C(5)	0.6012(4)	0.4012(4)	–0.0542(4)	38(2)
C(6)	0.6750(3)	0.2115(4)	–0.3132(4)	32(2)
[Cu(*N*-inicO)$_2$(H$_2$O)$_2$(py)$_2$]				
Cu(1)	0.0000	0.0000	0.0000	30.80(7)
O(1)	0.2483(1)	0.4039(1)	0.3201(1)	58.8(4)
O(2)	0.0539(1)	0.8406(1)	0.0599(1)	41.0(3)
O(3)	0.7375(1)	0.7281(1)	0.1401(1)	46.1(4)
O(4)	0.3167(1)	0.1583(1)	0.0660(1)	48.9(4)
N(1)	0.1707(1)	0.4822(1)	0.2707(1)	38.4(4)
N(2)	0.8254(1)	0.0818(1)	0.2089(1)	33.1(4)
C(1)	0.2959(1)	0.5650(1)	0.1793(1)	39.3(5)
C(2)	0.2182(1)	0.6511(1)	0.1304(1)	35.7(5)
C(3)	0.0114(1)	0.6518(1)	0.1712(1)	29.7(4)
C(4)	0.8859(1)	0.5635(1)	0.2615(1)	37.7(5)
C(5)	0.9686(2)	0.4813(1)	0.3121(1)	41.8(5)
C(6)	0.9226(1)	0.7466(1)	0.1195(1)	31.3(4)
C(7)	0.6471(1)	0.1236(1)	0.2286(1)	38.6(5)
C(8)	0.5236(2)	0.1789(1)	0.3702(1)	46.2(6)
C(9)	0.5803(2)	0.1897(1)	0.4963(1)	44.9(5)
C(10)	0.7625(2)	0.1468(1)	0.4765(1)	45.9(5)
C(11)	0.8802(1)	0.0941(1)	0.3319(1)	39.0(5)

[a] $U_{eq}=\frac{1}{3}(U_{11}+U_{22}+U_{33})$.

N-oxide anions are found in the crystal lattices.

This experiment sought to determine the structures of diaquabis(isonicotinato *N*-oxide)Cu(II), $[Cu(N\text{-inicO})_2(H_2O)_2]$ and diaquabis(isonicotinato *N*-oxide)bispyridinecopper(II), $[Cu(N\text{-inicO})_2(H_2O)_2(py)_2]$. The spectral and magnetic properties of the former have been studied earlier by Gelfand *et al.*[4] They described $[Cu(N\text{-ionicO})_2(H_2O)_2]$ as a tetracoordinated polymeric complex, where isonicotinato groups form single bridges between copper(II) ions through N–O oxygen and COO oxygen, the water molecules being exclusively lattice water. Magnetic susceptibility χ_g at 295 K is 1534×10^6 cgsu and the magnetic moment μ_{eff} is 1.91 B.M.[4]

EXPERIMENTAL

Preparation of the compounds. The royal blue crystals of $[Cu(N\text{-inicO})_2(H_2O)_2]$ (*1*) were prepared as reported earlier.[1,3]

Recrystallization of *1* from ethanolic pyridine solution gave beautiful blue crystals of an unstable pyridine derivative, $[Cu(N\text{-inicO})_2(H_2O)_2(py)_2]$ (*2*).

Table 3. Final positional parameters and isotropic thermal parameters ($\times10^2$) for hydrogen atoms and their standard deviations.

	x	*y*	*z*	*U*
$[Cu(N\text{-inicO})_2(H_2O)_2]$				
H(1)	0.113(5)	0.542(7)	0.075(7)	13(3)
H(2)	0.641(5)	0.992(7)	0.354(7)	10(2)
H(3)	0.358(5)	0.517(6)	0.214(6)	7(2)
H(4)	0.594(4)	0.493(6)	0.473(5)	6(2)
H(5)	0.626(5)	0.255(7)	0.313(6)	8(2)
H(6)	0.099(4)	0.775(6)	0.393(5)	8(2)
$[Cu(N\text{-inicO})_2(H_2O)_2(py_2)]$				
H(1)	0.445(2)	0.571(1)	0.165(1)	4.3(3)
H(2)	0.321(2)	0.707(1)	0.064(1)	5.5(3)
H(3)	0.723(1)	0.554(1)	0.297(1)	4.1(3)
H(4)	0.881(2)	0.420(1)	0.382(1)	5.4(3)
H(5)	0.601(2)	0.098(1)	0.130(1)	5.7(3)
H(6)	0.395(2)	0.210(1)	0.388(1)	8.0(4)
H(7)	0.504(2)	0.779(1)	0.411(1)	6.6(3)
H(8)	0.188(1)	0.842(1)	0.440(1)	4.8(3)
H(9)	0.029(1)	0.065(1)	0.306(1)	4.6(3)
H(10)	0.331(2)	0.175(1)	−0.004(1)	6.9(3)
H(11)	0.286(2)	0.219(1)	0.143(1)	7.2(4)

Copper was analyzed by standard EDTA titrations. The chemical analysis for C, N and H was performed by the Pulp and Paper Research Institute, Espoo, Finland.

Analytical results for $[Cu(N\text{-inicO})_2(H_2O)_2]$. Calculated: Cu 16.91 %, C 38.36 %, N 7.45 %,

Table 4. Selected interatomic distances (Å) and angles (°) and their standard deviations for $[Cu(N\text{-inicO})_2(H_2O)_2]$.

Environment of copper	
Cu(1)–O(2)	2.691(4)
Cu(1)–O(3)	1.934(4)
Cu(1)–O(4)	1.930(2)
O(2)–Cu(1)–O(3)	54.7(1)
O(2)–Cu(1)–O(4)	92.9(1)
O(3)–Cu(1)–O(2)	125.2(1)
O(3)–Cu(1)–O(4)	88.8(1)
O(4)–Cu(1)–O(2)	87.1(1)
O(4)–Cu(1)–O(3)	91.2(1)
Pyridine *N*-oxide group	
N(1)–O(1)	1.337(5)
N(1)–C(1)	1.371(6)
N(1)–C(5)	1.355(6)
C(1)–C(2)	1.369(8)
C(2)–C(3)	1.398(7)
C(3)–C(4)	1.404(7)
C(4)–C(5)	1.379(7)
O(1)–N(1)–C(1)	120.4(4)
O(1)–N(1)–C(5)	117.5(4)
C(1)–N(1)–C(5)	122.0(4)
N(1)–C(1)–C(2)	120.0(4)
C(1)–C(2)–C(3)	119.2(4)
C(2)–C(3)–C(4)	119.7(4)
C(3)–C(4)–C(5)	119.4(4)
Carboxylato group	
C(6)–C(3)	1.509(6)
C(6)–O(2)	1.229(6)
C(6)–O(3)	1.286(5)
O(2)–C(6)–O(3)	125.0(4)
O(2)–C(6)–C(3)	119.5(4)
O(3)–C(6)–C(3)	115.5(4)
H(1)–C(1)	1.49(7)
H(2)–C(2)	1.29(7)
H(3)–C(4)	1.22(6)
H(4)–C(5)	1.09(6)
H(5)–O(4)	0.68(7)
H(6)–O(4)	0.64(6)

Table 5. Selected interatomic distances (Å) and angles (°) and their standard deviations for $[Cu(N\text{-inicO})_2(H_2O)_2(py)_2]$.

Environment of copper	
Cu(1)–N(2)	2.006(1)
Cu(1)–O(2)	1.973(1)
Cu(1)–O(4)	2.509(1)
N(2)–Cu(1)–O(2)	88.63(3)
N(2)–Cu(1)–O(4)	92.39(2)
O(2)–Cu(1)–N(2)	91.37(3)
O(2)–Cu(1)–O(4)	91.34(3)
O(4)–Cu(1)–O(2)	88.66(3)
O(4)–Cu(1)–N(4)	87.61(2)
Pyridine *N*-oxide group	
N(1)–O(1)	1.314(1)
N(1)–C(1)	1.355(1)
N(1)–C(5)	1.344(1)
C(1)–C(2)	1.371(2)
C(2)–C(3)	1.379(1)
C(3)–C(4)	1.385(1)
C(4)–C(5)	1.376(2)
O(1)–N(1)–C(1)	119.52(8)
O(1)–N(1)–C(5)	120.07(8)
C(1)–N(1)–C(5)	120.41(10)
N(1)–C(1)–C(2)	120.33(9)
C(1)–C(2)–C(3)	120.33(8)
C(2)–C(3)–C(4)	118.33(10)
C(5)–C(4)–C(3)	120.02(9)
C(4)–C(5)–N(1)	120.53(9)
Carboxylato group	
C(6)–C(3)	1.510(1)
C(6)–O(2)	1.269(1)
C(6)–O(3)	1.228(1)
O(2)–C(6)–O(3)	127.06(10)
O(2)–C(6)–C(3)	114.05(8)
O(3)–C(6)–C(3)	118.87(8)
Pyridine ring	
N(2)–C(7)	1.346(1)
N(2)–C(11)	1.336(1)
C(7)–C(8)	1.374(1)
C(8)–C(9)	1.377(2)
C(9)–C(10)	1.377(2)
C(10)–C(11)	1.373(1)
C(7)–N(2)–C(11)	118.18(7)
N(2)–C(7)–C(8)	121.81(10)
C(7)–C(8)–C(9)	119.62(11)
C(8)–C(9)–C(10)	118.65(8)
C(9)–C(10)–C(11)	118.94(11)
N(2)–C(11)–C(10)	122.79(10)

O 34.06 %, H 3.22 %. Found: Cu 16.43 %, C 38.66 %, N 7.18 %, H 3.16 %.

Data collection. A Syntex $P2_1$, four-circle diffractometer employing graphite monochromatized Mo$K\alpha$-radiation was used to measure the crystal and intensity data of both compounds. The unit cell parameters were calculated by least squares refinement of 15 high order reflections.

After centering, the crystal of *2* was coated with glue to prevent decomposition in air by loss of pyridine.

Details of the data collections, including the crystal data, may be seen in Table 1. The data were corrected for Lorentz and polarization factors but not for absorption.

Structure determination. The structure of *1* was solved by direct methods[5] while for *2* the locations of the copper atom and three oxygen atoms were determined from a Patterson map. The refinement of the structures using unit weights was carried out by the X-Ray System programs.[6] All hydrogen atoms were located using difference Fourier syntheses. The final *R*-values were 0.047 and 0.040 for *1* and *2*, respectively. A refinement in space group *Cc* for *1* was also tried but it did not bring about any significant improvements. The scattering factors for Cu, C, N and O were those of Cromer and Mann[7] and for hydrogen atoms those reported by Stewart *et al.*[8]

Tables 2 and 3 present the final atomic coordinates and the thermal parameters with their standard deviations for both compounds. Lists of structure factors and anisotropic thermal parameters are available from the authors upon request.

DESCRIPTION AND DISCUSSION OF THE STRUCTURES

The labeling and the structure of the molecules are given in Fig. 1 for $[Cu(N\text{-inicO})_2(H_2O)_2]$ and in Fig. 2 for $[Cu(N\text{-inicO})_2(H_2O)_2(py)_2]$. Bond lengths and angles are listed in Tables 4 and 5.

Both copper(II) complexes are monomeric containing two chelating isonicotinato *N*-oxide and two aqua ligands per molecule for $[Cu(N\text{-inicO})_2(H_2O)_2]$ and two monodentate isonicotinato *N*-oxide, two aqua and two pyridine ligands per molecule for $[Cu(N\text{-inicO})_2(H_2O)_2(py)_2]$. The molecules are joined in the crystal lattice by

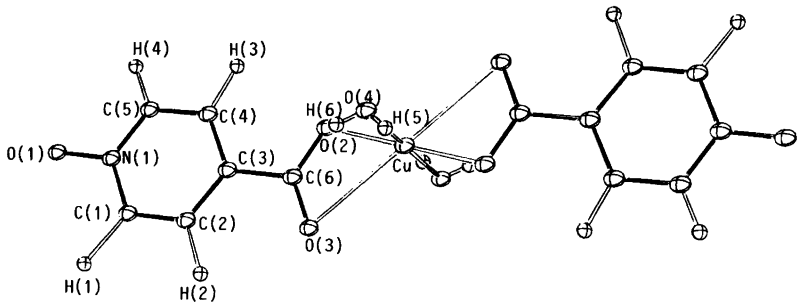

Fig 1. The labeling and structure of $[Cu(N\text{-inicO})_2(H_2O)_2]$. The ellipsoids are not scaled with thermal motion.

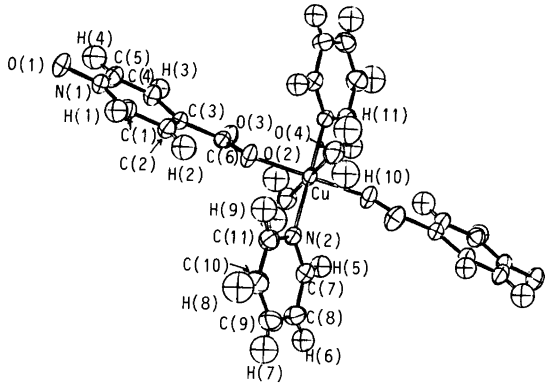

Fig. 2. The labeling and structure of $[Cu(N\text{-inicO})_2(H_2O)_2(py)_2]$. Thermal ellipsoids are drawn to enclose the 50 % probability level.

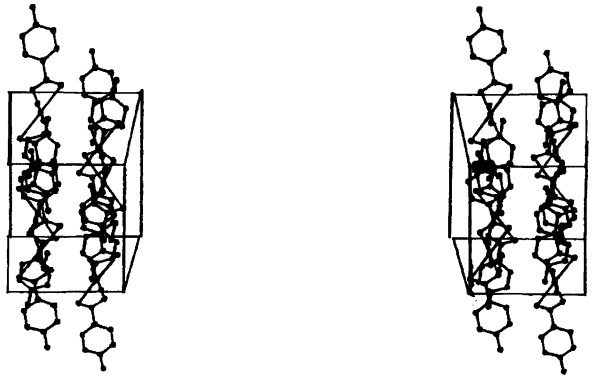

Fig. 3. Stereoview of the packing of $[Cu(N\text{-inicO})_2(H_2O)_2]$ within the unit cell. Hydrogen atoms have been excluded for clarity.

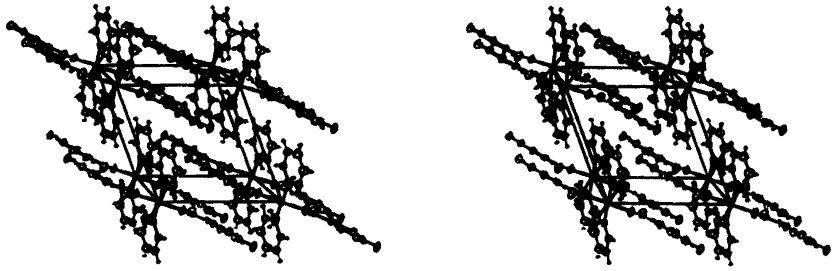

Fig. 4. Stereoview of the structure, illustrating the packing of $[Cu(N\text{-inicO})_2(H_2O)_2(py)_2]$ within the unit cell.

hydrogen bonds, Table 6. The packing in the crystals is shown in Figs. 3 and 4.

In the $[Cu(N\text{-inicO})_2(H_2O)_2]$ complex, oxygen atoms surround the copper ion forming a square planar arrangement. In addition there are two "out-of-plane" carboxylato oxygen atoms with very long Cu(1)–O(2) distances of 2.691(4) Å. The carboxylato oxygen–copper bond, Cu(1)–O(3) 1.934(4) Å and the aqua oxygen–copper bond, Cu(1)–O(4) 1.930(2) Å are equal. Angles O(3)–Cu(1)–O(4) and O(2)–Cu(1)–O(3) are 91.2(1) and 54.8(1)°, respectively. The angle O(2)–C(6)–O(3) in the carboxylato group is 125.0(4)°. The atoms C(3), C(6), O(2) and O(3) form a plane from which the copper atom is offset by 0.245 Å (Table 7).

The angle between the planes of the carboxylato group and pyridine ring is 1.7°. If the normal to the Cu(1), O(3), O(4) plane is considered as the "tetragonal" axis, then the angle between the "out-of-plane" Cu(1)–O(2) direction and the "tetragonal" axis is 35.5°.

The coordination geometry around the copper atom can be regarded as a square plane or a tetragonally distorted octahedron, depending upon whether or not the "out-of-plane" oxygen atoms are considered bonded to the Cu ion. However, we prefer to describe the coordination as a six-coordination with an extremely tetragonally distorted octahedral configuration although the long Cu(1)–O(2) distance indicates very weak interaction. Structures of copper(II) complexes have been presented where the geometry and coordination of the carboxylato group are similar to the coordination of the carboxylato group in $[Cu(N\text{-inicO})_2(H_2O)_2]$.[9–12] The lengths of the equatorial Cu–O bonds, the "out-of-plane" Cu–O bond, 2.691(4) Å and the angle of O(2)–Cu(1)–O(3) in $[Cu(N\text{-inicO})_2(H_2O)_2]$, have values close to the corresponding values found in *trans*-bis(chloroacetato)-bis(2-picoline)copper(II) (1.975(5), 2.707(7) Å, 53.9°),[9] in diaquabis(hydrogen *o*-phtalato)copper(II) (1.930(8), 1.967(8), 2.677(5) Å, 54.4(2)°),[11] and

Table 6. Hydrogen bonds.

	A–H···B	A–H	H···B	A–B	∠AHB(°)
$[Cu(N\text{-inicO})_2(H_2O)_2]$	O(4)–H(5)···O(1)	0.68(7)	2.09(6)	2.663(4)	143(6)
	O(4)^a–H(6)···O(1)^b	0.64(6)	2.19(6)	2.671(5)	133(6)
$[Cu(N\text{-inicO})_2(H_O)_2(py)_2]$	O(4)–H(10)···O(3)^c	0.72(1)	2.09(1)	2.757(1)	154(1)
	O(4)–H(11)···O(1)	0.78(1)	2.01(1)	2.782(1)	168(1)

Symmetry code *a*: $x-\frac{1}{2}, y+\frac{1}{2}, z$
b: $-x+\frac{1}{2}, y+\frac{1}{2}, -z+\frac{1}{2}$
c: $-x+1, -y+1, -z$

Table 7. Deviations (Å) of atoms from least-squares planes.

$[Cu(N\text{-inicO})_2(H_2O)_2]$									
Plane 1: O(2), O(3), C(6), C(3)									
O(2)	0.003	O(3)	0.003	C(6)	−0.008	C(3)	0.002	Cu(1)	0.245
Plane 2: N(1), C(1), C(2), C(3), C(4), C(5)									
N(1)	−0.006	C(1)	0.007	C(2)	−0.002	C(3)	−0.003	C(4)	0.004	C(5)	0.000
$[Cu(N\text{-inicO})_2(H_2O)_2(py)_2]$									
Plane 3: O(2), O(3), C(6), C(3)									
O(2)	0.001	O(3)	0.042	C(6)	−0.034	C(3)	−0.010	Cu(1)	0.247

in bis(chloroacetato)-(*N,N,N',N'*-tetramethylethylenediamine)copper(II) (1.975−1.977(3), 2.624−2.627(3) Å, 55.6−55.7(1)°).[12] However, the copper atom in bis(dichloroacetato)bis(2-picoline)copper(II) has been considered pentacoordinated since only one of the dichloroacetato groups coordinates through both carboxylato oxygen atoms.[10]

The structure of the pyridine derivative seems to favour an explanation based on hexacoordination, too. When diaquabis(isonicotinato *N*-oxide)copper(II) was crystallized from ethanolic pyridine solution, two pyridine molecules joined the coordination sphere of the copper atom so that both the long bond between carboxylato oxygen and copper disappeared and the bond between the aqua oxygen atom and the copper atom increased in length from 1.930(2) to 2.509(1) Å. The geometry around the copper atom is a distorted elongated octahedron with basal Cu−O bonds of 1.973(1) Å and Cu−N bonds of 2.001(1) Å. In both Cu(II) complexes under study the isonicotinato *N*-oxide ligand coordinates only through carboxylato oxygen atoms, being either bidentate or monodentate.

REFERENCES

1. Knuuttila, P. *Thesis,* University of Jyväskylä, Jyväskylä 1982.
2. Knuuttila, P. *Inorg. Chim. Acta 52* (1981) 141.
3. Knuuttila, P. *Inorg. Chim. Acta 58* (1982) 201.
4. Gelfand, L. S., Pytlewski, L. L., Cosgrove, D. L., Mikulski, C. M., Speca, A. N. and Karayannis, N. M. *Inorg. Chim. Acta 32* (1979) 59.
5. Main, P., Hull, S. E., Lessinger, L., Germain, G., Declercq, J.-P. and Woolfson, M. M. *MULTAN 80. A System for Automatic Solution of Crystal Structures from X-Ray Diffraction Data,* University of York, York 1980.
6. Stewart, J. M. *The X-Ray System, Version of 1976,* Technical Report TR-446, Computer Science Center, University of Maryland, College Park 1976.
7. Cromer, D. T. and Mann, J. B. *Acta Crystallogr. A 24* (1968) 321.
8. Stewart, R. F., Davidson, E. R. and Simpson, W. T. *J. Chem. Phys. 42* (1965) 3175.
9. Davey, G. and Stephens, F. S. *J. Chem. Soc. A* (1971) 1917.
10. Davey, G. and Stephens, F. S. *J. Chem. Soc. A* (1971) 2577.
11. Biagini Gingi, M., Guastini, C., Musatti, A. and Nardelli, M. *Acta Crystallogr. B 25* (1969) 1833.
12. Ahlgrén, M., Hämäläinen, R. and Turpeinen, U. *Acta Chem. Scand. A 32* (1978) 57.

Received July 26, 1982.

Acta Chemica Scandinavica A 37 (1983) 235–240

Preparation and Crystal Structures of *cis*-Dichlorobis-(thiourea)selenium(II) and *cis*-Dibromobis(thiourea)selenium(II)

STURLE VEGARD BJØRNEVÅG and SVERRE HAUGE

Department of Chemistry, University of Bergen, N-5000 Bergen, Norway

cis-Dichlorobis(thiourea)selenium(II), $Se(tu)_2Cl_2$ (Fig. 1) and *cis*-dibromobis(thiourea)selenium(II), $Se(tu)_2Br_2$, ($tu \equiv SC(NH_2)_2$) were prepared by reaction of Se(IV) with thiourea in strongly acidic solutions. The crystal structures were determined by X-ray methods and refined by full-matrix least-squares procedures. The structures are isomorphous, space group $P2_1/c$ (No. 14) with four formula units in the unit cell. The dichloride has the cell dimensions: $a=8.410(1)$, $b=16.522(3)$, $c=8.465(2)$ Å and $\beta=123.025(9)°$. The cell dimensions of the dibromide are: $a=8.731(2)$, $b=16.868(4)$, $c=8.777(2)$ Å and $\beta=125.10(1)°$.

The selenium atom has a distorted square planar environment, with long distances to halogen atoms which are *trans* to rather short bonds to sulfur atoms in thiourea. The Se–S bond lengths in $Se(tu)_2Cl_2$ are 2.175(1) and 2.196(1) Å and Se···Cl distances are 3.177(1) and 3.267(1) Å. In $Se(tu)_2Br_2$ the Se–S bond lengths are 2.191(2) and 2.206(2) Å and Se···Br distances are 3.261(1) and 3.335(1) Å. The Se–S bond lengths are near the expected length of a single covalent bond length, 2.18 Å. The selenium–halogen distances are much longer than the single covalent bond lengths, but shorter than van der Waals distances, 3.85 and 4.00 Å, respectively. The S–Se–S bond angle is 99.08(5)° in $Se(tu)_2Cl_2$ and 99.57(8)° in $Se(tu)_2Br_2$.

Within the errors of the determination, the thiourea groups are planar and the bond lengths are equal. The weighted mean value for the S–C bond lengths is 1.767(2) Å and for the C–N bond lengths 1.303(2) Å.

The reaction between tellurium(IV) and thiourea in acid aqueous solution, giving four coordinated complexes of divalent tellurium, is well known.[1] The corresponding reaction of selenium(IV) has not been reported. On the other hand, selenous acid has been used as test substance on the SH group in organic compounds.[2] In aqueous solution the thiomolecules are oxidized to disulfide while the selenium(IV) is reduced to the divalent state which disproportionates to free selenium and tetravalent selenium.[3] If the solution is strongly acidic, the reduction of tetravalent selenium stops at the divalent oxidation state,[4] *e.g.* in acidic solution one mol of selenous acid reacts with four mol of thiosulfate resulting in tetrathionate and selenopentathionate.[5] In the present work, where selenous acid reacts with thiourea, the reaction should be

$$H_2SeO_3 + 4tu + 4H^+ = Se(tu)_2^{2+} + (tu)_2^{2+} + 3H_2O$$

If the reaction goes as for the tellurium analog, the $Se(tu)_2X_2$ complex is expected instead of the cation $Se(tu)_2^{2+}$. In order to get information about the coordination around the selenium atom, the crystal structures were solved.

EXPERIMENTAL

Preparation of cis-*dichlorobis(thiourea)selenium(II),* 1. 5 mmol (0.55 g) SeO_2 was dissolved in 20 ml 8 M HCl, at room temperature. A solution of 20 mmol (1.52 g) thiourea dissolved in 20 ml 8 M HCl was added under vigorous stirring. A light yellow, finely crystallized precipitate was formed. Since it was difficult to find any solvent useful for recrystallization, the mother liquor was used as follows: The temperature was slowly raised to 45 °C under continued stirring. Undissolved precipitate was removed by filtration and

0302-4377/83 $2.50

the solution was set aside at 3 °C for 24 h.

Most of the crystals which deposited were identified as formamidinium disulfide dichloride. The crystals were removed from the solution and most of remaining light yellow precipitate was dissolved by heating and stirring. The solution was set aside at 3 °C for 24 h, yellow bipyramidal crystals were filtered off, washed with acetone, ether and dried in vacuum. The yield was 1.3 g or 87 % based on the amount of SeO_2 employed. The crystals were identified by X-ray methods.

Preparation of cis-*dibromobis(thiourea)selenium(II),* 2. Crystals of *cis*-dibromobis(thiourea)selenium(II), prepared in the same way as the corresponding dichloride compound, showed during the X-ray analysis unusual electron density around the position of the selenium atom, see the crystal data. A new product was made by dissolving 1 mmol (0.11 g) SeO_2 in 10 ml 47 % HBr, adding a solution of 4 mmol (0.31 g) of thiourea in 10 ml 47 % HBr. A yellow fine crystalline powder was formed. The solution was diluted under vigorous stirring and the temperature raised to 45 °C. Some undissolved precipitate was filtered off and the solution set aside at 3 °C for 10 h. Yellow bipyramidal crystals were filtered off, washed with acetone, ether and dried in vacuum. The yield was 0.34 g or 88 % based on the amount of SeO_2 employed. The crystals were identified by X-ray methods.

CRYSTAL DATA

Preliminary unit cell data were obtained from Weissenberg and precession photographs. Accurate unit cell parameters were determined on an Enraf-Nonius CAD-4 diffractometer from setting angles of 25 reflections, using least-squares analysis. The reflections were automatically located and centered. The space group was determined from systematically absent reflections and confirmed by the subsequent structure analysis. The reflection data were collected with graphite monocromatized Mo$K\alpha$ radiation. The reflections were scanned in the $\Delta\omega$ mode with variable scan rate. Of the total scan time 2/3 was used for scanning the peak and 1/3 for scanning the background on both sides of the peak. During the data collection the intensity variation with time was controlled by measuring two standard reflec-

Table 1. Crystal data and refinement characteristics.

Compound	$Se(tu)_2Cl_2$	$Se(tu)_2Br_2$
a (Å)	8.410(1)	8.731(2)
b (Å)	16.522(3)	16.868(4)
c (Å)	8.465(2)	8.777(2)
β (°)	123.025(9)	125.10(1)
V (Å^3)	986.2	1057.6
M	302.11	391.02
Space group	$P2_1/c$(No. 14)	$P2_1/c$(No. 14)
λMo$K\bar{\alpha}$ (Å)	0.71073	0.71073
Z	4	4
D_x (g cm^{-3})	2.035	2.456
D_{obs} (g cm^{-3})	2.00	2.47
μ (cm^{-1})	49.78	121.53
T (K)	293.0(5)	293.0(5)
F(000)	592	736
Sin θ/λ range (Å^{-1})	0–0.704	0–0.704
Scan width (°)	2.0+0.35 tgθ	1.5+0.35 tgθ
No. of refl.	3126	3380
No. of refl., $w\neq0$	1524	1327
Crystal dimensions (mm^3)	0.11×0.13×0.20	0.06×0.09×0.15
Scale factor, K	0.6672	1.0174
$R(F)$	0.044	0.039
$R_w(F)$	0.041	0.044
Goodness of fit	1.806	2.130
Difference Fourier max (e Å^{-3})	0.45	0.43

tions every hour of exposure time. A control of the centering of the crystal was made at every 100th observation by the use of these two standard and two additional reflections. If any angle for any of these reflections changed by more than 0.07°, a new orientation matrix was automatically determined, using the predetermined list of reflections.

The net intensity, $I=C-TB$ and the standard deviation $\sigma(I)=(S(C+T^2B+(pI)^2))^{1/2}$ where S is the scan rate, C is the total integrated peak count, T is the ratio of scan time to background counting time, B is the background counting and p is the instability factor and was set to 0.02. The intensities were corrected for Lorentz, polarization and absorption effects. The absorption corrections were carried out by the method of Coppens.[6] The subdivision in Gaussian points along *a*, *b* and *c* were 12×6×12 for *1* and 6×10×12 for *2*.

The calculations were carried out on a PDP-11 computer using Enraf-Nonius Structure Determination Package.[7,8] The two structures were solved by Patterson and Fourier methods and refined by full-matrix least-squares minimizing the function $r=\Sigma w(F_o-KF_c)^2$, where K is a scale factor and $w=1/\sigma^2_{Fo}$. The hydrogen atoms were placed and locked in position 0.87 Å from the nitrogen atoms and with fixed temperature factor $U=0.05$. The thiourea group was assumed to be planar and the nitrogen atoms were assumed to have a trigonal bonding system. The data for *1* and *2* showed no sign of secondary extinction.

Atomic scattering factors and anomalous dispersion values for non-hydrogen atoms were taken from Ref. 9. Crystal data and refinement characteristics are given in Table 1. A list of structure factors and anisotropic temperature factors is available from the authors on request.

Analysis of data taken from a crystal of the dibromo compound, prepared in the same way as the dichloro compound, showed a very high temperature factor for selenium. The bond distances selenium–sulfur were 2.12 and 2.13 Å which are shorter than the single covalent bond distances, 2.18 Å. Such an observation can probably be explained by the fact that some of the selenium positions in the crystals are occupied by sulfur. New crystals were prepared as described above.

RESULTS

From many crystal structure determinations of complexes of divalent tellurium, the configuration is known to be square planar.[1,10] The model of the bonding is two $3c-4e$ bonding systems at right angle to each other. Each system has only two bonding electrons for the two bonds, and the bonds are rather weak. The relative length of the two bonds depends on how efficient each of the ligands uses the common bonding orbital. With a ligand where sulfur is the complexing atom or with halogen as one of the ligands, the relative strengths of the two bonds are about equal. Divalent tellurium also forms very asymmetrical complexes, *i.e.* complexes with carbon as one of the complexing atoms.[10] Passing from tellurium to the less metallic element selenium, only a few structures are known, but from the known ones it seems that divalent selenium forms symmetrical bonds only when the two ligands are equal.[11] In the present structures with halogen in the *trans* position to sulfur the complexes are very asymmetric (Fig. 1).

Bond lengths and angles in the two crystal structures, based on the atomic coordinates in Table 2, are given in Table 3.

The environments of the selenium atoms in the two structures are given in Table 3. The Se–S bond lengths, 2.175(1) and 2.196(1) Å in *1* and 2.191(2) and 2.206(2) Å in *2*, are equal or a little longer than the sum of the covalent radii of selenium and sulfur, 2.18 Å. The dihedral angles SSeS/SeSC are 102.8 and 82.7° in *1* and 97.6 and 81.6° in *2*. As seen from Fig. 1, the environment

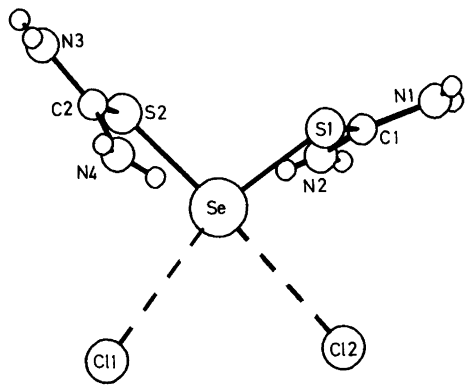

Fig. 1. ORTEP drawing of $Se(tu)_2Cl_2$ as seen normal to the SeSS plane.

Table 2. Atomic coordinates for *cis*-dichlorobis(thiourea)selenium(II) and *cis*-dibromobis(thiourea)selenium(II). Standard deviations from least squares are given in parantheses.

Atom	*x*	*y*	*z*
$Se(tu)_2Cl_2$			
Se	0.40601(8)	0.12792(4)	0.27845(8)
Cl1	0.7470(2)	0.00284(8)	0.4398(1)
Cl2	0.7075(2)	0.23298(8)	0.6511(2)
S1	0.3022(2)	0.06922(9)	0.0091(2)
S2	0.1472(2)	0.19289(9)	0.2069(2)
C1	0.2595(7)	−0.0322(3)	0.0404(7)
C2	0.1796(7)	0.2920(3)	0.1501(6)
N1	0.2491(6)	−0.0564(3)	0.1810(6)
N2	0.2374(6)	−0.0806(3)	−0.0922(6)
N3	0.0327(6)	0.3391(3)	0.0847(6)
N4	0.3392(6)	0.3171(3)	0.1782(6)
H1	0.2278	−0.1071	0.1905
H2	0.2635	−0.0218	0.2654
H3	0.2157	−0.1319	−0.0886
H4	0.2444	−0.0616	−0.1841
H5	0.0378	0.3887	0.0536
H6	−0.0707	0.3209	0.0722
H7	0.3491	0.3664	0.1482
H8	0.4363	0.2847	0.2271
$Se(tu)_2Br_2$			
Se	0.4037(1)	0.12694(6)	0.2782(1)
Br1	0.7498(1)	0.00176(6)	0.4467(1)
Br2	0.7018(1)	0.23394(5)	0.6566(1)
S1	0.2940(3)	0.0714(1)	0.0081(3)
S2	0.1501(3)	0.1899(1)	0.2100(3)
C1	0.2542(11)	−0.0288(5)	0.0348(11)
C2	0.1761(11)	0.2874(5)	0.1529(9)
N1	0.2430(10)	−0.0518(4)	0.1718(9)
N2	0.2383(10)	−0.0765(5)	−0.0913(9)
N3	0.0324(10)	0.3332(4)	0.0896(10)
N4	0.3314(9)	0.3118(4)	0.1814(9)
H1	0.2219	−0.1016	0.1795
H2	0.2608	−0.0185	0.2562
H3	0.2177	−0.1267	−0.0875
H4	0.2494	−0.0585	−0.1774
H5	0.0385	0.3817	0.0596
H6	−0.0684	0.3166	0.0776
H7	0.3378	0.3602	0.1512
H8	0.0483	0.2807	0.2298

of the selenium atom in the two compounds indicates a tendency to square-planar coordination at these atoms. The Se···Cl and Se···Br contacts which occur in the *trans* position to Se–S bonds, are 3.177(1), 3.267(1) Å and 3.262(1), 3.335(1) Å in *1* and *2*, respectively. The shortest selenium halogen contacts are *trans* to the longest Se–S bond. The S–Se···Cl angles are 154.94(4) and 164.51(4)°, and S–Se···Br angles are 156.06(6) and 163.42(6)°. The SeSSClCl and SeSSBrBr groups are approximately planar. The angles between the SeSS and SeXX planes are 25.6 and 26.0° in *1* and *2*, respectively. The halogen atoms are both about one Ångström out of the SeSS plane, one on each side of the plane.

Table 3. Bond lengths (Å) and bond angles (°). Standard deviations are given in parantheses.

	$Se(tu)_2Cl_2$	$Se(tu)_2Br_2$
Se–S1	2.175(1)	2.191(2)
Se–S2	2.196(1)	2.206(2)
Se···X1	3.267(1)	3.335(1)
Se···X2	3.177(1)	3.262(1)
S1–C1	1.763(4)	1.769(6)
S2–C2	1.769(4)	1.772(6)
C1–N1	1.303(5)	1.320(8)
C1–N2	1.307(5)	1.308(8)
C2–N3	1.301(5)	1.296(8)
C2–N4	1.297(5)	1.297(8)
S1–Se–S2	99.08(5)	99.57(8)
X1···Se···X2	83.50(3)	84.82(2)
S1–Se···X2	85.02(4)	85.90(6)
S2–Se···X1	97.90(4)	95.54(6)
S1–Se···X1	154.94(4)	156.06(6)
S2–Se···X2	164.51(4)	163.42(6)
Se–S1–C1	105.32(15)	105.2(2)
Se–S2–C2	104.52(15)	104.6(2)
S1–C1–N1	123.3(3)	121.7(5)
S1–C1–N2	113.5(3)	114.1(5)
N1–C1–N2	123.2(4)	124.2(6)
S2–C2–N3	114.7(3)	115.2(5)
S2–C2–N4	123.0(3)	122.0(5)
N3–C2–N4	122.3(4)	122.8(6)

The present crystal structures can be compared with structures of selenopentathionate ions,[12–14] selenium dithiocyanate [15] and with the dimerized selenium trithiocyanate ion.[16] The dihedral angles at Se–S in these structures are about the same as in the present structures. In selenopentathionates, the Se–S bond lengths are from 2.153(4) to 2.181(3) Å with 2.178(1) Å as weighted mean value. The angles S–Se–S are from 103.1(1) to 104.9(2)° with 103.9(1)° as the weighted mean value. There are no close contacts in the *trans* position to the Se–S bond. In

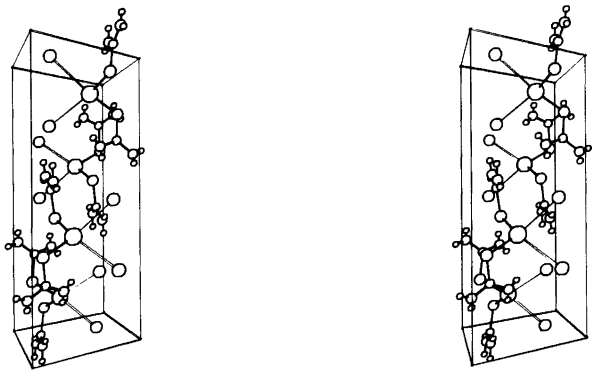

Fig. 2. A stereoscopic pair of drawings showing the content of the unit cell of $Se(tu)_2Cl_2$.

$Se(SCN)_2$, the Se–S bond length is 2.2136(10) Å and it has an N···Se–S approach of 3.000(3) Å and the angle S–Se–S is 101.59(4)°. The dimerized $Se(SCN)_3^-$ ion has S···Se–S approaches of 2.906(3) to 3.112(3) Å with Se–S bond lengths of 2.252(2) to 2.318(3) Å and S–Se–S angles of 95.50(11) to 98.52(12)°. From the bond lengths above, the influence of the halogen atoms on the Se–S bond length in the *trans* position should be less than that of the nitrogen atom in $Se(SCN)_2$. From the S–Se–S angles it can be seen that the influence is larger than from nitrogen in $Se(SCN)_2$, but less than from the bridging sulfur in $KSe(SCN)_3 \cdot 1/2H_2O$.

Bond lengths and angles in the thiourea groups do not deviate significantly from the values found in the crystals of thiourea itself.[17] Each of the thiourea groups is planar within the experimental errors. The carbon and nitrogen are all trigonal planar in accordance with the sp^2-hybridization of carbon atom. As seen from Table 3 the differences in the individual S–C bond lengths are not significant, nor are the differences in the individual C–N bond lengths. The weighted mean value of the S–C bond lengths is 1.767(2) Å and the weighted mean value of the C–N bond lengths is 1.303(2) Å. The N–C–N angles range from 122.3(4) to 124.2(6)° and the S–C–N angles from 113.5(3) to 123.3(3)°.

The packing in the crystals. The amino nitrogen atoms have short distances, probably involving hydrogen bonds, to halogen atoms (Table 4 and Fig. 2). The nitrogen atoms are assumed to have a trigonal planar bonding system, *i.e.* the hydrogen atoms lie in or close to the planes through the thiourea group. The interatomic distances and the distances of the halogen atoms from the thiourea planes are listed in Table 4.

Table 4. The geometry of the hydrogen bonding system.

Symmetry code:

1	$1+\bar{x}, \bar{y}, 1+\bar{z}$	4	$x-1, 1/2+\bar{y}, z-1/2$
2	$1+\bar{x}, \bar{y}, \bar{z}$	5	$1+\bar{x}, 1/2+y, 1/2+\bar{z}$
3	$1+\bar{x}, y-1/2, 1/2+z$	6	$x, 1/2+y, z-1/2$

D–H···A	D···A [Å]	Distance from thiourea plane [Å]
N1–H···$Cl2_1$	3.313(4)	0.147
N1–H···$Cl1_1$	3.178(4)	–0.821
N2–H···$Cl2_2$	3.279(4)	0.112
N2–H···$Cl1_3$	3.194(4)	–0.939
N3–H···$Cl2_4$	3.300(4)	–0.234
N3–H···$Cl2_5$	3.349(4)	–0.179
N3–H···$Cl1_4$	3.300(4)	–0.808
N4–H···$Cl2_5$	3.186(4)	–0.179
N4–H···$Cl1_6$	3.333(4)	1.179
N1–H···$Br2_1$	3.418(6)	0.035
N1–H···$Br1_1$	3.332(5)	–0.903
N2–H···$Br2_2$	3.421(6)	0.166
N2–H···$Br1_3$	3.343(5)	–0.925
N3–H···$Br2_4$	3.442(5)	–0.281
N3–H···$Br2_5$	3.535(5)	–0.108
N3–H···$Br1_4$	3.451(6)	–0.878
N4–H···$Br2_5$	3.335(5)	–0.108
N4–H···$Br1_6$	3.451(6)	1.174

REFERENCES

1. Foss, O. In Andersen, P., Bastiansen, O. and Furberg, S., Eds., *Selected Topics in Structure Chemistry,* Universitetsforlaget, Oslo 1967, p. 145.
2. Werner, A. E. *Sci. Proc. R. Dublin Soc. 22* (1941) 387.
3. Foss, O. *Acta Chem. Scand. 3* (1949) 708.
4. Ovsepyan, E. N., Shaposhnikova, G. V. and Galfayan, N. G. *Russ. J. Inorg. Chem. 16* (1967) 127.
5. Foss, O. *Acta Chem.Scand. 3* (1949) 435.
6. Coppens, P. In Ahmed, F. R., Hall, S. R. and Huber, C. P., Eds., *Crystallographic Computing,* Munksgaard, Cópenhagen 1970, p. 255.
7. *SDP-User's Guide,* Enraf-Nonius, Delft, Netherlands 1977.
8. Frenz, B. In Schenk, H., Olthof-Hazekamp, R., van Koningsveld, H. and Bassi, G., Eds., *Computing in Crystallography*, Delft University Press, Delft 1978, p. 64.
9. *International Tables for X-Ray Crystallography,* Kynoch Press, Birmingham 1962, Vol. 4, p. 86.
10. Foss, O. *Pure Appl. Chem. 24* (1970) 31.
11. Hauge, S. *Thesis,* University of Bergen, Bergen 1977.
12. Marøy, K. *Acta Chem. Scand. 26* (1972) 36.
13. Marøy, K. *Acta Chem. Scand. 26* (1972) 45.
14. Bøyum, K. and Marøy, K. *Acta Chem. Scand. 25* (1971) 2569.
15. Hauge, S. *Acta Chem. Scand. A 33* (1979) 313.
16. Hauge, S. *Acta Chem. Scand. A 29* (1975) 778.
17. Truter, M. R. *Acta Crystallogr. 10* (1957) 785.

Received August 13, 1982.

Acta Chemica Scandinavica A 37 (1983) 241–246

Liquid Phase Oxidation of Nitrous Acid by Hydrogen Peroxide

HANS T. KARLSSON

Department of Chemical Engineering, Lund Institute of Technology, Box 740, S-220 07 Lund, Sweden

The liquid phase oxidation of nitrous acid by hydrogen peroxide was investigated in a pH-stat. The results have revealed that the overall reaction includes a series of reactions and several intermediates. Nitrous acid decomposes to nitrogen oxide which in turn is oxidized to nitrogen dioxide by hydrogen peroxide. The dimer of nitrogen dioxide reacts with water to form the end product, *i.e.* nitric acid.

Nitrous acid is an important link in the complex aqueous chemistry of nitrogen oxides. If alkali is not present in the solution, nitrous acid decomposes into a variety of nitrogen oxides; alkali acts as a stabilizer due to nitrite ion formation. Hydrogen peroxide is thought to be an efficient species for oxidizing nitrous acid to nitric acid. Such an option is beneficial in air pollution control, not only because environmental impacts from nitrogen oxides are eliminated, but also because nitric acid can be recovered as a useful by-product.

At least two hydrogen peroxide based processes for control of air pollution by nitrogen oxides have been developed. Hydrogen peroxide can be used to enhance the absorption of nitrogen oxides in a wet scrubber.[1] Secondly, the release of nitrogen oxides to the ventilation gas in steel pickling can be suppressed by adding hydrogen peroxide to the pickling bath.[2]

The present study was undertaken to obtain kinetic data for the liquid phase oxidation of nitrous acid by hydrogen peroxide. Furthermore, an in-depth analysis of the chemistry was made to outline the reaction mechanism.

THEORY

If sodium nitrite is added to a water solution, complete dissociation is obtained:

$$NaNO_2 \rightleftarrows Na^+ + NO_2^- \qquad (a)$$

Hydrogen ions present in the solution produce nitrous acid by shifting the following equilibrium reaction to the right:

$$H^+ + NO_2^- \rightleftarrows HNO_2 \qquad (b)$$

From equilibrium data given by Skoog *et al.*[3] it can be inferred that the conversion of nitrite to nitrous acid is greater than 90 % at pH values below 2.3.

Hydrogen peroxide oxidizes the nitrous acid according to the following overall reaction:

$$HNO_2 + H_2O_2 \rightarrow HNO_3 + H_2O \qquad (c)$$

It is assumed that this reaction obeys an *m*-, *n*th-order rate expression of the following form:

$$r_c = -k_c(HNO_2)^n(H_2O_2)^m \qquad (1)$$

where the parentheses indicate aqueous phase concentration.

If a concentrated solution of sodium nitrite is added to the reaction mixture, the concentration of nitrous acid attains the following steady state value:

$$(HNO_2) = (H^+)_0 - (H^+) \qquad (2)$$

where (H^+) is given from the measured steady state pH value, and $(H^+)_0$ is the corresponding

0302-4377/83 $2.50

value before one starts to add nitrite to the solution.

The concentration of hydrogen peroxide can be calculated from the amount of this species charged to the solution, minus the amount consumed by reaction. The reaction rate can be estimated from the rate of added sodium nitrite solution and the concentration of the feed.

Thus the rate constant and the reactions orders can be obtained from steady state experiments by varying the concentrations of hydrogen peroxide and nitrous acid, *i.e.* hydrogen ion.

EXPERIMENTAL

Equipment. The experiments were performed by utilizing a pH-stat equipment (Radiometer). Hydrogen peroxide, water and nitric acid were charged to a glass beaker in desirable amounts. The pH-value of the solution was measured by an electrode connected to the pH-stat and the solution of sodium nitrite was added by an autoburette to obtain a preset pH value of the solution. The pH-stat adjusts the feed rate of the nitrite solution by a control loop based on a signal from the pH electrode.

The amount of nitrite fed to the solution was followed by continuously recording a signal from the burette on a strip chart recorder. The reaction rate was simply estimated by calculating the slope of the curve obtained on the strip chart numerically, and by multiplying by a calculated correction factor.

Procedure. The test runs were performed isothermally at 25 °C by cooling the glass beaker. Each experiment was run to completion, in order to allow a material balance calculation. It was found that the hydrogen peroxide was consumed stoichiometrically in all test runs with a deviation of roughly 5 %.

Preliminary experiments were performed in the absence of hydrogen peroxide to determine if any appreciable amount of nitrous acid was decomposed with subsequent stripping of nitrogen oxides; such a competing reaction path will lead to an overestimation of the reaction rate. However, negligible amounts of nitrite solution had to be added to the reaction mixture in order to maintain a constant pH value over an extended period of time. Thus, stripping of nitrogen oxides has a negligible impact on the result. This conclusion was further supported by the material balances.

Further tests were made to check the decomposition rate of hydrogen peroxide. Only small amounts were found to decompose at the pertinent concentration levels.

A total of 20 experiments were made under controlled conditions. The concentration of hydrogen peroxide was screened from 0.4 to 3.1 % by weight (115 to 920 mol m^{-3}). The steady state pH value was set below 2.3, and the concentration of nitrous acid was varied tenfold from about 5 to 50 mol m^{-3}.

RESULTS

Four series of data points were obtained, with constant concentration of hydrogen peroxide within each series. The data points are displayed in Fig. 1, as the reaction rate as a function of the concentration of nitrous acid. The plot reveals four straight lines with about equal slopes, but with intercepts increasing with the level of hydrogen peroxide. By rewriting eqn. (1) on a logarithmic form:

$$\log(-r_c) = \log[k_c(H_2O_2)^m] + n \log(HNO_2) \qquad (3)$$

it can be concluded that the findings are consistent with the suggested rate expression. Eqn. (3) predicts a straight line with a slope equaling the reaction order in nitrous acid. Furthermore, the intercept, corresponding to the first term of the right hand side, should increase with increasing concentration of hydrogen peroxide.

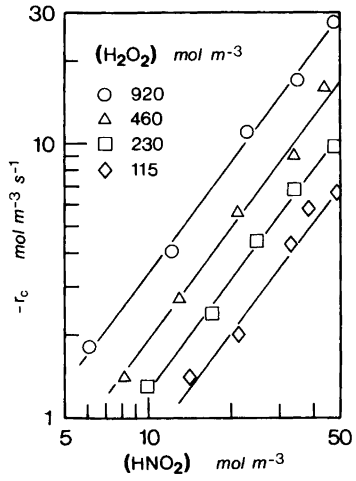

Fig. 1. The reaction rate as a function of the concentration of nitrous acid at 25 °C.

Each series of data points can, of course, be evaluated separately by simple least-square fits. However, based on the findings, a modified type of fit is more appropriate, in which case the slope is equal for all series. Such an approach is outlined in the Appendix.

By applying the procedure given in the Appendix, a slope of 1.35 was obtained. This value is equal to the reaction order with respect to nitrous acid. For convenience, justified later, it was rounded off to $n=4/3$. Based on this value, four straight lines have been inserted in Fig. 1.

In the limiting case $(HNO_2)=1$ mol m^{-3}, eqn. (3) is condensed to:

$$\log(-r_c) = \log(k_c) + m \log(H_2O_2) \quad (4)$$

By plotting the intercepts from Fig 1, obtained by extrapolating down to $(HNO_2)=1$ mol m^{-3}, the reaction order with respect to hydrogen peroxide can be obtained as shown in Fig. 2. The straight line was obtained from a simple least-square fit, yielding a slope of 0.685. This value was rounded off to $m=2/3$. The rate constant was calculated from the intercept to give a value of $k_c=1.56\times 10^{-3}$ mol^{-1} m^3 s^{-1}.

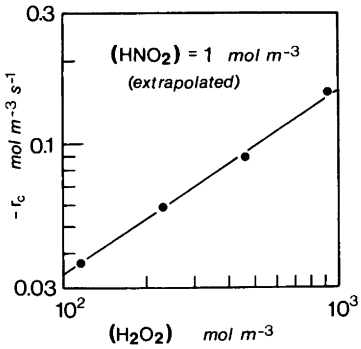

Fig. 2. Cross-plot of intercepts from Fig. 1.

REACTION MECHANISM

It was hypothesized that nitrous acid is inert with respect to oxidation by hydrogen peroxide directly. It was further alleged that the overall oxidation is a result of a reaction mechanism involving a series of reactions and several intermediates.

In the first step, nitrous acid is decomposed to nitric oxide and nitrogen dioxide according to the following two reactions:

$$2\,HNO_2 \rightleftarrows N_2O_3 + H_2O \quad (d)$$

$$N_2O_3 \rightleftarrows NO + NO_2 \quad (e)$$

Andrew *et al.*[4] studied the overall of these two reactions. They pointed out that the reactions are instantaneous and attain equilibrium in all points of the solution. It can clearly be concluded from work by Komiyama *et al.*[7] that N_2O_3 is an actual intermediate in the decomposition of nitrous acid.

It is well known from Sherwood *et al.*,[5] among others, that nitrogen dioxide reacts instantaneously to form a dimer:

$$2\,NO_2 \rightleftarrows N_2O_4 \quad (f)$$

The produced dimer is a reactive species. It reacts with water to form the end product, *i.e.* nitric acid, and to regenerate some nitrous acid:

$$N_2O_4 + H_2O \rightarrow HNO_3 + HNO_2 \quad (g)$$

In order to make the reactions proceed at steady state, the nitric oxide must be oxidized to nitrogen dioxide:

$$NO + H_2O_2 \rightarrow NO_2 + H_2O \quad (h)$$

The reaction mechanism is summarized in Fig. 3.

The rate expressions for reactions (g) and (h) can be written, respectively:

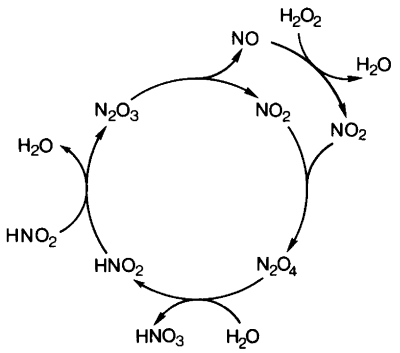

Fig. 3. Reaction mechanism for oxidation of nitrous acid by hydrogen peroxide.

$$r_g = -k_g (N_2O_4) \quad (5)$$

$$r_h = -k_h (NO)(H_2O_2) \quad (6)$$

The first rate expression has been verified by a large number of investigators during the last decades, for instance by Komiyama *et al.*[7] The second rate expression was suggested by Baveja *et al.*[8] and was later verified for low concentrations of nitrogen oxide.[1]

The equilibrium reactions can be represented by equilibrium constant expressions of the following forms:

$$\frac{(N_2O_3)}{(HNO_2)^2} = K_d \quad (7)$$

$$\frac{(NO)(NO_2)}{(N_2O_3)} = K_e \quad (8)$$

$$\frac{(N_2O_4)}{(NO_2)^2} = K_f \quad (9)$$

By a simple material balance, the pH values can be related to the concentrations of the various species:

$$(H^+)_o-(H^+) = (HNO_2)+(NO_2)+(NO)+ 2(N_2O_4)+2(N_2O_3) \quad (10)$$

This relationship is rather cumbersome to work with. However, by assuming that the concentration of nitrous acid is much greater than the concentrations of all other species, the following approximate equation is pertinent:

$$(H^+)_o-(H^+) \approx (HNO_2) \quad (11)$$

By this simplification, the concentration of nitrous acid can be calculated from observables explicitly.

If pseudo steady state is assumed, which is a reasonable approach at low concentrations, the following useful connection emerges:

$$r_c = r_g = r_h \quad (12)$$

By rearranging eqn. (5) through (9),(11) and (12), and by successively eliminating all species except nitrous acid, the reaction rate expression takes the following form:

Table 1. Rate constants and equilibrium data for pertinent reactions at 25 °C.

$K_dK_e(-)$	Andrew *et al.*:[4] 1.3×10^{-6}, and Nonhebel:[6] 1.5×10^{-6}.
K_f (mol^{-1} m^3)	Andrew *et al.*,[4] Sherwood *et al.*,[5] Nonhebel,[6] Komiyama *et al.*,[7] Wendel *et al.*[9] and Kramers *et al.*:[10] 13–73.
k_g (s^{-1})	Andrew *et al.*:[4] 48, Wendel *et al.*:[9] 290, Kramers *et al.*:[10] 415, Gerstacker:[11] 490, Komiyama *et al.*:[7] 591 and Nonhebel:[6] 670.
k_h (mol^{-1} m^3 s^{-1})	Baveja *et al.*[8] and Karlsson:[1] 0.57.
K_e (mol m^{-3})	Sherwood *et al.*:[5] 0.22.

$$r_c = -(k_hK_dK_e)^{2/3}(k_gK_f)^{1/3}(H_2O_2)^{2/3}(HNO_2)^{4/3} \quad (13)$$

It is concluded then, that this expression is equivalent to eqn. (1), with k_c replaced by:

$$k_c = (k_hK_dK_e)^{2/3}(k_gK_f)^{1/3} \quad (14)$$

From the experimental findings it was shown that the reaction orders with respect to hydrogen peroxide and nitrous acid were 2/3 and 4/3, respectively, which is consistent with the theoretical expression, *i.e.* eqn. (13).

DISCUSSION

Table 1 lists kinetic rate constants and equilibrium constants for the reactions involved in the detailed mechanism previously outlined. Data for K_f and k_g cover a wide range, mainly because solubility data for N_2O_4, obtained in the literature, appear to be rather unreliable.

The data allow a theoretical prediction of the rate constant for reaction (c) by utilizing eqn. (14). By inserting the extreme values in eqn. (14), the following limits can be obtained:

$$7.0\times10^{-4}<k_c<3.3\times10^{-3} \ (mol^{-1}\ m^3\ s^{-1})$$

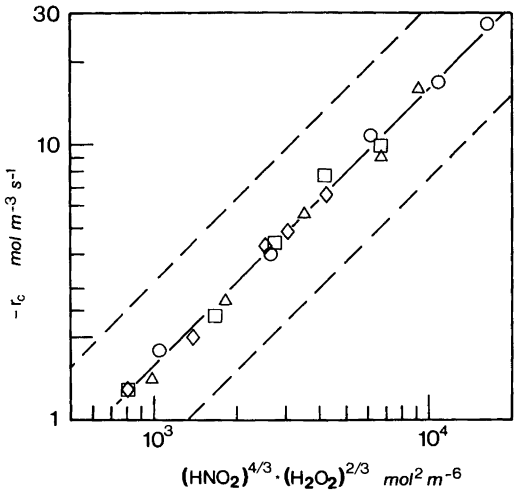

Fig. 4. Comparison of experimental results with theoretical predictions. The dashed lines represent the predicted upper and lower limits using the data given in Table 1.

while the experimentally determined rate constant is $k_c=1.56\times10^{-3}$ mol^{-1} m^3 s^{-1}.

All experimental data points have been plotted in Fig. 4 as the reaction rate as a function of $(HNO_2)^{4/3}(H_2O_2)^{2/3}$, along with the fitted curve. The dashed lines represent the limits for the predicted values based on the adapted literature data.

By evaluating the reliability of the literature data, it was concluded that the true data should generate a line between the one obtained from the present experiments and the upper limit.

Check of approximations. The literature data allow a check of the accuracy of the approximate equation describing the concentration of nitrous acid, *i.e.* eqn. (11). Using the most unfavorable data, the following set of information is obtained:

$(NO_2)<5.6\times10^{-3}\ (HNO_2)$
$(NO)<4.4\times10^{-3}\ (HNO_2)$
$2(N_2O_3)<6.8\times10^{-4}\ (HNO_2)$
$2(N_2O_4)<2.0\times10^{-2}\ (HNO_2)$

By simply adding these values, it can be concluded that the concentration of nitrous acid is never overpredicted by more than 3 %. However, the maximal errors given above do not appear simultaneously. Hence, the error is even smaller than 3 %. As the experimental conditions are altered, the error drops drastically.

The assumption concerning reactions (d) and (e) can be checked by writing the actual reaction rate for the overall reaction as:

$$r_{de} = -k'_{de}(HNO_2)^2+k'_{-de}(NO)(NO_2) \qquad (15)$$

If considering that:

$$r_{de} \approx r_c \qquad (16)$$

the following condition must be met to allow the assumption that reactions (d) and (e) are instantaneous:

$$-r_c \ll k'_{de}(HNO_2)^2 \qquad (17)$$

By utilizing eqn. (1), this can be rewritten to:

$$\frac{k'_{de}}{k_c} \gg \left\{\frac{(H_2O_2)}{(HNO_2)}\right\}^{2/3} \qquad (18)$$

A conservative estimate is given from the largest value of the right hand side, *i.e.* 150. From data by Komiyama *et al.*,[7] k'_{de} can be estimated to 27 mol^{-1} m^3 s^{-1} at 25 °C. Hence, $k'_{de}/k_c=1.8\times10^4\gg150$.

APPENDIX

Simultaneous least square fit of a number of series of data points. Eqn. (3) can be written in a simplified form:

$$Y = aX+b \qquad (A1)$$

p series of experiments are made, with q_j data points in series number j. b is unique for each series and attains a constant value within each series, but varies from one series to another. The slope, a, has the same value for all data points.

The square sum of the total error including all data points can be written:

$$S = \sum_j^p \sum_i^{q_j} (aX_{ij}+b_j-Y_{ij})^2 \qquad (A2)$$

The best fit is defined by:

$$\frac{dS}{da} = 0 \qquad (A3)$$

which leads to:

$$a \sum_{j}^{p} \sum_{i}^{q_j} X_{ij}^2 + \sum_{j}^{p} \left(b_j \sum_{i}^{q_j} X_{ij}\right) - \sum_{j}^{p} \sum_{i}^{q_j} (X_{ij} Y_{ij}) = 0 \quad \text{(A4)}$$

For each series:

$$S_j = \sum_{i}^{q_j} (aX_{ij} + b_j - Y_{ij})^2 \quad \text{(A5)}$$

with the following condition:

$$\frac{dS_j}{db_j} = 0 \quad \text{(A6)}$$

which leads to:

$$a \sum_{i}^{q_j} X_{ij} + b_j q_j - \sum_{i}^{q_j} Y_{ij} = 0 \quad \text{(A7)}$$

The intercept for each series is:

$$b_j = \left(\sum_{i}^{q_j} Y_{ij} - a \sum_{i}^{q_j} X_{ij} \right) / q_j \quad \text{(A8)}$$

This can be rewritten as:

$$\sum_{j}^{p} \left(b_j \sum_{i}^{q_j} X_{ij}\right) = \sum_{j}^{p} \left[\left(\sum_{i}^{q_j} Y_{ij}\right) \sum_{i}^{q_j} \left(X_{ij}/q_j\right)\right]$$
$$- a \sum_{j}^{p} \left[\left(\sum_{i}^{q_j} X_{ij} \right)^2 / q_j\right] \quad \text{(A9)}$$

The second term of eqn. (A4) can now be eliminated to give the slope explicitly:

$$a = \frac{\sum_{j}^{p} \sum_{i}^{q_j} \left(X_{ij} Y_{ij}\right) - \sum_{j}^{p} \left[\left(\sum_{i}^{q_j} Y_{ij} \right) \sum_{i}^{q_j} \left(X_{ij}/q_j\right)\right]}{\sum_{j}^{p} \sum_{i}^{q_j} X_{ij}^2 - \sum_{j}^{p} \left[\left(\sum_{i}^{q_j} X_{ij} \right)^2 / q_j\right]} \quad \text{(A10)}$$

From a known value of a, b_j can be calculated explicitly by eqn. (A8).

REFERENCES

1. Karlsson, H. T. *Mass Transfer and Engineering Aspects on Air Pollution Control Equipment,* Lund Institute of Technology, Lund 1981; Coden: LUTKDH/(TKKT/1002)/1–168/(1981).
2. Shuisky, G., Andersson, L., Eriksson, I., Karlsson, H., Moberg, A. and Nilsson, L.-I. *NO_x Emissions in Pickling of Stainless Steel,* Jernkontorets Forskning D 367, Jernkontoret, Stockholm 1981.
3. Skoog, D. A. and West, D. M. *Fundamentals of Analytical Chemistry,* Holt, Reinhart & Winston, London 1969.
4. Andrew, S. P. S. and Hanson, D. *Chem. Eng. Sci. 14* (1961) 105.
5. Sherwood, T. K., Pigford, R. L. and Wilke, C. R. *Mass Transfer,* McGraw-Hill, New York 1975.
6. Nonhebel, G. *Gas Purification Processes for Air Pollution Control,* Newness-Butterworth, London 1972.
7. Komiyama, H. and Inoue, H. *Chem. Eng. Sci. 35* (1980) 154.
8. Baveja, K. K., Rao, D. S. and Sarkar, M. K. *J. Chem. Eng. Jpn. 12* (1979) 322.
9. Wendel, M. M. and Pigford, R. L. *AIChE J. 4* (1958) 249.
10. Kramers, H., Blind, M. P. P. and Snoeck, E. *Chem. Eng. Sci. 14* (1961) 115.
11. Gerstacker *Chem. Eng. Sci. 14* (1961) 124.

Received August 13, 1982.

Acta Chemica Scandinavica A 37 (1983) 247–250

Characterization of a Mixed Valence Cyano-bridged Cobalt(III)iron(II) Complex

SVEN BAGGER and PER STOLTZE *

Chemistry Department A, Building 207, The Technical University of Denmark, DK-2800 Lyngby, Denmark

The mixed valence ion $[(en)_2(NH_3)Co{\cdot}{\cdot}NC{\cdot}Fe(CN)_5]^-$ has been isolated. Its optical and electrochemical properties have been studied. A comparison with the analogous cobalt(III)ruthenium(II) complex has been made.

The mixed valence complexes $[(NH_3)_5Co{\cdot}NC{\cdot}Ru(CN)_5]^-$ and $[(en)_2(NH_3)Co{\cdot}NC{\cdot}Ru(CN)_5]^-$, both of which contain the central unit {Co(III)·NC·Ru(II)}, have been described in the literature.[1,2] It would be of interest to compare these two ions with analogous iron complexes of composition $[(NH_3)_5Co{\cdot}NC{\cdot}Fe(CN)_5]^-$ and $[(en)_2(NH_3)Co{\cdot}NC{\cdot}Fe(CN)_5]^-$.

However, it has been reported that attempts to prepare $[(NH_3)_5Co{\cdot}NC{\cdot}Fe(CN)_5]^-$ were unsuccessful. We have confirmed the finding that $[Co(NH_3)_5(H_2O)]^{3+}$ reacts with $[Fe(CN)_6]^{4-}$ in aqueous solution to form a *greenish precipitate,* presumably consisting of cobalt(II)hexacyanoferrate(III) and cobalt(II)hexacyanoferrate(II).[1,3]

If *trans*-$[Co(en)_2(NH_3)(H_2O)]^{3+}$ is used instead of $[Co(NH_3)_5(H_2O)]^{3+}$ in a similar experiment, we observe a strikingly different behaviour. The reaction with $[Fe(CN)_6]^{4-}$ yields a *clear, intensely brown-red solution.* The appearance of this solution is stable for weeks on standing at room temperature. This observation encouraged us to search for the complex $[(en)_2(NH_3)Co{\cdot}NC{\cdot}Fe(CN)_5]^-$.

Notation and Terminology

In this paper *1* stands for $[(en)_2(NH_3)Co{\cdot}{\cdot}NC{\cdot}Fe(CN)_5]^-$; en is the abbreviation for 1,2-ethanediamine (ethylenediamine).

For the molar absorption coefficient, ε, the traditional dimension $M^{-1}\ cm^{-1}$ is used.

The characteristic strong colour of many mixed valence complexes arises from a charge-transfer transition which occurs between orbitals centered on different metal atoms.[4] This is called an IT-transition, IT being the abbreviation for intervalence transfer.

EXPERIMENTAL

An aqueous solution containing equimolar concentrations of *trans*-$[Co(en)_2(NH_3)(H_2O)]^{3+}$ and $[Fe(CN)_6]^{4-}$ develops a strong, brown-red colour within some hours. The colour is due to a broad absorption in the visible region, and after about 24 h the spectrum is virtually constant.

Ion-exchange chromatography of the brown-red solution shows that at least five strongly coloured, quite robust, anionic species are present. By column chromatography with the anion exchanger QAE-Sephadex as packing material and aqueous NaCl solution as eluent, five distinct zones are developed with relative R_f-values 127, 36, 9, 3 and 1.

During the chromatographic work it was discovered that the slow zones appeared somewhat sharper if O_2 was removed from the eluent.

All conditions being the same, it was found that the fastest moving component – in this paper named *1* – travels through the column at the same rate as $[(en)_2(NH_3)Co{\cdot}NC{\cdot}Ru(CN)_5]^-$.[2]

All five chromatographic zones contain cobalt and iron and were analyzed by atomic absorption

* Present address: Haldor Topsøe Research Laboratories, Nymøllevej 55, DK-2800 Lyngby, Denmark.

0302-4377/83 $2.50

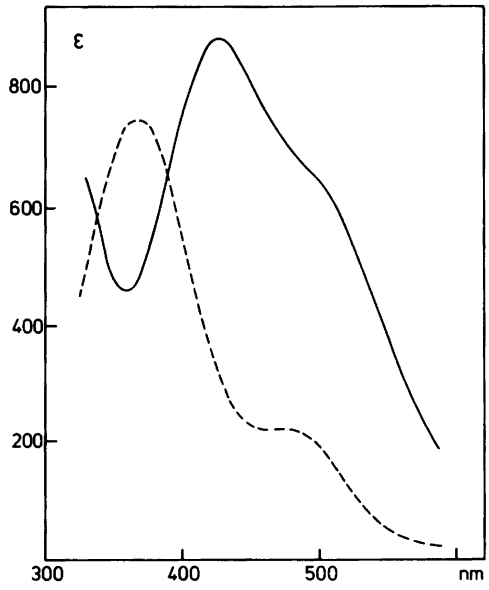

Fig. 1. Absorption spectra of solutions. ——, *1*; – – –, $[(en)_2(NH_3)Co{\cdot}NC{\cdot}Ru(CN)_5]^-$. The IT-transitions occur at 369 and 428 nm, respectively.

spectrometry.

The molar Co:Fe ratio of an eluted sample of *1* was found to be 1.

The remaining four zones were not eluted from the column before analysis, but after development all the content of the column was extruded and samples absorbed on Sephadex were obtained. The analysis showed Co:Fe molar ratios significantly lower than 1. Probably these four slow-moving species are cyano-bridged complexes with more than two metal centers, and they are not considered further in this paper.

The yield of chromatographically pure *1* is only *ca.* 10 %, relative to the complexes used for preparation of the initial raw solution.

An absorption spectrum and a single sweep triangular wave voltammogram of *1* are given in Figs. 1 and 2.

Like $[(en)_2(NH_3)Co{\cdot}NC{\cdot}Ru(CN)_5]^-$, *1* is photo-sensitive. A solution rapidly becomes cloudy when exposed to strong daylight.

1 is not so stable as its ruthenium analogue on standing at room temperature. In a day-old preparation changes are seen in the absorption spectrum and an extra wave has developed in the cyclic voltammogram.

Attempts to obtain IR- and NMR-spectra were hampered by partial decomposition of *1* during the procedure of preparing sufficiently concentrated samples. We have not succeeded in preparing a crystalline salt of *1*.

Experimental Details

General. Solutions of *1* were handled in subdued light and measurements were carried out on freshly chromatographed samples.

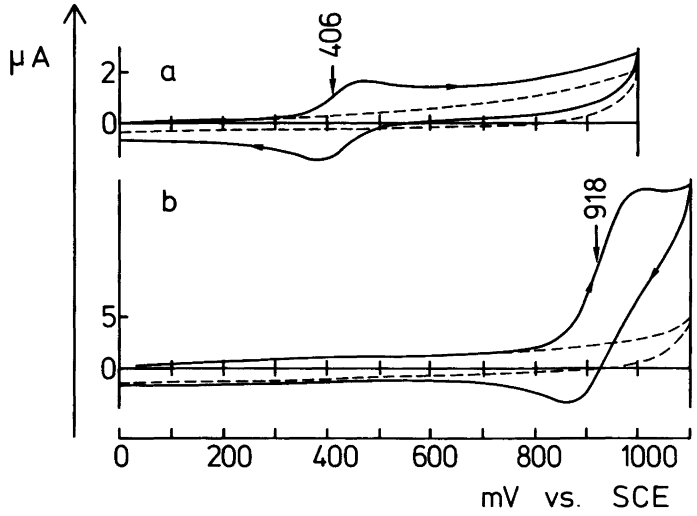

Fig. 2. Single-sweep triangular wave voltammograms. a, freshly eluted solution of *1*; b, $[(en)_2(NH_3)Co{\cdot}NC{\cdot}Ru(CN)_5]^-$. $E_{p/2}$-values for the anodic waves are indicated. Sweep rate: 100 mV s^{-1}. Supporting electrolyte: saturated NaCl. The dashed curves show the residual current. ($E_{p/2}$ for $[Fe(CN)_6]^{4-}$ and $[Ru(CN)_6]^{4-}$ are 287 mV and 904 mV, respectively, under the same conditions.[2])

Materials. *trans*-$[Co(en)_2(NH_3)(H_2O)](NO_3)_3$ was prepared according to a published procedure.[5] The anion exchanger used was QAE-Sephadex A-25 from Pharmacia (Sweden).

Synthesis and isolation of 1. An aqueous raw solution containing *1* was typically prepared as follows. Two solutions, 0.100 g *trans*-$[Co(en)_2(NH_3)(H_2O)](NO_3)_3$ (0.250 mmol) in 15 ml H_2O and 0.116 g $K_4[Fe(CN)_6].3H_2O$ (0.275 mmol) in 10 ml H_2O, were mixed in an Erlenmeyer flask. With these relatively concentrated solutions a yellow precipitate, probably $[Co(en)_2(NH_3)(H_2O)]_4[Fe(CN)_6]_3$, initially formed. After standing at room temperature in the dark for 24 h the precipitate had disappeared and an optically clear, strongly brown-red solution resulted. This solution was chromatographed.

For a preparative experiment a glass column of 50 mm internal diameter was packed with Sephadex ion exchanger to a height of about 40 mm. 25 ml of the solution described above was applied to the column. During this operation it was observed that some unreacted $[Co(en)_2(NH_3)(H_2O)]^{3+}$ passed through the Sephadex. After elution with about 350 ml 0.25 M aqueous NaCl solution a brown-red zone of *1* had separated from a dark-coloured band at the top of the column. As a precaution the eluent was deaerated by bubbling with N_2 before entering the column. The yield from an experiment like this was typically 0.02 mol *1* in 0.25 M NaCl.

Analyses. Solutions of *1* were analyzed for Co and Fe by atomic absorption spectrometry. A Perkin-Elmer model 305A spectrometer was used. Samples for analysis were prepared by evaporation, fuming with conc. HNO_3 and $HClO_4$, and finally appropriate dilution with H_2O.

The experimental Co:Fe molar ratio for *1* was 0.99.

Cyclic voltammetry. The method and the electrochemical apparatus of three-electrode design with a vitreous carbon indicator electrode was the same as described previously.[2] The supporting electrolyte was saturated NaCl in order to allow direct comparison with earlier results.[2]

DISCUSSION

On the basis of the available evidence *1* is formulated $[(en)_2(NH_3)Co{\cdot}NC{\cdot}Fe(CN)_5]^-$.

The absorption band at 428 nm with ε=883, which has no counterpart in either of the separate species $[Co(en)_2(NH_3)(H_2O)]^{3+}$ and $[Fe(CN)_6]^{4-}$, is assigned to an Fe(II)→Co(III) IT-transition mediated by the CN-bridge. The *d–d* transitions in Co(III) appear as a shoulder at about 500 nm.

Table 1. Data on IT-transitions of {Co(III)·NC·Fe(II)} species.

	IT-band	Ref.
$[(edta)Co{\cdot}NC{\cdot}Fe(CN)_5]^{5-}$ [a]	λ=565 nm ε=*ca.* 800	6
$[(cydta)Co{\cdot}NC{\cdot}Fe(CN)_5]^{5-}$ [b]	λ=540 nm ε=690	7
$[(NC)_5Co{\cdot}NC{\cdot}Fe(CN)_5]^{6-}$	λ=395 nm ε=700	6
1	λ=428 nm ε=883	This work

[a] edta=ethylenediaminetetraacetate. [b] cydta=*trans*-1,2-cyclohexanediaminetetraacetate.

In Table 1 the ε-value of the IT-absorption of *1* is compared with literature values for related {Co(III)·NC·Fe(II)} species.

$[(edta)Co{\cdot}NC{\cdot}Fe(CN)_5]^{5-}$ and $[(cydta)Co{\cdot}NC{\cdot}Fe(CN)_5]^{5-}$ have been detected as short-lived intermediates in electron transfer reactions between cobalt(II) complexes and hexacyanoferrate(III).

In the present study the reactants are a cobalt(III) complex and hexacyanoferrate(II). *1* is probably formed by a substitution reaction in which $[Fe(CN)_6]^{4-}$ displaces H_2O in $[Co(en)_2(NH_3)(H_2O)]^{3+}$.

Fig. 1 shows that in $[(en)_2(NH_3)Co{\cdot}NC{\cdot}Ru(CN)_5]^-$ the IT-band occurs at higher energy than in $[(en)_2(NH_3)Co{\cdot}NC{\cdot}Fe(CN)_5]^-$. This is in accordance with expectation, since $[Fe(CN)_6]^{4-}$ is more easily reduced than $[Ru(CN)_6]^{4-}$.

The redox reaction reflected in the waves of the cyclic voltammograms in Fig. 2 is

$$\{Co(III)\cdot NC\cdot M(II)\} \rightleftarrows \{Co(III)\cdot NC\cdot M(III)\}+e$$

In the voltammogram of *1* a simple behaviour is observed. The heights of the oxidation wave (outward scan) and the reduction wave (homeward scan) are the same. This was found to be the case even at much lower sweep rates.

In the case of $[(en)_2(NH_3)Co{\cdot}NC{\cdot}Ru(CN)_5]^-$ the reduction wave is almost absent; it becomes

more pronounced with faster sweeps. This indicates that the simple redox reaction is complicated by fast side-reactions of the {Co(III)·NC·Ru(III)} species.

$[(NH_3)_5Co{\cdot}NC{\cdot}Fe(CN)_5]^-$ does not exist as a stable species at room temperature because a spontaneous, intramolecular, thermal electron transfer would result in a labile Co(II) complex and hexacyanoferrate(III).[1] We have shown that *1* is moderately stable.

As deduced from the relative positions of the IT-bands of $[(en)_2(NH_3)Co{\cdot}NC{\cdot}Ru(CN)_5]^-$ and $[(NH_3)_5Co{\cdot}NC{\cdot}Ru(CN)_5]^-$ the group $(en)_2(NH_3)Co-$ is less liable to reduction than $(NH_3)_5Co-$.[2] This rationalizes that the tendency for $[(en)_2(NH_3)Co{\cdot}NC{\cdot}Fe(CN)_5]^-$ to disintegrate as a consequence of intramolecular electron transfer is less pronounced than for $[(NH_3)_5Co{\cdot}NC{\cdot}Fe(CN)_5]^-$.

Acknowledgement. The authors wish to acknowledge experimental contributions to the present study made by Ole Mogensen as part of his undergraduate work.

REFERENCES

1. Vogler, A. and Kunkely, H. *Ber. Bunsenges. Phys. Chem. 79* (1975) 83.
2. Bagger, S. and Stoltze, P. *Acta Chem. Scand. A 35* (1981) 509.
3. Gaswick, D. and Haim, A. *J. Am. Chem. Soc. 93* (1971) 7347.
4. Brown, D. B., Ed., *Mixed-Valence Compounds,* Reidel, Dordrecht 1980.
5. Tobe, M. L. and Martin, D. F. *Inorg. Synth. 8* (1966) 198.
6. Hester, R. E. and Nour, E. M. *J. Chem. Soc. Dalton Trans.* (1981) 939.
7. Huchital, D. H. and Hodges, R. J. *Inorg. Chem. 12* (1973) 998.

Received August 18, 1982.

Acta Chemica Scandinavica A 37 (1983) 251–257

Spin Equilibria in Some New *cis*-Diisothiocyanato Iron(II) Complexes with Tetradentate Ligands of the Tris(2-pyridylmethyl)amine Type

FREDE HØJLAND, HANS TOFTLUND and STEEN YDE-ANDERSEN

Department of Chemistry, University of Odense, DK-5230 Odense M, Denmark

The preparation of five new *cis*-[FeL(NCS)$_2$] complexes, where L is modified tetradentate ligands of the tris(2-pyridylmethyl)amine (tpa) type, is described.

Magnetic susceptibility measurements over the temperature range 80–300 K and infrared spectra at 77 and 300 K are reported.

The results show that two of the complexes exist in a temperature-dependent high-spin $^5T_2 \rightleftarrows$low-spin $^1A_1$ equilibrium. Two of the complexes show an intermediate spin state with a temperature independent magnetic moment. One complex is a pure high-spin $^5T_2$ complex at all temperatures.

The temperature-induced low-spin $^1A_1$ (Oh) $\rightleftarrows$ high-spin $^5T_2$ (Oh) transitions in iron(II) complexes of the type *cis*-[FeL$_2$(NCS)$_2$], where L are bidentate ligands as 2,2′-bipyridine (biby) or 1,10-phenanthroline (phen), have been extensively studied by several techniques as described in a recent review by Gütlich.[1] Some systems with modified phen or bipy ligands have been described [1,2] as well as a series of complexes where L is Schiff-base ligands.[3] All the previously investigated systems showing the spin-cross-over phenomenon contained four amine ligands of the conjugated diimine type. Recently it has been shown that iron(II) complexes of the hexadentate ligands of the tetrakis(2-pyridylmethyl)ethylenediamine (tpen) type are either low-spin or cross-over systems,[4] suggesting that the chelate effect may be as important as the conjugation in the ligand for the formation of cross-over iron(II) systems.

In order to investigate further some of the factors which can make a ligand capable of forming a spin-cross-over iron(II) complex we decided to make a systematic investigation on some new complexes of the *cis*-[FeL(NCS)$_2$] type (L is various tetradentate ligands of the tris(2-pyridylmethyl)amine (tpa) type). A large variation in magnetic behaviour turned out to be represented by these systems. Two new spin-cross-over systems were found for iron (II) complexes of L=tpa and (1-(2-pyridyl)ethyl)-bis(2-pyridylmethyl)amine (L(II)), whereas with L=(6-methyl-2-pyridylmethyl)-bis(2-pyridylmethyl)amine (L(IV)) a complex which is high-spin in the whole temperature range is formed. Two complexes with a temperature-constant intermediate spin, triplet ($^3T_1$(Oh)) or a mixture of singlet and quintet, were found for L=(2-(2-pyridyl)ethyl)-bis(2-pyridylmethyl)amine (L(III)) and bis(2-pyridylmethyl)amine (dpa) *plus* pyridine (py).

The spin states of the various iron(II) complexes were characterized by the variation of their magnetic susceptibility and their infrared spectra with the temperature.

EXPERIMENTAL

Instruments. Magnetic susceptibilities were measured by the Faraday method, using Hg [Co (SCN)$_4$] as calibrant. The equipment employs an electromagnet (Bruker-Physik), an electrical microbalance (Sartorius type 411) and a temperature unit (BVT-1000). Sample temperatures were measured using a chromel-alumel thermocouple.

0302-4377/83 $2.50

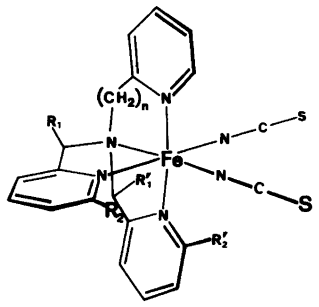

Fig. 1. Drawing of the *cis*-diisothiocyanato-tris(2-pyridylmethyl)amine iron(II) framework. The combination of substituents in the complexes used is given in Table 1.

Table 1. Combination of substituents.

R_1 or R_1'	R_2 or R_2'	Complex
$n=1$		
H	H	$[Fe(tpa)(NCS)_2]$
CH_3	H	$[FeL(II)(NCS)_2]$
H	CH_3	$[FeL(IV)(NCS)_2]$
$n=2$		
H	H	$[FeL(III)(NCS)_2]$
$n=0$		
H	H	$[Fe(dpa)(py)(NCS)_2]$

The molar susceptibilities were corrected for ligand diamagnetism by Pascal's constants.[18] The infrared spectra were obtained on a Perkin-Elmer 580 spectrometer calibrated with polystyrene. The samples were grounded in nujol and measured between KBr-plates. The low-temperature spectra were obtained with the samples placed *in vacuum* on a cold finger cooled with liquid nitrogen.

Preparation of ligands. Tris (2-pyridylmethyl)amine (tpa). This ligand was prepared by a method which was a slight modification of Anderegg's method.[5] A solution of 2-pyridylmethyl chloride hydrochloride prepared from α-picoline [19] (23.6 g, 144 mmol) in water (10 ml) was neutralized with a sodium hydroxide solution (29 ml, 5 M) and 2-pyridylmethylamine (Aldrich) (7.8 g, 72 mmol) was added. During the following days a sodium hydroxide solution (29 ml, 5 M) was added with stirring in so small portions that pH never exceeded 9. The resulting dark red solution was extracted with chloroform (3 times 150 ml). The combined extracts were dried (sodium sulfate) and the chloroform was removed on a rotary evaporator. The residue was purified by (short distance) high-vacuum distillation. The product was a yellow viscous oil, 4.2 g (35 %), b.p. 144–146 °C/0.01 mmHg.

1-(2-Pyridyl)ethyl-bis(2-pyridylmethyl)amine (L(II)). 2-Acetylpyridine (Aldrich) (9.3 g, 77 mmol) was dissolved in abs. ethanol (50 ml) and 2-aminomethylpyridine (Aldrich) (8.3 g, 77 mmol) was added and the solution was refluxed for 1 h. A viscous yellow oil remained after removal of solvent. It was dissolved in methanol (50 ml) and sodium tetrahydridoborate (Fluka) (1.6 g, 42 mmol) was added in small portions with stirring. The solution was left overnight. Hydrochloric acid (5 ml, 12 M) was added to the solution and when the gas evolution had ceased the solution was made alkaline with a sodium hydroxide solution (6 ml, 5 M). The solvent was evaporated *in vacuum* and water (20 ml) was added. A precipitate of sodium borate was filtered off. To the filtrate, 2-pyridylmethyl chloride hydrochloride (12.6 g, 77 mmol) was added and a sodium hydroxide solution (15 ml, 5 M) was added. During the following days sodium hydroxide solution (15 ml, 5 M) was added with stirring in such small portions that pH never exceeded 9. The resulting dark red solution was extracted with chloroform (3 times 100 ml). The combined extracts were dried (sodium sulfate) and the solvent was removed. The residue was purified by high vacuum distillation. The product was a yellow viscous oil, 2.3 g (10 %) b.p. 149–152 °C/0.01 mmHg.

2-(2-Pyridyl)ethyl-bis(2-pyridylmethyl)amine (L(III)). This ligand was prepared by the same method as used for tpa. 2-(2-Pyridyl)ethylamine (Aldrich) (9.8 g, 80 mmol) was treated with 2-pyridylmethyl chloride hydrochloride (30 g, 183 mmol) and sodium hydroxide (73 ml, 5 M). Purification by distillation gave a yellow viscous oil, 2.3 g (10 %), b.p. 154–256 °C/0.01 mmHg.

Bis(2-pyridylmethyl)amine (dpa). To a solution of 2-aminomethylpyridine (Aldrich) (10 g, 92 mmol) in abs. ethanol (20 ml) was added 2-pyridinecarbaldehyde (Aldrich) (10 g, 93 mmol). The solution was refluxed for 10 min. The solvent was removed and the residue dissolved in methanol (50 ml). Sodium tetrahydridoborate (Fluka) (1.9 g, 50 mmol) was added in small portions with stirring and the solution was left overnight. Excess of sodium tetrahydroborate was destroyed with hydrochloride acid (5 ml, 12 M). After removing the solvent and dissolving the residue in water (10 ml), the solution was made alkaline with a sodium hydroxide solution (7 ml,

5 M).

A precipitate of sodium borate was filtered off and the solution extracted with chloroform (3 times 100 ml). The combined extracts were dried (sodium sulfate) and the solvent was removed. The residue was distilled as above. The product was a pale yellow viscous oil, 2 g (21 %), b.p. 145 °C/0.2 mmHg.

(6-Methyl-2-pyridylmethyl)-bis(2-pyridylmethyl)amine (L(IV)). This ligand was prepared by the same method as used for tpa. Dpa, prepared as described above, (9.5 g, 48 mmol) was treated with 6-methyl-2-pyridylmethyl chloride hydrochloride, prepared from 2,6-lutidine and sodium hydroxide (19 ml, 5 M). The product was a pale yellow viscous oil, 2 g (14 %), b.p. 154–156 °C/0.01 mmHg.

Preparation of complexes. All iron(II) complexes were prepared under nitrogen in N_2-saturated solvents. *trans*-Diisothiocyanatotetrakispyridineiron(II), prepared as described in the literature.[19] was dissolved in boiling abs. ethanol (10 ml) and the ligand (2 mmol) dissolved in boiling abs. ethanol (5 ml) was added with stirring. The solution was slowly cooled to room temperature. The precipitated iron(II) complex was filtered off and washed with abs. ethanol and dried over sulphuric acid. The yields were in all cases about 3 g (65 %). (Anal. C,H,N,S).

RESULTS AND DISCUSSION

Preparations. The tetradentate ligands tris(2-pyridylmethyl)amine (tpa) and (2-(2-pyridyl)-ethyl)-bis(2-pyridylmethyl)amine [L(III)] were prepared by reacting 2-pyridylmethylamine or [2-(2-pyridyl)ethyl]amine with 2-pyridylmethyl chloride which is a modification of the method used by Anderegg for the preparation of tpa.[5] The ligand (6-methyl-2-pyridylmethyl)-bis(2-pyridylmethyl)amine [L(IV)] was prepared by reaction between bis(2-pyridylmethyl)amine and 6-methyl-2-pyridylmethyl chloride. [1-(2-Pyridyl)ethyl]-bis(2-pyridylmethyl)amine [L(II)] was prepared *via* the Schiff-base of 2-acetylpyridine and 2-pyridylmethylamine by reduction with sodium tetrahydridoborate. The remaining 2-pyridylmethyl group was introduced with 2-pyridylmethylchloride as above.

The bis-isothiocyanato iron(II) complexes were all prepared in a nitrogen atmosphere by reacting *trans*-[Fepy$_4$(NCS)$_2$] with the respective ligands in boiling absolute ethanol. The analytical data show good agreement between found and calculated values for all the metal complexes.

All the bis-isothiocyanato iron(II) complexes with the tetradentate ligands seem to be stable and resist air oxidation in the solid state at room temperature. Thus they show no change in coloration or IR spectra by storing for months.

The colour of the complexes varies from bright yellow for *cis*-[FeL(IV)(NCS)$_2$] to red brown for *cis*-[FeL(II)(NCS)$_2$]. *cis*-[Fe(tpa)(NCS)$_2$] and *cis*-[FeL(II)(NCS)$_2$] shows a very striking change in coloration on cooling from room temperature to liquid nitrogen temperature going from yellow to deep red.

Magnetic measurements. The magnetic measurements were made on solid samples in the temperture range 77 or 100 K to 300 or 350 K. All measurements were made at three different field strengths and no field dependence was observed. The data were recorded with ascending temperature. The compounds showed signs of decomposition at temperature above 350 K.

The temperature dependence of the effective magnetic moments μ_{eff} of the five iron(II) complexes are shown in Fig. 2. The highest and lowest μ_{eff} for each compound in this work as well as some relevant compounds from the literature are shown in Table 2.

cis-[FeL(IV)(NCS)$_2$] exhibits a behaviour typical for a high-spin pseudo-octahedral iron(II) complex (ground state $^5T_2$), with a nearly constant magnetic moment of 5.25–5.40 BM in the temperature range 77–300 K. However, strongly temperature dependent magnetic moments were observed for *cis*-[Fe(tpa)(NCS)$_2$] and *cis*-[FeL(II)(NCS)$_2$], changing from about 2.9 to 5.4 BM in the temperature range 80–300 K.

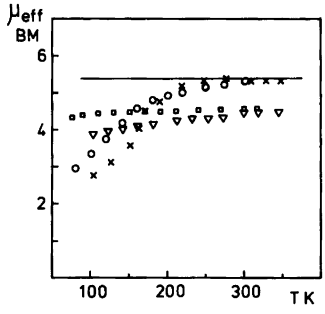

Fig. 2. The temperature dependence of the effective magnetic moment μ_{eff} BM. ——, *cis*-[FeL(IV)(NCS)$_2$]; ×, *cis*-[Fe(tpa)(NCS)$_2$]; ○, *cis*-[FeL(II)(NCS)$_2$];, □, *cis*-[FeL(III)(NCS)$_2$]; ▽, *cis*-[Fe(dpa)(py)(NCS)$_2$].

Table 2. Effective magnetic moment at liquid nitrogen temperature and at room temperature.

Compound	μ_{eff} BM at 80 K	μ_{eff} BM at 300 K	Ground state	Ref.
[FeL(IV)$(NCS)_2$]	5.25	5.40	$^5T_2$	This work
[Fe(2-CH_3phen)$_2(NCS)_2$]	5.37	5.42	$^5T_2$	17
[Fe(tpa)$(NCS)_2$]	2.83	5.46	$^5T_2 \rightleftarrows {}^1A_1$	This work
[FeL(II)$(NCS)_2$]	2.94	5.33	$^5T_2 \rightleftarrows {}^1A_1$	
[Fe(phen)$_2(NCS)_2$]	0.71	5.17	$^5T_2 \rightleftarrows {}^1A_1$	8
[FeL(III)$(NCS)_2$]	4.33	4.59	$^5T_2+{}^3T_1$	This work
[Fe{4,7(C_6H_5)$_2$(phen)}$_2(NCS)_2$]	4.13	4.28 [a]	$^5T_2+{}^3T_1$	3
[Fe(dpa)(py)$(NCS)_2$]	3.88 [b]	4.50	$^5T_2$, $^3T_1$, $^1A_1$	This work

[a] Value corresponding to 352 K. [b] Value corresponding to 100 K.

In contrast to *cis*-[Fe(phen)$_2(NCS)_2$] the spin changes are gradual and the residual paramagnetic moments at low temperature are relatively high. The residual magnetic moment presumably depends on the method of preparation. Thus, in the case of *cis*-[Fe(tpa)$(NCS)_2$], a sample of relatively large crystals precipitated from a pyridine solution shows a moment of 2.83 BM at 100 K whereas a sample of smaller crystals precipitated from absolute ethanol gave 3.76 BM at 100 K. Both samples crystallize without crystal solvent so the variation probably reflects some differences in the size of the domains in the crystals.[6]

The magnetic moment of *cis*-[FeL(III)$(NCS)_2$] changes only very slightly with the temperature, suggesting no spin change for this compound, but the effective magnetic moment is only 4.52 BM corresponding to 65 % of a pure high-spin phase $^5T_2$ mixed with 35 % of a pure low-spin phase $^1A_1$ or a mixture of equal amounts of a triplet phase $^3T_1$ and a quintet phase $^5T_2$. *cis*-[Fe(4,7(C_6H_5)$_2$phen)$_2(NCS)_2$] exhibits a very similar magnetic behaviour.[3] In this case a mixture of equal amounts of triplet and quintet is suggested.

The mixed ligand complex *cis*-[Fe(dpa)py$(NCS)_2$] also has a reduced magnetic moment at room temperature which gradually decreases to 3.88 at 77.

Infrared measurements. In order to have a microscopic criterium to supplement the macroscopic magnetic susceptibility information, we have measured the infrared spectrum at room temperature and at liquid nitrogen temperature in the region 4000–250 cm^{-1} for all the complexes. The region of the C–N stretching frequency of NCS is particularly useful in characterizing the ground state. It has been demonstrated that a $^5T_2$ ground state normally shows a strong doublet at 2060–2080 cm^{-1} whereas another strong doublet characteristic of a $^1A_1$ ground state appears at 2100–2120 cm^{-1}.[7,8] Fig. 3 shows the temperature variation of the IR spectrum of *cis*-[Fe(tpa)$(NCS)_2$] which is typical. It appears that each doublet is further split up presumably due to the fact that the two NCS groups are in different environments. The low-temperature spectrum shows lines both in the 2060–2080 cm^{-1} region and in the 2100–2120 cm^{-1} region. Therefore, we can conclude that the present transitions are characterized by the coexistence of the high-spin and low-spin ground state around and below the transition temperature T_c, ruling out any antiferromagnetic binuclear structure or any kind of admixed spin states. The frequencies for

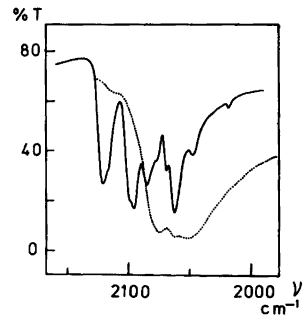

Fig. 3. The infrared spectra of *cis*-[Fe(tpa)$(NCS)_2$] in the CN stretching region. ···, Recorded at 300 K; ———, recorded at 77 K.

Table 3. Infrared stretching frequencies in the C–N and in the Fe–N region.

Compound	ν_{CN} cm^{-1} at 77 K					ν_{FeN} cm^{-1} at 77 K		ν_{CN} cm^{-1} at 300 K			ν_{FeN} cm^{-1} at 300 K	
	$^1A_1$		$^3T_1$		$^5T_2$	$^1A_1$		$^3T_1$		$^5T_2$		
[FeL(IV)(NCS)$_2$]				2078	2067	483			2073	2060	483	
[Fe(tpa)(NCS)$_2$]	2122	2095		2086	2062	532	480		2074	2060	479	
[FeL(II)(NCS)$_2$]	2108	2091		2081	2051	490	480		2074	2057	(534)	
[FeL(III)(NCS)$_2$]			2101	2086	2081 2062	528	483	2096	2082	2077	524	480
[Fe(dpa)(py)(NCS)$_2$]	2118		2099	2080	2059	530	482	2095	2076	2055	526	480

all the systems are shown in Table 3. In this table the low-spin Fe–NCS stretching frequencies are also shown. The corresponding high-spin frequencies are expected to appear at 250 cm^{-1} outside the detection region of our spectrometer.

cis-[FeL(IV)(NCS)$_2$] is clearly pure high-spin in the whole temperature range.

cis-[Fe(tpa)(NCS)$_2$], *cis*-[FeL(II)(NCS)$_2$] and *cis*-[Fe(dpa)py(NCS)$_2$] are seen to be spin-cross-over systems also according to the IR criterium. *cis*-[FeL(III)(NCS)$_2$], however, does not show any temperature dependence in the IR spectrum. In this case a constant 2:1 ratio of high-spin $^5T_2$ and low-spin $^1A_1$ species or a 1:1 ratio of $^5T_2$ and $^3T_1$ are in accordance with the position of the lines, but the equal intensity of the two sets of lines favours the last possibility. Thus a high-spin low-spin equilibrium does not occur here.

cis-[Fe(dpa)py(NCS)$_2$] also seems to contain approximately 30 % of a permanent low spin or intermediate spin component.

The increase in the C–N stretching frequencies of the NCS$^-$ ligand in the spin-cross-over system by 30–40 cm^{-1} when going from high-spin to low-spin is a little less than the 40–50 cm^{-1} observed for other similar systems,[8] whereas the intermediate spin systems are only shifted by 20–30 cm^{-1} compared to the high-spin systems. König and Madeja [9] explain the increase in the ν_{NC} as an increase of the Fe-NCS bond due to a decrease in π-acceptor ability of NCS$^-$ on going from high-spin to low-spin. However the isothiocyanate ion is not considered to be a good π-acceptor, the ligand field strength is even less than for ammonia so the increase in the ν_{NC} must be explained as mainly due to an increase in the σ-donation when going from high-spin to low-spin. According to the MO scheme of NCS$^-$ [10] the lone pair on N is slightly antibonding, so a σ-donation results in a net increase in the bond-order of the C–N bond, explaining the increase in the ν_{CN}. Madeja has suggested that the ν_{CN} of a diisothiocyanato iron(II) complex with a triplet ground state should be approximately 2050 cm^{-1}.[3,20] However, the true triplet nature of the complexes his measurements are made on, has been questioned.[1] If we assume that the ν_{NC} of a triplet ground-state iron(II) complex ($t_{2g}^5 e_g$) is the mean value of a high-spin case ($t_{2g}^4 e_g^2$) and a low-spin case (t_{2g}^6) a value of 2095–2085 cm^{-1} is suggested which is not far from the values found for *cis*-[FeL(III)(NCS)$_2$] (2101, 2086 cm^{-1}) and *cis*-[Fe(dpa)py(NCS)$_2$] (2099, 2087 cm^{-1}). As the occupancy of the e_g orbitals are expected to be crucial for the strength of the Fe–N bond the assignment given above is chemically reasonable.

Inspection of the Tanabe-Sugano diagrams for the d^6 configuration shows that at the cross-over point of $^5T_2$ and $^1A_1$ the lowest triplet state $^3T_1$ is not far above the ground state. A lowering of the symmetry will cause the $^3T_1$ state to split and a stabilization of a triplet state $^3A_2$ might be sufficient to make this the ground-state. König and Kremer have shown that with a tetragonal distortion, corresponding to Dt=1000 cm^{-1}, all three states can coexist for a rather large range of Dq values.[11] Cross-over behaviour involving triplet states has very rarely been observed (if ever) in iron(II) complexes so far,[12] but some [FeL$_2$X$_2$] complexes, where L are diimines and X=Cl$^-$, Br$^-$, NCS$^-$, N$_3^-$, and ½ mal (= half a molecule of malonate) are reported to have triplet ground states.[3,12,16] Recently, however, König has shown

that *e.g.* the mal complex has the composition $[Fe^{II}(phen)_3]_2[Fe^{III}(mal)_3]\cdot{}^1/_2(mal)(aq)$.[21]

Comparison of the systems. In the following we shall try to rationalize the various magnetical behaviour arising from chemical (steric and inductive) effects. We realize that the solid state effects (domain size) can be important, thus all the complexes discussed in this section are prepared under the same conditions.

Fig. 1 shows the various modifications of the ligand system dealt with in this work. The parent compound *cis*-[Fe(tpa)$(NCS)_2$] is, from the IR spectra, seen to possess a D_{2h} symmetry based on the octahedron and not a triagonal bipyramidal structure. The same is assumed to be the case for all the complexes in this work.

That the tpa complex is a spin-cross-over system like the bipy and phen complexes despite the fact that no conjugated diimine functions are present in the tpa ligand suggests that the additional chelate-ring in tpa, compared to two bipy or phen ligands, has compensated for the expected decrease in π-acceptor ability.

In the complex *cis*-[FeL(IV)$(NCS)_2$] (R_2 or $R_2'=CH_3$) where a methyl group is substituted in the 6-position of one of the pyridine rings, two geometrical isomers are possible. If the product is a mixture of these isomers both must be pure high-spin forms within the temperature range used. The high-spin nature of this complex is probably due to *intra*-molecular non-bonding interactions between the 6-methyl group and one of the isothiocyanate groups, resulting in an increase of the Fe−N distances and a reduction in the ligand field strength. The same argument has been used to explain that *cis*-[Fe(2-Me-phen)$_2$$(NCS)_2$] is a high-spin complex.[13] CH_3 has a stronger σ-donation power than hydrogen increasing the basicity of the nitrogen atom and making the Fe−N σ-bond somewhat stronger. This electronic effect is seen to be more than counterbalanced by the steric effect in the L(IV) case. However if the CH_3 group is substituted in one of the methylene groups as in L(II) (R_1 or $R_1=CH_3$) no steric interactions are present in the complexes and the electronic effect is expected *a priori* to dominate. Nevertheless, *cis*-[FeL(II)$(NCS)_2$] has a spin transition which is very similar to that for the corresponding tpa complex. This effect might be explained within the framework of the theory that the methylene group in the 2-pyridylmethyl amine chelate ring mediates an electronic conjugation in this ring.[14] Substituting H for CH_3 in the chelate ring is expected to break the conjugation resulting in a decrease in the π-acceptor abilily. *cis*-[FeL(II)$(NCS)_2$] can exist in 3 enantiomeric pairs due to a regio isomerism of the two CH_3 groups (R, or $R'=CH_3$). The product presumably is a mixture of these isomers.[1]

Expansion of one chelate ring from five-membered to six-membered (tpa *vs.* L(III)) is expected also to result in a decrease in the ligand field. On the other hand, the fusion of two five-membered chelate rings in a meridional plane is known to give rise to enough strain to distort the ligand field so much that the high-spin state will be favoured.[4] Meridional strain is probably also the explanation for the fact that only the facial isomers are formed when preparing the chromium(III) complexes of bis(2-pyridylmethyl)ethylenediamine.[15] The meridional strain is released if one six-membered ring is fused in a meridional fashion to one of the five-membered rings. Such a structure as the one indicated in Fig. 1 (n=2) is expected for *cis*-[FeL(III)$(NCS)_2$] and the structure of *cis*-[Fe(dpa)py$(NCS)_2$] will possess the same facial structure [corresponding to a removal of (CH_2)]. As explained earlier, these two complexes are characterized by having a permanent low-spin or intermediate spin component. Whether this behaviour is due to a coexistence of all three ground states in one geometrical isomer or if it is because the sample is a mixture of different geometrical isomers having different ground states is not possible to decide from the present data. But, as pointed out above, only one isomer is expected to be formed for each compound.

REFERENCES

1. Gütlich, P. *Struct. Bonding (Berlin) 44* (1981) 83.
2. Cunningham, A. J., Fergusson, J. E. and Powell, H. K. J. *J. Chem. Soc. Dalton Trans.* (1972) 2155.
3. Madeja, K., Böhmer, W. H., Nguyen-Trong Thúy, Oehme, G., El-Saghier, A. A., Vertes, A. and Burger, K. *Z. Anorg. Allg. Chem. 447* (1978) 5.
4. Toftlund, H. and Yde-Andersen, S. *Acta Chem. Scand. A 35* (1981) 575.
5. Anderegg, G. and Wenk, F. *Helv. Chim. Acta 50* (1967) 2330.

6. Gütlich, P., Köppen, H., Link, R. and Steinhäuser, H. G. *J. Chem. Phys. 70* (1979) 3977.
7. Baker, W. A., Jr. and Long, G. J. *Chem. Commun. 15* (1965) 368.
8. König, E. and Madeja, K. *Inorg. Chem. 6* (1967) 48.
9. König, E. and Madeja, K. *Spectrochim. Acta A 23* (1967) 45.
10. Rabalais, J. W., McDonald, J. R. and McGlynn, S. P. *Chem. Rev. 71* (1971) 73.
11. König, E. and Kremer, S. *Theor. Chim. Acta 22* (1971) 45.
12. König, E., Ritter, G., Goodwin, H. A. and Smith, F. E. *J. Coord. Chem. 2* (1973) 257.
13. Fleich, J., Gütlich, P., Hasselbach, K. M. and Müller, W. *Inorg. Chem. 15* (1976) 958.
14. Hancock, R. D. and McDougall, G. J. *J. Chem. Soc. Dalton Trans.* (1977) 67.
15. Michelsen, K. *Acta Chem. Scand. A 31* (1977) 429.
16. König, E., Ritter, G., Madeja, K. and Böhmer, W. H. *Ber. Bunsenges. Phys. Chem. 77* (1973) 390.
17. König, E. *J. Inorg. Nucl. Chem. 34* (1972) 2877.
18. Mathes, W. and Schütly, H. *Angew. Chem. 75* (1963) 235.
19. Mulay, L. N. and Boudreaus, E. A. *Theory and Applications of Molecular Diamagnetism,* Wiley, London 1976.
20. Böhmer, V. W. H., Madeja, K., Oehme, G., Vertes, A. and Burger, K. *Z. Anorg. Allg. Chem. 486* (1982) 153.
21. König, E., Ritter, G. and Kanellakopulos, B. *Inorg. Chim. Acta 59* (1982) 285.

Received August 18, 1982.

Acta Chemica Scandinavica A 37 (1983) 259–265

Short Communications

Properties of Binary Alcohol–Octane Solutions. Temperature Dependence of the Viscosities

JOHAN SJÖBLOM * and MICHAEL LILJESTRÖM

Department of Physical Chemistry, Åbo Akademi, Porthansgatan 3, SF-20500 Åbo 50, Finland

During the last few years, much effort has been focused on investigations on so-called microemulsions, which are defined as thermodynamically stable solutions of water, oil and surfactant and, frequently, an additional amphiphilic compound ("co-surfactant"). The solutions are transparent and homogeneous and the aggregates are reversibly formed. It has been clarified that the aggregates in these solutions vary in shape and structure as the polarity of the association medium undergoes changes. For the same surfactant a higher polarity in the medium brings about more open aggregates where aggregate geometries and strictly defined hydrophilic and hydrophobic domains have minor significance.

In previous papers we have viewed the behaviour of aqueous alcohol solutions.[1–3] These investigations were undertaken since it has been stressed how important the interaction between water and the polar alcohol molecules are when reversed micelles or so-called w/o microemulsions are formed in hydroxylic environments. When w/o microemulsion formation and stability is studied in quaternary systems with a non-polar solvent ("oil") as fourth component, we require information on the nature of the interaction between the oil and the alcohols. As a step in this direction we here present the temperature dependence of the viscosities together with activation energies of some binary alcohol-*n*-octane solutions. Octane has been used in many microemulsion investigations as a model hydrocarbon.

Experimental. Chemicals and preparation of samples. All chemicals together with the preparation of solutions have been described earlier.[4]

Apparatus. The viscosities were measured with capillary viscosimeters as described earlier.[4]

The calibration constants were determined separately at 298, 303 and 313 K.

Results. The effect of a dilution with octane at different temperatures on the viscosity of the alcohols (decanol, pentanol and ethanol) is shown in Fig. 1. For ethanol with or without octane we observe only a minor decrease in η as temperature is increased. Pentanol shows a reduction of 1.5 cP as T increases 15 K, while the value of pure decanol is almost halved for the same temperature change. Fig. 1 also illustrates the pronounced dilution effect on the alcohol with the longest hydrocarbon chain.

Assuming that the temperature dependence of viscosity follows the Arrhenius' equation [5]

$$\eta = A \exp(E^+/RT) \qquad (1)$$

where η is the viscosity, A a constant, and E^+ the activation energy, a linear behaviour of ln (η)

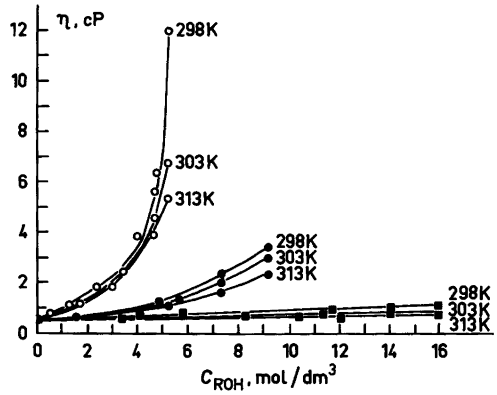

Fig. 1. The viscosities of alcohol–octane solutions at different temperatures. ○ decanol, ● pentanol, ■ ethanol.

* To whom correspondence should be addressed. Present address: Institute for Surface Chemistry, Box 5607, S-114 86 Stockholm, Sweden.

0302-4377/83 $2.50

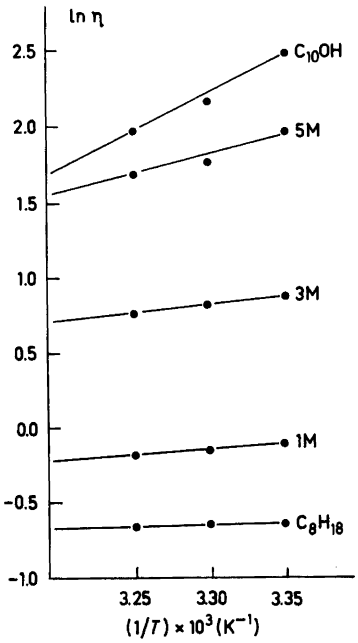

Fig. 2. A typical plot of $\ln(\eta)$ given in arbitrary units *versus* the inverse temperature T^{-1}. The molarity refers to the alcohol.

when plotted *versus* $1/T$, is predicted. This analysis is undertaken in Fig. 2. The prediction is fullfilled in all cases except for the highest contents of decanol.

The activation energies have been evaluated from Fig. 2 and are summarized in Table 1. The highest values are those of decanol. The values obtained for pure pentanol are in agreement with those given by D'Aprano *et al.*[6]

Table 1. Activation energies as calculated from eqn. (1).

$C_nOH+C_8H_{18}$	C_{ROH} mol dm^{-3}	E^+ kJ mol^{-1}
n=2	16[a]	10
	8	6
	4	3
n=5	9.1 [a]	19
	8	18
	4	3
n=10	5.4 [a]	39
	5	21
	3	3

[a] This concentration refers to the pure alcohol.

Discussion. In previous papers we have investigated the effect of an addition of water to different alcohols. Especially for long-chain alcohols we have observed a pronounced decrease of the alcohol self-association. In this study we have changed the polar additive to a completely nonpolar, *i.e.* octane. It is our intention to illustrate how changes in the hydrophobic interaction influence the self-association level of the alcohol. Although octane is a good representative for this purpose, a choice of just one solute can naturally not give a complete picture. The alcohols have been chosen to represent different self-association levels according to our previous data. A dilution with octane gives quite different results depending on the length of the hydrocarbon chain of the alcohol. Comparison of results at constant temperature (for instance 298 K) reveals that the reduction in viscosity is most pronounced for decanol and almost negligible for ethanol. A possible explanation is that the incorporation of octane into the hydrocarbon moiety of the alcohol does not leave the original self-association pattern invariant as long as the alcohol is hydrophobic enough. In the case of ethanol the viscosities could be explained by a "dilution" of the polymeric alcohol species with octane. Dielectric measurements have, however, shown that diluting ethanol with octane is accompanied by a large decrease in the dielectric constant indicating considerable reorientations in the OH-moments.[3] In the case of decanol the alkane does not obviously cause large deviations in the direction of the hydroxylic OH-moments.

Fig. 1 shows that the solutions poorest in octane are most sensitive to change in temperature. The magnitude of the reduction in viscosity decreases when proceeding from decanol to ethanol. In this respect a parallel can be drawn to the dilution with the alkane. An increase in temperature should be accompanied by a breaking of hydrogen bonds and an enhanced flexibility of the hydrocarbon chains. Both these effects should lower the extent of self-association in the alcohol. Therefore it is not so surprising that the value of E^+ for the long-chain alcohol in Table 1 exceeds 20 kJ/mol, which is usually needed for a rupture of hydrogen bonds. The activation energies of the pure compounds reveal that the associated species become much more bulky and flow less easily when one proceeds from ethanol to decanol. One cannot, however, conclude from the increased viscosity whether the reduced fluidity is due to a higher monomeric association

or to the increase in hydrocarbon chain length.

This study together with our earlier ones indicates that long-chain alcohols, like decanol, certainly retain traces of the strict molecular arrangements characterizing the solid lipid alkanols.[7] At the actual temperature a formation of linear complexes, probably even with a feature of a double-layer structure, seems to predominate in the solution. For short-chain alcohols, like ethanol, the solution structures seem to be more closed and compact, perhaps even with a cyclic character. A natural expansion of this picture would be the formation of clusters or clathrates in the shortest alcohol, *i.e.* water.

Acknowledgement. One of the authors (M.L.) thanks The Finnish Research Council for Natural Sciences for financial support.

1. Sjöblom, J. and Dyhr, H. *Acta Chem. Scand. A 35* (1981) 219.
2. Sjöblom, J., Dyhr, H. and Hansén, O. *Finn. Chem. Lett.* (1981) 110.
3. Sjöblom, J. and Liljeström, M. *Finn. Chem. Lett.* (1982) 168.
4. Sjöblom, J. and Liljeström, M. *Colloid Polym. Sci.* (1983). *In press.*
5. Arrhenius, S. *Medd. Vetensk. Nobel 3* (1916) 20.
6. D'Aprano, A., Donato, D. I. and Agaigento, V. *J. Solution Chem. 11* (1982) 259.
7. Chapman, D. *The Structure of Lipids,* Methuen & Co., London 1965.

Received November 18, 1982.

The Absolute Configuration of Hyperforin, an Antibiotic from *Hypericum perforatum* L., Based on the Crystal Structure Determination of its *p*-Bromobenzoate Ester

ILIA BRONDZ,[a] TYGE GREIBROKK,[a] PER GROTH [a] and ARNE J. AASEN [b]

[a] Department of Chemistry and [b] Department of Pharmacy, University of Oslo, Blindern, Oslo 3, Norway

The antibiotic properties of the antibacterial substances known to be present in species of the genus *Hypericum* (Hypericaceae (=Guttiferae)),[1] are well established.[2–4] Extracts from this plant have been used to preserve food [3] and to treat infections.[5] One active constituent designated hyperforin, was isolated and characterized in 1971.[5] The absolute configuration was suggested in 1975–1976.[6,7] A forthcoming report [8] presents arguments suggesting that a recent crystal structure determination of the 3,5-dinitrobenzoate ester [9] is in contradiction with the proposed absolute configuration. In order to obtain direct evidence for the absolute stereochemistry of hyperforin, a single crystal structure analysis of its *p*-bromobenzoate ester has been carried out.

The crystal data for $C_{42}H_{55}BrO_5$ are: a=11.692(4) Å, b=16.253(9) Å, c=10.233(4) Å, β=102.60(3)°, Z=2, space group $P2_1$, D_x=1.26 g cm^{-3}, D_m=1.23 g cm^{-3}, μ=1.19 mm^{-1} (Mo$K\alpha$). Data were collected on an automatic four-circle

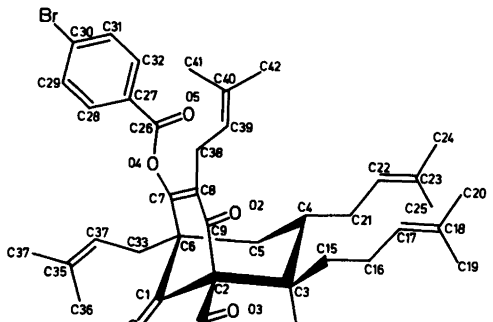

Fig. 1. Schematic drawing of the molecule showing the numbering of atoms.

Table 1. Final fractional coordinates with estimated standard deviations for non-hydrogen atoms.

ATOM	X	Y	Z
BR	.88298(3)	.73952(2)	.35632(4)
O1	.30912(23)	.82176(18)	1.03682(27)
O2	.03362(23)	.79540(17)	.79619(29)
O3	.00456(26)	.81537(20)	.99374(33)
O4	.42445(19)	.73957(23)	.66286(23)
O5	.32359(26)	.78297(21)	.45931(30)
C1	.27436(33)	.81595(24)	.91791(42)
C2	.14532(32)	.80554(25)	.85188(39)
C3	.10215(33)	.89247(25)	.78444(41)
C4	.18023(40)	.91151(28)	.67978(47)
C5	.31157(35)	.90993(27)	.74314(41)
C6	.35209(32)	.82792(25)	.81778(40)
C7	.32929(33)	.75535(26)	.72031(37)
C8	.23141(35)	.71644(24)	.69103(38)
C9	.12992(30)	.75668(33)	.74551(35)
C10	.08802(36)	.77555(27)	.95959(44)
C11	.11778(38)	.69156(28)	1.02427(45)
C12	.01838(44)	.62919(33)	.98316(61)
C13	.14813(41)	.70132(30)	1.17823(46)
C14	.12516(35)	.95838(26)	.89533(44)
C15	-.02839(33)	.88609(26)	.71176(41)
C16	-.10554(36)	.96294(27)	.71776(45)
C17	-.22187(38)	.95694(29)	.62096(47)
C18	-.32612(37)	.98188(28)	.63843(50)
C19	-.34757(41)	1.02320(32)	.76146(56)
C20	-.43221(40)	.97645(33)	.52581(54)
C21	.14812(37)	.99321(27)	.60391(46)
C22	.21939(36)	1.07867(27)	.49993(46)
C23	.26059(40)	.97786(31)	.37733(51)
C24	.10129(44)	.92630(35)	.32300(54)
C25	.27923(46)	.99784(38)	.28336(52)
C26	.41332(56)	.75904(26)	.52909(40)
C27	.52675(31)	.74886(31)	.48859(36)
C28	.53084(38)	.76487(28)	.35637(43)
C29	.63689(38)	.76114(28)	.31785(43)
C30	.73733(36)	.74163(37)	.41035(38)
C31	.73523(34)	.72219(27)	.54204(40)
C32	.62886(33)	.72566(28)	.58042(38)
C33	.48241(34)	.83176(27)	.89123(42)
C34	.52832(32)	.75297(30)	.95466(38)
C35	.63667(34)	.72149(28)	.96931(40)
C36	.73521(36)	.76459(30)	.92698(46)
C37	.66799(40)	.63852(32)	1.03485(48)
C38	.21535(37)	.63382(28)	.60457(45)
C39	.18779(49)	.55985(30)	.68438(54)
C40	.26595(40)	.52024(28)	.77602(49)
C41	.23080(44)	.44791(31)	.85211(52)
C42	.39347(43)	.54219(32)	.81801(53)

diffractometer at *ca.* −150 °C by the ω-scan technique ($2\theta_{max}$=*50°*, *MoKα*-radiation). 6686 reflections (Friedel equivalents included) were collected. With an observed-unobserved cutoff at 2.5$\sigma(I)$, 5661 reflections were regarded as observed. The intensities were corrected for absorption (crystal size 0.3×0.2×0.1 mm). The minimum and maximum transmission factors were 0.75 and 0.90, respectively. The phase problem was solved by direct methods.[11] Without taking into account anomalous dispersion, full-matrix least-squares refinement [12,*] converged at

* All programs used (except those for phase determination) are included in this reference.

0302-4377/83 $2.50

Table 2. Bond distances and angles with estimated standard deviations.

DISTANCE	(Å)	DISTANCE	(Å)
BR - C30	1.902(3)	O1 - C1	1.198(5)
O2 - C9	1.220(5)	O3 - C10	1.206(5)
O4 - C7	1.391(4)	O4 - C26	1.383(5)
O5 - C26	1.198(5)	C1 - C2	1.522(5)
C1 - C6	1.521(5)	C2 - C3	1.605(6)
C2 - C9	1.545(6)	C2 - C10	1.550(6)
C3 - C4	1.582(6)	C3 - C14	1.540(6)
C3 - C15	1.549(5)	C4 - C5	1.532(6)
C4 - C21	1.543(6)	C5 - C6	1.558(6)
C6 - C7	1.519(6)	C6 - C33	1.547(6)
C7 - C8	1.335(6)	C8 - C9	1.479(5)
C8 - C38	1.515(6)	C10 - C11	1.538(6)
C11 - C12	1.525(7)	C11 - C13	1.546(7)
C15 - C16	1.550(6)	C16 - C17	1.501(6)
C17 - C18	1.332(6)	C18 - C19	1.496(7)
C18 - C20	1.501(7)	C21 - C22	1.509(6)
C22 - C23	1.324(7)	C23 - C24	1.500(7)
C23 - C25	1.514(7)	C26 - C27	1.483(5)
C27 - C28	1.398(6)	C27 - C32	1.400(5)
C28 - C29	1.382(6)	C29 - C30	1.375(6)
C30 - C31	1.390(6)	C31 - C32	1.385(5)
C33 - C34	1.495(6)	C34 - C35	1.338(5)
C35 - C36	1.491(6)	C35 - C37	1.515(7)
C38 - C39	1.537(7)	C39 - C40	1.318(7)
C40 - C41	1.516(7)	C40 - C42	1.502(6)

ANGLE	(°)	ANGLE	(°)
C7 - O4 - C26	117.7(3)	O1 - C1 - C2	122.8(4)
O1 - C1 - C6	123.8(4)	C2 - C1 - C6	113.2(3)
C1 - C2 - C3	106.3(3)	C1 - C2 - C9	110.2(3)
C1 - C2 - C10	108.3(3)	C3 - C2 - C9	111.0(3)
C3 - C2 - C10	115.2(3)	C9 - C2 - C10	105.8(3)
C2 - C3 - C4	106.8(3)	C2 - C3 - C14	108.1(3)
C2 - C3 - C15	109.4(3)	C4 - C3 - C14	109.9(3)
C4 - C3 - C15	110.0(3)	C14 - C3 - C15	112.5(3)
C3 - C4 - C5	112.4(4)	C3 - C4 - C21	113.3(4)
C5 - C4 - C21	110.3(4)	C4 - C5 - C6	113.6(3)
C1 - C6 - C5	105.6(3)	C1 - C6 - C7	107.8(3)
C1 - C6 - C33	110.4(3)	C5 - C6 - C7	110.1(3)
C5 - C6 - C33	111.0(3)	C7 - C6 - C33	111.7(3)
O4 - C7 - C6	112.1(3)	O4 - C7 - C8	122.0(4)
C6 - C7 - C8	125.9(3)	C7 - C8 - C9	118.5(4)
C7 - C8 - C38	124.8(4)	C9 - C8 - C38	116.7(4)
O2 - C9 - C2	119.4(3)	O2 - C9 - C8	121.0(4)
C2 - C9 - C8	119.6(3)	O3 - C10 - C2	122.8(4)
O3 - C10 - C11	120.5(4)	C2 - C10 - C11	116.7(4)
C10 - C11 - C12	110.3(4)	C10 - C11 - C13	109.2(4)
C12 - C11 - C13	110.2(4)	C3 - C15 - C16	116.6(3)
C15 - C16 - C17	111.9(4)	C16 - C17 - C18	128.0(4)
C17 - C18 - C19	125.2(4)	C17 - C18 - C20	120.4(5)
C19 - C18 - C20	114.2(4)	C4 - C21 - C22	112.8(4)
C21 - C22 - C23	127.0(4)	C22 - C23 - C24	122.8(5)
C22 - C23 - C25	121.7(5)	C24 - C23 - C25	115.4(5)
O4 - C26 - O5	123.0(4)	O4 - C26 - C27	110.7(3)
O5 - C26 - C27	126.2(4)	C26 - C27 - C28	118.3(4)
C26 - C27 - C32	121.7(3)	C28 - C27 - C32	119.9(3)
C27 - C28 - C29	119.5(4)	C28 - C29 - C30	119.9(4)
BR - C30 - C29	119.3(3)	BR - C30 - C31	118.9(3)
C29 - C30 - C31	121.8(3)	C30 - C31 - C32	118.2(4)
C27 - C32 - C31	120.5(3)	C6 - C33 - C34	113.0(3)
C33 - C34 - C35	127.7(4)	C34 - C35 - C36	124.4(4)
C34 - C35 - C37	120.8(4)	C36 - C35 - C37	114.8(4)
C8 - C38 - C39	110.7(4)	C38 - C39 - C40	124.3(5)
C39 - C40 - C41	120.9(4)	C39 - C40 - C42	125.5(5)
C41 - C40 - C42	113.6(4)		

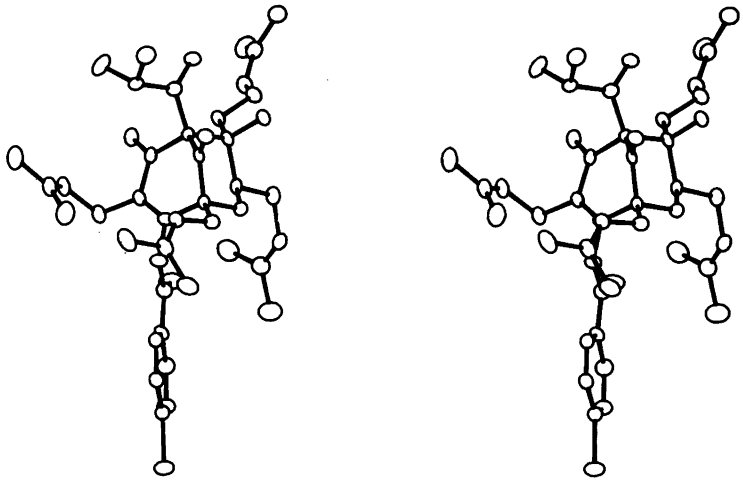

Fig. 2. Stereoscopic view of the molecule.

$R\sim10$ %. By introducing anomalous scattering factors for Br with $+\Delta f''=2.456$, further refinement led to $R=7.9$ % ($R_w=9.0$ %). When now changing the sign to $-\Delta f''$, the values dropped to $R=4.7$ % and $R_w=4.9$ %, respectively. The final values were $R=4.5$ % and $R_w=4.7$ %. The methyl hydrogen atoms were localized in a difference Fourier map while the positions of the other hydrogen atoms were calculated. Anisotropic temperature factors were introduced for all non-hydrogen atoms. The maximum r.m.s. amplitudes range from 0.15 to 0.26 Å. Weights in least squares were obtained from the standard deviations in intensities, $\sigma(I)$, taken as

$$\sigma(I) = [C_T+(0.02C_N)^2]^{1/2}$$

where C_T is the total number of counts, and C_N the net count. Only positional parameters for hydrogen atoms were refined.

Final fractional atomic coordinates for non-hydrogen atoms are given in Table 1. Bond distances and angles may be found in Table 2. Fig. 1 is a schematic drawing of the molecule showing the numbering of atoms. A stereoscopic view of the molecule is presented in Fig. 2. It may be noticed that the bond distances C2–C3 (1.605 Å) and C3–C4 (1.582 Å) are unusually long. However, the corresponding values for the 3,5-dinitrobenzoate ester [9] were also long (1.58 Å and 1.57 Å). The environment of the bond C8–C14 in the crystals of 3β,28-diacetoxy-18β,19β-epoxylupane [10] resembles that of C2–C3 in the present molecule. C8–C14 was found to be 1.605 Å. All other bond distances and angles have normal values within estimated limits of error. It may be pointed out that the difference between the earlier suggested absolute configuration [6,7] and the present one, is that the stereochemistry at the chiral centres C2 and C8 is opposite.

Lists of observed and calculated structure factors as well as the temperature factors are obtainable from Per Groth.

1. Osborne, E. M. *Br. J. Exp. Pathol. 24* (1943) 227.
2. Zellner, J. and Porodko, Z. *Arch. Pharm. 263* (1925) 170.
3. Jensen, L. B. and Miller, W. A. *US Pat.* 2,550,266, (1951).
4. Neuwald, F. and Hagenström, U. *Arch. Pharm. 287* (1954) 439.
5. Gurevich, A. I., Dobrynin, V. N., Kolosov, M. N., Papravko, S. A., Ryabova, I. D., Chernov, B. K., Derbentseva, N. A., Aizenman, B. E. and Garagulya, A. D. *Antibiotiki (Moscow) 16* (1971) 510.
6. Bystrov, N. S., Chernov, B. K., Dobrynin, V. N. and Kolosov, M. N. *Tetrahedron Lett.* (1975) 2791.
7. Bystrov, N. S., Dobrynin, V. N., Kolosov, M. N., Chernoy, B. K., Chervin, I. I. and Yakovlev, G. I. *Dokl. Akad. Nauk SSSR 226* (1976) 338.
8. Brondz, I., Greibrokk, T., Groth, P. A. and Aasen, A. J. *To be published.*
9. Brondz, I., Greibrokk, T., Groth, P. A. and Aasen, A. J. *Tetrahedron Lett. 23* (1982) 1299.
10. Hiltunen, L. and Niinistö, L. *Acta Crystallogr. B 35* (1979) 1530.
11. Germain, G., Main, P. and Woolfson, M. M, *Acta Crystallogr. A 29* (1971) 368.
12. Groth, P. *Acta Chem. Scand. 27* (1973) 1837.

Acta Chemica Scandinavica A 37 (1983) 267–275

Structure and Force Field of 1,3-Pentadiyne (Methyldiacetylene)

CLAUS J. NIELSEN and SVEIN SÆBØ

Department of Chemistry, University of Oslo, Oslo 3, Norway

Microwave spectra of 1,3-pentadiyne-5,5,5-d_3 ([5,5,5-$^2H_3$]-1,3-pentadiyne), including four of the ^{13}C isotopic species, and 1,3-pentadiyne-5,5-d_2 have been measured of the vibrational ground state. On the basis of the existing and the new spectroscopic data, the molecular structure (r_o, r_m, r_s) was derived and compared with results from *ab initio* calculations.

The infrared vapour spectrum of 1,3-pentadiyne-5,5,5-d_3 was reinvestigated and the Coriolis coupling constant ζ_{79}^a was determined. Far infrared spectra of the parent molecule were measured and the heretofore unobserved vapour phase frequencies for the $\nu_{13}(e)$ and $\nu_{14}(e)$ modes obtained. A symmetry force field was derived from the vibrational and rotational spectroscopic data.

1,3-Pentadiyne (methyldiacetylene, later to be called MDA) has been subjected to only a few spectroscopic investigations. The microwave spectra of the vibrational ground state and of the first vibrational excited state of $\nu_{14}(e)$ have been studied for MDA and the three deuterated molecules: MDA-1-*d*, MDA-5,5,5-d_3 and MDA-d_4.[1] This investigation was later extended to include a number of ^{13}C isotopes of the parent molecule and of the 1-*d* species.[2] From these data an r_o-structure assuming equal acetylenic bond lengths was proposed.[2] More recently, the microwave spectra of the vibrational excited states, ν_{13}, ν_{14}, $2\nu_{14}$ and $3\nu_{14}$, have been studied in greater detail [3] leading to very accurate rovibronic parameters.

The vibrational spectra of MDA, MDA-1-*d*, MDA-5,5,5-d_3 and MDA-d_4 have been reported.[4] The vibrational spectrum af MDA,[5] including the Coriolis coupling constants for the degenerate methyl vibrations, and a normal coordinate analysis [6] were reported from this laboratory.

EXPERIMENTAL

Small samples of MDA and MDA-5,5,5-d_3 were collected as "intermediates" in the synthesis of 2,4-hexadiyne (dimethyldiacetylene), 2,4-hexadiyne-1,1,1-d_3 and 2,4-hexadiyne-d_6.[7] The isotopic purity of MDA-5,5,5-d_3, checked by mass spectrometry, was *ca.* 97 %.

Microwave spectra were recorded on a Hewlett-Packard 8460A MRR spectrometer. Sample temperatures varied from −40 to −60 °C at pressures less than 0.01 Torr. Frequencies were measured to an accuracy of 0.05 MHz.

Infrared gas phase spectra were measured using a 10 cm cell (CsI windows) and a 20 cm cell (polyethylene windows) on a Bruker IFS 114C Fourier transform spectrometer.

MICROWAVE SPECTRA

The rotational spectra of MDA are those of a strictly symmetric top molecule with a positive value of D_{JK}. A number of strong lines due to vibrational excited states were observed but not studied in any detail. The spectrum of MDA-5,5-d_2, measured as an "isotopic impurity", is that of an extremely near prolate rotor with only the K=1 lines split.

Derived rotational parameters for MDA-5,5,5-d_3, four of the ^{13}C isotopic species and MDA-5,5-d_2 are presented in Table 1. In all cases the rotational constant and D_J are strongly correlated (0.9) and D_J poorly determined. A complete list of frequencies is available from the authors upon

0302-4377/83 $02.50

Table 1. Rotational parameters for 1,3-pentadiyne-5,5,5-d_3, ^{13}C isotopic species and 1,3-pentadiyne-5,5-d_2.

Molecule	B_o [MHz]	D_J [Hz]	D_{JK} [kHz]	N_{obs}	rms [MHz]
$D_3CCCCCH$	1834.8522(4) [a]	70.3(25)	14.553(5)	45	0.012
$D_3{}^{13}CCCCCH$	1795.8834(9)	62(5)	13.981(19)	29	0.023
$D_3C^{13}CCCCH$	1828.2555(23)	113(14)	14.52(6)	19	0.042
$D_3CCC^{13}CCH$	1818.587(3)	81(17)	14.26(5)	16	0.042
$D_3CCCC^{13}CH$	1785.0385(8)	70(4)	13.941(12)	21	0.015
$D_2HCCCCCH$	1899.3777(21) [C_o=1891.3084(21)]	64.(10)	14.189(21)	33	0.034

[a] Errors represent one standard deviation.

Table 2. Structure parameters for 1,3-pentadiyne (MDA) and butadiyne (DA).

	r_o [a]	r_m	r_s	*Ab initio*	
				MDA	DA
$r_{C_8-H_9}$	105.6(1) [b]	105.71(1)	105.5(1)	105.1	105.1
$r_{C_7\equiv C_8}$	120.8(1)	120.86(1)	120.9(1)	119.3	119.3
$r_{C_6-C_7}$	137.6(2)	137.22(1)	137.5(4)	137.9	137.8
$r_{C_5\equiv C_6}$	120.9(2)	120.82(2)	120.8(4)	119.4	119.3
$r_{C_4-C_5}$	145.4(1)	145.43(1)	145.6(3)	146.5	
$r_{C_4-H_1}$	110.7(1)	110.70(2)	110.5(1)	108.1	
$\alpha_{C_5C_4H_1}$	110.32(3)	110.46(1)	110.35(5)	110.6	

[a] Distances in pm. [b] Numbers in parantheses represent the standard deviation.

request or from NBS,* where it has been deposited.

STRUCTURE

The structures of more than 40 molecules containing the acetylenic group have been determined by spectroscopy and electron diffraction.[8] Disregarding the exceptionally short C≡C distance in fluoroacetylene [9] (r_s=119.8±0.3 pm), the C≡C bond distance appears to be almost unaffected by the substituents (r_s=120.4±0.3 and 120.9±0.2 pm in chloroacetylene [9] and *tert*-butylacetylene,[10] respectively). In spite of the experimental uncertainties, the expected trend of sigma electron donating substituents to lengthen and of sigma electron accepting substituents to shorten the C≡C bond is observed. For MDA, with two conjugated C≡C bonds, one would expect much smaller effects upon substitution, but the C≡C bond adjacent to the methyl group to be the longest.

Ab initio *calculations.* The fully optimized structures for 1,3-butadiyne (diacetylene, DA) and MDA were calculated by *ab initio* gradient calculations.

The calculations were carried out using the computer program MOLFORC,[11] in which the energy gradient with respect to the nuclear coordinates is calculated for a single-determinant SCF wavefunction and the molecular geometry determined by the force relaxation method.[12] This program is based on the program MOLECULE,[13] which solves the Roothaan-Hall equations for a basis set of contracted gaussian functions.

The basis set applied was the (7,3)→⟨4,2⟩ basis of Roos and Siegbahn [14] for the carbon atoms, and Huzinagas' (4)→⟨2⟩ [15] basis set scaled by the factor 1.2 for the hydrogen atoms.[16] This basis set is widely used and is expected to

* Microwave Data Center, Molecular Spectroscopy Section, National Bureau of Standards, Washington D. C. 20234, U.S.A.

give consistent descriptions of molecular geometries, with the CC triple bonds about 0.02 Å too short.

For DA the calculations were carried out starting with C_{2v} and C_{2h} symmetries. In both cases the calculations converged to the linear form. The geometry of MDA was optimized without symmetry restrictions. However, the geometry converged to the linear C_{3v} form with almost equal acetylenic bond lengths. In Table 2 the results from the *ab initio* calculations are compared with the experimental structure.

r_o-*structure.* The main problem in determining the structure of MDA is caused by the absence of experimental data for ^{13}C isotopic substitution of the central carbon atom (C_3). Hence, the (small) coordinate for C_3 has to be determined by the first moment equations which are not suited at all for small coordinates. The r_o-structure, given in Table 2, was derived by a least squares procedure using all the experimental moments of inertia for MDA and the isotopically substituted molecules (Table 3). The standard deviation of the fit, being five times larger than the experimental errors, indicates large zero-point vibrational effects. However, attempts to include bond shortening upon deuteration in the refinement leads to large correlation between the structural parameters and unreasonable values for $r_{CH}-r_{CD}$.

r_m-*structure.* It is possible to overcome the apparent inconsistency between the experimental moments of inertia and the structure parameters. This can be accomplished by assuming a functional mass dependence of the vibrational contribution to the effective moments of inertia.[17] As suggested by Watson,[17] a functional relationship of the form:

$$I^\circ = I'(r_m)+\varepsilon_1+\varepsilon_2$$

$$\varepsilon_1 = I'(r_m)^{1/2}$$

$$\varepsilon_2 = \left[\frac{m_1^3\, m_2^3\, m_3^3 \ldots m_N^3}{M^3 I'_a\, I'_b\, I'_c}\right]^{1/2(3N-6)}$$

should give (1) internal consistency between experimental data and structure parameters and (2) a better approximation to the equilibrium structure. As seen, both ε_1 and ε_2 are (as required) [18] homogeneous functions of degree ½ in the mass. Though this definition of the r_m-structure differs from that originally given by Watson,[18] the same labeling of the structure has been used in order to indicate the mass dependence.

In Table 2 are given the results of a least squares refinement where all experimental data (also I_c for MDA-5,5-d_2) have been fitted to the above expression. In view of the uncertainties in the r_o-structure, the differences in the r_m- and r_o-structures are insignificant. However, the parameters in the r_m-structure are far less correlated than in the r_o-structure and all the moments of inertia are reproduced within their experimental uncertainties.

r_s-*structure.* Five of the total of eight substitution coordinates in MDA can readily be determined from the Kraitchman equations [19] using either MDA, MDA-1-*d* or MDA-5,5,5-d_3 as the parent molecule. The two methyl group coordinates, the off-axis distances (x) and the along the axis coordinate (z), for the hydrogen atoms can be determined with either MDA or MDA-5,5,5-d_3 as the parent molecule. This can be accomplished by combining the Kraitchman equations for multiple substitution:

Table 3. Experimental values for the moments of inertia with standard errors for 1,3-pentadiyne.

Molecule	I_b° [u Å^2] [a]
$H_3CCCCCH$ [b]	248.25260(13)
$H_3{}^{13}CCCCCH$ [c]	254.897(6)
$H_3C^{13}CCCCH$ [c]	249.532(6)
$H_3CCC^{13}CCH$ [c]	250.317(6)
$H_3CCCC^{13}CH$ [c]	255.214(6)
$H_3CCCCCD$ [d]	261.8853(27)
$H_3{}^{13}CCCCCD$ [c]	268.829(7)
$H_3C^{13}CCCCD$ [c]	263.298(7)
$H_3CCC^{13}CCD$ [c]	263.790(7)
$H_3CCCC^{13}CD$ [c]	268.550(7)
D_3CCCCH	275.43314(6)
$D_3{}^{13}CCCCH$	281.40975(14)
$D_3C^{13}CCCH$	276.4270(4)
$D_3CCC^{13}CCH$	277.8966(5)
$D_3CCCC^{13}CH$	283.11945(13)
$D_3CCCCCD$ [d]	290.078(3)
$D_2HCCCCCH$	266.07615(29)
	[I_c°=267.2114(3)]

[a] Conversion factor: I B=505379.1 MHz u Å^2. 1 u Å^2=1.660531 10^{-47} kg m^2. [b] From Ref. 3. [c] From Ref. 2. [d] From Ref. 1.

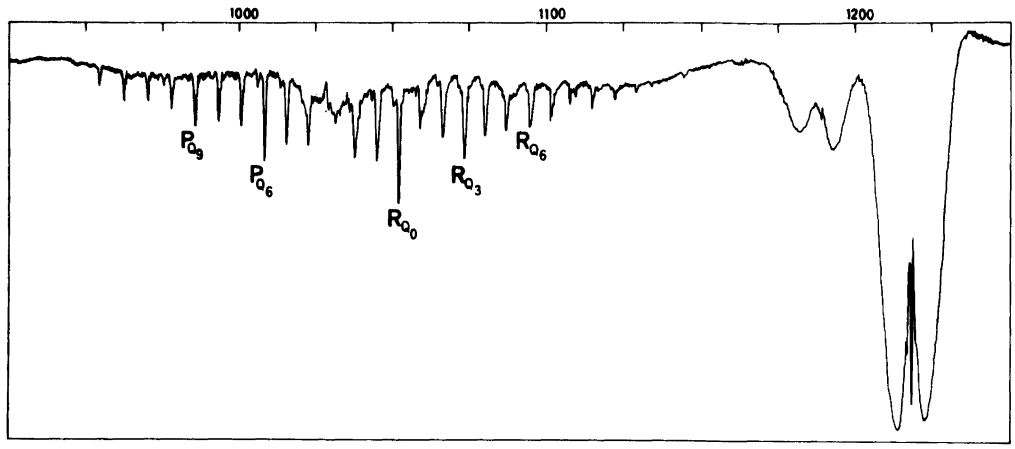

Fig. 1. Infrared spectrum in the region 1250–925 cm^{-1} of 1,3-pentadiyne-5,5,5-d_3 (resolution 0.25 cm^{-1}) showing the ν_6 (a_1) band at 1025 cm^{-1}, the ν_9(e) band at 1046 cm^{-1}, the ν_5(a_1) band at 1187 cm^{-1} and the $2\nu_{11}$(a_1+e) band at 1218 cm^{-1}.

$CH_3 \rightarrow CD_3$:

$$\Delta I_3 = \frac{3}{2}\Delta m x^2 + \mu_3 z^2,\ \mu_3 = \frac{3\,\Delta m M}{M+3\Delta m}$$

$CH_3 \rightarrow CD_2H$:

$$\Delta I_2 = \frac{1}{4}\mu_2 x^2 + \mu_2 z^2,\ \mu_2 = \frac{2\,\Delta m M}{m+2\Delta m}$$

$CD_3 \rightarrow CH_3$:

$$\Delta I_3 = \frac{3}{2}\Delta m x^2 + \mu_3 z^2,\ \mu_3 = \frac{3\,\Delta m M}{M+3\Delta m}$$

$CD_3 \rightarrow CD_2H$:

$$\Delta I_1 = \mu_1 x^2 + \mu_1 z^2,\ \mu_1 = \frac{\Delta m M}{M+\Delta m}$$

In both cases (the determinant being *ca.* 1.5) the equations are easily solved. If the x-coordinate for the methyl hydrogen is transferred from MDA or MDA-5,5,5-d_3 to MDA-1-*d*, then the corresponding z-coordinate in MDA-1-*d* can be found from the equation for the $CH_3 \rightarrow CD_3$ substitution.

The remaining coordinate for the central carbon atom has to be determined from the first moment equations. This coordinate was found to be +0.070±0.004, +0.204±0.001 and +0.013±0.005 Å in MDA, MDA-5,5,5-d_3 and MDA-1-*d*, respectively. The derived r_s-structure is compared with the r_o- and the r_m-structure in Table 2.

VIBRATIONAL SPECTRA

Coriolis coupling constants in MDA-5,5,5-d_3. The Coriolis coupling constants for the degenerate methyl vibrations have been determined for MDA.[5] For MDA-5,5,5-d_3 the corresponding vibrational bands (ν_8, ν_9 and ν_{10}) should all show resolvable rotational fine structure. However, due to the limited amount of sample, the ν_{10} band at *ca.* 850 cm^{-1} was too weak to be observed with any confidence. The ν_8 band at *ca.* 2250 cm^{-1} was partly obscured by the stronger ν_2(a_1) band at 2258 cm^{-1} and it was not possible to determine the band centre. Hence, only the ν_9 band at *ca.* 1050 cm^{-1} was studied in detail.

The Q-branches of the sub-bands that arise from the $\Delta K=\pm 1$, $\Delta J=0$ transitions are given by the expression:[20]

$$\nu_9^K = \nu_9 + [A'(1-\zeta_9)^2 - B'] \pm 2[A'(1-\zeta_9) - B']K + [(A'-A'') - (B'-B'')]K^2$$

Using the experimental value for B'', a value for A'' calculated from the r_o-structure (A''=2.590 cm^{-1}) and further assuming that $B'=B''$, ζ_9 and ν_9 can be calculated from the above equation.

As shown in Fig. 1, the ν_9 band is overlapped by the weak ν_6(a_1) band at *ca.* 1025 cm^{-1}. The intensity distribution among the sub-bands permits a choice of either *ca.* 1051 or *ca.* 1031 cm^{-1} as the $K=0\rightarrow 1$ transition. That the former is prob-

Table 4. ν_9 of 1,3-pentadiyne-5,5,5-d_3.

K-Value in sub-bands	P_{Q_K}		R_{Q_K}	
	Obs. [cm^{-1}]	Obs.−calc.	Obs. [cm^{-1}]	Obs.−calc.
0			1051.33	−0.24
1	1044.58	0.26	1058.56	−0.23
2	1037.34	0.31	1066.28	0.31
3			1073.03	−0.09
4	1021.91	−0.43	1080.26	0.03
5	1014.68	−0.26	1087.01	−0.30
6	1007.44	−0.07	1094.73	0.39
7	1000.21	0.17	1101.48	0.13
8	992.49	−0.04		
9	985.26	0.27	1114.99	−0.25
10	977.54	0.13	1122.22	0.08
11	969.83	0.03	1128.97	−0.26
12	962.11	−0.04		
13	954.39	−0.07		
14	946.68	−0.06		
	ν_9^0=1046.4±0.3 cm^{-1} [a]			
	ζ_9=−0.41±0.02			

[a] Estimated from an uncertainty in A′ of 5 %.

ably the correct assignment is supported by a solution/vapour shift of 20 cm^{-1} for this type of vibration.[5]

The observed Q-branches are listed in Table 4 together with the derived parameters. A standard error of 0.3 cm^{-1} for the fit is rather larger in view of the resolution used in obtaining the spectrum (*ca.* 0.25 cm^{-1}), but a secord order Coriolis coupling with ν_5 and/or ν_6 is a plausible explanation for this.

Vibrational fundamentals. From the two previous investigations of the vibrational spectra of MDA [4,5] and the deuterated molecules [5] a reliable assignment of most of the fundamental modes of vibration is known. Three obvious cases of Fermi resonance are observed. The ν_3 mode

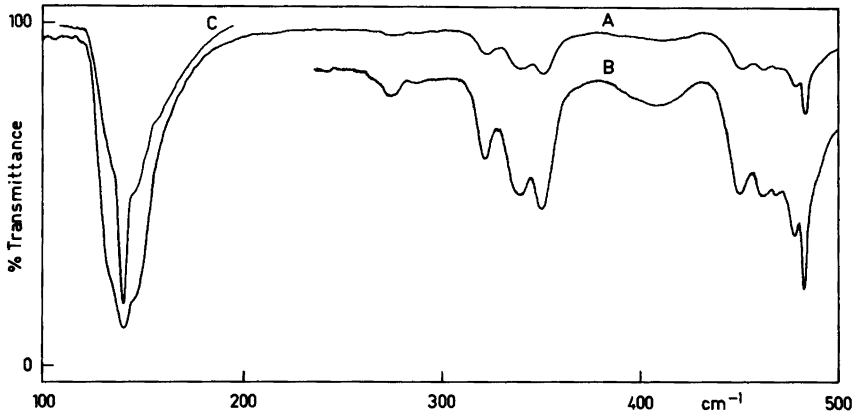

Fig. 2. Far infrared spectrum of 1,3-pentadiyne as a vapour. (A) 50 Torr, 20 cm, (B) scale expansion of A and (C) 10 Torr, 20 cm.

Table 5. Far infrared vapour phase spectral data for 1,3-pentadiyne.

Wavenumber	Interpretation [a]
482 w,⊥	ν_{12} *e*
476 w,⊥	$\nu_{11}-\nu_{14}=475$ A_1+E, $2\nu_{12}-\nu_{12}$ *E*
470 vw, sh,⊥	$3\nu_{12}-2\nu_{12}$ *E* ?
461, 449 w,∥	$\nu_{13}+\nu_{14}=459$ A_1+E
~420 vw,bd	$\nu_{10}-\nu_{11}=415$ A_1+E
349, 338 w,∥	$\nu_{12}-\nu_{14}=343$ A_1+E
320 w,⊥	ν_{13} *e*
~290 vvw ?	$\nu_{11}-\nu_{13}=294$ A_1+E
~274 vw,⊥ ?	$2\nu_{14}=278$ A_1+E
139 s,⊥	ν_{14} *e*

[a] Abbreviations: s: strong; v: very; w: weak; ||: parallel; ⊥: perpendicular; bd: broad; sh: shoulder.

(C≡C asym. stretch) in MDA and MDA-1-*d* is in resonance with the $2\nu_6$ mode.[4] Assuming an anharmonicity $X_6=0.001$, estimated from the 1-halogenated 1,5-pentadiynes,[5] corrections were made for the ν_3 fundamentals. Fermi resonance is also observed between ν_2 (≡C–D stretch) and $\nu_4+\nu_7$ in MDA-d_4. Since no frequency shift is expected for this mode in going from MDA-1-*d* to MDA-d_4, ν_2 is assumed to have the same frequency in these two molecules. In a few cases the fundamentals above 400 cm^{-1} have not been observed in the vapour phase. When possible, these fundamental frequencies were corrected by transferring the corresponding liquid/vapour shifts observed for the other isotopic species.

The two lowest degenerate fundamentals, ν_{13} and ν_{14}, have not been observed in the vapour phase previously. In Fig. 2 the far IR vapour phase spectrum of MDA is shown, while the wave numbers of the observed bands are given in

Table 6. Internal valence symmetry coordinates for 1,3-pentadiyne with reference to Fig. 3.

A_1

$$S_1=3^{-1/2}(\Delta r_1+\Delta r_2+\Delta r_3)$$
$$S_2=-(3(1+K^2))^{-1/2}(K(\Delta\alpha_1+\Delta\alpha_2+\Delta\beta_3)+(\Delta\beta_1+\Delta\beta_2+\Delta\beta_3))\ ^a$$
$$S_3=\Delta r_4$$
$$S_4=\Delta r_5$$
$$S_5=\Delta r_6$$
$$S_6=\Delta r_7$$
$$S_7=\Delta r_8$$

E

$$S_{8a}=6^{-1/2}(2\Delta r_1-\Delta r_2-\Delta r_3) \qquad S_{8b}=2^{-1/2}(\Delta r_2-\Delta r_3)$$
$$S_{9a}=6^{-1/2}(2\Delta\alpha_1-\Delta\alpha_2-\Delta\alpha_3) \qquad S_{9b}=2^{-1/2}(\Delta\alpha_2-\Delta\alpha_3)$$
$$S_{10a}=6^{-1/2}(2\Delta\beta_1-\Delta\beta_2-\Delta\beta_3) \qquad S_{10b}=2^{-1/2}(\Delta\beta_2-\Delta\beta_3)$$
$$S_{11a}=\Delta\gamma_x \qquad S_{11b}=\Delta\gamma_y$$
$$S_{12a}=\Delta\delta_x \qquad S_{12b}=\Delta\delta_y$$
$$S_{13a}=\Delta\varepsilon_x \qquad S_{13b}=\Delta\varepsilon_y$$
$$S_{14a}=\Delta\zeta_x \qquad S_{14b}=\Delta\zeta_y$$

[a] The angle redundancy has been removed: $\Delta\alpha=K\Delta\beta$, $K=3\sin\beta\cos\beta/\sin\alpha$.

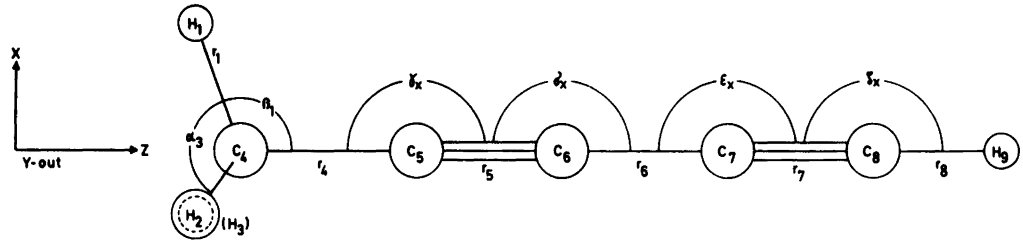

Fig. 3. Valence coordinates for 1,3-pentadiyne.

Table 7. Force constants and standard errors, in symmetry coordinate representation, for 1,3-pentadiyne. Stretching force constants in mdyn/Å, bending force constants in mdynÅ/rad^2 and stretch-bend interactions in mdyn/rad.

	F [a]	σ(F)	R,B,C [b]		F	σ(F)	R,B,C
$F_{1,1}$	4.953	0.034	4.96	$F_{8,8}$	4.777	0.032	4.71
$F_{1,2}$	0		0	$F_{8,9}$	0		0
$F_{2,2}$	0.5866	0.0070	0.51	$F_{8,10}$	0		0
$F_{2,3}$	–0.426	0.037	–0.34	$F_{9,9}$	0.559	0.014	0.53
$F_{3,3}$	5.54	0.23	5.57	$F_{9,10}$	–0.01	0.03	0
$F_{3,4}$	0.34	–	0	$F_{10,10}$	0.639	0.025	0.68
$F_{4,4}$	15.67	0.21	15.17	$F_{10,11}$	–0.062	0.019	0
$F_{4,5}$	1.14	–	0	$F_{11,11}$	0.316	0.029	0.42
$F_{4,6}$	0		0	$F_{11,12}$	0.071	0.017	0
$F_{5,5}$	7.23	0.35	7.52	$F_{12,12}$	0.314	0.021	0.38
$F_{5,6}$	0.72	0.30	0	$F_{12,13}$	0.015	0.015	0
$F_{6,6}$	15.14	0.31	14.39	$F_{13,13}$	0.348	0.036	0.37
$F_{6,7}$	0		0	$F_{13,14}$	0.127	0.009	0
$F_{7,7}$	5.979	0.047	5.95	$F_{14,14}$	0.212	0.002	0.17

[a] 1 mdyn/Å=10^2 N/m, 1 mdynÅ/rad^2=10^{-18} Nm/rad^2, 1 mdyn/rad=10^{-8} N/rad. [b] Rogstad, Benestad and Cyvin (Ref. 6) assumed tetrahedral angles and the following geometry: r_1=110.0, r_4=145.8, r_5=r_7=120.7, r_6=137.5 and r_8=105.7 pm.

Table 5 with the proposed assignment. Apart from the possible hot-band progression of the ν_{12} mode at 482 cm^{-1}, the rest of the observed bands are unambiguously assigned.

FORCE CONSTANT CALCULATION

In Table 6, internal valence symmetry coordinates are given which can be interpreted by reference to Fig. 3. The molecular geometry is taken as the r_s-structure given in Table 2 and the atomic masses are based upon the ^{12}C-scale.

All the available data on vibrational frequencies, centrifugal distortion constants and Coriolis coupling constants for the various isotopic species have been used for calculating the force field. Since anharmonicity constants for MDA are unknown, and the corrections to harmonic frequencies would have to be guessed, the anharmonic vapour phase frequencies have been used whenever possible.

The weights, w_i, assigned to the data were calculated from the equation: $w_i=1/\sigma_i^2$, where σ_i is the estimated probable error in the ith datum. σ_i has been taken equal to 0.01(frequency), but not less than 5 cm^{-1} for the vibrational frequencies. For the ζ constants, an uncertainty of 0.05 has been allowed to account for unknown anhar-

Table 8. 1,3-Pentadiyne; observed data and uncertainties (σ), calculated data and errors (ε). Fundamental modes of vibration in wavenumbers, D_J in Hz, D_{JK} in kHz, ζ-constants dimensionless and l-type doubling constants, q_i, in MHz.

	Obs.	σ	Calc.	ε
$H_3CCCCCH$ [a]				
ν_1	3333	33	3343	–10
ν_2	2935	29	2938	–3
ν_3	2257 [b]	23	2261	–4
ν_4	2079	21	2082	–3
ν_5	1385	14	1394	1
ν_6	1150	12	1170	–20
ν_7	696	7	687	–9
ν_8	2977	30	2996	–19
ν_9	1446	14	1449	–3
ν_{10}	1029	10	1031	–2
ν_{11}	614	6	616	–2
ν_{12}	484	5	486	–2
ν_{13}	320	5	320	0
ν_{14}	139	5	138	1
ζ_8	0.08	0.05	0.15	–0.07
ζ_9	–0.34	0.05	–0.37	0.03
ζ_{10}	0.40	0.05	0.36	0.04
ζ_{13}	0.94	0.05	0.93	0.01
ζ_{14}	0.96	0.05	0.96	0.

q_{13}	0.985	–	1.027	
q_{14}	2.108	–	2.161	
D_J	68.	15.	77.	–9.
D_{JK}	19.83	0.99	20.07	–0.24
$H_3CCCCCD$ [c]				
ν_1	2935	29	2938	–3
ν_2	2600	26	2588	12
ν_3	2244 [b]	22	2247	–3
ν_4	1968	20	1969	–1
ν_5	1385	14	1384	1
ν_6	1148	11	1161	–13
ν_7	681	7	678	3
ν_8	2976 [d]	30	2996	–20
ν_9	1446 [d]	14	1449	–3
ν_{10}	1029	10	1031	–2
ν_{11}	491	5	492	–1
ν_{12}	469	5	466	3
ν_{13}	314 [c]	5	315	–1
ν_{14}	131 [f]	5	134	–3
q_{14}	1.956	–	2.002	
D_J	62.	6.	67.	–5.
D_{JK}	18.31	0.92	18.47	–0.16
$D_3CCCCCH$ [c]				
ν_1	3334	33	3343	–9
ν_2	2258	23	2264	–6
ν_3	2123	21	2122	1
ν_4	2079	21	2076	3
ν_5	1187	12	1188	–1
ν_6	1025	10	1030	–5
ν_7	652	7	645	7
ν_8	2250	22	2234	16
ν_9	1046	10	1043	3
ν_{10}	827 [f]	8	825	2
ν_{11}	614	6	616	–2
ν_{12}	478	5	479	–1
ν_{13}	308 [e]	5	305	3
ν_{14}	134 [f]	5	131	3
ζ_9	–0.41	0.05	–0.44	0.03
q_{14}	1.804	–	1.913	
D_J	70.	5.	63.	7.
D_{JK}	14.55	0.73	14.51	0.04
$D_3CCCCCD$ [c]				
ν_1	2600 [b]	26	2588	12
ν_2	2250	23	2251	–1
ν_3	2121	21	2118	3
ν_4	1964	20	1968	–4
ν_5	1185	12	1181	4
ν_6	1028	10	1026	2
ν_7	646	6	638	6
ν_8	2250	23	2234	16
ν_9	1045 [d]	10	1043	2
ν_{10}	826	8	825	1
ν_{11}	490	5	485	5
ν_{12}	466	5	466	0
ν_{13}	298 [e]	5	301	–3
ν_{14}	125 [f]	5	127	–2
q_{14}	1.684	–	1.772	
D_J	103.	–	55.	
D_{JK}	13.48	0.67	13.41	0.07
$D_3{}^{13}CCCCCH$				
D_J	62.	10.	61.	1.
D_{JK}	13.98	0.70	13.89	0.09
$D_3C^{13}CCCCH$				
D_J	113.	–	62.	
D_{JK}	14.52	0.73	14.47	0.05
$D_3CCC^{13}CCH$				
D_J	81.	34.	62.	19.
D_{JK}	14.26	0.71	14.23	0.03
$D_3CCCC^{13}CH$				
D_J	70.	8.	59.	11.
D_{JK}	13.94	0.70	13.86	0.08
$D_2HCCCCCH$				
D_J	64.	20.	69.	–5.
D_{JK}	14.19	0.71	14.35	–0.16

[a] Vibrational frequencies from Ref. 5, Coriolis coupling constants from Ref. 5 and Ref. 3, *l*-type doubling constants from Ref. 2 and distortion constants from Ref. 1. [b] Corrected for Fermi resonance. [c] Vibrational frequencies from Ref. 4, distortion constants and *l*-type doubling constants from Ref. 1. [d] Corrected from (R_{Q_0}) to center frequency. [e] Solution data from Raman spectrum. [f] Corrected for liquid/vapour frequency shift.

monicity effects. The $\sigma(D_J)$ have been taken as two times the standard error on these constants (poorly determined) and the $\sigma(D_{JK})$ have been taken as 5 % of their values to allow for anharmonicity.

The results of a convergence to a 23 parameter force field are given in Table 7. In the A_1 species it was found necessary to constrain the

stretch–stretch interaction constants $F_{3,4}$ and $F_{4,5}$ to their values in 2,4-hexadiyne (dimethyldiacetylene).[21] The E species force constants are more reliably fixed, primarily due to the availability of D_{jk} for a number of ^{13}C isotopic substituted molecules. The reproduction of the observed data for all isotopes of MDA, calculated using the force field of Table 7, is given in Table 8.

Acknowledgements. The authors are grateful to the Department of Chemical Physics, University of Copenhagen, for the use of their microwave spectrometer. Financial support from the Norwegian Research Council for Science and the Humanities is acknowledged.

REFERENCES

1. Heath, G. A., Thomas, L. F., Sherrad, E. I. and Sheridan, J. *Discuss. Faraday Soc. 19* (1955) 38.
2. Thomas, L. F., Heeks, J. S. and Sheridan, J. *Arch. Sci. 10* (1957) 180.
3. Maier, M. *Thesis,* University of Sussex, Sussex 1977.
4. Lamotte, J., Lavalley, J. C. and Romanet, R. *J. Chim. Phys. Phys. Chim. Biol. 70* (1973) 1077.
5. Benestad, L., Augdahl, E. and Kloster-Jensen, E. *Spectrochim. Acta A 31* (1975) 1329.
6. Rogstad, A., Benestad, L. and Cyvin, S. J. *J. Mol. Struct. 23* (1974) 265.
7. Maier, J. P., Marthaler, O. and Kloster-Jensen, E. *J. Chem. Phys. 72* (1980) 701.
8. Callomon, J. H., Hirota, E., Kuchitsu, K., Lafferty, W. J., Maki, A. G. and Pote, C. S. *Structure Data of Free Polyatomic Molecules,* Springer, Berlin 1976.
9. Tyler, J. K. and Sheridan, J. *Trans. Faraday Soc. 59* (1963) 2661.
10. Nugent, L. J., Mann, D. E. and Lide, D. R. *J. Chem. Phys. 36* (1962) 965.
11. Sæbø, S. *The Program System MOLFORC,* Program Manual, Department of Chemistry, University of Oslo, Oslo 1979.
12. Pulay, P. *Mol. Phys. 17* (1969) 197.
13. Almlöf, J. *The Program System MOLECULE,* USIP Report 74–29, University of Stockholm, Stockholm 1974.
14. Roos, B. and Siegbahn, P. *Theor. Chim. Acta 17* (1970) 209.
15. Huzinaga, S. *J. Chem. Phys. 42* (1965) 1293.
16. Dunning, T. H., Jr., *J. Chem. Phys. 53* (1970) 2823.
17. Watson, J. K. G. *5th International Seminar on High Resolution Infrared Spectroscopy,* Prague 1978.
18. Watson, J. K. G. *J. Mol. Spectrosc. 48* (1973) 479.
19. Kraitchman, J. *Am. J. Phys. 21* (1953) 17.
20. Thomas, R. K. and Thompson, H. W. *Spectrochim. Acta A 24* (1968) 1337.
21. Nielsen, C. J. *To be published.*

Received August 30, 1982.

Acta Chemica Scandinavica A 37 (1983) 277–281

The Molecular Structure of Methylenimino Borane, $H_2C{=}N{-}BH_2$, Studied by *ab initio* Calculations

GRETE GUNDERSEN and SVEIN SÆBØ *

Department of Chemistry, University of Oslo, P.O.Box 1033, Oslo 3, Norway

Geometry optimizations of the title compound have shown that a linear orthogonal form is preferred over a planar one by about 50 kJ mol^{-1} (12 kcal mol^{-1}). The result is in contrast to the planar structure preferred for the iso-electronic $H_2B{-}O{-}BH_2$. The important geometrical parameters of the two forms of $H_2C{=}N{-}BH_2$ are $\angle$(C=N−B) 180 and 116.4°, r(C=N) 1.228 and 1.255 Å, and r(B−N) 1.374 and 1.476 Å, respectively. The B−N bond length and results of the population analysis reflect the importance of dative π-bonding in the B−N bond for the preferred structure. It appears that the C=N and B−N bonds are shorter in methylenimino borane than in methylenimine and aminoborane, respectively.

The planar arrangement of the bonds to nitrogen in aminoboranes has been related to effects from dative π-bonding. Thus, when the first monomeric iminoboranes were synthesized it was said that a structural consequence of such π-bonding for compounds with two-co-ordinate nitrogen ($R_2C{=}NBR'_2$) would be a linear configuration at nitrogen since in a perpendicular form this would maximize the π-bonding.[1,2] TThis was supported by results from infrared spectroscopic studies [1,2] and later corroborated by infrared data for several monomeric iminoboranes, as summarized elsewhere;[3] and by results of NMR spectroscopic investigations [4–8] and semi-empirical molecular orbital calculations.[8–10] Although dipole measurements are said to give results that demonstrate the lack of N⇒B π-bonding,[11,12] it seems that the evidence in favour of the linear structure is substantial and it has been shown by X-ray crystallography that the structure of $R_2C{=}N{-}BR'_2$ (R=mesityl and R′=phenyl) approximates very well to an allene-like configuration: $\angle$(C=N−B)=173(2)° and the dihedral angle (θ) between the $R_2C{=}N$ and $N{-}BR'_2$ planes is 87°.[10] The preliminary results of a gas-phase electron-diffraction study of $(CF_3)_2C{=}N{-}B(CH_3)_2$[13] initiated in connection with other studies of monomeric iminoboranes,[6–8] suggest a similar structure for this molecule, but more elaborate testing of interdependencies between the conformational parameters and assumptions regarding the torsional orientations of the CF_3-groups is needed to give more reliable structural data.

It has been speculated that also the derivatives of diboryloxide ($H_2B{-}O{-}BH_2$) would have allene-type structures, but electron-diffraction [14] and spectroscopic [15,16] studies showed that $[(CH_3)_2B]_2O$ has C_2 molecular symmetry in the gas phase. The molecule has $\angle$(B−O−B)=144(3)° and ϕ(B−O−B−C) = 38(4)° which corresponds to a dihedral angle between the two C_2B-planes of 72(7)°.[14] Moreover, *ab initio* calculations for the parent molecule ($H_2B{-}O{-}BH_2$) have shown that the minimum-energy geometry corresponds to a bent ($\angle$(B−O−B)=127°) *planar* form of C_{2v} symmetry.[17] Hence it was of interest to establish to which extent the iminoboranes are "true" allene analogues, *i.e.* whether the structures with angles approaching 180° at nitrogen and near perpendicular conformations in fact correspond

* Present address: Research School of Chemistry, The Australian National University, P.O. Box 4, Canberra, ACT 2600, Australia.

0302-4377/83 $02.50

to the preferred structure of the parent molecule. We have therefore studied $H_2C{=}N{-}BH_2$ by *ab initio* molecular orbital calculations, the results of which are presented in this paper. For comparison purposes we have supplemented previous *ab initio* studies of $H_2C{=}NH$ [18-20] with new calculations whereas results of compatible calculations for other related molecules such as $H_2B{-}NH_2$, $(H_2B)_2NH$ and $(H_2B)_2O$ already exist.[17]

CALCULATION PROCEDURE AND RESULTS

The calculations were initially (*A*) carried out using the computer program MOLECULE [21] which solves the Roothaan-Hall equations for a basis set of contracted Gaussian functions.

The minimum-energy geometries were determined from results of calculations for selected points on the energy surface assuming the energy to exhibit second order polynomial dependency upon the geometrical parameters. Subsequently, however, as MOLECULE was further developed so as to give a new *ab initio* gradient program MOLFORC [22] which calculates the energy gradient with respect to the nuclear coordinates for a single-determinant SCF wave function and fully optimizes the molecular geometry by the force-relaxation method,[23] new calculations (*B*) were carried out using this computer program. Initially (*A*) a basis set similar in size to one earlier used for H_2BNH_2 [24] was used, but in the course of the investigation a smaller basis set was found to reproduce rather well experimental molecular

Table 1. Minimum energy geometries, total energies(E_{tot}) and relative energies (ΔE) for methylenimino-borane and methylenimine.[a]

Type [b]	Geometrical parameters [d]	E_{tot}	ΔE
$H_2C{=}N{-}BH_2$			
A	Planar form [c] CN 1.250; BN 1.455; CNB 117.8; [CH1=CH2 1.08; NCH1=NCH2 122; BH3=BH4 1.20; NBH3=NBH4 120.] [d]	−119.31794	51.0 (12.2)
	Orthogonal (linear) form CN 1.224; BN 1.363; CNB 180 [CH1=CH2 1.08; NCH1=NCH2 122; BH3=BH4 1.20; BCH3=BCH4 120.] [d]	−119.33743	
B	Planar form CN 1.255; BN 1.476; CNB 116.4 CH1 1.086; CH2 1.090; NCH1 120.2; NCH2 124.4 BH3 1.195; BH4 1.185; NBH3 120.8; NBH4 119.1	−119.19591	46.9 (11.2)
	Orthogonal (linear) form CN 1.228; BN 1.374; CNB 180; CH1=CH2 1.086; NCH1=NCH2 121.8; BH3=BH4 1.185; NBH3=NBH4 119.3	−119.21374	
$H_2C{=}NH$			
B	Planar form CN 1.247 CH1 1.083; CH2 1.087; NCH1 119.5; NCH2 125.1 NH3 1.011; CNH3 110.5	−93.94904	

[a] Distances in Å, angles in degrees, E_{tot} in a.u., and ΔE in kJ mol^{-1} with values in parantheses in kcal mol^{-1}. [b] See text for explanation. [c] See text for *bent* nonplanar forms of $H_2C{=}N{-}BH_2$. [d] The numbering of the atoms are given in Fig. 1. Quantities in square brackets are assumed values.

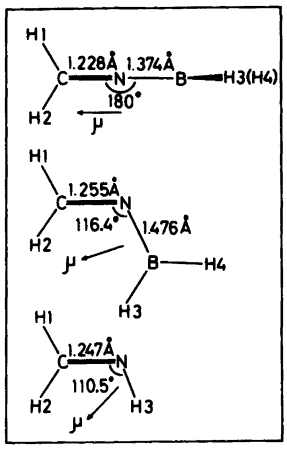

Fig. 1. Numbering of the atoms for methyleniminoborane and methylenimine. Important geometrical parameters and the directions of the dipole moments obtained in the *B*-type (see text) calculations.

geometries for H_2BNH_2, $HB(NH_2)_2$, H_2BOH and $HB(OH)_2$,[17] and a similar basis set was used in the *B*-calculations. The basis sets were for the nitrogen and carbon, boron, and the hydrogen atoms, respectively: *A* $(9s,5p,1d) \rightarrow \langle 4,3,1\rangle$, $(9s,5p) \rightarrow \langle 4,3\rangle$, and $(4s,1p) \rightarrow \langle 2,1\rangle$; and *B* $(7s,3p,1d) \rightarrow \langle 4,2,1\rangle$, $(7s,3p) \rightarrow \langle 4,2\rangle$ and $(4s) \rightarrow \langle 2\rangle$. The $(9s,5p)$ and $(7s,3p)$ basis sets were those given by Huzinaga [25] and Roos and Siegbahn,[26] respectively, and the Huzinaga $(4s)$ basis for the hydrogens [27] was scaled by a factor of 1.2.[30] The exponents of the polarization functions, 1*d* for carbon and nitrogen, and 1*p* for hydrogen, were 0.95 and 0.90, respectively.

The results of the geometry optimization are given in Table 1, whereas some results of the population analyses [28,29] for the *B*-calculations and corresponding values for H_2BNH_2 and $HN(BH_2)_2$ obtained in compatible calculations [17] are comprised in Table 2. The important geometrical parameters and the directions of the dipole moments defined as $q^- \rightarrow q^+$ are given in Fig. 1 which also shows the numbering of the atoms.

For $H_2C{=}NH$ only *B*-calculation on a planar form of the molecule was carried out whereas both types of calculations were performed for $H_2C{=}N{-}BH_2$.

A. $H_2C{=}N{-}BH_2$. Only r(C=N), r(B−N) and ∠(C=N−B) were optimized and the assumed values used for the remainder of the geometrical parameters are given in square brackets in Table 1. Initially r(C−N) and r(B−N) were assumed to be 1.27 and 1.38 Å, respectively. For the planar form ∠(C=N−B) was determined to 118.8° and subsequent coupled variations of r(C=N) and r(B−N) and re-optimization of ∠(C=N−B) gave the minimum-energy quoted in Table 1. For the orthogonal form calculations for ∠(C=N−B) of 170, 175 and 180° showed that there was an energy minimum at the linear configuration and the r(C=N) and r(B−N) values obtained for ∠(C=N−B) = 180° are given in Table 1. The energy differences were not pronounced around the linear form as bending of the linear form by 10 and 5°, required only 5.8 and 0.01 kJ mol^{-1} (1.4 and 0.003 kcal mol^{-1}), respectively.

B. $H_2C{=}N{-}BH_2$. The fully optimized structures of a planar and an orthogonal form are given in Table 1. The results given for the orthogonal form were obtained assuming a linear configuration. Subsequently, optimizations were carried out for a slightly bent, twisted form starting with ∠(C=N−B) = 170° and θ(B−N) = 80° and this optimization converged to the linear orthogonal form. This confirms that the linear allene form is a minimum on the potential surface. In agreement with the *A*-calculations it was also shown that the potential surface is very flat around this minimum. For example, with ∠(C=N−B) = 174° and θ(B−N) = 86° the total energy is only 0.13 kJ mol^{-1} (0.03 kcal mol^{-1}) above that of the linear orthogonal structure.

DISCUSSION

The two forms of $H_2C{=}N{-}BH_2$ have quite different electron distributions: one has a B−N bond with a high degree of double bonding (see below) whereas the other has a lone pair of electrons localized on nitrogen. Thus the neglect of correlation effects, *i.e.* the use of the Hartree-Fock model, may have introduced errors not only in the total energies, but also in the energy differences. Double bonds are generally poorly described in the Hartree-Fock model giving rise to a highish E(corr) term which is inherently also expected for a lone pair of electrons. The resultant impact on ΔE is, however, difficult to assess, but the relatively high energy difference (Table 1) of about 50 kJ mol^{-1} (12 kcal mol^{-1})

Table 2. Dipole moments (μ in D), gross atomic populations (N), B–N and C=N bond distances (r in Å) and corresponding net overlap populations (n) for $H_2C{=}N{-}BH_2$ and $H_2C{=}NH$ compared to results for $H_2B{-}NH_2$ and $H_2B{-}NH{-}BH_2$ (Ref. 17) obtained with the B-type (7s, 3p) basis.[a]

	$H_2C{=}N{-}BH_2$		$H_2C{=}NH$	$H_2N{-}BH_2$	$H_2B{-}NH{-}BH_2$
	Orthogonal [b]	Planar	Planar	Planar	Planar
$\lvert\mu\rvert$ [c]	2.21	2.05	2.08	2.00	1.23
N(N)	7.48	7.54	7.45	7.88	7.93
σ	4.77	6.46	6.36	6.18	6.35
π	1.10(z); 1.61(y)	1.08	1.09	1.70	1.58
N(B)	4.65	4.53	–	4.64	4.60
σ	4.33	4.40	–	4.34	4.39
π	0.33(y)	0.13	–	0.30	0.21
N(C)	6.17	6.18	6.24	–	–
σ	5.28	5.40	5.33	–	–
π	0.89(z)	0.78	0.91	–	–
$N(H_C)$	0.78	0.79	0.80	–	–
$N(H_B)$	1.06	1.08	–	1.07	1.06
$N(H_N)$	–	–	0.71	0.67	0.65
r(B–N)	1.374	1.476	–	1.398	1.435
n(B,N)	0.86	0.71	–	0.82	0.71
σ	0.54	0.60	–	0.52	0.50
π	0.32(y)	0.11	–	0.30	0.21
r(C=N)	1.228	1.255	1.247	–	–
n(C,N)	1.13	1.13	1.17	–	–
σ	0.62	0.68	0.65	–	–
π	0.51(z)	0.45	0.52	–	–

[a] Subscripts for H indicate the atoms to which the hydrogens are bonded. [b] π is considered to involve p_y for BH_2 and p_z for CH_2, thus giving two π components for nitrogens, p_y interacting with BH_2 and p_z with CH_2. [c] Experimental counterparts are μ_a=1.325 and μ_b=1.53 D,[34] 1.844(5) D,[30] and 1.245(17) D [35] for $H_2C{=}NH$, H_2NBH_2 and $H_2B{-}NH{-}BH_2$, respectively.

suggests that such effects cannot reverse the calculated conformational preference for the molecule. Hence it is concluded that an allene-type structure of $H_2C{=}N{-}BH_2$ is clearly favoured over a planar form. This is in contrast to the results for the isoelectronic $H_2B{-}O{-}BH_2$ which has a planar minimum energy geometry in which one lone pair of electrons remains uninvolved in bonding and the other is shared equally between the two BH_2 groups.[17]

Larger basis sets are known to yield the shorter bond distances, and this accounts for the differences in bond lengths obtained in the two sets of calculations (Table 1). For r(B–N) in the planar form the discrepancy is of the magnitude encountered for $H_2B{-}NH_2$ in which r(B–N) is 1.378 and 1.398 Å for A- [24] and B-type [17] calculations, respectively. The difference in r(B–N) is less for the orthogonal form and it is marginal for r(C=N). The calculated structure with B-basis for $H_2B{-}NH_2$ [17] is in good agreement with the experimental one which has r_s(B–N)=1.391(2) Å.[30] However, the calculated r(C=N) of 1.247 Å in $H_2C{=}NH$ is shorter than the experimental counterpart [31] by 0.026 Å. Consequently, the C=N bond length of 1.228 Å in $H_2C{=}N{-}BH_2$ is probably calculated too short. However, 1.374 Å should give a relatively good estimate of r(B–N) in the iminoborane, and it appears consistent with the somewhat unprecisely determined experimental values of 1.38(2) and 1.35(2) Å in $R_2C{=}N{-}BR'_2$ with R/R′ equal to mesityl/phenyl [12]0 and CF_3/CH_3,[13] respectively. The short B–N bond shows that it has strong π-bonding, and this is supported by results from the population analysis (Table 2). Corresponding quantities for the planar form reflect the slight possibility for the C=N bond to donate π-electrons to the BH_2-group. It appears that the C=N and B–N bonds in methyleniminoborane

are shorter than the corresponding bonds in $H_2C{=}NH$ and H_2BNH_2. This trend may be rationalized by the hybridization changes of nitrogen as related to the bonding in ethylene and allene which have r(C=C) values of 1.335(3)[32] and 1.312 Å,[33] respectively.

REFERENCES

1. Dorokhov, V. A. and Lappert, M. F. *Chem. Commun.* (1968) 250.
2. Jennings, J. R., Pattison, I., Summerford, C., Wade, K. and Watt, B. K. *Chem. Commun.* (1968) 250.
3. Weinstock, N. In Niedenzu, K. and Buschbeck, K., Eds., *Gmelin Handbuch der anorganischen Chemie, Erganzungwerk zur 8 Auflage,* Springer, Berlin-Heidelberg-New York 1975, Vol. 23, Borverbindungen, Teil 5, Chapter 3.9.
4. Summerford, C. and Wade, K. *J. Chem. Soc. A* (1970) 2010.
5. Collier, H. R., Lappert, M. F., Smith, R. and Wade, K. *J. Chem. Soc. Dalton Trans.* (1972) 370.
6. Gragg, B. R. and Niedenzu, K. *Synth. React. Inorg. Met. Org. Chem. 6* (1976) 275.
7. Emerick, D. P., Gragg, B. R. and Niedenzu, K. *J. Organomet. Chem. 153* (1978) 9.
8. Emerick, D. P., Komorowski, L., Lipinski, J., Nahm, F. C. and Niedenzu, K. *Z. Anorg. Allg. Chem. 468* (1980) 44.
9. Hoffmann, R. *Adv. Chem. Ser. 42* (1964) 78.
10. Bullen, G. J. *J. Chem. Soc. Dalton Trans.* (1973) 858; Bullen, G. J. and Wade, K. *Chem. Commun.* (1971) 1122.
11. Mikhailov, B. M., Ter-Sarkisyan, G.S., Nikolaeva, N. A. and Kieselev, V. G. *J. Gen. Chem. U.S.S.R. 43* (1973) 857.
12. Mikhailov, B. M., Ter-Sarkisyan, G. S., Govorov, N. N., Nikolaeva, N. A. and Kiselev, V. G. *Bull. Acad. Sci. USSR Div. Chem. Sci.* (1976) 848.
13. Almenningen, A., Gundersen, G. and Niedenzu, K. *Preliminary results in The Norwegian Electron Diffraction Group, Annual Report 1980,* Chapter 4, available upon request.
14. Gundersen, G. and Vahrenkamp, H. *J. Mol. Struct. 33* (1976) 97.
15. Lanthier, G. F. and Graham, W. A. G. *Chem. Commun.* (1968) 715.
16. Durig, J. R., Flanagan, M. J., Stampf, E. J. and Odom, J. *J. Mol. Struct. 42* (1977) 13.
17. Fjeldberg, T., Gundersen, G., Jonvik, T., Seip, H. M. and Sæbø, S. *Acta Chem. Scand. A 34* (1980) 547.
18. Macaulay, R., Barnelle, L. A. and Sandorfy, C. *Theor. Chim. Acta 29* (1973) 1.
19. Botschwina, P. Chem. Phys. Lett. 29 (1974) 580.
20. Howell, J. M. *J. Am. Chem. Soc. 98* (1976) 886.
21. Almlöf, J. *USIP Report 74–29,* University of Stockholm, Stockholm 1968.
22. Sæbø, S. *Internal Report,* Department of Chemistry, University of Oslo, Oslo 1979.
23. Pulay, P. *Mol. Phys. 17* (1969) 197.
24. Gropen, O. and Seip, H. M. *Chem. Phys. Lett. 25* (1974) 206.
25. Huzinaga, S. *J. Chem. Phys. 42* (1965) 1293.
26. Roos, B. and Siegbahn, P. *Theor. Chim. Acta 19* (1970) 209.
27. Dunning, T. H., Jr. *J. Chem. Phys. 53* (1970) 2823.
28. Mulliken, R. S. *J. Chem. Phys. 36* (1962) 3428.
29. Mulliken, R. S. *J. Chem. Phys. 23* (1955) 1833.
30. a. Sugie, M., Takeo, H. and Matsumura, C. *Chem. Phys. Lett. 66* (1979) 573; b. Matsumura, C. *Private communication.* (Revised structure).
31. Pearson, R., Jr. and Lovas, F. J. *J. Chem. Phys. 66* (1977) 4149.
32. Kuchitsu, K. *J. Chem. Phys. 44* (1966) 906.
33. Almenningen, A., Bastiansen, O. and Trætteberg, M. *Acta Chem. Scand. 13* (1959) 1699.
34. Kirchhoff, W. H., Johnson, D. R. and Lovas, F. J. *J. Phys. Chem. Ref. Data 2* (1973) 1.
35. Briggs, T. S., Gwinn, W. D., Jolly, W. L. and Thorne, L. R. *J. Am. Chem. Soc. 100* (1979) 7762; Thorne, L. R. and Gwinn, W. D. *J. Am. Chem. Soc. 104* (1982) 3822.

Received September 7, 1982.

Acta Chemica Scandinavica A 37 (1983) 283–291

The Crystal Conformation of 1,4,7,10-Tetra-(2-hydroxyethyl)-1,4,7,10-tetraazacyclododecane in Complexes with NaSCN and KSCN at −150 °C

P. GROTH

Department of Chemistry, University of Oslo, Oslo 3, Norway

The crystals of the NaSCN-complex are orthorhombic with space group $Pna2_1$ and cell dimensions $a = 24.980(5)$, $b = 9.304(2)$, $c=9.292(2)$ Å. Those of the KSCN-complex are monoclinic with space group $P2_1/n$ and cell dimensions $a=11.015(4)$, $b=31.863(10)$, $c=12.988(3)$ Å, $\beta=94.30(2)°$. Data were collected on an automatic four circle diffractometer. The structures were solved by direct methods and refined by full-matrix least squares technique. The ring conformation is [3 3 3 3] in both complexes. The Na cation is heptacoordinated, making use of the three *gauche* side-chains and the four ring nitrogens. In the KSCN-complex, which has a disordered structure, all four side-chains are bent in and K^+ is octacoordinated. In both complexes all side-arms bend off towards the ring corner atoms.

The aim of the single crystal X-ray crystallographic investigations of the molecule 1,4,7,10-tetra-(2-hydroxyethyl)-1,4,7,10-tetraazacyclododecane as a hydrate, and in complexes with Li^+, Na^+ and K^+, is to study conformational dissimilarities of this molecule and to correlate the findings with ^{13}C NMR results.[1] Crystal structure determinations of the dihydrated (2:1) LiCl-complex and the hydrate have been reported earlier.[2,3] The results obtained for the NaSCN- and KSCN-complexes are now reported.

Table 1. Final fractional coordinates with estimated standard deviations for the NaSCN-complex. Standard deviations for hydrogen atoms are about $\sigma_x=0.001$, $\sigma_y=0.003$ and $\sigma_z=0.004$. Hmn is bonded to Cm and HOm to Om.

ATOM	X	Y	Z
NA+	.91009(4)	−.09053(12)	−.17725(71)
S	.17353(4)	.61339(9)	.80099(70)
C	.1092(1)	.5826(3)	.8028(8)
N	.0632(1)	.5599(3)	.8040(8)
O1	.9576(1)	.0118(3)	.0246(8)
O2	.9710(1)	−.2810(3)	−.1232(8)
O3	.9838(1)	−.2975(3)	−.6143(8)
O4	.9652(1)	.1062(3)	−.2920(8)
N1	.8420(1)	−.0075(3)	.0123(8)
N2	.8553(1)	−.3123(3)	−.0945(8)
N3	.8611(1)	−.2079(3)	−.4000(8)
N4	.8476(1)	.0968(3)	−.2941(8)
C1	.8027(1)	−.1231(4)	.0349(8)
C2	.8277(1)	−.2722(4)	.0405(8)
C3	.8172(1)	−.3551(4)	−.2061(8)
C4	.8411(1)	−.3516(4)	−.3562(8)
C5	.8156(1)	−.1131(4)	−.4563(8)
C6	.8299(1)	.0455(4)	−.4561(8)
C7	.8011(1)	.1196(4)	−.1990(8)
C8	.8158(1)	.1249(4)	−.0391(8)
C9	.8720(1)	.0224(4)	.1460(8)
C10	.9246(1)	.0962(4)	.1181(8)
C11	.8948(1)	−.4277(4)	−.0655(8)
C12	.9475(1)	−.3676(4)	−.0141(8)
C13	.9970(1)	−.2258(4)	−.5249(8)
C14	.9524(1)	−.2790(4)	−.4857(8)
C15	.8787(1)	.2301(4)	−.3067(8)
C16	.9359(1)	.2072(4)	−.3717(8)
H11	.776	−.124	−.051
H12	.780	−.105	.124
H21	.800	−.344	.061
H22	.854	−.278	.127
H31	.784	−.292	−.205
H32	.805	−.462	−.195
H41	.813	−.588	−.428
H42	.871	−.418	−.358
H51	.785	−.130	−.372
H52	.800	−.154	−.536
H81	.800	.100	−.471

0302-4377/83 $02.50

H62	.858	.059	-.502
H71	.774	.041	-.220
H72	.781	.214	-.223
H81	.781	.140	.014
H82	.840	.209	-.014
H91	.879	-.073	.190
H92	.849	.082	.213
H101	.943	.113	.214
H102	.918	.196	.066
H111	.902	-.483	-.158
H112	.882	-.496	.006
H121	.972	-.452	.010
H122	.942	-.302	.072
H131	.901	-.128	-.568
H132	.879	-.288	-.603
H141	.953	-.374	-.430
H142	.971	-.206	-.425
H151	.883	.274	-.206
H152	.858	.307	-.369
H161	.952	.307	-.375
H162	.933	.171	-.474
HO1	.977	-.028	.078
HO2	.996	-.321	-.154
HO3	.972	-.391	-.656
HO4	.980	.155	-.207

EXPERIMENTAL

Crystal and intensity data, The crystal data for $(C_{16}H_{36}O_4N_4)\cdot NaSCN$ are: $a=24.980(5)$, $b=9.304(2)$, $c=9.295(2)$ Å, $Z=4$, space group $Pna2_1$, $D_x=1.32$ gcm^{-3}, $D_m=1.28$ gcm^{-3} (by flotation), $V=2160.29$ Å^3, $\mu=2.06$ cm^{-1} (MoK_α), λ(MoK_α)=0.71069 Å. The crystal data for $(C_{16}H_{36}O_4N_4)\cdot KSCN$ are: $a=11.015(4)$, $b=31.863(10)$, $c=12.988(3)$ Å, $\beta=94.30(2)°$, $Z=8$, space group $P2_1/n$, $D_x=1.30$ gcm^{-3}, $D_m=1.25$ gcm^{-3} (by flotation), $V=4545.32$ Å^3, $\mu=3.68$ cm^{-1} (Mo$K\alpha$), λ(Mo$K\alpha$)=0.71069 Å.

Data were collected on an automatic four-circle diffractometer at *ca.* −150 °C by the ω-scan technique ($2\theta_{max}=50°$) with Mo$K\alpha$ radiation. The scan rate varied from 2° to 23° min^{-1}, depending on the intensity of the reflection. The intensities of two test reflections remeasured after every 50 reflections showed no significant changes during data collection. The intensities were corrected for

Table 2. Bond distances and angles and dihedral angles with estimated standard deviations for the NaSCN-complex.

DISTANCE	(Å)	DISTANCE	(Å)	DIHEDRAL ANGLE	(°)
NA+ - O1	2.417(3)	NA+ - O2	2.388(3)	N1 - C9 - C10 - O1	-57.8(4)
NA+ - O4	2.526(3)	NA+ - N1	2.569(3)	N2 - C11 - C12 - O2	-63.4(4)
NA+ - N2	2.591(3)	NA+ - N3	2.643(3)	N3 - C13 - C14 - O3	177.4(3)
NA+ - N4	2.579(3)	N - O2'	2.820(4)	N4 - C15 - C16 - O4	-57.5(4)
N - O3"	2.812(4)	O1 - O4'	2.779(4)	C8 - N1 - C1 - C2	161.4(3)
S - C	1.632(3)	C - N	1.168(4)	C1 - N1 - C8 - C7	-77.4(4)
O1 - C10	1.432(4)	O2 - C12	1.424(4)	C9 - N1 - C1 - C2	-76.1(4)
O3 - C14	1.441(4)	O4 - C16	1.429(4)	C1 - N1 - C9 - C10	158.7(3)
N1 - C1	1.471(4)	N1 - C8	1.474(4)	C9 - N1 - C8 - C7	159.5(3)
N1 - C9	1.479(4)	N2 - C2	1.481(4)	C8 - N1 - C9 - C10	-78.1(4)
N2 - C3	1.464(5)	N2 - C11	1.482(4)	C3 - N2 - C2 - C1	-77.3(4)
N3 - C4	1.483(4)	N3 - C5	1.477(4)	C2 - N2 - C3 - C4	161.9(3)
N3 - C13	1.475(4)	N4 - C6	1.473(5)	C11 - N2 - C2 - C1	158.7(3)
N4 - C7	1.475(4)	N4 - C15	1.467(4)	C2 - N2 - C11 - C12	-84.6(4)
C1 - C2	1.521(5)	C3 - C4	1.519(6)	N1 - C1 - C2 - N2	-61.5(4)
C5 - C6	1.517(5)	C7 - C8	1.533(6)	C11 - N2 - C3 - C4	-75.0(4)
C9 - C10	1.505(5)	C11 - C12	1.504(5)	C3 - N2 - C11 - C12	151.3(3)
C13 - C14	1.520(5)	C15 - C16	1.521(5)	C5 - N3 - C4 - C3	-75.4(4)
ANGLE	(°)	ANGLE	(°)	C4 - N3 - C5 - C6	161.6(3)
S - C - N	179.7(3)	O1 - C10 - C9	111.0(3)	C13 - N3 - C4 - C3	163.4(3)
O2 - C12 - C11	110.2(3)	O3 - C14 - C13	109.7(3)	C4 - N3 - C13 - C14	-77.0(3)
O4 - C16 - C15	112.4(3)	N1 - C1 - C2	113.4(3)	N2 - C3 - C4 - N3	-59.5(4)
O1 - N1 - C8	113.8(3)	C1 - N1 - C9	110.8(3)	C13 - N3 - C5 - C6	-77.7(4)
N1 - C8 - C7	113.2(3)	C8 - N1 - C9	109.9(3)	C5 - N3 - C13 - C14	162.0(3)
N1 - C9 - C10	112.5(3)	N2 - C2 - C1	113.1(3)	C7 - N4 - C6 - C5	-78.0(4)
C2 - N2 - C3	111.6(3)	C2 - N2 - C11	109.7(3)	C6 - N4 - C7 - C8	161.3(3)
N2 - C3 - C4	113.0(3)	C3 - N2 - C11	111.4(3)	C15 - N4 - C6 - C5	159.5(3)
N2 - C11 - C12	111.7(3)	N3 - C4 - C3	113.8(3)	C6 - N4 - C15 - C16	-71.5(4)
C4 - N3 - C5	109.9(3)	C4 - N3 - C13	109.3(3)	N3 - C5 - C6 - N4	-62.0(4)
N3 - C5 - C6	113.5(3)	C5 - N3 - C13	110.3(3)	C15 - N4 - C7 - C8	-75.7(4)
N3 - C13 - C14	113.5(3)	N4 - C6 - C5	112.7(3)	C7 - N4 - C15 - C16	165.9(3)
C6 - N4 - C7	110.4(3)	C6 - N4 - C15	111.1(3)	N4 - C7 - C8 - N1	-59.2(4)
N4 - C7 - C8	113.5(3)	C7 - N4 - C15	110.1(3)		
N4 - C15 - C16	113.2(3)				

Lorentz and polarization effects, but no corrections for absorption or secondary extinction were made (crystal sizes 0.4×0.6×0.2 mm and 0.2×0.3×0.2 mm for the NaSCN-complex and the KSCN-complex, respectively). With an observed-unobserved cutoff at $2.5\sigma(I)$, 1709 and 5306 reflections were regarded as observed.

Determination and refinement of the structures. The phase problem was solved by direct methods.[4] For the KSCN-complex the *E*-map corresponding to the best figure of merit contained several split peaks indicating a disordered structure. The procedure from this map to the final structure was somewhat lengthy: repeated use of weighted Fourier calculations, parameter-shift refinements (to avoid singular-matrix problems in least-squares), intermediate introduction of anisotropic temperature factors (in order to calculate probable positions for partial atoms),[5] careful refinements of multiplicity factors, and calculation of partial hydrogen atom positions (to be used in structure factor calculations).[6,*] For the NaSCN-complex, anisotropic temperature factors were introduced for all non-hydrogen atoms. Maximum r.m.s. amplitudes lay between 0.13 and 0.22 Å. For the KSCN-complex, anisotropic temperature factors were used for the 21

* All programs used (except those for phase determination) are included in this reference.

Table 3. Final fractional coordinates with estimated standard deviations for the non-hydrogen atoms of the KSCN-complex. The two statistically disordered forms are labelled "A" and "B", respectively.

ATOM	X	Y	Z
K1	.92502(9)	.17886(5)	.51104(8)
K2	.25746(9)	.42236(5)	.78485(7)
S2	.1657(1)	.1109(0)	1.0021(1)
C34	.1418(4)	.1300(1)	1.1154(4)
N10	.1253(3)	.1432(1)	1.1970(3)
N1	1.1767(3)	.1949(1)	.5722(3)
N2	1.0192(3)	.2578(1)	.4442(3)
N3	.8222(3)	.2520(1)	.5994(3)
N4	.9815(4)	.1889(1)	.7304(3)
N5	.1714(3)	.5024(1)	.8401(3)
N6	.3756(3)	.4951(1)	.6931(3)
N7	.2175(3)	.4300(1)	.5617(2)
N8	.0115(3)	.4393(1)	.7077(3)
C10	1.1936(4)	.1277(1)	.4755(4)
C12	.9357(5)	.2273(1)	.2785(3)
C14	.6369(4)	.2182(1)	.5157(4)
C16	.8998(6)	.1165(1)	.7225(5)
C26	.2263(4)	.4754(1)	1.0154(3)
C28	.5561(4)	.4628(1)	.7954(4)
C30	.3102(4)	.3586(1)	.5803(3)
C32	-.0188(4)	.3696(1)	.7912(4)
S1A	1.0650(2)	.3788(0)	.2574(1)
S1B	.9968(8)	.3759(2)	.2835(5)
C33A	1.0258(10)	.3875(3)	.1542(17)
C33B	1.0382(21)	.3828(7)	.1686(31)
N9A	.9985(7)	.3942(2)	.0481(5)
N9B	1.0576(25)	.3863(6)	.0826(21)
O1A	1.0770(3)	.1103(1)	.5055(3)
O1B	1.0930(14)	.1330(4)	.3952(11)
O2A	.9436(3)	.1817(1)	.3036(3)
O2B	.8498(14)	.2089(4)	.3075(11)
O3A	.6928(4)	.2022(1)	.4295(3)
O3B	.6835(12)	.1793(4)	.4816(11)
O4A	.8184(4)	.1193(1)	.6395(3)
O4B	.9345(14)	.1054(5)	.6011(12)
O5A	.3210(4)	.4452(1)	.9892(3)
O5B	.2412(15)	.4318(4)	.9925(11)
O6A	.5085(3)	.4208(1)	.8080(3)
O6B	.4900(15)	.4460(5)	.8720(13)
O7A	.2506(3)	.3472(1)	.6720(3)
O7B	.3728(14)	.3621(4)	.6794(11)
O8A	.0795(3)	.3717(1)	.8656(3)
O8B	.1075(14)	.3522(5)	.7866(12)
C1A	1.2212(7)	.2259(2)	.5059(7)
C1B	1.2080(18)	.2418(7)	.5462(18)
C2A	1.1425(9)	.2650(3)	.4933(14)
C2B	1.1487(19)	.2628(6)	.4566(32)
C3A	.9331(6)	.2905(2)	.4616(6)
C3B	.9714(16)	.2944(5)	.5174(15)
C4A	.8999(14)	.2902(2)	.5759(8)
C4B	.8547(26)	.2896(5)	.5551(16)
C5A	.8198(10)	.2475(2)	.7088(5)
C5B	.8807(32)	.2489(7)	.7227(18)
C6A	.9404(8)	.2335(3)	.7648(6)
C6B	.9056(22)	.2099(8)	.7692(17)
C7A	1.1077(11)	.1833(6)	.7572(9)
C7B	1.1212(18)	.1966(10)	.7447(15)
C8A	1.1876(7)	.2096(3)	.6842(6)
C8B	1.2076(18)	.1851(7)	.6717(15)
C9A	1.2432(6)	.1547(2)	.5683(5)
C9B	1.2594(18)	.1723(6)	.4944(16)
C11A	1.0277(6)	.2521(2)	.3300(5)
C11B	.9635(22)	.2717(7)	.3424(17)
C13A	.6953(6)	.2581(2)	.5522(5)
C13B	.6922(21)	.2380(7)	.6079(19)
C15A	.9114(6)	.1586(2)	.7875(5)
C15B	.9810(23)	.1383(8)	.7612(18)
C17A	.2199(8)	.5362(2)	.7694(10)
C17B	.2351(16)	.5362(5)	.8147(22)
C18A	.3567(7)	.5304(2)	.7513(5)
C18B	.2940(21)	.5345(6)	.7172(16)
C19A	.3326(12)	.4971(2)	.5816(6)
C19B	.3818(33)	.4909(7)	.5909(17)
C20A	.3121(8)	.4554(3)	.5232(6)
C20B	.2779(22)	.4721(9)	.5317(15)
C21A	.0931(7)	.4486(3)	.5549(5)
C21B	.1000(17)	.4261(8)	.5296(14)
C22A	-.0080(8)	.4516(4)	.5988(6)
C22B	.0144(23)	.4462(10)	.5890(16)
C23A	-.0145(6)	.4860(2)	.7278(6)
C23B	-.0419(18)	.4675(7)	.7619(16)
C24A	.0440(6)	.5017(2)	.8526(8)
C24B	.0292(18)	.5053(6)	.7808(22)
C25A	.2209(6)	.5109(2)	.9487(5)
C25B	.1289(22)	.4985(7)	.9499(17)
C27A	.5100(6)	.4822(2)	.6974(5)
C27B	.4922(23)	.5044(8)	.7596(20)
C29A	.2224(6)	.3870(2)	.5167(4)
C29B	.3106(20)	.3980(6)	.5208(15)
C31A	-.0721(5)	.4138(2)	.7657(5)
C31B	-.0510(22)	.3927(8)	.7137(19)

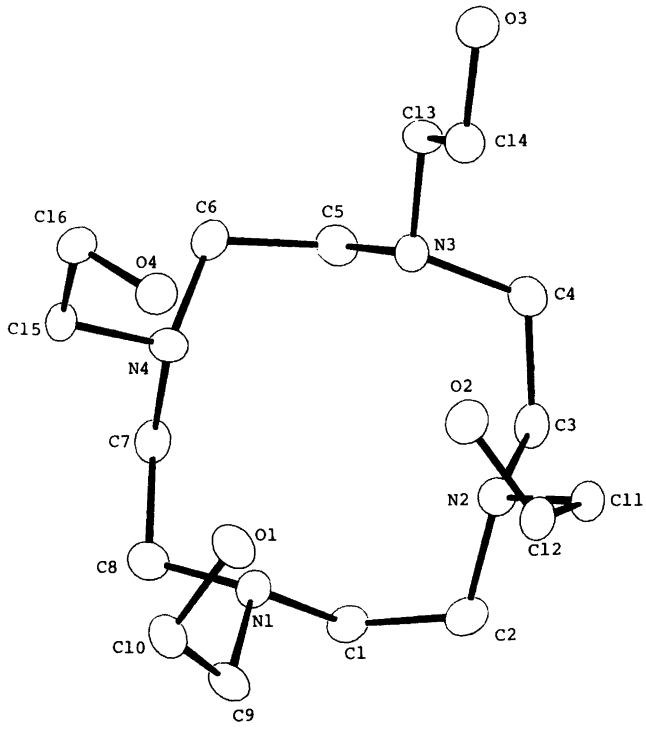

Fig. 1. Schematic drawing of the ligand of the NaSCN-complex showing the numbering of atoms.

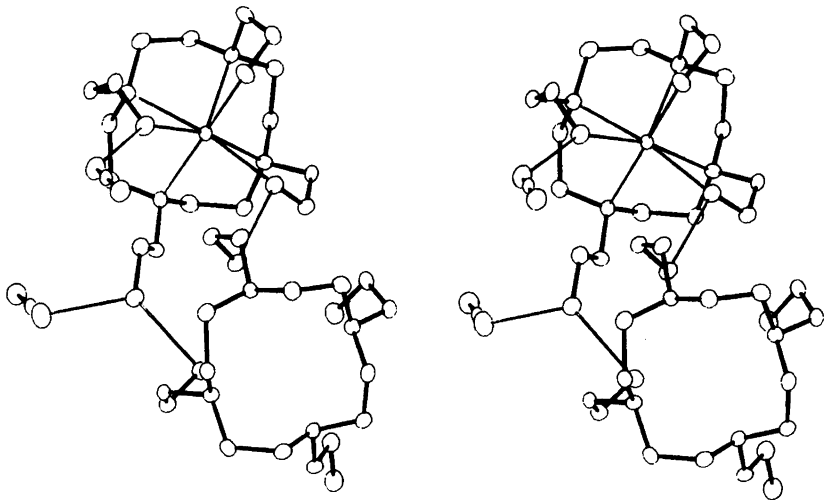

Fig. 2. Stereoscopic view of the NaSCN-complex, illustrating the coordination and hydrogen bonding system.

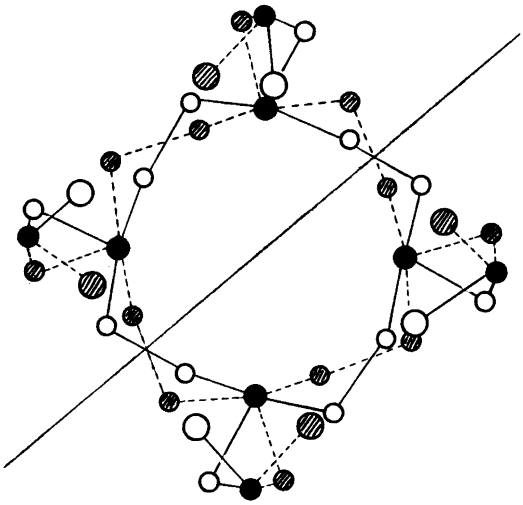

Fig. 3. Schematic drawing indicating the type of disorder (due to the presence of statistical pseudo mirror planes) for the ligands of the KSCN-complex.

atoms for which no disorder could be observed. For these atoms the maximum r.m.s. amplitudes range from 0.15 to 0.30 Å. The form factors used were those of Hanson *et al.*,[7] except for hydrogen.[8] Weights in least squares were obtained from the standard deviations in intensities, $\sigma(I)$, taken as $\sigma(I)=C_T+[(0.02C_N)^2]^{1/2}$, where C_T is the total number of counts, and C_N the net count. Methylene hydrogen positions were calculated. The hydroxyl hydrogen atoms of the NaSCN-complex were localized in a difference Fourier map. No attempt to find the corresponding partial hydrogens in the KSCN-complex was made. The final R-values were $R=3.5$ % ($R_w=3.0$ %) for the 1709 observed reflections of the NaSCN-complex, and $R=6.6$ % ($R_w=6.5$ %) for the 5306 observed reflections of the KSCN-complex. Standard deviations in bond distances and angles and torsional angles were calculated from the correlation matrixes of the final least-squares refinement cycles. Final fractional atomic coordinates are given in Tables 1 and 3, the latter containing only non-hydrogen atoms. Lists of observed and calculated structure factors, as well as the temperature factors, are obtainable from the author.

DISCUSSION

The NaSCN-complex. Fig. 1 is a schematic drawing of the ligand showing the numbering of atoms. The bond distances and angles of Table 2 have normal values within estimated limits of error. From the list of dihedral angles it may be seen that the 12-membered ring adopts the [3 3 3 3] conformation [2] and that three of the side-chains are *gauche* and the fourth *anti*. As to be expected from the ^{13}C NMR studies,[1] the ring conformation corresponds to that of the (2:1)

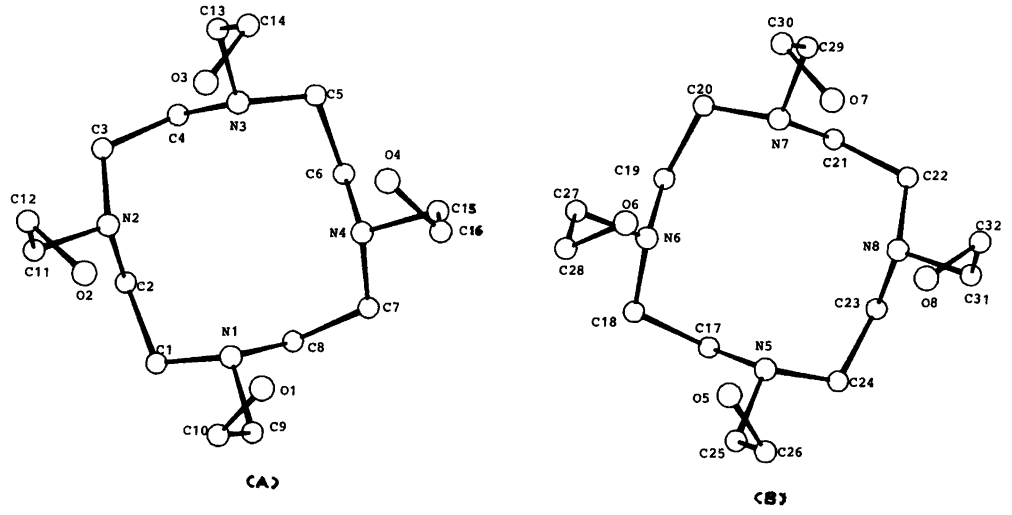

Fig. 4. Schematic drawings of the A-forms of the two crystallographically independent ligands, (A) and (B), of the KSCN-complex. The numbering of atoms (with the A's omitted) is indicated.

Table 4. Bond distances and angles and torsional angles with estimated standard deviations for the A-form of the KSCN-complex.

DISTANCE	(Å)	DISTANCE	(Å)
N1 - C1A	1.42(1)	N1 - C8A	1.52(1)
N1 - C9A	1.48(1)	N2 - C2A	1.47(1)
N2 - C3A	1.44(1)	N2 -C11A	1.5(1)
N3 - C4A	1.53(1)	N3 - C5A	1.43(1)
N3 -C13A	1.5(1)	N4 - C6A	1.57(1)
N4 - C7A	1.42(1)	N4 -C15A	1.47(1)
N5 -C17A	1.54(1)	N5 -C24A	1.4(1)
N5 -C25A	1.5(1)	N6 -C18A	1.42(1)
N6 -C19A	1.49(1)	N6 -C27A	1.52(1)
N7 -C20A	1.44(1)	N7 -C21A	1.51(1)
N7 -C29A	1.49(1)	N8 -C22A	1.44(1)
N8 -C23A	1.54(1)	N8 -C31A	1.48(1)
C10 - O1A	1.42(1)	C10 - C9A	1.53(1)
C12 - O2A	1.49(1)	C12 -C11A	1.43(1)
C14 - O3A	1.41(1)	C14 -C13A	1.49(1)
C16 - O4A	1.35(1)	C16 -C15A	1.59(1)
C26 - O5A	1.44(1)	C26 -C25A	1.47(1)
C28 - O6A	1.45(1)	C28 -C27A	1.47(1)
C30 - O7A	1.45(1)	C30 -C29A	1.52(1)
C32 - O8A	1.4(1)	C32 -C31A	1.55(1)
C1A - C2A	1.52(1)	C3A - C4A	1.5(1)
C5A - C6A	1.53(1)	C7A - C8A	1.58(2)
C17A -C18A	1.55(1)	C19A -C20A	1.54(1)
C21A -C22A	1.54(2)	C23A -C24A	1.55(1)

DIHEDRAL ANGLE	(°)
C8A - N1 - C1A - C2A	-70.(1)
N1 - C1A - C2A - N2	-63.(2)
C3A - N2 - C2A - C1A	161.(1)
C2A - N2 - C3A - C4A	-71.(1)
N2 - C3A - C4A - N3	-71.(1)
C5A - N3 - C4A - C3A	166.(1)
C4A - N3 - C5A - C6A	-70.(1)
N3 - C5A - C6A - N4	-63.(1)
C7A - N4 - C6A - C5A	161.(1)
C6A - N4 - C7A - C8A	-73.(1)
N4 - C7A - C8A - N1	-66.(1)
C1A - N1 - C8A - C7A	164.(1)
C24A - N5 -C17A -C18A	-164.(1)
N5 -C17A -C18A - N6	67.(1)
C19A - N6 -C18A -C17A	73.(1)
C18A - N6 -C19A -C20A	-161.(1)
N6 -C19A -C20A - N7	64.(1)
C21A - N7 -C20A -C19A	71.(1)
C20A - N7 -C21A -C22A	-163.(1)
N7 -C21A -C22A - N8	61.(1)
C23A - N8 -C22A -C21A	75.(1)
C22A - N8 -C23A -C24A	-160.(1)
N8 -C23A -C24A - N5	67.(1)
C17A - N5 -C24A -C23A	69.(1)

ANGLE	(°)	ANGLE	(°)
C1A - N1 - C8A	111.(1)	C1A - N1 - C9A	112.(1)
C8A - N1 - C9A	108.(1)	C2A - N2 - C3A	115.(1)
C2A - N2 -C11A	109.(1)	C3A - N2 -C11A	109.(1)
C4A - N3 - C5A	109.(1)	C4A - N3 -C13A	110.(1)
C5A - N3 -C13A	109.(1)	C6A - N4 - C7A	110.(1)
C6A - N4 -C15A	106.(1)	C7A - N4 -C15A	110.(1)
C17A - N5 -C24A	111.(1)	C17A - N5 -C25A	109.(1)
C24A - N5 -C25A	111.(1)	C18A - N6 -C19A	113.(1)
C18A - N6 -C27A	111.(1)	C19A - N6 -C27A	107.(1)
C20A - N7 -C21A	112.(1)	C21A - N7 -C29A	109.(1)
C21A - N7 -C29A	109.(1)	C22A - N8 -C23A	108.(1)
C22A - N8 -C31A	111.(1)	C23A - N8 -C31A	108.(0)
O1A - C10 - C9A	106.(0)	O2A - C12 -C11A	113.(0)
O3A - C14 -C13A	111.(0)	O4A - C16 -C15A	113.(1)
O5A - C26 -C25A	111.(0)	O6A - C28 -C27A	112.(0)
O7A - C30 -C29A	107.(0)	O8A - C32 -C31A	111.(0)
N1 - C1A - C2A	115.(1)	N2 - C2A - C1A	115.(1)
N2 - C3A - C4A	111.(1)	N3 - C4A - C3A	112.(1)
N3 - C5A - C6A	115.(1)	N4 - C6A - C5A	113.(1)
N4 - C7A - C8A	111.(1)	N1 - C8A - C7A	114.(1)
N1 - C9A - C10	112.(1)	N2 -C11A - C12	116.(1)
N3 -C13A - C14	113.(1)	N4 -C15A - C16	108.(1)
N5 -C17A -C18A	113.(1)	N6 -C18A -C17A	111.(1)
N6 -C19A -C20A	115.(1)	N7 -C20A -C19A	113.(1)
N7 -C21A -C22A	115.(1)	N8 -C22A -C21A	114.(1)
N8 -C23A -C24A	113.(1)	N5 -C24A -C23A	115.(1)
N5 -C25A - C26	114.(1)	N6 -C27A - C28	114.(1)
N7 -C29A - C30	112.(0)	N8 -C31A - C32	112.(0)

dihydrated LiCl-complex,[2] which also was found to be preferred in the hydrate.[3] The dissimilarity in conformation stems from the various number of *anti* and *gauche* side-chains. In the Li^+-complex there is one *gauche* chain while the hydrate has two. From Fig. 1 it may be seen that all side-arms bend off towards the "corner" atoms of the ring. The same pattern was observed in the earlier reported structures.[2,3]

Fig. 2 is a stereoscopic view of the complex. It shows that Na^+ is coordinated to four nitrogen atoms and to the three oxygens of the *gauche* side-chains. The nitrogen atom of the thiocyanate anion accepts hydrogen bonds from the hydroxyl group of the *anti* side-arm and from one of the *gauche* chains in a symmetry related ligand. The two remaining *gauche* side-chains are also hydrogen bonded to symmetry related ligands. (One of these hydrogen bonds, O3−O4'''=2.742(4) Å, is missing in Table 2.) The C−H and O−H bond distance ranges are 0.94−1.06 and 0.78−1.00 Å, respectively.

The KSCN-complex. There are two complexes in the asymmetric unit, both of which are

Table 5. Bond distances and angles and torsional angles with estimated standard deviations for the B-form of the KSCN-complex.

DISTANCE	(Å)	DISTANCE	(Å)
N1 - C1B	1.58(2)	N1 - C8B	1.35(2)
N1 - C9B	1.58(2)	N2 - C2B	1.43(2)
N2 - C3B	1.62(2)	N2 -C11B	1.48(2)
N3 - C4B	1.39(2)	N3 - C5B	1.68(3)
N3 -C13B	1.51(2)	N4 - C6B	1.21(2)
N4 - C7B	1.56(2)	N4 -C15B	1.66(3)
N5 -C17B	1.34(2)	N5 -C24B	1.70(2)
N5 -C25B	1.54(2)	N6 -C18B	1.64(2)
N6 -C19B	1.34(2)	N6 -C27B	1.54(3)
N7 -C20B	1.56(2)	N7 -C21B	1.34(2)
N7 -C29B	1.57(2)	N8 -C22B	1.56(2)
N8 -C23B	1.31(2)	N8 -C31B	1.64(2)
C1O - O1B	1.47(2)	C1O - C9B	1.61(2)
C12 - O2B	1.18(2)	C12 -C11B	1.66(2)
C14 - O3B	1.42(1)	C14 -C13B	1.45(2)
C16 - O4B	1.7O(2)	C16 -C15B	1.22(2)
C26 - O5B	1.37(2)	C26 -C25B	1.54(2)
C28 - O6B	1.38(2)	C28 -C27B	1.55(3)
C3O - O7B	1.42(2)	C3O -C29B	1.48(2)
C32 - O8B	1.5O(2)	C32 -C31B	1.28(2)
C1B - C2B	1.46(4)	C3B - C4B	1.42(3)
C5B - C6B	1.4O(4)	C7B - C8B	1.44(3)
C17B -C18B	1.47(3)	C19B -C20B	1.46(4)
C21B -C22B	1.41(3)	C23B -C24B	1.45(3)

DIHEDRAL ANGLE	(°)
C8B - N1 - C1B - C2B	-16O.(2)
N1 - C1B - C2B - N2	47.(4)
C3B - N2 - C2B - C1B	85.(2)
C2B - N2 - C3B - C4B	-157.(2)
N2 - C3B - C4B - N3	48.(3)
C5B - N3 - C4B - C3B	8O.(2)
C4B - N3 - C5B - C6B	-153.(2)
N3 - C5B - C6B - N4	63.(4)
C7B - N4 - C6B - C5B	76.(3)
C6B - N4 - C7B - C8B	-153.(3)
N4 - C7B - C8B - N1	46.(4)
C1B - N1 - C8B - C7B	83.(2)
C24B - N5 -C17B -C18B	-84.(2)
N5 -C17B -C18B - N6	-49.(3)
C19B - N6 -C18B -C17B	158.(2)
C18B - N6 -C19B -C20B	-82.(3)
N6 -C19B -C20B - N7	-47.(4)
C21B - N7 -C20B -C19B	153.(3)
C20B - N7 -C21B -C22B	-81.(3)
N7 -C21B -C22B - N8	-53.(4)
C23B - N8 -C22B -C21B	139.(3)
C22B - N8 -C23B -C24B	-76.(2)
N8 -C23B -C24B - N5	-57.(3)
C17B - N5 -C24B -C23B	156.(2)

ANGLE	(°)	ANGLE	(°)
C1B - N1 - C8B	112.(1)	C1B - N1 - C9B	99.(1)
C8B - N1 - C9B	113.(1)	C2B - N2 - C3B	1O3.(2)
C2B - N2 -C11B	114.(2)	C3B - N2 -C11B	1OO.(1)
C4B - N3 - C5B	111.(1)	C4B - N3 -C13B	124.(2)
C5B - N3 -C13B	1O2.(1)	C6B - N4 - C7B	125.(2)
C6B - N4 -C15B	115.(2)	C7B - N4 -C15B	98.(2)
C17B - N5 -C24B	1O9.(1)	C17B - N5 -C25B	120.(2)
C24B - N5 -C25B	95.(1)	C18B - N6 -C19B	1O8.(2)
C18B - N6 -C27B	99.(1)	C19B - N6 -C27B	118.(2)
C2OB - N7 -C21B	115.(1)	C2OB - N7 -C29B	1OO.(1)
C21B - N7 -C29B	119.(1)	C22B - N8 -C23B	119.(1)
C22B - N8 -C31B	1O2.(2)	C23B - N8 -C31B	113.(1)
O1B - C1O - C9B	1O8.(1)	O2B - C12 -C11B	113.(1)
O3B - C14 -C13B	12O.(1)	O4B - C16 -C15B	1O8.(1)
O5B - C26 -C25B	118.(1)	O6B - C28 -C27B	1O7.(1)
O7B - C3O -C29B	113.(1)	O8B - C32 -C31B	113.(1)
N1 - C1B - C2B	121.(2)	N2 - C2B - C1B	115.(2)
N2 - C3B - C4B	118.(1)	N3 - C4B - C3B	12O.(2)
N3 - C5B - C6B	121.(2)	N4 - C6B - C5B	115.(2)
N4 - C7B - C8B	125.(1)	N1 - C8B - C7B	116.(2)
N1 - C9B - C1O	1O3.(1)	N2 -C11B - C12	1O4.(1)
N3 -C13B - C14	114.(2)	N4 -C15B - C16	118.(2)
N5 -C17B -C18B	117.(2)	N6 -C18B -C17B	119.(2)
N6 -C19B -C2OB	117.(2)	N7 -C2OB -C19B	124.(2)
N7 -C21B -C22B	117.(2)	N8 -C22B -C21B	123.(2)
N8 -C23B -C24B	114.(2)	N5 -C24B -C23B	12O.(2)
N5 -C25B - C26	1O8.(1)	N6 -C27B - C28	1O8.(2)
N7 -C29B - C3O	11O.(1)	N8 -C31B - C32	118.(2)

disordered. The disorder arises from the presence of statistical pseudo mirror planes as indicated in Fig. 3. Least–squares refinement of multiplicity factors showed that there are about 75 % and 25 % of the two forms (labelled "A" and "B"), respectively. Fig. 4 (A) and (B) are schematic drawings of the A-ligands showing the numbering of atoms, (the A's being omitted). One of the thiocyanate anions is also disordered. The disorder was not observable for all the ligand atoms (black circles in Fig. 3), and these were refined anisotropically with multiplicity factors equal to 1.0. The same scheme was used for the potassium cations and the other thiocyanate anion.

Bond distances and angles and dihedral angles may be found in Tables 4, 5 and 6. Within the relatively large estimated limits of error all values are normal for the A-form. Problems connected with the design of a proper least–squares refinement scheme, due to close contacts between partial atoms, are probably responsible for some rather awkward values arrived at for the B-ligands. The torsional angles correspond to the

Table 6. Coordination bonds, hydrogen bonds and bond distances and angles of the anions with estimated standard deviations for the KSCN-complex.

DISTANCE	(Å)	DISTANCE	(Å)
S2 - C34	1.631(6)	S1A -C33A	1.64P(24)
S1B -C33B	1.615(38)	C34 - N10	1.167(6)
C33A - N9A	1.157(25)	C33B - N9B	1.158(49)
K1 - N1	2.872(4)	K1 - N2	2.878(4)
K1 - N3	2.868(4)	K1 - N4	2.889(4)
K1 - O1A	2.757(4)	K1 - O1B	2.871(15)
K1 - O2A	2.719(4)	K1 - O2B	2.874(15)
K1 - O3A	2.795(5)	K1 - O3B	2.659(14)
K1 - O4A	2.837(4)	K1 - O4B	2.673(16)
K2 - N5	2.833(4)	K2 - N6	2.904(4)
K2 - N7	2.91.(4)	K2 - N8	2.869(4)
K2 - O5A	2.79.(5)	K2 - O5B	2.734(15)
K2 - O6A	2.759(4)	K2 - O6B	2.824(17)
K2 - O7A	2.8.7(4)	K2 - O7B	2.726(16)
K2 - O8A	2.8[illegible](4)	K2 - O8B	2.781(16)
N10 - O1B	2.644(16)	N10 - O2A	2.801(6)
N1. - O6A	2.858(6)	N10 - O7B	2.779(16)
N9A - O8A	2.695(8)	N9B - O3B	2.878(31)
N9B - O5B	2.813(31)	O1A - O6A	2.800(6)
O2A - O7A	2.782(6)	O3A - O8A	2.763(6)
O4A - O5A	2.837(6)	O1B - O6B	2.767(23)
O2B - O7B	2.831(22)	O3B - O8B	2.794(22)
O4B - O5B	2.7.7(22)		

ANGLE	(°)	ANGLE	(°)
S1A -C33A - N9A	178.5(9)	S1B -C33B - N9B	173.6(25)
S2 - C34 - N10	179.2(5)		

familiar [3 3 3 3] conformation for all four 12-membered rings, and the N–N–C planes of the side-chains are again tilted towards the ring corner atoms. The profound conformational alteration suggested by the NMR investigation [1] is caused by the fact that all four side-arms are *gauche* in the KSCN-complex.

Fig. 5 is a stereoscopic view of the two A-complexes illustrating the eight-coordination of the potassium cations and the hydrogen bonding system. The potassium cation coordinates to four ring nitrogens and the four oxygens of the side-chains in both complexes. The thiocyanate anions are involved in four hydrogen bonds donated by two ligands. N10 accepts two bonds, while N9A and S1A accept one each. The same two ligands are finally linked by four hydrogen bonds to form the dimers shown in Fig. 5.

Concluding remarks. The modest upfield dis-

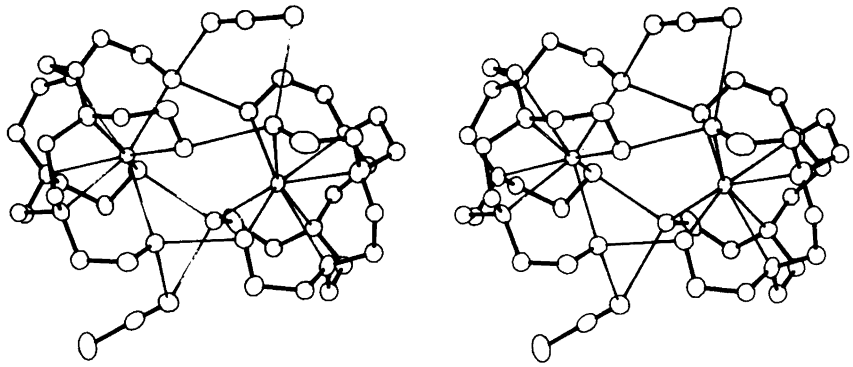

Fig. 5. Stereoscopic view of the A-form of the KSCN-complex illustrating the coordination and hydrogen bonding system.

placement of the ring ^{13}C signals [1] is in accordance with the recurrence of the same [3 3 3 3] ring conformation in the structures of the dihydrated (2:1) complex with LiCl,[2] the hydrate,[3] and the complexes with NaSCN and KSCN. The slight variations of torsional angles are a natural consequence of the adjustment of the donor–acceptor distances. The side-chains invariably bend off towards the corner atoms of the ring. When a side-arm is rejected, the C–C bond is anti, and when it coordinates to the cation (or water molecule), it is *gauche* of the same helicity as the corner bonds of the ring. Accommodation to the varying size of the cation occurs mainly by adjustment of this *gauche* torsional angle. In none of these structures is there any direct anion–cation contact. The ligand can thus be considered a sensitive probe for optimal coordination numbers of Li^+, Na^+ and K^+.

Acknowledgement. The author thanks S. Buøen for preparing the compounds.

REFERENCES

1. Buøen, S., Dale, J., Groth, P. and Krane, J. *Chem. Commun.* (1982) 1172.
2. Groth, P. *Acta Chem. Scand. A 37* (1983) 71.
3. Groth, P. *Acta Chem. Scand. A 37* (1983) 75.
4. Germain, G., Main, P. and Woolfson, M. M. *Acta Crystallogr. A 27* (1971) 368.
5. Kartha, G. and Ahmed, F. R. *Acta Crystallogr. 13* (1960) 532.
6. Groth, P. *Acta Chem. Scand. 27* (1973) 3131.
7. Hanson, H. P., Herman, F., Lea, J. D. and Skillman, S. *Acta Crystallogr. 17* (1964) 1040.
8. Stewart, R. F., Davidson, E. R. and Simpson, W. T. *J. Chem. Phys. 42* (1965) 3175.

Received September 7, 1982.

Acta Chemica Scandinavica A 37 (1983) 293–306

Solutions of Chlorine in Molten Chlorides. 2. Solubility and Diffusivity of Chlorine in Chloroaluminate Melts

O. WÆRNES and T. ØSTVOLD

Institutt for uorganisk kjemi, Norges tekniske høgskole, Universitetet i Trondheim, N-7034 Trondheim-NTH, Norway

The reduction of Cl_2 dissolved in basic as well as acidic $AlCl_3$–NaCl and $AlCl_3$–CsCl melts ($X_{AlCl_3} \lesssim 0.50$) has been investigated. The electrochemical techniques chronopotentiometry, chronoamperometry and voltammetry were employed.

The chronopotentiometric results obtained in $AlCl_3$–NaCl melts in the temperature range 160–450 °C did not obey the Sand equation, probably due to adsorption of chlorine on the electrode and/or a high value of the double layer capacity. The results have been corrected according to a model which implies simultaneous reaction of adsorbed and diffusing species (SAR model). Fair agreement with the chronoamperometric results was then obtained. The chlorine diffusivity in the $AlCl_3$–MCl mixtures is in the order of 10^{-5} cm^2 s^{-1}, and is not markedly different in acidic and basic melts.

In the $AlCl_3$–NaCl melts ($0.496 < X_{AlCl_3} < 0.52$) and in $AlCl_3$–CsCl melts where $X_{AlCl_3} > 0.50$, the reduction of chlorine is found to be irreversible with $\alpha n_a \approx 0.5$, *i.e.* one-electron transfer in the rate determining step. For the basic $AlCl_3$–CsCl mixtures a nearly reversible two-electron charge transfer was found.

The solubility of chlorine gas in molten $AlCl_3$–CsCl ($0.425 < X_{AlCl_3} < 0.52$) has been determined by a manometric technique. This involves keeping the gas volume above the melt constant and to measure the pressure decrease as the gas dissolves in the liquid. The solubility is around 5×10^{-6} mol cm^{-3} and is decreasing with increasing temperature. There is no tendency to a drastic change in the solubility around the melt composition corresponding to $X_{AlCl_3} = 0.50$.

In a recent paper from this laboratory solutions of chlorine in some alkali chloride melts were studied.[1] Solubilities and electrochemical diffusivities were measured. In the present paper analogous data in chloroaluminate melts are reported.

PRINCIPLES

Chlorine solubility measurements. The equilibrium (1) is studied:

$$Cl_2(g) = Cl_2(\text{dissolved}) \qquad (1)$$

Assuming that Henry's law is valid for the solute and that $Cl_2(g)$ obeys the ideal gas law with a standard state of 1 mol cm^{-3} for the dissolved gas and 1 atm for the pure gas, the equilibrium constant is equal to the Henry's law constant.

$$K_H = \frac{c_{Cl_2}(\text{diss})}{P_{Cl_2}(g)} = \frac{\Delta P V_o \rho}{RTw\Delta P_{eq}} \qquad (2)$$

ΔP is the pressure drop due to dissolution of chlorine. V_o is the volume of gas above the melt reduced to the volume this gas would have at the temperature T.[1-3] This temperature was normally 25 °C. ρ is the density of the melt, R the gas constant, w the weight of salt and ΔP_{eq} the change in equilibrium pressure after an addition of chlorine gas to the volume above the melt.

Chronopotentiometric measurements. The fundamental equation for chronopotentiometry (semiinfinite linear diffusion to a plane electrode) is the Sand equation [4]

$$\tau^{1/2} = \frac{\pi^{1/2} nFAcD^{1/2}}{2I} = \frac{\pi^{1/2} nFcD^{1/2}}{2i} \qquad (3)$$

0302-4377/83 $02.50

τ is the transition time, n the number of electrons in the overall electrochemical reaction, F the Faraday constant, A the electrode area, c the concentration of Cl_2 dissolved in the melt, D the chlorine diffusion constant, I the applied current and i the current density (I/A). The product $I\tau^{1/2}$ (or $i\tau^{1/2}$) should be independent of the applied current and the chlorine diffusion constant may be determined.

Corrections for the inconstancy of the chronopotentiometric constant ($I\tau^{1/2}$ in eqn. (3)) at short transition times have been considered by several authors.[5-11] The increase in $I\tau^{1/2}$ with decreasing transition time is most frequently caused by the distribution of the current between two or more simultaneous processes. The electrolysis of the electroactive species diffusing to the electrode may be complicated by the charging of the electrical double layer, formation or reduction of oxide films at the electrode and/or electrolysis of electroactive species adsorbed on the electrode. An approximate method of treating these effects is to consider the total current as the sum of four constant currents giving the equation (4) [8,9]

$$I\tau^{1/2} = \frac{\pi^{1/2}nFAcD^{1/2}}{2} + \frac{(C_l)_{av}\Delta EA}{\tau^{1/2}} + \frac{Q_{ox}A}{\tau^{1/2}} + \frac{nFA\Gamma}{\tau^{1/2}} \quad (4)$$

where $(C_l)_{av}$ is the average double layer capacity in the potential interval ΔE, Q_{ox} is the amount of electricity required for oxide film formation or reduction, and Γ is the amount of electroactive species adsorbed on the electrode. The other symbols have been defined previously. The first term on the right hand side of eqn. (4) is the "true" chronopotentiometric constant, while the additional correction terms are all of the same form. By rearranging this equation we get eqn. (5),

$$I\tau = \frac{nFAc(\pi D\tau)^{1/2}}{2} + B \quad (5)$$

where B is an overall correction factor. The assumption of constant currents for the different processes during electrolysis implies the simultaneous reaction of adsorbed reactant and diffusing species (SAR mechanism). Thus only a single transition time is expected.

If, however, the adsorbed species are completely reduced prior to the reduction of the diffusing species (AR, SR mechanism) [6,11] two transition times corresponding to the two processes should ideally be observed and $I\tau$ should be proportional to I^{-1}.

A third model requires that the adsorbed layer is being reduced at the end of the diffusion controlled reaction (SR, AR mechanism).[6,11] In this case $(I\tau)^{1/2}$ should be proportional to $I^{-1/2}$ and two distinct transition times would ideally be observed.

From eqn. (5) it is seen that a plot of $I\tau$ *versus* $\tau^{1/2}$ should give a straight line with finite intercept. The intercept may then give information on the amount of adsorbed species or some of the other terms in eqn. (4). From the slope of the line the "true" chronopotentiometric constant, $(I\tau^{1/2})_{corr}$, (or directly the diffusion coefficient) may be determined. Distinction between the various reaction mechanisms discussed is usually based on a best fit comparison of experimental data with the model equations.

Potential–time relations for a number of common reduction mechanisms, derived by several authors, have been summarized by Reinmuth.[12] For a reversible electrochemical reduction where the product of electrolysis is insoluble (or soluble with activity 1 at the electrode surface as in this case for the Cl^- ion) eqn. (6) may be derived from the Nernst equation [12,13]

$$E = E^\circ + \frac{RT}{nF}\ln\frac{2I}{nAF\pi^{1/2}D^{1/2}} + \frac{RT}{nF}\ln(\tau^{1/2}-t^{1/2}) \quad (6)$$

and a plot of the quantity $\ln(\tau^{1/2}-t^{1/2})$ *versus* E, where t is the time, should yield a straight line with the slope RT/nF.

The potential of the working electrode for an irreversible electrochemical reduction involving one rate-determining step is given by eqn. (7),[12,14]

$$E = E_o + \frac{RT}{\alpha n_a F}\ln\frac{2k_s}{\pi^{1/2}D^{1/2}} + \frac{RT}{\alpha n_a F}\ln(\tau^{1/2}-t^{1/2}) \quad (7)$$

where n_a is the number of electrons involved in the rate-determining charge transfer step, α is a transfer coefficient and k_s is the heterogeneous rate constant for the forward electrochemical process when $E=0$.

Chronoamperometry. In a chronoamperometric experiment, a potential step is applied to the

working electrode and the resulting current–time response is measured. In the simplest case the initial potential of the working electrode is sufficiently positive that the reduction does not proceed, and the potential attained by the step is sufficiently negative to immediately drive the surface concentration of the reactant to zero. Fick's law of diffusion solved with initial and boundary conditions for this case gives eqn. (8).[4]

$$It^{1/2} = \frac{nFAcD^{1/2}}{\pi^{1/2}} \tag{8}$$

This equation, known as the Cottrell equation, shows that a diffusion controlled electrolysis of a reactant gives a current decaying as a $t^{-1/2}$ function. If the current at any time, t_x, is plotted against the value of the applied potential, a current–potential curve for the reaction results. If the applied potentials correspond to the plateau of such a current–potential curve and the product $It^{1/2}$ is independent of time, the diffusion coefficient can be determined.

A current–potential curve, constructed from current–time curves, may yield information on the reduction mechanism. For a reversible electrochemical reduction where the product of electrolysis is insoluble (or soluble with activity 1 at the electrode surface as in the present case) eqn. (9) may be derived from the Nernst equation,[15]

$$E = E^\circ + \frac{RT}{nF} \ln \frac{(\pi t)^{1/2}}{nAFD^{1/2}} + \frac{RT}{nF} \ln(I_l - I) \tag{9}$$

where I_l is the limiting current corresponding to the plateau of the current–potential curve.

For an irreversible charge transfer reduction the analog equation is [16]

$$E = \text{const.} + \frac{RT}{\alpha n_a F} \ln \frac{I_l - I}{I} \tag{10}$$

The rate constant of the reaction may be determined from current–time curves at short times according to the method suggested by Oldham and Osteryoung.[17]

Voltammetry. Cyclic voltammetry provides several measurable parameters as function of scan rate: the net currents at the peaks of the cathodic and anodic response (I_p), the peak potentials (E_p), the separation between the cathodic and anodic peak (ΔE_p) and the half peak potential ($E_{p/2}$, the potential where $I = \frac{1}{2} I_p$).

For a reversible electrochemical reduction where the product is insoluble (or soluble with activity 1 at the electrode surface) Berzins and Delahay [18] and Mamantov *et al.*[15] derived the eqns. (11)–(13).

$$I_p = \frac{0.610(nF)^{3/2} AcD^{1/2} v^{1/2}}{(RT)^{1/2}} \tag{11}$$

$$E_p = E^\circ + \frac{RT}{nF} \ln \gamma c - 0.8540 \frac{RT}{nF} \tag{12}$$

$$E_p - E_{p/2} = -0.77 \frac{RT}{nF} \tag{13}$$

Corresponding relations for an irreversible electrochemical reduction are [19–21]

$$I_p = \frac{0.500 n(\alpha n_a)^{1/2} F^{3/2} AcD^{1/2} v^{1/2}}{(RT)^{1/2}} \tag{14}$$

$$E_p = E^\circ - \frac{RT}{\alpha n_a F}\left[0.780 + 0.5 \ln\left[\frac{D\alpha n_a F v}{RT}\right] - \ln k_s\right] \tag{15}$$

$$E_p - E_{p/2} = -1.857 \frac{RT}{\alpha n_a F} \tag{16}$$

From eqn. (15) it follows that the peak potential is a function of the potential scan rate, thus

$$(E_p)_2 - (E_p)_1 = 0.5 \frac{RT}{\alpha n_a F} \ln\left(\frac{v_1}{v_2}\right) \tag{17}$$

Subscript 1 and 2 corresponds to the different scan rates v_1 and v_2, respectively. An increase in the scan rate yields a cathodic shift in peak potential.

EXPERIMENTAL

Chemicals. Aluminium chloride from Fluka AG, was purified by distillation in evacuated and sealed quartz glass tubes furnished with quartz glass frits. The temperature was kept just above the melting point. The aluminium chloride vapour was transported through the frit by means of a small temperature gradient along the tube. The distillation was terminated when about 90 % of the material had been transported to the cool part of the tube. This procedure was repeated

three times. The purification of the alkali chlorides are described elsewhere.[1]

Mixtures of aluminium chloride and alkali chlorides (52 mol % $AlCl_3$) were made by melting and subsequent filtering of appropriate amounts of purified $AlCl_3$ and MCl in evacuated and sealed quartz glass tubes. After remelting, the filtrate was properly mixed and quenched to prevent any phase separation. An entire batch was used for one experiment.

All handling of purified salts were performed in an N_2-atmosphere glovebox where the water vapour level was constantly monitored and kept below 2 ppm.

Electrochemical measurements. The equipment and experimental procedure are described by Wærnes [2] and Wærnes *et al.*,[1] and only a few essential details will be given here.

The electrochemical experiments were performed with a potentiostat/galvanostat (Model 551) together with an analog function generator (Model 566) and a multifunction interface (Model 563) from AMEL, Milano, Italy. When operating in galvanostatic mode a puls generator (made in our workshop) was connected to a mercury-wetted relay in Model 551. This generator was introduced to cut the current at a certain time to prevent metal reduction at the working electrode.

A Nicolet Explorer 2090-3A digital storage oscilloscope with plug-in unit 206-1 (Nicolet Instrument Corp., Madison, Wisconsin) was used. This instrument provides numerical display of accurate voltage and time values for any selected waveform point, and the stored data could be recorded if necessary on an external Linseis LY 822 X–Y recorder.

For the $AlCl_3$–NaCl system (max. temp. 230 °C) the electrochemical cell was immersed in a Pyrex beaker (5 litre) containing a well-stirred eutectic KNO_3–$NaNO_2$ bath. The temperature was kept constant to ±0.5 °C by a heater, a stirrer and a Eurotherm PID regulator (Eurotherm Ltd., Sussex, England). The bath temperature was determined by a Pt/Pt10 %Rh thermocouple.

For the $AlCl_3$–CsCl system the cell was placed in a gold-plated transparent quartz glass tube furnace (Trans Temp., Inc., Cambridge, Massachusetts). The temperature profile in the middle zone of the furnace was $<\pm 1$ °C. The temperature was controlled by a Eurotherm PID regulator and was measured with a Pt/Pt10 %Rh thermocouple under the cell close to the outside cell wall. The actual melt temperature was found by calibration, correlating melt temperature and temperature outside the cell.

Using the gold furnace and the nitrate/nitrite bath, visual observation of the melt and electrodes was possible.

In the chloroaluminate melts the plane working electrode, sealed in a pyrex tube, as well as the cylindrical reference and counter electrodes were made of vitreous carbon since graphite showed considerable swelling and disintegration in these melts. To determine the composition in the $AlCl_3$–MCl mixture the following procedure was used: The starting composition was always 52 mol % $AlCl_3$. By adding MCl crystals to the mixture through the top of the cell at relatively high chlorine flowrate back diffusion of air was prevented. Solid MCl could visually be observed on the basic side ($X_{AlCl_3}<0.50$) after equilibration. The melt composition is thus given by the intercept between the liquidus line and the actual temperature.

Solubility measurements. The method used for measuring chlorine solubility is, in principle, the same as the one used by Wærnes *et al.*[1] and Andresen *et al.*[22] Due to high vapour pressures in chloroaluminate melts, however, the difference in chlorine solubility between two chlorine pressures were determined.[2,23] Due to the high vapour pressure the chlorine gas dissolved in these melts was removed by reducing the chlorine pressure to ~300 Torr, allowing the melt to remain at this pressure for equilibration. By again increasing the chlorine pressure to ~1000 Torr, a new solubility experiment could be performed.

RESULTS

Chlorine solubilities. The solubilities of chlorine in fused $AlCl_3$–CsCl mixtures have been determined in order to calculate the diffusion coefficients of chlorine. For comparison with literature data, solubility measurements in NaCl were also performed.[1]

The Henry's law test, based on the differential pressure change method,[2,23] is shown in Fig. 1 for Cl_2 dissolved in $AlCl_3$–CsCl melts. In this test, the upper and the lower pressure drop are plotted *versus* the upper and lower equilibrium pressures.[2,23] When four or more of these pressure drops (from the same experiment) lie on the same straight line through the origin Henry's law is confirmed.

The Henry's law constants, K_H, are determined from eqn. (2), where the recently measured density data [24] for $AlCl_3$–CsCl melts are used. The mean values of K_H with standard deviations are given in Table 1.

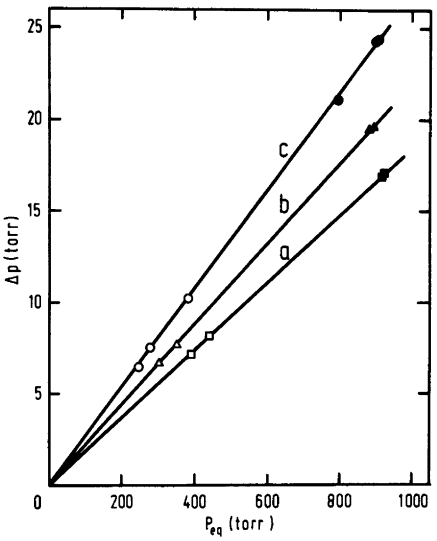

Fig. 1. Test of the validity of Henry's law based on the differential pressure change technique for Cl_2 in $AlCl_3$–CsCl. The filled and open symbols represent upper and lower equilibrium pressures, respectively. *a*–627 °C, X_{AlCl_3}=0.52; *b*–377 °C, X_{AlCl_3}=0.52; *c*–390 °C, X_{AlCl_3}=0.425.

Diffusion coefficients of chlorine.

Chronopotentiometry.

Chronopotentiometric measurements have been performed in $AlCl_3$–NaCl and $AlCl_3$–CsCl melts saturated with chlorine. Representative cathodic chronopotentiometric curves are shown in Fig. 2. The measured transition times, τ, together with the values of $I\tau^{1/2}$ are given by Wærnes.[2]

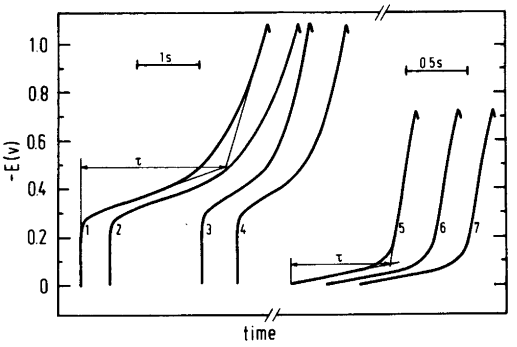

Fig. 2. Chronopotentiometric curves for the reduction of Cl_2 at a plane vitreous carbon electrode. Electrode area, A=0.0535 cm^2. Curves 1–4, acidic $AlCl_3$–NaCl melt at 229 °C, I=0.3, 0.3, 0.4, 0.4 mA. Curves 5–7, basic $AlCl_3$–CsCl melt at 448 °C, I=0.5 mA.

For the $AlCl_3$–CsCl system plots of $\tau^{1/2}$ *versus* inverse current were linear at all temperatures and compositions. As the curves also pass close to the origin eqn. (3) is valid, *i.e.* a single diffusion controlled reaction. The diffusion

Table 1. Solubility of chlorine in molten $AlCl_3$–CsCl mixtures.

Composition	Temp. (°C)	$(K_H \pm SD)10^6$ (mol cm^{-3} atm^{-1})
X_{AlCl_3}=0.52	377	5.22±0.12
	427	4.75
	477	4.21
	527	4.21
	627	3.73±0.01
	727	3.60
X_{AlCl_3}=0.435	360 [a]	5.59±0.29
X_{AlCl_3}=0.425	390 [a]	5.53±0.03

[a] Saturated with CsCl. Melt composition is given as the intercept between the liquidus line [25] and the actual melt temperature.

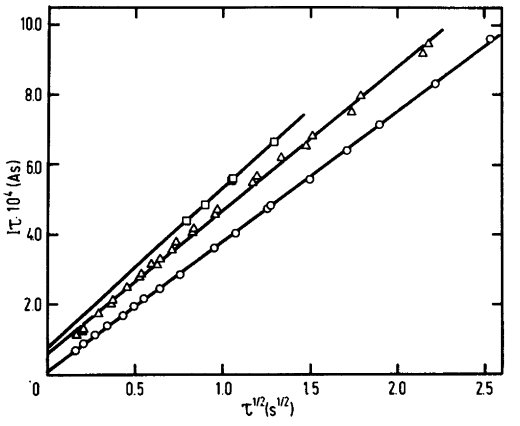

Fig. 3. Test of the SAR mechanism for the reduction of Cl_2 at a plane vitreous carbon electrode in $AlCl_3$–NaCl melts. Electrode area, A=0.0535 cm^2. □ – 157 °C, X_{AlCl_3}=0.51; △ – 187 °C, X_{AlCl_3}=0.51; ○ – 222 °C, X_{AlCl_3}=0.496.

Table 2. Diffusion coefficients of chlorine in molten chloroaluminate melts determined from chronopotentiometric measurements.

System	Temp. (°C)	Chronopot. constant $(i\tau^{1/2}\pm SD)10^3$ ($Acm^{-2}s^{1/2}$)	Number of curves	Diff.coeff. $(D\pm SD)10^5$ ($cm^2\ s^{-1}$)
$AlCl_3$–NaCl	157	8.56±0.07	6	2.22±0.04
X_{AlCl_3}=0.51	177	8.50±0.09	28	3.07±0.07
(Exp. A)	203	8.64±0.06	18	4.72±0.07
	229	8.26±0.04	20	6.16±0.06
X_{AlCl_3}=0.51	162	7.98±0.06	43	2.11±0.03
(Exp. B)	163	8.19±0.06	13	2.26±0.03
	187	7.68±0.06	33	2.94±0.05
	220	7.76±0.04	38	4.82±0.05
X_{AlCl_3}=0.496	163 [a]	7.12±0.04	23	2.01±0.02
(Exp. B)	190 [a]	7.40±0.04	20	3.37±0.04
	222 [a]	6.97±0.02	20	4.71±0.03
$AlCl_3$–CsCl				
X_{AlCl_3}=0.52	390	7.76±0.02	27	7.50±0.04
X_{AlCl_3}=0.435	362 [a]	7.93±0.04	20	7.02±0.07
X_{AlCl_3}=0.425	390 [a]	8.02±0.02	25	8.01±0.04
X_{AlCl_3}=0.40	448 [a]	8.26±0.02	34	10.40±0.05

[a] Saturated with MCl.

coefficients of chlorine are thus determined from the mean values of $i\tau^{1/2}$ at each temperature.

For the $AlCl_3$–NaCl system the product $I\tau^{1/2}$ increased with increasing current. As described previously, this generally indicates adsorption on the electrode or that other complicating processes occur. The experimental data are treated according to eqn. (5) and representative plots are shown in Fig. 3. Each plot gives a straight line with a finite intercept. By linear regression analysis, the "true" chronopotentiometric constant, $(I\tau^{1/2})_{corr}$, was determined from the slope of the curve. The choice of this model will be discussed later. In the following sections the $(i\tau^{1/2})_{corr}$ values for $AlCl_3$–NaCl melts are referred to as $i\tau^{1/2}$.

Calculated values of $i\tau^{1/2}$ along with standard deviations used in subsequent calculations of the diffusion coefficients of chlorine are presented in Table 2. The diffusion coefficients, D, are determined from the Sand equation, eqn. (3), where the concentration, c, is the chlorine solubility (eqns. (20)–(21)). As the overall electrochemical reaction is

$$Cl_2+2e^- \rightarrow 2Cl^- \qquad (18)$$

n in eqn. (3) is equal to 2.

In Table 2 Exp. A and Exp. B refer to different cell fillings. The composition of the acidic $AlCl_3$–NaCl melts ($X_{AlCl_3}>0.5$) given in the table is not exactly 51 mol % $AlCl_3$, and this is discussed later. For $AlCl_3$–NaCl melts saturated with NaCl, the given composition is the average saturation composition within the temperature range.[23] For $AlCl_3$–CsCl melts saturated with CsCl the melt composition is given as the intercept between the liquidus line [25] and the actual melt temperature. For the acidic $AlCl_3$–CsCl mixture negligible change in melt composition was observed, and the diffusion coefficient of Cl_2 is calculated for the initial composition (X_{AlCl_3}=0.52).

Chronoamperometry

Chronoamperometric data from $AlCl_3$–NaCl and $AlCl_3$–CsCl melts are given by Wærnes.[2] A typical current–time curve is shown in Fig. 4.

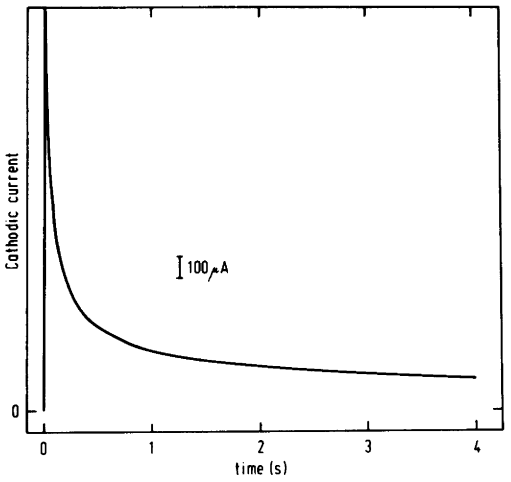

Fig. 4. Chronoamperometric curve for the reduction of Cl_2 at a plane vitreous carbon electrode in a basic $AlCl_3$–CsCl melt at 390 °C. Applied potential was −0.3 V measured against the chlorine reference electrode. Electrode area, A=0.0535 cm^2.

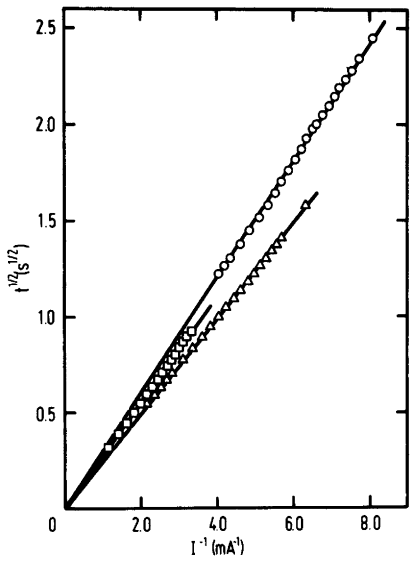

Fig. 5. Tests of the Cottrell equation for the reduction of Cl_2 at a plane vitreous carbon electrode with area A=0.0535 cm^2. ○ – 229 °C, acidic $AlCl_3$–NaCl; □ – 362 °C, basic $AlCl_3$–CsCl; △ – 187 °C, acidic $AlCl_3$–NaCl.

Table 3. Diffusion coefficients of chlorine in molten chloroaluminate melts determined from chronoamperometric measurements.

System	Temp. (°C)	Chronoamp. constant ($it^{1/2}$±SD)10^3 ($Acm^{-2}s^{1/2}$)	Number of curves	Diff.coeff. (D±SD)10^5 (cm^2s^{-1})
$AlCl_3$–NaCl	157	5.84±0.04	4	2.55±0.03
X_{AlCl_3}=0.51	177	5.48±0.07	5	3.15±0.08
(Exp. A)	203	5.62±0.06	11	4.93±0.11
	229	5.61±0.03	2	7.01±0.07
X_{AlCl_3}=0.51	162	5.02±0.03	5	2.06±0.02
(Exp. B)	163	5.49±0.04	7	2.50±0.04
	187	4.66±0.05	9	2.67±0.06
	220	4.68±0.03	7	4.33±0.06
X_{AlCl_3}=0.496				
(Exp. B)	163 [a]	4.73±0.09	12	2.19±0.08
$AlCl_3$–CsCl				
X_{AlCl_3}=0.52	390	5.26±0.01	6	8.50±0.03
X_{AlCl_3}=0.435	362 [a]	5.18±0.02	6	7.39±0.06
X_{AlCl_3}=0.425	390 [a]	5.19±0.02	4	8.28±0.06
X_{AlCl_3}=0.40	448 [a]	5.75±0.07	6	12.43±0.30

[a] Saturated with MCl.

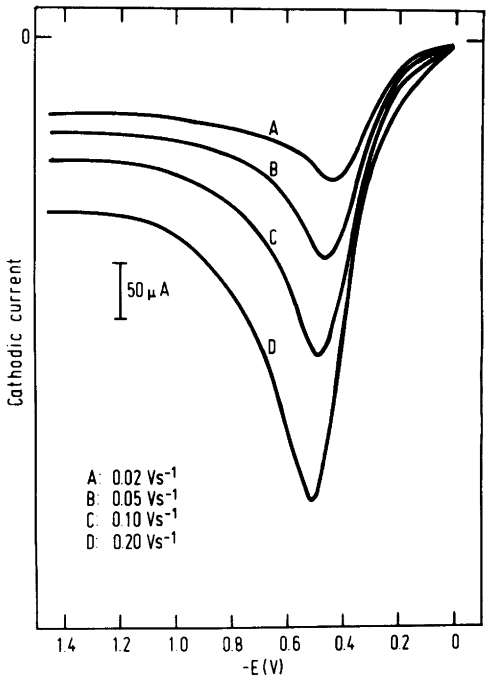

Fig. 6. Voltammograms at a plane vitreous carbon electrode in an acidic $AlCl_3$–NaCl mixture saturated with Cl_2 at 187 °C. Electrode area, A=0.0535 cm^2.

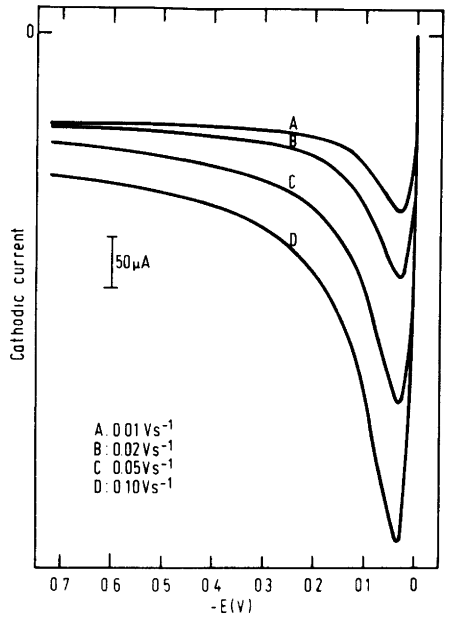

Fig. 7. Voltammograms at a plane vitreous carbon electrode in a basic $AlCl_3$–CsCl melt saturated with Cl_2 at 362 °C. Electrode area, A=0.0535 cm^2.

From each curve more than 15 corresponding I–t values were recorded using the numerical display of the oscilloscope. Fig. 5 shows that plots of $t^{1/2}$ *versus* inverse current were linear and pass close to the origin, thus confirming eqn. (8). The values of the product $it^{1/2}$ given in Table 3 are calculated from the mean values of $It^{1/2}$ obtained from several current–time curves. The diffusion coefficients given in the same table are determined by eqn. (8). The chlorine solubilities, the n value and the melt compositions are the same as those given previously for the chronopotentiometric measurements.

Voltammetry

The diffusion coefficient of chlorine may be determined from voltammetric measurements provided that the reduction mechanism is known. The results obtained in $AlCl_3$–NaCl and $AlCl_3$–CsCl melts using a plane working electrode are given by Wærnes,[2] and are only used in

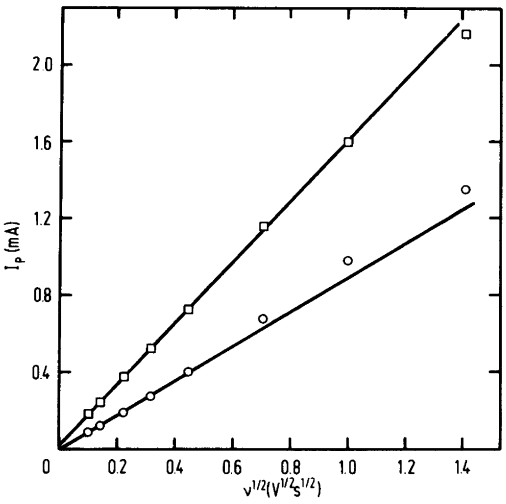

Fig. 8. Peak current *versus* the square root of the scan rate for the reduction of Cl_2 at a plane vitreous carbon electrode with area A=0.0535 cm^2. □ – 448 °C, basic $AlCl_3$–CsCl; ○ – 187 °C, acidic $AlCl_3$–NaCl.

the present paper in the discussion of the reduction mechanism of Cl_2. A series of typical voltammograms are shown in Figs. 6 and 7.

The sweep rate was varied between 0.01 and 2.00 V s^{-1}. The peak current, I_p, tends to show non-linear variation with $v^{1/2}$ at high sweep rates. This was most strongly pronounced for $AlCl_3$–NaCl melts. This is shown in Fig. 8.

DISCUSSION

Experimental accuracy. The relative error in $i\tau^{1/2}$ as expressed by the relation (19)

$$\frac{\Delta(i\tau^{1/2})}{i\tau^{1/2}} = \left[\left(\frac{\Delta I}{I}\right)^2 + \left(\frac{1}{2}\frac{\Delta\tau}{\tau}\right)^2 + \left(\frac{\Delta A}{A}\right)^2\right]^{1/2} \quad (19)$$

where Δ refers to error/uncertainty in the different parameters, is in fair agreement with the standard deviations of the chronopotentiometric constants given in Table 2. A similar equation may be used to estimate the relative error in the diffusion coefficients. The chlorine solubilities are given with a relative accuracy of ~5 % [2,23] and this gives a relative error in D_{Cl_2} of approximately 10–15 %.

The chronopotentiometric constant. Three possible models have been discussed for the correction of $I\tau^{1/2}$ at short transition times. However, the theoretical models are not widely different. There is no *a priori* way of distinguishing between the different mechanisms.

For $AlCl_3$–NaCl melts the increase in $I\tau^{1/2}$ with increasing current was significantly larger than can be attributed to errors arising from incorrect reading of transition times. Plots of the experimental data are well described by a straight line with a finite intercept of the Y-axis for each model. The recorded chronopotentiometric curves show a single transition time. This is expected if the SAR model is valid, while two distinct transition times would ideally be observed for both the AR, SR and SR, AR mechanisms. Since the plot of $I\tau$ *versus* $\tau^{1/2}$ (SAR mechanism) also resulted in intermediate values of the corrected chronopotentiometric constant, this model was preferred to avoid extreme errors.

Further support for the SAR model can be obtained from a comparison between the corrected values of $i\tau^{1/2}$ and the corresponding chronoamperometric constants, $it^{1/2}$. The theoretical value of the ratio $i\tau^{1/2}/it^{1/2}$ is 1.57. An average value of 1.55±0.02 is obtained from the data for the $AlCl_3$–NaCl system given in Tables 2 and 3.

The values of B in eqn. (5) obtained from the SAR model varied in the range 7–70 μA s. The correction decreased with increasing temperature and was highest for melts where $X_{AlCl_3}>0.5$.

Composition of acidic $AlCl_3$–NaCl melts. As previously described, the initial melt composition was 52 mol % $AlCl_3$ in the electrochemical studies. Due to the high vapour pressure of the melt and the flow of chlorine through the electrochemical cell, some $AlCl_3$ was lost during the measurements. Before changing the composition by adding NaCl crystals, melt samples were extracted for chemical analysis. From the amount of NaCl that had to be added to reach the saturation composition ($X_{AlCl_3}=0.496$) it was found that the melt composition had been changed to $0.505<X_{AlCl_3}<0.510$. The analysis of the samples did not, however, give a more accurate melt composition.

Although the solubility of chlorine in $AlCl_3$–NaCl melts changes with composition,[23] the diffusion coefficients seem to be constant in the concentration region $0.496<X_{AlCl_3}<0.52$ (at 160 °C).[2]

Due to the observed changes in the melt composition, all the D values for acidic $AlCl_3$–NaCl melts in Tables 2 and 3 are calculated by using solubility data for an average melt composition of 51 mol % $AlCl_3$. Thus an equation for the temperature dependence of D may be found.

Chlorine solubility. Fig. 9 shows semilogarithmic plots of K_H (mean values) *versus* inverse temperature. For comparison selected literature data [1,22,23] are included. Chlorine solubilities in $AlCl_3$–NaCl melts ($0.45<X_{AlCl_3}<0.6$) are given by eqn. (20).[23,26]

$$\log K_H = -7.927+2.554X_{AlCl_3}+709.7/T \quad (20)$$

(Note an error in eqn. (4) in Ref. 23).

Linear regression analysis of the present experimental data gives eqn. (21).

$AlCl_3$–CsCl($0.425<X_{AlCl_3}<0.52$):

$$\log K_H = -5.824+360.1/T \quad (21)$$

The relative standard deviation in K_H calculated from eqn. (21) is 5 %.

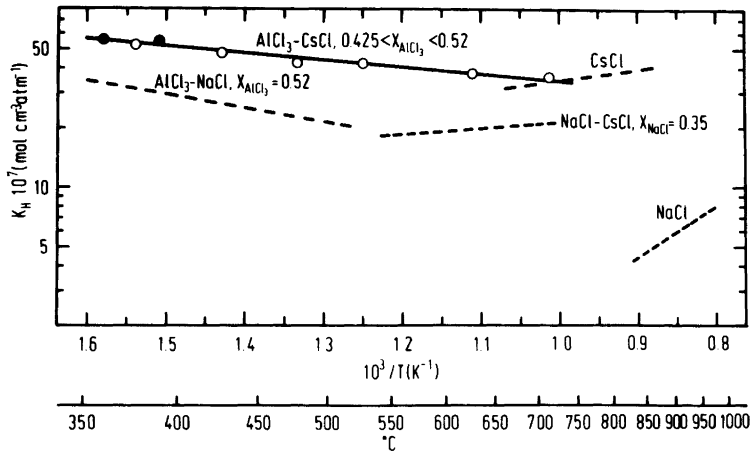

Fig. 9. Semilogarithmic plots of K_H *versus* inverse temperature. The filled symbols correspond to basic $AlCl_3$–CsCl melts where the composition is given by the intercept between the liquidus line [25] and the actual temperature. The dashed lines are results given by Wærnes *et al.*[1] (NaCl, NaCl–CsCl), Andresen *et al.*[22] (CsCl) and Carpio *et al.*[23,26] ($AlCl_3$–NaCl).

The standard enthalpy of dissolution, ΔH°_d, is calculated to be -6.9 ± 0.6 kJ mol^{-1} for chlorine in $AlCl_3$–CsCl melts. This means that the dissolution process is exothermic. Negative values of ΔH°_d are also reported for $AlCl_3$–MCl melts [23,27] and for $0.48<X_{KCl}<0.70$ in the system KCl–$PbCl_2$.[28] In $AlCl_3$–NaCl mixtures where $0.45<X_{AlCl_3}<0.6$, Carpio *et al.*[23] determined ΔH°_d to be -13.6 kJ mol^{-1}. The negative value was explained as due to the successive formation of $AlCl_4^-$, $Al_2Cl_7^-$, $Al_3Cl_{10}^-$ and Al_2Cl_6, which tends to make the melt structure looser and thus less energy is needed to form a void for Cl_2. Increasing polarization energy between Na^+ and Cl_2, and increasing van der Waals interaction forces between Cl_2 and the anions, will also tend to make ΔH°_d more negative when the melt becomes more covalent. This model implies that ΔH°_d decreases with increasing $AlCl_3$-content. Such a decrease was not observed in the relatively narrow composition range investigated by Carpio *et al.*[23] In $AlCl_3$–CsCl melts the polarization energy between Cs^+ and Cl_2 will decrease compared with forces between Na^+ and Cl_2. This will tend to make ΔH°_d less negative in $AlCl_3$–CsCl melts. On the other hand, CsCl may lead to a more "open" structure which results in decreased energy to form a void for Cl_2.

At 500 °C and $X_{AlCl_3}=0.52$ the chlorine solubility in $AlCl_3$–CsCl is twice that in $AlCl_3$–NaCl. The higher solubility in $AlCl_3$–CsCl is expected since the solubilities in pure CsCl are nearly one order of magnitude higher than in pure NaCl.[3,22] Compared with $AlCl_3$–NaCl the "free volume" in the melt may increase due to the larger Cs^+ ion, *i.e.* higher chlorine solubilities in $AlCl_3$–CsCl mixtures.

In molten $AlCl_3$–NaCl, which is assumed not to contain appreciable amounts of Cl_3^-, the chlorine solubility was highest in acidic melts.[23] The present investigation seems to give approximately the same chlorine solubilities in acidic and basic $AlCl_3$–CsCl mixtures (Fig. 9). The spectral changes around the equimolar composition indicates a different solute species as the $AlCl_3$ content is increased above 50 mol %.[24] However, a further discussion will have to be postponed until more spectra and solubility data are available.

Chlorine diffusivity. The temperature dependence of the diffusion coefficients of chlorine is well described by the Arrhenius-type eqn. (22),

$$D = D_o \exp(-E_a^D/RT) \qquad (22)$$

where D_o is a pre-exponential factor, and E_a^D is the activation energy of the diffusion process. Fig. 10 shows semilogarithmic plots of D *versus* inverse temperature. The filled symbols correspond to basic $AlCl_3$–MCl melts ($X_{AlCl_3}<0.5$),

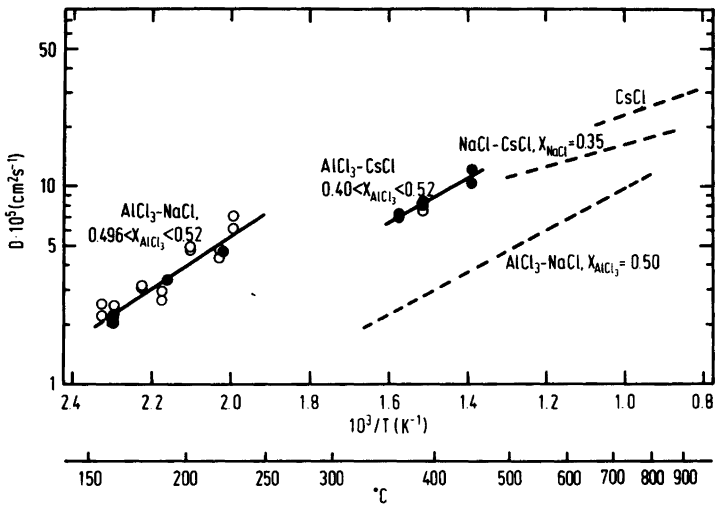

Fig. 10. Semilogarithmic plots of the diffusion coefficient of dissolved Cl_2 as function of inverse temperature. The filled symbols correspond to basic $AlCl_3$–MCl mixtures saturated with MCl. The dashed lines are results given by Wærnes *et al.*[1] (CsCl, NaCl–CsCl) and Mukliev *et al.*[29] ($AlCl_3$–NaCl).

and no drastic change in the diffusion coefficients is observed around the equimolar composition. For comparison selected literature data [1,29] are included.

Linear regression analysis of the data given in Tables 2 and 3 gives the eqns. (23)–(24).

$AlCl_3$–NaCl($0.496<X_{AlCl_3}<0.52$):

$$\log D = -1.593-1328/T \quad (23)$$

$AlCl_3$–CsCl($0.40<X_{AlCl_3}<0.52$):

$$\log D = -2.444-1087/T \quad (24)$$

The relative standard deviation in D calculated by eqns. (23)–(24) is 12 and 7 %, respectively. The activation energy of diffusion, E_a^D, is 25.4±2.0 kJ mol^{-1} for the $AlCl_3$–NaCl mixtures and 20.8±3.1 kJ mol^{-1} for $AlCl_3$–CsCl melts.

From Fig. 10 it is seen that the D values, reported by Mukliev *et al.*,[29] are significantly lower than the present results for $AlCl_3$–MCl melts. Mulkliev *et al.*[29] employed the technique of the weight loss of a platinum rotating disc, and do not report the chlorine solubility used in the calculations. A direct comparison is therefore difficult to perform.

Vetyukov *et al.*[30] have determined the diffusion coefficient of chlorine in basic $AlCl_3$–NaCl melts (790–880 °C) from impedance measurements. In the concentration range $0 \leq X_{AlCl_3} < 0.24$ the diffusion coefficient of chlorine varied one order of magnitude, decreasing to 5×10^{-5} cm^2 s^{-1} (820 °C) with increasing $AlCl_3$ content. In spite of the large differences in temperature and melt composition compared with the present measurements, the values reported by Vetyukov *et al.*[30] seem to be significantly lower than the present results for $AlCl_3$–MCl melts.

Taking into account the lower temperatures, the results for $AlCl_3$–MCl mixtures are not widely different from those found for alkali chlorides (Fig. 10). Moreover, no variation in D is observed close to the equimolar composition in spite of the large variation in the Cl^- activity.[31]

The absorption spectra of $AlCl_3$–NaCl melts ($0.45<X_{AlCl_3}<0.6$) saturated with chlorine did not change dramatically for compositions around $X_{AlCl_3}=0.50$.[23] A pronounced absorption peak at 30 200 cm^{-1}, close to that of gaseous chlorine, is observed. Together with solubility results, this points to Cl_2 as the dissolved species.[23] In $AlCl_3$–CsCl mixtures several spectral changes are observed around the melt composition corresponding to $X_{AlCl_3}=0.50$, probably due to formation of Cl_3^- on the basic side.[24] The absorbance of chlorine increases by a factor of 7 for a

basic melt relative to an acidic melt, while the ratio in molar absorptivity for $AlCl_3$–NaCl is 2 or less.[23]

The high values of the diffusion coefficient of chlorine dissolved in molten alkali chlorides have often been explained by a chain conduction mechanism.[1] This mechanism can not, however, explain the anomalously high diffusion coefficients ($D \geq 10^{-4}$ cm^2 s^{-1}) of other gaseous species like HCl in eutectic LiCl–KCl [32] and O_2 and H_2 in eutectic $NaNO_3$–KNO_3 melts.[33,34]

The results obtained for $AlCl_3$–MCl mixtures can not be explained either by the chain conduction mechanism, as these melts probably do not contain appreciable amounts of Cl_3^- on the acidic side ($X_{AlCl_3} > 0.50$). The relatively high values of D may be due to the "open" structure of these melts caused by the large anion and that diffusion of molecular chlorine therefore is facilitated.

Reduction mechanism of dissolved chlorine. A discussion of the mechanism for the overall reaction

$$Cl_2 + 2e^- \rightarrow 2Cl^-$$

will be given, although a detailed investigation has not been the main objective in the present study. The potentials are measured against a chlorine reference electrode, and the equilibrium potential of the vitreous carbon working electrode did not exceed ±1–3 mV. Equilibrium conditions were reestablished within one minute after each experimental run.

Fig. 6 shows representative voltammetric curves recorded in $AlCl_3$–NaCl melts saturated with chlorine. It is seen that the peak potential, E_p, varies with the scan rate, which is typical for an irreversible process. At each temperature αn_a is calculated by eqn. (17). The value of αn_a appears to be independent of temperature and melt composition, and an average value of 0.63±0.02 is obtained. According to eqn. (16) the peak to half peak separation gives a value of αn_a equal to 0.51±0.02.

From the ratio of voltametric $i_p v^{-1/2}$ to both the chronopotentiometric $i\tau^{1/2}$ and the chronoamperometric $it^{1/2}$, an average value of 0.54±0.02 is calculated for αn_a in the same melts.

As described previously, current–potential curves may be constructed from chronoamperometric curves recorded at different applied potentials. Fig. 11 shows such a curve where the current values are measured at t=2s. A well-defined plateau with a limiting current is obtained for the diffusion process. In the same figure a semilogarithmic plot of $(I_l - I)/I$ *versus* E

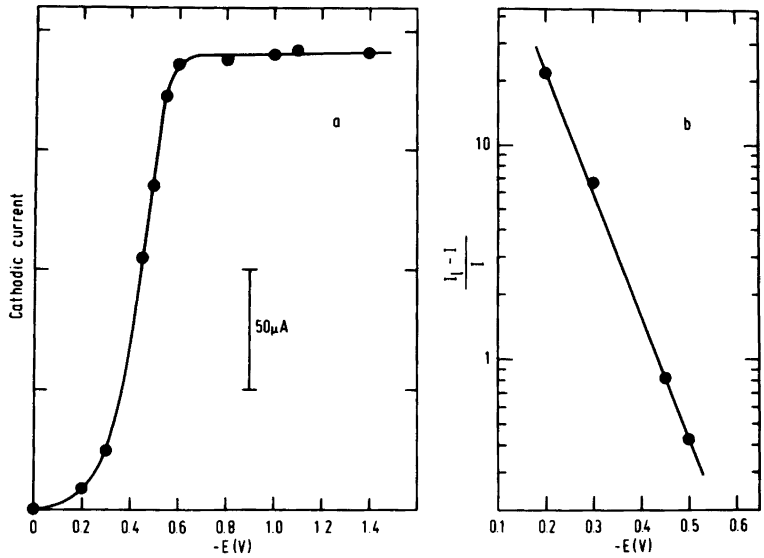

Fig. 11. (a) Current-potential curve constructed from chronoamperometric curves for the reduction of Cl_2 at a plane vitreous carbon electrode in acidic $AlCl_3$–NaCl melt at 162 °C. (b) Semilogarithmic plot of $(I_l - I)/I$ *versus* E for the same wave. Current measured at t=2s. Electrode area, A=0.0535 cm^2.

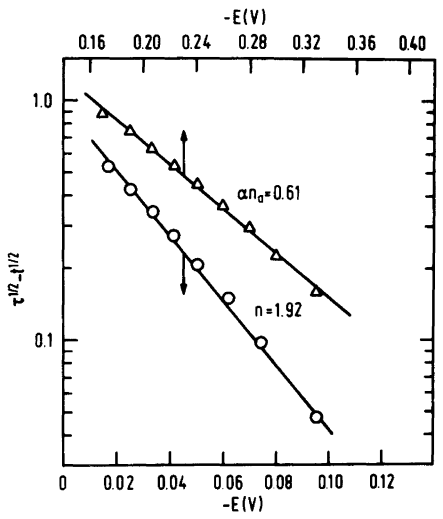

Fig. 12. Analysis of chronopotentiometric curves for the reduction of Cl_2 at a plane vitreous carbon electrode in $AlCl_3$–CsCl melts. △ – 390 °C, τ=1.95 s, acidic melt; ○ – 448 °C, τ=0.743 s, basic melt.

is shown. From the slope of the straight line αn_a is determined to be 0.50 (eqn. (10)).

For the reduction of chlorine in $AlCl_3$–NaCl melts, the αn_a values presented above suggest a one-electron transfer in the rate-determining step with $\alpha \approx 0.5$. This is in fair agreement with results reported for chlorine reduction in $AlCl_3$–NaCl–KCl mixtures.[35,36]

Voltammograms recorded in basic $AlCl_3$–CsCl melts appear to have a different shape relative to those recorded in acidic melts. Curves recorded in an acidic melt were similar to those obtained in $AlCl_3$–NaCl melts. Typical curves for a basic melt are shown in Fig. 7. For acidic melts the shift in peak potentials corresponds to αn_a=0.66. In basic melts the peaks are sharper, and for $v<1$ V s^{-1} E_p is nearly constant. Due to the apparent lack of an overpotential for the cathodic reaction, the curves are so steep that $E_p - E_{p/2} \approx E_p \approx -30$ mV. For a reversible two-electron reduction with soluble products at activity 1 the theoretical value at 262 °C is −21 mV (eqn. (13)). The experimental values of $i_p v^{-1/2}/i\tau^{1/2}$ and $i_p v^{-1/2}/it^{1/2}$ are also somewhat different from the expected results.

The same change in reduction mechanism with respect to melt composition is observed when an analysis of the chronopotentiometric curves is performed. This is illustrated in Fig. 12. The slopes of the curves [eqns. (6) and (7)] yield αn_a=0.61 (acidic melt) and n=1.92 (basic melt). Roughly the same values are obtained from analysis of current–potential curves like that shown in Fig. 7. The different reduction mechanism for chlorine in $AlCl_3$–CsCl melt may be due to the change in acid-base behaviour of the melt and/or if the complex ion Cl_3^- exists (basic melts), it may make the reaction more reversible.

CONCLUDING REMARKS

The diffusion coefficient of chlorine in molten chlorides does not seem to vary markedly with the nature of the salt. In the temperature range 160–890 °C the diffusion coefficient increases from $\sim 2\times10^{-5}$ to $\sim 3\times10^{-4}$ cm^2 s^{-1}.

The chlorine solubilities obtained in the $AlCl_3$–CsCl system indicate a constant solubility in the concentration range $0.425 < X_{AlCl_3} < 0.52$.

An interesting extension of the present work would be to investigate the magnesium chloride–alkali chloride systems where the literature data show a decreasing diffusion coefficient of chlorine with increasing $MgCl_2$ content.[37] These systems are also of interest with respect to the industrial magnesium electrolysis.

Acknowledgements. Experimental assistance of Bente Faaness is gratefully acknowledged. This work has been supported financially by *Norsk Hydro a.s.* and *Norges Teknisk–Naturvitenskapelige Forskningsråd.*

REFERENCES

1. Wærnes, O., Palmisano, F. and Østvold, T. *Acta Chem. Scand. A 37* (1983) 207.
2. Wærnes, O. *Thesis,* Universitetet i Trondheim, Norges tekniske høgskole, Institutt for uorganisk kjemi, Trondheim 1981.
3. Andresen, R. *Thesis,* Universitetet i Trondheim, Norges tekniske høgskole, Institutt for uorganisk kjemi, Trondheim 1976.
4. Delahay, P. *New Instrumental Methods in Electrochemistry,* Interscience, New York 1954.
5. Lorenz, W. *Z. Elektrochem. 59* (1955) 730.
6. Reinmuth, W. H. *Anal. Chem. 33* (1961) 322.
7. Laitinen, H. A. *Anal. Chem. 33* (1961) 1458.

8. Bard, A. J. *Anal. Chem. 33* (1961) 11.
9. Bard, A. J. *Anal. Chem. 35* (1963) 340.
10. Tatwawadi, S. V. and Bard, A. J. *Anal. Chem. 36* (1964) 2.
11. Laitinen, H. A. and Chambers, L. M. *Anal. Chem. 36* (1964) 5.
12. Reinmuth, W. H. *Anal. Chem. 32* (1960) 1514.
13. Paunovic, M. *J. Electroanal. Chem. 14* (1967) 447.
14. Delahay, P. and Berzins, T. *J. Am. Chem. Soc. 75* (1953) 2486.
15. Mamantov, G., Manning, D. L. and Dale, J. M. *J. Electroanal. Chem. 9* (1965) 253.
16. Laitinen, H. A. *Pure Appl. Chem. 15* (1967) 227.
17. Oldham, K. B. and Osteryoung, R. A. *J. Electroanal. Chem. 11* (1966) 397.
18. Berzins, T. and Delahay, P. *J. Am. Chem. Soc. 75* (1953) 555.
19. Nicholson, R. S. and Shain, I. *Anal. Chem. 36* (1964) 706.
20. Matsuda, H. and Ayabe, Y. *Z. Elektrochem. 59* (1955) 494.
21. Delahay, P. *J. Am. Chem. Soc. 75* (1953) 1190.
22. Andresen, R. E., Østvold, T. and Øye, H. A. In Pemsler, J. P., Braunstein, J., Morris, D. R., Nobe, K. and Richards, N. E., Eds., *Proc. Int. Symp. Molten Salts*, The Electrochem. Soc., Princeton, N. J. 1976, p. 111.
23. Carpio, R. A., King, L. A., Ratvik, A. P., Østvold, T. and Øye, H. A. *Light Metals 1981,* 110th AIME Annual Meeting, Chicago 1981, p. 325.
24. Ratvik, A. P. *Private communication,* Universitetet i Trondheim, Norges tekniske høgskole, Institutt for uorganisk kjemi, Trondheim 1982.
25. Van der Kamp, L. K. and van Spronsen, J. W. *Z. Anorg. Allg. Chem. 361* (1968) 328.
26. Øye, H. A. *Private communication.* Universitetet i Trondheim, Norges tekniske høgskole, Institutt for uorganisk kjemi, Trondheim 1981.
27. Stupina, A. M., Bezvoritnii, V. A., Baibakov, D. P., Mukliev, V. I. and Bezukladnikov, A. B. *Tr. Veses. Naucho Issled. Proektn. Inst. Alyumin., Magn. i Elektrod. Prom-sti 101* (1978) 82.
28. Kowalski, M. and Harrington, G. W. *Inorg. Nucl. Chem. Lett. 3* (1967) 121.
29. Mukliev, V. I., Stupina, A. M., Bezvoritnii, V. A., Baibakov, D. P. and Bezukladnikov, A. B. *Fiz. Khim. Elektrokhim. Rasplavl. Tverd. Elektrolitov, Tezisy Dokl. Vses. Konf. Fiz. Khim. Ionnykk Rasplavov Tverd. Elektrolitov, 7th 1* (1979) 48.
30. Vetyukov, M. M., Borisoglebskii, Yu. V. and Hung Bui Van, *Tsvetn. Met. 7* (1981) 45.
31. Boxall, L. G., Jones, H. L. and Osteryoung, R. A. *J. Electrochem. Soc. 120* (1973) 223.
32. Minh, N. Q. and Welch, B. J. *Aust. J. Chem. 28* (1975) 965.
33. Desimoni, E., Paniccia, F. and Zambonin, P. G. *J. Electroanal. Chem. 38* (1972) 373.
34. Desimoni, E., Palmisano, F. and Zambonin, P. G. *J. Electroanal. Chem. 84* (1977) 323.
35. Skundin, A. M., Palanker, V. Sh. and Bagotskii, V. S. *Sov. Electrochem. 2* (1966) 1325.
36. Holleck, G. L. *J. Electrochem. Soc. 119* (1972) 1158.
37. Ukshe, E. A., Leonova, L. S., Yavonova, G. N. and Bukhun, N. G. *Sov. Electrochem. 7* (1971) 373.

Received August 19, 1982.

Acta Chemica Scandinavica A 37 (1983) 307–314

Metal Ammine Formation in Solution. XXIII. Stability Constants of Protonated Non- and Partly-chelated Complexes in the Cadmium 1,2-Ethanediamine System

MICHAŁ WILGOCKI * and JANNIK BJERRUM

Chemistry Department, Inorganic Chemistry, H.C. Ørsted Institute, University of Copenhagen, Universitetsparken 5, DK-2100 Copenhagen Ø, Denmark

The cadmium 1,2-ethanediamine system was examined at 25 °C employing glass and Cd,Hg-electrode measurements in a 3 M $(Na,H)ClO_4$ medium with initial concentrations of $HClO_4$ varying from 0.01 to 1 M. The cumulative stability constants for the chelated complexes were determined from pH-titrations with low initial acid concentration, and the following constants were obtained: Cd en^{2+}, $\beta_{1,0}=10^{6.21}$; Cd en_2^{2+}, $\beta_{2,0}=10^{11.64}$; Cd en_3^{2+}, $\beta_{3,0}=10^{14.38}$. These constants were used to determine the stability constants for the protonated species from Cd,Hg-electrode measurements on solutions with high initial acid concentration (1 M). In this way the following values for the cumulative constants for the three most important species were obtained: Cd en H^{3+}, $\beta_{0,1}=10^{1.70}$; Cd en $(en\ H)^{3+}$, $\beta_{1,1}=10^{7.88}$; Cd en_2 $(en\ H)^{3+}$, $\beta_{2,1}=10^{12.23}$.

It was shown by Jannik Bjerrum [1] in 1941 that the successive formation constants for some 1,2-ethanediamine complexes of some metal-ions could be determined by pH-titrations of the acid metal salt solutions with the diamine. The procedure involves the tacit assumption that the formation of protonated non-chelate species can be neglected. In 1945 the method was applied by Bjerrum and Andersen[2] in a study of the zinc and cadmium ethanediamine systems, and in the following years many diamine systems were studied making this assumption.[3] Schwarzenbach and Szilard [4] have proven the existence of $Cd(tnH)^{3+}$ in the cadmium 1,2-propanediamine system, but for the more stable ethanediamine complexes with octahedral, tetrahedral or planar configuration it was assumed to be correct to neglect non-chelate complex formation. This is clearly not the case for the complexes formed with silver(I) and mercury(II) ions, with linear configuration, for which it has been shown [5,6] that ethanediamine is bound mainly as a monodentate ligand. However, in polarographic studies Biernat and Wilgocki [7–9] have shown that non-chelate complexes are also present to a great extent in the cadmium 1,2-diamine systems when the complex formation takes place under conditions where the concentration of the monoprotonated diamine is much higher than that of the diamine. The existence of complexes with monodentate bound ligands in zinc diamine systems was demonstrated similarly.[10] In the present study the cadmium 1,2-ethanediamine system has been studied by glass and Cd,Hg-electrode measurements in a 3 M $(Na,H)ClO_4$ medium. The stability constants for the chelate complexes have been obtained from measurements involving a low initial acid concentration, and the stability constants for the three most important protonated complexes $Cd(enH)^{3+}$, Cd en $(enH)^{3+}$ and Cd $en_2(enH)^{3+}$ have been determined from measurements involving a high initial acid concentration.

* On leave from The Institute of Chemistry, University of Wrocław, 507383 Wrocław, Poland

0302-4377/83 $02.50

EXPERIMENTAL

Reagents and solutions. All reagents were of analytical grade and were used without further purification. The ethylenediamine (Fluka, *puriss, p.a.*) was distilled before use. The various solutions were prepared in volumetric flasks by weighing or pipetting from analyzed stock solutions of cadmium perchlorate, sodium perchlorate, perchloric acid and ethylenediamine.

Glass electrode measurements were performed in a jacketed vessel with thermostatted water flow. pH (=$-\log [H^+]$) was measured relative to that of standard $HClO_4$-solutions (pH ~3) in 3 M $NaClO_4$. Selected Radiometer glass electrodes (G 202 C for pH <9 and G 202 B for pH >9) were used, both having nearly the theoretical pH-dependence. The potentiometer used was a Radiometer PHM 52 Digital pH-Meter, the mV-scale being preferred to the direct reading pH-scale. Sodium chloride calomel electrodes (1 and 0.05 M) prepared according to Gjaldbæk [11] and in electrode vessels of the type introduced by Lewis *et al.*[12] were used as reference electrodes.

Cd,Hg-electrode measurements were performed in a closed jacketed vessel with electrical connection to the reference electrode and with in- and outlet for nitrogen. A melted-in platinum wire provided contact to the liquid amalgam placed in a cavity in the bottom of the cell. The cadmium amalgam was prepared according to Szilard [13] by dissolving granulated cadmium metal in mercury placed in a 1 M perchloric acid solution under stirring at about 80 °C. The amalgam was stored under 10^{-3} M $HClO_4$. Dissolved oxygen was removed from the solution to be examined by bubbling with nitrogen before the amalgam was added to the cell. The nitrogen was purified by passing it consecutively through bubblers with spiral grooved fitted inner-tubes containing a concentrated solution of catechol in 50 % KOH and an acidic chromium(II) sulfate solution containing amalgamated zinc.[14] Cadmium amalgam potentials in oxygen-free solutions are well-defined and independent of the cadmium concentration in the two-phase range between 6 and 13 % of cadmium.[15] Our measurements of the cadmium ion concentration were performed with both a two-phase and (in most cases) a homogeneous 2 % amalgam with exactly the same result.

RESULTS

The acid-dissociation constants for the 1,2-ethanediammonium ion in 3 M (Na,H)ClO_4. The acid dissociation constants, $K_{en\ H_2^{2+}}$ and $K_{en\ H^+}$,

Table 1. Acid-base constants of 1,2-ethanediamine in 3 M (Na,H)ClO_4 with $[H^+]_o$=0.02 and 1 M at 25 °C.

C_{NaClO_4}	C_{HClO_4}	C_{en}	pH	$pK_{en\ H_2^+}$
2.98	0.02136	0.01365	7.843	7.959
2.98	0.02129	0.01429	7.972	7.958
			av.	7.95±0.01
2.00	1.0235	0.6648	7.855	7.927
2.00	1.0231	0.6717	7.884	7.927
			av.	7.93±0.01
				$pK_{en\ H^+}$
2.98	0.02126	0.03850	10.692	10.799
2.98	0.02114	0.04324	10.784	10.782
			av.	10.79±0.01
1.95	1.0551	1.4435	10.348	10.790
2.00	1.0257	2.0083	10.820	10.840
			av.	10.81±0.01

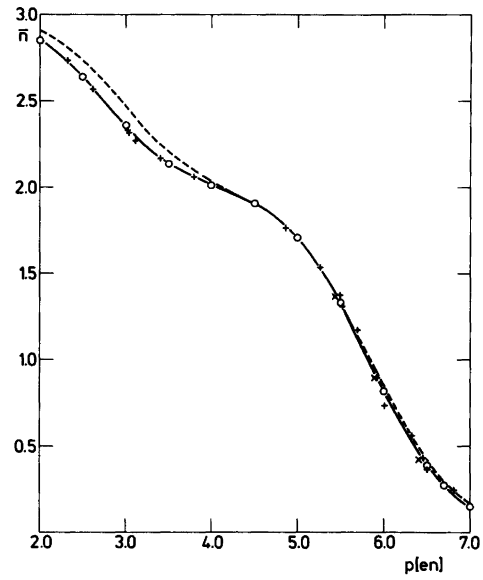

Fig. 1. Formation curve (n̄ *versus* p[en]) for the Cd^{2+}, en system in 3 M $NaClO_4$ at 25 °C. Experimental results with $C_{Cd(ClO_4)_2} \cong 0.02$ M, $C_{HClO_4} \cong 0.02$ M (+) and with $C_{Cd(ClO_4)_2} \cong 0.10$ M, $C_{HClO_4} \cong 0.01$ M (×). The full curve (○) is calculated with the constants derived from the pH-measurements ($\beta_{1,0}=10^{6.21}$, $\beta_{2,0}=10^{11.64}$, $\beta_{3,0}=10^{14.38}$) and the dotted curve with constants derived from the Cd,Hg-measurements ($\beta_{1,0}=10^{6.28}$, $\beta_{2,0}=10^{11.65}$, $\beta_{3,0}=10^{14.61}$).

Table 2. Results of glass and Cd,Hg-electrode measurements in ~3 M $NaClO_4$ at 25 °C. Data for 10 of 21 solutions studied. $C_{NaClO_4}=3.00-C_{HClO_4}-2C_{Cd(ClO_4)_2}$. $pK_{en\ H_2}=7.95$; $pK_{en\ H}=10.79$.

No.	C_{HClO_4}	$C_{Cd(ClO_4)_2}$	C_{en}	pH	$\bar{n}_{en}$	p[en]
1	0.02124	0.02002	0.01866	7.115	1.873	6.512
2	0.02121	0.02003	0.02263	7.213	1.845	6.327
3	0.02127	0.02000	0.02640	7.347	1.800	6.071
4	0.02112	0.02002	0.03888	7.647	1.667	5.519
5	0.02123	0.01999	0.04405	7.791	1.590	5.262
6	0.02122	0.02003	0.04995	8.026	1.455	4.865
7	0.02123	0.02001	0.06377	9.116	1.043	3.402
8	0.02133	0.02007	0.06695	9.379	0.999	3.113
9	0.02137	0.02003	0.07502	9.855	0.908	2.615
10	0.02144	0.02006	0.08105	10.140	0.823	2.322

No.	$\bar{n}_{Cd}$(exp)	$\bar{n}$(calc.) [a]	$\bar{n}$(calc.) [b]	$X_{(exp)}$	$X_{(calc.)}$ [a]	$X_{(calc.)}$ [b]
1	0.365	0.378	0.412	1.68	1.54	1.63
2	0.558	0.515	0.549	2.08	1.86	2.00
3	0.730	0.742	0.769	2.86	2.65	2.94
4	1.309	1.303	1.286	11.0	9.91	10.9
5	1.535	1.535	1,537	24.9	22.9	25.4
6	1.766	1.776	1.750	119	105	112
7	2.169	2.170	2.245	10.4×10^4	8.4×10^4	9.6×10^4
8	2.271	2.294	2.408	4.7×10^5	3.7×10^5	4.5×10^5
9	2.569	2.570	2.688	8.6×10^6	6.0×10^6	8.5×10^6
10	2.738	2.728	2.813	5.1×10^7	3.6×10^7	5.4×10^7

[a] Calc. with $\log\beta_{1,0}=6.21$, $\log\beta_{2,0}=11.64$, $\log\beta_{3,0}=14.38$. [b] Calc. with $\log\beta_{1,0}=6.28$, $\log\beta_{2,0}=11.65$, $\log\beta_{3,0}=14.61$.

for the 1,2-ethanediammonium ion were determined in the same way as in previous studies.[1,2] The results of some of the determinations are shown in Table 1. The data show in a convincing way that substitution of 1 M $NaClO_4$ with 1 M ($\frac{1}{2}$ en H_2, en H)ClO_4 has practically no influence on the values of $pK_{en\ H_2^{2+}}$ and $pK_{en\ H^+}$. It is therefore reasonable to assume that this change in medium also has no influence on the stability constants.

Estimation of the stability constants $\beta_{1,0}$, $\beta_{2,0}$ and $\beta_{3,0}$ *for the three chelate complexes in 3 M* $NaClO_4$. These measurements were made under conditions (low initial acid concentration) where the concentrations of the protonated non-chelated complexes could be assumed to be negligible. Some of the results are shown in Table 2. The calculations based on the glass electrode measurements were made as described previously.[1,2] $\bar{n}_{en}$ denotes the average number of protons bound per diamine and $\bar{n}_{Cd}$ the average number of diamine ligands bound to cadmium. p[en] is the negative exponent of the free diamine concentration. The agreement between the experimental results (with C_{Cd} 0.02, C_{HClO_4} 0.02 M (+), and with C_{Cd} 0.10, C_{HClO_4} 0.01 M (×)) and the formation curve derived from the calculated constants is shown in Fig. 1. Another set of stability constants was calculated from the measurements of the cadmium ion concentrations by means of eqn. (1)

$$X = \frac{C_{Cd}}{[Cd^{2+}]} = 1+\beta_{1,0}[en]+\beta_{2,0}[en]^2+\beta_{3,0}[en]^3 \quad (1)$$

employing the values of the free diamine concentration determined from pH-measurements. The formation curve derived from these constants (the dotted curve in Fig. 1) shows some deviation from the formation curve calculated solely on the basis of the pH-measurements. A plausible explanation for this is that the Cd,Hg-electrode shows deviations from Nernst' law for $[Cd^{2+}]\lesssim10^{-6}$ M.[4] This corresponds in our case to X-values higher than $\sim10^5$ and $\bar{n}\gtrsim2$, and explains the deviation between the two formation curves

Table 3. Results of glass and Cd,Hg-electrode measurements in 3 M (H,Na)ClO_4 with C_{HClO_4}=1.007 (Nos. 1–8, 10, 11), 1.013 (Nos. 9, 12), $C_{Cd(ClO_4)_2}$=0.00503 M and C_{NaClO_4}=3.00−C_{HClO_4}−2 $C_{Cd(ClO_4)_2}$. p$K_{en\ H_2}$=7.93, p$K_{en\ H}$=10.81.

No.	C_{en}	pH	p[en]	p[en H^+]	X_{exp}	Δ^a	Δ^b
1	0.5095	5.938	7.164	2.292	1.324	1.21	1.19
2	0.5170	6.330	6.383	1.904	2.647	1.90	1.78
3	0.5182	6.381	6.282	1.853	3.614	2.58	2.52
4	0.5250	6.559	5.929	1.678	6.282	3.77	3.42
5	0.5281	6.640	5.769	1.599	9.716	5.69	5.18
6	0.5347	6.793	5.467	1.451	24.73	14.1	13.0
7	0.5415	6.975	5.111	1.276	75.32	36.5	33.6
8	0.5865	7.433	4.236	0.859	2.728×10^3	1.11×10^3	1.03×10^3
9	0.6129	7.570	3.981	0.741	10.041×10^3	4.83×10^3	4.50×10^3
10	0.6607	7.815	3.549	0.554	8.656×10^4	4.59×10^4	4.12×10^4
11	0.6778	7.876	3.445	0.511	1.565×10^5	0.89×10^5	0.79×10^5
12	0.7097	8.001	3.237	0.426	3.831×10^5	1.89×10^5	1.53×10^5

[a] Calc. with log $\beta_{1,0}$=6.21, log $\beta_{2,0}$=11.64, log $\beta_{3,0}$=14.38. [b] Calc. with log $\beta_{1,0}$=6.28, log $\beta_{2,0}$=11.65, log $\beta_{3,0}$=14.61.

found at low p[en]-values. The two sets of constants were used to calculate $\bar{n}$ and X for each of the ten values in Table 2, and in the lower part of the table they are compared with the experimentally determined values.

Estimation of the stability constants for three of the protonated complexes. Apart from the chelate complexes Cd en^{2+}, Cd en_2^{2+} and Cd en_3^{2+}, it is most reasonable to assume the existence, among the numerous possibilities, of the following protonated species: Cd en H^{3+}, Cd en (en H)$^{3+}$ and Cd en_2 (en H)$^{3+}$ at high 1,2-ethaneammonium ion concentrations. It should then be possible knowing the stability constants for the chelated complexes to estimate the stability constants for the protonated complexes in the more acidic medium using eqn. (2)

Table 4. Results of calculations of stability constants for the protonated complexes.

	$\beta_{0,1}$	$\beta_{1,1}$	$\beta_{2,1}$
With Δ^a	52±3	$(7.8\pm0.5)\times10^7$	$(1.78\pm0.02)\times10^{12}$
With $\beta_{0,2}\equiv1000$	45±3	$(7.1\pm0.5)\times10^7$	$(1.80\pm0.02)\times10^{12}$
With Δ^b	48±3	$(7.3\pm0.5)\times10^7$	$(1.59\pm0.02)\times10^{12}$
Av. Δ^a and Δ^b	50	7.5×10^7	1.7×10^{12}

Table 5. Comparison of cadmium(II)–ethanediamine and ammonia stability constants.

Cd^{2+},en(en H^+) 3 M, 25 °C	Cd^{2+},NH_3 [1] 2 M, 25 °C	Found
log $\beta_{0,1}$=1.70	log K_1=2.69	log ($K_1/\beta_{0,1}$)=0.99
log $\beta_{1,0}$=6.21	log K_2=2.14	
log $\beta_{1,1}$=7.88	log K_3=1.48	log ($\beta_{1,1}/\beta_{1,0}$)=1.67
log $\beta_{2,0}$=11.64	log K_4=0.97	
log $\beta_{2,1}$=12.23	log K_5=−0.32	log ($\beta_{2,1}/\beta_{2,0}$)=0.59
log $\beta_{3,0}$=14.38	log K_6=−1.66	

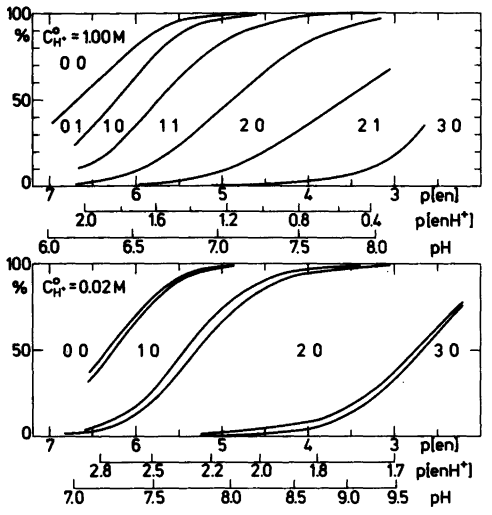

Fig. 2. Distribution of the six cadmium(II)–ethanediamine complexes at 25 °C. The ranges of existence of the six complexes from monoamine to hexaamine are plotted *versus* p[en]. The abscissa also shows the corresponding values of p[en H$^+$] and pH. *Upper figure.* In 3 M (NaH)ClO$_4$ for solutions with C_{Cd} 0.005, C_{HClO_4} 1.00, and C_{en} 0.01–0.1 M. *Lower figure.* In 3 M NaClO$_4$ for solutions with C_{Cd} 0.01–0.02, C_{HClO_4} 0.01–0.02, and C_{en} 0.01–0.1 M. The distribution curves in both figures are calculated with: $\beta_{0,1}=10^{1.70}$, $\beta_{1,0}=10^{6.21}$, $\beta_{1,1}=10^{7.88}$, $\beta_{2,0}=10^{11.64}$, $\beta_{2,1}=10^{12.23}$, $\beta_{3,0}=10^{14.38}$.

$$\Delta = X-\beta_{1,0}[\mathrm{en}]-\beta_{2,0}[\mathrm{en}]^2-\beta_{3,0}[\mathrm{en}]^3 = 1+\beta_{0,1}[\mathrm{en\,H^+}]+\beta_{1,1}[\mathrm{en}][\mathrm{en\,H^+}]+\beta_{2,1}[\mathrm{en}]^2[\mathrm{en\,H^+}] \quad (2)$$

and making the very plausible assumption that the stability constants in 3 M NaClO$_4$ are practically unchanged when 1 M NaClO$_4$ is replaced with 1 M ($\frac{1}{2}$en H$_2$,en H)ClO$_4$.

In the chosen medium with $C^o_{HClO_4}$=1 M the applied cadmium concentrations are so small compared with the concentrations of the 1,2-ethaneammonium ions that p[en] and p[en H$^+$] can be calculated directly from the pH-measurements irrespective of the fact that some of the protons are bound to the complexes. Under these circumstances it is not possible to calculate $\bar{n}_{Cd}$ from pH measurements and $X=C_{Cd}/[Cd^{2+}]$ is thus the sole basis for the calculations. The data for twelve of the solutions examined are shown in Table 3. The values of Δ^a and Δ^b were calculated knowing $\beta_{1,0}$, $\beta_{2,0}$ and $\beta_{3,0}$. Consequently, twelve equations are at our disposal for determining the three unknown ($\beta_{0,1}$, $\beta_{1,1}$ and $\beta_{2,1}$) of eqn. (2). A computer program was written for the purpose and the calculations were made using both sets of Δ-values. The results of the calculations are shown in Table 4. An attempt was also made to calculate $\beta_{0,2}$ and $\beta_{1,2}$ at the same time, but this placed too heavy a load on the data, and realistic values for these constants could therefore not be

Table 6. Chelation effects in metal(II)–ethanediamine systems relative to ammonia.

	Cd^{2+}	Zn^{2+}	Cu^{2+}	Ni^{2+}	Co^{2+}
log $\beta_{1,0}$(en)/K_1(NH$_3$)	3.0	3.6	6.6	4.7	3.8
log $\beta_{2,0}$(en)/β_2(NH$_3$)	6.5	6.4	12.4	8.9	7.1

Table 7. Stability constants for the chelated copper(II)–ethanediamine complexes [17] supplemented with empirically selected values for the protonated complexes.

Cu^{2+},en(en H$^+$) 1.3 M, 25 °C	Cu^{2+},NH$_3$ [1] 2 M, 25 °C	Assumption
log $\beta_{0,1}$= 3.20	log K_1=4.22	log ($K_1/\beta_{0,1}$)≅1.0
log $\beta_{1,0}$=10.75	log K_2=3.57	
log $\beta_{1,1}$=13.75	log K_3=2.96	log ($\beta_{1,1}/\beta_{1,0}$)≅3.0
log $\beta_{2,0}$=20.03	log K_4=2.20	

Table 8. Stability constants for the chelated nickel(II)–ethanediamine complexes [18] supplemented with empirically selected values for the protonated complexes.

Ni^{2+},en(en H^+) 1.3 M, 25 °C	Ni^{2+},NH_3 [1] 2 M, 25 °C	Assumption
log $\beta_{0,1}$= 1.80	log K_1=2.84	log $(K_1/\beta_{0,1})\cong 1.0$
log $\beta_{1,0}$= 7.66	log K_2=2.28	
log $\beta_{1,1}$= 9.16	log K_3=1.77	log $(\beta_{1,1}/\beta_{1,0})\cong 1.5$
log $\beta_{2,0}$=14.06	log K_4=1.23	
log $\beta_{2,1}$=14.86	log K_5=0.79	log $(\beta_{2,1}/\beta_{2,0})\cong 0.8$
log $\beta_{3,0}$=18.61	log K_6=0.07	

obtained. On the other hand, $K_{0,2}$, the constant for the uptake of the second en H^+-ligand by Cd en H^{3+}, can be estimated empirically to be <20, corresponding to $\beta_{0,2}<1000$. Table 4 demonstrates that the introduction of $\beta_{0,2}\equiv 1000$ in the calculations has very little influence on values of the other constants. It is therefore understandable that the data cannot be stretched to calculate stability constants for other than the three monoprotonated constants.

Fig. 2 shows the results of a calculation of the ranges of existence of the various cadmium species in the 3 M perchlorate solutions with different initial acid concentrations. The figure shows that formation of the protonated complexes is very considerable in the solutions with $C^{\circ}_{HClO_4}$=1 M and strongly suppressed in the solutions with $C^{\circ}_{HClO_4}$ as low as 0.02 M. This confirms on the whole our assumption that $\beta_{1,0}$, $\beta_{2,0}$ and $\beta_{3,0}$ can be determined at low initial acid concentration with only little interference from the formation of protonated complexes.

DISCUSSION OF RESULTS

The cumulative constants ($\beta_{n,1}$) found for the uptake of en- and en H^+-ligands are compared in Table 5 with the consecutive constants (K_n) for the corresponding cadmium-ammonia system.[1] It can be read from the table that the first en H^+-ligand is about 10 times more weakly bound to the cadmium ion than the first ammonia molecule. A decrease in affinity of this order of magnitude is also found in the corresponding silver(I) systems for which log K_1 is found to be 3.40 [1] in the ammonia system at 20 °C whereas log $\beta_{0,1}$ has the value 2.35 in the 1,2-ethanediamine system at the same temperature.[16]

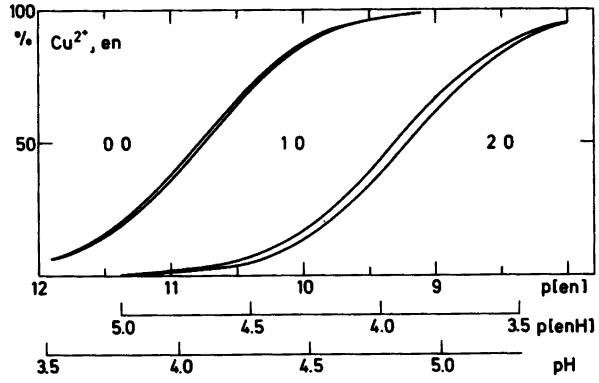

Fig. 3. Distribution of the complexes Cu(en H)$^{3+}$, Cu en^{2+}, Cu en (en H)$^{3+}$ and Cu en_2^{2+} estimated from the data of Bjerrum and Nielsen [17] ($\beta_{1,0}=10^{10.75}$, $\beta_{2,0}=10^{20.03}$) for solutions with: C_{KNO_3} 1.00, C_{Cu} 0.10, C_{HNO_3} 0.10 and C_{en} varying from 0.06 to 0.3 M at 25 °C. The stability constants for Cu (en H)$^{3+}$ and Cu en (en H)$^{3+}$ were assumed empirically to have the values: $\beta_{0,1}=10^{3.20}$ and $\beta_{1,1}=10^{13.75}$.

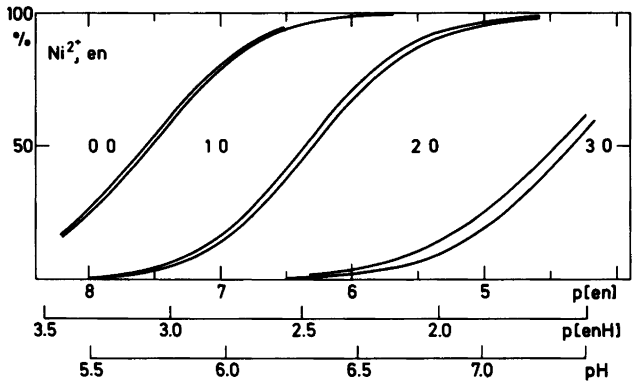

Fig. 4. Distribution of the six nickel(II)–ethanediamine complexes estimated from the data of Poulsen and Bjerrum [17] ($\beta_{1,0}=10^{7.66}$, $\beta_{2,0}=10^{14.06}$, $\beta_{3,0}=10^{18.61}$) for solutions with C_{KNO_3} 1.00, C_{Cu} 0.10, C_{HNO_3} 0.10 and C_{en} varying in the range 0.08–0.3 M at 25 °C. The stability constants for Ni(en H)$^{3+}$, Ni en (en H)$^{3+}$ and Ni en$_2$ (en H)$^{3+}$ were assumed empirically to have the values $\beta_{0,1}=10^{1.80}$, $\beta_{1,1}=10^{9.16}$ and $\beta_{2,1}=10^{15.06}$.

The influence of the positive charge on the protonated ligand ($NH_2CH_2CH_2NH_3^+$) is also of the same order in the Hg(II) systems.[1,6] The constant for the binding of an en H$^+$-ligand to Cd en^{2+} ($=\beta_{1,1}/\beta_{1,0}$) is seen to have a relatively high value comparable with the values for K_2 and K_3 in the ammonia system. This is tantamount to a considerable stabilization of the mixed complex Cd en (en H)$^{3+}$ relative to $Cd(NH_3)_3^{2+}$. The cadmium ion has only a very small affinity for more than four ammonia molecules [1] and it is therefore remarkable that the constant for binding of en H$^+$ to Cd en$_2^{2+}$ (log $\beta_{2,1}/\beta_{2,0}=0.59$) has a relatively high value. The reason for this must be that Cd en$_2^{2+}$, which has been shown recently [20] to have tetrahedral configuration, rather easily converts to octahedral configuration with Cd en$_2$ (en H)$^{3+}$ as an intermediate.

In the work of Jannik Bjerrum and coworkers on the determination of the stability constants for metal(II)–1,2-ethanediamine complexes [1,2,17–19] in 1.3 M chloride or nitrate solutions with the initial acid concentration as high as 0.10 M, the influence of protonated complexes has been neglected. It therefore has some interest to use the knowledge acquired for the cadmium system to estimate the error introduced by this omission. The chelation effects in the copper(II)– and nickel(II)–1,2-ethanediamine systems relative to the corresponding ammonia systems are higher than in the cadmium systems (see Table 6). It should therefore be expected that the formation of protonated complexes is of little importance in these systems. The basis for estimating the constants for the protonated complexes in the copper(II) and nickel(II) systems is given in Tables 7 and 8, and in Figs. 3 and 4 the probable ranges of existence of all of the species are calculated. The conclusion which can be drawn from the figures is that the needed correction to the previously determined stability constants for the copper(II)– and nickel(II)–ethanediamine systems are so small that they have kept their value within the accuracy of the determinations.

Acknowledgements. The authors are grateful to Morten Jannik Bjerrum for writing the computer programme and to Dr. Martin Hancock for correcting the English manuscript.

REFERENCES

1. Bjerrum, J. *Metal Ammine Formation in Aqueous Solution,* P. Haase and Son, Copenhagen 1941, reprinted 1957.
2. Bjerrum, J. and Andersen, P. *K. Dan. Vidensk. Selsk., Mat.-Fys. Medd. 22* (1945) No. 7.
3. Sillen, L. G. and Martell, A. E. *Chem. Soc. Spec. Publ. 17* (1964), *Suppl. 25* (1970).
4. Schwarzenbach, G. and Szilard, I. *Helv. Chim. Acta 45* (1962) 1222.
5. Schwarzenbach, G. *Helv. Chim. Acta 35* (1952) 2344.

6. Bjerrum, J. and Larsen, E. *Essays in Coordination Chemistry, Exper. Suppl. 9* (1964) 39.
7. Biernat, J. and Wilgocki, M. *Rocz. Chem. 48* (1974) 1663.
8. Wilgocki, M. *Dissertation,* Wrocław 1976.
9. Wilgocki, M. and Biernat, J. *Rocz. Chem. 51* (1977) 1297.
10. Wilgocki, M. and Biernat, J. *Congress on Polarography,* Prague 1980, Proc. II, p. 191.
11. Gjaldbæk, J. K. *K. Dan. Vidensk. Selsk., Mat.-Fys. Medd. 5* (1924) No. 9.
12. Lewis, G. N., Brighton, T. B. and Sebastian, R. L. *J. Am. Chem. Soc. 39* (1917) 2245.
13. Szilard, I. *Diss.* No. 3218, Zürich 1961.
14. Stone, H. W. *J, Am. Chem. Soc. 58* (1936) 2591.
15. Leden, I. *Diss.*, Lund 1943, p. 34.
16. Schwarzenbach, G. *Helv. Chim. Acta 36* (1952) 23.
17. Bjerrum, J. and Nielsen, E. J. *Acta Chem. Scand. 2* (1948) 297.
18. Poulsen, I. and Bjerrum, J. *Acta Chem. Scand. 9* (1955) 1407.
19. Pecsok, R. L. and Bjerrum, J. *Acta Chem. Scand. 11* (1957) 1419.
20. Fujita, T. and Ohtaki, H. *Bull. Chem. Soc. Jpn. 53* (1980) 930.

Received September 3, 1982.

Acta Chemica Scandinavica A 37 (1983) 315–322

Vibrational Spectra, Conformational Composition and Normal Coordinate Analysis of 3-Chloro-1-butene

S. H. SCHEI [a] and P. KLÆBOE [b]

[a] Department of Chemistry, University of Trondheim, NLHT, Rosenborg N-7000 Trondheim, Norway and [b] Department of Chemistry, University of Oslo, Oslo 3, Norway

The infrared spectra of 3-chloro-1-butene were recorded in the region 4000–50 cm^{-1} for the vapour, liquid, amorphous and annealed solid at 90 K. Raman spectra of the neat liquid, various solutions and amorphous and annealed solid were recorded. Intensity variations observed when going from the liquid to the solid state revealed that two or possibly three conformers were present. The predominant conformer in the vapour and liquid was also present in the crystal. Practically all the fundamentals of this conformer (the one where a hydrogen atom eclipses the double bond) were observed and interpreted. The interpretation was aided by a normal coordinate analysis. At high pressure (above *ca.* 1 kbar), partly isomerization to *trans*-1-chloro-2-butene took place. In an earlier vibrational study of 3-chloro-1-butene several impurity bands of *trans*-1-chloro-2-butene were reported.

Compared to the thorough vibrational study of 3-chloro-1-propene,[1–3] 3-chloro-1-butene (later to be called CB) has received little attention. A few years ago, certain infrared and Raman spectral data were reported.[4] The authors concluded that the two conformers with Cl and CH_3 eclipsing the double bond (II and III, Fig. 1) were nearly equally abundant and coexisted together with a third conformer, having a torsional angle of 180° relative to conformer II.

There is clear experimental evidence that both 3-chloro-1-propene [1–3,5] and 1-butene [6,7] exist predominantly as the conformer in which a hydrogen eclipses the double bond. Thus, the corresponding conformer (I, Fig. 1) is expected to be the most abundant for CB. Preliminary results from a gas phase electron diffraction study of CB [8] reveal that the vapour consists of *ca.* 80 % of conformer I.

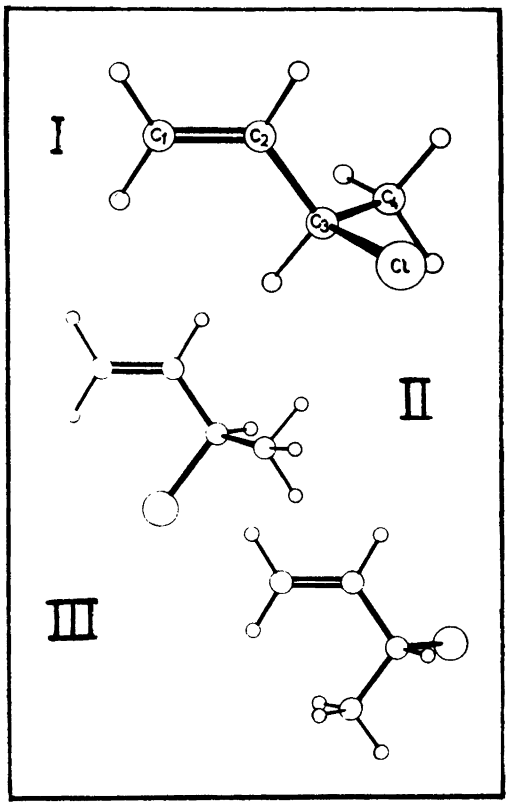

Fig. 1. The probable conformers of 3-chloro-1-butene (CB).

0302-4377/83 $02.50

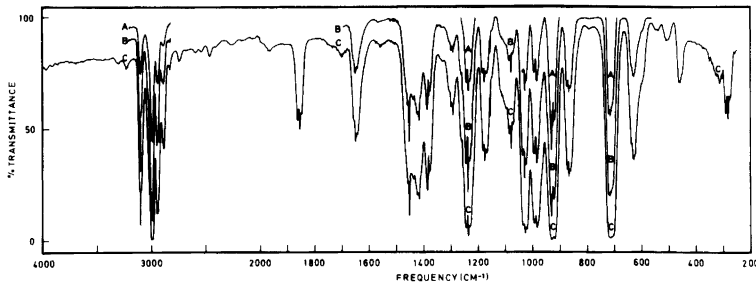

Fig. 2. Infrared spectra of 3-chloro-1-butene as a vapour; path length 10 cm; A, 10 Torr; B, 30 Torr; C, 100 Torr.

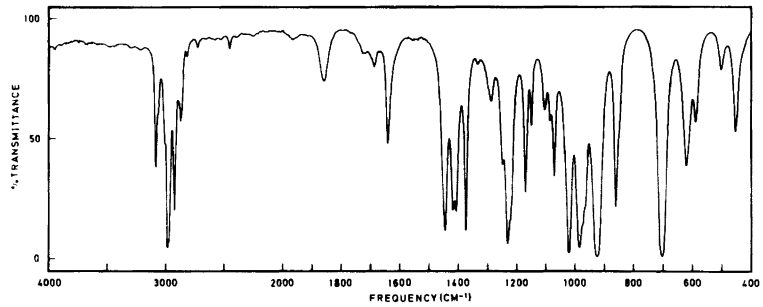

Fig. 3. Infrared spectrum of 3-chloro-1-butene as a liquid, 0.028 mm path length.

The spectra reported earlier [4] show a number of bands as expected when many conformers are present. However, the stronger band corresponding to C=C stretch was found as high as 1670 cm^{-1}, close to the C=C stretching frequency of *trans*-2-butene.[9] This seems surprising, since in propene,[10] 1-butene[11] and 3-chloro-1-propene[1-3] this frequency is close to 1650 cm^{-1}. Thus, it was found worthwhile to reinvestigate and to extend the vibrational study of CB. With three possible conformers coexisting, all of them without symmetry, it was regarded unlikely to discern completely the fundamentals of the less abundant conformers. However, it should be possible to identify the fundamentals of the main form.

EXPERIMENTAL

CB was a commercial product from Aldrich. The sample was purified by preparative gas chromatography, and the spectra were recorded as described previously.[12] The vapour spectra were recorded at 100, 30 and 12 torr in a 10 cm cell with CsI windows and in a 20 cm cell with polyethylene windows. High pressure infrared spectra were recorded in a diamond anvil cell, with spacers of copper and brass. No internal standard was used and the pressures are therefore highly approximative.

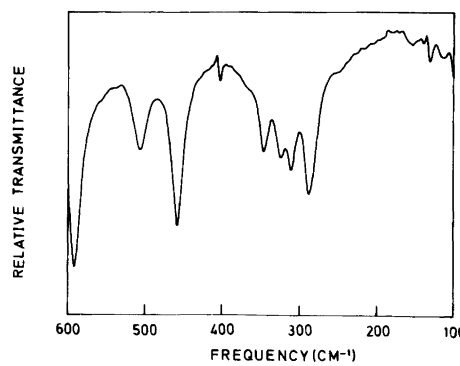

Fig. 4. Far infrared spectrum of 3-chloro-1-butene in benzene solution, path length 1 mm, 3.5 μm beamsplitter.

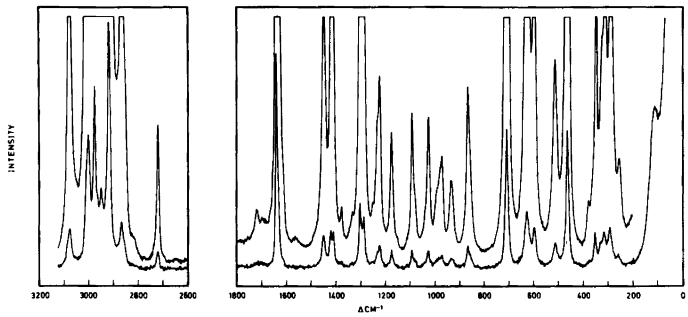

Fig. 5. Raman spectrum of liquid 3-chloro-1-butene.

RESULTS AND DISCUSSION

Infrared spectra of CB in the vapour and liquid states are shown in Figs. 2–4. The Raman spectra of the liquid and amorphous and crystalline solid are given in Figs. 5–6. The observed frequencies are listed in Table 1.

High pressure spectra. Isomerization. Application of high pressure (*ca.* 1 kbar) partly converted CB to *trans*-1-chloro-2-butene. The times before equilibrium composition was obtained were larger the lower the pressure. Within the pressure range used (*ca.* 1–20 kbar), the time varied from *ca.* two hours to practically instant conversion. From gas phase studies the activation energy at atmospheric pressure has been observed [14] to be 197 kJ mol^{-1}.

Approximately equal equilibrium mixtures were measured from a wide range of pressure conditions. The high pressure infrared spectrum (Fig. 7) was compared with liquid state spectra of CB+*trans*-1-chloro-2-butene mixtures. Such a comparison indicates that there is approximately 30 % CB and 70 % *trans*-1-chloro-2-butene in the equilibrium mixture in the high pressure cell. The same ratio was obtained earlier from a study of this equilibrium in toluene solution.[13]

The high pressure apparently reduces further the fairly low barrier (197 kJ mol^{-1}) of isomerization of CB to *trans*-1-chloro-2-butene, without significant changes in the isomeric composition. Therefore, the partial molar volumes $\bar{V}$ of CB and *trans*-1-chloro-2-butene must be almost

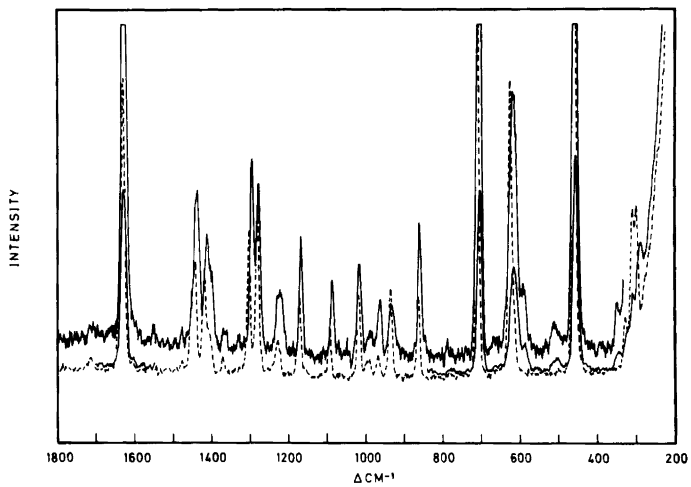

Fig. 6. Raman spectrum of amorphous (—) and crystalline (···) 3-chloro-1-butene at 90 K.

Table 1. 3-Chloro-1-butene, vibrational spectral data.

Infrared				Raman		Interpretation	
Vapour	Liquid	Amorphous (90 K)	Crystalline (90 K)	Liquid	Crystalline (90 K)	I	II/III
3108, 3103, 3098, 3091 s [a]	3090 m	3086 m	3085 m	3091 m	3087 s	ν_1	
3085 sh	3075 sh		*	3070 sh	*		fund.
3026 sh		3032 vvw	*	3025 sh	*		fund.
3001 sh	3014 sh	3012 w	3011 w	3016 s	3015 s	ν_2	
2997, 2994, 2990, 2988 vs	2990 vs	2987 s	2994, 2986 m	2991 vs	2999, 2993 s	ν_3	
2983 s	2978 sh,s	2975 s	2976 s	2979 sh,s	2977 s	ν_4	
2977 sh		2964 sh	2966 sh	2961 m	2965 s	ν_5	
2946, 2943, 2935 s	2931 s	2927 s	2926 s	2930 vs	2929 vs	ν_6	
					2909 w		
2894 m	2895 w		*				fund.
2882 m	2878 w	2877 w	2880 w	2879 m	2881 m	ν_7	
	2868 sh	2861 w	2865 w	2864 sh	2867 w		
2835, 2827 vw	2823 vw	2820 vw					
1860, 1853, 1846 m	1861 w	1874 m	1879 m			$2\times\nu_{21}$	
	1727 vw						
1700 vw	1718 vw	1699 vw	1696 w	1714 vw			
	1689 w	1673 w	1670 w				
1654, 1652, 1649, 1645 m	1644 m	1644, 1636 m	1646, 1634 m	1644 vs	1647, 1640 vs	ν_8	
1641				1635 sh			fund.
1617 sh	1616 sh			1616 sh	1618 vw		
1560 vw				1563 vw	1568 vvw		
1462, 1459 w	1454 sh	1454 sh	*	1450 m	1459 w (*)		fund.
1454, 1452 s	1449 s	1446 s	1448, 1446 s	1445 sh	1449 m	ν_9	
1438, 1430, 1423 s	1423 s	1424 s	1426, 1424 s	1422 m	1425 m	ν_{10}	
1423, 1416, 1411 s	1412 s	1410 s	1402 s	1411 m	1411 w	ν_{11}	
1385, 1380, 1376 s	1378 s	1375 s	1372 s	1380 w	1375 w	ν_{12}	
1338, 1329 vw	1337 vw			1328 vw			

1305 1299	sh	1394 sh	1304 w	1306 w	1304 s	1308 m	ν_{13}	
1294 1291 1287	m	1290 m	1286 w	1283 vw	1288 s	1286 m	ν_{14}	
1260 1258	sh	1253 sh,m	1249 sh	*	1251 vw	*		fund.
1243 1237 1232	vs	1234 vs	1234 s	1230 s	1232 sh,w	1232 w	ν_{15}	
1229 1223 1218	sh	1224 sh		*	1218 w	*		fund.
1183 1177 1169	m	1173 s	1175 s	1177 1175 s	1174 w	1175 w	ν_{16}	
1156 1149	sh	1153 w	1153 w	*	1157 vvw	*		fund.
1116 1112	sh	1107 w	1102 vw	*	1105 vw	*		fund.
1096	sh	1089 w	1092 m	1093 m	1089 w	1096 w	ν_{17}	
1086 1078 1071	m	1075 m	1075 m	1076 vw	1074 sh	*		fund.
1037 1031 1029 1023	vs	1024 vs	1022 vs	1017 vs	1024 w	1020 w	ν_{18}	
996 994	s	989 vs	992 s	994 s	989 sh	996 w	ν_{19}	
984 979	s	979 sh	976 sh	*	978 sh	*		fund.
967	sh	971 sh	967 s	964 s	971 w	968 w	ν_{20}	
935 931 927	vs	928 vvs,br	934 vs	937 vs	930 w	937 m	ν_{21}	
920	s				905 vvw			fund.
868 864 859	s	863 s	862 s	862 s	863 m	866 m	ν_{22}	
856	sh	852 sh		*	843 sh	*		fund.
			710 w	*				fund.
719 714 710 706	vvs	705 vvs	705 vvs	706 vs	708 vs	710 vs	ν_{23}	
636 629 626 622	m	622 m	620 m	620 m	622 s	625 s	ν_{24}	
596	sh	591 w	588 w	*	592 m	*		fund.
512 508 503 498	w	504 w	505 w	*	506 m	*		fund.

462							
456 } m	455 m	454 m	452 m	458 vs	456 vs	ν_{25}	
449							
	402 vw [b]						
	363 vvw		*	370 vw	*		fund.
350 vw	345 w	343 vvw	*	345 m	*		fund.
324 vw	323 w	325 w	325 w	324 sh	326 m	ν_{26}	
311 w	310 w	309 w	309 w	310 m	307 m	ν_{27}	
305 vvw	305 vw	302 vvw	*				fund.
290							
282 } m	286 m	289 w	289 w	289 m	296 m	ν_{28}	
274							
		272 vvw	272 vvw				
254 vw	252 vvw			252 w		ν_{29}	
235 vw							
					128 w		
					117 w		
				105 w		ν_{30}	

[a] Abbreviations: s, strong; m, medium; w, weak; v, very; sh, shoulder; br, broad; *, band vanishing in the crystalline state; fund., fundamental. [b] Liquid infrared observations below 450 cm^{-1} are benzene solution spectra.

equal, or the equilibrium would be displaced towards the isomer with the smallest volume. In the case of conformational equilibria of halocyclohexanes [15] and haloethanes [16,17] the equilibria are quite pressure dependent. The difference in partial molar volumes in these cases were calculated [15–17] from the pressure dependence of the conformational equilibria.

The isomerization of CB explains the large number of bands reported by earlier authors.[4] By comparison with our high pressure spectra, the additional bands were easily assigned to impurities of *trans*-1-chloro-2-butene.

Conformation. As expected, the vapour and liquid phase spectra of CB contain a large number of bands which may be regarded as fundamentals. Since many of these vanish nearly or completely in the crystalline sample, there are obviously at least two conformers present in the vapour and in the liquid. Most bands assigned as a fundamental of the predominant conformer, correspond to a nearby, less intense band of a second conformer. There is no definite evidence of a third conformer. But a third conformer cannot be excluded, since these bands must be of low intensity and may be hidden by bands of the other conformers.

Since all three conformers shown in Fig. 1 have C_1 symmetry, all the Raman lines are polarized and infrared vapour phase contours are *A/B/C*

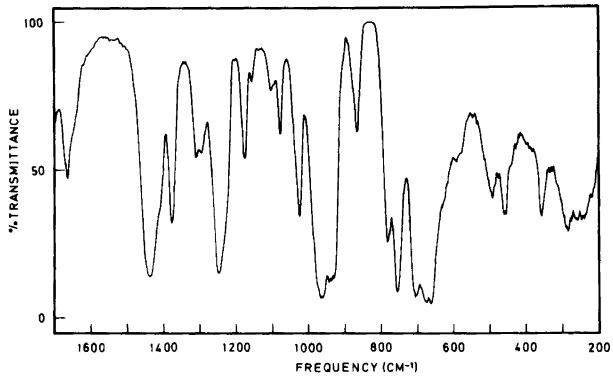

Fig. 7. Infrared spectrum of 3-chloro-1-butene, compressed to *ca.* 20 kbar pressure for *ca.* 4 h.

Table 2. 3-Chloro-1-butene, calculated frequencies for conformers I, II and III (Fig. 1), and corresponding potential energy distribution of I.

Assignment	Frequency				P.E.D.[a]
	I obs.	I calc.[b]	II calc.	III calc.	I
ν_1	3090	3095			$=C_1-H(99)$
ν_2	3014	3022			$=C_2-H(94)$
ν_3	2990	2982			$=C_1-H(95)$
ν_4	2978	2987			$C_4-H(100)$
ν_5	2961[c]	2987			$C_4-H(100)$
ν_6	2931	2931			$C_4-H(100)$
ν_7	2895	2916			$C_3-H(98)$
ν_8	1649	1645	1651	1644	$C=C(82)\ C_2-C_3(15)$
ν_9	1449	1489	1489	1489	$H-C_4-H(93)$
ν_{10}	1423	1488	1488	1488	$H-C_4-H(93)$
ν_{11}	1412	1418	1421	1420	$H-C_1-H(50)\ C=C_1-H(35)$
ν_{12}	1378	1370	1381	1387	$C-C_4-H(49)\ H-C_4-H(44)\ C-C_3-H(12)$
ν_{13}	1304	1362	1369	1369	$C-C_3-H(78)\ C-C_4-H(11)$
ν_{14}	1288	1316	1313	1306	$C=C_2-H(20)\ C_2-C_3(17)\ C-C_4-H(11)$
ν_{15}	1234	1229	1248	1233	$Cl-C-H(45)C-C_3-H(36)C-C_4-H(11)$
ν_{16}	1173	1160	1122	1194	$C_3-C_2-H(29)\ C_2-C_3(25)\ C=C_2-H(18)$
ν_{17}	1089	1078	1081	1007	$C_3-C_4(70)\ C=C_1-H(11)$
ν_{18}	1024	1019	1032	1046	$C-C_4-H(40)\ C=C_1H(19)\ Cl-C-H(11)$
ν_{19}	989	997	1011	1002	$w=CH_2(32)tC=C(31)\ w=CH(24)$
ν_{20}	979	979	984	990	$C-C_4-H(55)\ C=C_1-H(19)\ Cl-C-H(12)$
ν_{21}	928	924	932	931	$w=CH_2(52)\ tC=C(42)$
ν_{22}	863	885	887	872	$C-C_4-H(31)\ C_2-C_3(26)\ C=C_1-H(24)$
ν_{23}	705	747	713	738	$C-Cl(31)\ CC_4H(11)$
ν_{24}	622	618	610	591	$w=CH(38)\ tC=C(18)\ C-Cl(16)$
ν_{25}	455	410	522	501	$C=CC(32)\ C-Cl(21)$
ν_{26}	323	320	341	319	$C-C_3-H(21)\ C-C-C(21)\ Cl-C-C_2(18)\ C=C-C(18)$
ν_{27}	310	294	295	312	$Cl-C-C_4(54)\ Cl-C-C_2(25)$
ν_{28}	286	280	247	284	$C-C-C(38)\ Cl-C-C_2(24)\ Cl-C-C_4(15)$
ν_{29}	252	238	239	300	$tC_3-C_4(96)$
ν_{30}	105[c]	103	85	109	$tC_2-C_3(87)$

[a] Contributions of more than 10 % are included, given as $f_{ij}^2 F_{jj}\lambda_i$. w and t denote out-of-plane wag and torsion, respectively. [b] The force field will appear in Ref. 8. [c] Raman observation, other observed frequencies are infrared liquid data.

hybrids. Solution spectra from various solvents did not show intensity changes which were conformationally significant. It was not possible to decide which informer is predominant from the vibrational spectra alone.

All the bands which appeared in the liquid state spectra and vanished in the spectra of the crystalline sample, had low intensities. This observation strongly indicates that there is one abundant conformer. By comparison with the electron diffraction experiment,[8] this conformer is undoubtedly conformer I (Fig. 1).

Vibrational assignment. Most of the 30 fundamentals of conformer I were interpreted by comparison with the spectra of 3-chloro-1-propene [1-3] and 1-butene.[11] The frequencies associated with the $=CH_2$, $=CH$ and CH_3 groups are close to those of 3-chloro-1-propene and 1-butene. However, there is some uncertainty regarding the description of the C–H stretching modes and the frequencies in the region 1200–950 cm^{-1}.

The complexity of the spectrum in the 1200–950 cm^{-1} region is reflected in the potential

energy distribution of the vibrational modes in this region (Table 2). The calculation was based upon a valence force field, obtained as a combination of corresponding valence force fields for 3-chloro-1-propene and 1-butene (the force field will be published in a forthcoming paper [8]). The calculation shows that the normal modes approximately decribed as $=CH_2$ wag, =CH and C=C twist are highly mixed, as are C=C−H bend, CH_3 rock and C−C stretch. Nevertheless, the description given in Table 2 agrees quite well with those of 3-chloro-1-propene and 1-butene. The spectral interpretation relied heavily upon the results of the force constant calculations.

Normal coordinate calculations were also carried out for conformers II and III, by transferring the force constants from conformer I (Table 2). The calculations indicate that many fundamentals of the most abundant conformer I should overlap or lie very close to those of conformers II and III. 19 cases were observed for which infrared and/or Raman bands present in the liquid or amorphous spectra vanished in the crystal spectra. These bands are assigned as fundamentals of II and/or III, although we cannot exclude that some might be combination bands or overtones of conformers I and II.

Many of the bands which are attributed to conformers II and III agree quite well with the calculated wave numbers. It might have been possible to make systematic assignments of the fundamentals of conformers II and/or III, partly to the vanishing crystal bands and partly to bands of conformer I presumably overlapping those of conformers II and III. Since this procedure would be quite uncertain, it was not attempted.

Acknowledgements. We are grateful to Kerstin Nordby and Jann Samstad for technical assistance.

REFERENCES

1. McLachlan, R. D. and Nyquist, R. A. *Spectrochim. Acta A 24* (1968) 103.
2. Sourisseau, C. and Pasquier, B. *J. Mol. Struct. 12* (1972) 1.
3. Silvi, B. and Sourisseau, C. *Spectrochim. Acta A 31* (1975) 565.
4. Som, J. N. and Kastha, G. S. *Indian J. Phys. B 51* (1977) 77.
5. Hirota, E. *J. Mol. Spectrosc. 35* (1970) 9.
6. van Hemelrijk, D., van den Enden, L., Geise, H. J., Sellers, H. L. and Schäfer, L. *J. Am. Chem. Soc. 102* (1980) 2189.
7. Kondo, S., Hirota, E. and Morino, Y. *J. Mol. Spectrosc. 28* (1968) 471.
8. Schei, S. H. *To be published.*
9. Levin, I. W., Pearce, R. A. R. and Harris, W. C. *J. Chem. Phys. 59* (1973) 3048.
10. Silvi, B., Labarbe, P. and Perchard, J. P. *Spectrochim. Acta A 29* (1973) 263.
11. Durig, J. R. and Compton, D. A. C. *J. Phys. Chem. 84* (1980) 773.
12. Schei, S. H. and Klæboe, P. *J. Mol. Struct. 96* (1982) 9.
13. Dittmer, D. C. and Marcantonio, A. F. *J. Org. Chem. 29* (1964) 3473.
14. Nogier, J. P. and Blouri, B. *Bull. Soc. Chim. Fr.* (1973) 758.
15. Christian, S. D., Grundnes, J. and Klæboe, P. *J. Am. Chem. Soc. 97* (1975) 3864.
16. Christian, S. D., Grundnes, J. and Klæboe, P. *J. Chem. Phys. 65* (1976) 496.
17. Taniguchi, Y., Takaya, H., Wong, P. T. T. and Whalley, E. *J. Chem. Phys. 75* (1981) 4815, 4823.

Received August 11, 1982.

Acta Chemica Scandinavica A 37 (1983) 323–335

Matrix Infrared, *ab initio* and Normal Coordinate Study of the Association of Methanol, Considering Especially the Torsional Mode in Nitrogen and Carbon Monoxide Matrices

JUHANI MURTO, MARKKU RÄSÄNEN, ANTERO ASPIALA and EERO KEMPPINEN

Department of Physical Chemistry, University of Helsinki, Meritullinkatu 1 C, SF-00170 Helsinki 17, Finland

IR spectra of CH_3OH, CH_3OD and CD_3OD in N_2 matrices and of CH_3OH in CO matrices have been recorded in order to study the association of methanol. *Ab initio* STO–3G calculations have been carried out on open and cyclic dimers and trimers. Approximate normal coordinate GVFF calculations, based on the appropriately scaled *ab initio* force constants, have been carried out on open dimers and open and cyclic trimers. For the first time, a fine structure is found in the matrix IR spectrum of the OH torsional region of an alcohol, and is interpreted with the aid of the calculations. The results can be explained in terms of non-cyclic associates. In N_2 spectra the monomer τOH band is at 304 cm^{-1}, the dimer end group bands are at 386–325 cm^{-1}, the trimer end group bands at *ca.* 500 cm^{-1}, the dimer proton donor bands at 623–571 cm^{-1}, and the trimer and polymer proton donor bands at 800–700 cm^{-1}. The νOH and τOH dimer fine structures are proposed to be related to the different positions of the methanol molecules around the O···O axis. In CO only two non-cyclic dimer species were found, which interconvert reversibly in the temperature range 13–30 K. The IR-induced interconversion of the dimers in matrices is discussed, considering the possibility of cyclic intermediates.

There are several studies dealing with the matrix IR spectra of methanol,[1–10] the first paper being the classical one by Pimentel's group.[1] Barnes and Hallam [2] studied the association of methanol in argon, and they interpreted their results in terms of open chain dimers, trimers and tetramers, and cyclic tetramers, and dealt especially with the νOH, δOH and νCO regions. The influence of association on the τOH (torsion) band was not studied, obviously because of the low intensity of this band in argon.

Schriver *et al.*[8] made a thorough study of the νOH dimer region of methanol in nitrogen matrices. Four different νOH proton donor bands (called D_2 bands) were observed, together with the corresponding proton acceptor dimer end group bands (D_1 bands) near the monomer νOH peak (see Table 1), which proves conclusively that the methanol dimers are largely open (non-cyclic) in N_2 matrices. Using temperatures down to 8 K and a spectrophotometer whose IR beam is monochromatic at the sample, they found in N_2 (but not in Ar) both temperature-dependent and irradiation dependent processes. Upon increasing the temperature from 8 to 10 K, species A (see Table 1) was converted to species

Table 1. The open methanol dimers: νOH wavenumbers (in cm^{-1}) in the IR spectrum for four species in nitrogen matrices at 8 K.[8]

Ref. 8			This work	
Species	D_1	D_2		
A	3655.2	3519.5	Ic	Ib
B	3651.0	3504.0		
C	3658.7	3496.0	Ia	
D	3654.1	3488.8		

0302-4377/83 $02.50

B in a fast process; upon irradiation with broad band radiation, or with radiation of frequency 3489 cm^{-1} (the νOH value of the proton donor band of species D), the amount of the A and B species increased in the matrix. In the case of CH_3OD, the broad-band IR-induced process was ten times slower than the corresponding process of CH_3OH. It was found also that the majority of the mixed dimers has the structure $CH_3OD\cdots O(H)CH_3$.

We found two groups of sharp τOH association bands in our preliminary matrix IR study of methanol in N_2 and CO matrices,[9] one group (obviously due to end groups of open associates) being near the monomer band, and the other group at 600–800 cm^{-1}. These findings prompted us to carry out *ab initio* STO-3G calculations on methanol dimers and trimers, and to carry out normal coordinate calculations based on the diagonal force constants thus obtained. The purpose was to find support for the assignments of the τOH association bands, and to find an explanation for the quadruplet band structures of the dimer absorptions. The results are given in the present paper.

Methanol has no intramolecular absorption bands below 1000 cm^{-1} other than the τOH band, and since the molecule is small, it perturbs the matrix lattice only little.[10] Thus it is an ideal molecule for studying and calculating the association structure in the τOH region.

In a separate paper [10] we have discussed the specific influence of N_2 and CO on the νOH, δOH, νCO and τOH bands of monomeric methanol.

Association τOH bands of alcohols. Surprisingly little is known about the influence of association or heterodimer formation on the torsional vibration of alcohols.[11–19] Liquid alcohols display an extremely broad τOH band near 650 cm^{-1}, with a half-width of 200–300 cm^{-1}.[12] In the case of liquid CH_3OH the band occurs in the range 450–850 cm^{-1}, and in the case of CH_3OD in the range 350–630 cm^{-1}.[11,13] In the spectra of liquid ethanol the band is centred at 660 cm^{-1}, whereas in the spectra of crystalline ethanol a triplet with peaks at 725, 750 and 790 cm^{-1} is observed.[14]

In matrix spectra of alcohols at high concentra-

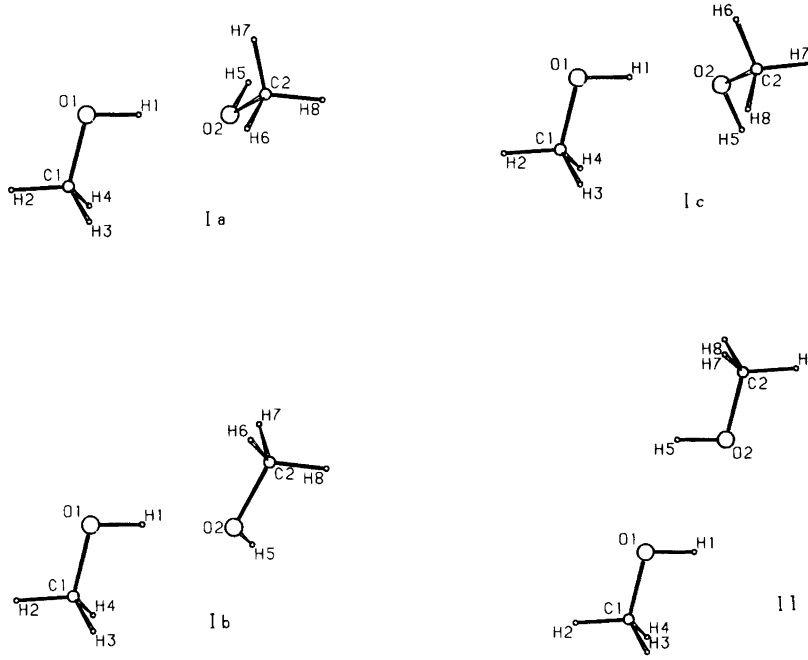

Fig. 1. Computer-drawn pictures of the optimized methanol dimers. Structures Ia, Ib and Ic' are open species (see Table 2); structure II is the cyclic dimer, for which $\Delta E = -7.1$ kJ mol^{-1}, and the optimized values of the coordinates are: OH 99.02 pm, CO 143.2 pm, OO 285 pm, COH 104.2° and COO 158.3°.

tions the association (polymer) τOH band is usually similar to those in the spectra of liquids, *i.e.*, it is a broad, indeterminate, structureless band at 600–700 cm^{-1}.[18,19] Thus it often remains unnoticed unless the concentration of the alcohol is quite high. There do not seem to exist cases where τOH dimer bands of alcohols in matrices have previously been definitely assigned.

Previous calculations on methanol dimers and trimers. There exist a few *ab initio* calculations [20–24] and one EPEN (empirical potential using electrons and nuclei) calculation [25] on methanol associates. The calculations have been carried out with rigid monomer geometries. The STO–3G dimerization energy of the open dimer (corresponding to structure Ia in Fig. 1) is –23.3 kJ mol^{-1}.[20,23] The cyclic dimer is considerably less stable, and an STO–3G dimerization energy of –9.0 kJ mol^{-1} has been reported.[22]

The *ab initio* STO–3G geometries and energies of trimers and higher associates up to hexamers have been estimated [24] on the basis of water polymer structures. In the case of trimers, the cyclic structure was found to be more stable than the lowest-energy open structure (the energies of formation from the monomers being –64.2 and –55.5 kJ mol^{-1}, respectively). The third type of trimers is the "double acceptor" species, the energy obtained for it being –37.5 kJ mol^{-1}.[24] EPEN calculations [25] yield similar energies as the STO–3G calculations for all of these trimers.

EXPERIMENTAL

The matrix IR measurements were carried out as previously,[18] using a Perkin-Elmer 621 spectrophotometer and a Displex CS-202 cryocooler. CH_3OH (E. Merck A.G., *pro analysi*), CH_3OD (Fluka A.G., *purum*) and CD_3OD (Fluka A.G., *puriss.*) were commercial products; they were dried with molecular sieves. The deposition temperature was 15 K; the heating and cooling rate of the matrices was 0.5 K min^{-1} (*cf.* Ref. 5). The lowest recording temperature was 13 K. The matrices were annealed by warming them 2–3 K above the highest recording temperature.

Ab initio CALCULATIONS

The *ab initio* calculations were carried out as previously described,[26] using the programme Gaussian 76 and the minimal STO–3G basis. By using this relatively small basis it was possible to optimize also the trimer structures. All intermolecular coordinates of the methanol associates, as well as intramolecular coordinates that relate to the COH groups of the methanol units, were carefully optimized by the usual iterative technique.

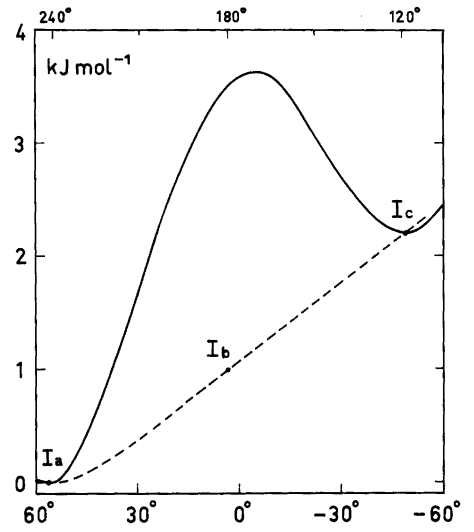

Fig. 2. STO–3G energies for the open methanol dimers: rotation of the second methanol molecule around the O···O axis (broken line, upper scale) and around the C_2O_2 bond (solid line, lower scale).

The four methanol *dimer* structures shown in Fig. 1 were optimized. For the structures Ia, Ib and Ic the dihedral angle τ_4 ($C_1O_1O_2C_2$) of the open dimer is –118° (or 242° in Fig. 2), 180° (planar $C_1O_1O_2C_2$ arrangement) and 118°, respectively. Structure Ia represents the total energy minimum of all methanol dimers, whereas structures Ib and Ic do not correspond to energy minima (with respect to τ_4); they were included to study the influence of variations in τ_4 on the total energy of the dimer. Structure Ic′ is the spectroscopically and energetically equivalent mirror image of structure Ic. Data on structures Ia and Ic are given in Table 2 (Del Bene [20] has reported values for quite different coordinates).

A picture and data on the cyclic dimer (structure II) are given in Fig. 1. This is the "planar" dimer [22] of C_{2h} symmetry.

Fig. 2 represents the variation of the STO–3G

Table 2. Ab initio STO–3G and normal coordinate results for the open dimers Ia and Ic. Units: bond lengths in picometres, angles in degrees, wavenumbers in cm^{-1}, stretching force constants in mdyn $Å^{-1}=10^2$ N m^{-1}, bending and torsion force constants in mdyn Å rad^{-2}=aN m rad^{-2}.

	Coord.	Opt. coord. value	Force const.	$\nu_{calc.}$ (PED)[a]	Opt. coord. value	Force const.	$\nu_{calc.}$ (PED)[a]
		Structure Ia			Structure Ic		
ν_1	O_1H_1	99.22	9.937[b,c]	3490 (98)	99.22	10.001[b,d]	3501 (98)
ν_2	O_2H_5	98.92	10.094	3659 (100)	98.95	10.077	3656 (100)
ν_3	C_1O_1	142.9	8.178	1048 (87)	142.9		
ν_4	C_2O_2	143.4	8.211	1064 (55) 1044 (42)	143.4		
δ_1	$C_1O_1H_1$	104.1	1.54	1386 (69)	104.1		
δ_2	$C_2O_2H_5$	104.8	1.34	1325 (65)	104.8		
τ_1	$H_2C_1O_1H_1$	180.0	0.320	625 (91)	180.1	0.290	597 (92)
τ_2	$H_6C_2O_2H_5$	180.1	0.103	385 (94)	180.0	0.092	361 (95)
ν_5	O_1O_2	274	0.336	192 (79)	275		
δ_3	$C_1O_1O_2$	103.9	0.193	85 (76)	101.1		
δ_4	$O_1O_2C_2$	117.4	0.086	65 (84)	117.8		
τ_3	$H_2C_1O_1O_2$	180.8	0.228	220 (89)[e]	−178.2		
τ_4	$C_1O_1O_2C_2$	−117.6	0.003	18 (99)	(118[f])		
τ_5	$O_1O_2C_2H_6$	56.3	0.044	108 (91)	47.9		
$-\Delta E$/(kJ mol^{-1})[g]		23.5			21.3		
μ/D[h]		2.91			3.45		

[a] The major potential energy contribution is due to the internal coordinate in question; the per cent value is given within parentheses. [b] The distance H_1O_2 was kept constant. [c] The angle $O_1H_1O_2$ is 179.6°, the dihedral angle $C_1O_1H_1O_2$ is 0.4°. [d] The angle $O_1H_1O_2$ is 176.1°, the dihedral angle $C_1O_1H_1O_2$ is −14.2°. [e] Value 0 for the coupling constant τ_1/τ_3 gives 221 (88), value −0.10 mdyn Å gives 177 (68). [f] Not an energy minimum. [g] The dimerization energy. The energy of the optimized monomer is −113.549 190 a.u. [h] The calculated dipole moment in Debye units. 1 D=3.335×10^{-30} C m.

Table 3. STO–3G optimized geometries for methanol trimers. See Table 2 for the units.

Coord.	Cyclic	Linear	Double accept.	Coord.	Cyclic	Linear	Double accept.
O_1H_1	99.27	99.60	99.13	$C_1O_1O_3$	122.5		
O_2H_5	99.46	99.43	98.84	$C_3O_3O_2$		117.7	108.7
O_3H_9	99.48	98.85	99.10	$O_1O_2C_2$	124.3	117.0	112.7
C_1O_1	143.1	142.8	143.0	$O_1O_3C_3$	115.9		
C_2O_2	143.0	142.9	143.6	$O_3O_2C_2$		105.4	108.8
C_3O_3	142.8	143.4	143.0	$O_1H_1O_2$	149	177.1	175
$C_1O_1H_1$	105.0	104.1	104.2	$O_1H_9O_3$	152		
$C_2O_2H_5$	105.4	104.7	104.9	$O_2H_5O_3$		175.6	171
$C_3O_3H_9$	105.9	104.8	104.4	$H_2C_1O_1O_2$	−153.0	181.5	
$H_2C_1O_1H_1$	186.9	180.1	180.2	$H_2C_1O_1O_3$	−86.6		
$H_6C_2O_2H_5$	180.0	180.2	178.6	$H_6C_2O_2O_1$	93.2	61.8	64.9
$H_{10}C_3O_3H_9$	178.2	180.4	180.8	$H_{10}C_3O_3O_1$	−163.9		
O_1O_2	260	265	279	$H_{10}C_3O_3O_2$		−57.2	180.0
O_1O_3	260			$C_1O_1O_2C_2$	−144.6	−98.9	−106
O_2O_3	259	264	279	$C_1O_1O_3C_3$	21.4		
$C_1O_1O_2$	110.2	105.3	106.9	$C_3O_3O_2C_2$		133.9	131.4
$-\Delta E$	66.2	58.3	39.4				
μ/D	0.87	3.51	1.68				

dimerization energy when rotating the second methanol molecule with respect to the first. The rotation Ia →Ic′ around the C_2O_2 bond (with respect to τ_5) involves a flat maximum [22] at τ_5 *ca.* 0°. The rotation around the O_1O_2 axis (in terms of τ_4) froom structure Ia to structure Ic involves an almost linear increase in energy, by *ca.* 2.2 kJ mol^{-1}.

The geometries of the three *trimers* were optimized (Table 3). In addition to the most stable species, the cyclic trimer (the same as in Ref. 25), also the double acceptor structure (open species I in Ref. 24) and an open "linear" structure (species II [24]) were optimized. The double acceptor species has a high energy compared to both the cyclic and linear species. However, matrices represent non-equilibrium systems, and also structures representing local energy minima may be formed (at least during diffusion within matrices). This was the reason for including the double acceptor structure in the calculations.

The trimer formation energies obtained (Table 3) are surprisingly similar to those found by Curtiss [24] without optimizations. Pictures of the cyclic and double acceptor species can be found in the literature.[25]

According to the calculations, the OH bond length increases upon H-bond formation from its optimized value in the monomer (99.12 pm; Table 4); in the free end group the bond is shorter than in the monomer. The calculated value of the COH angle increases in all cases from the value in the monomer, the increase being most marked in the strained cyclic trimer. The CO bond length changes only little from the monomer value upon association. The angles O–H···O differ slightly from 180° in the non-cyclic dimers and trimers.

Values for the diagonal force constants were also obtained for all optimized coordinates (*cf.* also Ref. 26). Their values for the open dimer species are given in Table 2.

NORMAL COORDINATE CALCULATIONS

The normal coordinate calculations were carried out using the modified Schachtschneider programmes described previously.[19] The torsional coordinate used was the simple *trans* dihedral angle HCOH, since the STO–3G force constant was calculated for this coordinate.

The calculations were based on the general valence force field of methanol monomer by Timidei and Zerbi.[27] Since the STO–3G geometries differ from the experimental geometries, the geometries used were based on the experimental data used by Timidei and Zerbi. For the CH_3 group the force constants of Timidei and Zerbi were used for all associates. The same force field was used for the protium and deuterium compounds.

It is well known that the harmonic STO–3G force constants are considerably larger than the experimental values. Thus the calculated STO–3G force constants were reduced by constant factors (*cf.* Ref. 28). The reduction factors used

Table 4. The COH vibrations of the CH_3OH monomer, calculated according to Timidei and Zerbi,[27] and according to the STO–3G calculations: evaluation of the force constant reduction factors. Units as in Table 2.

	Coord. value	Force const.	$\nu_{calc.}$	Opt. coord. value	Force const.	Force constant reduction factor	$\nu_{calc.}$	$\nu_{exp.}$[10] in N_2
	Experimental [27]			STO–3G				
νOH	95.6	7.623	3679	99.12	9.971	1.351 [a]	3637	3665
δOH	108.9	0.764	1339	103.9	1.387	1.815 [b]	1339	1348
νCO	142.7	5.221	1044	143.3	8.164	1.564 [b]	1044	1035
τOH	180	0.0342 [c,d]	304	180	0.0649	1.90 [d]	304	304

[a] Adjusted to give the experimental value for the linear dimer end group. [b] Adjusted to give the force constant given by Timidei and Zerbi. [c] Calculated in this paper. [d] Adjusted to give the experimental frequency.

for νOH, δOH, νCO and τOH vibrations of all dimers and trimers are given in Table 4. The value 1.90 obtained for τOH was used also for all intermolecular force constants (note that the value 1.82 for δOH is close to this value).

To keep the number of adjustable parameters as low as possible, only two interaction force constants between the coordinates were used. An interaction constant between the OH and the corresponding O···O stretching coordinates is required.[29] The value 0.383 mdyn Å^{-1} was used for it; the calculated H-donor νOH frequency of the open dimers then shifted downwards into the correct region, to *ca.* 3490 cm^{-1} in the case of species Ia (in the case of phenol–pyridine complexes the corresponding interaction constant was 0.3 mdyn Å^{-1} [29]).

A coupling constant of –0.05 mdyn Å was introduced in the case of the open dimers between the torsions τ_1 and τ_3; it shifted the bonded τOH frequency of species Ia from 641 to 625 cm^{-1} and improved the potential energy distribution (PED). This coupling constant was used also in the case of the double acceptor trimer. In the case of cyclic and linear trimers the value –0.10 mdyn Å was used, since the bonding is stronger than in the case of the open dimers.

RESULTS AND DISCUSSION

The experimental results are given in Table 5 and Figs. 3–7. Only the most important νOH, δOH and νCO association bands are considered,

Table 5. The most important νOH, δOH and νCO bands for CH_3OH and the τOH bands for CH_3OH, CH_3OD and CD_3OD in nitrogen matrix spectra. The letters A–D refer to the species in Table 1, the letter E to a proton acceptor end group. The wavenumbers are in cm^{-1}.

Wavenumber CH_3OH	Assignment	Wavenumber			Assignment
		CH_3OH	CH_3OD	CD_3OD	
νOH		τOH			
3673	dim. E	795	581	580	polym.
3665 s	monom.	792 br	570 br	570 br	polym.
3659–3488	dim., see Table 1	710–780	520–560	520–560	trim./tetram.
3445	trim./tetram.	644	478	478	multim. E
3430	trim./tetram.	623	468	466	dim. D
3390 [a]	trim./tetram.	609	457 vw	459 vw	dim.
3371	trim./tetram.	593	446 [d]	444 [d]	dim. B
3285 br	polym.	583	439 [c]	438 [c]	dim. C
3240	polym.	571	429 [d]	427 [d]	dim. A
δOH		550	414	413	water compl.?
1419	polym.	527	399	397	trim./tetram. E
1397	dim.	512	377 [a]	377	trim. E
1360	dim.	485 [a]	353	352	trim. E
1348 s	monom.	386	ca. 300 [c,e]	300 [c]	dim. E, D
1346 sh	dim. E	371 vw			dim.
1344	dim. E	359	282 [c]	278 [c]	dim. E, C
νCO		332 [b]			dim. E, A
1110	polym.	325 [a]	263 [a,d]	258 [d]	dim. E, B
1051	dim.	304 s	246 s	239 s	monom.
1040 [b]	dim.				
1035 vs	monom.				
1032	dim. E				
1029 [a]	dim. E				

[a] Maximum intensity decreases reversibly upon warming from 13 to 20 K (not indicated for all bands of this type). [b] Relative band intensity increases reversibly upon warming. [c] Band intensity decreases upon irradiation. [d] Band intensity increases upon irradiation. [e] The band is superposed on the monomer band of the protium compound.

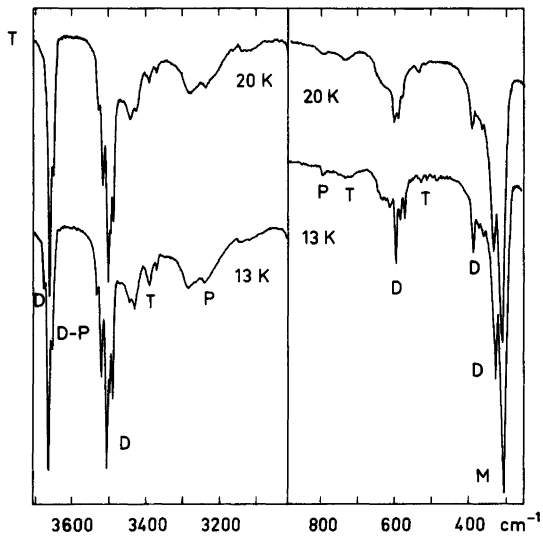

Fig. 3. The νOH and τOH regions of CH_3OH in N_2, M/A=100: influence of temperature. M=monomer, D=dimer, T=trimer/tetramer, P=polymer.

and are assigned analogously to the argon results.[2]

The νOH mode. It is significant that the νOH dimer D_2 bands in N_2 are quite sharp at low temperatures and concentrations ($\Delta\nu_{1/2}\approx 5$ cm^{-1}). Thus, in addition to monomers,[10] dimers do not perturb the N_2 lattice significantly.

Schriver *et al.*[8] considered multiple site trapping as an explanation for the quartet nature of the dimer D_2 νOH band, although it is observed both in Ar and N_2 spectra. Since the STO–3G energy of the dimer changes only little when varying the dihedral angle $C_1O_1O_2C_2$ (see Fig. 2), and simultaneously there are significant changes

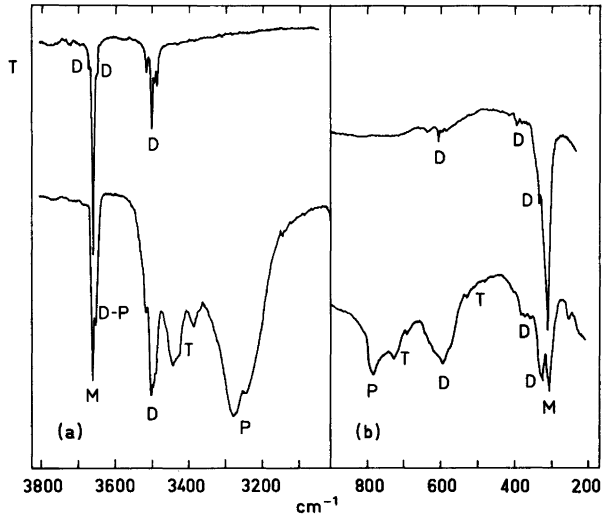

Fig. 4. The νOH and τOH regions of CH_3OH in N_2, temperature 13 K; influence of concentration. Upper curves: M/A=250, lower curves: M/A=20.

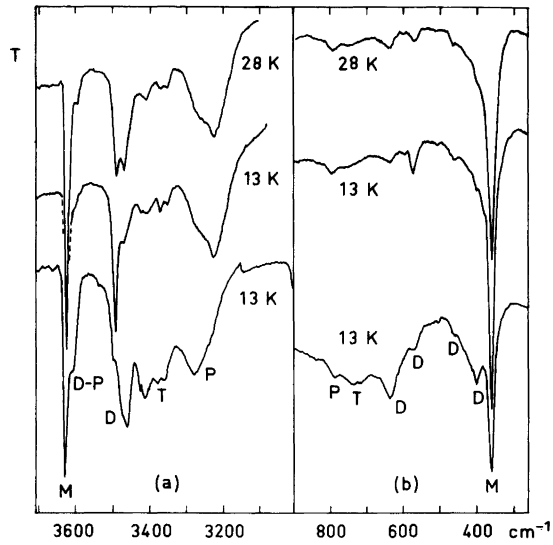

Fig. 5. The νOH and τOH regions of CH_3OH in CO. The two upper curves: M/A=100, annealed to 30 K; the lowest curves: M/A=20, unannealed (warming decreases the end group band at 400 cm^{-1} and increases the P bands considerably in the latter case).

in the νOH and τOH force constants, we conclude that the multiplet structures of the νOH dimer association bands are due to several different mutual positions of the two methanol molecules relative to the O···O axis. Only one of these positions (Ia) corresponds to an energy minimum in vapour; in matrices the other positions are stabilized by substitutional site effects. Interactions with the matrix molecules (see below) may change the relative energies of the species.

Inspection of the calculated νOH values given in Table 2 shows that the change Ia→Ic is accompanied by a small decrease of the νOH D_1 (end group) frequency ν_2 and by a somewhat larger increase of the D_2 νOH frequency ν_1 (these changes are continuous in the sequence Ia to Ib to Ic). The distance O···O increases and the bond weakens slightly during the rotation Ia→Ic.

The observed [8] thermal process, species A→species B, occurs largely between 8 and 10 K., *i.e.*, in a narrow temperature range, like phase transition processes;[8] this process in N_2 is not considered in the present paper. Our experimental results indicate that above 13 K (our lowest attainable temperature) the major influence of temperature on the νOH D_2 bands is a broadening of the bands, together with a slight decrease of the maximum absorbance. Thus it seems probable that considerable barriers are involved in the interconversion between the "sites".

There are interactions (more or less specific [10]) between the dimers and the matrix lattice, and their influence is seen especially in the τOH region (see below). Thus it is not possible to establish a direct correspondence between the species A–D in Table 1 and the species Ia–Ic discussed above. However, we propose an appoximate correspondence as shown in Table 1. Thus there is at least a qualitative agreement between experiments and the calculations.

Only two interconverting νOH proton donor dimer bands were found in the spectra of methanol in well-annealed *CO matrices* (see Fig. 5). The band at 3498 cm^{-1} decreases and that at 3478 cm^{-1} increases with increasing temperature; these will be called A and B type bands, respectively. The energy difference ΔH between the corresponding species is *ca.* 300–400 J mol^{-1}, as determined from the variation of the peak heights with temperature. Obviously the sites in CO are quite different from those in Ar or N_2, and the strong interactions with the polar CO matrix molecules may dominate (*cf.* Ref. 10). The bands are broader than those in N_2, especial-

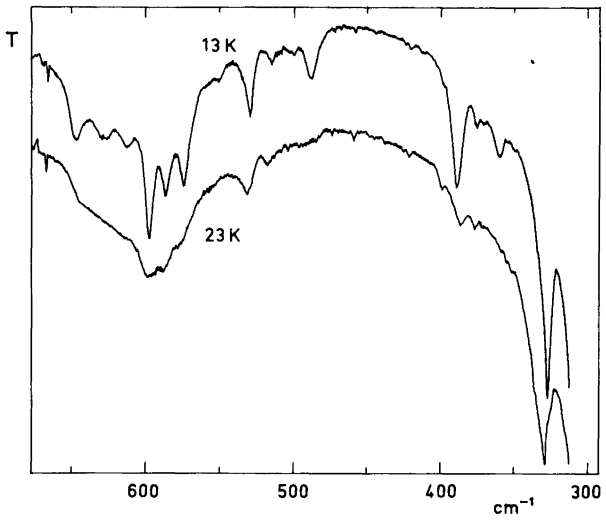

Fig. 6. Part of the τOH region of CH_3OH in N_2, M/A=100, recorded at two temperatures.

ly the lower-frequency band (in unannealed matrices it has a shoulder at 3460 cm^{-1}). The end-group (D_1) bands are obviously at 3618 cm^{-1} (*A*) and *ca.* 3595 cm^{-1} (*B*), indicating that the dimers are non-cyclic (see also Fig. 5).

It can be concluded that the changes corresponding to those which Schriver *et al.* [8]observed in N_2 between 8 and 10 K occur in CO at considerably higher temperatures.

The τ(OD) bands in N_2. The correspondence between the τOH and νOH regions is shown in Figs. 3 and 4, and details of the τOH region in Fig. 6.

The monomer band is at 304 cm^{-1} in N_2 matrix spectra. It is strongly and reversibly temperature dependent.[10]

The dimer τOH end group (D_1) bands are in the region 386–325 cm^{-1}, and the proton donor (D_2) bands in the region 623–572 cm^{-1} (see, *e.g.*, the upper curves in Fig. 4, and the results of the *ab initio* calculations). After the initial irradiation the most intense dimer peaks are those at 325 and 593 cm^{-1}.

There seem to be five τOH dimer D_2/D_1 pairs in the spectra of CH_3OH (Fig. 6, Table 5; the sixth band at 644 cm^{-1} in the D_2 group is due to multimers). The fifth D_2 band (at 459 cm^{-1} in Fig. 7) is weak in the spectra of the OD compounds. Since the conversions due to irradiation are slow also in the case of CD_3OD, it was possible to establish a correspondence between the τOH and νOH dimer fine structures (see Table 5).

To obtain some indication of the magnitude of the specific interaction between nitrogen and methanol, an STO–3G/normal coordinate calculation was carried out with an N_2 molecule bonded to H_5 of species Ia (linear O_2H_5NN arrangement [10]). The τ_2 frequency was then shifted from 385 cm^{-1} to 436 cm^{-1}. Thus it is seen that such interactions influence the "free" end group torsion frequency considerably. Small differences in the distances or angles between the OH group and the surrounding N_2 molecules or the smallness of the basis set used obviously explain why the experimental Δτ̃OH of τ_2 between species Ia and Ic is 61 cm^{-1}, whereas the calculated difference is only 24 cm^{-1}.

The spectra and the calculations (Table 6) suggest that the trimer end group bands are at *ca.* 500 cm^{-1}. A higher-associate end group band is at 644 cm^{-1}, and the polymer proton donor bands occur at *ca.* 800 cm^{-1}. Under favourable conditions a relatively sharp ($\Delta\nu_{1/2}$ *ca.* 10 cm^{-1}) polymer band is seen at 795 cm^{-1} (superimposed on a much broader band), which indicates that well-defined (probably open) polymer structures exist. This band corresponds to the νOH polymer peak at 3240 cm^{-1}.

As is seen in Fig. 6, the τOH association bands in N_2 spectra broaden considerably with increas-

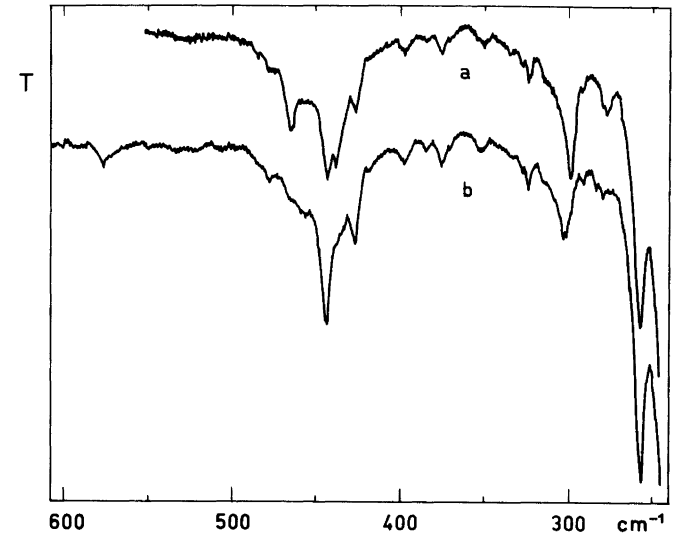

Fig. 7. The τOD region of CD_3OD in N_2, M/A=100. a, after deposition; b, after 20 h in the broad-band IR beam (Nernst irradiation) of the spectrometer.

ing temperature.

The τOD region for CH_3OD and for CD_3OD (see Fig. 7 and Table 5) is similar to the τOH region of CH_3OH, but the peaks are shifted to lower wavenumbers.

A comparison of the calculated τOH (τOD) bands of the associates with the experimental values in N_2 is presented in Table 6. A relatively good correspondence is seen to exist.

We have observed some indication of analogous torsional association fine structure in the spectra of 2-chloroethanol in Ar, and a correspondence between the νOH and τOH dimer fine structures in the spectra of allyl alcohol in Ar.[30] These findings are exceptional, and the dimers obviously involve specific structures other than

Table 6. Comparison of the calculated and observed wavenumbers (in cm^{-1}) of the OH torsion. E denotes the end group of an open associate.

Species	Tors. at	CH_3OH		CH_3OD		CD_3OD	
		Calc.	Obs.	Calc.	Obs.	Calc.	Obs.
Monom.	O_1	304	304	241	246	221	239
Open dim. Ia	O_1	625	623	486	468	455	466
	O_2(E)	385	386	310	~300	284	300
Open dim. Ic	O_1	597	593	463	446	435	444
	O_2(E)	361	325	290	263	266	258
Linear trim.	O_1	731	} 700–750	560	} 520–560	532	} 520–560
	O_2	762		587		557	
	O_3(E)	420	485	340	353	311	352
Cycl. trim.	O_1	774	} 700–800 possible	544		574	
	O_2	789		506	(650)	580	
	O_3	747		576		546	
Double accept. trim.	O_1	567		436		412	
	O_2(E)	494		406		363	
	O_3	570		440		414	

trapping site structures.

The τOH bands in CO. The quite symmetric monomer band is at 362 cm^{-1}. Its temperature dependence has been discussed previously.[10]

The τOH region of the IR spectrum of a CO matrix (Fig. 5) is similar to that of an N_2 matrix, but the association bands are much weaker and fewer bands are seen; the latter is to be expected, since only two νOH proton donor dimer bands were found. The dimer D_1 bands are at 400 cm^{-1} (type *A*) and at 450 cm^{-1} (type *B*), and the relatively broad D_2 bands are at 565 and 635 cm^{-1}, respectively. The sharp proton donor polymer band is at 785 cm^{-1}, and the other proton donor polymer/oligomer bands at 690–750 cm^{-1}. Methanol is less associated in CO than in N_2. The prevailing associates in CO are dimers and polymers, and thus trimer τOH bands could not be identified with certainty in the spectra.

The other fundamentals. The experimental results seem to indicate that the end group bands of the δOH and νCO vibrations of open associates occur at frequencies lower than the frequency of the monomer band (in accordance with the literature [2,31,32]). The calculations predict this effect for δOH but fail in the case of νCO (our calculations are too approximate to deal with the coupling of the δOH and νCO modes).

The calculated frequencies for the intermolecular modes of the open dimers (see Table 2) are as good as is the assumption of a common force constant reduction factor. The following comments can, however, be made:

(1). A good PED is obtained for these modes (considerably better than that obtained when the angle $O_1H_1O_2$ is used instead of the angle $C_1O_1O_2$). We thus conclude that the coordinates used are a meaningful approximation to the intermolecular normal modes.

(2). The value 222 cm^{-1} has been reported [2] for the H-bond stretching fundamental of the dimer in Ar; our calculated value is 192 cm^{-1}.

(3). The frequency for the torsion τ_4 around the O_1O_2 axis in the dimer is quite low (our calculated value is 18 cm^{-1}). The potential is very flat at the minimum, as is shown in Fig. 2.

(4). No bands in N_2 or CO matrix spectra were assigned to intermolecular modes.

IR-induced interconversion of dimers. In the case of 2-substituted ethanols, such as the 2-haloethanols,[33,26] 2-aminoethanol [34] and 2-nitroethanol,[35] IR radiation at the νOH frequency causes conformational changes in matrices, *i.e.*, the vibrational excitation energy must have been transferred into torsional states. The coupling between the νOH and torsional states is probably due to interactions with the matrix medium.

In the case of the methanol dimers, it is even more difficult to establish a mechanism for the IR-induced interconversion. The "bonded" νOH vibration of methanol dimer Ia is obviously responsible for the absorption of the IR energy. We assume that the initially excited state goes over into a highly excited state (or states) of torsion τ_1, the hydrogen bond $H_1\cdots O_2$ providing the necessary coupling term. In such states the amplitudes of the torsions are large, or there may exist almost free internal rotation. On the other hand, inspection of molecular models shows that relatively small motions of the molecules, or especially of the OH protons, are needed for the formation of a cyclic dimer. It represents a local energy minimum (at least the planar dimer II can be optimized on the STO–3G level with respect to all intermolecular coordinates), *i.e.*, it plays the role of an unstable intermediate (not transition state) often encountered in chemical kinetics. The cyclic (not necessarily planar) dimer decomposes into species Ic, or back into species Ia. Thus, although the intermediate is unstable, it is stable enough to facilitate the rearrangement of the dimer into species Ic.

Formation of a cyclic dimer from species Ic requires larger molecular motions than its formation from species Ia. This explains why the reverse reaction is slow.

The reaction is slow also in the case of OD methanols, since the deuterium atom is heavier than the hydrogen atom, and the amplitudes of the OD torsions are smaller than those of the corresponding OH torsions. This would explain also why the D-bonds prevail in the mixed dimers.

On the other hand, it is also possible that the energy pit of the cyclic dimer is relatively deep, and that its rearrangement into open species occurs primarily *via* tunnelling, which would be faster for a protium atom than for a deuterium atom. This latter mechanism would also explain the preference of D-bonding in the case of the mixed dimer, since the H-bond in the cyclic heterodimer is broken faster than the D-bond.

The energy of the νOH quantum (*ca.* 3500

cm^{-1}) corresponds to 42 kJ mol^{-1}, which is sufficient to dissociate the dimer into monomers. If such a dissociation occurs, it is followed by an immediate recombination inside the site cage, during which a rearrangement of the dimer is possible.

It may be mentioned in this connection that Fredin *et al.*[36] found that, in the case of HOD dimers in N_2 matrices, the species DOH···O(D)H is transformed into HOD···O(D)H in a thermal dark reaction, whereas the reverse reaction takes place due to IR irradiation. Also these processes may involved a cyclic (or bifurcated) intermediate, since it is impossible for the dimer to be broken into monomers in a thermal process under matrix conditions. It has been found,[37] using a large basis set and including a correlation correction, that a cyclic non-planar water dimer has an energy only *ca.* 4 kJ mol^{-1} higher than that of the linear dimer.

CONCLUDING REMARKS

The fine structure of the νOH and τOH dimer bands of methanol in matrices is obviously related to different positions of the two methanol units around the O···O axis.

Low-frequency modes such as the OH or NH_2 torsions have been studied very little using matrix infrared spectroscopy. However, such studies seem promising, since at least these torsional frequencies are sensitive to association and other intermolecular influences.

The approximate calculation method in this paper is successful in the case of τOH, since the relative frequency changes due to association are then large, and the torsions are only slightly coupled with each other or with other modes. Neglect of the variation (obviously small) of the torsional force constant reduction factor upon association does not lead to serious errors.

In the case of νOH the relative frequency changes due to association are much smaller, and the accompanying changes in the reduction factor cannot be neglected. Our calculations indicate that a coupling term is needed between the OH and H-bond stretchings in the linear dimers. There are coupling terms of unknown magnitude in the case of the cyclic dimer and all trimers (and of higher associates). For these reasons we did not attempt to predict the νOH wavenumbers for associates other than the linear dimers.

For the first time for an alcohol in matrices, a detailed τOH association fine structure has been found and the bands assigned. The dimer end group τOH band is shifted relatively little from the monomer band, whereas for the higher associates these shifts are considerable.

The calculations and the experimental evidence indicate for CH_3OH that the torsional dimer bands below 400 cm^{-1} and the trimer bands near 500 cm^{-1} are due to end groups of open dimers and trimers, respectively, and that the multimer band at 644 cm^{-1} is due to end groups of linear or branched species. The presence of cyclic or double acceptor trimers is not completely excluded. However, it can be concluded that the major features of the τOH region of the spectra of methanol in N_2 (and also in CO) can be explained in terms of non-cyclic associates. As the association proceeds, the alcohol chains become longer (and possibly branch). Raman spectra [38] and calculations using statistical mechanics [22,39] give the result that liquid methanol consists primarily of long H-bonded chains.

The cyclic trimer is predicted by the STO–3G calculations to be more stable than "linear" trimers. However, the calculated energy difference was only 8 kJ mol^{-1}, the basis used was small, and no supermolecule or dispersion energy corrections were made. Thus, more sophisticated calculations on the trimers are needed. The same applies to the cyclic dimer (the open dimer has been calculated using larger basis sets [23]).

On the other hand, although the cyclic trimer may be more stable in vapour than linear trimers, the cyclic species do not necessarily prevail in non-equilibrium systems like matrices.

REFERENCES

1. Van Thiel, M., Becker, E. D. and Pimentel, G. C. *J. Chem. Phys. 27* (1957) 95.
2. Barnes, A. J. and Hallam, H. E. *Trans. Faraday Soc. 66* (1970) 1920.
3. Mallinson, P. D. and McKean, D. C. *Spectrochim. Acta A 30* (1974) 1133.
4. Serrallach, A., Meyer, R. and Günthard, Hs. H. *J. Mol. Spectrosc. 52* (1974) 94.
5. Serrallach, E. and Meyer, R. *J. Mol. Spectrosc. 60* (1976) 246.

6. Burneau, A., Loutellier, A. and Schriver, L. *J. Mol. Struct. 61* (1980) 397.
7. Luck, W. A. P. and Schrems, O. *J. Mol. Struct. 60* (1980) 333.
8. Schriver, L., Burneau, A. and Perchard, J. P. *J. Chem. Phys. In press.*
9. Murto, J., Kemppinen, E. and Ovaska, M. *Abstract of paper presented at the 3rd International Meeting on Matrix Isolation,* Nottingham, England, 20–24th July, 1981.
10. Murto, J. and Ovaska, M. *Spectrochim. Acta. A 39* (1983) 149.
11. Stuart, A. V. and Sutherland, G. B. B. M. *J. Chem. Phys. 20* (1952) 1977.
12. Pimentel, G. C. and McClellan, A. L. *The Hydrogen Bond,* Freeman, San Francisco 1960, p. 128.
13. Falk, M. and Whalley, E. *J. Chem. Phys. 34* (1961) 1554.
14. Perchard, J. P. and Josien, M.-L. *J. Chim. Phys. Phys.-Chim. Biol. 65* (1968) 1856.
15. Rosenberg, M. Sh. and Iogansen, A. V. *Opt. Spektrosk. 31* (1971) 711.
16. McDonald, M. P. and Wilford, L. D. R. *Spectrochim. Acta A 29* (1973) 1407.
17. Rossarie, J., Gallas, J.-P., Binet, C. and Romanet, R. *J. Chim. Phys. Phys.-Chim. Biol. 74* (1977) 202.
18. Murto, J., Kivinen, A., Edelmann, K. and Hassinen, E. *Spectrochim. Acta A 31* (1975) 479.
19. Strandman-Long, L. and Murto, J. *Spectrochim. Acta A 37* (1981) 643.
20. Del Bene, J. E. *J. Chem. Phys. 55* (1971) 4633.
21. Curtiss, L. A. *Int. J. Quantum Chem. Symp. 11* (1977) 459.
22. Jorgensen, W. L. *J. Chem. Phys. 71* (1979) 5034.
23. Tse, Y.-C., Newton, M. D. and Allen, L. C. *Chem. Phys. Lett. 75* (1980) 350.
24. Curtiss, L. A. *J. Chem. Phys. 67* (1977) 1144.
25. Brink, G. and Glasser, L. *J. Comput. Chem. 2* (1981) 14.
26. Murto, J., Räsänen, M., Aspiala, A. and Homanen, L. *J. Mol. Struct. (Theochem.) 92* (1983) 45.
27. Timidei, A. and Zerbi, G. *Z. Naturforsch. Teil A 25* (1970) 1729.
28. Blom, C. E., Otto, L. P. and Altona, C. *Mol. Phys. 32* (1976) 1137.
29. Cummings, D. L. and Wood, J. L. *J. Mol. Struct. 20* (1974) 1.
30. Aspiala, A., Murto, J. and Räsänen, M. *Unpublished results.*
31. Kabish, G. and Pollmer, K. *J. Mol. Struct. 81* (1982) 35.
32. Felder, P. and Günthard, Hs. H. *Chem. Phys. Lett. 88* (1982) 473.
33. Pourcin, J., Davidovics, G., Bodot, H., Abouaf-Marguin, L. and Gauthier-Roy, B. *Chem. Phys. Lett. 74* (1980) 147.
34. Räsänen, M., Aspiala, A., Homanen, L. and Murto, J. *J. Mol. Struct. 96* (1982) 81.
35. Räsänen, M., Aspiala, A. and Murto, J. *J Chem. Phys. In press.*
36. Fredin, L., Nelander, B. and Ribbegård, G. *J. Chem. Phys. 66* (1977) 407.
37. Kistenmacher, H., Lie, G. C., Popkie, H. and Clementi, E. *J. Chem. Phys. 61* (1974) 546.
38. Perchard, C. and Perchard, J. P. *Chem. Phys. Lett. 27* (1974) 445.
39. Jorgensen, W. L. *J. Am. Chem. Soc. 102* (1980) 543; Jorgensen, W. L. and Ibrahim, M. *J. Am. Chem. Soc. 104* (1982) 373.

Received September 1, 1982.

Acta Chemica Scandinavica A 37 (1983) 337–339

Further *ab initio* Calculations on the Molecular Structure of Methylcyclopropane

ANNE SKANCKE

Department of Chemistry, Institute of Mathematical and Physical Sciences, University of Tromsø, Box 953, N-9001 Tromsø, Norway

The molecular structure of methylcyclopropane has been investigated *ab initio* calculations. The results are compared with earlier theoretical calculations, a microwave study and a recent electron diffraction work.

In a series of articles we have studied the effect of various substituents on the structure of the cyclopropane ring.[1] These studies were carried out within the Hartree-Fock approximation. In the first articles in the series, only the key structure parameters were optimized; the optimizations being carried out consecutively. When the computer programme TEXAS [2] became available to us, these calculations were carried out more efficiently and also more accurately, since the program calculates the forces on all atoms leading to a simultaneous optimization of all internal parameters. Also, we were now able to carry out complete geometry calculations including, for instance, deformations from local C_{2v} symmetry of methylene groups. In this way, more insight into the fine details of molecular structure is given. As for the accuracy of our calculations on these specific compounds, we have in several cases shown them to be at least as reliable as experimental works.[3–6]

In a recent paper by Klein and Schrumpf,[7] an electron diffraction study of methylcyclopropane and *trans*-1,2-dimethylcyclopropane is carried out, the former being compared to the results of our previous calculations.[3] Although the two works may be construed to be in essential agreement when the experimental errors are taken into account, the authors of the experimental work point out the difference in relative magnitude of the ring and exocyclic CC bonds between the two works. We have therefore recalculated the structure of methylcyclopropane using the computer programme TEXAS.

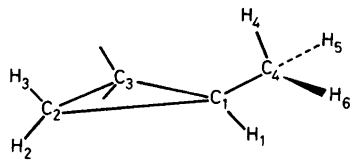

Fig. 1. Numbering of atoms in methyl cyclopropane.

We have, in the present calculation, carried out complete geometry optimizations for both the eclipsed and staggered forms. In our previous articles in this series, optimizations were carried out at the 4–21 level,[8] but since in the present work we are looking for very small variations in bond distances, we have carried out complete optimizations also with the 4–31G basis set which contains one extra primitive function at each of the heavy atoms, the number of contracted basis functions being the same as for the 4–21 set. A typical run with the latter basis set used about 20 % more computer time. The results of the calculations are given in Table 1.

RESULTS AND DISCUSSION

As is seen from Table 1, all C–C bonds are predicted to be larger in the 4–21 calculations compared to the slightly larger 4–31G basis set.

0302-4377/83 $02.50

Table 1. Calculated geometric parameters (in Å and degrees), dipole moments (in debyes) and barriers to internal rotation for methyl cyclopropane (in kJ/mol). See Fig. 1 for numbering of atoms).

Bond/angle	Eclipsed form		Staggered form	
	4–31G	4–21	4–31G	4–21
C_1-C_2	1.503	1.517	1.502	1.515
C_2-C_3	1.501	1.515	1.504	1.518
C_1-C_4	1.519	1.529	1.506	1.516
C_2-H_3	1.071	1.072	1.070	1.072
C_2-H_2	1.070	1.071	1.070	1.071
C_1-H_1	1.071	1.072	1.072	1.073
C_4-H_4	1.081	1.083	1.082	1.083
C_4-H_5	1.081	1.082	1.083	1.083
$\angle C_1C_4H_4$	110.7	110.8	111.3	110.8
$\angle C_1C_4H_5$	111.5	111.4	111.1	111.0
$\angle H_4C_4H_5$	107.3	107.5	107.5	107.9
$\angle H_5C_4H_6$	108.4	108.1	108.1	108.1
$\angle C_4$–ring plane	54.3	54.6	54.0	54.8
$\angle C_4C_1H_1$	114.4	114.9	114.3	114.8
$\angle H_2C_2H_3$	114.0	114.6	114.0	114.5
θ_{wag} [a]	0.0	0.0	0.0	0.1
θ_{rock} [b]	–0.5	–0.4	–0.2	–0.2
θ_{twist} [c]	0.2	0.6	0.0	0.5
$\lvert\mu\rvert$	0.15	0.13	0.14	0.10
V_3	11.29	11.23		

[a] $\theta_{wag}=(\alpha_{12}+\alpha_{13})-(\alpha_{32}+\alpha_{33})$;
[b] $\theta_{rock}=(\alpha_{12}+\alpha_{32})-(\alpha_{13}+\alpha_{33})$;
[c] $\theta_{twist}=(\alpha_{12}-\alpha_{32})-(\alpha_{13}-\alpha_{33})$; where $\alpha_{ik}=\angle C_iC_2H_k$.

Table 2. Key bond distances (Å) for methyl cyclopropane. Results from previous work.

Bond	Method M.W.[a]	E.D.[b](r_a)	SCF [c]
C_1-C_2	1.514	1.509(1)	1.517
C_2-C_3			1.519
C_1-C_4	1.513	1.517(2)	1.500

[a] Ref. 9. [b] Ref. 7. [c] Ref. 3.

Comparison with experimental values (see Table 2) gives us reason to believe that the 4–21 basis set may even be superior to the larger set when structure refinements are carried out. We have in this series of articles extensively been using molecular structures as indicators of intramolecular electronic interactions but, as we have pointed out before, it is especially important to have good quality trends in structures.

The internal consistency in Table 1 gives us reason to believe that trends are indeed well reproduced in the present work, although absolute values in C–C bond lengths may well differ by several thousands of an Ångström compared to experimental data. Our limited basis on hydrogen gives us C–H distances definitely too short, but since there is a systematic trend also in these, we believe their relative magnitudes to be of considerable better quality than their absolute values.

Our earlier calculation of this molecule [3] gave two nearly identical ring distances (1.517 and 1.519 Å for adjacent and opposite bond, respectively) and a C_1-C_4 bond distance of 1.500 Å. See Table 2. Calculations were carried out only for the staggered form. These results deviate from the present where the lowest energy form for both basis sets has an external C–C bond that must be considered as identical in length to the nearly identical ring bonds.

There is a microwave investigation of methyl cyclopropane,[9] but the number of observables did not suffice for a complete structure determination. Based on the assumption of an equilateral ring with distances equal to 1.514 Å, a C_1-C_4 bond of 1.513 Å was in agreement with observed data. A number of structures may be construed to be in agreement with this microwave work, depending on the actual ring size of the molecule. Thus, a lengthening of the C_1-C_2 bond would lead to a shortening of the C_1-C_4 bond and *vice versa,* the experimental moments of inertia giving a high precision determination of the overall size of the molecule. Thus, the results of our previous calculations as well as the electron diffraction results and the results from the present 4–21 calculations are equally well in agreement with the microwave work. Additional support of the latter is, however, given in the calculated, V_3 potential which agrees well with the experimental [9] of 11.95 kJ/mol and the total dipole moment that agrees well with the experimental [9] of 0.14 D.

Our results give nearly identical structures for the eclipsed and staggered forms, the only difference being in the C_1-C_4 which is lengthened in the high energy form.

The calculated value of the angle between the methyl group and the ring is 2 degrees smaller

than the electron diffraction result of 56.7°. The present result gives practically no distortions of the CH_2 groups; this was an assumption in the electron diffraction work. There is, however, a minute distortion from C_{3v} symmetry of the methyl group for the eclipsed form. This was apparently an additional assumption in the experimental work, although not explicitly mentioned therein. We believe that our computed distortions should be considered reliable, the calculated differences between bond angles and bond lengths being determined more reliably than their absolute values.

At this point an interesting comparison may be made to results of calculations on cyclopropylsilane.[10] This has been carried out with the same procedure and with a basis set compatible with the present work. The computed distortion of the methyl group closely parallels the SiH_3 group distortions.

In cyclopropylsilane, there is a lengthened C_1-C_2 bond and a C_2-C_3 bond unchanged from the parent compound. The authors of that work attribute this to the combined effect of pi and sigma donation from the substituent to the ring. From the results of the present work, it appears that any such charge flow must be negligibly small for methyl cyclopropane, a result compatible with the higher electronegativity of carbon as compared to silicon.

As a final comment, we find the present calculations to be in good agreement with both the electron diffraction work and the microwave study. Any disagreement of a few thousands of an Ångström may be attributed to the fact that the electron diffraction data give the r_a structure while our values are r_e values. Also, the slightly longer C_1-C_4 bond length in the electron diffraction work may be attributed to admixture of non-staggered forms, since it is seen from Table 1 that the eclipsed form has indeed a lengthened C_1-C_4 bond.

REFERENCES

1. Skancke, A. *Acta Chem. Scand. A 36* (1982) 637 and references therein.
2. Pulay, P. *Theor. Chim. Acta 50* (1979) 299.
3. Skancke, A. and Boggs, J. E. *J. Mol. Struct. 50* (1978) 173.
4. Skancke, A. *J. Mol. Struct. 42* (1977) 235.
5. Mathur, S. N. and Harmony, M.D. *J. Chem. Phys. 69* (1978) 4316.
6. Hedberg, L., Hedberg, K. and Boggs, J. E. *J. Chem. Phys. 77* (1982) 2996.
7. Klein, A. W. and Schrumpf, G. *Acta Chem. Scand. A 35* (1981) 425.
8. Pulay, P., Fogarasi, G., Pang, F. and Boggs, J. E. *Theor. Chim. Acta 50* (1979) 299.
9. Ford, R. G. and Beaudet, R. A. *J. Chem. Phys. 48* (1968) 4671.
10. Oberhammer, H. and Boggs, J. E. *J. Mol. Struct. 57* (1979) 175.

Received August 30, 1982.

Acta Chemica Scandinavica A 37 (1983) 341–352

On the Molecular Structure of Bis(trichloromethyl) Sulfone from Electron Diffraction and Vibrational Spectra of Bis(trichloromethyl) and Bis(tribromomethyl) Sulfone

MAGDOLNA HARGITTAI,[a] ERZSÉBET VAJDA,[a] CLAUS J. NIELSEN,[b] PETER KLÆBOE,[b] RAGNHILD SEIP [b] and JON BRUNVOLL [c]

[a] Department of Structural Studies, Research Laboratory for Inorganic Chemistry, Hungarian Academy of Sciences, P.O.B. 117, Budapest, H-1431, Hungary,[b] Department of Chemistry, University of Oslo, Blindern, Olso 3, Norway and [c] Department of Physical Chemistry, The University of Trondheim, N-7034 Trondheim NTH, Norway

Gaseous $(CCl_3)_2SO_2$ was studied by electron diffraction at a nozzle temperature of 100 °C, while $(CBr_3)_2SO_2$ decomposed at a temperature of 140 °C.

Infrared spectra of the two sulfones as pellets, as melts and as solutes in various solvents were recorded in the region 4000–50 cm^{-1}. Raman spectra of the sulfones as polycrystalline solids, as saturated solutions in benzene and carbon tetrachloride, as a melt ($(CCl_3)_2SO_2$) and as a single crystal ($(CBr_3)_2SO_2$) were obtained. The electron diffraction analysis of $(CCl_3)_2SO_2$ yielded C_2 symmetry with the two CCl_3 groups twisted in the opposite direction from the C_{2v} position by 12° and tilted by 5° from each other. The most important geometrical data in terms of r_g and $\angle_\alpha$ parameters are: S=O 1.419(3) Å, S–C 1.894(5) Å, C–Cl 1.757(4) Å, ∠O–S–C 106.5(3)°, ∠C–S–C 109.8(4)°, ∠O–S–O 120.8(1.0)°, ∠Cl–C–Cl 110.2(1)°.

For both compounds the vibrational spectra could be interpreted either in terms of C_{2v} or C_2 symmetry. Apart from the two torsional modes expected below 50 cm^{-1}, the fundamentals for both compounds have been assigned.

The molecular structures of a relatively large series of sulfone derivatives with various ligands have recently been determined.[1,2] The observed structural variations were interpreted primarily in terms of the valence shell electron pair repulsion model.[2,3] The molecular structures and vibrational spectra of halogenated sulfones $(CX_3)_2SO_2$ seemed interesting for testing these observations on molecules with relatively bulky substituents.

EXPERIMENTAL

Commercial samples (K&K ICN Pharmaceuticals) were used in the electron diffraction, infrared and Raman experiments without further purification. Gas chromatographic analysis revealed that both compounds were more than 99 % pure.

The electron diffraction patterns of both compounds were recorded on the Balzers Eldigraph KD–G2 in Oslo. For $(CCl_3)_2SO_2$ (TCMS) the standard experimental conditions [4,5] were applied with a nozzle temperature of 100 °C. The reduced molecular intensities are shown in Fig. 1. Neither the experiment nor the structure analysis showed any indication of decomposition of the TCMS sample during the electron diffraction experiment. For $(CBr_3)_2SO_2$ (TBMS) both the standard [4,5] and the low pressure [6] techniques were used for recording the electron diffraction pattern, the latter in order to keep the experimental temperature as low as possible to prevent decomposition of the compound in the vapour phase. Nevertheless, the data analysis of the bromine compound showed a considerable degree of decomposition in the vapour. Since we were not able to overcome this difficulty, the molecular geometry of TBMS could not be determined.

0302-4377/83 $02.50

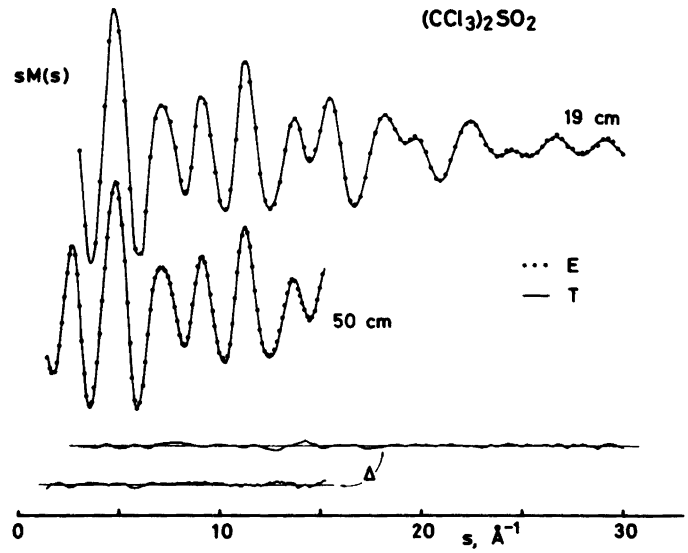

Fig. 1. Experimental (E) and theoretical (T) molecular intensities and their differences (△D) for $(CCl_3)_2SO_2$.

The infrared spectra were recorded with a Perkin-Elmer model 225 (4000–200 cm^{-1}) spectrometer and an evacuable, fast scan Fourier transform spectrometer (Bruker 114c) (600–50 cm^{-1}). Crystalline solids of TCMS and TBMS were recorded as KBr, KI and polyethylene pellets. Solutions in CCl_4, CS_2, C_6H_6 and C_6H_{12} were recorded in sealed cells with windows of KBr and polyethylene. Both compounds were recorded as melts between CsI plates, TCMS was perfectly stable as a melt. For TBMS a slight decomposition occurred at 100 °C, at 150 °C the spectrum changed considerably in 30 min.

The Raman spectra were recorded on a modified Cary 81 spectrometer, excited by an argon ion laser (CRL 52 G) using the 5145 Å line for excitation.

RESULTS

Structural analysis. The molecular model and numbering of the atoms in TCMS are shown in Fig. 2. Since TBMS decomposed during the ED experiments, no structural results for this compound were obtained. Although in similar symmetrically substituted X_2SO_2 sulfones the molecular symmetry is usually C_{2v} (either determined or assumed) with such bulky ligands as CCl_3 and CBr_3, we did not feel justified in making such an assumption. The IR and Raman spectra of TCMS and TBMS could be reasonably well interpreted in terms of C_{2v} symmetry, but small deviations due to arrangements of the trichloromethyl groups could not be excluded.

Keeping these arguments in mind for the electron diffraction structure refinement, the rotation of the CCl_3 groups around the S–C axis as well as the tilt of the trichloromethyl groups from the same axis were taken into account. In this way the C_{2v} symmetry was decreased to either C_2, C_s or even C_1. The only assumptions regarding the molecular geometry were: (i) The OSO plane bisects the CSC plane, (ii) The local symmetry of the CCl_3 groups is C_{3v}.

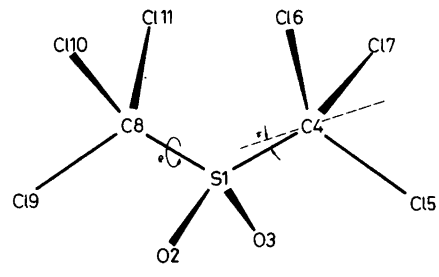

Fig. 2. C_{2v} symmetry molecular model for $(CCl_3)_2SO_2$.

The geometry of the molecule was then determined by the following eight parameters: r(S=O), r(C−Cl), r(S−C), ∠O−S−O (or r(O···O), see later), ∠S−C−Cl, ∠O−S−C, ρ (rotation angle of the CCl_3 groups around the S−C axis; the angle is zero in the C_{2v} position shown in Fig. 2) and τ (tilt of the CCl_3 groups; *i.e.* rotation of CCl_3 in the CSC plane around an axis through C and perpendicular to the CSC plane; the positive sign of this angle means the two CCl_3 groups move away from each other).

Our experience with the structure analysis of simple sulfones [7] showed that one of the most sensitive and not very well determined parameters is the O=S=O angle. At the first stage of the structure refinement we therefore made use of the observed invariance of the r(O···O) distances in the sulfone series [1,2] and kept it at 2.485 Å. In the final stage of the refinement, however, this constraint was removed. Although the O···O non-bonded distance decreased considerably (about 0.02 Å) this parameter influenced the other structural parameters only within their experimental errors.

Normal coordinate analysis was carried out based upon the experimental vibrational frequencies. Since the two lowest torsional frequencies were not observed in the spectra and the calculated vibrational amplitudes (both parallel and perpendicular) are quite sensitive to the torsional force constant, we proceeded in the following way. The value of the torsional force constant was varied in a wide range 0.005−0.030 mdyn Å rad^{-2} and the calculated parallel mean vibrational amplitudes were compared with the experimental values. The set closest to the experimental one and corresponding to τ=0.025 mdyn Å rad^{-2} was selected and its perpendicular amplitudes were used to transform the r_a to r_α parameters. The least squares refinement of the molecular structure was carried out on the r_α structure. Although the large amplitude torsional motion of the CCl_3 groups introduces some uncertainty into these correction terms, our test calculations for this molecule as well as our experience with other CCl_3 derivatives, *viz.* CCl_3SO_2Cl,[11] showed no appreciable bond angle changes in terms of r_a/r_α refinements.

The best agreement with the experimental data was achieved with a C_2 symmetry model, in which the two CCl_3 groups were rotated 12° in the opposite direction from the C_{2v} position shown in Fig. 2 and tilted away from each other about 5°.

The experimental radial distribution curve and the difference between the experimental and the theoretical curve for the final C_2 symmetry model is shown in Fig. 3. The positions of the interatomic distances with their relative weights are also indicated.

The geometrical parameters determined for TCMS together with the experimental and calculated vibrational amplitudes are collected in Table 1.

Spectral interpretations. IR spectrum of a capillary film of molten TCMS between CsI plates at

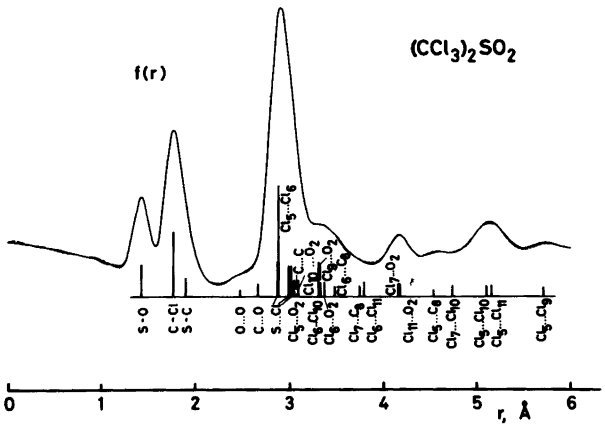

Fig. 3. Experimental (E) and theoretical (T) radial distribution curves for the final C_2 symmetry model of $(CCl_3)_2SO_2$.

Table 1. Structural parameters of $(CCl_3)_2SO_2$.

Parameters	r_a,$\angle_\alpha$ Å, degree	l(ED) Å	l(calc) Å	K(calc) Å
Independent				
S=O	1.418(3)	0.038(2)	0.036	0.0085
C–Cl	1.756(4)	0.046(2)	0.055	0.0154
S–C	1.892(5)	0.059(6)	0.056	0.0049
O···O	2.464(15)	0.099(16) [c]	0.060	0.0124
O–S–C	106.5(3)			
S–C–Cl [a]	108.8(1)			
ρ [b]	12.4(4)			
τ [b]	4.9(3)			
Dependent				
O···C	2.665(8)	0.122 [c]	0.084	0.0081
S···Cl_5	2.873(10)	0.091(2) [d]	0.094	0.0121
Cl_5···Cl_6	2.878(6)	0.074 [d]	0.077	0.0224
S···Cl_7	2.989(6)	0.080 [e]	0.078	0.0119
S···Cl_6	3.022(7)	0.077(3) [e]	0.076	0.0115
Cl_5···O_2	3.052(13)	0.168 [e]	0.163	0.0145
C···C	3.091(9)	0.099 [l]	0.099	0.0028
Cl_{10}···O_2	3.092(13)	0.152 [e]	0.151	0.0146
Cl_6···Cl_{10}	3.309(14)	0.271 [f]	0.285	0.0204
Cl_9···O_2	3.326(12)	0.143 [f]	0.157	0.0130
Cl_6···O_2	3.371(12)	0.137(6) [f]	0.151	0.0125
Cl_6···C_8	3.482(11)	0.163 [f]	0.177	0.0092
Cl_7···C_8	3.746(11)	0.151(16) [g]	0.178	0.0072
Cl_6···Cl_{11}	3.799(20)	0.295 [g]	0.318	0.0082
Cl_7···O_2	4.160(9)	0.090(5) [h]	0.081	0.0106
Cl_{11}···O_2	4.168(9)	0.094 [h]	0.084	0.0103
Cl_5···C_8	4.539(12)	0.113(13) [i]	0.106	0.0037
Cl_7···Cl_{10}	4.740(18)	0.269 [i]	0.258	0.0033
Cl_5···Cl_{10}	5.112(12)	0.173(6) [j]	0.197	0.0053
Cl_5···Cl_{11}	5.156(12)	0.141 [j]	0.165	0.0040
Cl_5···Cl_9	5.726(19)	0.129(14) [k]	0.148	0.0045
O–S–O	120.8(10)			
C–S–C	109.8(3)			
Cl–C–Cl	110.2(1)			

[a] Mean value, refers to the untilted position of the CCl_3 groups. [b] For definition, see the text. [c–k] Mean amplitudes refined in groups. [l] Fixed at the calculated value.

60 °C is shown in Fig. 4, while a far IR spectrum of a saturated solution in cyclohexane is presented in Fig. 5. A Raman spectrum of TCMS melted in an evacuated tube is shown in Fig. 6.

For TBMS IR spectra of KBr and polyethylene pellets are shown in Figs. 7 and 8, respectively. A far IR spectrum of TBMS in benzene solution is given in Fig. 9, whereas a Raman spectrum of a single crystal is presented in Fig. 10. The wave numbers of the observed IR and Raman bands of TCMS and TBMS are listed in Tables 2 and 3, respectively.

As discussed above, the present compounds can have C_{2v}. C_2, C_s or C_1 symmetry. In principle it should be possible to determine the molecular symmetry from the vibrational spectra. However, no vapour spectra could be recorded due to the very low volatilities. Moreover, there was a

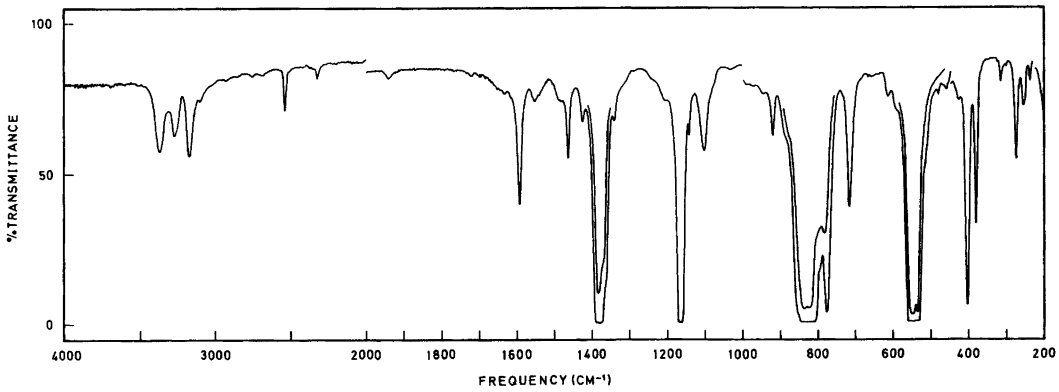

Fig. 4. Infrared spectrum of $(CCl_3)_2SO_2$ as a capillary melt at *ca.* 70 °C between CsI plates.

considerable overlap of bands particularly in the low frequency region, making the spectral data incomplete. For both compounds the IR and Raman data could be interpreted in terms of C_{2v} symmetry (9 a_1, 5 a_2, 7 b_1 and 6 b_2) as previously done for dimethylsulfone [8] and diphenylsulfone.[9] The a_2 modes should in this case be depolarized in Raman and inactive in IR, and very few such cases were observed in the spectra. Preliminary force constant calculations revealed that practically all the a_2 modes overlapped other modes. Both for TCMS and TBMS the spectra were easily interpreted in terms of C_{2v} symmetry and the number of polarized Raman bands agreed quite well with the 9 a_1 modes expected.

Since the results obtained from electron diffraction favoured C_2 symmetry for TCMS (see above), we have interpreted the spectra of both compounds in terms of this symmetry. The vibrational fundamentals should divide themselves between 14 *a* and 13 *b*, the former should be polarized, the latter depolarized in Raman. The assigned fundamentals for TCMS and TBMS are listed in Table 4, together with the calculated frequencies.

As is apparent from Table 4, the majority of

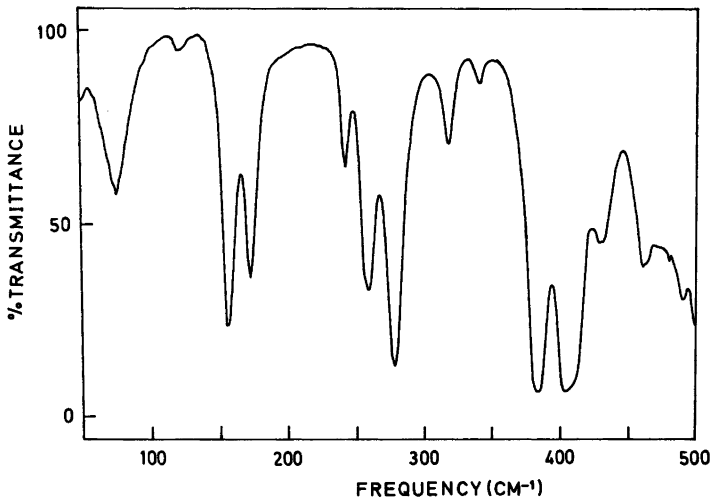

Fig. 5. Infrared spectrum of $(CCl_3)_2SO_2$ as a saturated solution in C_6H_{12}, 1 mm polyethylene cell, 6 μm beamsplitter.

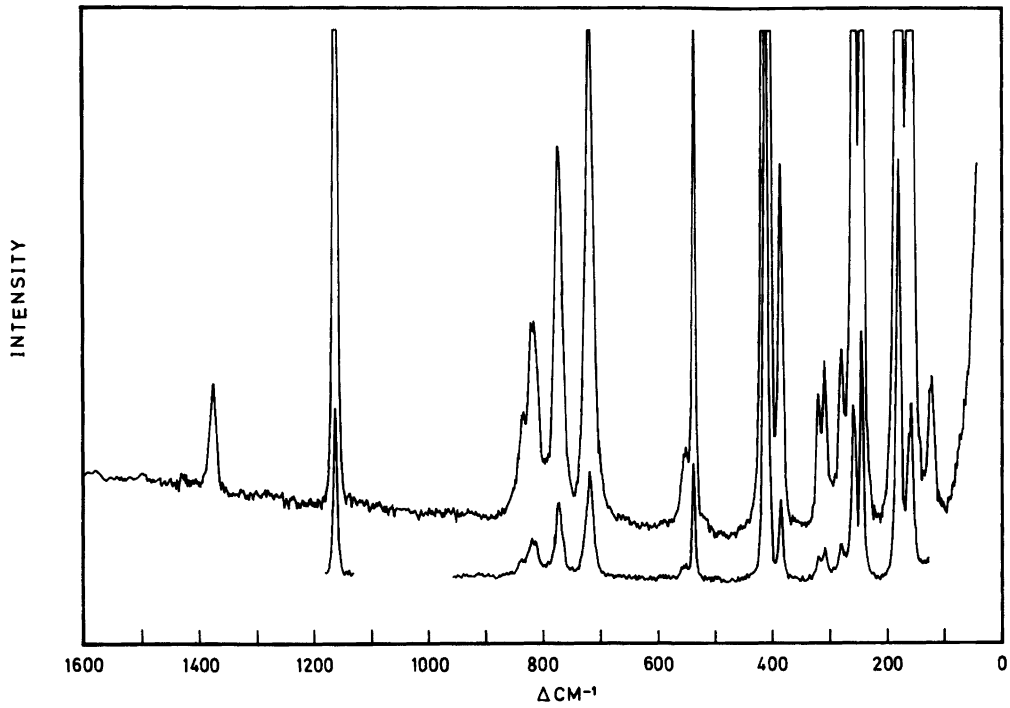

Fig. 6. Raman spectrum of $(CCl_3)_2SO_2$ as a melt at *ca.* 70 °C.

the *a*-fundamentals of TCMS and TBMS were experimentally observed as polarized in Raman. Since the polarization ratios of *a*-fundamentals can lie close to 3/4, the apparent depolarized bands assigned as ν_7 and ν_8 of TCMS and as ν_4 of TBMS represent no serious objection to the interpretations. On the other hand, no polarized Raman bands were assigned as *b*-fundamentals except those overlapping *a*-fundamentals.

Some of the fundamentals are good group frequencies like ν_1, ν_5 and ν_{15} connected with O=S=O, symmetric stretch, bend and asymmetric stretch, respectively. Various correlations between the wave numbers of these modes and

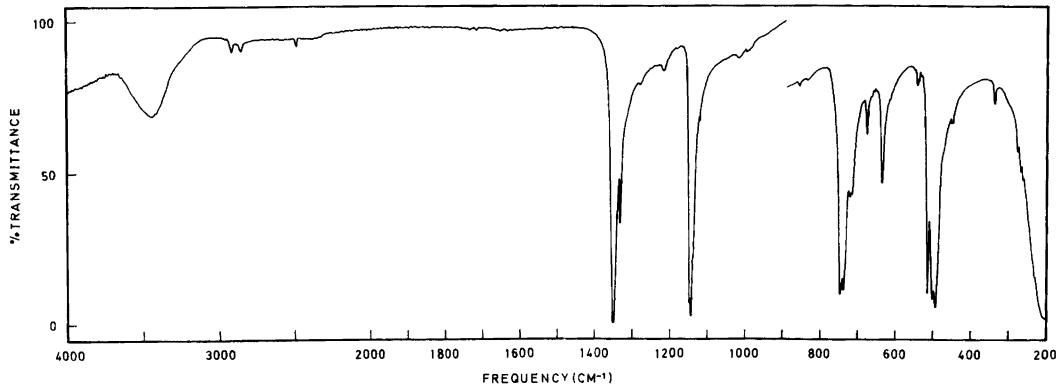

Fig. 7. Infrared spectrum of $(CBr_3)_2SO_2$ in a KBr pellet.

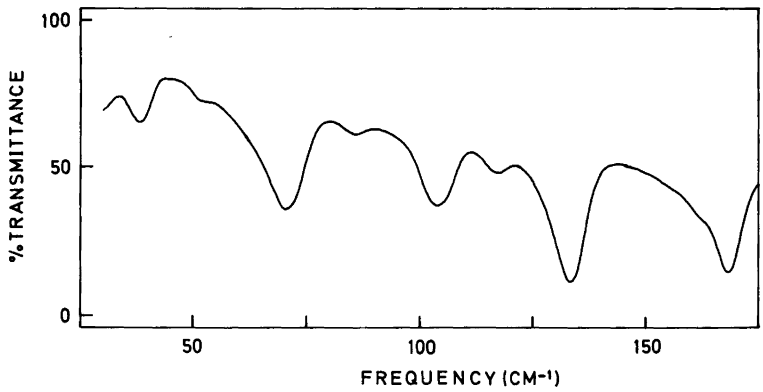

Fig. 8. Infrared spectrum of $(CBr_3)_2SO_2$, 50 mg in a polyethylene pellet, 12 μm beamsplitter.

the O=S=O bond angle and bond distance have been proposed.[1,2] The six C-halogen stretching modes for thhese compounds are spread over a large frequency region and are mixed with C–S stretch. The various CX_3 bending modes give rise to a number of distinct IR and Raman bands below *ca.* 380 cm^{-1} for TCMS and 240 cm^{-1} for TBMS. Although the positions of the torsional frequencies ν_{14} and ν_{27} are very uncertain, they are probably situated below 35 cm^{-1} for both compounds. With local C_{3v} symmetry they are probably quite weak both in IR and in Raman, and it is not surprising that they remain unobserved.

As is apparent from Table 4, the agreement between the observed and calculated fundamentals was quite satisfactory. The result of the force constant calculations was a great help

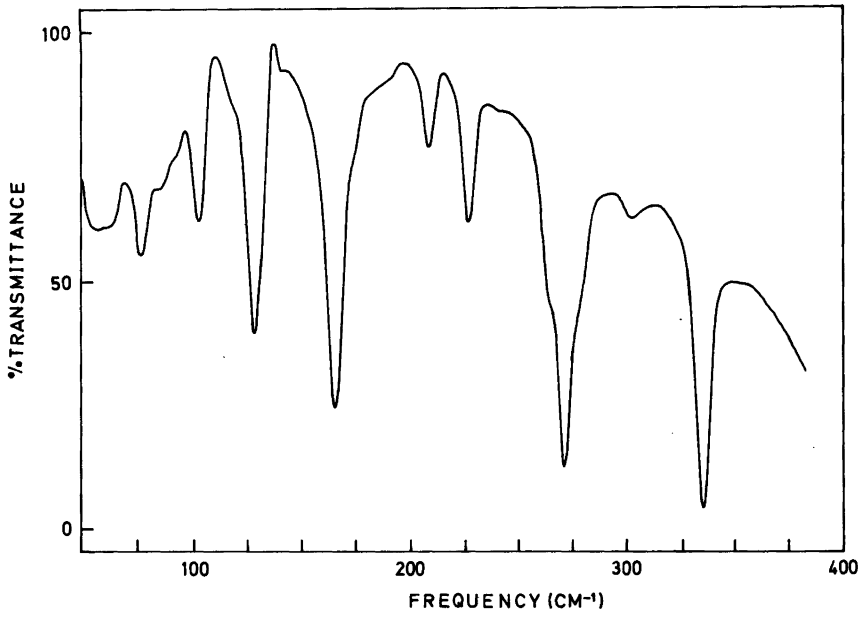

Fig. 9. Infrared spectrum of $(CBr_3)_2SO_2$ as a saturated solution in C_6H_6, 1 mm polyethylene cell, 3 μm beamsplitter.

Table 2. Infrared and Raman spectral data [a] for bis(trichloromethyl) sulfone (TCMS).

IR				Raman		Interpretation
Melt	Solution		Solid Pellet	Melt	Solution CCl_4	
	CCl_4 [b]	C_6H_6				
1464 m [c]	1470 m					
				1445 vw P?	1445 vw	
1426 w						
1382 vs,bd	1392 vs		1384 s	1384 w D	1389 w D	ν_{15} *b*
1366 m,sh	1373 m		1366 w,sh			
1340 vw			1341 vw,bd?			
1167 s	1168 s		1268 s	1168 s P	1169 s P	ν_1 *a*
1161 m,sh	1165 m		1266 w,sh			
1143 vw			1133 vw			
1104 vw	1108 vw,bd		1105 vw,bd			
947 vw	944 vw					
921 w	921 w		922 vw			
886 w	888 w					
858 s,sh	858 s,sh		860 vw,sh		859 vw ?	
836 vs,bd	837 vs		836 s	836 w D	838 w D	ν_2 *a*, ν_{16} *b*
820 vs,bd	822 vs		821 ms,sh	821 w P	822 w P	ν_3 *a*
794 w					795 w,sh P?	ν_{17} *b*
778 s			777 mw	774 m D	778 m D	ν_{18} *b*
				755 vw D?	755 vw,sh	
717 m	719 m		718 mw	723 s,bd P	723 m,bd P?	ν_4 *a*
614 vw	615 vw					
592 vw	592 vw					
561 s,sh						
549 vs	554 vs		554 vs	555 w D	555 w D	ν_{19} *b*
	544 vw					
536 vs	536 s		538 vs	542 s P	540 m P	ν_5 *a*
512 w,sh	512 w,sh			517 vw P	520 vw P?	
481 vw						
458 vw	457 vw	459 m?				
					438 vw P?	
429 vw	418 w	426 m	428 vw	418 vs P	417 vs P	ν_6 *a*
406 s	404 s	410 s	406 s			ν_{20} *b*
383 s	384 s	386 vs	385 s	387 m D	387 m D	ν_{21} *b*
318 w		317 w	318 w	320 m D?		ν_7 *a*
302 vw?				308 m D?		ν_8 *a*
277 m	278 m	277 m	276 m	280 m D?	281 w D?	ν_{22} *b*
258 w	258 w	256 m	258 w	259 vs D	258 vs D	ν_9 *a*, ν_{23} *b*
253 vw,sh						ν_{24} *b*
241 vw	237 vw	241 w	243 w	245 vs P	245 vs P	ν_{10} *a*
	227 vw			225 vw?		
	172 m	173 m	172 m	180 vs P	180 vs P	ν_{11} *a*, ν_{25} *b*
	154 m	155 m	155 m	162 s D	158 s D	ν_{26} *b*
		120 w	118 w	122 m P	122 m P	ν_{12} *a*
		82 vw				
		73 w	74 m			ν_{13} *a*
			50 vw?			

[a] Data listed in the region 1500–40 cm^{-1}. [b] C_6H_{12} solution employed in the region 500–40 cm^{-1}. [c] Abbreviations used: s, strong; m, medium; w, weak; v, very; bd, broad; sh, shoulder; P, polarized; D, depolarized.

Table 3. Infrared and Raman spectral data [a] for bis(tribromomethyl) sulfone (TBMS).

IR		Raman			Interpretation
Solution CS_2 [b]	Solid Pellet	Solution		Solid	
		CS_2	C_6H_6		
1374 vs [c]	1353 vs	1374 m D	1376 m D	1351 m	ν_{15} *b*
	1344 vw?				
1358 m	1336 m				
	1151 s				
1156 vs	1146 vs	1155 s P	1156 s P	1150 s	ν_1 *a*
1149 m,sh	1141 m				
1132 vw	1123 vw		1124 vw?		
	1015 vw				
	857 vw				
784 w					
762 w					
	748 vs				
736 vs		736 m P	737 m P	742 m	ν_2 *a*, ν_{16} *b*
	739 vs				
	723 m			725 w	
720 m		718 m,bd D	718 m D		ν_3 *a*, ν_{17} *b*
	717 m			716 m	
675 w	678 w	675 m D?	678 m D?	678 m	ν_4 *a*
653 vw				656 vw	
637 m	638 m		638 w D?	642 w	ν_{18} *b*
548 vw	546 vw				
536 w	524 vw		534 vw?		
515 s	517 vs	516 w	517 w P?	518 m	ν_5 *a*
502 vs	503 vs	503 w D?	505 w D	505 vw	ν_{19} *b*
493 s	494 vs			493 w	
452 vw	453 vw				
		395 w,bd?			
334 w	340 w	333 w D	334 w D	342 m	ν_{20} *b*
277 vw,sh	281 w				ν_6 *a*
270 m	272 w	275 s P	277 s P	283 s	ν_7 *a*
262 w,sh	266 w	263 vs P	263 vs P	266 vs	ν_8 *a*, ν_{21} *b*
226 w	227 w	226 vs P	227 s P	229 s	ν_9 *a*
207 w	211 w	208 w D?	208 w D	213 w	ν_{22} *b*
				175 m,sh	ν_{23} *b*
165 m	168 m	163 s D	164 s D	165 s	ν_{10} *a*, ν_{24} *b*
	160 vw,sh?				
140 vw?	144 vw				
126 m	132 m	132 vw	132 vw?	133 vw	ν_{11} *a*
	116 vw	113 w P	113 w P	104 s	ν_{12} *a*
101 vw	103 w	100 vw,sh	100 vw D	119 m	ν_{25} *b*
81 vw	85 vw				ν_{26} *b*
61 vw,bd	69 m			67 w	ν_{13} *a*
	51 vw				
	37 w				

[a] Data listed in the region 1500–40 cm^{-1}. [b] C_6H_6 solution employed in the region 500–40 cm^{-1}. [c] Abbreviations: see footnote to Table 2.

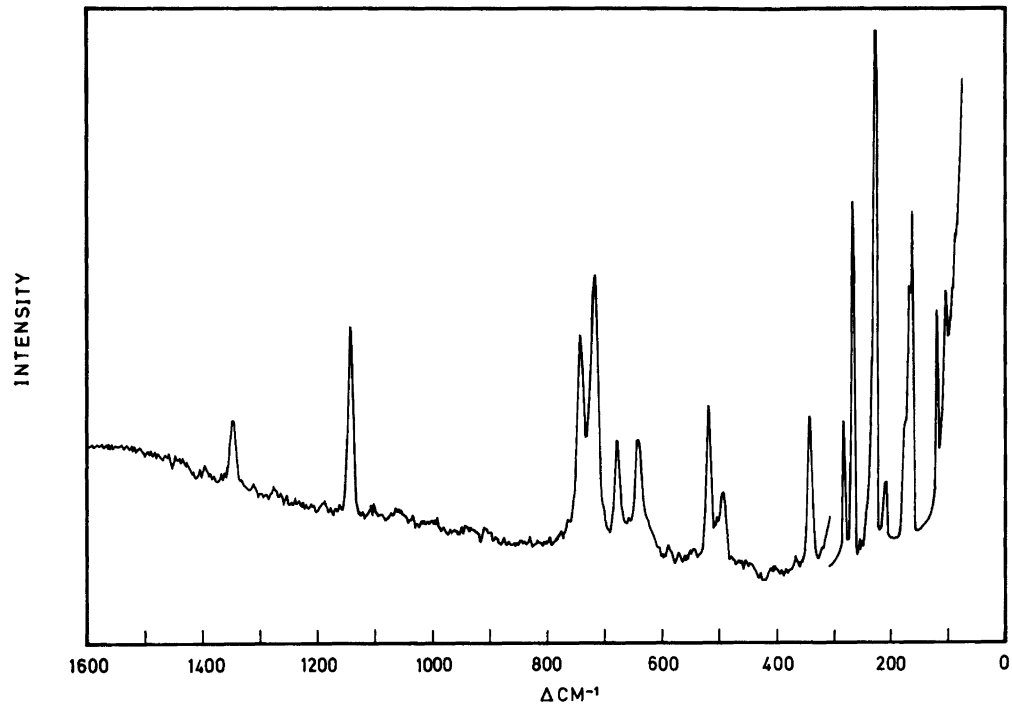

Fig. 10. Raman spectra of a single crystal of $(CBr_3)_2SO_2$.

Table 4. Observed and calculated fundamental vibrations of $(CCl_3)_2SO_2$ (TCMS) and $(CBr_3)_2SO_2$ (TBMS).

	TCMS			TBMS		
	Obs.	Calc.	Approx.description	Obs.	Calc.	Approx.description
[a]						
ν_1	1167	1158	SO_2 stretch	1156	1158	SO_2 stretch
ν_2	836 [a]	807	CCl_3 stretch	736 [a]	742	CBr_3 stretch
ν_3	820	803	CCl_3 stretch	720 [a]	729	CBr_3 stretch
ν_4	719	734	CS stretch	675	698	CS stretch
ν_5	536	554	OSO bend	515	537	OSO stretch
ν_6	418	419	CCl_3 stretch	277	296	CBr_3 stretch
ν_7	318	329		275	267	SO_2 twist
ν_8	308	326		263 [a]	235	
ν_9	258 [a]	250	SO_2 twist	226	178	
ν_{10}	245	242	CCl_3 def	165 [a]	170	CBr_3 def
ν_{11}	172 [a]	174		132	105	
ν_{12}	122	169		113	102	
ν_{13}	74	69	CSC bend	61	45	CSC bend
ν_{14}		39 [b]	torsion	–	–	torsion

ν_{15}	1382	1357	SO_2 stretch	1374	1356	SO_2 stretch
ν_{16}	836 [a]	785	CCl_3 stretch	736 [a]	759	CS stretch
ν_{17}	794	785	CCl_3 stretch	720 [a]	708	CBr_3 stretch
ν_{18}	778	757	CS stretch	637	693	CBr_3 stretch
ν_{19}	554	578	SO_2 wag	502	524	SO_2 wag
ν_{20}	404	407	CCl_3 stretch	334	297	SO_2 rock
ν_{21}	384	357	SO_2 rock	263 [a]	274	CBr stretch
ν_{22}	278	283		207	198	
ν_{23}	258 [a]	241		175	179	
ν_{24}	253	239	CCl_3 def	165 [a]	162	CBr_3 def
ν_{25}	172 [a]	171		101	113	
ν_{26}	154	146		81	103	
ν_{27}		54 [b]	torsion	–	–	torsion

[a] Used twice. [b] Estimated from the electron diffraction data (see text).

for the assignments.

The force field was evaluated from the spectroscopic data on dimethyl sulfone,[8] 1,1,1-trichloroethane [15] and 1,1,1-tribromoethane.[16] Since the CS distance in TCMS is lengthened by the halogen substitution, the force constant, K_{cs}, was estimated 10 % lower for TCMS than for dimethyl sulfone. The force field is listed in Table 5.

DISCUSSION

A relatively large body of experimental data has been accumulated on the geometries of sulfone derivatives.[1,2] The most noteworthy feature of the TCMS structure is the longest S–C bond in this series and the rather large C–S–C bond angle. The lengthening of the S–C bond from 1.76 to 1.86 Å in the CH_3SO_2Cl/CF_3SO_2Cl pair as well as in the CH_3SO_2Cl/CCl_3SO_2Cl pair has already been noted.[10,11] Substitution of one of the methyl groups of dimethyl sulfone, S–C 1.771(4) Å [12] by a chlorine barely influences the length of the remaining S–C bond in CH_3SO_2Cl, S–C 1.763(5) Å.[7] The S–C bond length of CCl_3SO_2Cl has been determined, unfortunately, with relatively large uncertainty. The origin of the CH_3SO_2Cl/CF_3SO_2Cl change has been examined in detail.[2] Semiempirical molecular orbital calculations in the CNDO/2 approximation [13] have agreed with the observed changes in bond length. They were attributed primarily to the difference between the electron withdrawing ability of the CF_3 group and the electron donating ability of the CH_3 group. The somewhat smaller C–S–Cl bond angle (98.7±0.4°) of CF_3SO_2Cl as compared with the analogous bond angle of CH_3SO_2Cl (101.0±1.4°) is consistent with what could be expected from the elec-

Table 5. Suggested valence force constants for $(CCl_3)_2SO_2$ (TCMS) and $(CBr_3)_2SO_2$ (TBMS).

Constant	Value [a] TCMS	TBMS
K_{CS}	3.00	3.00
K_{SO}	9.54	9.54
K_{CX} [b]	3.35	2.83
H_{CSC}	0.83	0.83
H_{OSO}	1.39	1.39
H_{CSO}	1.10	1.10
H_{SCX}	1.12	1.13
H_{XCX}	1.21	1.25
$F_{CX/CX}$	0.35	0.30
$F_{CS/CX}$	0.32	0.29
$F_{CS/CSO}$	0.19	0.19
$F_{CS/SCX}$	0.51	0.51
$F_{CX/SCX}$	0.64	0.56
$F_{CX/XCX}$		
$F_{CSO/CSO'}$	0.21	0.21
$F_{CSO/C'SO}$	–0.19	–0.19
$F_{SCX/SCX}$	0.10	0.16
$F_{SCX/XCX}$		
$F_{XCX/XCX}$		
$\tau_{torsion}$	0.025 [c]	

[a] Stretch and stretch–stretch force constants in mdyn Å^{-1}; bending and torsional force constants in mdyn Å rad^{-2} and stretch–bend force constants in mdyn · rad^{-1}. [b] X=Cl,Br. [c] Estimated from electron diffraction data (see text).

tronegativity rule of the VSEPR model. This trend is also consistent with the supposedly greater double bond character of the S–C bond *versus* that in CF_3SO_2Cl. If the C–S–C angles of $(CH_3)_2SO_2$ and TCMS are compared, similar reasoning would suggest a smaller angle in TCMS which is clearly not the case. The only explanation may be found in the strong steric effects caused by the large space requirements of the two trichloromethyl groups in TCMS. The Cl_6---Cl_{10} non-bonded distance is 3.309(14) Å, considerably smaller than the sum of the van der Waals radii (3.60 Å). A more typical C–S–C angle would correspond to yet a smaller Cl---Cl non-bonded distance (*e.g.* 100° to 2.96 Å). The C–S–C bond angle in this molecule is, in fact, so large that the relationship <XSY≪X(Y)SO≪OSO generally observed for XSO_2Y sulfones is not valid here. A similarly large XSX bond angle was observed for only one molecule, *viz.* N–S–N 110.5±0.4° in $(CH_3)_2NSO_2N(CH_3)_2$,[14] also with unusually large ligands on the SO_2 group.

Acknowledgements. We are grateful to Anne Horn, Hans Volden and Jann Samstad for technical assistance.

REFERENCES

1. Hargittai, I. *Sulphone Molecular Structures, Lecture Notes in Chemistry,* Springer, Berlin 1978, Vol. 6.
2. Hargittai, I. *The Structure of Volatile Sulphur Compounds,* Akadémiai Kiadó, Budapest and Reidel Publ. Co., Dordrecht. *In press.*
3. Schmiedekamp, A., Cruickshank, D. W. J., Skaarup, S., Pulay, P., Hargittai, I. and Boggs, J. E. *J. Am. Chem. Soc. 101* (1979) 2002.
4. Zeil, W., Haase, J. and Wegmann, L. *Z. Instrumentenkd. 74* (1966) 84.
5. Bastiansen, O., Graber, R. and Wegmann, L. *Balzers' High Vacuum Rep. 25* (1969) 1.
6. The Norwegian Electron Diffraction Group, *Annual Report,* NAVF, Oslo 1980.
7. Hargittai, M. and Hargittai, I. *J. Chem. Phys. 59* (1973) 2513.
8. Geiseler, G. and Hanschmann, G. *J. Mol. Struct. 8* (1971) 293; *11* (1972) 283.
9. Nagel, B., Steiger, Th., Fruwert, J. and Geiseler, G. *Spectrochim. Acta A 31* (1975) 255.
10. Brunvoll, J., Hargittai, I. and Kolonits, M. *Z. Naturforsch. Teil A 33* (1978) 1236.
11. Brunvoll, J., Hargittai, I. and Seip, R. *Z. Naturforsch. Teil A 33* (1978) 222.
12. Hargittai, M. and Hargittai, I. *J. Mol. Struct. 20* (1974) 283.
13. Mayer, I. and Hargittai, I. *Z. Naturforsch. Teil A 34* (1979) 911.
14. Hargittai, I., Vajda, E. and Szöke, A. *J. Mol. Struct. 18* (1973) 381.
15. Evans, J. C. and Bernstein, H. J. *Can. J. Chem. 33* (1955) 1746.
16. Durig, J. R., Craven, S. M., Hawley, C. W. and Bragin, J. *J. Chem. Phys. 57* (1972) 131.

Received August 26, 1982.

Acta Chemica Scandinavica A 37 (1983) 353–358

Crystal Structure of *N*(6),*N*(6)-Dimethyladeninium Tricyanoethenolate Dioxane Solvate

TOR DAHL

Institute of Mathematical and Physical Sciences, University of Tromsø, P.O.Box 953, N-9001 Tromsø, Norway

The title compound crystallizes with 1/2 dioxane molecule per formula unit in the monoclinic space group *C2/m* with cell parameters a=14.473(2) Å, b=6.862(1) Å, c=17.493(3) Å, β=111.04(1)°. The structure was refined to R=0.069 for 792 observed reflections. The structure is disordered with each ion and molecule in two orientations. The *N*(6),*N*(6)-dimethyladeninium ion has H atoms bonded to N(3) and N(7) which is different from what has been observed in other adeninium derivatives. The two ions are linked by several hydrogen bonds along (010) and are stacked alternately in infinite columns along [010].

Crystal structure investigations [1–5] show that in most molecular complexes of adenine derivatives the partner molecules are hydrogen bonded to each other and, in addition, associated by stacking interactions. Spectroscopic measurements [6,7] indicate charge transfer interactions in complexes of adenine and its derivatives with π^*-acceptors. The intention of the present work was to study the interactions in a crystalline complex with tetracyanoethylene as the acceptor. Unexpected reactions during the crystallization, however, gave the title compound. As there might be hydrogen bonds and stacking interactions of interest even in this compound, the crystal structure was investigated.

EXPERIMENTAL

By evaporation in the atmosphere of a dioxane solution of equimolecular amounts of *N*(6),*N*(6)-dimethyladenine and tetracyanoethylene a brown residue was formed, mainly as a powder, but with a few needle-shaped crystals. Because of instability and difficulties in making a sufficient amount of the crystals, the composition was not found by the usual analytical methods, but as a result of the structure analysis. The formation of the compound may be explained in accordance with what is known from the literature [8] by assuming hydrolysis of tetracyanoethylene, using water from the atmosphere, and subsequent protonation of the adenine derivative. The crystal chosen for data collection had the dimensions 0.12×0.8×0.3 mm in the axial directions.

The cell parameters and X-ray intensities were measured on an Enraf-Nonius CAD4 diffractometer using Cu$K\alpha$ radiation (λ=1.5418 Å). The cell parameters were determined from the setting angles of 25 reflections. The intensities were collected by an $\omega/2\theta$ scan at a rate in ω of 0.3–2.9° min^{-1}. Although the crystals were kept in sealed capillaries, there was a continuous reduction of intensity of the standard reflections down to 56 % of their original values and a considerable decrease of the quality of the crystals during the data collection. 793 reflections with $I>1.5\sigma(I)$ were used for the structure determination. Lp and absorption corrections were performed.

CRYSTAL DATA

N(6),*N*(6)-Dimethyladeninium tricyanoethenolate dioxane solvate, $C_7H_{10}N_5^+$ $C_5N_3O^-$ 1/2 $C_4H_8O_2$, F.W.=326.33. Space group *C2/m*, a=14.473(2) Å, b=6.862(1) Å, c=17.493(3) (Å), β=111.04(1)°, V=1621.5 Å^3, Z=4, D_x=1.34 g cm^{-3}, D_m=1.35 g cm^{-3} (by flotation), μ(Cu$K\alpha$)=8.15 cm^{-1}.

0302-4377/83 $02.50

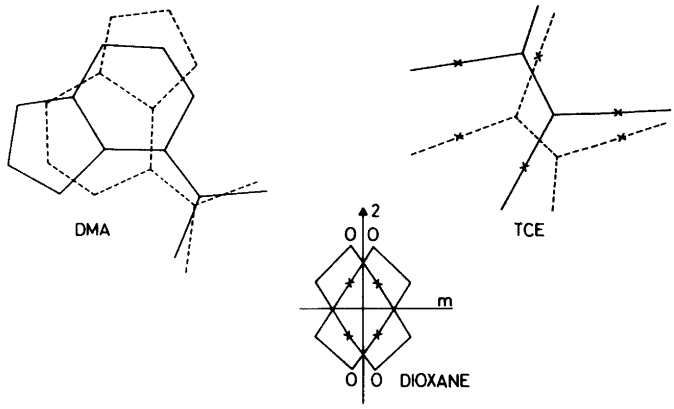

Fig. 1. The disorder of the molecules. Minor orientations with broken lines.

STRUCTURE DETERMINATION AND REFINEMENT

Three space groups, *C*2, *Cm* and *C*2/*m*, are possible from the systematic absences. A sharpened Patterson map indicated that most of the atoms are situated in the planes $y=0$ and $y=1/2$. From this, as well as a more detailed analysis of the Patterson map and packing considerations it was possible to conclude that *C*2/*m* is the most probable space group, and also to find a position and orientation of the adenine derivative which could be used as a starting point for the structure determination. The interpretation of the subsequent Fourier maps led to the deduction of the composition of the compound and to the conclusion that both the tricyanoethenolate ion (TCE) and the dioxane molecule are disordered, each with two different orientations. The orientations of TCE are non-equivalent whereas those of dioxane are related by symmetry and therefore equivalent. Least squares refinements performed at this stage could not bring *R* below 12 % and gave unreasonable thermal parameters for some atoms of the *N*(6),*N*(6)-dimethyladeninium ion (DMA). By assuming a second orientation also of this ion the structure was refined to the final *R*-value and the thermal parameters of DMA became reasonable. The disorder of the molecules is shown in Fig. 1.

A difference map (Fig. 2) shows clearly the positions of the non-methyl H atoms of the major orientation of DMA. Surprisingly, two of these are bonded to N(3) and N(7), rather than to N(1) and N(9) as in other adeninium derivatives.[9,10] No H atom bonded to N'(7) in the minor orientation can be seen in the map. As protonation at N'(7) and at N'(1) both seem possible for steric reasons, the possibility that the disorder is accompanied by tautomerism cannot be excluded, and one H position of the minor orientation is therefore regarded as uncertain. All the other H positions not found from the difference map were calculated with C–H distances of 0.95 Å and disorder due to rotation of the methyl groups assumed. The *U* values used for the H atoms were 0.10 $Å^2$ for those bonded directly to the ring system of DMA and 0.13 $Å^2$ for the others. The parameters of these atoms were not refined, but included in the structure factor calculations.

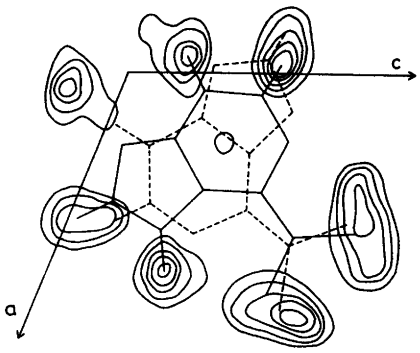

Fig. 2. Section through a difference Fourier map showing the H atoms. Contours are at intervals of 0.05 e $Å^{-3}$, starting at 0.05 e $Å^{-3}$.

Table 1. Positional parameters and equivalent or isotropic temperature factors (Å^2). $U_{eq}=1/3\sum_i\sum_j U_{ij}a_i^*a_j^*a_ia_j\cos a_{ij}$, or $U_{iso}+1/3\Delta U$ for atoms where the method of Kartha and Ahmed [12] has been used. Standard deviations in parentheses. Occupancy factors are 0.70 for N(1)–C(11), 0.30 for N′(1)–C′(11), 0.58 for O(1)–C(16), 0.42 for O′(1)–C′(16) and 0.50 for O(2)–C(18).

	x	*y*	*z*	U_{eq} or U_{iso}
N(1)	0.1193(7)	0	0.2596(5)	0.093
C(2)	0.0408(8)	0	0.1972(8)	0.097
N(3)	0.0322(6)	0	0.1159(5)	0.086
C(4)	0.1194(6)	0	0.1052(6)	0.081
C(5)	0.2120(7)	0	0.1702(6)	0.087
C(6)	0.2134(7)	0	0.2508(6)	0.080
N(6)	0.2924(6)	0	0.3184(5)	0.094
N(7)	0.2795(6)	0	0.1328(6)	0.095
C(8)	0.2305(7)	0	0.0530(7)	0.097
N(9)	0.1345(5)	0	0.0338(5)	0.086
C(10)	0.2853(8)	0	0.4018(6)	0.112
C(11)	0.3926(8)	0	0.3166(6)	0.121
N′(1)	0.2864	0	0.1781	0.062
C′(2)	0.2306	0	0.1015	0.071
N′(3)	0.1292	0	0.0693	0.082
C′(4)	0.0883	0	0.1269	0.077
C′(5)	0.1417	0	0.2117	0.058
C′(6)	0.2448	0	0.2392	0.070
N′(6)	0.3037	0	0.3160	0.074
N′(7)	0.0703	0	0.2465	0.087
C′(8)	–0.0162	0	0.1852	0.062
N′(9)	–0.0095	0	0.1130	0.070
C′(10)	0.4113	0	0.3393	0.075
C′(11)	0.2650	0	0.3823	0.087
O(1)	0.4754(7)	0	0.1644(6)	0.101
N(10)	0.5902(16)	0	0.0327(9)	0.209
N(11)	0.8184(14)	0	0.2168(16)	0.158
N(12)	0.6492(12)	0	0.3874(9)	0.112
C(12)	0.5561(10)	0	0.1675(9)	0.073
C(13)	0.6564(12)	0	0.2391(13)	0.090
C(14)	0.5755(11)	0	0.0895(8)	0.119
C(15)	0.7460(26)	0	0.2252(31)	0.151
C(16)	0.6550(12)	0	0.3207(10)	0.092
O′(1)	0.8222(15)	0	0.2820(11)	0.133
N′(10)	0.6700(18)	0	0.3816(14)	0.110
N′(11)	0.4904(12)	0	0.1873(11)	0.089
N′(12)	0.7291(12)	0	0.0728(11)	0.134
C′(12)	0.7309(20)	0	0.2616(14)	0.085
C′(13)	0.6607(16)	0	0.1871(10)	0.075
C′(14)	0.6923(20)	0	0.3346(16)	0.115
C′(15)	0.5764(20)	0	0.1894(16)	0.082
C′(16)	0.6953(12)	0	0.1223(11)	0.093
O(2)	0.0113(8)	0.2009(10)	0.5156(6)	0.120(3)
C(17)	–0.0249(11)	0.0860(34)	0.5641(8)	0.129
C(18)	0.0724(10)	0.0894(29)	0.4813(9)	0.119

In the last part of the least squares refinement the positions of all non-hydrogen atoms were varied independently, except those of the minor orientation of DMA which were refined as a rigid group with bond distances and angles as those found for the major orientation. Anisotropic thermal parameters were used for all non-hydrogen atoms, except for O(1), N(12), C(12), C(16), N′(10), N′(11), C′(14), C′(15) and O(2) which are close to atoms from other orientations, and for those of the minor orientation of DMA. As the refinement showed that the vibrations in this compound are greatest along [010], all these atoms except O(2) were given additional vibrations in this direction by introducing "half atoms" and refining the y-values.[12] As N(6) and N′(6) of the major and minor orientation of DMA are very close, alternating cycles were performed in which the thermal parameters of N(6) were varied while those of all non-hydrogen atoms of the minor orientation were kept constant, and *vice versa*. The number of variable parameters in these cycles were 193 and 201, respectively. The reflection 404 turned out to have a great systematic error and was left out of the refinement. Occupancy factors of 0.70 and 0.58 for the major orientations of DMA and TCE, respectively, were arrived at after systematic variation of the factors and least squares refinement of the structure with these factors kept constant for each set of values.

The weights used in the refinement were $w=XY$, where $X=1$ for sin $\theta>0.5$, else $X=\sin\theta/0.5$, $Y=1$ for $|F_o|\leq 10$, else $Y=10/|F_o|$. The final $R=0.069$ and $R_w=[\Sigma w(F_o-F_c)^2/\Sigma wF^2]^{1/2}=0.089$. Lists of observed and calculated structure factors and anisotropic thermal parameters may be obtained from the author on request. The final parameters are given in Table 1. Bond distances and angles are shown in Fig. 3, the molecular

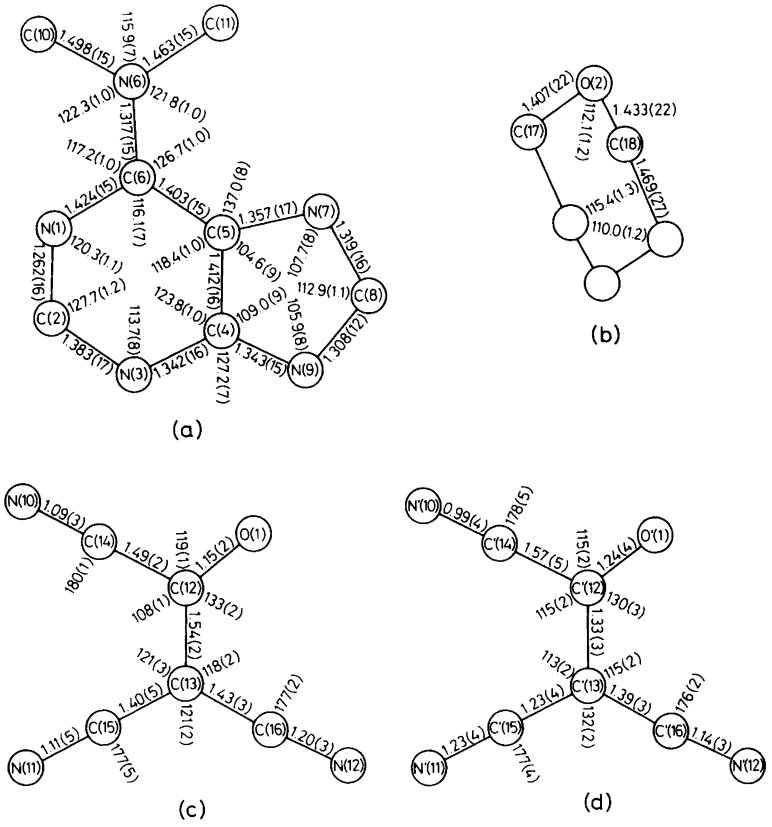

Fig. 3. Bond distances (Å) and angles (°) in DMA, major orientation (a), dioxane (b) and TCE, major orientation (c) and minor orientation (d). Standard deviations in parentheses.

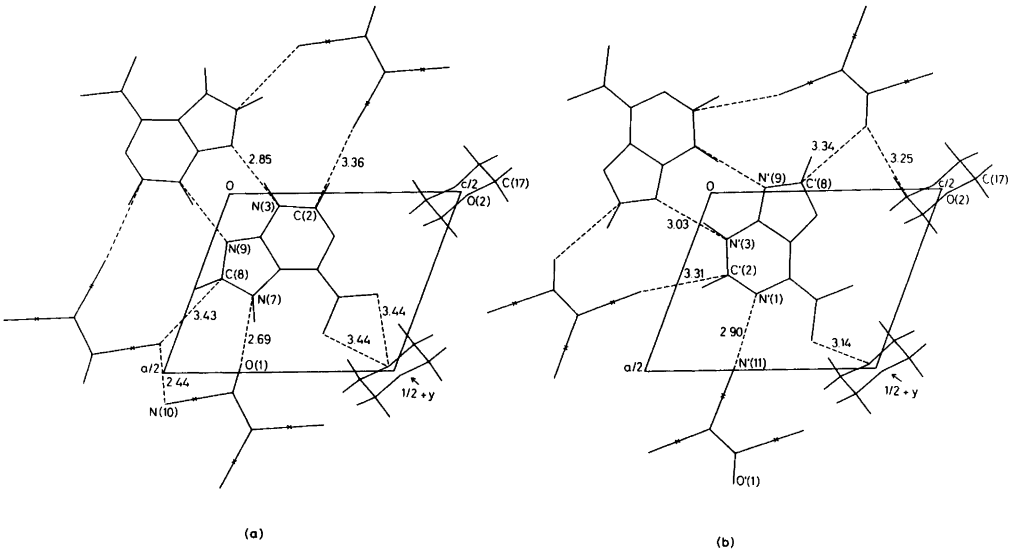

Fig. 4. The packing of the molecules in their major orientations (a) and minor orientations (b) in a layer along (010). One H atom of the DMA ion in the minor orientation, which position is uncertain, and methyl H atoms are not included. Short intermolecular distances (Å) are given.

packing and intermolecular distances in Fig. 4 and the overlap of the molecules in Fig. 5.

Scattering factors for the H atoms are taken from Ref. 13, those used for the other atoms are taken from Ref. 14. All calculations have been performed at the CYBER 171 MP at the University of Tromsø. The computer program used for data reduction has been written at the University of Lund and modified at the University of Tromsø. The other programs used are included in the X-RAY 76 system.[15]

DISCUSSION

The bond distances and angles in DMA deviate significantly from those found in other adeninium derivatives.[9–11] This would be expected from the different H positions, and it appears from the resonance picture in Fig. 6 that there is full agreement between the bond distances and the observed H positions. It also appears from this picture that the N(1)–C(2) bond, which has a very short bond length, is an approximately pure double bond.

It is remarkable that even in the closely related *N*(6)-methyladeninium chloride [9] the H atoms are bonded as in other adeninium derivatives. The unusual bonding in the present compound may thus possibly be a result of interactions between the DMA ion and its environments. This hypothesis will be tested by structure investigations of other DMA-compounds.

Because of large standard deviations and high correlation between parameters of TCE, bond distances and angles of this ion are very uncertain and will not be subject to any further comments.

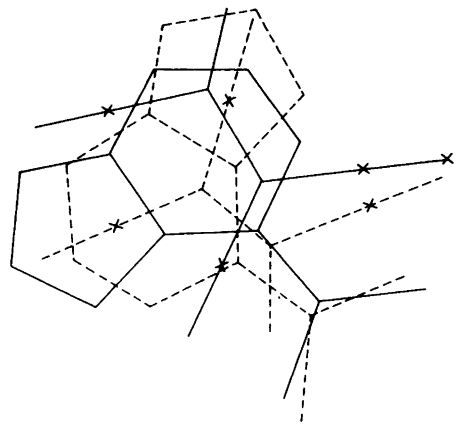

Fig. 5. The overlap of the molecules. Minor orientations with broken lines.

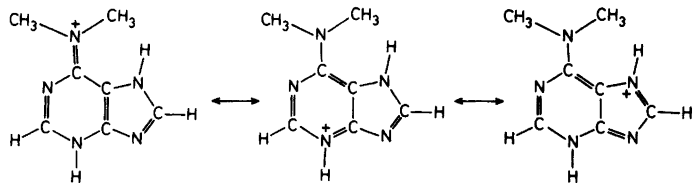

Fig. 6. Resonance structures of the DMA ion.

If the orientations of neighbouring DMA and TCE ions are independent of each other, two unreasonably short C–H···N bonds with C–N distances of 2.47 and 2.64 Å would have to exist. It is therefore believed that in layers along (010) the contacts are mainly between the major orientations and between the minor orientations, although this assumption cannot be strictly correct as the occupancy factors are not equal for the two ions. The two ways of molecular packing are shown in Fig. 4. In both cases DMA forms dimers held together by hydrogen bonds, and there are also many hydrogen bonds along (010) between DMA and TCE. The short distance of 2.44 Å between two equivalent positions of N(10) in the major orientation is hard to explain.

Despite the large number of hydrogen bonds along (010) the crystals are elongated in the [010]-direction, along which the ions are stacked alternately in infinite columns. The interplanar distance, 3.431 Å, is greater than expected if charge transfer interactions had been present. The overlap (Fig. 5) gives no clear indication of an important influence of electrostatic forces. The close contact and nearly parallel orientation of the double bonds N(1)–C(2) and C(12)–C(13) in the major orientations are worth noticing and may be an effect of dispersion or polarization forces.

Acknowledgement. The author thanks cand. real. Lars K. Hansen for help in the use of the diffractometer.

REFERENCES

1. Voet, D. and Rich, A. *Proc. Natl. Acad. Sci. U.S.A. 68* (1971) 1151.
2. Shieh, H.-S. and Voet, D. *Acta Crystallogr. B 31* (1975) 2192.
3. Scarbrough, F. E., Shieh, H.-S. and Voet, D. *Proc. Natl. Acad. Sci. U.S.A. 73* (1976) 3807.
4. Fuji, S., Kawasaki, K., Sato, A., Fujiwara, T. and Tomita, K.-I. *Arch. Biochem. Biophys. 181* (1977) 363.
5. Takenaka, A. and Sasada, Y. *Bull. Chem. Soc. Jpn. 55* (1982) 680.
6. Slifkin, M. A. In Ratajczak, H. and Orville-Thomas, W. J., Eds., *Molecular Interactions*, Wiley, New York 1980, Vol. 2, Chapter 6.
7. Sheina, G. G., Radchenko, E. D., Egupov, S. A., Blagoy, Yu. P. and Orlov, V. M. *Int. J. Quantum Chem. 16* (1979) 387.
8. Middleton, W. J., Little, E. L., Coffman, D. D. and Engelhardt, V. A. *J. Am. Chem. Soc. 80* (1958) 2795.
9. Sternglanz, H. and Bugg, C. E. . *Cryst. Mol. Struct. 8* (1978) 263.
10. Hingerty, B. E., Einstein, J. R. and Wei, C. H. *Acta Crystallogr. B 37* (1981) 140.
11. Taylor, R. and Kennard, O. *J. Mol. Struct. 78* (1982) 1.
12. Kartha, G. and Ahmed, F. R. *Acta Crystallogr. 13* (1960) 532.
13. Stewart, R. F., Davidson, E. R. and Simpson, W. T. *J. Chem. Phys. 42* (1965) 3175.
14. Cromer, D. and Mann, J. *Acta Crystallogr. A 24* (1968) 321.
15. Stewart, J. M., Machin, P. A., Dickinson, C., Ammon, H. L., Heck, H. and Flack, H. *The X-Ray System, Version of 1976,* Technical Report TR-446, Computer Science Center, University of Maryland, College Park 1976.

Received September 14, 1982.

Acta Chemica Scandinavica A 37 (1983) 359–365

Studies on Metal Carbonate Equilibria. 5. The Cerium(III) Carbonate Complexes in Aqueous Perchlorate Media

DIEGO FERRI,* INGMAR GRENTHE, SIRKKA HIETANEN and FRANCESCO SALVATORE *

Department of Inorganic Chemistry, Royal Institute of Technology, S-100 44 Stockholm 70, Sweden

The complex formation equilibria were studied by solubility measurements at 25 °C in a 3 M $Na(ClO_4)$ ionic medium. Two different solid phases were used, $Ce_2(CO_3)_3 \cdot 8H_2O$ which is the thermodynamically stable phase at $[CO_3^{2-}] < 10^{-4.8}$ M, and $NaCe(CO_3)_2 \cdot 2H_2O$ which is stable at $[CO_3^{2-}] > 10^{-4.8}$ M. The solubility of $Ce_2(CO_3)_3(s)$ was measured as a function of $[H^+]$ in solutions with $[H^+] > 10^{-8}$ M saturated with CO_2 or mixtures of CO_2-H_2.

The solubility data were explained by assuming the following equilibria

$$Ce_2(CO_3)_3(s) + 6H^+ \rightleftarrows 2Ce^{3+} + 3CO_2(g) + 3H_2O$$
$$\log K_{s,I} = 21.80 \pm 0.05$$

$$Ce^{3+} + H_2O + CO_2(g) \rightleftarrows CeCO_3^+ + 2H^+$$
$$\log \beta_{2,1} = -11.30 \pm 0.05$$

$$Ce^{3+} + 2H_2O + 2CO_2(g) \rightleftarrows Ce(CO_3)_2^- + 4H^+$$
$$\log \beta_{4,2} = -24.1 \pm 0.1$$

The solubility of $NaCe(CO_3)_2 \cdot 2H_2O$ was measured in Na_2CO_3 solutions with $[H^+] < 10^{-8}$ M as a function of $[CO_3^{2-}]$.

The data were explained with the following equilibria

$$NaCe(CO_3)_2(s) \rightleftarrows Ce^{3+} + Na^+ + 2CO_3^{2-}$$
$$\log K_{s,II} = -17.5 \pm 0.1$$

$$Ce^{3+} + 3CO_3^{2-} \rightleftarrows Ce(CO_3)_3^{3-}$$
$$\log \beta_3 = 12.6 \pm 0.2$$

$$Ce^{3+} + 4CO_3^{2-} \rightleftarrows Ce(CO_3)_4^{5-}$$
$$\log \beta_4 = 13.7 \pm 0.1$$

No evidence was found for the formation of mixed species.

A short review of thermodynamic data for complex formation reactions in lanthanoid(III)–CO_3^{2-}–H_2O systems was given in part 3 of this series,[1] where an emf study of the La(III)–CO_3^{2-}–H_2O system in concentrated solutions of La(III) was reported. The acidity range investigated was $3.1 < -\log[H^+] < 4.1$, the upper limit was determined by the precipitation of $La_2(CO_3)_3(s)$. The stability constants for the formation of $La_2CO_3^{4+}$, $LaHCO_3^{2+}$ and $LaCO_3^+$ were determined. To extend the measurements to lower acidities, *i.e.* higher carbonate concentrations, it is necessary to use a different experimental approach. Dumonceau *et al.*[2] used an extraction technique to determine the stability constant for the limiting complex $Ln(CO_3)_4^{5-}$ for all lanthanoids except Ce and Pm. The measurements refer to a 2.5 M NH_4NO_3 medium.

A number of solid phases, *e.g.* $Ln_2(CO_3)_3(s)$, $Ln(OH)CO_3(s)$ and $MeLn(CO_3)_2(s)$ (Me=an alkali ion) [3] are formed in the Ln(III)–CO_3^{2-}–H_2O system. From the solubility of these phases [4] as a function of the carbonate concentration, one can obtain information on solubility products as well as on the composition and the stability constants of the complexes formed in solution. The Ce(III)–CO_3^{2-}–H_2O system was selected as a model for a solubility study in a wide carbonate concentration range. Data of this type are needed to decide whether the concentration of tervalent lanthanoids and actinoids in ground water may be limited by solubility factors or not.

* Permanent address: Istituto Chimico dell'Università Via Mezzocannone 4, 80134 Napoli, Italy.

0302-4377/83 $02.50

This, in turn, is related to problems of radionuclide migration from nuclear waste repositories.

NOTATIONS

Previous studies of the La(III)$-CO_3^{2-}-H_2O$ [1] and Y(III)$-CO_3^{2-}-H_2O$ [5] systems indicate that the concentration of polynuclear complexes should be negligible at the low metal ion concentrations encountered in this solubility study. The equilibria in the presence of CO_2(g) may then be written

$$Ce^{3+}+pH_2O+rCO_2(g) \rightleftarrows Ce(OH)_p(CO_2)_r^{3-p}+pH^+ \quad (1)$$

with $(OH)CO_2^- \equiv HCO_3^-$ and $(OH)_2CO_2^{2-} \equiv CO_3^{2-}$

where B=the total concentration of Ce(III), *i.e.* the measured solubility, H=analytical proton concentration excess:

$$H \simeq [ClO_4^-]-[Na^+] = h-[HCO_3^-]-2c-\sum_n 2n[Ce(CO_3)_n^{3-2n}] \quad (2)$$

where the last term is negligible throughout this study, b,h=molar concentrations of Ce^{3+} and H^+, respectively, c=molar concentration of CO_3^{2-}, a=partial pressure of CO_2(g), $\beta_{p,r}$=the equilibrium constant for the reaction (1), $K_p=\sum_r \beta_{p,r} \cdot a^r$, a conditional equilibrium constant at constant a, β_n=the equilibrium constant for the reaction

$$Ce^{3+}+nCO_3^{2-} \rightleftarrows Ce(CO_3)_n^{3-2n}$$

$\alpha=\log(B\,a^{3/2}h^{-3})$, $\psi=\log(B[Na^+])$, $K_{a1}=10^{-7.987}$ is the equilibrium constant [1] for $CO_2(g)+H_2O \rightleftarrows H^+ + HCO_3^-$ $K_{a2}=10^{-9.63}$ is the constant [1] for

$$HCO_3^- \rightleftarrows H^+ + CO_3^{2-} \quad (3)$$

$K_{s,I}$, $K_{s,II}$ are the equilibrium constants for the reactions (4) and (5) respectively.

$$Ce_2(CO_3)_3(s)+6H^+ \rightleftarrows 2Ce^{3+}+3CO_2(g)+3H_2O \quad (4)$$

$$NaCe(CO_3)_2(s) \rightleftarrows Na^+ + Ce^{3+} + 2CO_3^{2-} \quad (5)$$

METHOD

The solubility of two different solid phases, $Ce_2(CO_3)_3 \cdot 8H_2O$ and $NaCe(CO_3)_2 \cdot 2H_2O$ were studied at 25±1 °C in a 3 M $Na(ClO_4)$ medium.

The solubility of the $Ce_2(CO_3)_3$ phase was measured as a function of the hydrogen ion concentration, in solutions of acidity $10^{-8}<h\,t1<10^{-4}$ *M. These were saturated with* CO_2-H_2 *mixtures of known partial pressure,* a, of CO_2. Gas mixtures containing H_2 were chosen because Ce(III) in carbonate media is easily oxidized to Ce(IV) by air. The oxidation could be avoided by passing the H_2 gas mixture over a Pd sponge in the test solution of the general composition:

H M H^+, (3.000$-H$) M Na^+, 3.000 ClO_4^- saturated with $Ce_2(CO_3)_3$(s) and CO_2(g, a atm).

At acidities lower than 10^{-8} M, $NaCe(CO_3)_2 \cdot 2H_2O$ is the stable solid phase. Its solubility was measured in solutions of the general composition:

H M H^+, 3.000 M Na^+, (3.000+H) M ClO_4^- saturated with $NaCe(CO_3)_2$(s)

as a function of the carbonate ion concentration in the range $10^{-3}<c<1$ M.

H_2 was passed through these solutions in the presence of a Pd catalyst, only for the time necessary to remove O_2, every time the reaction vessel was opened for sampling. We were thus able to avoid both oxidation and significant changes of h due to removal of CO_2.

c was calculated from H and h by using eqns. (2) and (3). H is a known analytical quantity, while h was obtained by means of the cell

Ref | test solution | glass electrode (A)

where Ref indicates

$$Ag,AgCl \left| \begin{matrix} 2.99\ M\ NaClO_4, \\ 0.01\ M\ AgClO_4 \end{matrix} \right| 3\ M\ NaClO_4$$

or, for combined glass electrodes

$$Ag,AgCl \left| \begin{matrix} 2.99\ M\ NaClO_4, \\ 0.01\ M\ NaCl \end{matrix} \right| 3\ M\ NaClO_4$$

The emf of cell (A) is equl to

Table 1. Survey of the experimental data.

i. Solutions equilibrated with $Ce_2(CO_3)_3 \cdot 8H_2O(s)$

a=0.97 atm

α, log ($h^{-2}a$): 10.81, 8.01; 10.84, 8.09; 10.90, 8.15; 10.80, 8.17; 10.88, 8.32; 10.93, 8.33; 10.83, 8.35; 10.92, 8.62; 10.85, 8.65; 10.93, 8.72; 10.86, 8.74; 10.88, 9.07; 10.90, 9.09; 10.87, 9.26; 10.91, 9.38; 10.90, 9.41; 10.80, 9.49; 10.83, 9.55; 10.96, 9.63; 10.72, 9.65; 10.92, 9.72; 10.96, 9.88; 10.94, 10.13; 10.94, 10.21; 10.97, 10.37; 11.13, 10.58; 10.98, 10.65; 11.02, 10.71; 11.05, 10.76; 10.96, 10.92; 11.07, 11.02; 11.20, 11.04; 11.23, 11.24; 11.01, 11.25; 11.23; 11.25; 11.58, 11.42; 11.45, 11.54; 11.72, 11.59; 11.67, 11.78; 12.06, 12.19; 12.26, 12.42; 12.71, 12.67; 12.97, 12.97; 13.85, 13.51; 14.20, 13.75; 14.66, 13.83; 15.05, 13.89; 14.92, 14.02; 15.01, 14.07; 15.69; 14.31; 15.71, 14.41; 15.99, 14.48; 16.85, 14.89.

a=0.097 atm

α, log ($h^{-2}a$): 10.85, 9.42; 10.88, 10.09; 10.85, 10.13; 10.86, 10.24; 11.10, 10.86; 11.20, 11.48; 11.74, 11.62; 11.92, 12.02; 12.51, 12.52; 12.66, 12.60; 13.66, 13.22; 14.17, 13.54; 14.53, 13.66; 15.56, 14.32.

ii. Solutions equilibrated with $NaCe(CO_3)_2 \cdot 2H_2O(s)$

$-\psi$, $-\log c$: 4.02, 0.16_5; 4.26, 0.29; 4.32, 0.30; 4.37, 0.30; 4.39, 0.34; 4.54, 0.42; 4.75, 0.53; 4.80, 0.58_5; 5.01, 0.68; 5.04, 0.72; 5.15, 0.77; 5.29, 0.87; 5.50, 1.04; 5.63, 1.11; 5.64, 1.18_5; 5.67, 1.20; 5.69, 1.19_5; 5.74, 1.24; 5.80, 1.31_5; 5.92, 1.50; 6.03, 1.64; 6.08, 1.66; 6.22, 1.91; 6.23, 1.98_5; 6.36, 2.35.

$$E = E_o - 59.16 \log h + E_j$$

E_o is a constant which was determined in solutions of known h. E_j is the liquid junction potential between the test solutions and 3 M $NaClO_4$ which we found to be well approximated by $E_j = -7.2 \cdot H$. We have neglected E_j for solutions with $h > 10^{-11}$ M since the largest correction introduced in log h(0.04 units) hardly exceeds the present accuracy of the measurements. For solutions with $h < 10^{-11}$ M, we can write eqn. (2) as

$$-H = 2c \qquad (6)$$

since h is negligible and $[HCO_3^-]$ amounts to, at most, 4 % of c.

However, the value of c obtained from eqn. (6) always agreed with that obtained from eqns. (2) and (3) within 0.01 logarithmic units.

The solubility, B, was calculated by measuring the γ-activity of test solutions and by comparing it with the known specific activity of radioactive Ce(III) stock solutions. The solubility of the most acidic solutions were measured by a direct titration of Ce(III) with EDTA.

To ensure the attainment of equilibrium in the test solutions, we checked that the same value of the solubility was obtained in solutions which were initially undersaturated or supersaturated, after stirring them from one day to one week with the solid phase.

The primary data $B(h,a)$ for the $Ce_2(CO_3)_3 \cdot 8H_2O(s)$ and $B(h,H)$ for the $NaCe(CO_3)_2 \cdot 2H_2O$ phases recalculated in the form of $\alpha(\log h^{-2} a)$ and $\psi(\log c)$, respectively, are collected in Table 1 and plotted in Figs. 1 and 2. They form the basis of the following mathematical treatment.

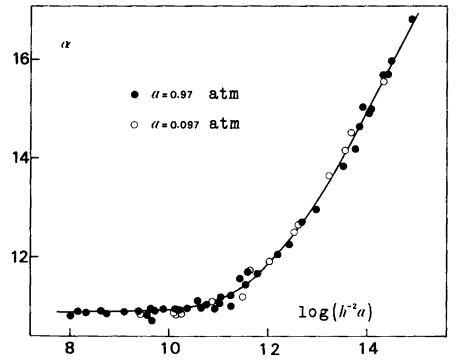

Fig. 1. The $\alpha(\log h^{-2}a)$ data at two different a, the partial pressure of CO_2. For clarity every second experimental point has been reported in the horizontal part of the plot. The curve has been calculated using the values of $\beta_{2,1}$, $\beta_{4,2}$ and $K_{s,I}$ given in Table 2.

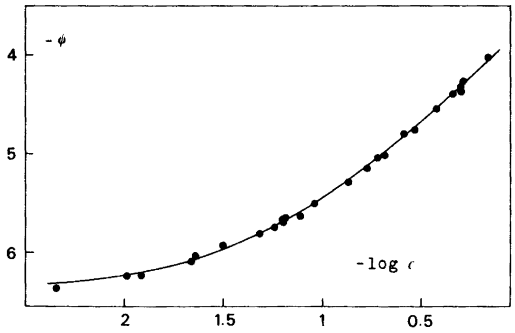

Fig. 2. The $\psi(\log c)$ data. The curve has been calculated using the values of β_2, β_3, β_4 and $K_{s,II}$ given in Table 2.

EXPERIMENTAL

A stock solution of $Ce(ClO_4)_3$ was prepared from $Ce(NO_3)_3$ (BDH, analytical grade) and perchloric acid (Merck, *p.a.*) by repeated evaporations under a heating lamp. The cerium and hydrogen ion concentrations were determined as described previously.[1] An active stock solution, used for the preparation of the solid phases, was obtained by adding a small known amount of cerium tracer to the Ce(III) stock solution. All other reagents were analyzed by standard methods.

$Ce_2(CO_3)_3 \cdot 8H_2O$ was prepared by adding $NaHCO_3$ to 0.1 M active Ce(III) stock solution. CO_2 was bubbled through the resulting slurry for 1–2 days. The precipitate was filtered, washed with water and finally dried with acetone. Analyses of Ce and carbonate confirmed the composition given above.

$NaCe(CO_3)_2 \cdot 2H_2O$ was prepared by shaking $Ce_2(CO_3)_3 \cdot 8H_2O$ with a 0.5–1 M Na_2CO_3 solution for 2 days. In order to avoid the oxidation of Ce(III) to Ce(IV), $H_2(g)$ was bubbled through the slurry in the presence of a Pd-catalyst. Analyses of Na, Ce and CO_3^{2-} confirmed the formula. Both solids were also characterized by their X-ray powder patterns.

Ce(III) stock solutions containing tracer amounts of Ce-144, Ce-141 or Ce-139 were used for the solubility measurements. These were made either by preparing individual test solutions in glass-stoppered flasks or by using a vessel where the composition of the test solution was varied in a titration procedure. Clear samples of known volume were withdrawn from these solutions with a pipette on which a G3 filter had been fitted. Contact between solution and air was prevented before separation from the solid phase. We found the titration technique to be superior and most of the experimental data were collected by using this method.

A Tracerlab scintillation counter, model Compumatic V or Scaler Sc-57 was used. E was measured by using a Radiometer Phm 4 with Beckman, Jena or Metrohm glass electrodes.

All the glass electrodes were calibrated against the hydrogen electrode in separate experiments in the acidity range $10^{-12} < h < 10^{-3}$ M. Correction for the sodium error was negligible, down to $h = 10^{-10}$ M.

TREATMENT OF THE DATA AND RESULTS

The solubility data for the two solid phases were treated separately.

In our treatment, we assumed that only mononuclear complexes are formed.

Solubility data do not in general [4] provide information as to the nuclearity of the species formed. However, the results of previous studies on lanthanum [1] and yttrium [5] indicate that this assumption is valid at the metal concentrations encountered in this study.

I. The solubility of $Ce_2(CO_3)_3(s)$ can be written

$$B = [Ce^{3+}] + \sum_p \sum_r [Ce(OH)_p(CO_2)_r] = b(1 + \sum_p \sum_r \beta_{p,r} h^{-p} a^r) \quad (7)$$

with p and r integer.

Introducing into eqn. (7) the equilibrium constant for reaction (4)

$$k_{s,I} = b^2 a^3 h^{-6}$$

and

$$K_p = \sum_r \beta_{p,r} a^r$$

valid for a series of measurements at constant a, we recalculated the experimental data in the form (8).

$$\alpha_a = \log (B a^{3/2} h^{-3})_a = \tfrac{1}{2} \log K_{s,I} + \log(1 + \sum_p K_p h^{-p}) \quad (8)$$

The $\alpha(-\log h)_a$ curves proved to be parallel, with the spacing

$$((\Delta \log a)/(\Delta \log h))_a = 2.0$$

This indicates [6,7] that the complexes contain 2OH groups per CO_2, *i.e.* $r=p/2$. Thus, eqn. (8) may be written as

$$a = \tfrac{1}{2} \log K_{s,I} + \log (1+\sum_p \beta_{p,p/2}(h^{-2}a)^{p/2}) \quad (9)$$

Fig. 1 shows, as eqn. (9) suggests, that the $a[\log (h^{-2}a)]$ data yield a single curve.

From its slope at the lowest h values,we deduce that the upper limit of p is 4. This means that the most probable values of p are 2 and 4, since $r(=p/2)$ must be an integer.

This hypothesis was tested by comparing the data with normalized model functions.

Assuming $p=2$ and 4,eqn. (9) takes the form

$$a = \tfrac{1}{2} \log K_{s,I} + \log (1+\beta_{2,1}h^{-2}a+\beta_{4,2}h^{-4}a^2) \quad (10)$$

Introducing in eqn. (10) the normalized variable

$$u = \beta_{2,1}\, h^{-2}a \quad (11)$$

the theoretical $Y(\log u)$ curves

$$Y = \log (1+u+Lu^2) \quad (12)$$

with $L=\beta_{4,2}\beta_{2,1}^{-2}$

were calculated for various L values and compared to the experimental $a[\log (h^{-2}a)]$ data.

In the position of best fit, shown in Fig. 1, $\log K_{s,I}$ was obtained from the difference of the ordinates, $\log \beta_{2,1}$ as the difference of the abscissas and $\beta_{4,2}$ from the value of L (=0.03) which gave the best fit.

The results are collected in Table 2. The errors are maximum deviations from the average.

II. At lower acidities, $[Ce^{3+}]$ is negligible and the solubility of $NaCe(CO_3)_2(s)$ can be expressed as

$$B = \sum_p \sum_n [Ce(OH)_p(CO_3)_n] = \sum_p \sum_n \beta_{p,n}\, b h^{-p} c^n \quad (13)$$

where $\beta_{p,n}$ is the equilibrium constant of the reaction

$$Ce^{3+} + pH_2O + nCO_3^{2-} \rightleftarrows Ce(OH)_p(CO_3)_n^{3-p-2n} + pH^+ \quad (14)$$

Introducing into eqn. (13) the equilibrium constant for reaction (5)

$$K_{s,II} = [Na^+]b\, c^2$$

and rearranging, we obtain

$$\psi = \log (B[Na^+]) = \log K_{s,II} + \log (\sum_p \sum_n \beta_{p,n} h^{-p} c^{(n-2)}) \quad (15)$$

In Fig. 2, the $\psi(\log c)$ data are seen to fall on a single curve, although h was varied independently of c. This indicates that p, in eqns. (13)–(15), is equal to zero.

Eqn. (15) can then be more simply written as

$$\psi = \log K_{s,II} + \log (\sum_n \beta_n c^{(n-2)}) \quad (16)$$

From the limiting slopes of the $\psi(\log c)$ function, we deduced that $2 \leq n \leq 4$.

Assuming the formation of three complexes with $n=2$, 3, 4, eqn. (16) takes the form

$$\psi = \log K_{s,II} + \log \beta_2 + \log (1+\frac{\beta_3}{\beta_2}c+\frac{\beta_4}{\beta_2}c^2) \quad (17)$$

The $\psi(\log c)$ data were compared to the normalized model function $X(\log v)$

$$X=\log (1+\rho v+v^2),\ v^2=\beta_4\beta_2^{-1}c^2 \text{ and } \rho=\beta_3(\beta_2\beta_4)^{-1/2} \quad (18)$$

Table 2. Survey of the equilibrium constants.

$-\log \beta_{p,p/2}$	$p=2$ 11.30±0.05	$p=4$ 24.1±0.1		
	$n=1$	$n=2$	$n=3$	$n=4$
$\log \beta_n$	6.32±0.08	11.1±0.1	12.6±0.2	13.7±0.1
$\log K_{s,I}$	21.80±0.05			
$-\log K_{s,II}$	17.5±0.1			

constructed for various values of ρ.

A satisfactory fit (Fig. 2) was obtained with $\rho=1.8$. Since

$$\log \beta_2=\log \beta_{4,2}-2 \log(K_{a1}K_{a2})$$

where $\beta_{4,2}$ refers to $Ce(OH)_4(CO_2)_2^-$, $K_{s,II}$, β_3 and β_4 were calculated as shown previously in this section.

The values of the equilibrium constants and their maximum deviations are reported in Table 2.

DISCUSSION

From the magnitude of the stability constants given in Table 2, one finds that the $Ce(CO_3)_2^-$ complex is predominant over a very wide $[CO_3^{2-}]$ range ($2\cdot10^{-5}$ M$<c<3\cdot10^{-2}$ M). Experimental measurements must be made outside this range in order to provide information on the formation of lower and higher carbonato complexes. This has not always been done in previous studies.

Lundqvist [8] studied the Eu^{3+} and Am^{3+} systems at $c<10^{-2}$ M. Hence, he only obtained information about the formation of $M(CO_3)^+$ and $M(CO_3)_2^-$. His data are in agreement with ours.

Bidoglio [9] studied a more limited c range, where $Am(CO_3)_2^-$ is predominant. He also reports the formation of hydrogen carbonato and mixed hydroxide, carbonate species. Taking the experimental errors into account, it seems possible to describe the largest part of his data with only one complex, $Am(CO_3)_2^-$.

Dumonceau *et al.*[2] find that the limiting complex in the $Ln^{3+}-CO_3^{2-}$ system is the presumably 8-coordinate $Ln(CO_3)_4^{5-}$ which is in agreement with our findings.

Polynuclear complexes seem to form only at rather high total metal ion concentrations in the lanthanoid(III) and actinoid(III) carbonate systems.[1] Weak hydrogen carbonate complexes are formed at $h\simeq10^{-3}$ M.[1]

$Ce_2(CO_3)_3$(s) transforms into $NaCe(CO_3)_2$(s) according to $Ce_2(CO_3)_3(s)+2Na^++CO_3^{2-} \rightleftarrows 2NaCe(CO_3)_2(s)$.

We were not able to make a direct experimental determination of the carbonate concentration, when the two solids are in equilibrium with one another. This is probably due to slow equilibria as observed previously in some lanthanoid–oxalate systems.[10] The equilibrium concentration, $[CO_3^{2-}]=10^{-4.8}$ M, was instead calculated from the solubility products of the two phases.

Some solubility data (at $\log(h^{-2}a)>12.97$) for the $Ce_2(CO_3)_3$-phase have been collected at $[CO_3^{2-}]>10^{-4.8}$ M. Because of the slow rate of phase transformation, these data still represent (metastable) equilibria with $Ce_2(CO_3)_3$(s).

Most deep ground waters have $10^{-9}<h<10^{-6}$ M and total carbonate concentrations in the range 10–200 ppm.[11] Hence, tervalent lanthanoids and actinoids should occur mainly as $Me(CO_3)^+$ and $Me(CO_3)_2^-$ with $Me_2(CO_3)_3$(s) as the most stable solid carbonate phase.

The equilibrium data obtained in a medium of high and constant ionic strength must be recalculated in order to be useful for the description of a ground water. We have previously utilized the specific ion interaction theory for this purpose.[12] Many ground waters have a low content of dissolved electrolytes and equilibrium constants valid for $I=0$ can then be used. From the following values for the interaction parameters

$$\varepsilon(Ce^{3+},HCO_3^-) \simeq \varepsilon(Ce^{3+},ClO_4^-) \simeq \varepsilon(La^{3+},ClO_4^-) = 0.47^{1}$$

$$\varepsilon(CeCO_3^+,ClO_4^-) \simeq \varepsilon(YCO_3^+,ClO_4^-) = 0.17^{11}$$

$\varepsilon(Ce(CO_3)_2^-,Na^+)\simeq0$ (taken as the average of $\varepsilon(A^-,Na^+)$ in Table 5 of Ref. 13.

$$\varepsilon(Na^+,CO_3^{2-}) = -0.05^{13}$$

we obtain

$$\log K_{s,I}\ (I=0)=18.9\pm0.4$$

$$\log \beta_1(I=0)=8.4\pm0.4$$

$$\log \beta_2(I=0)=13.7\pm0.4$$

Acknowledgements. This work was financed through grants from the Swedish Natural Science Research Council, The National Council for Radioactive Waste (PRAV) and the Swedish Nuclear Fuel Supply Co., Div. KBS.

REFERENCES

1. Ciavatta, L., Ferri, D., Grenthe, I., Salvatore, F. and Spahiu, K. *Acta Chem. Scand. A 35* (1981) 403.
2. Dumonceau, J., Bigot, S., Treuil, M., Faucherre, J. and Fromage, F. *Rev. Chim. Miner. 16* (1979) 583.
3. Wakita, H. *Bull. Chem. Soc. Jpn. 51* (1978) 2879.
4. Johansson, L. *Coord. Chem. Rev. 3* (1968) 293.
5. Spahiu, K. *Thesis*, Royal Institute of Technology, Stockholm 1983.
6. Sillén, L. G. *Acta Chem. Scand. 8* (1954) 299.
7. Sillén, L. G. *Acta Chem. Scand. 8* (1954) 318.
8. Lundqvist, R. *Acta Chem. Scand. A 36* (1982) 741.
9. Bidoglio, G. *Radiochem. Radioanal. Lett. To be published.*
10. Grenthe, I., Gårdhammar, G. and Rundcrantz, E. *Acta Chem. Scand. 23* (1969) 93.
11. Swedish Nuclear Fuel Supply Co., Div. KBS, *Technical Reports.*
12. Biedermann, G., Bruno, J., Ferri, D., Salvatore, F. and Spahiu, K. *Proc. Fifth Int. Symp. on the Scientific Basis for Radioactive Waste Management, Berlin 1982, In press.*
13. Ciavatta, L. *Ann. Chim. Rome 70* (1980) 551.

Received October 20, 1982.

Acta Chemica Scandinavica A 37 (1983) 367–381

X-Ray Diffraction Studies of the Structures of Melts within the System (Ag,K,Na)–(I,NO_3)

BERTIL HOLMBERG [a] and GEORG JOHANSSON [b]

[a] Physical Chemistry 1, Chemical Center, P.O. Box 740, S-220 07 Lund 7, Sweden and [b] Department of Inorganic Chemistry, Royal Institute of Technology, S-100 44 Stockholm 70, Sweden

The structures of 11 melts of different compositions in the system (Ag,K,Na)–(I,NO_3) have been studied by X-ray diffraction methods at 280 °C. For pure $AgNO_3$ and $AgNO_3$–$(K,Na)NO_3$ mixtures the scattering data indicate a preferred orientation of the nitrate groups around the silver ions with one O closely bonded (2.45 Å) and another O more distant (3.0 Å). For the binary mixed anion system AgI–$AgNO_3$ a model based on a close-packed arrangement of the I^- and NO_3^- ions, with Ag^+ occupying tetrahedral holes can explain the scattering data over the whole range of compositions investigated. This is similar to the anion arrangement in the solids Ag_2INO_3 and $Ag_3I(NO_3)_2$ in which, however, the Ag^+ ions occupy octahedral holes.

For systems AgI–$AgNO_3$–$(K,Na)NO_3$ the short-range cationic arrangement around each I^- is characterized by about four distinct Ag–I distances of 2.8 Å irrespective of the overall Ag^+ fraction (0.38 and 0.75). The non-random cation distribution is consistent with previous thermodynamic data. No specific Ag–Ag correlations in the coordination sphere of I^- can be observed, however.

The formation of cationic complexes Ag_2I^+, Ag_3I^{2+}, and Ag_4I^{3+} has been proposed by different authors to account quantitatively for the increase in solubility of AgI with increasing concentration of Ag^+ in aqueous $AgClO_4$ and $AgNO_3$ solutions.[1,2] The existence of complex cations $Ag_mX^{(m-1)+}$ in binary melts AgX–$AgNO_3$ was suggested by Schwartz already in 1941,[3] and dinuclear silver halide species Ag_2X^+ have often been considered in tests of the quasi-lattice models for ternary melts, dilute in Ag^+ and X^-. This field of chemistry has been briefly reviewed by Holmberg.[4]

From a recent study [5] of the solubility of AgI at 280 °C in molten equimolar mixtures of KNO_3 and $NaNO_3$, containing various amounts of $AgNO_3$, it was concluded that silver and iodide form a series of complex ions $Ag_mI^{(m-1)+}$, with formal charges of +1, +2 and +3. This conclusion was supported by emf measurements of the Ag(I) activity as a function of I^- added to $(K,Na)NO_3$ melts with a high concentration of $AgNO_3$. The average number $\overline{m}$ of Ag(I) in the cationic complexes was estimated to be 3.5–4.0 [5] and the thermodynamic stability of cationic silver iodide complexes in molten $(K,Na)NO_3$ would thus be of the same order of magnitude as that of anionic species, $AgI_n^{(n-1)-}$.

The structure of complex cations of this kind is not known and the present study was made in an attempt to clarify the arrangement of Ag^+ ions around the iodide ions in melts of various compositions in the quasi-ternary system Ag,(K,Na)–I,NO_3 and in the binary subsystems AgI–$AgNO_3$. The temperature chosen for the investigation was the same as that used for the equilibrium measurements, *i.e.* 280 °C. In a parallel research project the crystal structures of a number of compounds $Ag_mX_nA_y$ (X=halide, A=other anion, $m>n$) have been determined,[6] including Ag_2ClNO_3,[7] Ag_2BrNO_3,[8] Ag_2INO_3,[9] $Ag_3I(NO_3)_2$,[10] $Ag_2IF \cdot H_2O$,[11] $Ag_7I_2F_5 \cdot 2.5H_2O$[12] and $Ag_3I(ClO_4)_2$.[13] The structure of the analogous compound $Ag_{13}I_9(WO_4)_2$ is also known.[14] No uniform geometrical arrangement of Ag^+ around the halide atoms is found,

0302-4377/83 $02.50

however, in these structures. In Ag_2ClNO_3 and Ag_2BrNO_3 each Cl^- and Br^- is surrounded by five Ag forming a trigonal bipyramid. In Ag_2INO_3 and $Ag_3I(NO_3)_2$ six Ag^+ form distorted trigonal prisms around I^-. In the fluoride and the perchlorate compounds no well-defined Ag^+ coordination geometry around I^- seems to occur, and $Ag_{13}I_9(WO_4)_2$ is an ionic conductor with Ag^+ freely moving within a network of iodide tetrahedra. Structural relations between the compounds can, however, be found by considering the packing of the anions, which, for example, in Ag_2INO_3, $Ag_3I(NO_3)_2$ and β-$AgNO_3$ (the high-temperature modification of silver nitrate [15]) can be described as close-packed arrangements with Ag^+ ions occupying available holes.

X-Ray diffraction data for 11 different compositions of melts in the Ag,(K,Na)–I,NO_3 system will be presented and discussed in the present paper. It follows from the 553 K isotherm for this system [16] that at this temperature binary melts $AgI-AgNO_3$ can be studied over the composition range $0 \leqq X_I \leqq 0.74$, X_I being the anion fraction of iodide. The general structural change caused by a gradual replacement of NO_3^- with I^- has been followed from pure liquid $AgNO_3$ to a melt of composition $AgI_{2/3}(NO)_{1/3}$. Two of the compositions investigated were chosen to correspond to those of the crystalline compounds Ag_2INO_3 and $Ag_3I(NO_3)_2$ (melting points: 109 and 119 °C, respectively [17]) to allow a direct comparison with the structure of the solids. Previous diffraction studies of multicomponent ionic melts are limited to binary systems with a common anion and the present study seems to be the first report on X-ray diffraction in mixed anion melts. Ternary melts $(K,Na)NO_3-AgI-AgNO_3$ have also been included in the investigation. In order to obtain sufficiently high iodide concentrations in these melts, we have worked with systems having contents of $AgNO_3$ considerably higher than those used in the thermodynamic study.[5] A straightforward extrapolation of the thermodynamic data into this range gives a ligand (Ag^+) number $\bar{m} \approx 4$, *i.e.* each I^- should on an average have four Ag^+ as nearest neighbours irrespective of the overall cationic Ag^+ fraction in the melts.

An analysis of the radial distribution functions (RDF) for the ternary melts requires information on the RDFs for simpler subsystems of similar compositions. Accordingly, binary melts $(K,Na)NO_3-AgNO_3$ and $(K,Na)NO_3-(K,Na)I$ as well as pure equimolar $(K,Na)NO_3$ have also been investigated. Previous structure information on such nitrate melts has emerged essentially from spectral studies and diffraction measurements on single component molten salts.

Although numerous studies of vibrational spectra have presented evidence for strong interactions between silver and nitrate ions in pure liquid $AgNO_3$ and mixtures with alkali metal nitrates,[18–33] no precise information on the nature of the silver-nitrate interaction is available. The spectral characteristics have been considered as due to collective vibrational motions of a quasi-lattice-like structure. The lowering of the nitrate ion symmetry to C_{2v} or C_s, which is generally observed, has also been attributed to the existence of specific contact ion pairs in the melt.[22] Brooker [32] recently considered non-equivalent sets of nitrate ions in molten $AgNO_3$– one associated with a particular cation and one in a non-specific cation environment. Clarke [29] attributed the $AgNO_3$ Raman band at 107 cm^{-1} to a librational oscillation of the nitrate ion around the C_2 axis due to restricted out-of-plane rotation and concluded that Ag^+ is capable of simultaneous association with more than one nitrate ion in mixtures with alkali metal nitrate.

Suzuki and Fukushima [34] investigated the structure of the nitrate ion in pure molten $AgNO_3$ from pulsed neutron diffraction data and found slightly different O–O distances in NO_3^- giving a C_{2v} symmetry. Previous X-ray diffraction studies of related molten salt systems include single component $AgNO_3$ and alkali metal nitrates only.[35–38] Ohno and Furukawa [37] studied molten $AgNO_3$ at 260 °C and proposed a simple cubic (NaCl-like) packing arrangement of ions, but no specific conclusion about any preferential $Ag^+-NO_3^-$ interaction geometry could be drawn from their data.

EXPERIMENTAL

All melts were prepared from *p.a.* grade chemicals, predried, fused under vacuum, purged with dry N_2 and filtered as described previously.[39] The mass density was determined volumetrically in a Pyrex glass vessel, calibrated with $AgNO_3$ by use of the data of Boardman *et al.*[40]

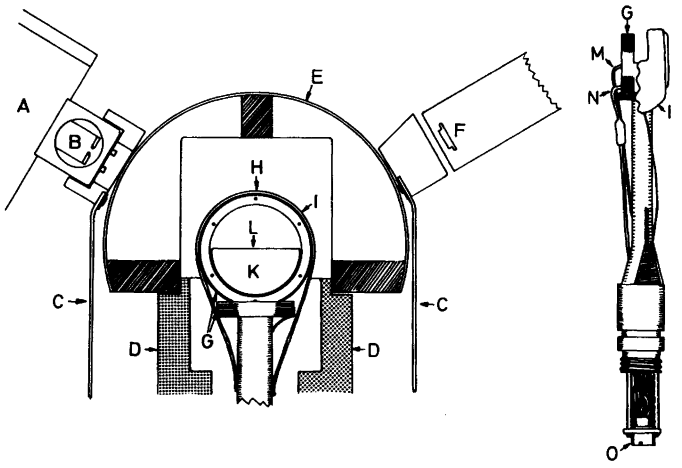

Fig. 1. The experimental arrangement used for the molten salt diffraction measurements. A, X-ray tube; B, Zoller slit; C, lead rubber protection; D, water-cooled metal cylinder; E, beryllium window; F, scatter slit; G, thermocoax heating coil; H, aluminum framed Al window; I, aluminum covered glass fiber; K, glass fiber reinforced teflon container; L, melt; M, Fe-const. thermocouple; N, Pt-100 element; O, connector.

The arrangement used to keep the melt at a constant temperature, usually 280 °C, during the scattering measurements is illustrated in Fig. 1. The sample was kept in a glass-fiber reinforced teflon container shaped as a half cylinder with the open surface 25×30 mm and a depth of 20 mm. It was placed inside a cylinder of aluminum provided with a thermocoax heating element (~25 Ω) and isolated from the surroundings by a layer of glass fiber covered by aluminum foil. An opening for the X-rays about 15 mm wide was covered by 0.01 mm thick aluminum foil. This isolated chamber was positioned inside a cylindrical radiation shield having a 15 mm wide opening for the X-rays covered with a 0.5 mm thick beryllium window. A copper-constantan thermocouple and a Pt-100 resistance thermometer, placed close to the teflon container, were used to measure the temperature. The resistance thermometer also served as a sensor to regulate the temperature which could be kept constant within ±0.1 °C from a preselected value.

The diffractometer has been described in previous papers.[41] Mo$K\alpha$ radiation (λ=0.7107 Å) was used for the diffraction measurements. The radiation scattered from the free surface of the melt was reflected in a curved single crystal monochromator of lithium fluoride before being measured in a scintillation counter provided with a pulse height discriminator. The scattered radiation was measured at discrete intervals of 0.1° for $1°<\theta<20°$ and 0.25° for $20°<\theta<70°$. Three different slit combinations were used to cover the entire θ region. For each point 100 000 counts were collected and each melt was scanned twice, which corresponds to a statistical error of 0.22 % in observed intensity values. Corrections were made for absorption when necessary, for polarization in the sample and in the monochromator, for contributions from incoherent scattering slipping through the monochromator and for multiple scattering. Normalization to a stoichiometric unit of volume containing one formula weight of MX (M=Ag, Na, K and X=NO_3, I) was done by comparing measured intensities in the high-angle region with calculated values for the sum of independent coherent and incoherent scattering. Reduced intensities $i(s)$, where $s=4\pi\lambda^{-1}\sin\theta$, were obtained as

$$i(s) = KI(s) - \sum_{i=1}^{N} n_i \{(f_i(s)+\Delta f_i')^2+(\Delta f_i'')^2+\mathrm{del}(s)I_i^{\mathrm{incoh}}(s)\}$$

Here K is the normalization factor, $I(s)$ the observed intensities corrected for absorption, polarization, and multiple scattering, N is the number of different atomic species in the melt, n_i the number of atoms "i" in the stoichiometric unit of volume, $f_i(s)$ the scattering factors for atom "i", $\Delta f_i'$ and $\Delta f_i''$ the real and the imaginary parts of the anomalous dispersion corrections, $I_i^{\mathrm{incoh}}(s)$ the incoherent scattering and del(s) the

estimated fraction of incoherent scattering passing through the monochromator. The del(s) function was estimated from the spectrum of the X-ray tube and was checked in the high-angle region by comparing measurements done with a Zr filter placed before and after the sample, respectively.

Scattering factors, $f_i(s)$, for the neutral atoms were used.[42,43] Anomalous dispersion corrections, $\Delta f_i'$ and $\Delta f_i''$, were taken from Cromer.[44] Values for incoherent scattering were those given by Cromer.[45] Corrections for the Breit-Dirac factors were applied. All calculations were done with the use of programs described previously.[46]

The reduced intensities were corrected for low-frequency contributions leading to spurious peaks in the D(r) functions below about 1 Å and not ascribable to interatomic distances.[46] The electronic radial distribution functions were calculated from the expression:

$$D(r) = 4\pi r^2\rho_o + \frac{2r}{\pi}\int_0^{s_{max}} si(s)\,(\sin rs)M(s)\mathrm{d}s$$

with the modification function

$$M(s) = [f_I^2(0)/f_I^2(s)]\,\exp(-0.01\,s^2).$$

For an assumed structural model, theoretical intensities were calculated from the Debye expression for discrete intramolecular interactions:

$$i(s)_{calc} = \sum_p \sum_q f_p(s)f_q(s)\frac{\sin(s\,r_{pq})}{sr_{pq}}\exp(-b_{pq}s^2).$$

r_{pq} is the distance between the atoms p and q, and b_{pq} is related to the rms variations l_{pq} of the distance: $b_{pq}=1/2\cdot l_{pq}^2$. Intermolecular interactions were approximated by assuming an evenly distributed electron density outside a sphere of radius R.[46] Corresponding shape functions were calculated by a Fourier inversion analogous to the one used for the experimental intensity data.

Compositions of the melts investigated are given in Table 1 and are indicated in the phase diagrams in Fig. 2.

RESULTS AND DISCUSSION

Systems $AgNO_3$–(K,Na)NO_3. Changes in the radial distribution curves caused by a gradual replacement of the cations in equimolar (K,Na)NO_3 by Ag^+ from (K,Na)NO_3(l) to $AgNO_3$(l) are illustrated in Fig. 3 for the melts A to D.

Table 1. Compositions of the melts investigated.

	Melt	Density/(g cm^{-3})	Stoichiom. vol., V/Å^3	Ag mol l^{-1}	Atoms in V	(K,Na) mol l^{-1}	Atoms in V	NO_3 mol l^{-1}	Atoms in V	I mol l^{-1}	Atoms in V
A	(K,Na)NO_3	1.918±0.004	80.5			20.62	1	20.61	1		
B	$Ag_{0.38}(K,Na)_{0.62}NO_3$	2.663±0.006	76.1	8.24	0.378	13.56	0.622	21.81	1		
C	$Ag_{0.75}(K,Na)_{0.25}NO_3$	3.390±0.007	74.0	16.92	0.754	5.53	0.246	22.45	1		
D	$AgNO_3$	3.890	72.5	22.90	1			22.90	1		
E	$Ag_6I(NO_3)_5$	4.202±0.008	71.4	23.26	1			19.38	0.833	3.88	0.167
F1	$Ag_3I(NO_3)_2$ 280 °	4.536±0.008	70.1	23.68	1			15.79	0.667	7.89	0.333
F2	$Ag_3I(NO_3)_2$ 140°	4.861±0.008	65.4	25.38	1			16.92	0.667	8.45	0.333
G	Ag_2INO_3	4.869±0.010	69.0	24.06	1			12.03	0.500	12.03	0.500
H	$Ag_3I_2NO_3$	5.203±0.010	68.0	24.41	1			8.14	0.333	16.27	0.667
I	$(K,Na)I_{0.05}(NO_3)_{0.95}$	1.974±0.005	81.2			20.44	1	19.35	0.946	1.097	0.054
J	$Ag_{0.38}(K,Na)_{0.62}I_{0.05}(NO_3)_{0.95}$	2.628–0.006	79.4	7.91	0.378	13.02	0.622	19.80	0.946	1.123	0.054
K	$Ag_{0.75}(K,Na)_{0.25}I_{0.05}(NO_3)_{0.95}$	3.495±0.008	73.4	17.05	0.754	5.57	0.246	21.41	0.946	1.214	0.054

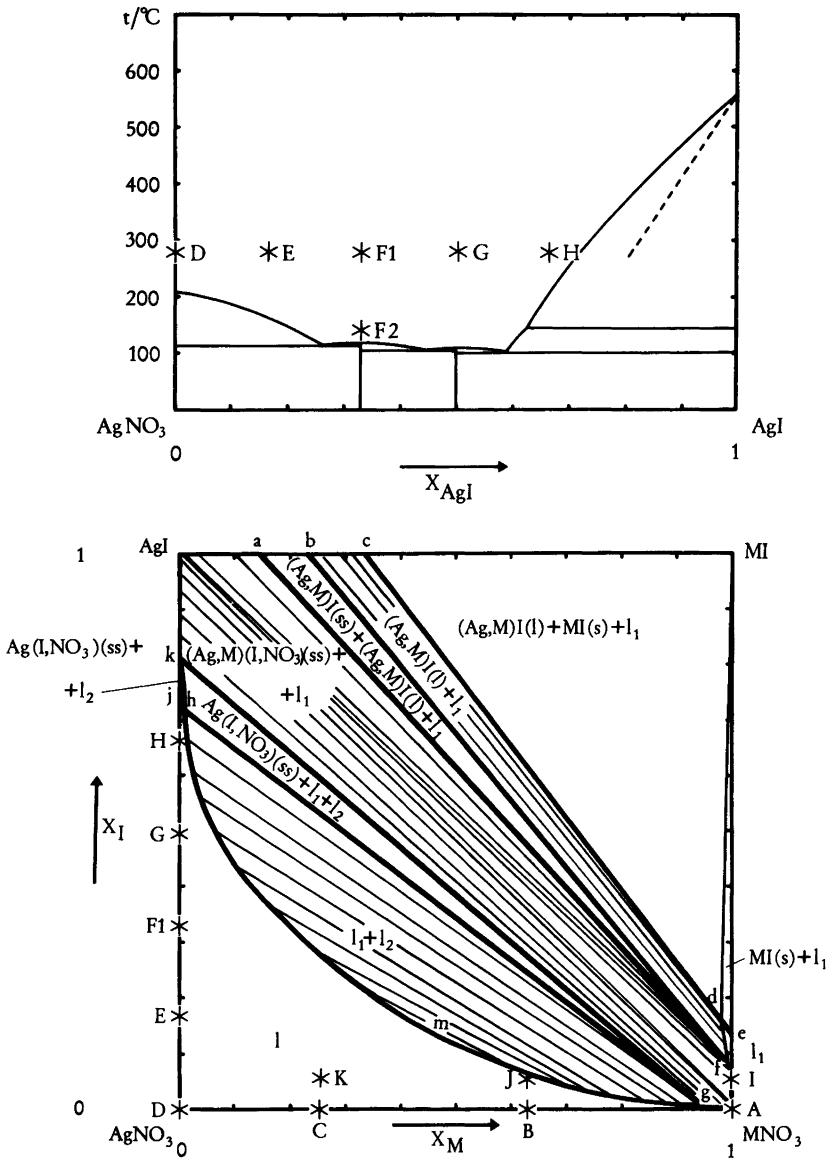

Fig. 2. (a) Phase diagram for the $AgNO_3$–AgI system constructed from data of Refs. 5 and 17. (b) The M,Ag–I,NO_3 isotherm at 280 °C (M=(K,Na)) from Ref. 16. The compositions of all investigated melts are indicated.

The first two peaks in the RDF for pure (K,Na)NO_3 (=A) are observed at 1.2 and 2.1 Å, corresponding to the expected N–O and O–O distances within the nitrate ion. The corresponding peaks for the melts B to D are much less pronounced because of the large concentration of Ag^+ in these systems. The interatomic distances within the planar nitrate ion, which have been used in the model calculations, were set to N–O=1.24 Å and O–O=2.14 Å in accordance with these and previous findings.

For (K,Na)NO_3 the next two peaks occur at about 2.9 Å and 4.3 Å. The first of these most probably corresponds to cation–NO_3^- interac-

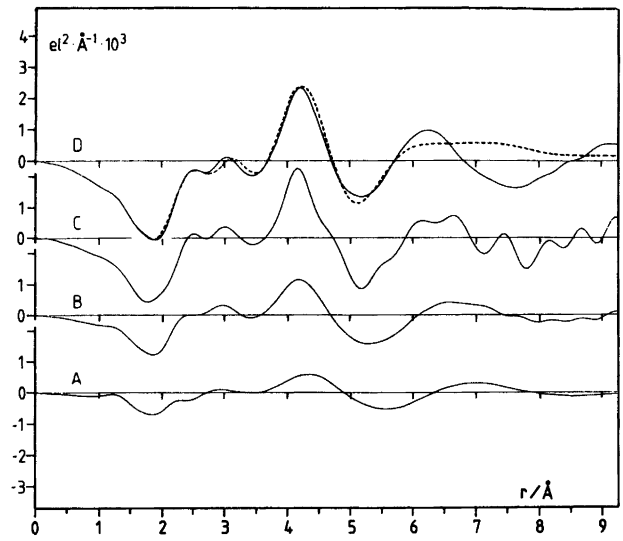

Fig. 3. $D(r)-4\pi r^2\rho_0$ functions for the melts A to D (see Table 1 and Fig. 2). The dashed line for "D" is a theoretical curve calculated with parameter values given in Table 2.

tions. For pure $NaNO_3$(l) (340 °C) and KNO_3(l) (360 °C) the corresponding distance has been reported to be 2.65 and 3.00 Å, respectively.[37] In the mixed cation system (K,Na)NO_3 these two peaks are not resolved and only one broad peak with a maximum at the intermediate value of 2.9 Å appears. The maximum at 4.3 Å also falls between the values 4.00 and 4.35 Å, previously reported for $NaNO_3$(l) and KNO_3(l). These features indicate that the modified close-packed type of ionic arrangement suggested by Ohno and Furukawa [37] for the single component melts might also be a good model description of the mixed alkali metal nitrate melt.

The changes in the radial distribution function caused by replacing alkali metal ions in (K,Na)NO_3 with Ag^+ are illustrated in Fig. 3. An increasing fraction of Ag^+ from 0.38 in "B" to 1.0 in "D" results in increasing peaks at about 2.5 Å, 3.0 Å and 4.2 Å. In crystals, such as Ag_2INO_3,[4] $Ag_3I(NO_3)_2$,[10] β-$AgNO_3$ [15] and $KAg(NO_3)_2$,[47] nitrate groups are often found to be coordinated to Ag^+ in the way illustrated in Fig. 4. One oxygen is closely bonded with an Ag–O distance of about 2.5 Å. Another oxygen occurs at a distance of about 3.0 Å, approximately the same as the Ag–N distance, and the third Ag–O distance is about 4.2 Å. The radial distribution curves in Fig. 3 seem to indicate a similar coordination in molten $AgNO_3$ and $AgNO_3$–(K,Na)NO_3 mixtures.

Two crystalline modifications of $AgNO_3$ have been described and their crystal structures have been determined. In the modification stable at room temperature,[48] Ag^+ ions are joined by shared nitrate groups into pairs with an Ag–Ag distance of 3.22 Å, not much longer than the distance of 2.89 Å found in silver metal. Similar short Ag–Ag distances occur in several other silver compounds.[11] The other modification, β-$AgNO_3$, is unstable at room temperature but can be obtained by rapid supercooling of molten $AgNO_3$. Here the shortest Ag–Ag distances are 4.06 Å and each Ag atom is in close contact (2.45–2.58 Å) with six nitrate oxygens.[15]

The scattering data from the $AgNO_3$ melt can be closely reproduced by a model in which an Ag^+ ion is assumed to coordinate about four

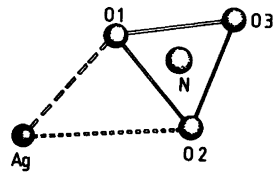

Fig. 4. Suggested model for the coordination of a nitrate group to Ag^+.

nitrate groups in the way shown in Fig. 4. This is sufficient to explain the peaks at 2.5 Å and 3.1 Å in the distribution curves for $AgNO_3$(l) and the presence of short Ag–Ag distances of the type found in many crystals does not have to be assumed. This is shown by the comparison in Fig. 3 of calculated and experimental $D(r)-4\pi r^2\rho_o$ functions for $AgNO_3$(l) (="D"). The parameters used for the theoretical model are given in Table 2 and assume all nitrate groups to be coordinated in the same way with Ag^+ in the plane of the group. The rather limited information contained in the scattering data does not justify a more detailed model in particular, since the light atom interactions cannot be distinguished as separate peaks. Also the calculations are not sensitive towards limited movements of the Ag^+ ion out of the plane of the nitrate group. Thus, the scattering data for $AgNO_3$(l) are consistent with a model with a preferred orientation of the nitrate groups around Ag^+ with frequent Ag–O interactions occurring at about 2.45 Å and 3.0 Å. Significant deviations from this geometry for a large number of nitrate groups are unlikely as

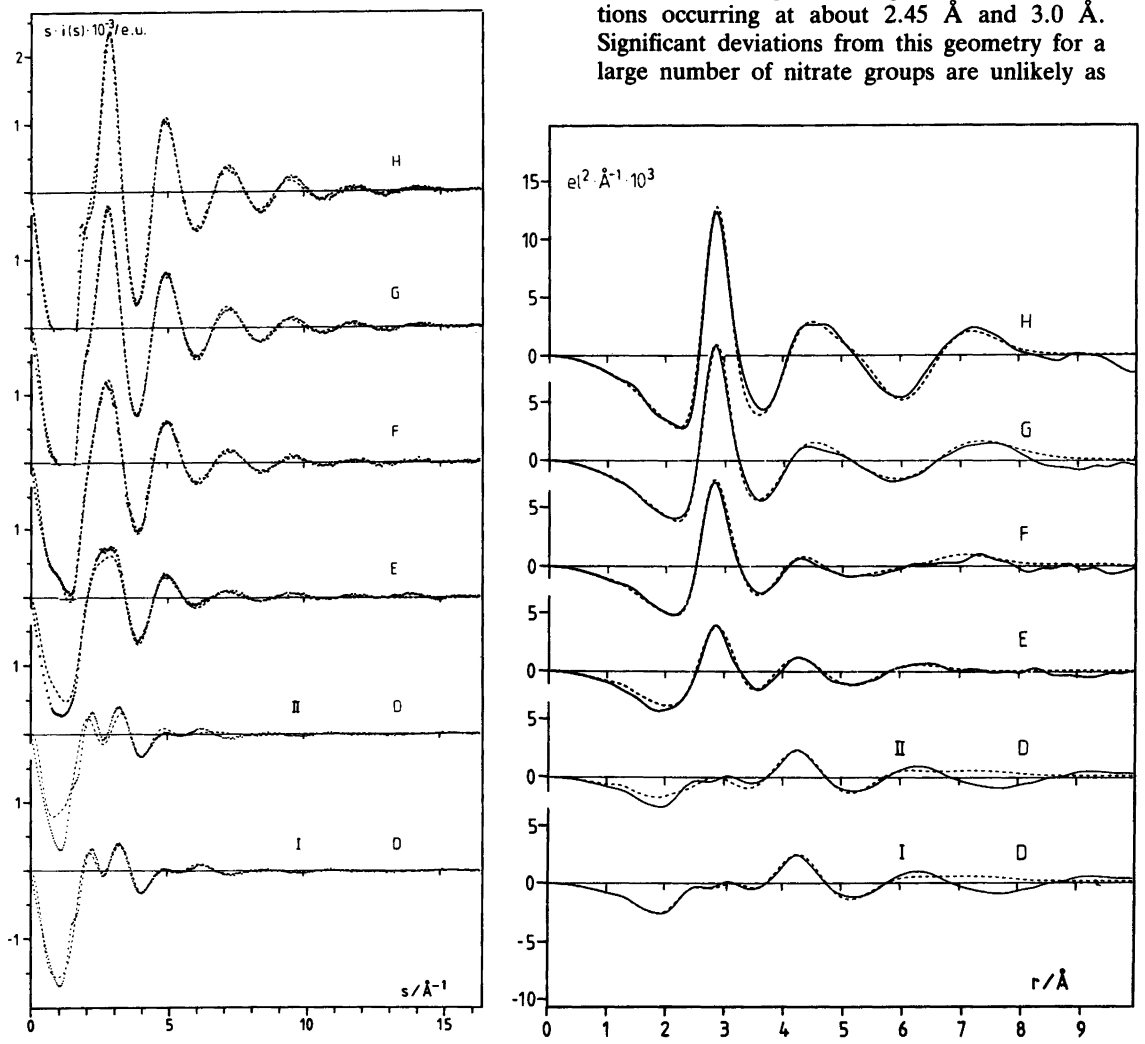

Fig. 5. (a) Comparison between observed (dots) and calculated (dashes) $s\cdot i(s)$ functions for the melts D to H (see Table 1 and Fig. 2). Parameters used for the theoretical curves are given in Table 4 for DII, E, F, G and H and in Table 2 for DI. (b) Corresponding observed (solid lines) and calculated (dashed lines) $D(r)-4\pi r^2\rho_o$ functions.

Table 2. Parameters used for the model calculations for $AgNO_3$(l) in Fig. 3 (D) and Fig. 5 (D:I). The assumed Ag–NO_3 coordination is illustrated in Fig. 4. d=interatomic distance in Å, b=temp. coeff. in Å^2, and n=number of interactions referred to one Ag atom. R=the radius in Å for the emergence of the continuum and B=the corresponding temp. coefficient.

	d	b	n	R	B
Ag–N	3.13	0.04	3.8		
Ag–O1	2.45	0.022	3.8		
Ag–O2	3.05	0.022	3.8		
Ag–O3	4.32	0.06	3.8		
Ag–Ag NO_3–NO_3	4.07	0.17	3.5		
Ag–NO_3	5.4	0.2	8.3		
Ag^+				5.5	0.4
NO_3^-				5.5	0.4

they should result in other peaks than those now observed in the region between 2.5 and 4 Å in the RDF. Freely rotating or randomly oriented nitrate groups cannot explain the two peaks at 2.5 and 3.2 Å, as shown by the comparison in Fig. 5 (DII), which will be discussed later. In the crystal structure of $MAg(NO_3)_2$ (M=K,NH_4 or Rb) [47] and in the high temperature form β-$AgNO_3$, nitrate groups are coordinated approximately as shown in Fig. 4 and for Ag atoms sharing nitrate oxygens the shortest Ag–Ag distances are ~4.1 Å. This distance corresponds to the position of the dominant peak at 4.1 Å in the RDFs for the Ag containing melts (Fig. 3), which has, therefore, been identified with Ag–Ag interactions in the model used (Table 2).

The $D(r)-4\pi r^2\rho_0$ functions for the melts "B" and "C" in Fig. 3 show that the same type of Ag^+–NO_3^- interaction occurs in the mixed $AgNO_3$–(K,Na)NO_3 melts.

Systems AgI–AgNO$_3$. Addition of AgI to $AgNO_3$(l) results in a marked peak at about 2.8 Å in the distribution curves which can be related to Ag–I contact distances in the melts. Other changes are less pronounced as seen by a comparison between the distribution curves given

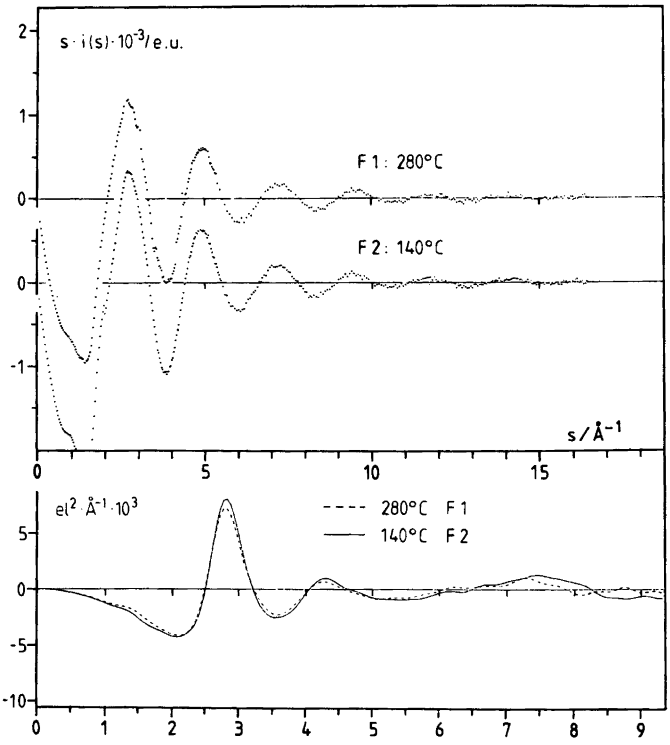

Fig. 6. Comparison between observed $si(s)$ values and $D(r)-4\pi r^2\rho_0$ functions for the melt F at two different temperatures.

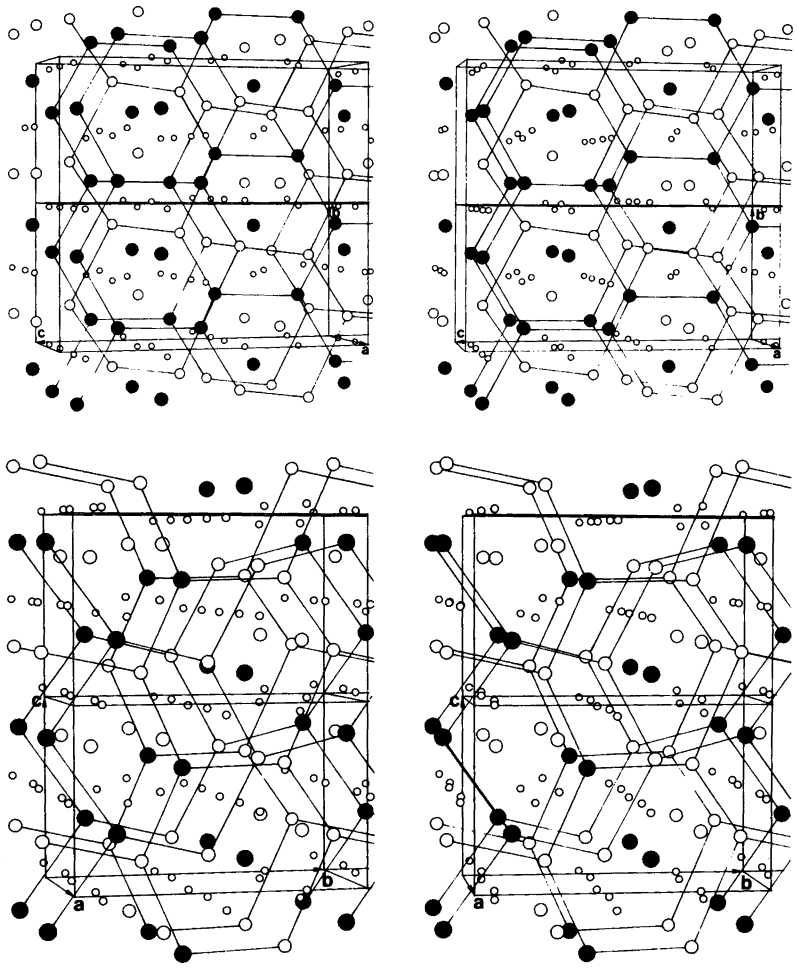

Fig. 7. Stereoscopic views of the ion packings in Ag_2INO_3 (a) and $Ag_3I(NO_3)_2$, (b). Large circles are I^- (filled) and N (open), and small circles represent the Ag^+ positions. The oxygens of the NO_3^- groups are omitted.

in Fig. 5b.

For two of the melts investigated, "F" and "G" in Fig. 5, the compositions correspond to the two solid compounds $Ag_3I(NO_3)_2$ and Ag_2INO_3 (Fig. 2), the crystal structures of which have been determined.[9,10] For the melt "F" with the composition $Ag_3I(NO_3)_2$ diffraction measurements were also made at 140 °C, which is only about 20 K above the melting point of the solid. A comparison between the results obtained for "F" at the two different temperatures is given in Fig. 6. The peaks in the $si(s)$ and the $D(r)-4\pi r^2\rho_o$ functions are slightly less distinct at the higher temperature, but the differences are minor and seem to be limited primarily to a slight broadening of the Ag–I peak at 2.8 Å towards longer distances. The slightly unsymmetrical broadening is probably due to an increased exchange frequency between nearest Ag–I neighbours at the higher temperature, increasing the upper range of distances in the average distribution, whereas the lower range is limited by repulsive forces. Thus no significant structural change takes place in the melt between 280 °C and the melting point.

By assuming the short range order in the crystals to be retained in the melts, distribution

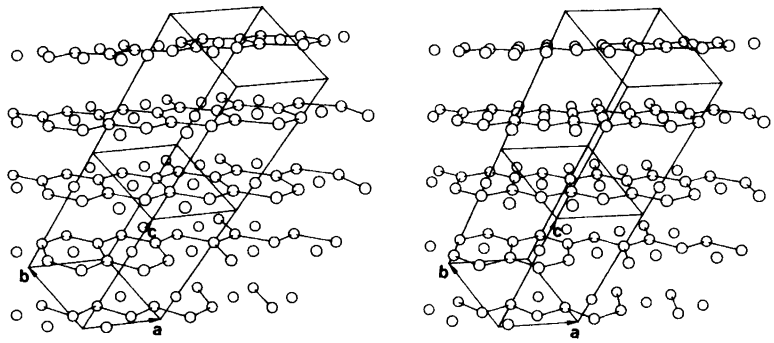

Fig. 8. The nitrate ion arrangement in β-$AgNO_3$, schematically shown by the N positions of the NO_3^- groups.

curves were calculated and were compared with the experimental curves. This comparison showed the degree of order in the melt to be much less than in the crystals. Hence this approach is not very useful for an analysis of the experimental data. It did bring out, however, that the number of Ag–I contacts per I atom is smaller in the melt than in the corresponding crystals and the Ag–I contact distances, which fall in the range 2.865–3.295 Å in the crystals with an average value of 2.99 Å, are shortened to about 2.8 Å in the melts. Also the many Ag–Ag

Table 3. Frequency of distances, *d*, in a regular hexagonal close-packing of anions, X, with cations, M, occupying all tetrahedral holes. *R*=radius of the close-packed anion.

d/*R*	M–M	M–X	X–X	*d*/Å values for *R*=2.15 Å	Peaks in D(r) for melts E–H
0.816	1			1.75	
1.225		8		2.63	2.8
1.414	3			3.04	
2	12		12	4.30	4.2
2.041		2		4.39	
2.160	6			4.64	
2.345		18		5.04	5.2
2.448	4			5.26	
2.708	3			5.82	
2.828	6		6	6.08	
2.858		12		6.14	
3.082		18		6.63	6.8
3.162	12			6.80	
3.266	2		2	7.02	
3.367	3			7.24	
3.464	18		18	7.45	
3.559	6			7.65	
3.674		18		7.90	
3.830	12		12	8.23	
3.851		6		8.28	
3.916	6			8.42	
4	6		6	8.60	
4.021		12		8.65	

distances at around 4 Å in the crystals are much less pronounced in the melts and do not appear as discrete peaks.

For interpreting the distribution curves in terms of a structural model the following approach was found more useful. An analysis of the crystal structures of the two compounds Ag_2INO_3 and $Ag_3I(NO_3)_2$ shows that the anions occupy positions corresponding approximately to a hexagonal close-packing with the NO_3^- ions and the I^- ions distributed over the available anion positions. This is demonstrated in Fig. 7, showing stereoscopic views of the structures. The NO_3^- groups are represented by the N positions only, in order to make the overall anion packing more clear. In these close-packed arrangements the Ag^+ ions occupy the octahedral holes, which lead to the trigonal prisms of Ag atoms surrounding the anions, which were discussed in the original papers on the crystal structure determinations.[9,10]

In the β-$AgNO_3$ structure the nitrate ions are arranged in layers of a close-packed type as shown in Fig. 8, but the stacking of the layers differs from that of a close-packed structure.

The peaks in the radial distribution curves for the melts (Fig. 5) occur at distances approximately corresponding to those expected for a close-packed arrangement (Table 3) of the anions. The peak at about 2.8 Å should then correspond to cation–anion distances, the second peak, at 4.2 Å, to anion–anion and cation–cation distances, and the diffuse peak at about 5.2 Å to cation–anion distances. In Table 3 a comparison is made with the expected distribution of distances for a perfect hexagonal close-packing. Very similar values are obtained for a cubic close-packing, since the most prominent differences in packing statistics between hcp and ccp occur for distances larger than $3R$, with R being the radius of the close-packed anion.

For all of the melts, theoretical curves in satisfactory agreement with those observed could be obtained on the basis of this packing model, assuming I^- and NO_3^- ions to be randomly distributed over the anion sites and using spherical symmetric scattering factors for the nitrate ion. An arbitrarily chosen value of R=5.5 Å was used

Table 4. Parameter values used for the theoretical curves in Fig. 5. X=I^- or NO_3^-, assumed to be randomly distributed.

Type of interaction	Param.	H	G	F1	E	DII
	d	2.82	2.82	2.77	2.70	
Ag–I	*b*	0.015	0.015	0.015	0.021	
	n	3.8	3.8	4.2	4.1	
	d	3.10	3.10	3.10	3.00	2.9
Ag–NO_3	*b*	0.015	0.015	0.015	0.021	0.08
	n	3.8	3.8	4.2	4.1	4.2
	d	3.35	3.35	3.3		
Ag–Ag	*b*	0.03	0.03	0.03		
	n	0.9	0.3	0.2		
	d	4.23	4.19	4.19	4.12	4.07
Ag–Ag X–X	*b*	0.11	0.18	0.17	0.17	0.17
	n	3.5	3.8	4.0	3.6	3.5
	d	5.16	5.20	5.35	5.20	5.50
Ag–X	*b*	0.14	0.21	0.17	0.20	0.16
	n	6.7	6.8	6.2	5.8	7.5
	d	6.8	6.9	6.5	5.9	
Ag–X	*b*	0.18	0.25	0.24	0.22	
	n	1.5	1.5	1.2	2.0	

for the emergence of the continuum around each ion, with a corresponding "temperature coefficient" of B=0.4 Å^2, also arbitrarily chosen, to account for the diffuseness of the beginning of the continuum. For each melt, the distance, d, the temperature coefficient, b, and the frequency, n, of each interaction, were adjusted until the best fit was obtained. The final parameter values are given in Table 4 and a comparison between observed and calculated curves is given in Fig. 5.

For $AgNO_3$(l) the DII and the DI curves in Fig. 5 demonstrate the differences in the theoretical curves when the coordinated nitrate groups in the model discussed above (Figs. 3 and 4) are replaced by randomly oriented nitrate groups. The poor agreement between calculated and experimental curves, when spherically symmetric nitrate groups are used can be observed also in the high-angle part of the $si(s)$ curves (Fig. 5a) for melt "E", where the I^- concentration is not yet sufficiently large to hide this effect.

Other values for R and B than those used can be chosen, which will affect the parameter values associated with the longer distances but may lead to equally good fits between observed and calculated values. The parameter values obtained for the first coordination sphere will not be affected as long as the limit for the continuum is chosen sufficiently large. The parameter values for the "best fit" (Table 4) are found to be approximately equal for the different melts which means that over the whole range of composition investigated the differences in the $si(s)$ and the $D(r)$ functions (Fig. 5) can be fully accounted for by the changing mol fractions of I^- and NO_3^-. The structural change when AgI is introduced into $AgNO_3$(l) thus seems to be limited primarily to a random replacement of NO_3^- ions by I^- on the anion sites.

The analysis shows also (Table 4) that the number of I^- and NO_3^- ions in the first coordination sphere around an Ag^+ ion is close to four in all the melts, which indicates that the cations occupy tetrahedral holes in the close-packed arrangement rather than octahedral holes as in the crystal structures. This change in coordination is indicated also by the shortening of the Ag–I bonds to about 2.8 Å in the melts compared to an average value of 2.99 Å in the crystals.

The number of tetrahedral holes in a close-packed arrangement is twice the number of close-packed anions and, therefore, only 50 % of the tetrahedral holes can be occupied by Ag^+ ions. For the most iodide rich melts an Ag–Ag interaction at about 3.3 Å, had to be included in the model (Table 4) in order to improve the fit to the experimental data. This may be an indication that in these melts the Ag^+ ions tend to occupy two adjacent tetrahedral holes (Table 3) with shared I^-, leading to the short Ag–Ag distances found to be present also in many crystal structures.

Systems AgI–$AgNO_3$–$(K,Na)NO_3$. The coordination around an I^- ion dissolved as (K,Na)I in molten $(K,Na)NO_3$ and $AgNO_3$–$(K,Na)NO_3$ mixtures was studied by comparison of the distribution curves for the melts A, B and C with those for the melts I, J and K (Fig. 2b). This comparison is summarized in Fig. 9.

An introduction of a small amount (~5 mol %) of I^- into the $(K,Na)NO_3$ melt causes only minor changes in the distribution function as seen from the comparison between the melts I and A in Fig. 9. An analogous substitution of NO_3^- by I^- in the Ag^+ containing melts B and C leads to significant changes only in the region around 2.8 Å, corresponding to the Ag–I contact distances (Fig. 9). By comparing the size of the 2.8 Å peak as it appears in the difference curves illustrated in Fig. 9, with peaks calculated by assuming each I^- ion to replace an NO_3^- ion in contact with Ag^+, it is found to correspond to about four I^-–Ag^+ contacts per I^- ion. The curves in Fig. 9 show this number to be independent, within the accuracy of the determination, of the total Ag^+ cation fraction in the melts. This indicates a non-random distribution of cations over the available cation positions and the I^- ion thus associates preferentially with Ag^+. This would seem to be in accordance with the interpretation of thermodynamic data in terms of complex ions $Ag_mI^{(m-1)+}$.[5] An extrapolation of the thermodynamic data into the composition range for the present study gives Ag_4I^{3+} as the dominant species and the interpretation of the thermodynamic and the X-ray diffraction data thus seems to be consistent. However, a remarkable feature in the radial distribution functions for the melts J and K is the virtual absence of significant new contributions from distinct Ag^+–Ag^+ interactions within the coordination sphere around the I^- ion. Such interactions should be expected in the region around 4.5 Å (4.6 Å for a tetrahedral

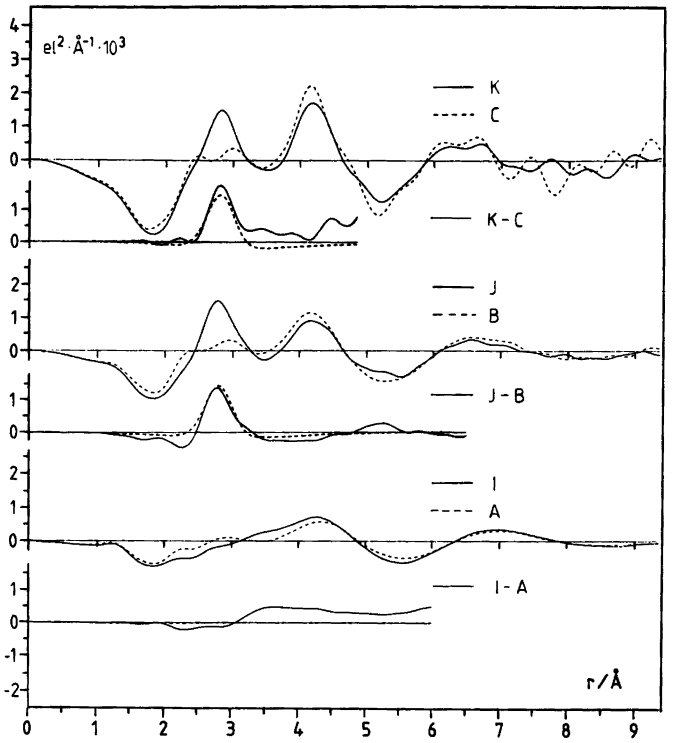

Fig. 9. $D(r)-4\pi r^2\rho_o$ function for the melts A, B and C before (dashed lines) and after (solid lines) addition of about 5 mol % I^-. Differences between the corresponding $D(r)$ functions are given below (solid lines) and are compared with calculated peak shapes (dashed lines) assuming a nitrate group to be replaced by an I^-, bonded to four Ag^+.

arrangement, 4.06 Å for a square planar arrangement), where Ag–Ag interactions occur for the iodide-free melts B and C (Table 2 and Fig. 3). Although unlikely, it cannot be excluded that their formation could be balanced by a breaking up of already existing interactions between Ag atoms sharing a nitrate group. The most likely explanation is, however, a considerable tendency to a random spread in Ag–Ag distances among the Ag^+ ions in contact with an I^-, either becauce of a high mobility or an irregular arrangement of the Ag^+ ions within the I^- coordination sphere.

CONCLUDING REMARKS

It is inherent in the method of liquid X-ray diffraction that it leads to only a one-dimensional representation of the structure, which is not sufficient to resolve the many different types of interactions occurring in a complex system. Even with this limitation, however, valuable structural information can be obtained by following changes in the RDFs with changes in the composition of the system, especially when heavy atoms, which dominate the scattering, are present as the case in the present study.

By comparing the radial distribution functions for various $AgNO_3$–$(K,Na)NO_3$ melts the peaks in the RDFs associated primarily with the Ag^+–NO_3^- interactions can be identified, and a model for the interaction geometry can be derived. This is illustrated in Fig. 4 and it is consistent with the arrangement in the solid high-temperature form of β-$AgNO_3$ as well as in several other crystal structures containing Ag^+ and NO_3^- ions. Such a preferential Ag^+–NO_3^- arrangement would seem to lower the apparent NO_3^- symmetry in accordance with previous

vibrational spectroscopy findings. A coordination of four NO_3^- to Ag^+ in pure molten $AgNO_3$ seems to rule out any description of the melt based on the existence of discrete ion pairs, however, and no distinct nitrate ion symmetry can be deduced from such considerations, since there must be an extensive sharing of NO_3^- ions between Ag^+ ions.

The analysis of distribution functions for binary mixed anion melts $AgI-AgNO_3$ has shown that the close-packed arrangement of anions in the solids Ag_2INO_3 and $Ag_3I(NO_3)_2$ is retained in the melts, although the order in the melt is effectively averaged out beyond a distance of about $3R$, where R is the radius of the anions. On melting, the Ag^+ ions are transferred from the octahedral holes in the solids to a preferential occupation of 50 % of the tetrahedral sites in the corresponding melts.

Changes in the radial distribution functions caused by variations in the I^-/NO_3^- ratio in the $AgI-AgNO_3$ binaries can be satisfactorily accounted for by assuming a random distribution of the two kinds of anions over the sites of a close-packed arrangement. Structural models, based on close-packing geometry, have previously been suggested to account for the structural features of single component molten salts, such as alkali nitrates,[37] sulfates,[49,50] and $ZnCl_2$.[51] The present diffraction study, where mixed anion melts have been investigated for the first time, has thus demonstrated the usefulness of similar approaches to melts with two rather different kinds of close-packed ions.

The results for the quasi-ternary systems $AgI-AgNO_3-(K,Na)NO_3$ indicate a non-random distribution of cations due to a preferential association of I^- with approximately four Ag^+ irrespective of the total cation fraction of Ag^+ in the melts. This finding is in agreement with a straight-forward extrapolation of thermodynamic data for melts considerably more dilute in I^- and Ag^+.[5] On the other hand, no indication of a preferential structural Ag–Ag correlation within a cationic coordination sphere of I^- can be found. Hence, there is no basis for a description of $Ag_mI^{(m-1)+}$ units in these melts by use of classical coordination chemistry concepts. The influence of the structuring properties of the bulk nitrate melt on the total short range order within the closest I^- environment may be of importance. In that perspective, structural studies of analogous systems in other solvents, such as aqueous solutions, should be of value for the clarification of the nature of the proposed $Ag_mI^{(m-1)+}$ species.

Acknowledgements. The work has been supported by the Swedish Natural Science Research Council (NFR).

We thank Mr Ernst Hansen for skilful technical assistance.

REFERENCES

1. Leden, I. and Parck, C. *Acta Chem. Scand. 10* (1956) 535.
2. Lieser, K. H. *Z. Anorg. Allg. Chem. 292* (1957) 114; *Ibid. 304* (1960) 296.
3. Schwartz, K. G. *Z. Electrochem. 47* (1941) 144.
4. Holmberg, B. *Acta Chem. Scand. A 30* (1976) 680.
5. Holmberg, B. *Acta Chem. Scand. A 30* (1976) 797.
6. Persson, K. *Structural Studies on Some Silver(I) and Mercury(II) Halide Compounds in the Solid State,* Thesis, Lund 1981.
7. Persson, K. *Acta Crystallogr. B 35* (1979) 1432.
8. Persson, K. and Holmberg, B. *Acta Crystallogr. B 33* (1977) 3768.
9. Persson, K. *Acta Crystallogr. B 35* (1979) 302.
10. Birnstock, R. and Britton, D. *Z. Kristallogr. 132* (1970) 87.
11. Persson, K. and Holmberg, B. *J. Solid State Chem. 42* (1982) 1.
12. Persson, K. and Holmberg, B. *Acta Crystallogr. B 38* (1982) 1065.
13. Persson, K. and Holmberg, B. *To be published.*
14. Chan, L. Y. Y. and Geller, S. *J. Solid State Chem. 21* (1977) 331.
15. Meyer, P., Rimsky, A. and Chevalier, R. *Acta Crystallogr. B 32* (1976) 1143.
16. Holmberg, B. *Acta Chem. Scand. A 34* (1980) 151.
17. Berg, L. and Lepeshkov, I. N. *Ann. Sect. Anal. Phys. Chim. USSR 15* (1947) 144.
18. Janz, G. J. and James, D. W. *J. Chem. Phys. 35* (1961) 739.
19. Wilmshurst, J. K. and Senderoff, S. *J. Chem. Phys. 35* (1961) 1078.
20. Walrafen, G. E. and Irish, D. E. *J. Chem. Phys. 40* (1964) 911.
21. Janz, G. J. and Kozlowski, T. R. *J. Chem. Phys. 40* (1964) 1699.
22. Wait, S. C., Ward, A. T. and Janz, G. J. *J. Chem. Phys. 45* (1966) 133.

23. Wait, S. C. and Ward, A. T. *J. Chem. Phys. 44* (1966) 448.
24. Devlin, J. P., Williamson, K. and Austin, G. *J. Chem. Phys. 44* (1966) 2203.
25. Li, P. and Devlin, J. P. *J. Chem. Phys. 49* (1968) 1441.
26. Vallier, J. *J. Chim. Phys. Phys.-Chim. Biol. 65* (1968) 1762.
27. James, D. W. and Leong, W. H. *J. Chem. Phys. 51* (1969) 640.
28. Clarke, J. H. R. *Chem. Phys. Lett. 4* (1969) 39.
29. Clarke, J. H. R. and Hartley, P. J. *J. Chem. Soc. Faraday Trans. 2, 68* (1972) 1634.
30. Eluard, A., Balasubrahmanyam, K. and Janz, G. *J. Chem. Phys. 59* (1973) 2756.
31. Kawamura, K. *Trans. Jpn. Inst. Met. 16* (1975) 281.
32. Huang, C.-H. and Brooker, M. *Spectrochim. Acta A 32* (1976) 1715.
33. Prisyazhnyi, V. D., Baranov, S. P. and Kirillov, S. A. *Ukr. Khim. Zh. 45* (1979) 387.
34. Suzuki, K. and Fukushima, Y. *Z. Naturforsch. A 32* (1977) 1438.
35. Danilov, V. I. and Krasnitskii, S. I. *Dokl. Akad. Nauk SSSR 101* (1955) 661.
36. Furukawa, K. *Discuss. Faraday Soc. 32* (1961) 53.
37. Ohno, H. and Furukawa, K. *J. Chem. Soc. Faraday Trans. 1, 74* (1978) 297.
38. Shvets, V. S. and Klintsov, N. Ya. *Ukr. Khim. Zh. 46* (1980) 1152.
39. Hemmingsson, S. and Holmberg, B. *Inorg. Chem. 19* (1980) 2242.
40. Boardman, N. K., Dorman, F. H. and Heyman, E. *J. Phys. Chem. 53* (1949) 375.
41. Johansson, G. *Acta Chem. Scand. 25* (1971) 2787; *20* (1966) 553.
42. Cromer, D. T. and Waber, J. T. *Acta Crystallogr. 18* (1965) 104.
43. *International Tables for X-Ray Crystallography*, Kynoch Press, Birmingham 1968 (Vol. 3) and 1974 (Vol. 4).
44. Cromer, D. T. *Acta Crystallogr. 18* (1965) 17.
45. Cromer, D. T. *J. Chem. Phys. 50* (1969) 4857.
46. Johansson, G. and Sandström, M. *Chem. Scr. 4* (1973) 195.
47. Zobetz, E. *Monatsh. Chem. 111* (1980) 1253.
48. Meyer, P., Rimsky, P. and Chevalier, R. *Acta Crystallogr. B 34* (1978) 1457.
49. Ohno, H. and Furukawa, K. *J. Chem. Soc. Faraday Trans. 1, 74* (1978) 795.
50. Morikawa, H., Miyake, M., Okada, K., Ohno, H. and Furukawa, K. *J. Chem. Soc. Faraday Trans. 1, 76* (1980) 1185.
51. Triolo, R. and Narten, A. H. *J. Chem. Phys. 74* (1981) 703.

Received September 13, 1982.

Acta Chemica Scandinavica A 37 (1983) 383–391

Radicals Formed from α-Tocopherol under Oxidizing and Reducing Conditions. An EPR and ENDOR Study

JORMA ELORANTA, EILA HÄMÄLÄINEN, ESA SALO, REIJO MÄKELÄ and ULLA KEKÄLÄINEN

Department of Chemistry, University of Jyväskylä, SF-40100 Jyväskylä 10, Finland

Oxidation of α-tocopherol with linoleic acid as hydrogen acceptor gave the neutral radical of the corresponding semiquinone in acetic acid. The hyperfine structure was well resolved. The neutral radical was also formed in methanol in the presence of sodium hydroxide and linoleic acid. The anion radical of the semiquinone appeared when the concentration of the sodium hydroxide was sufficiently high.

EPR and ENDOR spectra showed α-tocopherol to yield a single radical with two different proton couplings under the reducing conditions of a sodium–ammonia system at room temperature. At 193 K the EPR spectrum showed the spectral lines of 12 equivalent protons and the ENDOR spectrum only one proton coupling. The effect of temperature was reversible.

The splitting pattern of ^{13}C in natural abundance was also seen in the EPR spectrum. The 6 coupling constants of the 10 carbon atoms appeared in the satellite spectrum.

The oxidation of α-tocopherol has been studied earlier by EPR but resolution of the spectrum was poor.[1,10] Alkali metal reduction of the quinone of α-tocopherol has given the corresponding anion radical of the semiquinone.[2] The spin relaxation processes have been investigated by EPR and ENDOR spectra.[3] A comprehensive treatise on vitamin E has been edited by Machlin.[4]

α-Tocopherol (=RH_2)

$R_1=CH_2-(CH_2-CH_2-\underset{\displaystyle CH_3}{\underset{|}{CH}}-CH_2)_3H$

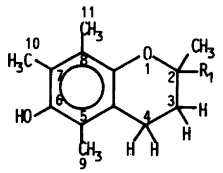

α-Tocopherol produces radicals under oxidizing conditions[4] and we have now extended the studies to cover also the reducing conditions. Two proton and two electron transfers take place in the oxidizing reactions as in the system hydroquinone→quinone. When a hydroquinone loses only one electron it becomes a semiquinone. In this study we used linoleic or oleic acid as the unsaturated compound needed as electron and proton acceptor.

$R_2=CH_2-CH=C(CH_3)-R_1$ and L is the hydrogen acceptor. I is the anion radical of the α-tocopherol, which dimerizes into II in liquid ammonia. III is the cation radical of the corresponding semiquinone, IV the neutral radical, V the anion radical of the semiquinone, and VI α-tocopherolquinone. I and III were not seen in this study. IV can polymerize in many different ways.[4]

EXPERIMENTAL

We employed Varian E-12 and E-9 EPR spectrometers equipped with a Varian gaussmeter and a high frequency counter TR 5211 from Takeda Riken Industry Co. The equipment was connected to a computer programmed to

0302-4377/83 $02.50

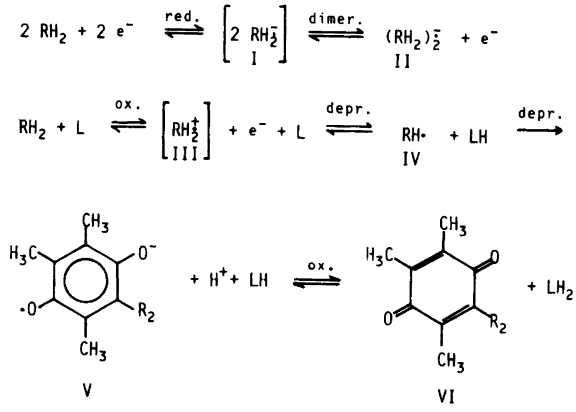

calibrate the changes in high frequency during the measurements. The computer prints out the *g*-values and intensities, and lists the values of the coupling constants in order of magnitude. The coupling constant measured in the different parts of the spectrum differed by less than ±0.01 G. The position of the sample relative to the probe of the gaussmeter proved critical and the sample was carefully adjusted for each measurement. As standards in the *g*-value measurements we used the anion radicals of pyrene, naphtacene and perylene.[5,6] The reproducibility was good to six decimals. Second order corrections were not used. The ENDOR spectra were measured with a Varian E-12 spectrometer equipped with a Bruker Physik ENDOR system B-EN200S. The variable temperature regulators from Varian were controlled with a digital thermometer. The INDO calculations were carried out on a UNIVAC 1100/60 computer.

DL-*α*-Tocopherol for biochemical use was a product of Merck. IR, NMR and UV spectra were identical with spectra in the literature.[4,7,8] The linoleic acid was from Fluka AG (*puriss*) and the oleic acid from Merck. The samples were prepared in nitrogen atmosphere and the high vacuum samples were prepared as before.[9] The ammonia was a Merck product of 99.9 % purity. It was distilled into the ampoule under nitrogen atmosphere.

RESULTS AND DISCUSSION

In ethanol with dissolved oxygen, *α*-tocopherol gave a poorly resolved EPR-spectrum. When the sample was illuminated with a UV-lamp, the radical concentration increased slightly. At room temperature the radical disappeared within half an hour. The lifetime of the radical in the corresponding high vacuum sample was clearly longer, but the radical formation was more difficult.

When linoleic acid was added to a sample of *α*-tocopherol in ethanol with dissolved oxygen, the resolution of the EPR spectrum clearly improved and the hyperfine structure appeared. The radical concentration at room temperature as a function of time seemed to decrease in two steps and the signal disappeared entirely in five hours.

In an attempt to increase the lifetime of IV, methanol, carbon tetrachloride and acetic acid were used instead of ethanol in the above system. In all these solvents the hyperfine structure of the EPR spectra was well resolved. Signal intensity was highest in methanol but the signal disappeared in four hours at room temperature. The resolution was poor when the temperature de-

Table 1. The coupling constants (G) of the neutral radical of *α*-tocopherol (IV), linoleic acid as hydrogen acceptor, 295 K, in different solvents.

	CH_3COOH	CCl_4	CH_3OH	CH_3CH_2OH	CH_3COCH_3[10]	Indo A	Indo B
$-CH_3(11)$	0.54	0.75	0.57	0.65	0.90	−2.65	−2.69
$-CH_3(9)$	4.13	4.41	4.20	4.23	4.75	4.20	4.18
$-CH_3(10)$	5.63	5.94	5.72	5.79	5.75	4.34	4.38
$-CH_2(4)$	0.98	1.39	1.13	1.09	0.90	−3.48	−3.75

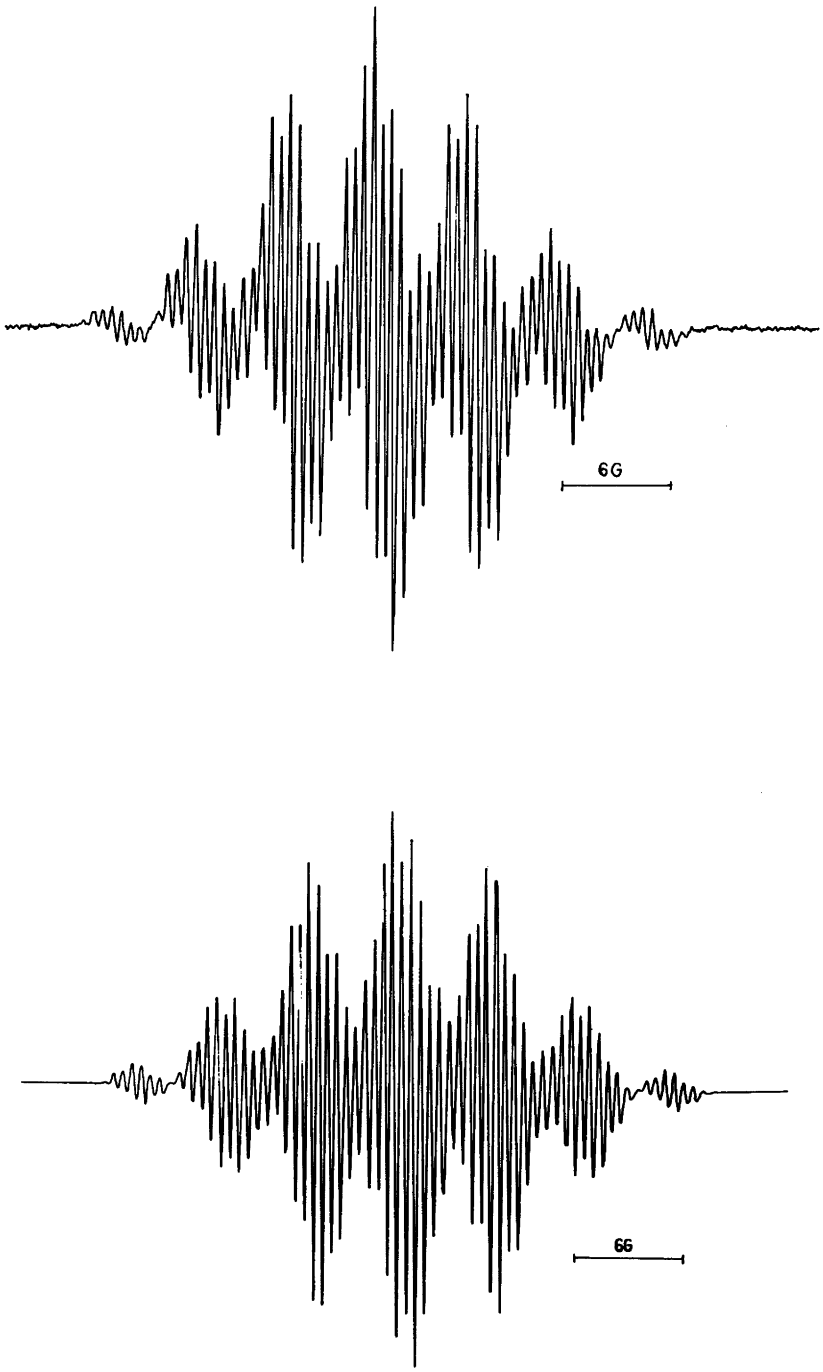

Fig. 1. The EPR spectrum of the neutral radical of α-tocopherol semiquinone (IV) in acetic acid, with linoleic acid as the proton acceptor, at room temperature. (a) Measured spectrum, (b) simulated spectrum.

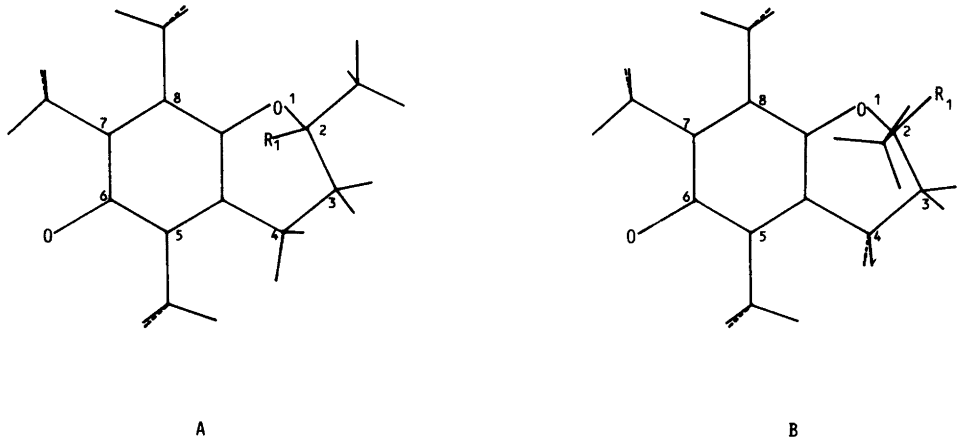

Fig. 2. The two projected conformations of the α-tocopherol structure.

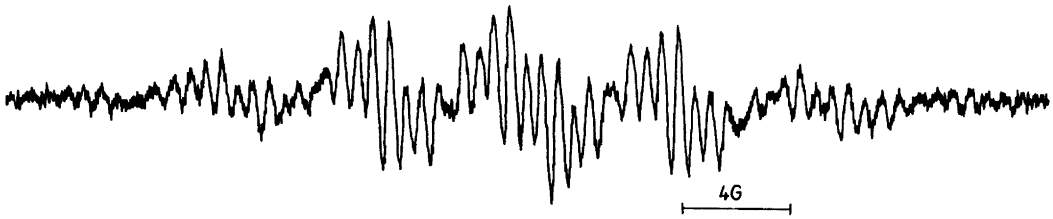

Fig. 3a. The EPR spectrum of the neutral radical of α-tocopherol (IV) in weak alkaline methanol solution at room temperature with linoleic acid as proton acceptor.

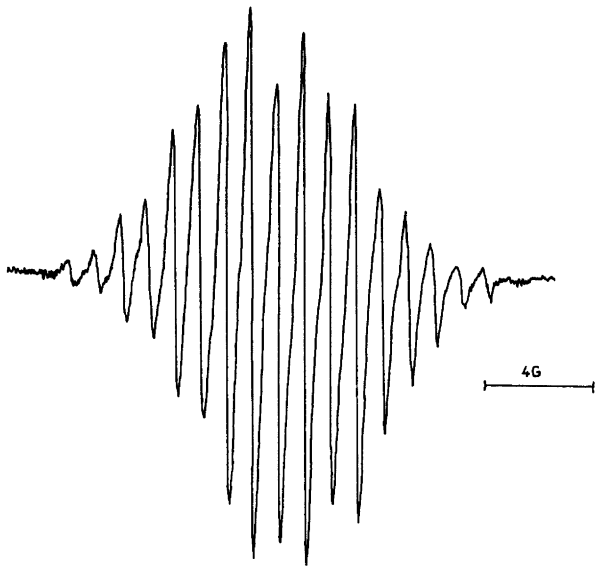

Fig. 3b. The EPR spectrum of the anion radical of the semiquinone (V) in strong alkaline methanol solution at room temperature with linoleic acid as proton acceptor.

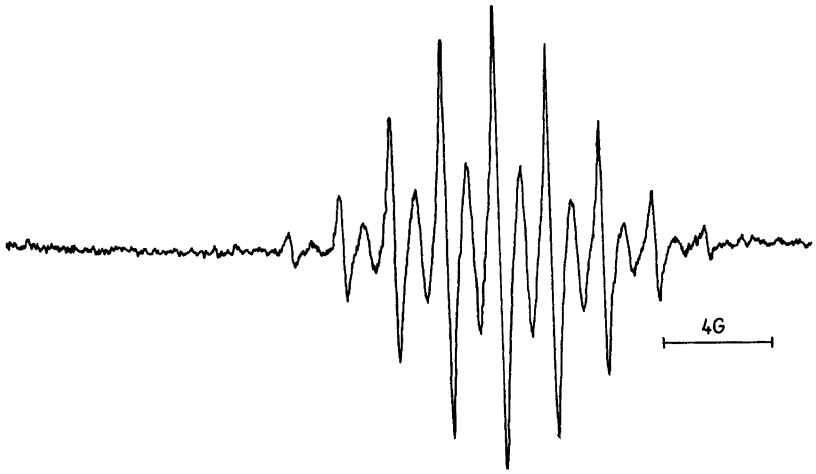

Fig. 4. The EPR spectrum of the anion radical of the α-tocopherol dimer (II) in the sodium–ammonia at room temperature.

creased to 268 K, and increase of the temperature above room temperature accelerated the disappearance of the signal. The best resolved spectrum of IV was obtained in acetic acid (Fig. 1).

When the hydrogen acceptor was oleic acid instead of linoleic acid, the resolution of the EPR spectra was poorer, but the coupling constants were similar. When the solvent was trifluoroacetic acid the EPR spectra showed 7 broad peaks without hyperfine structure.

The coupling constants (Table 1) were somewhat solvent dependent and differed slightly from the values given in the literature.[10] The coupling constants were assigned with INDO calculations. Bond lengths and bond angles were given standard values.[11] Projections of the two conformations of α-tocopherol in the plane of the aromatic ring are seen in Fig. 2. According to INDO calculations the conformation A is energetically a little more favourable than the conformation B. The spin densities of both conformations differ only slightly and in the side chains the spin densities are very small.

α-Tocopherol and linoleic acid in methanol with sodium hydroxide initially gave a poorly resolved spectrum of the neutral radical of the semiquinone (Fig. 3a). When the solution was saturated with sodium hydroxide and the sample was kept for several hours at room temperature, the spectrum of the anion radical of the semiquinone appeared (V, Fig. 3b). The coupling constants were $a(CH_2)=0.95$ G and $a(3CH_3)=1.90$ G, which agree with the values measured by other methods.[2] The semiquinone anion radical was stable for several days at room temperature

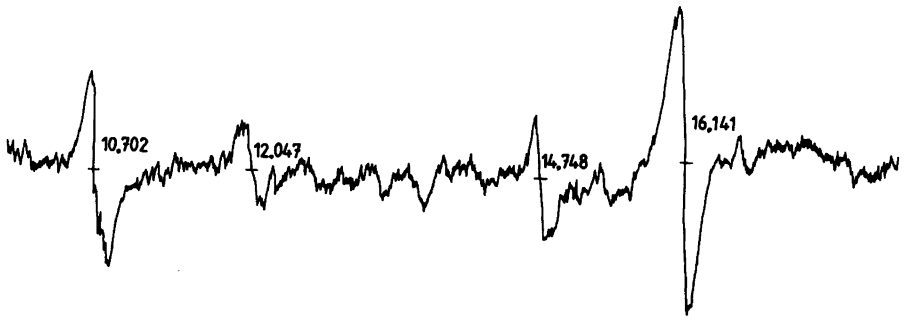

Fig. 5. The ENDOR spectrum of the same sample as in Fig. 4.

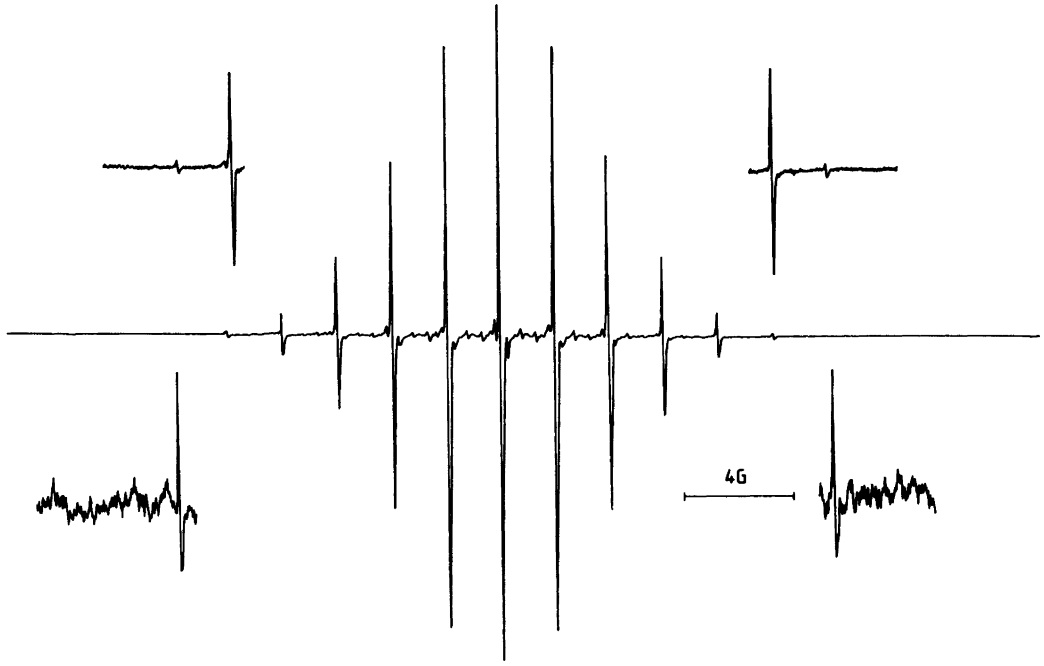

Fig. 6. The EPR spectrum of the same sample as in Fig. 4, at 193 K.

and when the temperature was decreased the hyperfine structure of the EPR spectrum disappeared.

If the concentration of the natrium hydroxide was inadequate the neutral radical disappeared and the spectrum of the anion was not seen. Apparently the neutral radical also may polymerize without anion formation.[4]

Under the reducing conditions in high vacuum in sodium–ammonia without linoleic acid, at room temperature α-tocopherol gave the EPR spectrum seen in Fig. 4 and the ENDOR spectrum seen in Fig. 5. The ENDOR spectrum shows two proton couplings $a(CH_3)=1.94$ G and $a(CH_2)=0.95$ G.

The EPR and ENDOR spectra of the same sample but at 193 K are reproduced in Figs. 6 and 7. There is only one proton coupling $a=1.91$ G in the ENDOR spectrum. In the EPR spectrum in Fig. 6 there are 12 equivalent protons (13 lines). Table 2 shows the effect of temperature on the intensities of the lines. The intensities were

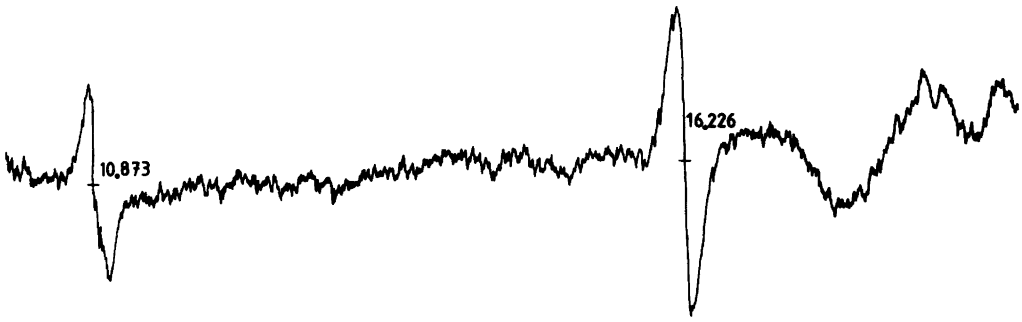

Fig. 7. The ENDOR spectrum of the same sample as in Fig. 4, at 193 K.

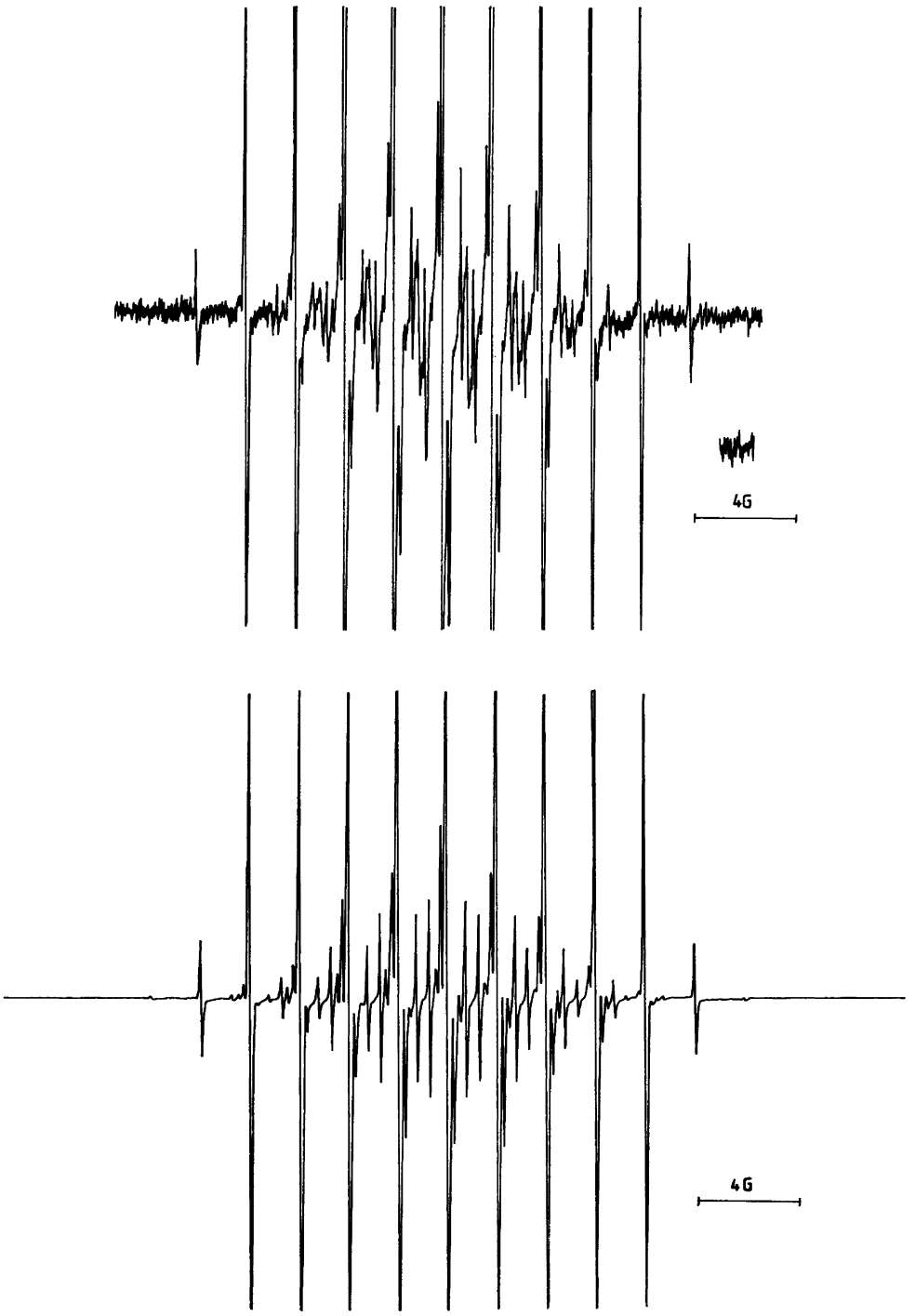

Fig. 8. The EPR ^{13}C satellite spectrum of the anion radical of the α-tocopherol dimer (II) recorded at 193 K. (a) Recorded spectrum, (b) simulated spectrum.

Table 2. The effect of temperature on the relative intensities of EPR spectral lines of α-tocopherol in sodium–ammonia (II).

12 prot. calc. *I*/K	0.0011	0.013	0.071	0.238	0.536	0.857	1.00
295	g=2.00482 a=1.91 G a=0.95 G	–	0.069	0.226	0.531	0.845	1.00
253	g=2.00482 a=1.92 G	–	0.060	0.240	0.521	0.862	1.00
243	g=2.00482 a=1.92 G	–	0.070	0.243	0.530	0.860	1.00
233	g=2.00482 a=1.92 G	–	0.069	0.239	0.531	0.887	1.00
213	g=2.00481 a=1.92 G	0.009	0.065	0.236	0.531	0.856	1.00
193	g=2.00482 a=1.92 G	0.013	0.060	0.237	0.536	0.858	1.00

measured both using a computer and manually from spectra. The measured intensities agree well with the calculated intensities of 12 equivalent protons even at room temperature. Fig. 4 shows that between the main lines there appear new lines. According to the computer analysis the smaller coupling constant at room temperature is 0.95 G, the same as the value measured by ENDOR. The effect of temperature was reversible. The ENDOR measurements did not show the existence of two radicals, even when the magnetic field was locked to different lines.

The coupling constants (1.94 and 0.95 G) are similar in value to those of the anion radical of the semiquinone (V) (1.90 and 0.95 G). However, intensity analysis of the EPR spectrum and the presence of the 12 equivalent protons clearly prove that they are due to different radicals. Indeed it would be hard to believe that the reduction and oxidation reactions followed by ring opening could lead to the same results.

From the structure of the α-tocopherol it can be deduced that the anion radical of α-tocopherol (I) dimerizes to radical II. Otherwise it would be difficult to explain the 12 equivalent protons. Apparently the dimerization takes place at the hydroxyl groups. The 12 equivalent protons are then the methyl protons of the dimer in the positions 9, 10, 9′, 10′. As the temperature increases toward room temperature, the dimer remains stable, but the protons in position 4 start to appear in the spectrum.

Fig. 8a shows the EPR satellite spectrum of the ^{13}C isotope in natural abundance of the anion radical of the α-tocopherol dimer and Fig. 8b the simulated spectrum. Coupling constants of at least ten carbon atoms can be observed. Such a high receiver gain was used in recording the spectrum that between the main lines one can also see the proton coupling of 0.95 G.

The peaks between the main lines become clearly visible near room temperature. The assignment of the methyl carbons (9, 10, 9′, 10′) and (5, 7, 5′, 7′) has been made by INDO calculations on I (Table 3). The INDO calcula-

Table 3. The ^{13}C coupling constants (G) of the satellite EPR spectrum of the anion radical dimer of α-tocopherol (II).

	Positions	INDO
a(4 carbons)=0.44 G	9,10,9′,10′	−4.1
a(4 carbons)=1.40 G	5,7,5′,7′	9.0
a(1 carbon) =4.82 G	6 or 6′	–
a(1 carbon) =4.40 G	6 or 6′	–

tions on the monomer cannot be valid for the largest coupling constant if the dimer is formed through hydroxyl groups, as proposed. The symmetry of the dimer in positions 6,6′ is not complete.

REFERENCES

1. Boguth, W. and Niemann, H. *Biochim. Biophys. Acta 248* (1971) 121.
2. Das, M. R., Connor, H. D., Leniart, D. S. and Freed, J. H. *J. Am. Chem. Soc. 92* (1970) 2258.
3. Leniart, D. S., Connor, H. D. and Freed, J. H. *J. Chem. Phys. 63* (1975) 165.
4. Machlin, L. J. *Vitamin E,* Dekker, New York 1980.
5. Segal, B. G., Kaplan, M. and Fraenkel, G. K. *J. Chem. Phys. 43* (1965) 4191.
6. Allendoerfer, R. D. *J. Chem. Phys. 55* (1971) 3615.
7. *The Sadtler Standard Grating Spectra* 18246 K.
8. *The Sadtler Standard NMR Spectra* 14713 M.
9. Eloranta, J., Salo, E. and Mäkinen, S. *Acta Chem. Scand. A 34* (1980) 42.
10. Kohl, D., Wright, J. and Weissman, M. *Biochim. Biophys. Acta 180* (1969) 536.
11. Pople, J. and Beveridge, D. *Approximate Molecular Orbital Theory,* McGraw-Hill, New York 1970, p. 111.

Received September 23, 1982.

Acta Chemica Scandinavica A 37 (1983) 393–397

Partial Molar Volumes of Some 1-Alcohols in Micellar Solutions

OVE KVAMMEN,[a] GJERMUND KOLLE,[a] SUNE BACKLUND [b] and HARALD HØILAND[a]

[a] Department of Chemistry, University of Bergen, N-5014 Bergen-U, Norway and [b] Department of Physical Chemistry, Åbo Akademi, SF-20500 Åbo 50, Finland

The volumetric behaviour of 1-pentanol, 1-hexanol and 1-heptanol were investigated by means of density measurements in micellar solutions of sodium decanoate, disodium 2-carboxytetradecanoate, sodium dodecylsulfate and hexadecyltrimethylammonium bromide at 298.15, 303.15 and 313.15 K. The partial molar volumes of the alcohols in the different micellar solutions have been compared with the molar volumes of the pure alcohols and the partial molar volumes at infinite dilution in water and in heptane. The results show a greater tendency for the higher alcohols to be solubilized in the micelles. The degree of solubilization seems to be a function of the surfactant molality.

The partial molar volume has proved to be a useful quantity in obtaining information about surfactant solutions.[1–13] The surfactant molar volumes increase on passing from the aqueous environment below the c.m.c. to the nonpolar one above the c.m.c.[2,7,11,12] It has been concluded that the micellar interior is liquid-like and that the hydrocarbon chains acquire a slightly looser structure than in liquid hydrocarbon.[1,4] Corkill *et al.*[4] also suggest that the hydration of the methylene groups adjacent to the hydrophilic group is retained in the micellar state.

The partial molar volume of the surfactant has also been studied under the influence of various additives.[1,14–25] Added neutral salts [1,18,19] and higher alcohols [1] had very little effect on the partial molar volumes of the surfactants. As lower alcohols were added, it was observed that the partial molar volumes of the surfactant molecules in the singly dispersed state first decreased and then increased.[17,21,25] Adddition of these alcohols apparently affected the solvent structure and solute–solvent interactions by changing the composition and dielectric constant of the environment.[25] On the other hand, the partial molar volumes of the surfactants in the micellar state increase gradually upon addition of lower alcohols.[17,21,24,25]

There have, however, been rather few investigations [1,21,26–29] of the volumetric behaviour of the additives. Vikingstad *et al.*[21,28,29] report that the partial molar volumes of *n*-alkanes and *n*-alcohols in sodium alkanoate micelles are higher than those in water but close to those of pure alkanes and alcohols, respectively. For alcohols the volumes descrease with increasing chain length of the surfactant [1,29] and with increasing surfactant concentration.[29]

When an alcohol is added to an aqueous micellar solution, it will be partitioned between the aqueous and micellar phases. The measured partial molar volume will be affected by this partitioning, and it is thus possible to obtain information about the degree of solubilization. Manabe *et al.*[26] have even calculated distribution coefficients of some alcohols in sodium dodecylsulfate from partial molar volume data.

It thus seems worth while to carry out systematic studies of the partial molar volumes of solubilizates in surfactant solutions. In this work we present data for pentanol, hexanol and heptanol in various surfactants.

EXPERIMENTAL

Chemicals. Sodium decanoate (NaC_{10}) was prepared by neutralization of decanoic acid with NaOH. Disodium 2-carboxytetradecanoate (Na_2C_{15}) was made from malonic ester synthesis

0302-4377/83 $02.50

using dodecylbromid and diethyl malonate. The details have been described elsewhere.[10,12] Hexadecyltrimethylammonium bromide (HTAB) was from Sigma and sodium dodecylsulfate (NaDDS) was BDH-"specially pure". The surfactants were dried in an evacuated desiccator at about 340 K for 48 h before they were used. 1-Pentanol (C_5OH), 1-hexanol (C_6OH) and 1-heptanol (C_7OH) were *puriss* quality from Fluka and were used without further purification.

Measurements. All solutions were made by weight. The densities of the solutions were measured with a Paar DMA 601 density meter. The temperature was controlled to better than ±0.005 K as measured by a Hewlett-Packard quartz thermometer.

RESULTS AND DISCUSSION

All measurements were made in homogeneous solutions in the water-rich region of the different water–surfactant–alcohol systems.

The apparent molar volumes of the alcohols, V_{ϕ,C_nOH}, were calculated by eqn. (1).

$$V_{\phi,C_nOH} = \frac{\rho^* - \rho}{m_{C_nOH}\rho^*\rho} + \frac{M_{C_nOH}}{\rho} \qquad (1)$$

Here M_{C_nOH} is the molar mass and m_{C_nOH} the molality of the alcohol, calculated as mol kg^{-1} solvent (water+surfactant). In eqn. (1) ρ and ρ^* are the densities of the solution and solvent, respectively.

Fig. 1 shows typical plots of V_{ϕ,C_nOH} *versus* m_{C_nOH} in different surfactant solutions. The partial molar volumes of the alcohols at infinite dilution, $V^{\infty}_{C_nOH}$, were obtained from linear extrapolations. The concentration dependence of the apparent molar volume is generally considered to reflect solute–solute interactions other than the long-range Debye-Hückel type.[30] From Fig. 1 it can be seen that the slope of V_{ϕ,C_nOH} *versus* m_{C_nOH} is larger in the NaDDS and HTAB solutions than in NaC_{10} solutions. In the latter case, the concentration ratio between alcohol and surfactant never exceeds 1:1. However, for the NaDDS and HTAB systems this ratio may become as large as 5:1. It is therefore possible that the larger slope observed for these systems reflects interactions between alcohol molecules in the micellar phase.

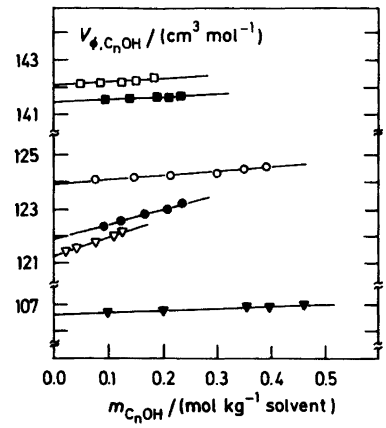

Fig. 1. Apparent molar volumes of 1-alcohols plotted *versus* the alcohol molality in different surfactant solutions at 303.15 K: 1-Heptanol in 0.15 m Na_2C_{15} (□), in 0.45 m NaC_{10} (■); 1-hexanol in 0.45 m NaC_{10} (○); in 0.1 m NaDDS (●), in 0.02 m HTAB (▽); 1-pentanol in 0.45 m NaC_{10} (▼).

Table 1. Partial molar volumes of some 1-alcohols, $V^{\infty}_{C_nOH}$, in micellar solutions of sodium decanoate at 303.15 and 313.15 K. The errors in measured $V^{\infty}_{C_nOH}$ were within ∓0.4 cm^3 mol^{-1}.

Alcohol	T / K	$V^{\infty}_{C_nOH}$, cm$_3$ mol^{-1} 0.30 m	0.45 m	0.60 m	0.90 m
C_7OH	303.15	142.0	141.5	141.2	140.7
	313.15	143.5	142.9	142.5	142.1
C_6OH	303.15	124.6	124.1	123.9	123.7
	313.15	125.5	125.1	125.0	124.8
C_5OH	303.15	106.6	106.6	106.6	106.6
	313.15	107.7	107.6	107.6	107.6

The partial molar volumes of 1-heptanol, 1-hexanol and 1-pentanol in micellar solutions are given in Table 1 as a function of $m_{NaC_{10}}$ at 303,15 and 313,15 K. Vikingstad [29] has measured the corresponding values in 1 m NaC_{10} at 298.15 K. By extrapolation of our data, we find good agreement with his values. It can be seen from Table 1 that for C_7OH and C_6OH there is a small decrease in the volumes as $m_{NaC_{10}}$ increases.

$V^{\infty}_{C_nOH}$ apparently varies with the surfactant molality. In order to compare data for various alcohols in various surfactants a common reference point, with regard to surfactant concentration, must be found. The natural choice seems to be an extrapolation of $V^{\infty}_{C_nOH}$ to the c.m.c. of the surfactant concerned. One thus obtains the partial molar volume of the alcohol infinitely diluted in a surfactant at its c.m.c., $V^{\infty}_{C_nOH\,(cmc)}$. An example of such an extrapolation is given in Fig. 2.

Since the alcohol is distributed between the micellar and aqueous phases, the following expression can be set up for the measured partial molar volume

$$V_{C_nOH} = \alpha V^{mic}_{C_nOH} + (1-\alpha) V^{ag}_{C_nOH} \qquad (2)$$

Here α is the fraction of alcohol molecules solubilized in the micelles. $V^{mic}_{C_nOH}$ and $V^{ag}_{C_nOH}$ are the partial molar volumes of alcohol in the micellar and aqueous phases, respectively. Manabe *et al.*[26] have measured partial molar volumes of alcohols in NaDDS solutions below the c.m.c., obtaining a partial molar volume equal to the one in pure water. $V^{ag}_{C_nOH}$ in eqn. (2) may therefore be taken as equal to the partial molar volume of the alcohol in water. $V^{mic}_{C_nOH}$ cannot be measured. However, Manabe *et al.*[26] have calculated distribution coefficients from eqn. (2) by assuming that $V^{mic}_{C_nOH}$ is equal to the molar volume of the pure alcohol, $V^{*}_{C_nOH}$. This appeared to be a reasonable assumption since the partial molar volumes of nonanol and decanol were almost equal to $V^{*}_{C_9OH}$ and $V^{*}_{C_{10}OH}$, respectively, and very little nonanol or decanol are believed to be dissolved in the aqueous phase. Our results, however, show that even $V^{\infty}_{C_7OH(cmc)}$ in NaC_{10} at 303.15 K is almost equal to $V^{*}_{C_7OH}$. Using the argument of Manabe *et al.*[26] this equality indicates that practically all heptanol is solubilized in the micelles. In our opinion this is not reasonable. Vikingstad [29] has measured $V^{\infty}_{C_{10}OH}$ in 2 m

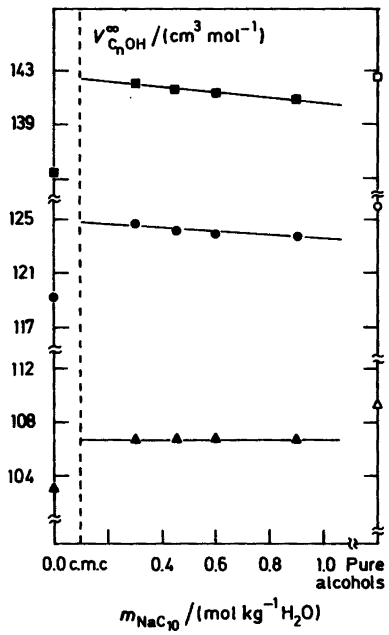

Fig. 2. Partial molar volumes of 1-heptanol (■), 1-hexanol (●) and 1-pentanol (▲) in micellar solutions of sodium decanoate at 303.15 K plotted *versus* the surfactant molality. The partial molar volumes of the alcohols infinitely diluted in water are also plotted in the figure together with the molar volumes of the pure alcohols (open symbols).

sodium octanoate and obtained a value of 193.6 cm^3 mol^{-1} which exceeds the value of $V^{*}_{C_{10}OH}$ by 2 cm^3 mol^{-1}. Accordingly, we think that it is not correct to identify $V^{mic}_{C_nOH}$ with $V^{*}_{C_nOH}$. The correct value of the partial molar volume of an alcohol in the micellar phase, $V^{mic}_{C_nOH}$, probably lies between the value in pure alcohol and the value in liquid alkane. The partial molar volumes of alcohols in liquid heptane are given in Table 2, and they are seen to be larger than $V^{*}_{C_nOH}$.

Because $V^{mic}_{C_nOH}$ in eqn. (2) is unknown, the volumetric results presented in this work cannot at present be used in any quantitative calculations of the distribution of the alcohols in micellar solutions. From the results, it is, however, possible to give a qualitative description of the distribution process. From Fig. 2 and Table 2 it turns out that $V^{ag}_{C_nOH} < V^{\infty}_{C_nOH(cmc)} < V^{*}_{C_nOH}$. The difference between $V^{ag}_{C_nOH}$ and $V^{\infty}_{C_nOH(cmc)}$ is smallest for pentanol increasing with the chain

Table 2. Partial molar volumes of some 1-alcohols in different solvents at 303.15 K and the molar volumes of the same alcohols and at the same temperature.

Alcohol	Volume, $cm^3\ mol^{-1}$						
	H_2O [a]	NaC_{10} [b] at c.m.c.	Na_2C_{15} [c] at c.m.c.	Nadds [b] at c.m.c.	HTAB [b] at c.m.c.	Pure [d] alcohol	Heptane [b]
C_7OH	135.10	142.4	143	–	–	142.51	147.5
C_6OH	119.02	124.7	125	121.9	121.3	125.89	131.4
C_5OH	102.94	106.6	106	–	–	109.17	115.1

[a] The values are estimated from Refs. 31 and 34 and are assumed to be better than $\pm 0.10\ cm^3\ mol^{-1}$. [b] The errors are within $\pm 0.4\ cm^3\ mol^{-1}$. [c] The values have been calculated from a few experimental data. [d] The error margin is less than $\pm 0.10\ cm^3\ mol^{-1}$.

length of the alcohol. It means that the higher the alcohol, the larger is the fraction of alcohols solubilized in the micellar state. If $V^{aq}_{C_nOH}$ and $V^{mic}_{C_nOH}$ are constants in eqn. (2), the variation in $V^{\infty}_{C_nOH}$ with surfactant molality in Figs. 2 and 3 means that both α and the distribution coefficient depend on the surfactant molality. Thermodynamic and emf measurements also indicate such a dependence upon surfactant molality.[32,33]

From Table 2 it can be seen that $V^{\infty}_{C_nOH}$ depends on the surfactant. First it appears that the various polar groups of the surfactants could be a significant factor for this difference in $V^{\infty}_{C_nOH}$. However, Vikingstad [29] has observed similar differences in $V^{\infty}_{C_nOH}$ for homologous series of surfactants. It was suggested that this was caused by differences in the packing of the alcohol molecules in the interior of the micelle. Consequently, a second explanation is that $V^{\infty}_{C_nOH}$ depends on the micellar size. Thirdly, differences in the solubilization equilibria may also lead to different values of $V^{\infty}_{C_nOH}$ in different surfactant solutions. The latter effect can be estimated since distribution coefficients have been determined for alcohol–surfactant systems saturated with respect to the alcohol.[32] This contribution turns out to be quite small and works in the opposite direction of the observed differences. The effects of various polar groups or micellar size cannot be separated at this stage, but Vikingstad's argument on the size effects [29] still seems the most plausible.

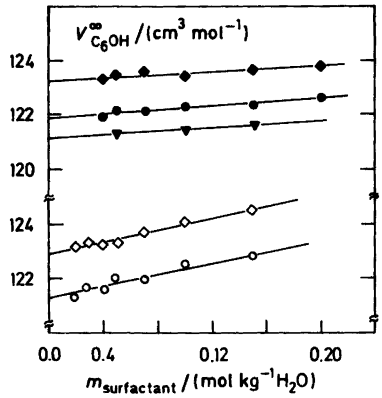

Fig. 3. Partial molar volumes of 1-hexanol in micellar surfactant solutions at 313.15 K (◆), 303.15 (●) and 298.15 K (▼) plotted *versus* the surfactant molality. Filled symbols NaDDS and open symbols HTAB.

Acknowledgement. One of us, S.B., thanks *Nordisk Forskarkurs* for financial support.

REFERENCES

1. Hutchinson, E. and Mosher, C. S. *J. Colloid Sci. 11* (1956) 352.
2. Shinoda, K. and Soda, T. *J. Phys. Chem. 67* (1963) 2072.
3. Benjamin, L. *J. Phys. Chem. 70* (1966) 3790.
4. Corkill, J. M., Goodmann, J. F. and Walker, T. *Trans. Faraday Soc. 63* (1967) 768.
5. Desnoyers, J. E. and Arel, M. *Can. J. Chem. 45* (1967) 359.
6. Leduc, P. A. and Desnoyers, J. E. *Can. J. Chem. 51* (1973) 2993.
7. Musbally, G. M., Perron, G. and Desnoyers, J. E. *J. Colloid Interface Sci. 48* (1974) 494.
8. Sakurai, M., Komatsu, T. and Nakagawa, T. *Bull. Chem. Soc. Jpn. 48* (1975) 3491.
9. Brun, T., Høiland, H. and Vikingstad, E. *J. Colloid Interface Sci. 63* (1978) 89.

10. Vikingstad, E., Skauge, A. and Høiland, H. *J. Colloid Interface Sci. 66* (1978) 240.
11. De Lisi, R., Perron, G. and Desnoyers, J. E. *Can. J. Chem. 58* (1980) 959.
12. Vikingstad, E. and Sætersdal, H. *J. Colloid Interface Sci. 77* (1980) 407.
13. Backlund, S., Hormi, O., Kvammen, O., Høiland, H. and Sjöblom, J. *Finn. Chem. Lett.* (1982) 147.
14. Lee, I. and Hyne, J. B. *Can. J. Chem. 46* (1968) 2333.
15. Philip, P. R., Desnoyers, J. E. and Hade, A. *Can. J. Chem. 51* (1973) 187.
16. Musbally, G. M., Perron, G. and Desnoyers, J. E. *J. Colloid Interface Sci. 54* (1976) 80.
17. Kaneshina, S., Manabe, M., Sugihara, G. and Tanaka, M. *Bull. Chem. Soc. Jpn. 49* (1976) 876.
18. Høiland, H. and Vikingstad, E. *J. Colloid Interface Sci. 64* (1978) 126.
19. Vikingstad, E., Skauge, A. and Høiland, H. *Acta Chem. Scand. A 33* (1979) 235.
20. Vikingstad, E. and Bakken, J. *J. Colloid Interface Sci. 74* (1980) 8.
21. Vikingstad, E. and Kvammen, O. *J. Colloid Interface Sci. 74* (1980) 16.
22. Vikingstad, E. *J. Colloid Interface Sci. 73* (1980) 500.
23. Ogino, K. and Takeshita, N. *Bull. Chem. Soc. Jpn. 53* (1980) 611.
24. Güveli, D. E., Kayes, J. B. and Davis, S. S. *J. Colloid Interface Sci. 82* (1981) 307.
25. Güveli, D. E. *J. Chem. Soc. Faraday Trans. 1 78* (1982) 1377.
26. Manabe, M., Shirahama, K. and Koda, M. *Bull. Chem. Soc. Jpn. 49* (1976) 2904.
27. Vikingstad, E. and Høiland, H. *J. Colloid Interface Sci. 64* (1978) 510.
28. Vikingstad, E. *J. Colloid Interface Sci. 68* (1979) 287.
29. Vikingstad, E. *J. Colloid Interface Sci. 72* (1979) 75.
30. Redlich, O. and Meyer, D. M. *Chem. Rev. 64* (1964) 221.
31. Høiland, H. *J. Solution Chem. 9* (1980) 857.
32. Kvammen, O., Backlund, S. and Høiland, H. In Birdi, K. S., Ed., *Proc. VII Scand. Symp. Surf. Chem.*, Copenhagen 1981, p. 243.
33. Backlund, S. and Rundt, K. In Birdi, K. S., Ed., *Proc. VII Scand. Symp. Surf. Chem.*, Copenhagen 1981, p. 255.
34. Høiland, H. and Vikingstad, E. *Acta Chem. Scand. A 30* (1976) 182.

Received October 15, 1982.

Acta Chemica Scandinavica A 37 (1983) 399–407

The Crystal Structures of Two Forms of $BaBi_2S_4$

BENGT AURIVILLIUS

Division of Inorganic Chemistry 2, The Lund Institute of Technology, P.O.Box 740, S-220 07 Lund, Sweden

Two forms of $BaBi_2S_4$ have been prepared on reacting BaS and Bi_2S_3 at 640 °C, and their crystal structures have been determined. Both forms crystallize in the space group $P6_3/m$. $Z=9$ for 9-$BaBi_2S_4$ and 12 for 12-$BaBi_2S_4$. 9-$BaBi_2S_4$ contains a slight excess of Bi_2S_3 and 12-$BaBi_2S_4$ a slight excess of BaS in relation to the stoichiometric formula. A compound $SrBi_2S_4$ was prepared and was found to be isotypic to 12-$BaBi_2S_4$. The intensity data were collected by means of Weissenberg photographs. The cell dimensions for 9-$BaBi_2S_4$ and 12-$BaBi_2S_4$ are in turn: $a=21.705(7)$ Å, $c=4.158(3)$ Å and $a=25.272(8)$ Å, $c=4.1825(3)$ Å. The corresponding R-factors and numbers of independent reflections are 0.0952(608) and 0.1079(1085), respectively. Comparisons are made to other structures of formula AB_2S_4.

Compounds in the systems $CaS-Bi_2S_3$, $SrS-Bi_2S_3$ and $BaS-Bi_2S_3$ have been discussed by Schenk.[1] He showed that an equilibrium $MeS+Bi_2S_3 \rightleftarrows MeBi_2S_4$ exists for Me=Sr,Ba in the temperature range 456–706 °C and concluded the existence of the compounds $SrBi_2S_4$ and $BaBi_2S_4$. Bok and de Wit [2] reacted BaS, Bi and S at 600 °C for 3 days and obtained a product whose powder photograph was different from those of BaS and Bi_2S_3. The relative intensities and d values of the powder photograph were published but no indexing was made. The present author found that the lines could be interpreted with a hexagonal unit cell with $a=25.14(1)$ Å and $c=4.170(2)$ Å. A systematic study of the systems $SrS-Bi_2S_3$ and $BaS-Bi_2S_3$, using X-ray methods, was started and the present paper reports the results.

EXPERIMENTAL

Preparation and composition. In most experiments SrS or BaS was reacted with Bi_2S_3 in evacuated pyrex tubes at 640, 680 or 780 °C for various lengths of time. Bi_2S_3, 99.999 % (metals basis) and SrS 98 % both from Alfa Division and BaS 98 % from Ventron were used for these experiments. Another way of synthesis was also tried. To prepare $Ba_2Bi_2Se_5$ which later proved to have the composition $BaBiSe_3$,[3] Gattow [4] reacted Bi, $BaAc_2$ and Se in the weight ratio 1:5:5 in closed crucibles at 550 °C. A similar procedure was used here substituting Se by S and in some cases $BaAc_2$ by $SrAc_2$. Powder photographs were taken for all samples. In spite of many efforts, single crystals could not be obtained for the Sr compound. It was, however, noticed that whisker-like crystals were sometimes formed in the $BaS-Bi_2S_3$ samples and reaction times, temperatures and compositions were therefore varied. Small thread-like single crystals were obtained when $BaS{\cdot}1.25Bi_2S_3$ was heated for 7 days at 640 °C. Intensity data could be collected by means of the Weissenberg method. The unit cell was found to be hexagonal with $a=21.705(7)$ and $c=4.158(3)$ Å. Thus the single crystals so obtained had not the same cell dimensions as could be deduced from the data of Bok and de Wit.[2] Inspection of all the powder photographs taken indicated that the two hexagonal phases generally coexisted but with different proportions. Single crystals of the other hexagonal phase were obtained on heating $BaS{\cdot}Bi_2S_3$ for 10 days at 670 °C and the Weissenberg photographs taken indicated a cell with $a=25.3$ and $c=4.18$ Å. The corresponding powder photographs gave $a=25.272(8)$ and $c=4.1825(3)$ Å. 90 % of the lines present could be indexed by the phase. Making reasonable assumptions starting from the cell volumes, $Z=9$ and $Z=12$ were obtained for the two phases.

0302-4377/83 $02.50

They will hereafter be denoted 9-$BaBi_2S_4$ and 12-$BaBi_2S_4$. To elucidate the relations between the two phases, series of measurements were made on samples with ratios $BaS-Bi_2S_3$ 4:1, 2:1, 1:1, 1:1.25, 1:1.50, 1:1.75, 1:2 and 1:4. The samples were first prepared on heating the components to 640 °C for 24 h. They were then recrystallized for 2 h at 420, 680 and 780 °C. 4 batches of BaS were used with different ages from the openings of the bottles. The corresponding powder photographs were indexed using the unit cells of 9-$BaBi_2S_4$, 12-$BaBi_2S_4$ and Bi_2S_3. The fraction $Q(1)$ of indexed lines corresponding to each unit cell was calculated. Due to the fact that a certain line may be indexed in more than one way, the sums of the $Q(1)$ values are larger than 1. Thus pure Bi_2S_3 shows the fractions 0.49, 0.56 and 1.00 for 9-$BaBi_2S_4$, 12-$BaBi_2S_4$ and Bi_2S_3, respectively. The corresponding values for 9-$BaBi_2S_4$ and 12-$BaBi_2S_4$ are in turn 1.00, 0.40, 0.36 and 0.37, 1.00, 0.25. An alternative way of treating the data is as follows. For each phase the fractions, $Q(2)$, of the lines that could solely be indexed by that specific phase was calculated. The fractions so obtained for the pure compounds 9-$BaBi_2S_4$, 12-$BaBi_2S_4$ and Bi_2S_3 are in turn 0.41, 0, 0; 0, 0.52, 0; 0, 0, 0.27. Two of the 4 batches were fresh or nearly so and two were aged. The two groups differed somewhat in

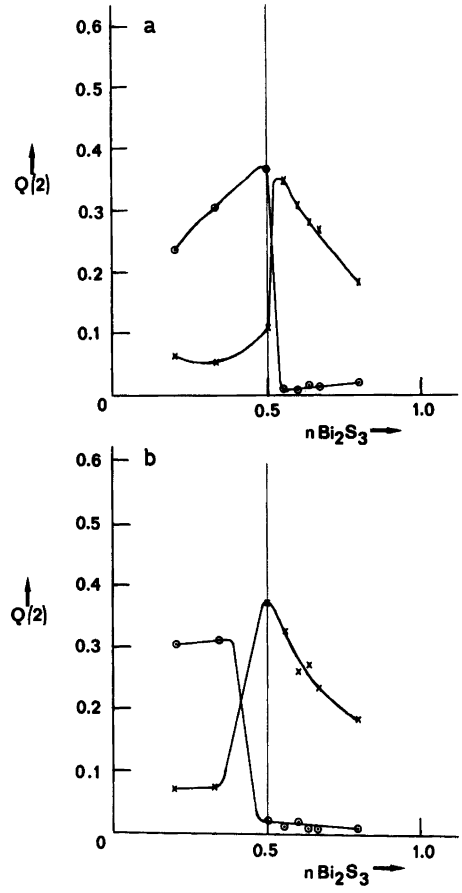

Fig. 1. The fractions $Q(2)$, see the text, for 9-$BaBi_2S_4$ (×) and 12-$BaBi_2S_4$ (○) are plotted against the mol fraction of Bi_2S_3 in the samples. Average values are taken for samples prepared at 420, 640 and 680 °C. a. Average value of two nearly fresh batches of BaS. b. Average values of two aged batches of BaS.

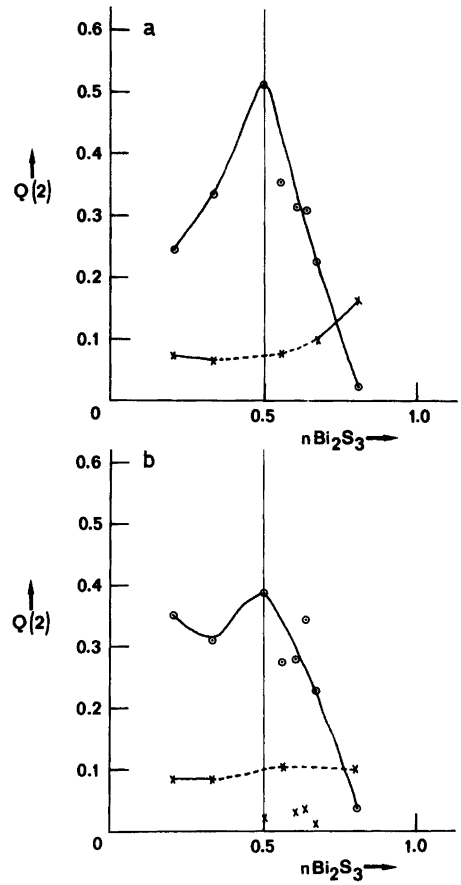

Fig. 2. The fractions $Q(2)$ for 9-$BaBi_2S_4$ (×) and 12-$BaBi_2S_4$ (○) are plotted against the mol fraction of Bi_2S_3 in the samples. Temperature of synthesis is 780 °C. a. Average values for two nearly fresh samples of BaS. b. Average values for two aged samples of BaS.

behaviour. $Q(2)$ was plotted against the mol fraction of Bi_2S_3 in the samples in Figs. 1 and 2. Figs. 1a and 1b show the averaged results for measurements made at 420, 640 and 680 °C for fresh and aged samples respectively. It is seen that 12-$BaBi_2S_4$ is formed for compositions $(1+\varepsilon_{12})BaS{\cdot}Bi_2S_3$ and 9-$BaBi_2S_4$ for $BaS{\cdot}(1+\varepsilon_9)Bi_2S_3$, where $\varepsilon_9, \varepsilon_{12} \geq 0$. Figs. 2a and 2b show the corresponding behaviour for samples recrystallized at 780 °C. The equilibria have shifted drastically and 12-$BaBi_2S_4$ is the predominant phase. The syntheses according to Gattow [4] always led to 12-$BaBi_2S_4$.

SrS and Bi_2S_3 were reacted at 640 °C in the molar ratios 4:1, 3:1, 2:1, 1:1, 1:2 and 1:3. In all cases the powder photographs could be explained by the 12-phase in combination with SrS and/or Bi_2S_3. The same result was obtained in the syntheses according to Gattow.[4] The $Q(1)$ values, see above, for 12-$SrBi_2S_4$ seemed to have maximum for the 1:1 samples. The cell dimensions of 12-$SrBi_2S_4$ prepared on reacting SrS and Bi_2S_3 for 15 min at 640 °C are a=24.925(2) Å, c=4.0954(8) Å. The 9-phase does not seem to exist in the system $SrS-Bi_2S_3$. Efforts to prepare $CaBi_2S_4$ either on reaction of CaS with Bi_2S_3 or using the method of Gattow have hitherto failed.

Single crystal work. On reaction in pyrex tubes 9-$BaBi_2S_4$ and 12-$BaBi_2S_4$ sintered to rods and single crystals were formed on their surfaces. The 12-$BaBi_2S_4$ single crystal had a length of 0.7 mm. Its cross-section was slightly elliptical with an average diameter of 0.008 mm. The single crystal of 9-$BaBi_2S_4$ was lost before measuring but had about the same dimensions. Both single crystals were mounted along their needle axes (4 Å) in Weissenberg cameras and the layers 0–3 were registered using Cu$K\alpha$ radiation. The multiple film technique was used and the intensities were estimated visually by the aid of a calibrated scale. The intensities were corrected for $(Lp)^{-1}$ but not for the absorption. The Laue symmetry was found to be $6/m$. The absence of the reflections 001 and 003 in the powder photographs gave the condition limiting possible reflections: $00l$: $l=2n$ which is characteristic of the space groups $P\,6_3$ and $P\,6_3/m$. A sample of composition $BaBi_2S_4$ with $Q(1)$=0.90 for the 9-phase had an observed density of 5.88 Mg m^{-3}, whereas the calculated value for Z=9 was 6.02 Mg m^{-3}. The sample from which the single crystal of 12-$BaBi_2S_4$ was picked out had $Q(1)$=0.90 and its observed density was 5.71 Mg m^{-3} in good agreement with the calculated value 5.89 Mg m^{-3}. Using the observed intensity data and the Z-values derived, three-dimensional Patterson functions were utilized to find the positions of the bismuth atoms. Space group $P6_3/m$ was assumed. Assuming the formula to be $BaBi_2S_4$ or close to it the structures were then worked out in the conventional way. Refinements in space group $P6_3$ were not tried. In both cases isotropic temperature factors were used for all atoms, the weighting scheme of Hughes was applied and the restriction $0.3<|F_o/F_c|<3$ was made. For the 9-phase the final R-factor was 0.0952 for all 608 reflections and 0.0906 for 602 reflections. For the 12-phase the corresponding values were 0.1079(1085) and 0.1040(1080). In this last case, however, the Fourier maps showed the presence of an "extra" metal atom at the position 0, 0, ¼; 0, 0, ¾. This extra atom was more or less arbitrarily assumed to be Ba. Positional and thermal parameters are summarized in Table 1. Observed and calculated structure amplitudes are available on request.

Table 1. Final positional parameters and isotropic temperature factors in 9-$BaBi_2S_4$ and 12-$BaBi_2S_4$. Standard deviations are given within parentheses.

Atom	x	y	z	B (Å^2)
9-$BaBi_2S_4$				
Bi(1)	0.8821(2)	0.4426(2)	¼	1.69(8)
Bi(2)	0.6273(2)	0.9696(2)	¼	1.73(8)
Bi(3)	0.1933(2)	0.2011(2)	¾	1.92(9)
Ba(1)	⅓	⅔	¼	0.9(2)
Ba(2)	0.2376(3)	0.8215(3)	¼	1.8(1)
Ba(3)*	0	0	¼	4.8(7)
S(1)	0.2995(13)	0.2347(13)	¼	1.7(4)
S(2)	0.0470(12)	0.4414(12)	¼	1.5(4)
S(3)	0.5407(11)	0.3145(11)	¼	0.9(4)
S(4)	0.0969(14)	0.1577(14)	¼	2.0(5)
S(5)	0.3488(11)	0.5203(11)	¼	1.1(4)
S(6)	0.3509(11)	0.1045(11)	¼	0.6(3)
12-$BaBi_2S_4$				
Bi(1)	0.2743(1)	0.9414(1)	¼	1.28(6)
Bi(2)	0.6488(1)	0.1448(1)	¼	1.09(6)
Bi(3)	0.4596(1)	0.0500(1)	¼	1.27(6)
Bi(4)	0.8449(1)	0.0236(1)	¼	1.52(6)
Ba(1)	0.3226(2)	0.5546(2)	¼	0.61(7)
Ba(2)	0.2279(2)	0.3495(2)	¼	1.00(8)
Ba(3)*	0	0	¼	4.5(6)
S(1)	0.1770(9)	0.4490(9)	¼	1.1(3)
S(2)	0.4529(8)	0.1483(7)	¼	0.6(3)
S(3)	0.0940(9)	0.5479(9)	¼	1.2(3)
S(4)	0.2474(8)	0.0324(8)	¼	0.7(3)
S(5)	0.6344(8)	0.0017(8)	¼	0.9(3)
S(6)	0.6566(8)	0.2495(8)	¼	0.6(3)
S(7)	0.3069(8)	0.1918(8)	¼	0.8(3)
S(8)	0.0623(12)	0.1351(12)	¼	2.7(5)

* The site is half-occupied.

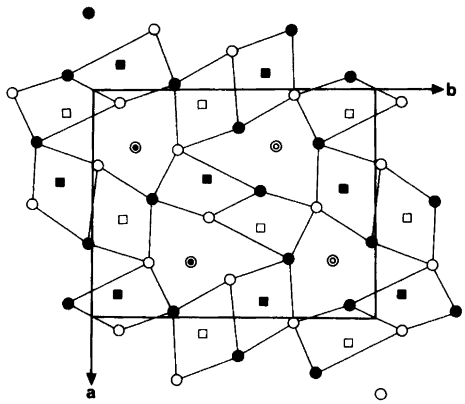

Fig. 3. Projection of the structure of galenobismutite on the *ab*-plane. The Bi–S octahedra are indicated. Single empty circles, squares and double circles indicate S, Bi and Pb at $z=¼$. Filled circles and squares indicate the respective atoms at $z=¾$.

DESCRIPTION AND DISCUSSION OF THE STRUCTURES

Architecture. The building principles of lead bismuth sulfosalts and of heavy metal sulfides in general have recently been elaborately discussed by Makovicky [5] and by Makovicky and Hyde.[6] The present discussion will be limited and starts from the octahedral Bi–S or Sb–S skeletons of the compounds. Thus the Ba(Pb) atoms will be omitted at this stage. Comparisons will be made to compounds of related stoichiometry, *e.g.* $PbBi_2S_4$, galenobismutite,[7] $6PbS{\cdot}7Sb_2S_3$, zinckenite,[8,9] $BaSb_2Se_4$[10] and $PbCr_2Se_4$.[11] To describe the octahedral blocks of the compounds, use will be made of layers *H* and *T* cut out from the PbS(NaCl) structure parallel to (111) and (100), respectively.[5] Use will also be made of the concept of chemical twinning [12] though in a slightly modified form. In galenobismutite [7] Bi(1) is coordinated by 6 sulfur atoms and Bi(2) by 7. In the following description the contact Bi(2)–S(1)=3.10 Å is somewhat arbitrarily neglected. It is seen from Fig. 3 that the octahedral skeleton consists of pairs of edge-sharing octahedra extending to rows in the *c*-axis direction. These rows could be cut out from single layers *H*. The rows are formed through the action of centre of symmetry at 0, 0, 0; ½, 0, 0; 0, ½, 0; ½, ½, 0 and each row contains either Bi(1) or Bi(2). 4 rows are joined by corner-sharing which

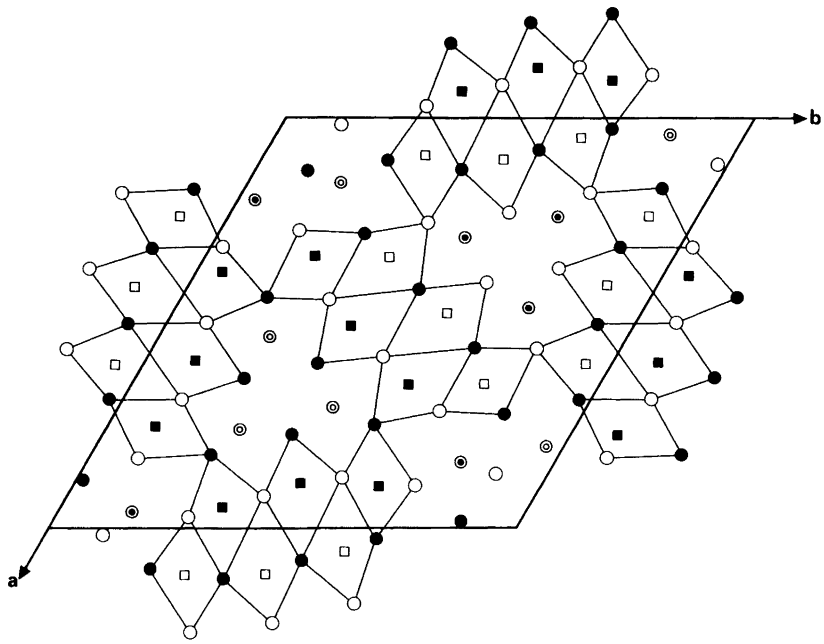

Fig. 4. Projection of the structure of zinckenite according to Takeda and Horiuchi on the *ab*-plane. The Sb–S octahedra are indicated. Single empty circles, squares and double circles indicate S, Sb, Pb or (Pb,Sb), respectively, at $z=¼$. Filled circles and squares indicate the respective atoms at $z=¾$.

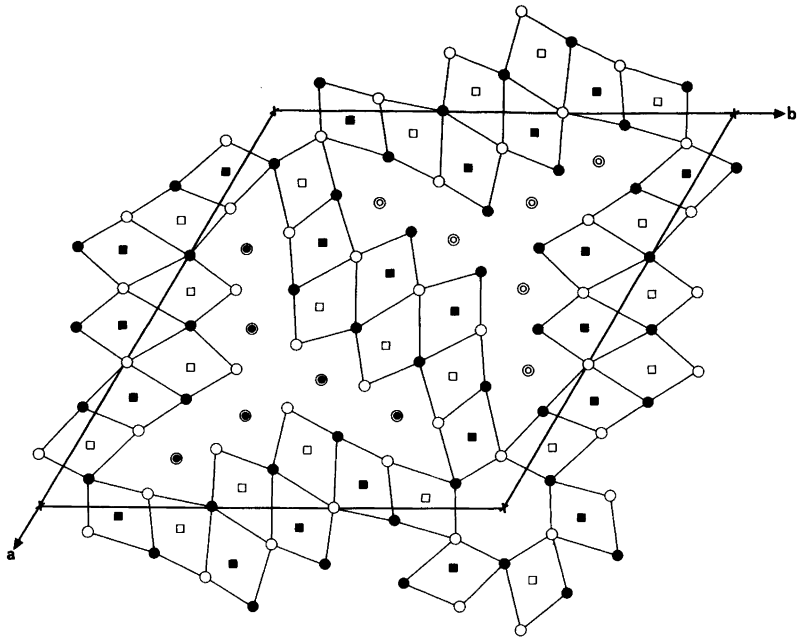

Fig. 5. Projection of the structure of 12-$BaBi_2S_4$ on the *ab*-plane. The Bi–S octahedra are indicated. Single empty circles, squares and double circles indicate S, Bi and Ba, respectively, at $z=¼$. Filled circles and squares indicate the respective atoms at $z=¾$. The Ba and/or Bi atoms at 0, 0, ¼; 0, 0, ¾ are denoted by crosses.

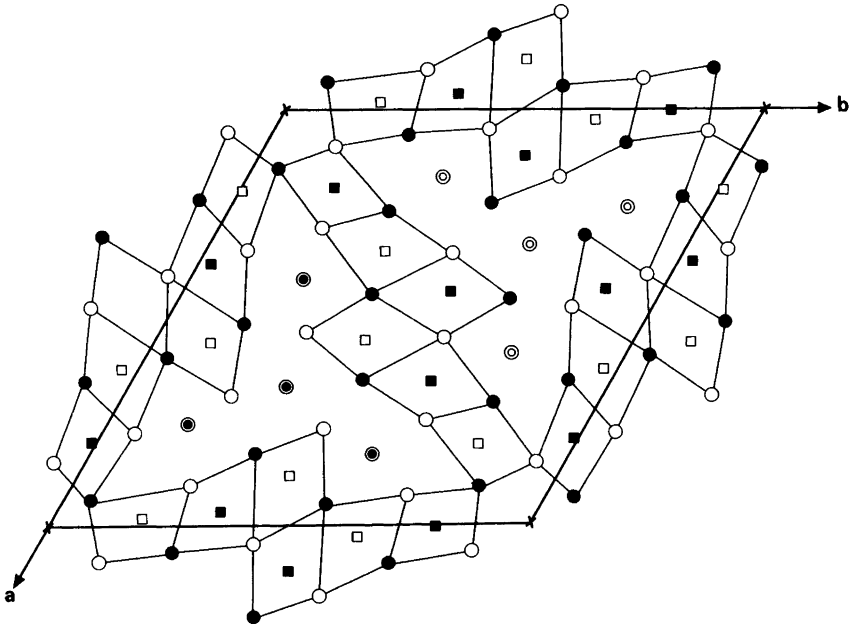

Fig. 6. Projection of the structure of 9-$BaBi_2S_4$ on the *ab*-plane. Bi–S octahedra are shown and the notations of the atoms are the same as in Fig. 5.

leads to tunnels where the Pb atoms are situated. Zinckenite will be described here according to Takeda and Horiuchi [9] and its real composition $6PbS \cdot 7Sb_2S_3$ will be approximated to $PbSb_2S_4$ and the correct space group $P6_3$[8] to $P6_3/m$. The *ab*-projection is shown in Fig. 4. The octahedral skeleton is built up from blocks of edge-sharing octahedra, 6 octahedra wide, which can be cut out from two consecutive layers *T*. The blocks are joined by corner-sharing which leads to tunnels where Pb or (Pb,Sb) and extra S atoms are situated. The blocks of octahedra are generated from the positions of the atoms in the asymmetric part of the unit cell through the action of centra of symmetry at ½, 0, 0; 0, ½, 0; ½, ½, 0; ½, 0, ½; 0, ½, ½; ½, ½, ½. The joining of 3 blocks by corner-sharing is accomplished by the threefold axes at ⅔, ⅓, *z*; ⅓, ⅔, *z*. The architectures of 12-$BaBi_2S_4$ and 9-$BaBi_2S_4$ are closely related to that of zinckenite. Both compounds crystallize in $P6_3/m$. The *ab*-projection of 12-$BaBi_2S_4$ is shown in Fig. 5. As seen, the central parts of the blocks are identical to those of zinckenite. Each block contains $2Z/3=8$ octahedra. Added to the zinckenite parts of the blocks are on each side single rows of edge-sharing octahedra. The octahedral skeleton is built up from the atoms of the asymmetric part of the unit cell in the same way as for zinckenite, namely be means of centra of symmetry and of 3-fold axes. The *ab*-projection of 9-$BaBi_2S_4$ is shown in Fig. 6. The central part of the octahedral blocks contain here only 4 octahedra instead of 6 as found in 12-$BaBi_2S_4$ and in zinckenite. Added to the 4-membered blocks are on each side single rows of edge-sharing octahedra as in 12-$BaBi_2S_4$. Totally the blocks contain $2Z/3=6$ octahedra. Since $BaBi_2S_4$ occurs in two forms with $Z=9$ and $Z=12$ one might ask if samples with $Z=3$ or 6 could prepared. Spatial considerations show that this is impossible. Higher polymorphs with $Z=15...$ may exist but there is hitherto no experimental proof that such phases could be formed.

$BaSb_2Se_4$[10] is a layer structure. The unit cell is monoclinic, $P\,2_1/n$ with the general point position *x*, *y*, *z* (1); $\bar{x}$, $\bar{y}$, $\bar{z}$ (2); ½−*x*, ½+*y*, ½−*z* (3); ½+*x*, ½−*y*, ½+*z* (4). 2 of the 4 Sb atoms of the asymmetric part of the unit cell are coordinated by 3 S and 2 by 4 S. To accomplish a comparison to $BaBi_2S_4$ all Sb atoms have, however, been regarded as formally 6-coordinated. Starting

Table 2. Distances Sb−S in the deformed Sb−S octahedra assumed here for $BaSb_2Se_4$.[10] Values above the horizontal lines are from [10], those below are calculated here.

Sb(11)−Se(84)	2.59	Sb(21)−Se(21)	2.56
Sb(11)−Se(13)	2.58	Sb(21)−Se(33)	2.65
Sb(11)−Se(62)	2.60	Sb(21)−Se(51)	2.85
		Sb(21)−Se(84)	2.92
Sb(11)−Se(33)	3.41		
Sb(11)−Se(51)	3.49	Sb(21)−Se(62)	3.31
Sb(11)−Se(52)	3.66	Sb(21)−Se(34)	3.95
Sb(31)−Se(53)	2.55	Sb(41)−Se(71)	2.61
Sb(31)−Se(42)	2.67	Sb(41)−Se(41)	2.70
Sb(31)−Se(31)	2.67	Sb(41)−Se(63)	2.80
		Sb(41)−Se(72)	2.85
Sb(31)−Se(71)	3.10		
Sb(31)−Se(81)	3.30	Sb(41)−Se(53)	3.12
Sb(31)−Se(41)	3.51	Sb(41)−Se(31)	3.72

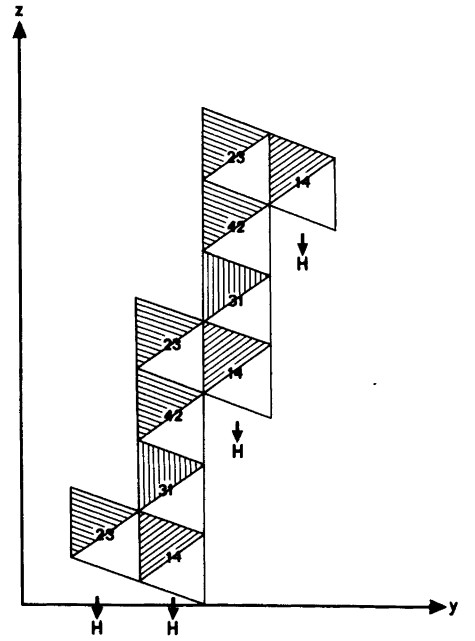

Fig. 7. A slightly idealized projection of one octahedral Sb−S layer with $0.35<y<0.65$ in $BaSb_2Se_4$. The two-membered figures indicate Sb atoms within the octahedra. The first number is the number of the respective Sb atom as it occurs in the list of coordinates in [10], the second number refers to the general point position in $P2_1/n$ in the order *x*, *y*, *z*; $\bar{x}$, $\bar{y}$, $\bar{z}$; ½−*x*, ½+*y*, ½−*z*; ½+*x*, ½−*y*, ½+*z*. The different slabs of type *H*, see the text, are marked out.

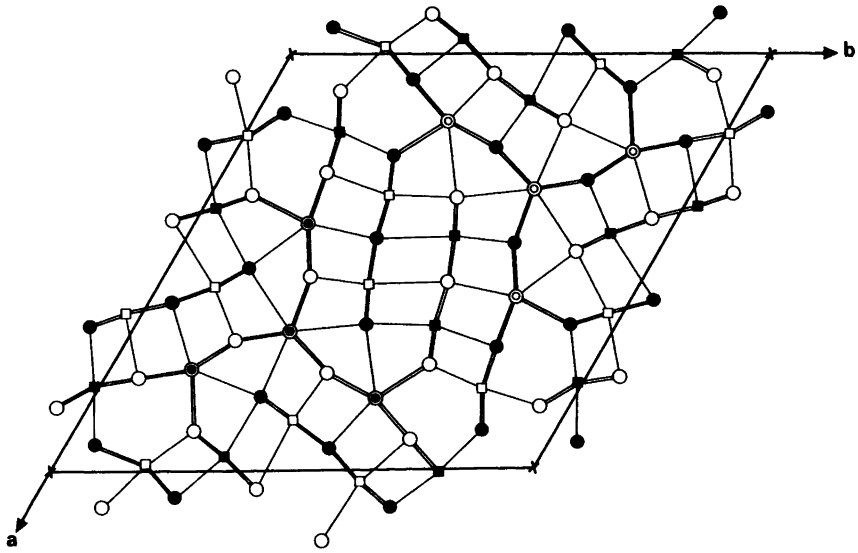

Fig. 8. The bonding scheme in 9-$BaBi_2S_4$. The notations of the atoms are the same as in Fig. 5.

from the coordinates given in Ref. 10 as x, y, z and using the numbering of the atoms in the general point position as given above as subscripts the 6-coordination of the Sb atoms was obtained as shown in Table 2. Fig. 7 shows a slightly idealized projection of the Sb–S layer with $0.35<y_{Sb}<0.65$ on the y,z-plane. As seen, the layer is built up from 4-membered strips of type *H* which are joined stepwise. At each junction the arrangements of the octahedra are the same as in two consecutive layers of type *H*. Thus even if formal octahedra are introduced there is very little similarity between $BaSb_2Se_4$ and the hexagonal compounds $BaBi_2S_4$ and

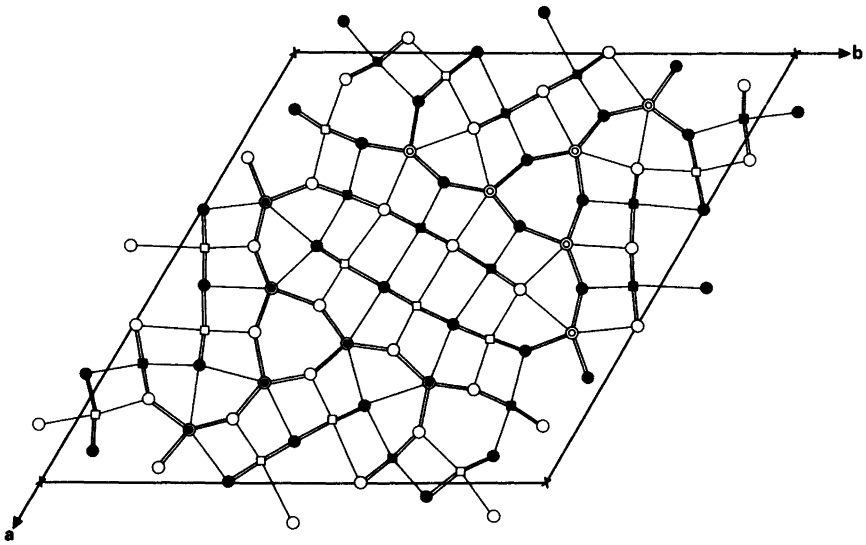

Fig. 9. The bonding scheme in 12-$BaBi_2S_4$. The notations of the atoms are the same as in Fig. 5.

Table 3. Selected distances (Å) with standard deviations in parentheses of 9-$BaBi_2S_4$ and 12-$BaBi_2S_4$. Average values are calculated for the bismuth-sulfur distances within each octahedron and the sums of the squares of the departures from these values are also given.

9-$BaBi_2S_4$		Average value	$\Sigma\Delta^2$	12-$BaBi_2S_4$		Average value	$\Sigma\Delta^2$
Bi(1)–S(3)	2.55(2)			Bi(1)–S(4)	2.70(2)		
Bi(1)–2S(5)	2.73(1)			Bi(1)–2S(7)	2.79(1)		
Bi(1)–2S(2)	3.03(2)	2.98	0.62	Bi(1)–2S(5)	2.91(1)	2.84	0.04
Bi(1)–S(2)	3.59(2)			Bi(1)–S(1)	2.96(2)		
Bi(2)–S(1)	2.66(3)			Bi(2)–S(6)	2.55(2)		
Bi(2)–2S(6)	2.81(1)			Bi(2)–2S(1)	2.72(1)		
Bi(2)–2S(2)	2.86(2)	2.87	0.12	Bi(2)–2S(3)	3.07(1)	2.95	0.48
Bi(2)–S(5)	3.14(2)			Bi(2)–S(5)	3.45(2)		
Bi(3)–S(4)	2.74(3)			Bi(3)–S(2)	2.57(2)		
Bi(3)–2S(4)	2.76(2)			Bi(3)–2S(3)	2.82(1)		
Bi(3)–S(6)	2.86(2)	2.82	0.02	Bi(3)–2S(5)	2.94(1)	2.98	0.54
Bi(3)–2S(1)	2.91(2)			Bi(3)–S(3)	3.57(2)		
Ba(1)–6S(3)	3.29(2)			Bi(4)–S(8)	2.73(3)		
Ba(1)–3S(5)	3.36(2)			Bi(4)–2S(8)	2.76(2)		
				Bi(4)–S(7)	2.89(2)	2.83	0.03
Ba(2)–2S(3)	3.15(2)			Bi(4)–2S(4)	2.92(1)		
Ba(2)–S(2)	3.16(2)						
Ba(2)–S(5)	3.23(2)			Ba(1)–2S(2)	3.16(1)		
Ba(2)–2S(1)	3.25(2)			Ba(1)–2S(6)	3.18(1)		
Ba(2)–2S(6)	3.25(2)			Ba(1)–2S(6)	3.24(1)		
				Ba(1)–S(1)	3.29(2)		
Ba(3)*–3S(4)	2.99(3)			Ba(1)–S(3)	3.39(2)		
Ba(3)*–6S(4)	3.64(2)			Ba(2)–2S(2)	3.15(1)		
				Ba(2)–2S(4)	3.21(1)		
Closest S–S approach				Ba(2)–2S(7)	3.25(1)		
S(1)–S(6)	3.52(3)			Ba(2)–S(5)	3.34(2)		
				Ba(2)–S(1)	3.35(2)		
				Ba(3)*–3S(8)	2.96(3)		
				Ba(3)*–6S(8)	3.63(2)		
				Closest S–S approach			
				S(6)–2S(6)	3.47(3)		

zinckenite.

In $Eu_{1-p}Cr_2Se_{4-p}$[11] the Cr–Se skeleton, space group $P\ 6/m$, consists of 5-membered single layers *H* which are fused by face-sharing of the terminal octahedra and there is no similarity to $BaBi_2S_4$.

Stoichiometry of the $BaBi_2S_4$ phases. As discussed above, 9-$BaBi_2S_4$ has the composition $BaS\cdot(1+\varepsilon_9)Bi_2S_3$ for samples prepared at 640 °C and also for those recrystallized at 420 or 680 °C. 12-$BaBi_2S_4$ has the composition $(1+\varepsilon_{12})BaS\cdot Bi_2S_3$ for samples prepared in the same way. For both phases the Fourier maps show the presence of atoms, presumably cations in the tunnels around 0, 0, *z*. The composition $BaS\cdot(1+\varepsilon_9)Bi_2S_3$ for 9-$BaBi_2S_4$ may be attained with the present structure if there are slight vacancies in the cation lattice. The composition $(1+\varepsilon_{12})BaS\cdot Bi_2S_3$ for 12-$BaBi_2S_4$ may result if

some extra Ba is inserted at the point position 0, 0, ¼; 0, 0, ¾ and the charge is compensated by some vacancy in the Bi lattice or in the stoichiometric case if ≤1 Ba atom per unit cell is moved from its 6-fold position to a half-occupied site at 0, 0, ¼; 0, 0, ¾ leaving a vacancy at its former site. The mechanisms proposed here are based on the assumption that the sulfur lattice remains intact. Neither mechanism could, however, be proved by means of the intensity data.

Coordination of the metal atoms. For both polymorphs the cations Ba and/or Bi at the position 0, 0, ¼ are coordinated by 9 sulfur atoms in the form of a three-capped trigonal prism, see Table 3, Ba(3)*, and Figs. 8 and 9. The atoms Ba(2) 9-$BaBi_2S_4$, and Ba(1) and Ba(2) 12-$BaBi_2S_4$, are 8-coordinated in the form of a bicapped trigonal prism. The coordination polyhedra are fairly regular with distances Ba–S 3.15–3.39 Å, see Table 3 and Figs. 8 and 9. The Ba(1) atom of 9-$BaBi_2S_4$ is situated at the position ⅓, ⅔, ¼; ⅔, ⅓, ¾ and its coordination polyhedron is a regular three-capped trigonal prism. The coordination polyhedra of bismuth are as expected irregular octahedra. The Bi–S distances vary between 2.55 and 3.59 Å. The departure from regularity of the octahedra was estimated as follows. Average values of the 4 independent Bi–S distances were calculated for each octahedron and the sums of the squares of the departures $\Sigma\Delta^2$ were derived and used as a measure of the irregularity. The average Bi–S distance and corresponding $\Sigma\Delta^2$ are given for each Bi octahedron in Table 3. It is seen that $\Sigma\Delta^2$ for 9-$BaBi_2S_4$ grows in the order Bi(3), Bi(2), Bi(1). For 12-$BaBi_2S_4$ the corresponding order is Bi(4), Bi(1), Bi(2), Bi(3). These orders are, however, the same as when one starts from the outermost of the octahedra in the octahedral blocks shown in Figs. 5 and 6 and moves to the centra of the blocks. Thus in 9-$BaBi_2S_4$ and 12-$BaBi_2S_4$ the central octahedra are the most deformed ones. This is contrary to what was found by Makovicky [5] for bismuth sulfosalts containing other cations *e.g.* Ag, Cu, Pb.

Finally it ought to be mentioned that all S–S distances are normal though some of them are quite short, see Table 3.

Acknowledgements. Mr. Christer Jönsson is thanked for his skill and for the interest he has taken in this work. This investigation has been supported financially by grants from the Swedish Natural Science Research Council.

REFERENCES

1. Schenk, R. *Naturwissenschaften 25* (1937) 260.
2. Bok, L. D. C. and de Wit, J. H. *Z. Anorg. Allg. Chem. 324* (1963) 162.
3. Volk, K., Cordier, G., Cook, R. and Schäfer, H. *Z. Naturforsch. Teil B 35* (1980) 136.
4. Gattow, G. *Naturwissenschaften 52* (1965) 104.
5. Makovicky, E. *Fortschr. Mineral 59(2)* (1981) 137.
6. Makovicky, E. and Hyde, B. G. *Struct. Bonding (Berlin) 46* (1981) 103.
7. Iitaka, Y. and Nowacki, W. *Acta Crystallogr. 15* (1962) 691.
8. Portheine, J. C. and Nowacki, W. *Z. Kristallogr. 141* (1975) 79.
9. Takeda, H. and Horiuchi, H. *J. Mineral. Soc. Jpn. 10* (1971) 283.
10. Cordier, G. and Schäfer, H. *Z. Naturforsch. Teil B 34* (1979) 1053.
11. Brouwer, R. and Jellinek, F. *J. Phys., Suppl. 12 Tome 38* (1977) C7.
12. Andersson, S. and Hyde, B. G. *J. Solid State Chem. 9* (1974) 92.

Received October 4, 1982.

Acta Chemica Scandinavica A 37 (1983) 409–413

On the Phase Transformation in Ta_3P

J.-O. WILLERSTRÖM, Y. ANDERSSON and S. RUNDQVIST

Institute of Chemistry, University of Uppsala, Box 531, S-751 21 Uppsala, Sweden

In an earlier paper, [*Acta Chem. Scand. A 32* (1978) 515], it was suggested that Ta_3P transforms from a high temperature modification β-Ta_3P, crystallizing with the β-V_3S-type structure (space group $P4_2/nbc$), into a low temperature modification α-Ta_3P, crystallizing with the Ti_3P-type structure ($P4_2/n$). A reinvestigation of the X-ray powder patterns of Ta_3P revealed that the reflections with an odd value of $h+k+l$ were broader and weaker in β-Ta_3P compared to α-Ta_3P. This observation indicates that β-Ta_3P could in fact be a transitional structure, with regions of a body-centered high temperature modification, crystallizing with either the Fe_3P-(space group $I\bar{4}$) or the α-V_3S-type structure ($I\bar{4}2m$), and regions of the Ti_3P-type low temperature modification occurring simultaneously within a common coherent lattice. An estimation of the relative amounts of the high and low temperature modifications in the transitional structure was made using a Rietveld-type full profile analysis of Guinier-Hägg X-ray powder diffraction film intensity data. Analysis of the line broadening of the reflections with an odd value of $h+k+l$ yielded a second estimate of the proportions of the two modifications. The good agreement between the two independently determined results supports the proposed existence of a transitional structure in Ta_3P, corresponding to the phase formerly denoted by β-Ta_3P.

A phase transformation in Ta_3P was reported in Ref. 1. The transformation temperature was estimated to be less than 100 °C below the melting point of Ta_3P which is close to 2100 °C.

On the basis of single-crystal X-ray data obtained by the Weissenberg method, which indicated a primitive tetragonal symmetry and Laue symmetry $4/mmm$, it was suggested [1] that the high temperature modification (β-Ta_3P) crystallizes with the β-V_3S-type structure [space group $P4_2/nbc$ (No. 133)]. A crystal structure refinement based on X-ray diffractometer data converged in a satisfactory manner with normal values of the isotropic temperature factors but with somewhat high R values (*e.g.* $R_w(F^2)$= 0.224). The low temperature modification (α-Ta_3P) crystallizes with the Ti_3P-type structure [space group $P4_2/n$ (No. 86)]. A single-crystal structure refinement of α-Ta_3P is reported in Ref. 2.

The unit cell dimensions, determined from X-ray powder diffraction data, are almost equal for the two forms; for β-Ta_3P: a=10.1542(4) Å, c=5.0137(3) Å and for α-Ta_3P: a=10.1550(3) Å, c=5.0128(2) Å.[2]

The proposed structures of the two modifications are very similar, and movements of the atoms of the order of some hundredths of an Ångström are sufficient to convert one structure into the other. In view of this, the transformation from the high to the low temperature form should occur so readily that it is surprising that the high temperature form can be retained by quenching. Furthermore, a heat treatment at 1100 °C for three days was not sufficient to complete the transformation from β-Ta_3P into α-Ta_3P.[2]

Recent studies of the phase transformations in Ta_3Ge [3,4] and V_3S [5] have revealed the occurrence of a novel type of transition between structures belonging to the Fe_3P–Ti_3P–V_3S family. The X-ray data did not show a separation into two distinct phases during the transformation but a continuous change in the unit cell parameters from the values of the body-centered high temperature modification to the values of the primitive low temperature modification. This observation suggested the existence of a tran-

0302-4377/83 $02.50

sitional structure with regions of the high temperature modification alternating with regions of the low temperature modification within a common coherent lattice. At a stage of the transformation when the number and extent of the regions of the low temperature modification have become sufficiently large, reflections with an odd value of $h+k+l$ appeared in the diffraction patterns. The intensities and halfwidths of this category of reflections varied considerably. With a decreasing amount of the high temperature modification in the transitional structure the intensities and halfwidths of these reflections increased and decreased, respectively. With this new information at hand it seemed worthwhile to re-examine the phase transformation in Ta_3P in greater detail.

The X-ray powder diffraction films of Ta_3P showed that reflections with an odd value of $h+k+l$ were broader and weaker in β-Ta_3P compared to α-Ta_3P. The observed differences in intensity between corresponding reflections for β-Ta_3P and α-Ta_3P as reported earlier [2] cannot be explained by the difference in structure type. In fact, powder diffraction data calculated on the basis of positional parameters taken from the single-crystal structure refinements [1,2] differ insignificantly between the β-V_3S- and the Ti_3P-type structures of Ta_3P. (Due to an input error in the computer program used, the calculated powder diffraction intensities for β-Ta_3P as published in Table 1 of Ref. 2 are incorrect. Values calculated in the correct manner are almost identical to the calculated intensities for α-Ta_3P listed in the same table.)

The appearance of the broader and weaker reflections with an odd value of $h+k+l$ suggests, in analogy with the Ta_3Ge and V_3S transformations, that β-Ta_3P might be regarded as a transitional structure with regions of a body-centered high temperature form, in the following denoted by γ-Ta_3P, crystallizing with either the Fe_3P- or α-V_3S-type structure, alternating with regions of the low temperature modification α-Ta_3P. Whether γ-Ta_3P really is an equilibrium phase in the Ta-P system is not known. The transitional structure may be an intermediate step in the transformation from pure γ-Ta_3P into α-Ta_3P or due to stacking faults formed during the solidification of Ta_3P.

EXPERIMENTAL

The preparation of the samples of Ta_3P was described in Ref. 1. The intensity data for the Rietveld-type full profile analysis [6] and the line broadening analysis were obtained by scanning X-ray powder diffraction films using a SAAB automatic film scanner [7,8] connected to a Nord 100 computer. The films used were recorded using a Philips XDC 1000 or 700 Guinier-Hägg type focusing camera with $CuK\alpha_1$ (Rietveld analysis) and $CrK\alpha_1$ radiation (line broadening analysis), respectively.

The sample contained small amounts of tantalum metal. The tantalum reflections were removed from the intensity data without serious loss of intensity information for Ta_3P.

The halfwidths of certain reflections were obtained by plotting the intensity values obtained from the film scan against 2θ and measuring the full widths at half-maximum intensity in the graphs. The halfwidth for a reflection with an odd value of $h+k+l$ was corrected for instrumental broadening and particle size effects by simply subtracting the halfwidth of a neighbouring reflection with an even value of $h+k+l$.

STRUCTURE REFINEMENT

The details in the determination of the relative amounts of the high and low temperature forms in the transitional structure of Ta_3P using the Rietveld method are identical to the description given for the analogous determination in Ta_3Ge in Ref. 4. The refinement was performed assuming that the γ-Ta_3P-type regions have the Fe_3P-type structure.

The following parameters were refined: the profile parameters, which comprise the halfwidth (six parameters, three parameters for reflections with an even value of $h+k+l$ and three parameters for reflections with an odd value of $h+k+l$), the asymmetry (two parameters) and the 2θ zero point (one parameter), and the structure parameters which comprise the overall scale factor (one parameter), the lattice parameters (two parameters), the positional parameters (nine parameters, since only the tantalum positions were refined), the occupancy (one parameter) and the overall temperature factor (one parameter). Scattering factors corrected for the real part of the anomalous dispersion were interpolated from values given in the *International Tables for X-Ray Crystallography*.[9] No

Table 1. Structure data for the transitional structure, corresponding to the phase formerly denoted by β-Ta_3P.[a]

Atom	x	y	z	n_p	B (Å^2)
Ta(1)	1598(6)	6542(6)	7458(17)		
Ta(2)	1053(3)	2539(13)	4873(12)	0.96(1)	1.29(6)
Ta(3)	0521(7)	5449(6)	2363(12)		
P [b]	0420	2583	0064	0.96(1)	

[a] Space group $P4_2/n$ (No. 86); all atoms in position 8*g*; origin at $\bar{1}$. Positional parameters $\times 10^4$, standard deviations in parentheses. [b] Positional parameters from Ref. 2.

attempt was made to correct for absorption. The overall temperature factor obtained therefore includes the combined effects of thermal vibration and absorption.

Positional parameters from the α-Ta_3P structure [2] were used as starting values in the refinement. The final residual values obtained were; for the reflections with an even value of $h+k+l$ (for definitions see Ref. 10): R_I=0.092 and R_F=0.071, and for the reflections with an odd value of $h+k+l$: R_I=0.149 and R_F=0.139. The R values for the total profile (197 reflections) were R_p=0.180 and R_{wp}=0.259.

Structure data are presented in Table 1. The z-coordinates of the Ta(2) and Ta(3) atoms obtained using the Rietveld method differ by 14 and 9 standard deviations, respectively, from those of α-Ta_3P obtained using the single-crystal method.[2] The differences between the other positional parameters are within three standard deviations.

The occupancy parameter n_p is equivalent to the relative number of unit cells of α-Ta_3P in the transitional structure, while $1-n_p=N$ is thus equal to the relative number of unit cells of the high temperature modification γ-Ta_3P.

An identical refinement of a sample of pure α-Ta_3P [no broadening of the reflections with odd values of $h+k+l$ was visible in the X-ray powder pattern] resulted in an n_p value of 1.01(2), the estimated standard deviation in parenthesis.

RESULTS AND DISCUSSION

The transitional structure proposed for Ta_3P is very similar to the transitional structures in Ta_3Ge and V_3S. A detailed description of the transitional structure in Ta_3Ge was given in Ref. 4. The regions of γ-Ta_3P type in the transitional structure of Ta_3P can adopt either the Fe_3P- or α-V_3S-type structure without affecting the main features of the discussion below.

The halfwidths of the reflections with an odd value of $h+k+l$ depend on the number and extensions of the regions of γ-Ta_3P in the transitional structure. Only γ-Ta_3P-type regions with an extension of ma in a direction parallel to an a axis, where m is an integer and a is equal to the length of the a axis, contribute to the broadening of the reflections with an odd value of $h+k+l$. This is because the atoms in one of the regions of α-Ta_3P surrounding such a region of γ-Ta_3P are shifted by approximately $(a+a+c)/2$ from the positions corresponding to the other region.[4]

If the extension of the region of γ-Ta_3P is equal to $(m+1/2)a$ in a direction parallel to an a axis, there are no shifts in the atomic positions of the surrounding regions of α-Ta_3P with respect to each other. This type of region will thus not contribute to the line broadening of the reflections with odd values of $h+k+l$.

The relation between the integral breadth of the reflections with an odd value of $h+k+l$ and the relative number γ of regions of the high temperature modification with an extension of ma was given in Ref. 4,

$$\beta(2\theta) = -\frac{\lambda(|h|+|k|)\ln(1-2\gamma)}{2a\cos\theta\,(h^2+k^2+(a/c)^2l^2)^{1/2}} \qquad (1)$$

where $\beta(2\theta)$ is the integral breadth in radians, λ is the wavelength of the radiation used, a and c are the lengths of the a and c axes, respectively, θ is the diffraction angle (in degrees) for the hkl reflection. The values of γ calculated using eqn. (1) for some reflections are presented in Table 2.

The line broadening in powder patterns from different parts of the same sample varies. This

Table 2. The breadth of some reflections with an odd value of $h+k+l$ and the corresponding γ values calculated using eqn. (1) for a sample of the transitional structure (β-Ta_3P) and α-Ta_3P.

Sample and heat treatment						
	h k l	201 [d]	311	412 [d]	511	
β-Ta_3P [a,b]	β(rad) [c]	0.0016	0.0021	0.0022	0.0032	
arc-melted	γ	0.009	0.008	0.008	0.010	
	$\bar{\gamma}$ [e]					0.009(1)
β-Ta_3P [a]	β(rad) [c]	0.0021	0.0046	0.0074	0.0057	
arc-melted	γ	0.012	0.017	0.022	0.018	
	$\bar{\gamma}$ [e]					0.017(4)
α-Ta_3P	β(rad) [c]	– [f]	0.0	– [f]	0.0001	
1700 °C 20 min	γ	–	–	–	0.0005	

[a] Samples from different parts of the same master alloy. [b] Sample used in the Rietveld analysis. [c] The halfwidths corrected for instrumental broadening and particle size effects. [d] Reflection overlapped by a reflection with an even value of $h+k+l$. The halfwidth of the reflection with an odd value of $h+k+l$ was obtained by resolving the reflections by means of a least-squares method assuming an asymmetric Lorentzian peak shape. [e] Arithmetic mean value with standard deviation in parenthesis. [f] Reflection not measured.

variation indicates that the amount of γ-Ta_3P varies between different parts of the same sample which, for instance, might be due to local differences in the cooling rate.

Because of the low amount of the γ-Ta_3P-type regions in the transitional structure, around 4 % according to the Rietveld analysis (Table 1), it is reasonable to assume that the regions of γ-Ta_3P type are very narrow and m is of the order of unity. Furthermore, by assuming that γ-Ta_3P occurs with equal probability in regions with an extension of either a or $3a/2$ in directions parallel to an a axis, it is possible to estimate the fraction γ of regions of extension a using the value of $N(=1-n_p)$ as obtained from the Rietveld analysis:

$\gamma+3\gamma/2=N$; $\gamma=0.4N=0.4\cdot0.04=0.016(5)$, the estimated standard deviation in parenthesis. This value should thus be compared to 0.009(1) as obtained from the line broadening analysis (Table 2).

The close agreement between the two independently determined results supports the view that the β-Ta_3P modification is, in fact, a transitional structure with regions of α-Ta_3P alternating with regions of the body centered γ-Ta_3P within a common coherent lattice.

No significant broadening of reflections with odd values of $h+k+l$ was observed in α-Ta_3P (Table 2), which is in accordance with the value of $N=-0.01(2)$ as obtained using the Rietveld method.

Weissenberg films showed that single-crystals of β-Ta_3P apparently possessed the Laue symmetry *4/mmm*.[1] Single-crystals with this symmetry seem to occur frequently in these samples since they have been isolated both at our institute in Uppsala and by the X-Ray Crystallography Group at Chulalongkorn University in Bangkok, Thailand. The appearance of the Laue symmetry *4/mmm* of the transitional structure, consisting primarily (96 %) of regions with the Ti_3P-type structure, which possesses the lower Laue symmetry *4/m*, may seem rather surprising. However, this observation may be explained considering the regions of γ-Ta_3P type with an extension of a. As was mentioned above, the atomic positions in one of the regions of α-Ta_3P surrounding such a region of γ-Ta_3P are shifted by approximately $(a+a+c)/2$ from the positions corresponding to the other region. The relation between the two regions of α-Ta_3P can also be described as a rotation of one of the regions by 90° around the tetragonal axis with respect to the other region. In reciprocal space, this rotation means that the $(hkl)_1$ reflections will be overlapped by the $(khl)_2$ reflections (the subscripts 1 and 2 are used to distinguish between the reflections scattered from the two different regions of α-Ta_3P). Assuming that the regions of γ-Ta_3P, with an extension of a, are distributed randomly over the transitional structure, the amount of the two types of α-Ta_3P regions will be almost equal.

Accordingly, on a Weissenberg film, $I_{hkl}=I_{(hkl)_1}+I_{(khl)_2}$ will thus be equal to $I_{(khl)}=I_{(khl)_1}+I_{(khl)_2}$ and the transitional structure will appear to possess the Laue symmetry 4/*mmm*, although both its constituents possess the lower Laue symmetry 4/*m*.

The Laue symmetry 4/*mmm* of the transitional structure can possibly be explained in another way. The actual structure of the regions of γ-Ta_3P in the transitional structure is not known and, as was mentioned above, they could adopt the α-V_3S structure type. The free energy of the transitional structure may then be lowered if the low temperature modification adopts the β-V_3S-type structure instead of the Ti_3P structure type. The Laue symmetry 4/*mmm* of the transitional structure is then easily understood, since both α-V_3S and β-V_3S possess the Laue symmetry 4/*mmm*.[11] A β-V_3S-type structure of the low temperature modification may thus be stabilized by the α-V_3S-type structure of the regions of γ-Ta_3P. However, in the instance when all regions of γ-Ta_3P have transformed into the low temperature modification, all atoms can shift over into the Ti_3P-type structure and the Laue symmetry 4/*m* is then observed.

The alternative model of the transitional structure consisting of regions adopting the α-V_3S and β-V_3S structure types has also been refined using the Rietveld method but no significant improvement was obtained.

There is no increase in the *c*/*a* ratio on passing from the transitional structure into α-Ta_3P although the *c*/*a* ratio increases with an increasing degree of transformation in both the Ta_3Ge and V_3S transformations.[3,5] This difference between the transformation in Ta_3P and the Ta_3Ge and V_3S transformations may simply be due to the specific effect of the relative amounts of the high and low temperature modifications on the cell parameters of the transitional structure in Ta_3P. In the Ta_3Ge transformation the relative change in the cell dimensions of the transitional structure decreased with an increasing degree of transformation.[4] This indicates that when the last regions of the high temperature modification disappear in the transitional structure of Ta_3P, the effect on the cell dimensions may be too small to be observed.

The transformation in Ta_3P, whether it is from pure γ-Ta_3P into pure α-Ta_3P or from the transitional structure into α-Ta_3P, is very similar to the transformations in Ta_3Ge and V_3S, and the Ta_3P transformation may thus occur through a similar shear type mechanism.[3,5] The more extensive atomic movements needed in this type of transformation compared to those involved in a transition from the β-V_3S- into the Ti_3P-type structure explain the low rate of transformation observed in annealing experiments of β-Ta_3P.

Acknowledgement. Financial support from the Swedish Natural Science Research Council is gratefully acknowledged.

REFERENCES

1. Phavanantha, P., Pontchour, C., Pramatus, S., Andersson, Y. and Rundqvist, S. *Acta Chem. Scand. A 32* (1978) 515.
2. Andersson, Y., Pramatus, S. and Rundqvist, S. *Acta Chem. Scand. A 32* (1978) 811.
3. Willerström, J.-O. *J. Less Common Met. 86* (1982) 85.
4. Willerström, J.-O. *J. Less Common Met. 86* (1982) 105.
5. Willerström, J.-O. *J. Less Common Met. 92* (1983) 41.
6. Werner, P.-E., Salomé, S., Malmros, G. and Thomas, J. O. *J. Appl. Crystallogr. 12* (1979) 107.
7. Abrahamsson, S. *J. Sci. Instrum. 43* (1966) 931.
8. *SAAB Film Scanner Manual,* SAAB AB, Datasaab, Linköping, Sweden 1967.
9. Ibers, J. A. and Hamilton, W. C. *International Tables for X-Ray Crystallography,* Kynoch Press, Birmingham 1974, Vol. 4, p. 71.
10. Malmros, G. and Thomas, J. O. *J. Appl. Crystallogr. 10* (1977) 7.
11. Pedersen, B. and Grønvold, F. *Acta Crystallogr. 12* (1959) 1022.

Received October 19, 1982.

Acta Chemica Scandinavica A 37 (1983) 415–422

Metal Complexes with Mixed Ligands. 26. Complex Formation between Cadmium(II) Imidazoles and Chloride Ions. A Potentiometric and Solubility Study in Mixed 3.0 M $(Na)ClO_4$, Cl Media

INGER GRANBERG and STAFFAN SJÖBERG

Department of Inorganic Chemistry, University of Umeå, S-901 87 Umeå, Sweden

Stability constants of ternary Cd^{2+}-complexes with the ligands imidazole ($C_3H_4N_2$,L) and chloride ions were studied at 25 °C. The measurements were performed as potentiometric titrations [glass and Cd(Hg) electrodes] in ionic media consisting of mixtures of 3.0 M $(Na)ClO_4$ and 3.0 M (Na)Cl. Besides pure binary species CdL_n^{2+}, n=1, 2, 3, 4 and $CdCl_s^{(2-s)+}$, s=1, 2, 3, data can be explained with the ternary complexes $CdLCl^+$, $CdLCl_3^-$, CdL_2Cl^+, CdL_2Cl_2 and CdL_3Cl^+ with formation constants $\log \beta_{111}$= 4.33±0.01, $\log \beta_{113}$=5.11±0.06, $\log \beta_{121}$=6.26± 0.03, $\log \beta_{122}$=6.57±0.06 and $\log \beta_{131}$= 7.95±0.03. In addition, two stable solid phases were obtained, $CdLCl_2(s)$ with

$$\log \beta(Cd^{2+}+L+2Cl^- \rightleftarrows CdLCl_2(s))=7.76\pm0.07$$

and $CdL_6(ClO_4)_2$ with

$$\log \beta(Cd^{2+}+6L+2ClO_4^- \rightleftarrows CdL_6(ClO_4)_2(s))=13.8\pm0.2.$$

In the calculations the computer programs LETAGROPVRID and SOLGASWATER were employed.

Complexation in the Cd^{2+}–imidazole ($C_3H_4N_2$,L)–OH^- system was presented in a preceding publication.[1] By using glass and Cd(Hg) electrodes it was shown that besides pure binary species, CdL_n^{2+} (n=1...4), a mixed hydroxo complex $CdLOH^+$ was formed. A comparison between acidities of the Cd^{2+}- and CdL^{2+}-ions clearly showed CdL^{2+} to be a stronger acid. This fact indicates that a coordinated imidazole ligand enhances the affinity for OH^- in the complex. This behaviour has earlier been found in the corresponding Zn^{2+} and Hg^{2+} systems investigated by Forsling [2] and Sjöberg,[3] respectively. In these two systems the stability of several mixed Me^{2+}–L–Cl^- complexes was also evaluated.

It was also found, as in the case of $ZnOH^+$, that $ZnCl^+$ is a stronger complexing agent to imidazole than the Zn^{2+}-ion. In the mercury(II) system no pronounced enhancement for Cl^- in the different Hg^{2+}–L and Hg^{2+}–L–Cl^- complexes was found.

The aim of the present investigation was to determine compositions and stabilities of possible mixed chloro complexes in the Cd^{2+}–L–Cl^- system. Furthermore, the solubility products of crystalline precipitates, obtained during the experimental conditions, were determined.

By means of the results obtained, a comparison of stabilities of different binary and ternary complexes within the 2B group was performed.

EXPERIMENTAL

Chemicals and analysis. All solutions used were prepared and analyzed as described earlier.[1] A protolytic impurity in 3 M $NaClO_4$ and 3 M NaCl solutions was determined amounting to 10^{-4} M with an acidity constant of $\sim10^{-8}$ M.

0302-4377/83 $02.50

Corrections for this impurity have been made in the calculations described below.

Method. The titrations were performed as potentiometric titrations (glass and Cd(Hg) electrodes) as 25 °C. The titration procedures and the experimental details of the measurements are fully described in Ref. 1.

The equilibrium solutions were made to contain $[ClO_4^-]+X=3.0$ M, where X is the total concentration of chloride ions. The general compositions of solutions were: B M Cd^{2+}, C M HL^+, H M H^+, X M Cl^-, (3.00−X) M ClO_4^- and ($[ClO_4^-]$+X−2B−C−H) M Na^+. B, C and X are the total concentrations of cadmium(II), imidazole and chloride and H stands for the total concentration of protons calculated over the zero level Cd^{2+}, HL^+, Cl^- and H_2O. The free hydrogen ion concentration, h, and the free cadmium ion concentration, b, were measured with a glass electrode and a cadmium−amalgam electrode, respectively.

Solid phases. Most of the titrations were ended by the formation of crystalline precipitates. Three different phases were identified, $CdLCl_2$(s), CdL_2Cl_2(s) and $CdL_6(ClO_4)_2$(s), by using powder X-ray techniques.

The solid phase CdL_2Cl_2 was transformed to $CdLCl_2$ after a while. Due to this instability, CdL_2Cl_2 was not further examined and no attempts were made to determine the solubility product for this phase.

To determine the solubility products of $CdLCl_2$ and $CdL_6(ClO_4)_2$, the solutions were equilibrated with these phases for several months, filtered and then analyzed with respect to H and the free concentrations of Cd^{2+} (b) and Cl^- (x). H in the solutions was determined by adding H^+ from a burette and evaluated using a Gran [4] plot. b was determined by using a cadmium ion−selective electrode (Orion, model 94-48A) and x was measured by means of an Ag,AgCl electrode. In a few solutions x was too high to be accurately measured. Instead X was determined (precipitated as AgCl in acidified solutions) and x was calculated as described below.

Speciation and equilibria. We will assume the presence of four component equilibria of the general form

$$pH^+ + qCd^{2+} + rHL^+ + sCl^- \rightleftarrows H_pCd_qHL_rCl_s^{(2q+p+r-s)+};\ \beta_{pqrs} \quad (1)$$

In addition to the four component equilibria we have:

(i) Complex formation between cadmium(II) and chloride

$$Cd^{2+} + sCl^- \rightleftarrows CdCl_s^{(2-s)+};\ \beta_s \quad (2)$$

In 3.0 M (Na)ClO_4,Cl medium the formation constants were determined to be log $\beta_1=1.55(1)$, log $\beta_2=2.19(2)$ and log $\beta_3=2.34(3)$, in good agreement with those determined by Biedermann *et al.*[5] The equilibrium constant for the complex $CdCl_4^{2-}$, log β_4, turned out with great uncertainty. However, within the concentration range investigated the complex $CdCl_4^{2-}$ could be neglected, and no further attempts to determine the value of the formation constant were made.

(ii) The imidazole equilibria, which within the concentration range $0\leq X\leq 3.0$ M with (ClO_4^- +X)=3.0 M are determined by Sjöberg,[3] and could be described as

$$HL^+ \rightleftarrows L + H^+;\ k_a \quad (3)$$

$$HL^+ + Cl^- \rightleftarrows LCl^- + H^+;\ \beta_{-1011} \quad (4)$$

$$HL^+ + 2Cl^- \rightleftarrows LCl_2^{2-} + H^+;\ \beta_{-1012} \quad (5)$$

with log $k_a=-7.913$, log $\beta_{-1011}=-8.641$ and log $\beta_{-1012}=-9.279$.

(iii) The cadmium(II) imidazole equilibria [1]

$$pH^+ + qCd^{2+} + rHL^+ \rightleftarrows H_pCd_q(HL)_r^{(2q+p+r)+} \quad (6)$$

with log $\beta_{-111}=-4.820$, log $\beta_{-212}=-10.327$, log $\beta_{-313}=-16.451$ and log $\beta_{-414}=-23.14$.

In the present study the hydrolytic equilibria of the cadmium(II) ion as well as the formation of ternary cadmium(II)−OH^--imidazole complexes could be neglected provided $C/B>6$ or $B\gtrsim 0.010$ M. Equilibria (2)−(6) were assumed to be known in the calculations concerning the four component equilibria.

Computer programs used. The mathematical analysis of the experimental data were performed with the least-squares computer program LETAGROPVRID [6] (version ETITR [7,8]). As input to this program *h, b, H, C* and *X* or *h, b, B, C* and *X* were given. The error squares sums $U=\Sigma(H_{calc}-H_{exp})^2$ and $U=\Sigma(B_{calc}-B_{exp})^2$, respectively, were minimized. The different standard deviations were defined and calculated according to Sillén.[9,10]

Calculations of the free concentrations of imidazole, [L], and chloride for obtaining the solubility products, were performed by using the computer program SOLGASWATER.[11] As input to this program *b, H, X*-data and formation constants β_{nqs} defined according to the equilibria

$$qCd^2 + nL + sCl^- \rightleftarrows Cd_qL_nCl_s^{(2q-s)+} \quad (7)$$

were given. [L]and *x* were then calculated using the expressions

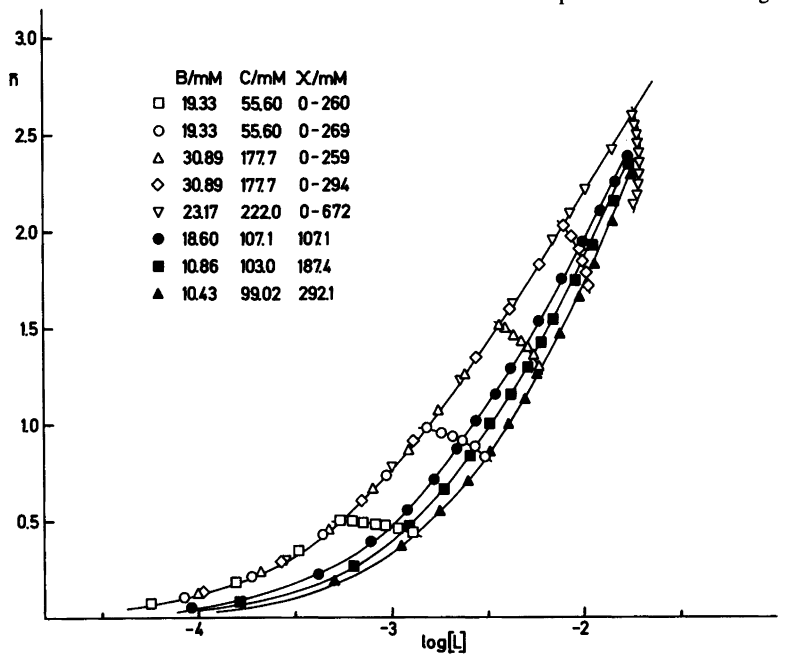

Fig. 1. Experimental data plotted as curves $\bar{n}(\log [L])$. Open symbols refer to titrations in 3.0 M $(Na)ClO_4$ and mixed media at defined $\bar{n}$-values. Filled symbols refer to titrations at constant Cl^- concentrations. The full curves were calculated with β_n values given in the final model.

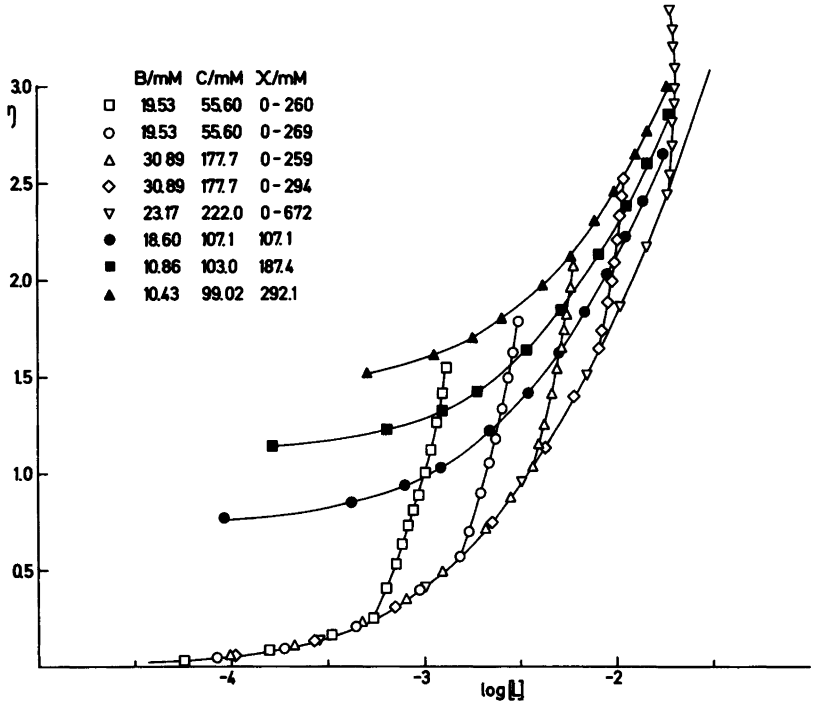

Fig. 2. Experimental data plotted as curves $\eta(\log [L])$.

$$-H=[L]+[LCl^-]+[LCl_2^{2-}]+\Sigma n[CdL_nCl_s^{(2-s)+}]$$

$$X=x+[LCl^-]+2[LCl_2^{2-}]+\Sigma s[CdCl_s^{2-s}]+\Sigma s[CdL_nCl_s^{2-s}]$$

The program SOLGASWATER was also used to calculate distribution diagrams and predominance area diagrams in order to visualize the amounts of the different species.

The mathematical analysis of powder X-ray data was performed using a least-squares program.[12] As input the cell parameters given in the structure determination of $(CdLCl_2)_\infty$[13] and $(CdL_2Cl_2)_\infty$[14] and those for $CdL_6(ClO_4)_2^1$ were used. Clear evidence for the existence of these solid phases was given.

The computations were performed on a CD 6600 computer.

DATA, CALCULATIONS AND RESULTS

Experimental data were collected by performing titrations with OH^- or H^+ at constant Cl^- concentrations (X=0, 0.11, 0.15, 0.19, 0.22 and 0.3 M) and at defined $\bar{n}$ values ($\bar{n}$=0.25, 0.5, 0.75, 1, 1.2, 1.5, 1.7, 2, 2.3 and 2.6) where solutions 3.0 M in $(Na)ClO_4$ were titrated with solutions 3.0 M in $(NaCl+NaClO_4)$. The quotients C/B were kept constant and had the values 3, 6 and 10. The concentration ranges investigated were $4<-\log h<8$, $0.01\leq B\leq 0.03$ M, $0.05\leq C\leq 0.22$ M and $0<X\leq 0.6$ M, comprising 15 different titrations with 284 experimental points.

The analysis of data was started by making $\bar{n}(\log [L])$ plots and $\eta(\log [L])$ plots, by using E_H data and (E_B+E_H) data, respectively. These are shown in Figs. 1 and 2. Systematic deviations from the $\bar{n}$ and η curves indicate formation of ternary mixed complexes of type $Cd_qL_nCl_s^{(2q-s)+}$.

The different LETAGROP calculations showed that the "best" explanation of the experimental data was obtained with the ternary complexes $CdLCl^+$, $CdLCl_3^-$, CdL_2Cl^+, CdL_2Cl_2 and CdL_3Cl^+. The complexes $CdLCl_2$, $CdLCl_4^{2-}$, $CdL_2Cl_3^-$, CdL_3Cl_2, CdL_4Cl^+ and CdL_4Cl_2 were also tested one at a time. Formation constants of these complexes came out with large standard deviations. The results of these calculations are summarized in Table 1. At higher Cl^- concentrations (2.25 M) a titration was performed in order to find out whether there were any additional complexes formed at high Cl^- concentration. However, data could satisfactorily be explained

Table 1. Results of LETAGROP calculations concerning formation of ternary $Cd^{2+}-L-Cl^-$ complexes. The formation constants are defined according to the equilibrium.

$$pH^+ + qCd^{2+} + rHL^+ + sCl^- \rightleftarrows H_pCd_qHL_rCl_s^{(2q+p+r-s)+};\ \beta_{pqrs}$$

When no $3\sigma(\log \beta_{pqrs})$ is given the formation constant has not been varied. R denotes a rejected complex ($\beta_{pqrs}\leq 0$).

No. of titr/ No. of points	$CdLCl^+$ $\log(\beta_{1111}\pm 3\sigma)$	$CdLCl_3^-$ $\log(\beta_{1113}\pm 3\sigma)$	CdL_2Cl^+ $\log(\beta_{2121}\pm 3\sigma)$	CdL_2Cl_2 $\log(\beta_{2122}\pm 3\sigma)$	CdL_3Cl^+ $\log(\beta_{3131}\pm 3\sigma)$	$CdL_nCl_s^{(2-s)+}$ $\log(\beta_{pqrs}\pm 3\sigma)$	p,r,s	U [a]	$\sigma(y)$
15/284	−3.58(1)	−2.80(6)	−9.60(3)	−9.26(6)	−15.79(3)			2.93 [c]	0.10
	−3.60(2)	−2.84(5)	−9.50(5)	−9.29(5)	−15.82(9)			4.77 [b]	0.13
	−3.61(3)	−2.94(9)	−9.60	−9.29	−15.79	−3.77(14)	−1,1,2	2.82	0.10
	−3.58(1)	−2.80(2)	−9.60	−9.29	−15.79	R	−1,1,4	2.93	0.10
	−3.58	−2.80	−9.60(2)	−9.28(10)	−15.79	−10.28−9.58 [d]	−2,2,3	2.93	0.10
	−3.58	−2.80	−9.59(3)	−9.30(9)	−15.80(4)	−16.51−16.06 [d]	−3,3,2	2.90	0.10
	−3.58	−2.80	−9.59(3)	−9.26(4)	−15.80(7)	−23.61−22.88 [d]	−4,4,1	2.93	0.10
	−3.58	−2.80	−9.59(3)	−9.29(6)	−15.80(3)	−22.90−22.53 [d]	−4,4,2	2.88	0.10

[a] $Y=H_{CALC}-H_{EXP}$. Calculations are based on E_H+E_B data with data set *h, b, H, C, X* used. [b] $(Y)=B_{CALC}-B_{EXP}$. Calculations are based on E_H+E_B data with data set *h, b, B, C, X* used. [c] Proposed constants. [d] Min and max values in log β.

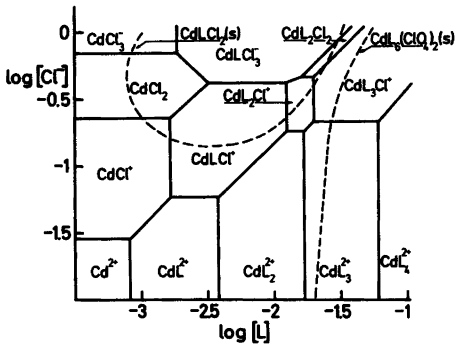

Fig. 3. Predominance area diagram for different cadmium(II) complexes and solid phases for B=0.01 M, ([ClO_4^-]+X)=3.0 M. Log [L]≳−1.8 and log [Cl^-]≳−0.4 denote extrapolated ranges.

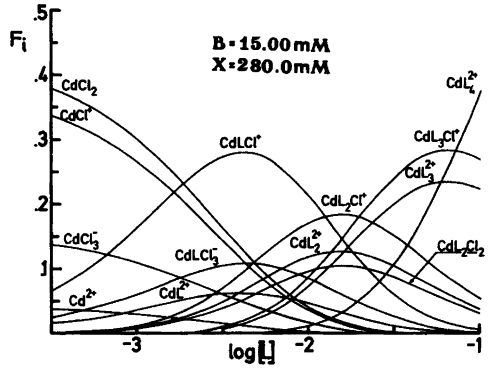

Fig. 4. Distribution diagram $F_i(\log [L])_{B,X}$ for the different cadmium(II) complexes.

with the complex $CdLCl_3^-$ besides the binary $CdCl_s^{(2-s)+}$, s=1...4, complexes and no further measurements in this area up to 3.0 M Cl^- were performed. (In this calculation log β_4=2.2 according to Biedermann [5] was used.)

In order to visualize the amounts of the different Cd(II) species in this system a distribution diagram as well as a predominance area diagram have been constructed (see Figs. 3 and 4).

For the solid phases $CdLCl_2$ and $CdL_6(ClO_4)_2$, solutions were analyzed to determine their solubility products. The measurements include seven solutions for the phase $CdLCl_2$ and three solutions for $CdL_6(ClO_4)_2$. The solubility products were defined according to the relation

$$Cd^{2+}+L+2Cl^- \rightleftarrows CdLCl_2(s);$$
$$\log(\beta\pm3\sigma)=7.76(7)$$

and

$$Cd^{2+}+6L+2ClO_4^- \rightleftarrows CdL_6(ClO_4)_2(s);$$
$$\log(\beta\pm3\sigma)=13.8(2)$$

As this determination is based on rather few data, the resulting standard deviations are quite large.

The extent to which the solid phases are formed is demonstrated in the predominance area diagram for B=0.01 M (Fig. 3).

DISCUSSION

The present emf investigation has clearly shown the existence of ternary cadmium(II)-imidazole-Cl^- complexes. Besides the series CdL_nCl^+, n=1, 2, 3 the complexes CdL_2Cl_2 and $CdLCl_3^-$ were formed. These ternary complexes are all formed in significant amounts and do in fact predominate within specified ranges (*cf.* Fig. 3). The results can be interpreted as stepwise reactions in which Cl^- ions are successively coordinated to each of the CdL_n^{2+} species (n=0, 1, 2, 3). Stepwise constants for the reactions

$$CdL_nCl_{s-1}^{(3-s)+}+Cl^- \rightleftarrows CdL_nCl_s^{(2-s)+};$$
$$K_{1ns} \quad s=1, 2, 3$$

Table 2. Some stepwise reactions with constants calculated by means of formation constants given in this paper. The different reactions define the stepwise uptake of Cl^- and are to be read horizontally. (CdL^{2+} 1.24 $CdLCl^+$ stands for $CdL^{2+}+Cl \rightleftarrows CdLCl^+$ with log K=1.24.)

Cd^{2+}	1.55	$CdCl^+$	0.65	$CdCl_2$	0.15	$CdCl_3^-$
CdL^{2+}	1.24	$CdLCl^+$		0.78		$CdLCl_3^-$
CdL_2^{2+}	0.72	CdL_2Cl^+	0.35	CdL_2Cl_2		
CdL_3^{2+}	0.66	CdL_3Cl^+				

Table 3. Logarithms of the statistical stability constants of the complexes compared with the corresponding experimental stability constant.

Formula	Stat. value of log β_{ns}	Exp. value of log β_{ns}
$CdLCl^+$	4.15	4.33
CdL_2Cl^+	6.12	6.24
CdL_3Cl^+	7.53	7.94
CdL_2Cl_2	6.13	6.57
$CdLCl_3^-$	4.38	5.09

with different values of n and s are given in Table 2. A comparison between the different K_{1ns} values directly shows the Cd^{2+} ion to be a stronger complexing agent for Cl^- than the binary CdL_n^{2+} as well as the ternary CdL_nCl_s complexes. However, it can be noted that for the reaction

$$CdL_nCl^+ + 2Cl^- \rightleftarrows CdL_nCl_3^-$$

log K (n=0)=0.80 and log K (n=1)=0.78, thus almost the same values. The high stability of this ternary complex is most probably due to a coordination shift leading to a tetrahedral configuration as in $CdCl_3^-$.

A decreased stability of the ternary complexes in comparison with the binary $CdCl_s^{2-s}$ species has also been found in other ternary $Cd^{2+}-L-X^-$ systems, where L stands for organic ligands such as thiourea,[15] glycine,[16] ethylenediamine,[16] the inorganic ligand sulfate [17] and X^- stands for the halides Cl^-, Br^- and I^-.

To determine whether there is any mutual influence between imidazole and Cl^- in the ternary complexes or if statistical reasons alone determine their formation, statistical equilibrium constants β_{ns} ($Cd^{2+}+nL+sCl^- \rightleftarrows CdL_nCl_s^{(2-s)+}$) have been calculated according to the formula [17]

$$\log \beta_{ns} = \frac{n \log \beta_{N0} + s \log \beta_{0N}}{N} + \log \frac{N!}{n!s!}$$

where $N=n+s$.

Table 4. Some stepwise reactions for the Zn group by means of formation constants given in Ref. 2, this paper and Ref. 3, and proposed configuration. The different reactions define the stepwise uptake of the ligands Cl^-, $C_3H_4N_2$(L) are to be read horizontally.

ex. $MeCl^+$	3.64 (o) 2.60 (o) 9.18 (l)	$MeLCl^+$ stands for	$ZnCl^+ + L \rightleftarrows ZnLCl^+$ $CdCl^+ + L \rightleftarrows CdLCl^+$ $HgCl^+ + L \rightleftarrows HgLCl^+$	log K=3.64 log K=2.60 log K=9.18

(o), (t) and (l) stand for octahedral, tetrahedral and linear coordination, respectively.

$MeCl_3^-$	−0.15(t) 1.07(t)	$MeCl_4^{2-}$										
$MeCl_2$	0.75(t) 0.15(t) 1.07(t)	$MeCl_3^-$	3.45(t) 2.77(t) 3.08(t)	$MeLCl_3^-$								
$MeCl^+$	0.41(t) 0.65(o) 6.78(l)	$MeCl_2$	− − 3.15(t)	$MeLCl_2$	7.53[a](t) 4.38[a](o) 6.23[a](t)	MeL_2Cl_2						
Me^{2+}	0.19(o) 1.55(o) 7.22(l)	$MeCl^+$	3.64(o) 2.60(o) 9.18(l)	$MeLCl^+$	2.52(o,t)? 1.93(o) 2.48(t)	MeL_2Cl^+	3.61(t) 1.69(o) −	MeL_3Cl^+				
		Me^{2+}	2.93(o) 3.09(o) 9.18(l)	MeL^{2+}	2.00(t) 2.41(o) 9.01(l)	MeL_2^{2+}	3.79(t) 1.79(o) −	MeL_3^{2+}	2.82(t) 1.22(o) −	MeL_4^{2+}		

[a] The formation constants given include the uptake of two ligands ($MeCl_2+2L \rightleftarrows MeL_2Cl_2$).

By using proposed formation constants for CdL_n^{2+}, n=2, 3, 4 and $CdCl_s^{(2-s)+}$, s=2, 3, 4 and assuming that log $\beta_{CdCl_4^{2-}}$=2.2 [5,17] it is possible to calculate statistical values for all ternary complexes found in this system. The result is given in Table 3.

It can be seen from this table that the two- and three-coordinated complexes $CdLCl^+$ and CdL_2Cl^+ are formed by statistical reasons, while the four-coordinated complexes CdL_3Cl^+, CdL_2Cl_2 and $CdLCl_3^-$ are significantly stronger than predicted from statistical reasoning. Thus the formation of four-coordinated complexes are determined by entropy as well as enthalpy changes.

It is interesting to note that similar behaviour is found for the ternary complexes $HgLCl^+$ and $HgOHCl^+$ which are formed by statistical reasons, while Zn^{2+} forms ternary complexes with imidazole and chloride which are considerably stronger than are predicted from statistical values.

Stabilities of Zn, Cd, Hg complexes. By means of the results obtained in this investigation, it has become possible to compare stabilities of different binary and ternary complexes with the ligands imidazole and chloride in the 2B group (Zn, Cd, Hg). Complexation in the corresponding Zn^{2+} (Forsling) and Hg^{2+} system (Sjöberg) [3] has earlier been studied under similar experimental conditions.

It is well-known that Zn and Cd usually form complexes with octahedral or tetrahedral configuration. Mercury, on the other hand, shows a preference for linear and tetrahedral coordination.

In the Zn^{2+}-imidazole-Cl^- system coordination shifts seem to occur frequently. Besides a shift at the second step in the $ZnCl_s^{2-s}$ series, octa- and tetrahedral complexes are formed in the binary ZnL_n^{2+} series as well as among the ternary $Zn^{2+}-L-Cl^-$ species.

In the Hg^{2+} system the most stable species are linear, and three- and four-coordinated complexes have much lower stability.

In the present system, the validity of the 2-parameter approximation within the CdL_n^{2+} series indicates no coordination shift. These complexes are most probably octahedral, as has been shown for $Cd(H_2O)_6^{2+}$ [18] and CdL_6^{2+} [1] from structural investigations. Octahedral configuration has also been found in the solid phases $(CdLCl_2)_n$[13] and $(CdL_2Cl_2)_n$[14] and it seems likely that the corresponding mononuclear complexes in aqueous solution have a similar coordination. From NMR [19] and calorimetric [20] measurements, tetrahedral configuration in $CdCl_3^-$ and $CdCl_4^{2-}$ has been proposed.

A review of the stabilities of the different species formed in the 2B group is given in Table 4. Most probable configuration of the complexes are also indicated. As can be seen, it is possible to compare stabilities of different types of complexes (tetrahedral (t), octahedral (o) and linear (l)) within this group. For tetrahedral binary and ternary chloro complexes, *e.g.* $MeCl_3^-$ and $MeLCl_3^-$, the stability seems to increase within the series:

$$Zn_t > Cd_t < Hg_t$$

Irrespective of type of configuration all ternary complexes show the same trend in stability, *i.e.* Zn>Cd<Hg. For the different imidazole complexes, the tetrahedral Zn species are more stable than the corresponding octahedral Cd species.

Acknowledgements. We wish to thank Professor Nils Ingri for his great interest and for all the facilities placed at our disposal. The English of the present paper has been corrected by Dr. Michael Sharp. The work forms part of a program financially supported by the Swedish Natural Science Research Council.

REFERENCES

1. Granberg, I. and Sjöberg, S. *Acta Chem. Scand. A 35* (1981) 193.
2. Forsling, W. *Thesis,* Umeå, Sweden 1978.
3. Sjöberg, S. *Thesis,* Umeå, Sweden 1976.
4. Gran, G. *Acta Chem. Scand. 4* (1950) 559.
5. Biedermann, G., Lagrange, J. and Lagrange, P. *Chem. Scr. 5* (1974) 153.
6. Ingri, N. and Sillén, L. G. *Ark. Kemi 23* (1964) 97.
7. Arnek, R., Sillén, L. G. and Wahlberg, O. *Ark. Kemi 31* (1969) 353.
8. Brauner, P., Sillén, L. G. and Whiteker, R. *Ark. Kemi 31* (1969) 365.
9. Sillén, L. G. *Acta Chem. Scand. 16* (1962) 159.
10. Sillén, L. G. and Warnqvist, B. *Ark. Kemi 31* (1969) 341.
11. Eriksson, G *Anal. Chim. Acta 112* (1979) 375.

12. Werner, P.-E. *Ark. Kemi 31* (1969) 513.
13. Nassimbeni, L. R. and Rodgers, A. L. *Acta Crystallogr. B 32* (1976) 257.
14. Flook, R. J., Freeman, H. C., Huq, F. and Rosally, J. M. *Acta Crystallogr. B 29* (1973) 903.
15. De Marco, D., Bellamo, A. and De Roberts, A. *J. Inorg. Nucl. Chem. 43* (1981) 137.
16. Fridman, Ya. D. and Danilova, T. V. *Russ. J. Inorg. Chem. 16* (1971) 34.
17. Feodorov, V. A., Chernikova, G. E., Kuzechikina, M. A. and Kuznetsova, T. I. *Russ. J. Inorg. Chem. 20* (1975) 1613.
18. West, C. D. *Z. Kristallogr. 88* (1934) 150.
19. Ackerman, J. J. H., Orr, T. V., Bartuska, V. J. and Maciel, G. E. *J. Am. Chem. Soc. 101* (1979) 341.
20. Persson, I. *Thesis,* Lund, Sweden 1980.

Received October 8, 1982.

Acta Chemica Scandinavica A 37 (1983) 423–430

The Mechanisms of the Dimerization of Sulfur Dioxide Anion Radical in the Presence of Tetraalkylammonium Ions in DMF

VERNON D. PARKER

Laboratory for Organic Chemistry, Norwegian Institute of Technology, University of Trondheim, N-7034 Trondheim-NTH, Norway

In the presence of tetraethylammonium ion $SO_2^{\cdot-}$ undergoes reversible dimerization with an apparent rate constant of 1.5×10^7 M^{-1} s^{-1} at 0 °C and an apparent activation energy of −7 kcal/mol. Due to the reversibility of the anion radical–dimer equilibrium the reaction appears to be relatively slow at long measurement times. When the counter ion is tetrabutylammonium ion a different mechanism was observed consisting of the reversible association (i) followed by reaction (ii).

$$SO_2^{\cdot-}+SO_2 \overset{K_i}{\rightleftarrows} (SO_2^{\cdot-})SO_2 \qquad \text{(i)}$$

$$(SO_2^{\cdot-})SO_2+SO_2^{\cdot-} \xrightarrow{k_{ii}} {}^-O_2S-SO_2^-+SO_2 \qquad \text{(ii)}$$

Reaction (ii) could either be an electron transfer or the displacement of SO_2 by $SO_2^{\cdot-}$. The latter pathway is deemed most likely on the basis of an apparent activation energy of the order of 5 kcal/mol since ΔH_i° is expected to be negative and the E_a for electron transfer to be small. K_i was observed to be equal to 1640 M^{-1} at 293 K and k_{ii} was estimated to be equal to 1.7×10^7 M^{-1} s^{-1} at the same temperature. In the presence of Et_4N^+, K_i was observed to be equal to or less than about 200 M^{-1}. The data are discussed in context with other recent studies of the reactions of sulfur dioxide anion radical in DMF.

The electroreduction of SO_2 in nonaqueous media has been investigated intensively over the past fifteen years.[1–13] In DMF containing Et_4N^+ ion, ESR and electrochemical measurements have shown that $SO_2^{\cdot-}$ exists along with the anion radical complex $(SO_2^{\cdot-})SO_2$ according to equilibrium (1).[7,1–3]

$$SO_2^{\cdot-}+SO_2 \overset{K_1}{\rightleftarrows} (SO_2^{\cdot-})SO_2 \qquad (1)$$

However, the value of K_1 was found to depend strongly on the particular technique used in the study. Kastening and Gostisa-Mihelcic [7] reported a value of 230 M^{-1} for K_1 based on a combination of polarographic and e.s.r. measurements. Gardner, Fouchard and Fawcett [2] determined K_1 to be 8400 M^{-1} by *a.c.* polarography, while the most recent study by Laman, Gardner and Fouchard using simultaneous electrochemical and e.s.r. measurements [14] resulted in a value of 611 M^{-1}.[1] The latter study also resulted in an estimate of the forward rate constant for reaction (1) of 10^5 $M^{-1}s^{-1}$.

Another interesting aspect of the reactions of $SO_2^{\cdot-}$ was reported by Gardner, Fouchard and Fawcett.[3] They found that in the presence of either Et_4N^+ or Bu_4N^+ the reactions of $SO_2^{\cdot-}$ could be described by reaction (1) but in the presence of Li^+ only dimerization to dithionate ion (2) takes place.

$$2\,SO_2^{\cdot-} \xrightarrow{k_2} S_2O_4^{2-} \qquad (2)$$

The dependence of the reaction pathway upon both the supporting electrolyte cation and the solvent was interpreted in terms of the relative importance of ion pairing.

The previous studies all involved measurements at relatively long times and thus the details of the primary processes taking place are not evident. The competition between the reaction with substrate and dimerization of anion radicals is of interest with regard to some of our related

0302-4377/83 $02.50

Table 1. The effect of substrate concentration on apparent rate constants for the dimerization of sulfur dioxide anion radical in DMF in the presence of tetraethylammonium ion.[a]

$[SO_2]$/mM	$v_{0.3}$	$10^{-6}k/M^{-1}s^{-1}$	$-E^p$(100 V s^{-1})[b]/mV
0.095	35.5	9.22	1073
0.190	64.6	8.39	1073
0.285	90.7	7.85	1073
0.428	114.5	6.60	1073

[a] Measurements by DCV at 291.9 K in solvent containing Et_4NBF_4 (0.1 M). [b] Peak potential *vs.* Ag/Ag^+ in acetonitrile.

work.[15–18] The study of the association of ion radicals to neutral molecules and the effect this has on kinetics and mechanism is pertinent to our recent work in other systems.[19–22] Finally, we have been concerned with reversible dimerizations of ion radicals and the mechanisms of the reactions.[23,24] Thus, because of interest in this general area of chemistry as well as the uncertainties remaining in the $SO_2^{\cdot-}$ system, a re-investigation of the kinetics and mechanism of the dimerization of $SO_2^{\cdot-}$ in DMF was undertaken.

RESULTS

At voltage sweep rates of 200 mV/s or less, the cyclic voltammogram for the reduction of SO_2 in DMF containing Et_4NClO_4 takes the form expected for a reversible charge transfer followed by a slow homogeneous reaction of the anion radical (see Fig. 1 of Ref. 2). Nearly identical results are obtained when the supporting electrolyte is Et_4NBF_4. However, at higher voltage sweep rate (v) the peak current ratio is much less than unity indicating a very rapid follow-up reaction of $SO_2^{\cdot-}$. Results for the measurement of $v_{0.3}$, the sweep rate necessary for the current derivative ratio to equal 0.300, are summarized in Table 1.* The peak potential measured at 100 V/s was constant at 1073±1 mV *vs.* an Ag/Ag^+ reference electrode. The latter indicates that the association of $SO_2^{\cdot-}$ with SO_2 is not favorable enough under the measurement conditions for a shift in reversible potential to be evident. The value of $v_{0.3}$ was observed to be concentration dependent and the rate constants given in column 3 of Table 1 are assuming a dimerization mechanism, eqn. (2), and were calculated from theoretical relationships previously reported.[25] A decreasing trend with increasing substrate concentration is found in the rate constants. This is not consistent with the interference of the dissocia-

* See Ref. 27 for a discussion of DCV mechanism analysis.

Table 2. The effect of temperature on the apparent rate constant for the dimerization of sulfur dioxide anion radical in DMF in the presence of tetraethylammonium ion.[a] $E_a = -7.1$ kcal/mol (r=0.9993).[b]

T/K	$v_{0.3}$/V s^{-1}	$10^{-6}k/M^{-1}$ s^{-1}
291.9	114.5	6.60
282.9	168	9.99
273.1	249	15.3
253.9	>500	>33.1

[a] Measurements of DCV on solutions containing Et_4NBF_4 (0.1 M) and SO_2 (0.428 mM). [b] Linear regression correlation coefficient.

Table 3. Evidence for the reversibility of the dimerization of sulfur dioxide in the presence of tetraethylammonium ion in DMF.[a]

v/V s^{-1}	R_I' [b]
100.0	0.354
60.0	0.333
40.0	0.323
20.0	0.322
10.0	0.321
5.00	0.347
2.00	0.395
1.00	0.430

[a] In solvent containing Et_4NBF_4 (0.1 M) and SO_2 (0.428 mM) at 304.6 K. [b] The ratio of first derivative peaks of the reverse and forward cyclic voltammetry scans.

tion of the dimer, dithionate ion, which would be expected to cause the opposite trend in the rate constants. Although there is some deviation from second order kinetics, the effect is relatively small.

The data in Table 2 show the effect of temperature on the apparent rate constants. It was possible to measure $v_{0.3}$ at temperatures ranging from 292–273 K and the resulting rate constants gave an Arrhenius plot with an apparent activation energy of −7.1 kcal/mol and a linear regression correlation coefficient of 0.9993. The linearity of the Arrhenius plot suggests that the dissociation of the dimer is not seriously affecting the values of the observed rate constants. This has also been demonstrated to be the case in the reversible dimerization of 9-substituted anthracenes.[23,24] At 253.9 K the reaction rate was observed to be so great that a reliable value of the rate constant could not be determined. Since the reaction continues to increase in rate with decreasing temperature at temperatures where the dissociation is surely not a problem, the apparent activation energy for the dimerization does indeed have a negative value.

The reversibility of the dimerization reaction is demonstrated by the data in Table 3. At 304.6 K the ratio of the derivative peaks of the cyclic voltammogram, R_I', decreases as v is decreased from 100 V/s and reaches a minimum value of about 0.321 in the region near 10 V/s. Further decreases in v are then accompanied by increasing R_I' values. Similar behaviour has been shown to be due to the dissociation of the dimer dianion in a related case.[23]

When Bu_4NBF_4 was the supporting electrolyte, quite a different situation was encountered. The peak potential measured by derivative cyclic voltammetry (DCV) at 100 V/s was observed to depend strongly on the substrate concentration. The data in Table 4 show this effect. If the shift in the peak potential with increasing substrate concentration is caused by the association equilibrium (1), the equilibrium constant (K_1) is related to the shift in reversible potential (ΔE_{rev}) by eqn. (3).

$$\Delta E_{rev} = RT/F \ln(1+K_1[SO_2]) \quad (3)$$

This equation has been derived earlier [2] using an analysis similar to that employed by Peover and Davies for the determination of ion pair equilibrium constants.[26] When the substrate is involved in the equilibrium as in (1) a special problem is encountered since the direct determination of E_{rev} under conditions where it is not affected by the association reaction is not possible if K_1 is large. The values of K_1 listed in the last column of Table 4 were obtained assuming E_{rev} was 4.0 mV less negative than that measured at a substrate concentration of 0.000211 M. The standard deviation in the calculated K_1 values was observed to be only ±5.4 % of the mean value. Assuming either higher or lower values of ΔE_{rev} resulted in a larger standard deviation and hence a poorer fit of the data to eqn. (3).

Table 4. The equilibrium constant for the association of sulfur dioxide anion radical with substrate in DMF in the presence of tetrabutylammonium ion.[a]

$10^4[SO_2]$/M	$-E_p$[b]/mV	ΔE_{rev}[c]/mV	K[d]/M^{-1}
2.11	522.7(0.9)	4.0	1631
3.16	522.3(1.6)	4.4	1513
4.21	518.8(0.5)	7.9	1749
5.26	518.0(0.6)	8.7	1568
6.32	516.1(1.1)	10.6	1655
7.37	514.2(0.8)	12.5	1743
8.42	513.8(1.6)	12.9	1588
			1635±5.4 %

[a] Measurements by derivative cyclic voltammetry at 293 K. [b] The peak potential, refered to a bias potential of −600 mV *vs.* Ag/Ag^+ in acetonitrile, measured by DCV at 100 V s^{-1}. The numbers in parentheses refer to the standard deviations in five replicate measurements. [c] The values giving the best fit to eqn. (3). [d] Calculated according to eqn. (3).

Table 5. The effect of substrate concentration on the rate of dimerization of sulfur dioxide anion radical in DMF in the presence of tetrabutylammonium ion.[a]

$[SO_2]$/mM	$v_{0.3}$/V s^{-1}	$v_{0.3}/[SO_2]^2$	$10^{-10}k^b$/$M^{-2}s^{-1}$
0.421	35.0	197.5	1.72
0.526	47.2	170.6	1.49
0.632	75.2	188.3	1.64
0.737	107.9	198.7	1.73
0.842	121.0	170.7	1.49
		185.2(13.8)	1.61(0.12)
0.211	7.45	167.3	1.46
0.316	18.6	186.1	1.63
0.421	39.1	220.6	1.93
0.526	49.6	179.3	1.57
		188.3(22.8)	1.65(0.20)

[a] Measurements by DCV in solvent containing Bu_4NBF_4 (0.1 M) at 293.0 K. [b] Calculated from theoretical data reported in Ref. 25.

The effect of substrate concentration on the rate of reaction of $SO_2^{\cdot-}$ in DMF in the presence of Bu_4N^+ ion was also observed to be markedly different than when the counter ion was Et_4N^+. The data are summarized in Table 5 for two independent series of experiments. The third column gives $v_{0.3}$ divided by the square of the substrate concentration. According to the principles of DCV mechanism analysis [27] the overall reaction order, $R_{A/B}$, is given by eqn. (4) where z is the number necessary for the term in parentheses to be constant.

$$R_{A/B} = 1+z \quad (v_{0.3}/C_A^z = \text{constant}) \tag{4}$$

The data fit relationship (4) with $z=2$ indicating that $R_{A/B}$ is 3. This result is consistent with rate law (5) where R_B, the reaction order in primary intermediate, or $SO_2^{\cdot-}$ in this case is 2, and R_A the reaction order in substrate is 1.

$$\text{Rate} = k_{app}[SO_2^{\cdot-}]^2[SO_2] \tag{5}$$

This rate law is that expected for the association of $SO_2^{\cdot-}$ with SO_2 followed by rate determining reaction between the complex and anion radical (6) in which case $k_{app}=k_6K_1$.

$$(SO_2^{\cdot-})SO_2+SO_2^{\cdot-} \xrightarrow{k_6} S_2O_4^{2-}+SO_2 \tag{6}$$

Theoretical data are available for the DCV analysis of this mechanism.[25] The rate constants listed in the last column of Table 5 were calculated assuming mechanism (1)+(6) and rate law (5). The apparent rate constants for the two independent sets of experiments were nearly identical at 1.61(±0.12) and 1.65(±0.20)×10^{10} $M^{-2}s^{-1}$.

The effect of temperature on the reaction rate of $SO_2^{\cdot-}$ in DMF in the presence of Bu_4N^+ is illustrated by the data in Table 6. There was some scatter in the data and the correlation coefficient for the Arrhenius plot was only 0.96. The apparent activation energy was 5.5 kcal/mol.

According to mechanism (1)+(6) the linear sweep voltammetry (LSV) peak potential is predicted to shift by 39.4 mV per decade change in substrate concentration at 298 K. This value can be derived from eqn. (7) where a is the reaction order in substrate and b that in primary intermediate.[28]

$$\text{d log } E^p/\text{d log } C_A = RT/F\,(a+b-1)/(b+1) \tag{7}$$

The LSV data shown in Table 7 were obtained to further test the compatibility of rate law (5) with the data. At 292 K the theoretical value of the slope is −38.6 mV. The value observed was −51.6 mV/decade. However, we must keep in mind that the reversible potential also changes

Table 6. The effect of temperature on the apparent third order rate constants for the dimerization of sulfur dioxide anion radical in DMF in the presence of Bu_4N^+.[a] E_a=5.5 kcal/mol.

T/K	$v_{0.3}$/V s^{-1}	$10^{-10}k/M^{-2}s^{-1}$
292.6	53.8	2.66
273.1	44.5	2.35
252.7	40.0	2.29
242.7	36.0	2.14

[a] Measurements by DCV on solutions containing SO_2 (0.421 mM) and Bu_4NBF_4 (0.1 M).

with substrate concentration and this must be corrected for. The corrections in the third column reflect the reversible potential changes in this concentration range. After correction a slope of −33.9 mV/decade was obtained. Deleting the data at the highest concentration improved the linearity of the analysis and a slope of −37.2 mV/decade with a correlation coefficient of 0.9993 was found. We can safely conclude that the LSV data are consistent with rate law (5).

DISCUSSION

The cause of some of the inconsistencies in previously reported values of K_1 in DMF in the presence of Et_4N^+ is now obvious. The highest value 8,400 M^{-1}, was calculated from polarographic half-wave potentials assuming the dimerization reaction (2) is so slow that the cyclic voltammogram is essentially reversible at only 200 mV/s.[2] The apparent reversibility of the electrode process has been shown in this work to be due to the reversibility of reaction (2) and under the conditions of the polarographic work [2] the reversible reaction can be described by (8).

$$2\ SO_2 + 2\ e^- \rightleftarrows S_2O_4^{2-} \qquad (8)$$

However, eqn. (8) only holds when the time scale of the experiment is long compared to the rate of dissociation of dithionate ion. The influence of the time scale of the experiment is shown clearly by the data in Table 3. The high value of the apparent ΔE_{rev} which led to the assumption of the high K_1 value [2] was simply due to the fact that the potential for reaction (8) is concentration dependent and the reversible potential shift is a reflection of that. In order to derive the equilibrium constant for (9) it would be advisable to work on a time scale where other reactions are not interfering. Further work is necessary along these lines.

$$2\ SO_2^{\cdot-} \overset{K_9}{\rightleftarrows} S_2O_4^{2-} \qquad (9)$$

Reversible potential shifts were calculated assuming each of the previously reported K_1 values and are compared to that observed in this work in Table 8. The peak potential measured by DCV at 100 V/s was observed to be independent of substrate concentration ranging from 0.095 to 0.428 mM within the limits of experimental error which was estimated to be about ±1 mV. The two higher values, 8400 and 611 M^{-1}, are clearly ruled out under the conditions of the measure-

Table 7. The effect of substrate concentration on the linear sweep voltammetry peak potential during the dimerization of sulfur dioxide anion radical in DMF containing Bu_4N^+.[a]

$[SO_2]$/mM	$-E_p$	Correction [b]	$-E_p$(corr)/mV
0.211	380.4(0.5)	4.0	384.4
0.422	366.4(0.2)	7.5	373.9
0.844	348.8(0.1)	13.2	362.0
1.266	341.0(0.1)	17.9	358.9
$(dE_p/d \log [SO_2])$/(mV/decade)	−51.6		−33.9 [c]

[a] Measurements at 200 mV/s in solvent containing Bu_4NBF_4 (0.1 M) at 292 K. [b] The shift in the reversible potential calculated from the equilibrium constant for: $SO_2^{\cdot-} + SO_2 \rightleftarrows (SO_2^{\cdot-})SO_2$. [c] Omitting the data at the highest concentration results in a value of −37.2 mV/decade with a correlation coefficient of 0.9993.

Table 8. Calculated reversible potential shifts (ΔE_{rev}/mV) from equilibrium constants reported in the literature for the association of $SO_2^{\cdot-}$ with SO_2 in DMF containing Et_4N^+.

$[SO_2]$/mM	Ref. 2 K=8400 M^{-1}	Ref. 1 K=611 M^{-1}	Ref. 7 K=230 M^{-1}	This work Observed [a]
0.095	8.5	0.72	0.27	±1
0.190	14.8	1.42	0.54	±1
0.285	19.8	2.10	0.81	±1
0.428	25.9	3.10	1.28	±1

[a] From measurements by DCV at 100 V s^{-1}.

ments used. The value reported by Kastening and Gostisa-Mihelcic [7] appears to be just a little bit higher than is compatible with the peak potential shift data. It is likely that the value is 200 M^{-1} or less. The very large equilibrium constant for reaction (9) would have to be taken into account in the analysis of all of the previous data in order to come up with a reasonable estimate of K_1.

On the other hand, K_1 is sufficiently large in DMF in the presence of Bu_4N^+ to completely change the situation. A value of 1635 M^{-1} was estimated from the shift in peak potential measured at 100 V/s (Table 4). The equilibrium constant expression for reaction (1) can be rearranged to (10),

$$[(SO_2^{\cdot-})SO_2]/[SO_2^{\cdot-}] = K_1[SO_2] \quad (10)$$

which gives the relative concentrations of complexed to uncomplexed anion radical at a given substrate concentration. Since the concentrations employed in the experiments ranged from 2.11 to 8.42×10^{-4} M, there was always an appreciable fraction of uncomplexed $SO_2^{\cdot-}$ in the reaction layer. Thus, the magnitude of K_1 in the presence of Bu_4N^+ cannot be responsible for the exclusion of dimerization reaction (2). This can also be deduced from considering the first entries in Tables 2 and 5. At the same $[SO_2]$ and temperature, $v_{0.3}$ was observed to be nearly 3 times as great in the presence of Et_4N^+ than in the presence of Bu_4N^+ which means that the lifetime of $SO_2^{\cdot-}$ under these conditions is about 3 times as great in the presence of Bu_4N^+. The reaction order data indicate that dimerization is the predominant reaction in the presence of Et_4N^+ (Table 1) and that the third order mechanism (1)+(6) is the nearly exclusive pathway in the presence of Bu_4N^+ (Table 5). It appears that the electrolyte effect is best described by the influence of Et_4N^+ on reaction (2) and on the magnitude of equilibrium constant K_9 as well as on the magnitude of K_1. A plausible explanation of these observations is that ion pairing is much more pronounced in the case of Et_4N^+ as the counter ion than when Bu_4N^+ is the supporting electrolyte cation. This suggests that the dimerization reaction can be described by a mechanism involving equilibrium (11) and coupling reactions (12) and (13), the latter depending upon the magnitude of K_{11}.

$$SO_2^{\cdot-} + R_4N^+ \overset{K_{11}}{\rightleftarrows} (SO_2^{\cdot-})R_4N^+ \quad (11)$$

$$(SO_2^{\cdot-})R_4N^+ + SO_2^{\cdot-} \xrightarrow{k_{12}} S_2O_4^{2-}(R_4N^+) \quad (12)$$

$$2\,(SO_2^{\cdot-})R_4N^+ \xrightarrow{k_{13}} S_2O_4^{2-}(R_4N^+)_2 \quad (13)$$

In fact, this is essentially the same interpretation that Gardner, Fouchard and Fawcett [3] presented for the dimerization reaction in the presence of Li^+. However, they assumed that ion pairing was insignificant in the presence of Et_4N^+. The pre-equilibrium mechanism (11)−(13) also accounts for the apparent negative activation energy (Table 2). The apparent activation energy for this mechanism is the sum of ΔH°_{11} and E_a for the coupling reactions (12) or (13) depending upon which is important under the conditions of the measurements.

One of the features of the previous work that was of special interest to the author was that the forward rate constant for reaction (1) was proposed to be equal to only 10^5 $M^{-1}s^{-1}$.[1] This value appeared to be quite low for a reaction which only involves the formation of a non-bonded association complex. However, in this work we

see that forward reaction (1) is fast enough so that (1) is in equilibrium in spite of the occurrence of a very rapid further reaction (6). The apparent rate constant for mechanism (1)+(6) is equal to k_6K_1 and was found to be 1.63×10^{10} $M^{-2}s^{-1}$ at 293 K (Table 5). Since K_1 was estimated to be equal to 1635 at the same temperature (Table 4) this results in a value of 10^7 $M^{-1}s^{-1}$ for k_6. Since rate law (5) requires that (1) is at equilibrium, we can estimate the value of k_1 from eqn. (14),

$$k_1[SO_2^{\cdot-}][SO_2]>10\,k_6[(SO_2^{\cdot-})SO_2][SO_2^{\cdot-}] \quad (14)$$

which results in a value of the order $k_1>10^8$ $M^{-1}s^{-1}$ assuming that average ratio of the concentrations of SO_2 and the anion radical complex is about 1 in the reaction layer. Thus, it is quite probable that forward reaction (1) is diffusion controlled.

Reaction (6) is an intriguing one. At first glance one might assume that it is a simple electron transfer with $SO_2^{\cdot-}$ donating an electron to the complex. This could indeed be the case. However, the apparent activation energy for the process was observed to be of the order of 5.5 kcal/mol (Table 6). Since reaction (1) is a simple association which would be expected to be exothermic, an overall activation energy of 5.5 kcal/mol implies that E_a for reaction (6) may be somewhat greater after accounting for ΔH_1°. If reaction (6) only involves the transfer of an electron, the activation energy would be expected to be considerably smaller. On this basis it would appear to be more likely that (6) is not an electron transfer reaction but rather a displacement of SO_2 from the complex by $SO_2^{\cdot-}$. The relatively large activation energy, *i.e.* for a reaction with a rate constant of 10^7 $M^{-1}s^{-1}$, could then be due to the charge repulsion in the transition state leading to the formation of dithionate ion. Still another possibility is that the reaction does involve electron transfer but that (6) is a two-step process. The first step could be electron transfer (15) which is then followed by the formation of dithionate ion (16).

$$(SO_2^{\cdot-})SO_2+SO_2^{\cdot-} \underset{}{\overset{K_{15}}{\rightleftarrows}} (SO_2^{\cdot-})SO_2^{\cdot-}+SO_2 \quad (15)$$

$$(SO_2^{\cdot-})SO_2^{\cdot-} \xrightarrow{k_{16}} S_2O_4^{2-} \quad (16)$$

This sequence would also account for the activation energy but would give rise to rate law (17) and overall second order kinetics.

$$\text{Rate} = k_{16}K_1K_{15}[SO_2^{\cdot-}]^2 \quad (17)$$

Mechanism (15)+(16) can be ruled out on this basis. Thus, the most likely mechanism appears to be the displacement reaction.

In conclusion, it should be emphasized that the reaction pathway followed by $SO_2^{\cdot-}$ in DMF depends very much upon the reaction conditions. A change from Et_4N^+ to Bu_4N^+ as counter ion brought about a change in mechanism. It is quite likely that other factors such as the presence and concentration of proton donors could cause equally dramatic changes.

EXPERIMENTAL

The instrumentation, electrodes, cells and data handling procedures were those described earlier.[29] Reagent grade DMF containing the supporting electrolyte (Bu_4NBF_4) were passed through a column containing neutral alumina before use. Anhydrous SO_2 from Matheson was used as received. A stock solution of SO_2 in DMF was added to the electrolyte solution after oxygen had been removed by purging with nitrogen. Derivative cyclic voltammetry experiments were carried out as previously described.[30]

REFERENCES

1. Laman, F. C., Gardner, C. L. and Fouchard, D. T. *J. Phys. Chem. 86* (1982) 3130.
2. Gardner, C. L., Fouchard, D. T. and Fawcett, W. R. *J. Electrochem. Soc. 128* (1981) 2337.
3. Gardner, C. L., Fouchard, D. T. and Fawcett, W. R. *J. Electrochem. Soc. 128* (1981) 2345.
4. Geronov, V., Moshtev, R. V. and Puresheva, B. *J. Electroanal. Chem. 108* (1980) 335.
5. Shembel, E. M., Litvinova, V. I., Maksyuta, I. M. and Ksezhek, O. S. *Sov. Electrochem. 15* (1980) 1534.
6. Shembel, E. M., Litvinova, V. I., Maksyuta, I. M. and Ksezhek, O. S. *Sov. Electrochem. 15* (1980) 1435.
7. Kastening, B. and Gostisa-Mihelcic, B. *J. Electroanal. Chem. 100* (1979) 801.

8. Magno, R. P., Mazzoccin, G. A. and Bontempelli, G. *J. Electroanal. Chem. 57* (1974) 89.
9. Martin, R. P. and Sawyer, D. T. *Inorg. Chem. 11* (1972) 2644.
10. Bonnaterre, R. and Cauquis, G. *J. Electroanal. Chem. 32* (1971) 215.
11. Rinker, R. G. and Lynn, S. *Ind. Eng. Chem. Prod. Res. Dev. 8* (1969) 338.
12. Rinker, R. G. and Lynn, S. *J. Phys. Chem. 72* (1968) 4706.
13. Dinse, K. P. and Möbius, K. *Z. Naturforsch. A 23* (1968) 695.
14. Goldberg, I. B. and Bard, A. J. *J. Phys. Chem. 75* (1971) 3281.
15. Parker, V. D. *Acta Chem. Scand. B 35* (1981) 149.
16. Parker, V. D. *Acta Chem. Scand. B 35* (1981) 279.
17. Margaretha, P. and Parker. V. D. *Acta Chem. Scand. B 36* (1982) 260.
18. Parker, V. D. Adv. *Phys. Org. Chem. 19* (1983) 131.
19. Parker, V. D. *Acta Chem. Scand. B 35* (1981) 147.
20. Lerflaten, O. and Parker, V. D. *Acta Chem. Scand. B 36* (1982) 193.
21. Parker, V. D. *Acta Chem. Scand. B 37* (1983). *In press.*
22. Lerflaten, O. and Parker, V. D. *Acta Chem. Scand. B 37* (1983). *In press.*
23. Hammerich, O. and Parker, V. D. *Acta Chem. Scand. B 35* (1981) 341.
24. Hammerich, O. and Parker, V. D. *Acta Chem. Scand. B 37* (1983). *In press.*
25. Ahlberg, E. and Parker, V. D. *Acta Chem. Scand. B 35* (1981) 117.
26. Peover, M. E. and Davies, J. D. *J. Electroanal. Chem. 6* (1963) 46.
27. Parker, V. D. *Acta Chem. Scand. B 35* (1981) 233.
28. Parker, V. D. *Acta Chem. Scand. B 35* (1981) 259.
29. Ahlberg, E. and Parker, V. D. *Acta Chem. Scand. B 34* (1980) 97.
30. Ahlberg, E. and Parker, V. D. *J. Electroanal. Chem. 121* (1981) 73.

Received October 29, 1982.

Acta Chemica Scandinavica A 37 (1983) 431–436

Resonance Energies of Unsaturated Cyclophanes with 4N and (4N+2) Perimeters

ULF NORINDER * and OLOF WENNERSTRÖM

Department of Organic Chemistry, Chalmers University of Technology and University of Göteborg, S-412 96 Göteborg, Sweden

The resonance energies of a series of paracyclophanes with unsaturated perimeters have been calculated by the methods of Hess and Schaad (RE) and Trinajstić *et al.* (TRE). The two methods give similar results. The resonance energies (TRE) of some dianions of the paracyclophanes were also evaluated. An alternating effect of the resonance energies as a function of the size of the perimeter, whether it is of the $4n$ or $(4n+2)$ type, was observed for a series of paracyclophanes with one benzene ring. The effect is almost quenched in cyclophanes with three or four benzene rings. However, it is somewhat restored in the dianions of paracyclophanes with four benzene rings. It can be concluded that calculated resonance energies are dominated by the effect of the local aromatic rings and that the effect of the size of the perimeter is somewhat masked. The chemistry of these large cyclophanes appears to be better understood in terms of frontier orbital considerations.

Since the first concept of extra stability of conjugated compounds appeared in the literature,[1] a steady flow of papers has appeared on the subject. Many of them deal with the failure of the original Hückel delocalisation energies (DE) in predicting this extra stability, often called aromaticity. This fact was proved by the synthesis of compounds such as fulvene,[2] heptafulvene [3] and fulvalene,[3] which all have large DE values,[4] although none of them are to be considered aromatic. This lack of agreement led to new concepts in estimating resonance energies. Dewar and co-workers calculated a new type of resonance energies (DRE) using a semi-empirical SCF MO-method.[5] The DRE-values predict aromaticity or lack of it rather successfully. It soon became apparent that it was not the changeover to more sophisticated calculations, but rather the change of reference system, that made these new resonance energies more reliable. Hess and Schaad have proposed an elegant method within the Hückel framework, which predicts the amount of extra stability present in a conjugated structure.[6] They classified the bonds of acyclic polyenes into eight different types, which they correlated against twenty-two such structures.[7] These values were then used to calculate π resonance energies (*RE*) using the equation

$$RE = E_{HMO} - E_{LOC}$$

where E_{HMO} is the total HMO π energy and E_{LOC} the π energy of the corresponding "localised" structure.[8] To obtain a comparable quantity, compensating the variation in size of molecules investigated, Hess and Schaad proposed the resonance energy per π electron (REPE) as such. Trinajstić *et al.* have proposed a similar idea, the HMO index of aromatic stabilisation (A_s), using correlated values of only one type of polyene double and single bonds.[9] A comparison between the REPE and the HMO index per π electron (A_s/e) gives in most cases similar results.[10] A most promising topological interpretation of resonance energies has lately appeared through the works of Aihara [11] and Trinajstić *et al.*[12] Using

* To whom correspondence should be addressed.

0302-4377/83 $02.50

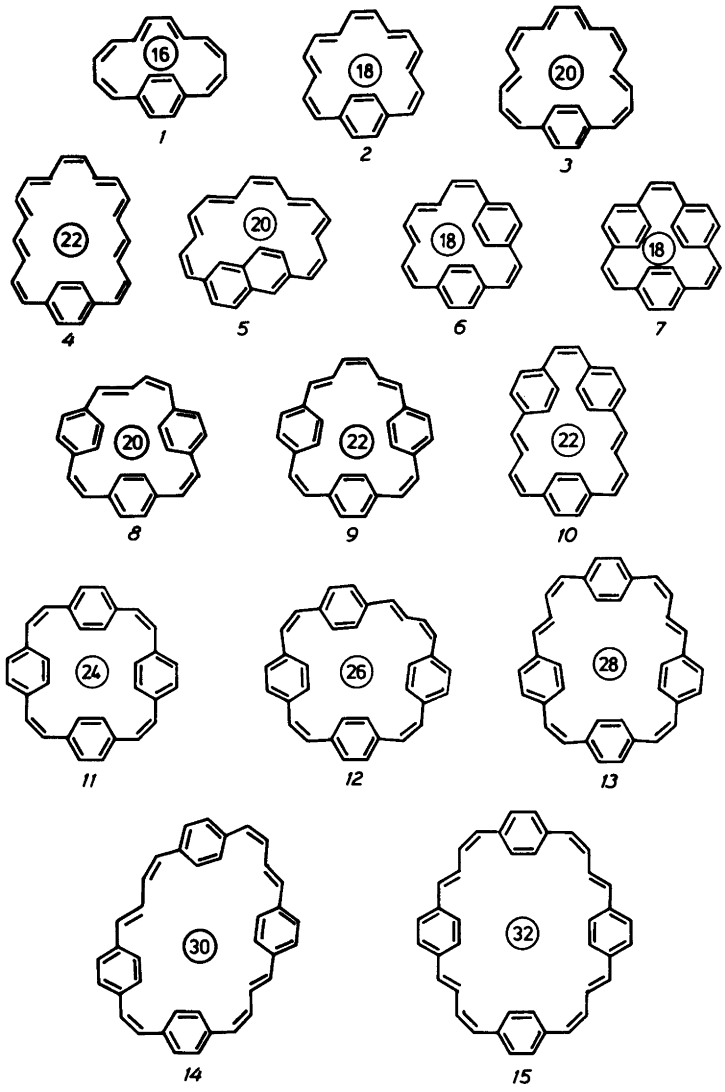

Scheme 1.

graph theory,[13] they have extended the previous ideas of predicting aromatic stability. Utilizing topological resonance energies (TRE), one can treat any conjugated system, neutral or ion, cyclic or acyclic in a nonempirical way. TRE-values are calculated using the equation

$$TRE = \sum_{j=1}^{N} g_j(x_j - x_j^{ac})$$

where g_j is the occupancy number of the jth MO, x_j the Hückel eigenvalues, and x_j^{ac} the roots of the reference polynomial. TRE gives exactly $TRE=0$ for all acyclic structures. To compensate for size, Trinajstić *et al.* have proposed a quantity similar to REPE, namely the topological resonance energy per π electron [TRE(PE)].

Recently we have found that a series of cyclophanes with unsaturated bridges on reduction gives a new type of dianion with aromatic

Table 1. Resonance energies (in β) of conjugated cyclophanes.

Compound	*TRE*	*TRE(PE)*	*RE*	*REPE*	Predicted status [21]
1	0.0117	0.0007	0.1980	0.0110	NA
2	0.2482	0.0124	0.4416	0.0221	A
3	0.0418	0.0019	0.2451	0.0111	NA
4	0.2322	0.0097	0.4418	0.0184	NA/A
5	0.2041	0.0085	0.4197	0.0175	NA
6	0.4328	0.0197	0.7130	0.0324	A
7	0.6378	0.0266	1.0195	0.0425	A
8	0.5510	0.0212	0.9349	0.0360	A
9	0.6143	0.0219	1.0410	0.0359	A
10	0.6105	0.0218	0.9979	0.0356	A
11	0.7864	0.0246	1.2877	0.0402	A
12	0.8100	0.0238	1.3138	0.0386	A
13	0.7694	0.0214	1.2773	0.0355	A
14	0.7876	0.0207	1.2982	0.0342	A
15	0.7422	0.0186	1.2675	0.0317	A

character, *e.g.* having a perimeter of $(4n+2)$ π-electrons, sustaining large diamagnetic ring currents in strong magnetic fields.[14] We now report an evaluation of the relative amounts of extra stabilisation in these large dianions, their parent cyclophanes and some smaller members based upon RE and TRE calculations.

RESULTS AND DISCUSSION

The resonance energies RE and TRE for paracyclophanes with one, two, three and four benzene rings connected by unsaturated bridges to give compounds with conjugated perimeters ranging from 16 to 32 π-electrons have been calculated within the Hückel framework (Table 1). Thus, we assumed that the minimum energy conformations of the paracyclophanes are near planar, which may be doubtful in some cases. The structures of the cyclophanes are depicted in Scheme 1, and the topological resonance energies (*TRE*) for some selected dianions are shown in Table 2.

Table 2. Resonance energies (in β) of dianions of some selected cyclophanes.

Compound	*TRE*	*TRE(PE)*	Predicted status [21]
11	0.5912	0.0174	A
12	0.4544	0.0126	A
13	0.6218	0.0164	A
14	0.4822	0.0121	A
15	0.6186	0.0147	A

Although the theoretical foundations for the topological resonance energy method have been questioned recently,[15] it has generally been observed that TRE values and RE values are proportional.[12c] Other methods suggested by Haddon [16] and Aihara [11] give, for annulenes, essentially the same results. We have found the correlation between TRE and RE values to exist for the series of cyclophanes discussed in this paper as well (Fig. 1, *TRE* and *RE* values for some annulenes have been included for comparison).

Only a few [18]annulene derivatives with para-substituted benzene rings as a part of the π-system have been reported. A bridged [18]annulene prepared by photocyclisation of [2.2](3,6)phenanthrenoparacyclophanediene shows a large diamagnetic ring current in a strong magnetic field.[17] For the neutral paracyclophanes with three or four benzene rings the situation is different. They do not show any significant ring current effects regardless if they formally have $4n$ or $(4n+2)$ perimeters. Most of these cyclophanes do not attain a planar conformation to allow for an efficient overlap between the rings and the unsaturated bridges. Their spectroscopic prop-

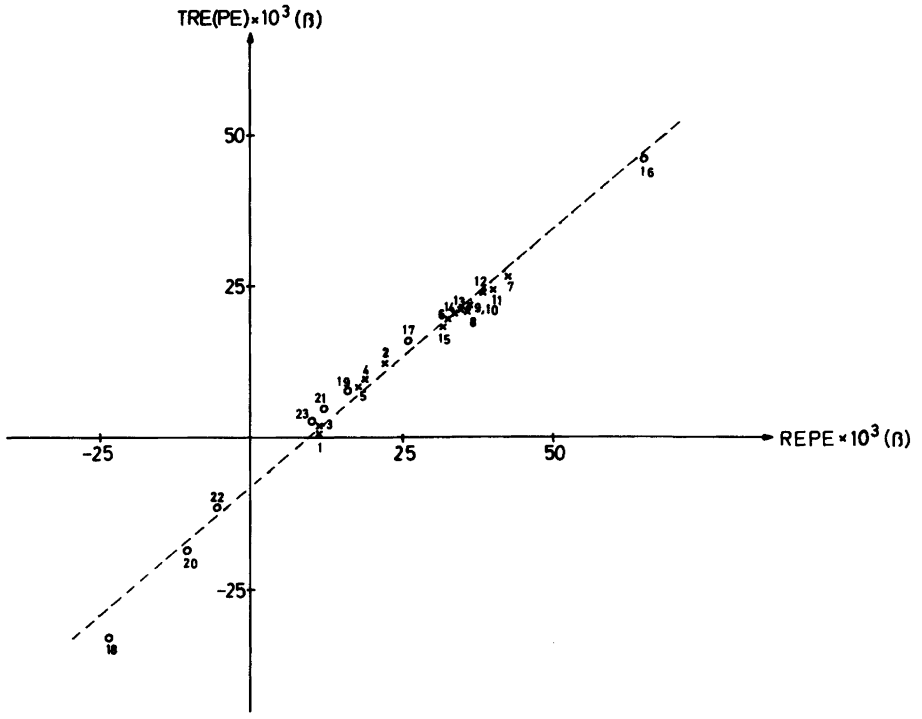

Fig. 1. A plot of *TRE(PE) vs. REPE* of cyclophanes with unsaturated bridges. (Annulenes included for comparison: 16=benzene, 17=[10]annulene, 18=[12]annulene, 19=[14]annulene, 20=[16]annulene, 21=[18]annulene, 22=[20]annulene, 23=[22]annulene.)

erties are very much those expected for normal aromatic compounds.[18] Whether the preferred conformations are due solely to steric effects or result from the lack of resonance stabilisation of the more planar conformations, cannot be determined without more extensive quantum mechanical calculations. The simple resonance arguments presented here are, however, consistent with the experimental findings.

The [6]–[22]annulenes with one parasubstituted benzene ring, compounds *1–4*, show a distinct alternation of their RE and TRE values, although less pronounced than in the annulene series (Fig. 1).

The change of the aromatic unit from benzene to naphthalene within the same size of the perimeter, cyclophanes *3* and *5*, increases the calculated resonance energies (Table 1). In the naphthalenophane the influence of the aromatic unit dominates the total resonance energy. The same trend is observed on increasing the number of benzene rings within the [18]annulene perimeter, cyclophanes *2*, *6* and *7*. Both methods give a regular increase in the calculated resonance energies, which for the [2.2.2]paracyclophanetriene, *7*, is very large and dominated by the three benzene rings.

The resonance energies of the cyclophanes with three benzene rings and perimeters of 18, 20 and 22 π-electrons, compounds *7–10*, are similar but slightly smaller for the [20]annulene derivative, cyclophane *8*. On further increase of the number of benzene rings and size of the perimeter, the calculated resonance energies show even less alternation between Hückel and Möbius systems, as expected. The RE and TRE values for the series of cyclophanes *11–15* differ by only a few per cent within each method of calculation. The total resonance energies are dominated by the influence of the benzene rings. The results demonstrate that it is irrelevant to consider these paracyclophanes as annulene derivatives even if they were planar. This conclusion is consistent with the chemical and spectro-

scopic properties (especially NMR data) of the cyclophanes, as pointed out above. It seems safe to conclude, not only from this investigation but also from previous studies of benzannulenes with more than one aromatic unit,[19] that the local aromatic units dominate the character of the total π-electron structure. On the other hand, the cyclophanes with only one benzene ring are more interesting and might well be considered as annulene derivatives.

What is true for the neutral cyclophanes may, however, not hold for the charged species. Recently, we have shown that certain cyclophanes readily form dianions with complete delocalisation of the charge over the total π-system and that these dianions are of the $(4n+2)$ type and show large diamagnetic ring current effects.[14] The resonance energies (*TRE*) of the dianions from cyclophanes *11–15* show a more pronounced alternating behaviour than the neutral cyclophanes, although all of them should be characterised as aromatic (Table 2). Even in these dianions, which must be nearly planar to sustain large ring currents in strong magnetic fields, the total resonance energy is dominated by the contributions form the local aromatic rings. It may be questioned whether resonance arguments are of use for the understanding of these types of dianions. There are certainly severe problems with the definition of resonance energy and the choice of reference structure for compounds of this type. Such problems, already large for neutral cyclophanes, are even more important for the dianions. At present, there is also a lack of experimental data with which to verify the various recent theories of large π-systems.[11,12b–c,20] These theories generally predict similar behaviour for the neutral and charged species with the same number of π-electrons, which does not seem to be consistent with the, admittedly limited, experimental findings.

There have been numerous attempts to correlate ring currents and resonance energy [16] or more generally aromaticity. Such correlations are necessarily more complicated for cyclophanes with an annulene character due to the presence of the local aromatic subunit. For example, the dianion of cyclophane *11* shows a large diatropic shift of the signals from the inner and outer protons, whereas the tetra-anion shows somewhat smaller paratropic shifts.[14b] Both species are aromatic, much more so than the neutral annulenes with the same π-electron perimeters due to the benzene rings.

In cyclophanes with an annulene character, regardless of charge, the effect of the aromatic unit must clearly be eliminated when discussing the effect of the size of the total perimeter, regardless if it is of the Hückel or the Möbius type. One approach to this problem is to limit the discussion to frontier orbitals rather than to consider the total resonance energies. The simplest approach is to correlate energies of the Hückel HOMO and LUMO orbitals with experimental observables, *e.g.* the reduction potentials for the reversible formation of dianions, which results in an unexpectedly good correlation.[14a]

Acknowledgement. Financial support from the Swedish Natural Science Research Council is gratefully acknowledged.

REFERENCES

1. Hückel, E. *Z. Physik 70* (1931) 204; *Z. Physik 72* (1931) 310.
2. Thiec, J. and Wiemann, J. *Bull. Soc. Chim. Fr.* (1956) 177.
3. Doering, W. v. E. *Theor. Org. Chem., Kekulé Symp. 1958,* Butterworth, London 1959.
4. Streitwieser, A. *Molecular Orbital Theory for Organic Chemists,* Wiley, New York 1962.
5. Dewar, M. J. S. and Gleicher, G. J. *J. Am. Chem. Soc. 87* (1965) 685.
6. Hess, B. A., Jr. and Schaad, L. J. *J. Am. Chem. Soc. 93* (1971) 305; *J. Am. Chem. Soc. 93* (1971) 2413; *J. Am. Chem. Soc. 94* (1972) 3068; *J. Org. Chem. 30* (1971) 3418.
7. Two bond types had to be arbitrarily assigned due to linear dependence.
8. For greater detail, see Ref. 6.
9. Milun, M., Sobotka, Ž. and Trinajstić, N. *J. Org. Chem. 37* (1972) 139.
10. Hess, B. A., Jr. and Schaad, L. J. *J. Org. Chem. 37* (1972) 4180.
11. Aihara, J. I. *J. Am. Chem. Soc. 98* (1976) 2750; *Bull. Chem. Soc. Jpn. 49* (1976) 1427.
12. a. Trinajstić, N. *Croat. Chem. Acta 49* (1977) 593; b. Gutman, I., Milun, M. and Trinajstić, N. *Croat. Chem. Acta 49* (1977) 441; c. Gutman, I., Milun, M. and Trinajstić, N. *J. Am. Chem. Soc. 99* (1977) 1692.
13. For a review, see Harary, F. *Graph Theory,* Addison-Wesley, Reading, Mass. 1969.

14. a. Norinder, U., Tanner, D., Thulin, B. and Wennerström, O. *Acta Chem. Scand. B 35* (1981), 403; b. Huber, W., Müller, K. and Wennerström, O. *Angew. Chem. 92* (1980) 636.
15. a. Gutman, I. *Chem. Phys. Lett 66* (1979) 595; b. Gutman, I. and Mohar, B. *Chem. Phys. Lett. 69* (1980) 375; c. Heilbronner, E. *Chem. Phys. Lett. 85* (1982) 377.
16. Haddon, R. C. *J. Am. Chem. Soc. 101* (1979) 1722.
17. DuVernet, R. B., Wennerström, O., Lawson, J., Otsubo, T. and Boekelheide, V. *J. Am. Chem. Soc. 100* (1978) 2457.
18. Thulin, B. *J. Chem. Soc. Perkin Trans. 2* (1980) 664.
19. Mitchell, R. H. *Isr. J. Chem. 20* (1980) 294.
20. Bates, R. B., Hess, B. A., Jr., Ogle, C. A. and Schaad, L. J. *J. Am. Chem. Soc. 103* (1981) 5052.
21. According to the TRE(PE) values.

Received October 27, 1982.

Acta Chemiea Scandinavica A 37 (1983) 437–445

Short Communications

On the Crystal Structure of the Tetrabutylammonium Tetraiodothallate(III) $[N(C_4H_9)_4][TlI_4]$

JULIUS GLASER,[a] PETER L. GOGGIN,[b] MAGNUS SANDSTRÖM[a] and VLADIMIR LUTSKO[c]

[a] Department of Inorganic Chemistry, Royal Institute of Technology, (KTH), S-100 44 Stockholm, Sweden, [b] Department of Inorganic Chemistry, The University, Bristol BS8 1TS, England and [c] Institute for Physico-Chemical Research, Byelorussian State University, 220080 Minsk-80, USSR

We have previously published results of the crystal structure determination of the title compound.[1] Following publication, we received a letter from Dr. R. E. Marsh,* in which he kindly pointed out that the crystal structure which we described in the space group $P2_1$, could possibly be better described in $P2_1/n$ (non-standard setting of $P2_1/c$, equivalent positions: $\pm(x, y, z)$, $\pm(1/2-x, 1/2+y, 1/2-z)$). The additional glide plane in $P2_1/n$ requires the systematic absence of all reflexions $h0l$ with $(h+l)$ odd.

In our original data set, the $h0l$'s with $(h+l)$ odd included 11 reflections having $F_{obs} \geq 3.92\sigma(F_{obs})$, leading us to describe the structure in $P2_1$. We have now measured all the equivalent $h0l$ reflections, and are convinced that they are systematically extinguished; the intensities that appear to be non-zero arise, we believe, from splitting of the crystal or from a small satellite. As a consequence, we have re-refined the structure in $P2_1/n$, using the same data as previously but with the eleven odd $h0l$'s removed.

* California Institute of Technology, Pasadena, California 91125, Bldg. 127-72, USA.

Table 1. Final fractional atomic positional parameters for the heavy atoms. Estimated standard deviations are given in parentheses.

$P2_1/n$	($P2_1$)	x	y	z
Tl	(Tl1, Tl2)	0.23476(8)	0.68332(5)	0.46103(9)
I1	(I1, I7)	0.2805(2)	0.6848(1)	0.2368(2)
I2	(I2, I5)	0.4325(2)	0.7030(1)	0.6133(2)
I3	(I3, I6)	0.0711(2)	0.7742(1)	0.4883(2)
I4	(I4, I8)	0.1435(2)	0.5669(1)	0.5099(2)

Table 2. Final anisotropic thermal parameters with estimated standard deviations in parentheses. The expression used is $\exp[-2\pi^2(U_{11}h^2a^{*2}+\ldots+2U_{12}hka^*b^*+\ldots)]$.

Atom	U_{11}	U_{12}	U_{33}	U_{12}	U_{13}	U_{23}
Tl1	0.0719(6)	0.0775(6)	0.0754(6)	0.0009(6)	0.0082(5)	0.0013(6)
I1	0.1469(20)	0.1673(23)	0.0840(14)	0.0024(18)	0.0287(14)	0.0028(15)
I2	0.0675(11)	0.1526(20)	0.1017(15)	0.0081(11)	0.0056(10)	–0.0252(14)
I3	0.0778(11)	0.0899(14)	0.1145(15)	0.0103(10)	–0.0043(10)	–0.0120(11)
I4	0.1088(15)	0.0818(14)	0.1463(19)	–0.0022(13)	0.0019(14)	0.0279(14)

0302-4377/83 $2.50

Table 3. Some interatomic distances in Ångströms and angles in degrees. Estimated standard deviations are given in parentheses.

Distance	Å [a]	Å [b]	Angle	deg.[a]
Tl–I1	2.752(2)	2.782(3)	I1–Tl–I2	110.72(8)
Tl–I2	2.748(2)	2.766(2)	I1–Tl–I3	109.62(7)
Tl–I3	2.764(2)	2.775(3)	I1–Tl–I4	109.93(8)
Tl–I4	2.770(2)	2.791(2)	I2–Tl–I3	110.95(7)
			I2–Tl–I4	108.43(7)
			I3–Tl–I4	107.11(7)

[a] Non-corrected values. [b] Corrected for thermal motion assuming the I atom to ride on the Tl atom.

The refinements were performed in the same way as in the previous paper.[1] Some, mostly terminal, carbon atoms obtained rather high temperature factors and probably have alternative positions. However, it was not necessary to keep positional parameters constant for any carbon atom, as was the case for $P2_1$ (probably because of the near singularities which arise when an approximately centrosymmetric structure is refined in a non-centrosymmetric space group). The final refinement cycle (114 refined parameters, the heavy atoms anisotropic, the nitrogen and carbon atoms isotropic) led to $R=5.4$ % ($R_w=8.0$ %, $S=1.82$) thus not significantly better than for $P2_1$. The results are given in Tables 1–3. Full parameter listings and structure factors are available from the authors on request. As can be seen, the distances and angles between the heavy atoms are not significantly different from the values of $P2_1$ when the mean values are taken in $P2_1$ (*e.g.* r_{Tl-I1} in $P2_1/n$ corresponds to $(r_{Tl-I1}+r_{Tl-I7})/2$ in $P2_1$), but the TlI_4 tetrahedron is more regular in $P2_1/n$. The standard deviations are about 50 % lower in the latter space group.

1. Glaser, J., Goggin, P. L., Sandström, M. and Lutsko, V. *Acta Chem. Scand. A 36* (1982) 55.

Received April 20, 1983.

The Crystal Structure of Imidotetraphenyldithiodiphosphinic Acid, a Compound with an N–H···S Hydrogen Bond

STEINAR HUSEBYE and
KNUT MAARTMANN-MOE

Department of Chemistry, University of Bergen, Realfagbygget, Allegt. 41, N-5000 Bergen, Norway

In recent work, we have used the imidotetraphenyldithiodiphosphinate anion as a ligand.[1,2] In the parent acid $H\{N(Ph_2PS)_2\}$, it has been assumed from IR spectral work that the acid proton was bonded to nitrogen rather than to sulfur.[3] The present work was undertaken to locate this proton and see if it is involved in hydrogen bonding. Another reason was that the structure of the acid would serve as a reference to further use of its anion as a ligand.

Table 1. Atomic coordinates for the molecule in fractions of cell edges with estimated standard deviations.

Atom	*x*	*y*	*z*
S1	0.48100(7)	0.76775(8)	0.51748(8)
S2	−0.00376(7)	0.91574(7)	0.35162(7)
P1	0.29746(7)	0.77394(7)	0.59586(7)
P2	0.17583(7)	0.93543(7)	0.34715(7)
N	0.2072(2)	0.8998(2)	0.4978(2)
H	0.162(2)	0.939(2)	0.529(2)
C111	0.2216(3)	0.6188(2)	0.6412(3)
C112	0.0868(3)	0.6172(3)	0.6691(3)
C113	0.0287(3)	0.5015(3)	0.6947(3)
C114	0.1028(4)	0.3861(3)	0.6939(4)
C115	0.2352(4)	0.3862(3)	0.6672(4)
C116	0.2950(3)	0.5014(3)	0.6424(3)
C121	0.2609(2)	0.8133(3)	0.7430(2)
C122	0.3119(3)	0.9297(3)	0.7308(3)
C123	0.2816(4)	0.9693(3)	0.8368(3)
C124	0.2017(4)	0.8925(4)	0.9565(3)
C125	0.1542(4)	0.7781(4)	0.9693(3)
C126	0.1825(3)	0.7369(3)	0.8644(3)
C211	0.2244(3)	1.1084(3)	0.2444(2)
C212	0.1679(3)	1.1917(3)	0.1362(3)
C213	0.2038(4)	1.3249(3)	0.0591(3)
C214	0.2950(4)	1.3756(3)	0.0886(3)
C215	0.3536(3)	1.2933(3)	0.1937(3)
C216	0.3195(3)	1.1600(3)	0.2723(3)
C221	0.2852(3)	0.8245(2)	0.2804(2)
C222	0.4017(3)	0.8682(3)	0.1897(3)
C223	0.4813(3)	0.7798(3)	0.1393(3)
C224	0.4456(3)	0.6493(3)	0.1801(3)
C225	0.3311(3)	0.6054(3)	0.2698(3)
C226	0.2495(3)	0.6936(3)	0.3183(3)

The acid was prepared by published methods [3] and recrystallized from CH_2Cl_2. The crystals are triclinic with a=10.688(2) Å, b=10.852(2) Å, c=11.192(2) Å, α=64.50(1)°, β=75.14(1)°, γ=80.81(1)°, Z=2, D_m=1.31 and D_x=1.32 g/cm^3. Absence of systematic extinctions implies space groups $P1$ or $P\bar{1}$.

Based on 3845 observed reflections [$I>2\sigma(I)$], the structure was solved by direct methods (MULTAN) and refined by full-matrix least squares methods to a final conventional R value of 0.042 (R_w=0.043; Table 1). Data collection procedures and programs used in structure determination are similar to those used earlier in this laboratory.[4] The choice of $P\bar{1}$ as the correct space group was justified by the successful refinement of the structure. All hydrogen atoms were located and refined. Tables of structure factors, temperature factors and phenyl hydrogen coordinates are available from the authors upon request.

Fig. 1. shows the molecule as seen nearly along the normal to the central P1N1P2 plane. The S–P–N–P–S backbone of the acid has a *trans* conformation relative to the central –P–N–P– group as opposed to the *cis* conformation found when its anion acts as a bidentate, chelating ligand.[1] This is not unexpected as the *non*-bonded intramolecular interactions will be reduced in the *trans* as compared to the *cis* conformation. On the other hand, the S–S separation in the anion will be too large in the *trans* conformation if it is to act as a chelating

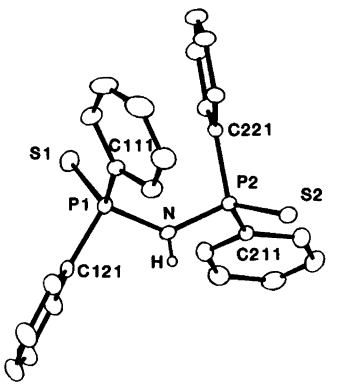

Fig. 1. The imidotetraphenyldithiodiphosphinic acid molecule as seen along the normal to the C221P2N plane.

0302-4377/83 $2.50

Table 2. Some bond lengths (Å) and angles (°) with standard deviations.

S1–P1	1.937(1)	S1–P1–N	115.49(9)
S2–P2	1.950(1)	S2–P2–N	114.59(9)
N–P1	1.683(2)	P1–N–P2	132.68(14)
N–P2	1.672(2)	S1–P1–C111	113.37(9)
P1–C111	1.800(3)	S1–P1–C121	113.53(9)
P1–C121	1.808(3)	S2–P2–C211	112.16(9)
P2–C211	1.807(3)	S2–P2–C221	111.20(9)
P2–C221	1.803(2)	N–P1–C111	105.27(12)
N–H	0.711(24)	N–P1–C121	99.97(11)
H···S2′	2.638(25)	N–P2–C211	104.28(11)
N···S2′	3.349(2)	N–P2–C221	106.32(11)
		P1–N–H	117(2)
		P2–N–H	109(2)
		N–H···S2′	178(3)
Torsional angles		S1–P1–N–P2	62.4
		S2–P2–N–P1	112.8
		S1–P1–N–H	−133.1
		S2–P2–N–H	−52.7

ligand. A similar behaviour has been observed in oxamide and dithiooxamide ligands.[5] The average P–S and P–N bond lengths are 1.944(9) and 1.678(8) Å, respectively (Table 2). These lengths may be compared to 2.02 and 1.59 Å which are the corresponding bond lengths found in metal complexes of the anionic ligand.[1] They may also be compared to P=S double bond lengths around 1.95 Å observed in phosphine sulfides [6] and to a P–N single bond of 1.77 Å.[4] Thus the P–N bonds have some double bond character. This agrees with the observation that the H-atom bonded to N is only 0.17 Å below the PNP plane, indicating a tendency toward sp^2 hybridization of nitrogen. Consequently it is found that the sum of the nitrogen bond angles is 358.7°. Possible resonance forms of the acid could then be of the types I–III with I dominating.

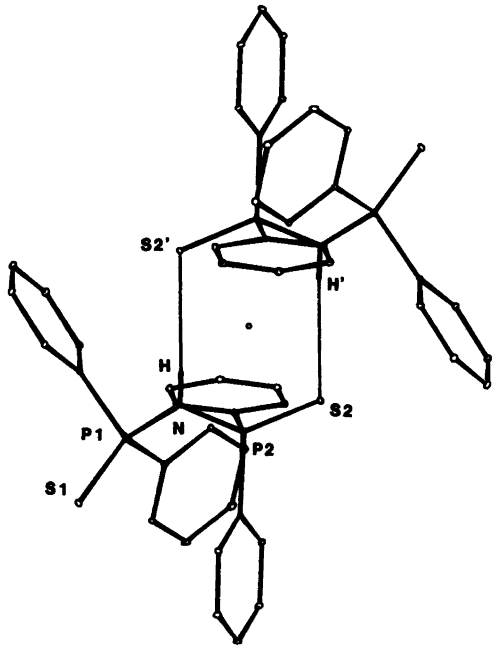

Fig. 2. Pairs of hydrogen bonded molecules seen along the normal to the plane through S2···H′ and S2′···H. Primed letters denote atoms in a molecule related to the original one (Table 1) by a center of symmetry in 0,0,1/2.

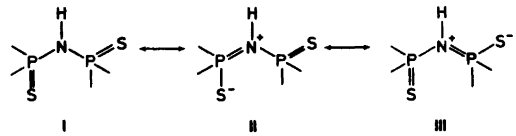

I II III

A positive charge on nitrogen will increase the acidity of the hydrogen bonded to it and enhance the possibility of hydrogen bonding to a partially negative and thus better hydrogen bond accepting sulfur atom. This is also observed in the present investigation where pairs of molecules are bonded together across centers of symmetry by N–H···S2′ bonds (Fig. 2). The N···S2′ and H···S2′ distances of 3.349(2) and 2.64(3) Å, respectively, agree well with previous investigations.[7] The angle N–H···S2′ is 178(3)°. Resonance form III which puts negative charge

on S2, contributes more than II which puts negative charge on S1, the sulphur atom not involved in hydrogen bonding. This is reflected in the observed bond lengths in the SPNPS group (Table 2). Thus hydrogen bonding explains why P2–S2 is longer than P1–S1. Similar effects are observed in thioamides where conjugated systems strengthen hydrogen bonding.[8–10] An IR spectrum (KBr) of the acid shows absorptions at 2680 (w) and 2623 cm^{-1} (ms) probably due to N–H··· stretch and in this region differs from the first reported spectrum.[3] Bonds and angles in the phenyl groups have normal values.

1. Bjørnevåg, S., Husebye, S. and Maartmann-Moe, K. *Acta Chem. Scand. A 36* (1982) 195.
2. Husebye, S. and Maartmann-Moe, K. *Acta Chem. Scand. A 37* (1983) 219.
3. Schmidpeter, A. and Groeger, H. *Z. Anorg. Allg. Chem. 345* (1966) 106.
4. Aaberg, A., Gramstad, T. and Husebye, S. *Acta Chem. Scand. A 34* (1980) 717.
5. Drew, M. G. B., Kisenyi, J. M. and Willey, G. R. *J. Chem. Soc. Dalton Trans.* (1982) 1729.
6. Codding, P. W. and Kerr, K. A. *Acta Crystallogr. B 34* (1978) 3785.
7. Hamilton, W. C. and Ibers, J. A. *Hydrogen Bonding in Solids*, Benjamin, New York 1968, p. 168.
8. Griffiths, P. J. F., Morgan, G. D. and Ellis, B. *Spectrochim. Acta A 28* (1972) 1899.
9. Kulevsky, N. and Reineke, W. *J. Phys. Chem. 72* (1968) 3339.
10. Moeller, T. and Kokalis, S. G. *J. Inorg. Nucl. Chem. 25* (1963) 875.

Received January 31, 1983.

Specific Equatorial Photolabilization of Ammonia in Cyanopentaamminerhodium(III)

J. S. SVENDSEN and L. H. SKIBSTED

Chemistry Department, Royal Veterinary and Agricultural University, Thorvaldsensvej 40, DK-1871 Copenhagen V, Denmark

In octahedral complexes belonging to the pentaammine series two different ammonia ligands can be distinguished, and the ammonia which becomes substituted by water as a result of ligand field excitation in aqueous solution can be either

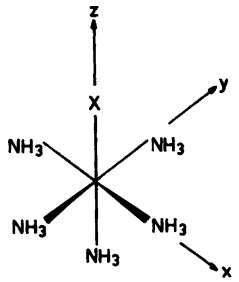

in the axial position on the unique tetragonal axis or in an equatorial position. The product stereochemistry found for such reactions [1-3]

$$[Rh(NH_3)_5Br]^{2+} + H_3O^+ \xrightarrow{h\nu} \textit{trans}\text{-}[Rh(NH_3)_4(H_2O)Br]^{2+} + NH_4^+$$

$$[Cr(NH_3)_5Cl]^{2+} + H_3O^+ \xrightarrow{h\nu} \textit{cis}\text{-}[Cr(NH_3)_4(H_2O)Cl]^{2+} + NH_4^+$$

$$[Rh(NH_3)_5(CN)]^{2+} + H_3O^+ \xrightarrow{h\nu} \textit{cis}\text{-}[Rh(NH_3)_4(H_2O)(CN)]^{2+} + NH_4^+$$

is not, however, indicative of whether axial or equatorial ammonia is substituted, owing to the high stereomobility of such excited state reactions.[4-6]

trans-$[Rh(en)_2(NH_3)Br]^{2+}$ has been used as a model for $[Rh(NH_3)_5Br]^{2+}$, and the observation that ammonia, rather than ethylenediamine (en), photoaquates in the mixed amine complex was considered indicative of axial labilization also in the pentaammine complex $[Rh(NH_3)_5Br]^{2+}$.[1] A more direct proof of axial labilization and, consequently, of photoisomerization was provided by the use of isotopic labelling in $[Cr(NH_3)_5Cl]^{2+}$.[2] In both of the complexes in which axial labilization has been identified, the heteroligand has been the weaker field ligand. In order to establish the origin of the photolabilized ammonia in a pentaammine complex containing a ligand of greater ligand field strength than ammonia, we have ^{15}N-labelled *trans*-NH_3 in $[Rh(NH_3)_5(CN)]^{2+}$ and report here the result of an isotopic analysis of the ammonia released during photoaquation.

trans-$[Rh(NH_3)_4Cl(CN)]^+$ was heated in a ^{15}N-enriched (2.69 %) aqueous NH_3/NH_4^+ buffer solution, and the enrichment of the complex was confirmed by a $^{15}N/^{14}N$ analysis of the isolated and recrystallized $[Rh(NH_3)_5(CN)]Cl_2$. The $^{15}N/^{14}N$ analysis showed that only one mol of enriched ammonia per mol of complex had entered the coordination sphere, indicating that exchange between coordinated and solution ammonia was insignificant. Since thermal substitution of ammonia for choride at Rh(III) centers is stereoretentive,[7-9] scrambling among the five ammonia ligands was excluded. Thus, the procedure employed resulted in specific *trans*-labelling:

$$\textit{trans}\text{-}[Rh(NH_3)_4Cl(CN)]^+ + {}^{15}NH_3 \longrightarrow \textit{trans}\text{-}[Rh(NH_3)_4({}^{15}NH_3)(CN)]^{2+} + Cl^-$$

Table 1. Fraction of equatorial NH_3 released during photoaquation of $[Rh(NH_3)_5(CN)]^{2+}$ in aqueous 0.10 M $HClO_4$ calculated from isotopic analysis of NH_3 released from 2.69 % ^{15}N *trans*-enriched $[Rh(NH_3)_5(CN)]^{2+}$.

λ_{irr} nm	$[Rh(NH_3)_5(CN)]^{2+}$ [a] μmol	NH_3 [b] μmol	^{15}N %	Equatorial NH_3 [c]
254	9.6	8.4	0.46	0.96
254	9.6	8.8	0.43	0.97
254	9.6	8.9	0.46	0.96
313	8.9	9.3	0.54	0.93

[a] Amount of $[Rh(NH_3)_5(CN)]^{2+}$ photolyzed. [b] Amount of released NH_3 separated from photolysis solution. [c] Equatorial NH_3 released as a fraction of total released NH_3.

0302-4377/83 $2.50

2 mM solutions of the ^{15}N *trans*-enriched $[Rh(NH_3)_5(CN)]Cl_2$ in aqueous 0.10 M $HClO_4$ were irradiated with 254 or 313 nm monochromatic light until at least 90 % was converted to *cis*-$[Rh(NH_3)_4(H_2O)(CN)]^{2+}$ (as monitored by UV-spectroscopy). 254 nm excitation (^1E, $^1B_2 \leftarrow {}^1A_1$; C_{4v} symmetry) was found to result in the same photoproducts, *viz.* *cis*-$[Rh(NH_3)_4(H_2O)(CN)]^{2+}$ and NH_4^+, with the same photoreaction quantum yield, 0.10±0.01 mol/einstein at 25 °C, as the previously investigated [3] excitation at 313 and 334 nm (^1E, $A_2 \leftarrow {}^1A_1$). NH_4^+ was separated from the reaction mixture by a procedure (*vide infra*) which was known to liberate no further ammonia, and was subsequently subjected to $^{15}N/^{14}N$ analysis.

With the present experimental design, a natural $^{15}N/^{14}N$ ratio corresponding to 0.36 % ^{15}N is expected in the photoaquated ammonia from equatorial labilization, whereas 2.69 % is indicative of axial labilization. Experimental results are found in Table 1. The observed $^{15}N/^{14}N$ ratios are only slightly greater than corresponding to 0.36 % and indicate that as much as 96±1 % of the ammonia separated from the reaction mixture originates from equatorial positions. From these results we conclude that photolabilization in $[Rh(NH_3)_5(CN)]^{2+}$ takes place almost exclusively in the equatorial plane.

In Rh(III) low-spin complexes the photochemically reactive state has been identified as the lowest ligand field excited state.[4,5] In $[Rh(NH_3)_5(CN)]^{2+}$ this triplet state is $^3A_2$, corresponding to the configuration $(d_{xz},d_{yz})^4$ $(d_{xy})^1(d_{x^2-y^2})^1$ $(d_{z^2})^0$, and the σ-antibonding e_g orbital eventually populated as a result of ligand field excitation is therefore located in the $x-y$ plane. Labilization is consequently expected to occur among the four equatorial ammonia ligands.[3] In the more detailed theoretical treatment by Vanquickenborne and Ceulemans [10,11] for d^6 (Rh(III)) and d^3 (Cr(III)) complexes, excited state bond indices I*(ML) are calculated from spectroscopic σ- and π-parameters for metal–ligand bonds and provide a quantitative indication of which ligand becomes labilized. I*(ML) calculated for the individual bonds in $[Rh(NH_3)_5(CN)]^{2+}$ clearly predicts equatorial labilization,[3,11] in agreement with the qualitative arguments presented above and, which is more significant, in agreement with our experimental observations. These results therefore serve as an important verification of the predictive power of the Vanquickenborne-Ceulemans model for a C_{4v} complex with the strong field ligand in an axial position.

It should also be noted that despite the common photoproduct stereochemistry, the photoaquated ammonia originates from different coordination sites in the two octahedral pentaammine complexes in which the stereochemical origin has been established by direct experiment. In $[Cr(NH_3)_5Cl]^{2+}$ axial ammonia is preferentially labilized, whereas equatorial ammonia is almost exclusively labilized in $[Rh(NH_3)_5(CN)]^{2+}$. These results are both accommodated within Adamson's photochemical rules,[12] which are based empirically on the relative strength of the ligand field, and they are also well understood on the basis of more recent theories,[4,5] as discussed above for $[Rh(NH_3)_5(CN)]^{2+}$.

Isotopic labelling. A 125 mg portion of *trans*-$[Rh(NH_3)_4(CN)Cl]Cl\cdot 1½\ H_2O$, prepared and purified as described previously,[3] was dissolved together with 125 mg of 96.3 % ^{15}N NH_4Cl (VEB Berlin Chemie, GDR) in 7.70 ml of 12.1 M aqueous NH_3 (natural $^{15}N/^{14}N$ ratio corresponding to 0.36 %) and the solution was maintained at 90 °C in the dark under reflux for 75 min. The product, which precipitated upon slow cooling to room temperature, was filtered off and recrystallized from aqueous HCl. Yield 100 mg (83 %). The UV spectrum was identical to that previously reported [3] for $[Rh(NH_3)_5(CN)]Cl_2$. Calculated ^{15}N enrichment: 0.748 %. Found: 0.755 %.

Photolysis experiments. The quantum yield for the photoreaction of $[Rh(NH_3)_5(CN)]^{2+}$ resulting from 254 nm irradiation was determined by experimental and numerical procedures outlined previously,[13] using an Oriel 6035 low-pressure Hg–Ar penlight equipped with an Oriel 6041 short-wave filter. The exhaustive or nearly exhaustive photolyses were performed with ≈10 μmol samples of enriched $[Rh(NH_3)_5(CN)]Cl_2$ dissolved in 5.00 ml of 10^{-1} M $HClO_4$ in a Rayonet RMR-500 photochemical reactor with an RMA-400 Merry-Go-Round Unit (254 nm), or in the Spindler and Hoyer optical train described previously (313 nm).[13] After quantitative transfer of the photolyzed solution to a distillation flask, the excess acid was neutralized with NaOH and the solution buffered with 0.5 g of $Na_2B_4O_7\cdot 10H_2O$. By means of a gentle N_2 flow through the solution for 8 h, the photoproduct NH_3 was separated from the other principal photoproduct, *cis*-$[Rh(NH_3)_4(H_2O)(CN)]^{2+}$, and trapped in standardized 10^{-2} M HCl. The amount of NH_3 thus separated was determined by titration, and the $^{15}N/^{14}N$ ratio was subsequently determined.

Isotopic analysis. The $^{15}N/^{14}N$ ratio in the labelled compound and in the photochemically liberated NH_3 was determined by optical emission analysis at the Physics Laboratory of the Royal Veterinary and Agricultural University.

The analytical procedure (a detailed description is found in Ref. 14) involved a Dumas destruction of the material.

Acknowledgements. This research was supported by grants from the Danish Natural Science Research Council and by a grant from the Carlsberg Foundation. The authors wish to thank the Physics Laboratory of the Royal Veterinary and Agricultural University, in particular Dr. H. Saaby Johansen, for carrying out the isotopic analyses, and Drs. Marta Willems and Martin Hancock for helpful advice. We are grateful to Johnson Matthey for a loan of the rhodium used in these studies.

1. Clark, S. F. and Petersen, J. D. *Inorg. Chem. 18* (1979) 3394.
2. Zinato, E., Riccieri, P. and Adamson, A. W. *J. Am. Chem. Soc. 96* (1974) 375.
3. Skibsted, L. H. and Ford, P. C. *Inorg. Chem. 22* (1983). *In press.*
4. Vanquickenborne, L. G. and Ceulemans, A. *Coord. Chem. Rev. 48* (1983) 157.
5. Ford, P. C. *Coord. Chem. Rev. 44* (1982) 61.
6. Skibsted, L. H. and Ford, P. C. *Inorg. Chem. 19* (1980) 1828.
7. Johnson, S. A. and Basolo, F. *Inorg. Chem. 1* (1962) 925.
8. Balt, S. and Jelsma, A. *J. Chem. Soc. Dalton Trans.* (1981) 1289.
9. Ogino, H. and Bailar, J. C. *Inorg. Chem. 17* (1978) 1118.
10. Vanquickenborne, L. G. and Ceulemans, A. *J. Am. Chem. Soc. 99* (1977) 2208.
11. Vanquickenborne, L. G. and Ceulemans, A. *Inorg. Chem. 17* (1978) 2730.
12. Adamson, A. W. *J. Phys. Chem. 71* (1967) 798.
13. Howland, K. and Skibsted, L. H. *Acta Chem. Scand. A 37* (1983). *In press.*
14. Johansen, H. S. and Middelboe, V. *Appl. Spectrosc. 36* (1982) 221.

Received April 20, 1983.

Acta Chemica Scandinavica A 37 (1983) 447–451

Acid-catalyzed Hydrolyses of Bridged Bi- and Tricyclic Compounds. XXI. Kinetics of Hydration of *exo*- and *endo*-5-Nitro-2-norbornenes and 3-Nitronortricyclane

MARTTI LAJUNEN and HELENA KUKKONEN

Department of Chemistry and Biochemistry, University of Turku, SF-20500 Turku 50, Finland

The activation parameters, solvent deuterium isotope effects, and dependences of rates on acid concentration measured for the hydration of *exo*- and *endo*-5-nitro-2-norbornenes and 3-nitronortricyclane agree with the rate-determining protonation of the carbon–carbon double bond or the three-membered carbon ring ($A-S_E2$ mechanism). The product analysis supports the conclusion. The hydration rate of *endo*-5-nitro-2-norbornene seems abnormally high considering the correlation between the hydration rates of 5-X-substituted 2-norbornenes and 3-X-substituted nortricyclanes (X=H, CH_2OH, CH_2Cl, OH, Ac, CN, and NO_2).

The alkali metal salts of 2-nitronorbornanes and 5-nitro-2-norbornenes react easily with aqueous acids yielding 2-norbornanone (80 %) in the former case [the Nef reaction, eqn. (1)] and rearranged products. *e.g. cis*-cyclopentena[*e*]-tetrahydro-1,2-oxazin-3-one (42 %), in the latter case [eqn. (2)].[1,2] The nitro group is destroyed in both reactions. The reactive structure is evidently the *aci* form of the nitro compound (nitronic acid) formed in the acid-base equilibria [eqn. (3)].[3]

$$R_2CH-N=O \rightleftharpoons R_2C=N^{+}(-O^{-}) + H^{+} \rightleftharpoons R_2C=N-OH \qquad (3)$$

In the *nitro* form the secondary nitro group is probably much more resistant against aqueous acids. Thus it may be apt for a strongly electronegative substituent in acid-catalyzed hydrolysis reactions. However, the *nitro* form may

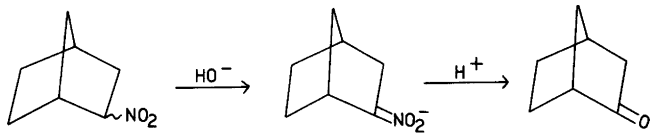

(1)

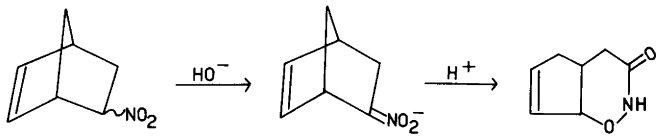

(2)

0302-4377/83 $02.50

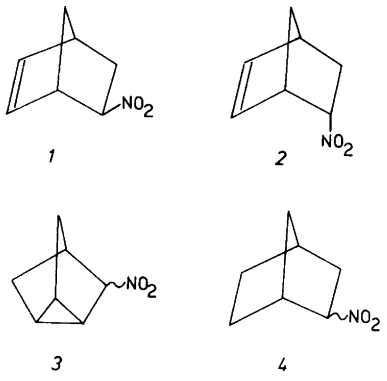

1 2 3 4

produce a minute concentration of the much more energetic *aci* form,[3] thus this route must be taken into account.

The present work expands our studies on the acid-catalyzed hydration of substituted norbornenes and nortricyclanes to *exo*- and *endo*-5-nitro-2-norbornenes (*1* and *2*) and 3-nitronortricyclane (*3*). The effects of temperature and acid concentration on the reaction rates, and solvent deuterium isotope effects are recorded. The reaction products are also studied and the low reactivity of 2-nitronorbornanes (*4*) is checked.

EXPERIMENTAL

Syntheses. A mixture of *exo*- and *endo*-5-nitro-2-norbornenes was prepared from cyclopentadiene and nitroethene.[2] An effort to separate the epimers on a preparative gas chromatograph (FFAP column) caused the isomerization of the 1:4 mixture producing a new one where the *exo* and *endo* epimers had the equilibrium ratio of *ca.* 2:1 (*cf.* Ref. 4). The *exo* epimer was obtained from this mixture with the purity of 95 % by GLC. The *endo* epimer used in the investigations contained *ca.* 17 % of the *exo* form. The retention times (*exo* 5.6 min and *endo* 8.1 min in a FFAP column at 130 °C) were so different that the epimers did not disturb each other.

3-Nitronortricyclane was prepared as follows. The addition of acetic acid to 2,5-norbornadiene produced a mixture of *exo*-5-acetoxy-2-norbornene and 3-acetoxynortricyclane.[5] The acetates were separated by distillation on a Perkin Elmer 251 Auto Annular Still and the tricyclic acetate was hydrolyzed by aqueous potassium hydroxide to 3-hydroxynortricyclane, which was oxidized to 3-nortricyclanone.[6] The ketone was turned to the corresponding oxime by hydroxylamine hydrochloride.[7] The oxime was recrystallized from liquid petroleum (b.p. 50–70 °C) and oxidized to 3-nitronortricyclane by the method of Emmons and Pagano,[8] but the oxidant used by them, peroxytrifluoroacetic acid, was replaced by 3-chloroperbenzoic acid. The yield was 63 % from the oxime, which is of the same magnitude as those obtained by peroxytrifluoroacetic acid oxidation of aliphatic oximes,[8] and 24 % from the starting materials.

A mixture (*exo*–*endo*=1:5) of 2-nitronorbornanes was prepared by hydrogenating the corresponding mixture of 5-nitro-2-norbornenes in acetone with palladium on carbon as catalyst at room temperature and in atmospheric pressure.

The substrates were identified from their IR (NO_2: 1545 and 1375 cm^{-1}) and ^1H and/or ^{13}C NMR spectra.[4,9,10]

Kinetics. The disappearance of the substrates (initial concentration 3×10^{-3} mol dm^{-3}) in aqueous perchloric acid was followed during about 2.5 half-lives by taking samples after appropriate intervals, by neutralizing them with concentrated ammonia and Sörensen phosphate buffer (pH 6.8), and by analyzing them by GLC (FFAP column) using camphor as inert internal standard. The *exo* and *endo* epimers isomerized quite easily to each other in the gas chromatograph. The very careful manner of working reduced but did not totally eliminate the epimerization, which caused scattering in rate constants. Thus the standard errors of the mean were larger for nitronorbornenes (2–4 %, av. 3 %) than for nitronortricyclane (1–2 %, av. 1.3 %). Several duplicate or triplicate runs, however, showed that the measured rate coefficients were reproducible within 10 %. The reaction medium turned slightly reddish brown during the runs and in the case of nitronorbornenes small dark brown flakes appeared during long runs ($t_{1/2}\geq5$ h).

Product analysis. 0.70 g of a 1:5 mixture of *exo*- and *endo*-5-nitro-2-norbornenes was hydrolyzed over ten half-lives by efficiently stirring in 50 cm^3 of 5 mol dm^{-3} $HClO_4$ at 75 °C. The solution was cooled and extracted with CH_2Cl_2 four times. The organic phase was washed with water three times and dried on sodium sulphate. The solvent was distilled off *in vacuo* and the residue (0.40 g) was analyzed by GLC and by IR, ^1H and ^{13}C NMR spectroscopy: the product was a 48:52 (±2) mixture of *exo*- and *endo*-5-nitro-*exo*-2-norbornеols (see Table 1).

The solid flakes were separated from the aqueous phase after extraction with CH_2Cl_2 by repeatedly decanting acidic water off and by adding fresh water until the solvent was neutral,

Table 1. Comparison of the ^{13}C chemical shifts for *exo-* and *endo*-5-nitro-*exo*-2-norborneols (calculated by addition of the effects of the *exo*-2-hydroxyl and *exo-* and *endo*-5-nitro groups on the chemical shifts of norbornane) with the observed ^{13}C chemical shifts in $CDCl_3$ for the product of hydration of *exo-* and *endo*-5-nitro-2-norbornenes.

	C(1)	C(2)	C(3)	C(4)	C(5)	C(6)	C(7)	Ref.
Norbornane	36.8	30.1	30.1	36.8	30.1	30.1	38.7	10
$\Delta\delta$(*exo*-2-OH)	+7.7	+44.3	+12.3	−1.0	−1.3	−5.2	−4.1	10
$\Delta\delta$(*exo*-5-NO_2)	+0.2	−2.0	−3.7	+6.8	+58.0	+5.7	−2.9	[a]
$\Delta\delta$(*endo*-5-NO_2)	±0.0	−1.8	−7.0	+6.1	+57.5	+3.3	+0.2	[a]
exo-5-Nitro-*exo*-2-norborneol (calc.)	44.7	72.4	38.7	42.6	86.8	30.6	31.7	
exo-5-Nitro-*exo*-2-norborneol (obs.)	43.6	72.7	38.3	42.7	86.9	31.7	31.7	[a]
endo-5-Nitro-*exo*-2-norborneol (calc.)	44.5	72.6	35.4	41.9	86.3	28.2	34.8	
endo--5-Nitro-*exo*-2-norborneol (obs.)	44.3	72.8	35.5	42.0	85.8	29.1	34.9	[a]

[a] This work.

thereafter the flakes were filtered off and dried (yield 20 mg). According to the IR spectrum the nitro group had mainly but not entirely disappeared and a hydroxyl group had appeared.

RESULTS AND DISCUSSION

The disappearance rate coefficients of *exo-* and *endo*-5-nitro-2-norbornenes (*1* and *2*) and 3-nitronortricyclane (*3*) in 5 mol dm^{-3} perchloric acid at different temperatures are listed in Table 2 together with the activation parameters calculated from the second-order rate coefficients ($k_2=k_1/c_{HClO_4}$). The solvent deuterium isotope effects are also given. The activation entropies (−18 to −39 J mol^{-1} K^{-1}) and isotope effects (k_H/k_D 1.1 to 1.2) are in agreement with the rate-determining proton transfer from the hydronium ion to the carbon–carbon double bond of the nitronorbornenes and to the three-membered carbon ring of nitronortricyclane (A-S_E2 or Ad_E2 mechanism), but not with the initial protonation of the nitro group (A-1 or A-2 mechanisms).[11–15] The isotope effects are close to unity, which points to a late "intermediate-like" transition state. This agrees, according to the Hammond postulate,[16] with the slow reaction rate caused by the very electronegative nitro group. In the A-S_E2 hydration of *exo-* and *endo*-5-cyano-2-norbornenes and 3-cyanonortricyclane, where the reaction rates are equal or slightly greater ($k_1/10^{-4}$ s^{-1}: 11.4, 10.25 and 20.0, respectively, in 5 mol dm^{-3} $HClO_4$ at 75 °C), the isotope effects are, however, larger: 1.4 to 1.6.[12]

The disappearance rate constants in different

Table 2. Rate constants for the disappearance of 5-nitro-2-norbornenes, 3-nitronortricyclane, and 2-nitronorbornanes in aqueous 5.03 mol dm^{-3} $HClO_4$ at different temperatures, and their solvent deuterium isotope effects at 75 °C and activation parameters at 25 °C.

Temp. °C	k_1 10^{-4} s^{-1}	Isotope effects and activation parameters
exo-5-Nitro-2-norbornene		
25	0.0169 [a]	
45	0.234	
55	0.698	$k_H/k_D=1.09(7)$
65	2.08	$\Delta H^{\ddagger}=99.8(26)$ kJ mol^{-1}
75	6.49	$\Delta S^{\ddagger}=-34(8)$ J mol^{-1} K^{-1}
75	5.93 [b]	
endo-5-Nitro-2-norbornene		
25	0.0261 [a]	
45	0.385	
55	1.240	$k_H/k_D=1.11(5)$
65	4.10	$\Delta H^{\ddagger}=103.5(12)$ kJ mol^{-1}
75	11.68	$\Delta S^{\ddagger}=-18(4)$ J mol^{-1} K^{-1}
75	10.47 [b]	
3-Nitronortricyclane		
25	0.00884 [a]	
55	0.383	
65	1.116	$k_H/k_D=1.22(4)$
75	3.32	$\Delta H^{\ddagger}=99.9(11)$ kJ mol^{-1}
75	2.73 [b]	$\Delta S^{\ddagger}=-39(3)$ J mol^{-1} K^{-1}
85	8.58	
2-Nitronorbonanes (*exo–endo*=1:5)		
75	0.0175(6)	

[a] Calculated from the activation parameters. [b] Measured in 5.01 mol dm^{-3} $DClO_4(D_2O)$.

Table 3. Rate constants for the disappearance of *exo-* and *endo*-5-nitro-2-norbornenes at 75 °C and 3-nitronortricyclane at 85 °C in different perchloric acid concentrations, and slopes for the plots log k_1 *vs.* $-H_o$ (Slope) and log k_1+H_o *vs.* $H_o+\log c_{HClO_4}$ (ϕ).

c_{HClO_4} / mol dm^{-3}	$-H_o$	k_1 / 10^{-4} s^{-1}	Slopes
exo-5-Nitro-2-norbornene			
0.996	0.33	0.0463	
2.05	0.84	0.166	
3.03	1.33	0.600	Slope=1.09(1)
4.02	1.81	1.85	ϕ=−0.13(2)
5.03	2.33	6.49	
6.02	2.92	33.0	
endo-5-Nitro-2-norbornene			
1.002	0.33	0.203	
2.02	0.83	0.403	
3.03	1.33	1.28	Slope=0.98(1) [a]
4.02	1.81	3.76	ϕ=0.02(1) [a]
5.03	2.33	11.68	
6.02	2.92	46.4	
3-Nitronortricyclane			
1.002	0.33	0.0529	
2.02	0.83	0.208	
3.03	1.33	0.697	Slope=1.04(2)
4.02	1.81	2.36	ϕ=−0.05(3)
5.03	2.33	8.58	
6.02	2.92	30.8	
7.04	3.55	120.5	

[a] An exceptional value in 1.00 mol dm^{-3} $HClO_4$ has been excluded.

acid concentrations are listed in Table 3 together with the slopes for the plots log k_1 *vs.* $-H_o$ and log k_1+H_o *vs.* $H_o+\log c_{HClO_4}$. The former plots are fairly linear (correlation coefficients 0.9992 to 0.9999) and their slopes (0.98 to 1.09) are typical of the $A-S_E2$ mechanism as are also the Bunnett-Olsen ϕ values (the slopes of the latter plots: −0.13 to +0.02).[11–15,17]

All the kinetic parameters are thus in agreement with the hydration of the carbon–carbon double bond and the three-membered carbon ring of the substrates. The rate constants are 190–670 times greater than the disappearance rate constant of 2-nitronorbornane (an *exo–endo* mixture; see Table 2). 2-Nitronorbornane yields 2-norbornanone [analyzed by GLC; *cf.* eqns. (1) and (3)]. Thus this rate constant gives a rough estimate of the reaction *via* the *aci* form, and it seems negligible.

The product analysis for the hydrolysis of nitronorbornenes (*exo–endo*=1:5) showed that the reaction yields at least 50 % of 5-nitro-*exo*-2-norborneols (*exo–endo*=1:1; see Experimental) probably *via* protonation of C(3), Wagner-Meerwein rearrangement, and hydration of C(2) [eqn. (4)].

Besides, *ca.* 3 % of an unidentified saturated polymeric product was isolated. Other products were not observed, but the formation of up to 50 % of rearranged and/or fragmented products (soluble in acidic water but insoluble in CH_2Cl_2 and invisible in the GLC analysis of the neutralized samples), *e.g. via* protonation of C(2) [eqn. (5)], can not be entirely excluded (*cf.* Ref. 18).

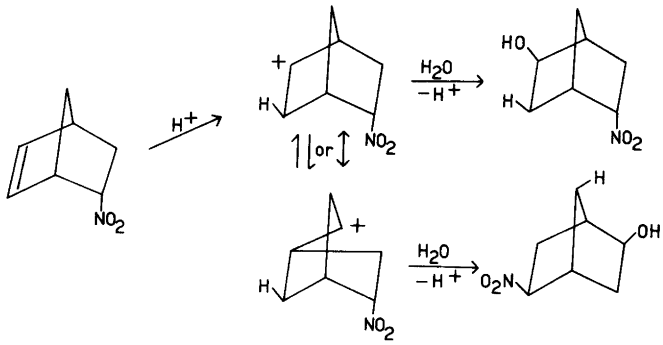

(4)

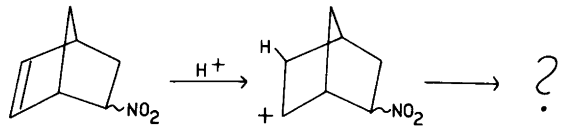

(5)

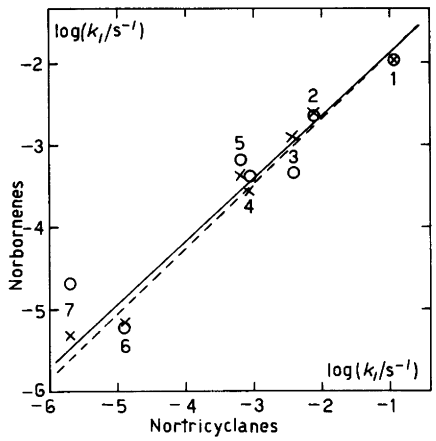

Fig. 1. The logarithms of rate constants of hydration for *exo-* and *endo*-5-substituted 2-norbornenes *versus* those for 3-substituted nortricyclanes (1 mol dm^{-3} $HClO_4$ at 75 °C). Symbols: ×, *exo* substituent and ○, *endo* substituent; 1, hydrogen; 2, hydroxymethyl; 3, chloromethyl (unpublished preliminary values); 4, hydroxyl; 5, acetyl (unpublished values); 6, cyano, and 7, nitro; ———, *exo*-substituted norbornenes (slope=0.765, r=0.989) and – – –, *endo*-substituted norbornenes (slope=0.794, r=0.965, point No. 7 has been excluded).

There is a hint of a possible side reaction in the case of *endo*-5-nitro-2-norbornene (*2*). It is a somewhat exceptional behavior of *endo*-nitronorbornene in the otherwise fairly linear correlation between the logarithms of rate constants for 5-substituted 2-norbornenes and 3-substituted nortricyclanes in 1 mol dm^{-3} $HClO_4$ at 75 °C (Fig. 1). The observed disappearance rate of *endo*-nitronorbornene (Table 3) is about eight times greater than the predicted value. However, this high rate is in the agreement with the observation made by Grob *et al.* that the solvolysis rate of *endo*-6-nitro-*exo*-2-norbornyl tosylate is abnormally high (42 times greater than that of *exo*-6-nitro-*exo*-2-norbornyl tosylate).[18] The reason may be the same, *e.g.* the neighboring-group participation of the oxygen atoms of the *endo* nitro group.

Acknowledgement. Financial aid from the Academy of Finland, Research Council for the Natural Sciences, is gratefully acknowledged.

REFERENCES

1. Wildman, W. C. and Hemminger, C. H. *J. Org. Chem. 17* (1952) 1641.
2. Noland, W. E., Cooley, J. H. and McVeigh, P. A. *J. Am. Chem. Soc. 81* (1959) 1209.
3. Nielsen, A. T. In Feuer, H., Ed., *The Chemistry of the Nitro and Nitroso Groups,* Interscience, New York 1969, Chapter 7 and references therein.
4. Ouellette, R. J. and Booth, G. E. *J. Org. Chem. 30* (1965) 423.
5. Krieger, H. *Suom. Kemistil. B 33* (1960) 183.
6. Brown, H. C. and Garg, C. P. *J. Am. Chem. Soc. 83* (1961) 2952.
7. Vogel, A. I. *Practical Organic Chemistry,* 3rd Ed., Longman, London 1970, p. 343.
8. Emmons, W. D. and Pagano, A. S. *J. Am. Chem. Soc. 77* (1955) 4557.
9. Paasivirta, J. *Suom. Kemistil. B 38* (1965) 130.
10. Levy, G. C., Lichter, R. L. and Nilson, G. L. *Carbon-13 Nuclear Magnetic Resonance Spectroscopy,* 2nd Ed., Wiley, New York 1980, pp. 60–62.
11. Lajunen, M. and Hirvonen, P. *Finn. Chem. Lett.* (1978) 38.
12. Lajunen, M. and Sura, T. *Finn. Chem. Lett.* (1979) 233.
13. Lajunen, M. and Wiksten, P. *Finn. Chem. Lett.* (1980) 17.
14. Lajunen, M. and Tallgren, J. *Finn. Chem. Lett.* (1981) 106.
15. Allen, A. D. and Tidwell, T. T. *J. Am. Chem. Soc. 104* (1982) 3145.
16. Hammond, G. S. *J. Am. Chem. Soc. 77* (1955) 334.
17. Rochester, C. H. *Acidity Functions,* Academic, London 1970.
18. Grob, C. A., Günther, B. and Hanreich, R. *Helv. Chim. Acta 64* (1981) 2312.

Received November 4, 1982.

Acta Chemica Scandinavica A 37 (1983) 453–459

The Crystal Structure of α-Sodium Hexafluorooxoniobate(V), α-$Na_3[NbF_6O]$

ROLF STOMBERG

Department of Inorganic Chemistry CTH/GU, Chalmers Tekniska Högskola, S-412 96 Göteborg, Sweden

Crystals of α-$Na_3[NbF_6O]$ are orthorhombic, space group $P2_12_12_1$ (No. 19), with a=5.6481(4) Å, b=5.7661(5) Å, c=16.9340(13) Å and Z=4. The axial ratio is 1:1.0209:2.9982. Reflexion intensities were registered at room temperature with an automatic single-crystal X-ray diffractometer using Mo$K\alpha$ radiation. Least-squares refinement of structural and thermal parameters yielded a final R-value of 0.034 for 1173 observed reflexions.

Another orthorhombic phase with the approximate cell dimensions a=5.60(1), b=11.65(2), c=8.46(1) Å and V=552(3) Å^3 appeared in the system $NaF-Nb_2O_5-HF-H_2O$ after α-$Na_3[NbF_6O]$ had begun to separate on evaporation of the solvent. Within experimental errors the two phases have the same cell volumes.

The crystals contain sodium ions and hexafluorooxoniobate(V) ions. In the complex anion niobium is surrounded by a pentagonal bipyramidal arrangement of ligands with five fluorine atoms forming the equatorial plane and one fluorine atom and the oxygen atom occupying the apical positions. This is thus not in accord with the monocapped octahedral structure proposed for $[NbF_6O]^{3-}$ in the disordered cubic $K_3[NbF_6O]$.

Bond distances are: $Nb-F_{equatorial}$ 2.016–2.050(3) Å, $Nb-F_{apical}$ 2.084(3) Å and Nb=O 1.738(3) Å. Coordination distances to the sodium ions range from 2.221(3) Å to 2.677(4) Å.

About ten extremely weak reflexions, indicating the existence of a superstructure, were observed on the Weissenberg photographs taken in the initial stage; they were, however, too weak to be registered as significant reflexions by the diffractometer.

0302-4377/83 $02.50

Based on the result of their structure investigation using powder diffraction data, Williams *et al.*[1] claim that the geometrical arrangement of the $[NbF_6O]^{3-}$ ion in $K_3[NbF_6O]$ is a capped octahedron, as was also deduced by Hampson *et al.*[2] for the $[ZrF_7]^{3-}$ ion in $(NH_4)_3[ZrF_7]$ and $K_3[ZrF_7]$. Since all these compounds crystallize in the cubic system, space group $Fm3m$, their structures are incompatible with ordered orientations of the anions. Zachariasen pointed out that $(NH_4)_3[ZrF_7]$ and $K_3[ZrF_7]$ are isostructural with the disordered cubic form of $K_3[UF_7]$.[3] The ordered tetragonal form of $K_3[UF_7]$ contains pentagonal bipyramidal $[UF_7]^{3-}$ ions.[3] Zachariasen, therefore, found it likely that the $[UF_7]^{3-}$ and $[ZrF_7]^{3-}$ ions in the cubic structures should exhibit the same geometry. The disorder of $(NH_4)_3[ZrF_7]$ has been further investigated by Hurst *et al.*,[4] who also proposed a model with a pentagonal bipyramidal geometry. The same situation was also observed by Stomberg *et al.* in $(NH_4)_3[TiF_5(O_2)]$.[5] This compound was later investigated by Massa *et al.*,[6] who preferred to describe the disorderly orientated anion as octahedral.

Besides the above-mentioned geometrical arrangements of ligands, the capped octahedron and the pentagonal bipyramid, there is a third possibility, the capped trigonal prism, exemplified by the $[ZrF_7]^{2-}$ ion in $K_2[ZrF_7]$.[7,8] The available structural data indicate that none of these three geometrical arrangements is particularly favoured unless a bias might be built into a polydentate ligand. Also, all three will, in general, have similar stability.

As already pointed out by Baker *et al.*,[9] it would be of interest to determine the geometry of the $[NbF_6O]^{3-}$ ion by single-crystal studies. In connection with structural work on fluoroperoxoniobates performed at this department, mainly with sodium as cation, fluorooxoniobates are intermediates.[10–13] It, therefore, seemed natural to consider these. The structure of one of these, $(C_9H_8NO)_2[NbF_5O]\cdot 2H_2O$, containing a disorderly orientated octahedral anion, has already been published,[14] while that of α-$Na_3[NbF_6O]$ is reported in this paper.

EXPERIMENTAL

Preparation. 8 g sodium fluoride and 12 g niobium(V) oxide were dissolved in an excess of boiling 38 % hydrofluoric acid in a platinum crucible. Most of the hydrofluoric acid was expelled by repeated addition of water and subsequent evaporation to almost dryness. The final volume was adjusted to 200 ml. When half of the solvent had been evaporated at room temperature, a crystalline mass had begun to separate out. pH was then about 2. From this mass, crystals were picked out for the single-crystal X-ray work. Only a few could be used, most being multiple crystals. The rest, which proved to be a single phase (α), was separated from the solution and analysed. Further crystallization yielded at least one other phase (β) intergrown with the first one.

Analysis. Niobium was determined gravimetrically by precipitation as the hydroxide with ammonia and ignition to the oxide. Sodium was determined by flame emission spectroscopy. Fluoride was determined by potentiometric titration with lanthanum nitrate at pH 5.4 using a fluoride selective electrode (Radiometer fluoride selectrode^R F1052F). (Found: Nb 31.9; Na 22; F 39.3. Calc. for $Na_3[NbF_6O]$: Nb 31.8; Na 23.6; F 39.1).

X-Ray methods. X-Ray powder photographs were obtained by the Guinier-Hägg method (Cu$K\alpha_1$ radiation) using $Pb(NO_3)_2$ (a=7.8566 Å at 21 °C) as an internal standard.

Rotation photographs showed that reflexions with l odd were considerably weaker than those with l even. Weissenberg photographs with rotation about the c axis were registered for l=0–8, 10 and 12, using graphite-monochromatized Cu$K\alpha$ radiation. With a few exceptions the observed reflexions could be indexed according to an orthorhombic cell with a=5.65, b=5.77 and c=16.9 Å. Eleven clearly visible, very weak reflexions could be indexed only by doubling the a and b axes, thus indicating the existence of a superstructure. None of these reflexions (with indices 110, 101, 011, 112, 132, 312, 103, 303, 503, 114, 116 referring to the superstructure cell) was stronger than the weakest observed reflexion due to the smaller cell. Other crystals showed the same situation.

Intensity data were recorded at room temperature for the larger cell (a=11.307(4) Å, b=11.541(5) Å and c=16.919(4) Å, determined from a least-squares fit of refined diffractometer setting angles for 15 reflexions) with a SYNTEX $P2_1$ automatic four-circle single-crystal X-ray diffractometer using graphite-monochromatized Mo$K\alpha$ radiation and a crystal with the dimensions 0.15×0.15×0.26 mm. The θ–2θ method was used and the 2θ scan speed was allowed to vary between 3 and 20 °/min, depending on the intensity of the measured reflexion. Data were collected for $2\theta \leq 78°$. Three test reflexions, measured after each forty-seventh reflexion, showed no significant difference in intensity during the data collection. A profile analysis based on the Lehmann-Larsen method [15] was applied to the 96-step profile collected for each reflexion.

Of the 6580 measured, independent reflexions 1173, having $I_o \geq 3\sigma(I_o)$, were regarded as being observed and were used in the subsequent calculations. All observed reflexions could be indexed according to the smaller cell. Thus, none of the above-mentioned very weak, photographically registered reflexions was strong enough to be registered by the diffractometer. The structure solution is, therefore, based upon the smaller cell. The intensities were corrected for Lorentz, polarization and absorption effects. For the absorption correction the crystal was divided into a 6×6×6 grid. The transmission factor varied between 0.60 and 0.65.

The unit cell parameters were determined by a least-squares fit of observed and calculated $\sin^2\theta$-values for 57 unequivocally indexed reflexions obtained from two independent powder photographs.

Preliminary crystallographic data for the β-phase, which appeared on further crystallization (*vide supra*), were obtained from rotation and Weissenberg photographs. These indicated an orthorhombic cell with the approximate cell dimensions a=5.60(1), b=11.65(2), c=8.46(1) Å and V=552(3) Å^3. The crystal used was intergrown with the α-phase, the respective axes being parallel (*i.e.* $a_\alpha \| a_\beta$, etc.), as far as could be judged from the photographs. The axial ratio for the β-phase is 1:2.080:1.511 and the ratios a_α:a_β, b_α:b_β, and c_α:c_β are 0.991, 2.020 and 0.500, respectively. The cell volumes, V_α=551.50(8) Å^3 and V_β=552(3) Å^3, do not differ significantly.

The above evidence supports the view that the two phases are isostoichiometrical. Since the α-phase could be obtained pure, the single-crystal study was performed on that phase.

CRYSTAL DATA

α-Sodium hexafluorooxoniobate(V), α-$Na_3[NbF_6O]$; *F.W.*=291.87
Space group $P2_12_12_1$ (No. 19)
a=5.6481(4) Å, b=5.7661(5) Å, c=16.9340(13) Å, V=551.50(8) Å^3, Z=4, D_o=3.53 g cm^{-3}, D_c=3.52 g cm^{-3}, μ(Mo$K\alpha$)=2.38 mm^{-1}, λ(Mo$K\alpha$)=0.7107 Å, λ(Cu$K\alpha_1$)=1.54051 Å.

A list of observed lines in the powder photograph of α-$Na_3[NbF_6O]$, giving *hkl*, d_o, d_c and I_o, as well as lists of observed and calculated structure factors and anisotropic thermal parameters are available from the author upon request.

STRUCTURE DETERMINATION

As none of the few very weak reflexions indicating a supercell, observed on the Weissenberg photographs, was strong enough to be registered as significant by the diffractometer, the structure determination is based on the smaller cell.

The positions of the niobium atom and two sodium atoms were obtained from the Patterson function and the third sodium atom from the first electron density map. Since these atoms have rather special positions, a lot of false symmetry was introduced in the subsequent electron density map. A tedious trial method in identifying this map led to a plausible structure, which could be successfully refined.

Full-matrix least-squares refinement of an overall scale factor and positional and isotropic thermal parameters for all atoms yielded an R-value of 0.057 ($R=\Sigma||F_o|-|F_c||/\Sigma|F_o|$). When anisotropic thermal parameters were introduced for all atoms, the R-value was reduced to 0.034. The weighting scheme used was that of Cruickshank:[16] $w=(a+|F_o|+c|F_o|^2+d|F_o|^3)^{-1}$ with a=15, c=0.01 and d=0.001. The scattering factors for Nb, Na^+, F, and O were taken from Ref. 17 as were the dispersion corrections.

The largest peak in a difference synthesis calculated after the final cycle of refinement, appeared at 0.8 Å from niobium with a peak height of 2 e/Å^3. No other peak had a height exceeding 0.7 e/Å^3.

Calculations were carried out on an IBM 3033 computer using the crystallographic programmes described by Lindgren.[18]

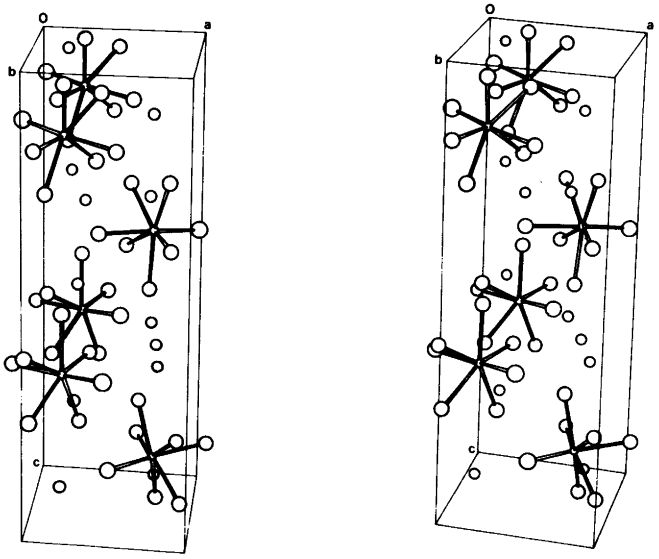

Fig. 1. Stereoscopic drawing of the unit cell of α-$Na_3[NbF_6O]$.

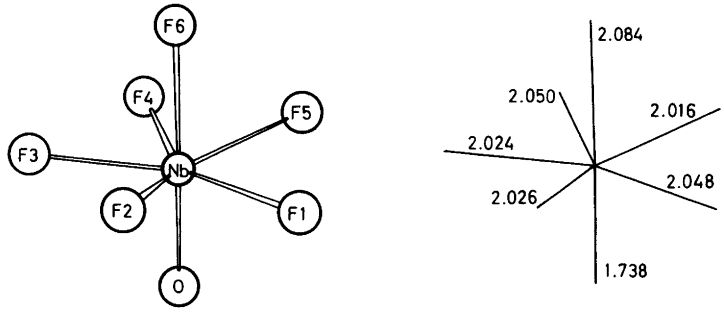

Fig. 2. The ion $[NbF_6O]^{3-}$.

RESULTS AND DISCUSSION

The positional and thermal parameters obtained in the last refinement cycle are given in Table 1. A stereoscopic drawing of the unit cell is shown in Fig. 1 and the anion in Fig. 2. Bond distances and angles are given in Table 2 and coordination distances to the sodium ions in Table 3.

The crystals of α-sodium hexafluorooxoniobate(V), α-$Na_3[NbF_6O]$, are composed of sodium ions and hexafluorooxoniobate(V) ions, held together by ionic forces.

Niobium is seven-coordinated to six fluorine atoms and one oxygen atom. The arrangement of the ligands in $[NbF_6O]^{3-}$ is somewhat distorted pentagonal bipyramidal with five fluorine atoms, F1–F5, forming the pentagonal plane and one fluorine atom, F6, and one oxygen atom occupying the apical positions. This investigation thus contradicts the monocapped octahedral configuration proposed by Williams *et al.* based on a structure determination of $K_3[NbF_6O]$.[1] The distances from the least-squares plane through F1–F5 to these atoms and to Nb, F6 and O are in order 0.163, −0.124, 0.040, 0.069, −0.148, 0.187, −1.893 and 1.926 Å, respectively. The largest observed deviation from the 72° angle between neighbouring Nb–F bonds in the pentagonal plane, expected for full C_5 symmetry, is 1.2°. The geometry of the $[NbF_6O]^{3-}$ ion is, therefore, completely different from that of the $[NbF_7]^{2-}$ ion observed in $K_2[NbF_7]$.[8] The latter is described as a distorted monocapped trigonal prism. Seven-coordinated complexes are considered to be stereochemically nonrigid, since, according to theory, interconvertions between the three geometrical arrangements of ligands can occur without difficulty. One might, therefore, expect considerable distortions in such systems, $[NbF_7]^{2-}$ being one example. In $[NbF_6O]^{3-}$ the five equatorial atoms deviate significantly (by $20-60\sigma$) from coplanarity. This may be compared with the situation in seven-coordinated transition metal peroxo compounds, the five equatorial atoms

Table 1. Positional and thermal parameters for α-$Na_3[NbF_6O]$. $U_{eq}=\frac{1}{3}(U_{11}+U_{22}+U_{33})$.

Atom	x	y	z	$U_{eq}/Å^2$
Nb	0.25348(6)	−0.00913(4)	0.12488(2)	0.0101(1)
Na1	0.2638(4)	0.0124(3)	0.3749(1)	0.0204(4)
Na2	0.2371(3)	0.4688(3)	0.2562(1)	0.0195(3)
Na3	0.2198(4)	0.4908(3)	−0.0034(1)	0.0239(4)
F1	0.1566(5)	0.0768(5)	0.2377(2)	0.0208(5)
F2	0.1243(5)	0.3187(4)	0.1235(1)	0.0226(5)
F3	0.2693(6)	0.1017(4)	0.0116(1)	0.0239(5)
F4	0.4459(5)	−0.2436(5)	0.0604(2)	0.0206(5)
F5	0.4193(5)	−0.2289(4)	0.1992(1)	0.0233(5)
F6	0.5780(5)	0.1608(4)	0.1341(1)	0.0199(5)
O	−0.0098(5)	−0.1608(5)	0.1123(2)	0.0188(6)

Table 2. Bond distances and angles in α-$Na_3[NaF_6O]$.

Distance/Å		Angle/°	
Nb–F1	2.048(3)	F2–Nb–F3	73.1(1)
Nb–F2	2.026(2)	F2–Nb–F4	143.1(1)
Nb–F3	2.024(2)	F2–Nb–F5	139.6(1)
Nb–F4	2.050(3)	F3–Nb–F6	83.1(1)
Nb–F5	2.016(3)	F2–Nb–O	99.2(1)
Nb–F6	2.084(3)	F3–Nb–F4	71.3(1)
Nb–O	1.738(3)	F3–Nb–F5	140.3(1)
Angle/°		F3–Nb–F6	83.3(1)
		F3–Nb–O	94.6(1)
F1–Nb–F2	71.9(1)	F4–Nb–F5	70.8(1)
F1–Nb–F3	145.0(1)	F4–Nb–F6	83.3(1)
F1–Nb–F4	143.0(1)	F4–Nb–O	93.2(1)
F1–Nb–F5	72.2(1)	F5–Nb–F6	80.8(1)
F1–Nb–F6	92.9(1)	F5–Nb–O	99.1(1)
F1–Nb–O	90.4(1)	F6–Nb–O	176.4(1)

Table 3. Cation environment in α-$Na_3[NbF_6O]$.

Distance/Å		Distance/Å	
Na1···F1	2.429(3)	Na2···F5^{iii}	2.374(3)
Na1···F2^{i}	2.461(3)	Na2···F6^{iii}	2.401(3)
Na1···F3^{ii}	2.414(3)	Na2···O$_v$	2.677(4)
Na1···F4^{iii}	2.423(3)	Na3···F2	2.427(3)
Na1···F5^{iii}	2.646(3)	Na3···F3	2.275(3)
Na1···F6^{iv}	2.221(3)	Na3···F3^{vii}	2.603(4)
Na1···O^{v}	2.378(3)	Na3···F4^{vi}	2.269(3)
Na2···F1^{v}	2.312(3)	Na3···F4^{vii}	2.334(3)
Na2···F1	2.327(3)	Na3···F6^{vii}	2.510(3)
Na2···F2	2.492(3)	Na3···O^{viii}	2.587(4)
Na2···F5^{vi}	2.243(3)		

Symmetry codes

i	$(\bar{x},-\frac{1}{2}+y,\frac{1}{2}-z)$	v	$(\bar{x},\frac{1}{2}+y,\frac{1}{2}-z)$
ii	$(\frac{1}{2}-x,\bar{y},\frac{1}{2}+z)$	vi	$(x,1+y,z)$
iii	$(1-x,\frac{1}{2}+y,\frac{1}{2}-z)$	vii	$(-\frac{1}{2}+x,\frac{1}{2}-y,\bar{z})$
iv	$(1-x,-\frac{1}{2}+y,\frac{1}{2}-z)$	viii	$(\frac{1}{2}+x,\frac{1}{2}-y,\bar{z})$

being much nearer to coplanarity. The bidentate peroxo group thus seems to stabilize the pentagonal bipyramidal geometry.

The niobium atom is displaced 0.19 Å from the equatorial plane towards the oxygen atom. The effect of this is that the distances between the apical positions to the equatorial plane deviate by only 0.033 Å. Such displacements are often observed in pentagonally bipyramidal configurations when the apical atoms are different,or are differently coordinated, numerous examples being found among transition metal peroxo complexes exhibiting this geometry with displacements ranging from 0.2 to 0.4 Å (see Table 6 in Ref. 19). In pentagonal pyramidal complexes the displacement may be as large as 0.5 Å, examples being $[CrO(O_2)_2py]$[20] and $[VO(O_2)_2(NH_3)]^-$.[21]

The $Nb-F_{equatorial}$ bond distances, 2.016–2.050 Å, are somewhat shorter than the $Nb-F_{apical}$ bond distance, 2.084 Å. This is contrary to the observations made for fluoroperoxometallates with both apical positions being occupied by fluorine atoms. In these cases the average $Nb-F_{equatorial}$ bond distances are

2.00 Å and the Nb–F_{apical} ones are 1.92 Å. In the seven-coordinate monocapped trigonal prismatic $[NbF_7]^{2-}$ ion the Nb–F bonds range between 1.911 and 1.971 Å, which is normal for Nb–F single bond distances in seven-coordinate fluoroniobates. In $[NbF_6O]^{3-}$, the Nb–F_{apical} bond distance, 2.084 Å, is thus considerably longer. This seems to be due to the presence of the oxygen atom, the Nb=O bond being a double bond, as can be judged from the short Nb=O bond distance of 1.738 Å. In seven-coordinate complexes with a pentagonal bipyramidal geometry and with an Me=O_{apical} bond, the opposite Me–L_{apical} bond distance is significantly longer than a normal single bond, examples being $[CrO(O_2)_2bipy]$,[22] $[CrO(O_2)_2phen]$,[23] $K_2[O\{MoO(O_2)_2(H_2O)\}_2]\cdot 2H_2O$,[24] $K_2[MoO(O_2)_2(C_2O_4)]$,[25] $(NH_4)_4[O\{VO(O_2)_2\}_2]$,[19] $K_6[Mo_7O_{22}(O_2)_2\cdot 8H_2O$,[26,27] $(NH_4)[VO(O_2)(H_2O\{C_5H_3M(COO)_2\}]\cdot xH_2O$,[28] $K_3[VO(O_2)_2(C_2O_4)]\cdot H_2O$,[29] and $K_2[O\{WO(O_2)_2(H_2O)\}_2]\cdot 2H_2O$.[30] In the six-coordinate, tetragonally bipyramidal complex $[NbF_5O]^{2-}$ the Nb–F_{trans} (trans corresponds here to apical) bond distance is 2.06 Å in $K_2[NbF_5O]$,[31] *i.e.* about the same as in the $[NbF_6O]^{3-}$ ion (2.084 Å), while it is considerably longer, being 2.21 Å, in $(N_2H_6)[NbF_5O]\cdot H_2O$.[32] In both $(C_9H_8NO)_2[NbF_5O]\cdot 2H_2O$ [14] and Li_2NbF_5O [33] the $[NbF_5O]^{2-}$ ions are disordered, the average Nb–(F,O) distances being 1.92(1) Å and 1.95 Å, respectively. That the Nb–$F_{equatorial}$ bond distances are persistently significantly longer in the pentagonal planes, being 1.97–2.05 Å,[10–13] than in the tetragonal ones, lying in the range of 1.84–1.93 Å for a number of cases,[31,32,34] is understandable on purely geometrical grounds, the repulsive effect being larger in the more crowded pentagonal case.

The Nb=O distance in $[NbF_6O]^{3-}$ is 1.738(3) Å and compares well with the value 1.71±0.02 Å, which is the average Nb=O double-bond distance calculated from data for $(N_2H_6)[NbF_5O]\cdot H_2O$,[32] $K_2[NbF_5O]$,[31] $[NbCl_2O(OC_2H_5)(C_{10}H_8N_2)]$,[35] $[(C_6H_5)_4As]_2[Nb(NCS)_5O]$,[35] and $(NH_4)_3[Nb(C_2O_4)_3O]\cdot H_2O$.[36,37]

The observed coordination distances between the sodium and fluoride ions range from 2.221 to 2.646 Å; this is to be compared with the radii sum of 2.31 Å. The shortest Na···F interaction involves the fluorine atom with the longest coordination distance to the niobium atom. The coordination distances between the sodium atoms and the oxygen atom lie between 2.378 and 2.677 Å; in this case the radii sum is 2.35 Å.

In the system $NaF–Nb_2O_5–HF–H_2O_2–H_2O$ three distinct crystalline phases were isolated and identified by Stomberg.[10–12] They all appeared during the same crystallization experiment on total evaporation of the solvent. Their structures were determined and their formulae are $Na_2[NbF_5(O_2)]\cdot H_2O$,[10] $Na_3[HF_2][NbF_5(O_2)]$,[11] and $Na_2[NbF_5(O_2)]\cdot 2H_2O$.[12] They all contain the anion $[NbF_5(O_2)]^{2-}$. The situation might be similar in the system $NaF–Nb_2O_5–HF–H_2O$. Two phases have hitherto been observed, namely the α-phase, whose structure is described in this paper, and another phase, called the β-phase. The latter has the same cell volume as the α-phase well within experimental errors, and there is a simple ratio between the corresponding cell edges. The β-phase appeared intergrown with the α-phase with the respective axes parallel to each other. The above evidence might indicate identical stoichiometry.

Acknowledgement. I wish to express my gratitude to Mrs. Solveig Olson for technical assistance.

REFERENCES

1. Williams, M. B. and Hoard, J. L. *J. Am. Chem. Soc. 64* (1942) 1139.
2. Hampson, G. C. and Pauling, L. *J. Am. Chem. Soc. 60* (1938) 2702.
3. Zachariasen, W. H. *Acta Cryst. 7* (1954) 792.
4. Hurst, H. J. and Taylor, J. C. *Acta Cryst. B 26* (1970) 417.
5. Stomberg, R. and Svensson, I.-B. *Acta Chem. Scand. A 31* (1977) 635.
6. Massa, W. and Pausewang, G. *Mater. Res. Bull. 13* (1978) 361.
7. Hoard, J. L. *J. Am. Chem. Soc. 61* (1939) 1252.
8. Brown, G. M. and Walker, L. A. *Acta Cryst. 20* (1966) 220.
9. Baker, A. E. and Haendler, H. M. *Inorg. Chem. 1* (1962) 127.
10. Stomberg, R. *Acta Chem. Scand. A 34* (1980) 193.
11. Stomberg, R. *Acta Chem. Scand. A 35* (1981) 389.
12. Stomberg, R. *Acta Chem. Scand. A 35* (1981) 489.

13. Stomberg, R. *Acta Chem. Scand. A 36* (1982) 101.
14. Stomberg, R., Svensson, I.-B. and Trysberg, L. *Acta Chem. Scand. A 35* (1981) 779.
15. Lehmann, M. S. and Larsen, F. K. *Acta Crystallogr. A 30* (1974) 580.
16. Cruickshank, D. W. J. *Crystallographic Computing,* Munksgaard, Copenhagen 1970, p. 195.
17. *International Tables for X-Ray Crystallography Vol. IV,* Kynoch Press, Birmingham, England 1974.
18. Lindgren, O. *Thesis,* University of Göteborg and Chalmers University of Technology, Göteborg 1977.
19. Svensson, I.-B. and Stomberg, R. *Acta Chem. Scand. 25* (1971) 898.
20. Stomberg, R. *Arkiv Kemi 22* (1964) 29.
21. Drew, R. E. and Einstein, F. W. B. *Inorg. Chem. 11* (1972) 1079.
22. Stomberg, R. and Ainalem, I.-B. *Acta Chem. Scand. 22* (1968) 1439.
23. Stomberg, R. *Arkiv Kemi 24* (1965) 111.
24. Stomberg, R. *Acta Chem. Scand. 22* (1968) 1076.
25. Stomberg, R. *Acta Chem. Scand. 24* (1970) 2024.
26. Stomberg, R., Trysberg, L. and Larking, I. *Acta Chem. Scand. 24* (1970) 2678.
27. Larking, I. and Stomberg, R. *Acta Chem. Scand. 26* (1972) 3708.
28. Drew, R. E. and Einstein, F. W. B. *Inorg. Chem. 12* (1973) 829.
29. Begin, D., Einstein, F. W. B. and Field, J. *Inorg. Chem. 14* (1975) 1785.
30. Einstein, F. W. B. and Penfold, B. R. *Acta Crystallogr. 17* (1964) 1127.
31. Pinsker, G. Z. *Kristallografiya 11* (1966) 741; *Soviet Phys. Crystallogr. 11* (1967) 634.
32. Gorbunova, Ju. E., Pakhomov, V. I., Kuznetsov, V. G. and Kovaleva, E. S. *Zh. Strukt. Khim. 13* (1972) 165; *J. Struct. Chem. 13* (1972) 154.
33. Galy, J., Andersson, S. and Portier, J. *Acta Chem. Scand. 23* (1969) 2949.
34. Pakhomov, V. I. and Kaidalova, T. A. *Kristallografyia 19* (1974) 733; *Soviet Phys. Crystallogr. 19* (1975) 454.
35. Kamenar, B. and Prout, C. K. *J. Chem. Soc. A* (1970) 2379.
36. Mathern, G., Weiss, R. and Rohmer, R. *Chem. Comm. D* (1969) 70.
37. Mathern, G. and Weiss, R. *Acta Crystallogr. B 27* (1971) 1610.

Received November 19, 1982.

Acta Chemica Scandinavica A 37 (1983) 461–475

A Very Simple One-Variable Flip-flop Model of the Belousov-Zhabotinskii Reaction

TORBEN SMITH SØRENSEN

Fysisk-Kemisk Institut, Technical University of Denmark, DK-2800 Lyngby, Denmark

On the basis of the socalled "Oregonator" model by Field and Noyes for the oscillating Belousov-Zhabotinskii reaction, a very simple one-variable model is proposed with virtually the same behaviour as the three-variable Oregonator model. The present model is inspired by the classical treatment of relaxation-oscillations by van der Pol.

The model involves quasi-stationarity assumptions for the intermediary compound $HBrO_2$ and for Br^-. Bromide is stationary except at two critical concentrations, where the concentration "flips" and "flops" almost instantaneously between two separate branches of the stationarity curve for Br^-. The limit cycle then involves a rapid movement in the phase plane along an "A-branch" triggered by a pulse of $HBrO_2$ followed by a slow restoring movement along a "B-branch". The time spent on the two branches can be calculated simply as two integrals (chronomals) in dimensionless units(θ_A and θ_B). The sum $\theta_A+\theta_B$ is equal to the dimensionless period of the limit cycle (θ_p). The period of the limit cycle in real time is determined exclusively by the inverse rate constant k_5 of the fifth reaction in the Oregonator-model: The oxydative decarboxylation reaction between Ce^{4+} and bromomalonic acid.

Experimentally, the influence of bromate concentration and temperature on the period and on the fraction of time spent on the A-branch (low bromide concentration) in the full cycle has been studied. Together with the experimental findings of Field, Körös and Noyes and the theoretical results of the present study we conclude from this that the value for parameter $q=2k_1k_4/k_2k_3$ should be in the interval $2.5\cdot10^{-2}-7.6\cdot10^{-2}$.

The inverse period of the relaxation-oscillations has a simple Arrhenius dependence on the absolute temperature which is also explained by the model. The activation energy for the oscillations is composed by the activation energy of k_5 and a term proportional to the activation energy of the q-parameter.

When chemical reactions occur outside the quite narrow range of applicability of the reciprocity relations of Onsager, numerous instabilities leading to spatial and/or temporal structures may occur induced by nonlinearities in the reaction system.[1] One of such possibilities is the appearance of *limit cycles* first discussed by Poincaré 100 years ago.[2] In 1958, Belousov reported on oscillations in the ratio of Ce^{4+} to Ce^{3+} ions during the cerium ion catalyzed oxidation of citric acid by bromate in aqueous sulfuric acid solution.[3] The study was some years later taken up by Zhabotinskii *et al.*[4–7] who elucidated the mechanism and showed that citric acid could be replaced by malonic acid or by another organic material with an active methylenic hydrogen and that Ce^{4+}/Ce^{3+} could be replaced with other redox couples as Mn^{3+}/Mn^{2+} or ferroin/ferriin indicator. It was also shown that spatial structures could appear in unstirred solution in the form of propagating chemical waves. Henceforth, the reaction system was called the Belousov-Zhabotinskii (BZ) system.

Further elucidation of the mechanism was made by Degn,[8] Kasperek and Bruice [9] and Busse.[10] However, it was the very careful experimental study and data collection of Field, Körös and Noyes [11] in 1972 which enabled Field and Noyes [12] from the University of Oregon to propose their socalled "Oregonator" model of the BZ-oscillator, a name chosen to match with

0302-4377/83 $02.50

$$Br^- + HOBr + H^+ \longrightarrow Br_2 + H_2O \quad (R1)$$
$$Br^- + HBrO_2 + H^+ \longrightarrow 2HOBr \quad (R2)$$
$$Br^- + BrO_3^- + 2H^+ \longrightarrow HBrO_2 + HOBr \quad (R3)$$
$$2HBrO_2 \longrightarrow HOBr + BrO_3^- + H^+ \quad (R4)$$
$$BrO_3^- + HBrO_2 + H^+ \longrightarrow 2BrO_2\cdot + H_2O \quad (R5)$$
$$Ce^{3+} + BrO_2\cdot + H^+ \longrightarrow Ce^{4+} + H_2O + HBrO_2 \quad (R6)$$
$$4Ce^{4+} + BrM + HOBr + H_2O \longrightarrow 2Br^- + 4Ce^{3+} + 3CO_2 + 6H^+ \quad (R7) = (R10) + (R11)$$
$$Br_2 + M \longrightarrow BrM + Br^- + H^+ \quad (R8)$$
$$6Ce^{4+} + M + 2H_2O \longrightarrow 6Ce^{3+} + HCOOH + 2CO_2 + 6H^+ \quad (R99)$$
$$4Ce^{4+} + BrM + 2H_2O \longrightarrow 4Ce^{3+} + HCOOH + 2CO_2 + 5H^+ + Br^- \quad (R10)$$
$$HOBr + HCOOH \longrightarrow Br^- + CO_2 + H_2O + H^+ \quad (R11)$$

Scheme 1. The 11 most important reactions in the BZ-reaction system. M=malonic acid; BrM=bromomalonic acid.

the well known "Brusselator" of the Brussels school of thermodynamics. The "Oregonator" is basically a five-reaction/three-variable model representing the oscillations very well. Therefore, in the light of the fact that there are at least 10 important reactions occurring simultaneously (see Scheme 1), the Oregonator constitutes a tremendous simplification and intellectual effort. However, the model is still not simple to explain pedagogically, and simulations have to be done by computer.

It has often been pointed out that the saw-tooth oscillations of the BZ-system are very like the relaxation-oscillations of the well known bistable multivibrators in electronics. Some time ago, I therefore started to speculate on the possibility of treating the BZ-system in analogy with the paradigm of relaxation-oscillations, *i.e.* the harmonic oscillator with negative and non-linear friction introduced by van der Pol in 1920 to describe relaxation-oscillations in electron tube oscillators, see Minorsky.[13] The present paper will show that it is indeed possible to give a very similar description of the BZ-reaction. Actually, the solution of the three-variable Oregonator system can be reduced – without any significant loss of precision – to the solution of a simple, one-variable kinetic equation along two quasi-stationarity branches with virtually instantaneous "jumps" from one branch to the other at critical positions on the two branches. The two branches are branches of a certain "H-curve", which has also a middle, unstable branch. The jumps occur at the maximum and the minimum of the H-curve, in precise analogy with the situation for the van der Pol oscillator.

THE OREGONATOR

The five reactions selected from the list in Scheme 1, which were considered by Field and Noyes to be the important "bottlenecks" in the reaction scheme, are the following:

$$A + Y \xrightarrow{k_1} X + P \quad (1)$$
$$X + Y \xrightarrow{k_2} 2P \quad (2)$$
$$A + X \xrightarrow{k_3} 2X + 2Z \quad (3)$$
$$2X \xrightarrow{k_4} P + A \quad (4)$$
$$Z \xrightarrow{k_5} f \cdot y \quad (5)$$

The meaning of the symbols is given by eqns. (6):

$$A = BrO_3^-,\ P = HOBr,\ X = HBrO_2,\ Y = Br^-,\ Z = Ce^{4+} \quad (6)$$

It has been used that the ratio of ceri to cero-ions is always very small. Account has therefore only to be taken of the ceri-ions. In the following, the reaction labels (R1)–(R11) refer to Scheme 1. Concentrations of H^+ and H_2O have everywhere been built into the rate constants, since the reaction medium is about 1 mol/dm^3 with respect to sulfuric acid, which is a much larger concentration than all the other concentrations.

By reaction (1) – which is identical to (R3) – the intermediate compounds $HBrO_2$ and HOBr are formed by reaction between Br^- and BrO_3^-.

$HBrO_2$ is reacting further through reaction (2) with Br^- to form two moles of HOBr. Reaction (2) is identical to (R2). Reaction (3) is an *autocatalytic* reaction for formation of $HBrO_2$. It is equivalent with the reaction (R5)+2(R6)=(G) shown below. (R5) is the rate determining step.

$$2Ce^{3+}+BrO_3^-+HBrO_2+3H^+ \rightarrow 2Ce^{4+}+H_2O+2HBrO_2 \quad (G)$$

Reaction (4) is a sink for $HBrO_2$ which is equivalent to (R4). The last reaction (5) is a kind of pooled reaction representing the oxydation of organic matter by Ce^{4+} (formed in the autocatalytic reaction) and release of Br^- from bromomalonic acid (BrM). BrM is formed through Br_2 in reactions (R1) and (R8). In the original Oregonator model, reaction (5) was assumed to be a mixture of (R9) and (R10). The stoichiometric factor f for Br^- release would then vary between 0 (pure R9) and 1/4 (pure R10). The problem is, however, that f has to be between 0.25 and 1.206 in order to have possibility of oscillations in the Oregonator, see Murray.[14] (Note that we have followed the definition of f given in the book of Murray rather than the definition in the original Oregonator-model). Also, Bornmann *et al.*[15] failed to detect formic acid among the reaction products which should be the case if (R9) or (R10) was followed. In order to remedy this mismatch, Noyes and Jwo [16] postulated the reaction (R11) between HCOOH and HOBr. When (R10) is followed by (R11) with (R10) as the rate determining step, the kinetics is as given in reaction (5) and the net reaction is as (R7) where f=0.5. It has been assumed that the concentration of BrM is virtually constaant over a cycle, so that [BrM] can be built into k_5.

The more detailled kinetics of the oxidation of BrM by Ce^{4+} were elucidated by Jwo and Noyes.[17] They found the following dependence of k_5 on [BrM]:

$$k_5 = k_{05} \cdot [BrM]/(K_M+[BrM]) \quad (k_{05} = 0.015\ s^{-1}) \quad (7)$$

where k_{05} is a catalytic constant and K_M a "Michaelis-Menten" constant. The kinetics were really found to be first order with respect to Ce^{4+}. The value of K_M is dependent on the reaction time in an unexplained way. Before a certain "break point" K_M is 0.107 mol/dm^3 and after K_M is 0.033 mol/dm^3. The "break point" seems to occur after a time of the order of magnitude of 10 min, so it is hardly reached with the normal oscillations of the BZ reaction of order of magnitude 1 min. We therefore conclude, that k_5 is varying between the value given in eqn. (8) for very low [BrM] to the value given in eqn. (9) for high values of [BrM], where the catalyst is saturated.

$$k_5 = 0.140\,[BrM]\ s^{-1},\ [BrM] \ll 0.1\ mol/dm^3 \quad (8)$$

$$k_5 = 0.015\ s^{-1},\ [BrM] \gg 0.1\ mol/dm^3 \quad (9)$$

In normal experimental cases for the BZ reaction, the condition given in eqn. (8) prevails. The activation energy found for k_{05}/K_M was the value given in eqn. (10) (before the "break point"):

$$E_5^{\neq} = 54.5 \pm 2.0\ kJ/mol \quad (10)$$

We have been quite critical with k_5 here, since the present model will show that the period of the oscillations is largely determined by the rate constant k_5.

NONDIMENSIONALIZATION AND QUASI-STATIONARITY APPROXIMATION

Assuming that only X, Y and Z vary during a cycle, we obtain from the reactions (1)−(5) a set of three coupled differential equations in X, Y and Z:

$$dX/dt=(k_1A)\cdot Y-k_2\cdot X\cdot Y+(k_3A)\cdot X-2k_4\cdot X^2 \quad (11)$$

$$dY/dt=-(k_1A)\cdot Y-k_2\cdot X\cdot Y+f\cdot k_5\cdot Z \quad (12)$$

$$dZ/dt=2(k_3A)\cdot X-k_5\cdot Z \quad (13)$$

Here, t is real time and X, Y and Z are the molar concentrations of X, Y and Z, where the square brackets have been left out for brevity. We can simplify the equations by introducing dimensionless concentrations:

$$x \equiv (k_2/k_1A)\cdot X \quad (14)$$

$$\eta \equiv (k_2/k_3A)\cdot Y \quad (15)$$

$$\zeta \equiv \{k_4k_5/(k_3A)^2\}\cdot Z \tag{16}$$

Now, equations (11) to (13) transform to:

$$\varepsilon dx/d\tau = x+\eta-x\cdot\eta-qx^2 \tag{17}$$

$$d\eta/d\tau = (2f/q)\cdot\zeta-\eta-x\cdot\eta \tag{18}$$

$$(p/q)d\zeta/d\tau = x-(1/q)\cdot\zeta \tag{19}$$

We have also introduced a dimensionless time given by (20) and three dimensionless parameters given by (21):

$$\tau \equiv k_1A\cdot t \tag{20}$$

$$\varepsilon \equiv k_1/k_3 \sim 2\cdot10^{-4},\ p \equiv k_1A/k_5 \sim 3.1\cdot10^2,$$
$$q \equiv 2k_1k_4/k_2k_3 \sim 8.4\cdot10^{-6} \tag{21}$$

The values given for ε, p and q are approximate values valid at 25 °C, see Refs. 12 and 14.

Since $\varepsilon \ll 1$ the approximation suggests itself to take the left hand side of eqn. (17) to be zero. This amounts to a quasi-stationarity approximation for $HBrO_2$, and the approximation has been discussed under the name "stiffly coupled approximation" by Field and Noyes.[12] In this manner we obtain a system of only two equations which we shall reformulate as eqns. (22) and (23):

$$d\eta/d\tau = (2f/q)\cdot\{\zeta-[H(\eta)/2f]\} \tag{22}$$

$$d\zeta/d\tau = (1/p)\cdot\{U(\eta)-\zeta\} \tag{23}$$

We have introduced two functions of η which become of crucial importance, $U(\eta)$ and $H(\eta)$, defined by eqns. (24) and (25):

$$U(\eta) \equiv \tfrac{1}{2}\{1-\eta+\sqrt{(1-\eta)^2+4q\eta}\} \tag{24}$$

$$H(\eta) \equiv [q+U(\eta)]\cdot\eta \tag{25}$$

We have further a supplementary stationarity condition for x:

$$x = U(\eta)/q \tag{26}$$

(The positive sign has to be chosen in the solution of the quadratic equation in order to obtain a positive x).

We shall further simplify eqn. (22) by taking $2f=1$, since $f=0.5$ seems to be a quite realistic stoichiometric factor.[16] The functions $U(\eta)$ and $H(\eta)$ can now be seen to play the role of nullclines separating upward and downward motion or motion to the right and to the left of a phase point in the (η,ζ) phase plane. Indeed, we have:

$$d\zeta/d\tau \gtrless 0 \quad \text{for} \quad \zeta \lessgtr U(\eta) \tag{27}$$

$$d\eta/d\tau \gtrless 0 \quad \text{for} \quad \zeta \gtrless H(\eta)\ (2f=1) \tag{28}$$

Stationary points in the phase plane have to be intersections in the positive quadrant between the U and the H-curves.

A second stationarity approximation may be introduced. Since $q \ll 1$ and $p \gg 1$, the η-variable will equilibrate itself very rapidly according to eqn. (22) in comparison to the ζ-variable. We would therefore tend to have eqn. (29) satisfied whenever possible (we shall see that it is not always possible and then we have the "jumps"):

$$\zeta \cong H(\eta) \quad (2f=1) \tag{29}$$

The problem is then reduced to a one-variable problem, since the phase point just "slides" along the H-curve. It is now important to study the properties of the U and the H-curves, their intersection points and the stability of the intersection points. This will be the topic of the two next sections.

PROPERTIES OF THE U AND H FUNCTIONS

Fig. 1 exhibits some of the properties of the U and H functions for a q-value less than unity, but not much less. The U function decreases monotonously, but H has a maximum. In the case of Fig. 1, this maximum is positioned at a higher η-value than the intersection point. It is easy to see that the intersection point in that case is a *stable* stationary point since phase points in all directions around the intersection point will move towards that point due to the relative position of the nullclines. Basically, the slope of the H curve has to be negative in the intersection point in order to obtain instability, see the discussion in the next section.

The expression for U may be reformulated as eqn. (30):

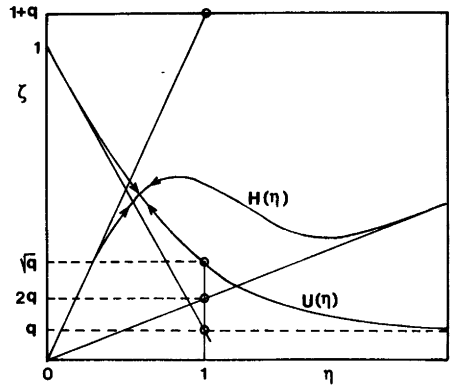

Fig. 1. Phase plane with the U-nullcline between upwards and downwards motion and the H-nullcline between motion to the right and to the left. The H-curve is also the curve of quasi-stationarity for Br^-. The dimensionless bromide concentration is η and the dimensionless Ce^{4+} concentration ζ. The intersection between the U- and H-curve is a stationary point. The stationary point is stable here, since the U- and H-curves cross at lower η than η_{max} corresponding to the maximum in the H-curve. For $q \ll 1$ this will not be the case.

$$U(\eta)=\tfrac{1}{2}(1-\eta)\cdot[1+\mathrm{sign}(1-\eta)\cdot \sqrt{1+4q\eta/(1-\eta)^2}] \quad (30)$$

If the condition (31) is satisfied, the square root can be Taylor-expanded, so that we obtain eqn. (32):

$$4q\eta/(1-\eta)^2 \ll 1 \quad (31)$$

$$U(\eta)\cong\tfrac{1}{2}(1-\eta)\cdot[1+\mathrm{sign}(1-\eta)\cdot \{1+[2q\eta/(1-\eta)^2]\}] \quad (32)$$

We therefore have two approximate equations for U, eqn. (33) for $\eta<1$ and eqn. (34) for $\eta>1$:

$$U(\eta)\cong(1-\eta)\cdot[1+\{q\eta/(1-\eta)^2\}]\cong 1-\eta \quad (\eta<1) \quad (33)$$

$$U(\eta)\cong q\eta/(\eta-1) \quad (\eta>1) \quad (34)$$

Condition (31) will be satisfied for any q with η close enough to zero, so the initial slope of the U-curve will be $-(1-q)$. If $q \ll 1$, condition (31) will be satisfied for all $\eta<1$ except for η-values very close to 1, and in that case U will be $1-\eta$ in the interval $\eta\in[0|1-\delta]$, where δ is a small quantity. On the other hand, condition (31) will also be satisfied for any q and $\eta \gg 1$. In that case, approximation (34) is valid, and $U \to q$ for $\eta \to +\infty$.

For the function $H(\eta)$ we obtain under the same condition (31) the eqns. (35) and (36) for $\eta<1$ and $\eta>1$, respectively:

$$\frac{H}{\eta}\cong 1+q-[1-\{q/(1-\eta)\}]\eta \quad [\eta<1, \text{cond. (31)}] \quad (35)$$

$$\frac{H}{\eta}\cong\{(2\eta-1)/(\eta-1)\}\cdot q \quad [\eta>1, \text{cond. (31)}] \quad (36)$$

From eqn. (35) we see that the limiting slope for $\eta \to 0_+$ and any q for the H-function is $1+q$. For very small q-values H will be approximately equal to $(1-\eta)\cdot\eta$ in the interval $\eta\in[0|1-\delta]$ and the maximum in H will fall at $\eta_{max}=0.5$ with $H_{max}=0.25$. From eqn. (36) we see that the limiting value of H for very large η and any q will be $H=2q\cdot\eta$. The approximation (36) is also valid for all $\eta>1$ when q is very small, except for η-values very close to 1. The function in eqn. (36) has extrema at $\eta=1\pm(\sqrt{2}/2)$, but only the plus sign yields an η in the correct range. The extremum is here a minimum. In summary we have for $q \ll 1$:

$$\eta_{max}=0.5; \quad H_{max}=0.25 \quad (q \ll 1) \quad (37)$$

$$\eta_{min}=1+\sqrt{2}/2=1.7071; \quad H_{min}=(2q/\sqrt{2})(1+\sqrt{2}/2)(1+\sqrt{2})= 5.828q \quad (q \ll 1) \quad (38)$$

Thus, for very small q (which is the case for the Oregonator), the maximum and the position of the minimum of the H-curve do not depend on the precise value of q. Only H_{min} depends proportionally on q.

The points of intersection between $H/2f$ and U are stationary points. Their η-values will be designated by η_o. The problem of finding roots of $H(\eta_o)/2f=U(\eta_o)$ can be recast into the problem of finding roots in eqn. (39):

$$U(\eta_o)=g(\eta_o)\equiv(q/2f)\cdot\eta_o/[1-(\eta_o/2f)] \quad (39)$$

(The relation (25) between U and H has been used). The function $g(\eta_o)$ grows up from 0 at $\eta_o=0$ to $+\infty$ at $\eta_o=2f$. From $2f+\delta$ to $+\infty$, g grows from $-\infty$ to $-q$. Therefore, there can only be one intersection point between $H/2f$ and U, and there *will* always be one which is positioned at $\eta_o<2f$. For $f=0.5$, the stationary point will always be positioned for $\eta_o<1$. For very small values of q, and $\eta<1$ we have $U=1-\eta$ and $H=(1-\eta)\cdot\eta$. U is 0.5 at η_{max} with $H_{max}=0.25$ and it is seen that H will continue to be less than U when η is growing towards 1. Therefore, the root η_o has to be positioned extremely close to 1, where the approximation breaks down.

LINEAR STABILITY OF STATIONARY POINT

The first step in the investigation of the stability of a stationary point will always be to investigate the *linear stability* of small perturbations from that point. We express the two variables as in eqn. (40) where δ signifies a small deviation:

$$\eta=\eta_o+\delta\eta \quad \zeta=\zeta_o+\delta\zeta \tag{40}$$

($\zeta_o=U(\eta_o)=H(\eta_o)/2f$). Introducing eqn. (40) into eqns. (22) and (23) throwing away all second and higher order terms in the perturbation, we obtain the linearised equations written in matrix form in eqn. (41):

$$\begin{bmatrix} \delta\dot{\eta} \\ \delta\dot{\zeta} \end{bmatrix} = \begin{bmatrix} -(H'_o/q) & (2f/q) \\ U'_o/p & -1/p \end{bmatrix} \begin{bmatrix} \delta\eta \\ \delta\zeta \end{bmatrix} \tag{41}$$

U'_o and H'_o are the derivates of the U and H functions with respect to η taken at $\eta=\eta_o$. The stability and the oscillatory behaviour in the region of validity of the linearisation is determined by the nature of the eigenvalues to the coefficient matrix of eqn. (41). The two eigenvalues are given by eqn. (42):

$$\lambda = \tfrac{1}{2}[-(H'_o/q+1/p) \pm \sqrt{(H'_o/q-1/p)^2+(8f/qp)U'_o}] \tag{42}$$

The quadratic equation to which the eigenvalues n eqn. (42) are solutions is given by eqn. (43):

$$\lambda^2+a_1\cdot\lambda+a_o = 0 \tag{43}$$

The coefficients a_1 and a_2 are given in eqn. (44):

$$a_1 = (1/q)\cdot(H'_o+q/p)$$
$$a_o = (/q\cdot p)\cdot(H'_o-2fU'_o) \tag{44}$$

Using the Hurwitz stability criterion,[18] we find the conditions for having the real parts of $\lambda\geqq 0$ (marginal stability or instability) as given in the conditions (45) and (46):

$$a_0\leqq 0 \quad \text{(unstable node)} \tag{45}$$

$$a_1\leqq 0 \quad \text{(unstable focus)} \tag{46}$$

The condition (45) corresponds to an unstable node (no oscillations) and (46) to an unstable focus (oscillations, complex eigenvalues). The stability behaviour according to eqn. (43) is summed up in Fig. 2.

Examining first the conditions (45) and using that

$$H' = q+U+U'\cdot\eta \tag{47}$$

we transform condition (45) to the form (48):

$$U'_o \geqq \frac{U_o+q}{2f-\eta_o} \tag{48}$$

This is clearly impossible, since U'_o is negative whereas the right hand side of (48) is positive since it was demonstrated in the previous section that $2f-\eta_o$ is always positive. Thus, the instability will always break out oscillatory, and condition (46) is the important one. Therefore, we have condition (49):

$$H'_o \leqq -q/p \tag{49}$$

The intersection point between the H-curve and the U-curve has to be positioned at $\eta_o>\eta_{max}$, where H'_o is negative, in order to have linear instability. With $q/p\ll 1$, the critical slope $H'_o=-q/p$ will be close to zero. Therefore, the separation between stability and instability will be made by the value q_{max} with *coincidence* between η_o and η_{max} in the limit $p\to\infty$. One finds the value $q_{max}=7.62\cdot10^{-2}$. For $q>q_{max}$ it is not possible to have any oscillations with the present model.

The final point to be discussed in the framework of linear stability theory is the angular

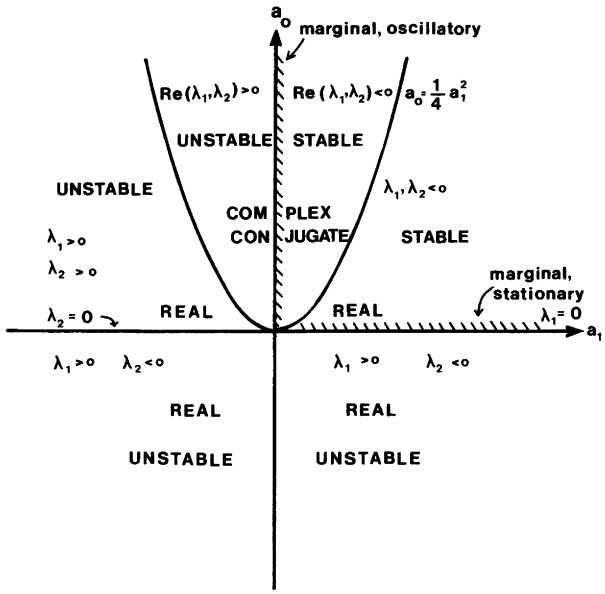

Fig. 2. Stability-instability diagram corresponding to the characteristic equation (43).

frequency (ω) for the marginally stable focus, *i.e.* $a_1=0$ or $H'_o=-q/p$. According to the bifurcation theorem of Hopf,[19] there will exist a *limit cycle* (stable or unstable) with the period $2\pi/\omega$ when we diminish the slope H'_o slightly below the critical value given by $-q/p$. This value is the only estimate for the period of the real limit cycle which we are able to extract from linear theory.

Inserting $\lambda=\pm i\omega$ in eqn. (43) we obtain $a_1=0$ and eqn. (50):

$$\omega = \sqrt{a_0} = \sqrt{\frac{H'_o-2f\cdot U'_o}{qp}} \tag{50}$$

Using the relation (47) we have:

$$H'_o-2f\cdot U'_o=q+U_o+(1-2f)\,U'_o \tag{51}$$

For $2f=1$ we therefore have for the Hopf angular frequency:

$$\omega_{Hopf} = \sqrt{\frac{q+U_o}{q\cdot p}} = \sqrt{\frac{H_o}{\eta_o\cdot q\cdot p}} = \sqrt{\frac{U_o}{\eta_o\cdot q\cdot p}} \tag{52}$$

From eqn. (39) and eqn. (52) we obtain for the dimensionless Hopf-period:

$$\tau_{Hopf}=2\pi/\omega_{Hopf}=2\,\pi\sqrt{p(1-\eta_o)} \tag{53}$$

Passing to real time through eqn. (20) we have:

$$t_{Hopf}=(2\pi/k_1A)\sqrt{p}\cdot\sqrt{1-\eta_o} \tag{54}$$

Using eqn. (21) for the parameter p we obtain:

$$t_{Hopf}=2\pi\sqrt{1-\eta_o}/\sqrt{k_1\cdot k_5A} \tag{55}$$

For comparison with experiments we write for the inverse period:

$$1/t_{Hopf} = \frac{\sqrt{k_1k_5}}{2\pi\sqrt{1-\eta_o}}\cdot\sqrt{A} \tag{56}$$

The value of $1-\eta_o$ depends solely on the value assumed for q. The rate constant k_1 has a value given in eqn. (57):[12,14]

$$k_1\simeq 2.1\ s^{-1}\cdot dm^3\cdot mol^{-1}\quad (25\ °C) \tag{57}$$

The rate constant k_5 was given by the relation (7). It is independent of the bromate concentration (A) if either a) the concentration of BrM is much greater than 0.1 mol/dm^3 or b) if BrM is only slightly dependent on BrO_3^-, so that k_5 in eqn. (56) may be replaced by k_5 (mean).

We shall indeed find a dependence of the experimental inverse period on the bromate concentration of the form (58):

$$1/t_p = \text{constant} \cdot [BrO_3^-]^{0.5} \quad (58)$$

A more detailled comparison with experimental facts will be carried out in the final section. Here, I shall just warn the reader not to take the comparison between t_p (experimental) and t_{Hopf} too seriously. The experimentally observed relaxation-oscillations ("saw tooth" oscillations) are indeed far from the uniformly rotating Hopf cycle near the critical point. Therefore, the experimental conditions are probably too *supercritical* for the Hopf estimate to be more than an order of magnitude calculation. A better approximation to the period of the relaxation-oscillations will be derived in the next section.

THE CHRONOMALS OF THE RELAXATION-OSCILLATION

For the value $q=8.4\cdot10^{-6}$ given in eqn. (21), the H-curve has been drawn, see Fig. 3. The U-curve is also drawn, and they have an intersection point extremely close to $\eta=1$ as inferred also from the previous section. The slopes U'_o and H'_o are extremely large and negative. Actually, it is necessary to plot the (η,ζ) phase plane in logarithmic units as shown on Fig. 3. The intersection point will be unstable, but because of the enormous difference in magnitude of the rate of the two processes (22) and (23), the H-curve will be followed as far as possible according to eqn. (29). Then, the phase point will move up or down on the unstable C-branch of the H-curve according to the sign of the initial perturbation from stationary point O. Let us assume that it moves up. When H_{max} is reached, the phase point

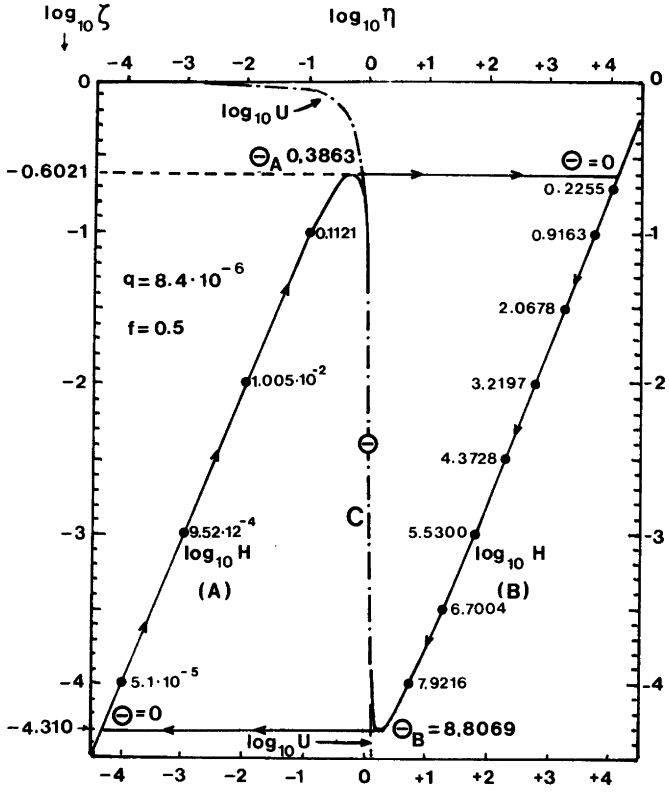

Fig. 3. Phase plane plot of relaxation oscillations for a very low value of q. The phase point is jumping back and forth between the A- and the B-branch of the H-curve at the two extrema. The C-branch with the stationary point (O) is unstable. The time consumed at some points along the A- and B-branches is indicated.

should still move upwards, since we are still below the *U*-nullcline (cf. conditions (27)). Thus, we have to leave the *H*-curve in the upwards direction. As soon as this happens, the very fast process (22) sets in, and a very rapid motion of the phase point in the η-direction starts. During the "jump", the "slow" ζ-variable does not change its value significantly. When we hit the *B*-branch we are above the *U*-nullcline, and we therefore move slowly downwards along the *B*-branch of the *H*-curve. When H_{min} is reached, the story repeats itself and we jump to the *A*-branch of the *H*-curve, where we move slowly upwards until H_{max} is reached. We are now in the relaxation-oscillation limit cycle and we never again follow the unstable branch *C* of the *H*-curve.

The situation here may be described as a *non-equilibrium phase transition:* The quasi-stationary curve for the Br^- concentration is followed smoothly up to an upper critical Br^- concentration ("superheating"). Another branch is followed smoothly down to a lower critical Br^- concentration ("supercooling").

The problem is now reduced solely to find the motion along the *A* and the *B*-branch of the *H*-curve, which is an almost trivial one parameter problem. In such cases, the concentration variable can be separated from the time variable. Then, the time consumption on each branch or the so called *chronomal* (a word introduced in connection with steady state kinetics by J. A. Christiansen [20]) can be calculated by analytic or numerical integration.

Thus, using eqn. (23) in connection with the inverse of eqn. (29) and introducing a new dimensionless time be eqn. (59), we obtain immediately eqn. (60) for the chronomal:

$$\theta \equiv \tau/p = k_5 \cdot t \tag{59}$$

$$\theta = \int_{\zeta_{initial}}^{\zeta} \frac{dx}{U[H^{-1}(x)]-x} \tag{60}$$

The inverse function $\eta = H^{-1}(\zeta)$ is not unique. In eqn. (60) it has to be chosen for the appropriate branch (A or B) of the *H*-curve. For the numerical integration to be more feasible, it is better to integrate in terms of $\log_{10} x$:

$$\theta = \int_{\log_{10}\zeta_{initial}}^{\log_{10}\zeta} F(u)\, du \tag{61}$$

$$F(u) = \ln 10 \cdot [(1/10^u)\, U(H^{-1}(10^u)) - 1]^{-1} \tag{62}$$

Since $q \ll 1$ we can use $U = 1-\eta$ on branch *A* and $H = (1-\eta)\cdot\eta$ from which follows eqns. (63) and (64):

$$\eta_A = H_A^{-1}(\zeta_A) \simeq \tfrac{1}{2} \cdot (1 - \sqrt{1-4\zeta_A}) \tag{63}$$

$$U[H_A^{-1}(\zeta_A)] \simeq \tfrac{1}{2} + \tfrac{1}{2}\sqrt{1-4\zeta_A} \tag{64}$$

On the *B*-branch we can use the approximation (36) to which corresponds the inverse function (65):

$$\eta_B = H_B^{-1}(\zeta_B) \simeq (1/4q)[(\zeta_B+q) + \sqrt{(\zeta_B+q)^2 - 8q\zeta_B}] \tag{65}$$

and we can use eqn. (34) as an approximation for *U*. However, we actually used the full expression for *U* in the numerical integration.

The numerical integrations were performed by a HP-41C microprocessor using a standard Simpson rule routine.[21] The precision of the chronomal values was checked by varying the step length. The results are given in Table 1. Some of the θ-values are also indicated on the phase plane plot, Fig. 2. For branch A, $\zeta_{initial} = H_{min} = 5.828q$ and $\zeta_{final} = H_{max} = 0.25$. For branch B, the values are in inverse order.

The time spent on branch *A* for $q = 8.4\cdot10^{-6}$ is $\theta_A = 0.3863$. In comparison, the time spent on branch *B* for the same *q* is $\theta_B = 8.8069$. Therefore, we shall call branch *A* the "fast branch" and branch *B* the "slow branch". The total period of the relaxation-oscillations is given by eqn. (66):

Table 1. Time consumption on A- and B-Branch of *H*-curve for $q = 8.4\cdot10^{-6}$.

$\log_{10}\zeta$	Branch A θ	Branch B θ
−4.31016	0	$8.8069 = \theta_B$
−4.00	$5.1050\cdot10^{-5}$	7.9216
−3.50	$2.6737\cdot10^{-4}$	6.7004
−3.00	$9.5204\cdot10^{-4}$	5.5300
−2.50	$3.1234\cdot10^{-3}$	4.3728
−2.00	$1.0053\cdot10^{-3}$	3.2197
−1.50	$3.2631\cdot10^{-2}$	2.0678
−1.00	$1.1208\cdot10^{-1}$	0.9163
−0.70	–	0.2255
−0.60206	$3.8626\cdot10^{-1} = \theta_A$	0

$$\theta_p = \theta_A + \theta_B = 9.1932 \quad (66)$$

When q becomes even lower, H_{min} will be lower and both θ_A and θ_B will increase somewhat. Thus, the number corresponding to the dimensionless period will be greater than 9.1932 for smaller q and smaller for greater q than $8.4 \cdot 10^{-6}$. This,we have to remember when we want to discuss temperature dependence of the period of the BZ-reaction.

Fig. 4 shows the dimensionless concentration as a function of dimensionless time for the species Ce^{4+}, Br^- and $HBrO_2$. The concentrations are in logarithmic units and the curve form will be representative for the form of experimental curves of electromotive force of Pt and Br^- electrodes against a reference electrode (Nernst equation). The curves are remarkably similar to the experimental ones – though not in all details. They seem to be identical to the curves obtained by simulations on the full three-variable Oregonator.[12] It is interesting that even the sharp pulses of $HBrO_2$ seem to be well reproduced in spite of the fact that we used the quasi-stationary approximation for that species.

The mechanism of the pulses seems to be the following: Br^- is slowly consumed by reaction (1). Hereby, $HBrO_2$ is produced. This triggers the autocatalytic production of more $HBrO_2$ through process (3). At the same time Ce^{4+} is produced and Br^- consumption is rapidly increased due to the reaction between Br^- and $HBrO_2$ in process (2). All this happens during the very short pulse of $HBrO_2$ (branch A) which terminates due to reaction (4). The Br^- concentration is then restored by reaction (5) and the play starts all over again at the upper critical Br^- concentration, where Br^- consumption again becomes dominating by reaction (1).

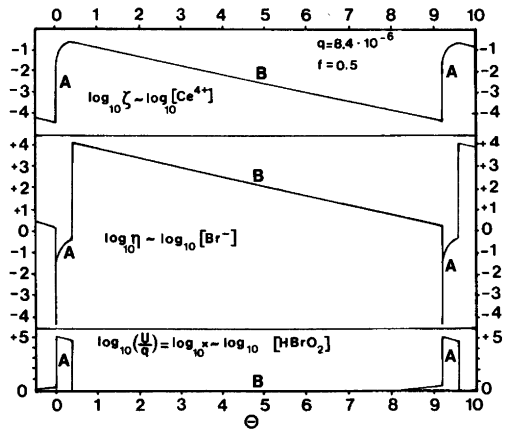

Fig. 4. The dimensionless concentrations of Ce^{4+}, Br^- and $HBrO_2$ as a function of dimensionless time for $q=8.4 \cdot 10^{-6}$ corresponding to the phase plane plot in Fig. 3.

COMPARISON WITH EXPERIMENTAL DATA

The main purpose of the paper has been to demonstrate, that the simplified flip-flop model of the BZ-system yields results almost identical to the solutions to the full Oregonator-model. Another question is whether the Oregonator itself is a sensible model, and if it is, whether the values of the parameters used in the Oregonator are correct. Since the present model represents a much more simple picture of the situation than the Oregonator-model, one might hope that the parameters (especially the q-parameter) could be judged with greater reliability.

First, it should be noticed that the rate constant of the fifth Oregonator reaction according to our model should be directly evaluable from the real time consumption for a period (t_p):

$$k_5 = \theta_p / t_p \quad (67)$$

θ_p is a *number* depending only on the parameter q. The smaller the value of q the lower is H_{min} (see eqn. (38)). Therefore, the chronomal integration paths are longer and θ_p increases. Fig. 5 shows that there is a linear relation between the dimensionless period and $\log_{10} q$. Integrations have only been performed up to $q=10^{-2}$ since some of the approximations used for the inverse H-function do not work well at high q-values. However, the extrapolated linear part of the curve is probably a good approximation anyway. The intersection point for $\theta_p=0$ corresponds well to the value $q_{max}=7.62 \cdot 10^{-2}$ at which the maximum of the H-curve coincides with the intersection point between the U-curve and the H-curve. According to the linear stability analysis, this is the highest value q can have for oscillations to occur. Just below q_{max}, the flip-flop model will still be valid if only $p \gg q$. Fig. 5 also shows that the time consumption on the A-branch with low

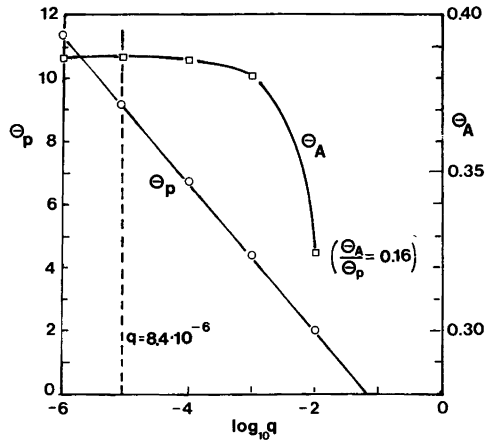

Fig. 5. The dimensionless period and the dimensionless time consumption on the *A*-branch as a function of the dimensionless parameter q. No oscillations are possible above $q_{max}=7.62\cdot10^{-2}$ where the maximum in the *H*-curve and the intersection between the *H*-curve and the *U*-curve coincide.

bromide concentration is approximately constant for very low q-values but decreases with increasing q, when q_{max} is approached. The fraction θ_A/θ_p increases drastically when q_{max} is approached, see Table 2.

Some experimental findings are listed in Table 3. FKN refers to values estimated from Figs. 1–6 in the paper of Field, Körös and Noyes.[11] The other values have been determined for this paper, since it was found important to elucidate the influence of BrO_3^- and the temperature on the period t_p. In the FKN-paper no measures were apparently taken to thermostat the reaction vessel and only two bromate concentrations were used. The experimental conditions for the present measurements differ from the ones in the FKN-paper only with regard to the thermostating and the following (insignificant) details: Here, $Ce(SO_4)_2\cdot4H_2O$ was used as a catalyst (Ferak, Berlin, analytical grade) instead of $Ce(NH_4)_2(NO_3)_5$. The ratio Ce^{4+}/Ce^{3+} was monitored with a Pt-electrode instead of a tungsten electrode. The Br^- concentration was monitored by a third-order $Ag/Ag_2S/AgBr$ electrode.[22] Finally, the reference electrode was a $Hg/HgSO_4$ electrode with saturated K_2SO_4 as salt bridge.

Table 2. Relative duration of period with low Br^- to total period.

q	θ_p	θ_A/θ_p
10^{-6}	11.322	0.0341
$8.4\cdot10^{-6}$	9.193	0.0420
10^{-4}	6.716	0.0575
10^{-3}	4.404	0.0864
10^{-2}	2.004	0.1619

It is evident from Table 3, that the ratio t_A/t_p is closer to 0.5 than the value 0.04 found theoretically for $q=8.4\cdot10^{-6}$, which is the q-value chosen in the Oregonator.[12,14] According to Fig. 5, the real q-value should therefore be in the region between 10^{-2} and $q_{max}=7.62\cdot10^{-2}$. The evidence from calculated values of k_5 points in the same direction. In Table 3, k_5 has been calculated from eqn. (67) using $\theta_p=9.19$ and 1, respectively. The former values (corresponding to $q=8.4\cdot10^{-6}$) are far too high, since the maximum value for k_5 at 25 °C should be 0.015 s^{-1} at saturating concentrations of BrM, see eqn. (9). For $\theta_p=1$ (corresponding to q around $2.5\cdot10^{-2}$), the values of k_5 are much better, although a few are too high. Therefore, q can be localized in the region between $2.5\cdot10^{-2}$ and $7.6\cdot10^{-2}$ by means of two independent criteria. If p can still be assumed to be of order of magnitude 10^2, the flip-flop model is still a reasonable approximation, though not as exact as before. Indeed, the "vertical" sections of the log c *vs.* time curves are found not to be completely vertical in the experiments. In other words, the "jumps" take some time.

In the experiments performed here, the inverse period was found to increase approximately as the square root of the bromate concentration, see Fig. 6. From the FKN-data, a dependence on the malonic acid concentration as [M] to the power 0.69 could be inferred. The "activation energy" ($E_p^{\neq}$) for $1/t_p$ was found to be practically independent on the level of bromate concentration, see Fig. 7, and equal to $8.8\cdot10^3\cdot R$. Assuming $E_p^{\neq}$ to be also independent of [M] (which is not proven by the present data), we may summarize the empirical findings in the formula (68):

$$1/t_p = k[BrO_3^-]^{0.48}\cdot[M]^{0.69}\cdot\exp[8.8\cdot10^3 (1/298.16-1/T)] \quad (68)$$

Eqn. (68) is valid for [Ce]=0.001 mol/dm^3. From the data in Table 3, we can see that the influence

Table 3. Experimental data for the Belousov-Zhabotinskii reaction.[a]

Temp. °C	$[BrO_3^-]$	[M] mol/dm^3	[Ce]	t_p s	t_A/t_p	$100/t_p$ s^{-1}	$(100/t_p)$ calcd.[b] s^{-1}	$(919/t_p)$ s^{-1}	Comments
	0.063	0.032	0.001	120	0.5	0.833	0.839	7.66	FKN,[c] Fig. 1
	0.063	0.013	0.001	215	0.4–0.6	0.465	0.451	4.27	FKN, Fig. 2
Ambient	0.063	0.500	0.001	18	0.5	5.55	5.59	51.0	FKN, Fig. 3
	0.016	0.130	0.001	93	0.2	1.075	1.143	9.88	FKN, Fig. 4
	0.063	0.130	0.005	66	0.5	1.515	–	13.9	FKN, Fig. 5
	0.063	0.130	0.0001	50	0.5	2.00	–	18.4	FKN, Fig. 6
15.0	0.040	0.0167	0.001	870	0.5	0.115	0.0910	–	Own experiments
	0.060			840	0.5	0.119	0.111	–	
	0.080			743	0.6	0.135	0.127	–	
	0.100			570	0.8	0.175	0.141	–	
	0.133			570	0.8	0.175	0.162	–	
20.0	0.060	0.0167	0.001	465	0.4	0.215	0.186	–	Own experiment
25.0	0.020	0.0167	0.001	450	0.5	0.222	0.182	2.04	Own experiments
	0.040			390	0.5	0.256	0.253	2.36	
	0.060			308	0.7	0.325	0.308	2.98	
	0.080			300	0.7	0.333	0.353	3.06	
	0.100			245	0.7	0.408	0.393	3.75	
	0.133			218	0.7	0.459	0.451	4.22	
	0.167			180	0.7	0.555	0.503	5.10	
30.0	0.060	0.0167	0.001	203	0.5	0.492	0.501	–	Own experiment
35.0	0.020	0.0167	0.001	240	0.3	0.417	0.473	–	Own experiments
	0.040			123	0.6	0.813	0.660	–	
	0.060			110	0.7	0.910	0.802	–	
	0.080			101	0.8	0.991	0.921	–	
	0.100			92	0.8	1.086	1.025	–	

[a] $[H_2SO_4]$=0.8 mol/dm^3. [b] Calculated from eqns. (68) and (69). [c] Field, Körös and Noyes, Ref. 11.

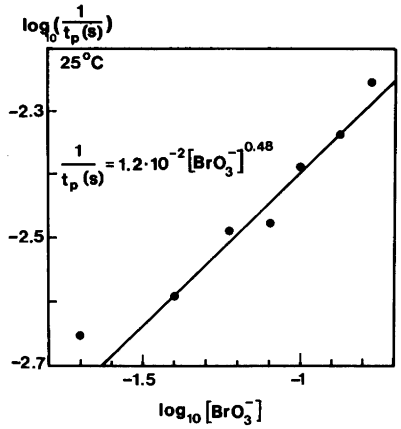

Fig. 6. Dependence of the inverse period found in experiments on bromate concentration.

of [Ce] is very small. Increasing [Ce] from 0.0001 to 0.0050 mol/dm^3 (50 fold), the inverse period decreases only 25 % (from 2 s^{-1} to 1.5 s^{-1}). The values of k differ somewhat for the FKN experiments and the present experiments:

$$k = \begin{cases} 0.34\ \text{s}^{-1} & \text{(FKN)} \\ 0.20\ \text{s}^{-1} & \text{(TSS)} \end{cases} \qquad (69)$$

The higher value found by FKN might be due to the exothermicity of the BZ-reaction and the apparent lack of thermostating in the FKN-investigation.

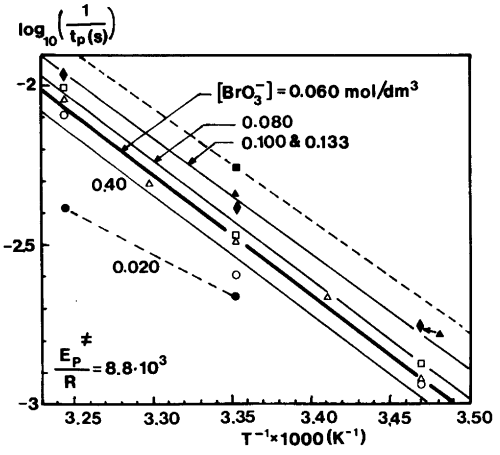

Fig. 7. Temperature dependence of inverse period at various levels of initial bromate concentrations. [BrO_3^-]: 0.020, 0.040, 0.060, 0.080, 0.100, 0.133, 0.167 mol/dm^3.

The dependence of $1/t_p$ on the bromate and the malonic acid concentration might well reflect the dependence of k_5 on the concentration of bromomalonic acid, see eqn. (7), indicating that we are somewhere in the transition region between the first and the zeroth order region of the Ce-catalyst in reaction (5).

In the section concerning the linear stability analysis it was mentioned, that the Hopf-estimate was able to produce an expression for $1/t_{\text{Hopf}}$ proportional to the square root of the bromate concentration, see eqn. (56). Since the constant in eqn. (58) is found to be $1.2\cdot10^{-2}$ (see Fig. 6), we should have:

$$\sqrt{k_1\cdot k_5(\text{mean})}/(2\pi\sqrt{1-\eta_o}) \simeq 1.2\cdot10^{-2} \qquad (70)$$

In Table 4, $1-\eta_o$ and values of $k_1\cdot k_5$(mean) calculated from eqn. (70) are listed for various values of q. Taking the value of k_1 from eqn. (57), we can calculate approximate values of k_5(mean). Those values are all much lower than the maximum value of k_5. Therefore, a mean value of the concentration of bromomalonic acid can be estimated from eqn. (8) for all values of q. We are not able to say something about the correct value of q by this method. However, the bromomalonic acid concentration appears to be unrealistically low for $q=8.4\cdot10^{-6}$. For $q=q_{\max}$, we still have [BrM] much less than [BrO_3^-] and [M]. If our conclusion from before (that we are in the transition region between first and zeroth order region for the Ce-catalyst) is correct, then the real values of [BrM] must be greater than the values in Table 4. Thus, if those greater values are used in eqn. (56) to calculate k_5, the values of $1/t_{\text{Hopf}}$ will be greater than the experimental values $1/t_p$. Most probably, the Hopf-periods will therefore be considerably shorter than the real periods of the relaxation-oscillations. Relaxation-oscillation is a highly nonlinear phenomenon, so it is no surprise that the (almost) linear Hopf limit cycle is a bad approximation. Nevertheless, the square root dependence on [BrO_3^-] of $1/t_{\text{Hopf}}$ as well as $1/t_p$ (exp) seems quite remarkable.

Finally, it is understandable that we obtain a straight line Arrhenius plot for the logarithm of the inverse period against $1/T$. Differentiating eqn. (67) we obtain:

$$E_p^{\neq}/R \equiv -\text{d}\ln(1/t_p)/\text{d}(1/T) = E_5^{\neq}/R - (\text{d}\ln\theta_p/\text{d}\ln q)\cdot E_q^{\neq}/R \qquad (71)$$

Table 4. Comparison between experimental data and the period of the Hopf limit cycle.

q	$1-\eta_o$	$k_1 \cdot k_5$(mean) [a] s^{-2} dm^3 mol^{-1}	k_5(mean) [b] s^{-1}	$[BrM]_{mean}$ [c] mol/dm^3
$8.4 \cdot 10^{-6}$	$2.05 \cdot 10^{-3}$	$1.16 \cdot 10^{-5}$	$5.53 \cdot 10^{-6}$	$3.95 \cdot 10^{-5}$
10^{-5}	$2.23 \cdot 10^{-3}$	$1.27 \cdot 10^{-5}$	$6.05 \cdot 10^{-6}$	$4.32 \cdot 10^{-5}$
10^{-4}	$7.05 \cdot 10^{-3}$	$4.00 \cdot 10^{-5}$	$1.905 \cdot 10^{-5}$	$1.36 \cdot 10^{-4}$
10^{-3}	$2.21 \cdot 10^{-2}$	$1.26 \cdot 10^{-4}$	$5.98 \cdot 10^{-5}$	$4.27 \cdot 10^{-4}$
10^{-2}	$6.83 \cdot 10^{-2}$	$3.88 \cdot 10^{-4}$	$1.85 \cdot 10^{-4}$	$1.32 \cdot 10^{-3}$
$2.5 \cdot 10^{-2}$	0.1057	$6.00 \cdot 10^{-4}$	$2.86 \cdot 10^{-4}$	$2.04 \cdot 10^{-3}$
$5 \cdot 10^{-2}$	0.1461	$8.29 \cdot 10^{-4}$	$3.95 \cdot 10^{-4}$	$2.82 \cdot 10^{-3}$
$7.62 \cdot 10^{-2}$ (q_{max})	0.1771	$1.007 \cdot 10^{-3}$	$4.80 \cdot 10^{-4}$	$3.43 \cdot 10^{-3}$ ($\ll 0.1$)

[a] Calculated from eqn. (56) with $t_{Hopf}=t_p$ (experimental), *i.e.* eqn. (70). [b] Assuming the value $k_1=2.1$ s^{-1} dm^3 mol^{-1}. [c] Calculated from eqn. (8).

We have used the following definition:

$$E_q^{\neq}/R \equiv -\mathrm{d} \ln q/\mathrm{d}(1/T) \tag{72}$$

The value of $\mathrm{d} \ln \theta_p/\mathrm{d} \ln q$ can be obtained straightaway from Fig. 4:

$$\mathrm{d} \ln \theta_p/\mathrm{d} \ln q = -2.33 \tag{73}$$

With $E_p^{\neq}/R=8.8 \cdot 10^3$ and $E_5^{\neq}/R=6.6 \cdot 10^3$ (see eqn. (10)), we therefore calculate the activation energy for q:

$$E_q^{\neq}/R = 9.4 \cdot 10^2 \tag{74}$$

The activation energy for q is about an order of magnitude smaller than the activation energy for reaction (5) and it is positive. Both of those features are physically possible, since q is equal to $2k_1k_4/k_2k_3$ (see eqn. (21)). The activation energy for q is therefore given as eqn. (75):

$$E_q^{\neq} = E_1^{\neq}+E_4^{\neq}-(E_2^{\neq}+E_3^{\neq}) \tag{75}$$

Since $E_q^{\neq}$ is a difference between the sum of two activation energies and the sum of two other activation energies, it should be small and it might be positive. The relations (74) and (75) should be tested by independent experiments in the future. For the present, we cannot push the comparison between the simple flip-flop version of the Oregonator and the real experiments any further. However, a considerable amount of clarification seems to have come with the investigation performed in this paper.

After the performance of the present calculations I have become aware, that J. J. Tyson [23–24] has made quite similar approximations to the relaxation-oscillations of the Oregonator (see especially Ref. 23 pp. 54–62). Tyson mostly stresses the importance of f (called h in his treatment). The parameter q is treated as a very small parameter and only the first terms in the power expansions in q of the various expressions are retained. However, it is hinted that q should perhaps be higher than $\sim 10^{-5}$. A value $q \sim 4 \cdot 10^{-3}$ is mentioned on p. 61. This value is based on comparison with the experimental value of the upper critical Br^--concentration. I would not trust the absolute amplitudes of the bromide electrode so much. As already mentioned by Field, Körös and Noyes,[11] this electrode is in fact part of the time outside of its thermodynamic range of stability (too low Br^--concentration).

Tyson also suggests, that p should rather be ~ 2 than ~ 300. For such a p-value there are significant deviations from simple flip-flop behaviour (Ref. 23, p. 64). However, the suggested value of p is estimated from the slope of the experimental $\log_{10}[Br^-]$ *vs.* time curve for the B-branch. In the experiments reported here, this curve is not a straight line and any estimation of p is very uncertain.

In a very recent paper by Edelson and Thomas,[25] a sensitivity analysis of the Oregonator has been performed. Those authors found that k_5 was of prime importance for the period time in complete agreement with the quasi-analytical results found in the present paper.

Acknowledgements. Stud.polyt. Finn Madsen is thanked for technical assistance with the experimental work. Dr. J. B. Jensen and Dr. P. Schack are thanked for useful discussions. One of the referees is thanked for particularly useful comments.

REFERENCES

1. Nicolis, G. and Prigogine, I. *Self-Organization in Nonequilibrium Systems* Wiley-Interscience, New York 1977.
2. Poincaré, H. *J. des Math. 3* (1881) 7.
3. Belousov, B. P. *Ref. Radiats Med. 1958, Medgiz, Moscow* (1959) 145.
4. Zhabotinskii, A. M. *Dokl. Akad. Nauk SSSR 157* (1964) 392.
5. Zhabotinskii, A. M. *Biofizika 9* (1964) 306.
6. Vavilin, V. A. and Zhabotinskii, A. M. *Kinet. Katal. 10* (1969) 83, 657.
7. Zaikin, A. N. and Zhabotinskii, A. M. *Nature (London) 225* (1970) 535.
8. Degn. H. *Nature (London) 213* (1967) 589.
9. Kasparek, G. J. and Bruice, T. C. *Inorg. Chem. 10* (1971) 382.
10. Busse, H. G. *J. Phys. Chem. 73* (1969) 750.
11. Field, R. J., Körös, E. and Noyes, R. M. *J. Am. Chem. Soc. 94* (1972) 8649.
12. Field, R. J. and Noyes, R. M. *J. Chem. Phys. 60* (1974) 1877.
13. Minorsky, N. *Nonlinear Problems in Physics and Engineering.* In Margenau, H. and Murphy, G. M., Eds., *The Mathematics of Physics and Chemistry,* Van-Nostrand-Reinhold, New York 1964, Vol. 2, Chapter 6, Section 11.
14. Murray, J. D. *Lectures on Nonlinear-Differential-Equation Models in Biology,* Clarendon Press, Oxford 1977. Sections 4.5–4.6.
15. Bornmann, L., Busse, H. and Hess, B. *Z. Naturforschung, Teil C 28* (1973) 514.
16. Noyes, R. M. and Jwo, J.-J. *J. Am. Chem. Soc. 97* (1975) 5431.
17. Jwo, J.-J. and Noyes, R. M. *J. Am. Chem. Soc. 97* (1975) 5422.
18. Netushil, A. *Theory of Automatic Control,* MIR Publishers, Moscow 1973, pp. 145–149.
19. Hopf, E. *Ber. Math.-Phys. Kl. Sächs. Akad. Wiss., Leipzig 94* (1942) 3.
20. Christiansen, J. A. *Z. Phys. Chem. 196* (1950) 12.
21. Hewlett-Packard, HP-41C "Math Pac" (Instruction book for mathematics module), 1982, pp. 25–28.
22. Jensen, J. B. *Anal. Chim. Acta 91* (1977) 149.
23. Tyson, J. J. *The Belousov-Zhabotinskii Reaction. Lecture Notes in Biomathematics Vol. 10.* Springer-Verlag, Berlin-Heidelberg-New York 1976, pp. 54–62.
24. Tyson, J. J. *Ann. N.Y. Acad. Sci. 316* (1979) 279.
25. Edelson, D. and Thomas, V. M. *J. Phys. Chem. 85* (1981) 1555.

Received November 8, 1982.

Acta Chemica Scandinavica A 37 (1983) 477–486

Microwave Spectrum, Conformational Equilibrium, Intramolecular Hydrogen Bonding and Centrifugal Distortion of 3-Mercaptopropionitrile

K.-M. MARSTOKK and HARALD MØLLENDAL

Department of Chemistry, The University of Oslo, P.O.Box 1033, Blindern, Oslo 3, Norway

The microwave spectra of 3-mercaptopropionitrile, CH_2SHCH_2CN, and one deuterated species, CH_2SDCH_2CN, have been investigated in the 12.0–18.0 GHz and 20.3–28.5 GHz spectral regions at −5 °C. Two conformations were assigned. The heavy atom *gauche* conformation has a very weak hydrogen bond formed between the mercapto group hydrogen atom and the cyano group. The other identified conformation, which has no hydrogen bond, has the heavy atoms in *anti* position and the mercapto group is *gauche* to the plane formed by the heavy atoms. The hydrogen-bonded conformation is the more stable of the two by 1.3(20) kJ/mol. The two conformations together make up at least 90 % of the gas at −5 °C.

The SCCC dihedral angle is 65(3)° from *syn*, and the C≡N and S–H bonds are about 7° from being parallel in the *gauche* form. The CCS angle is 114.0(15)° in this rotamer, while the CCS angle takes the value of 111.5(10)° in the *anti* conformation.

Five vibrationally excited states belonging to two different normal modes were assigned for the hydrogen-bonded *gauche* rotamer. The C–C torsional frequency was determined to be 118(20) cm^{-1} by relative intensity measurements in fair agreement with 97(10) cm^{-1} found using the quartic centrifugal distortion constants in a force field calculation. The C–S torsional frequency was found to be 178(30) cm^{-1} by relative intensity measurements.

Three vibrationally excited states of the C–C torsional mode was found for the *anti* conformation, and this frequency was determined to be 121(20) cm^{-1} by relative intensity measurements.

An extensive centrifugal analysis was carried out for the ground vibrational state of the *gauche* form and accurate values were determined for the quartic and four sextic centrifugal distortion constants.

Intramolecular hydrogen bonding of free molecules has in recent years been studied for many alcohols and amines. However, only few reports exist for thiols. In allyl mercaptan,[1] $CH_2=CHCH_2SH$, the preferred conformation has what could perhaps be called a very weak intramolecular hydrogen bond. In CH_2OHCH_2SH [2] the one identified conformation has an internal hydrogen bond with the hydroxyl group acting as proton donor and the mercapto group as proton acceptor. Two rotamers were identified for $CH_2NH_2CH_2SH$;[3] one of these, which is also the less stable, has a hydrogen bond with the −SH group being proton donor. Only one heavy-atom *anti* form without a hydrogen bond was assigned in the case of CH_2SHCH_2Cl.[3] This molecule possesses a weak, but crowded microwave spectrum and the stable coexistence of a hydrogen-bonded heavy-atom *gauche* conformation as well as a second *anti* form was by no means ruled out in this study.

3-Mercaptopropionitrile, CH_2SHCH_2CN, was chosen for study because hydrogen bonding might exist between the mercapto and the cyano groups. In addition, the existence of *anti* conformations without hydrogen bonds was considered to be quite probable, because the mercapto group is a weak proton donor. The three most probable conformations are shown in Fig. 1. The hydrogen-bonded heavy-atom *gauche* conforma-

0302-4377/83 $02.50

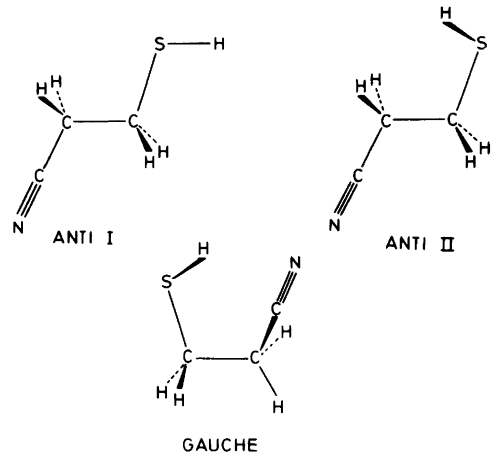

Fig. 1. Selected conformations of CH_2SHCH_2CN. The hydrogen-bonded heavy-atom *gauche* conformation was found to be more stable than *anti II* by 1.3(20) kJ/mol. *Anti I* was not identified and shown to be less stable than *anti II* by at least 1 kJ/mol.

tion as well as *anti II* were assigned. The former is more stable than the latter by 1.3(20) kJ/mol. *Anti I* was not identified and it is estimated to be at least 2.3 kJ/mol less stable than the *gauche* rotamer if it exists at all as a stable conformation of the molecule.

EXPERIMENTAL

CH_2SHCH_2CN was purchased from Parish Chemical Company, Orem, Utha, U.S.A. The sample was checked by gas chromatography and found to be pure. The deuterated species, CH_2SDCH_2CN, was produced by direct exchange by heavy water in the wave guide. In this manner, about 30 % deuteration was achieved. Measurements were made on a conventional microwave spectrometer in the 12.0–18.0 and 20.3–28.5 GHz spectral regions. A few spectral measurements were also made above 28.5 GHz. A pressure of roughly 20 Pa was used. The spectra were measured at about −5 °C. Lower temperatures could not be utilized due to insufficient vapour pressure of the compound.

RESULTS

Assignment of the ground vibrational state of anti II. The rotational constants of both *anti I* and *anti II* were predicted using structural parameters taken from related molecules (see later section). Both these conformations were predicted to be very nearly symmetrical tops with the asymmetry parameter $\kappa \approx -0.99$. The dipole moment components along the principal axes were predicted to be μ_a=2.8 D, μ_b=0.2 D and μ_c=0.0 D (for symmetry reasons) for *anti I*, and μ_a=2.4 D, μ_b=1.1 D and μ_c=0.6 D for *anti II*, respectively, using the bond-moment method.[4] Both these

Table 1. Microwave spectrum of the ground vibrational state of *anti II* of CH_2SHCH_2CN.

Transition	Observed frequency [a] (MHz)	Obs.−calc. frequency (MHz)	Centrifugal distortion (MHz)
$5_{0,5} \rightarrow 6_{0,6}$	17643.34	−0.02	−0.10
$5_{1,4} \rightarrow 6_{1,5}$	17790.42	0.03	−0.10
$5_{1,5} \rightarrow 6_{1,6}$	17500.54	0.06	−0.10
$6_{1,5} \rightarrow 7_{1,6}$	20755.13	0.01	−0.15
$6_{1,6} \rightarrow 7_{1,7}$	20416.93	0.04	−0.15
$7_{0,7} \rightarrow 8_{0,8}$	23521.36	−0.14	−0.23
$7_{1,6} \rightarrow 8_{1,7}$	23719.74	0.04	−0.23
$7_{1,7} \rightarrow 8_{1,8}$	23333.26	0.10	−0.23
$8_{0,8} \rightarrow 9_{0,9}$	26459.60	−0.06	−0.32
$8_{1,7} \rightarrow 9_{1,9}$	26249.21	−0.04	−0.32
$8_{2,6} \rightarrow 9_{2,7}$	26476.66	−0.09	−0.32
$9_{0,9} \rightarrow 10_{0,10}$	29397.12	0.02	−0.44
$9_{1,8} \rightarrow 10_{1,9}$	29648.40	0.11	−0.44
$9_{1,9} \rightarrow 10_{1,10}$	29165.17	0.02	−0.44

[a] ±0.10 MHz.

Table 2. Spectroscopic constants for *anti II* of CH_2SHCH_2CN.[a]

Vibrational state	Ground	First ex. C−C tors.	Second ex. C−C tors.
Number of transitions	15	13	6
rms (MHz) [b]	0.078	0.106	0.132
A_v (MHz)	24200.6(1107)	22514.5(2092)	22176.0(3643)
B_v (MHz)	1494.6723(54)	1495.9761(83)	1497.289(16)
C_v (MHz)	1446.3525(54)	1449.5251(77)	1452.709(15)
Δ_J (kHz) [c]	0.111(30)	0.034(45)	−0.156(85)
$I_a+I_b-I_c$ [u(nm)^2]	0.09587(96)	0.1162(21)	0.1243(37)

[a] Uncertainties represent one standard deviation. [b] rms is the root-mean square deviation. [c] Further quartic centrifugal distortion constants were kept at zero in the least squares fit.

conformations were thus predicted to have relatively strong, simple *R*-branch *a*-type spectra characterized by strong pile-ups of all the $K_{-1}\neq1$ transitions. These pile-ups should also have very rapid Stark effects. The $K_{-1}=1$ transitions, however, are placed almost symmetrical on the high and low frequency sides of the $K_{-1}\neq1$ pile-ups.

The observed microwave spectrum of CH_2SHCH_2CN was found to be very dense and of moderate intensity. The strongest lines observed had peak absorption coefficients of roughly 4×10^{-7} cm^{-1}. Despite its density, one series of *R*-branch *a*-type $K_{-1}\neq1$ pile-ups was readily assigned due to their strengths, spectral positions, and rapid Stark effects. The $K_{-1}=1$ transitions were then found after some searching and identified by their spectral positions and Stark effects. The spectrum is shown in Table 1.* Only the well-resolved low-K_{-1} lines have been included in this table. The derived spectroscopic constants are shown in Table 2.

A search was made for *b*- and *c*-type lines, but none was identified. This was expected, because both μ_b and μ_c were predicted to be much smaller than μ_a by the bond-moment method as discussed above. Very low intensities are thus predicted for the *b*- and *c*-type lines.

There is no great difference between the predicted values of the rotational constants for each of the conformations *anti I* and *anti II*. However, *anti I* should have $\mu_c=0$ D, while μ_c of *anti II* is different from zero. Unfortunately, attempts to resolve the Stark effect of several $K_{-1}=1$ transitions and thereby determine the dipole moment were futile because of the absolute weakness of these transitions. No determination of the dipole moment could thus be made.

Another method which may be used to differentiate between *anti I* and *anti II* is based on the value of $I_a+I_b-I_c$. The calculated value for *anti I*, which has two out-of-plane hydrogen atoms, is 0.0642 u(nm)^2 while 0.0887 u(nm)^2 is computed for *anti II*. (See structure section below). The latter is quite close to the observed value of 0.09587(96) u(nm)^2 as shown in Table 2. Moreover, the study of the deuterated species, CH_2SDCH_2CN, as discussed below also strongly indicates that the assigned *anti* form is undoubtedly *anti II* and not *anti I*.

There are two identical forms of *anti II*. The mercapto group proton might be expected to tunnel between these two identical forms. The *c*-type transitions would then be expected to occur between (+) and (−)-states with resulting large splittings, whereas the *a*- and *b*-type transitions would be of the (+)→(+) or (−)→(−) type. These last-mentioned transitions should then have small splittings which would not perhaps be resolved. Such spectral features have been observed for other thiols, *e.g.* ethyl mercaptan,[5,6] isopropyl mercaptan,[7] propargyl mercaptan [8,9] and in *anti-gauche* propyl mercaptan.[10–12] However, in the case of *anti II*, no splittings were observed for the assigned *a*-type transitions. The $K_{-1}=1$ lines were especially scrutinized for this effect, however, with negative result. It is concluded that these lines are split by 0.6 MHz at most. This resembles the findings for propyl mercaptan [11,12] where only a

* The complete microwave spectra of CH_2SHCH_2CN and CH_2SDCH_2CN are available from the authors upon request or from the Molecular Spectra Data Center, National Bureau of Standards, Bld. 221, Rno. B 265, Washington D.C. 20234, USA, where they have been deposited.

few *a*-type lines were seen to be split by a small amount, due to accidental degeneracy between the (+) and (−) states, whereas ethyl mercaptan,[5,6] isopropyl mercaptan [7] and propargyl mercaptan [8,9] typically displayed splittings of a few megahertz for the majority of this kind of transition.

Vibrationally excited states of anti II. Three vibrationally excited states presumably belonging to successively excited states of the C−C torsional mode were assigned for *anti II*. The spectroscopic constants of the first and the second excited states are shown in Table 2. Only the high $K_{-1}\neq1$ pile-ups were identified for the third excited state of this motion and $B+C\approx2954.98(10)$ MHz was determined using the peak absorption frequencies of the pile-ups. The fourth excited state of this fundamental was tentatively assigned. This state was found to have $B+C\approx2959.45(20)$ MHz. No splittings were observed for any of these excited state transitions.

The B and C rotational constants increase almost linearly with increasing excitation as can be seen from Table 2. The values of $I_a+I_b-I_c$ also increase upon excitation. This is typical for a harmonic mode. Relative intensity measurements were made for this C−C torsional mode following the prescription of Esbitt and Wilson.[13] A value of 121(20) cm^{-1} was found.

As will be shown below, a C−S torsional frequency of 178(30) cm^{-1} was found for the hydrogen-bonded heavy-atom *gauche* conformation. Searches were made for the corresponding excited state of *anti II* which was expected to have roughly 1/3 of the intensity of the ground state lines. No identifications could be made for this excited state. One explanation for this could be that the rotational transitions of this state are split which would result in intensities of only about 1/6 of the corresponding ground state lines. Such weak lines would be very difficult to identify in this dense spectrum. This is especially true for the $K_{-1}=1$ transitions. The first excited state lines of the C−S torsion are furthermore expected to lie close to their ground state counterparts since little reduced mass is involved in this mode. Overlapping by ground state lines is thus considered to be quite likely.

Assignment of the ground vibrational state of the gauche *conformation.* A large number of unassigned lines remained in the spectrum after *anti II* had been assigned. Search for the hydrogen-bonded *gauche* rotamer was therefore made. The dipole moment components of this conformation were predicted using the bond-moment method [4] as $\mu_a=1.3$ D, $\mu_b=3.6$ D and $\mu_c=0.3$ D, respectively. Searches were then initiated for the $K_{-1}=1\rightarrow2$ and $K_{-1}=2\rightarrow3$ *b*-type *Q*-branch series whose high-*J* members are among the strongest lines of the spectrum. The low *J* members of these series were not so strong that well-resolved Stark effects were observed. The initial assignments were made for the $K_{-1}=1\rightarrow2$ *Q*-branch series in the 12−18 GHz spectral region and readily extended to the $K_{-1}=2\rightarrow3$ and $K_{-1}=3\rightarrow4$ *Q*-branch series. The *b*-type low *J* *R*-branch lines were then found after some searching. None of these transitions displayed well-resolved Stark splitting due to insufficient intensities and crowded neighbourhoods. Medium *J*-, *P*- and *R*-branch lines which are of moderate intensities were then predicted and found using a trial and error procedure. Spectral positions of high *J*-, *P*- and *R*-branch lines, none of which are strong, were now predicted and identified by their spectral positions and fit to a centrifugally distorted asymmetric rotor. Their very rapid Stark effects produced by a non-zero value of μ_a were also a considerable aid for their assignments. In this manner, *P*-branch lines up to the coalescing $70_{29,41}\rightarrow69_{30,40}$ and $70_{29,42}\rightarrow69_{30,39}$ pair of transitions, and *R*-branch lines including the $75_{28,47}\rightarrow76_{27,50}$ and $75_{28,48}\rightarrow76_{27,49}$ pair were identified. *P*- and *R*-branch lines with even higher *J* quantum numbers were searched for but not identified presumably because of too low intensities. A total of about 290 *b*-type transitions were assigned in this manner for the ground state. 50 selected transitions are shown in Table 3. 251 transitions, of which 35 are *Q*-branch and 216 *P*- or *R*-branch, were used to determine the spectroscopic constants shown in Table 4.

These constants predict the frequencies of *a*- and *c*-type transitions very accurately. However, no such transitions were identified with certainty, presumably because μ_a and μ_c are too small and thus produce lines of insufficient intensities.

The Stark effects of many low and medium *J*-lines were studied in an attempt to determine the dipole moment of the *gauche* conformation. Unfortunately, no lines with adequately resolved Stark effects were found, and thus no dipole moment could be measured.

Vibrationally excited states of the gauche *con-*

Table 3. Selected transitions for the ground vibrational state of the hydrogen-bonded *gauche* conformation.

Transition	Observed frequency[a] (MHz)	Obs.−calc. frequency (MHz)	Centrifugal distortion	
			Total (MHz)	Sextic (MHz)
$1_{1,0} \rightarrow 2_{2,1}$	25280.65	0.11	−0.40	
$1_{1,1} \rightarrow 2_{2,0}$	25752.77	−0.06	−0.42	
$2_{0,2} \rightarrow 3_{1,3}$	17357.76	0.18	0.06	
$4_{1,4} \rightarrow 5_{0,5}$	17623.37	−0.12	−1.41	
$5_{0,5} \rightarrow 6_{1,6}$	27635.72	−0.03	−0.08	
$5_{2,3} \rightarrow 5_{3,2}$	27316.11	−0.06	−0.14	−0.01
$6_{1,6} \rightarrow 6_{2,5}$	21615.52	−0.14	−0.08	−0.01
$7_{2,5} \rightarrow 7_{3,4}$	26012.46	−0.03	3.38	−0.02
$7_{0,7} \rightarrow 7_{1,6}$	13968.53	0.01	−3.39	
$7_{1,7} \rightarrow 7_{2,6}$	23260.86	−0.08	−0.50	−0.01
$7_{2,6} \rightarrow 8_{1,7}$	25042.81	−0.02	−9.41	
$8_{0,8} \rightarrow 8_{1,7}$	16808.28	−0.02	−5.94	
$8_{1,7} \rightarrow 8_{2,6}$	14237.67	0.21	1.01	−0.01
$9_{1,9} \rightarrow 9_{2,8}$	27245.45	−0.16	−2.71	−0.02
$9_{2,7} \rightarrow 9_{3,6}$	24030.80	0.05	8.44	−0.04
$10_{1,9} \rightarrow 10_{2,8}$	16111.87	0.03	−3.80	−0.02
$10_{2,8} \rightarrow 10_{3,7}$	22996.13	0.15	10.82	−0.06
$11_{1,10} \rightarrow 11_{2,9}$	17823.35	−0.05	−8.92	−0.02
$11_{2,9} \rightarrow 11_{3,8}$	22099.09	−0.14	12.30	−0.08
$12_{2,10} \rightarrow 12_{3,9}$	21471.45	0.01	12.12	−0.10
$12_{4,8} \rightarrow 13_{3,11}$	17174.50	−0.08	−22.32	−0.02
$13_{2,11} \rightarrow 13_{3,10}$	21229.77	0.07	9.44	−0.12
$14_{1,13} \rightarrow 14_{2,12}$	26111.66	0.06	−37.65	−0.01
$15_{2,13} \rightarrow 15_{3,12}$	22260.50	−0.05	−6.67	−0.13
$17_{2,15} \rightarrow 17_{3,14}$	25666.30	0.09	−41.68	−0.09
$18_{3,15} \rightarrow 18_{4,14}$	28310.93	0.12	39.75	−0.66
$18_{8,10} \rightarrow 17_{9,9}$	15599.27	−0.03	−5.89	0.03
$18_{8,11} \rightarrow 17_{9,8}$	15599.27	−0.10	−5.90	0.03
$19_{3,16} \rightarrow 19_{4,15}$	28045.20	−0.03	25.33	−0.68
$20_{3,17} \rightarrow 20_{4,16}$	28368.85	0.08	2.00	−0.65
$23_{8,15} \rightarrow 24_{7,18}$	23835.29	−0.06	−190.24	0.32
$23_{8,16} \rightarrow 24_{7,17}$	23965.66	−0.04	−195.33	0.37
$27_{12,15} \rightarrow 26_{13,14}$	20579.66	0.08	4.02	0.08
$27_{12,16} \rightarrow 26_{13,13}$	20579.66	0.08	4.02	0.08
$36_{16,20} \rightarrow 35_{17,19}$	25577.29	−0.01	36.44	0.04
$36_{16,21} \rightarrow 35_{17,18}$	25577.29	−0.01	36.44	0.04
$44_{19,25} \rightarrow 43_{20,24}$	23812.05	0.00	217.69	−1.94
$44_{19,26} \rightarrow 43_{20,23}$	23812.05	0.00	217.69	−1.94
$49_{18,31} \rightarrow 50_{17,34}$	25957.06	0.03	−1387.27	13.31
$49_{18,32} \rightarrow 50_{17,33}$	25957.06	0.03	−1387.27	13.31
$54_{23,31} \rightarrow 53_{24,30}$	24549.88	0.00	538.39	−7.87
$54_{23,32} \rightarrow 53_{24,29}$	24549.88	0.00	538.39	−7.87
$61_{23,38} \rightarrow 62_{22,41}$	22037.48	0.01	−2391.80	37.92
$61_{23,39} \rightarrow 62_{22,40}$	22037.48	0.01	−2391.80	37.92
$66_{28,38} \rightarrow 65_{29,37}$	27879.64	0.13	1075.13	−23.84
$66_{28,39} \rightarrow 65_{29,36}$	27879.64	0.13	1075.13	−23.84
$72_{27,45} \rightarrow 73_{26,48}$	24785.28	0.09	−3866.73	84.85
$72_{27,46} \rightarrow 73_{26,47}$	24785.28	0.09	−3866.73	84.85
$75_{28,47} \rightarrow 76_{27,50}$	26481.54	−0.02	−4391.67	103.70
$75_{28,48} \rightarrow 76_{27,49}$	26481.54	−0.02	−4391.67	103.70

[a] ±0.10 MHz.

Table 4. Spectroscopic constants of the ground vibrational state of the *gauche* conformation of CH_2SHCH_2CN and CH_2SDCH_2CN.[a]

Species	CH_2SHCH_2CN	CH_2SDCH_2CN
Number of transitions	251	31
rms (MHz) [b]	0.076	0.115
A_v (MHz)	7773.9116(41)	7521.020(24)
B_v (MHz)	2404.9015(13)	2401.280(19)
C_v (MHz)	1959.2031(15)	1941.588(18)
Δ_J (kHz)	2.4141(44)	2.55(24)
Δ_{JK} (kHz)	−17.855(34)	−17.50(18)
Δ_K (kHz)	48.232(18)	52.3(27)
δ_J (kHz)	0.7696(23)	0.7473(67)
δ_K (kHz)	3.502(79)	4.44(23)
H_J (Hz)	−0.0475(49)	– [d]
H_{JK} (Hz)	−0.865(86)	– [d]
H_{KJ} (Hz)	−1.137(60)	– [d]
H_K (Hz) [c]	1.070(43)	– [d]

[a,b] Comments as for Table 2. [c] Further sextic constants preset at zero. [d] Sextic constants preset at zero.

Table 5. Spectroscopic constants of vibrationally excited states of the *gauche* conformation of CH_2SHCH_2CN.[a]

rms (MHz) [b]	First ex. C−C tors. 0.15	Second ex. C−C tors. 0.19	Third ex. C−C tors. 0.69	First ex. C−S tors. 0.15	Comb. C−C and C−S tors. 0.01
A_v (MHz)	7852.945(24)	7933.925(63)	8015.04(42)	7768.266(45)	7846.000(11)
B_v (MHz)	2392.848(14)	2381.217(38)	2369.42(19)	2405.846(30)	2393.246(14)
C_v (MHz)	1952.030(13)	1944.993(35)	1937.66(18)	1959.788(31)	1952.915(20)
Δ_J (kHz)	2.30(16)	2.83(45)	[c]	1.30(37)	[c]
Δ_{JK} (kHz)	−18.80(41)	−18.90(39)	[c]	−17.06(24)	[c]
Δ_K (kHz)	64.9(50)	38.6(72)	[c]	48.3(33)	[c]
δ_J (kHz)	0.723(10)	0.731(14)	[c]	0.778(11)	[c]
δ_K (kHz)	4.27(51)	5.07(55)	[c]	3.04(37)	[c]
No. of Q-branch lines	28	21	9	25	8
No. of R-branch lines	9	4	2	3	1
J_{max} Q-branch	19	18	18	20	19
J_{max} R-branch	8	7	7	7	7

[a,b] Comments as for Table 2. [c] Fitted, but too inaccurate to be reported.

formation. Five vibrationally excited states were assigned for this conformation as shown in Table 5. The most intense of these vibrational satellites is the first excited state of the C−C torsional mode which has about 50 % of the ground state intensity. Low J,R-branch and low medium J,Q-branch lines were assigned for this mode as seen in Table 5. Many attempts were made to assign the medium and high J,P- and R-branch lines for this excited state in the same manner as described for the ground vibrational state. However, these attempts were unsuccessful presumably because P- and R-branch lines with J between 10 and 25 are quite weak and also overlap with other lines in many cases.

Relative intensity measurements yielded 118(20) cm^{-1} for this C−C torsional fundamental. This is close to 121(20) cm^{-1} found for the *anti II* conformation as expected.

A rough force field (Table 6) was constructed

Table 6. Assumed diagonal force field,[a] centrifugal distortion constants and torsional frequency for the heavy-atom *gauche* conformation of CH_2SHCH_2CN.

Stretching (10^2 N m^{-1})			
C≡N	17.4	H_2C-CH_2	4.6
C–CN	5.5	C–S	1.7
S–H	3.5	C–H	4.8
Bending (aJ rad^{-2})			
S–C–C	1.0	C–S–H	0.58
S–C–H	0.76	H–C–CN	0.67
C–C–C	1.1	C–C–H	0.61
H–C–H	0.50	C–C≡N	0.16
Torsion (aJ rad^{-2})			
C–S	0.25		
C–C	0.270 [b]		

Centrifugal distortion constants (kHz)	Obs.	Calc.
Δ_J	2.414	2.664
Δ_K	−17.86	−17.65
Δ_K	48.23	48.23
δ_J	0.7696	0.7796
δ_K	3.50	4.30

[a] See text. [b] Obtained from least-squares fit yielding a C–C torsional frequency of 97 cm^{-1} as compared to 118(20) cm^{-1} found by relative intensity measurements.

for *gauche* CH_2SHCH_2CN in order to calculate the torsional frequency utilizing the quartic centrifugal distortion contants in the manner described previously.[14]

A value of 97 cm^{-1} was found as compared to 118(20) cm^{-1} obtained by relative intensity measurements. It is difficult to estimate uncertainty limits with this method, but ±10 cm^{-1} appears reasonable. All quartic centrifugal distortion constants, with the exception of δ_K, are well reproduced as can be seen in Table 6.

No similar calculation could be made for *anti II* because no accurate centrifugal distortion constants are available.

Attempts were also made to reproduce the changes of the rotational constants upon excitation by opening up the SCCC dihedral angle by 3° with the other structural parameters kept fixed. The calculated values were ΔA=+165.83 MHz, ΔB=−51.59 MHz and ΔC=−19.94 MHz as compared to ΔA=+79.04 MHz, ΔB=−12.06 MHz and ΔC=−7.17 MHz, respectively, found experimentally (Tables 4 and 5). The agreement is not very good. This presumably means that the C–C torsional motion is considerably more complex than just a simple rotation about the central C–C bond. Further torsional motions or bending vibrations seem to be involved.

The second and third excited states of the heavy-atom torsional motion were also assigned as shown in Table 5. The successive changes of the rotational constants upon progressive excitation are very constant. This is typical for a harmonic mode.

Another excited state having approximately one third of the intensity of the ground state was also identified. Relative intensity measurements [13] yielded 178(30) cm^{-1} for this fundamental. This state is assigned as the first excited state of C–S torsional motion because the changes of the rotational constants upon excitation are small as compared to the C–C torsional motion (Tables 4 and 5). Moreover, its frequency of 178(30) cm^{-1} is typical for the C–S torsion of thiols.[15] Splitting of any of its lines was searched for, but not observed. Attempts to assign the second excited state of this normal mode were futile.

The fifth excited state assigned (Table 5) is presumably a combinational mode where both the C–C and C–S torsional modes simultaneously are excited, because its rotational constants are very close to what is found when both the changes of the rotational constants upon excitation of each of the C–C and C–S torsions are added to the ground vibrational state rotational constants.

Further excited vibrational states were searched for. In particular, a search was made for the first excited state of the heavy atom bending mode. In the isoelectronic compound 2-chloro propionitrile [16] the lowest of these modes is found at 307 cm^{-1}. The Boltzmann factor at −5 °C would then be 0.19 for the first excited state of this bending mode of 2-chloro propionitrile. It is likely that a similar situation exists for 3-mercaptopropionitrile. However, no excited state of about 20 % of the ground state intensity could be identified.

Searches for further conformations. A total of about 600 transitions making up about 400 well-resolved lines were assigned for the two

conformations. All "strong" lines, *i.e.* lines with peak absorption coefficients larger than roughly 1×10^{-7} cm^{-1}, were assigned. The great majority of "medium" intensity (peak absorption coefficients between approximately 5×10^{-8} and 1×10^{-7} cm^{-1}) were also identified. Many "weak" lines with absorption coefficients less than about 5×10^{-8} cm^{-1} were also assigned. Stark effect studies were made for the remaining unassigned lines of medium intensity, but no resolution was seen.

In particular, attempts were made to find the coalescing $K_{-1}\neq1$ pile-ups of the hypothetical *anti I* conformation. However, no assignments could be made.

There are probably small differences between the rotational constants of the *anti II* and the hypothetical *anti I* conformations. If the $K_{-1}\neq1$ pile-ups were well-separated for these two rotamers, identification would probably have been made provided that the intensities of the *anti I* pile-ups were 20 % or more of the corresponding transitions of *anti II*. If overlap does occur, the presence of *anti I* would probably have been noted provided that the concentration of this rotamer were 1/3 of that of *anti II*. *Anti I*, which has half the statistical weight of *anti II*, is then conservatively estimated to be at least 1.0 kJ/mol less stable than the latter assigned conformation if it exists at all as a stable conformation.

3-Mercaptopropionitrile is not the only thiol which prefers the *gauche* form for the HSCC dihedral angle. Ethyl mercaptan has the *gauche* form more stable than *anti* by about 1.7 kJ/mol.[5] The *anti–gauche* conformation of propyl mercaptan is also more stable than the *anti–anti* rotamer by 1.8 kJ/mol.[12]

The majority of the unassigned lines of the spectrum are believed to belong to unidentified vibrationally excited states of the heavy-atom hydrogen-bonded *gauche* conformation. Presumably, *anti II* and the *gauche* form together make up at least 90 % of the gaseous composition of CH_2SHCH_2CN at −5 °C.

Energy differences between the heavy-atom gauche *and* anti II *conformations*. Relative intensity measurements were made following the procedure of Ref. 17 in order to determine the energy difference between the two conformers. Strong lines of the heavy-atom *gauche* conformation lying relatively close to $K_{-1}\neq1$-lines of *anti II* were selected. The lines were checked for overlap with other lines or Stark components and were presumably not significantly contaminated by such effects. Unfortunately, the dipole moments of the two conformations were not available, and the bond–moment values cited above were assumed in order to derive an energy difference. ΔH°_3 was thus found to be 1.3(20) kJ/mol with the hydrogen-bonded form as the more stable. Uncertainties resulting from the fact that the principal axes dipole moment components have to be assumed, are included in the above uncertainty limit of 2.0 kJ/mol.

Deuterated species. The deuterated species, CH_2SDCH_2CN, was studied to obtain information about the mercapto group hydrogen position. 31 transitions were readily assigned for the hydrogen-bonded conformation and the spectroscopic constants shown in Table 4 were determined. Kraitchman's coordinates [18] were then calculated for the mercapto group hydrogen atom. They are reported in Table 7.

In the case of *anti II*, only the $K_{-1}\neq1$ pile-ups were assigned and $B+C\approx2895.55(5)$ MHz was determined. The $K_{-1}=1$-lines were too weak to be assigned with certainty.

The changes of $B+C$ upon deuteration were calculated to be −65.74 MHz for *anti I* and −42.77 MHz for *anti II* using the plausible structure discussed later. The observed value was −45.47 MHz. Deuteration thus clearly shows that assignment has been made for *anti II* and not for *anti I*.

^{34}S is present in about 4 % concentration. The spectrum is relatively weak and dense, and assignment of this isotopic species of both rotamers would therefore be very difficult and no attempts were made to this end.

Structure of the two conformations. Only two isotopic species were studied for the two rotamers. A complete geometrical structure cannot, therefore, be determined for each of the two conformations. A selection of geometrical parameters to be fitted must be made. The S−H bond length, the CCS angle and the SCCC dihedral angle were fitted for the heavy-atom hydrogen-bonded *gauche* conformation, while only the CCS angle was fitted for *anti II*. The remaining bond lengths and angles were kept fixed as shown in Table 7. These structural parameters were selected from recent accurate studies. The CCN angle was assumed to be 180°, although it is realized that small deviations from linearity have

Table 7. Plausible structural parameters [a] (bond lengths in *pm*, angles in *degrees*) of *anti II* and of the hydrogen-bonded *gauche* conformation of CH_2SHCH_2CN.

Assumed structural parameters common for both conformations

C–S	182.0	∠CCC	110.5
C–C	153,0	∠CSH	96.2
C–CN	147.4	∠CCN	180.00
C≡N	115.7	∠CCH	109.48
C–H	109.3	∠HCH	109.48
		∠HSCC	120.00 from *anti*

Fitted structural parameters

Conformation	*Gauche*	*Anti II*
S–H	137(10)	132.2 [b]
∠CCS	114.0(15)	111.5(10)
∠SCCC from *syn*	65(3)	180.00 [b]

Hydrogen bond parameters of the *gauche* conformation

$H\cdots C_N$	267	H···N	301
$S\cdots C_N$	324	S···N	394
∠S–H···N	124	∠S–H···C	101
∠S–H,CN	7		

Sum of van der Waals radii [c]

H···C	290 [d]	H···N	270
S···C	355 [d]	S···N	335

Rotational constants (MHz) of the *gauche* conformation

	CH_2SHCH_2CN			CH_2SDCH_2CN		
	Obs.	Obs.-calc.	Diff (%)	Obs.	Obs.-calc.	Diff(%)
A	7773.9116	5.04	0.06	7521.020	−4.17	0.06
B	2404.9015	5.18	0.22	2401.280	6.84	0.24
C	1959.2031	3.57	0.18	1941.588	4.69	0.24

Kraitchman's coordinates of mercapto group hydrogen atom of the *gauche* form

	|*a*|	|*b*|	|*c*|
From rotational constants	48.31(15)	145.448(53)	29.23(27)
From plausible structure	65.1	144.4	19.6

Rotational constants (MHz) of the *anti II* conformation of CH_2SHCH_2CN

	Obs.	Obs.-calc.	Diff(%)
A	24200.6(1107)	−889.8	3.7
B	1494.6723(54)	−1.30	0.08
C	1446.3525(54)	−1.28	0.09

B+*C* for *anti II* of CH_2SDCH_2CN

	Obs.	Calc.
B+*C*	2895.55(5)	2900.83

[a] See text. [b] Not fitted, held fixed. [c] Taken from Ref. 21. [d] van der Waals radius of carbon assumed to be 170 pm as for aromatic carbon atoms.

been found for several molecules containing the cyano groups.

The CCS angle of *anti II* was fitted in steps of 0.5°. The A rotational constant is much less accurately determined than B and C, and the fit was made using only these two constants. A value of 111.5(10)° was found for the CCS angle (see Table 7).

The SCCC angle of the heavy-atom *gauche* conformation was fitted in steps of 1° and the CCS angle in steps of 0.5°. The best values were found to be 65(3)° from *syn* and 114.0(15)°, respectively, for these two angles (Table 7).

A rough reproduction of the Kraitchmann coordinates of the mercapto group hydrogen atom shown in Table 7 was attempted by varying the S–H bond length. However, a reproduction of the *a*-axis coordinate would have required an abnormally long S–H bond length as well as an unrealistically small CSH angle.

A similar situation was found for $CH_2OHCH_2NH_2$.[19] This anomaly was explained [20] as resulting from a shortening of the non-bonded O···N distance upon deuteration of the hydroxyl hydrogen atom. It seems that a similar situation exists for 3-mercaptopropionitrile. The S–H bond length becomes very uncertain as a result of this effect.

DISCUSSION

The present work demonstrates that the mercapto group is capable of forming some sort of weak attractive interaction to the cyano group leaving the heavy-atom *gauche* conformation more stable than *anti II* by 1.3(20) kJ/mol. This stabilization is presumably mainly electrostatic in origin, as the S–H and C≡N bonds are about 7° from being parallel (Table 7) which is ideal for dipole–dipole interaction. Covalent forces may play a small role in stabilizing the *gauche* conformation. If the van der Waals radius of the carbon atom of the cyano group is taken to be 170 pm, which is the value often quoted for aromatic carbon atoms,[21] the non-bonded H···C distance is about 20 pm shorter than the sum of the van der Waals radii of hydrogen and carbon. Likewise, the S···C distance is shorter than the sum of the van der Waals radii [21] by about 30 pm.

No explanation can be offered for the finding that *anti II* is more stable than *anti I* by at least 1 kJ/mol. It should be pointed out, however, that molecules of the type $X-CH_2SH$ have a propensity for forming stable *gauche* rotameric forms. This has been found for ethyl mercaptan,[5] propyl mercaptan [10–12] and propargyl mercaptan [8,9] in addition to the title compound.

REFERENCES

1. Sastry, K. V. L. N., Dass, S. C., Brooks, W. V. F. and Bhaumik, A. *J. Mol. Spectrosc. 31* (1969) 54.
2. Sung, E. M. and Harmony, M. D. *J. Am. Chem. Soc. 99* (1977) 5603.
3. Nandi, R. N., Boland, M. F. and Harmony, M. D. *J. Mol. Spectrosc. 92* (1982) 419.
4. Smyth, C. P. *Dielectric Behaviour and Structure,* McGraw-Hill, New York 1955, p. 244.
5. Schmidt, R. E. and Quade, C. R. *J. Chem. Phys. 62* (1975) 3864.
6. Nakagawa, J., Kuwada, K. and Hayashi, M. *Bull. Chem. Soc. Jpn. 49* (1976) 3420.
7. Griffiths, J. H. and Boggs, J. E. *J. Mol. Spectrosc. 56* (1975) 257.
8. Bolton, K. and Sheridan, J. *Spectrochim. Acta A 26* (1970) 1001.
9. Scappini, F., Mäder, H. and Sheridan, J. *Z. Naturforsch. A 28* (1973) 77.
10. Ohashi, O., Ohnishi, M., Tagui, A., Sakaizumi, T. and Yamaguchi, I. *Bull. Chem. Soc. Jpn. 50* (1977) 1749.
11. Nakagawa, J. and Hayashi, M. *Chem. Lett.* (1979) 1321.
12. Nakagawa, J. and Hayashi, M. *J. Mol. Spectrosc. 85* (1981) 327.
13. Esbitt, A. S. and Wilson, E. B., Jr. *Rev. Sci. Instrum. 34* (1963) 901.
14. Braathen, O.-A., Marstokk, K.-M. and Møllendal, H. *Acta Chem. Scand. A 36* (1982) 173.
15. Inagaki, F., Harada, I. and Shimanouchi, T. *J. Mol. Spectrosc. 46* (1973) 381.
16. Klæboe, P. and Grundnes, J. *Spectrochim. Acta A 24* (1968) 1905.
17. Wilson, E. B., *et al. To be published.*
18. Kraitchman, J. *Am. J. Phys. 21* (1953) 17.
19. Penn, R. E. and Curl, R. F., Jr. *J. Chem. Phys. 55* (1971) 651.
20. Penn, R. E. and Olsen, R. J. *J. Mol. Spectrosc. 62* (1976) 423.
21. Pauling, L. *The Nature of the Chemical Bond,* 3rd. Ed. Cornell University Press, New York 1960, p. 260.

Received October 11, 1982.

Acta Chemica Scandinavica A 37 (1983) 487–491

The Surface Tension of Molten Mixtures Containing Cryolite. I. The Binary Systems Cryolite–Alumina and Cryolite–Calcium Fluoride

D. BRATLAND, C. M. FERRO * and T. ØSTVOLD

Institutt for uorganisk kjemi, Norges tekniske høgskole, Universitetet i Trondheim, -7034 Trondheim-NTH, Norway

Surface tension has been measured in the two molten systems:
(1) Na_3AlF_6–Al_2O_3 (0.4–12wt%Al_2O_3) and (2) Na_3AlF_6–CaF_2 (0–15wt%CaF_2) in the temperature range 1000–1100 °C. The results may be expressed by:

$$\gamma_1/(\text{mN m}^{-1}) = 264.3-0.1318\ t/°C - 4.6\log(C_{Al_2O_3}/\text{wt\%}) - (3.29-0.00329\ t/°C)\cdot C_{Al_2O_3}/\text{wt\%}$$

and

$$\gamma_2/(\text{mN m}^{-1}) = 274.8-0.1392\ t/°C - (0.19-0.00056\ t/°C)C_{CaF_2}/\text{wt\%}$$

The relative standard deviation is 0.2 %.

Molten cryolite is the basic electrolyte in the electrowinning of aluminium. The degree of wetting of carbon materials (anode carbon, carbon particles in the bath) by cryolite-based melts depends, partly, on the surface tension of the electrolyte.[1] Knowledge of surface tension data for cryolite systems, therefore, is important for gaining a deeper insight into the process.

In this work the surface tension in some molten salt mixtures containing cryolite has been measured by means of the pin detachment method. This method was first described by Janz and Lorenz,[2] and was later used by Lillebuen and co-workers at this laboratory.[3] It involves a metal sinker with a pin (Fig. 1), dipping into the melt. When the sinker is lifted out of the melt, the apparent weight of the sinker will decrease abruptly the moment it is detached from the melt surface. This weight change is the detachment force, equal to the weight of the liquid column lifted by the pin just before detachment. Lillebuen showed that the surface tension of the liquid may be calculated when the detachment force,

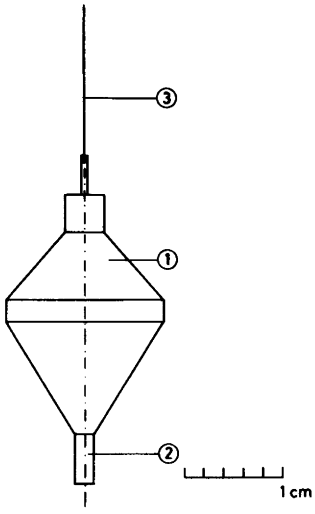

Fig. 1. Platinum sinker for measurement of surface tension in molten salts. 1, Sinker, Pt-10%Rh; 2, Pin for surface tension measurements; 3, Tungsten wire.

* Present address: ALUAR Aluminio Argentino S.A.I.C., Puerto Madryn, Chubut, Argentina.

0302-4377/83 $02.50

the radius of the pin and the specific gravity of the liquid is known.[4]

The specific gravity data were taken from the work by Edwards *et al.*[5]

EXPERIMENTAL

Apparatus. The essential features of the thermobalance and the vacuum system have been described elsewhere,[3,6] although the design has been somewhat altered. In the previous design the crucible supporter could be moved vertically relative to the furnace and the suspended sinker. Now the supporter is fixed to the furnace, and the furnace with the supporter can be moved. A bellow connects the furnace to the balance housing. The original balance is replaced by a Mettler electronic weighing cell.

The sinker was made from platinum–10 % rhodium alloy and was suspended by a 0.3 mm diameter tungsten wire, previously annealed from an electronic balance into a furnace. The pin diameter (approximately 2.2 mm) was measured at room temperature before each experiment with a precision of a thousandth of one millimeter, and extrapolated to the working temperature using data for thermal expansion of the alloy.

Chemicals. Hand-picked cryolite, calcined alumina and analytical grade calcium fluoride were stored and handled in a glove-box containing nitrogen with less than 5 ppm moisture.

Procedure. The salts were premelted in a platinum crucible under high purity nitrogen atmosphere and stirred for 30 min with a platinum stirrer. Then the covered crucible with contents was quenched in cold water, and the salt crushed before the experiment. The crushing would ensure a thorough mixing of the components. It was very important to avoid carbon in the system as carbon particles floating on the melt surface would dramatically alter the wetting properties of the liquid.

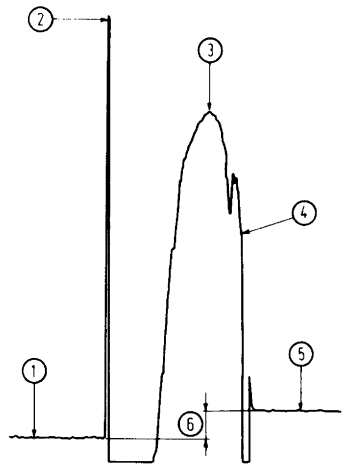

Fig. 2. Example of a weight–time record. 1, Base line before the first contact with the melt; 2, Contact between pin and melt; 3, Peak value; 4, Detachment of pin from melt; 5, Base line after detachment; 6, Difference between base lines before and after contact.

With the salt mixture in a platinum crucible in place inside the furnace, the whole system was evacuated to 10^{-4} mbar. The salt was heated to 200 °C and kept at that temperature for a few hours. The apparatus was then back-filled with high purity nitrogen. For the remainder of the experiment nitrogen flowed through the system at a rate of 50 cm^3 min^{-1}.

The salt was kept at constant temperature (±0.2 °C) for one hour before each set of measurements.

The crucible was raised or lowered by means of a reversible electric motor connected to a gear box from which a shaft moved the furnace at an adjustable speed, maximum 0.4 mm min^{-1}. When the pin touched the surface the weight of the sinker increased abruptly. By slowly lowering the

Table 1. Surface tension (mN m^{-1}) and temperature coefficient $d\gamma/dT$ (mN m^{-1} $degree^{-1}$) for pure supercooled liquid cryolite, Na_3AlF_6, at 1000 °C.

Method of investigation	Ref.	$\gamma(\pm SD)$	$d\gamma/d\ T(\pm SD)$
Pin detachment	This work	135.6 (0.3)	−0.137 (0.003)
Ring detachment	7	148.3	−0.135
Max. bubble press.	8	134.0	−0.128
Capillary	9	145.5	−0.130
	10	145.4	−0.124

furnace from this position, the weight increased steadily and passed through a well-defined maximum before a stable minimum was attained after detachment. The latter is the weight of the sinker in nitrogen atmosphere. The accuracy of the weighing was ±0.1 mg. The measurements at each temperature were reproducible within 0.1 %. The weight change was recorded on a strip chart recorder.

Fig. 2 shows a typical weight–time record.

After detachment the weight of the sinker includes the weight of a melt droplet attached to the tip of the pin. As a consequence, a difference is observed in the base line recorded before the very first contact between pin and melt and after the first detachment. A correction must be made for this discrepancy. The weight of the droplet so determined may be compared after the experiment with the weight of the easily removeable frozen droplet attached to the tip of the pin. It may well amount to 2 % of the detachment force, and consequently introduce a substantial systematic error.

RESULTS

In Table 1 the surface tension data for the pure supercooled fused cryolite at 1000 °C from this work are compared with available literature data. The overall standard deviation of our surface tension measurements was ±0.2 %.

The present results for pure molten cryolite were obtained in three separate runs, and the data are given in Fig. 3 where the surface tension

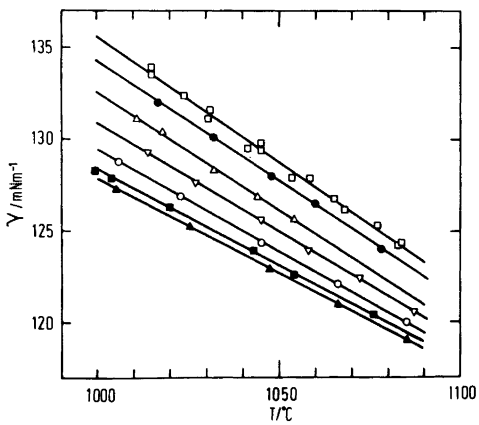

Fig. 3. Surface tension in Na_3AlF_6–Al_2O_3 melts. □, Na_3AlF_6; ●, 0.4 wt% Al_2O_3; △, 1 wt% Al_2O_3; ▽, 2 wt% Al_2O_3; ○, 5 wt% Al_2O_3; ■, 8 wt% Al_2O_3; ▲, 10 wt% Al_2O_3.

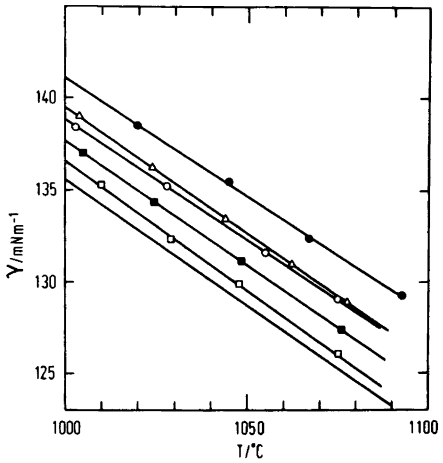

Fig. 4. Surface tension in Na_3AlF_6–CaF_2 melts. —, Na_3AlF_6; □, 3 wt% CaF_2; ■, 5 wt% CaF_2; ○, 8 wt% CaF_2; △, 10 wt% CaF_2; ●, 15 wt% CaF_2.

is plotted *versus* temperature. The whole temperature region was covered by making 5 measurements in each run; a total of 15 measurements.

Results for the two binary mixtures of Na_3AlF_6 with Al_2O_3 and CaF_2, respectively, are given in Fig. 3 and Fig. 4. In Fig. 5 the surface tension is plotted *versus* solute concentration for the two binary mixtures at 1000 °C. As can be observed from Fig. 5, the surface tension appears to reach

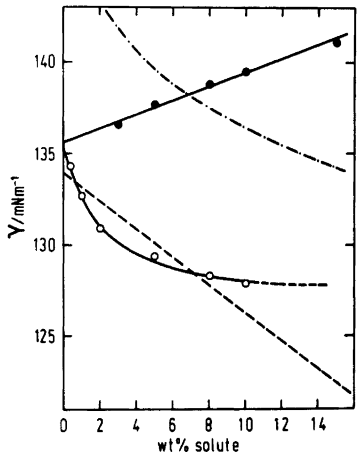

Fig. 5. Surface tension in Na_3AlF_6–Al_2O_3 and Na_3AlF_6–CaF_2 melts at 1000 °C. ●, Present work, CaF_2; ○, Present work, Al_2O_3; – – –, Bloom and Burrows,[8] Al_2O_3; –·–·, Vajna,[7] Al_2O_3.

Table 2. Constants in eqn. (1). Temp. range: 1000–1100 °C.
Concentration ranges: 0.4≤wt% Al_2O_3<12, 0≤wt% CaF_2<15.

System	a_0	a_1	a_2	a_3	a_4	SD_{rel}%
Na_3AlF_6	272.5	−0.1369	0	0	0	±0.19
$Na_3AlF_6-Al_2O_3$	264.3	−0.1318	−3.29	−4.6	0.00329	±0.18
$Na_3AlF_6-CaF_2$	274.8	−0.1392	−0.19	0	0.00056	±0.21

a constant value in the $Na_3AlF_6-Al_2O_3$ melt when the concentration of Al_2O_3 approaches saturation (12.5 %).[11]

The surface tension values in the cryolite systems investigated have been fitted to an equation of the form (1).

$$\gamma/\text{mN m}^{-1} = a_0+a_1t/°\text{C}+a_2(C_{\text{solute}}/\text{wt\%})+ a_3 \log (C_{\text{solute}}/\text{wt\%})+a_4t/°\text{C}(C_{\text{solute}}/\text{wt\%}) \quad (1)$$

In Table 2 the constants in this equation are given together with the relative standard deviation in per cent.

As can be observed from Table 1, there is a considerable disagreement between the present results for pure cryolite and previously published data. An exception is the data of Bloom and Burrows.[8] This is also reflected in Fig. 5 where the present data in the $Na_3AlF_6-Al_2O_3$ system are compared with the data of Vajna [7] and Bloom and Burrows.[8]

DISCUSSION

We believe that the discrepancy between the surface tension data reported by us and those given in the literature must be due to experimental uncertainties in the literature data.

As can be observed from the data of Vajna [7] and Bloom and Burrows [8] given in Fig. 5, the limiting slopes of γ plotted *versus* wt% Al_2O_3 do not approach zero at saturation. Moreover, a variation in the surface tension can be observed even for Al_2O_3 concentrations above the saturation limit.

As mentioned previously, it is very important to have a clean melt with no insoluble particles floating on the melt surface. The melting point of the cryolite used in the present work was 1010 °C which is equal to that reported by Holm [12] and slightly above the value given by Foster [13] (1009 °C). Bloom and Burrows report an approximate melting point of 1004 °C and indicated a 99.6 % purity of their cryolite, while Vajna does not give any data for the cryolite used. The experimental set-up of Vajna indicates that he must have had large temperature gradients across his cell. This makes his temperatures uncertain and therefore also his surface tension values since γ has a significant temperature coefficient. Bloom and Burrows report severe corrosion on their stainless steel tube. It is not clear, however, if this corrosion influenced the purity of their melts.

Gibbs surface tension equation [14] [eqn. (2)] gives a relation between the surface concentration Γ_1 of component 1 and the activity of this component. Accordingly, the surface concentration of Al_2O_3 or Al–O containing species must be positive since γ decreases when the Al_2O_3 content of the melt is increasing (Fig. 5).

$$\Gamma_1 = -\frac{d\gamma}{RT\, d \ln a_1} \quad (2)$$

When Al_2O_3 dissolves in a cryolite melt, ionic species are formed. The most plausible species are $Al_2O_2F_4^{2-}$ and $Al_2OF_6^{2-}$.[15–17] These ionic

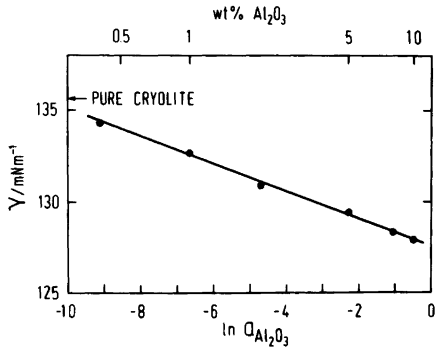

Fig. 6. Surface tension in $Na_3AlF_6-Al_2O_3$ melts at 1000 °C plotted *versus* the natural logarithm of the Al_2O_3 activity in the melt.

species will thus be enriched in the surface until surface-phase saturation.

In Fig. 6 γ is plotted *versus* ln $a_{Al_2O_3}$. A straight line is obtained down to 0.4 wt% Al_2O_3. This shows that surface saturation occurs at very low bulk concentration of Al_2O_3 (eqn. 2). From the slope of the line the surface-phase concentration of Al_2O_3 is calculated to be $\Gamma_{Al_2O_3}=7.2\cdot10^{-8}$ mol/m^2. If we, as a first approximation, assume that a monolayer of the solute species covers the surface, this surface concentration gives an area per formula unit Al_2O_3 on the surface $1/\Gamma_{Al_2O_3}=2.3\cdot10^5$nm^2/$Al_2O_3$. This area is too large to match any possible oxygen–containing ionic species in the $Na_3AlF_6-Al_2O_3$ system. It does, however, show that the oxygen–containing complex ions are far apart from each other on the surface of the melt. This is consistent with the long range coulomb repulsion between the ions.

The conductivity of liquid cryolite is reduced when alumina is added.[18] This reflects an increase of the covalency of the liquid cryolite structure, and thus formation of species with lower surface tension, in agreement with observations. When CaF_2 is added to cryolite, the melt becomes more ionic and the surface tension increases accordingly.

Acknowledgements. This work has been financially supported by *Norges teknisk-naturvitenskapelige forskningsråd* (NTNF.), grant 0511.00581. Dr. Carlos Ferro expresses his appreciation to NTNF for a research grant which made his stay in Norway possible.

REFERENCES

1. Grjotheim, K., Krohn, C., Malinovský, M., Matiašovský, K. and Thonstad, J. *Aluminium Electrolysis. Fundamentals of the Hall-Héroult Process,* 2nd Ed., Aluminium-Verlag GmbH, Düsseldorf 1982, p. 138.
2. Janz, G. J. and Lorenz, M. R. *Rev. Sci. Instrum. 31* (1960) 18.
3. Grjotheim, K., Holm, J. L., Lillebuen, B. and Øye, H. A. *Trans. Faraday Soc. 67* (1971) 640.
4. Lillebuen, B. *Acta Chem. Scand. 24* (1970) 3287.
5. Edwards, J. D., Taylor, C. S., Cosgrove, L. A. and Russell, A. S. *J. Electrochem. Soc. 100* (1953) 508.
6. Bratland, D., Grjotheim, K., Krohn, C. and Motzfeldt, K. *Acta Chem. Scand. 20* (1966) 1811.
7. Vajna, A. *Alluminio 20* (1951) 29.
8. Bloom, H. and Burrows, B. H. *Proc. First Australian Conf. Electrochem.,* Pergamon, Sydney, Hobart, Australia 1963, p. 882.
9. Kazantsev, G. E., Lepinskikh, B. M. and Kozhevnikov, G. N. *Tr. Inst. Metall Akad. Nauk SSSR Ural Fil. 20* (1969) 63.
10. Zhivov, V. G. *Tr. VAMI 13* (1936) 12.
11. Grjotheim, K., Krohn, C., Malinovský, M., Matiašovský, K. and Thonstad, J. *Aluminium Electrolysis. Fundamentals of the Hall-Héroult Process,* 2nd Ed., Aluminium-Verlag GmbH, Düsseldorf 1982, p. 29.
12. Holm, J. L. and Holm, B. J. *Acta Chem. Scand. 27* (1973) 1410.
13. Foster, P. A. *J. Am. Ceram. Soc. 53* (1970) 599.
14. Gibbs, J. W. *The Scientific Papers of J. Willard Gibbs,* Dover, New York 1961, Vol. 1, p. 230.
15. Grjotheim, K., Krohn, C., Malinovský, M., Matiašovský, K. and Thonstad, J. *Aluminium Electrolysis. Fundamentals of the Hall-Héroult Process,* 2nd Ed., Aluminium-Verlag GmbH, Düsseldorf 1982, p. 122.
16. Sterten, Å. *Electrochim. Acta 25* (1980) 1673.
17. Julsrud, S., Førland, T. and Kleppa, O. J. *Private communication.*
18. Zhivov, V. G. *Tr. VAMI 13* (1936) 133.

Received November 8, 1982.

Acta Chemica Scandinavica A 37 (1983) 493–501

Microwave Spectrum, Conformational Equilibrium, Intramolecular Hydrogen Bonding and Centrifugal Distortion of 3-Aminopropionitrile

OLE-ANDERS BRAATHEN, K.-M. MARSTOKK and HARALD MØLLENDAL

Department of Chemistry, The University of Oslo, P.O.Box 1033, Blindern, Oslo 3, Norway

The microwave spectrum of 3-aminopropionitrile, $CH_2NH_2CH_2CN$, has been investigated in the 18.0–32.0 GHz spectral region at 0 °C. The two C–C–C–N *gauche* conformations denoted I and II and shown in Fig. 1, were assigned. Both these rotamers are stabilized by an intramolecular hydrogen bond formed between the amino group hydrogen atom and the cyano group. The energy difference between I and II is 0(2) kJ/mol. The two identified conformations are each at least 4 kJ/mol more stable than any one of the three further forms shown in Fig. 1.

The C–C–C–N dihedral angles are 63(3)° from *syn* in I and 59(3)° from *syn* in II, respectively. The C–C–NH_2 angle has a "normal" value of 108.0(15)° in I, while this angle opens up to 114.0(15)° in II. The angle between the N–H bond involved in hydrogen bonding and the cyano group is about 4° from being parallel in both rotamers.

One vibrationally excited state was found for I, while two such states were identified for II. Accurate centrifugal distortion constants were determined for II and used to determine the C–C torsional frequency as 100(10) cm^{-1} for this conformation.

The amino group may act as proton donor in molecules capable of forming weak internal hydrogen bonds. Several such amines have recently been studied by microwave spectroscopy. These studies include $CF_3CH_2NH_2$,[1] H_2NCH_2CN,[2] $H_2NCH_2C{\equiv}CH$,[3] $CH_2NH_2CH_2NH_2$,[4] CH_2NH_2COOH,[5] $CH_3OCH_2CH_2NH_2$,[6] $CH_2FCH_2NH_2$[7] and $CHF_2CH_2NH_2$.[8]

0302-4377/83 $02.50

Amines may use both amino group hydrogen atoms in hydrogen bond formation. More than one hydrogen-bonded conformation may thus exist in most cases. Two hydrogen-bonded rotamers involving the amino group acting as proton donor have been assigned in the cases of $CH_2NH_2CH_2NH_2$[4] and $CH_2NH_2CH_2F$,[7] while three hydrogen-bonded conformations were found for $CHF_2CH_2NH_2$.[8] In the remainder of the above cited molecules, only one hydrogen-bonded rotamer where the amino group acts as proton donor, has been identified in each case.

3-Aminopropionitrile, $CH_2NH_2CH_2CN$, has five different all-staggered conformational possibilities as shown in Fig. 1. Conformations I and II each possesses an intramolecular hydrogen bond, whereas this interaction is not possible in the other three cases. This work was undertaken in order to see which of the five conformations of $CH_2NH_2CH_2CN$ are favoured. It was found that rotamers I and II, which are stabilized by weak hydrogen bonds formed between the amino group hydrogen atoms and the cyano group, are preferred by the molecule. The energy difference between I and II is 0(2) kJ/mol. No further conformations were identified. The hydrogen bond is so strong in each of I and II that they both are more stable than any one of III, IV and V by at least 4 kJ/mol.

EXPERIMENTAL

3-Aminopropionitrile was purchased from K&K Laboratories. The molecule was difficult to

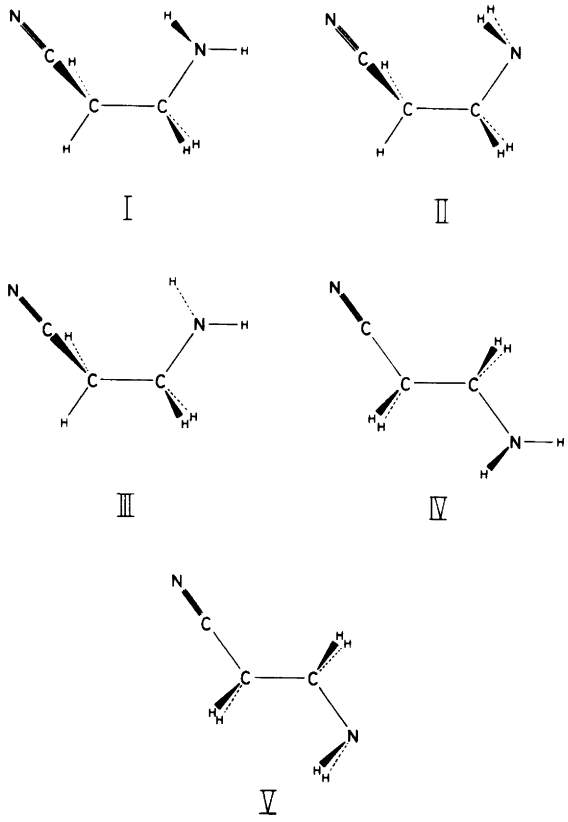

Fig. 1. Possible conformations of $CH_2NH_2CH_2CN$ with all-staggered atomic arrangements. I and II, both containing intramolecular hydrogen bonds, were assigned and the energy difference between them determined to be 0(2) kJ/mol. I and II are each at least 4 kJ/mol more stable than any one of III, IV or V.

handle because decomposition and/or polymerization reactions frequently occurred even during the registration of the microwave spectra where the compound was kept in a brass cell at a pressure of a few tenths of a pascal and a temperature of about 0 °C. Attempts to purify the compound by gas chromatography were unsuccessful because of polymerization reactions in the columns. The compound was kept at liquid nitrogen temperature when not in use, but decomposition/polymerization was always observed when the sample tubes were heated to room temperature in order to yield fresh samples. Ammonia appeared to be one decomposition product, but no further decomposition products were identified by their microwave spectra.

The spectrum was recorded on a conventional spectrometer in the 18–32 GHz spectral range. The spectrum was quite weak. The strongest lines appeared to have roughly 2×10^{-7} cm^{-1} intensity under these somewhat unfavourable experimental conditions. The cell could not be cooled below 0 °C because of insufficient vapour pressure of $CH_2NH_2CH_2CN$.

RESULTS

Assignment of conformation I. Preliminary rotational constants of I were computed using structural data taken from related molecules. Bond moment calculations using the values of Ref. 9 yielded μ_a=3.0 D, μ_b=1.6 D, and μ_c=0.4 D. The relatively strong *a*-type *R*-branch J=3→4 and J=4→5 transitions were therefore searched for and identified by their partially resolved Stark effects and rigid rotor fit. The assignments were

Table 1. Microwave spectrum of the ground vibrational state of conformation I of $CH_2NH_2CH_2CN$.

Transition	Observed frequency [a] (MHz)	Obs.-calc. frequency (MHz)	Centrifugal distortion (MHz)
$2_{1,1}\rightarrow 3_{1,2}$	19391.27	−0.09	−0.48
$3_{1,3}\rightarrow 4_{1,4}$	23393.96	−0.03	−0.42
$3_{0,3}\rightarrow 4_{0,4}$	24313.71	0.06	−0.82
$3_{2,2}\rightarrow 4_{2,3}$	24646.91	0.06	−0.30
$3_{2,1}\rightarrow 4_{2,2}$	25008.11	0.11	−0.53
$4_{1,4}\rightarrow 5_{1,5}$	29181.85	−0.02	−0.94
$4_{0,4}\rightarrow 5_{0,5}$	30142.79	0.02	−1.43
$4_{2,3}\rightarrow 5_{2,4}$	30761.82	0.04	−1.03
$4_{2,2}\rightarrow 5_{2,3}$	31461.44	−0.04	−1.65
$4_{1,3}\rightarrow 5_{1,4}$	32180.15	−0.05	−2.35
$5_{1,4}\rightarrow 5_{2,3}$	19197.44	−0.02	1.57
$7_{1,6}\rightarrow 7_{2,5}$	18608.57	0.07	1.87
$8_{1,7}\rightarrow 8_{2,6}$	19002.41	−0.06	0.55
$9_{1,8}\rightarrow 9_{2,7}$	19992.23	−0.12	−2.57
$10_{1,9}\rightarrow 10_{2,8}$	21653.99	0.10	−8.22
$11_{1,10}\rightarrow 11_{2,9}$	24039.08	0.07	−17.12
$13_{1,12}\rightarrow 13_{2,11}$	30995.81	−0.04	−46.14
$8_{2,6}\rightarrow 8_{3,5}$	33248.68	0.03	8.86
$9_{2,7}\rightarrow 9_{3,6}$	31839.96	−0.13	12.53
$10_{2,8}\rightarrow 10_{3,7}$	30459.26	0.17	15.68
$11_{2,9}\rightarrow 11_{3,8}$	29285.39	−0.01	17.25
$12_{2,10}\rightarrow 12_{3,9}$	28497.36	−0.03	15.97
$13_{2,11}\rightarrow 13_{3,10}$	28252.16	−0.06	10.52
$14_{2,12}\rightarrow 14_{3,11}$	28675.71	0.01	−0.46
$15_{2,13}\rightarrow 15_{3,12}$	29860.85	0.01	−18.24

[a] ±0.10 MHz.

then extended to include the *b*-type *Q*-branch $K_{-1}=1\rightarrow 2$ and $K_{-1}=2\rightarrow 3$ transitions. No *c*-type lines were identified presumably owing to their low intensities produced by a small μ_c. The high *J* *b*-type *P*- and *R*-branch lines were also too weak to be identified. No quadrupole fine structure was observed. The spectrum * is reported in Table 1 and the derived spectroscopic constants are listed in Table 2.

The first excited C−C torsional state was also identified as indicated in Table 2. Searches were made for the second excited state of this mode as well as for the first excited state of the C−N torsional mode, but no assignments could be made presumably because of the weakness of the spectrum.

* The microwave spectra of the vibrationally excited states of conformations I and II are available from the authors upon request or from Molecular Spectra Data Center, Bldg. 221, Room B 265, National Bureau of Standards, Washington D.C. 20234, U.S.A., where they have been deposited.

Rough relative intensity measurements were made for the C−C torsional mode, and a frequency of 140(50) cm^{-1} was determined. Attempts to calculate the same frequency by assuming the rough force field shown in Table 3 and using the centrifugal distortion constants of Table 2 in the manner described in Ref. 10, were rather inconclusive. A poor fit was obtained, and it is believed that the experimentally determined centrifugal distortion constants are too inaccurate to produce a reliable C−C torsional frequency.

Attempts to measure the dipole moments of both conformations I and II were futile because of insufficient intensities.

Assignment of conformation II. After the completion of the assignment of conformation I, it became clear that at least one further rotamer had to be present. Searches were therefore made for II. This conformation was computed to have $\mu_a=2.2$ D, $\mu_b=2.1$ D and $\mu_c=1.5$ D by the bond-moment method.[9] The strong *b*-type *Q*-branch lines were first identified for this confor-

Table 2. Spectroscopic constants for conformation I of $CH_2NH_2CH_2CN$.[a]

Vibrational state		Ground	First ex. C–C torsion
Numbers of transition		26	16
rms (MHz) [b]		0.0856	0.0872
A_v	(MHz)	10526.455(38)	10612.720(97)
B_v	(MHz)	3387.403(13)	3374.049(27)
C_v	(MHz)	2781.573(13)	2773.412(18)
Δ_J	(kHz)	4.11(30)	4.80(41)
Δ_{JK}	(kHz)	−22.48(58)	−15.5(17)
Δ_K	(kHz)	52.8(60)	−22(24)
δ_J	(kHz)	1.313(17)	1.453(46)
δ_K	(kHz)	7.20(75)	−1.0(14)

[a] Uncertainties represent one standard deviation. [b] rms is the root-mean-square deviation.

mer. The low J *a* and *b*-type *R*-branch lines were now readily assigned. High J *b*-type *R*-branch transitions were then identified by a trial and error procedure amongst lines of suitable intensity with very fast Stark effects. As shown in Table 4, it was possible to assign 53 transitions with a maximum J of 50. Even higher J transitions were searched for but not identified presumably because of insufficient intensities. No lines split by quadrupole coupling were observed. The frequencies of *c*-type transitions could be very accurately predicted, but none were found with certainty presumably because of a low *c*-axis dipole moment component. The spectroscopic constants are listed in Table 5.

Table 3. Assumed diagonal force field,[a] centrifugal distortion constants and torsional frequency for conformation II of $CH_2NH_2CH_2CN$.

Stretching (10^2 Nm^{-1})			
C≡N	17.7	H_2C-CH_2	4.4
C–CN	5.2	H_2N-C	5.1
C–H	4.7	N–H	6.4
Bend (aJ rad^{-2})			
C–C≡N	0.16	C–C–N	1.3
C–C–C	2.14	H–C–N	0.90
C–C–H	0.66	C–N–H	0.85
H–C–H	0.53	H–N–H	0.47
Torsion (aJ rad^{-2})			
C–C	0.11 [b]	C–N	0.25

Centrifugal distortion constants (kHz)

	Obs.	Calc.
Δ_J	4.066	4.084
Δ_{JK}	−22.94	−21.31
Δ_K	66.41	66.51
δ_J	1.2335	1.3327
δ_K	8.33	10.09

[a] See text. [b] Obtained from least-squares fit yielding a C–C torsional frequency of 100(10) cm^{-1} as compared to 140(50) cm^{-1} found by relative-intensity measurements.

Vibrationally excited states of II. Two vibrationally excited states were assigned for conformation II as indicated in Table 5. The strongest excited state which has roughly 50 % of the intensity of the ground state, is presumed to be the first excited state of the C–C torsional mode. Apart from its intensity, the changes of the rotational constants upon excitation are fairly similar to the changes found for conformation I (Table 2). Rough relative intensity measurements yielded 140(40) cm^{-1} for this mode. Force field calculations using the centrifugal distortion constants [10] resulted in a C–C torsional frequency of 100(10) cm^{-1} as shown in Table 3. In this case, a rather good fit was obtained (Table 3) presumably because much more accurate centrifugal distortion constants are available for conformation II than for conformation I.

The second excited state of the C–C torsional mode was searched for and a tentative assignment was made. The rotational constants (not included in Table 5) derived from 8 tentatively assigned lines were: A=10427.4(16) MHz, B=3348.905(72) MHz, and C=2748.088(81) MHz.

Another excited state having about 1/3 of the

Table 4. Microwave spectrum of the ground vibrational state of conformation II of $CH_2NH_2CH_2CN$.

Transition	Observed frequency (MHz)	Obs.-calc. frequency (MHz)	Centrifugal distortion Total (MHz)	Sextic (MHz)
$2_{1,1}\rightarrow 3_{1,2}$	19271.43	0.07	−0.47	
$2_{2,0}\rightarrow 3_{2,1}$	18538.32	−0.02	0.05	
$3_{0,3}\rightarrow 4_{1,4}$	28793.68	−0.04	0.02	
$3_{1,2}\rightarrow 4_{1,3}$	25646.40	−0.01	−1.16	
$3_{2,1}\rightarrow 4_{2,2}$	24858.17	−0.05	−0.50	0.01
$3_{2,2}\rightarrow 4_{2,3}$	24485.43	0.10	−0.26	0.01
$4_{0,4}\rightarrow 5_{1,5}$	33626.88	−0.01	−0.11	0.01
$4_{1,3}\rightarrow 4_{2,2}$	19257.39	0.03	0.68	
$4_{1,3}\rightarrow 5_{1,4}$	31975.05	−0.06	−2.28	0.01
$4_{1,4}\rightarrow 5_{0,5}$	25268.21	−0.11	−2.21	0.01
$4_{1,4}\rightarrow 5_{1,5}$	28974.64	0.12	−0.93	0.01
$4_{2,2}\rightarrow 5_{2,3}$	31279.39	0.00	−1.60	0.01
$4_{2,3}\rightarrow 5_{2,4}$	30558.36	0.02	−0.97	0.01
$6_{1,5}\rightarrow 6_{2,4}$	18114.53	−0.04	1.79	0.01
$7_{1,6}\rightarrow 7_{2,5}$	18060.24	−0.04	1.58	0.02
$7_{1,7}\rightarrow 7_{2,6}$	30489.02	−0.05	−1.65	0.03
$7_{2,5}\rightarrow 7_{3,4}$	33343.95	−0.06	4.65	0.07
$8_{0,8}\rightarrow 8_{1,7}$	22604.14	−0.10	−10.05	0.01
$8_{1,7}\rightarrow 8_{2,6}$	18518.85	0.05	0.22	0.03
$8_{2,6}\rightarrow 8_{3,5}$	32059.29	0.08	8.04	0.10
$9_{0,9}\rightarrow 9_{1,8}$	26970.69	−0.04	−15.35	0.01
$9_{1,8}\rightarrow 9_{2,7}$	19585.86	0.13	−2.90	0.03
$9_{2,7}\rightarrow 9_{3,6}$	30664.24	0.01	11.57	0.14
$10_{0,10}\rightarrow 10_{1,9}$	31683.83	0.09	−21.54	0.02
$10_{1,9}\rightarrow 10_{2,8}$	21335.26	0.13	−8.48	0.04
$10_{2,8}\rightarrow 10_{3,7}$	29323.28	−0.03	14.47	0.18
$10_{4,7}\rightarrow 11_{3,8}$	21179.06	0.03	−36.46	0.03
$11_{1,10}\rightarrow 11_{2,9}$	23815.02	−0.04	−17.19	0.04
$11_{2,9}\rightarrow 11_{3,8}$	28220.71	−0.03	15.69	0.22
$12_{1,11}\rightarrow 12_{2,10}$	27034.30	0.04	−29.41	0.03
$12_{2,10}\rightarrow 12_{3,9}$	27535.45	−0.04	14.00	0.26
$13_{1,12}\rightarrow 13_{2,11}$	30948.18	−0.05	−44.98	0.03
$13_{2,11}\rightarrow 13_{3,10}$	27421.96	0.08	8.12	0.28
$13_{5,8}\rightarrow 14_{4,11}$	22594.21	0.01	−49.90	0.18
$14_{2,12}\rightarrow 14_{3,11}$	28000.98	−0.04	−3.20	0.29
$15_{2,13}\rightarrow 15_{3,12}$	29360.26	−0.05	−21.18	0.27
$16_{2,14}\rightarrow 16_{3,13}$	31552.91	0.02	−46.73	0.22
$18_{7,12}\rightarrow 19_{6,13}$	25554.82	−0.14	−131.53	0.29
$20_{8,13}\rightarrow 21_{7,14}$	23205.12	0.09	−159.32	0.30
$32_{13,19}\rightarrow 33_{12,22}$	25139.29	−0.08	−522.34	1.42
$32_{13,20}\rightarrow 33_{12,21}$	25139.29	−0.11	−522.35	1.42
$33_{13,20}\rightarrow 34_{12,23}$	31577.86	0.04	−622.23	1.83
$33_{13,21}\rightarrow 34_{12,22}$	31577.86	−0.02	−622.24	1.83
$37_{15,22}\rightarrow 38_{14,25}$	27148.45	0.11	−777.76	2.77
$37_{15,23}\rightarrow 38_{14,24}$	27148.45	0.11	−777.76	2.77
$39_{16,23}\rightarrow 40_{15,26}$	24949.86	0.10	−859.23	4.39
$39_{16,24}\rightarrow 40_{15,25}$	24949.86	0.10	−859.23	4.39
$44_{18,26}\rightarrow 45_{17,29}$	26876.36	−0.17	−1204.96	8.04
$44_{18,27}\rightarrow 45_{17,28}$	26876.36	−0.17	−1204.96	8.04
$47_{19,28}\rightarrow 48_{18,31}$	30955.51	−0.02	−1509.95	9.03
$47_{19,29}\rightarrow 48_{18,30}$	30955.51	−0.02	−1509.95	9.03
$49_{20,29}\rightarrow 50_{19,32}$	28723.90	0.07	−1631.58	13.83
$49_{20,30}\rightarrow 50_{19,31}$	28723.90	0.07	−1631.58	13.83

[a] ±0.10 MHz.

Table 5. Spectroscopic constants for conformation II of $CH_2NH_2CH_2CN$.[a]

Vibrational state		Ground	First ex. C–C tors.	First ex. C–N tors.
No. of transitions		53	18	12
rms [b]	(MHz)	0.0854	0.091	0.058
A_v	(MHz)	10281.375(19)	10353.694(70)	10285.280(66)
B_v	(MHz)	3367.7496(43)	3357.962(19)	3373.9074(66)
C_v	(MHz)	2761.0828(39)	2754.208(16)	2763.256(11)
Δ_J	(kHz)	4.066(38)	2.92(32)	– [c]
Δ_{JK}	(kHz)	−22.94(40)	−25.15(85)	−23.27(79)
Δ_k	(kHz)	66.41(46)	90(11)	66(10)
δ_J	(kHz)	1.2335(71)	1.176(22)	1.249(21)
δ_K	(kHz)	8.33(27)	10.28(94)	8.52(80)
H_J	(Hz)	0.329(99)	– [c]	– [c]
H_{JK}	(Hz)	1.1(18)	– [c]	– [c]
H_{KJ}	(Hz)	21.9(35)	– [c]	– [c]
H_K	(Hz)	−44.9(74)	– [c]	– [c]

[a,b] Comments as for Table 2. [c] Not fitted. Kept at zero in least-squares fit.

intensity of the ground state was also assigned. Its spectroscopic constants are displayed in Table 5. Relative intensity measurements yielded 210(50) cm^{-1} for this mode. This frequency is typical for an amino group torsional mode.[11] The fact that the changes of the rotational constants upon excitation of this mode are quite small (Table 5), also indicates that this is indeed the first excited state of the C–N torsional vibration.

Searches for further conformations. About 130 transitions were assigned and approximately 10 more lines were tentatively identified as described above. This include all the strongest lines of the spectrum as well as the majority of the transitions of intermediate intensity. Some 20 lines of intermediate intensity could not be accounted for. None of these displayed resolved Stark splittings. Attempts to ascribe these transitions to conformations III, IV, or V of Fig. 1 turned out to be futile.

Predicted rotational constants of III were: A=10.4 GHz, B=3.3 GHz, and C=2.8 GHz. The dipole moment components were predicted [9] to be μ_a=4.2 D, μ_b=2.4 D, and μ_c=1.1 D using the bond-moment method. The unidentified lines could in no way be compatible with the strong *a*-type *R*-branch feature predicted for the hypothetical III conformation. The large μ_a predicted for this rotamer lead us to conclude that I and II each are at least 4 kJ/mol more stable than the hypothetical conformation III.

The hypothetical rotamers IV and V are very nearly prolate tops. A=25.2 GHz, B=2.3 GHz and C=2.2 GHz were predicted for IV, and A=24.5 GHz, B=2.3 GHZ and C=2.2 GHz predicted for V. The *a*-axis dipole moment components were calculated to be 4.2 D for conformation IV and 3.5 D for V, respectively, using the bond-moment method.[9] The microwave spectra of IV and V should then have strong and simple characteristic pile-ups of the $K_{-1}\neq 1$ *a*-type *R*-branch transitions. No such simple spectral features were seen. It is again concluded that I and II each are more stable than the hypothetical conformations IV and V by at least 4 kJ/mol. The unassigned lines are then believed to originate from either unidentified vibrationally excited state transitions or impurities.

Energy difference between I and II. Unfortunately, the dipole moment of neither conformation I nor II could be determined, and the values calculated by the bond-moment method [9] and reported above had to be used in order to derive the energy difference between I and II. Intensity comparisons as described in Ref. 12 were made between low K_{-1} *a*-type *R*-branch transitions because they are presumed to be very little split by nitrogen nuclei quadrupole effects. The energy difference was found to be zero with a liberally estimated uncertainty limit of ±2 kJ/mol.

Structure. Only one isotopic species was studied for both rotamers and only three rotational constants are thus available for each conformation. A complete geometrical structure cannot,

Table 6. Plausible structural parameters [a] (bond lengths in *pm*, angles in *degrees*) and observed and calculated rotational constants of conformations I and II of $CH_2NH_2CH_2CN$.

Assumed structural parameters common for I and II

C≡N	115.7	C–C≡N	180.0	H–N–C–C 60 or 180 from *syn*
C–N	147.5	C–C–H	109.5	
C–CN	146.3	C–N–H	111.0	
C–C	154.8	C–C–C	110.5	
C–H	109.1			
N–H	101.7			

Fitted structural parameters

	Conformation I	Conformation II
N–C–C–C	63(3) from *syn*	59(3) from *syn*
N–C–C	108.0(15)	114.0(15)

Rotational constants (MHz)

Conformation I			Conformation II		
Obs.	Calc.	Diff.(%)	Obs.	Calc.	Diff.(%)
10526.46	10502.44	0.23	10281.38	10289.27	0.08
3387.40	3389.32	0.06	3367.75	3362.23	0.16
2781.57	2789.67	0.29	2761.08	2767.15	0.22

Hydrogen bond parameters

	Conformation I	Conformation II
H···CN	255	270
H···NC	302	312
N···CN	290	298
N···NC	366	372
N–H···C [b]	100	98
N–H···N [b]	122	118
N–H, C≡N [c]	4	4

Sum of van der Waals radii [d]

H···C [e]	290	H···N	270
N···C [e]	320	N···N	300

[a] See text. [b] Angles around hydrogen atom involved in hydrogen bonding. [c] Angle between N–H bond involved in hydrogen bonding and cyano group. [d] Taken from Ref. 13. [e] van der Waals radius of carbon assumed to be 170 pm as in aromatic systems.[13]

Table 7. Selected results for some $CH_2XCH_2NH_2$-type molecules involving hydrogen bonding.

X	$\Delta H°$ [a] (kJ/mol)	∠X–C–C–N (Degrees)	∠N–C–C (Degrees)	Ref.
NH_2	1.3(8)	63(2) for I and II	109(1) for I; 111.5(10) for II [b]	4
F	0.4(13)	64(2) for I; 63(2) for II	110.0(10) for I; 114.5(10) for II	7
CN	0(2)	63(3) for I; 59(3) for II	108.0(15) for I; 114.0(15) for II	– [c]
OCH_3	<−7.2	61.5(12) for II [d]	112.2(12) for II [d]	6

[a] Positive value for $\Delta H°$ means that I is more stable than II. [b] Average values. [c] Present work. [d] Only II was found.

therefore, be determined for the two rotamers. A selection of parameters to be fitted must be made. The NCCC dihedral angle and the CCN angle were chosen because the rotational constants are sensitive to variation in these chemically interesting parameters and because they are among the structural parameters most prone to change from one conformer to another. In contrast, structural parameters likely to vary among conformers, namely the HNCC dihedral angles as well as the HNH and HNC angles, cannot be accurately fitted because the rotational constants are relatively insensitive to variation in these angles. The amino group was therefore assumed to be in exactly staggered positions in both I and II. Furthermore, the C–C≡N angle was assumed to be exactly 180°, even though it is realized that small deviations from linearity normally do occur. The bond lengths and angles, which are shown in Table 6 and kept fixed in the fitting procedure, were taken from recent accurate studies of related compounds.

The dihedral angle NCCC was varied in steps of one degree and the NCC angle in steps of 0.5 degree. The dihedral angles were found as 63(3)° in I and 59(3)° in II, and the NCC angles as 108.0(15)° in I and 114.0(15)° in II, respectively, as seen in Table 6. The error limits have been derived taking into account the inherent uncertainties of the assumed structural parameters.

DISCUSSION

The fact that both conformation I and II each are at least 4 kJ/mol more stable than any other conformation of 3-aminopropionitrile, presumably means that the amino and cyano groups attract each other rather strongly. This attraction is clearly considerably stronger than for thiol and cyano groups as demonstrated in the case of CH_2SHCH_2CN.[14]

The covalent contribution to the hydrogen bonds of the two rotamers of $CH_2NH_2CH_2CN$ must be of minor importance as can be inferred from the hydrogen-bond parameters of Table 6. However, the geometrical arrangement of the N–H bond involved in hydrogen bonding and the cyano groups is very favourable for dipole–dipole interactions in both rotamers because these bonds are about 4° from being parallel in both conformations.

Amines of the $CH_2XCH_2NH_2$ type may possess two hydrogen bonded conformations similar to conformations I and II of Fig. 1. Results for four compounds including $CH_2NH_2CH_2CN$ are collected in Table 7. With the exception of $CH_3OCH_2CH_2NH_2$,[6] conformations I and II are almost equally stable. $CH_2NH_2CH_2CN$ has the NCC angle about 6° smaller in I than in II. Similar results have been found for $CH_2NH_2CH_2NH_2$[4] and $CH_2FCH_2NH_2$[7] as seen in Table 7. The NCC angle is also quite large (112.2(12)°) in conformation II of $CH_3OCH_2CH_2NH_2$ in keeping with the trend seen for the other three molecules of Table 7.

The rather large NCC angles observed for the II conformations of Table 7 are hardly the result of 1,3-repulsion because the non-bonded distance of the hydrogen atoms in question is somewhat larger than the sum of the van der Waals radii. It is also interesting to note that rather large NCC angles have been found for the one identified conformation of $CF_3CH_2NH_2$[1] as well as in conformation III of $CHF_2CH_2NH_2$.[8] In both these two cases, attraction – and not repulsion – between two hydrogen and two fluorine atoms presumably exists. Perhaps the rather large H_2N–C–C angle of II resultts mainly from a slight rehybridization of the carbon atom carrying the amino group and is not a result of repulsion within the molecule.

The heavy-atom dihedral angle XCCN is close to 60° from *syn* in all the molecules of Table 7. It is also characteristic that no heavy-atom *anti* forms have been identified for any of the four molecules in the gaseous state. This points to a rather strong interaction between the amino group and the four proton accepting groups of Table 7. High-temperature electron-diffraction work has been made for $CH_2NH_2CH_2NH_2$ in an attempt to find the heavy-atom *anti* conformation,[15] however, with negative result. It is hoped that such work will be carried out for the remainder of the molecules of Table 7 in order to learn more about the hydrogen bonding ability of the amino group.

REFERENCES

1. Warren, I. D. and Wilson, E. B., Jr. *J. Chem. Phys. 56* (1972) 2137.
2. Pickett, H. M. *J. Mol. Spectrosc. 46* (1973) 335.

3. Cervellati, R., Caminati, W., Degli Esposti, C. and Mirri, A. M. *J. Mol. Spectrosc. 66* (1977) 389.
4. Marstokk, K.-M. and Møllendal, H. *J. Mol. Struct. 49* (1978) 221.
5. Suenram, R. D. and Lovas, F. J. *J. Am. Chem. Soc. 102* (1980) 7180.
6. Caminati, W. and Wilson, E. B., Jr. *J. Mol. Spectrosc. 81* (1980) 356.
7. Marstokk, K.-M. and Møllendal, H. *Acta Chem. Scand. A 34* (1980) 15.
8. Marstokk, K.-M. and Møllendal, H. *Acta Chem. Scand. A 36* (1982) 517.
9. Smith, C. P. *Dielectric Behavior and Structure,* McGraw-Hill, New York 1955, p. 244.
10. Braathen, O.-A., Marstokk, K.-M. and Møllendal, H. *Acta Chem. Scand. A 36* (1982) 173.
11. Tamagake, K., Tsuboi, M. and Hirakawa, A. Y, *J. Chem. Phys. 48* (1968) 5536.
12. Wilson, E. B., Jr. *et al. To be published.*
13. Pauling, L. *The Nature of the Chemical Bond,* 3rd. Ed., Cornell University Press, New York 1960, p. 260.
14. Marstokk, K.-M. and Møllendal, H. *Acta Chem. Scand. A 37* (1983) 477.
15. Yokozeki, A. and Kuchitsu, K. *Bull. Chem. Soc. Jpn. 44* (1971) 2926.

Received November 16, 1982.

Acta Chemica Scandinavica A 37 (1983) 503–508

Crystal and Molecular Structure of the Chloropalladation Adduct ($Pd_2Cl_2(C_{10}H_{16}Cl)_2$) of a Vinylcyclopropane

EVA E. BJÖRKMAN and JAN-E. BÄCKVALL

Department of Organic Chemistry, Royal Institute of Technology, S-100 44 Stockholm, Sweden

The compound $Pd_2Cl_2(C_{10}H_{16}Cl)_2$ crystallizes in the orthorhombic space group $P2_12_12_1$ (No. 19) with $a=10.556(6)$, $b=16.984(10)$, $c=13.229(4)$ Å and $z=4$. The X-ray investigation was based on 2423 independent reflections collected with an automatic computer controlled, Syntex $P2_1$ four-circle diffractometer. The structural parameters were refined by least-squares methods to a conventional R-value of 0.038.

The molecular structure is dimeric and contains a non-planar double palladium-chloro bridge, with a dihedral angle of 125.2°. A π-allyl group is coordinated to each of the palladium atoms, with the π-allyl groups arranged *cis* to one another. The Pd–Pd distance is 3.125 Å.

The palladium and the chlorine atoms on the ring are *trans* to one another showing that a *trans*-chloropalladation of the cyclopropane ring has occurred.

The present work is part of an investigation of the stereochemistry of the opening of cyclopropanes by palladium chloride complexes to give chloropalladation adducts. It has been reported that chloropalladation of a homoallylic cyclopropane occurs *cis*, but that the analogous chloropalladation of an allylic cyclopropane occurs *trans*.[2] Recently *cis*-chloropalladation of a methylene cyclopropane was established.[3] We have recently studied the mechanism of chloropalladation of vinylcyclopropanes [4] and we now report an X-ray crystal structure of one of the adducts (*1*) obtained from reaction of (+)-2-carene with bis(acetonitrile)palladium dichloride.

Reaction of (+)-2-carene with bis(acetonitrile)palladium dichloride gives two isomeric π-allylpalladium complexes *1* and *2* as products,

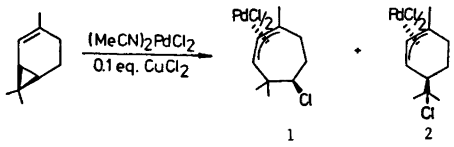

1 2

with a solvent dependent product ratio.[4] The stereochemistry of complex *2* was previously established by NMR spectroscopy.[4a] The X-ray analysis of complex *1*, reported in the present paper,* shows that the elements of Pd and Cl have added *trans* across the cyclopropane moiety in this case.

EXPERIMENTAL

Preparation of crystals. $(MeCN)_2PdCl_2$ and (+)-2-carene were stirred in benzene for 60 h. The solvent was evaporated, and the residue was purified by flash chromatography on silica gel, using CCl_4–CH_2Cl_2 (3:2) as eluate. Recrystallization from hexane–chloroform gave the desired π-allylpalladium complex *1*, as yellow prismatic crystals, stable at room temperature.

X-Ray data. The intensity data were collected at ambient temperature by a computer-controlled four-circle diffractometer of type Syntex $P2_1$, using graphite-monochromatized Mo$K\alpha$-radiation ($\lambda=0.71069$ Å).

A crystal with maximum dimensions of about 0.3 mm was used. A preliminary determination of the symmetry and the unit cell was made from Weissenberg photographs. The lattice constants were refined by centering 20 selected reflections on the diffractometer. An orthorhombic unit cell was found with $a=10.556(6)$, $b=16.989(10)$,

* A preliminary report of this work has appeared.[4b]

0302-4377/83 $02.50

c=13.229(4) Å and V=2367.6 Å^3. The calculated density was 1.76 g/cm^3 for Z=4. Systematically absent reflections were $h00$ for $h=2n+1$; $0k0$ for $k=2n+1$, and $00l$ for $l=2n+1$ which are characteristic for the non-centrosymmetric space group $P2_12_12_1$ (No. 19).[5]

For the intensity data collection the ω-scan mode was used, with intensity dependent variable scan speeds from 0.49° min^{-1} up to 29.5 min^{-1}.

All hkl reflections up to 2θ=50° and part of the $hk\bar{l}$ reflections ($1k\bar{l}$ and $2k\bar{l}$) were measured. Of 2791 reflections, 2423 had intensities larger than $1.96\sigma(I)$ and were considered observed. Averaging the Friedel pairs gave 2390 independent reflections, 2072 with $I>1.96\ \sigma(I)$. The intensities were corrected for Lorentz and polarization effects and converted to scaled $|F_o|$ values. After every 50th reflection, three check reflections were measured. No systematic variation in their intensities was observed during the data collection.

The absorption coefficient μ(Mo$K\alpha$) is 19.3 cm^{-1}. A semiempirical absorption correction was used,[6] based on a rotation around the diffraction vector for a few selected reflections. The measured relative variation in transmission ratio was from 1 to 0.74.

The program system supplied by Syntex (XTL version 2) [7] for a NOVA 1200 computer with a disk memory unit, was used for all calculations. In addition, the thermal-ellipsoid plot program for crystal structure illustration, ORTEP 2,[8] was used.

The scattering factors used for all nonhydrogen atoms were calculated from analytical expressions for the neutral atoms.[5] For the hydrogen atoms the spherical form factors proposed by Stewart *et al.* were used.[9] Anomalous dispersion corrections were included for palladium and chlorine.[5]

STRUCTURE DETERMINATION AND REFINEMENT

The positions of the palladium atoms were found from the three dimensional Patterson map,

Table 1. Final fractional atomic positional parameters and the isotropic temperature factors. The estimated standard deviations are given in parentheses.

Atom	x	y	z	B_{iso}
Pd1	0.06795(6)	0.19699(4)	0.10210(5)	3.04(3)
Pd2	−0.22982(6)	0.21068(3)	0.10782(5)	2.69(3)
Cl1	0.0525(3)	0.1359(2)	0.4703(2)	4.8(1)
Cl2	−0.2016(3)	−0.0257(2)	0.3185(2)	4.4(1)
Cl3	−0.0651(2)	0.3130(1)	0.1205(2)	3.5(1)
Cl4	−0.0935(2)	0.1471(2)	−0.0143(2)	3.2(1)
C1	0.2530(9)	0.1593(7)	0.1333(6)	3.6(4)
C2	0.1804(9)	0.0899(6)	0.1167(7)	3.2(4)
C3	0.1194(11)	0.0409(6)	0.1943(7)	3.4(4)
C4	0.1430(11)	0.0611(6)	0.3040(7)	4.1(5)
C5	0.0941(10)	0.1398(6)	0.3353(6)	3.3(4)
C6	0.1838(10)	0.2102(6)	0.3170(7)	3.3(4)
C7	0.2191(9)	0.2163(6)	0.2056(7)	3.8(4)
C8	0.1206(12)	0.2895(6)	0.3486(8)	4.5(5)
C9	0.3098(11)	0.2011(9)	0.3753(8)	5.6(6)
C10	0.2018(11)	0.0486(8)	0.0164(8)	4.9(5)
C11	−0.4118(8)	0.2038(6)	0.1645(7)	3.2(4)
C12	−0.3427(10)	0.2461(6)	0.2372(7)	2.9(4)
C13	−0.2781(10)	0.2081(5)	0.3301(7)	3.2(4)
C14	−0.2962(11)	0.1206(6)	0.3488(7)	3.8(5)
C15	−0.2531(9)	0.0677(5)	0.2628(7)	3.0(4)
C16	−0.3485(9)	0.0527(5)	0.1815(7)	2.6(3)
C17	−0.3833(10)	0.1299(6)	0.1265(7)	2.9(4)
C18	−0.2941(12)	−0.0031(6)	0.1000(8)	4.4(5)
C19	−0.4734(12)	0.0180(7)	0.2176(9)	5.6(6)
C20	−0.3626(13)	0.3321(6)	0.2487(8)	5.0(6)

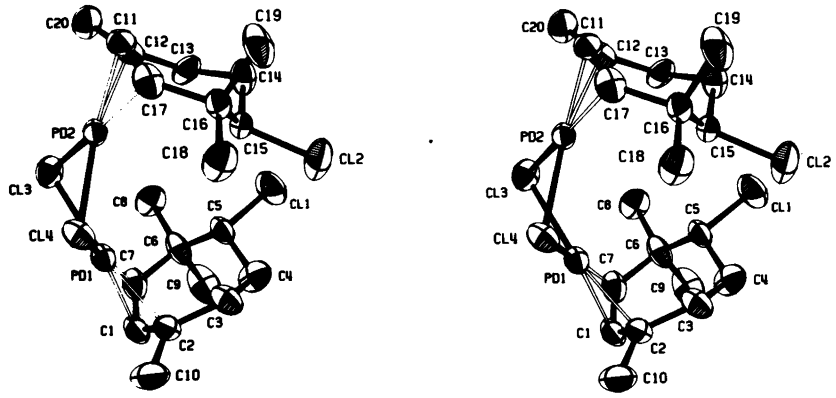

Fig. 1. A stereoscopic view of the molecular structure of $Pd_2Cl_2(C_{10}H_{16}Cl)_2$.

assuming the space group $P2_12_12_1$, and used as the starting point for a full-matrix least-squares refinement. The function minimized was $\Sigma w||F_o|-|F_c||^2$ including reflections with $F_o>3.92\ \sigma(F_o)$. The weighting scheme used was $w=1/[\sigma^2(F_o)+(0.04\ F_o)^2]$ which, according to a weight analysis, gave a satisfactory error distribution.

The chlorine and the carbon atoms were found from a subsequent Fourier difference synthesis. Full matrix least-squares refinements with all atoms isotropic and with mean values of the Friedel pairs gave $R=0.068$.* New refinements with anisotropic temperature coefficients gave $R=0.047$. The present limited set of data do not allow the determination of the absolute configuration of the molecule. Thus, the R_w values without averaging over the Friedel pairs were 0.073(0.074)* for isotropic atoms and 0.052(0.053)* for anisotropic atoms *i.e.* no significant differences.

From another Fourier difference synthesis 12 of the 32 hydrogen atoms could be located and refined ($R=0.040$). The final refinement with an additional 17 hydrogen atoms, geometrically inserted with fixed parameters ($B=5$ Å^2), gave $R=0.038$ ($R_w=0.055$). Three hydrogen atoms belonging to a methyl group, C20, were not included.

Positional and thermal parameters are given in Table 1. Listings of structure factors, anisotropic temperature factors and hydrogen positions are available from the authors on request.

The highest remaining peak in a final difference electron density map was 0.6 e/Å^3 close to Pd1.

* The conventional R-value is defined as $R=\Sigma||F_o|-|F_c||/\Sigma|F_o|$, and the weighted as $R_w=(\Sigma w||F_o|-|F_c||^2/wF_o^2)^{1/2}$. The values in parentheses are for the enantiomorphous structure.

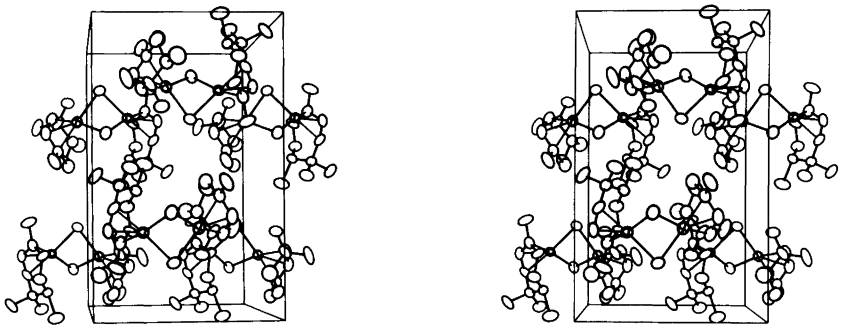

Fig. 2. A stereoscopic view of the unit cell. The *a* axis is horizontal, the *b* axis is vertical and origo is the lower, left rear corner.

Table 2. Selected interatomic distances, Å.[a]

(i) The chloro-palladium bridge			
Pd1–Cl3	2.431(2)	Pd2–Cl3	2.463(2)
Pd1–Cl4	2.448(2)	Pd2–Cl4	2.418(2)
Pd1–Pd2	3.153(1)		
Cl3–Cl4	3.347(3)		
(ii) The π-allyl groups			
Pd1–C1	2.10(1)	Pd2–C11	2.07(1)
Pd1–C2	2.18(1)	Pd2–C12	2.17(1)
Pd1–C7	2.13(1)	Pd2–C17	2.14(1)
C1–C2	1.42(1)	C11–C12	1.41(1)
C1–C7	1.41(1)	C11–C17	1.39(1)
(iii) The carbon–carbon and carbon–chloro σ-bonds			
C2–C3	1.48(1)	C12–C13	1.55(1)
C3–C4	1.51(1)	C13–C14	1.52(1)
C4–C5	1.49(2)	C14–C15	1.52(1)
C5–C6	1.55(2)	C15–C16	1.50(1)
C6–C7	1.53(1)	C16–C17	1.54(1)
C6–C8	1.56(1)	C16–C18	1.57(1)
C6–C9	1.54(2)	C16–C19	1.52(2)
C2–C10	1.51(2)	C12–C20	1.48(1)
C5–Cl1	1.84(1)	C15–Cl2	1.83(2)
(iiii) Intermolecular distance			
Pd1–Pd2[b]	3.838(1)		

[a] Estimated standard deviations in parentheses. [b] Symmetry code 1/2+x, 1/2−y, z̄.

DISCUSSION

The molecular structure and the packing of the unit cell are shown in Figs. 1 and 2. Selected interatomic distances are given in Table 2, selected angles in Table 3.

The molecule is a dimeric complex, with the palladium atoms linked together by a double chloro bridge. Each palladium atom further coordinates a π-allyl group as an organic ligand. From the ORTEP drawing of the molecular structure, Fig. 1, it can be seen that the chloro bridge is bent, with an angle of 125.2°, *cf.* Table 3. Fig. 1 also shows that the allyl groups are arranged *cis* to one another. The conformation usually observed [10–17] in dimeric π-allylpalladium chloride complexes is one with a planar bridge, with a *trans* arrangement of the allyl groups and with a center of symmetry. However, two reported structures, $[\eta^3$-cycloheptenyl-PdBr$]_2$[18] and $[\eta^3$-(2,3,4)-pentenyl-PdCl$]_2$[19] resemble the complex *1*. They have a non-planar bridge and a *cis* arrangement of the π-allyl groups. To our knowledge, no structure with a *cis* arrangement of the allyl groups and a planar chloropalladium bridge has been reported.

The reason for the bending of the halide bridge in *cis*-complexes is not clear. The Pd–Pd intramolecular distance, 3.152 Å, (Table 2), is shorter than in corresponding dimeric complexes having a planar Pd–Cl bridge. This indicates some non-bonding interactions between the metal centers. [20] (The Pd–Pd distance in elemental palladium is 2.75 Å[21] and in $Pd(NH_3)_4PdCl_4$ 3.25 Å.[22]) Packing forces could be one reason why bending occurs in the *cis*-complexes. From Fig. 3, which shows the possible *cis* and *trans* conformations, it can be seen that the *trans* conformation (*4*) loses its center of symmetry on bending, whereas the bending of the *cis* conformation (*3*) occurs within the C_{2v}-symmetry. In Table 4 we have summarized the π-allyl groups that lead to dimeric *cis*- and *trans*-complexes, respectively.

For each of the two allyl groups in compound

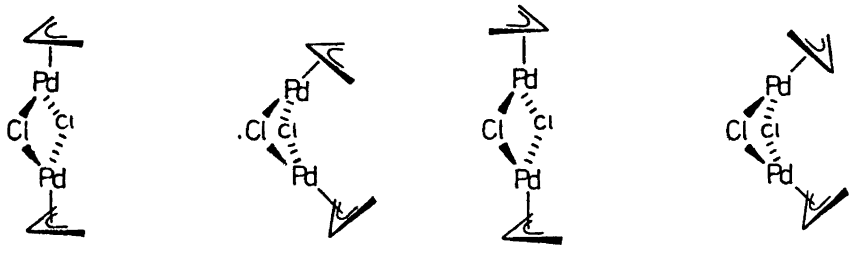

3 4

Fig. 3. Possible *cis* (3) and *trans* (4) conformations for a dimeric chlorobridged π-allylpalladium complex.

Table 3. Selected angles, in degrees. [a]

(i) The chloro-palladium bridge			
Pd1–Cl3–Pd2	80.19(8)		
Pd1–Cl4–Pd2	80.77(8)		
Cl3–Pd1–Cl4	86.62(8)		
Cl3–Pd2–Cl4	86.58(8)		
(ii) The π-allyl groups			
C2–C1–C7	122.5(9)	C12–C11–C17	126.8(9)
C1–C2–C3	126.7(9)	C11–C12–C13	124.0(8)
C6–C7–C1	132.3(9)	C16–C17–C11	130.5(8)
(iii) The σ-bond angles of the organic ligand			
C2–C3–C4	118.0(9)	C12–C13–C14	118.8(8)
C3–C4–C5	114.4(9)	C13–C14–C15	114.6(8)
C4–C5–C6	116.1(8)	C14–C15–C16	115.4(8)
C5–C6–C7	110.7(8)	C15–C16–C17	110.9(8)
C3–C2–C10	114.1(9)	C13–C12–C20	113.0(8)
C5–C6–C8	111.2(8)	C15–C16–C18	110.6(8)
C5–C6–C9	111.9(9)	C15–C16–C19	115.6(8)
C8–C6–C9	108.5(9)	C18–C16–C19	106.6(8)
C4–C5–Cl1	108.6(7)	C14–C15–Cl2	107.3(6)
(iiii) Dihedral angles			
Cl3–Pd1–Cl4/Cl3–Pd2–Cl4	125.2	Cl3–Pd1–Cl4/C7–C1–C2	118.6
Cl3–Pd2–Cl4/C17–C11–C12	120.7		

[a] Estimated standard deviations in parentheses.

Table 4. Conformation of bis (π-allylpalladium) complexes, (*cf.* Fig. 3).

cis conformation	Ref.	*trans* conformation	Ref.
	18		10
	19		11
			12
	This work	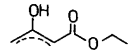	13
		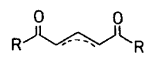	14
		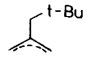	15
		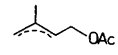	16
		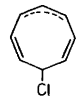	17

1, the three Pd–C distances (Table 2) are found to be different, but with similar variations. The shortest Pd–C distance is the one to the central carbon atom, with an average distance of 2.08 Å. To the terminal carbon atoms the average distances are 2.18 Å and 2.13 Å, with the longest distance to the most substituted carbon. A similar variation is reported for [η^3-(2,3,4)-pentenyl-PdCl]$_2$[19] *5* and π-allylpalladium complexes *6* with nonidentical ligands.[23] This asymmetry may have

5

6

different origins. In the latter case it may be due to *trans* effects from the ligands, but in complex *1*, reported in this paper, it is probably a steric effect.

The remainder of the molecule is in accordance with previous reports. For example, the dihedral angles between the plane through the allyl group and the palladium-chloro plane (Cl–Pd–Cl) are 118.6 and 120.7°, which are only slightly larger than the corresponding angle in [η^3-(1,2,3)-propenyl-PdCl]$_2$,[10] 111.5°.

Acknowledgements. We thank the Swedish Natural Science Research Council, *Stiftelsen för Bengt Lundqvists Minne* and *Tryggers Stiftelse* for financial support. This structure determination was part of a graduate course in crystallography given by the Department of Inorganic Chemistry. We thank Drs. Georg Johansson and Magnus Sandström for their guidance throughout the work.

REFERENCES

1. Albelo, G. and Rettig, M. F. *J. Organomet. Chem. 42* (1972) 183.
2. Albelo, G., Wiger, G. and Rettig, M. F. *J. Am. Chem. Soc. 47* (1975) 4510.
3. Clemens, P. R., Hughes, R. P. and Morgerum, L. D. *J. Am. Chem. Soc. 103* (1981) 2428.
4. a. Ahmad, M. U., Bäckvall, J. E., Nordberg, R. E., Norin, T. and Strömberg, S. *J. Chem. Soc. Chem. Commun.* (1982) 321; b. Bäckvall, J. E. and Björkman, E. E. *J. Chem. Soc. Chem. Commun.* (1982) 693.
5. *International Tables for X-Ray Crystallography,* Kynoch Press, Birmingham 1969 and 1974, Vols. 1 and 4 respectively.
6. Kopfmann, G. and Huber, R. *Acta Crystallogr. A 24* (1968) 348; North, A. C. T., Phillips, D. C. and Scott Mattews, F. *Ibid.* 351.
7. *Nicolet SRD Corporation,* 10061 Bubb Road, Cupertino, California 95014, USA.
8. Johnson, C. K. *A FORTRAN Thermal-Ellipsoid Plot Program for Crystal Structure Illustrations,* ORNL-5138, Oak Ridge National Laboratory, Oak Ridge 1976.
9. Stewart, R. F., Davidsson, E. R. and Simpson, W. T. *J. Chem. Phys. 42* (1965) 3175.
10. Smith, A. E. *Acta Crystallogr. 18* (1965) 331.
11. Mason, R. and Wheeler, A. G. *J. Chem. Soc. A* (1968) 2549.
12. Broadbent, T. A. and Pringle, G. E. *J. Inorg. Nucl. Chem. 33* (1971) 2009.
13. Oda, K., Yasuoka, N., Ueki, T., Kasai, N. and Kakudo, M. *Bull. Chem. Soc. Jpn. 43* (1970) 362.
14. Uhkin, L. Yu., Il'in, V. I. and Orlova, Zh. I. *J. Organomet. Chem. 113* (1976) 167.
15. Murphy, J. B., Holt, S. L. Jr., and Holt, E. M. *Inorg. Chim. Acta 48* (1981) 29.
16. Manchand, P. S., Wong, H. S. and Blount, J. F. *J. Org. Chem. 43* (1978) 4769.
17. Baenziger, N. C., Goebel, C. V., Foster, B. H. and Doyle, J. R. *Acta Crystallogr. B 34* (1978) 1681.
18. Kilbourn, B. T., Mais, R. H. B. and Owston, P. G. *J. Chem. Soc. Chem. Commun.* (1968) 1438.
19. Davies, G. R., Mais, R. H. B., O'Brien, S. and Owston, P. G. *J. Chem. Soc. Chem. Commun.* (1967) 1151.
20. Kruger, C., Sekutowski, J. C., Berke, J. and Hoffmann, R. *Z. Naturforsch. B 33* (1978) 1110.
21. Fordham, S. and Khalsa, R. G. *J. Chem. Soc.* (1939) 406.
22. Miller, J. R. *Proc. Chem. Soc.* (1960) 318.
23. Wong-Ny, W. and Nyburg, S. C. *J. Chem. Soc. Dalton Trans.* (1981) 1935 and references therein.

Received November 4, 1982.

Acta Chemica Scandinavica A 37 (1983) 509–518

The Vibrational Spectra and Molecular Structure of *trans*- and *cis*-1,2-Diethynylcyclobutane

H. HOPF,[a] P. KLÆBOE,[b] C. J. NIELSEN,[b] H. PRIEBE,[a] D. L. POWELL [b,*] and R. SUCHI [b]

[a] Institute of Organic Chemistry, The Technical University of Braunschweig, D-3300 Braunschweig and [b] Department of Chemistry, University of Oslo, Oslo 3, Norway

The infrared spectra of *trans*- and *cis*-1,2-diethynylcyclobutane were recorded for the vapour, liquid and crystalline states. Raman spectra of the liquid and crystalline compounds were obtained.

The *trans* compound was shown to exist in only one conformer in all phases. The evidence strongly favours this conformer being that with both acetylenic groups equatorial. The fundamental frequencies were assigned for both compounds, supported by normal coordinate calculations.

The two title compounds offer an interesting pair. If a non-planar ring is present in the *trans* isomer, two different conformers may result, while a planar ring implies only one conformer. On the other hand, the *cis* compound exists only in one conformer whether the ring is planar or not (Fig. 1).

For many years we have been studying the spectra of compounds which may exist in more than one conformation. In a loose sense this work is an extension of our earlier work on bipropargyl,[1,2] which can be seen clearly if one mentally substracts the two carbon atoms which are not attached to acetylenic groups along with their associated hydrogen atoms. Two conformers were expected for the *trans* isomer in accordance with gas phase electron diffraction results on *trans*-1,3-bromochlorocyclobutane [3] and vibrational spectroscopic results on 1,1,2-trichloro-2,3,3-trifluorocyclobutane,[4] for which two conformers were found. However, only one conformer was found for *cis*-1,3-dibromocyclobutane and for *cis*-1,3-bromochlorocyclobutane by electron diffraction.[3]

EXPERIMENTAL

The samples used for the spectral measurements were prepared by photodimerization of

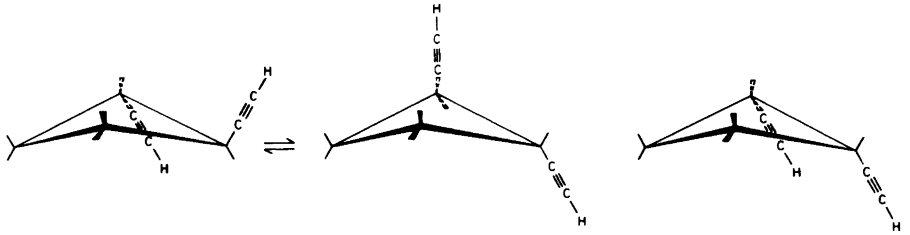

ee-trans *aa-trans* *ae-cis*

Fig. 1. The *ee* and *aa* conformers of *trans*-1,2-diethynylcyclobutane and the *ae* conformer of *cis*-1,2-diethynylcyclobutane.

* On leave of absence from The College of Wooster, Wooster, Ohio, U.S.A.

0302-4377/83 $02.50

Table 1. Symmetry species and possible conformers for *cis*- and *trans*-diethynylcyclobutane.

	cis			*trans*		
	Symmetry	Symmetry species	Possible conformers	Symmetry	Symmetry species	Possible conformers
Planar ring	C_s	21A'+21A''	1	C_2	22A+20B	1
Non-planar ring	C_1	42A	1 (ae)	C_2	22A+20B	2 (aa, ee)

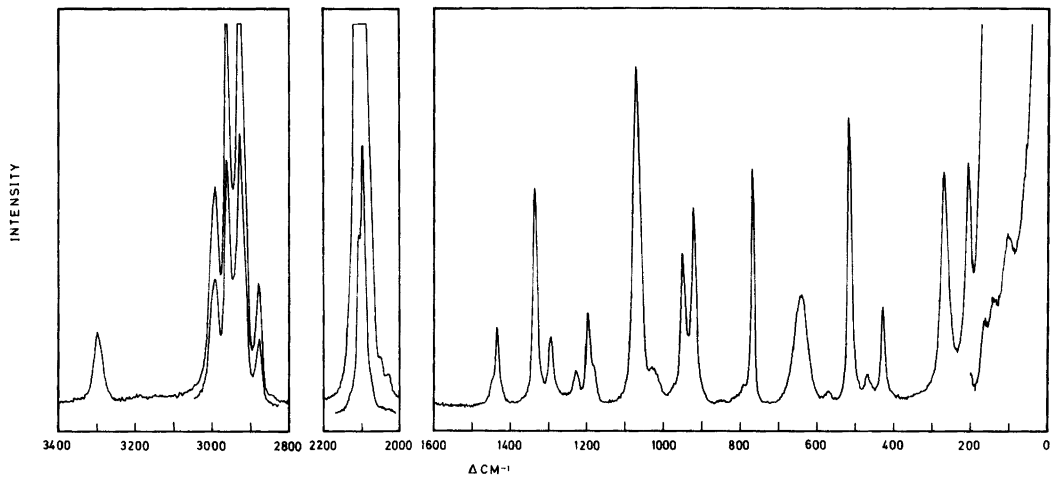

Fig. 2. Raman spectrum of *trans*-1,2-diethynylcyclobutane as a liqquid.

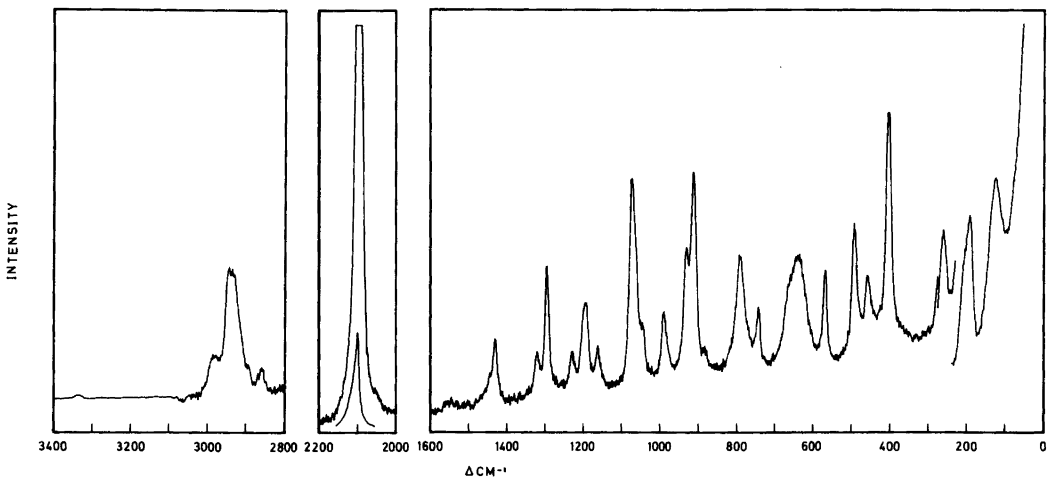

Fig. 3. Raman spectrum of *cis*-1,2-diethynylcyclobutane as a liquid.

vinylacetylene.[5] The pure isomers were obtained by preparative gas chromatographic separation.

The infrared spectra were recorded with a Perkin-Elmer model 225 spectrometer (4000–200 cm^{-1}) and a Bruker IFS-114C evacuable fast scan Fourier spectrometer (700–50 cm^{-1}). Spectra were taken of both compounds as vapours (4000–400 cm^{-1}) and as unannealed and annealed solids (4000–250 cm^{-1}). The *trans* isomer was studied as a pure liquid and as a solute in CCl_4 solution (4000–400 cm^{-1}), and in cyclohexane solution (400–50 cm^{-1}). The *cis* isomer was studied in CCl_4 solution (4000–400 cm^{-1}) and in benzene solution (400–50 cm^{-1}).

The Raman spectra were recorded with a Cary model 81 Raman spectrometer equipped with a Spectra Physics 125A helium-neon laser and a CRL model 52G argon ion laser. The spectrum of the liquid phase of the *trans* isomer, including semi-quantitative polarization measurements, was obtained with the argon ion laser. Because of problems with decomposition in the argon ion laser beam, the spectrum of the liquid phase of the *cis* isomer, including semiquantitative polarization measurements, was obtained with the helium-neon laser. Unannealed and annealed solids of both compounds were studied at 90K with the argon ion laser.

RESULTS AND DISCUSSION

The spectral alternatives for planar and non-planar rings for both compounds are shown in Table 1. For the *cis* compound, only one conformer can exist. This has, in principle, both polarized and depolarized bands in Raman if the ring is planar, but only polarized bands if the ring is non-planar. For the *trans* compound, all reasonable structures have the same symmetry (Fig. 1).

The experimental results obtained are shown in Table 2 (*trans*) and Table 3 (*cis*). Liquid phase Raman spectra for the two compounds are shown in Figs. 2 and 3, far infrared spectra for both compounds in the liquid phase in Figs. 4 and 5, and mid infrared spectra for the *trans* isomer in both unannealed and the crystalline solid phases in Fig. 6.

Conformation of the ring. Our assumption is that both rings are non-planar. Any of three different events could have occurred which would have provided information on planarity. First, observation of a series of puckering transitions either in the far infrared or in the Raman spectra or a series of combination bands involving puckering frequencies can give aid for deciding on planarity. Second, reliable polarization measurements on the *cis* compound would have helped to distinguish between planar C_s (21 polarized fundamentals and 21 depolarized fundamentals) and non-planar C_1 (all 42 fundamentals polarized). Finally, evidence for two conformers in the *trans* compound would clearly have demonstrated the existence of a non-planar ring.

A careful inspection of our spectra reveals no series of bands which we can interpret as a puckering series. The two compounds were not

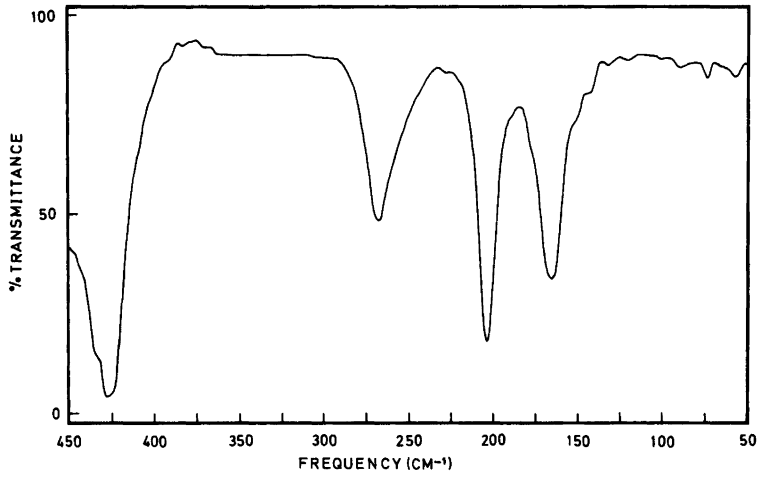

Fig. 4. Far infrared spectrum of *trans*-1,2-diethynylcyclobutane dissolved in cyclohexane, path 1 mm.

Table 2. Infrared and Raman spectral data for *trans*-1,2-diethynylcyclobutane (cm^{-1}).

Infrared [a]			Raman		Interpretation
Vapour	Liquid	Solid, 90 K	Liquid	Solid 90 K	
3335 vs 3330 vs 3324 vs	3300 vs [b]	3284 vs 3272 vs	3296 m, P	3284 w 3276 w	ν_1, ν_{23}
3310 m,sh 3304 m,sh		3257 w			
3010 s,sh 3002 vs C	2994 s	2999 s	2993 m,sh,D	3304 2998 m	ν_{24}
2994 s 2987 s	2986 s,sh	2987 s	2983 s,P	2985 m	ν_2
2970 s 2966 s,A 2959 s	2954 s	2955 s 2951 s,sh	2953 vs,P	2955 m,sh 2953 m	ν_3
2945 m	2934 m,sh	2940 w,sh		2940 m	
2919 w,sh	2910 w,sh	2923 w	2920 vs,P	2924 s	ν_{25}
2893 w		2894 w		2898 w	ν_{26}
2889 m 2884 m	2874 m	2867 w 2858 w	2872 m P	2868 w 2861 w	ν_4
		2131 vw		2145 w	
2128 m,bd	2119 m	2120 w	2116 vs,sh,P?	2120 vs	ν_5, ν_{27}
			2106 vs,P	2109 vs 2090 m	FR
1469 w	1460 w	1453 w	1458 w,sh,P	1455 w	ν_6
1459 w,sh 1452 m A 1446 w	1446 m	1434 m 1431 w,sh	1445 s D	1440 w 1437 w	ν_{28}
		1378 m			
1352 m 1344 m	1345 m	1359 w 1350 w	1344 vs P	1355 w 1349 s	ν_7
1311 m 1307 m A 1301 m	1302 m	1307 w 1301 m	1301 m D	1306 m	ν_{29}
1275 w,sh	1270 m,bd	1281 m,bd			ν_8
1261 s 1255 s 1251 s		1267 w			
1231 w,sh	1234 w	1240 w 1233 m	1233 w,D	1244 w 1235 w	ν_{30}
1203 w	1200 w	1217 m 1203 w	1203 s P	1215 vw 1203 m	ν_9
1185 w,sh	1182 w,bd	1192 w	1188 m P	1190 w	ν_{10}
1110 w		1093 w	1095 vw,D	1097 w	ν_{32}
			1075 vs P	1087 s 1080 m	ν_{11}

		1071 w		1070 w	
1070 w	1063 w	1062 w	1064 s,sh		ν_{33}
		1060 m		1062 w	
1033 w		1023 w	1036 w P		
1023 w	1021 w	1020 w	1024 w D	1022 w	
982 vw	981 vw	986 vw	978 w,sh D	982 vw	
963 vw	955 w	961 w	955 s D	960 s	ν_{34}
956 vw		953 w	948 w,sh P?	950 w,sh	ν_{12}
915 w		922 s			
912 w	926 vw		925 vs P	926 vs	ν_{13}
906 w		920 m			
	911 m	917 m	917 vw?	916 w,sh	ν_{14}
			858 vw P	859 vw	
823 vw	821 vw		814 vw P		
801 w					
797 w, C	796 w	798 s	795 w D	800 w	ν_{35}
792 w,sh					
	771 vw	774 w	772 vs P	774 m	ν_{15}
736 vw?		750 w			
		694 vs		692 m	Interactions
		680 vw			in the
	675 w,sh	668 m	672 w,sh	668 m	crystal
		666 s			
		663 vs			
638 vs		646 vs			
636 vs	640 vs	633 s	643 m P?	635 m	ν_{16}, ν_{17}, ν_{36}, ν_{37}
632 vs					
582 w,sh					
569 w,Q	572 w	569 s	573 w D	572 vw	ν_{38}
522 vw,sh	517 m,sh	519 s	519 vs P	523 m	ν_{18}
511 m					
	507 s	508 s	509 w,sh D	513 w	ν_{39}
504 m,sh					
481 w,sh					
472 m,C	472 s	476 s	472 w D	479 w	ν_{40}
464 w,sh					
		468 vw	465 w		
430 w					
	429 m	433 s	430 m P	436 w	ν_{19}
422 w					
	269 w	274 w	271 vs P?	278 s	ν_{20}
			251 w,sh		
	203 m		207 s D	215 m	ν_{41}
				179 w	
	165 m		169 w D		ν_{42}
				164 w	
	147 vw		143 w P	120 m	ν_{21}
			105 w P?	95 w	ν_{22}
				80 w	
				59 w	lattice modes
				53 w	

[a] Infrared data not obtained below 300 cm^{-1} in the vapour state and 220 cm^{-1} in the solid state. [b] s=strong, m=medium, w=weak, v=very, sh=shoulder, bd=broad, P=polarized, D=depolarized, A, B and C are vapour contours, FR=Fermi resonance.

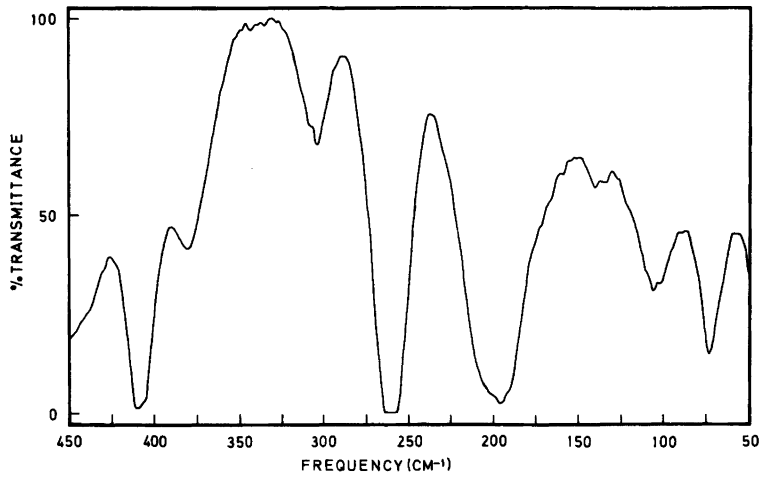

Fig. 5. Far infrared spectrum of *cis*-1,2-diethynylcyclobutane dissolved in benzene, path 1 mm.

Table 3. Infrared and Raman spectral data for *cis*-1,2-diethynylcyclobutane (cm^{-1}).[a]

Infrared			Raman		Interpretation
Vapour	Solution	Solid, 90 K	Liquid	Solid, 90 K	
~3360 m,sh					
3338 vs 3332 vs,Q 3325 vs	3304 vs	3280 vs		3284 m	ν_1, ν_2
3325 vs 3312 m,Q 3306 m,sh				3274 w,sh	
3010 s 3004 vs,Q 2297 s 2983 s,sh	2996 s ~2985 m,sh	2998 s 2984m,sh	2997 m ~2980 m,sh	2995 m 2984 m	ν_3 ν_4
2968 s 2962 vs,Q 2953 s	2954 s	2955 s	2956 vs	2953 s	ν_5
2951 vs,Q 2942 s	2940 m,sh	~2910 m,sh	2943 s	2941 s	ν_6
2931 m,Q 2924 m	~2920 m,sh	~2920 m,sh	~2920 m,sh	2913 s	ν_7
2888 m 2885 m,Q 2879 m	2901 m,sh 2870 m	~2900 w,sh 2870 m	2905 m 2870 m	~2900 w,sh 2870 m	ν_8
2125 m	2116 m ~1460 w,sh	2112 m ~1460 w	2116 vs,P	2110 vs	ν_9, ν_{10}
1461 m,Q	1453 m	1454 w	~1455 w,sh	~1455 w,sh	ν_{11}
1453 m 1447 m,Q 1446 m	1442 m	1441 m	1443 m	1445 w	ν_{12}

	1437 w,sh	1437 w,sh			
1340 m 1334 m,Q 1328 m	1330 m	1331 m	1331 w	1332 w	ν_{13}
	1320 vw,sh				
1315 w 1307 w	1304 m	1306 m	1305 m,P	1305 m	ν_{14}
~1280 vs	~1275 w,sh	1292 m,bd			ν_{15}
1256 s 1248 s	~1245 s,bd				
1243 s,sh	1238 s	1240 m	1237 w	1242 w	ν_{16}
1214 w	1207 m	1205 w	1206 m	1208 m	ν_{17}
~1185 vw					
1170 m	1155 m	~1170 w	1170 w	1174 w	ν_{18}
1118 m	1106 m	1098 m			ν_{19}
~1090 vw	~1090 vw				
	~1085 vw	~1080 w	1082 s,P	1084 s	ν_{20}
	1070 w	~1070 w	~1070 m,sh	1071 m	ν_{21}
	1051 w	1052 w	1054 m	1052 m	ν_{22}
983 w	~ 995 w	988 w	996 m	994 w,bd	ν_{23}
939 w,Q	938 m	942 m	938 m,P	945 m	ν_{24}
	~ 920 vw,sh	~ 920 vw	921 vs	923 s	ν_{25}
892 w,Q	888 m	892 m	889 w	892 w	ν_{26}
841 w	~ 835 w				
797 w	~ 790 vw	~ 790 w	794 s,P	791 m,bd	ν_{27}
746 w,Q	747 m	752 m	749 m	752 w	ν_{28}
718 w,sh					
710 s	702 m	710 s			ν_{29}
		692 s		693 w,sh	ν_{30}, ν_{31}, ν_{32}, ν_{33}
~ 675 w	673 s	670 s	672 m,sh		
		661 s		666 m,bd	
630 vs	632 vs	638 vs	640 m,bd		
		624 s		633 w	
578 m 572 m,Q 567 m	573 m	578 m	572 m,P	577 w	ν_{34}
	520 vw				
500 m 492 s,Q 485 m	495 s	501 m	496 m,P	503 w	ν_{35}
	461 m	465 m	462 w	467 w	ν_{36}
		432 vw			
408 w,Q	410 m	410 m	407 s	409 m	ν_{37}
	~ 305 vw				
	262 m		261 m	269 m	ν_{38}
	204 m		204 m,sh	216 m,sh	ν_{39}
	190 m		191 s	200 s	ν_{40}
			125 s	150 s,bd	ν_{41}
	~ 105 vw		~ 110 m,sh	113 m	ν_{42}
				78 m	

[a] For meaning of abbreviations, see Table 2.

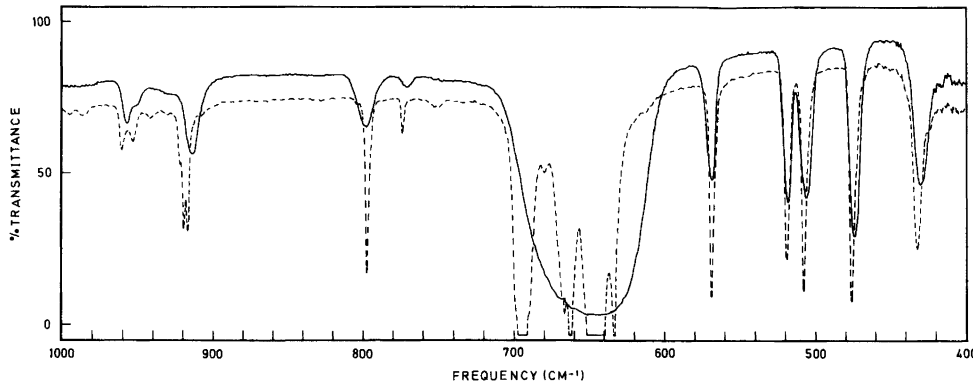

Fig. 6. Infrared spectra of *trans*-1,2-diethynylcyclobutane as an unannealed (solid curve) and annealed solid (dashed curve) at 90 K.

volatile enough and certainly not stable enough at elevated temperatures to attain the pressures necessary for such observations to be made. We did attempt polarization measurements with the *cis* compound, but its instability forced us to run the liquid phase spectra with the less intense helium-neon laser. The necessity of using axial illumination gives polarization measurements of lesser quality. And, even with this laser, there was some evidence of polymerization during the course of the determination. Thus, we have only labelled a few of the bands which were obviously polarized because of the uncertainty in this determination. Finally, as mentioned earlier, variations in the spectra on phase changes are of the sort to be associated with hydrogen bonding differences, not with changes in ring conformation or conformational abundance.

Conformation of substituents. If the ring is non-planar one acetylenic group must always be axial and the other equatorial in the *cis* isomer. However, in the *trans* isomer the two substituents are either both axial or both equatorial (Fig. 1).

To repeat a point just made in connection with the conformation of the ring, we note that there is no simplification of the spectra, no disappearance of either infrared or Raman bands upon crystallization of the *trans* isomer. To illustrate this point, the regions of the infrared spectra of amorphous and crystalline *trans*-1,2-diethynylcyclobutane which are shown in Fig. 6 display as usual a great change near 630 cm^{-1} associated [1,2] with the ≡C−H bending frequencies when the sample crystallizes. Otherwise the spectra are very similar. Our interpretation is that only one conformer is present in the liquid. It is very probably the conformer with the two acetylenic groups in equatorial positions as expected [3] and this prediction is supported by our normal coordinate calculations.

As seen from Table 4 the observed infrared and Raman bands believed to be fundamentals agree much better with those calculated for the *ee* than for the *aa* conformer. Particularly, the *b* fundamentals ν_{35}, ν_{36} and ν_{38}, but also the *a* fundamentals ν_{12}, ν_{14} and ν_{21} agree well with the calculated *ee* modes, but they can hardly be fitted to the *aa* frequencies. All together 14 bands assigned as fundamentals in the *trans* isomer agree best with the calculated *ee* frequencies, 4 agree best with the *aa* values, while the remaining bands can be equally well correlated with both sets. We feel that these data firmly support our conclusion that *trans*-diethynyl cyclobutane exists in the *ee* conformation in the vapour, liquid and crystalline states. A possible second conformer (*aa*) is probably present in less than 5 % abundance.

Spectra and vibrational assignment. The C_2 axis of the *trans* isomer coincides with the *B*-axis of inertia. The vapour phase infrared bands of species *a* are expected to have type *B* band contours and bands of species *b* are expected to have type *A*/*C* hybrid band contours. While in general the band contours were not of much help in the assignment, those bands with really prominent central maxima (3002, 1452, 1307, 797 and 472 cm^{-1}) were all assigned to species *b* fun-

Table 4. Observed and calculated fundamentals for *trans*- and *cis*-1,2-diethynylcyclobutane.

	trans			*cis*	
	Calc. (aa)	Obs.[a]	Calc. (ee)	Calc.	Obs.
a					
ν_1	3301	3300	3301	3301	3304
ν_2	2973	2983 [b]	2973	3301	3304
ν_3	2949	2954	2926	2993	2996
ν_4	2897	2874	2893	2974	2985
ν_5	2122	2116 [b]	2122	2957	2954
ν_6	1444	1460	1460	2939	2941 [b]
ν_7	1312	1345	1314	2917	2913 [b]
ν_8	1291	1275 [d]	1274	2896	2870
ν_9	1225	1200	1226	2125	2116
ν_{10}	1078	1188 [b]	1151	2123	2116
ν_{11}	1067	1075 [b]	1061	1456	1453
ν_{12}	1001	948 [b]	965	1443	1442
ν_{13}	910	926	925	1325	1330
ν_{14}	812	911	1283	1304	
ν_{15}	759	771	762	1280	1275
ν_{16}	637	640	637	1248	1238
ν_{17}	637	640	626	1233	1207
ν_{18}	522	522	525	1145	1155
ν_{19}	436	429	430	1117	1106
ν_{20}	274	269	369	1084	1082 [b]
ν_{21}	181	143 [b]	149	1076	1070
ν_{22}	82	105 [b]	93	1042	1051
b					
ν_{23}	3301	3300	3301	977	996 [b]
ν_{24}	2994	2994	2992	954	938
ν_{25}	2965	2920 [b]	2952	917	921 [b]
ν_{26}	2919	2893	2917	842	888
ν_{27}	2126	2116 [b]	2125	796	794
ν_{28}	1445	1446	1449	738	747
ν_{29}	1320	1302	1292	699	702
ν_{30}	1236	1234	1271	638	632
ν_{31}	1188	1161	1155	637	632
ν_{32}	1038	1110 [d]	1109	636	632
ν_{33}	1011	1063	1018	635	632
ν_{34}	946	955	933	568	573
ν_{35}	868	796	809	504	495
ν_{36}	713	640	639	472	461
ν_{37}	638	640	637	416	410
ν_{38}	636	572	580	273	262
ν_{39}	511	507	521	222	204
ν_{40}	445	472	502	202	190
ν_{41}	223	203	225	115	125
ν_{42}	145	165	182	89	113 [c]

[a] Wave numbers given are IR solution values except when noted. [b] Raman liquid values. [c] Raman solid values. [d] IR vapour values.

damentals. The bands at 1348 and 426 cm^{-1} which clearly do not contain central maxima were assigned to fundamentals of species *a*.

As in the case of 1,5-hexadiyne,[1,2] for both compounds studied, the ≡C−H stretching region of the liquid phase spectrum is a little unusual since all three compounds deviate from the characteristic pattern for a terminal alkyne. Usually the liquid phase spectrum has a strong peak near 3315 cm^{-1} with a weak shoulder near 3300 cm^{-1}, the shoulder probably arising from the CH stretching of an acetylenic hydrogen which is hydrogen-bonded to the triple bond of another molecule.[6] In the pure liquid both of these compounds show only a strong singlet at or near 3300 cm^{-1}, implying complete or nearly complete association in the liquid phase. In a dilute solution in an inert solvent, the equilibrium is expected to shift toward the monomer; in spectra of such a solution we do observe the expected behaviour.

For both compounds the assignments, with the aid of the normal coordinate assignments were quite straightforward. For the *trans* isomer, the criteria of polarized and depolarized bands and of infrared vapour contours needed to be satisfied as well as the numerical predictions.

The assignments proposed for the two diethynylcyclobutanes are listed in Tables 2 and 3 and only a few uncertainties will be mentioned. Two very strong Raman bands were observed at 2116 and 2106 cm^{-1} of the *trans* isomer. The former band, also observed in the IR, was attributed to coinciding C≡C stretching modes ν_5 and ν_{27}, found at 2116 cm^{-1} in the *cis* isomer. Thus, the 2106 cm^{-1} band which is the more intense, was interpreted as a combination band of species *A*, enhanced by Fermi resonance.

In spectra of both compounds strong infrared vapour bands around 1250 cm^{-1} were interpreted as overtone and combination bands of the C≡C−H bending modes, as commonly observed for acetylenes. Also, very intense infrared bands observed between 640 and 700 cm^{-1} of the crystalline compounds are characteristic of the C≡C−H bending modes interacting in the crystal.[1,2] The mode ν_{14} of the *trans* isomer was assigned to the infrared and Raman bands around 915 cm^{-1}, although the Raman band at 858 cm^{-1} which had no infrared counterpart agreed slightly better with the calculated frequency of 879 cm^{-1}.

Because of the chemical instability of *cis*-1,2-diethynylcyclobutane, its infrared and Raman spectra were not as completely studied as those for the *trans* isomer. Since there is no symmetry in this molecule, the infrared vapour contours or the Raman polarization measurements are not informative. We believe that our assignments are essentially correct, since they are in good agreement with the results of the normal coordinate analysis.

FORCE CONSTANT CALCULATIONS

Force fields for the two title compounds were constructed by transferring force constants *without* modification from ethynylcyclohexane [7] and from cyclobutane. We derived the latter force field (a 25 parameter VFF) by a least squares procedure from the spectroscopic data given by Miller *et al.*[8]

As seen from Table 4 the agreement between the observed and calculated fundamental frequencies is quite satisfactory. The few obvious discrepancies are those for the bending modes at the substituted sites of the cyclobutane ring. Only small changes in the force constants are necessary in order to obtain a perfect agreement between the observed and calculated fundamental modes of vibration. For the sake of brevity the force constants are not presented here, but they are available from the authors (Oslo) upon request.

Acknowledgements, We are grateful to J. E. Gustavsen and J. Samstad for technical help. DLP wishes to thank the Norwegian Marshall Fund for financial support.

REFERENCES

1. Powell, D. L., Klæboe, P., Phongsatha, A., Cyvin, B. N., Cyvin, S. J. and Hopf, H. *J. Mol. Struct. 41* (1977) 203.
2. Braathen, G. O., Nielsen, C. J., Klæboe, P. and Hopf, H. *J. Mol. Struct. 74* (1981) 233.
3. Almenningen, A., Bastiansen, O. and Wallöe, L. In Andersen, P., Bastiansen, O. and Furberg, S. Eds., *Selected Topics in Structure Chemistry,* Universitetsforlaget, Oslo 1967, p. 91.
4. Powell, D. L. and Klæboe, P. *Acta Chem. Scand. A 32* (1978) 71.
5. Eisenbuth, L. and Hopf, H. *J. Am. Chem. Soc. 96* (1974) 5667; Eisenbuth, L., Siegel, M. and Hopf, H. *Chem. Ber. 114* (1981) 3772.
6. West, R. and Kraihanzel, C. S. *J. Am. Chem. Soc. 83* (1961) 765.
7. Woldbæk, T., Nielsen, C. J. and Klæboe, P. *To be published.*
8. Miller, F. A., Capwell, R. J., Lord, R. C. and Rea, D. G. *Spectrochim. Acta A 28* (1972) 603.

Received November 16, 1982.

Acta Chemica Scandinavica A 37 (1983) 519–522

Preparation and Characterization of Mo_3Si and Mo_5Si_3

A. NØRLUND CHRISTENSEN

Department of Inorganic Chemistry, Aarhus University, DK-8000 Aarhus C, Denmark

Crystals of Mo_3Si were grown from a melt using the travelling solvent method and crystals of Mo_5Si_3 were grown from the melt using the Czochralski growth method.

Mo_3Si was characterized by neutron single crystal diffractometry and Mo_5Si_3 by neutron powder diffraction methods. Mo_3Si is cubic, *Pm3n* (No. 223), a=4.897(1) Å. Shortest Mo–Mo distance is 2.449(1) Å. Mo_5Si_3 is tetragonal, *I4/mcm* (No. 140), a=9.650(2), c=4.911(1) Å. Shortest Mo–Mo distance is 2.456(2) Å.

A large number of intermetallic compounds with the nominal composition A_3B are isostructural with β-W and have the so-called A15 structure. This structure belongs to the space group *Pm3n*, and has the A-atoms in site 6*c* and the B-atoms in site 2*a*. However, a major fraction of these intermetallic compounds are not strictly stoichiometric but exist in broad composition ranges. Mo_3Si is one of the few A15 compounds that has the stoichiometric A_3B composition at room temperature according to the literature [1–4] concerning the binary phase diagrams of the corresponding A–B system. Most of the intermetallic A15 compounds melt incongruently and this is also the case for Mo_3Si. In a project concerning development of crystal growth methods for incongruently melting compounds large single crystals of Mo_3Si were obtained. As Mo_3Si belongs to the stoichiometric A15 compounds it was decided to characterize the compound using neutron diffraction techniques.

Mo_5Si_3 is one of the congruently melting compounds in the Mo–Si systems. This compound was prepared as well and characterized by neutron diffraction technique.

EXPERIMENTAL

Crystal growth of Mo_3Si. The following compounds can be found in a zone melted rod of the composition Mo_3Si: The first part of the specimen contains a polycrystalline core of Mo_5Si_3 and Mo_3Si. The rest of the specimen is Mo_3Si and the frozen zone is a mixture of Mo_3Si and Mo. This shows without ambiguity that the phase diagram published for the Mo–Si system in Ref. 5 is in error. It demonstrates in addition that Mo_5Si_3 isostructural with W_5Si_3[6] is formed instead of a compound with the composition Mo_3Si_2.[1] The structure of that compound has not been confirmed. In Fig. 1 is shown a fraction of the Mo–Si phase diagram reproduced from literature data [1] and with Mo_5Si_3 as one of the solid phases. The hatched area represents a two phase temperature composition range where the melt is in equilibrium with solid Mo_3Si. Single crystals of Mo_3Si can be made by a modified floating zone growth procedure, the so-called travelling solvent method where the molten zone of solvent has the nominal composition Mo_4Si, indicated by an arrow, z, in Fig. 1. The feed rod and the grown crystal have the composition Mo_3Si. The volume of the molten zone of solvent must be kept

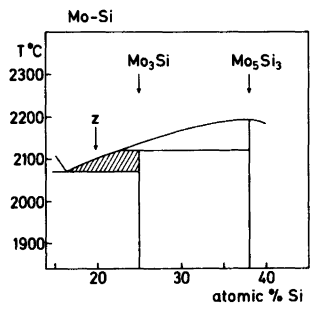

Fig. 1. Fraction of the phase diagram of the Mo–Si system (data from Ref. 1).

0302-4377/83 $02.50

constant in the floating zone like growth procedure. The crystals of Mo_3Si were made in an ADL–MP crystal growth unit at an ambient He pressure of 2 MPa. With a typical growth rate of 1 mm h^{-1} single crystals of Mo_3Si with a volume of up to 1 cm^3 were obtained.

Crystal growth of Mo_5Si_3. As can be seen from the phase diagram Fig. 1, the compound Mo_5Si_3 melts congruently and a normal Czochralski growth technique can be used in preparation of single crystals of Mo_5Si_3. Crystals of volume of up to 1 cm^3 were pulled from the melt kept in a cold crucible. The pulling rate was 1 mm h^{-1} and an ambient He pressure of 1 MPa was used.

Diffraction experiments. X-Ray diffraction powder patterns of Mo_3Si and Mo_5Si_3 were recorded on a Guinier camera with silicon as an internal standard using Cu$K\alpha_1$ radiation. From these measurements the following unit cell parameters were calculated: a_{Mo_3Si}=4.897(1) Å, $a_{Mo_5Si_3}$=9.650(2) Å, $c_{Mo_5Si_3}$=4.911(1) Å.

Mo_3Si was characterized by single crystal neutron diffractometry. A single crystal of dimensions 2×2×2 mm was cut from a large crystal of Mo_3Si using spark erosion and this crystal was used in measuring neutron intensities using a four-circle neutron diffractometer at Risø. Neutrons of 0.8 Å wave length were used, and the ω-2θ scan technique was applied. Two standard reflections were measured for each 50 reflections, and a total of 1496 reflections were measured in a half sphere out to sin θ/λ=1.16 $Å^{-1}$. After correction for absorption (μ=0.065 cm^{-1}) and data reduction, the number of reflections with $I>3\sigma(I)$ was 154. However, 26 of these were weak and space group forbidden, but apparently present due to multiple scattering. These reflections were omitted in the structure factor calculations. The parameters refined and the values arrived at for these parameters are listed in Table 1. A list of observed and calculated structure factors is available on request.

The least-squares program LINUS [7] was used in the structure factor calculations with the scattering lengths 0.695 and 0.4149 (in units of 10^{-12} cm),[8] respectively, for molybdenum and silicon.

Mo_5Si_3 was characterized by neutron diffraction powder methods. Powder patterns were measured at room temperature on the D1B spectrometer at the Laue-Langevin Institute in Grenoble, using neutrons of wavelength λ=2.5186 Å. The pattern of Mo_5Si_3 was measured in the 2θ interval 10.0 to 89.8° in steps of 0.2°. Mo_5Si_3 was housed in a 12 mm vanadium container. The structure was refined using the Hewat version of the Rietveld profile refinement programme.[9,10] The values of the scattering length used for the two elements were as reported above. A list of observed and calculated intensities is available on request.

RESULTS AND DISCUSSIONS

Mo_3Si. The A15 structure, space group *Pm3n* (No. 223), has the B-atoms placed in a body centered unit cell and the A-atoms in strings on the cubic faces of the unit cell. The direction of the strings are parallel to the axis of the unit cell and the interatomic distances between the metal atoms in the strings are approximately 10–15 % smaller than the interatomic distances in the corresponding pure metal.[11] For the A15 compounds the parameters of the thermal ellipsoide of the A-atoms have lower values in the direction of the strings than perpendicular to this direction, so in general U_{11} (Å) is smaller than U_{33} (Å). For compounds that are superconductors, the ratio U_{11}/U_{33} is smaller than the ratio $a/4r$ where a is the unit cell parameter and r the Goldschmidt radius of the A-atom. For Nb_3Al and V_3Si the values are 0.645<0.887, and 0.792<0.881,

Table 1. Mo_3Si, *Pm3n*, Mo in site 6*c*, Si in site 2*a*. Standard deviations in parentheses.

$h^2+k^2+l^2>$	No. of reflections	R %	Scale factor	Isotropic ext. parameters	Mo-atom U_{11} U_{33} $\times10^4$	Si-atom U_{11} $\times10^4$
1	128	2.1	54.6(5)	6.9(4)	15(1) 22(1)	27(1)
25	112	1.9	55.6(5)	7.2(4)	17(1) 24(1)	29(1)
50	92	1.9	57.3(7)	8.0(6)	20(1) 27(1)	34(2)
75	64	1.9	60.5(1.4)	8.6(9)	26(2) 32(2)	42(3)
85	56	1.9	64.1(1.8)	8.8(1.1)	32(3) 38(3)	50(3)
95	45	2.0	72.2(3.2)	11.2(1.6)	41(4) 47(4)	62(5)
100	41	1.9	72.9(3.3)	9.7(1.6)	43(4) 49(4)	64(5)

Table 2. Atomic coordinates of Mo_5Si_3 from neutron diffraction powder pattern, $R=10.1$ %. Standard deviations in parentheses.

Atom	Site	x	y	z	B (Å^2)
Mo 1	16*k*	0.0786(6)	0.2247(6)	0	0.9(2)
Mo 2	4*b*	0	1/2	1/4	0.9(2)
Si 1	8*h*	0.1710(10)	0.6710(10)	0	0.9(2)
Si 2	4*a*	0	0	1/4	0.9(2)

respectively.[12] For A15 compounds that show no superconductivity at moderately high temperatures, the values of the two ratios are close to each other. For Cr_3Si as an example, U_{11}/U_{33} is 0.879 and $a/4r$ is 0.876.[12] Mo_3Si belongs to this group of compounds and has $a/4r$ equal to 0.875 and U_{11}/U_{33} equal to 0.878. Table 1 lists the results of the least-squares refinement of the Mo_3Si structure, including all the 128 observed reflections and selections of high angle data. The isotropic extinction parameter used assumes a Nelmes-Thornly formalism.[7]

Refinement of the occupancy factor of the silicon atom showed that the composition did not deviate significantly from the stoichiometry of A_3B.

Mo_5Si_3. The compound was first reported to have the composition Mo_3Si_2,[1] but later Aronsson [6] showed Mo_5Si_3 to be isostructural with tetragonal W_5Si_3. According to this, the space group of Mo_5Si_3 is *I4/mcm* (No. 140) and the molybdenum atoms are placed in site 16*k* and 8*b*. The silicon atoms are placed in site 8*h* and 4*a*. The powder pattern of Mo_5Si_3 had fourteen resolved peaks and the profile refinement yielded the values of the parameters listed in Table 2. As starting parameters, the atomic coordinates for W_5Si_3 reported by Aronsson were used.[6] The structure investigation of Mo_5Si_3 shows a good agreement between the atomic parameters of Mo_5Si_3 derived from a neutron diffraction powder pattern and the atomic parameters of W_5Si_3 obtained from a single crystal X-ray investigation.[6]

The following Mo–Mo distances are found in Mo_5Si_3: 2.456(2) Å in a string of atoms parallel to the *c*-axis, 2.684(5) Å in the *ab*-plane, and 3.023(5) and 3.163(5) Å between atoms placed in planes spaced *c*/4 and *c*/2, respectively, from each other. In Mo_3Si the Mo–Mo distances are 2.449(1) and in molybdenum the interatomic distances are 2.725(1) Å.[13] The Mo–Mo distances in Mo_3Si are thus 10 % shorter than in pure molybdenum.

Acknowledgements. The Danish Natural Science Research Council is acknowledged for financial support concerning the four-circle diffractometer at Risø, and for support to the author in connection with a visit to the Institute Max von Laue–Paul Langevin in Grenoble. *Carlsbergfondet* is acknowledged for the spark erosion machine. The Institute Max von Laue–Paul Langevin is acknowledged for the use of the spectrometer DlB and for hospitality during a long time visit to the Institute.

REFERENCES

1. Hansen, M. *Constitution of Binary Alloys,* McGraw-Hill, New York 1958.
2. Elliott, R. P. *Constitution of Binary Alloys. First Supplement,* McGraw-Hill, New York 1965.
3. Shunk, F. A. *Constitution of Binary Alloys. Second Supplement,* McGraw-Hill, New York 1969.
4. Moffatt, W. G. *The Handbook of Binary Phase Diagrams,* Vol. 1–3, General Electric Company Corporate Research and Development Technology Marketing Operation, Scenectady 1978.
5. Smithells, C. J. *Metals Reference Book II,* 4th Ed., Butterworth, London 1967.
6. Aronsson, B. *Acta Chem. Scand. 9* (1955) 1107.
7. Busing, W. R., Martin, K. O. and Levy, H. A. *ORFLS, A Fortran Crystallographic Least-Squares Program,* Report ORNL-TM 305, Oak Ridge National Laboratory, Oak Ridge 1962. LINUS is a 1971 version of *ORFLS.*
8. Koester, L. and Rauch, H. *Summary of Neutron Scattering Lengths,* KFA, Jülich 1981.

9. Hewat, A. W. *Harwell Report AERE, R7350,* Harwell 1973.
10. Rietveld, H. M. *J. Appl. Crystallogr. 2* (1969) 65.
11. Lehmann, M. *Thesis,* Friedrich-Alexander-Universität, Erlangen-Nürnberg 1981.
12. Flükiger, R., Staudenmann, J.-L. and Fischer, P. *J. Less-Common Met. 50* (1976) 253.
13. *International Tables for X-Ray Crystallography,* Kynoch Press, Birmingham 1968, Vol. 3, p. 281.

Received November 11, 1982.

Acta Chemica Scandinavica A 37 (1983) 523–530

The Disordered Structure of Bis(8-hydroxyquinolinium) Pentafluoroperoxoniobate(V) Trihydrate, $(C_9H_8NO)_2[NbF_5(O_2)] \cdot 3H_2O$. A Redetermination at 170 and 275 K

ROLF STOMBERG

Department of Inorganic Chemistry CTH/GU, Chalmers Tekniska Högskola, S-412 96 Göteborg, Sweden

The crystal structure of $(C_9H_8NO)_2[NbF_5(O_2)] \cdot 3H_2O$, originally solved using the film method, has been reinvestigated. The structure determination is based on reflexion intensities collected by an automatic four-circle single-crystal X-ray diffractometer using Mo$K\alpha$ radiation. Crystals of $(C_9H_8NO)_2[NbF_5(O_2)] \cdot 3H_2O$ are monoclinic, space group $P2_1/c$ (No. 14), with a=6.717(1), b=24.683(8), c=13.703(3) Å, β=103.35(1)°, V=2210.6(9) Å^3 at 170 K and a=6.761(2), b=24.707(15), c=13.737(8) Å, β=103.35(4)°, V=2233(2) Å^3 at 275 K. Z=4. Least-squares refinement of structural and thermal parameters yielded a final R-value of 0.061 for 3315 observed independent reflexions at 170 K and of 0.067 for 2079 reflexions at 275 K.

The investigation indicates a disordered orientation of the pentagonal bipyramidal $[NbF_5(O_2)]^{2-}$ ion, also met with in some other pentafluoroperoxoniobates, at both 170 and 275 K. Two different, mutually overlapping orientations seem to predominate. Because of the disorder, the interatomic distances obtained are considerably less accurate than those usually obtained using diffractometer data. The ranges of interatomic distances at 170 K, being the more accurate ones, are: Nb–O 1.87–2.02 Å, Nb–F 1.89–2.01 Å, O–O 1.45–1.47 Å, C–O 1.34–1.36 Å, C–N 1.32–1.38 Å, and C–C 1.36–1.42 Å. Disregarding the structure of the anion and its orientation, the possible disorder of one water molecule, and the conclusions drawn about the peroxo group, the structural results previously obtained have been confirmed.

0302-4377/83 $2.50

The $[NbF_5(O_2)]^{2-}$ ion in $(C_9H_8NO)_2[NbF_5(O_2)] \cdot 3H_2O$ has a very distorted geometry according to a crystal structure analysis by Ružić-Toroš *et. al.* (R–T).[1] On the other hand, in $Na_2[NbF_5(O_2)] \cdot H_2O$,[2–4] $Na_3[HF_2][NbF_5(O_2)]$,[2,5] $Na_2[NbF_5(O_2)] \cdot 2H_2O$,[6] and $(C_{12}H_{10}N_2)[NbF_5(O_2)]$,[7] the $[NbF_5(O_2)]^{2-}$ ion is quite symmetrical (approximately C_{2v}). Moreover, the reported (R–T) occupation numbers, 1.0 and 0.3, for the peroxo oxygen atoms O1 and O2 are unreasonable from a chemical point of view, despite the well-known fact that peroxo complexes are unstable. A more natural model would have been a peroxo group with the occupation number 0.3 and an oxide oxygen atom with the occupation number 0.7 (the IR spectrum of the fresh sample does not, however, show an absorption typical for Nb=O), but this does not explain the distortion of the ion. It is the author's experience that a number of pentafluoroperoxo complexes,[6–8] as well as pentafluorooxoniobates, *e.g.* $(C_9H_8NO)[NbF_5O] \cdot 2H_2O$,[9] are disordered. It was therefore thought worthwhile to undertake a reinvestigation.

EXPERIMENTAL

Preparation and thermogravimetrical analysis. 5.3 g (0.02 mol) niobium(V) oxide was dissolved in 20 ml hot 40 % hydrogen fluoride in a platinum crucible and 11.6 g (0.08 mol) 8-hydroxyquinoline was added. $(C_9H_8NO)_2$-

$[NbF_5O] \cdot 2H_2O$ was obtained as a crystalline mass. Part of this was dissolved in water and to the solution, which had been filtered to remove small amounts of remaining undissolved niobium(V) oxide, an excess of hydrogen peroxide was added. Crystals suitable for the X-ray work were obtained by slow evaporation of the solvent. They were formed as thin plates with the crystallographic *b*-axis perpendicular to the plate plane. Many of the crystals were twins; these were twice as thick as the single crystals.

The niobium content was determined by carefully heating a weighed sample in a platinum crucible to red heat. (Found: Nb 16.37. Calc. for $(C_9H_8NO)_2[NbF_5(O_2)] \cdot 3H_2O$: 16.41). A thermogravimetrical analysis was carried out on the substance between 20 and 680 °C with a universal thermobalance (Mettler TA1). Water is lost between 50 and 110 °C (Found: 9.1 Calc.: 9.5). At 140 °C a general disintegration begins, which becomes rapid above 450 °C. Just below 600 °C a constant weight is obtained [niobium(V) oxide].

X-ray methods. The collection of intensity data was performed by a SYNTEX $P2_1$ automatic single-crystal X-ray diffractometer at 170 and 275 K. For the two data sets different crystals, with the dimensions 0.14×0.32×0.44 mm (at 170 K) and 0.04×0.14×0.33 mm (at 275 K), were used. The X-ray intensities were measured by the ω scan technique at 170 K ($2\theta \leqq 58°$) and by the $\theta-2\theta$ scan technique at 275 K ($2\theta \leqq 50°$) using graphite-monochromatized Mo$K\alpha$ radiation. Two test reflexions measured after each fiftieth reflexion showed no decrease in intensity at 170 K and only a minor one at 275 K during the collection of the data. The ω scan speed was varied between 3 and 30°/min and the 2θ scan speed between 2 and 8°/min depending on the intensity of the measured reflexion. A 19-step and a 96-step profile at 170 and 275 K, respectively, were recorded for each reflexion. A profile analysis based on the Lehmann-Larsen method was then applied to each reflexion.[10] A total of 6030 independent reflexions at 170 K and 4068 at 275 K were measured. Of these, 3315 and 2079 reflexions at 170 and 275 K, respectively, for which $I_o \geqq 3\sigma(I_o)$, were regarded as being observed and were used in the subsequent calculations. The intensities were corrected for Lorentz, polarisation and absorption effects.

The unit cell parameters were determined from a least-squares fit of refined diffractometer setting angles for 15 reflexions.

CRYSTAL DATA

Bis(8-hydroxyquinolinium) pentafluoroperoxoniobate(V) trihydrate, $(C_9H_8NO)_2[NbF_5(O_2)] \cdot 3H_2O$. F.W.= 566.28. Space group $P2_1/c$ (No. 14).

	At 170 K	At 275 K	At 298 K (Ref. 1)
a (Å)	6.717(1)	6.761(2)	6.771(2)
b (Å)	24.683(8)	24.707(15)	24.785(5)
c (Å)	13.703(3)	13.737(8)	13.768(3)
β (°)	103.35(1)	103.35(4)	103.3(3)
V (Å^3)	2210.6(9)	2232.7(20)	2248.6
D_c (g cm^{-3})	1.702	1.685	1.666

$Z=4$, μ(Mo$K\alpha$)=0.611 mm^{-1}, λ(Mo$K\alpha$)=0.71069 Å.

STRUCTURE REFINEMENT

Three cycles of block-diagonal least-squares refinement of positional and isotropic thermal parameters using the 275 K data set and the parameters reported by R–T[1] led to an R-value of 0.119 ($R=\Sigma||F_o|-|F_c||/\Sigma|F_o|$). A few atoms showed unreasonably high B-values (B(O1)=10, B(O2)=21, B(Ow3)=12 Å^2), some quite large (B(F2)–B(F4) 9–10 Å^2), while all other 27 non-hydrogen atoms had normal B-values (3–6 Å^2), and the peroxo bond distance appeared unacceptably short, 1.00 Å. Thus, the model proposed by R–T could not be completely correct. R–T put forward the opinion that oxygen is lost by disintegration of the peroxo group, and introduced unequal occupation numbers, 0.3 and 1.0, for the peroxo oxygen atoms. If oxygen is lost the corresponding amount of peroxide is replaced by oxide. Thus, such a model was tested with, at the start, equal occupation numbers, 0.5, for the oxo and peroxo oxygen atoms. This led to more reasonable B-values and a peroxo bond distance of 1.33 Å (R=0.072 with anisotropic thermal parameters). The Nb–"O"$_{oxo}$ bond distance of 1.91 Å obtained at this stage indicates a normal single bond and thus supports the observation made from IR-data that an Nb=O bond does not seem to exist. The idea of a complex with part of the peroxide being replaced by oxide was therefore abandoned for the moment.

It was observed by the author that the anion in $(C_{12}H_{10}N_2)[NbF_5(O_2)]$ as well as in

$(C_9H_8NO)_2[NbF_5O] \cdot 2H_2O$ is disorderly orientated.[7,9] The same situation might prevail also in this case. Inspection of the difference electron density map, the signs of the F's being determined by all but the coordinated atoms (R=0.22), and refinement of occupation numbers, led to a model with the complex orientated in mainly two ways. One orientation, comprising the atoms denoted Nb, F1–F5, O1 and O2, is very close to the one observed by R–T and the other, comprising the atoms denoted Nb, F1–F3, F5, F6, O3 and O4, has the centre of the peroxo group approximately at F4, both orientations having occupation numbers 0.5. Nb, F1–F3, and F5 are thus common to both orientations; the corresponding peaks could not be resolved into two parts. Further least-squares refinement of positional and anisotropic thermal parameters for all non-hydrogen atoms as well as an overall scale factor reduced the R-value to 0.067. A difference synthesis calculated after the final cycle of refinement showed no peak higher than 1.0 e Å^{-3}.

The structure was further studied at low temperature (170 K) in order to explore whether the disorder still existed and to obtain more reliable interatomic distances. It was soon found

Table 1. Atomic coordinates for $(C_9H_8NO)_2[NbF_5(O_2)] \cdot 3H_2O$ at 170 K and 275 K. All atoms occupy the general four-fold site of space group $P2_1/c$. The occupation number is 0.5 for F4, F6, O1, O2, O3 and O4; 0.6 for Ow3; 0.4 for Ow4; and 1.0 for all other atoms. $U_{eq}=\frac{1}{3}\sum_i\sum_j U_{ij}a_i^*a_j^*a_ia_j\cos\alpha_{ij}$

	170 K				275 K			
Atom	x	y	z	U_{eq}	x	y	z	U_{eq}
Nb	0.4212(1)	0.11575(2)	0.25000(4)	0.0281(1)	0.4164(2)	0.11715(4)	0.24858(7)	0.0441(2)
F1	0.2848(7)	0.1686(2)	0.1472(3)	0.044(1)	0.2818(11)	0.1691(3)	0.1458(5)	0.069(2)
F2	0.2113(10)	0.0678(2)	0.1830(5)	0.076(2)	0.2146(15)	0.0686(4)	0.1821(8)	0.125(3)
F3	0.2327(8)	0.1410(3)	0.3282(4)	0.082(2)	0.2374(14)	0.1441(5)	0.3271(7)	0.134(4)
F4	0.5498(18)	0.0726(4)	0.3608(7)	0.064(3)	0.5570(26)	0.0773(7)	0.3625(13)	0.094(5)
F5	0.5834(9)	0.1815(2)	0.3067(4)	0.059(1)	0.5843(13)	0.1808(3)	0.3025(6)	0.087(2)
F6	0.6074(13)	0.1002(4)	0.1684(7)	0.047(2)	0.5837(23)	0.1077(7)	0.1573(11)	0.089(5)
O1	0.5228(21)	0.0740(5)	0.1493(11)	0.064(4)	0.5359(37)	0.0783(9)	0.1585(19)	0.112(7)
O2	0.6668(18)	0.1153(5)	0.1963(11)	0.092(4)	0.6775(23)	0.1124(9)	0.2048(14)	0.085(5)
O3	0.6285(17)	0.0940(4)	0.3750(7)	0.037(2)	0.6261(33)	0.0932(8)	0.3672(16)	0.090(6)
O4	0.4770(31)	0.0531(5)	0.3285(11)	0.097(5)	0.4675(56)	0.0598(10)	0.3347(23)	0.173(10)
Ow1	0.8678(10)	0.1786(2)	0.0990(4)	0.049(1)	0.8665(15)	0.1763(4)	0.0983(7)	0.080(3)
Ow2	0.9676(9)	0.1731(3)	0.4323(4)	0.069(2)	0.9668(13)	0.1717(5)	0.4293(6)	0.084(3)
Ow3	−0.0125(17)	0.0349(4)	0.3812(8)	0.058(3)	−0.0172(40)	0.0314(9)	0.3873(16)	0.109(6)
Ow4	−0.0885(29)	0.0078(5)	0.4263(9)	0.065(4)	−0.0981(69)	0.0132(16)	0.4158(27)	0.144(11)
Ox1	0.6639(8)	0.2977(2)	0.4151(3)	0.034(1)	0.6689(12)	0.2986(3)	0.4143(6)	0.055(2)
Ox2	0.0070(9)	0.3932(2)	0.0842(3)	0.046(1)	0.0102(13)	0.3929(3)	0.0825(6)	0.062(2)
N1	0.5661(8)	0.2799(2)	0.2163(4)	0.031(1)	0.5699(12)	0.2802(3)	0.2160(6)	0.044(2)
N2	0.0956(9)	0.4533(2)	0.2521(5)	0.036(1)	0.0991(13)	0.4521(3)	0.2507(7)	0.049(2)
C1	0.5227(11)	0.2675(3)	0.1184(5)	0.038(2)	0.5243(18)	0.2675(5)	0.1196(9)	0.056(3)
C2	0.4953(12)	0.3100(4)	0.0470(5)	0.048(2)	0.4985(17)	0.3092(5)	0.0475(8)	0.058(3)
C3	0.5107(11)	0.3622(4)	0.0784(6)	0.044(2)	0.5167(17)	0.3625(5)	0.0802(9)	0.058(3)
C4	0.5538(10)	0.3759(3)	0.1813(5)	0.034(1)	0.5583(16)	0.3757(4)	0.1804(10)	0.055(3)
C5	0.5850(10)	0.3325(2)	0.2511(5)	0.029(1)	0.5875(15)	0.3319(4)	0.2497(8)	0.040(2)
C6	0.5748(11)	0.4292(3)	0.2180(7)	0.045(2)	0.5788(18)	0.4292(5)	0.2192(11)	0.066(4)
C7	0.6235(11)	0.4388(3)	0.3208(6)	0.041(2)	0.6218(19)	0.4378(5)	0.3184(11)	0.070(4)
C8	0.6521(10)	0.3950(3)	0.3888(5)	0.036(2)	0.6577(17)	0.3950(5)	0.3867(9)	0.058(3)
C9	0.6361(10)	0.3420(3)	0.3552(5)	0.028(1)	0.6420(15)	0.3428(5)	0.3539(8)	0.048(3)
C10	0.1354(12)	0.4850(3)	0.3316(8)	0.057(2)	0.1379(18)	0.4841(5)	0.3312(11)	0.070(4)
C11	0.1786(15)	0.4629(4)	0.4292(7)	0.067(2)	0.1804(21)	0.4616(6)	0.4266(10)	0.076(4)
C12	0.1769(13)	0.4082(4)	0.4390(6)	0.051(2)	0.1825(19)	0.4085(6)	0.4355(9)	0.067(4)
C13	0.1393(9)	0.3740(3)	0.3558(5)	0.033(1)	0.1379(15)	0.3730(5)	0.3540(8)	0.052(3)
C14	0.0926(9)	0.3977(2)	0.2590(5)	0.026(1)	0.0951(15)	0.3978(4)	0.2586(8)	0.039(2)
C15	0.1361(11)	0.3164(3)	0.3619(6)	0.041(2)	0.1420(17)	0.3151(5)	0.3587(9)	0.057(3)
C16	0.0979(12)	0.2862(3)	0.2770(7)	0.045(2)	0.0982(18)	0.2863(5)	0.2740(10)	0.062(3)
C17	0.0522(10)	0.3101(3)	0.1807(6)	0.037(2)	0.0547(16)	0.3099(4)	0.1792(9)	0.051(3)
C18	0.0477(10)	0.3659(3)	0.1707(5)	0.031(1)	0.0523(16)	0.3663(4)	0.1688(8)	0.046(3)

that the situation is the same as at 275 K. The electron density peaks about niobium were more fully examined in a series of difference electron density maps, calculated by omitting the ligand atoms one at a time in determining the *F*-signs. The omitted atoms showed up at the same positions as those found at 275 K. Thus, the same model is applicable both at 170 and 275 K. Furthermore, in both cases the water oxygen Ow3 was found statistically to occupy two positions, denoted Ow3 and Ow4, with the occupation numbers 0.6 and 0.4, respectively. Introduction of the hydrogen atoms belonging to the ring systems with calculated positions and $B=5$ Å^2 and least-squares refinement of positional and anisotropic thermal parameters for all non-hydrogen atoms as well as a common scale factor, gave a final *R*-value of 0.061. In this case the highest peak in an electron density difference map was less than 1.2 e Å^{-3}.

The weighting scheme used was that of Cruickshank:[11] $w=(a+|F_o|+c|F_o|^2+d|F_o|^3)^{-1}$ with $a=20.0$, $c=0.005$, and $d=0$ at 275 K and $a=30.0$, $c=0.008$, and $d=0$ at 170 K. The atomic scattering factors were taken from Ref. 12 as were the dispersion corrections.

Calculations were carried out on an IBM 3033 computer using a set of crystallographic programmes in use at this department.[13] Lists of structure factors and anisotropic thermal parameters are available from the author upon request.

RESULTS AND DISCUSSION

The positional parameters as well as U_{eq}'s obtained in the last refinement cycles are given in Table 1. Within the limits of experimental error the structures at 170 and 275 K are the same. All distances and angles quoted in this discussion refer to the 170 K data set, since this is the more accurate one. With the exception of the orientations of the anion and the positions of one water molecule, Fig. 3 in Ref. 1, showing the unit cell content, is applicable. The relative orientations of the anion are shown in Fig. 1. Bond distances and angles are given in Table 2 and hydrogen bond distances in Table 3.

The crystals of bis(8-hydroxyquinolinium) pentafluoroperoxoniobate(V) trihydrate, $(C_9H_8NO)_2[NbF_5(O_2)] \cdot 3H_2O$, consist of 8-hydroxyquinolinium and pentafluoroperoxoniobate(V) ions and water of crystallization, held

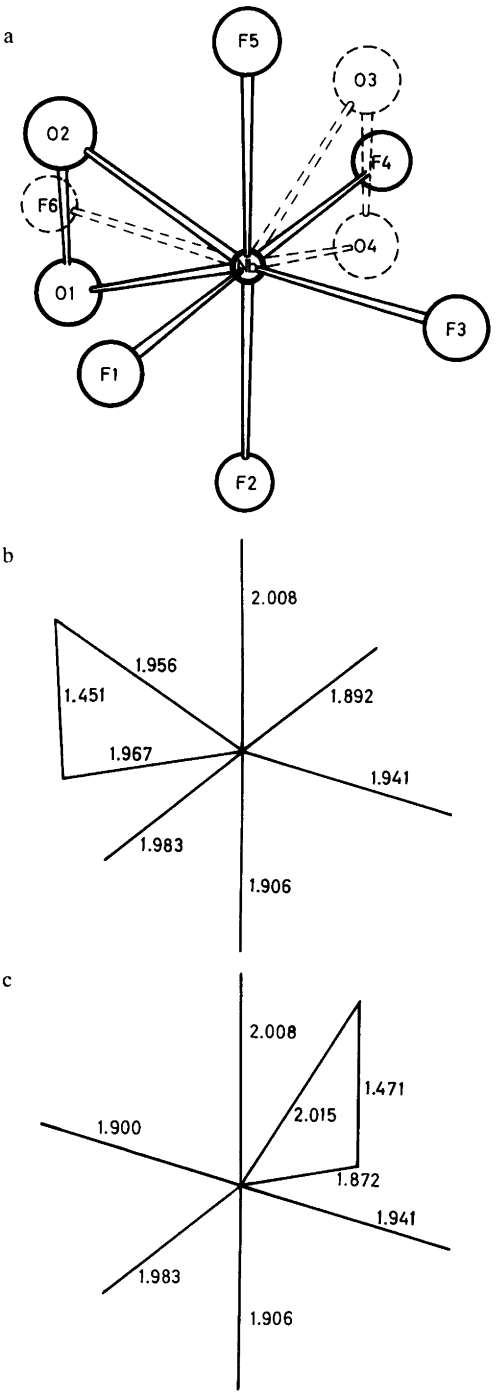

Fig. 1. (a) The two orientations **A** and **B** of the disordered anion. Orientation **A** comprises the atoms Nb, F1–F5, O1 and O2 and **B** the atoms Nb, F1–F3, F5, F6, O3 and O4. (b) Bond distances in **A** at 170 K. (c) Bond distances in **B** at 170 K.

Table 2. Bond distances at 170 and 275 K and angles at 170 K in $(C_9H_8NO)_2[NbF_5(O_2)] \cdot 3H_2O$. Nb, F1, F2, F3, F4, F5, O1 and O2 comprise one anionic complex, Nb, F1, F2, F3, F5, F6, O3 and O4 the other.

	170 K	275 K				
Distance/Å			Angle (°)			
Nb–F1	1.983(4)	1.97(1)	F1–Nb–F2	84.1(2)	C1–N1–C5	123.0(6)
Nb–F2	1.906(6)	1.89(1)	F1–Nb–F3	85.9(2)	N1–C1–C2	118.8(7)
Nb–F3	1.941(6)	1.92(1)	F1–Nb–F4	172.3(3)	C1–C2–C3	119.8(7)
Nb–F4	1.892(10)	1.91(2)	F1–Nb–F5	82.2(2)	C2–C3–C4	121.8(7)
Nb–F5	2.008(5)	1.98(1)	F1–Nb–F6	88.5(3)	C3–C4–C5	117.2(7)
Nb–F6	1.900(9)	1.89(2)	F1–Nb–O1	91.4(4)	C3–C4–C6	124.1(7)
Nb–O1	1.967(14)	1.89(2)	F1–Nb–O2	91.6(4)	C5–C4–C6	118.7(7)
Nb–O2	1.956(13)	2.00(2)	F1–Nb–O3	153.5(3)	N1–C5–C4	119.4(6)
Nb–O3	2.015(10)	1.99(2)	F1–Nb–O4	161.9(6)	N1–C5–C9	119.3(6)
Nb–O4	1.872(14)	1.83(3)	F2–Nb–F3	87.7(3)	C4–C5–C9	121.4(6)
O1–O2	1.451(19)	1.32(3)	F2–Nb–F4	100.8(4)	C4–C6–C7	120.1(7)
O3–O4	1.471(19)	1.35(4)	F2–Nb–F5	164.3(2)	C6–C7–C8	120.2(7)
N1–C1	1.342(9)	1.33(1)	F2–Nb–F6	96.1(3)	C7–C8–C9	121.1(7)
C1–C2	1.420(12)	1.41(2)	F2–Nb–O1	71.0(4)	C5–C9–Ox1	116.5(6)
C2–C3	1.355(13)	1.39(2)	F2–Nb–O2	114.2(5)	C8–C9–Ox1	124.9(6)
C3–C4	1.413(11)	1.38(2)	F2–Nb–O3	122.2(3)	C5–C9–C8	118.6(6)
C4–C5	1.419(10)	1.42(2)	F2–Nb–O4	78.0(6)	C10–N2–C14	122.6(7)
C5–N1	1.378(8)	1.36(1)	F3–Nb–F4	88.4(4)	N2–C10–C11	120.7(7)
C4–C6	1.406(11)	1.42(2)	F3–Nb–F5	83.8(3)	C10–C11–C12	118.3(8)
C6–C7	1.391(12)	1.34(2)	F3–Nb–F6	172.9(3)	C11–C12–C13	121.7(8)
C7–C8	1.411(11)	1.40(2)	F3–Nb–O1	158.8(4)	C12–C13–C14	118.4(7)
C8–C9	1.383(10)	1.36(2)	F3–Nb–O2	157.6(5)	C12–C13–C15	123.9(7)
C9–C5	1.407(9)	1.42(2)	F3–Nb–O3	91.5(3)	C14–C13–C15	117.6(6)
C9–Ox1	1.355(8)	1.36(1)	F3–Nb–O4	91.0(6)	N2–C14–C13	118.2(6)
N2–C10	1.317(12)	1.34(2)	F4–Nb–F5	92.2(4)	N2–C14–C18	119.8(6)
C10–C11	1.413(14)	1.39(2)	F4–Nb–O1	95.8(5)	C13–C14–C18	122.0(6)
C11–C12	1.357(14)	1.32(2)	F4–Nb–O2	91.8(6)	C13–C15–C16	120.2(7)
C12–C13	1.394(11)	1.40(2)	F5–Nb–F6	91.1(3)	C15–C16–C17	121.8(7)
C13–C14	1.416(9)	1.42(2)	F5–Nb–O1	116.7(4)	C16–C17–C18	120.2(7)
C14–N2	1.377(8)	1.35(1)	F5–Nb–O2	73.8(4)	C14–C18–Ox2	116.1(6)
C13–C15	1.424(11)	1.43(2)	F5–Nb–O3	71.3(3)	C17–C18–Ox2	125.8(6)
C15–C16	1.356(11)	1.34(2)	F5–Nb–O4	115.3(5)	C14–C18–C17	118.2(6)
C16–C17	1.413(12)	1.40(2)	F6–Nb–O3	91.6(4)		
C17–C18	1.384(10)	1.40(2)	F6–Nb–O4	95.7(6)		
C18–C14	1.415(9)	1.43(2)	O1–Nb–O2	43.4(6)		
C18–Ox2	1.335(8)	1.33(1)	O3–Nb–O4	44.3(6)		

together by ionic and hydrogen bond forces. The anion and one water molecule show disorder at 275 K as well as at 170 K. The anion has two equally occupied orientations with a common centre and one water molecule occupies two positions with the occupation numbers 0.6 and 0.4, respectively.

The two 8-hydroxyquinolinium ions are planar within the experimental errors. These planes form an angle of 0.6° to each other. The corresponding bond distances in the two non-equivalent 8-hydroxyquinolinium ions are equal; the largest difference is less than 3σ. The three carbon-carbon distances C2–C3, C6–C7 and C8–C9, and the corresponding ones in the other cation, are significantly shorter than the other carbon-carbon distances; the average ones * are 1.371(15) and 1.413(7) Å, respectively. They compare well with the corresponding values of 1.364(6) and 1.410(10), 1.365(12) and 1.404(13), and 1.369(12) and 1.415(10) for $(C_9H_8NO)_2[NbF_5O] \cdot 2H_2O$,[9] $(C_9H_8NO)[Mo(C_9H_6NO)Cl_3O]$,[14] and $[V(C_9H_6NO)_2(i\text{-}OC_3H_7)O]$,[15] respectively. One C–N distance is shorter than the other in both cations; the mean distance is 1.330(13) Å for the shorter and 1.378(1) Å for the larger one. The same observations were made

* R.m.s. deviations from the mean are given in parentheses.

Table 3. Hydrogen bond distances (Å) in $(C_9H_8NO)_2[NbF_5(O_2)] \cdot 3H_2O$.

	170 K	275 K
Ow1···F1^{i}	2.737(8)	2.74(1)
Ow1···F6	2.912(11)	2.81(2)
Ow1···O2	2.621(15)	2.67(2)
Ow1···Ox1^{ii}	2.641(7)	2.65(1)
Ow2···F3^{i}	2.647(8)	2.64(1)
Ow2···F5	2.759(8)	2.77(1)
Ow2···O3	2.964(12)	2.98(2)
Ow2···Ox2^{iii}	2.612(9)	2.60(1)
Ow3···Ow4^{iv}	2.776(16)	2.86(5)
Ow3^{i}···O3	2.803(15)	2.81(3)
Ow3···N2^{v}	2.690(12)	2.69(3)
Ow4^{i}···F4	2.875(20)	2.77(5)
Ow4^{i}···O3	2.832(18)	2.69(5)
Ow4···Ox2^{v}	2.892(15)	3.03(5)
Ow4···N2^{v}	2.781(14)	2.74(4)
N1···F5	2.717(7)	2.72(1)

Symmetry codes

i	$1+x,y,z$
ii	$x,\frac{1}{2}-y,-\frac{1}{2}+z$
iii	$1+x,\frac{1}{2}-y,\frac{1}{2}+z$
iv	$\bar{x},\bar{y},1-z$
v	$\bar{x},-\frac{1}{2}+y,\frac{1}{2}-z$

for the other three compounds mentioned above; the corresponding distances are 1.326(5) and 1.373(6) Å,[9] 1.321(3) and 1.367(3) Å,[14] and 1.329(5) and 1.362(1) Å,[15] respectively. All bond distances and angles in the 8-hydroxyquinolinium ion agree well with other observations for this ion and the 8-hydroxyquinolinato ligand.[9,14–18]

The pentafluoroperoxoniobate(V) anions are disorderly orientated in the crystal; this was not realised by R–T. Two main orientations, denoted A and B, both with occupancies 0.5, were observed (Fig. 1). The possibility of the existence of still other orientations with small occupation numbers cannot, however, be ruled out. It should be noted that the situation is the same at 275 and 170 K; one of the orientations might have been stabilized at the lower temperature. The disorder may be compared to the ones observed in $(C_{12}H_{10}N_2)[NbF_5(O_2)]$[7] and $Na_2[NbF_5(O_2)] \cdot 2H_2O$,[6] where two main orientations of the anions also were observed. Though having a common central atom position in all three cases, the relative orientations of the anions are, however, quite different. In $(C_{12}H_{10}N_2)[NbF_5(O_2)]$ the equatorial planes of the two disorderly orientated pentagonal bipyramidal anions almost coincide, forming an angle of 3° with one another, and the pentagons are mutually twisted 61°. In $Na_2[NbF_5(O_2)] \cdot 2H_2O$, turning the complex 90° about a line through niobium and the midpoint of the peroxo group gives the other orientation of the anion. Finally, the present investigation has shown that in $(C_9H_8NO)_2[NbF_5(O_2)] \cdot 3H_2O$, orientation B is reached from orientation A by rotating the anion 87° about a line through niobium, parallel to the O–O bond in the peroxo group (Fig. 1). The disorder in, *e.g.*, $(NH_4)_3[TiF_5(O_2)]$ is completely different, the complex assuming random orientations.[8,19]

The geometry of the anion $[NbF_5(O_2)]^{2-}$ is pentagonally bipyramidal as was found in $Na_2[NbF_5(O_2)] \cdot H_2O$,[4] $Na_3[HF_2][NbF_5(O_2)]$,[5] $Na_2[NbF_5(O_2)] \cdot 2H_2O$[6] and $(C_{12}H_{10}N_2)[NbF_5(O_2)]$.[7] The consistency of this geometry for the pentafluoromonoperoxometallates is evident from Table 5 in Ref. 6, listing interatomic distances in some compounds of this type, and is further supported by the values obtained for $(C_{12}H_{10}N_2)[NbF_5(O_2)]$,[7] $K_3[HF_2][TaF_5(O_2)]$,[20] and in the present investigation (see Table 5). Table 4 shows that the equatorial atoms are significantly displaced from the respective pentagonal planes; this has been found for other pentafluoroniobates, also.[4–7] The pentagonally bipyramidal configuration has been observed for all seven coordinated transition metal peroxo complexes hitherto investigated (see, *e.g.*, Refs. 4–8, 20–25). Since there are three, energetically about equally favourable, geometries for seven coordination, the pentagonal bipyramid, the monocapped octahedron and the monocapped trigonal prism, the bidentate ligand O_2^{2-} obviously stabilizes the pentagonal bipyramidal arrangement.

The Nb–F and Nb–O bond distances, ranging from 1.892 to 2.008 Å and from 1.872 to 2.015 Å, respectively, are considered to be metal-ligand single-bond distances, comparable to other observations.[4–7,9,25] The anion orientation A comprises the positions denoted Nb, F1–F5, O1 and O2 and B those denoted Nb, F1–F3, F5, F6, O3 and O4. Nb, F1–F3, and F5 thus belong to both orientations. Each of these experimentally observed positions is probably split into two unresolvable ones. As a consequence of this, the interatomic distances involving these atoms are considered to be more uncertain than can be judged from the e.s.d.'s.

Table 4. Displacements (Å) of the atoms from certain least-squares planes in $(C_9H_8NO)_2[NbF_5(O_2)] \cdot 3H_2O$. Defining atoms, given equal weights, are: Plane I F2, F3, F5, O2 and O1
Plane II F5, F1, F2, O4 and O3

	Plane I			Plane II	
Atom	170 K	275 K	Atom	170 K	275 K
F2	0.102(6)	0.10(1)	F5	0.063(5)	0.06(1)
F3	−0.110(6)	−0.13(1)	F1	−0.055(4)	−0.02(1)
F5	0.108(5)	0.15(1)	F2	0.038(6)	−0.03(1)
O2	−0.065(13)	−0.12(2)	O4	0.008(14)	0.12(3)
O1	−0.036(14)	0.00(2)	O3	−0.054(10)	−0.14(2)
Nb	−0.120(1)	−0.07(1)	Nb	−0.081(1)	−0.06(0)
F1	1.858(4)	1.88(1)	F3	1.856(6)	1.85(1)
F4	−2.006(10)	−1.96(2)	F6	−1.977(9)	−1.92(2)

Table 5. The length of the edges of the pentagonal bipyramidal coordination polyhedron in $(C_9H_8NO)_2[NbF_5(O_2)] \cdot 3H_2O$ at 170 K. The designation of the edges conforms to Fig. 3 in Ref. 6. Compare with Table 5 in Refs. 6 and 7 and with Table 4 in Ref. 20.

Edge		Distance/Å		Distance/Å
a	F2···F3	2.666(9)	F5···F1	2.622(7)
b	F3···F5	2.638(8)	F1···F2	2.605(8)
c	F5···O2	2.379(15)	F2···O4	2.377(19)
d	O2···O1	1.451(19)	O4···O3	1.471(19)
e	O1···F2	2.250(15)	O3···F5	2.344(10)
f	F1···F2	2.605(8)	F3···F5	2.638(8)
g	F1···F3	2.673(7)	F3···F1	2.673(7)
h	F1···F5	2.622(7)	F3···F2	2.666(9)
i	F1···O2	2.823(14)	F3···O4	2.720(17)
j	F1···O1	2.827(14)	F3···O3	2.834(12)
k	F4···F2	2.926(13)	F6···F5	2.790(10)
l	F4···F3	2.672(13)	F6···F1	2.709(10)
m	F4···F5	2.810(11)	F6···F2	2.829(10)
n	F4···O2	2.763(18)	F6···O4	2.797(18)
o	F4···O1	2.862(17)	F6···O3	2.807(13)

The peroxo oxygen bond distances, 1.471(19) and 1.451(19) Å, compare well with other observations. In the pentafluoroperoxoniobates hitherto investigated, the following distances were observed: 1.476(7) Å in $Na_2[NbF_5(O_2)] \cdot H_2O$,[4] 1.481(4) Å in $Na_3[HF_2][NbF_5(O_2)]$,[5] 1.506(26) and 1.411(31) Å in $Na_2[NbF_5(O_2)] \cdot 2H_2O$ (disordered),[6] and 1.483(8) and 1.440(16) Å in $(C_{12}H_{10}N_2)[NbF_5(O_2)]$ (disordered).[7] Comparable values have been found in other transition metal peroxo complexes (see Tables of O–O bond distances in, *e.g.*, Refs. 21–23). The distances obtained at 275 K in the present investigation are rather short, though, owing to their large standard deviations, it is doubtful whether they are significantly different from other observations. There is, in fact, evidence for O–O bond distances determined at room temperature to appear a bit short, not only those obtained using film data but also diffractometer data, a recent example being 1.419(6) Å, observed in $[Ti(O_2)(C_6H_4NO_2)_2(OPN_3C_6H_{18})]$.[24] Possible reasons for this effect may be thermal motion and partial decomposition of the compound during the data collection, both these factors being less pronounced at low temperatures.

Substantial hydrogen bonding stabilizes the structure; the shortest hydrogen bond is 2.612(9) Å. One of the water molecules (w3 according to R–T) was observed to be disordered; this molecule occupies two positions, denoted w3 and w4,

with the occupancies 0.6 and 0.4, respectively. This together with the existence of two orientations of the anion (four new atomic positions were introduced), leads to a modification of the hydrogen bonding scheme put forward by R–T, and is evident from Table 3.

Acknowledgements. I wish to express my gratitude to Mrs. Solveig Olson for technical assistance.

REFERENCES

1. Ružić-Toroš, Ž., Kojić-Prodić, B., Gabela, F and Šljukić, M., *Acta Crystallogr. B33* (1977) 692.
2. Svensson, I-B. and Stomberg, R., *7:e Nordiska Strukturkemistmötet,* Göteborg (1970) 97.
3. Stomberg, R., Internal report, Chalmers tekniska högskola, 1974.
4. Stomberg, R., *Acta Chem. Scand. A34* (1980) 193.
5. Stomberg, R., *Acta Chem. Scand. A35* (1981) 389.
6. Stomberg, R., *Acta Chem. Scand. A35* (1981) 489.
7. Stomberg, R., *Acta Chem. Scand. A36* (1982) 101.
8. Stomberg, R. and Svensson, I-B., *Acta Chem. Scand. A31* (1977) 635.
9. Stomberg, R., *Acta Chem. Scand. A35* (1981) 779.
10. Lehmann, M. S. and Larsen, F. K., *Acta Crystallogr. A30* (1974) 580.
11. Cruickshank, D. W. J. In *Crystallographic Computing,* Munksgaard, Copenhagen 1970, p. 195.
12. *International Tables for X-Ray Crystallography,* Kynoch Press, Birmingham 1974, Vol. 4.
13. Program library of the Dept. of Inorg. Chem., Chalmers Tekniska Högskola and Göteborgs universitet: LELA, SYN written by Lindqvist, O. and Ljungström, E., DRF by Zalkin, A., BLOCK by Lindgren, O., LINUS (Hamilton and Ibers' version of the Busing-Levy-Martin program ORFLS), DISTAN by Zalkin, A. and PLANEFIT by Wengelin, F.
14. Yamanouchi, K., Huneke, J. T., Enemark, J. H., Taylor, R. D. and Spence, J. T. *Acta Crystallogr. B35* (1979) 2326.
15. Scheidt, W. R. *Inorg. Chem. 12* (1973) 1758.
16. Hoy, R. C. and Morris, R. H. *Acta Crystallogr. 22* (1967) 476.
17. Schlemper, E. O. *Inorg. Chem. 6* (1967) 2012.
18. Atovmayan, L. O. and Sokolova, Y. A. *Zh. Strukt. Khim. 12* (1971) 851.
19. Massa, W. and Pausewang, G. *Mater. Res. Bull. 13* (1978) 361.
20. Stomberg, R. *Acta Chem. Scand. A36* (1982) 423.
21. Svensson, I-B. and Stomberg, R. *Acta Chem. Scand. 25* (1971) 898.
22. Larking, I., and Stomberg, R. *Acta Chem. Scand. 26* (1972) 3708.
23. Begin, D., Einstein, F. W. B. and Field, J. *Inorg. Chem. 14* (1975) 1785.
24. Mimoun, H., Postel, M., Casabianca, F., Fischer, J. and Mitschler, A. *Inorg. Chem. 21* (1982) 1303.
25. Pakhomov, V. I. and Kaidalova, T. A. *Kristallografiya 19* (1974) 733.

Received November 24, 1982.

Acta Chemica Scandinavica A 37 (1983) 531–534

Studies on Metal Carbonate Equilibria. 6. On the Solubility Equilibria of Rare-earth Carbonates: The Lanthanum Carbonate, $La_2(CO_3)_3 \cdot 8H_2O(s)$

DIEGO FERRI* and FRANCESCO SALVATORE*

The Royal Institute of Technology, Department of Inorganic Chemistry, S-100 44 Stockholm 70, Sweden

A general method for the accurate evaluation of the solubility equilibria of rare-earth carbonates from emf measurements is proposed. Its application to $La_2(CO_3)_3 \cdot 8H_2O(s)$ is described in detail and the equilibrium constant

$$K=[La^{3+}]^2[H^+]^{-6}P_{CO_2}^3=10^{(22.65\pm0.03)}$$

for the reaction

$$La_2(CO_3)_3(s)+6H^+ \rightleftharpoons 2La^{3+}+3CO_2(g)+3H_2O$$

is determined in 1 M $La(ClO_4)_3$ medium, at 25 °C.

Equilibria of the type

$$Ln_2(CO_3)_3(s) \rightleftharpoons 2Ln^{3+}+3CO_3^{2-} \quad (1)$$

have usually been investigated by solubility measurements.[1] The attainment of equilibrium is the critical stage when studying heterogeneous equilibria. The time for equilibration is often several days long, particularly if an initially amorphous phase recrystallizes. Thus serious effort has to be devoted to ascertain that true equilibrium is reached.

The attainment of a constant solubility value is certainly a simple equilibrium criterium, but a tedious one because of the manipulations involved.

In this communication, we have chosen the lanthanum carbonate system to describe how the emf method can conveniently ensure the reliable attainment of equilibrium and the accurate evaluation of the solubility equilibria.

METHOD

The equilibrium constant of the reaction

$$La_2(CO_3)_3(s)+6H^+ \rightleftharpoons 2La^{3+}+3CO_2(g)+3H_2O \quad (2)$$

has been determined at 25 °C in 1 M $La(ClO_4)_3$ by measuring the emf of the cell

$$-\text{glass electrode} \mid \text{test solution} \mid \text{RE}+ \quad (A)$$

where RE is the reference half cell

$$\begin{array}{l|l|l} 1\ M & 0.01\ M\ AgClO_4, & AgCl(s), \\ La(ClO_4)_3 & 0.997\ M\ La(ClO_4)_3 & Ag \end{array}$$

The emf of cell (A) can be written

$$E=E_o - 59.16 \log h + E_j \quad (3)$$

In (3) h is the proton concentration. E_j is the liquid junction potential between the test solution and 1 M $La(ClO_4)_3$ which was considered negligible. Actually E_j did not exceed 0.1 mV, since the initial h was always smaller than 10^{-2} M. E_o is a constant determined in the initial part of

* Permanent address: Istituto Chimico dell'Università, via Mezzocannone 4, 80 134 NAPOLI, Italy.

0302-4377/83 $2.50

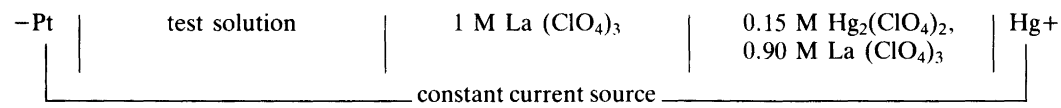

Scheme 1.

the experiments. These were carried out as titrations, where the total lanthanum concentration was kept constant, whereas the analytical concentration excess of protons, H,* was varied by stepwise reduction on a Pt gauze by means of the coulometric circuit (Scheme 1).

In order to avoid local formation of lanthanum oxide on the cathode, current densities lower than $1 \cdot 10^{-3}$ A/cm^2 were used.

The test solutions had the general composition

TS=1.000 M La^{3+}, H M H^+, (3.000+H) M ClO_4^-

In the first part of the titration, H was only varied within the range where $h=H$ can be assumed, *i.e.* no appreciable hydrolysis of La^{3+} takes place.

E_o could thus be determined from the $E(H)$ data by using eqn, (3) and the relation

$$H=H_o - w/V \qquad (4)$$

In (4) H_o is the initial analytical concentration excess of protons and V (dm^3) the volume of the test solution; w represents the total number of mol of protons removed after each step of electrolysis.

Then a stream of CO_2–N_2 gas of known composition, presaturated with the proper H_2O vapour pressure (0.0276 atm) by equilibration with 1 M $La(ClO_4)_3$, was passed through TS. H was decreased in a single step to a value where the incipient formation of a solid phase, recognized a $La_2(CO_3) \cdot 8H_2O$, was observed. The electrolysis was then discontinued. Equilibrium was reached in a few days as indicated by the emf of cell (A) which eventually reached a value that remained constant within 0.1 mV for several days.

* The analytical variable H is equal to the analytical concentration of $HClO_4$ at the beginning of the titration minus the total OH^- concentration coulometrically generated.

Table 1. $h(P_{CO_2})$ data at $[La^{3+}]=1.000$ M.

P_{CO_2} (atm)	$h \cdot 10^3$ (M)	log K_s (eqn. 6)
0.978	0.164	22.68
0.099_5	0.052	22.69
0.298_5	0.093	22.62
0.995	0.168	22.64

The equilibrium was also re-established in a few days, when the CO_2–N_2 mixture was replaced with another of different partial pressure of carbon dioxide, P_{CO_2}. Experiments performed by letting P_{CO_2} span repeatedly the values 1, 0.1, 0.3, 1 atm indicate that the emf of cell (A) is the same within the experimental errors on approaching equilibrium both from supersaturated and undersaturated solutions. Thus true equilibrium is attained.

From the $h(P_{CO_2})$ data, K can easily be calculated with a high degree of accuracy, as shown in the next section.

CALCULATIONS

Determination of K. The coulometric alkalification of the test solution is carried out until the incipient precipitation of the solid phase. Only a negligible fraction of the lanthanum ion is thus removed from the solution to enable the formation of $La_2(CO_3)_3$(s). In addition from the $h(P_{CO_2})$ data (see Table 1), we can deduce that the concentration of the hydroxo[3] and carbonate[2] complex species in the test solutions equilibrated with the solid $La_2(CO_3)_3$ are always several orders of magnitude lower than the total metal concentration.

Consequently, no loss of accuracy is introduced by assuming that the concentration of non-bound lanthanum stays constant at the 1 M level throughout the experiment, *i.e.*

$$[La^{3+}]=1.000\ M \quad (5)$$

From the $h(P_{CO_2})$ data and from (5), we can calculate

$$K=[La^{3+}]^2 P_{CO_2}^3 h^{-6} \quad (6)$$

From a series of measurements of which a sample is reported in Table 1, we obtained

$$\log K=22.65\pm0.03$$

The error represents the maximum deviation from the mean.

Extrapolation of the results. The value of K for reaction (2) determined above refers to a 1 M $La(ClO_4)_3$ medium.

The medium dependence of equilibrium constants is usually evaluated by estimating the activity factors of the species involved.

The specific interaction (SI) theory has satisfactorily been used[4,5] for this purpose. Its application is shown here to the calculation of the constant of reaction (2) at infinite dilution, K_o, from its value valid in 1 M $La(ClO_4)_3$. The relation between K and K_o expressed in molal units is given by

$$\log K_o=\log K+\log(\gamma_{La^{3+}}^2 \cdot \gamma_{H^+}^{-6}) -4\log(d-0.4373) \quad (7)$$

where γ_i is the molal activity coefficient of species i at the molality m_i, $d=1.328$ g cm^{-3} is the density of 1 M $La(ClO_4)_3$ at 25 °C and 0.4373 is the weight of 1 mmol of $La(ClO_4)_3$. The activity coefficients ratio in (7) can be evaluated by applying the SI theory:

$$\log(\gamma_{La^{3+}}^2 \cdot \gamma_{H^+}^{-6})=-6.131\sqrt{I}(1+1.5\sqrt{I})^{-1}+ +[2\varepsilon(La^{3+},ClO_4^-)_I - 6\varepsilon(H^+,ClO_4^-)_I]m_{ClO_4^-} \quad (8)$$

where I is the ionic strength of the solution and $\varepsilon(i,K)_I$ is the interaction coefficient at ionic strength I of the species i with the species K at the molality m_K.

In (8) the terms accounting for the interaction between La^{3+} and H^+ with HCO_3^- and CO_3^{2-} have been neglected because of the very low values attained by $m_{HCO_3^-}$ and $m_{CO_3^{2-}}$ in this study. By introducing in (8) the values

$$\varepsilon(H^+,ClO_4^-)_{6.7}=0.16\ \text{kg mol}^{-1}$$

$$\varepsilon(La^{3+},ClO_4^-)_{3.5}\simeq\varepsilon(La^{3+},ClO_4^-)_{6.7}=0.47\ \text{kg mol}^{-1}$$

evaluated from osmotic coefficients reported in the literature,[6,7] we obtain

$$\log(\gamma_{La^{3+}}^2 \cdot \gamma_{H^+}^{-6})=-3.3\pm0.2 \quad (9)$$

Consequently,

$$\log K_o=19.1_5\pm0.2 \quad (10)$$

The errors in (9) and (10) have been estimated by varying the interaction coefficients within ±10 %. The magnitude of K_o in molar units obviously coincides with the value given in (10).

Further evidence for the convenience of the emf method for the evaluation of solubility equilibria will be given in a forthcoming paper on the yttrium carbonate system.[8] This extensive study carried out at several ionic strengths also corroborates the numerical treatment illustrated above.

EXPERIMENTAL

Lanthanum, carbon and water in a sample of the air-dried precipitate were analysed using elemental analytical techniques. The results showed ratios corresponding to $La_2(CO_3)_3 \cdot 8H_2O(s)$. In addition, X-ray powder diffraction data, compared with those reported by Wakita,[9] also indicated $La_2(CO_3)_3 \cdot 8H_2O(s)$.

The details of the emf measurements as well as the methods of preparation and analysis of solutions have been described elsewhere.[2,3]

Acknowledgements. This investigation was financially supported by PRAV (The Swedish National Council for Radioactive Waste), KBS (The Swedish Nuclear Fuel Supply Co.) and by C.N.R. (The Italian National Research Council).

REFERENCES

1. Sillén, L. G. and Martell, E. A., *Eds. Stability Constants of Metal Complexes, Chem. Soc., Spec. Publ. 17* (1964) and *25* (1971).
2. Ciavatta, L., Ferri, D., Grenthe, I., Salvatore, F. and Spahiu, K. *Acta Chem. Scand. A 35* (1981) 403.

3. Biedermann, G. and Ciavatta, L. *Acta Chem. Scand. 15* (1961) 1347.
4. Biedermann, G. In Goldberg, E.D., Ed. *On the Nature of Sea Water, Dahlem Konferenzen,* Berlin 1975.
5. Ciavatta, L. *Ann. Chim. Rome 70* (1980) 551.
6. Robinsons, R. A. and Stokes, R. H. *Electrolyte Solutions,* Butterworth, London 1955.
7. Pitzer, K. S. and Mayorga, G. *J. Phys. Chem. 77* (1973) 2300.
8. Spahiu, K. *To be published.*
9. Wakita, H. *Bull. Chem. Soc. Jpn. 51* (1978) 2879.

Received November 22, 1982.

Acta Chemica Scandinavica A 37 (1983) 535–538

Short Communication

Formal Potentials of Importance for Iodometry in 3 M NaCl and 4 M HBr Media

GEORG BIEDERMANN and SIGNAR SUNDSTRAND

Department of Inorganic Chemistry, The Royal Institute of Technology, S-100 44 Stockholm, Sweden

New methods for iodine analysis, involving the coulometric formation of IBr_2^- and $HgICl_3^{2-}$, have been described in Refs. 1 and 2.

In order to optimize our experimental conditions we constructed redox diagrams of different types in the ionic media 3 M NaCl and 4M HBr.

The reliable calculation of these diagrams required the evaluation of several formal (standard) potentials ($E^{0\prime}$) in the actual media.

The formal redox potentials and the corresponding equilibrium constants, K, which were determined, are collected in Tables 1 and 2.

We have assumed that each of the reacting species occurs entirely in the form written in Tables 1 and 2. The uncertainty thus arising was one of the reasons to not provide lg K values more accurately than 0.1 units.

The reference states have been chosen so that the activity coefficients tend to unity as the composition of the test solutions, TS, approaches 4 M HBr and 3 M NaCl, respectively. Hence our two pE scales are different.

To convert the data to a common scale, it is required to estimate the trace activity coefficient of H^+, and of the other reacting species, and the mean activity coefficient of 4 M HBr.

The emf measurements were carried out with the equipment and the reagents that were used in the iodine analyses.[1,2]

The reversible emf data are presented in Tables 1 and 2. They may be regarded as correct first estimates of the standard potentials but with wide limits of uncertainty (typically 5 mV).

Each $E^{0\prime}$, determination started with a calibration step. The glass electrode, or the external reference half-cell, was compared with the hydrogen electrode using the cell arrangements shown in Tables 1 and 2.

Table 1. Survey of formal redox potentials in 4M HBr medium at 25 °C.

Calibration step: H_2 (1atm) | Pt(Platinized) | 4 M HBr | Glass electrode +
Measuring cell: Glass electrode | TS | Ir +.

Cell reaction, No.	lg K,	$E^{0\prime}$ V,	$E^{0\prime}$ V, (est.[a])	Comments
$Br_3^- + H_2$(1 atm) $\rightleftharpoons$ 3 Br^-(4 M) +2 H^+ (4 M), (1)	$33._0$	0.97_6	0.99	Coulometric oxidation of bromide. $[Br_3^-]$=0.02–0.5 mM
$I_2Br^- + H_2$(1 atm)$\rightleftharpoons 2I^- + Br^-$(4 M) +2$H^+$(4 M), (2)	$17._4$	0.51_4	0.52	Potentiometric titration
2 $IBr_2^- + H_2$(1 atm)$\rightleftharpoons I_2Br^-$ +3 Br^-(4 M)+2H^+(4 M), (3)	$26._2$	0.77_6	0.75	Coulometric oxidation and potentiometric titration
$IBr_2^- + H_2$(1 atm)$\rightleftharpoons I^- +2$ Br^-(4 M) +2H^+(4 M), (4)	$21._8$	0.64_5	0.64	Dilution of an iodine solution

[a] See text and Tables 3 and 4.

0302-4377/83 $2.50

Table 2. Survey of formal redox potentials in 3 M NaCl medium at 25 °C.

Calibration step:
H_2 (1 atm) | Pt(Platinized) (and glass electrode) | TS | RE+ TS: 3 M Cl^-, (3 M–*h*) Na^+, $h=[H^+]$ (h=1.7–7.7 mM)
RE= ⋮ 3M NaCl ⋮ 3 M NaCl saturated with AgCl (*s*) | AgCl(*s*) | Ag
The calibration was made with coulometric alkalification of the test solution.
Measuring cell: RE | TS | Ir+(and glass electrode)

Cell reaction, No.	lg *K*,	$E^{0\prime}$ V	$E^{0\prime}$ V, (est.[a])	Comments
$Cu(II)+\frac{1}{2}\,H_2(1\ atm)\rightleftharpoons Cu(I)+H^+$, (5)	8.6_4	0.51_1	—,	Coulometric reduction [Cu(I)]=0.3–1.3 mM, [Cu(II)]=66.7–65.7 mM
$2\,ICl_2^-+H_2$ (1 atm)$\rightleftharpoons I_2Cl^-+3\,Cl^-$ (3 M)$+2\,H^+$, (6)	$32._8$	0.97_1	0.97	Potentiometric titration
$I_2Cl^-+2\,HgCl_4^{2-}+H_2$ (1 atm)$\rightleftharpoons 2\,HgICl_3^{2-}+3\,Cl^-$(3 M)$+2\,H^+$, (7)	$28._9$	0.85_4	0.88	Potentiometric titration
$ICl_2^-+HgCl_4^{2-}+H_2$ (1 atm)$\rightleftharpoons HgICl_3^{2-}+3\,Cl^-$(3M)$+2\,H^+$, (8)	$30._8$	0.91_1	0.93	Dilution of an iodine solution

[a] See text and Tables 3 and 4.

Table 3. Data needed to estimate the equilibrium constants of Table 1 and 2. The superscript zero denotes a value valid at low ionic strengths.

Reaction		lg K^0	Ref.
$I_2(s)\rightleftharpoons I_2\ (aq)$	(9)	–2.9	4–6 (S.C.)
$\frac{1}{2}\,I_2(s)+e\rightleftharpoons I^-$	(10)	9.05	3 (Latimer)
$\frac{1}{2}\,Br_2(aq)+e\rightleftharpoons Br^-$	(11)	18.35	3
$Br_2(aq)+Br^-\rightleftharpoons Br_3^-$	(12)	1.2	4–6
$I_2(aq)+Br^-\rightleftharpoons I_2Br^-$	(13)	1.1	4–6
$I_2(aq)+I^-\rightleftharpoons I_3^-$	(14)	2.9	4–6
$IBr_2^-+e\rightleftharpoons\frac{1}{2}\,I_2(s)+2\,Br^-$	(15)	14.7	3
$ICl_2^-+e\rightleftharpoons\frac{1}{2}\,I_2(s)+2Cl^-$	(16)	17.8	3
$I_2(s)+Cl^-\rightleftharpoons I_2Cl^-$	(17)	–2.69	17
lg K (3M NaCl)		–3.05	17
$I_2(s)+I^-\rightleftharpoons I_3^-$ 1 g K (3M Na^+ (ClO_4^-, I^-))	(18)	–0.3	Present work
$HgCl_4^{2-}+nI^-\rightleftharpoons HgI_nCl_{4-n}^{2-}+n\,Cl^-$ lg K_n (3M)	(19)	4.3 n=1 8.2 n=2 11.7 n=3 14.8 n=4	Present work

After the calibration step, the platinum electrode was removed from the vessel and the hydrogen gas was expelled overnight by nitrogen or argon. The redox potential measurements were then undertaken with an iridium electrode. This technique was used throughout.

Tribromide ions (reaction 1), IBr_2^- (3) and Cu(I) (5), were generated by coulometry with

iridium electrodes.

Equilibria involving I(+I) and I(–I), (4) and (8), could conveniently be studied by preparing an iodine solution and diluting it stepwise with the ionic medium. The remaining reactions were investigated by potentiometric titrations of iodine with I^- or ICl_2^-.

The validity of our assumptions concerning equilibrium concentrations and of our experimental approach in general, may be tested by the thermodynamic criteria:

$$2\ E^{0\prime}(4)=1.29=E^{0\prime}(2)+E^{0\prime}(3)=0.51+0.78\ \text{V}$$

$$2E^{0\prime}(8)=1.82=E^{0\prime}(6)+E^{0\prime}(7)=0.97+0.85\ \text{V}$$

Comparison with previous results. Many equilibrium constants and standard potentials involving iodine and bromine are available in dilute aqueous solutions. These may be combined to estimate the equilibrium constants of Tables 1 and 2. Most of the information required is easily available in Latimer's treatise,[3] and in the volumes of Stability Constants.[4,5,6]

The data needed for our purpose are gathered in Table 3.

The triiodide formation constant at 3 M $[Na^+]$ level, represents our preliminary result. The mixed formation constants (K_n of (19)) were estimated by using Sillén's,[7] Arnek's[8] and Ciavatta's[9] results concerning tetrachloro and tetraiodo complexes at different ionic strengths. We introduced the hypothesis that the medium effect on $\beta(HgCl_4^{2-})$ equals that of $\beta(HgI_4^{2-})$, *i.e.* that the activity coefficient quotient

$$y^4(I^-)\times y(HgCl_4^{2-})/[y^4(Cl^-)\times y(HgI_4^{2-})]$$

remains uninfluenced by the medium.

Further, we assumed according to Spiro and Hume[10] (*cf.* also Ref. 11), that the equilibrium constants for the formation of mixed complexes can be calculated assuming a statistical distribution of the ligands.

Hence,

$$\lg K_n=n/4\times(\lg\beta(HgI_4^{2-})-\lg\beta(HgCl_4^{2-}))+\lg 4!-\lg((4-n)!n!) \quad \text{(i)}$$

Spiro and Hume showed that this hypothesis explained both their own spectroscopic and Marcus'[12] distribution data.

The chemical significance of our lg K_n calculation is visualized in Fig. 1 . It is clear from this figure, that at the low $[I^-]/[Cl^-]$ ratios chosen for analysis, it is permissible to set $[I^-]_{tot}$ equal to $[HgICl_3^{2-}]$ as was done in Table 2.

The activity coefficient data and the estimates necessary to calculate the constants of Tables 1 and 2 from those of Table 3 are summarized in Table 4.

The medium effect estimates were carried out by employing the specific interaction theory essentially in the form developed by Scatchard.[13–15]

Table 4. Activity coefficient data and estimates needed to calculate the $E^{0\prime}$ values of Tables 1 and 2. y^0 denotes the activity coefficient of an electrolyte in its own solution in volume concentration terms.

(1)	4M (4.5m) hydrogen bromide medium	
	y^0(4M HBr)=3.39	(Ref. 18)
	y^0(4M HI)=4.31	(Ref. 18)
	postulates:	
	$y(I_2Br^-)=y(Br^-)$	
	$y(IBr_2^-)=y(Br^-)$	
	$y(Br_3^-)=y(Br^-)$	
	(these postulates are not likely to be far from the truth as the salting out by HBr is small [a])	
(2)	3M (3.2m) sodium chloride medium	
	y^0(3M NaCl)=0.77	(Ref. 19)
	y^0(3M HCl)=1.48	(Ref. 19)
	$y(I_2Cl^-)/y(Cl^-)=2.31$	(Ref. 17)
	postulates:	
	$y(I_2Cl^-)=y(ICl_2^-)$	
	$y(HgICl_3^{2-})=y(HgCl_4^{2-})$	

[a] The salting out by HBr is generally small as it may be estimated by considering solubility data for nonpolar gases and approximating its Setschenow parameter k_{HBr} with $k_{HBr}=k_{HCl}+k_{MeBr}-k_{MeCl}$[13,20].

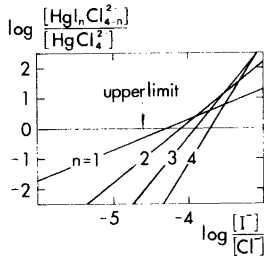

Fig. 1. Concentration ratio diagram for the formation of mixed iodide- and chloride-bearing mercury complex species in 3 M Na^+ (Cl^-, I^-) medium. The lines have been calculated with equation (i) using the formation constant data discussed in the text. The arrow indicates the maximum $[I^-]/[Cl^-]$ ratio reached in the titrations.

The activity coefficients reported in the literature have been recalculated to the volume molarity scale by using density data recommended by the Gmelins Handbook of Inorganic Chemistry.[16]

Comparison of $E^{0\prime}$ and $E^{0\prime}$(estimated) in Tables 1 and 2, demonstrates that the deviation between the values hardly exceeds the experimental uncertainty. As the distributions of copper(I) and copper(II) ions over different complexes are not known with certainty, we have not been able to estimate lg K (5).

The triiodide formation constants (reactions 14 and 18), also included in Table 3, are needed for the estimates of the $[I_3^-]$ in the redox diagrams shown in Refs. 1 and 2.

In the light of the close agreement generally obtained, we may have little doubt that our experiments may be regarded to be consistent with the numerous results of the classical investigators.

Acknowledgements. This work has been supported by a grant from *Statens Naturvetenskapliga Forskningsråd* (The Swedish Natural Science Research Council). We are grateful to Professor Ingmar Grenthe for his valuable comments on the manuscript.

1. Sundstrand, S. *Acta Chem. Scand. A 37* (1983). *In press.*
2. Sundstrand, S. *Acta Chem. Scand. A 37* (1983). *In press.*
3. Latimer, W. M. *Oxidation Potentials*, 2nd Ed., Prentice-Hall, New York 1952.
4. *Stability Constants*, Special Publication No. 17, The Chemical Society, London 1964.
5. *Stability Constants*, Supplement No. 1, Special Publication No 25, The Chemical Society, London 1971.
6. *Stability Constants*, Part A: Inorganic Ligands, (Supplement No. 2), IUPAC Chemical Data Series, No. 21, Pergamon, Oxford 1982.
7. Sillén, L. G. *Acta Chem. Scand. 3* (1949) 539.
8. Arnek, R. *Ark. Kemi 24* (1965) 531.
9. Ciavatta, L. and Grimaldi, M. *J. Inorg. Nucl. Chem. 30* (1968) 197.
10. Spiro, T. G. and Hume, D. N. *Inorg. Chem. 2* (1963) 340.
11. Marcus, Y. and Eliezer, I., *J. Phys. Chem. 66* (1962) 1661.
12. Marcus, Y. *Acta Chem. Scand. 11* (1957) 599.
13. Scatchard, G. *Equilibrium in Solutions, Surface and Colloid Chemistry*, Harvard University Press, Cambridge, London 1976, pp. 136–148.
14. Biedermann, G., Bruno, J., Ferri, D., Grenthe, I., Salvatore, F. and Spahiu, K. In Lutze, W., Ed., *Scientific Basis for Radioactive Waste Management – V*, North-Holland, New York, Amsterdam, Oxford 1982, pp. 791–799.
15. Biedermann, G. In Goldberg, E. D., Ed., *Dahlem Workshop on the Nature of Seawater 2*, Physical and Chemical Sciences Research, Report 1, Berlin 1975, pp. 339–362.
16. *Gmelins Handbook of Inorganic Chemistry, 8th Ed., Syst. No. 6*, 1927, p. 140, (HCl), *Syst. No. 7*, 1931, p. 217, (HBr), *Syst. No. 8*, 1933, p. 296, (HI), *Syst. No. 21*, 1928, p. 336, (NaCl).
17. Cason, D. L. and Neumann, H. M. *J. Am. Chem. Soc. 83* (1961) 1822.
18. Haase, R., Naas, H. and Thumm, H. *Z. Phys. Chem. 37* (1963) 210.
19. Robinson, R. A. and Stokes, R. H., *Electrolyte Solutions*, 2nd Ed., (revised), 5th impression, Butterworth, London 1970.
20. Long, F. A. and McDevit, W. F. *Chem. Rev. 51* (1952) pp. 119–169, (*cf.* esp. p. 134).

Received February 28, 1983.

Acta Chemica Scandinavica A 37 (1983) 539–543

The Crystal Structure of $Ni_2P_4O_{12}$

ANDERS G. NORD

Section of Mineralogy, Swedish Museum of Natural History, P.O. Box 50007, S-104 05 Stockholm 50, Sweden

$Ni_2P_4O_{12}$ belongs to a group of isostructural $M_2P_4O_{12}$ tetrametaphosphates with monoclinic $C2/c$ space group symmetry. The cell constants of $Ni_2P_4O_{12}$ are: a=11.642(3), b=8.239(2), c=9.850(2) Å, β=118.47(2)°, V=830.6(5) Å^3 (Z=4); D_x=3.465 g cm^{-3}. The structure has been profile-refined with neutron powder diffraction data down to R_I=0.059 on the basis of 138 independent reflections. The two distinct cation sites have fairly regular octahedral environments with average Ni-O distances of 2.06(1) and 2.07(1) Å, respectively. The $P_4O_{12}^{4-}$ ions have P-O-P angles of 133.6° and 130.2°. A comparison with other known $M_2P_4O_{12}$ structures is made, showing good correlation between metal-oxygen distances and cation radii.

$Al_4(P_4O_{12})_3$ was the first tetrametaphosphate structure to be investigated; it was determined in 1937 by Pauling and Sherman.[1] Since then about thirty inorganic tetrametaphosphate structures have been published. Some pioneer work on divalent-metal metaphosphates was done by Thilo and Grunze.[2] They showed, from X-ray powder diffraction data and paper chromatography, that many of these compounds were isomorphous with each other and probably were tetrametaphosphates of the type $M_2P_4O_{12}$. Some unit cell dimensions were later published by Beucher and Grenier,[3] indicating monoclinic symmetry. The crystal structure for this group of tetrametaphosphates was finally solved independently by means of the compounds $Cu_2P_4O_{12}$ (Patterson methods)[4] and $Mg_2P_4O_{12}$ (direct methods),[5] thus settling the space group symmetry as $C2/c$. A study of $Co_2P_4O_{12}$ has also been completed recently.[6]

The present structural study of $Ni_2P_4O_{12}$ has been undertaken for two reasons. The first is a desire to improve the general crystallographic knowledge of divalent-metal phosphates (*cf.* Ref. 7) and to try to correlate observed metal-oxygen distances and cation radii in various groups of isomorphous compounds. The second reason is that the structure will be used as a reference for future cation distribution studies of some $(Ni,M)_2P_4O_{12}$ solid solutions. Such results will then be included in a more general survey of the distribution of M^{2+} cations in solid solutions of oxosalt structures, so far restricted by the present author to orthophosphates (*e.g.* Refs. 8–11).

EXPERIMENTAL

A sample of $Ni_2P_4O_{12}$ (~10 g) was prepared by thermal decomposition and reaction of a mixture of reagent grade NiO and $NH_4H_2PO_4$("Baker's Analyzed" Chemical Reagents) in the molar proportion 1:2. The mixture was slowly (24 h) heated to 1200 K in an open platinum crucible, ground, and heated again at 1100 K for two weeks. X-ray powder diffraction data were recorded with a Guinier-Hägg type focusing camera (Cu$K\alpha_1$ radiation, λ=1.5405 Å, 295 K, KCl internal standard). The unit cell dimensions (see next section) were determined utilizing conventional least-squares techniques (programs LAZY and CELREF by A. G. Nord). Because of pronounced difficulties in preparing single crystals (*cf.* Refs. 3–5), the structural study reported here was based on neutron powder diffraction data. These were collected at room temperature at the 2 MW JEEP-2 nuclear research reactor at Kjeller (Lillestrøm, Norway), with the sample kept in a thin-walled vanadium cylinder and using a "squashed" germanium monochromator crystal (λ≈1.882 Å). The data were recorded with an OPUS-3 powder diffractometer, equipped with five ^{3}He detectors, in the

0302-4377/83 $2.50

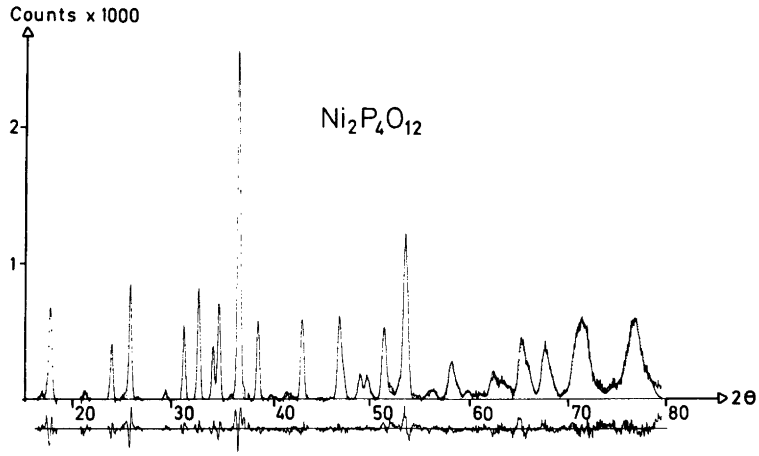

Fig. 1. The least-squares fit obtained between the observed intensities (continuous curve) and calculated intensities (points) for $Ni_2P_4O_{12}$ (neutron powder diffraction data). The discrepancy in the fit, defined as $\Delta I = I_{obs} - I_{calc}$, is plotted below to the same scale.

range $5 \leq \theta \leq 39.5°$ ($\Delta\theta = 0.025°$). The raw data from the various detectors were averaged with a NORD-10 computer at Kjeller.

STRUCTURE ANALYSIS

Crystal data. Nickel(II) tetrametaphosphate, $Ni_2P_4O_{12}$. Space group $C2/c$ (No. 15)

$a = 11.642(3)$ Å, $b = 8.239(2)$ Å,
$c = 9.850(2)$ Å, $\beta = 118.47(2)°$

$V = 830.6(5)$ Å^3, $Z = 4$, $D_x = 3.465$ g · cm^{-3}
(at 295 K); $M_w = 433.30$ *u*.

The neutron diffraction intensity profile contained 138 partly overlapping, independent Bragg reflections. After subtraction of the background, the data were processed with Rietveld's full-profile refinement procedure.[12] Some trial refinements were made to settle the wavelength, scale factor *etc.* In the final stages, the complete crystal structure was refined with 32 parameters: one scale factor, 25 atomic positional parameters (starting with those of $Mg_2P_4O_{12}$[5]), three parameters defining the Gaussian shape of the peaks as a function of θ, and three isotropic temperature factors (for nickel, phosphorus, and oxygen). The final R values (*cf.* Ref. 12) were $R_I = 0.059$, $R_p = 0.103$, and $R_{wp} = 0.111$.

Table 1. Fractional atomic coordinates and thermal parameters for $Ni_2P_4O_{12}$ (space group $C2/c$). The estimated standard deviations are given within parentheses and refer to the last digit of the respective value.

Atom	Point set	x	y	z	B (Å^2)
Ni1	4(*d*)	1/4	1/4	1/2	0.2(2)
Ni2	4(*e*)	0	0.053(1)	1/4	0.2(2)
P1	8(*f*)	0.188(2)	0.501(2)	0.194(2)	0.7(3)
P2	8(*f*)	0.010(2)	0.264(2)	–0.018(2)	0.7(3)
O1	8(*f*)	0.069(1)	0.613(2)	0.153(2)	0.4(1)
O2	8(*f*)	0.148(1)	0.362(2)	0.074(2)	0.4(1)
O3	8(*f*)	0.230(1)	0.418(2)	0.348(2)	0.4(1)
O4	8(*f*)	0.304(2)	0.575(2)	0.183(2)	0.4(1)
O5	8(*f*)	–0.050(2)	0.247(2)	0.085(2)	0.4(1)
O6	8(*f*)	0.029(1)	0.119(2)	–0.093(2)	0.4(1)

A table of observed and calculated integrated intensities is available from the author. The observed and calculated intensity profiles are shown in Fig. 1. The refined atomic parameters are listed in Table 1. Note that the labelling is *not* the same as for $Mg_2P_4O_{12}$;[5] it has been changed to accord with the labelling of the $Cu_2P_4O_{12}$ atoms[4] which better agrees with the generally adopted nomenclature used in cation distribution studies of olivines, orthopyroxenes, *etc.*

DISCUSSION

The crystal structure of $Ni_2P_4O_{12}$ is built up of two kinds each of crystallographically non-equivalent NiO_6 octahedra and PO_4 tetrahedra. The octahedra are linked by edge-sharing in $-(Ni1)O_6-(Ni2)O_6-(Ni1)O_6-(Ni2)O_6-$ chains parallel to $10\bar{1}$; the common edge O4–O5 is the shortest O–O distance within each octahedron, *viz.* 2.72(2) Å. Two PO_4 tetrahedra of each kind are linked together in a ring to form a $P_4O_{12}^{4-}$ ion with a crystallographically imposed $\bar{1}$ symmetry. The NiO_6 and PO_4 polyhedra share corners with each other, thus building up a three-dimensional framework. Illustrations of the crystal structure have been given previously (*cf.* Refs. 4,5); the tetrametaphosphate anion is shown in Fig. 2.

Some interatomic distances and angles in $Ni_2P_4O_{12}$ are given in Table 2. The PO_4 tetrahedra are distorted, with the bridging P–O distances significantly longer than the terminal ones. The two P–O–P angles are 133.6° and 130.2° respectively, so that the bridging angle at O1 is about 3° larger than at O2. The same tendency was observed in $Mg_2P_4O_{12}$ (X-ray single-crystal data)[5] and $Co_2P_4O_{12}$ (neutron powder data)[6], but for $Cu_2P_4O_{12}$ (X-ray single-crystal data)[4] both P–O–P angles are around 137°. In $Ni_2P_4O_{12}$ and $Mg_2P_4O_{12}$ (P2)O_4 is more distorted than (P1)O_4, while the converse is true for $Cu_2P_4O_{12}$ and $Co_2P_4O_{12}$.

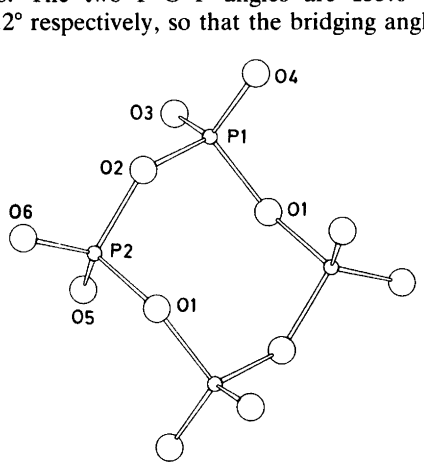

Fig. 2. The centrosymmetrical tetrametaphosphate ion.

Ni1 and Ni2 have the point symmetries $\bar{1}$ and *2*, respectively. The two NiO_6 octahedra are fairly regular (*cf.* Table 2). The metal-oxygen distance ranges and average values within each type of metal-oxygen polyhedron are compared for the four known $M_2P_4O_{12}$ tetrametaphosphate structures. This is done in Table 3. (Note that the atoms are labelled as in Ref. 4). In addition, the unit cell dimensions of these compounds are also given for comparison. It is obvious that the metal-oxygen octahedra in the nickel, magnesium, and cobalt tetrametaphosphates are fairly regular, while in $Cu_2P_4O_{12}$ the CuO_6 octahedra are very distorted, probably due to the Jahn-Teller effect. Generally, the *M*-O mean distances correspond well with what might be expected considering the values of the cation radii (see Table 3). This agreement between ionic radii and geometrical dimensions is also expressed, although less explicitly, in the unit cell dimensions. Again $Cu_2P_4O_{12}$ is a slight exception.

As mentioned in the introductory section, I have performed some cation distribution studies utilizing various orthophosphates as "base structures" for the solid solutions. In a neutron diffraction study of the olivine-related solid solution $(Ni_{0.75}Zn_{0.25})_3(PO_4)_2$,[9] with two distinct octahedral cation sites, it was shown that Ni^{2+} was partially ordered at the somewhat smaller and more regular M1 sites, with $K_D(Ni,Zn)\approx 4$. A study of isostructural $(Ni,Mg)_3(PO_4)_2$ phases[15] gave $K_D(Ni,Mg)=4.0$. The metal-oxygen octahedra in $Ni_2P_4O_{12}$ are similar in shape as well as symmetry to those of the orthophosphates mentioned, and also to the MO_6 octahedra in olivine, an important rock-forming mineral. It would therefore be interesting to use nickel tetrametaphosphate as a "base structure" for cation distribution studies of some suitable $(Ni,M)_2P_4O_{12}$ solid solutions, to see if the same cation ordering tendencies will appear here. Some investigations are already in progress; preliminary results show that in $NiZnP_4O_{12}$ there is a slight tendency for nickel to prefer the M1

Table 2. Interatomic distances (Å) and angles (°) in $Ni_2P_4O_{12}$. The standard deviations are around ±0.02 Å for the P–O distances, ±0.01 Å for the Ni-O distances, and ±0.6° or less for the angles.

P1–O1	1.56	P2–O1	1.58
P1–O2	1.56	P2–O2	1.63
P1–O3	1.51	P2–O5	1.48
P1–O4	1.53	P2–O6	1.48
Average:	1.54	Average:	1.54
O1–P1–O2	109.3	O1–P2–O2	100.1
O1–P1–O3	110.2	O1–P2–O5	111.5
O1–P1–O4	116.9	O1–P2–O6	105.3
O2–P1–O3	105.6	O2–P2–O5	109.0
O2–P1–O4	101.3	O2–P2–O6	109.3
O3–P1–O4	112.0	O5–P2–O6	119.9
Average:	109.2	Average:	109.2
P1–O1–P2	133.6	P1–O2–P2	130.2
Ni1–O3	1.97 (×2)	Ni2–O4	2.06 (×2)
Ni1–O4	2.15 (×2)	Ni2–O5	2.15 (×2)
Ni1–O5	2.07 (×2)	Ni2–O6	2.00 (×2)
Average:	2.06	Average:	2.07
O3–Ni1–O3′	180	O5–Ni2–O6	173.6 (×2)
O4–Ni1–O4′	180	O4–Ni2–O4′	170.0
O5–Ni1–O5′	180	O4–Ni2–O6	93.7 (×2)
O4–Ni1–O5	99.8 (×2)	O5–Ni2–O6	93.4 (×2)
O3–Ni1–O4	92.7 (×2)	O4–Ni2–O6′	93.4 (×2)
O3–Ni1–O5	90.1 (×2)	O4–Ni2–O5	92.0 (×2)
O3–Ni1–O5′	89.9 (×2)	O6–Ni2–O6′	89.8
O3′–Ni1–O4	87.3 (×2)	O5–Ni2–O5′	84.0
O4′–Ni1–O5	80.2 (×2)	O4′–Ni2–O5	80.6 (×2)

Table 3. Unit cell parameters and averaged metal-oxygen distances for four $M_2P_4O_{12}$ tetrametaphosphates. The standard deviation of the average distances refer to the estimated values for each separate *M*–O distance. The cited cation radii, r_M, are those for octahedrally coordinated M^{2+} ions published by Shannon and Prewitt.[13,14]

	$Ni_2P_4O_{12}$	$Mg_2P_4O_{12}$	$Cu_2P_4O_{12}$	$Co_2P_4O_{12}$
Reference	This work	Ref. 5	Ref. 4	Ref. 6
r_M (Å)	0.69	0.72	0.73	0.74
a (Å)	11.642(3)	11.756(2)	12.552(8)	11.809(2)
b (Å)	8.239(2)	8.285(1)	8.083(3)	8.297(1)
c (Å)	9.850(2)	9.917(1)	9.573(3)	9.923(2)
β (°)	118.47(2)	118.96(2)	118.66(1)	118.72(1)
V (Å^3)	830.6(5)	845.1(3)	852.3(8)	852.6(4)
M1-O mean (Å)	2.06(1)	2.065(3)	2.092(6)	2.08(2)
M2-O mean (Å)	2.07(1)	2.092(3)	2.122(6)	2.11(2)
M1-O range (Å)	1.97–2.15	2.01–2.10	1.94–2.37	2.03–2.14
M2-O range (Å)	2.00–2.15	1.99–2.16	1.91–2.47	2.03–2.16

site of the structure, and the same situation is also noted in $NiMgP_4O_{12}$.[16] Crystallographic work on some pure $M_2P_4O_{12}$ phases is also in progress.

Acknowledgements. I am very grateful to Professor Eric Welin for his kind interest in my work and for the excellent laboratory and computing facilities placed at my disposal. It is a great pleasure to thank Dr Arne F. Andresen (Kjeller, Norway) for his valuable help with the collection and processing of the neutron diffraction data. Many thanks are also due to my colleagues Dr Knut Christiansson for his helpful and inspiring discussions, and to Mr David Mills for the illustrations.

This work has in some part been financially supported by the Swedish Natural Science Research Council (NFR).

REFERENCES

1. Pauling, L. and Sherman, J. *Z. Kristallogr. 96* (1937) 481.
2. Thilo, E. and Grunze, I. *Z. Anorg. Allg. Chemie 290* (1957) 209.
3. Beucher, M. and Grenier, J. C. *Mater. Res. Bull. 3* (1968) 643.
4. Laügt, M., Guitel, J. C., Tordjman, I. and Bassi, G. *Acta Crystallogr. B28* (1974) 201.
5. Nord, A. G. and Lindberg, K. B. *Acta Chem. Scand. A29* (1975) 1.
6. Nord, A. G. *Cryst. Struct. Commun. 11* (1982) 1467.
7. Nord, A. G. and Kierkegaard, P. *Chem. Scr. 15* (1980) 27.
8. Nord, A. G. and Stefanidis, T. *Acta Crystallogr. B37* (1981) 1509.
9. Nord, A. G. *Neues Jahrb. für Mineral.*, (1982) 422.
10. Nord, A. G. and Ericsson, T. *Amer. Mineral. 67* (1982) 826.
11. Nord, A. G. *Acta Chem. Scand. A36* (1982) 95.
12. Rietveld, H. M. *J. Appl. Crystallogr. 2* (1969) 65.
13. Shannon, R. D. and Prewitt, C. T. *Acta Crystallogr. B25* (1969) 925.
14. Shannon, R. D. and Prewitt, C. T. *Acta Crystallogr. B26* (1970) 1046.
15. Nord, A. G. and Stefanidis, T. *Phys. Chem. Minerals* (1983). *In press.*
16. Nord, A. G. *To be published.*

Received November 22, 1982.

Acta Chemica Scandinavica A 37 (1983) 545–552

Acid-catalyzed Hydrolyses of Bridged Bi- and Tricyclic Compounds. XXII. Kinetics of Epimerization and Hydration of *exo*- and *endo*-5-Acetyl-2-norbornenes and Hydration of 3-Acetylnortricyclane

MARTTI LAJUNEN and ASKO HINTSANEN

Department of Chemistry and Biochemistry, University of Turku, SF-20500 Turku 50, Finland

In aqueous perchloric acid *exo*- and *endo*-5-acetyl-2-norbornenes react by competing epimerization of the acetyl group and hydration of the carbon-carbon double bond. The four rate constants which control the reactions are evaluated at different temperatures. 3-Acetylnortricyclane reacts under similar conditions by hydration of the three-membered carbon ring. Kinetic parameters indicate that epimerization occurs via enolic intermediates and that the mechanism of hydration is $A-S_E2$, *i.e.* slow protonation of a carbon atom. The reaction products support the conclusions.

In a recent study 5-oxo-2-norbornene (dehydronorcamphor) was observed to disappear in aqueous acid by slow protonation and subsequent hydration of the carbon-carbon double bond ($A-S_E2$ mechanism, eqn. 1).[1] Thus its reaction differs from the acid-catalyzed reactions of other β,γ-unsaturated ketones, which generally isomerize to α,β-unsaturated ketones by initial pre-equilibrium protonation of the carbonyl oxygen followed by deprotonation and protonation steps, one of which is rate-limiting (A-2 mechanism, eqn. 2).[2,3]

In the case of other 5-x-substituted 2-norbornenes (x=H, CH_2OH, OH, CN, and NO_2) the mechanism of hydration is $A-S_E2$.[4–9] Thus 5-oxo-2-norbornene reacts similarly as the other bicyclic compounds.

In the acid-catalyzed hydration of 3-x-substituted nortricyclanes (x=H, CH_2OH, OH, CN, and NO_2) protonation of the cyclopropane ring is also the rate-determining step ($A-S_E2$ mechanism, eqn. 3).[5,7–9] The hydration mechanism of

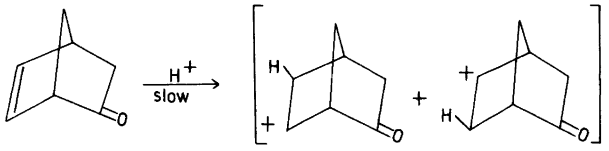

(1)

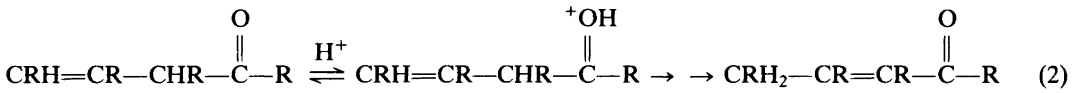

(2)

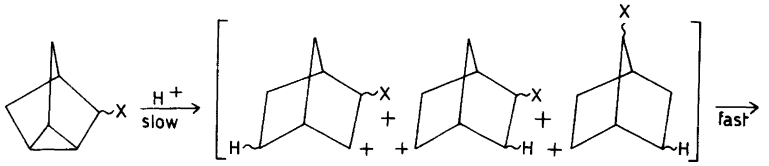

(3)

0302-4377/83 $2.50

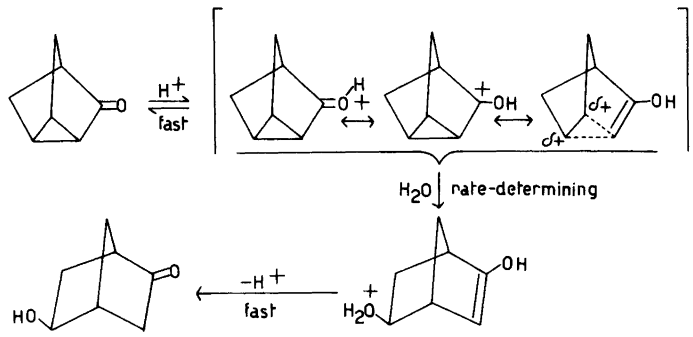

Scheme 1.

3-oxonortricyclane (3-nortricyclanone) is, however, different: it occurs mainly by fast initial protonation of the carbonyl oxygen followed by rearrangement and hydration steps (*A*-2 mechanism, Scheme 1).[10,11] Thus the carbonyl group may account for the different routes of the hydration reactions.

The aim of the present work is to study the effect of the carbonyl group situated outside but second to the bi- and tricyclic skeleton upon the hydration mechanisms of norbornenes and nortricyclanes. Therefore *exo*- and *endo*-5-acetyl-2-norbornenes (*1* and *2*) and 3-acetylnortricyclane

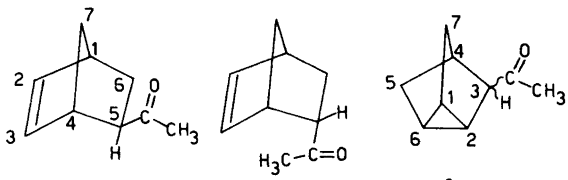

1 *2* *3*

(*3*) were prepared, their disappearance rates in perchloric acid were measured, and reaction products were identified in the case of acetylnorbornenes.

EXPERIMENTAL

Syntheses. A 1:4 mixture of *exo*- and *endo*-5-acetyl-2-norbornenes was prepared by the Diels-Alder reaction of monomerized cyclopentadiene and methyl vinyl ketone.[12] The isomers were enriched by distillation and separated on a preparative gas chromatograph (FFAP column).

3-Acetylnortricyclane was synthesized as follows. A 27:73 mixture of *exo*-5-acetoxy-2-norbornene and 3-acetoxynortricyclane was obtained by addition of acetic acid to norbornadiene.[13] The mixture was hydrolyzed in aqueous potassium hydroxide to the corresponding alcohols, which were turned into the corresponding chlorides by treating them with thionyl chloride in pyridine. The chlorides were isomerized totally to 3-chloronortricyclane with titanium tetrachloride in methylene chloride.[14] The chloride was transformed into nortricyclyl magnesium chloride with magnesium turnings in diethyl ether and addition of acetaldehyde into the solution produced 3-(1-hydroxyethyl)nortricyclane, which was oxidized to 3-acetylnortricyclane with chromic acid.[15] The yield was 33 % from the starting materials.

A 3:7 mixture of *exo*- and *endo*-2-acetylnorbornanes for a ^{13}C NMR spectrum was obtained by hydrogenating the corresponding mixture of acetylnorbornenes in acetone with palladium on carbon as catalyst at room temperature and in atmospheric pressure.

The products were identified from their IR (C=O 1710 cm^{-1}), ^1H and ^{13}C NMR spectra.[12,16]

Kinetics. The disappearance of the substrates (initial concentration *ca.* 2×10^{-3} mol dm^{-3}) in aqueous $HClO_4$, was followed by taking samples after appropriate intervals, by neutralizing them with concentrated ammonia (final pH ca. 7), and by analyzing them by GLC (FFAP column) using norcamphor or 1-methylnorcamphor as inert internal standard. In the case of acetylnorbornenes, where mutual isomerization occurred, the peak areas of both epimers were measured and the rate constants of isomerization (k_i) and hydration (k_h, Scheme 2) were computed from

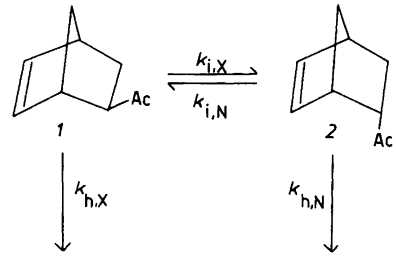

Scheme 2.

$$(1)= \frac{k_{1,N}(2)_o-(k_{i,X}+k_{h,X}+m_2)(1)_o}{m_1-m_2} \exp(m_1t) + \frac{(k_{i,X}+k_{h,X}+m_1)\ (1)_o-k_{i,N}(2)_o}{m_1-m_2} \exp(m_2t) \quad (4)$$

$$(2)= \frac{(k_{i,X}+k_{h,X}+m_1)\ [k_{i,N}(2)_o-(k_{i,X}+k_{h,X}+m_2)\ (1)_o]}{k_{i,N}(m_1-m_2)} \exp\ (m_1t) + \frac{(k_{i,X}+k_{h,X}+m_2)\ [(k_{i,X}+k_{h,X}+m_1)\ (1)_o-k_{i,N}(2)_o]}{k_{i,N}(m_1-m_2)} \exp(m_2t) \quad (5)$$

$$m_1=\tfrac{1}{2}\left\{-(k_{i,X}+k_{i,N}+k_{h,X}+k_{h,N})-[(k_{i,X}+k_{i,N}+k_{h,X}+k_{h,N})^2 -4(k_{i,N}k_{h,X}+k_{i,X}k_{h,N}+k_{h,X}k_{h,N})]^{\frac{1}{2}}\right\} \quad (6)$$

$$m_2=\tfrac{1}{2}\left\{-(k_{i,X}+k_{i,N}+k_{h,X}+k_{h,N})+[(k_{i,X}+k_{i,N}+k_{h,X}+k_{h,N})^2 -4(k_{i,N}k_{h,X}+k_{i,X}k_{h,N}+k_{h,X}k_{h,N})]^{\frac{1}{2}}\right\} \quad (7)$$

eqns. (4) and (5)[17] by iteration.

In these equations (*1*) and (*2*) are the peak areas of the *exo* and *endo* epimers divided by the peak area of the internal standard at time t, the subindex 0 refers to the first sample (t=0), and m_1 and m_2 are defined by eqns. (6) and (7).

Each sample was analyzed several times and the mean values were used in the calculations. Measurements at different temperatures were made three or more times by starting with the pure epimers (purity ≥ 99 % by GLC). The means of $k_{i,X}$, $k_{i,N}$, $k_{h,X}$, and $k_{h,N}$ and their standard deviations were calculated.

Efforts to measure the rate constants in 1.00 mol dm^{-3} $DClO_4(D_2O)$ for solvent deuterium isotope effects were unsuccesful in the case of acetylnorbornenes, but there were no difficulties in the case of 3-acetylnortricyclane. The measurements of the rate constants for acetylnortricyclane (purity > 99 %) were much more accurate than those for acetylnorbornenes.

Equilibration of acetylnorbornenes. 5-Acetyl-2-norbornenes (0.05 mol dm^{-3}) were equilibrated in methanol under catalysis of sodium methoxide (0.1 mol dm^{-3}). The ratio of isomers was analyzed by GLC from samples neutralized by aqueous perchloric acid (final pH *ca.* 7).

Product analysis. 1.00 g of the 24:76 mixture of *exo*- and *endo*-5-acetyl-2-norbornenes was hydrolyzed for over ten half-lives by stirring efficiently in 70 cm^3 of 1 mol dm^{-3} $HClO_4$ at 75 °C. The solution became brown and a black tarry substance was formed. The mixture was cooled and extracted with CH_2Cl_2 three times when the tarry material was dissolved as well. The organic phase was washed with water three times and dried on sodium sulphate. The solvent was distilled off in vacuo and the black residue (0.75 g) was analyzed by GLC and by IR and ^{13}C NMR spectroscopy. The product is mainly a mixture of 5- and 6-acetyl-*exo*-2-norborneols and its ^{13}C NMR spectrum agrees with the following positions of the acetyl group: 37 % of *exo*-5, 23 % of *endo*-5, 22 % of *exo*-6, and 18 % of *endo*-6 (±3 %, see Table 1). There are several other minor signals which do not fit in the calculated chemical shifts of 5- and 6-acetyl-*endo*-2-norborneols and are, at least partly, due to the unidentified impurity (5 %) of the acetylnorbornenes used as starting material.

RESULTS AND DISCUSSION

The aqueous acid causes both *exo-endo* isomerization (epimerization) and disappearance of *exo*- and *endo*-5-acetyl-2-norbornenes (*1* and *2*). The isomerization (k_i) and disappearance (k_h)

Table 1. Comparison of the ^{13}C chemical shifts for *exo*- and *endo*-5- and -6-acetyl-*exo*-2-norborneols (calculated by addition of the effects of the *exo*-2-hydroxyl and *exo*- and *endo*-5- and -6-acetyl groups on the chemical shifts of norbornane) with the observed ^{13}C chemical shifts in $DCCl_3$ for the hydration products of *exo*- and *endo*-5-acetyl-2-norbornenes.

	C(1)	C(2)	C(3)	C(4)	C(5)	C(6)	C(7)	C=O	CH_3	Ref.
Norbornane	36.8	30.1	30.1	36.8	30.1	30.1	38.7			15
$\Delta\delta$ (*exo*-2-OH)	+7.7	+44.3	+12.3	−1.0	−1.3	−5.2	−4.1			15
$\Delta\delta$ (*exo*-5-Ac)	−0.8	−0.6	−1.2	+3.9	+24.8	+2.3	+1.2	+209.9	+29.8	[a]
exo-5-acetyl-*exo*-2-norborneol (calc.)	43.7	73.8	41.2	39.7	53.6	27.2	35.8	209.9	29.8	
exo-5-acetyl-*exo*-2-norborneol (obs.)	44.1	74.2	42.2	39.2	53.7	27.1	36.8	209.5	28.9	[a]
$\Delta\delta$ (*endo*-5-Ac)	+0.4	−1.0	−5.6	+3.9	+24.7	−0.3	+1.6	+209.6	+29.8	[a]
endo-5-acetyl-*exo*-2-norborneol (calc.)	44.9	73.4	36.8	39.7	53.5	24.6	36.2	209.6	29.8	
endo-5-acetyl-*exo*-2-norborneol (obs.)	45.8	73.9	37.8	39.4	53.0	25.3	35.3	209.3	29.8	[a]
$\Delta\delta$ (*exo*-6-Ac)	+3.9	−1.2	−0.6	−0.8	−0.3	+24.8	+1.2	+209.9	+29.8	[a]
exo-6-acetyl-*exo*-2-norborneol (calc.)	48.4	73.2	41.8	35.0	28.5	49.7	35.8	209.9	29.8	
exo-6-acetyl-*exo*-2-norborneol (obs.)	48.9	74.5	42.0	34.4	28.1	51.2	35.1	209.0	29.5	[a]
$\Delta\delta$ (*endo*-6-Ac)	+3.9	−5.6	−1.0	+0.4	+2.3	+24.7	+1.6	+209.6	+29.8	[a]
endo-6-acetyl-*exo*-2-norborneol (calc.)	48.4	68.8	41.4	36.2	31.1	49.6	36.2	209.6	29.8	
endo-6-acetyl-*exo*-2-norborneol (obs.)	47.5	71.9	41.8	37.2	31.2	50.4	37.1	208.7	28.7	[a]

[a] This work.

Table 2. Rate constants of isomerization (k_i) and disappearance (k_h) for *exo*- and *endo*-5-acetyl-2-norbornenes (Scheme 2) in 1.00 mol dm^{-3} $HClO_4$ at different temperatures and activation parameters at 25 °C.

Reaction	Temp./ °C	k_1/ 10^{-5} s^{-1} [a]	Activation parameters
exo→*endo*	25	0.40(4)[b]	
($k_{i,X}$)	55	9.9(5)	$\Delta H^{\neq}$=84(2) kJ mol^{-1}
	65	24(1)	$\Delta S^{\neq}$= −67(5) J mol^{-1} K^{-1}
	75	56(3)	
	85	137(3)	
endo→*exo*	25	0.24(5)[b]	
($k_{i,N}$)	55	7.0(5)	$\Delta H^{\neq}$=89(4) kJ mol^{-1}
	65	17.0(9)	$\Delta S^{\neq}$= −55(12) J mol^{-1} K^{-1}
	75	51(2)	
	85	107(4)	
exo→products	25	0.051(16)[b]	
($k_{h,X}$)	55	3.7(6)	$\Delta H^{\neq}$=114(6) kJ mol^{-1}
	65	11.7(11)	$\Delta S^{\neq}$=+17(17) J mol^{-1} K^{-1}
	75	49(4)	
	85	119(8)	
endo→products	25	0.14(3)[b]	
($k_{h,N}$)	55	6.8(4)	$\Delta H^{\neq}$=104(4) kJ mol^{-1}
	65	22(1)	$\Delta S^{\neq}$= −9(11) J mol^{-1} K^{-1}
	75	56(3)	
	85	184(17)	

[a] The standard deviations are given in parenthesis. [b] Calculated from the activation parameters.

rate constants (see Scheme 2) in 1.00 mol dm^{-3} aqueous $HClO_4$ are listed in Table 2 together with the activation parameters. The epimerization rates are somewhat greater than the disappearance rates at lower temperatures (*e.g.* 25 °C), but all the four rates are of the same magnitude at the higher temperature used (*e.g.* 75 °C). These results agree with the activation enthalpies being higher for disappearance (104 to 114 kJ mol^{-1}) than for isomerization (84 to 89 kJ mol^{-1}). The latter values are similar to those measured for the acid-catalyzed enolization of aliphatic and alicyclic ketones and aldehydes (82 to 87 kJ mol^{-1} in aqueous acids and 75 to 97 kJ mol^{-1} in 90 % acetic acid – HCl solutions).[18,19] The activation entropies of isomerization (−55 to −67 J mol^{-1} K^{-1}) are also in accordance with those measured for enolization of the ketones (−30 to −62 J mol^{-1} K^{-1} in 90 % acetic acid – HCl solutions).[19] Thus it is evident that the epimerization occurs via enolic structures (*4* and *5* in Scheme 3). Considering the equilibrium ratios for the corresponding methyl enol ethers (*6*–*9*) at 25 °C [20] the intermediates (*4* and *5*) are energetically close to each other and only somewhat less stable than the corresponding methylene enols, 5-(1-hydroxyvinyl)-2-norbornenes.

The ratio of the epimerization rate constants ($k_{i,X}$:$k_{i,N}$) differs slightly from the equilibrium ratio of the *exo* and *endo* epimers (K=[*endo*]/[*exo*]): $k_{i,X}$:$k_{i,N}$= 1.10±0.09 and K=0.96±0.02 at 75 °C. The equilibrium ratio of acetylnorbornenes is very similar to that measured for *exo* and *endo*-5-carbomethoxy-2-norbornenes (K=0.95±0.02 at 75 °C).[21] The discrepancy above may be due to the inaccuracy of the isomerization rate constants presented in Table 2.

The corresponding reaction via enolic structures is also probable in the case of 3-acetylnortricyclane (*3*), but it causes only a racemization of

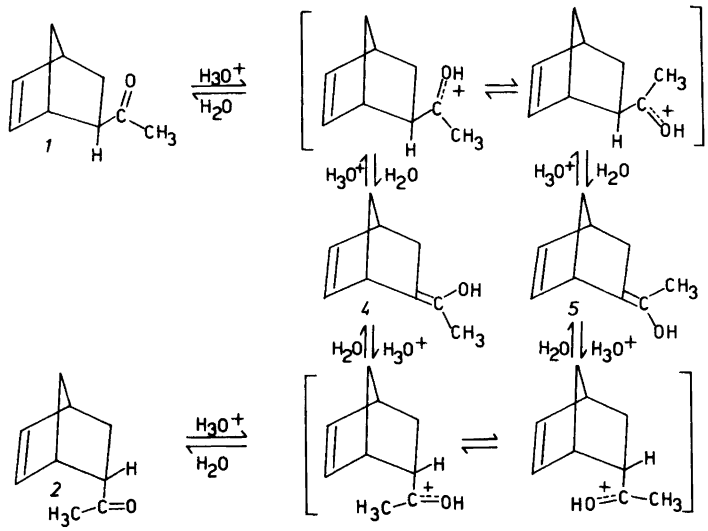

Scheme 3.

the substrate. Since the tricyclic compound is already an optically inactive mixture of two enantiomers, there is no change in the composition of the substrate. Evidently the amounts of the enolic forms are so minor[22] that they have no effect on the disappearance rates of acetylnorbornenes (Table 2) and acetylnortricyclane (Table 3).

The activation entropies of disappearance for 5-acetyl-2-norbornenes are close to zero (−9 to +17 J mol^{-1} K^{-1}) and are thus in agreement with the slow protonation of the carbon-carbon double (A–S_E2 mechanism).[1,4–9] The activation entropy measured for the disappearance of 3-acetylnortricyclane is of the same magnitude (−7 J mol^{-1} K^{-1}, Table 3). The activation enthalpies for acetylnorbornenes and -nortricyclane are also similar (104 to 114 kJ mol^{-1}). The other kinetic parameters of disappearance measured only for acetylnortricyclane (the solvent deuterium isotope effect, k_H/k_D=1.35, and the slopes for log k_1 *vs.* $-H_o$, 1.19, and for log k_1+H_o *vs.* H_o+log c_{HClO_4}, −0.27) are also in accordance with the slow protonation of the three-membered carbon ring (A–S_E2 mechanism).[5,7–9] Besides, the rate constants of disappearance for 5-acetyl-2-norbornenes and 3-acetylnortricyclane are in agreement with the hydration rate constants of other 5-*x*-substituted 2-norbornenes and 3-*x*-substituted nortricyclanes (*x*=H, CH_2OH, CH_2Cl, OH, CN, and NO_2).[9]

The main reaction products of acid-catalyzed hydration of 5-acetyl-2-norbornenes were identified to be 5- and 6-acetyl-*exo*-2-norborneols (see Experimental). The observed amounts of the acetyl group at different positions are 60±4 % at C(5) and 40±4 % at C(6) [the acetyl group may evidently shift between the *exo* and *endo* positions as it does in the substrates, (*1* and *2*), and the Wagner-Meerwein rearrangement may occur, at least, in the 5-acetyl-2-norbornyl cation (see Scheme 4)].

The ratio indicates that about 60 % of protonation occurs at C(3) and about 40 % at C(2) of 5-acetyl-2-norbornenes, which is just the same ratio as was recently observed for the hydrations

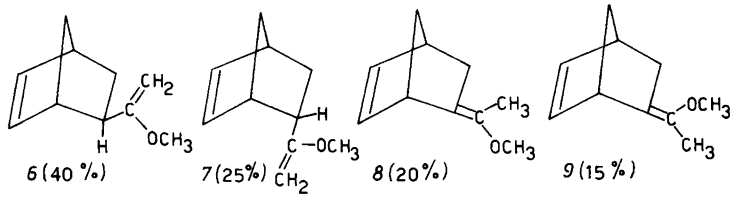

Table 3. Disappearance rate constants for 3-acetylnortricyclane in aqueous perchloric acid at different temperatures and acid concentrations, activation parameters at 25 °C, solvent deuterium isotope effect, and slopes for the plots log k_1 *vs.* $-H_o$ (Slope) and log k_1+H_o *vs.* $H_o+\log c_{HClO_4}$ (Ø).

Temp./ °C	$^cHClO_4$/ mol dm^{-3}	$-H_o$	k_1/ 10^{-5} s^{-1}	Activation parameters, isotope effect, and slopes
25	1.00		0.129(6)[a]	
45	1.01		1.89(4)	
55	1.01		6.73(12)	$\Delta H^{\neq}$=104.5(9) kJ mol^{-1}
65	1.01		20.6(4)	$\Delta S^{\neq}$= −7(3) J mol^{-1} K^{-1}
75	1.01		63.6(12)	k_H/k_D=1.35(6)
75	1.01		47.1(12)[b]	
85	1.01		168(3)	
45	1.01	0.33	1.89(4)	
45	2.02	0.83	9.50(7)	Slope=1.19(3)
45	3.03	1.33	34.6(2)	Ø= −0.27(7)
45	4.02	1.81	125(2)	
45	5.03	2.33	468(5)	

[a] Calculated from the activation parameters. [b] Measured in $DClO_4(D_2O)$.

of *endo*-5-hydroxy- and 5-methyl-*endo*-5-hydroxy-2-norbornenes.[23] The similarity of the ratios is rational considering the similar inductive effects of the acetyl and hydroxyl groups,[24] but it is strange that the same ratio was also measured for the hydration of 5-oxo-2-norbornene.[1] The oxo substituent is much more electronegative than the hydroxyl or acetyl groups, *e.g.* the hydration rates of 5-hydroxy- and 5-acetyl-2-norbornenes are *ca.* 10^3 times higher than that of 5-oxo-2-norbornene.[1,7] According to Carrupt and Vogel[25] the oxo group at C(5) may, however, stabilize the positive charge at C(3) by a hyperconjugative interaction, although the protonation of C(3) and the subsequent formation of a positive charge at C(2) would seem more probable in view of the homoconjugation present in the initial state of 5-oxo-2-norbornene, which already causes a partial positive charge at C(2).[26]

Thus both the kinetic and product-analytic results indicate that *exo*- and *endo*-5-acetyl-2-norbornenes and 3-acetylnortricyclane disappear

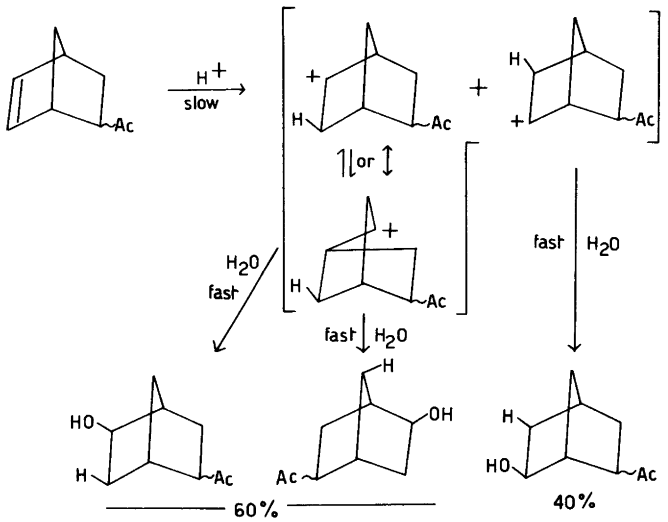

Scheme 4.

in the aqueous acid by the rate-determining protonation of the carbon-carbon double bond or the three-membered carbon ring (A-S_E2 mechanism, eqn. 3 and Scheme 4). In the case of acetylnorbornenes the epimerization of the *exo* and *endo* isomers via the enolic forms (A-2 mechanism, see Scheme 3), however, competes with the hydration reaction. The enolization in deuterioperchloric acid also results in an exchange of the hydrogen atom at C(5) to deuterium, which causes a primary isotope effect and is the reason for the failure in the attempt to measure solvent deuterium isotope effects for acetylnorbornenes (see Experimental).

Acknowledgements. The authors are grateful to Dr. Esko Taskinen for valuable discussions and to Miss Helena Kukkonen, B. A., for her assistance in kinetic measurements. One of us (M. L.) is indebted to the Academy of Finland, Research Council for the Natural Sciences, for financial aid.

REFERENCES

1. Lajunen, M. and Sura, T. *Tetrahedron 34* (1978) 189.
2. Noyce, D. S. and Evett, M. *J. Org. Chem. 37* (1972) 394 and 397.
3. Whalen, D. L., Weimaster, J. F., Ross, A. M. and Radhe, R. *J. Am. Chem. Soc. 98* (1976) 7319.
4. Chwang, W. K., Nowlan, V. J. and Tidwell, T. T. *J. Am. Chem. Soc. 99* (1977) 7233.
5. Lajunen, M. and Hirvonen, P. *Finn. Chem. Lett.* (1978) 38.
6. Lajunen, M. and Peuravuori, J. *Ibid.* (1976) 99.
7. Lajunen, M. and Hirvonen, P. *Ibid.* (1974) 245.
8. Lajunen, M. and Sura, T. *Ibid.* (1979) 233.
9. Lajunen, M. and Kukkonen, H. *Acta Chem. Scand. A 37* (1983) 447.
10. Lajunen, M. and Wiksten, P. *Finn. Chem. Lett.* (1980) 17.
11. Paasivirta, J. *Suom. Kemistil. B 36* (1963) 156.
12. Kobuke, Y., Fueno, T. and Furukawa, J. *J. Am. Chem. Soc. 92* (1970) 6548.
13. Meinwald, J., Crandall, J. and Hymans, W. E. *Org. Synth. 45* (1965) 74.
14. Reetz, M. T. and Sauerwald, M. *Chem. Ber. 114* (1981) 2355.
15. Brown, H. C. and Garg, C. P. *J. Am. Chem. Soc. 83* (1961) 2952.
16. Levy, G. C., Lichter, R. L. and Nelson, G. L. *Carbon-13 Nuclear Magnetic Resonance Spectroscopy,* 2nd Ed., Wiley, New York 1980, pp. 60–62.
17. Alberty, R. A. and Miller, W. G. *J. Chem. Phys. 26* (1957) 1231.
18. Palm, V. A., Haldna, Ü. L. and Talvik, A. J. in Patai, S., Ed., *The Chemistry of the Carbonyl Group,* Vol. 1, Interscience, London 1966, Chapter 9 and references therein.
19. Shechter, H., Collis, M. J., Dessy, R., Okuzumi, Y. and Chen, A. *J. Am. Chem. Soc. 84* (1962) 2905.
20. Taskinen, E. *Personal communication.*
21. Ouellette, R. J. and Booth, G. E. *J. Org. Chem. 30* (1965) 423.
22. Forsen, S. and Nilsson, M. in Zabicky, J., Ed., *The Chemistry of the Carbonyl Group,* Vol. 2, Interscience, London 1970, Chapter 3.
23. Lajunen, M. and Lyytikäinen, H. *Acta Chem. Scand. A 35* (1981) 139.
24. Grob, C. A., Schaub, B. and Schlageter, M. G. *Helv. Chim. Acta* 63 (1980) 57.
25. Carrupt, P.-A. and Vogel, P. *Tetrahedron Lett. 23* (1982) 2563.
26. Werstiuk, N. H., Taillefer, R., Bell, R. A. and Sayer, B. *Can. J. Chem. 51* (1973) 3010.

Received December 7, 1982.

Acta Chemica Scandinavica A 37 (1983) 553–559

The Crystal Structure of Ammonium (2,2′-Bipyridine)oxodiperoxovanadate(V) Tetrahydrate, $NH_4[VO(O_2)_2(C_{10}H_8N_2)] \cdot 4H_2O$, at −100 °C

HELGA SZENTIVANYI and ROLF STOMBERG

Department of Inorganic Chemistry CTH/GU, Chalmers Tekniska Högskola, S-412 96 GÖTEBORG, Sweden

The crystal structure of ammonium (2,2′-bipyridine)oxodiperoxovanadate(V) tetrahydrate, $NH_4[VO(O_2)_2(C_{10}H_8N_2)] \cdot 4H_2O$, has been determined at −100 °C by single-crystal X-ray methods. The compound crystallizes in the monoclinic space group $P2_1/n$ with a=7.089(2) Å, b=18.087(7) Å, c=12.798(3) Å, β=90.57(2)°, V=1640.8(9) Å^3 and Z=4. Refinement by the least-squares method gave a final R-value of 0.050 for 2221 observed independent reflexions.

The structure is comprised of ammonium ions, (2,2′-bipyridine)oxodiperoxovanadate(V) ions and water of crystallization, held together by ionic and hydrogen bond forces. Vanadium is seven-coordinated. The geometry of the anion is a distorted pentagonal bipyramid with the vanadyl oxygen atom and one nitrogen atom from 2,2′-bipyridine at the apices and the peroxo groups and the other nitrogen atom forming the pentagonal plane. The vanadium atom is displaced 0.32 Å from this plane towards the vanadyl oxygen atom. Interatomic distances within the anion are: V−$N_{equatorial}$ 2.149(4) Å, V−N_{apical} 2.288(3) Å, V=O 1.619(3) Å, V−O_{peroxo} 1.880(3)−1.911(3) Å and $(O-O)_{peroxo}$ 1.465(4) and 1.471(4) Å.

As part of a project on transition metal peroxo complexes at this department, attention has been focused on the structures of mixed-ligand vanadium(V) peroxo complexes. Of this type, only the structures of $NH_4[VO(O_2)_2(NH_3)]$,[1] $NH_4[VO(O_2)_2(H_2O)\{C_5H_3N(COO)_2\}] \cdot xH_2O$,[2] and $K_3[VO(O_2)_2(C_2O_4)] \cdot H_2O$,[3] all being monomeric, have been published to date. Beiles *et al.* report a compound, which they denote $(NH_4)_2(bipy)_2 \cdot H_2V_2O_{11} \cdot H_2O_2 \cdot 3H_2O$,[4] and Sala-Pala *et al.* another with the formula $NH_4[V(O_2)_3bipy] \cdot 3H_2O$.[5] According to Vuletić *et al.*, these two compounds seem to resemble $NH_4[VO(O_2)_2bipy] \cdot 4H_2O$, which they have prepared.[6] It was, therefore, thought worthwhile to determine their crystal structures in order to elucidate the nature of these three compounds.

EXPERIMENTAL

Preparation. Crystals were prepared according to Beiles *et al.*,[4] Sala-Pala *et al.*,[5] as well as Vuletić *et al.*,[6] those obtained by the first method were recrystallized from a 15 % aqueous solution of hydrogen peroxide.

X-Ray methods. X-Ray powder photographs were obtained by the Guinier-Hägg method and single crystal photographs by the multiple film, equi-inclination Weissenberg technique, using Cu$K\alpha$ radiation at room temperature. These photographs indicated that the compounds obtained in the three different preparations are identical, shown in the present investigation to be $NH_4[VO(O_2)_2bipy] \cdot 4H_2O$.

The single crystal photographs were taken with rotation about [100] (layer lines 0–6) and [010] (layer line 0). Because of the low stability of the compound, new crystals had to be mounted for each layer line. A total of 1177 independent reflexions were registered. The intensities were corrected for Lorentz and polarization effects.

For the refinement of the crystal structure, intensity data were recorded with a SYNTEX $P2_1$ automatic four-circle single-crystal X-ray dif-

0302-4377/83 $2.50

fractometer, using graphite-monochromatized Mo$K\alpha$ radiation and a crystal with the dimensions 0.19×0.19×0.28 mm. The temperature was maintained at −100 °C with the SYNTEX LT1 low-temperature device. The ω–2θ scan method was used and the 2θ scan speed was allowed to vary between 2 and 15° min^{-1}, depending on the intensity of the measured reflexion. Data were collected for $2\theta \leq 55°$. A profile analysis based on the Lehmann-Larsen method [7] was applied to the 96-step profile collected for each reflexion. A reflexion measured after each twenty-fourth reflexion showed no significant difference in intensity during the collection of the data.

A total of 3792 independent reflexions were measured. Of these, 2221 having $I_o \geq 3\sigma(I_o)$ were regarded as being observed and were used in the subsequent calculations. The intensities were corrected for Lorentz and polarization effects but not for absorption.

The unit cell parameters were determined from a least-squares fit of refined diffractometer setting angles for 15 reflexions.

CRYSTAL DATA

Ammonium (2,2′-bipyridine)oxodiperoxovanadate(V) tetrahydrate, $NH_4[VO(O_2)_2(C_{10}H_8N_2)] \cdot 4H_2O$. F.W.=377.22. Space group: $P2_1/n$ (No. 14; non-standard setting). General positions: $\pm(x,y,z)$, $\pm(\frac{1}{2}+x,\frac{1}{2}-y,\frac{1}{2}+z)$.

	At −100 °C	At 18 °C (Ref. 19)
a (Å)	7.089(2)	7.114(1)
b (Å)	18.087(7)	18.142(2)
c (Å)	12.798(3)	12.845(1)
β (°)	90.57(2)	90.52(1)
V (Å^3)	1640.8(9)	1657.8

$Z=4$, $D_x=1.52$ g cm^{-3}, μ(Mo$K\alpha$)=0.69 mm^{-1}, μ(Cu$K\alpha$)=5.8 mm^{-1}.

STRUCTURE DETERMINATION

Single crystal photographs showed, with a few minor deviations, that $I(hkl)$ and $I(hk\bar{l})$ are almost equal. On all films, reflexions of the type $h0l$ with $h+l=2n+1$ and $0k0$ with $k=2n+1$ were missing. With the exception of nine weak reflexions, $hk0$-reflexions with $k=2n+1$ were also missing. The effect of the angle β deviating slightly from 90° could clearly be observed on upper-level photographs. Thus, though undoubtedly monoclinic, the crystals exhibit almost orthorhombic symmetry (approximately space group $Pmnb$ or $P2_1nb$). While waiting for an automatic single-crystal diffractometer to be installed at the department, a preliminary structure analysis was performed, taking advantage of the pseudo orthorhombic symmetry.

Since the true space group, $P2_1/n$, is centrosymmetric, $Pmnb$ was first tested. The positions of all non-hydrogen atoms were determined from a Patterson map and subsequent electron density calculations. Least-squares refinement of positional and anisotropic thermal parameters yielded an R-value of 0.13 ($R=\Sigma||F_o|-|F_c||/\Sigma|F_o|$), a reasonable value considering that film data and unstable crystals had been used. No attempt was made to refine the structure in space group $P2_1/n$ using film data.

Refinement of the structural parameters, based on diffractometer data, was performed later. Because of the instability of the crystals at room temperature, data were collected at −100 °C. Least-squares refinement of an overall scale factor and positional and isotropic thermal parameters for all the non-hydrogen atoms yielded an R-value of 0.10. Refinement of positional and anisotropic thermal parameters for the non-hydrogen atoms and positional parameters for the non-water hydrogen atoms reduced R to 0.050. The B_{iso}'s of the carbon and ammonium nitrogen atoms were used as the B_{iso}'s for the corresponding hydrogen atoms, and were not refined. The weighting scheme used was that of Cruickshank:[8] $w=(a+|F_o|+c|F_o|^2+d|F_o|^3)^{-1}$, with $a=10.0$, $c=0.020$ and $d=0.0$. The scattering factors for V, O, N, C and H were taken from the *International Tables for X-Ray Crystallography, Vol. IV.*

The highest peak in the final electron density difference synthesis, 0.86 e Å^{-3}, appeared 1.05 Å from vanadium.

Calculations were carried out on an IBM 3033 computer, using the crystallographic programmes described in Ref. 9.

Lists of structure factors and anisotropic thermal parameters are available from R.S. upon request.

RESULTS AND DISCUSSION

According to the literature three peroxovanadates have been found in the system $NH_4^+-VO_3^-$

Table 1. Atomic coordinates and thermal parameters ($Å^2$) for $NH_4[VO(O_2)_2(C_{10}H_8N_2)] \cdot 4H_2O$ at −100 °C. Space group $P2_1/n$.
$U_{eq}=\frac{1}{3}\sum_i\sum_j U_{ij}a^*_i a^*_j a_i a_j \cos\alpha_{ij}$

Atom	x	y	z	U_{eq}
V	0.24868(10)	0.55911(4)	0.26888(5)	0.0244(2)
O1	0.5147(4)	0.5608(2)	0.2460(2)	0.0373(7)
O2	0.4392(4)	0.6308(2)	0.2851(2)	0.0364(7)
O3	−0.0159(4)	0.5649(2)	0.2408(3)	0.0378(7)
O4	0.0662(4)	0.6339(2)	0.2813(2)	0.0368(7)
O5	0.2429(5)	0.5183(2)	0.3813(2)	0.0416(8)
Ow1	0.4431(5)	0.3540(3)	0.5088(3)	0.0689(12)
Ow2	0.7568(5)	0.8406(2)	0.1138(2)	0.0427(8)
Ow3	0.7541(5)	0.2152(2)	0.2790(3)	0.0603(10)
Ow4	0.0584(5)	0.3533(2)	0.5147(3)	0.0540(10)
N1	0.2447(5)	0.4558(2)	0.1860(3)	0.0312(8)
N2	0.2543(5)	0.5862(2)	0.0943(2)	0.0284(8)
N3	0.7406(5)	−0.0029(2)	0.1067(3)	0.0340(8)
C1	0.2400(8)	0.3910(3)	0.2378(4)	0.0424(11)
C2	0.2356(9)	0.3235(3)	0.1866(5)	0.0534(14)
C3	0.2342(8)	0.3230(3)	0.0778(4)	0.0506(13)
C4	0.2376(7)	0.3888(3)	0.0244(4)	0.0401(11)
C5	0.2438(6)	0.4550(2)	0.0798(3)	0.0280(9)
C6	0.2509(6)	0.5277(2)	0.0287(3)	0.0273(9)
C7	0.2557(6)	0.5371(3)	−0.0799(3)	0.0342(10)
C8	0.2629(7)	0.6082(3)	−0.1200(3)	0.0398(11)
C9	0.2652(7)	0.6675(3)	−0.0529(4)	0.0423(11)
C10	0.2607(7)	0.6543(3)	0.0534(4)	0.0385(11)
H(C1)	0.232(9)	0.395(4)	0.326(5)	
H(C2)	0.240(9)	0.281(4)	0.236(6)	
H(C3)	0.246(9)	0.274(4)	0.032(6)	
H(C4)	0.235(9)	0.383(4)	−0.047(6)	
H(C7)	0.251(8)	0.494(4)	−0.122(5)	
H(C8)	0.258(9)	0.616(4)	−0.195(6)	
H(C9)	0.265(10)	0.713(4)	−0.065(6)	
H(C10)	0.275(9)	0.690(4)	0.098(5)	
H1(N3)	0.756(7)	−0.052(3)	0.117(4)	
H2(N3)	0.750(7)	0.004(3)	0.039(4)	
H3(N3)	0.639(8)	0.014(3)	0.143(4)	
H4(N3)	0.864(8)	0.016(3)	0.135(4)	

$-H_2O_2$–bipy$-H_2O$.[4–6] The aim of the present investigation was to deduce their structures. The crystalline products obtained from the three different synthetic procedures were shown, however, to be identical. Sala-Pala *et al.* found, from Weissenberg photographs, that their crystalline product, which they formulate $NH_4[V(O_2)_3bipy] \cdot 3H_2O$, is orthorhombic with $a=12.83(5)$ Å, $b=18.13(3)$ Å, $c=7.11(2)$ Å, $D_m=1.49$ g cm^{-3}, $Z=4$, and $D_c=1.51$ g cm^{-3}.[5] Within 1σ these data are the same as those found in this work for $NH_4[VO(O_2)_2bipy] \cdot 4H_2O$, which was found to be monoclinic (see crystal data). That Sala-Pala *et al.* found their substance to be orthorhombic is understandable, since normal care taken in the interpretation of the Weissenberg films might easily lead to that conclusion (this is more fully explained under the heading Structure Determination). There is a plausible explanation to the question why the formulæ deduced by Beiles *et al.* and by Sala-Pala *et al.* probably are wrong. In determining the peroxide content they have used iodometry and might have overlooked the fact that also vanadium(V) oxidizes iodide ions.

The positional parameters obtained for

Table 2. Bond distances (Å) and angles (°) in $NH_4[VO(O_2)_2(C_{10}H_8N_2)] \cdot 4H_2O$. Values in square brackets refer to film data.

	Distance			Angle
V–O1	1.911(3)	[1.90(1)]	O1–V–O2	45.4(1)
V–O2	1.883(3)	[1.86(1)]	O1–V–O3	159.9(1)
V–O3	1.909(3)	[1.90(1)]	O1–V–O4	133.0(1)
V–O4	1.880(3)	[1.86(1)]	O1–V–O5	100.2(2)
V–O5	1.619(3)	[1.61(1)]	O1–V–N1	86.9(1)
V–N1	2.149(4)	[2.15(1)]	O1–V–N2	79.6(1)
V–N2	2.288(3)	[2.28(1)]	O2–V–O3	133.3(1)
O1–O2	1.465(4)	[1.47(1)]	O2–V–O4	89.3(1)
O3–O4	1.471(4)	[1.47(1)]	O2–V–O5	104.0(2)
N1–C1	1.347(6)	[1.32(2)]	O2–V–N1	131.2(1)
N1–C5	1.359(5)	[1.32(2)]	O2–V–N2	86.6(1)
C1–C2	1.386(7)	[1.42(3)]	O3–V–O4	45.7(1)
C2–C3	1.392(8)	[1.40(4)]	O3–V–O5	99.1(2)
C3–C4	1.373(7)	[1.32(3)]	O3–V–N1	86.9(1)
C4–C5	1.392(6)	[1.44(2)]	O3–V–N2	80.3(1)
C5–C6	1.470(6)	[1.46(2)]	O4–V–O5	103.3(2)
C6–C7	1.401(6)	[1.39(2)]	O4–V–N1	131.5(1)
C7–C8	1.385(7)	[1.38(3)]	O4–V–N2	87.0(1)
C8–C9	1.374(7)	[1.38(3)]	O5–V–N1	92.4(2)
C9–C10	1.381(7)	[1.35(2)]	O5–V–N2	165.2(1)
N2–C10	1.338(6)	[1.36(2)]	N1–V–N2	72.8(1)
N2–C6	1.351(5)	[1.33(2)]	V–O1–O2	66.2(2)
C1–H(C1)	1.14(7)		V–O2–O1	68.2(3)
C2–H(C2)	1.00(8)		V–O3–O4	66.1(2)
C3–H(C3)	1.07(7)		V–O4–O3	68.2(2)
C4–H(C4)	0.93(8)		C1–N1–C5	118.9(4)
C7–H(C7)	0.95(6)		C6–N2–C10	118.6(4)
C8–H(C8)	0.97(7)		N1–C1–C2	122.2(4)
C9–H(C9)	0.85(7)		C1–C2–C3	118.6(5)
C10–H(C10)	0.86(6)		C2–C3–C4	119.4(5)
N3–H1(N3)	0.90(5)		C3–C4–C5	119.5(4)
N3–H2(N3)	0.88(5)		N1–C5–C4	121.3(4)
N3–H3(N3)	0.91(5)		N1–C5–C6	115.8(3)
N3–H4(N3)	1.01(5)		C4–C5–C6	123.0(4)
			N2–C6–C5	115.2(3)
			N2–C6–C7	121.3(4)
			C5–C6–C7	123.5(4)
			C6–C7–C8	118.9(4)
			C7–C8–C9	119.5(4)
			C8–C9–C10	118.7(5)
			N2–C10–C9	123.0(4)

$NH_4[VO(O_2)_2bipy] \cdot 4H_2O$ in the last refinement cycle, as well as U_{eq} are given in Table 1. The content of the unit cell is shown in Fig. 1 and the anion in Fig. 2. Bond distances and angles are given in Table 2 and hydrogen bond distances in Table 3.

Table 1 shows that the largest deviation from *Pmnb*-symmetry, exhibited by C3, is 0.112(6) Å. Bond distances obtained by refining the parameters in space group *Pmnb* using film data do not differ significantly from those obtained by refining the parameters in space group $P2_1/n$ using diffractometer data (see Table 2).

The crystals of ammonium (2,2′-bipyridine)-oxodiperoxovanadate(V) tetrahydrate consist of ammonium ions, (2,2′-bipyridine)oxodiperox-

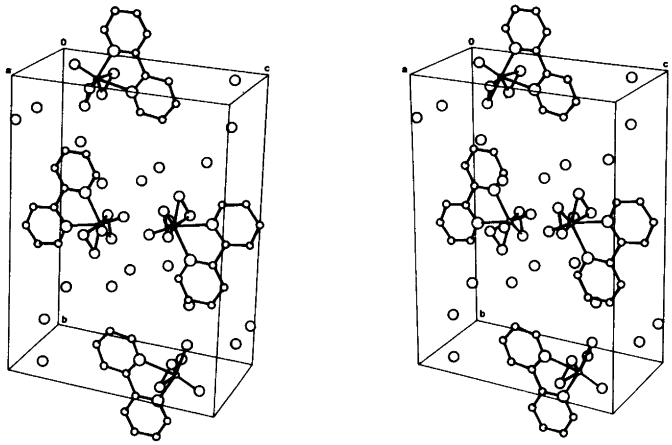

Fig. 1. Stereoscopic drawing of the unit cell of $NH_4[VO(O_2)_2bipy] \cdot 4H_2O$.

ovanadate(V) ions and water of crystallization, held together by ionic and hydrogen bond forces.

$[VO(O_2)_2(bipy)]^-$ has a pentagonal bipyramidal arrangement of ligands, as shown in Fig. 2, a configuration observed in several transition metal peroxo complexes (see, *e.g.*, Refs. 2,3,10–16). The distances from the equatorial plane (plane I), defined by O1, O2, O3, O4 and N1, to these atoms and to V, O5 and N2 are given in Table 4. Within the limits of experimental error the defining atoms all lie in this plane. The atoms V, O5, N1 and N2 and the midpoints between O1 and O3 and O2 and O4 also lie in a plane (plane II). Planes I and II form an angle of 89.6° with one another.

Table 3. Hydrogen bond distances (Å). Ow1–Ow4 are water oxygen atoms and N3 is the ammonium nitrogen atom.

		Distance
N3···O1	$(\frac{3}{2}-x,-\frac{1}{2}+y,\frac{1}{2}-z)$	2.797(5)
N3···O3	$(\frac{1}{2}-x,-\frac{1}{2}+y,\frac{1}{2}-z)$	2.813(5)
N3···O5	$(\frac{1}{2}+x,\frac{1}{2}-y,-\frac{1}{2}+z)$	2.897(4)
N3···Ow2	$(x,-1+y,z)$	2.835(5)
Ow1···O2	$(1-x,1-y,1-z)$	2.772(5)
Ow1···Ow2	$(\frac{3}{2}-x,-\frac{1}{2}+y,\frac{1}{2}-z)$	2.667(5)
Ow1···Ow4	(x,y,z)	2.729(5)
Ow2···Ow3	$(\frac{3}{2}-x,\frac{1}{2}+y,\frac{1}{2}-z)$	2.653(5)
Ow2···Ow4	$(\frac{1}{2}-x,\frac{1}{2}+y,\frac{1}{2}-z)$	2.771(5)
Ow3···O2	$(\frac{3}{2}-x,-\frac{1}{2}+y,\frac{1}{2}-z)$	2.786(5)
Ow3···O4	$(\frac{1}{2}-x,-\frac{1}{2}+y,\frac{1}{2}-z)$	2.806(5)
Ow4···O4	$(-x,1-y,1-z)$	2.774(5)

The vanadium atom is displaced 0.318 Å from the pentagonal plane towards the vanadyl oxygen atom. Such a displacement is usually observed for transition metal peroxo compounds (see, *e.g.*, Table 6 in Ref. 11). When the apical atoms are different, or one is missing, this displacement is in the range 0.2–0.5 Å, the latter value being observed for pentagonal pyramidal complexes like $[CrO(O_2)_2py]$ and $[VO(O_2)_2(NH_3)]^-$, while 0.3 Å is commonly encountered in pentagonal bipyramidal compounds.

The $V-O_{peroxo}$ bond lengths, 1.880–1.911 Å, lie in the range of $V-O_{peroxo}$ distances previously reported[1–3,11] and are normal vanadium-oxygen single bond distances.

The distances between the oxygen atoms in the peroxo groups, 1.465 and 1.471 Å, compare well with other observations (see, *e.g.*, Refs. 1–3 and Table 7 in Ref. 11).

The V=O bond length, 1.619 Å, is in good agreement with the corresponding values reported for vanadium peroxo compounds.[1–3,11]

Each pyridine ring in the bipyridine ligand is planar and the planes intersect each other at 1.4°. The deviations of the atoms from the respective plane, as well as from the plane $x=\frac{1}{4}$, are given in Table 4. Bond distances and angles within the bipyridine group are in good agreement with data peviously reported.[14,17] The difference between $V-N_{equatorial}$ and $V-N_{apical}$ distances, 2.149 and

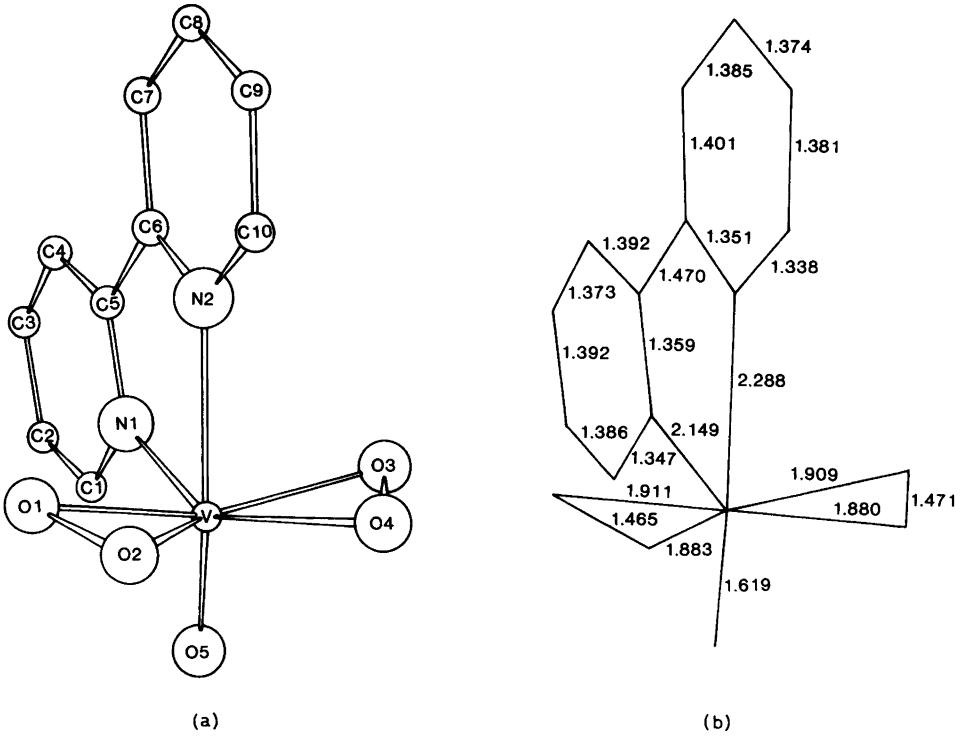

Fig. 2. The anion $[VO(O_2)_2bipy]^-$.

Table 4. Displacements (Å) of atoms from least-squares planes in $NH_4[VO(O_2)_2(C_{10}H_8N_2)] \cdot 4H_2O$.

Defining atoms are:
Plane I O1, O2, O3, O4, N1
Plane II V, O5, N1, N2, the midpoints between O1 and O3 (O1/O3) and O2 and O4 (O2/O4)
Plane III N1, C1–C5
Plane IV N2, C6–C10
Plane V $x=\frac{1}{4}$

Atom	Plane I	Atom	Plane II	Atom	Plane III	Atom	Plane IV	Atom	Plane V
O1	0.011(3)	V	−0.001(1)	N1	−0.001(4)	N2	−0.003(4)	N1	0.037(4)
O2	−0.007(3)	O5	0.002(4)	C1	0.004(5)	C6	0.003(4)	C1	0.071(5)
O3	0.010(3)	N1	−0.002(4)	C2	−0.003(6)	C7	−0.001(5)	C2	0.102(6)
O4	−0.006(3)	N2	0.002(4)	C3	−0.001(6)	C8	−0.001(5)	C3	0.112(6)
N1	−0.008(4)	O1/O3	0.000(3)	C4	0.004(5)	C9	0.001(5)	C4	0.088(5)
V	−0.318(1)	O2/O4	−0.002(3)	C5	−0.003(4)	C10	0.001(5)	C5	0.044(4)
N2	−1.928(4)	O1	−1.881(3)					C6	−0.006(4)
O5	1.943(4)	O2	−1.324(3)					C7	−0.041(5)
		O3	1.881(3)					C8	−0.091(5)
		O4	1.321(3)					C9	−0.108(5)
								C10	−0.076(5)
								N2	−0.030(4)

2.288 Å, is also in good agreement with earlier results.[14,17,18]

The ammonium ion is hydrogen bonded to the two peroxo oxygen atoms O1 and O3, the vanadyl oxygen atom, O5, and one of the water molecules, with bond distances ranging from 2.80 to 2.90 Å. The X···H–N angles are almost linear (144–168°).

Acknowledgement. We wish to express our gratitude to Mrs. Solveig Olson for technical assistance.

REFERENCES

1. Drew, R. E. and Einstein, F. W. B. *Inorg. Chem. 11* (1972) 1079.
2. Drew, R. E. and Einstein, F. W. B. *Inorg. Chem. 12* (1973) 829.
3. Begin, D., Einstein, F. W. B. and Field, J. *Inorg. Chem. 14* (1975) 1785.
4. Beiles, R. G., Malysheva, V. V. and Beiles, E. M. *Russ. J. Inorg. Chem., Engl. Transl. 15* (1970) 794.
5. Sala-Pala, J. and Guerchais, J. E. *J. Chem. Soc. A* 1971, 1132.
6. Vuletić, N. and Djordjević, C. *J. Chem. Soc., Dalton Trans.* 1973, 1137.
7. Lehmann, M. S. and Larsen, F. K. *Acta Crystallogr. A 30* (1974) 580.
8. Cruickshank, D. W. J. *Crystallographic Computing,* Copenhagen 1970, p. 195.
9. Lindgren, O. *Thesis,* University of Göteborg and Chalmers University of Technology, Göteborg 1977.
10. Stomberg, R. and Svensson, I.-B. *Acta Chem. Scand. A 31* (1977) 635.
11. Svensson, I.-B. and Stomberg, R. *Acta Chem. Scand. 25* (1971) 898.
12. Stomberg, R. *Acta Chem. Scand. A 36* (1982) 101.
13. Stomberg, R. *Acta Chem. Scand. A 36* (1982) 423.
14. Stomberg, R. and Ainalem, I.-B. *Acta Chem. Scand. 22* (1968) 1439.
15. Trysberg, L. and Stomberg, R. *Acta Chem. Scand. A 35* (1981) 823.
16. Einstein, F. W. B. and Penfold, B. R. *Acta Crystallogr. 17* (1964) 1127.
17. Edwards, A. J., Slim, D. R., Guerchais, J. E. and Sala-Pala, J. *J. Chem. Soc., Dalton Trans.* 1977, 984.
18. Stomberg, R. *Arkiv. Kemi 24* (1965) 111.
19. Campbell, N. J., Capparelli, M. V., Griffith, W. P. and Skapski, A. C. *Private communication.*

Received December 3, 1982.

Acta Chemica Scandinavica A 37 (1938) 561–568

Equilibrium and Structural Studies of Silicon(IV) and Aluminium(III) in Aqueous Solution. 7. Redox, Hydrolysis and Complexation Equilibria in the System Al^{3+}–1,2-Naphthoquinone-4-sulfonate/1,2-Dihydroxy-naphthalene-4-sulfonate–OH^-. A Potentiometric Study in 0.6 M Na(Cl)

LARS-OLOF ÖHMAN, STAFFAN SJÖBERG and NILS INGRI

Department of Inorganic Chemistry, University of Umeå, S-901 87 Umeå, Sweden

Equilibria between aluminium(III) and 1,2-naphthoquinone-4-sulfonate (Q^-), aluminium(III), 1,2-dihydroxynaphthalene-4-sulfonate (H_2L^-) and OH^- as well as redox equilibria between the two organic substances were studied in 0.6 M Na(Cl) medium at 25 °C in the 1–10 mM, the 9.5–6.8 $-\lg\{e^-\}$ and the 1.5–9 $-\lg[H^+]$ ranges. The measurements were performed as emf titrations (glass and platinum electrodes) in which H_2L^- was generated coulometrically from Q^- by means of an integrating potentiostat. In the $Al^{3+}-Q^-$ system no stable complexes were found. In the $Al^{3+}-H_2L^--OH^-$ system data could be explained with the complexes AlL^o, $Al(OH)L^-$, AlL_2^{3-}, $Al(OH)L_2^{4-}$ and AlL_3^{6-}. Apart from these complexes, it was also possible to determine the stability constant for the aluminate ion, $Al(OH)_4^-$. The redox reaction between Q^- and H_2L^- was found to be $Q^-+2H^++2e^- \rightleftarrows H_2L^-$ for $-\lg[H^+] \lesssim 4.5$, while, at higher $-\lg[H^+]$, Q^- seems to decompose irreversibly. A full compilation of experimental results with equilibrium constants and corresponding standard deviations are given in Table 1. Data were analyzed with the least-squares computer program LETAGROPVRID.

In a current project at this department, the ability of Si(IV) and Al(III) to form aqueous complexes with ligand types occurring in natural waters, is being studied. In the $Al^{3+}-OH^--$gallic acid system [1] it was found that strong complexes were formed between Al^{3+} and two phenolic groups in *ortho*-position. In a natural water containing oxidizing agents, this type of ligand originating from lignin degradation, will always, at least partially, be oxidized to the corresponding *ortho*-diquinone. Indirect proofs have also been given that these types of organic compounds could act as ligands toward metal ions.[2] We have found it interesting to determine whether or not this is the case for Al(III). In the search for a suitable *o*-diphenolic/*o*-diquinonic redox couple[3] it was found necessary to choose an *o*-dihydroxynaphthalenic/*o*-naphthoquinonic system as the quinonic state of the simple phenolics (*e.g.* pyrocatechol, gallic acid) is not stable but polymerizes irreversibly to some kind of synthetic humic acid.[4]

A suitable choice for the present investigation seems to be the compounds Q^-/H_2L^- (structures given in Scheme 1), a couple whose redox and acid-base properties have been found to be reversible in earlier investigations.[3,5]

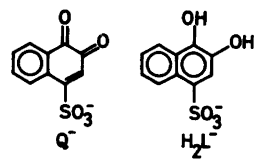

Scheme 1.

0302-4377/83 $2.50

EXPERIMENTAL

Chemicals and analysis. Potassium 1,2-naphthoquinone-4-sulfonate (KQ) was synthesized and purified according to Fieser[6] from *1-amino-2-naphthol-4-sulfonic acid* (Merck *p.a.*). As it was found that aqueous solutions of Q^- deteriorated on standing, fresh solutions prepared from the solid were always used in the measurements. The content of Q^- was determined potentiometrically using the Gran extrapolation method[7] after reduction of Q^- to 1,2-dihydroxynaphthalene-4-sulfonate (H_2L^-). The titrated amount was somewhat lower than that expected from the weighed amount (0.8 %) and was assumed to be correct.

Stock solution of *sodium chloride* and *aluminium chloride* as well as the dilute *hydrochloric acid* and *sodium hydroxide* solutions were prepared and standardized as described earlier.[1]

Apparatus. The automatic system for precise emf titrations, the thermostat and the glass, hydrogen and Ag/AgCl electrodes were described in Ref. 1. The platinum electrodes were cleaned in boiling *aqua regia,* rinsed in distilled water and heated in an ethanol flame before use. The reduction of Q^- to H_2L^- was performed coulometrically at +240 mV *vs.* NHE with an integrating potentiostat, built at our department.

Special precautions. Since the system under study is extremely redox active it is necessary to perform the experiments in an inert environment. We have taken the same precautions as in Ref. 1 and in addition to these, performed the experiments in dark coloured vessels.

METHOD

The present study was carried out as a series of titrations at 25 °C in a constant ionic medium of 0.6 M Na(Cl). The free H^+ concentration, h, and the (hypothetical) electron activity, $\{e^-\}$, were determined by measuring the emf of the cell −RE// equilibrium solution/ME+, where ME denotes a glass or platinum electrode and RE=Ag, AgCl/0.6 M NaCl. $-\lg h$ is in this cell given by the expression $-\lg h=(E_{o,gl}+E_j-E_{gl})(59.157)^{-1}$ where $E_{o,gl}$ is a constant which was determined in each titration where complex formation could be neglected. $-\lg\{e^-\}$ is defined as $(E_H)(59.157)^{-1}$ where $E_H=E_{o,Pt}+E_j-E_{Pt}$. $E_{o,Pt}$ was determined separately by measuring the emf between the reference electrode and NHE($E_{NHE}\equiv 0$). $E_{o,Pt}$ was found to be −250.5 mV, *i.e.* $E_{RE}=+250.5$ mV *vs* NHE. The liquid junction potential, E_j, could in 0.6 M Na(Cl) be written[8] $E_j=-77h+42k_wh^{-1}$, where $k_w=1.875\cdot 10^{-14}$ M^2 is the ionic product of water. According to the different types of equilibria which must be considered, the present study can be divided into parts as follows:

(i) redox and acid-base equilibria of Q^-/H_2L^-. The reduction of Q^- can be written

$$Q^-+2H^++2e^-\rightleftarrows H_2L^-;\ K_{red} \qquad (1)$$

in acid solution. Knowing the total amount of Q^-, generating a known amount of H_2L^- and measuring $-\lg h$ and $-\lg\{e^-\}$ the equilibrium constant could be determined. 8 titrations with 64 experimental points within the ranges $0.001\ M\leq C+D\leq 0.010$ M; $0.025\leq D/C\leq 20$ were performed. (C and D stand for the total concentration of H_2L^- and Q^-, respectively.) After complete reduction to H_2L^-, $-\lg h$ was increased gradually by means of a coulometer in order to study the equilibrium

$$H_2L^-\rightleftarrows HL^{2-}+H^+;\ k_1 \qquad (2)$$

These experiments comprise 5 titrations with 103 experimental points within the concentration range 0.001−0.01 M. No attempts were made to evaluate the second acidity constant of H_2L^-, as this would require such a high $-\lg h$ that the glass electrode would yield inaccurate values ($-\lg k_2\sim 12.7$).[5] The redox behaviour at higher $-\lg h$ was studied by adding OH^- solution to Q^-/H_2L^- buffers.

(ii) Three component equilibria in the system $H^+-Al^{3+}-H_2L^-$ of the general form

$$pH^++qAl^{3+}+r(H_2L^-)\rightleftarrows H_pAl_q(H_2L)_r^{p+3q-r};\ \beta_{pqr} \qquad (3)$$

The system was investigated through 11 titrations with 504 experimental points where OH^- was generated coulometrically after complete reduction of Q^- to H_2L^-. The ranges $1.5\leq -\lg h\leq 9$; $0.0005\ M\leq B\leq 0.004$ M and $0.002\ M\leq C\leq 0.009$ M with the C/B ratios 15, 10, 7.5, 5, 2.5, 2.25 and 2 were covered. (B stands for the total concentration of Al^{3+}.)

(iii) Two component equilibria in the system $Al^{3+}-Q^-$ of the general form

$$qAl^{3+}+sQ^-\rightleftarrows Al_qQ_s^{3q-s};\ \beta_{q,s} \qquad (4)$$

With knowledge of equilibria under (i) and (ii), it is possible to perform two types of potentiometric experiments in order to investigate this system: (I) By increasing $-\lg h$ with OH^- solution in an Al^{3+}, H_2L^- solution containing different amounts of Q^-. Two titrations (B=0.001 M; C=0.005 M; D=0.005 M and 0.02 M, respectively) were performed. (II) By studying changes in $-\lg \{e^-\}$ when Al^{3+} solution is added to a Q^-/H_2L^- buffer at constant and low $-\lg h$ (no $Al-H_2L$ complexes present). One titration with $0 \leq B/D \leq 17$ was performed.

Apart from these equilibria, the hydrolysis of Al^{3+}:

$$pH^+ + qAl^{3+} \rightleftarrows H_pAl_q^{p+3q}; \beta_{pq} \quad (5)$$

have to be considered under (ii) and (iii). In Part 3 of this series,[9] the complexes $AlOH^{2+}$ (lg $\beta_{-1,1}$= −5.52), $Al_3(OH)_4^{5+}$ (lg $\beta_{-4,3}$= −13.57) and $Al_{13}O_4(OH)_{24}^{7+}$ (lg $\beta_{-32,13}$= −109.2) were found to explain the hydrolysis for $-\lg h \lesssim 4.2$. In neutral solution, small amounts of $Al(OH)_2^+$ and eventually (*cf.* May *et. al.*[10]) $Al(OH)_3^o$ occurs. Finally, in alkaline solution, the dominating species is $Al(OH)_4^-$. Formation constants proposed by Baes and Mesmer[11] (recalculated to be valid in 0.6 M medium) are lg $\beta_{-2,1}$= −10.3; lg $\beta_{-3,1}$= −16.1 and lg $\beta_{-4,1}$= −23.7, respectively.

Data treatment. In the evaluation of the experimental data, we have used standard graphical methods as well as least squares computer calculations (LETAGROPVRID,[12] version ETITR [13,14]). As "best" model or models we will consider those giving the lowest error squares sum $U=\Sigma(H_{calc}-H_{exp})^2$. The LETAGROP calculations also give standard deviations $\sigma(H)$, $\sigma(\beta)$ and $3\sigma(\lg \beta)$, calculated and defined according to Sillén.[15,16] The computations were performed on a CYBER 172 computer.

DATA, CALCULATIONS AND RESULTS

Redox and acid-base equilibria of Q^-/H_2L^-. Some of the data used to evaluate the redox equilibrium constant K_{red} (eqn. (1)) are illustrated in Fig. 1. A least-squares adjustment of the data gave $\lg(K_{red} \pm 3\sigma) = 21.27 \pm 0.09$ (E^o=629±2.7 mV).

The study of redox behaviour at higher $-\lg h$ showed that eqn. (1) could explain data for $-\lg h \lesssim 4.5$. At higher $-\lg h$, the colour of the solutions slowly changed from bright yellow to reddish-brown in connection with a release of protons. Even after 24 h no stable potential could be obtained and, upon standing, a precipitate was formed. This behaviour must be explained by a degradation of Q^- as the same result was obtained with a pure Q^- solution while a pure H_2L^- solution gave stable potentials in this range.

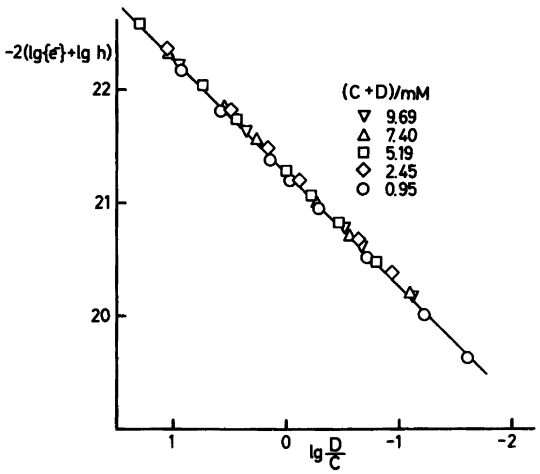

Fig. 1. A part of experimental data used to evaluate the redox equilibrium constant K_{red}. The figure visualizes the validity in the assumption of equilibrium reaction (eqn. (1)) as all the data points can be described by the expression $-2(\lg \{e^-\}+\lg h)=\lg K_{red}+\lg (D/C)$. The full curve has been calculated using the proposed constant lg K_{red}=21.27.

The evaluation of the first acidity constant of H_2L^- (eqn. (2)) was performed as a LETAGROP calculation. The analysis ended at $\sigma(H)$=0.02 mM giving $\lg(k_1 \pm 3\sigma) = -7.798 \pm 0.002$.

These results will be considered as known in all the following calculations and no attempt will be made to adjust these equilibrium constants.

The $H^+-Al^{3+}-H_2L^-$ system. In order to visualize the experimental results, data sets $Z_c(-\lg h)$ were calculated and some of them are given in Fig. 2. Z_c is defined as the average number of OH^- reacted per C and is given by the relation $Z_c=(h-H-k_w h^{-1})/C$ where H denotes the total concentration of protons calculated over

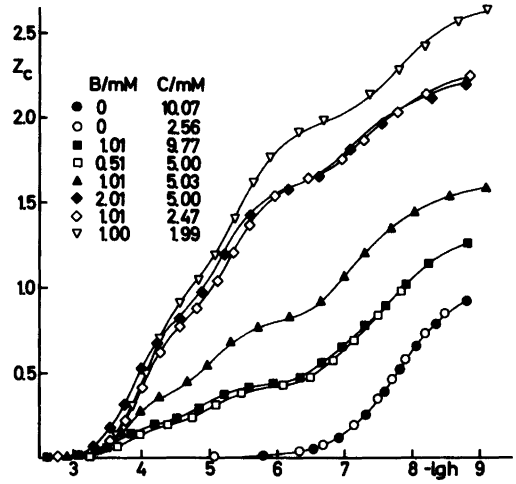

Fig. 2. A part of the experimental data in the system $H^+-Al^{3+}-H_2L^-$ plotted as curves $Z_c(-\lg h)$ for *C/B* ratios 2, 2.5, 5, 10 and ∞. The full curves have been calculated using the set of proposed constants in Table 1.

the zero level H_2O, Al^{3+}, H_2L^-. In addition, the Bjerrum plot $\bar{n}(\lg[L^{3-}])$, where $\bar{n}$ denotes the average number of L^{3-} coordinated per Al^{3+}. was constructed (Fig. 3).

From this latter figure it could be concluded

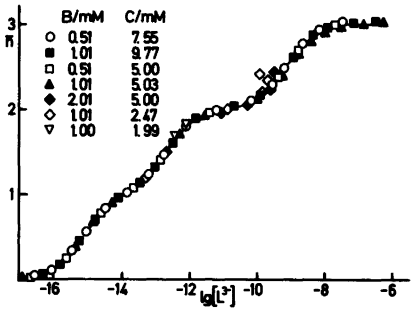

Fig. 3. Experimental data in the system $H^+-Al^{3+}-H_2L^-$ plotted as curves $\bar{n}(\lg [L^{3-}])$ for *C/B* ratios 2, 2.5, 5, 10 and 15. In the calculation, the value $\lg k_2 = -12.66$, obtained for the second acidity constant of H_2L^- by Buffle and Martell,[5] has been used. The chosen value affects the scale on the x-axis but not the shape of the $\bar{n}$ curves. For ratio 2 and 2.5, the experimental data fulfilling the condition $Z_c>2$ have not been possible to visualize with this function.

that the main complexes in the system are AlL^0, AlL_2^{3-} and AlL_3^{6-}. There are, however, deviations and the fact that Z_c passes 2 at low *C/B* quotients (Fig. 2) makes it obvious that some hydrolytic ($Al(OH)_4^-$) or ternary hydroxo species are formed in appreciable amounts.

The assumption of three mononuclear complexes at high quotients (5–15) was confirmed by a LETAGROP calculation. The analysis ended at $\sigma(H)=0.02$ mM giving $\lg \beta_{-2,1,1} = -5.34\pm0.01$; $\lg \beta_{-4,1,2} = -13.12\pm0.02$ and $\lg \beta_{-6,1,3} = -24.48\pm0.02$ (*p,q,r* notations according to eqn. (3)). Applying these species to the titrations at lower quotients (upper part of Fig. 4) showed that minor systematic deviations remained. (In this calculation, the Al^{3+} hydrolytic species with formation constants given earlier were included). As the deviations showed two well-separated broad peaks divided at $-\lg h \sim 6$, we decided to test the simple hypothesis that each peak could be explained by a single complex $H_pAl_q(H_2L)_r^{p+3q-r}$. The search for composition and equilibrium constants for these complexes was performed as *pqr*-analyses (systematic testing of *pqr* combinations) using the LETAGROP-VRID program.

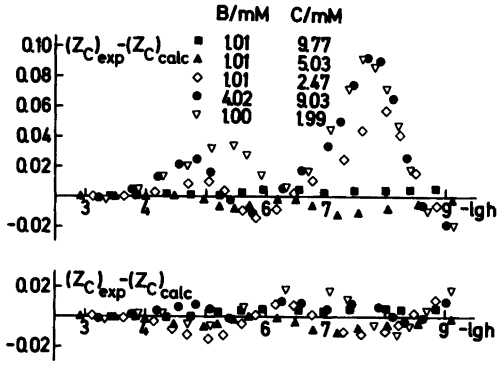

Fig. 4. Residual plots $\Delta Z_c(-\lg h)$ for the system $H^+-Al^{3+}-H_2L^-$. The upper part of this figure shows the residuals obtained when aluminium(III) hydrolysis with equilibrium constants given under "METHOD" and the complexes (−2,1,1): $\lg \beta_{-2,1,1} = -5.34$; (−4,1,2): $\lg \beta_{-4,1,2} = -13.12$ and (−6,1,3): $\lg \beta_{6,1,3} = -24.48$ are applied. The lower part of the figure shows the same quantity when the final model with equilibrium constants given in Table 1 are applied.

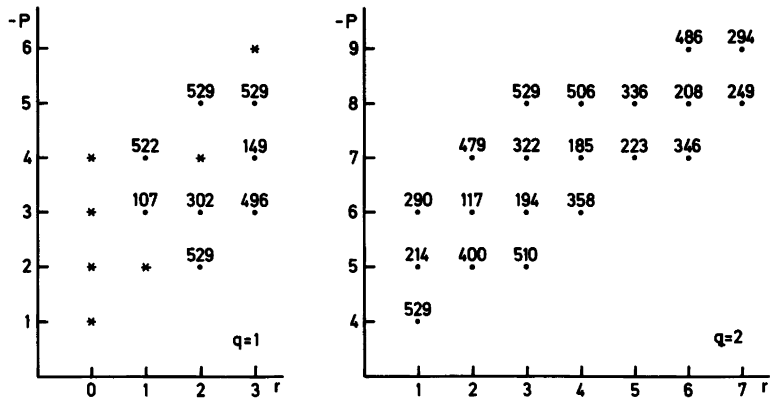

Fig. 5. Result of the first *pqr*-analysis concerning the acid ($-\lg h \lesssim 6$) peak in the system $H^+-Al^{3+}-H_2L^-$. The diagrams give the error squares sums $U_H(pr)_q \cdot 10^3$ assuming one new complex. In the calculations, aluminium hydrolysis and (−2,1,1), (−4,1,2) and (−6,1,3) (marked in the left diagram with asterisks) have been assumed to be known. The calculations are based on 117 points giving $U_H(00)_0 = 529 \cdot 10^{-3}$.

The result of the first analysis, performed on the acid peak, is given in Fig. 5 and it was found that the lowest value of U was obtained for the complex $H_{-3}Al(H_2L)^-$ with $\lg \beta_{-3,1,1} = -11.19 \pm 0.07$. The alkaline peak was, in the same manner, best explained with the complex $H_{-5}Al(H_2L)_2^{4-}$; $\lg \beta_{-5,1,2} = -21.12 \pm 0.08$ (Fig. 6).

Model calculations, performed with the computer program SOLGASWATER,[17] had shown that significant amounts of $Al(OH)_4^-$ were formed at the lowest quotients. In the final LETAGROP calculation on the whole data material, the formation constant for this species, as well as the equilibrium constants for all three component complexes found above, were refined. This calculation, which provides the final proposed model and corresponding equilibrium constants for the system, is presented in Table 1.

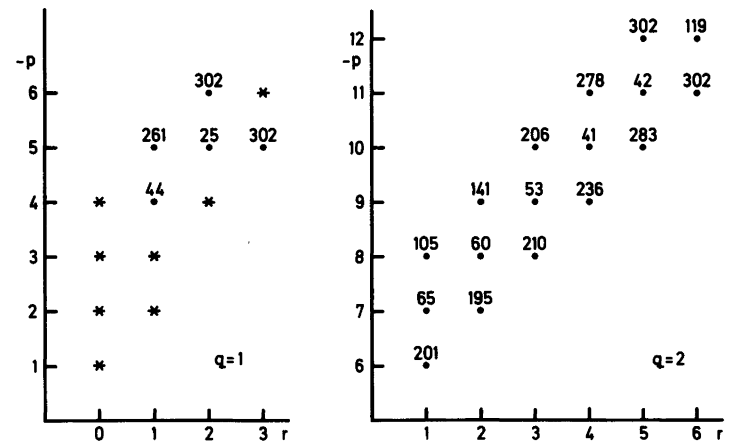

Fig. 6. Result of the second *pqr*-analysis on the alkaline ($-\lg h \gtrsim 6$) peak in the system $H^+-Al^{3+}-H_2L^-$. The complex $H_{-3}Al(H_2L)^-$ has, in addition to those complexes mentioned in the first *pqr*-analysis, been assumed to be known and the diagrams give $U_H(pr)_q \cdot 10^2$ assuming one new complex. The calculations are based on 49 points giving $U_H(00)_0 = 302 \cdot 10^{-2}$.

Table 1. A compilation of final results. Q^- stands for 1,2-dinaphthoquinone-4-sulfonate and H_2L^- stands for 1,2-dihydroxynaphthalene-4-sulfonate.

System	No. of titr./ No. of points	Equilibrium reaction	Tentative formula	lg($\beta\pm3\sigma$)
$e^--H^+-Q^-$	8/64	$Q^-+2H^++2e^- \rightleftarrows H_2L^-$ for $-\lg h \lesssim 4.5$ Q^- decomposes at $-\lg h \gtrsim 4.5$		21.27±0.09
$H^+-Al^{3+}-H_2L^-$		$pH^++qAl^{3+}+r(H_2L^-) \rightleftarrows H_pAl_q(H_2L)_r^{p+3q-r}$		
	5/103	p,q,r: −1,0,1	HL^{2-}	−7.798±0.002
	11/504	−4,1,0	$Al(OH)_4^-$	−23.46±0.11
		−2,1,1	AlL^o	−5.343±0.006
		−3,1,1	$Al(OH)L^-$	−11.24±0.08
		−4,1,2	AlL_2^{3-}	−13.115±0.009
		−5,1,2	$Al(OH)L_2^{4-}$	−21.15±0.04
		−6,1,3	AlL_3^{6-}	−24.47±0.02
$Al^{3+}-Q^-$	3/41	$qAl^{3+}+sQ^- \rightleftarrows Al_qQ_s^{3q-s}$ No stable complexes are formed		

The analysis ended at $\sigma(H)=0.03$ mM, indicating a good fit, and from the lower part of Fig. 4 it is clear that no systematic deviations remain.

The $Al^{3+}-Q^-$ system. The two experimental procedures to investigate this system are described under "METHOD". In procedure I, where Q^- competes with H_2L^- for Al^{3+}, the occurrence of a complex $Al_qQ_s^{3q-s}$ would lower $\bar{n}$ (the average number of L^{3-} coordinated per Al^{3+}) at a given $-\lg [L^{3-}]$. The experimental results are shown in Fig. 7 and indicate no such tendencies. In procedure II, a complex $Al_qQ_s^{3q-s}$ would lower the free Q^- concentration and consequently (eqn. (1)) cause a decrease in $-\lg \{e^-\}$. As seen in Fig. 8, neither does this experiment indicate the existence of any complex between Al^{3+} and Q^-. (It could be mentioned that a satisfactory check of the validity of this latter procedure was obtained in procedure I, where H_2L^- was bound to Al^{3+}.)

On the basis of these two types of experiments, we find it credible to conclude that Al^{3+} does not form stable complexes with Q^-.

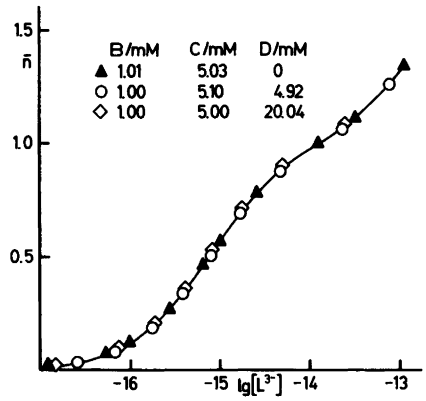

Fig. 7. $\bar{n}(\lg [L^{3-}])$ curves for the system $H^+-Al^{3+}-H_2L^-$ in the presence of different amounts of Q^-. The full curve has been calculated with the set of proposed constants given in Table 1 and the figure indicates that the amount of Q^- is quite insignificant to the complex formation between Al^{3+} and H_2L^-. Thus the figure indicates that no complexes between Al^{3+} and Q^- are formed.

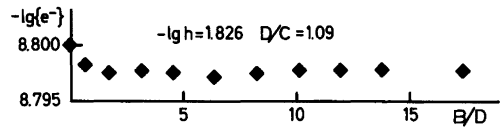

Fig. 8. The figure shows that $-\lg\{e^-\}$ is unaffected when aluminium(III) solution is added to a Q^-/H_2L buffer at low $-\lg h$ where no $Al^{3+}-H_2L^-$ complexes are formed (*cf.* Fig. 2), thus again indicating the absence of any complex $Al_qQ_s^{3q-s}$.

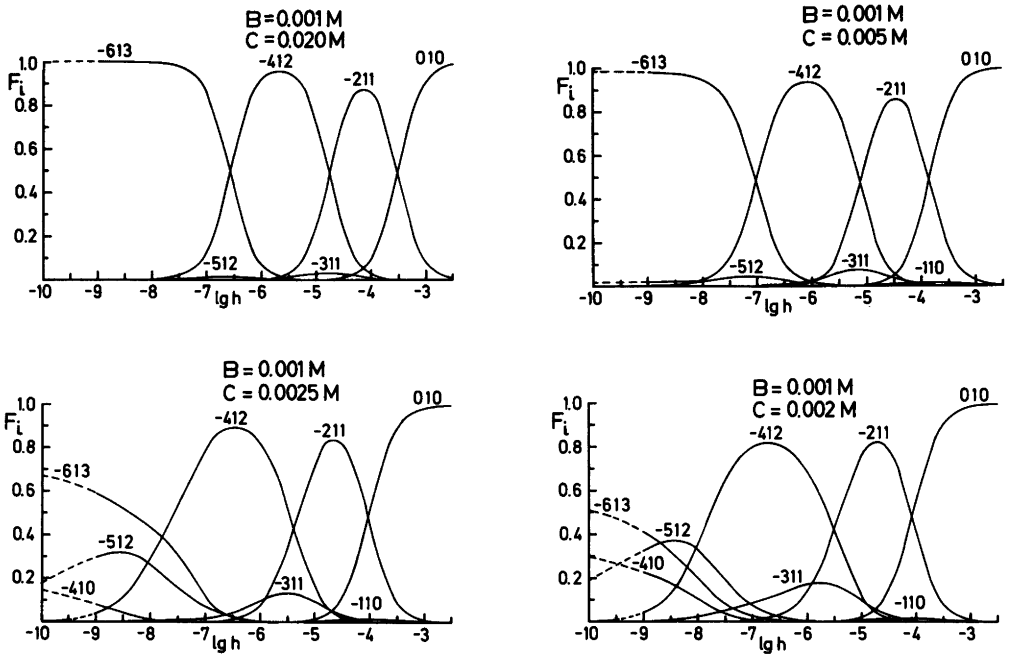

Fig. 9. Distribution diagrams $F_i(\lg h)_{B,C}$ in the system $H^+-Al^{3+}-H_2L^-$. F_i is defined as the ratio between aluminium(III) in a species and total aluminium(III). The calculations have been performed using the computer program SOLGASWATER [17] with constants given in Table 1. Broken lines in the figures denote ranges where no measurements have been performed.

DISCUSSION

The main purpose of the present study was to investigate whether complexes are formed between aluminium(III) and *o*-diquinones. As a model system, we chose the system $Al^{3+}-1,2$-naphthoquinone-4-sulfonate(Q^-) and found, on the basis of two independent types of potentiometric experiments, that no stable complexes were formed. We believe that this is a general observation and that it could be concluded that *o*-diquinones do not complexate aluminium(III) in any appreciable amount. Thinking in terms of soft and hard acids and bases,[18] the result is in no way surprising, but our investigation has provided the experimental proof.

Concerning complex formation between Al^{3+} and the reduced state of the *o*-dinaphthoquinone, *i.e.* 1,2-dihydroxynaphthalene-4-sulfonate (H_2L^-), the study has given evidence for the formation of a main series of complexes $(-2,1,1)$, $(-4,1,2)^{3-}$, $(-6,1,3)^{6-}$ together with two hydrolyzed species $(-3,1,1)^-$ and $(-5,1,2)^{4-}$. The amounts of the different species are illustrated in Fig. 9. It must be pointed out that although the species $(-3,1,1)^-$ gave the closest fit on the acid peak, an almost equal low error squares sum was obtained for the dimer of this complex, $(-6,2,2)^{2-}$. It is possible that these two species actually co-exist in solution, although we have no possibility to analyse this on the present data material. Regarding the other species, the fact that these are formed in great amounts (Fig. 9) and that the standard deviations of the equilibrium constants are low, (Table 1) makes it possible to consider these as well determined.

Although an emf investigation gives no structural information but merely gross compositions and formation constants of the species formed, we find it most credible that the species in the main series formed are chelates between Al^{3+} and the two orthocoordinated phenolic groups on the naphthalene and that these species could be written AlL_n^{3-3n}; $n=1,2,3$. As the ligand only

offers two hydrolyzable protons, we also conclude that the species (−3,1,1) and (−5,1,2) are hydroxo complexes and could be written $Al(OH)L^-$ and $Al(OH)L_2^{4-}$ respectively.

The formation constant for the aluminate ion, $Al(OH)_4^-$, has hitherto mainly been determined indirectly, by measurements of the solubility of $Al(OH)_3(s)$ in alkaline solution. Baes and Mesmer[11] have discussed experimental difficulties and uncertainties with this method and estimate one standard deviation in the formation constant to be 0.3 logarithmic units. A revision of the constant with 0.24 log units therefore seems by no means unrealistic, especially since the complex is formed in considerable amounts in some of the experiments (Fig. 9). The fact that the resultant standard deviation is moderate ($3\sigma(\lg\beta)=0.11$), (Table 1) also gives support for this revision.

The reduction of Q^- to H_2L^- is a two-electron, two-proton transfer reaction. The relatively large standard deviation obtained in the equilibrium constant ($3\sigma(\lg K_{red})=0.09$) (Table 1) seems to depend upon a variation in $E_{o,Pt}$ between the titrations. It was found that the standard deviations were an order of magnitude lower within single titrations. As $E_{o,Pt}$ had to be determined separately and indirectly, the phenomenon is, however, beyond our control.

The results found in this acid area are in accordance with those found by Buffle *et. al.*[5] On the other hand, while we have found that Q^- decomposes irreversibly in neutral and alkaline solution, they claim that the reversibility holds to at least $-\lg h=10$ and that at higher $-\lg h$ a semiquinone is formed. We believe that this difference in results could be explained by the different experimental procedures used. As their experiments lasted only a few minutes it is most probable that they had a negligible decomposition of Q^- during that time.

As pointed out in Part I of this series, the occurrence of organic ligands in a natural water could change the speciation and significantly increase the solubility of Al-containing minerals. It was shown that with a total concentration of gallic acid equal to 30 μM, the solubility of the clay mineral kaolinite was increased by an average factor of 5 with respect to Al in the pH-region 5–9. (When we renewed this calculation, using the revised formation constant for $Al(OH)_4^-$, the Part 3[9] hydrolysis model and literature values for $Al(OH)_2^+$ and $Al(OH)_3$, the average increase factor became 3.4.) In the present study we have confirmed the powerful complexing ability of two *ortho*-coordinated phenolic groups (an analogous calculation as above, ended at an average increase in Al-solubility of 4.8) and in addition, showed that the corresponding oxidized compounds, *i.e. o*-diquinones, do not form any stable complexes with Al(III).

Acknowledgements. The English of the present paper has been corrected by Dr. Michael Sharp. The work forms part of a program financially supported by the Swedish Natural Science Research Council.

REFERENCES

1. Öhman, L.-O. and Sjöberg, S. *Acta Chem. Scand. A 35* (1981) 201.
2. Rashid, M. A. *Chem. Geol. 9* (1972) 241.
3. Clark, W. M. *Oxidation-Reduction Potentials of Organic Systems,* Williams & Wilkins, Baltimore 1960, p. 373.
4. Gieseking, J. E., Ed., *Soil. Components, Vol. 1, Organic Components,* Springer, New York 1975.
5. Buffle, J. and Martell, A. E. *Inorg. Chem. 16* (1977) 2221.
6. Fieser, L. F. *Org. Synth. 21* (1941) 91.
7. Gran, C. *Acta Chem. Scand. 4* (1950) 559.
8. Sjöberg, S., Nordin, A. and Ingri, N. *Mar. Chem. 10* (1981) 521.
9. Öhman, L.−O. and Forsling, W. *Acta Chem. Scand. A 35* (1981) 795.
10. May, H. M., Helmke, P. A. and Jackson, M. L. *Geochim. Cosmochim. Acta 43* (1979) 861.
11. Baes, C. F. and Mesmer, R. E. *The Hydrolysis of Cations,* Wiley, New York 1976, p. 112.
12. Ingri, N. and Sillén, L. G. *Ark. Kemi 23* (1964) 97.
13. Arnek, R., Sillén, L. G. and Wahlberg, O. *Ark. Kemi 31* (1969) 353.
14. Brauner, P., Sillén, L. G. and Whiteker, R. *Ark. Kemi 31 (1969) 365.*
15. *Sillén, L. G. Acta Chem. Scand. 16* (1962) 159.
16. Sillén, L. G. and Warnqvist, B. *Ark. Kemi 31* (1969) 341.
17. Eriksson, G. *Anal. Chim. Acta 112* (1979) 375.
18. Ahrland, S., Chatt, S. J. and Davis, W. R. *Quart. Rev. 12* (1958) 265.

Received December 7, 1982.

Acta Chemica Scandinavica A 37 (1983) 569–578

The Structures of two Oxalato-bridged Cu-Dimers; $[Cu_2(Me_4en)_2(C_2O_4)(H_2O)_2](PF_6)_2 \cdot 2H_2O$ and $[Cu_2(Et_5dien)_2(C_2O_4)](PF_6)_2$

JORUNN SLETTEN

Department of Chemistry, University of Bergen, Realfagbygget, N-5000 Bergen, Norway

The structures of $[Cu_2(Me_4en)_2(C_2O_4)(H_2O)_2](PF_6)_2 \cdot 2H_2O$ and $[Cu_2(Et_5dien)_2(C_2O_4)](PF_6)_2$, where Me_4en is *N,N,N',N'*-tetramethylethylenediamine and Et_5dien is *N,N,N',N'',N''*-pentaethyldiethylenetriamine, have been determined using heavy atom X-ray methods. The Me_4en-compound crystallizes in the triclinic space group $P\bar{1}$ with cell dimensions $a=7.932(5)$ Å, $b=8.117(7)$ Å, $c=12.089(15)$ Å, $\alpha=96.89(9)°$, $\beta=97.03(8)°$, $\gamma=102.44(6)°$, $Z=1$. The structure was refined to an R of 0.053 using 1353 observed reflections. The Et_5dien compound is monoclinic, space group $I2/c$ (conventional setting $C2/c$) with cell dimensions $a=13.436(9)$ Å, $b=22.29(2)$ Å, $c=14.59(1)$ Å, $\beta=103.68(7)°$, $Z=4$, and was refined to an R of 0.045 using 2112 observed reflections. Both compounds are centrosymmetric binuclear complexes bridged by an oxalate group. The Cu-coordination in the Me_4en compound is slightly distorted square pyramidal with the bridging group occupying two equatorial coordination sites and a water molecule in the apex position; while in the Et_5dien compound a geometry intermediate between square pyramidal and trigonal bipyramidal is found; the oxalate oxygen atoms occupying one equatorial and one axial position.

Magnetic exchange interactions in transition metal dimers, and structural properties of such complexes have been studied extensively over the last few years. Much work has been focused on systems with single atom bridges.[1-2] However, metal-metal interaction is also found in dimers containing various polyatomic bridging groups like *e.g.* formate and oxalate, and with geometries such that no short metal-metal contact is present. Attempts have been made to find correlations between magnetic properties and coordination geometry in such complexes.[3-8] The magnetic properties apparently depend upon both the type of bridging ligand and outer ligand involved, the counter ion, as well as the coordination geometry.[3] More data is needed in order to sort out the various factors involved. Recently a series of dimeric Cu and Ni complexes with μ-oxamido, μ-oxamato and μ-oxalato bridges were synthesized by Nonoyama *et al.*[9,10] Most of these complexes have subnormal magnetic moments at room-temperature, indicating metal-metal magnetic interaction. The present paper presents structural data on two of these compounds containing μ-oxalato-bridges. In a previous paper the structures of two complexes with μ-oxamido-bridges were reported.[11]

EXPERIMENTAL

Both compounds were synthesized by Nonoyama *et. al.*[9] Crystals suitable for X-ray investigations grew by slow evaporation from methanol/water solutions at room temperature. The Me_4en complex crystallized as bright blue, tiny platelets which fractured easily and had a high mosaic spread. The crystal used for X-ray measurements was lost at the end of the data collection, hence dimensions were not measured. The Et_5dien complex crystallized as dark blue prisms; dimensions of the crystal used were $0.45\times0.38\times0.24$ mm. Intensity data were collected at 85 K and 140 K, respectively, on a

0302-4377/83 $2.50

Table 1. Measurement of intensity data.

Compound	Me_4en	Et_5dien
Temperature (K)	85	140
Scan type	ω	ω
Scan range (°)	$\Delta\omega$=3.5	$\Delta\omega$=2.0
Scan speed (°/min)	10	60
Max. 2θ (°)	45	45
No. of unique refl. measured	1957	2787
"Observed" refl.	1353	2112
Cutoff	$3\sigma_c$	$2\sigma_c$

Syntex $P2_1$ diffractometer using monochromatized Mo$K\alpha$-radiation. A summary of the data collection parameters is listed in Table 1. The intensities were corrected for Lorentz and polarizations effects; no absorption correction was carried out.

CRYSTAL DATA

Me_4en complex. (μ-oxalato-[bis{aqua-*N,N,N',N'*-tetramethylethylenediaminecopper(II)}]phosphorhexafluoride dihydrate, $Cu_2C_{14}H_{40}F_{12}N_4O_8P_2$, triclinic, $P\bar{1}$ (No2). a=7.932(5) Å, b=8.117(7) Å, c=12.089(15) Å, α=96.89(9)°, β=97.03(8)°, γ=102.44(6)°, V=745.7(1.3) Å^3, M=809.51, Z=1, D_m=1.78 g cm^{-3}, D_x(85K)=1.803 g cm^{-3}, μ(Mo$K\alpha$)=16.51 cm^{-1}.

Et_5dien complex. [μ-oxalato-bis{*N,N,N',N'',N''*-pentaethyldiethylenetriaminecopper(II)}]phosphorhexafluoride, $Cu_2C_{30}H_{66}F_{12}N_6O_4P_2$, monoclinic, *I2/c* (No 15, standard setting *C2/c*). a=13.436(9) Å, b=22.29(2) Å, c=14.59(1) Å, β=103.68(7)°, V=4244(6) Å^3, M=991.91, Z=4, D_m=1.54 g cm^{-3}, D_x(140K)=1.553 g cm^{-3}, μ(Mo$K\alpha$)=11.70 cm^{-1}.

STRUCTURE DETERMINATIONS

Both structures were solved using the heavy atom technique, and refined by least-squares methods. All hydrogen atoms, except one on the water of crystallization in the Me_4en compound, were localized in difference Fourier maps, and were refined isotropically. For non-hydrogen atoms anisotropic thermal parameters were employed. The weight assigned to each reflection in the refinement is $w=[\sigma_F^2+(kF_o)^2]^{-1}$ where $\sigma_F=\sigma_c(I\cdot \mathrm{Lp})^{-1/2}$ and k=0.02. Final R-factors are 0.053 and 0.045 for the Me_4en and Et_5dien complex, respectively. Weighted R-factors are 0.051 and 0.044, and the standard deviations of an observation of unit weight 2.00 and 1.29, respectively.

Atomic scattering factors were taken from International Tables IV.[12] All calculations were carried out on an Eclipse computer employing the SHELXTL program system.[13]

Final atomic parameters are listed in Tables 2 and 3, bond lengths and angles in Tables 4 and 5. Bond distances and angles involving hydrogen atoms are not listed, they are all normal within the limits of errors. C–H bond lengths in the range 0.83–1.11 Å are found in the Me_4en compound and in the range 0.73–1.19 Å in the Et_5dien compound. Standard deviations in these bond lengths are in the range 0.05–0.11 Å. Molecular framework and numbering schemes are shown in Figs. 1 and 2, packing diagrams in Figs. 3 and 4. Lists of observed and calculated structure factors and of anisotropic thermal parameters may be obtained from the author.

RESULTS AND DISCUSSION

Each complex consists of a dimeric unit with two metal ions being bridged centrosymmetri-

Table 2. Final coordinates and equivalent U-values of non-hydrogen atoms with estimated standard deviations in parentheses. Equivalent U-values are defined by: $U_{eq}=1/3\,\Sigma_i\Sigma_j U_{ij}a_i^*a_j^*\mathbf{a}_i\mathbf{a}_j$. Fractional atomic coordinates have been multiplied by a factor of 10^4 and thermal parameters by 10^3, except the parameters of Cu in the Et_5dien compound which have been multiplied by factors of 10^5 and 10^4, respectively.

Atom	x	y	z	U_{eq}
Me_4en compound				
Cu	2450(1)	1329(1)	1722(1)	25(1)
O1	242(7)	1806(7)	1007(5)	28(2)
O2	1870(7)	−670(7)	446(5)	24(2)

Table 2. Continued.

OW1	3876(8)	3190(7)	732(6)	36(3)
OW2	2727(9)	−6031(8)	119(7)	36(3)
N1	4519(9)	611(8)	2481(6)	25(3)
N2	2493(9)	2823(8)	3209(7)	29(3)
C1	−455(11)	715(11)	165(7)	23(3)
C2	5926(11)	621(12)	1782(9)	37(4)
C3	3971(11)	−1177(11)	2746(8)	30(3)
C4	5178(14)	1843(14)	3519(10)	39(4)
C5	3682(13)	2266(12)	4059(9)	40(4)
C6	728(11)	2636(11)	3568(8)	29(3)
C7	3138(12)	4655(11)	3107(10)	35(4)
P	−1233(3)	−2877(3)	2935(2)	29(1)
F1	−1947(6)	−1518(6)	3721(4)	35(2)
F2	−2954(6)	−3211(6)	2039(4)	38(2)
F3	486(6)	−2563(6)	3828(4)	34(2)
F4	−2178(7)	−4391(6)	3560(5)	42(2)
F5	−293(6)	−1368(6)	2306(4)	37(2)
F6	−518(7)	−4232(6)	2143(5)	42(2)
Et_5dien compound				
Cu	16986(5)	6693(3)	49941(4)	246(2)
O1	1085(3)	208(2)	5874(2)	26(1)
O2	288(3)	324(2)	4007(2)	28(1)
N1	2814(3)	8(2)	4955(3)	25(2)
N2	2291(3)	1131(2)	4058(3)	26(2)
N3	1210(3)	1500(2)	5417(3)	30(2)
C1	222(4)	−37(2)	5536(4)	23(2)
C2	3683(4)	56(3)	5825(4)	34(2)
C3	3425(5)	−160(3)	6726(4)	41(2)
C4	2386(4)	−613(2)	4828(4)	31(2)
C5	3165(5)	−1105(3)	4761(4)	40(2)
C6	3212(4)	182(3)	4118(4)	30(2)
C7	3306(4)	856(2)	4072(4)	32(2)
C8	1581(4)	1090(3)	3099(4)	31(2)
C9	1864(4)	1471(3)	2341(4)	36(2)
C10	2396(4)	1765(3)	4413(4)	35(2)
C11	1411(5)	1932(3)	4685(4)	37(2)
C12	1813(4)	1701(3)	6367(4)	43(2)
C13	1641(5)	1351(3)	7195(4)	55(3)
C14	75(4)	1479(2)	5369(4)	33(2)
C15	−405(5)	2083(3)	5519(5)	48(3)
P1	0(0)	2990(1)	2500(0)	30(1)
P2	5000(0)	1537(1)	7500(0)	43(1)
F1	0(0)	2270(2)	2500(0)	36(2)
F2	−567(3)	2988(2)	3349(2)	44(1)
F3	0(0)	3708(2)	2500(0)	54(2)
F4	−1086(2)	2985(1)	1754(2)	41(1)
F5	4216(3)	2042(2)	7636(3)	74(2)
F6	4498(3)	1531(2)	6387(2)	55(1)
F7	4218(3)	1029(2)	7646(3)	67(2)

Table 3. Atomic parameters of hydrogen atoms. Isotropic temperature factors are defined by $\exp[-8\pi^2 U \sin^2 \theta/\lambda^2]$. All values are multiplied by 10^3.

Atom	*x*	*y*	*z*	*U*
Me_4en compound				
H21	682(9)	42(9)	213(6)	17(20)
H22	547(12)	−4(13)	104(8)	58(31)
H23	620(13)	169(13)	163(9)	64(32)
H31	359(8)	−178(8)	196(5)	1(17)
H32	505(9)	−141(9)	326(6)	25(21)
H33	310(10)	−114(10)	318(7)	38(24)
H41	577(12)	146(12)	409(8)	42(29)
H42	592(13)	290(14)	332(9)	66(34)
H51	412(10)	299(10)	483(7)	32(24)
H52	347(12)	131(12)	425(8)	58(29)
H61	79(9)	322(9)	437(6)	19(20)
H62	−3(8)	298(8)	304(5)	3(16)
H63	37(9)	158(10)	361(7)	28(22)
H71	243(11)	498(11)	246(7)	45(26)
H72	448(11)	482(11)	290(8)	43(26)
H73	353(16)	530(16)	391(11)	101(43)
HW11	509(12)	333(11)	51(8)	52(28)
HW12	350(10)	375(10)	50(7)	35(24)
HW21	−209(14)	−572(14)	61(9)	8(41)
Et_5dien compound				
H21	390(4)	49(2)	591(3)	42(15)
H22	427(4)	−15(2)	569(3)	36(15)
H31	404(4)	−7(2)	724(4)	52(17)
H32	338(4)	−54(2)	671(3)	29(14)
H33	283(4)	11(3)	684(4)	64(19)
H41	183(3)	−58(2)	418(3)	20(12)
H42	205(3)	−64(2)	532(3)	15(11)
H51	350(4)	−100(2)	420(3)	36(15)
H52	364(4)	−118(2)	533(3)	35(15)
H53	273(4)	−148(2)	460(4)	52(17)
H61	384(3)	−1(2)	417(2)	0(10)
H62	276(3)	2(2)	355(3)	16(12)
H71	351(3)	93(2)	359(3)	3(10)
H72	386(4)	103(2)	466(3)	39(15)
H81	154(4)	70(2)	288(3)	34(14)
H82	92(4)	117(2)	311(4)	47(16)
H91	249(3)	143(2)	229(3)	14(11)
H92	140(4)	140(2)	171(4)	42(16)
H93	188(4)	188(2)	252(3)	39(15)
H101	253(3)	202(2)	392(3)	25(13)
H102	302(4)	178(2)	501(3)	31(14)
H111	85(4)	191(2)	410(3)	33(14)
H112	150(4)	231(2)	504(3)	42(16)
H121	180(4)	218(2)	658(3)	39(15)
H122	243(5)	161(2)	634(4)	58(18)
H131	159(5)	82(3)	715(4)	84(22)
H132	202(5)	152(2)	771(4)	52(19)
H133	90(5)	138(3)	729(4)	87(20)
H141	3(3)	119(2)	589(3)	5(10)
H142	−23(4)	136(2)	473(4)	56(18)
H151	−31(4)	232(3)	490(4)	68(19)
H152	−95(4)	203(3)	542(4)	55(18)
H153	−12(4)	221(2)	617(4)	51(17)

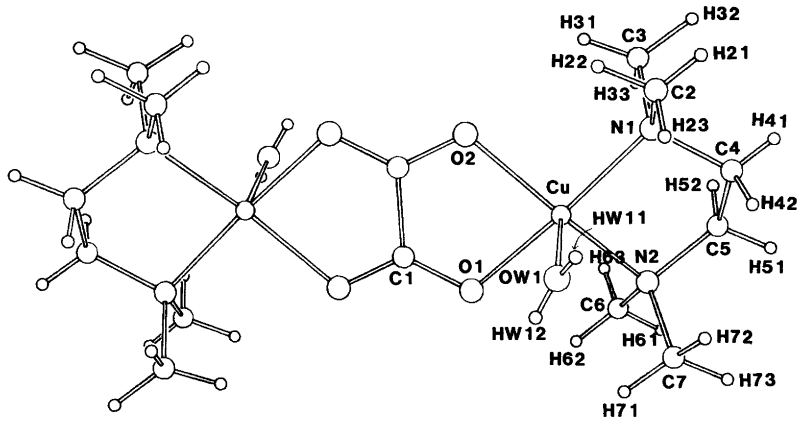

Fig. 1. Dimeric unit of $[Cu_2(Me_4en)_2(C_2O_4)(H_2O)_2]^{2+}$.

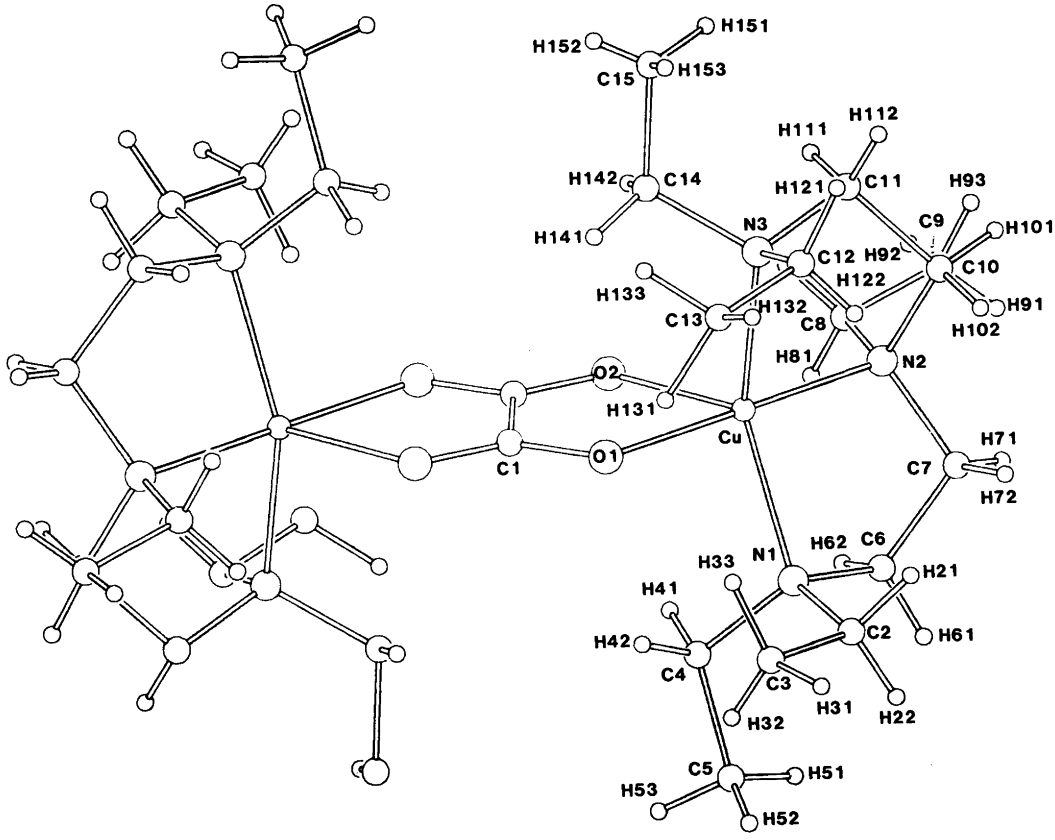

Fig. 2. Dimeric unit of $[Cu_2(Et_5dien)_2(C_2O_4)]^{2+}$.

Table 4. Bond lengths (Å).

Me_4en compound			
Cu–O1	1.992(6)	N1–C2	1.480(13)
Cu–O2	2.032(6)	N1–C3	1.508(11)
Cu–N1	2.011(8)	N1–C4	1.469(13)
Cu–N2	2.037(8)	C4–C5	1.505(16)
Cu–OW1	2.241(7)	N2–C5	1.486(13)
O1–C1	1.249(9)	N2–C6	1.497(12)
O2–C1′	1.257(10)	N2–C7	1.490(11)
C1–C1′	1.533(18)		
Et_5dien compound			
Cu–O1	1.971(4)	C4–C5	1.534(8)
Cu–O2	2.229(4)	C6–C7	1.511(8)
Cu–N1	2.113(5)	N2–C7	1.490(7)
Cu–N2	2.017(5)	N2–C8	1.499(6)
Cu–N3	2.104(5)	N2–C10	1.501(7)
O1–C1	1.271(6)	C8–C9	1.512(9)
O2–C1′	1.241(7)	C10–C11	1.515(9)
C1–C1′	1.545(10)	N3–C11	1.508(8)
N1–C2	1.511(6)	N3–C12	1.500(7)
N1–C4	1.494(7)	N3–C14	1.511(7)
N1–C6	1.495(8)	C12–C13	1.501(9)
C2–C3	1.515(9)	C14–C15	1.529(9)

cally by an oxalate ion (Figs. 1 and 2). The Cu···Cu distances within the dimers are 5.232(4)Å and 5.457(3)Å for the Me_4en and Et_5dien complex, respectively.

The coordination geometry. In the Me_4en compound a somewhat distorted square pyramidal (SP) coordination geometry is found with oxalate and diamine coordinating in the equatorial plane. Cu is displaced 0.208 Å from a best least-squares plane through the equatorial ligand atoms towards the apical water oxygen OW1; while O1, O2, N1, N2 deviate 0.106, −0.105, 0.101, −0.101 Å, respectively, from this plane, showing a significant tetrahedral distortion. The sixth position, opposite to OW1 is blocked by the proximity of F5 of the PF_6-group (see Fig. 3); Cu···F5 being 2.953 Å and ∠F5···Cu − OW1=160.3°. The coordination geometry is similar to that found in a copper dimer containing an oxamido bridge and bipyridyl as outer ligand, $([Cu_2(oa)(bipy)_2](NO_3)_2 \cdot 3H_2O)$,[11] although in the latter case the apical position is occupied by the anion. Both of these compounds are reported to have subnormal magnetic moments at room temperature (1.00 B.M. for the oxamido, 1.47 B.M. for the oxalato bridged dimer),[9] indicating magnetic interaction between metal ions. No study on temperature dependence of the magnetic susceptibility has been done for these two compounds. However, for a structurally closely related SP complex with a dithiooxamide derivative as bridging group equatorially, very strong antiferromagnetic coupling has been shown to be present in two different modifications.[8,17] A mechanism for a σ-type magnetic exchange through the bridging ligand has been proposed for such complexes with SP geometry, $d_{x^2-y^2}$ Cu(II)ion ground state, and the bridging ligand occupying two equatorial coordination sites.[8] Strong antiferromagnetism has also been measured in cases of square planar[6] and elongated octahedral[14] geometry with equatorial oxalate bridges.

In the Et_5dien compound the coordination geometry is intermediate between SP and trigonal bipyramidal (TBP). If regarding the complex as SP, oxalate oxygen O2 occupies the apical position with the other oxalate oxygen atom and the nitrogen atoms in the basal plane. Deviations from a best least-squares plane through O1, N1, N2, N3 are 0.238, −0.251, 0.264, −0.251 Å, respectively; the Cu atom deviating by 0.218 Å towards the axial ligand. The values listed here as well as the bond angles (Table 5) show that the

Table 5. Bond angles (°)

Me_4en compound, copper coordination			
O1–Cu–O2	83.4(2)	O2–Cu–N2	162.3(3)
O1–Cu–N1	173.8(3)	O2–Cu–OW1	94.9(2)
O1–Cu–N2	93.6(3)	N1–Cu–N2	87.2(3)
O1–Cu–OW1	87.6(2)	N1–Cu–OW1	98.3(3)
O2–Cu–N1	93.9(3)	N2–Cu–OW1	102.4(3)
Me_4en compound, oxalate bridge			
Cu–O1–C1	111.1(6)	O1–C1–C1′	118.5(9)
Cu–O2–C1′	111.0(5)	O2–C1–C1′	115.9(8)
O1–C1–O2′	125.6(8)		
Me_4en compound, tetramethylethylenediamine			
Cu–N1–C2	113.2(6)	Cu–N2–C6	113.0(5)
Cu–N1–C3	110.3(5)	Cu–N2–C7	110.0(6)
Cu–N1–C4	105.8(6)	Cu–N2–C5	105.8(6)
C2–N1–C3	107.0(7)	C6–N2–C7	107.2(7)
C2–N1–C4	109.5(7)	C6–N2–C5	109.5(7)
C3–N1–C4	111.0(8)	C7–N2–C5	111.4(6)
N1–C4–C5	110.3(8)	N2–C5–C4	108.9(9)
Et_5dien compound, copper coordination			
O1–Cu–O2	79.5(1)	O2–Cu–N2	98.6(2)
O1–Cu–N1	93.6(2)	O2–Cu–N3	102.5(2)
O1–Cu–N2	178.1(2)	N1–Cu–N2	86.6(2)
O1–Cu–N3	93.5(2)	N1–Cu–N3	153.4(2)
O2–Cu–N1	104.0(2)	N2–Cu–N3	87.2(2)
Et_5dien compound, oxalate bridge			
Cu–O1–C1	117.1(3)	O1–C1–C1′	116.4(6)
Cu–O2–C1′	108.9(3)	O2–C1′–C1	118.0(5)
O1–C1–O2′	125.6(4)		
Et_5dien compound, pentaethyldiethylenetriamine			
Cu–N1–C2	109.9(3)	Cu–N3–C14	110.0(3)
Cu–N1–C4	113.3(3)	Cu–N3–C12	113.3(3)
Cu–N1–C6	103.5(3)	Cu–N3–C11	103.5(3)
C2–N1–C4	111.6(4)	C14–N3–C12	111.8(4)
C2–N1–C6	108.2(4)	C14–N3–C11	109.6(4)
C4–N1–N6	109.9(4)	C12–N3–C11	108.3(4)
N1–C2–C3	114.6(5)	N3–C14–C15	114.9(4)
N1–C4–C5	114.9(5)	N3–C12–C14	115.8(5)
N1–C6–C7	110.3(5)	N3–C11–C10	110.0(4)
C6–C7–N2	108.8(4)	C11–C10–N2	107.8(5)
Cu–N2–C7	106.8(3)	C7–N2–C8	111.5(4)
Cu–N2–C8	109.6(3)	C7–N2–C10	111.8(4)
Cu–N2–C10	105.4(3)	C8–N2–C10	111.5(4)

distortion from idealized SP geometry is appreciable. Viewing the complex as distorted TBP, N1, N3 and O2 define the equatorial plane, with Cu 0.035 Å out of this plane in the direction of O1.

The room temperature magnetic moment of this compound is reported to be normal (1.82 B.M).[9] However, temperature dependent magnetic susceptibilities and EPR measurements have shown that antiferromagnetic interaction is present,[3] although to an appreciably smaller

extent than in the compounds referred to above.[6,8] Felthouse *et al.*[3] have discussed the difference in magnetic exchange mechanisms between dimers with TBP and SP geometry, where the oxalate-type bridge in both cases occupies one axial and one equatorial coordination site. The authors suggest the greatest antiferromagnetic interaction is likely to be found in TBP complexes, with a gradual decrease as the geometry is distorted towards SP. Comparing the present Et_5dien compound with two closely related compounds, $[Cu_2(Et_5dien)_2(C_2O_4)](BPh_4)_2$ and $[Cu_2(dien)_2(C_2O_4)](ClO_4)_2$,[3,15] for which structures as well as magnetic properties are known, we find indeed such a variation. $[Cu_2(Et_5dien)_2(C_2O_4)](BPh_4)_2$ has a geometry fairly close to TBP, and a magnetic exchange parameter of $J = -37.4$ cm^{-1}.[3]

$(Cu_2(dien)_2(C_2O_4)](ClO_4)_2$ approximates SP geometry,[15] and in this case the susceptibility shows no sign of exchange interaction down to 4.2 K ($|J| < \sim 0.5$ cm^{-1}).[3] The present Et_5dien compound with the described intermediate geometry has intermediate magnetic properties as well, $J = -9.6$ cm^{-1}.[3]

From the data referred to in the preceeding paragraphs it appears that the strongest antiferromagnetic interaction is found in the complexes with $d_{x^2-y^2}$ Cu(II) ion ground state (square planar, square pyramidal or elongted octahedral geometry) and the oxalate type bridging group occupying two equatorial sites. Somewhat weaker exchange interaction is present when there is a d_{z^2} Cu(II) ion ground state (TBP geometry) and oxalate is occupying one equatorial and one axial site. The weakest interaction is found in a $d_{x^2-y^2}$ ground state complex with oxalate in one equatorial and one axial site.

The oxalate ion. The bridging oxalato group is in each case planar within the experimental error, with Cu displaced 0.027 and 0.077 Å from the plane in the two compounds. In the Me_4en complex the oxalate occupies two equatorial sites while in the Et_5dien complex it occupies one equatorial and one axial site.

The C–C bond lengths are found within the

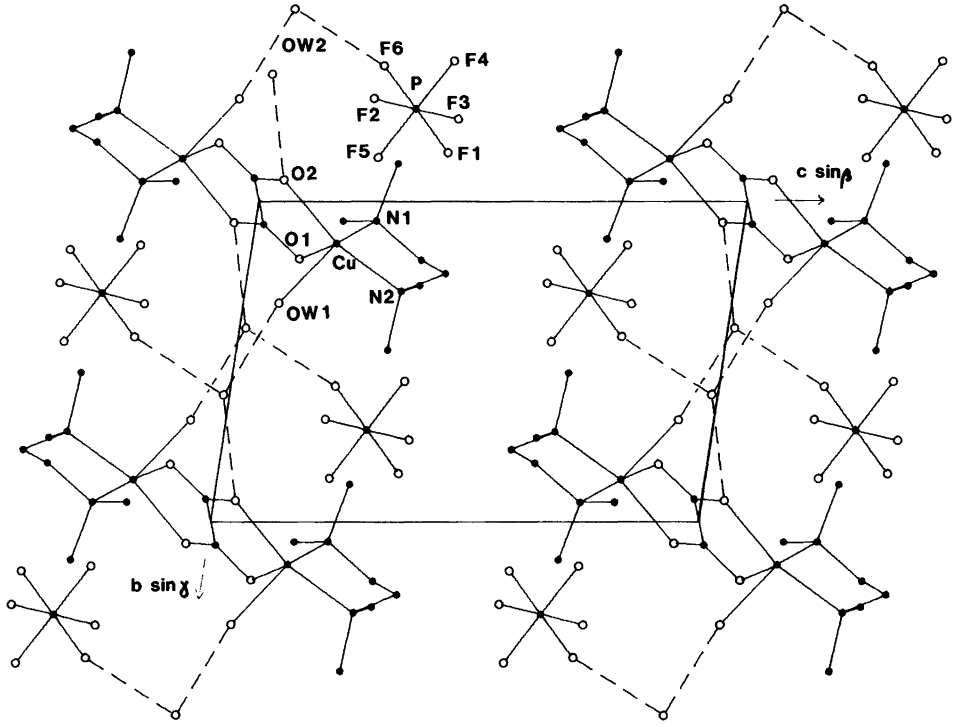

Fig. 3. Crystal packing of $[Cu_2(Me_4en)_2(C_2O_4)(H_2O)_2](PF_6)_2 \cdot 2H_2O$ as viewed down the *a*-axis. Hydrogen atoms are not drawn.

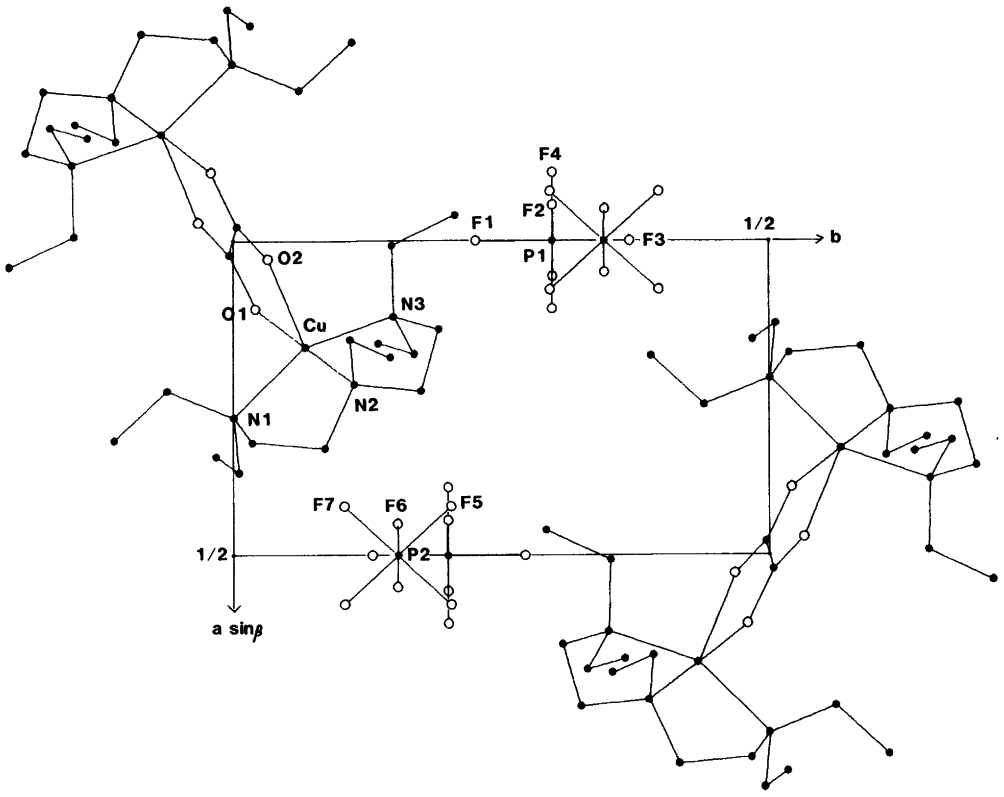

Fig. 4. Crystal packing of $[Cu_2(Et_5dien)_2(C_2O_4)](PF_6)_2$ as viewed down the *c*-axis. Hydrogen atoms are not drawn.

range normally observed for oxalic acid and oxalates (1.53–1.56 Å).[3,15,16] In the μ-oxamido complexes, on the other hand, the C–C bonds were observed to be slightly shorter than the corresponding bond in neutral oxamide.[11] In the Me_4en compound the two C–O bond lengths [1.249(9), 1.257(10) Å] are not significantly different. In the Et_5dien compound, on the other hand, there is a slight difference in C–O bond lengths [1.271(6), 1.241(7) Å] as well as in Cu–O–C angles [117.1(3), 108.9(3)°], reflecting the difference in coordination of the axial and equatorial oxygen atoms.

Phosphorhexafluoride ion. In both compounds the bond angles of the phosphorhexafluoride ions do not deviate significantly from the expected 90 and 180°. In the Me_4en compound where there is a short Cu···F5 contact as well as a hydrogen bond involving F6, the P – F bond lengths in the linear sequences F1 – P – F6 and F4 – P – F5 [1.609(6) – 1.615(6) Å] appear to be slightly different from those in the sequence F2 – P – F3 (1.585(5), 1.587(6) Å.) In the Et_5dien compound where there are no such short contacts to the fluorine atoms, the variation in P – F bond lengths of the two crystallographically independent PF_6-ions (each situated on a two-fold axis) is within the experimental error [1.587(5) – 1.603(5) Å].

Hydrogen bonding and molecular packing. In the Me_4en compound the presence of water molecules gives rise to a hydrogen bond network as depicted in Fig. 3. The coordinated water, OW1, participates in two hydrogen bonds to two water of crystallization molecules related by a centre of symmetry

$(OW1(HW11)\cdots OW2_{x+1,y+1,z}=2.842$ Å,

$OW1(HW12)\cdots OW2_{-x,-y,-z}=2.908$ Å).

The water of crystallization participates in four hydrogen bonds. In addition to the two already

mentioned, there is one hydrogen bond to F6 (OW2-(HW21)···F6=2.860 Å) and another one to O2 of the oxalate ion (OW2-(HW22)···$O2_{-x,-y-1,-z}$=2.925 Å). Only one of the hydrogen atoms on OW2 was unequivocally localized, the one pointing towards F6. However, from the remaining hydrogen bonding scheme it is clear that OW2 is a donor also in the OW2···O2 hydrogen bond. The hydrogen bonding laces the complex units together in a two dimensional network parallel to the *ab* plane, while there are no such connections parallel to *c*. This explains why the crystals easily fracture into thin platelets.

In the Et_5dien compound there is no hydrogen bonding, the structure shows discrete PF_6^- anions and dimeric cations, held together by ionic and van der Waals forces. A packing diagram is shown in Fig. 4.

Acknowledgements. Thanks are due to Professor M. Nonoyama for supplying samples of the compounds and to Professor H. Hope for placing X-ray equipment and computer facilities at my disposal during my sabbatical stay at the University of California, Davis.

REFERENCES

1. Hodgson, D. J. *Prog. Inorg. Chem. 19* (1975) 173.
2. Hatfield, W. E. *Theory and Application of Molecular Paramagnetism* E. A. Bourdeaux and L. N. Mulay, Ed., Wiley-Interscience, New York, N. Y., 1976 pp. 349–449.
3. Felthouse, T. R., Laskowski, E. J. and Hendrickson, D. N. *Inorg. Chem. 16* (1977) 1077.
4. Hay, P. J., Thibeault, J. C. and Hoffman, R. *J. Am. Chem. Soc. 97* (1975) 4884.
5. Pierpont, C. G., Francesconi, L. C. and Hendrickson, D. N. *Inorg. Chem. 16* (1977) 2367.
6. Michalowvicz, A., Girerd, J. J. and Goulon, J. *Inorg. Chem. 18* (1979) 3004.
7. Girerd, J. J., Kahn, O. and Verdaguer, M. *Inorg. Chem. 19* (1980) 274.
8. Girerd, J. J., Jeannin, S., Jeannin, Y. and Kahn, O. *Inorg. Chem. 17* (1978) 3034.
9. Nonoyama, K., Ojima, H., Ohki, K. and Nonoyama, M. *Inorg. Chim. Acta 41* (1980) 155.
10. Nonoyama, M. and Nonyama, K. *J. Inorg. Nucl. Chem. 43* (1981) 2567.
11. Sletten, J. *Acta Chem. Scand. A 36* (1982) 345.
12. *International Tables of X-Ray Crystallography,* Kynoch Press, Birmingham 1974, Vol. IV, pp. 55, 99, 149.
13. Sheldrick, G. M. (1981) *Nicolet SHELXTL Operations Manual.* Cupertino, Calif.: Nicolet XRD Corp.
14. Cavalca, L., Chiesi Villa, A., Gaetani Manfredotti, A., Mangia, A. and Thomlinson, A. A. G. *J. Chem. Soc. Dalton Trans.* (1972) 391.
15. Curtis, N. F., McCormick, I. R. N. and Waters, T. N. *J. Chem. Soc. Dalton Trans.* (1973) 1537.
16. Delaplane, R. G. and Ibers, J. A. *Acta Crystallogr. B 25* (1969) 2423.
17. Chauvel, C., Girerd, J. J., Jeannin, Y., Kahn, O. and Lavigne, G. *Inorg. Chem. 18* (1979) 3015.

Received November 26, 1982.

Acta Chemica Scandinavica A 37 (1983) 579–584

Chromium(III) Complexes of Macrocyclic Ligands. II. Preparation and Properties of Chromium(III) Complexes of *rac*-5,5,7,12,12,14-Hexamethyl-1,4,8,11-tetraazacyclotetradecane

J. ERIKSEN and O. MØNSTED

Department I. Inorganic Chemistry, H. C. Ørsted Institute, University of Copenhagen, Universitetsparken 5, DK-2100 Copenhagen Ø, Denmark

The reaction between anhydrous chromic chloride and the title amine, cyc*b*, in non-aqueous solvents gives green insoluble *cis*-[Cr(cyc*b*)Cl_2]Cl. This compound has been used as the starting material for a number of new *cis*-compounds all containing the Cr(cyc*b*)-moiety, and all apparently having an identical cyc*b*-ligand configuration. Visible absorption spectra and acid dissociation constants are given and are compared with and rationalized in relation to data for other more normally behaving *cis*-tetraaminechromium(III) systems.

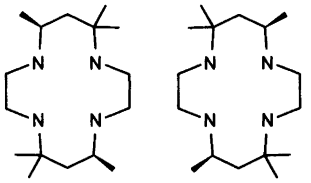

cyc *b*

Fig. 1. rac-5,5,7,12,12,14-Hexamethyl-1,4,8,11-tetraazaccyclotetradecane.

The title amine, Fig. 1, Table 1, is readily obtained by reduction of a condensation product between 1,2-ethanediamine and acetone.[1] This condensation reaction was first performed by dissolving tris(1,2-ethanediamine)nickel(II) salts in acetone[2,3] but is now more easily carried out without nickel(II), but at a suitable pH.[4] Many transition metal complexes of this amine have been studied, and the present work extends these studies to include the preparation of a number of new chromium(III) complexes, with the particular intention to further study the influences from non-reacting ligands on the kinetic behaviour of metal complexes.

Table 1. List of ligand name abbreviations.

cyc*a*	*meso*-5,5,7,12,12,14-hexamethyl-1,4,8,11-tetraazacyclotetradecane
cyc*b*	*rac*-5,5,7,12,12,14-hexamethyl-1,4,8,11-tetraazacyclotetradecane
cyclam	1,4,8,11-tetraazacyclotetradecane
H(acac)	2,4-pentanedione
H_2(mal)	malonic acid
H_2(ox)	oxalic acid
en	1,2-ethanediamine
trien	1,4,7,10-tetraazadecane

0302-4377/83 $2.50

RESULTS AND DISCUSSION

Solutions of anhydrous chromium(III) chloride react with cyc*b* to give an insoluble green product. This reaction, which is complete after about two hours in boiling *N*-methylformamide, is significantly slower than the similar reactions with a number of other amines, such as 1,2-ethanediamine, 1,3-propanediamine, and *trans*-1,2-cyclohexanediamine.[5] These latter reactions are all complete after 1 hour in *N,N*-dimethylformamide, DMF, or dimethylsulfoxide, DMSO, at 150 °C, whereas even after 8 hours in boiling DMF some unreacted cyc*b* and Cr(III) is still present. In DMSO, at temperatures near the boiling point where the complex formation reaction is fast, amine decomposition apparently takes place in competition with complexation, and dark brown solutions result. The same green insoluble material analyzing as 1 Cr(III): 1 cyc*b*: 3 Cl^- is obtained, however, in all three solvents. Further reactions of this material produce *cis*-tetraamine derivatives and the product is therefore most likely formulated as *cis*-$[Cr(cycb)Cl_2]Cl$, although a formulation as *fac*-$[Cr(cycb^*)Cl_3]$, with the amine bound as a tridentate ligand cannot immediately be excluded, and is in better agreement with both colour and solubility characteristics of other chromium(III) complexes.

The green compound can be treated with hot aqueous hydroxide without loss of coordinated amine, which is an unusual robustness for a chromium(III) amine complex. This produces a blue solution from which blue-violet *cis*-$[Cr(cycb)(OH)_2]ClO_4 \cdot 2H_2O$ can be precipitated. The cation of this compound has the structure shown in Fig. 2 [6], and in aqueous solution it behaves as a divalent base. From potentiometric titrations the acid dissociation

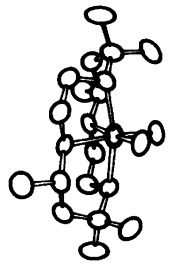

Fig. 2. Configuration of the *cis*-$[Cr(cycb)(OH)_2]^+$-cation, hydrogen atoms omitted, in *cis*-$[Cr(cycb)(OH)_2]ClO_4 \cdot 2\ H_2O$.[6]

constants have been determined, and in Table 2 it is seen that the *cis*-$[Cr(cycb)(OH_2)_2]^{3+}$ cation is a significantly stronger acid than a number of other *cis*-tetraaminediaquachromium(III) cations. This marked difference is most plausibly associated with differences in cation-solvent interactions as the differences in solvation energies as function of charge are probably smaller for the less hydrated complexes with the more organic amine ligands, which will make these types of complexes stronger acids.

The increased acidity of these types of complexes compared to more traditional ones, is also demonstrated by the *cis*-$[Cr(cycb)(mal)]^+$ cation, which in strongly basic solution shows the variation of visible absorption spectra exhibited in Fig. 3. In view of a greatly increased intensity of the second absorption band, this spectral change probably reflects the equilibrium shown on the Fig. Interpretation of the data using this model gives $K \sim 1.76 \pm 0.04$ M^{-1}, which using $K_w \sim 10^{-13.80}$ M^2 [8] yields the acidity constant $K_A \sim 10^{-13.55}$ M at 25 °C, which is unusually acid for a malonato ligand in aqueous solution.

The spectral characteristics of *cis*-$[Cr(cycb)(OH)_2]^+$ and its protonation products are

Table 2. Acid dissociation constants for some *cis*-tetraaminediaquachromium(III) complexes at 25.0 °C in 1.00 M sodium perchlorate solution.

Complex[a]	$-\log K_1$[b]	$-\log K_2$[b]
cis-$[Cr(NH_3)_4(OH_2)_2]^{3+}$	4.961±0.015	7.53±0.03
cis-$[Cr(en)_2(OH_2)_2]^{3+}$	4.75±0.03	7.35±0.05
cis-$[Cr(trien)(OH_2)_2]^{3+}$	4.47±0.03	7.14±0.05
cis-$[Cr(cyclam)(OH_2)_2]^{3+}$	4.212±0.013	7.25±0.03
cis-$[Cr(cycb)(OH_2)_2]^{3+}$	3.331±0.012	7.019±0.014

[a] Ref. 7 and this work. [b] The *K*'s are measured in mol l^{-1}.

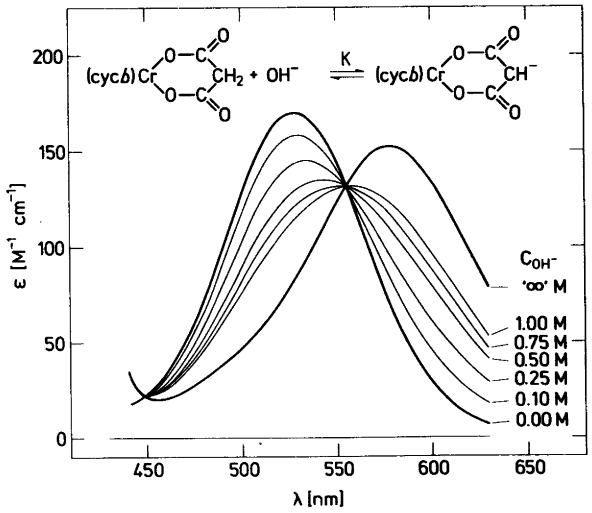

Fig. 3. Spectral changes of *cis*-[Cr(cyc*b*)(mal)]$^+$ in 1.00 M Na(ClO_4,OH). The absorption spectrum of the deprotonated species is calculated from the series of spectra given in the figure assuming the equilibrium shown.

summarized in Fig. 4 A. All three spectra are characterized by an increased intensity and a red-shift of the absorption bands compared to other *cis*-tetraaminechromium(III) complexes such as those of both ammonia and 1,2-ethanediamine, and also of the macrocyclic *cis*-(1,4,8,11-tetraazacyclotetradecane)chromium(III) derivatives, as shown in Fig. 4 B. Both these effects may qualitatively be accounted for with reference to Fig. 2 which shows a pronounced tetrahedral distortion of the CrN_2O_2-plane apparently induced by the two methyl groups above and below this plane.

In the experimental section results are given for a number of preparative experiments of the general type:

$$cis\text{-}[Cr(cyc\mathit{b})(OH)_2]^+ + yH_2c \rightarrow cis\text{-}[Cr(cyc\mathit{b})(c)_y]^{(3-yz)}$$

The preference for ligands which can be expected not to interact significantly with the methyl groups above and below the CrN_2O_2-plane should be noted. For coordinated ammonia and 1,2-ethanediamine, models indicate that hydrogen atoms of these ligands will point in directions towards these methyl groups, and it is therefore noteworthy that several attempts to coordinate these two ligands to the Cr(cyc*b*)-moiety were unsuccessful. For cobalt(III) a *cis*-

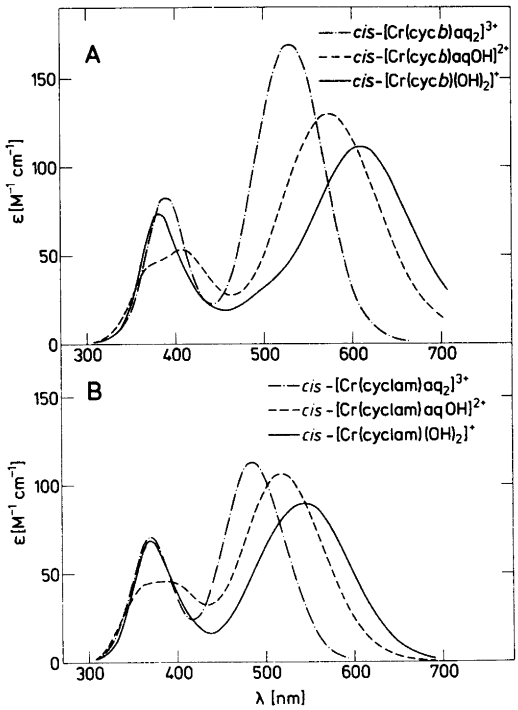

Fig. 4. Visible absorption spectra of diaqua-cyc*b*- and -cyclam-Cr(III) complexes and their deprotonation products. Further details of the solutions for the cyc*b* complexes are given in Table 3. The cyclam complexes are measured in 0.5 M $HClO_4$+0.5 M $NaClO_4$, 1 M NaCl with $\log[H^+] \sim \frac{1}{2}(\log K_1 + \log K_2)$ *cf.* Table 2, and 0.95 M NaCl+0.05 M NaOH, respectively.

$[Co(cyc\textit{b})(en)]^{3+}$ cation has been reported,[9] which is a manifestation of the differences between the cobalt(III)- and the chromium(III)-cyc*b* complexes, which is also apparent when the relatively easy transformation between a *trans* isomer and several *cis* isomers in the cobalt(III) system[10] is contrasted to the presence, so far at least, of only one geometric ligand arrangement in the Cr(cyc*b*)-moiety, as demonstrated both by the structural studies of the $[Cr(cyc\textit{b})(OH)_2]^+$- and $[Cr(cyc\textit{b})(O_2CO)]^+$-cations[6] and the inability so far to detect more than one isomer in any of the compounds from the preparative studies.

EXPERIMENTAL

Chemicals. *rac*-5,5,7,12,12,14-Hexamethyl-1,4,8,11-tetraazacyclotetradecane hydrate: cyc*b*·H_2O, was prepared and separated from the corresponding *meso*-isomer dihydrate: cyc*a*·$2H_2O$ according to a literature method.[4] *cis*-$[Cr(cyclam)Cl_2]Cl$ was prepared directly from $CrCl_3$ and cyclam by a modification of a literature method.[11] All other chemicals were commercial products.

Preparations. The following compounds were all made with kinetic and thermodynamic investigations in solution in mind. Whenever possible fairly soluble compounds were therefore made, and greater yields than reported can therefore normally be obtained by precipitation with other anions. For the 1+ cations the solubility decreases fairly regularly along the series: $Cl^- > Br^- > ClO_4^-$. This provides an opportunity for recovery of the *cis*-Cr(cyc*b*)-moiety even from fairly dilute solutions by precipitation of either *cis*-$[Cr(cyc\textit{b})Cl_2](ClO_4,Cl)$ in acid or *cis*-$[Cr(cyc\textit{b})(O_2CO)]ClO_4$ in base.

1. *cis*-$[Cr(cyc\textit{b})Cl_2]Cl$. 10 g $CrCl_3$ is warmed with about 10 mg Zn-powder in 50 ml *N*-methylformamide until it dissolves. 18 g cyc*b*, dried in vacuum over conc H_2SO_4, is added and the resulting solution refluxed for 2 h. During this treatment a bluish-green precipitate slowly forms. The resulting mixture is cooled in ice after which the precipitate is filtered off and washed twice with cold water * and then with ethanol. The yield is 25 g (89 %). Analyses: Cr, Cl, N, C, H.

2. *cis*-$[Cr(cyc\textit{b})(OH)_2]^+$-solution. 10 g *cis*-$[Cr(cyc\textit{b})Cl_2]Cl$, preparation no. 1, is dissolved in a solution of 4 g NaOH in 100 ml water at 100 °C. The resulting blue solution is cooled to room temperature and filtered to remove traces of undissolved material. This solution is the starting material for the following preparations.

3. *cis*-$[Cr(cyc\textit{b})(OH)_2]ClO_4 \cdot 2H_2O$. 20 ml saturated $NaClO_4$ (aq)-solution is slowly added to 100 ml *cis*-$[Cr(cyc\textit{b})(OH)_2]^+$-solution, preparation no. 2. The mixture is cooled in ice, and the bluish-black crystals are filtered off and washed quickly twice with ice-cold acetone in which it is somewhat soluble. Yield 10 g corresponding to 88 %. Analyses: Cr, Cl, N, C, H. This material is analytically pure but can be recrystallized by dissolving it in 250 ml 0.1 M NaOH(aq) at 80 °C and slowly adding 40 ml saturated $NaClO_4$(aq)-solution while cooling to 0 °C. Yield 6.0 g (53 %).

4. *cis*-$[Cr(cyc\textit{b})(OH_2)_2]Br_3 \cdot 2\frac{1}{2}H_2O$. 100 ml *cis*-$[Cr(cyc\textit{b})(OH)_2]^+$-solution, preparation no. 2, is cooled in ice and made strongly acid by the slow addition of 100 ml 63 % HBr(aq). The temperature should be kept below 10 °C. A reddish-violet precipitate is formed, and after standing at 0 °C for 30 min it is filtered off and washed twice with ice-cold acetone. The yield is about 12 g of impure material containing varying amounts of chloride ions. It is purified by dissolution in 80 ml 0.5 M NaOH(aq) solution at 80 °C and reprecipitating the bromide salt by the addition of 50 ml 63 % HBr(aq) in the cold, as described above. The yield of recrystallized material is about 10 g (65 %). Analyses: Cr, Br, (Cl), N, C, H.

5. *cis*-$[Cr(cyc\textit{b})(OH_2)Cl](ClO_4)_2 \cdot xaq\cdot y HClO_4$. 15 ml *cis*-$[Cr(cyc\textit{b})(OH)_2]^+$-solution, preparation no. 2, is acidified with 5 ml 70 % $HClO_4$(aq) at room temperature and left for some weeks. A violet precipitate is slowly formed. This is filtered off and washed twice with diethylether. Yield 2.5 g. This product is recrystallized by dissolving it in 65 ml 0.1 M HCl(aq), and reprecipitating the perchlorate by the slow addition of 8 ml saturated $NaClO_4$(aq) solution. Yield 1.25 g, which is 56 % based upon a formulation as *cis*-$[Cr(cyc\textit{b})(OH_2)Cl](ClO_4)_2 \cdot 0.4\ HClO_4 \cdot 3\ H_2O$ suggested by Cr, Cl, Cl^-, N, C, H analyses.

6. *cis*-$[Cr(cyc\textit{b})Cl_2]Cl \cdot H_2O$. 100 ml *cis*-$[Cr(cyc\textit{b})(OH)_2]^+$-solution, preparation nr. 2, is acidified with 100 ml concentrated HCl(aq), and the resulting solution boiled to precipitate the green chloride until the solution is almost colourless. This takes about 5 min. After cooling the mixture to room temperature the precipitate is filtered off and washed twice with cold water and

* cyc*a* is the most common impurity in cyc*b* preparations. The primary reaction products between the two amines: cyc*a* and cyc*b* and $CrCl_3$ have, however, such different solubilities in water that small amounts of soluble *trans*-$[Cr(cyc\textit{a})Cl_2]Cl$ are easily removed from insoluble *cis*-$[Cr(cyc\textit{b})Cl_2]Cl$ by washing the crude product with water.

then with ethanol. Yield 8.8 g (86 %). Analyses: Cr, Cl, N, C, H.

7. *cis*-[Cr(cyc*b*)F_2]ClO_4. 50 ml *cis*-[Cr(cyc*b*)$(OH)_2$]$^+$-solution, preparation no 2, is acidified with 40 % HF(aq). 4 g NaF is dissolved in this solution which is then kept at 80 °C for 10 min. A violet precipitate forms, and after cooling the mixture to room temperature it is filtered off and washed twice with cold acetone. Yield 3.6 g. More material is obtained by adding 3 ml saturated $NaClO_4$(aq) to the mother liquor. Yield 2.3 g. The two fractions were reprecipitated from the minimum amount of water at 80 °C by the slow addition of saturated $NaClO_4$(aq) solution. Yield 2.2 and 1.5 g, respectively, which is a total of 68 %. Analyses: Cr, Cl, N, C, H. The two fractions have identical analyses, visible absorption spectra in both acid and basic solution, and powder diffraction patterns, and are also, by the same criteria, identical to the compound which can be prepared in lower yield from *trans*-[Cr(py)$_4F_2$]ClO_4 and cyc*b* in *N*-methylformamide.

8. *cis*-[Cr(cyc*b*)O_2CO]Cl · H_2O. 5 g of solid NH_4Cl is dissolved in 100 ml *cis*-[Cr(cyc*b*)$(OH)_2$]$^+$-solution, preparation no. 2, which is then saturated with CO_2 at 0 °C. The red-violet precipitate is filtered off and washed twice with ethanol. Yield 8.0 g corresponding to 78 %. The compound is recrystallized by dissolving it in 120 ml water at 80 °C. This solution is saturated with CO_2 and then reduced in volume to about 20 ml by vacuum evaporation of solvent. Yield 6.0 g of recrystallized material (59 %). Analyses: Cr, Cl, N, C, H.

9. *cis*-[Cr(cyc*b*)(ox)]Cl · 2 H_2O. 50 ml *cis*-[Cr(cyc*b*)$(OH)_2$]$^+$-solution, preparation no. 2, is acidified with a solution of 10 g $(COOH)_2$ · 2 H_2O in 60 ml of water. The resulting solution is kept at 100 °C for 5 min and then cooled to 0 °C. The precipitate is filtered off and washed twice with acetone. Yield 8.2 g of crude material which contains excess oxalic acid. It is purified by dissolution in about 200 ml of water at 90 °C and precipitated by the slow addition of 50 ml saturated NaCl solution and cooling to 0 °C. Yield 4.1 g (74 %). Analyses: Cr, Cl, N, C, H.

10. *cis*-[Cr(cyc*b*)(mal)]ClO_4. 50 ml *cis*-[Cr(cyc*b*)$(OH)_2$]$^+$-solution, preparation no. 2, is acidified with a solution of 10 g malonic acid in 20 ml of water. 20 ml of a saturated $NaClO_4$(aq) solution is added, and the resulting mixture kept at 100 °C for 2 minutes and then cooled to 0 °C. The violet precipitate is filtered off and washed twice with acetone. Yield 4.5 g. The compound is recrystallized by extraction with 100 °C warm water on the filter, slow addition of 1/10 vol saturated $NaClO_4$(aq) solution and cooling to 0 °C. Yield 3.6 g (59 %). Analyses: Cr, Cl, N, C, H.

11. *cis*-[Cr(cyc*b*)(acac)]Br_2 · 3 H_2O. A mixture of 25 ml *cis*-[Cr(cyc*b*)$(OH)_2$]$^+$-solution, preparation no. 2, and 5 ml acetylacetone is left at room temperature overnight. The resulting solution is precipitated with 10 ml saturated NaBr(aq)-solution and cooled to 0 °C. The precipitate is filtered off and washed twice with acetone. Yield 2.1 g. The compound is recrystallized by dissolving it in 25 ml of water at 80 °C, and precipitated by the addition of 3 ml saturated NH_4Br-solution and cooling to 0 °C. Yield 1.6 g (43 %). Analyses: Cr, Br, N, C, H.

Analyses, spectra and potentiometric measurements. Microanalyses were performed by the analytical sections of the Chemistry Departments I and II of the Institute: I: Cr and II: C, H, N, Cl,

Table 3. Summary of spectral characteristics of some *cis*-cyc*b*-Cr(III) complexes in aqueous solution.

Complex	Medium	$\lambda_{1,max}$ [nm]	$\varepsilon_{1,max}$ [M^{-1} cm^{-1}]	$\lambda_{2,max}$ [nm]	$\varepsilon_{2,max}$ [M^{-1} cm^{-1}]
cis-[Cr(cyc*b*)$(OH)_2$]$^+$	1 M NaOH	609	111	380	73
cis-[Cr(cyc*b*)(OH)(OH_2)]$^{2+}$ [a]	~1 M NaCl	572	130	407	53
cis-[Cr(cyc*b*)$(OH_2)_2$]$^{3+}$	1 M $HClO_4$, 0.1 M $HClO_4$+0.9 M $NaClO_4$	529	169	388	82
cis-[Cr(cyc*b*)(OH_2)Cl]$^{2+}$	1 M HCl	554	173	405	105
cis-[Cr(cyc*b*)F_2]$^+$	1 M HCl, 1 M NaOH	541	145	379	58
cis-[Cr(cyc*b*)(O_2CO)]$^+$	0.1 M NaOH+0.9 M NaCl	521	145	382	106
cis-[Cr(cyc*b*)(ox)]$^+$	Water, 1 M NaOH	516	157	384	102
cis-[Cr(cyc*b*)(mal)]$^+$	1 M HCl, 0.01 M NaOH+0.99 M NaCl	527	167	387	82
cis-[Cr(cyc*b*)(acac)]$^{2+}$	1 M HCl, 1 M NaOH	535	161	390	256

[a] *cis*-[Cr(cyc*b*)$(OH)_2$]$^+$ solution titrated to $\log[H^+] \sim \frac{1}{2}(\log K_1 + \log K_2)$.

Br. Samples were further tested for impurities by acid-base titrations and cation exchange chromatography on Sephadex SP-C-25.

Visible absorption spectra were measured on a Cary 118 C spectrophotometer at room temperature (20–25 °C), *cf.* Table 3.

Potentiometric measurements and the processing of these measurements to give acid dissociation constants for the *cis*-$[Cr(cyclam)aq_2]^{3+}$ – and *cis*-$[Cr(cyc\textit{b})aq_2]^{3+}$-cations were performed as previously described.[7] *Cis*-$[Cr(cyc\textit{b})aq_2]^{3+}$-solutions were prepared by dissolving *cis*-$[Cr(cyc\textit{b})(OH)_2]ClO_4 \cdot 2\ H_2O$ in acid perchlorate solution. Solutions of *cis*-$[Cr(cyclam)aq_2]^{3+}$ were prepared as follows: 25 mg of recrystallized *cis*-$[Cr(cyclam)Cl_2]Cl$ was heated to boiling with 2 ml 0.25 M NaOH-solution. The resulting solution was cooled to room temperature and made slightly acid, pH~3, by the addition of perchloric acid. This solution was charged onto a 2×15 cm Sephadex SP–C–25 filled column, and the *cis*-$[Cr(cyclam)aq_2]^{3+}$-cation eluted by 1.0 M $NaClO_4$ or 1.0 M NaCl.

REFERENCES

1. Curtis, N. F. *J. Chem. Soc.* (1964) 2644.
2. Curtis, N. F. *J. Chem. Soc.* (1960) 4409.
3. Blight, M. and Curtis, N. F. *J. Chem. Soc.* (1962) 3016.
4. Hay, R. W., Lawrance, G. A. and Curtis, N. F. *J. Chem. Soc. Perkin Trans. I* (1975) 591.
5. Pedersen, E. *Acta Chem. Scand. 24* (1970) 3362.
6. Bang, E. and Mønsted, O. *Acta Chem. Scand. A. To be published.*
7. *Mønsted, L. and Mønsted, O. Acta Chem. Scand. A 30* (1976) 203.
8. Fischer, R. and Byé, J. *Bull. Soc. Chim. Fr.* (1964) 2920.
9. Whimp, P. O. and Curtis, N. F. *J. Chem. Soc. A* (1966) 1827.
10. Kane-Maguire, N. A. P., Endicott, J. F. and Rillema, D. P. *Inorg. Chim. Acta 6* (1972) 443 and references therein.
11. Ferguson, J. and Tobe, M. L. *Inorg. Chim. Acta 4* (1970) 109.

Received December 10, 1982.

Acta Chemica Scandinavica A 37 (1983) 585–593

Semiclassical Calculation of Activation Parameters for Elementary Steps in Catalytic Olefin Hydrogenation in Liquid Media

P. SØGAARD-ANDERSEN and J. ULSTRUP

Chemistry Department A, Building 207, The Technical University of Denmark, DK-2800 Lyngby, Denmark

We have applied general electron and atom group transfer theory to calculate activation energies and pre-exponential nuclear tunnelling factors for the oxidative addition and insertion steps in olefin hydrogenation catalyzed by low-valent rhodium complexes. Nuclear tunnelling is important for bond stretching in the hydrogen molecule, in Rh–H, and in C–C bonds, while other modes contribute fully to the activation energy. Explicit activation parameter expressions in terms of structural and thermodynamic properties of the complexes can be obtained when the nuclear motion is represented by harmonic potentials, and rate parameters calculated on the basis of available data are found to be similar for oxidative addition and insertion.

Calculation of activation energies for elementary steps (dissociation, addition, insertion *etc.*) in catalytic processes by quantum chemical methods, is presently attracting much attention.[1–13] Frequently, motion of a few molecular fragments is considered, while synchronous motion of other fragments and the solvent has to be disregarded. It is, however, necessary to provide a prescription for incorporating all molecular and solvent modes. In addition, attention should be given to nuclear tunnelling for the transfer of hydrogen atoms and other small groups. In this work we shall show how this can be achieved by means of recent theoretical formulations of electron and atom group transfer in condensed media.[14–17] More specifically, we shall calculate activation energies and nuclear tunnelling factors for representative models of elementary steps in the hydrogenation of olefins catalyzed by $RhClL_3$ (L=triphenylphosphine). This approach can be complemented by representing the molecular modes by nuclear potentials obtained by quantum chemical methods.

PROCEDURE FOR THE CALCULATION OF ACTIVATION PARAMETERS

We introduce potential energy surfaces for the initial (i) and final (f) states

$$U_i=U_i(\{Q_i\},\{q\});U_f=U_f(\{Q_f\},\{q\})+\Delta U_o \qquad (1)$$

where $\{Q_i\}$ and $\{Q_f\}$ are sets of intramolecular coordinates, $\{q\}$ the "collective" solvent coordinates, and ΔU_o the difference between the minima of the surfaces. In general $\{Q_f\}$ are related to $\{Q_i\}$ by a linear transformation, *i.e.*

$$Q_f^k=\sum_{j=1}^{N}\alpha_{kj}Q_i^j,$$

where the superscripts refer to components of $\{Q_i\}$ and $\{Q_f\}$, N is the number of molecular degrees of freedom, and $\{\alpha_{kj}\}$ a transformation matrix.[14,15] In most cases the solvent can be regarded as "linear". This implies that $\{q\}$ span harmonic potentials subject to equilibrium shifts only. All coordinates for most organic solvents at room temperature are furthermore classical,[18] as are most intramolecular modes, with stretching and deformation of bound hydrogen and C–C stretching as exceptions.

When the electron exchange integral between

0302-4377/83 $2.50

the zero order states is small the rate probability per unit time takes the form [15]

$$W = A \exp[-H(\theta^*;\{Q_i^*\},\{q^*\};\Delta U_o)] \approx$$
$$A \exp[-\sigma(\{Q_{iq}^*\})] \times$$
$$\exp[-U_i'(\{Q_{ic}^*\},\{Q_{iq}=0\},\{q^*\};\Delta U_o)/k_B T] \quad (2)$$

A is a constant which depends on the topology of the surfaces close to the intersection region and represents the activation entropy, k_B is Boltzmann's constant and T the absolute temperature. The strongest dependence on the structural and thermodynamic parameters is, however, reflected in the quantities σ and U_i^*. The activation energy U_i^* is the energy at the saddle point of the intersection between the "classical" parts of U_i and U_f, the coordinates of which, $\{Q_{ic}^*\}$ and $\{Q_{fc}^*\}$, are determined by the equations

$$(1-\theta^*)\frac{\partial U_i}{\partial Q_{ic}^j} + \theta^* \frac{\partial U_f}{\partial Q_{ic}^j} = 0 \quad (3)$$

$$U_i(\{Q_{ic}^*\},\{Q_{iq}=0\},\{q^*\}) =$$
$$U_f(\{Q_{fc}^*\},\{Q_{iq}=0\},\{q^*\}) + \Delta U_o \quad (4)$$

where θ^* is the transfer coefficient, $\theta^* = \partial U_i(\{Q_i^*\},\{q^*\})/\partial \Delta U_o$.

The high-frequency coordinates $\{Q_{iq}\}$ (the equilibrium values are taken as zero initially and as $\{Q_{fqo}\}$ in the final state) determine the temperature independent nuclear tunnelling factor $\sigma(\{Q_{iq}^*\})$. Although interconversion between high-frequency quantum and low-frequency classical modes can be handled generally, we use here the harmonic approximation which provides compact rate expressions and is at the same time a reasonable approximation for the modes in question here (*cf.*, however, section 5). For $\{Q_{iq}\}$ eqn. (3) must then be replaced by the following equation [15]

$$Q_{iq}^* \, th\,[\beta\hbar\Omega_\lambda(1-\theta^*)]/2 +$$
$$\sum_\rho \tau_{\rho\lambda}(Q_{pq}^{\rho*} - Q_{fqo}^\rho) th\,\beta\hbar\Omega_\rho\theta^*]/2 = 0 \quad (5)$$

where Q_{iq}^λ are the high-frequency coordinates in the initial state which are converted to the final state coordinates Q_{fq}^ρ by the transformation matrix $\{\tau_{\rho\lambda}\}$, Ω_λ *and* Ω_ρ are vibrational frequencies and $\hbar$ Planck's constant divided by 2π.

If the exchange integral is not small, the activation energy is given by the maximum of the lowest adiabatic surface.[14] For atom group transfer it can be expected that this modification is frequently necessary, but we shall disregard it in the present approach.

ELEMENTARY STEPS IN CATALYTIC HYDROGENATION

The sequence of steps in Scheme 1 has emerged from many investigations.[19,20]

Structural data are only available for the original catalyst molecule (i). A T-shaped structure for RhL_3^+, presumably similar to that of $RhClL_2$, has been reported,[21] and SCF calculations suggest that the two possible ligand arrangements in a T-shaped structure for $RhClL_2$ are about equally stable.[12a] NMR data suggest that the structure of (iii) is III in Fig. 1.[22,23] This is borne out by isolated complexes containing bulkier phosphine ligands[24,25] and by SCF calculations.[12a] Steps involving this intermediate could furthermore be solvent dependent due to the vacant coordination site. The existence of (iv)

(i) $RhClL_3$	$\rightarrow RhClL_2+L$	Dissociation	(6)
(ii) $RhClL_2+H_2$	$\rightarrow H_2RhClL_2$	Oxidative Addition	(7)
(iii) H_2RhClL_2+olefin	$\rightarrow H_2RhClL_2$(olefin)	Association	(8)
(iv) H_2RhClL_2(olefin)	$\rightarrow HRhClL_2$(alkyl)	Insertion	(9)
(v) $HRhClL_2$(alkyl)	$\rightarrow RhClL_2$+alkane	Reductive Elimination	(10)

Scheme 1.

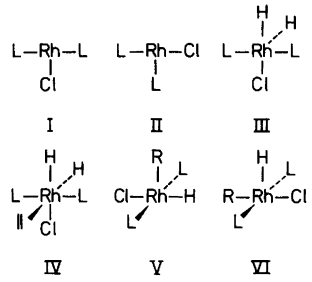

Fig. 1. Isomers of intermediates in $RhClL_3$-catalyzed olefin hydrogenation.

and (v) has been inferred from kinetic data. SCF calculations indicate that among isomers which originate from III with little molecular reorganization energy expenditure, IV is significantly more stable than other isomers.[12a] The most stable isomers of (v) are finally V and VI.[12] Formation of V from IV requires, however, far less intramolecular activation energy than conversion between other energetically accessible isomers. In the following we therefore restrict our considerations to I, III, IV and V.

ACTIVATION PARAMETER EXPRESSIONS

The rate determining step for $RhClL_3$-catalyzed hydrogenation of ethylene is believed to be insertion,[19,20] but either this step or oxidative addition could conceivably be rate determining for different olefins, catalysts or solvents. We therefore derive activation parameters for the four steps (6)–(9).

(A) Dissociation and association. The potential energy surfaces for dissociation are

$$U_i=v_i(Q_L)+\tfrac{1}{2}\sum_{j=1}^{N-1}M_j\Omega_j^2Q_j^2+\tfrac{1}{2}\sum_{\varkappa}\hbar\omega_\varkappa q_\varkappa^2 \qquad (11)$$

$$U_f=u_f(Q_L)+\tfrac{1}{2}\sum_{j=1}^{N-1}M_j\Omega_j^2(Q_j-Q_{jo})^2+ \tfrac{1}{2}\sum_{\varkappa}\hbar\omega_\varkappa(q_\varkappa-q_{\varkappa o})^2+\Delta U_o \qquad (12)$$

The first term represents the outgoing ligand, the second ones the other ligands, and the third terms the solvent, where q_κ and ω_κ are (dimensionless) coordinates and vibrational frequencies. Equilibrium values for all coordinates have been taken as zero initially, while the zero subscripts refer to the final state. The coordinates Q_j (taken as identical for U_i and U_f) are represented by the harmonic approximation in view of their small shifts. M_j are effective masses, and the vibrational frequencies Ω_j are related to the actual frequencies in the initial and final states, $\Omega_j^{(i)}$ and $\Omega_j^{(f)}$, by the equation

$$\Omega_j=2\Omega_j^{(i)}\Omega_j^{(f)}/(\Omega_j^{(i)}+\Omega_j^{(f)}).$$

Q_L represents initially a bound state. In the final state L is weakly bound in a solvent cage. As a consequence $\partial v_i/\partial Q_L>>\partial u_f/\partial Q_L$, and provided that θ^* is not close to zero or unity, eqn. (3) shows that Q_L^* practically coincides with the initial equilibrium value of Q_L.[26,27] Eqn. (4) then gives

$$\theta^*=\tfrac{1}{2}+\frac{\Delta U_o+E_{rL}^f}{2(E_s+E_r)};$$

$$E_A=(E_s+E_r+E_{rL}^f+\Delta U_o)^2/4(E_s+E_r) \qquad (13)$$

where we have introduced reorganization energies for the solvent, $E_s=\frac{1}{2}\sum_{\varkappa}\hbar\omega_\varkappa q^2{}_{\varkappa o}$, the molecular modes, $E_r=\frac{1}{2}\sum_{j=1}^{N-1}M_j\Omega_j^2Q_{jo}^2$, and the outgoing ligand, $E_{rL}^f=u_f(Q_L=O)$.

A similar calculation gives for association[26,27]

$$\theta^*=\tfrac{1}{2}+\frac{\Delta U_o-E_{rc}^i}{2(E_s+E_r)};$$

$$E_A=(E_s+E_r+\Delta U_o-E_{rc}^i)^2/4(E_s+E_r) \qquad (14)$$

where $E_{rC}^i=v_i(Q_L=Q_{LO})$ is the reorganization energy for the incoming substrate molecule.

(B) Oxidative addition. We represent the solvent and non-hydride ligands as above. However, the state of the hydrogen atoms for *cis*-addition – which we consider here – changes drastically. Initially there are three hindered translational and two hindered rotational degrees of freedom largely involving H_2, and one stretching mode of this molecule. In the final state these

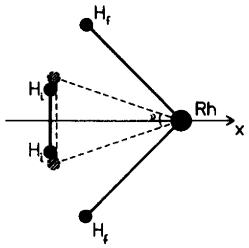

Fig. 2. Oxidative addition. The fully drawn lines indicate the equilibrium configuration of the H_2 molecule at the transition configuration for the coordinate x, and the equilibrium configuration of the dihydrido complex. The hydrogen atoms in these two states are characterized by the subscripts i (initial) and f (final), respectively. The filled circles show the positions of the hydrogen and rhodium atoms. In the transition configuration, shown by the dashed lines, the H_2 bond is less distorted than the H−Rh−H bending mode.

modes are converted to a symmetric and an asymmetric stretching, a bending mode of the H−Rh−H unit and three orientational modes of the complex. Secondly, H_2 stretching is a high-frequency quantum mode,[14–17] while other initial state modes are classical. In the final state Rh−H stretchings are of quantum nature, the bending mode in the intermediate range, while the orientational modes are classical. *cis*-Addition of H_2 thus involves both "mixing" and "interconversion" of quantum and classical modes.

We consider approach of H_2 to $RhClL_2$ in a plane perpendicular to the L−Rh−L axis. The orientation shown in Fig. 2 requires the smallest reorganization, but different configurations could be suitably averaged. In this figure the chlorine ligand is thus in *trans* position with respect to one of the hydride ligands H_f, and the Rh−L bonds perpendicular to the plane shown. We then only need to consider the following simplified potential energy expression for the initial state

$$U_i=\tfrac{1}{2}(2M_H)\Omega_x^2Q_x^2+\tfrac{1}{2}(\tfrac{1}{2}M_H)\Omega_i^{s2}Q_i^{s2}+\tfrac{1}{2}\sum_{j=1}^{N'}M_j\Omega_j^2Q_j^2+\tfrac{1}{2}\sum_{\varkappa}\hbar\omega_\varkappa q_\varkappa^2 \quad (15)$$

The first term represents hindered translation of H_2 along the x axis, the second one stretching of H_2, the Ω's are vibrational frequencies, and M_H the mass of a hydrogen atom. The potential energy of the final state is

$$U_f=\tfrac{1}{2}(2M_H)\Omega_f^{s2}(Q_f^s-Q_{fo}^s)^2+\tfrac{1}{2}(2M_H)\Omega_f^{b2}(Q_f^b-Q_{fo}^b)^2+\tfrac{1}{2}\sum_{j=1}^{N'}M_j\Omega_j^2(Q_j-Q_{jo})^2+\tfrac{1}{2}\sum_{\varkappa}\hbar\omega_\varkappa(q_\varkappa-q_{\varkappa o})^2+\Delta U_o \quad (16)$$

where the first two terms now refer to symmetric stretching (s) and bending (b). The relation between the "mixed" coordinates is

$$\begin{Bmatrix} Q_f^s \\ Q_f^b \end{Bmatrix} = \begin{Bmatrix} \tfrac{1}{2}\sin\nu & -(1+\cos\nu) \\ (1+\cos\nu) & \sin\nu \end{Bmatrix} \begin{Bmatrix} Q_i^s \\ Q_x \end{Bmatrix} \quad (17)$$

where ν is the angle of the H−Rh−H unit close to the transition configuration.

Eqns. (3)−(5) and (15)−(17) give the following coordinates for the transition configuration

$$q_\varkappa^*=\theta^* q_{\varkappa o};\quad Q_j^*=\theta^* Q_{jo} \quad (18)$$

$$Q_j^{s*}\approx Q_{io}^s-Q_{io}^s\Big/\left[1+(1+\cos\nu)^2(\Omega_f^b\Omega_f^s/\Omega_i^{s2})^{1/2}\mathrm{th}\,\frac{\beta\hbar\Omega_f^b\theta^*}{2}\right] \quad (19)$$

$$Q_x^*-Q_{xo}\approx \tfrac{1}{2}[\sin\nu/(1+\cos\nu)][1-(\Omega_f^b/\Omega_f^s)th\beta\hbar\Omega_f^b\theta^*/2]\times(Q_i^{s*}-Q_{io}^s) \quad (20)$$

$$Q_f^{b*}-Q_{fo}^b\approx(1+\cos\nu)(Q_i^{s*}-Q_{io}^s) \quad (21)$$

$$Q_f^{s*}-Q_{fo}^s\approx\tfrac{1}{2}\sin\nu(\Omega_f^b/\Omega_f^s)\mathrm{th}\,\frac{\beta\hbar\Omega_f^b\theta^*}{2}\,(Q_i^{s*}-Q_{io}^s) \quad (22)$$

where Q_{xo} and Q_{io}^s are the equilibrium values of Q_x and Q_i^s in the final state (we have here ignored $\sin^2\nu$ compared with $(1+\cos\nu)^2$ close to the saddle point where Q_f^b is significantly distorted). These equations suggest the following sequence of events. The classical modes, *i.e.* those of the solvent, the Rh−Cl and Rh−L modes, and x are

first reorganized to the configuration given by eqns. (18) and (20), providing most of the activation energy. This is followed by H_2 bond stretch by nuclear tunnelling to the configuration given by eqn. (19). For reported or suggested frequency values[22-25] ($\Omega_f^b \approx 600-1000$ cm^{-1}, $\Omega_f^s \approx 2000$ cm^{-1} and $\Omega_i^s \approx 4000$ cm^{-1}) and $\theta^* \approx 0.1-0.3$ (*cf.* the concluding section) it amounts to 15–30 % of the total shift of Q_i^s. Subsequent to changes of the electronic structure the dihydrido complex is formed, with instantaneous Q_f^s and Q_f^b values given by eqns. (21) and (22). Q_f^b is much more vibrationally excited than Q_f^s which is shifted by nuclear tunnelling to its vibrational ground level.

The exponent H in eqn. (3) is now found by solving the following equation with respect to θ^*

$$(2\theta^*-1)(E_s+E_r)+\tfrac{1}{2}(2M_H)\Omega_x^2 Q_x^{*2}= \tfrac{1}{2}(2M_H)\Omega_f^{b2}(Q_f^{b*}-Q_{fo}^b)ch^{-2}(\beta \mathrm{th}\Omega_f^b\theta^*/2)+\Delta U_o \quad (23)$$

where the explicit dependence of Q_x^* and Q_f^{b*} on θ^* is given by eqns. (20) and (21). This equation can be handled numerically, and the resulting θ^* inserted in eqns. (1) and (3) to give the activation energy and tunnelling factor. Analytical expressions can, however, be obtained in the following two limiting cases:

(1) For $\beta\hbar\Omega_f^b\theta^*/2 >> 1$, corresponding to a high bending frequency. The activation energy and the nuclear tunnelling factor are then

$$E_A = E_{rh}^x+(E_s+E_r+\Delta U_o-E_{rh}^x)^2/4(E_s+E_r) \quad (24)$$

$$\sigma \approx \tfrac{1}{2}(M_H/\hbar)(1+\cos\nu)^2\times \frac{4(\Omega_f^b/\Omega_f^s)+(\Omega_f^b/\Omega_i^s)(1+\cos\nu)^2}{[1+(1+\cos\nu)^2(\Omega_q^b\Omega_f^s/\Omega_i^{s2})^{1/2}]^2}\, Q_{io}^s \quad (25)$$

where E_{rh}^x is the reorganization energy for H_2 motion along the coordinate x, from its initial equilibrium position to the position given by eqn. (20) with th($\beta\hbar\Omega_f^b\theta^*/2$) replaced by unity.

(2) In the opposite limit $\beta\hbar\Omega_f^b\theta^*/2 << 1$. The tunnelling factor now vanishes, while E_A is

$$E_A = (E_s+E_r+E_r^b+\Delta U_o-E_{rl}^x)^2/4(E_s+E_r) \quad (26)$$

E_r^b is the energy required to distort Q_f^b – at fixed Q_f^s identical to its final equilibrium value – from final state equilibrium to the value which corresponds to a distance between the two hydrogen atoms identical to the equilibrium bond length of the H_2 molecule. E_{rl}^x is the energy required to bring an H_2 molecule from its initial equilibrium location, along x, to the position which corresponds to such a deformation of Q_f^b.

(C) Insertion. This step is viewed as planar motion of coordinated ethylene and a *cis*-located hydride ligand (Fig. 3). We again only include coordinates subject to equilibrium shifts. The initial state potential energy is then

$$U_i = \tfrac{1}{2}M_{et}\Omega_{is}^{et2}Q_s^{et2}+\tfrac{1}{2}\mu_{et}\Omega_{is}^{cc2}Q_{is}^{cc2}+ \tfrac{1}{2}M_{et}\Omega_b^{et2}Q_b^{et2}+\tfrac{1}{2}\mu_{et}^i\Omega_{ib}^{cc2}Q_{ib}^{cc2}+ \tfrac{1}{2}M_H\Omega_{is}^{H2}Q_{is}^{H2}+\tfrac{1}{2}M_H\Omega_{ib}^{H2}Q_{ib}^{H2}+ \tfrac{1}{2}\sum_{j=i}^{N'}M_j\Omega_j^2Q_j^2+\tfrac{1}{2}\sum_x\hbar\omega_x q_x^2 \quad (27)$$

The first two terms represent stretching and bending (the angle β in Fig. 3) of the bond between Rh and the mass centre of ethylene (with Ω's referring to vibrational frequencies and M's and μ's to masses or reduced masses), the third term stretching of the olefin C–C bond, and the fourth bending of ethylene around the angle χ. The fifth and sixth terms refer to stretching and bending of the Rh–H bond, and the last two terms have the same meaning as before. All modes except C–C stretching and those involving the Rh–H bond can furthermore be regarded as classical.

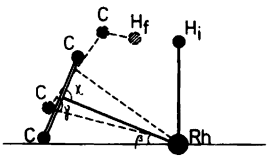

Fig. 3. Insertion. The fully drawn lines show the initial state equilibrium configuration of coordinated ethylene and hydrogen (H_i). The dashed line shows the transition configuration formed by motion along the angle β and providing the shortest possible distance for hydrogen atom transfer. The position of the hydrogen atom after transfer is also indicated (H_f). This distance would be shortened by compression of the Rh-ethylene bond and twisting around the angle χ.

The potential energy surface for the final state is

$$U_f=\tfrac{1}{2}M_{et}\Omega_{fs}^{et2}(Q_s^{et}-Q_{so}^{et})^2+\tfrac{1}{2}M_{et}\Omega_{fb}^{et2}(Q_b^{et}-Q_{bo}^{et})^2+$$

$$\tfrac{1}{2}\mu_{et}\Omega_{fs}^{cc2}(Q_s^{cc}-Q_{so}^{cc})^2+\tfrac{1}{2}\mu_{et}^{f}\Omega_{fb}^{cc2}(Q_{fb}^{cc}-Q_{fbo}^{cc})^2+$$

$$\tfrac{1}{2}M_u\Omega_{fb}^{H2}(Q_{is}^{H}-Q_{iso}^{H})^2+\tfrac{1}{2}M_H\Omega_{fs}^{H2}(Q_{ib}^{H}-Q_{ibo}^{H})^2+$$

$$\tfrac{1}{2}\sum_{j=1}^{N'}M_j\Omega_j^2(Q_j-Q_{jo})^2+\tfrac{1}{2}\sum_{\varkappa}\hbar\omega_{\varkappa}(q_{\varkappa}-q_{\varkappa o})^2+\Delta U_o \quad (28)$$

Stretching and bending of the bond between Rh and the mass centre of coordinated alkyl, and C–C stretching (the first three terms in eqn. (28) are given by the same coordinates as for the initial state. The hydride ligand is converted to a bound state at the β-carbon atom. The transition configuration favours an orientation where this motion is conversion of Rh–H bending to C–H stretching and of Rh–H stretching to C–H bending (the fifth and sixth terms). This path could be generalized to incorporate the remaining hydrogen atoms at carbon. The hybridization change thus causes equilibrium change in the C–H bending modes in the plane, but this is of minor importance compared with reorganization in other parts of the molecule. The fourth term refers to bending of the Rh–C–C unit (the angle γ). For small fluctuations this coordinate is "proportional" to Q_{ib}^{cc} (bending at the angle χ), so that the coordinate change essentially involves equilibrium and frequency shift.

All classical saddle point coordinates are then given by equations of the same kind as eqn. (18). The following equation is valid for high-frequency C–C stretching

$$Q_s^{cc*}+(\Omega_{fs}^{cc}/\Omega_{is}^{cc})^{1/2}(Q_s^{cc*}-Q_{so}^{cc})=0 \quad (29)$$

where we have put $Q_{ib}^{cc}=Q_{fb}^{cc}=Q_b^{cc}$. The effect of this mode is thus reflected solely in the tunnelling factor. The equilibrium geometries of the Rh–C–C framework in the initial and final states corresponds to widely separated positions of the hydrogen atom which is transferred. The hydrogen atom transfer path therefore depends explicitly on the instantaneous position of the Rh–C–C unit. In view of the expected low vibrational frequency of the bending mode of this unit and the high frequencies of the modes involving bound hydrogen, it is a good approximation to regard the coordinates for hydrogen atom transfer as referring to the intermediate configuration for the rest of the molecule, as determined by the effects of repulsive interactions between strongly distorted Rh–C–C and weakly distorted Rh–H bonds. Improvement of this point would require that we introduce the explicit dependence of the hydrogen transfer probability on the transfer distance and the parameters of a repulsive potential. The saddle point coordinates for the Rh–H are now

$$Q_{is}^{H*}+(\Omega_{fb}^{H}/\Omega_{is}^{H})^{1/2}(Q_{is}^{H*}-Q_{iso}^{H})=0 \quad (30)$$

$$Q_{ib}^{H*}\,\mathrm{th}\frac{\beta\hbar\Omega_{ib}^{H}\theta^*}{2}+(\Omega_{fs}^{H}/\Omega_{ib}^{H})^{1/2}(Q_{ib}^{H*}-Q_{ibo}^{H})=0 \quad (31)$$

Q_{ib}^{H} furthermore coincides approximately with Q_{ibo}^{H} ($\beta\hbar\Omega_{ib}^{H}\theta^*/2\approx 0.3-0.4$, *cf.* the following section). The activation energy and tunnelling factor are then

$$E_A\approx(E_s+E_r+E_{r,st}^{et}+E_{r,b}^{et}+E_{r,b}^{cc}+\Delta U_o-E_{r,b}^{H})^2/$$
$$4(E_s+E_r+E_{r,st}^{et}+E_{r,b}^{cc}) \quad (32)$$

$$\sigma\approx\sigma_s^{cc}+\sigma_s^{H} \quad (33)$$

where $E_{r,st}^{et}$, $E_{r,b}^{et}$, $E_{r,b}^{cc}$ and $E_{r,b}^{H}$ are the reorganization energies for stretching and bending of the Rh–C–C unit, for C–C bending, and for Rh–H bending, respectively, and σ_s^{cc} and σ_s^{H} the tunnelling contributions from C–C and Rh–H stretching, *i.e.*

$$\sigma_s^{cc}\approx(\mu_{et}/\hbar)\Omega_{is}^{cc}\Omega_{fs}^{cc}/(\Omega_{is}^{cc}+\Omega_{fs}^{cc})Q_{so}^{cc2} \quad (34)$$

$$\sigma_s^{H}\approx(M_H/\hbar)[\Omega_{is}^{H}\Omega_{fb}^{H}/(\Omega_{is}^{H}+\Omega_{fb}^{H})]Q_{iso}^{H2} \quad (35)$$

CONCLUDING REMARKS

We have provided rate parameter expressions for several steps in catalytic olefin hydrogenation, in terms of rate theory for chemical processes in liquid solutions.[14–17] This approach is general in the sense that it incorporates all nuclear modes including those of the solvent. It also accounts for both thermal activation and nuclear tunnelling, and for the effects of high- and low-frequency mode "mixing" and "interconversion".

In addition to the geometric restrictions inherent in the planar motion shown – which could obviously be relaxed – our most important

simplifying assumptions are firstly that we have ignored the electron exchange integral and determined the many-dimensional barrier for nuclear motion as the saddle point between two zero order potential energy surfaces, and secondly, application of the harmonic approximation for "mixing" and "interconversion". With these assumptions, rather compact and transparent expressions for the activation energy and nuclear tunnelling factors can be derived. However, the major conclusions are not affected, and numerical treatment of the procedure can be provided if rather general molecular potentials, including potentials calculated by quantum chemical methods, are used. For example, the nuclear wave functions of the high-frequency modes can be combined with the electron exchange integral in an adiabatic approach with respect to separation between low-frequency modes on one hand and the combined electronic and high-frequency nuclear system on the other.[28] Also, the transition configuration coincides with the equilibrium configuration for the high-frequency state for general molecular potentials, when a particular nuclear mode is converted from a high-frequency to a low-frequency state or *vice versa*.

The high- and low-frequency modes for the insertion step are separated in the approach which we have taken. From reported experimental values of the activation energy in the range 7–18 kcal[29–31] for insertion of cyclohexene and SCF calculations of $\Delta U_o = -17$ kcal for the step represented by eqn. (9)[12b] values of both θ^* and the combined reorganization energy terms can be calculated by means of eqn. (32). We can here disregard the contribution from the Rh–H bending mode which is small for the insertion step. The resulting values are thus $\theta^* \approx 0.2-0.3$ corresponding to 50–100 kcal for the combined reorganization energy.

The tunnelling factors are about 10^{-3} for C–C stretching and $10^{-3}-10^{-2}$ for hydrogen atom transfer in insertion. These values were obtained from eqns. (34) and (35). Stretching frequencies of 1600 cm^{-1} and 1100 cm^{-1} for C–C double and single bonds, respectively, and a bond length difference of 0.16 Å were taken for the former while 600 cm^{-1} and 3000 cm^{-1}, and a transfer distance of 0.7 Å (Fig. 3), were taken for the hydrogen atom. The tunnelling probability for the hydrogen atom may be decreased at the expense of additional activation energy expenditure by compression and twisting of the Rh-ethylene unit. The fairly exothermic nature of the process also implies that kinetic deuterium isotope effects are not necessarily large even though tunnelling distances for hydrogen atoms are significant.[32,33]

The activation energy for bending of coordinated ethylene is finally calculated to be 25–30 kcal if we use a bending frequency of 200 cm^{-1} representative of metal–ligand bending modes with a ligand mass corresponding to that of ethylene, and the bending angle is 25° (Fig. 3 and Ref. 12b). Anharmonic effects are, however, undoubtedly important here due to very high vibrational excitation. The activation energy could thus be lowered by more than 10 kcal by using for example a squared hyperbolic tangent potential[32] (the Morse-Rosen potential[34]) and brought close to experimental values[29,31] and the value of 15–18 kcal which emerges from SCF calculations.[12b]

Extraction of rate parameters is less straightforward for oxidative addition due to the "mixing" of the nuclear modes and the nature of Rh–H bending as intermediate between the classical and quantum limits. This mode is thus thermally excited to a certain vibrational level from which further distortion occurs by tunnelling. In order to specify as few of the inaccessible structural parameters as possible, estimates were made in the following way. Q_i^{s*} was calculated for different values of θ^* by means of eqn. (19). This also provides a value of Q_f^{b*} from eqn. (21), and upper limits for the right hand side of eqn. (23). Ω_f^b was also here taken to be 600 cm^{-1}, the Rh–H bond length 1.65 Å,[12b] and $-\Delta U_o > 13$ kcal. When the right hand side of eqn. (23) is compared with the left hand side for values of the reorganization energy terms in the range 5–15, kcal, ignoring here the small value of the term which represents the mode Q_x, it is found that $\theta^* \approx 0.2-0.3$ are upper limits for solutions of eqn. (23). Larger values are thus only found for unrealistically large values of $E_s + E_r$.

This value of θ^* gives an upper limit of 1.15 Å for the H_2 bond length in the intermediate state corresponding to about 25 % of the total change of this bond length when going from from the initial to the final state (Fig. 2). Using a vibrational frequency of 4000 cm^{-1} the tunnelling factor for H_2 stretching is found to be $10^{-3}-0.1$, while the activation energy for Rh–H bending is

10–15 kcal if the bending frequency is again 600 cm^{-1} and the Rh–H bond length 1.65 Å. The activation energy value would be lowered by 1–4 kcal if we used an anharmonic potential such as the squared hyperbolic tangent potential.[32]

Eqns. (13), (24) and (32)–(35) finally provide indications as to the rate determining step of the overall reaction. In spite of the somewhat endothermic nature of the dissociation step ($\Delta U_o > 5-6$ kcal[19]) this step represents rapid pre-equilibrium, largely because of low reorganization energies for the solvent and intramolecular modes. Both oxidative addition and insertion are accompanied by large restructuration, but in different nuclear parts, while differences in the solvent contributions are likely to be less important in view of the apolar nature of the reaction media and the small charge redistribution in the reacting complexes. Furthermore, since E_r and ΔU_o are also similar, the difference between the activation parameters must be contributed largely by H_2 stretching and Rh–H bending in oxidative addition, and by Rh-ethylene-ethyl bending and C–C stretching in insertion.

When we insert the activation energies and nuclear tunnelling factors estimated, in the rate expressions, it appears that the insertion step is rate determining primarily due to the large activation energy for bending of the coordinated olefin. The dominance of this particular mode to the activation energy of the insertion step also emerges from quantum chemical calculations of the energy changes which accompany the motion of the different molecular fragments in this step.[12b] The total rate difference between insertion and oxidative addition originating from the calculated activation energies and tunnelling factors seems, however, to be small enough that the latter step could be rate determining for other related systems.

REFERENCES

1. Sakaki, S., Kato, H., Hanai, H. and Tamara, K. *Bull. Chem. Soc. Japan. 48* (1975) 813.
2. Novaro, O., Chow, S. and Magnonat, P. *J. Catal. 41* (1976) 91.
3. Grima, J. P., Choplin, F. and Kaufmann, G. *J. Organomet. Chem. 129* (1977) 221.
4. Lauher, J. W. and Hoffmann, R. *J. Am. Chem. Soc. 98* (1976) 1729.
5. Fonnesbech, N., Hjortkjær, J. and Johansen, H. *Int. J. Quant. Chem. 12 Suppl. 2* (1977) 95.
6. Novaro, O., Blaisten-Barojas, E., Clementi, E., Giunchi, S. and Ruiz-Vizcaya, M. E. *J. Chem. Phys. 68* (1978) 2337.
7. Thorn, D. L. and Hoffmann, R. *J. Am. Chem. Soc. 100* (1978) 2079.
8. Cassoux, P., Crasnier, F. and Labarre, J. F. *J. Organomet. Chem. 165* (1979) 303.
9. McKinney, D. J. and Pensak, D. A. *Inorg. Chem. 18* (1979) 3413.
10. Dedieu, A. and Strich, A. *Inorg. Chem. 18* (1979) 2940.
11. McKinney, D. J. *J. Chem. Soc. Chem. Commun.* (1980) 490.
12. a. Dedieu, A. *Inorg. Chem. 19* (1980) 375; b. *20* (1981) 2803.
13. Johansen, H. *Chem. Phys. Lett. 84* (1981) 580.
14. Dogonadze, R. R. and Urushadze, Z. D. *J. Electroanal. Chem. 32* (1971) 235.
15. a. Dogonadze, R. R., Kuznetsov, A. M. and Vorotyntsev, M. A. *Phys. Status Solidi B 54* (1972) 125; b. *54* (1972) 425.
16. Dogonadze, R. R. and Kuznetsov, A. M. *Prog. Surf. Sci. 5* (1975) 1.
17. Ulstrup, J. *Charge Transfer Processes in Condensed Media, Lecture Notes in Chemistry,* Springer, Berlin 1979, Vol. 10.
18. Ulstrup, J., *In preparation.*
19. Henrici-Olivé, G. and Olivé, S. *Coordination and Catalysis,* Verlag Chem., New York 1977.
20. James, B. R. *Adv. Organomet. Chem. 17* (1979) 319.
21. Yared, Y. W., Miles, S. L., Bau, R. and Reed, C. A. *J. Am. Chem. Soc. 99* (1977) 7076.
22. Meakin, P., Jesson, J. P. and Tolman, C. A. *J. Am. Chem. Soc. 94* (1972) 3240.
23. Tolman, C. A., Meakin, P. Z., Lindner, D. L. and Jesson, J. P. *J. Am. Chem. Soc. 96* (1974) 2762.
24. Masters, C. and Shaw, B. L. *J. Chem. Soc. A* (1971) 3679.
25. Van Gaal, H. L. M., Verlaak, J. M. J. and Posno, T. *Inorg. Chim. Acta 23* (1977) 43.
26. German, E. D. and Dogonadze, R. R. *J. Res. Inst. Catal. Hokkaido Univ. 20* (1972) 34.
27. German, E. D. and Dogonadze, R. R. *Int. J. Chem. Kinet. 6* (1974) 457.
28. Vorotyntsev, M. A., Dogonadze, R. R. and Kuznetsov, A. M. *Dokl. Akad. Nauk SSSR Ser. Fiz. Khim. 209* (1973) 1135.

29. Osborn, J. A., Jardine, F. H., Young, J. F. and Wilkinson, G. *J. Chem. Soc. A* (1966) 1711.
30. Demortier, Y. and de Aguirre, I. *Bull. Soc. Chim. Fr.* (1974) 1673.
31. Rousseau, C., Evrard, M. and Petit, F. *J. Mol. Catal. 3* (1977) 309.
32. Brüniche-Olsen, N. and Ulstrup, J. *J. Chem. Soc. Faraday Trans. 1, 75* (1979) 205.
33. German, E. D. and Kuznetsov, A. M. *J. Chem. Soc. Faraday Trans. 2, 77* (1981) 397.
34. Rosen, N. and Morse, P. *Phys. Rev. 42* (1932) 210.

Received December 9, 1982.

Acta Chemica Scandinavica A 37 (1983) 595–599

The Molecular Structures of Trimethylarsenic, Trimethylantimony and Dimethyltellurium Determined by Gas Electron Diffraction

RICHARD BLOM, ARNE HAALAND and RAGNHILD SEIP

Department of Chemistry, University of Oslo, Blindern, Oslo 3, Norway

The molecular structures of trimethylarsenic, trimethylantimony and dimethyltellurium have been determined by gas electron diffraction. The bond distances (r_a) are As–C=1.968(3) Å, Sb–C=2.163(3) Å, and Te–C=2.142(5) Å, the valence angles ∠CAsC=96.1(5)°, ∠CSbC= 94.1(5)° and ∠CTeC=94(2)°.

While making a survey of bond distances and valence angles in simple methyl derivatives of main group elements,[1] $El(CH_3)_k$, we discovered that accurate values were missing for $As(CH_3)_3$, $Sb(CH_3)_3$ and $Te(CH_3)_2$. The present study was undertaken in order to close the gap.

EXPERIMENTAL

Reagent grade $As(CH_3)_3$ (Strem Chemicals) and $Sb(CH_3)_3$ and $Te(CH_3)_2$ (Alpha/Ventron) were used without further purification.

The scattering patterns were recorded on Balzers Eldigraph KDG-2 with nozzle temperatures of about 20 °C and nozzle-to-plate distances of 50 and 25 cm. For the structure determination of $As(CH_3)_3$ we used six plates from each set, for $Sb(CH_3)_3$ we used six 50 cm and eleven 25 cm plates, and for $Te(CH_3)_2$ we used five 50 cm and four 25 cm plates. The scattering data were processed by standard procedures. The molecular intensity curves obtained for each nozzle-to-plate distance were averaged, but not connected. The curves extended from s=2.00 to 14.00 Å^{-1} with increment Δs=0.125 Å^{-1} (50 cm) and from s=4.00 to 28.00 Å^{-1} with increment Δs=0.250 Å^{-1}.

The complex atomic scattering factors of Sb were obtained by interpolation of tabulated values.[2] The scattering factors of As, Te, C and H were calculated from the atomic potentials[3] by the partial wave method.[4]

STRUCTURE ANALYSIS

Structure refinements of $As(CH_3)_3$ and $Sb(CH_3)_3$ were based on models of C_{3v} symmetry, structure refinement of $Te(CH_3)_2$ on a model of C_{2v} symmetry. The methyl groups in each molecule were assumed to have C_{3v} symmetry with the threefold axes coinciding with the El-C bonds. Finally, the orientation of the methyl groups was assumed to be staggered with respect to the bond(s) radiating from the heteroatom. See Figs. 1, 2 and 3. The structure of each molecule is then determined by four parameters; the bond distances El-C and C–H and the valence angles ∠CElC and ∠ElCH.

Simple valence force fields were adjusted to reproduce the normal modes of vibrations assigned for the three molecules,[5] and root-mean-square vibrational amplitudes, l, and the vibrational correction coefficients $D=r_\alpha-r_a$ calculated at T=293 K using a program written by Hilderbrandt.[6] The values obtained (Table 1) were similar to those reported by Beagley and Medwid.[5]

The molecular structures were refined under the constraints of geometrically consistent r_a structures by least squares calculations on the molecular intensities with non-diagonal weight matrices.[7] Those vibrational amplitudes which

0302-4377/83 $2.50

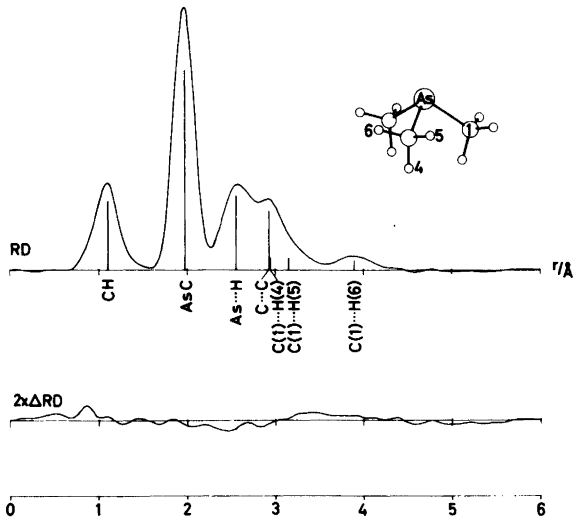

Fig. 1. Above: Experimental radial distribution curve for $As(CH_3)_3$. Artificial damping constant $k=0.003$ Å^2. Major interatomic distances are indicated by bars of height proportional to the *area* under the corresponding peak. *Below:* Difference between experimental curve and the theoretical curve calculated for the best model.

could not be refined were fixed at their calculated values. The refinements converged to yield the parameter values listed in Table 1. The estimated standard deviations have been expanded to include scale uncertainty of 0.1 %.

Experimental radial distribution (RD) curves calculated by Fourier inversion of experimental modified molecular intensity curves, are shown in Figs. 1, 2 and 3 along with the difference between the experimental RD curves and their theoretical counterparts calculated for the best model.

Table 1 shows that the structure of $Te(CH_3)_2$ has been determined with lower accuracy than expected from studies of this kind. We feel that

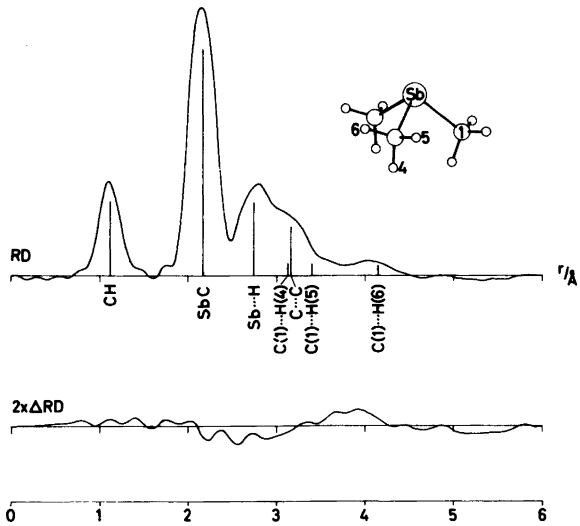

Fig. 2. Experimental radial distribution curve for $Sb(CH_3)_3$. $k=0.002$ Å^2.

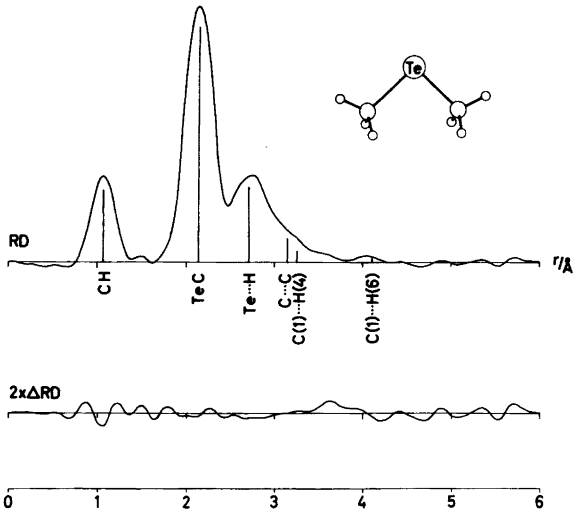

Fig. 3. Experimental radial distribution curve for $Te(CH_3)_2$. k=0.003 Å^2.

Table 1. Internuclear distances (r_a), valence angles, and root mean square vibrational amplitudes (l) of $As(CH_3)_3$, $Sb(CH_3)_3$ and $Te(CH_3)_2$ obtained by least squares refinement on gas electron diffraction (GED) data. Estimated standard deviations in parentheses in units of the last digit. Root mean square vibrational amplitudes and vibrational correction terms ($D=r_a-r_a$) calculated from a molecular force field (FF).

	r_a (Å)	l (Å) (GED)	l (Å) (FF)	D (Å) (FF)
$As(CH_3)_3$				
As–C	1.968(3)	0.062(3)	0.050	−0.0012
C–H	1.100(6)	0.080(6)	0.078	−0.0316
As···H	2.54	0.119(6)	0.118	−0.0111
C···C	2.92	0.100(8)	0.103	0.0018
$C_1\cdots H_4$	2.93	(0.204)	0.204	0.0022
$C_1\cdots H_5$	3.15	0.22(7)	0.208	0.0034
$C_1\cdots H_6$	3.89	0.14(3)	0.126	−0.0061
∠CAsC(°)	96.1(5)			
∠AsCH(°)	109.0(6)			
$Sb(CH_3)_3$				
Sb–C	2.163(3)	0.051(1)	0.053	−0.0017
C–H	1.113(6)	0.080(6)	0.078	−0.0363
Sb···H	2.74	0.122(9)	0.122	−0.0126
C···C	3.16	0.13(1)	0.117	0.0022
$C_1\cdots H_4$	3.15	(0.226)	0.226	0.0031
$C_1\cdots H_5$	3.40	(0.227)	0.227	0.0038
$C_1\cdots H_6$	4.15	0.16(3)	0.138	−0.0067
∠CSbC(°)	94.1(5)			
∠SbCH(°)	110.1(8)			
$Te(CH_3)_2$				
Te–C	2.142(5)	0.06(2)	0.055	−0.0003
C–H	1.07(2)	0.07(2)	0.078	−0.0388
Te···H	2.71	(0.119)	0.119	−0.0121
C···C	3.14	(0.114)	0.114	0.0035
C···H	3.25	(0.229)	0.229	0.0055
C···H	4.10	(0.131)	0.131	−0.0055
∠CTeC(°)	94(2)			
∠TeCH(°)	112(2)			

the poor result is due to a combination of several effects; the background of atomic scattering is high, the beat-out corresponding to $\Delta\eta_{TeC}=\pi/2$ occurs somewhat below $s=20$ Å^{-1}, and the multiplicity of the C–C distance is unity as compared to three in $Sb(CH_3)_3$. The refinement of the latter was based on eleven 25 cm plates, the refinement of $Te(CH_3)_2$ on four. It would clearly have been advantageous to include a larger number of 25 cm plates for $Te(CH_3)_2$, but when this became clear, we had already destroyed the sample.

RESULTS AND DISCUSSION

The structure parameters of $As(CH_3)_3$, $Sb(CH_3)_3$ and $Te(CH_3)_2$ are listed in Table 1. The results for $As(CH_3)_3$ are in agreement with an early gas electron diffraction study which yielded R(As–C)=1.98(2) Å and ∠CAsC=95(5)°.[8] Later, Lide determined the principal moment of inertia, which together with an assumed value for ∠CAsC=96°, gave R(As–C)=1.96(1) Å.[9] We are not aware of any previous gas phase studies of $Sb(CH_3)_3$ or $Te(CH_3)_2$.

We have already made use of the results of the present study when discussing period and group variations of main-group-element-to-carbon, -hydrogen and -chlorine bond distances in homoleptic compounds $El(CH_3)_k$, ElH_k and $ElCl_k$.[1] It was then noted that the bonding radius of a fourth period element between Cd and I appears to be 0.19±0.01 Å greater than the third period element in the same group. The El–C bond distances reported here conform to the rule; R(Sb–C) $-R$(As–C)=0.195(4) Å; combination with the published Se–C bond distance in $Se(CH_3)_2$[10] gives R(Te–C)$-R$(Se–C)= 0.202(6) Å.

In our discussion of the periodic variation of El–C bond distances, we limited ourselves to trivalent compounds of group VB elements and divalent compounds of group VI B elements. In Table 2 we compare the bond distances in triorganyl-derivatives of P, As and Sb with equatorial and axial bond distances in corresponding pentaorganyl-derivatives with trigonal bipyramid structure: It is seen that the equatorial bond distances in the pentavalent compounds are very similar to the bond distances in the trivalent compounds, while the axial bonds are 0.10 to 0.15 Å longer. The bond distances, therefore, are in good agreement with the view that the equatorial bonds may be regarded as normal single bonds while the $C_{ax}ElC_{ax}$-fragment is held together by a three-center, four electron bond.[23]

Very recently Titus, Zialo and co-workers have reported the crystal and molecular structure of the first tetraorganyl Te(IV) compound, tetraphenyltellurium 1/8 benzene.[24] The structure is that of a distorted trigonal bipyramid with an electron pair occupying an equatorial site. The mean equatorial Te–C bond distance, 2.13(0) Å, is indistinguishable from the bond distance in $Te(CH_3)_2$, while the mean Te–C_{ax} bond distance is 2.29(1) Å.

Table 2. El-C bond distances in homoleptic compounds of type ElR_3 and equatorial and axial bond distances in ElR_5 compounds of trigonal bipyramid symmetry.[a] El=P, As and Sb.

Compound	R (Å)	Ref.	Compound	R_{eq} (Å)/R_{ax} (Å)	Ref.
$P(CH_3)_3$	1.85	11			
PPh_3	1.83	12	PPh_5	1.85/1.99	18
$PMes_3$	1.84	13			
$As(CH_3)_3$	1.97				
$AsPh_3$	1.96	14	$AsPh_5$[b]	1.96/2.11	19
$AsTol_3$	1.95	15			
$Sb(CH_3)_3$	2.16		$Sb(CH_3)_5$	2.15/2.25	20
$SbTol_3$	2.14	16	$SbPh_5$	2.13/2.25	21
$SbXyl_3$	2.19	17	$SbTol_5$	2.16/2.26	22

[a] Ph = phenyl, Tol=*p*-tolyl, Xyl = 2,6-dimethylphenyl, Mes = mesityl. [b] Crystallized with 0.5 mol cyclohexane.

Acknowledgements. We are grateful to the Norwegian Research Council for Science and the Humanities (NAVF) for financial support and to Dr. Chr. Römming and Dr. Tor G. Strand for permission to quote unpublished results.

REFERENCES

1. Haaland, A. *J. Mol. Struct. 97* (1983) 115.
2. Bonham, R. A. and Schäfer, L. *International Tables for X-Ray Crystallography,* Kynoch Press, Birmingham 1974, Vol. 4.
3. As and C; Strand, T. G. and Bonham, R. A. *J. Chem. Phys. 47* (1967) 2599; Te; Liberman, D., Wader, J. T. and Cramer, D. T. *Phys. Rev. A 140* (1965) 1133; H; Steward, R. F., Davidson, E. R. and Simpson, W. T. *J. Chem. Phys. 42* (1965) 3175.
4. Yates, A. C., *Comput. Phys. Commun. 2* (1971) 175.
5. $As(CH_3)_3$; Park, P. J. D. and Hendra, P. J. *Spectrochim. Acta A 24* (1968) 2081; Rojhantalab, H. and Nibler, J. W. *Ibid. A 32* (1976) 947. $Sb(CH_3)_3$; Siebert, H. *Z. Anorg. Allg. Chem. 273* (1953) 16. $Te(CH_3)_2$; A Ulcius, J. R. and Hendra, P. J. *Spectrochim. Acta 22* (1966) 2075. Normal coordinate calculations on $As(CH_3)_3$ and $Sb(CH_3)_3$; Beagley, B. and Medwid, A. R. *J. Mol. Struct. 38* (1977) 229.
6. Hilderbrandt, R. L. and Wieser, J. D. *J. Chem. Phys. 55* (1971) 4648.
7. Seip, H. M., Strand, T. G. and Stølevik, R. *Chem. Phys. Lett. 3* (1969) 617; Gundersen, G. *Annual Report of the Norwegian Electron Diffraction Group,* Oslo 1977.
8. Spingall, H. D. and Brockway, L. O. *J. Am. Chem. Soc. 60* (1938) 996.
9. Lide, D. R. *Spectrochim. Acta 15* (1959) 473.
10. Beecher, J. F. *J. Mol. Spectrosc. 21* (1966) 414.
11. Bryan, P. S. and Kuczkowski, R. L. *J. Chem. Phys. 55* (1971) 3049 L; Bartell, L. S. and Brockway, L. O. *Ibid. 32* (1960) 512.
12. Daly, J. J. *J. Chem. Soc.* (1964) 3799.
13. Blount, J. F., Maryanoff, C. A. and Mislow, K. *Tetrahedron Lett. 11* (1975) 913.
14. Römming, C. and Songstad, J. *Unpublished result*; Sobolev, A. N., Belsky, V. K., Chernikova, N. Yu. and Akhmadulina, F. Yu. *J. Organomet. Chem. 244* (1983) 129.
15. Sobolev, A. N. and Belsky, V. K. *J. Organomet. Chem. 214* (1981) 41.
16. Sobolev, A. N., Romm, I. P., Belsky, V. K. and Buryanova, E. N. *J. Organomet. Chem. 179* (1979) 153.
17. Sobolev, A. N., Romm, I. P., Belsky, V. K., Syutkina, O. P. and Guryanova, E. N. *J. Organomet. Chem. 209* (1981) 49.
18. Wheatley, P. J. *J. Chem. Soc.* (1964) 2206.
19. Brock, C. P. and Webster, D. F. *Acta Crystallogr. B 32* (1976) 2089.
20. Strand, T. G. *Preliminary results.*
21. Brabant, C., Blanck, B. and Beauchamp, A. L. *J. Organomet. Chem. 82* (1974) 231.
22. Brabant, C., Hubert, J. and Beauchamp, A. L. *Can. J. Chem. 51* (1973) 2952.
23. Keil, F. and Kutzelnigg, W. *J. Am. Chem. Soc. 97* (1975) 3623; Kutzelnigg, W., Wallmeier, H. and Wasilowski, J. *Theor. Chim. Acta 51* (1979) 261.
24. Smith, C. S., Lee, J. S., Titus, D. D. and Ziolo, R. F. *Organometallics 1* (1982) 350.

Received December 10, 1982.

Acta Chemica Scandinavica A 37 (1983) 601–607

Preliminary Structure and Force Field of 4-Fluoro-benzonitrile from Microwave, Raman and Infrared Spectra

BØRGE BAK, DANIEL HØJGAARD CHRISTENSEN, NIELS ARNT KRISTIANSEN, FLEMMING NICOLAISEN and OLE FAURSKOV NIELSEN

Chemical Laboratory V, University of Copenhagen, The H. C. Ørsted Institute, 5, Universitetsparken, DK-2100 Copenhagen Ø, Denmark

Microwave spectra of vapours from solid 4-fluoro-benzonitrile (I), C_7H_4FN, are reported for the 18.6–39.0 GHz region and analyzed in terms of rotational and distortion constants and inertial defect $I_c-I_b-I_a$ of the ground state. Rotational constants and inertial defects for the 2 lowest vibrationally excited levels were found and analyzed. Since it is well established that the perturbing effects of one substituent such as F and CN on the benzene ring geometry is small, we present a model of I found by joining fluorobenzene and benzonitrile moities to fit with the experimentally established rotational constants. This model would seem to represent the most rational starting structure for obtaining an *ab initio* geometry-optimized model of I. Earlier vibrational assignments are confirmed from infrared gas spectra (3240–50 cm^{-1}) and Raman (liq.) spectra (50 °C) now including depolarization measurements. A quadratic force field has been constructed and used with confidence to calculate inertial defects for I and its vibrationally excited states, thus establishing an unambiguous assignment between a particular microwave spectrum and a vibrational level.

Determination of molecular structure, dynamics, dipole moment etc. are now increasingly being taken over by computers.[1] Complementary use of experimental and computer techniques is, however, still of current interest. As an example this paper wants, in the first place, to derive a 'first order' (incomplete) model of 4-fluoro-benzonitrile (I), or 1-cyano-4-fluorobenzene (Fig. 1), simply by joining moieties of fluorobenzene[2] and benzonitrile[3] (Fig. 2). An acceptable model should agree with the experimental rotational constants B and C of I while possessing an 'aromatic' $d\sim1.39-1.41$ Å. The text of Fig. 2 states this to be possible. A *para* substituted benzene such as I was chosen for its conceivable non-overlap domain C4, C6, C10 and C12 (Fig. 1), un-parallelled in *ortho* and *meta* derivatives. In the second place, a 'first-order' force field of I was obtained by the combined use of the preliminary model and of force constants for benzene, obtained *ab initio*,[1] and conventionally derived constants for fluorobenzene[4] and benzonitrile.[5] A complete harmonic force field for I contains 158 constants as compared to

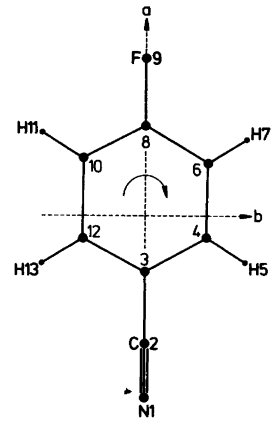

Fig. 1. Numbering of atoms in planar 4-fluoro-benzonitrile (point group C_{2v}) as applied in Fig. 2 and in Tables 6 and 7. Principal axes *a,b* (and *c*, not shown).

0302-4377/83 $2.50

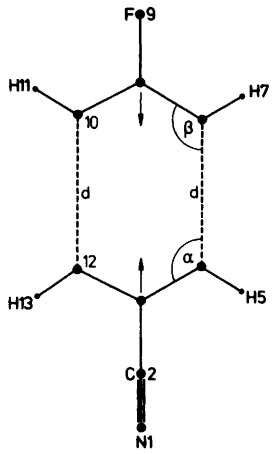

Fig. 2. Joining a fluorobenzene moiety (upper part) with a supplementary benzonitrile moiety (bottom part) to 4-fluoro-benzonitrile of C_{2v} symmetry varying the distance d. Agreement with the experimental rotational constants B and C of 4-fluoro-benzonitrile occurred for d=1.401 Å. α=119.3° and β=118.1°.

its 33 normal vibration frequencies, ν_i. Thus, information from other sources such as benzene are quite necessary. Adaption of the initially assumed iterative field to the normal vibration frequencies, ν_i, of I produced the desired 'first-order' field. By using this force field inertial defects, $I_c-I_b-I_a$, for I in its ground state and in a number of vibrationally excited states could be calculated, three of them being compared to experimentally obtained defects. This linked the structural and dynamic aspects presented.

In the absence of economic restrictions a rather accurate, complete structure and force field of I could simply have been computed. The resulting molecular model would, however, not produce rotational constants (A,B,C) comparable in precision to experimental values (Table 1).

SAMPLE

Commercial I (Fluka, purity > 98 %) was used throughout, its m.p.=32–34 °C and its IR spectrum being as published.[6] Its equilibrium vapor pressure, vp_{eq}, is 0.65 and 0.20 Torr at 25 and 0 °C, respectively (LKB Autovac). If I was kept at liquid nitrogene temperature for 2–3 h. followed by spontaneous heating to room temperature, a higher vp was observed, slowly decreasing to 0.65 Torr at 25 °C. Possibly, more than one crystalline form of I exist.

MICROWAVE SPECTRA. ASSIGNMENTS. DIPOLE MOMENT.

Microwave (mw) spectra of I have not yet been reported. They were recorded in a 'flow' system

Table 1. Calculated (ROTFIT [8]) ground state rotational constants A,B,C, (MHz) and distortion constants (τ_{aaaa} etc.) in kHz of 4-fluoro-benzonitrile from 65 experimental $J_{K_{-1}K_{+1}}\rightarrow J_{K_{-1}K_{+1}+1}$ ($9\leq J\leq 22$) microwave transitions between 18.4 and 40 GHz.[a] RMS deviation 0.031(3) MHz. Asymmetry parameter κ= –0.94028(3). Inertial defect [b] $I_c-I_b-I_a$=0.016(2) μÅ^2. Identification frequencies (MHz), ANALYT.

A		B	C	
5627.638(59)		972.39469(120)	829.10806(86)	
τ_{aaaa}	τ_{bbbb}	τ_{cccc}	τ_{abab}	τ_{caca}
–1.000(fixed)	–0.0810(90)	–0.0406(31)	–0.5272(18)	0
–4.755[c]	–0.0896[c]	–0.0428[c]	–0.6543[c]	0

ANALYT

Transition	Experimental	Exp-Calc.
$10_{2,8}\rightarrow 11_{2,9}$	20317.38(20)	0.001
$14_{2,12}\rightarrow 15_{2,13}$	27941.74(20)	−0.005
$17_{2,15}\rightarrow 18_{2,16}$	33571.76(20)	0.130
$20_{2,19}\rightarrow 21_{2,20}$	37078.13(20)	−0.026

[a] Available on request. [b] Conversion factor 505376 uÅ^2. Inertial defect from vibrational spectra, 0.028uÅ^2. [c] From vibrational spectra.

described earlier,[7] at cell temperatures 25° and pressure p=30 mTorr, and at *ca.* −60 °C (p=3−5 mTorr). The results obtained by pumping I(gas) through a conventional Stark modulated cell are reported in Table 1. 65 ground state transitions were measured of which only 4 prominent lines are included for identification purposes. The numerically small inertial defect shows I to be planar as expected. In addition, the observed intensity alternation, 5:3 for K_{-1} even: odd, agreed with spin exchange of two pairs of equivalent protons about a C_2 axis. Thus, I has at least C_{2v} symmetry.

The microwave spectra of I at 25 °C had rather intense patterns of vibrational satellites, due to low-energy vibrational states (Table 2) and to a large dipole moment. Experimental dipole moments of gaseous fluorobenzene and benzonitrile are 1.59 and 4.39 D, respectively.[9] A predicted dipole moment of I would be 2.80 D. The conveniently located transition $10_{2,8} \rightarrow 11_{2,9}$ (Table 1) showed 5 distinct Stark lobes towards lower frequencies not coinciding with the satellite pattern concerned at higher than 20318 MHz. For M=0,1,2,3,4 the shifts were −2.57, −4.06, −9.14, −17.28 and −28.78 MHz fitting with a dipole moment of 2.88±0.05 D (program STARK[8]). The measurements were taken at −60°, p=3−5 mTorr and at 2924 V cm^{-1} electric field intensity.

Based partly on an assignment of normal vibration frequencies of I (*vide infra*), Table 2 predicts relative mw spectral intensities and inertial defects of I in its ground state and in 9 moderately populated vibrationally excited levels, thus suggesting the working strategy to be applied. For each 'K_{-1} even' mw transition (Table 2, Int[c]) the ground state line is easy to distinguish even at room temperature (see Table I, ANALYT) whereas the satellites are much harder to assign. To identify 'K_{-1} odd' ground state transitions, cooling of the mw cell is necessary (Table 2, Int[d]). Hereafter, Table 1 resulted. The 'K_{-1} odd' transitions for molecules in the level at 104 cm^{-1} could subsequently be identified at 25° because of their high intensity. This produced rotational constants permitting calculation of 'K_{-1} even' transitions and subsequent experimental location. The experimental $I_c - I_b - I_a$ of −1.66(3) uÅ^2 is in satisfactory agreement with −1.59 uÅ^2 from vibrational data (Table 3). The mw spectrum of I in the level at 152 cm^{-1} was analyzed correspondingly (Table 3). The rotational constants of vibrationally excited levels are less accurate than for the ground level, partly due to Stark lobe perturbances. The analyses for further satellite spectra will be postponed.

VIBRATIONAL SPECTRA. NORMAL VIBRATION FREQUENCIES.

Raman and IR spectra of dissolved I have been published earlier and analyzed in terms of 33

Table 2. Energies (cm^{-1}) of the lowest vibrational levels of 4-fluorobenzonitrile from IR and Raman spectra, E; normal vibration numbers as in ref. 6, i; sum levels, Sums; 'Boltzmann' population at 300K, Boltz; C_{2v} vibrational species a_1(e), b_2(o), a_2(e), b_1(o), even-odd referring to C_2,[a,b] Species; spin weight factors for K_{-1} even or odd, $S(e)$ and $S(o)$; relative intensities, Int; calculated inertial defects, i.d. in uÅ^2.

E	i	Sums	Boltz	Species[b]	$S(e)$	Int[c]	$S(o)$	Int[d]	i.d.
0			1.00	a_1(e)	5	1.00	3	0.60	+0.028
104	22		0.59	b_1(o)	3	0.35	5	0.58	−1.59
152	33		0.47	b_2(o)	3	0.28	5	0.47	+1.49
208		2×22	0.35	a_1(e)	5	0.35	3	0.21	−3.21
256		22+33	0.28	a_2(e)	5	0.28	3	0.17	−0.13
265	21		0.26	b_1(o)	3	0.16	5	0.27	−0.48
304		2×33	0.22	a_1(e)	5	0.22	3	0.13	+2.95
312		3×22	0.21	b_1(o)	3	0.13	5	0.22	−4.83
360		2×22+33	0.17	b_2(o)	3	0.10	5	0.17	−1.75
369		21+22	0.15	a_1(e)	5	0.15	3	0.09	−2.10

[a] Axis of minimum moment of inertia. [b] Capital letters, A_1, B_2, A_2, B_1 used in most literature. [c] 'K_{-1} even' transitions. [d] 'K_{-1} odd' transitions.

Table 3. Calculated (ROTFIT [8]) rotational constants A,B,C (MHz) for the two lowest vibrational levels at 104 and 152 cm^{-1}, respectively, of 4-fluoro-benzonitrile based on 39 and 43 experimental microwave transitions; vibrational levels in cm^{-1}, Levels; rms deviations, r.m.s.; experimental inertial defects, i.d., in u$Å^2$.

Levels	A	B	C	r.m.s.	i.d.[a]
104	5545.0(1.1)	973.203(17)	830.153(14)	0.4575(563)	−1.66(3)
152	5705.5(1.2)	973.570(17)	829.629(14)	0.4680(544)	+1.49(3)

[a] Calculated from force field −1.59 and +1.49 u$Å^2$, respectively.

Table 4. Distribution of 4-fluoro-benzonitrile normal vibrations ν_i on C_{2v} species a_1, b_2 (planar), a_2 and b_1, Species; Raman polarization (pol/depol), Pol; i.r. activity (±), i.r.; band contour branches *P, Q, R;* types A, B, C, TYPE (κ= −0.94, Table 1).

Species	i [a]	Pol [b]	i.r.	P,Q,R[b]	TYPE
a_1	1–12	pol	+	*PQR*	A
b_2	23–33	depol	+	*PR*	B
a_2	13–15	depol	−		
b_1	16–22	depol	+	P^cQR^c	C

[a] Numbered as in ref. 6. [b] Experimental spectra, available on request. [c] Weak. *Q*-branch dominates.

normal vibration frequencies, ν_i (i=1−33), distributed on C_{2v} species a_1, b_2, a_2 and b_1.[6] To ensure that no serious disagreement concerning the ν_i's of Ref. 6 exists, readily available Raman equipment was used by us to obtain Raman spectra (50−3200 cm^{-1}) of I (liq.) at 50 °C, and IR spectra at 25 °C of I(gas) at p=0.60 Torr, recorded interferometrically 50−500 cm^{-1} (path length 4.6 m) and conventionally 400−3240 cm^{-1} (path length 20 m). The expected spectral features are reported in Table 4, the assignments of ν_i's in Table 5. Referring to Ref. 6, Table 2, page 1282, acceptable agreement was obtained comprising our measurements of Raman line polarization and i.r. band contours (not explicitly reported in Ref. 6). Only a few questions remain. We suggest to replace ν_{22}=118 cm^{-1} by the FIR observed 104 cm^{-1} (Fig. 3) for I(gas). Further, we definitely interpret the contour of the IR spectrum around 540 cm^{-1} as necessarily due to a *C*-type band (b_1 species) superimposed by a *B*-type band (b_2) excluding the presence of *A*-type contour. Thus, ν_{31}=540 cm^{-1}. The three IR inactive a_2 vibrations ν_{13}, ν_{14} and ν_{15} are Raman active. Within the limits of the reliability of our force field (*vide infra*) their predicted locations are at 965, 840 and 392 cm^{-1}. Observed polarized Raman bands at 948 (weak), 840 (strong) and 400 cm^{-1} (strong) might hide weak depolarized ν_{13}, ν_{14} and ν_{15}.

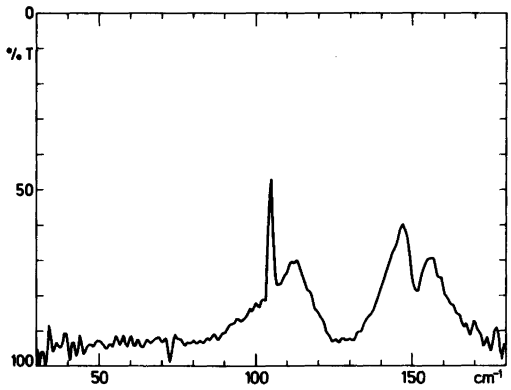

Fig. 3. Far infrared spectrum of gaseous 4-fluoro-benzonitrile obtained interferometrically by subtraction of an experimental 'background' of 4 superimposed runs from 3 averaged interferograms of I(gas). No further bands were observed 160–400 cm^{-1}. ν_{21}=269 cm^{-1} was seen only in Raman (Table 5).

Table 5. Present assignment of 4-fluor-benzonitrile gas phase normal vibration frequencies (cm^{-1}) ν_i numbered as in ref. 6. If unobserved in the IR gas spectrum the uncorrected value from the Raman spectrum (liq.) has been inserted marked by Ra. C_{2v} species a_1, b_2, a_2, b_1.

a_1-species			b_2-species			a_2-species			b_1-species		
Exp.	i	Calc.[c]	Exp.	i	Calc.[c]	Exp.[a]	i	Calc.[c]	Exp.	i	Calc.[c]
3081	1	3085	3078	23	3081	—	13	965	922	16	948
3062	2	3061	3062	24	3064	—	14	840	842	17	822
2240	3	2242	1607	25	1616	—	15	392	728	18	740
1612	4	1620	1407	26	1419	—			538	19	537
1514	5	1510	1300	27	1312	—			Ra 469	20	472
1253	6	1262	1245	28	1260	—			Ra 269	21	265
Ra 1193	7	1210	1095	29	1118	—			104	22[b]	106
1159	8	1147	Ra 645	30	638	—					
1018	9	1019	540	31	540	—					
838	10	830	405	32	404	—					
678	11	688	152[b]	33	152	—					
411	12	398									

[a] See text. [b] Calculated inertial defect in Table 3. [c] From Table 6 ADAPT constants.

Table 6. Adopted (ADOPT) and adjusted (ADAPT) force field constants for 4-fluoro-benzonitrile (Fig. 1). Experimental and calculated normal vibration frequencies in Table 5. Possible alternative, ALTER.

Deformations	Units	ADOPT	ADAPT	ALTER
Stretchings	mdyn/Å			
C–F		5.80[4]	5.77(52)	7.1(9)
C–N		16.80[5]	16.1[a]	17.0(8)
C2–C3		5.39[5]	7.18(57)	5.39(fixed)
Angles (in plane)	mdyn Å			
β-CF[b]		1.89[4]	1.99(7)	
β-C3C2[b]		1.36[5]	1.09(8)	
∠CCN		0.35[5]	0.42(3)	
Interactions (in plane)				
C–F/C6–C8	mdyn/Å	0.43[4]	0.54(25)	
C2–C3/C3–C4	—	0.18[5]	0.2[a]	
C–F/q^c_{19}	mdyn	−0.11[1]	−0.39(21)	
C–F/q^c_{20a}	—	−0.10[1]	−0.66(28)	
β-CF/β-CH[b]	mdyn Å	0.02[1]	0.13(5)	
β-C3C2/β-CH[b]	—	0.02[1]	−0.21(6)	
Angles (out of plane)				
γ-CF	mdyn Å	0.6	0.54(7)	
γ-C3C2	—	0.48[5]	0.38(5)	
∠CCN	—	0.37[5]	0.49(7)	
γ-C3C2/∠CCN	—	0.01[5]	−0.05(3)	

[a] Fixed, but changed in succeeding calculations until optimal fit was obtained. [b] β is defined as in Ref. 4; for example, β-CF is defined as ½(∠C6C8F−∠C10C8F). For sign conventions see Ref. 1 and 4. [c] See ref. 1.

Table 7. Preliminary structure of 4-fluoro-benzonitrile (rotational constants B_{mod} and C_{mod} MHz) agreeing with experimental B and C (Table 1). Selected structure elements from fluorobenzene [2] and benzonitrile.[3] Atom numbering in Fig. 1, fragments approach in Fig. 2.

Distances	(Å)	Angles (degrees)	
N≡C	1.1581[a]	C3C4H5	120.64[a]
C2C3	1.4509[a]	C4C3C12	121.82[a]
C3C4	1.3876[a]	C3C4C6	119.30[c] (α)
C4H5	1.0803[a]		
C4C6	1.401[c] (d)	C6C8C10	123.4[b]
FC	1.354[b]	C8C6H7	120.0[b]
C6C8	1.383[b]	C8C6C4	118.1[c] (β)
C6H7	1.081[b]		
	B^d	C^d	
	972.394	829.108	
	B_{mod}	C_{mod}	
	972.120	829.429	

[a] Ref. 3. [b] Ref. 2. [c] Derived parameters d,α,β. [d] Table 1.

CHOICE AND CHECK OF FORCE FIELD

A tentative force field for I (C_{2v}) was constructed by first redistributing the quantum mechanically calculated field for benzene (D_{6h})[1] according to C_{2v} symmetry, the result being checked by satisfactory recalculation of the benzene normal frequencies (VIBROT [8]). Hereafter, values of force field constants from Ref. 4 and 5 connected with the substituents F and CN, respectively, were introduced (Table 6, ADOPT), taking the remaining necessary constants from Ref. 1. For the redundant set of ring CC stretch and CCC bending coordinates, symmetry coordinates were used.[1,4]. The benzene part of the field was unchanged during a following least-square fit (FLINDA[8]) except for the constants under ADOPT, Table 6. The adapted constants are reported in Table 6, ADAPT, stating possible numerical values of the desired tentative force field constants. The corresponding ν_i's are reported in Table 5 showing acceptable agreement with the assigned ν_i's. The ADAPT constants produce satisfactory agreement between calculated and experimental inertial defect (~0) and the distortion constants τ_{aaaa} etc. for I in its ground level (Tables 1 and 2), and between the inertial defects of I in its ν_{22} and ν_{33} levels (Table 3). Thus, the remaining inertial defects given in Table 2 may prove useful for future work.

DISCUSSION

Table 7 summarizes assumed and calculated geometric parameters of I assembled as in Fig. 2. The resulting d=1.401 Å, α=119.3° and β=118.1°. The C3–C8 distance is 2.7309 Å compared to 2.7338 Å in $C_6H_5NO_2$.[10] The ADAPT field is, of course, far from unique and only moderately different from expectations except, perhaps, the C2–C3 stretching constant of 7.18 mdyn/Å. It is larger than in benzonitrile (5.39)[5] and in *p*-chloro-benzonitrile (6.0)[11] and actually quite comparable to the C–C stretching constant in benzene. Taking the C2–C3 constant at its 'face' value of 7.85 suggests taking a shorter C2–C3 distance than assumed (1.45 Å, Table 7). Simply taking it from vinylcyanide, N≡C–CH=CH_2,[12] where C–C is 1.425 Å and proceeding as above, leads to d=1.420 Å, α=119.3° and β=118.1°. If felt necessary, an 'aromatic' d in the 1.39–1.41 Å range is easily obtainable by small adjustments of the chosen fluorobenzene and benzonitrile fragments. As shown in column ALTER of Table 6 a similar discussion could be centered around the force constant and the assumed length of the C8–F bond, 'freezing' the C2–C3 stretching constant at the benzonitrile value (5.39). The force constants of C–F, C≡N and C2–C3 stretchings are strongly correlated. Presently we have no intention of going further.

Acknowledgements. The Danish National Science Research Council is acknowledged for its support. Thanks are due to N. W. Larsen, T. Pedersen and G. O. Sørensen of this laboratory for helpful discussions.

REFERENCES

1. Pulay, P., Fogarasi, G. and Boggs, J. E. *J. Chem. Phys. 74* (1980) 3999.
2. Nygaard, L., Bojesen, I., Pedersen, T. and Rastrup-Andersen, J. *J. Mol. Struct. 2* (1968) 209.
3. Casado, J., Nygaard, L. and Sørensen, G. O. *J. Mol. Struct. 8* (1971) 211.
4. Duincker, J. C. *Thesis,* Amsterdam (1964); Duincker, J. C. and Mills, I. M. *Spectrochim. Acta A 24* (1968) 417.
5. Kuwae, A. and Machida, K. *Spectrochim. Acta A 35* (1979) 841.
6. Green, J. H. S. and Harrison, D. J. *Spectrochim. Acta A 32* (1976) 1279.
7. Bak, B., Svanholt, H. and Holm, A. *Acta Chem. Scand. A 34* (1980) 625.
8. Sørensen, G. O., this laboratory.
9. Smyth, C. P., *Dielectric Behavior and Structure,* McGraw-Hill Book Co., New York, 1955, p. 314.
10. Høg, J. H. *Thesis,* Copenhagen (1971), this laboratory; Larsen, N. W. *J. Mol. Struct. 51* (1979) 175.
11. Gates, P. N., Steele, D., Pearce, R. A. R. and Radcliffe, K., *J. Chem. Soc. Perkin Trans. II* (1972) 1607.
12. Costain, C. C. and Stoicheff, B. P. *J. Chem. Phys. 30* (1959) 777.

Received November 26, 1982.

Acta Chemica Scandinavica A 37 (1983) 609–616

Short Communications

On the Homogeneity Ranges of LaB_6, EuB_6 and SmB_6

YU. B. PADERNO * and T. LUNDSTRÖM

Institute of Chemistry, Box 531,
S-751 21 Uppsala, Sweden

The width of the homogeneity ranges of the rare earth hexaborides has been determined in only a few cases.[1] For SmB_6 a relatively large decrease has been found in the cell dimension with decreasing metal content,[2] which has been taken to indicate the occurrence of metal vacancies in the boron-rich compositions, a conclusion supported by density measurements. For LaB_6 no cell dimension variations have been found.[3,4] Johnson and Daane[3] reported that the range of homogeneity of cubic LaB_6 extends from $La_{0.99}B_6$ to $La_{0.82}B_6$ although the a axis was unchanged. Storms and Mueller[4] concluded that two phases occur, denoted LaB_6 and LaB_9, which have the same X-ray diffraction pattern (as regards intensities and cell dimensions), although the phases differ in colour and thermodynamic properties. Iso-structural non-stoichiometric $Th_{1-x}B_6$ has, however, been studied in detail using neutron diffraction techniques and density measurements.[5] For this compound it was demonstrated that thorium vacancies occur up to $x \sim 0.22$ and that the unit cell volume increases with increasing number of thorium vacancies.

In the present work, the hexaborides were prepared by reaction in vacuum between rare earth sesqui-oxide (RE_2O_3) and boron (so-called boro-thermal reduction) at 1700–1800 °C for approximately 4 h according to

$$(1-x)RE_2O_3+3(5-x)B\rightarrow$$
$$2RE_{1-x}B_6+3/2\cdot(1-x)B_2O_2$$

The compositions $Sm_{0.97}B_6$ and $Sm_{0.94}B_6$ were obtained from SmB_6 and $Sm_{0.9}B_6$ in the required proportions using ZrB_2 crucibles at 1800 °C for 4h. The unit cell dimensions were determined using a Guinier-Hägg powder X-ray camera with strictly monochromatic $CuK\alpha_1$ radiation (λ=1.540598 Å) and zone-refined silicon as an internal calibration substance (a=5.431065 Å). The unit cell dimensions were least-squares refined using a local program.[6] Most of the samples were analysed chemically. The boron and RE content of the borides was determined using conventional mannitol and EDTA titration respectively.

The results of the cell dimension determinations (including standard deviations) and chemi-

* On leave from Institute of Materials Problems, Ukrainian Academy of Sciences, Krzyzhanovski Street 3, 252142 Kiev, USSR.

Table 1. Chemical analyses and cell dimensions for SmB_6 samples.

Composition	Chemical analyses % Sm	% B	Cell dimensions a (Å)	V (Å^3)
SmB_6	69.76	30.19	4.1334(2)	70.62(1)
$Sm_{0.97}B_6$[a]	n.a.	n.a.	4.1317(2)	70.53(1)
$Sm_{0.94}B_6$[a]	n.a.	n.a.	4.1301(2)	70.45(1)
$Sm_{0.90}B_6$	67.1	32.2	4.1280(2)	70.35(1)
$Sm_{0.89}B_6$	67.35	32.49	4.1272(1)	70.30(1)
$Sm_{0.81}B_6$	65.0	34.4	4.1281(1)	70.35(1)
$Sm_{0.79}B_6$	64.36	35.34	4.1272(2)	70.30(1)
$Sm_{0.71}B_6$	62.17	37.63	4.1277(1)	70.33(1)

[a] Prepared from SmB_6 and $Sm_{0.90}B_6$ (master alloys).

0302-4377/83 $2.50

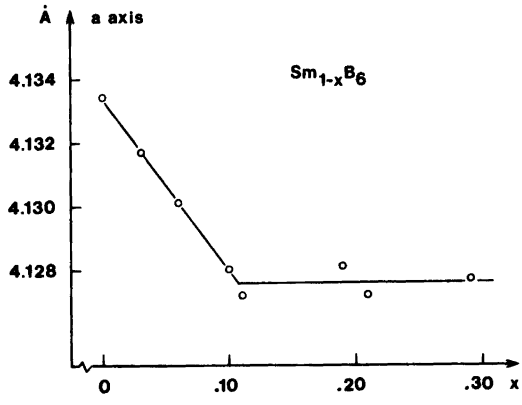

Fig. 1. The unit cell parameter a of $Sm_{1-x}B_6$ as a function of x.

cal analyses are in Tables 1–3. The X-ray photographs were taken at a temperature of (21±1) °C. The uncertainty in the temperature determination introduces a relative error of $5/10^6$, that can be neglected in comparison with one standard deviation.

The cell dimensions and chemical analyses for SmB_6 are given in Fig. 1 and Table 1. The cell parameter of SmB_6 decreases linearly from 4.1337 Å at the stoichiometric composition to 4.1276 Å at the composition $Sm_{0.89}B_6$ (Fig. 1). In samples with higher boron content the cell parameter of SmB_6 is constant indicating the occurrence of a two-phase regime. A considerable excess of boron was required for the SmB_{66} diffraction lines to occur in the powder pattern of a boron-rich sample due to the low scattering power of SmB_{66}. In boron-rich samples, prepared by arc-melting mixtures of $Sm_{0.90}B_6$ and crystalline boron and subsequently by heat treating the alloy at 1800 °C for 8h, SmB_{66} and SmB_6 occurred simultaneously, the latter with a=4.1274(3) Å (see Table 3). The unit cell dimension of stoichiometric SmB_6 in the present study is in close agreement with the values reported in other recent investigations.[7–9]

The present results differ significantly from those reported by Niihara[2] for samples prepared at 1650 °C using the same method of synthesis as

Table 2. Chemical analyses and cell dimensions for some LaB_6 and EuB_6 samples.

Composition	Chemical analyses % La	% B	Cell dimensions a (Å)
LaB_6	68.2	31.7	4.1563(1)
$La_{0.94}B_6$	66.9	33.0	4.1565(1)
$La_{0.9}B_6$	65.4	34.4	4.1561(2)
$La_{0.81}B_6$	63.1	36.4	4.1562(2)
$La_{0.75}B_6$	61.2	38.4	4.1567(2)
EuB_6	n.a.[a]	n.a.	4.1844(5)[b]
$Eu_{0.79}B_6$[c]	64.77	35.10	4.1849(2)

[a] Stoichiometric. [b] As measured with the Debye-Scherrer technique. [c] After arc-melting of the EuB_6 sample.

Table 3. Cell dimensions of phases in two-phase regimes. The samples were heat-treated at 1800 °C for 8 h.

Phases in equilibrium	Phase	Cell dimensions (Å)
$SmB_{66}+Sm_{1-x}B_6$	SmB_{66}	a=23.4683(5)
	$Sm_{1-x}B_6$	a=4.1274(3)
β-rh. B+$La_{1-x}B_6$	β-rh. B	a=10.929(1)
		c=23.821(3)
	$La_{1-x}B_6$	a=4.1565(1)
β-rh. B+$Eu_{1-x}B_6$	β-rh. B	a=10.928(2)
		c=23.823(4)
	$Eu_{1-x}B_6$	a=4.1849(2)

in this work. Niihara reported a cubic unit cell dimension of 4.1305 Å for stoichiometric SmB_6 and a non-linear decrease to 4.1278 Å for the composition $Sm_{0.68}B_6$. It is not easy to understand the large difference between Niihara's results and ours, in particular not the width of the homogeneity range. The temperatures used are nearly the same. The smaller unit cell of stoichiometric SmB_6, reported by Niihara, might be due to impurities of other rare earth elements and/or the grinding of crystalline boron in a sardonyx mortar prior to heat treatment. According to our experience, such a procedure contaminates the sample with abraded particles from the mill. These particles may then react with the sample at the high temperatures of the heat treatment.

Stoichiometric SmB_6 displays valence fluctuations between Sm^{3+} and Sm^{2+} with a nearly temperature independent concentration ratio.[15] Paderno *et al.*[9] have observed that the main part of the valence change in $Sm_{1-x}B_6$ occurs in the composition region $x=0.0$ to $x=0.1$, which closely coincides with the region of variable cell dimensions as determined in the present investigation.

Table 2 shows that the average of the cubic unit cell parameter for LaB_6 is 4.1564(2) Å and that no significant variations occur within the homogeneity range. This result is in agreement with several recent reports.[4,10,11] The chemical analyses, however, indicate a variable composition (B/La ratio, see Table 2) for LaB_6. The structural mechanism behind the compositional changes has not been established. Since the cell dimensions do not change significantly with composition, it does not seem probable that the composition is changed by the occurrence of a variable number of vacancies at the metal position. An experimental study of this question is currently in progress.

The cell dimensions of phases participating in two-phase equilibria are given in Table 3. The unit cell dimensions of β-rhombohedral boron saturated with lanthanum and europium respectively do not differ significantly from those of the pure β-rh. boron used ($a=10.9276(5)$ Å; $c=23.8141(15)$ Å).[12] The solid solubility of lanthanum and europium respectively in β-rh. boron is consequently very small (probably less than 0.1 atomic per cent) while that of several of the transition elements has been found to lie between one and four atomic per cent.[12]

The cubic unit cell dimension $a=23.4683(5)$ Å for the samarium-rich compound SmB_{66} (see Table 3) is smaller than the value 23.474(2) Å for single-phase SmB_{66} reported by Soloviev and Spear[13] and also smaller than the value 23.487(3) Å for boron-rich SmB_{66} reported by Schwetz *et al.*[14] It is notable that the unit cell parameter of SmB_{66} *increases* with *decreasing* samarium.

Acknowledgements. The authors wish to thank Drs. N. I. Perepelitza, E. M. Dudnik and A. V. Kovalev, Kiev, as well as Dr. L.-E. Tergenius, Uppsala, for skillful assistance in preparation and X-ray work. The support of the Swedish Natural Science Research Council is gratefully acknowledged.

The stay in Uppsala of Yu.B.P. took place within the framework of the scientific exchange between the Academy of Sciences of USSR, the Royal Swedish Academy of Sciences and the Royal Swedish Academy of Engineering Sciences.

1. Spear, K. E., *in* A. M. Alper (ed.), *Phase Diagrams: Materials Science and Technology*, Vol. IV. Academic, New York, 1976, pp. 91–159.
2. Niihara, K., *Bull. Chem. Soc. Jap. 44* (1971) 963.
3. Johnson, R. W. and Daane, A. H., *J. Phys. Chem. 65* (1961), 909.
4. Storms, E. and Mueller, B., *J. Phys. Chem. 82* (1978) 51.
5. Etourneau, J., Naslain, R. and LaPlaca, S., *J. Less-Common Metals 24* (1971) 183.
6. Ersson, N.-O., Institute of Chemistry, University of Uppsala, Uppsala. *Unpublished.*
7. Solovyev, G. I. and Spear, K. E., *J. Am. Ceram. Soc. 55* (1972) 475.
8. Eick, H. A. and Gilles, P. W. *J. Am. Chem. Soc. 81* (1959) 5030.
9. Paderno, Yu. B., Konovalova, E. S., Baturniskal, I. L., Dudnik, E. H., Finkel'shtein, L. D. and Efremova, N. N., *Neorgan. Mater. 18* (1982) 37.
10. Gurin, V. N., Korsukova, M. M., Nikanorov, S. P., Smirnov, I. A., Stepanov, N. N. and Shul'man, S. G., *J. Less-Common Metals 67* (1979) 115.
11. Futamoto, M., Aita, T. and Kawabe, U., *Jap. J. Appl. Phys. 14* (1975) 1263.
12. Jiminez-Crespo, A., Tergenius, L.-E. and Lundström, T., *J. Less-Common Metals 77* (1981) 147.
13. Soloviev, G. I. and Spear, K. E., *J. Am. Ceram. Soc. 55* (1972) 475.
14. Schwetz, K. A., Ettmayer, P., Kieffer, R. and Lipp, A., *J. Less-Common Metals 26* (1972) 99.

15. Kasaya, M., Kimura, H., Isikawa, Y. and Kasuya, T. In Falicov, L. M., Hanke, W. and Maple, M. B., Eds., *Valence Fluctuations in Solids,* North-Holland, Amsterdam, 1981, pp. 251–254.

Received June 20, 1983.

Amineanionogold(III) Complexes. III. Kinetics of the Substitution of Ammonia by Bromide in Amminetribromidogold(III) in Acid Aqueous Solution

L. H. SKIBSTED

Chemistry Department, Royal Veterinary and Agricultural University, Thorvaldsensvej 40, DK-1871 Copenhagen V, Denmark

Two distinct stages with rates differing by five orders of magnitude are observed in the reaction sequence in which the four ammonia ligands in the square planar tetraamminegold(III) ion are replaced by bromide.[1] The first stage giving *trans*-diamminedibromidogold(III) as product consists of two consecutive reactions of comparable rates,

$$[Au(NH_3)_4]^{3+} + Br^- \xrightarrow{k_1} [AuBr(NH_3)_3]^{2+} + NH_3 \quad (1)$$

$$[AuBr(NH_3)_3]^{2+} + Br^- \xrightarrow{k_2} \textit{trans}\text{-}[AuBr_2(NH_3)_2]^+ + NH_3 \quad (2)$$

The second and slower stage appears as a simple pseudo first-order reaction when bromide is in excess, and the replacement of one ammonia in *trans*-$[AuBr_2(NH_3)_2]^+$ has been identified as the experimentally observed slow reaction of the overall process in acid solution,

$$\textit{trans}\text{-}[AuBr_2(NH_3)_2]^+ + Br^- \xrightarrow{k_3} [AuBr_3NH_3] + NH_3 \quad (3)$$

The last ammonia is replaced by bromide,

$$[AuBr_3NH_3] + Br^- \xrightarrow{k_4} [AuBr_4]^- + NH_3 \quad (4)$$

at a rate which is fast compared to the rate of reaction (3).

The rate constants and activation parameters for the first three reactions in the reaction sequence (1)–(4) in 1.0 M $H(Br,ClO_4)$ have been determined previously, but since reaction (4) is preceded by a much slower reaction, the kinetic parameters for this reaction were not accessible from kinetic experiments in which solutions of $[Au(NH_3)_4](NO_3)_3$ or *trans*-$[AuBr_2(NH_3)_2]Br$ were allowed to react with bromide.[1]

Strähle *et al.*[2] have recently prepared $[AuCl_3NH_3]$ by thermal decomposition of $NH_4[AuCl_4]$. Since halide exchange reactions at Au(III) centers are fast compared to reactions (1)–(4),[3–5] $[AuCl_3NH_3]$ can be used as a precursor for $[AuBr_3NH_3]$, thus allowing a direct study of reaction (4) and thereby a completion of the work started in Ref. 1. The results from such kinetic studies are reported here together with a discussion based on activation parameters of the factors which control the rate of replacement of ammonia by bromide at Au(III) centers.

The rate of replacement of ammonia by bromide in $[AuBr_3NH_3]$ was monitored spectrophotometrically. All kinetic experiments were performed with excess of bromide ion in acidic solution, and simple pseudo first-order kinetics were observed in all experiments. The observed pseudo first-order rate constants, which are given in Table 1 together with the experimental conditions, are more than a factor 10^3 greater than those expected for Cl^-/Br^- exchange reactions,[3,5] and any interference from halide exchange reactions on reaction (4) could therefore be excluded. From experiments 2–4, 8, and 9 of Table 1 it is seen that the first-order constants are directly proportional to $[Br^-]$, indicating that the substitution reaction takes place as a direct displacement without any significant contribution from a solvent path.[1,3,5] Experiments 4–7 indicate, in accordance with the results previously obtained for reactions (1)–(3), that both NH_4^+ and H^+ in the concentration range studied have only minor effects on the reaction rate. From the dependence of the pseudo first-order rate constants on $[Br^-]$ and from the temperature dependence (experiments 1,3,10, and 11), the second-order rate constant and the activation parameters for reaction (4) at 25 °C were estimated. These values are compared in Table 2 with those previously obtained for reactions (1)–(3).

Effects due to the charge of the nucleophile in combination with the charge of the substrate as well as separate effects due to *cis*- and *trans*-ligands have been used in parameterization of the reactivity of d^8 low-spin square planar complexes. The influence of these different factors is normally discussed on the basis of rate constants for consecutive ligand substitution reactions in series of complexes such as $[Pt(H_2O)_x(NH_3)_yCl_{4-x-y}]$, and $[AuBr_xCl_{4-x}]^-$[3,6,7] obtained at one

0302-4377/83 $2.50

Table 1. Pseudo first-order rate constants for the substitution reaction $AuBr_3NH_3+Br^- \xrightarrow{k_4} AuBr_4^-+NH_3$ in acidic aqueous solution. A 1.00 M $H(Br,ClO_4)$ medium was used in all experiments except Nos. 5, 6, and 7.

No.	t/°C	$[Br^-]$/M	pH	k_4'/s^{-1}
1	19.5	0.0150	0.00	$2.18(3) \times 10^{-4}$
2	25.0	0.0100	0.00	$2.52(14) \times 10^{-4}$
3	25.0	0.0150	0.00	$3.76(15) \times 10^{-4}$
4	25.0	0.0200	0.00	$5.01(7) \times 10^{-4}$
5[a]	25.0	0.0200	0.52	$5.09(9) \times 10^{-4}$
6[b]	25.0	0.0200	0.52	$4.02(3) \times 10^{-4}$
7[c]	25.0	0.0200	1.10	$3.98(5) \times 10^{-4}$
8	25.0	0.0300	0.00	$7.54(10) \times 10^{-4}$
9	25.0	0.0400	0.00	$1.04(1) \times 10^{-3}$
10	29.6	0.0150	0.00	$6.89(13) \times 10^{-4}$
11	34.4	0.0150	0.00	$1.19(5) \times 10^{-3}$

[a] $[NH_4^+]=0.70$ M, $[H^+]=0.30$ M, $[Br^-]=0.0200$ M, $[ClO_4^-]=0.98$ M. [b] $[Na^+]=0.70$ M, $[H^+]=0.30$ M, $[Br^-]=0.0200$ M, $[ClO_4^-]=0.98$ M. [c] $[Na^+]=0.92$ M, $[H^+]=0.080$ M, $[Br^-]=0.0200$ M, $[ClO_4^-]=0.98$ M.

Table 2. Rate constants and activation parameters for the reaction of tetraamminegold(III) ions with bromide in aqueous 1.0 M $H(Br,ClO_4)$ at 25 °C.

Reaction	k_n/l mol^{-1}s^{-1}	$\Delta H_n^{\ddagger}$/kJ mol^{-1}	$\Delta S_n^{\ddagger}$/J mol^{-1}K^{-1}	Ref.
$[Au(NH_3)_4]^{3+}+Br^- \xrightarrow{k_1} [AuBr(NH_3)_3]^{2+}+NH_3$	3.40(8)	73(3)	8(3)	1
$[AuBr(NH_3)_3]^{2+}+Br^- \xrightarrow{k_2}$ *trans*-$[AuBr_2(NH_3)_2]^+ + NH_3$	6.5(4)	69(3)	2(10)	1
trans-$[AuBr_2(NH_3)_2]^+ + Br^- \xrightarrow{k_3} [AuBr_3NH_3]+NH_3$	$9.3(3) \times 10^{-5}$	88(3)	−26(8)	1
$[AuBr_3NH_3]+Br^- \xrightarrow{k_4} [AuBr_4]^- + NH_3$	$2.68(9) \times 10^{-2}$	84(4)	7(9)	Present work [a]

[a] The correlation coefficient between the two activation parameters is −0.9998.

fixed temperature. However, the data of Table 2 provide an opportunity for a discussion of these factors in relation to the activation parameters for a series of Au(III) substrates.

The difference between the rates of bromide substitution of the two first and the subsequent and more robust ammine ligands is primarily a consequence of a higher enthalpy of activation. However, for the third ammine ligand it is also a consequence of a more negative entropy of activation. It is noteworthy that the enthalpies of activation for the substitution of the two first ammine ligands are identical within the experimental uncertainties, and that the enthalpies of activation for substitution of the last two ammine ligands are likewise equal. Thus, the remarkably high *cis*-effect of ammonia relative to bromide in Au(III) complexes, which has been shown to be purely kinetic in nature,[4] is mainly an enthalpy effect. The labilizing effect of two *cis*-ammonia relative to two *cis*-bromide ligands thus corresponds to≈15 kJ/mol, *viz.* the difference between $\Delta H_4^{\ddagger}$ ($\approx \Delta H_3^{\ddagger}$) and $\Delta H_2^{\ddagger}$ ($\approx \Delta H_1^{\ddagger}$).

The rate constants and the entropies of activation given in Table 3 have been corrected statistically for the number of equivalent leaving ligands. The *trans*-labilizing effect of bromide relative to ammonia is 575 calculated from the

Table 3. Statistically corrected rate constants and entropies of activation for the successive substitution of ammonia with bromide in tetraamminegold(III) ions in aqueous 1.0 M H(Br,ClO_4) at 25 °C.[a]

Reaction	m	$k_n m^{-1}$/l mol^{-1}s^{-1}	$\Delta S^{\ddagger}_{n,corr}$/J mol^{-1}K^{-1}
$[Au(NH_3)_4]^{3+}+Br^- \xrightarrow{k_1}$ $[AuBr(NH_3)_3]^{2+}+NH_3$	4	0.85	−3
$[AuBr(NH_3)_3]^{2+}+Br^- \xrightarrow{k_2}$ *trans*-$[AuBr_2(NH_3)_2]^+ + NH_3$	1	6.5	2
trans-$[AuBr_2(NH_3)_2]^{2+}+Br^- \xrightarrow{k_3}$ $[AuBr_3NH_3]+NH_3$	2	4.7×10^{-5}[b]	−32
$[AuBr_3NH_3]+Br^- \xrightarrow{k_4}$ $[AuBr_4]^- + NH_3$	1	2.7×10^{-2}	7

[a] m is the number of equivalent leaving ligands in the complex. [b] Incorrectly given as 4.7×10^{-6} in Ref. 1.

corrected rate constants for reactions (3) and (4). This difference in rate is mainly an entropy effect, since $\Delta H_4^{\ddagger}-\Delta H_3^{\ddagger}=-4\pm5$ kJ/mol whereas $-298(\Delta S_{4,corr}^{\ddagger}-\Delta S_{3,corr}^{\ddagger})=-12\pm4$ kJ/mol. However, the *trans*-effect of bromide relative to ammonia is only 8 when calculated from the results for the two first substitution reactions. The expected acceleration of the second substitution reaction relative to the first due to an entropy effect is hardly observed, since -298 $(\Delta S_{2,corr}^{\ddagger}-\Delta S_{1,corr}^{\ddagger})=-2\pm3$ kJ/mol. Charge neutralization during bond formation generally makes a positive contribution to the entropy of activation for substitution reactions with associative activation. The data of Table 3 do indeed show this effect to be significant for the present series of Au(III) substrates. It is remarkable that the partial charge neutralization in the transition state of the tripositive $[Au(NH_3)_4]^{3+}$ accelerates the substitution of the first ammine to essentially the same extent as the presence of a *trans*-bromide ligand accelerates the substitution of the second ammine ligand. However, it should be noted that the *trans*-directing influence of bromide relative to ammonia is not affected, since only *trans*-$[AuBr_2(NH_3)_2]^+$*) was observed as a product of reaction (2).[1]

In conclusion, the present results suggest that the high *cis*-effect of ammonia relative to bromide is an enthalpy effect whereas the more modest *trans*-effect of bromide relative to ammonia is an entropy effect. Bond formation in the transition state has been shown to be more important in Au(III) complexes than in other square planar complexes.[5] Charge neutralization appears to play a significant role during this bond formation step.

In the mixed chlorido-bromido complexes $[AuBr_xCl_{4-x}]^-$, bromide is about 65 times better than chloride as an entering ligand and the Br^-/Cl^- *trans*-effect is ~14.[3] If these trends are assumed to be valid also for mixed ammine-halogenido complexes, then the prediction can be made that in the anation of $[Au(NH_3)_4]^{3+}$ with chloride, the relative rates of the two first ammonia/chloride exchange reactions should be reversed compared to the analogous ammonia/bromide exchange reactions. This would be a unique substitution behaviour for a square planar complex, and it would be an important verification of the significance of charge neutralization during bond formation in the transition state of ligand substitutions in cationic Au(III) complexes. An investigation of the reaction of $[Au(NH_3)_4]^{3+}$ with chloride is now in progress.[9]

Experimental. $[AuCl_3NH_3]$ synthesized by the method of Strähle *et al.*[2] was dissolved in the various reaction media prepared from analytical grade chemicals and analyzed using standard methods. Prethermostatted solutions with $c_{Au}\approx10^{-4}$ M were placed in a 1 cm quartz cell in the thermostatted cell-holder of a Zeiss DMR 21 spectrophotometer and UV-spectra were recorded at known times. All experiments were run in duplicate.

Calculations. The recorded spectra were read off at the four wavelengths 360, 380, 400, and 420 nm and the calculations were done by non-linear regression analysis, as described previously.[1] Under the present conditions the reaction showed pseudo first-order kinetics (goodness-of-fit test). An Arhenius-type plot showed linearity within the estimated uncertainty and the activation parameters were evaluated using reaction rate theory.

* The *trans*-configuration of this product has now been confirmed by an X-ray single-crystal structure determination of the bromide salt.[8]

Acknowledgements. The author is grateful to Jacob Ventegodt for assistance in the experimental work and to Dr. Martin Hancock for linguistic help.

1. Skibsted, L.H. *Acta Chem. Scand. A 33* (1979) 113.
2. Strähle, J., Gelinek, J. and Kölmel, M. *Z. Anorg. Allg. Chem. 456* (1979) 241.
3. Elding, L. I. and Gröning, A.-B. *Acta Chem. Scand. A 32* (1978) 867.
4. Mønsted, O. and Skibsted, L. H. *Acta Chem. Scand. A 38* (1984). *In press.*
5. Baddley, W. H. and Basolo, F. *Inorg. Chem. 3* (1964) 1087.
6. Elding, L. I. and Gröning, A.-B. *Chem. Scri. 11* (1977) 8.
7. Elding, L. I. *Inorg. Chim. Acta 7* (1973) 581.
8. Kaas, K. and Skibsted, L. H. *To be published.*
9. Øby, B. and Skibsted, L. H. *To be published.*

Received July 18, 1983.

Acta Chemica Sandinavica A 37 (1983) 617-629

Precipitation Reactions between Silver Nitrate and Sodium Tungstate in 1.0 mol dm^{-3} Aqueous Sodium Nitrate Solution at 25 °C

JØRGEN BIRGER JENSEN and JØRGEN LOU

Fysisk-Kemisk Institut, DTH 206, DK-2800 Lyngby, Denmark

Precipitation reactions of silver tungstate have been followed by simultaneous potentiometric registration of pAg and pH. The reactions were initiated by addition of 1.0 cm^3 of 1.0 mol dm^{-3} sodium tungstate to 1.0 cm^3 of 1.0 mol dm^{-3} silver nitrate in 125 cm^3 1.0 mol dm^{-3} sodium nitrate at 25 °C. The experimental results indicate formation of at least four sparingly soluble silver tungstate compounds. X-Ray powder diffraction, quantitative silver and tungstate analyses and electron microscopy were used to characterize the precipitates. By combining the experimental results with protolytic equilibria given in the literature, a model is outlined which can describe a possible reaction pattern.

A survey of the existing literature [1-6] shows that the precipitation of silver tungstate from sodium tungstate–silver nitrate mixtures must be regarded as somewhat more complicated than expressed by the following reaction:

$$2Ag^+(aq)+WO_4^{2-}(aq)\rightarrow Ag_2WO_4(s) \qquad (1)$$

Saxena and Gupta [5] describe in a paper, where potentiometric titration between silver nitrate and sodium tungstate has been treated, that the "direct titration", *i.e.* addition of sodium tungstate from a burette to silver nitrate, can be performed at different concentrations with no problems, whereas the "reverse titration" only succeeds in concentrated solution. The lower limit for the titrant concentration was given to 0.01 mol dm^{-3}. During the titration, two other observations concerning the precipitate were made: (1) a change in the nature of the precipitate; before the end-point, the silver tungstate was formed as colloid particles which in the vicinity of the end-point began to coagulate and (2) a change in the colour from white to yellow.

Buchholz [3] has carried out conductometric titration of sodium tungstate with silver nitrate and during these experiments he observed that silver tungstate has a great tendency to form supersaturated solutions, especially when it is precipitated from dilute solution (*i.e.* below 0.01 mol dm^{-3}). A similar observation was made by Varughese and Rao [6] who found it necessary to heat the solution in a steam bath for 7–8 h in order to complete the precipitation.

Several titrations – both direct and reverse – have been carried out at this institute. Our experiences from these titrations can be concluded in the following way. Titration of 0.01 mol dm^{-3} sodium tungstate in 1.0 mol dm^{-3} sodium nitrate with 1.0 mol dm^{-3} silver nitrate in 1.0 mol dm^{-3} sodium nitrate solution could be performed problem-free although it was obvious that the precipitation of silver tungstate was not complete at the end of the titration curve. However, contrary to Saxena and Gupta, we did not succeed in getting reproducible results from titration of 0.01 mol dm^{-3} silver nitrate in 1.0 mol dm^{-3} sodium nitrate with 1.0 mol dm^{-3} sodium tungstate in 1.0 mol dm^{-3} sodium nitrate. Twelve experiments gave twelve different titration curves, *i.e.* different with respect to the position of end-points and different with respect to the appearance. Some of the curves showed two

0302-4377/83 $2.50

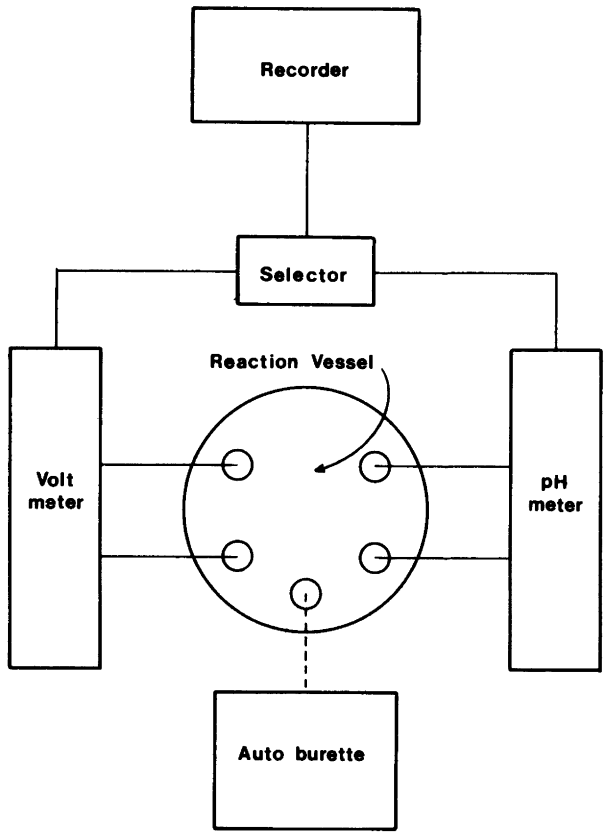

Fig. 1. Diagram of the experimental equipment.

end-points. During the "direct titration", we observed colour-change of the precipitate from yellow to white. Based on the fact that our observations to some extent were contrary to those made by Saxena and Gupta,[5] we decided to study the precipitation mechanism of silver tungstate somewhat more in detail. Some preliminary results from this study have already been published in this journal.[7] The main purpose of the present paper is to include the latest experimental results in order to suggest a precipitation mechanism of silver tungstate.

EXPERIMENTAL

Sodium tungstate *p.a.* was obtained from Riedel de Haén, Ferak and Merck. The three samples were used at random in the experiments. No differences could be observed in the precipitation experiments. In order to remove traces of sodium hydroxide (about 0.1 weight %), the sodium tungstate was recrystallized three times by dissolving in distilled and deionized water. From this solution, sodium tungstate was slowly precipitated by adding three times the volume of ethanol. Sodium determination on a flame photometer showed that the sodium tungstate used in the experiments had the formula $Na_2WO_4 \cdot 2H_2O$. The nitric acid and the sodium hydroxide solutions were made by dilution from titrisol ampulae (Merck), containing 1 mol. Silver nitrate and sodium nitrate were from Merck (*p.a.*) and used without purification. Silver tungstate was delivered from Alfa Products.

During the precipitation reactions, the continuous measuring and registration of pAg and pH was performed by means of an equipment shown graphically in Fig. 1. pH was measured with a glass electrode with an Hg(l), Hg_2Cl_2(s), KCl(sat), $NaNO_3$(1.0 mol dm^{-3})-reference elec-

trode. Both electrodes were obtained from Radiometer A/S, Copenhagen, Denmark (G202C and K701, respectively). (Due to Cl^--contamination a "normal" saturated calomel electrode could not be used as reference-electrode.) pAg was measured with an Ag-electrode (P 4011) and an $Hg(l),Hg_2SO_4(s)$, $Na_2SO_4(sat)$-reference electrode (K501) from Radiometer. By means of a selector unit, made at this institute, both pAg and pH were continuously recorded on a Servograph-recorder (REC 51 from Radiometer A/S). The selector unit also allowed us to place the pAg- and pH-signals arbitrary and independent of each other on the recorder paper, whereas the sensitivity of both signals was determined by the recorder. The reaction vessel consists of a water-jacketed 250 cm^3 glass tube with lid, thermostated at 25.0±0.1 °C. Through the lid the electrodes were immersed into the reaction mixture. An additional hole in the lid was used for addition of reactants. In order to stabilize the ionic strength, all experiments were carried out in 1.0 mol dm^{-3} sodium nitrate. Initial concentration of silver nitrate was selected to $8 \cdot 10^{-3}$ mol dm^{-3} achieved by adding 1.0 cm^3 of 1.0 mol dm^{-3} $AgNO_3$ to 125 cm^3 of 1.0 mol dm^{-3} $NaNO_3$. (According to Saxena and Gupta,[5] it is expected that the greatest difficulties in explaining the precipitation reactions of silver tungstate should arise from solutions with initial concentrations below 0.01 mol dm^{-3}.) To this solution a 1.0 mol dm^{-3} Na_2WO_4 was added, sometimes at once with a 1 cm^3 Carlsberg-pipette, and sometimes from an autoburette (ABU 13 from Radiometer A/S) with a speed of $31.25 \cdot 10^{-3}$ cm^3 min^{-1}. This autoburette was also used in experiments with

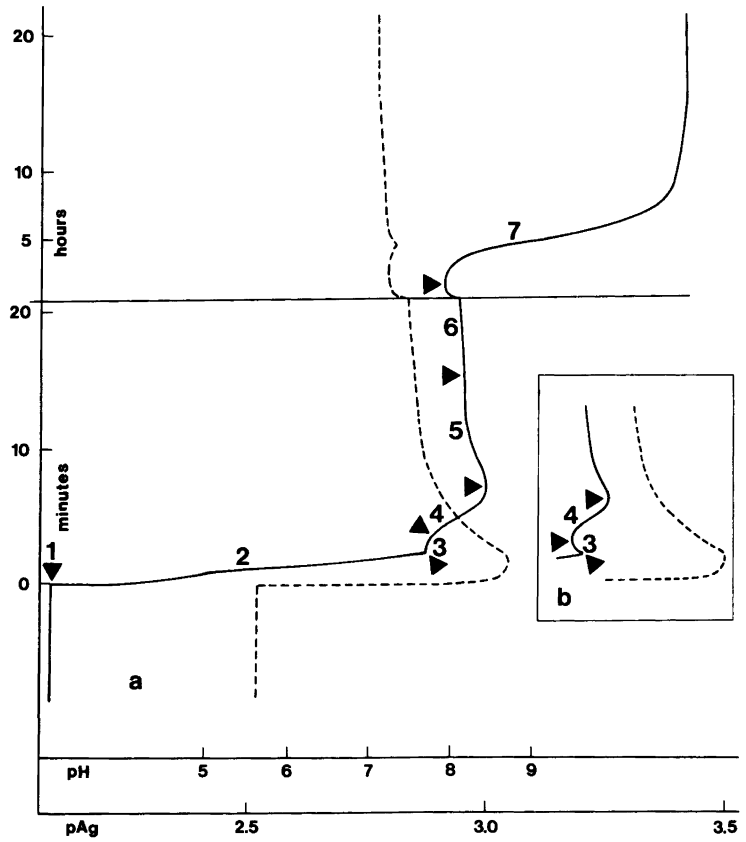

Fig. 2. Time variation of pAg (fully drawn line) and pH (dotted line). Precipitation reactions started at $t=0$, when 1.0 cm^3 of 1.0 mol dm^{-3} sodium tungstate quickly was added to a solution of 1.0 cm^3 of 1.0 mol dm^{-3} silver nitrate in 125 cm^3 of 1.0 mol dm^{-3} sodium nitrate. Two slightly different patterns (indicated by a and b) are shown of the initial course of the reactions. The horizontal line indicates a change in recorder velocity from 1 cm min^{-1} to 0.5 cm h^{-1}.

continuous addition of NaOH.

Titration curves were performed by an automatic titration equipment (Radiometer A/S) which was also used in experiments carried out with constant pH.

Sodium determinations were carried out on a flame photometer (FLM 3, Radiometer A/S).

The X-ray powder diffractometer was a vertical type (Philips PW 1049/01). The copper target was operated at 40 kV and 20 mA.

Photos of precipitates were taken by application of a scanning electron microscope (Philips SEM 505), operated at 19.0 and 24.4 kV.

Silver content of the precipitate was determined in two ways: (a) by dissolving the precipitate in an aqueous NH_3-solution and potentiometric titration of the $Ag(NH_3)_2^+$-complex with aqueous KI-solution, (the strength of the KI-solution was determined by means of $AgNO_3$ dissolved in aqueous NH_3) and (b) by electron micro probe analysis (Applied Research Laboratories, type EMX).

Tungstate content of the precipitate was determined by electron micro probe analysis.

RESULTS AND DISCUSSION

Precipitation reaction between sodium tungstate and silver nitrate in 1.0 mol dm^{-3} sodium nitrate has been followed during a period of about 24 h by continuously registrating changes in pAg- and pH-values. The results are shown in Fig. 2. Immediately after the reactants have been brought together, a yellow precipitate appeared. The yellow colour gradually changed to white and later to light grey. The instantaneous changes in both pAg- and pH-values together with colour changes of the precipitate and the peculiar appearance of both curves during the first 10–15 min of the reaction, strongly indicate that the precipitate initially formed *cannot* be described with the (simple) formula Ag_2WO_4. The S-shape on the pAg-curve (period 7 on Fig. 2a) formed during the following 5–6 h might indicate the dissolution of one sparingly soluble silver tungstate compound followed by formation of another (more sparingly soluble) compound.

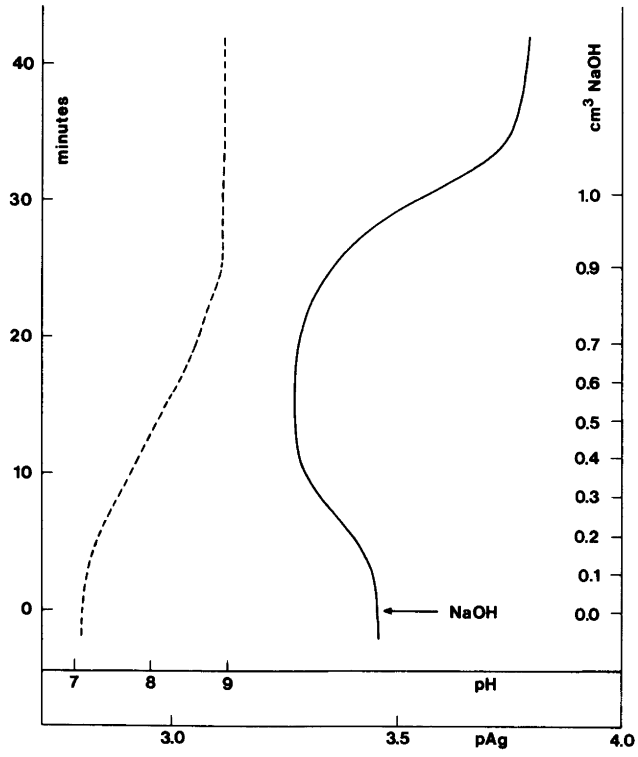

Fig. 3. Continuation of Fig. 2 after a reaction period of 24 h. By slow addition of 1.0 mol dm^{-3} sodium hydroxide (autoburette) pH was raised from about 7.1 to 9.0 after which pH was kept constant at this value.

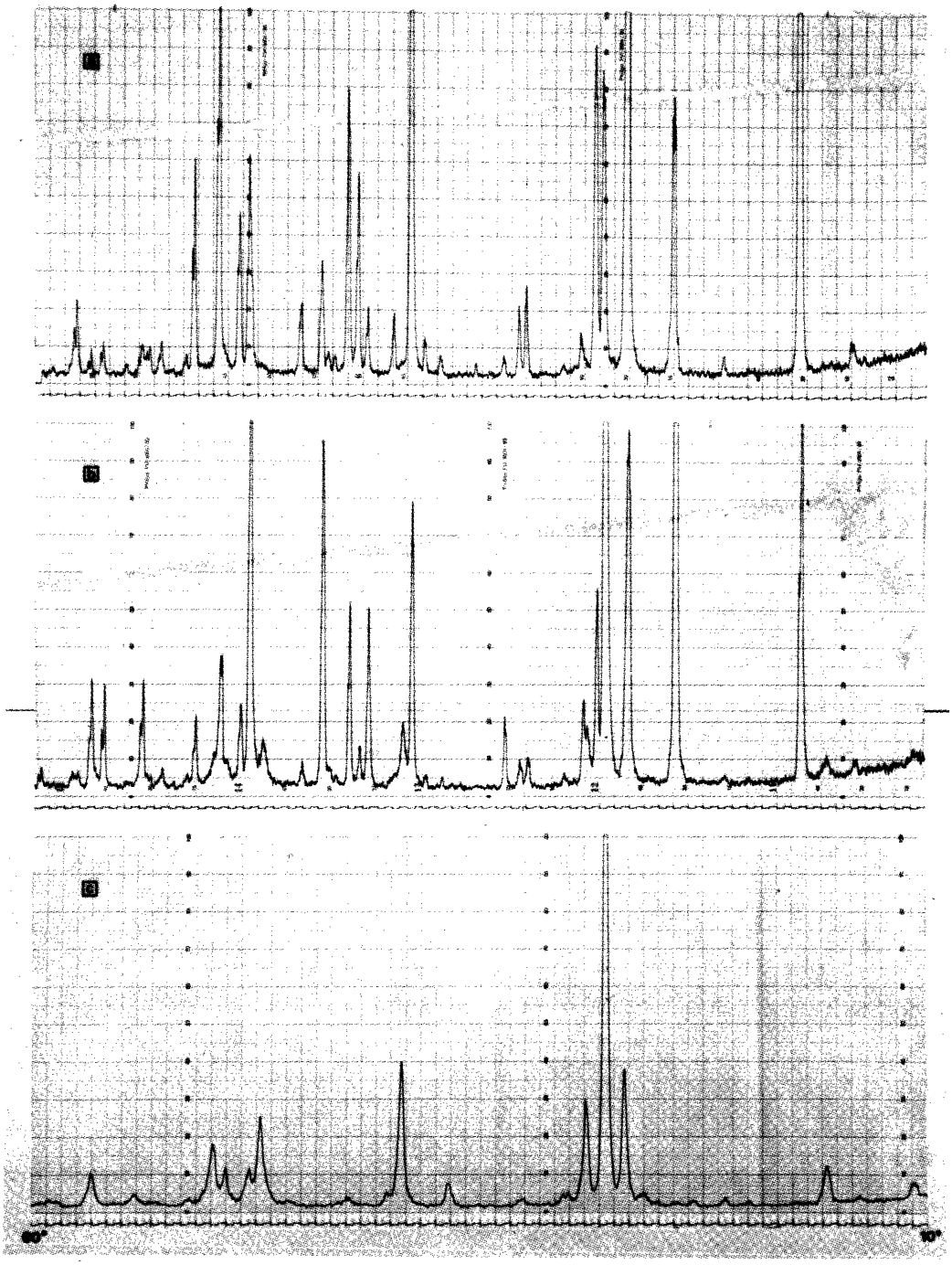

Fig. 4. X-Ray diffraction patterns of precipitates isolated from (a) period 6 (*cf.* Fig. 2), (b) period 7 (*cf.* Fig. 2) and (c) commercial Ag_2WO_4 from Alfa Products.

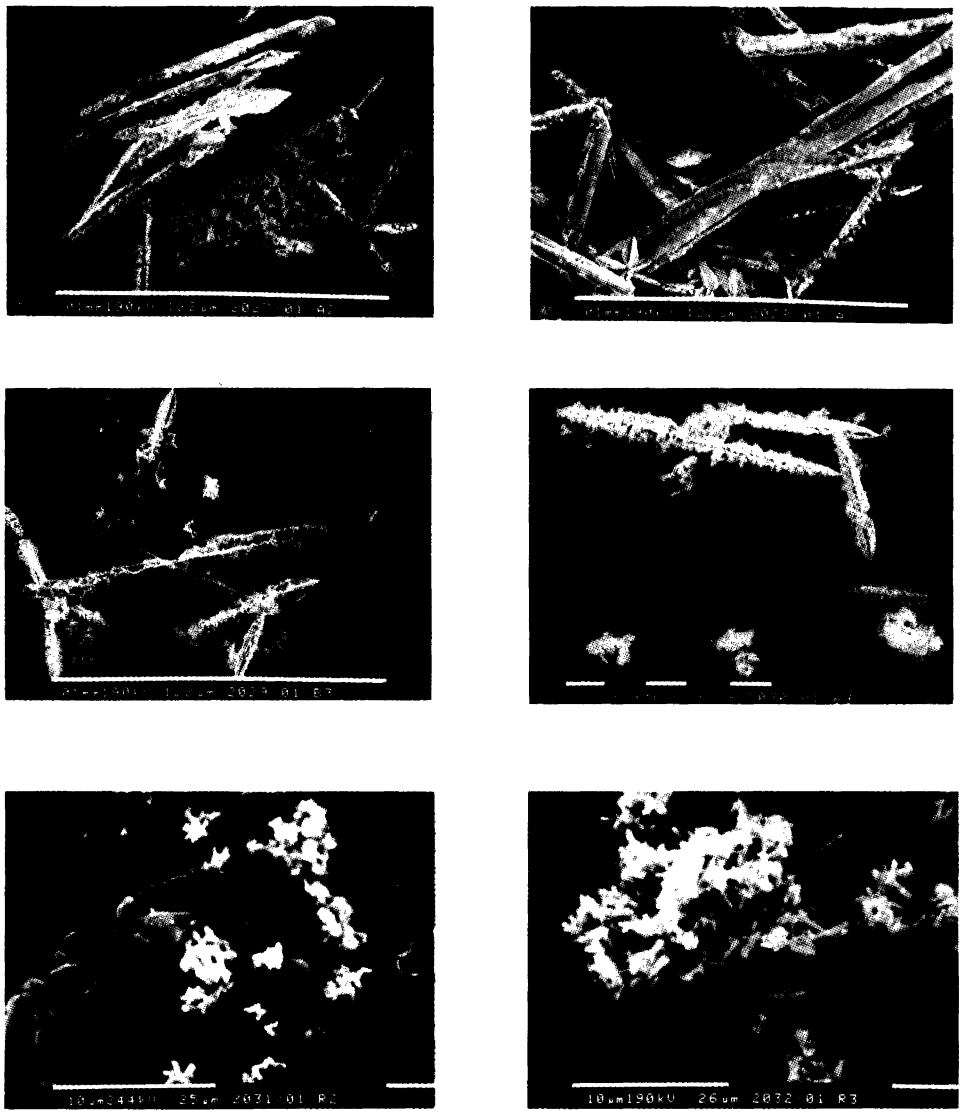

Fig. 5. Electron microscopy of precipitates from period 6 and 7 (*cf.* Fig. 2) and of commercial Ag_2WO_4. The dimensions are indicated by the white bars at the bottom of the pictures.

Two upper pictures. Precipitate from period 6, white bar=100 μm.

Two middle pictures. Precipitate from the end of period 7, white bar=100 μm (left-hand) and=10 μm (right hand).

Two lower pictures. Precipitate isolated after one year of reaction (left-hand) and crystals from commercial Ag_2WO_4 (right-hand), white bars=10 μm.

Note: The crystals in the two lower figures must be regarded as identical confirming the statement that the final product consists of pure Ag_2WO_4.

During this period the white to light grey colour change of the precipitate was observed.* The observation that both pAg and pH, after a reaction period of 24 h, obviously approach stable values, might suggest that an equilibrium is to be established, which means that the final step (formation of Ag_2WO_4 only[7]) of the reaction is approached. However, the following facts reject this suggestion:

(1) Using the pAg-value at the end of period 7 (Fig. 2), the solubility product of Ag_2WO_4 is calculated to be about $4 \cdot 10^{-9}$ mol^3 cm^{-9}. This value is quite different and much higher than the value previously reported ($1.63 \cdot 10^{-11}$ mol^3 cm^{-9}).[7]

(2) If Ag_2WO_4 – and only Ag_2WO_4 – was formed at the end of period 7, then an increase in pH (addition of NaOH to the reaction vessel) must be followed by either no change or by an increase of pAg. (Increase is due to further precipitation of Ag_2WO_4 or a possible precipitation of Ag_2O.) The actual situation is illustrated in Fig. 3. About 24 h after mixing the reactants, almost stable values are read for pAg and pH (pH=7.1 and pAg=3.5). When pH was raised to 9 by addition of NaOH, it was seen that pAg initially decreased, then later increased, obviously going towards a new steady state, (maybe an equilibrium). This means that the precipitate at the end of period 7 must consist of a mixture of at least two sparingly soluble silver tungstate compounds which again means that the final step of the precipitation reaction has not yet been reached after a reaction of 24 h.

* A possible explanation of the pAg and pH variations in Fig. 2 and the colour changes could be that an ion exchange takes place between protons from the precipitates and sodium ions from the solution. However, precipitates isolated from periods 6 and 7 contained not even traces of sodium (determined by flame photometry), which means that mechanisms involving ion exchanges can totally be excluded.

(3) X-Ray measurements on precipitate isolated from this period showed a completely different pattern compared with the curve on pure Ag_2WO_4 (from Alfa Products) (Fig. 4).

(4) Electron microscopy on precipitate relating to this period shows a mixture of crystals – different in both shape and size – compared with Ag_2WO_4 crystals (Fig. 5).

(5) Quantitative silver and tungstate analyses on precipitates isolated from periods 6 and 7 show nearly identical composition. The calculated average formula is $Ag_{1.93}WO_4$ (Table 1).

(6) An experiment similar to that shown in Fig. 2 was carried out and pAg and pH were recorded for three weeks. During this period pH was almost constant (a slight increase of about 0.2 pH was observed), whereas a slow and continuous increase in pAg was observed. Sometimes the pAg increase followed an S-curve. At the end of the three-week period pAg was about 3.9 but still not enough to explain the saturation equilibrium of Ag_2WO_4 (=4.2).

In order to try to give some reasonable semi-quantitative explanation of the precipitation reactions between sodium tungstate and silver nitrate under the present experimental conditions, the protolytic equilibria of sodium tungstate in aqueous solutions must be taken into account.[3,8–16] Arnek and Sasaki[16] found the following protolytic equilibria in 3 M $Na(ClO_4)$ at 25 °C:

$$2H^+ + WO_4^{2-} \rightleftarrows H_2WO_4 \quad (2)$$
$$6H^+ + 6WO_4^{2-} \rightleftarrows W_6O_{21}^{6-} + 3H_2O \quad (3)$$
$$7H^+ + 6WO_4^{2-} \rightleftarrows HW_6O_{21}^{5-} + 3H_2O \quad (4)$$
$$14H^+ + 12WO_4^{2-} \rightleftarrows W_{12}O_{41}^{10-} + 7H_2O \quad (5)$$

and determined the equilibrium constants, K_2, K_3, K_4, K_5. Further, Arnek and Sasaki found the non proton-involving equilibrium to be "practically instantaneously" established:

Table 1. Quantitative analyses of precipitates from period 6 and 7 together with analyses of Ag_2WO_4 (own preparation). The theoretical figures for pure Ag_2WO_4 are: Ag 46.54 and W 39.66.

	Potentiometric, % Ag	Electron micro probe % Ag	% W
Precipitate from period 6 (A2)	45.6±0.1	45.4±0.5	40.7±0.3
Precipitate from period 7 (B3)	45.5±0.1	45.1±1.0	40.3±0.6
Ag_2WO_4 (own preparation, R2)	46.6±0.2	46.6±0.5	39.7±0.2

$$2HW_6O_{21}^{5-} \rightleftarrows W_{12}O_{41}^{10-} + H_2O \quad (6)$$

The protolytic equilibria (2)–(5) are also assumed to be practically instantaneously established, *e.g.* faster than the considered precipitation reactions. Assuming also that the values for K_2, K_3, K_4 and K_5 are valid in 1.0 mol dm^{-3} $NaNO_3$ solution at 25 °C – maybe a somewhat bold assumption – then concentrations of the various tungstate compounds can be calculated at different pH-values.

The following mass-balance holds:

$$C_0 = C_{WO_4^{2-}} + C_{H_2WO_4} + 6C_{HW_6O_{21}^{5-}} + 6C_{W_6O_{21}^{6-}} + 12C_{W_{12}O_{41}^{10-}} \quad (7)$$

Introducing (2)–(5) in eqn. (7):

$$C_0 = C_{WO_4^{2-}} + K_2(C_{H^+})^2 C_{WO_4^{2-}} + 6K_3(C_{H^+})^6(C_{WO_4^{2-}})^6 + 6K_4(C_{H^+})^7(C_{WO_4^{2-}})^6 + 12K_5(C_{H^+})^{14}(C_{WO_4^{2-}})^{12} \quad (8)$$

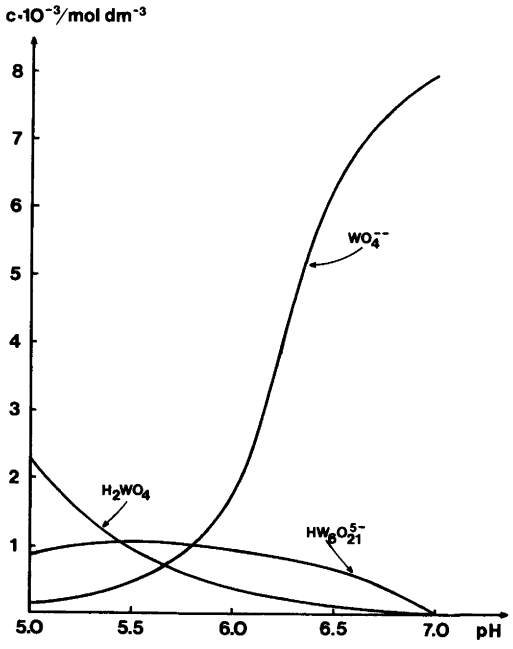

Fig. 6. Calculated distribution of H_2WO_4, $HW_6O_{21}^{5-}$ and WO_4^{2-} as a function of pH utilizing equilibrium constants determined by Arnek and Sasaki.[16] Total concentration of tungstate=8 · 10^{-3} mol dm^{-3} (calculated as WO_4^{2-}).

where C_0 denotes the initial concentration of tungstate calculated as WO_4^{2-}. In our experiments C_0=8 ·10^{-3} mol dm^{-3}. Utilizing eqn. (8), the complete distribution among the five different tungstate ions can be calculated at different pH-values. The result is shown in Fig. 6. Above pH 7 the WO_4^{2-} ion is totally dominating and is practically equal to C_0. Therefore the distribution is only shown for the pH-interval 5<pH<7. The two ionic species $W_6O_{21}^{6-}$ and $W_{12}O_{41}^{10-}$ turn out to be present in so small concentrations that they cannot be shown on the figure. A consequence of this could be that only two ions, *i.e.* $HW_6O_4^{5-}$ and WO_4^{2-} were able to take part in the precipitation processes.

However, according to the experimental results above and the three to four plateaus in the pAg-curve mentioned in Fig. 7, two different sparingly soluble silver tungstate compounds are probably not enough to explain the results shown in Fig. 2. (Two sparingly soluble silver tungstate compounds are in this paper defined to be different when they create two different saturated concentrations of silver ions at the same pH.) The initial conditions in Fig. 7 were exactly the same as those in Fig. 2, *i.e.* 1.0 cm^3 of 1.0 mol dm^{-3} sodium tungstate was quickly added to a solution consisting of 1.0 cm^3 of 1.0 mol dm^{-3} silver nitrate in 125 cm^3 sodium nitrate, but now a pH-state equipment was attached to the reaction vessel. By means of NaOH pH was not allowed to go below 8.0, so when this value was reached (about 5 min after the reaction was started) and during the following 48 h, pAg was registrated at constant pH (8.0). During this registration, three distinct plateaus were observed on the pAg-curve and, at the end of the registration period, plateau number four was obviously approached (Fig. 7). This can be explained by formation of at least four different sparingly soluble silver tungstate compounds being created during the precipitation reactions either before or during the pH-state conditions. Further information of the different silver tungstate compounds can be obtained from Figs. 8 and 9. In Fig. 8 the reactants, *i.e.* silver nitrate and sodium tungstate, were mixed together at pH 5.25. No visible precipitate was formed at the mixing, but gradually a slightly visible precipitate was created. To this mixture a solution of 1.0 mol dm^{-3} NaOH was gradually added from an autoburette. Initially a moderate increase in pAg was registrated,

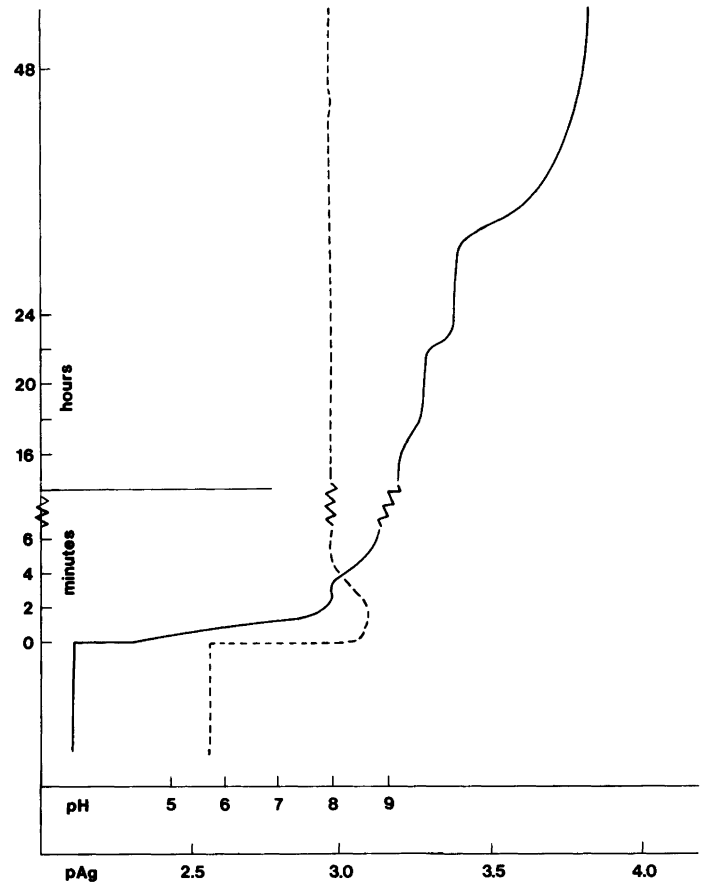

Fig. 7. Initial conditions as in Fig. 2. From t≈5 min pH was kept constant (8.0) in the reaction vessel by means of a pH-state. During the progress of the reactions three plateaus were formed by the pAg curve and obviously the fourth plateau was approached.

but at pH≈6.6 a considerable increase in pAg suddenly occurred, followed by a small decrease. After this an increase in pAg again is observed. We interpret this behaviour in the following way: initially an acidic silver tungstate compound is quickly precipitated (*cf.* Fig. 2). When the precipitation of this compound is almost completed, the precipitation of a second silver tungstate compound is initiated at higher pAg and pH values. However, at these new values the acidic compound is unstable and dissolves initially faster than the second compound precipitates, with the result that both pAg and pH decrease. Later on, the acidic compound is completely dissolved and an increase in both pAg and pH is again observed. The interpretation above is supported by the results shown in Fig. 9, where a solution of sodium tungstate gradually was added to a silver nitrate–sodium nitrate solution. The transistory decrease in pH observed at pH≈6.7 can be explained by dissolution of the acidic silver tungstate compound, due to the fact that this component becomes unstable at higher pH.

Based on the experimental facts, we found it permissible to assume that at least four different silver tungstate compounds must be considered in order to explain the precipitation reaction shown in Fig. 2. Assuming further the protolytic equilibria (2)–(5) to be valid, we suggest that the following precipitations take place:

$$5Ag^+(aq)+HW_6O_{21}^{5-}(aq)\rightleftarrows Ag_5HW_6O_{21}(s) \quad (9)$$

$$10Ag^+(aq)+W_{12}O_{41}^{10-}(aq)\rightleftarrows Ag_{10}W_{12}O_{41}(s) \quad (10)$$

$$6Ag^+(aq)+W_6O_{21}^{6-}(aq)\rightleftarrows Ag_6W_6O_{21}(s) \quad (11)$$

$$2Ag^+(aq)+WO_4^{2-}(aq)\rightleftarrows Ag_2WO_4(s) \quad (12)$$

The solubility products are denoted by the letter L and defined in the following way:

$$L_9=(C_{Ag^+})^5 C_{HW_6O_{21}^{5-}} \quad (13)$$

$$L_{10}=(C_{Ag^+})^{10} C_{W_{12}O_{41}^{10-}} \quad (14)$$

$$L_{11}=(C_{Ag^+})^6 C_{W_6O_{21}^{6-}} \quad (15)$$

$$L_{12}=(C_{Ag^+})^2 C_{WO_4^{2-}} \quad (16)$$

When L is known and utilizing eqns. (7) and (8), the saturation concentration of the silver ions, $C_{Ag^+,sat}$, belonging to each of the four slightly soluble silver tungstate compounds can be calculated at different pH-values. The shape of the curves is determined from the pH-distribution of the different tungstate ions. This distribution is known (eqn. (8)). The exact position of the curves is determined from the L-values. However, only L_{12} is known precisely[7] ($1.63 \cdot 10^{-11}$ mol^3 dm^{-9} in 1.0 mol dm^{-3} $NaNO_3$). $C_{Ag^+,sat(12)}$ is calculated and shown as 1 in Fig. 10. Concerning L_9, L_{10} and L_{11}, no exact values can be given. Reasonable estimates might possibly be made from the experimental results shown in Figs. 2, 8 and 9. Utilizing the pH–pAg relation L_9 and L_{10} can roughly be estimated to 10^{-15} and 10^{-48}, and two saturation curves 2 and 3 can be drawn in

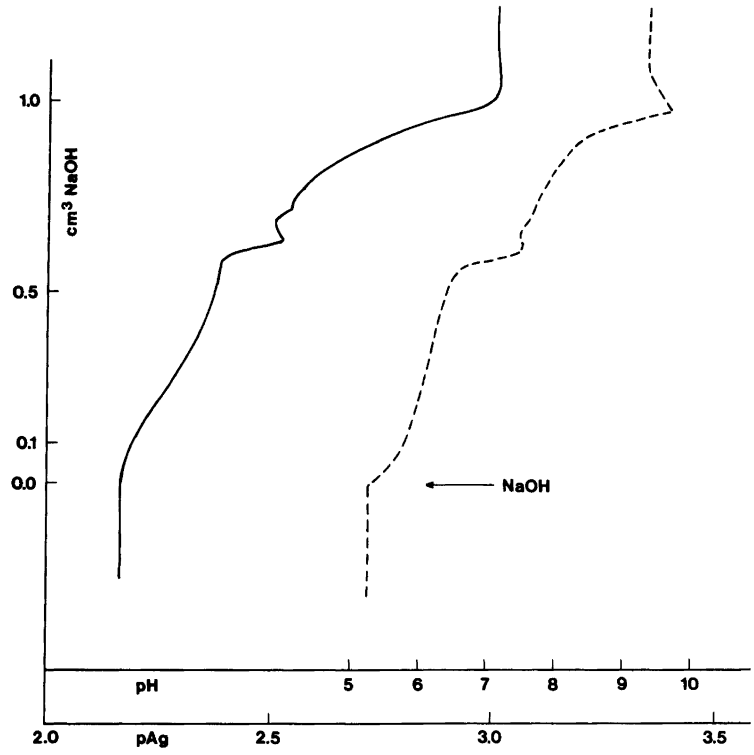

Fig. 8. Time variations of pAg (fully drawn line) and pH (dotted line) when 1.0 mol dm^{-3} sodium hydroxide from an autoburette is slowly added to a mixture of (1.0 cm^3 of 1.0 mol dm^{-3} sodium tungstate +1.0 cm^3 of 1.0 mol dm^{-3} silver nitrate) in 125 cm^3 of 1.0 mol dm^{-3} sodium nitrate. Initial pH value 5.25. Note the small decrease in both pAg and pH at pH≈7.5.

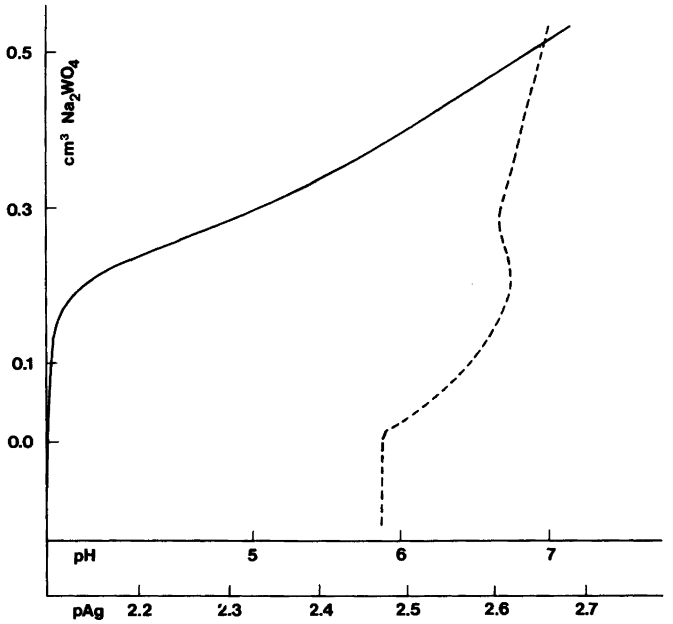

Fig. 9. Time variations of pAg (fully drawn line) and pH (dotted line) when 1.0 mol dm^{-3} sodium tungstate from an autoburette is slowly added to a mixture of 1.0 cm^3 of 1.0 mol dm^{-3} silver nitrate in 125 cm^3 1.0 mol dm^{-3} sodium nitrate. Initial pH value 5.9. Note the decrease in pH at pH=6.7.

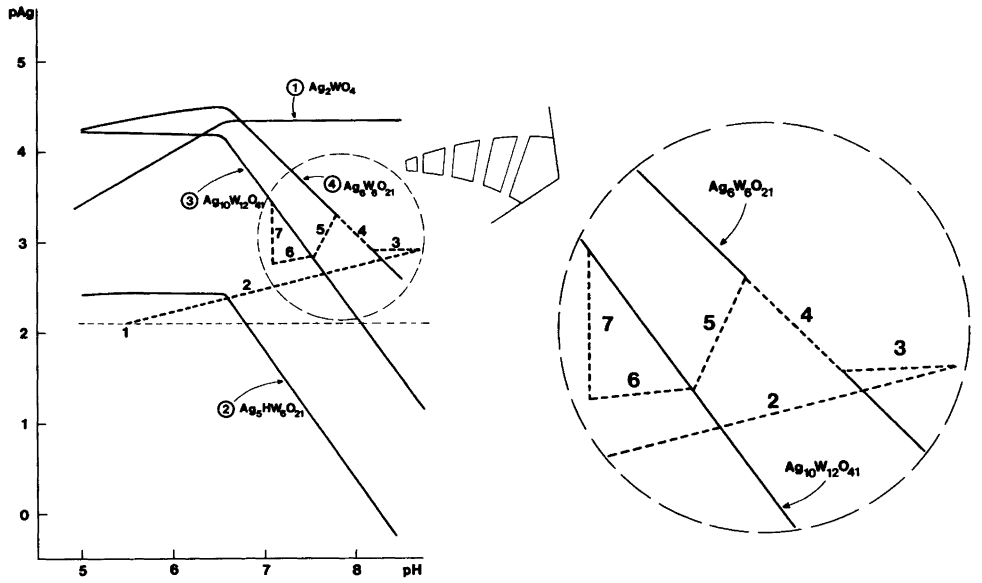

Fig. 10. Calculated saturation concentrations of silver ions corresponding to four different sparingly soluble silver tungstate compounds [eqns. (9)–(12)] as a function of pH. The solubility products of the silver tungstate compounds are estimated from experimental data.

Fig. 10. The position of 4 is restrained to lie between curve 1 and curve 3 for pH>7. In Fig. 10, L_{11} is selected to be 10^{-32}. Fig. 5 shows that the precipitate from period 6 (two upper pictures) consists of rod-shaped crystals. No traces of Ag_2WO_4-crystals (shown on the two lower pictures) can be seen. The two middle pictures show that the rod-shaped crystals are not stable (under the present pH-values) but dissolve into smaller crystals. The final result of this process is pure Ag_2WO_4-crystals (two lower pictures).

In order to interpret these results in accordance with the proposed equilibria (9)–(12) we shall assume that the sparingly soluble silver tungstate compounds formed according to these equilibria do not exist as monomers in acidic medium but are built together in a polymer structure (forming rod-shaped crystals). In alkaline medium the polymer structure breaks down (slowly) under formation of the monomer compounds. Utilizing the results from Table 1, it must be concluded that the polymer is built up mainly of Ag_2WO_4-units. This again means that only small amounts of $Ag_5HW_6O_{21}$, $Ag_{10}W_{12}O_{41}$ and $Ag_6W_6O_{21}$ are formed during the dissolution of the polymer. However, it must be emphasized that the pure existence of these compounds is enough to create a silver ion concentration different from that defined by pure Ag_2WO_4.

The precipitation is initiated in acidic medium (Fig. 2), so it must be expected that the rod-shaped crystals are created at the initial stage of the reaction. According to this a semi-quantitative consistent explanation of the reactions * shown in Fig. 2 can be given with simultaneous reference to Fig. 10. The progress of the reaction is divided into seven periods indicated by the numbers 1 to 7 on both figures. These periods shall be discussed separately.

Period 1. Registration of pAg and pH in an aqueous nitrate–sodium nitrate solution.

Period 2. The protolytic equilibria (2)–(5) are established and the precipitation reactions (9)–(12) occur from left to right, immediately followed by a polymerization of the precipitate.

Period 3. Due to the high pH-value, the polymer will start to dissolve and reactions (9)–(11) occur from right to left. At the end of this period the system can be described with a point on the saturation curve 4 for $Ag_6W_6O_{21}$.

Period 4. The polymer still dissolves. Reactions (9) and (10) occur from right to left and reaction (11) occurs from left to right. The system moves along the saturation curve for $Ag_6W_6O_{21}$. (According to Buchholz[3] practically no further precipitation of Ag_2WO_4 occurs.)

Period 5. Reactions as in period 4, but reactions (9) and (10) are now "faster" than reaction (11), so an increase in the concentration of silver ions is observed and the system moves from curve 4 to curve 3 (precipitation curve for $Ag_{10}W_{12}O_{41}$). The system "delays" a short time on curve 3. This is visualized by the very small shoulder seen in Fig. 2a between periods 5 and 6.

Period 6. The polymer still dissolves and is still the main component as can be seen from Fig. 5. The results from Table 1 seem to indicate that the polymer here mainly consists of Ag_2WO_4-units. The following reactions are proposed:

Reaction (9) occurs from right to left and reactions (10)–(12) occur from left to right. The dissolution of $Ag_5HW_6O_{21}$ goes "faster" than the precipitation of $Ag_{10}W_{12}O_{41}$, $Ag_6W_6O_{21}$ and $AgWO_4$ so a decrease in both pAg and pH is observed. At the end of this period $Ag_5HW_6O_{21}$ is completely dissolved so that in:

Period 7. Reactions (10) and (11) occur from left to right and the system will move towards the saturation curve for $Ag_{10}W_{12}O_{41}$. The results from Table 1 say that the average composition of the precipitate from the start of this period is almost identical with the average composition of the precipitate from period 6. At the end of this period the precipitate probably consists of a mixture of $Ag_{10}W_{12}O_{41}$, $Ag_6W_6O_{21}$ and pure Ag_2WO_4. We know that the reactions continue until the precipitate consists of pure Ag_2WO_4.

CONCLUSIONS

Since the appearance of the paper of Zettnow[17] concerning the precipitation of silver tungstate from sodium tungstate–silver nitrate solutions, only little attention has been paid to explain the reaction mechanism of this reaction.[1–6] The complexity of the reaction is illustrated by Fig. 2 in this paper. We found the behaviour of the silver ion concentration in the solution during

* By the term "consistent explanation" we mean an explanation consistent with our experimental results and the protolytic equilibria from literature. Other "consistent explanations" might probably exist.

the precipitation very strange. In order to explain the experimental results shown in Fig. 2 and the following figures, we were forced to operate with the theory that the precipitate consists of a mixture of silver tungstate components of which one should have a polymer structure. Based on reported protolytic equilibria the following sparingly soluble silver tungstates are assumed to be formed: $Ag_5HW_6O_{21}$, $Ag_6W_6O_{21}$, $Ag_{10}W_{12}O_{21}$, Ag_2WO_4 and a polymer which, according to Table 1, can be given the formula $(Ag_{1.93}WO_4)_n$. The relations between these compounds are given by (9)–(12). Previously it has been reported[7] that at the final step of the precipitation reactions the precipitate consists of pure Ag_2WO_4.

Acknowledgements. Thanks are due to lektor Torben Knudsen, *Instituttet for Mineralindustri,* lektor R. Norbach Nielsen and Inger Søndergaard, *Instituttet for Metallære,* for valuable technical assistance and discussions during the X-ray measurements and electron microscopy. Civ.ing. Keld West, *Fysisk-Kemisk Institut,* has carried out the sodium determinations. The authors also thank civ. ing. Ole Lindegaard Knudsen for advice and skilled technical assistance and lektor O. V. Glistrup, *Fysisk-Kemisk Institut,* for assistance in making Fig. 4.

REFERENCES

1. Pan, K. *J. Chin. Chem. Soc. Taipei 1* (1954) 1.
2. Britton, H. T. S. and German, W. L. *J. Chem. Soc. 2* (1934) 1156.
3. Buchholz, E. *Z. Anorg. Allg. Chem. 244* (1940) 149.
4. Weiner, R. and Boriss, P. *Z. Anal. Chem. 168* (1959) 195.
5. Saxena, R. S. and Gupta, C. M. *J. Sci. Ind. Res. Hardwar India B 17.* (1958) 505.
6. Varughese, K. and Rao, K. S. *Anal. Chim. Acta 57* (1971) 219.
7. Jensen, J. B. and Buch, J. R. S. *Acta Chem. Scand. A 34* (1980) 99.
8. Jander, G. and Heukeshoven, W. *Z. Anorg. Allg. Chem. 187* (1930) 60.
9. Rosenheim, A. and Wolff, A. *Z. Anorg. Allg. Chem. 193* (1930) 47.
10. Vallance, R. H. and Pritchett, E. G. K. *J. Chem. Soc.* (1934) 1586.
11. Buchholz, E. *Z. Anorg. Allg. Chem. 244* (1940) 168.
12. Jander, G. and Krüerke, U. *Z. Anorg. Allg. Chem. 265* (1951) 244.
13. Freedman, M. L. *J. Am. Chem. Soc. 80* (1958) 2072.
14. Szarvas, P. and Kukri, E. C. *Z. Anorg. Allg. Chem. 305* (1960) 55.
15. Duncan, J. F. and Kepert, D. L. *J. Chem. Soc.* (1962) 205.
16. Arnek, R. and Sasaki, Y. *Acta Chem. Scand. A 28* (1974) 20.
17. Zettnow, E. *Pogg. Ann. 130* (1867) 16 and 241.

Received December 9, 1983.

Acta Chemica Scandinavica A 37 (1983) 631–638

The Complex Formation between Nickel(II) and 2-Aminoacetamidoxime and Its *N*-Methylated Derivatives

HEIKKI SAARINEN, MARJATTA ORAMA, TUOVI RAIKAS and JORMA KORVENRANTA

Division of Inorganic Chemistry, University of Helsinki, SF-00100 Helsinki 10, Finland

The complex formation equilibria of nickel(II) with 2-aminoacetamidoxime *1*, 2-(methylamino)acetamidoxime *2* and 2-(dimethylamino)-acetamidoxime *3* have been studied in 1.0 M $Na(ClO_4)$ medium at 25 °C by potentiometric titrations with the use of a glass electrode. Experimental data collected from acid, neutral and weakly alkaline solutions were analyzed with respect to the complexes formed and their stability constants using the least-squares computer program MINIQUAD. With ligands *1* and *2*, nickel(II) forms octahedral stepwise complexes $Ni(HL)^{2+}$, $Ni(HL)_2^{2+}$, $Ni(HL)_3^{2+}$, and a square-planar complex $Ni(HL)L^+$ with the intramolecular O···O hydrogen bridge between the oxime oxygen atoms. Data for system *3* can be explained with the octahedral mononuclear binary complexes $Ni(HL)^{2+}$, $Ni(HL)_2^{2+}$ together with the hydrolytic ternary species $H_{-1}Ni(HL)_2^+$ and $H_{-6}Ni_4(HL)_4^{2+}$.

The metal complexes of different oxime ligands in the solid state as well as in aqueous solution have been described in several reports from this laboratory. The investigation has now been extended to include the nickel(II) complexes formed with 2-aminoacetamidoxime *1* and with two of its derivatives containing one *2* and two *3* methyl groups on the amine nitrogen.

The amidoxime group is capable of binding metal ions as such or in the form of the amidoximate anion and can behave as bidentate ligand through the amide nitrogen and oxime oxygen (or nitrogen) atoms. The colour reactions of this grouping with several transition metals were already noted in the early days of coordination chemistry.[1] However, when the amidoxime ligand contains an additional –NRR′ donor site allowing a five-membered chelate ring *via* the amine nitrogen to be formed, the second coordinating atom can be either the oxime nitrogen or the amide nitrogen. In both modes of chelation the stabilities of the complexes would be expected to decrease with increasing *N*-methylation. It could also be presumed that coordination through the oxime nitrogen would easily lead to the formation of a bis complex species with the strong intramolecular hydrogen bridge between the oxime oxygen atoms. Such a bond would stabilize the planar dsp^2 hybridization of nickel(II) and thereby limit the maximum number of binding ligands to two.

In this communication we report the results of a potentiometric study on complex formation equilibria of ligands *1*–*3* with divalent nickel in aqueous 1.0 M $Na(ClO_4)$ medium. During the investigation we also isolated some of these chelates in the solid state and determined their structures by X-ray methods. The details of the X-ray diffraction data will be published in a forthcoming paper. There are apparently no previous reports on the metal complexes formed with these ligand systems.

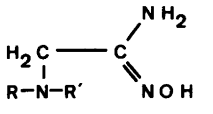

1 R = R′ = H

2 R = H, R′ = CH_3

3 R = R′ = CH_3

EXPERIMENTAL

Ligand preparations. 2-Aminoacetamidoxime *1* was prepared by action of hydroxylamine on

0302-4377/83 $2.50

2-aminoacetonitrile applying the method first described by Tiemann.[2] To a suspension of hydroxylammonium chloride (1.0 mol) and 2-aminoacetonitrile hydrochloride (0.8 mol) in 200 ml of absolute ethanol was slowly added a sodium ethoxide solution (prepared by dissolving 1.8 mole of sodium to *ca.* 500 ml of absolute ethanol) with vigorous stirring. After completion of the reaction the solid sodium chloride was filtered off and the clear colourless solution was stirred for about 48 hours at room temperature. When anhydrous HCl was passed into the solution cooled to 0 °C, *1* was precipitated as its monohydrochloride; yield *ca.* 60 % of the theoretical.

2-(Methylamino)acetamidoxime *2* and 2-(dimethylamino)acetamidoxime *3* were prepared similarly to *1* using 2-(methylamino)acetonitrile hydrochloride and 2-(dimethylamino)acetonitrile, respectively, as starting reagents. Both compounds were obtained in good yields (70–80 %) in the form of their monohydrochlorides. Recrystallizations from hot ethanol gave all three hydrochlorides as white needle-like crystals. Analyses: C, H, N, Cl. The formula weights of the air dried products as determined by potentiometric titrations were 126.1 (calc. 125.6), 139.4 (calc. 139.6) and 153.6 (calc. 153.6) for ligands *1*, *2* and *3*, respectively.

Method. The present investigation was carried out as a series of potentiometric titrations at 25 °C and in a constant 1.0 M $Na(ClO_4)$ medium. The free hydrogen ion concentration, h, was determined by measuring the emf of the cell

$$-RE \mid \text{equilibrium solution} \mid GE+$$

where GE denotes a glass electrode (Beckman, type 40495) and $RE=Hg,Hg_2Cl_2 \mid 0.01$ M Cl^-, 0.99 M ClO_4^-, 1.00 M $Na^+ \mid 1.00$ M $NaClO_4$. Assuming the activity coefficients to be constant, the following expression is valid:

$$E=E_o+59.157 \log h+E_j \quad (1)$$

For each separate titration the electrode system was calibrated against the background electrolyte by means of E_o, E_j-titration, after which the main run was started. For the liquid junction potential we used $E_j=j_h h$; the values of the coefficient j_h varied slightly in different runs and the average value was -60 mV M^{-1}. The changes in the values of E_o caused by the concentration changes during the titrations were considered negligible.

In the binary titrations made to determine acidity constants of the oxime groups it was necessary to obtain potential readings from relatively high $-\log h$ ranges (values of $-\log h$ up to *ca.* 11.8 were used). Employment of the glass electrode under such conditions has often been questioned. However, the value of the ionic product of water ($pk_w=13.74(1)$) obtained during the calculations was found to be in satisfactory agreement with the literature value of k_w valid in 1 M $NaClO_4$ ($pk_w=13.770$)[3] and we considered it unnecessary to replace the glass electrode by a hydrogen electrode, especially since the complex formation reactions studied occurred in consider-

Table 1. Initial total concentrations (10^3 mol/l) of metal (C_M) and ligand (C_L), number of titration points, and rough $-\log h$ ranges used in the calculations.

Ligand	C_M	C_L	No. of points	$-\log h$	Range	Ligand	C_M	C_L	No. of points	$-\log h$	Range
1		13.65	67	2.36	11.72	*2*	4.931	11.09	36	4.38	8.50
		18.26	72	2.68	11.73		4.369	18.46	55	5.13	9.26
		25.00	81	2.44	11.68		4.369	22.61	32	5.69	9.38
		33.23	80	2.50	11.72		3.218	26.32	39	3.62	8.76
	14.98	15.04	23	2.69	4.47		2.434	36.22	32	4.04	8.80
	8.320	16.30	60	2.78	5.97	*3*		10.80	42	2.09	11.66
	4.362	17.18	75	2.75	8.89			13.57	56	2.27	11.73
	4.369	23.61	66	2.82	8.59			16.41	40	2.01	11.63
	6.399	17.60	35	2.87	6.80			20.32	62	1.89	11.73
2		12.54	60	2.19	11.71		10.71	10.84	26	4.77	6.99
		19.31	71	2.49	11.75		2.623	27.34	48	4.32	8.84
		25.38	78	2.25	11.80		2.633	17.97	48	4.67	8.82
		27.31	82	2.07	11.78		3.404	14.40	42	4.84	8.81
	12.59	12.55	24	3.93	5.73		4.522	14.08	34	4.70	8.85
	9.339	13.98	34	3.90	7.03		5.763	11.67	40	4.69	8.86
	8.334	17.34	48	3.86	8.31		7.388	8.734	21	4.91	7.41

ably lower $-\log h$ regions. Thus the inaccuracy in the values of the NOH acidity constants could hardly lead to erroneous selection of the complex models.

During the measurements h was varied by adding hydroxide or hydrogen ions to the solution. The compositions of the starting solutions, number of the titration points, and the $-\log h$ ranges used in the calculations are quoted in Table 1. The upper limits of the reactants and the $-\log h$ ranges in the metal-ligand systems were largely determined by formation of precipitates or by very slow attainment of equilibria.

Data treatment. In evaluating the equilibrium constants, H^+, Ni^{2+} and HL (the neutral oxime) were chosen as components. The general three-component equilibrium (2) and the two-component equilibria (3–5) are the following:

$$pH^+ + qNi^{2+} + r(HL) \rightleftharpoons (H^+)_p(Ni^{2+})_q(HL)_r;\ \beta_{pqr} \quad (2)$$

$$nH^+ + HL \rightleftharpoons (H^+)_n(HL);\ \beta_{n01},\ n=1,2 \quad (3)$$

$$HL \rightleftharpoons L^- + H^+;\ k_a \quad (4)$$

$$pH^+ + qNi^{2+} \rightleftharpoons (H^+)_p(Ni^{2+})_q;\ \beta_{pq0} \quad (5)$$

For the binary hydrolytic equilibrium (5) we used the results summarized by Baes and Mesmer.[4] Inclusion of the proposed complexes and equilibrium constants (recalculated values valid in 1 M $NaClO_4$) in the calculations showed that the Ni^{2+} hydrolysis was negligible in our conditions. Since the ligands were added to the titration solution as their hydrochlorides the formation of the chloro complexes of nickel had also to be taken into consideration. On the basis of known weakness of these complexes[5] and the low concentrations of Cl^- in our solutions it can be estimated that no significant amounts of $(H^+)_p(Ni^{2+})_q(HL)_r(Cl^-)_s$ species were formed.

The calculational problem is to find the sets of pqr that best explain the experimental data. The search for the best model was made with the least-squares computer program MINIQUAD,[6] which minimizes the sum of the squares of residuals, $U=\Sigma(\Delta C_M^2+\Delta C_L^2+\Delta C_H^2)$, where C_M, C_L and C_H are the total molar concentrations of metal, ligand and proton, respectively. The computational work was performed on a Univac 1108 computer.

CALCULATIONS AND RESULTS

The H^+-ligand systems. In the concentration ranges used in the measurements no association products were found and each of the separate systems could be well explained in terms of the equilibrium constants β_{101}, β_{201} and k_a. The results are presented in Table 2. Although the calculated standard deviations even in the constants referring to the oxime dissociations were relatively low, the experimental technique used does not permit accurate measurements in alkaline solutions. Very wide error limits have therefore been estimated for the values given for the constant k_a. To facilitate comparisons between the different acid functions of the ligands, the stepwise protonation constant k_2 has been included in Table 2. In subsequent calculations all the ligand-proton equilibria were assumed to be exactly known and no attempts were made to adjust the corresponding equilibrium constants.

The H^+–Ni^{2+}–ligand 1 system. The analysis of the data was begun with construction of the Bjerrum plot, $\bar{n}(\log[HL])$, shown in Fig. 1. At sufficiently low $-\log[HL]$ values the data can reasonable be explained by formation of the stepwise mononuclear complexes $Ni(HL)_n^{2+}$ with $n=1-3$. At higher $-\log h$ values (>5.5), the titration solutions change from pale green to orange with increasing basicity. The data points

Table 2. Values of the proton–ligand equilibrium constants relating to the reactions (3)–(4). The errors $3\sigma(\log\beta_{n01})$ are given for $\log\beta_{101}$ and $\log\beta_{201}$. The error estimated for $\log k_a$ corresponds to *ca.* $10\sigma(\log k_a)$.

	Ligand *1*	Ligand *2*	Ligand *3*
$\log\beta_{101}$	7.942±0.004	8.260±0.007	7.606±0.005
$\log\beta_{201}$	10.409±0.006	10.372±0.012	9.365±0.009
$\log k_a$	−12.5 ±0.1	−12.4 ±0.1	−12.3 ±0.1
*$\log k_2$	2.467	2.112	1.759

* $\log k_2=\log\beta_{201}-\log\beta_{101}$

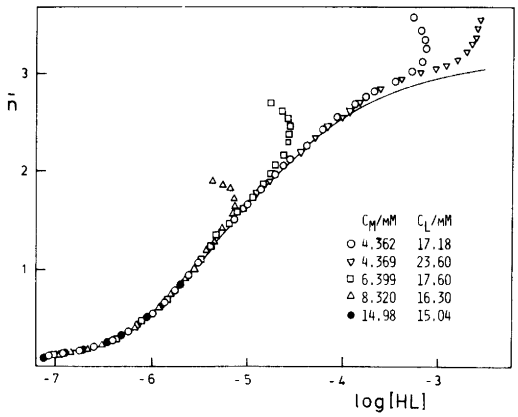

Fig. 1. Experimental data for ligand *1* plotted as curves $\bar{n}(\log[HL])$. In order to make the figure clear only part of the data points used in the calculations have been plotted.

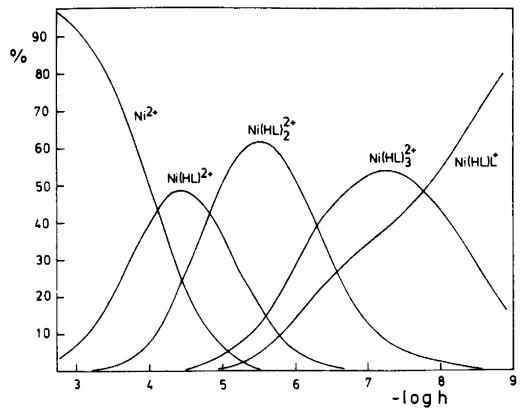

Fig. 2. Percentage distribution of nickel among various species in the Ni^{2+}-ligand *1* system with C_M=4.362 mM and C_L=17.18 mM.

no longer fall on a single curve, indicating the presence of deprotonated or polynuclear complex species. Since the $Ni(HL)_n^{2+}$ compexes clearly possessed acidic properties and the formation of planar bis complex was expected, a complex model comprising species $Ni(HL)^{2+}$, $Ni(HL)_2^{2+}$, $Ni(HL)_3^{2+}$ and $H_{-1}Ni(HL)_2^{+}$ was tested using the complete data set (Table 1, 259 experimental points). The results are given in Table 3. The low error squares sum indicated a very satisfactory fit. Since the standard deviations in the constants are relatively low $[3\sigma(\log\beta_{pqr}) \leq 0.02]$ and all the complexes occur in great amount (Fig. 2), we regard them as well established.

Further analysis showed the detection of any other deprotonated complex species besides $H_{-1}Ni(HL)_2^{+}$ in the system to be impossible. The same was true for all the polynuclear species tested. We then concluded that the experimental data are describable in terms of the complexes $Ni(HL)^{2+}$, $Ni(HL)_2^{2+}$, $Ni(HL)_3^{2+}$ and $H_{-1}Ni(HL)_2^{+}$ alone, with the equilibrium constants given in Table 3.

The limiting factor for these complex formation studies was the relatively low solubility of the perchlorate salt of $H_{-1}Ni(HL)_2^{+}$, and most of the titrations were ended by the appearance of an orange-coloured NiL_2HClO_4 precipitate. Limited concentration ranges had therefore to be used in the measurements.

The $H^+-Ni^{2+}-$ligand 2 system. The essential features of the complex formation with this ligand are largely the same as with ligand *1*. The $\bar{n}(\log[HL])$ plot is given in Fig. 3. The MINIQUAD analysis showed that the same complex species as for ligand *1* could explain the 300 data points in Table 1 fairly well.

A representative distribution diagram of the complexes is shown in Fig. 4. In this system $Ni(HL)_3^{2+}$ was found only as a minor species in most of our titrations, and even at the highest

Table 3. Final values of the complex formation constants relating to the reaction (2). The errors given are $3\sigma(\log\beta_{pqr})$.

	Ligand *1*	Ligand *2*	Ligand *3*
$\log\beta_{011}$	5.720±0.005	5.253±0.004	3.979±0.004
$\log\beta_{012}$	10.843±0.007	9.505±0.007	5.52 ±0.02
$\log\beta_{013}$	14.74 ±0.02	11.88 ±0.08	
$\log\beta_{-121}$	4.27 ±0.02	2.406±0.006	−3.24 ±0.05
$\log\beta_{-644}$			−26.77 ±0.02

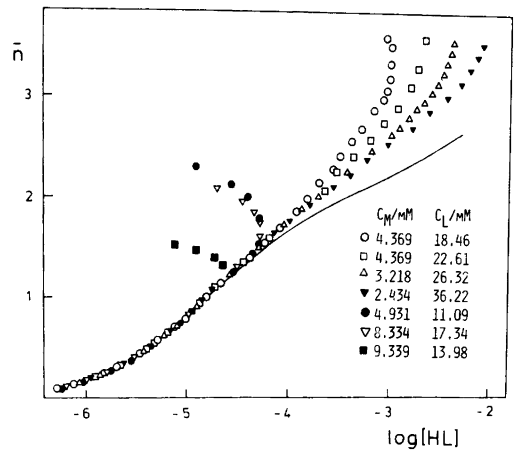

Fig. 3. A part of the experimental data for ligand *2* plotted as curves $\bar{n}(\log[HL])$.

ligand–metal ratio (15:1) the maximum concentration of $Ni(HL)_3^{2+}$ was only 20 % of the total nickel concentration. This is also reflected in the relatively large standard deviation in the value of $\log\beta_{013}$.

The H^+–Ni^{2+}–ligand 3 system. The behaviour of ligand *3* towards nickel ions deviates significantly from that of ligands *1* and *2*. This is already noticed in the colour of the solutions which gradually change from green-blue to green-brown, as $-\log h$ is raised. There is no sign of the orange colour found in the previous system. With this ligand the reactions at quotients $C_L/C_M<2$ and $C_H<0$ (the zero level of the ligand was calculated according to HL) were extremely slow and the achievement of stable potential readings remained uncertain. When such titrations were performed batchwise using a series of bottles, it was found that after a few days the solutions turned cloudy and the corresponding titration points had to be omitted in the calculations.

The Bjerrum plot is shown in Fig. 5. At low values of [HL] the function $\bar{n}(\log[HL])$ seems to be independent of C_M and C_L and refers to the formation of the mononuclear complexes $Ni(HL)^{2+}$ and $Ni(HL)_2^{2+}$. When the data fulfilling these conditions were treated separately using 216 data points from 7 different titrations the MINIQUAD analysis gave an entirely satisfactory fit and yielded the following formation constants with their standard deviations (3σ): $\log\beta_{011}=3.978\pm0.003$ and $\log\beta_{012}=5.595\pm0.018$. The values of these constants were assumed to be known during the search for the additional complexes and were not varied until the final calculations.

The shape of the titration curves indicated that the system must contain hydrolytic complex species. A noticeable inflection point which appeared on each of the titration curves when C_H/C_M approached –1.5 further indicated that these complexes cannot be mononuclear. This

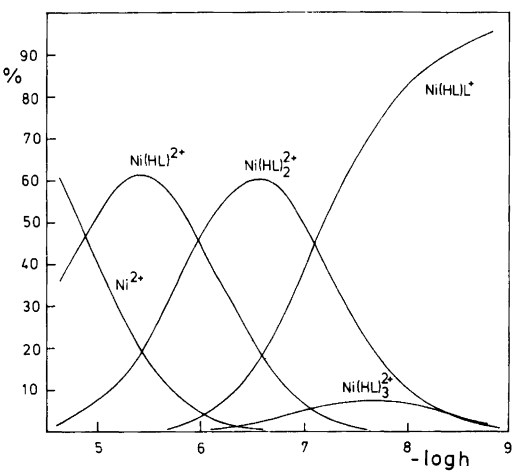

Fig. 4. Percentage distribution of nickel among various species in the Ni^{2+}-ligand *2* system with $C_M=4.369$ mM and $C_L=18.46$ mM.

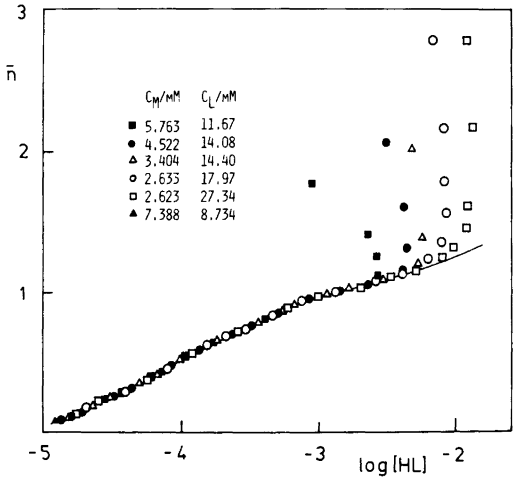

Fig. 5. A part of the experimental data for ligand *3* plotted as curves $\bar{n}(\log[HL])$.

was confirmed in the calculations, in which hydrolysis of $Ni(HL)^{2+}$ to $H_{-1}Ni(HL)^{+}$ or $Ni(HL)_2^{2+}$ to $H_{-1}Ni(HL)_2^{+}$ could not be traced.

The following search for the best complexes to describe the remaining experimental data was started with the simple hypothesis that in addition to $Ni(HL)^{2+}$ and $Ni(HL)_2^{2+}$ only one predominant complex was present. The error squares sum U was taken as the criterion for the best explanation. It was soon found that by far the best fit of the experimental data was obtained if the complex formed up to the inflection point mentioned had the stoichiometric relation H^+:Ni^{2+} equal to -3:2. The calculations fulfilling this condition are summarized in Fig. 6, and it is found that the lowest value of U is obtained for the tetranuclear complex $H_{-6}Ni_4(HL)_4^{2+}$. All the data in Table 1, in fact, proved to be quite satisfactorily described by assuming the complex species $Ni(HL)^{2+}$, $Ni(HL)_2^{2+}$ and $H_{-6}Ni_4(HL)_4^{2+}$ alone. There were, however, systematic drifts in the magnitudes of the residuals ΔC_H and ΔC_L in the regions where C_H approaches zero and the χ^2-statistics[6] were unsatisfactory. This clearly pointed to the presence of one or more additional complexes. Using a systematic trial and error procedure we found that the best single complex was $H_{-1}Ni(HL)_2^{+}$. Although the maximum pre-

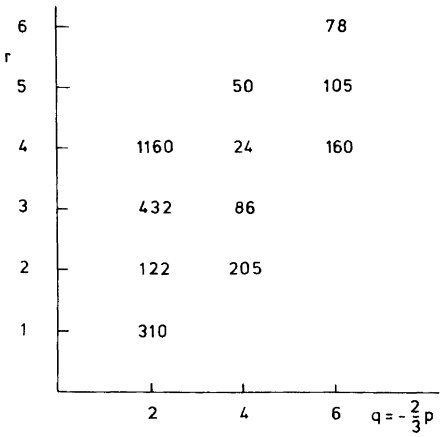

Fig. 6. Search for the ternary $H_pNi_q(HL)_r^{p+2q}$ complex with HL=*3* assuming $q = -\frac{2}{3}p$. The diagram gives the error square sum $U(qr)_p \times 10^{-8}$ assuming one new complex. The calculations are based on 214 points chosen to cover as great a concentration range as possible. The nickel(II) hydrolysis and the complexes $Ni(HL)^{2+}$ and $Ni(HL)_2^{2+}$ are supposed to be known.

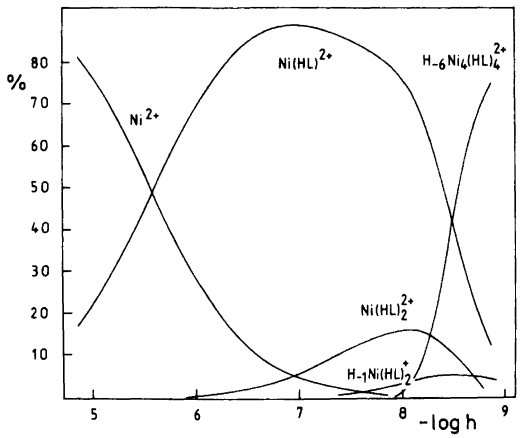

Fig. 7. Percentage distribution of nickel among various species in the Ni^{2+}-ligand *3* system with C_M=3.404 mM and C_L=14.40 mM.

sence of this new species was only 13 % relative to the total nickel concentration, its inclusion in the complex model resulted in an error squares sum 66 % lower than with only three complexes present. At the same time χ^2 improved dramatically from 216 to 19. This implies that there are no obvious systematic errors left in the data. Since the remaining effects seemed to be too small to justify a more detailed analysis, we propose, for inclusion in the final complex model, the species $Ni(HL)^{2+}$, $Ni(HL)_2^{2+}$, $H_{-1}Ni(HL)_2^{+}$ and $H_{-6}Ni_4(HL)_4^{2+}$ with the formation constants given in Table 3. A distribution diagram of the complexes in one of the titrations is shown in Fig. 7.

DISCUSSION

The values of the stepwise protonation constants in Table 2 show that the ligands are moderately strong bases as regards the addition of the first proton to HL, while the species H_2L^+ show no significant basicity. The obvious resonance of the oxime group with the adjacent amide group makes it clear that the values β_{101} refer to the protonation of the amine nitrogens and the values of k_2 to the protonation of the amide nitrogens.

Examination of the effects of *N*-substitution on the different protonation reactions shows that the basic strengths of the ligands do not strictly follow the number of the methyl groups: the

order of ligands with increasing k_2 is *3<2<1* while the order with increasing β_{101} is *3<1<2*. These trends are also found for the corresponding ethylenediamine compounds,[7] and can be attributed mainly to the inductive effect (+I) of the alkyl substituents and to reduction of hydrogen bonding.[8]

From the complex formation data the existence of the species $Ni(HL)^{2+}$ and $Ni(HL)_2^{2+}$ was established for all three ligands studied. The species $Ni(HL)_3^{2+}$ was also found in systems *1* and *2* but not in *3*. The decrease of the complex stabilities of these successive complexes with increasing *N*-substitution is clearly seen in the values of the formation constants in Table 3. It can be judged that with ligand *1* all three complexes are readily formed, with *2* formation of the tris complex is considerably hindered, and with *3* the tris complex is not formed at all and the bis complex only with great difficulty. These substituent effects are somewhat greater than those found for *N*-methylated ethylenediamines[7] but they clearly demonstrate the participation of the amine nitrogen atoms in the coordination.

The potentiometric data do not directly indicate which of the remaining nitrogen atoms is involved in the coordination. The more negative character of the oxime group would nevertheless suggest that the oxime nitrogen has the preference. Strong support of this hypothesis is provided by the solid state complexes. During the investigation we isolated the $Ni(HL)_2^{2+}$ complexes of ligands *1* and *3* as chlorides in the crystalline state and determined their structures by X-ray methods. For ligand *1* the compound analysed was $[Ni(HL)_2(H_2O)_2]Cl_2$ and the following centrocymmetric *trans*-octahedral coordination was found:

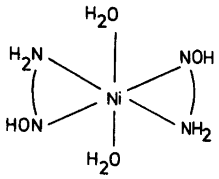

The same chelating groups are also present in the structure of $[Ni(HL)_2(H_2O)_2]Cl_2 \cdot H_2O$ formed by *3* but here the coordination about nickel proved to be *cis*-octahedral.

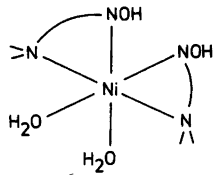

In summary, we find it credible that the aqueous $Ni(HL)_n^{2+}$ complexes are all octahedral and coordination is through the oxime nitrogen and amine nitrogen atoms.

The species $H_{-1}Ni(HL)_2^+$ was found in all the present systems. With ligands *1* and *2* it is orange coloured, occurs in great amounts and usually represents the final product in the alkalimetric measurements. In system *3*, in contrast, $H_{-1}Ni(HL)_2^+$ is of uncertain colour and only a minor species. Thus even its real existence can be questioned.

It is evident that the complex $H_{-1}Ni(HL)_2^+$ with HL=*1* and *2* is square-planar with the following structure:

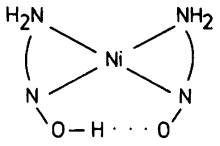

The proof for this complex moiety was obtained from X-ray analysis of solid $[Ni(HL)L]Cl \cdot 1\frac{1}{2}H_2O$, where HL is *1*. This orange complex was obtained from a neutral solution where $H_{-1}Ni(HL)_2^+$ was known to be the predominant species. The same characteristic colour of the complex in the solid state strongly argues for the presence of a like coordination of nickel in the liquid and solid states.

In the structure of $Ni(HL)L^+$ there is still one dissociable proton left, and one could assume the existence of the species NiL_2 in solution of sufficient alkalinity. Under the conditions used in our measurements no such complexes were found, however. This is probably because the intramolecular hydrogen bond formed between the oxime oxygen atoms is very strong (O···O distances usually below 2.5 Å),[9] with the result that the acidities of the $Ni(HL)L^+$ complexes must be very weak.

It is of interest to note that the formation of square-planar bis complexes does not prevent the co-existence of octahedral tris complexes in

suitable solutions. Figures 2 and 4 show that, as $-\log h$ is raised, the sequence of the complex formation can be different: in system *1* the species $Ni(HL)L^+$ starts to form after the formation of the tris complex, whereas in system *2*, where $Ni(HL)L^+$ is considerably lower in stability, the situation is the reverse.

For ligand *3* two ternary complexes of composition $H_{-1}Ni(HL)_2^+$ and $H_{-6}Ni_4(HL)_4^{2+}$ are proposed. Possibly the structure of the minor complex $H_{-1}Ni(HL)_2^+$ is not the same as for ligands *1* and *2*. This is already suggested by the acidity constants calculated from Table 3 for the different $Ni(HL)_2^{2+}$ complexes: the pK_a-value with ligand *3* (8.76) is considerably higher than with ligands *1* (6.57) and *2* (7.10).

A look at the molecular models of the complexes shows that the spatial requirements of the two adjacent $(CH_3)_2N$ groups of *3* make it impossible, without considerable strain in the molecule, to construct a planar $Ni(HL)L^+$ complex containing the intramolecular O···O hydrogen bond. Evidently complex $H_{-1}Ni(HL)_2^+$ with ligand *3* is still octahedral. In the same way the tendency of *3* toward polymerization reactions could be understood to originate from steric factors.

The low standard deviation in the value of the formation constant of the dominating ternary species $H_{-6}Ni_4(HL)_4^{2+}$ ($3\sigma(\log\beta_{-644}=0.02$) allows it to be regarded as well established. We cannot, however, suggest any plausible scheme for its formation from simple components and, in principle, it is possible that $H_{-6}Ni_4(HL)_4^{2+}$ represents only a kind of one-parameter approximation of a more complicated system. The uncertainty is mainly due to the necessary omission of titration points at low C_L/C_M ratios from the calculations and thus the limited amount of experimental data.

Since we have not been successful in our attempts to prepare a suitable crystal of the tetranuclear compound for X-ray analysis, suggestions for the actual structure of $H_{-6}Ni_4(HL)_4^{2+}$ will be highly speculative. The often found connection between the compositions of the ternary hydrolytic complexes and binary hydroxo species of the metal[10–15] would suggest the formula $Ni_4(OH)_4(HL)_2L_2^{2+}$, but an equally plausible formula is $Ni_4L_2(L-H)_2^{2+}$ which would denote that two of the amidoxime NH_2 groups are deprotonated and involved in the coordination in the form of the negative $-NH^-$ anion. Such a coordination has recently been found in a solid tetrameric copper(II) complex formed by *3*.[16]

REFERENCES

1. Eloy, F. and Lenaers, R. *Chem. Rev. 62* (1962) 155.
2. Tiemann, F. *Ber. 17* (1884) 126.
3. Näsänen, R. and Paakkola, K. *Suom. Kemistil. B 34* (1961) 20.
4. Baes, C. F. and Mesmer, R. E. *The Hydrolysis of Cations,* Wiley, New York 1976, p. 246.
5. Sillén, L. G. and Martell, A. E. (compilers), *Stability Constants of Metal-Ion Complexes, Chem. Soc.* London, Spec. Publ. No. 17 (1964) and No. 25 (1971).
6. Gans, P., Vacca, A. and Sabatini, A. *Inorg. Chem. Acta 18* (1976) 237.
7. Näsänen, R., Koskinen, M., Tilus, P. and Ilomäki, A. *Suom. Kemistil. B 43* (1970) 34.
8. King, E. J. *Acid-base Equilibria,* Pergamon, Oxford 1965, p. 151.
9. Fair, C. K. and Schlemper, *Acta Crystallogr. B 34* (1978) 436.
10. Forsling, W. *Acta Chem. Scand. A 32* (1978) 857.
11. Sjöberg, S. *Acta Chem. Scand. 27* (1973) 3721.
12. Forsling, W. *Acta Chem. Scand. A 31* (1977) 759.
13. Sjöberg, S. *Acta Chem. Scand. A 31* (1977) 729.
14. Öhman, L-O. and Sjöberg, S. *Acta Chem. Scand. A 36* (1982) 47.
15. Granberg, I. and Sjöberg, S. *Acta Chem. Scand. A 35* (1981) 193.
16. Korvenranta, J. and Saarinen, H. *Unpublished results.*

Received December 15, 1982.

Acta Chemica Scandinavica A 37 (1983) 639–645

Copper(II) Catalysed Oxidation of Hydroxylamine. A Kinetic Study of the Reaction between Vanadium(V) and Hydroxylamine in Strongly Acid Solutions

GÖSTA BENGTSSON

Inorganic Chemistry 1, Chemical Center, University of Lund, P.O.B. 740, S-220 07 Lund 7, Sweden

The previous kinetic studies of the oxidation of hydroxylamine by vanadium(V) in strongly acid solutions have been continued by a corresponding study of this reaction in the presence of copper(II), acting as a catalyst with only a moderate catalytic effect. The experimental rate law of the catalysed reaction is analogous to that of the uncatalysed reaction, *i.e.*

$$-d[VO_2^+]/dt = k[VO_2^+][NH_3OH^+] + k'[VO_2^+]^2[NH_3OH^+]$$

Both rate constants increase with increasing copper(II) concentration and finally reach limiting values such that $k_{lim}/k_0=3$ and $k'_{lim}/k'_0=2$ (index 0 represents [Cu(II)]=0). At the same time, the stoichiometry increases to the limiting value $\Delta[VO_2^+]/\Delta[NH_3OH^+]=2.0$. The limiting values of both the stoichiometry and the rate constants are attained at much lower copper(II) concentrations in the presence of chloride ions or bromide ions than in the absence of halide ions.

A reaction mechanism of the catalysed reaction, giving a reasonable interpretation of the experimental results, is proposed. This includes the same initial steps as those of the uncatalysed reaction, *i.e.* a rapid reversible complex formation between the reactants, followed by two parallel slow electron transfer steps. In the catalysed reaction, these are followed by rapid reactions between copper(II) and nitrogen-containing intermediates. At sufficiently large copper(II) concentrations, all intermediates formed in the slow reaction steps are oxidised by copper(II). The copper(I) formed is reoxidised by vanadium(V).

0302-4377/83 $2.50

Previous studies[1–3] of the reaction between hydroxylamine and vanadium(V) in strongly acid solution ($[H^+]=0.005-1.0$ M) have shown that this reaction is slow, yields vanadium(IV) and dinitrogen and probably some dinitrogen oxide, and for $[H^+]\geq 0.2$ M obeys the rate equation

$$-d[VO_2^+]/dt = k[VO_2^+][NH_3OH^+] + k'[VO_2^+]^2[NH_3OH^+]$$

At lower hydrogen ion concentrations the reaction is still slow, but the kinetics become more complicated.[3] Within the hydrogen ion concentration range of these studies, vanadium(V) is present as VO_2^+ and hydroxylamine as hydroxylammonium ion NH_3OH^+.[2,4,5] The studies at $[H^+]=0.2-1.0$ M[1,2] indicate a mechanism with a rapid, reversible complex formation between VO_2^+ and NH_3OH^+ followed by two parallel rate-determining electron transfer reactions. The k term of the rate law might be supposed to correspond to the reaction path yielding dinitrogen, and the k' term to the one yielding dinitrogen oxide. The rate of nitrogen gas evolution and the fact that the stoichiometry $\Delta[VO_2^+]/\Delta[NH_3OH^+]$ *decreases* with increasing initial vanadium(V) concentration indicate, however, that nitrogen gas is formed also in the reaction path corresponding to the third order term, possibly as a result of the reaction between an intermediate in this reaction series and NH_3OH^+.

According to Gowda *et al.*[6] the rate of the

oxidation of hydroxylamine by vanadium(V) is increased by the addition of copper sulfate to solutions being 5–6 M with respect to hydrochloric acid. In these catalytic reactions, dinitrogen oxide is the only product emanating from hydroxylamine, while in the absence of copper(II) one obtains a mixture of nitrogen gas and dinitrogen oxide. These observations indicate that a kinetic study of the copper(II) catalysed reaction might give some further information about the mechanism of the oxidation of hydroxylamine with vanadium(V).

EXPERIMENTAL

The chemicals used were of the same kind and quality as those described in Refs. 1–3, *i.e.* vanadium pentoxide, hydroxylammonium chloride (Riedel de Haën), hydroxylammonium sulfate (Merck), perchloric acid and sodium perchlorate, all of analytical grade. So were the methods used to prepare stock solutions and to determine the concentrations of these.

Besides the chemicals used previously the following ones were also used in this study: Copper perchlorate, $Cu(ClO_4)_2 \cdot 6H_2O$ (G. Frederick Smith Chemical Co., Columbus, Ohio) for the preparation of copper(II) stock solutions. The copper concentrations of these were determined electrogravimetrically or by a spectrophotometric method. In the latter, the absorbance of a sample of the solution to be analysed was measured at the wavelength 610 nm in the presence of 5 M ammonia (molar absorption coefficient: 53.1 ± 0.1 M^{-1} cm^{-1}). The two methods gave consistent results. Sodium chloride and sodium bromide were used in those measurements in which the effect of halide ions on the reaction rate was investigated.

For one series of measurements, solutions of hydroxylammonium perchlorate were prepared by addition of equivalent amounts of barium perchlorate ($Ba(ClO_4)_2 \cdot 3H_2O$; G. F. Smith Chemical Co.) to hydroxylammonium sulfate solutions and filtering out the barium sulfate precipitated. These solutions gave within the experimental error limits the same results as hydroxylammonium sulfate solutions. Also the chemicals described here were of analytical grade.

The kinetic and stoichiometric measurements were carried out spectrophotometrically using a Zeiss PMQ II Spektralphotometer, mainly at the wavelength 340 nm. Some kinetic measurements (with the vanadium(V) concentration 0.2–0.4 mM) were, however, carried out at 280 nm. The reactions were initiated by mixing the proper volumes of reactant solutions by pipette or, for more rapid reactions, by means of an all-glass syringe equipped with a device to allow the delivery of a well-defined volume of the solution in question directly into the absorption cell.

Initial rates were evaluated graphically from absorbance *versus* time plots or, for more rapid reactions, reciprocal absorbance *versus* time plots which give a more gentle curvature. In general, the rate did not change appreciably during the first 5 % of a complete run. Every initial rate value given in this paper represents the mean value of 3–5 separate measurements. Rate constants were calculated from linear relationships by means of a least squares program. The error limits given in this paper represent a confidence level of 99.9 %.

The temperature was 25.0 ± 0.1 °C and the ionic strength for most of the measurements 1.0–1.1 M. At copper perchlorate concentrations exceeding 30 mM and when sodium perchlorate, sodium chloride or sodium bromide was added, the ionic strength could be much larger. The effect of minor changes of the ionic strength fell within the normal experimental error limits, whereas major changes had appreciable effects.

SYMBOLS, NOTATIONS, AND EQUATIONS

$M =$ $V(V) = VO_2^+$

$L =$ NH_3OH^+

$C_M =$ overall initial concentration of vanadium(V) ($mol \cdot l^{-1}$). $C_M = [M] + [ML] = [M]\ (1 + \beta_1[L]) \approx [M]\ (1 + \beta_1 C_L)$ where $\beta_1 = 12.5 \pm 0.4$ M^{-1} (*cf.* Ref. 2) is the stability constant of ML.

$C_L =$ overall initial concentration of hydroxylamine ($mol \cdot l^{-1}$). $C_L = [L]\ (1 + \beta_1[M]) \approx [L](1 + \beta_1 C_M)$.

$C_{Cu} =$ overall concentration of copper(II) ($mol \cdot l^{-1}$).

$C_{Cl} =$ overall concentration of chloride ions ($mol \cdot l^{-1}$).

$C_{HClO_4} =$ overall concentration of perchloric acid ($mol \cdot l^{-1}$). Generally, $[H^+] = C_{HClO_4} - C_M$.

$b =$ path length of the absorption cell (cm).

$A =$ absorbance.

ε_M; $\varepsilon_{ML} =$ molar absorption coefficients of the species indicated (M^{-1} cm^{-1}).

$\varepsilon =$ formal molar absorption coefficient of a solution containing both M and ML (M^{-1} cm^{-1}). $\varepsilon = A/bC_M$.

t= time (s).
v_o= initial reaction rate ($M s^{-1}$). $v_o = -(\Delta A/b\varepsilon \cdot \Delta t)_{t=0} = -(\Delta C_M/\Delta t)_{t=0} = -(1+\beta_1[L])\ (\Delta[M]/\Delta t)_{t=0} \approx -(1+\beta_1 C_L)(d[M]/dt)_{t=0}$ $(\Delta A/b\Delta t)_{t=0} = -(A^2\Delta(1/A)/\Delta t)_{t=0}$.
μ= ionic strength ($mol \cdot l^{-1}$).

Indices $_o$, $_t$, and $_\infty$ denote the time after mixing of the reactants.

MEASUREMENTS AND RESULTS

Stoichiometry. The stoichiometry of the reaction was determined by measuring the decrease in absorbance at complete reaction for solutions initially containing both vanadium(V) (in excess, $C_L/C_M \leq 0.4$) and hydroxylamine, as compared to solutions with the same value of C_M but $C_L=0$. The stoichiometry is independent of the proportion between the reactants and of the hydrogen ion concentration ($0.2\ M \leq [H^+] \leq 1.0\ M$). It increases with increasing values of C_{Cu} and finally reaches the limiting value $\Delta C_M/\Delta C_L=2.0$. The results shown in Table 1 have been obtained with hydroxylammonium chloride. A similar trend, and the same limiting value, is obtained with hydroxylammonium sulfate, but the increase is less rapid than in the presence of chloride ions.

Rate equation. The rate law with respect to hydroxylamine and vanadium(V), respectively, was determined by the method of initial rates at different values of C_{Cu}. Fig. 1 shows v_o *versus* C_L at constant C_M for $C_{Cu}=0$ and 24.7 mM, respectively. It can be noted that, at least for low values of C_L, the initial rate is proportional to C_L. Fig. 2 shows $v_o(1+\beta_1 C_M)/C_M$ *versus* C_M at a constant value of C_L for a series of C_{Cu} values. $v_o(1+\beta_1 C_M)/C_M$ is a linear function of C_M, and it appears that both the intercept and the slope increase with increasing values of C_{Cu} and tend towards limiting values. The rate equation of the

Table 1. The stoichiometry $\Delta C_M/\Delta C_L$ as a function of $C_{Cu} \cdot C_M=5.00$ mM; $C_L=(0.50-2.00)$ mM; $C_{Cl}=C_L$; $[H^+]=1.00$ M.

C_{Cu}/mM	$\Delta C_M/\Delta C_L$	C_{Cu}/mM	$\Delta C_M/\Delta C_L$
0	1.21	5.92	1.98
0.99	1.62	11.84	1.98
1.97	1.78	17.8	2.01
2.96	1.86	24.7	2.00

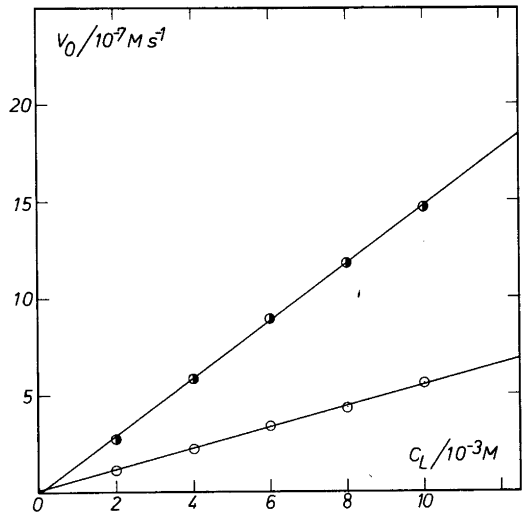

Fig. 1. v_o *versus* $C_L \cdot C_M=5.00$ mM; $C_{Cl}=C_L$; $C_{HClO_4}=1.00$ M; $C_{Cu}=0$ ○, 24.7 mM ◑.

catalysed reaction is, accordingly, analogous to that of the uncatalysed reaction, and can be written as

$$-(\Delta[M]/\Delta t)_o = k[M]\,[L] + k'[M]^2[L]$$

or

$$v_o = k\,\frac{C_M C_L}{1+\beta_1 C_M} + k'\,\frac{C_M^2\,C_L}{(1+\beta_1 C_L)\,(1+\beta_1 C_M)}$$

Both the second order and the third order term increase with increasing C_{Cu} and the experimental rate constants at sufficiently large copper concentrations attain limiting values such that $k_{lim}/k_0=3.1\pm0.4$ and $k'_{lim}/k'_0=2.1\pm0.3$ (*cf.* Table 2). k_{lim} and k'_{lim} have been calculated from the initial rates at $C_{Cu}=19.8$ and 24.7 mM which can be accommodated to the same straight line $v_o(1+\beta_1 C_M)/C_M$ *versus* C_M.

For an actual verification of the rate law given above as regards the dependence on C_L at constant C_M, it should be shown that the experimental values of quantities such as v_o/C_L or $v_o(1+\beta_1 C_L)/C_L$ are linearly dependent on $1/(1+\beta_1 C_L)$ and C_L, respectively. Although these functions do fit straight lines, they are very sensitive to experimental error, because v_o/C_L and $v_o(1+\beta_1 C_L)/C_L$ do not change more than, at

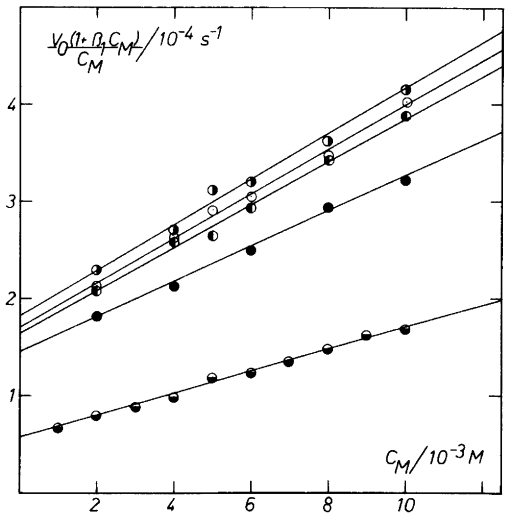

Fig. 2. v_o $(1+\beta_1 C_M)/C_M$ *versus* C_M. C_L=10.0 mM; $C_{Cl}=C_L$; C_{HClO_4}=1.00 M; C_{Cu}=0 ◒, 4.94 mM ●, 9.81 mM ◐, 14.8 mM ○, 24.7 mM ◑.

most, about 40 % within the C_L range where reliable measurements of v_o could be made ($C_L \leq 50$ mM). The linearity of these functions is, therefore, of only limited value in establishing the detailed dependence of v_o on C_L. At low hydroxylamine concentrations, v_o should, according to the rate law, be expected to be proportional to C_L. The two plots in Fig. 1 have the slopes $5.5 \cdot 10^{-5}$ s^{-1} and $15 \cdot 10^{-5}$ s^{-1} for C_{Cu}=0 and 24.7 mM, respectively, in good agreement with the values that can be calculated with the appropriate rate constant values of Table 2.

The reaction rate is independent of $[H^+]$ within the hydrogen ion concentration range of this study. It is also unaffected by the removal of dissolved air from the solutions.

Table 2. The experimental rate constants k and k' as functions of C_{Cu}. C_M=(1−10) mM; C_L=10.0 mM; $C_{Cl}=C_L$; C_{HClO_4}=1.00 M.

C_{Cu}/mM	$k/10^{-3}M^{-1}s^{-1}$	$k'/M^{-2}s^{-1}$
0	5.7±0.5	1.28±0.07
4.94	14±1	2.0±0.2
9.87	16±2	2.5±0.3
14.8	17±2	2.6±0.3
19.8	17±2	2.7±0.3
24.7	18±1	2.6±0.2

Table 3. The rate constant k, obtained from pseudo first order plots, as a function of C_{Cu}. C_M=0.200 mM; C_L=20.0 mM; $C_{Cl}=C_L$; C_{HClO_4}=1.00 M.

C_{Cu}/mM	$k/10^{-3}M^{-1}s^{-1}$	C_{Cu}/mM	$k/10^{-3}M^{-1}s^{-1}$
0	5.9	14.7	16.1
2.45	14.7	19.6	17.2
4.91	15.9	39.5	16.8
9.81	16.8	49.5	17.6

At very low C_M values ($C_M \leq 5 \cdot 10^{-4}$ M) the k' term of the rate law can be neglected, and if $C_L \gg C_M$ the reaction becomes pseudo first order with the rate constant kC_L. Table 3 shows the values obtained.

Effect of halide ions. The results of Tables 2 and 3 have been obtained with hydroxylammonium chloride, *i.e.* $C_{Cl}=C_L$=10.0 or 20.0 mM, respectively. In solutions free from chloride ions, the increase of the reaction rate with increasing C_{Cu} is considerably less marked, as it is illustrated by the rate constant values of Table 4. Furthermore, the attainment of the limiting values of the rate constants seems to be masked by an increase of the reaction rate which might be due to the large increase of ionic strength obtained at high copper perchlorate concentrations.

Table 5 shows the dependence of the initial rate on C_{Cu} and C_{Cl}. The effect of chloride ions in the absence of copper(II) falls almost within the error limits. In the presence of copper(II), there is, however, a marked influence of C_{Cl}.

Bromide ions have about the same effect as chloride ions.

Table 4. The experimental rate constants k and k' as functions of C_{Cu} in the absence of chloride ions. C_M=(2−10) mM; C_L=10.0 mM; C_{Cl}=0, C_{HClO_4}=1.00 M.

C_{Cu}/mM	$k/10^{-3}M^{-1}s^{-1}$	$k'/M^{-2}s^{-1}$
0	6±1	1.4±0.2
19.6	11±2	1.8±0.5
49.5	13±2	2.3±0.3
99.0	18±2	2.3±0.4
196	17±2	3.2±0.4
379	19±4	4.1±0.6
543	22±2	4.7±0.4

Table 5. The dependence of the initial rate on C_{Cl} and C_{Cu}. C_M=5.00 mM; C_L=10.0 mM; C_{HClO_4}=1.00 M.

C_{Cl}/mM	$v_o/10^{-7}$ M s^{-1}						
C_{Cu}/mM	0	4.91	9.82	14.7	19.6	24.7	39.6
0	5.4	6.4	7.9	8.7	9.0	9.4	10.3
2.00	5.4	8.0	9.3	10.6	11.1	11.6	12.2
10.0	5.6	11.4	12.4	12.7	14.9	14.7	17.0
20.0	5.7	12.7	14.8	14.7	16.2	15.3	17.5
40.0	5.7	14.0	15.2	16.9	16.6	16.0	17.1
60.0	5.8	14.9	15.9	16.9	16.3	16.4	17.1
80.0	5.9	15.4	16.9	16.8	17.0	17.0	18.3
100	5.9	14.9	17.0	16.7	16.8	17.4	16.6

No detailed study of the effect of C_{Cl} on the individual rate constants k and k' was carried out, but the values in Tables 4 and 6 (*e.g.* at C_{Cu}=19.6 mM) show that, in the presence of Cu(II), both constants depend on C_{Cl}.

Effect of ionic strength. The experimental rate constants were determined at a series of different ionic strengths for C_{Cu}=0 and 19.8 mM, *i.e.*, for the uncatalysed and fully catalysed reaction, respectively. The results are shown in Table 6. k is only slightly affected by even large changes of the ionic strength. The effects fall within the error limits. The effect on k' is, however, much more pronounced.

Table 6. The experimental rate constants k and k' as functions of the ionic strength at C_{Cu}=0 and 19.8 mM. C_M=(2–10) mM; C_L=10.0 mM; C_{Cl}=C_L; C_{HClO4}=1.00 M.

μ/M	C_{Cu}/mM	$k/10^{-3}M^{-1}s^{-1}$	$k'/M^{-2}s^{-1}$
1.07	0	6±1	1.2±0.2
1.07	19.8	17±2	2.7±0.3
2.05	0	6±1	1.5±0.2
2.05	19.8	17±2	3.2±0.2
2.88	0	6±1	2.0±0.2
2.88	19.8	19±2	3.9±0.3
3.62	0	6±2	2.5±0.5
3.62	19.8	18±2	5.7±0.3

DISCUSSION

The mechanism suggested in Ref. 1 for the uncatalysed reaction may be represented by the following simplified formulae:

Path 1 (k term).

$$V(V)+N(-I)\rightleftharpoons V(V)\cdot N(-I) \quad (1)$$
$$V(V)\cdot N(-I)\rightarrow V(IV)+N(O) \quad \text{(slow)} \quad (2)$$
$$N(O)\rightarrow \tfrac{1}{2}N_2 \quad (3)$$

Path 2 (k' term).

$$V(V)+N(-I)\rightleftharpoons V(V)\cdot N(-I) \quad (1)$$
$$V(V)\cdot N(-I)+V(V)\rightarrow 2\,V(IV)+N(I) \quad \text{(slow)} \quad (4)$$
$$N(I)\rightarrow \tfrac{1}{2}N_2O \quad (5)$$
$$N(I)+N(-I)\rightarrow N_2 \quad (6)$$

In these formulæ $V(V)=VO_2^+$, $N(-I)=NH_3OH^+$, and $V(V)\cdot N(-I)=VO_2NH_3OH^{2+}$. The nature of N(O) and N(I) will be discussed below.

The fact that the rate law of the copper(II) catalysed reaction is analogous to that of the uncatalysed reaction implies that the initial steps of the two reactions are the same. The catalytic action of copper(II) must then be due to reactions between the catalyst and intermediates formed from hydroxylamine in the slow steps, or subsequent steps. Copper(I) is probably formed and rapidly reoxidised by reaction with vanadium(V). Since both terms of the rate law are increased by the presence of copper(II), intermediates from both reaction paths must be assumed to react with copper(II). Such a mechanism will give a proper explanation to the moderate catalytic effect of copper(II). To obtain the stoichiometry $\Delta C_M/\Delta C_L$=2, one must assume that the nitrogen–containing intermediates, formed by the oxidations with copper(II), react with hydroxylammonium ion, yielding dinitrogen oxide as the ultimate product. The mechanism outlined here can be summarised, using the same kind of simplified formulæ as before:

Path 3 (k term; catalysed).

$$V(V)+N(-I)\rightleftharpoons V(V)\cdot N(-I) \quad (1)$$
$$V(V)\cdot N(-I)\rightarrow V(IV)+N(O) \quad \text{(slow)} \quad (2)$$
$$2\,Cu(II)+N(O)\rightarrow 2\,Cu(I)+N(II) \quad (7)$$
$$2x[Cu(I)+V(V)\rightarrow Cu(II)+V(IV)] \quad (8)$$
$$N(II)+\tfrac{1}{2}N(-I)\rightarrow \tfrac{3}{4}N_2O \quad (9)$$

Path 4 (k' term; catalysed).

$$V(V)+N(-I) \rightleftharpoons V(V)\cdot N(-I) \quad (1)$$

$$V(V)\cdot N(-I)+V(V) \rightarrow 2V(IV)+N(I) \quad \text{(slow)} \quad (4)$$

$$2\,Cu(II)+N(I) \rightarrow 2\,Cu(I)+N(III) \quad (10)$$

$$2x[Cu(I)+V(V) \rightarrow Cu(II)+V(IV)] \quad (8)$$

$$N(III)+N(-I) \rightarrow N_2O \quad (11)$$

The identity of the intermediates denoted as N(O), N(I), N(II) and N(III) has not been established. These intermediates are supposed to be present only in very low concentrations and, in general, the identification of such species is difficult. Gutch and Waters[7] have shown the existence of the radical $NH_2O\cdot$ as an intermediate in the oxidation of hydroxylamine by cerium(IV) in methanol and methanol–water solutions by means of ESR measurements. In these reactions, dinitrogen is the product formed, and it seems reasonable that $N(O)=NH_2O\cdot$ (*cf.* however Ref. 8, where $:\dot{N}HOH$ is suggested as a better alternative in the oxidation of hydroxylamine with $IrCl_6^{2-}$). The participation of free radicals in this reaction is implied by the fact that the reacting solution induces polymerisation of acrylonitrile. Nitroxyl, HNO, has been suggested as an intermediate in several reactions yielding dinitrogen oxide as the product of oxidation of hydroxylamine,[9–17] although no real evidence for this has been put forward. The intermediate N(I) might be nitroxyl, or some species derived from it.

The presence of chloride or bromide ions makes the rate attain the limiting value at lower copper(II) concentrations than in the absence of halide ions. This effect may, according to the mechanisms proposed above, be attributed to reactions (7) and (10) or perhaps reaction (8) being favoured at the expense of reactions (3) and (5), respectively.

The effect of ionic strength on the experimental rate constants is in agreement with the mechanisms suggested above. The value of k is only slightly dependent on the ionic strength, just as it might be expected if the rate-limiting step is monomolecular. The effect that does exist, may be a secondary salt effect. The fact that k changes little with increasing ionic strength indicates that β_1 changes only slightly with μ. The value of β_1 used for the calculation of the values of Table 6 is the one determined at μ=1.00 M. The values of k and k' obtained from $v_o(1+\beta_1 C_M)/C_M$ *versus* C_M are not, however, very sensitive to the value of β_1 used in these calculations.

Reaction (4) might in fact be two consecutive reactions; a rapid reversible formation of a binuclear complex followed by a rate-limiting electron transfer reaction. The strong dependence of k' on the ionic strength indicates, however, that this reaction is truly bimolecular. Since the reacting species in reaction (4) are both positively charged, k' should be expected to increase with increasing ionic strengths. The studies on the pre-equilibrium reported in Ref. 2 gave no evidence for the rapid formation of any binuclear complex.

Acknowledgements. The author is indebted to Professor Sture Fronæus for a positive criticism of this work, and to Mrs. Christina Oskarsson for technical assistance in most of the measurements.

REFERENCES

1. Bengtsson, G. *Acta Chem. Scand. 26* (1972) 2494.
2. Bengtsson, G. *Acta Chem. Scand. 27* (1973) 2554.
3. Bengtsson, G. *Acta Chem. Scand. 27* (1973) 3053.
4. Rossotti, F. J. C. and Rossotti, H. *Acta Chem. Scand. 10* (1956) 957.
5. Lumme, P., Lahermo, P. and Tummavuori, J. *Acta Chem. Scand. 19* (1965) 2175.
6. Gowda, H. S., Bhaskara Rao, K. and Gopal Rao, G. *Z. Anal. Chem. 160* (1958) 117.
7. Gutch, J. W. and Waters, W. A. *J. Chem. Soc. A* (1965) 751.
8. Sen, P. K., Maiti, S. and Sen Gupta, K. *Indian J. Chem. 19A* (1980) 865.
9. Scott, R. A., Haight, G. P. and Cooper, J. N. *J. Am. Chem. Soc. 96* (1974) 4136.
10. Waters, W. A. and Wilson, I. R. *J. Chem. Soc. A* (1966) 534.
11. Anderson, J. H. *Analyst. London 91* (1966) 532.
12. Hughes, M. N. *Q. Rev. Chem. Soc. 22* (1968) 1.
13. Erlenmeyer, H., Flierl, C. and Sigel, H. *J. Am. Chem. Soc. 91* (1969) 1065.
14. Jindal, V. K., Agrawal, M. C. and Mushran, S. P. *J. Chem. Soc. A* (1970) 2060.

15. Hughes, M. N. and Nicklin, H. G. *J. Chem. Soc. A* (1971) 164.
16. Swaroop, R. and Gupta, Y. K. *J. Inorg. Nucl. Chem. 36* (1974) 169.
17. Sen Gupta, K. K. and Sen, P. K. *J. Inorg. Nucl. Chem. 39* (1977) 1651.

Received January 4, 1983.

Acta Chemica Scandinavica A 37 (1983) 647-657

Aqueous Solution Photochemistry of *cis*- and *trans*-Diaquabis(ethylenediamine)rhodium(III) Ions and Their Conjugated Bases. Photoisomerization and Photostationary States and Their Correlation with Spectroscopic Properties

KATHERINE HOWLAND and L. H. SKIBSTED

Chemistry Department, Royal Veterinary and Agricultural University, Thorvaldsensvej 40, DK-1871 Copenhagen V, Denmark.

Upon ligand field excitation the *cis*-diaquabis(ethylenediamine)-rhodium(III) ion isomerizes to the corresponding *trans*-complex with a quantum yield of 0.27 mol/Einstein in acidic 1.0 M perchlorate aqueous solution at 25 °C. Under the same conditions the *trans*-isomer appears photoinert. The aquahydroxobis(ethylenediamine)rhodium(III) ions photoisomerize *trans* to *cis* with a quantum yield of 0.61 mol/Einstein and *cis* to *trans* with 0.048 mol/Einstein, whereas the dihydroxo species are photoinert. The photoisomerization has been investigated in the pH region 0 to 12 and the composition of the *cis*/*trans*-photostationary states is described quantitatively as a function of pH. The ethylenediamine complexes differ qualitatively in their photochemical properties from the analogous, previously investigated ammonia complexes, and this difference is discussed in relation to the σ-donor strength of the amine ligands.

According to recent theories [1-4] on ligand-field (LF) excited states of rhodium(III) and other d^6 low-spin complexes, the stereochemical consequences of LF photosubstitution reactions are related to the nature of the ligand field of the pentacoordinate intermediate generated by ligand dissociation from a hexa-coordinate triplet excited state. This intermediate is capable of *apical*/*basal* rearrangements prior to deactivation to the ground state and trapping by a solvent molecule. In this context, the observation that tetraamminerhodium(III) complexes undergo *cis* to *trans* photoisomerizations,[2-5] *i.e.*,

$$cis\text{-}[Rh(NH_3)_4Cl_2]^+ + H_2O \xrightarrow{h\nu} trans\text{-}[Rh(NH_3)_4(H_2O)Cl]^{2+} + Cl^-$$

as well as *trans* to *cis* photoisomerizations,[6,7] *i.e.*,

$$trans\text{-}[Rh(NH_3)_4(OH)Cl]^+ + H_2O \xrightarrow{h\nu} cis\text{-}[Rh(NH_3)_4(OH)_2]^+ + H^+ + Cl^-$$

can be explained by the relative energies of the *apical* and *basal* triplet excited-state isomers of the pentacoordinate intermediate. MO calculations suggest [1-4] that the isomer with the weakest σ-donor ligand in the apical position has the lowest energy. Thus, in accordance with the proposed σ-donor strength series $OH^- > NH_3 > H_2O > Cl^-$, the more stable excited-state intermediates in the two above-mentioned photoreactions would be *apical*-$[Rh(NH_3)_4Cl]^{2+*}$ and *basal*-$[Rh(NH_3)_4(OH)]^{2+*}$, respectively.

The photochemical behaviour of *cis*- and *trans*-$[Rh(NH_3)_4(H_2O)_2]^{3+}$ confirms that water and ammonia have comparable σ-donor strengths and that the energy separation between *basal*- and *apical*-$[Rh(NH_3)_4(H_2O)]^{3+*}$ is small, as LF excitation of *cis*- or *trans*-$[Rh(NH_3)_4(H_2O)_2]^{3+}$ leads to a *cis*/*trans*-photostationary state,[7]

0302-4377/83 $2.50

$$cis\text{-}[Rh(NH_3)_4(H_2O)_2]^{3+} \underset{h\nu}{\overset{h\nu}{\rightleftharpoons}} trans\text{-}[Rh(NH_3)_4(H_2O)_2]^{3+}$$

Substitution of ammonia with other amine ligands in diaquatetraaminerhodium(III) complexes is expected to influence the *apical/basal* excited-state equilibrium in accordance with the water amine σ-donor strength difference. The composition of the *cis/trans* photostationary states should therefore correlate with the amine σ-donor strength and in principle be predictable from the LF spectra.

An investigation of the photochemistry of a series of diaquatetraminerhodium(III) complexes in which the amine σ-donor strength is systematically varied is therefore of importance in the evaluation of excited-state properties and processes of rhodium(III) complexes and of d^6 low-spin complexes in general. As the first part of such studies we here report the results for the *cis*- and *trans*-diaquabis(ethylenediamine)rhodium(III) ions and their conjugated bases.

EXPERIMENTAL

Matrials. The ethylenediamine (en=1,2-diaminoethane) complex *cis*-$[Rh(en)_2(H_2O)(OH)]S_2O_6$ was prepared from *cis*-$[Rh(en)_2Cl_2]Cl_{½}(ClO_4)_{½}$ by a literature method.[8,9,16] The precursor to *trans*-$[Rh(en)_2(H_2O)(OH)](ClO_4)_2$, *trans*-$[Rh(en)_2Cl_2]NO_3$, was also prepared by a (somewhat modified) literature method.[8] Other chemicals were of analytical grade.

Synthesis. *trans*-$[Rh(en)_2(H_2O)(OH)](ClO_4)_2$, for which several methods of preparation have been suggested,[10–13] was prepared and purified by the following method. A 400 mg portion of *trans*-$[Rh(en)_2Cl_2]NO_3$ and 1.0 g of HgO were dissolved in 60 ml of 0.33 M $HClO_4$ and heated at reflux for 2 h. Then the volume was reduced to 15 ml by evaporation and the resulting solution cooled in ice. 10 M NaOH was added slowly until pH≈10 and the precipitated HgO was removed by filtration through a G-4 sintered glass filter. While kept at ≈0 °C, pH was adjusted by addition of 5 M $HClO_4$ to ≈6. The product formed, crude *trans*-$[Rh(en)_2(H_2O)(OH)](ClO_4)_2$, was filtered off, washed with ice-cold water and subsequently with 96 % ethanol then ether. The crude product (yield 300 mg) was dissolved in 0.8 ml of 1 M HBr and the resulting solution was filtered through a G-4 sintered glass filter. 0.8 ml of an ice-cold saturated aqueous LiBr solution was added in order to precipitate *trans*-$[Rh(en)_2(H_2O)_2]Br_3$. Yield of this compound after washing with ice-cold absolute ethanol was 270 mg. After dissolving the product in 1.0 ml of boiling water, 1.0 ml of a saturated, aqueous $LiClO_4$ solution was immediately added and pH adjusted to≈6 with 0.2 M NaOH. After cooling in ice for 2 h, a 200 mg yield of *trans*-$[Rh(en)_2(H_2O)(OH)](ClO_4)_2$ was filtered off and washed as before. This product was reprecipitated twice by dissolution in 1.0 ml of 0.5 M $HClO_4$ and subsequent adjustment of pH to≈6 with 2 M NaOH. After cooling in ice for 2 h the product was filtered off, washed with ice-cold water, then with 96 % ethanol and finally with ether. A third reprecipitation did not change the absorption spectrum. Yield 160 mg (30 %). Anal. C, H, N, Cl.

Absorption spectra. Electronic spectra were recorded on a Zeiss DMR 21 or a Cary 219 spectrophotometer.

pH measurements. A Radiometer PHM 52 pH-meter with a combination glass electrode with 1.0 M NaCl in the reference part was used for the pH measurements. Since all measurements were made in a 1.0 M (H,Na)(ClO_4,OH) medium, the definition pH= $-\log[H^+]$ was used throughout by using standardized perchloric acid in 1.0 M $NaClO_4$ as pH standards.

Photolyses. The optical train consisted of the light source, an Osram HBO 100/2 high pressure mercury lamp, a light condenser, a heat filter (a 5 cm water-filled cell), an interference filter, a precision shutter connected to an electronic timer and lenses focusing the light into the thermostatted photolysis cell. All optical parts and cells were of quartz (Spindler und Hoyer, Göttingen, GFR). Photolyses were carried out with monochromatic light (312 or 334 nm) at 25±0.5 °C. Light intensities were determined by standard ferrioxalate actinometry.[7,17]

For all the complex ions under investigation, experiments were made to ensure that no significant thermal reactions ("dark reactions") occurred during photolysis.

Calculation of quantum yield. The calculations of quantum yields were based on spectral changes at four different wavelengths in principle by Method B of Ref. 7 with some minor modifications.[19] The molar absorptivities at the monitoring wavelengths λ_{mon} are given in Table 3 for the relevant complex ions.

RESULTS

The results reported here are a quantitative description of the aqueous solution ligand field excitation photochemistry of *cis*- and *trans*-

Table 1. pK_a value for *cis*- and *trans*-$[Rh(en)_2(H_2O)_2]^{3+}$ in aqueous solution.

$pK_{a,1}$	$pK_{a,2}$	Medium	*t*/°C	Ref.
trans-$[Rh(en)_2(H_2O)_2]^{3+}$				
4.43	7.81	0.20 M $NaNO_3$	≈20	10
4.37	7.64	1.0 M $NaClO_4$	26.4	11
4.33	7.72	0.5 M $NaClO_4$	25	13
4.47	7.91	1.0 M $NaClO_4$	25.0	This work[a]
cis-$[Rh(en)_2(H_2O)_2]^{3+}$				
5.82	7.98	0.01 M $NaClO_4$	25	15
6.09	8.08	0.5 M $NaClO_4$	25	15
6.34	8.24	1.0 M $NaClO_4$	25.0	16[a]

[a] Values used in the present study.

$[Rh(en)_2(H_2O)_2]^{3+}$ and their conjugated bases in a 1.0 M perchlorate medium at 25 °C. Also reported is an improved preparation and purification procedure for *trans*-$[Rh(en)_2(H_2O)(OH)](ClO_4)_2$ and the pK_a values of this complex together with the electronic spectra determined in aqueous 1.0 M (H,Na)(ClO_4,OH) solution in comparison with the same characteristics for the *cis*-isomer.

Acid dissociation and ligand field spectra. Weighed amounts of *trans*-$[Rh(en)_2(H_2O)(OH)](ClO_4)_2$ (between 0.02 and 0.05 mmol) were dissolved in 25.00 ml of 0.00200 M $HClO_4$ plus 1.00 M $NaClO_4$ and titrated with 0.0200 M NaOH in 0.98 M $NaClO_4$. $pK_{a,1}$ and $pK_{a,2}$ were calculated by standard numerical procedures[18] from 8 full titration curves (estimated standard deviation on the pK_a-values 0.02) and are com-

Table 2. UV-visible absorption spectra of *trans*-$[Rh(en)_2(H_2O)_2]^{3+}$ and conjugated bases. [λ in nm (ε in l $mol^{-1}cm^{-1}$)].

$\lambda_{max}(\varepsilon_{max})$	$\lambda_{min}(\varepsilon_{min})$	Medium	Ref.
trans-$[Rh(en)_2(H_2O)_2]^{3+}$			
342 (64), 262(148)		pH=2	10
351 (61.6), 274(138)		0.02 M $HClO_4$, 1.0 M $NaClO_4$	11
342 (66), 272(125)		0.1 M $HClO_4$	12
350 (60), 274(130)		0.01 M $HClO_4$	13
352 (58.4), 274(130)	330(51.5), 251(96)	0.10 M $HClO_4$, 0.90 M $NaClO_4$	This work[a]
trans-$[Rh(en)_2(H_2O)(OH)]^{2+}$			
337 (88), 270(158)		pH=6	10
343 (89), 282(154)			13
344 (87), 284(149)	326(79), 244(59)	1.0 M $NaClO_4$, pH=6.2	This work[a]
trans-$[Rh(en)_2(OH)_2]^{+}$			
346 (99), 297(130)		0.7 M NaOH	14
336 (94), 289(154)		pH=11	10
338 (136), 290(136)		0.1 M NaOH	12
344 (99), 296(134)		0.01 M NaOH	13
344 (97), 295(132)	327(91), 244(48)	0.04 M NaOH, 0.96 M $NaClO_4$	This work[a]

[a] *trans*-$[Rh(en)_2(H_2O)(OH)](ClO_4)_2$ dissolved in the media quoted.

Table 3. Spectral characteristics of *cis*- and *trans*-diaquabis(ethylenediamine)rhodium(III) ions and their conjugated bases in aqueous 1.0 M (Na,H)(ClO_4,OH) [λ in nm (ε in l $mol^{-1}cm^{-1}$)].

Complex ion[a]	$\lambda_{max}(\varepsilon_{max})$	$\lambda_{irr}(\varepsilon_{irr})$	$\lambda_{mon}(\varepsilon_{mon})$[d]
cis-$[Rh(en)_2(H_2O)_2]^{3+}$	318(175), 271(137)	312(166), 334(142)	320(174), 330(155) 340(120)
cis-$[Rh(en)_2(H_2O)(OH)]^{2+}$ [b]	323(203), 280(161)[c]	312(196), 334(192)	320(209), 330(202) 340(170)
cis-$[Rh(en)_2(OH)_2]^{+}$	329(179), 278.5(171)	312(150), 334(177)	320(170), 330(179) 340(166)
trans-$[Rh(en)_2(H_2O)_2]^{3+}$	352(58.4), 274(130)	312(71), 334(52)	320(58), 330(52) 340(55)
trans-$[Rh(en)_2(H_2O)(OH)]^{2+}$ [b]	344(87), 284(149)	312(100), 334(82)	320(83), 330(80) 340(86)
trans-$[Rh(en)_2(OH)_2]^{+}$	344(97), 295(132)	312(109), 334(97)	320(95), 330(92) 340(97)

[a] Medium for the diaqua complexes: 0.10 M $HClO_4$, 0.90 M $NaClO_4$; for the aquahydroxo complexes: 1.00 M $NaClO_4$ adjusted to $pH=\frac{1}{2}(pK_{a,1}+pK_{a,2})$; for the dihydroxo complexes: 0.04 M NaOH, 0.96 M $NaClO_4$. [b] $\lambda_{max}(\varepsilon_{max})$ reported is that measured for a mixture at $pH=\frac{1}{2}(pK_{a,1}+pK_{a,2})$, whereas $\lambda_{irr}(\varepsilon_{irr})$ and $\lambda_{mon}(\varepsilon_{mon})$ has been corrected for the presence of the diaqua and the dihydroxo species. [c] Shoulder. [d] λ_{mon} are the wavelengths used in the calculations of quantum yields and of the composition of photostationary states and ε_{mon} are the molar absorptivities at these wavelengths.

pared in Table 1 with literature values for the same compound and for its *cis*-isomer. In Table 2, λ_{max} (ε_{max}) and λ_{min} (ε_{min}) for the ligand field spectra of *trans*-$[Rh(en)_2(H_2O)_2]^{3+}$, of *trans*-$[Rh(en)_2(H_2O)(OH)]^{2+}$ and of *trans*-$[Rh(en)_2(OH)_2]^{+}$ are compared with the available literature data.

cis- *and* trans-*$[Rh(en)_2(H_2O)_2]^{3+}$ photoreactions.* LF photolysis of *cis*-$[Rh(en)_2(H_2O)_2]^{3+}$ in aqueous acidic 1.0 M perchlorate solution ($[H^+]\geq 0.010$ M) led cleanly and efficiently to *trans*-$[Rh(en)_2(H_2O)_2]^{3+}$. 6.00 ml of a $2.124 \cdot 10^{-3}$ M solution of *cis*-$[Rh(en)_2(H_2O)_2]^{3+}$ in 0.10 M $HClO_4$, 0.90 M $NaClO_4$ exhaustively photolyzed ($\lambda_{irr}=334$ nm, light intensity $I_0=9.08 \cdot 10^{-7}$ Einstein/min over a front window of 3.5 cm^2, 7 h of irradiation, 25 °C) had the following spectral characteristics: λ_{max} (ε_{max})=352 nm (58.9 l/mol cm); 274(127); $\lambda_{min}(\varepsilon_{min})$=330 (52.0); 251 (93) which within experimental uncertainties are identical with the spectral characteristics of *trans*-$[Rh(en)_2(H_2O)_2]^{3+}$ under the same conditions, see Tables 2 and 3. An analysis of the product spectrum (4 characteristic wavelengths, see Table 3) showed that no more than 0.6 % of the *cis*-isomer was left in the product solution. Isosbestic points at 358, 290, 278 and 258 nm were maintained throughout the photolysis, see Fig. 1. The photoreaction of *cis*-$[Rh(en)_2(H_2O)_2]^{3+}$ under the present conditions is thus a clean isomerization without any detectable competing or secondary reactions of thermal or photochemical nature.

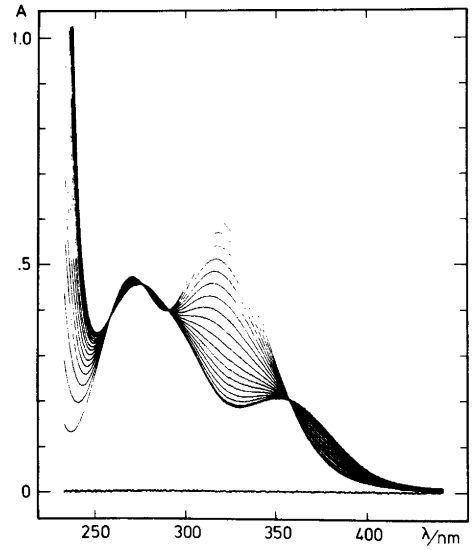

Fig. 1. Absorption spectra recorded during 334 nm photolysis at 25 °C of *cis*-$[Rh(en)_2(H_2O)_2]^{3+}$ (λ_{max}=318 and 271 nm) in 0.10 M $HClO_4$ plus 0.90 M $NaClO_4$ to give *trans*-$[Rh(en)_2(H_2O)_2]^{3+}$ (λ_{max}=352 and 274 nm), see Results.

Table 4. Photoisomerization quantum yields for *cis*- and *trans*-$[Rh(en)_2(H_2O)_2]^{3+}$ and their conjugated bases in aqueous 1.0 M (Na,H)(ClO_4,OH) at 25 °C.

Complex ion	Principal photoproduct	λ_{irr}/nm	pH	Φ/mol Einstein^{-1}	Number of exp.
cis-$[Rh(en)_2(H_2O)_2]^{3+}$	*trans*-$[Rh(en)_2(H_2O)_2]^{3+}$	334	0.0	0.27±0.01	2
		334	1.0	0.26±0.01	4
		312	1.0	0.26±0.01	3
		334	2.0	0.28±0.01	2
trans-$[Rh(en)_2(H_2O)_2]^{3+}$	*cis*-$[Rh(en)_2(H_2O)_2]^{3+}$	334	1.0	<0.002	2
cis-$[Rh(en)_2(H_2O)(OH)]^{2+}$	*trans*-$[Rh(en)_2(H_2O)(OH)]^{2+}$	334	8.25[a]	0.052[b,c]	1
		334	8.37[a]	0.048[b,c]	1
		334	8.48[a]	0.043[b,c]	1
trans-$[Rh(en)_2(H_2O)(OH)]^{2+}$	*cis*-$[Rh(en)_2(H_2O)(OH)]^{2+}$	334	6.1–6.2[a]	0.62±0.04[c]	5
		312	6.1–6.2[a]	0.59±0.02[c]	2
cis-$[Rh(en)_2(OH)_2]^{+}$	*trans*-$[Rh(en)_2(OH)_2]^{+}$	334	12.6	<0.002	2
trans-$[Rh(en)_2(OH)_2]^{+}$	*cis*-$[Rh(en)_2(OH)_2]^{+}$	334	12.6	<0.002	2

[a] Initial pH, see Results. [b] Corrected for photoreaction of *cis*-$[Rh(en)_2(H_2O)_2]^{3+}$. [c] Calculated on the basis of the light absorbed by the complex ion mentioned.

Evaluation of quantum yields was made from spectral changes and the results (experiments at three different acid concentrations and two different wavelengths of irradiation) are seen in Table 4. No acid concentration or wavelength dependence was observed and an average value of $\Phi=0.27\pm0.01$ mol/Einstein was calculated for the *cis* to *trans* photoisomerization.

LF photolysis of *trans*-$[Rh(en)_2(H_2O)_2]^{3+}$ under the same conditions as the *cis*-isomer resulted in very minor spectral changes and a generous upper limit of $\Phi=0.002$ mol/Einstein for a *trans* to *cis* photoisomerization was estimated.

The *cis*/*trans* ratio in the product solutions after exhaustive photolysis was <0.006 as calculated from the product spectrum (see above) and <0.003 as calculated from $(\varepsilon^{irr}_{trans}\,\Phi_{trans})/(\varepsilon^{irr}_{cis}\,\Phi_{cis})$ (see Ref. 7), and it was concluded that whereas *cis*-$[Rh(en)_2(H_2O)_2]^{3+}$ photoisomerizes efficiently to the *trans*-isomer, *trans*-$[Rh(en)_2(H_2O)_2]^{3+}$ is photoinert (except for the possibility of photochemical water exchange [17]).

cis- *and* trans-*$[Rh(en)_2(OH)_2]^+$ photoreactions.* Long term LF photolysis of either dihydroxobis(ethylenediamine)rhodium(III) ion in aqueous 0.04 M NaOH, 0.96 M $NaClO_4$ led to minor and uncharacteristic spectral changes and these changes did not indicate any photoisomerization. The photoisomerization quantum yield presented in Table 4 for the dihydroxo species are estimated upper limits.

cis- *and* trans-*$[Rh(en)_2(H_2O)(OH)]^{2+}$ photoreactions.* Aqueous 1.0 M $NaClO_4$ solutions of *trans*-$[Rh(en)_2(H_2O)(OH)]^{2+}$ showed a very high photoreactivity, whereas *cis*-$[Rh(en)_2(H_2O)(OH)]^{2+}$ were but moderately photoreactive. This indicated a different photochemical behavior for the aquahydroxo complex ions in comparison to both the diaqua and to the dihydroxo complex ions.

A $9.95\ 10^{-4}$ M *trans*-$[Rh(en)_2(H_2O)(OH)]^{2+}$ solution with pH=6.00 was photolyzed with 312 nm monochromatic light until no further spectral changes were observed. Throughout the photolysis isosbestic points at 259, 292, and 366 nm were maintained. The product solution had a pH value of 7.00 and the following spectral characteristics: $\lambda_{max}(\varepsilon_{max})=322$ nm (180 l/mol cm), $\lambda_{sh}(\varepsilon_{sh})=280$ (139), and $\lambda_{min}(\varepsilon_{min})=246$ (83). An analogous experiment with the *cis*-isomer (initial pH=7.30) gave a product solution with pH=7.16 and $\lambda_{max}(\varepsilon_{max})=322$ nm (201 l/mol cm), $\lambda_{sh}(\varepsilon_{sh})=280$ (164), and $\lambda_{min}(\varepsilon_{min})=247$ (110). Both the spectral and pH changes in these two experiments indicated *trans* to *cis* photoisomerization for the *trans*-isomer and *cis* to *trans* photoisomerization for the *cis*-isomer. Numerical analysis of the product solution absorption spectra in combination with solution pH's at this and different λ_{irr} demonstrated the photoproduct to be solely $[Rh(en)_2(H_2O)(OH)]^{2+}$ in a *cis*/*trans* photostationary state, both isomers in thermal acid/base equilibria with the corresponding diaqua and dihydroxo complex ions.

Quantum yields for the *trans* to *cis* photoisomerization process were determined from photolysis of *trans*-$[Rh(en)_2(H_2O)(OH)]^{2+}$ solutions with initial $pH=\frac{1}{2}(pK_{a,1}+pK_{a,2})$. At pH=6.19 the aquahydroxo ion fraction of the *trans*-isomer is 0.963 and $\delta_{(H_2O)(OH)}$, the light fraction absorbed by this ion, is 0.970 at 334 nm and 0.966 at 312 nm, respectively, as calculated from eqn. (1):

$$\delta_{(H_2O)(OH)}=\frac{\varepsilon^{irr}_{(H_2O)(OH)}[H^+]K_{a,1}}{\varepsilon^{irr}_{(H_2O)_2}[H^+]^2+\varepsilon^{irr}_{(H_2O)(OH)}[H^+]K_{a,1}+\varepsilon^{irr}_{(OH)_2}K_{a,1}K_{a,2}} \quad (1)$$

where ε^{irr} are the molar absorptivities of the different complex ions at the wavelength of irradiation. The quantum yield for the *trans* to *cis* isomerization, $\Phi^{(H_2O)(OH)}_{trans}$, had the value 0.61 mol/Einstein (Table 4) as calculated from spectral changes correcting for both inner filter effects and for *cis* to *trans* photoisomerization, *cf.* Method B of Ref. 7.

In order to separate the photoreaction of *cis*-$[Rh(en)_2(H_2O)(OH)]^{2+}$ from that of *cis*-$[Rh(en)_2(H_2O)_2]^{3+}$, photolysis experiments to establish the *cis* to *trans* photoisomerization of the aquahydroxo ion as well as to determine the quantum yield of this process were carried out at pH≥8.25. At pH=8.25 the light fractions absorbed for the three *cis*-species calculated from eqn. (1) and the two analogous formulas are $\delta_{(H_2O)_2}=0.005$, $\delta_{(H_2O)(OH)}=0.512$, and $\delta_{(OH)_2}=0.483$, respectively. The observed quantum yield corrected for *trans* to *cis* photoisomerization was $\Phi^{obs}_{cis}=0.0232$ mol/Einstein at pH=8.25. Correcting this value by eqn. (2).

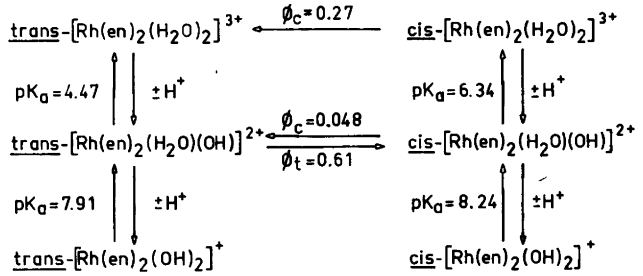

Scheme 1.

$$\Phi_{cis}^{(H_2O)(OH)} = \frac{\Phi_{cis}^{obs} - \Phi_{cis}^{(H_2O)_2}\delta_{(H_2O)_2} - \Phi_{cis}^{(OH)_2}\delta_{(OH)_2}}{\delta_{(H_2O)(OH)}} \quad (2)$$

the value $\Phi_{cis}^{(H_2O)(OH)}=0.052$ reported in Table 4 was obtained.

cis/trans-*Photostationary states.* *trans*-$[Rh(en)_2(H_2O)(OH)]^{2+}$, *cis*-$[Rh(en)_2(H_2O)_2]^{3+}$, and *cis*-$[Rh(en)_2(H_2O)(OH)]^{2+}$ are each photoreactive with respect to isomerization and the quantum yields for these photoreactions are shown in Scheme 1. The difference in photoreactivity of the different acid/base-forms of the two isomers leads to photostationary states in which the *cis*/*trans* composition depends on the product solution pH.

Solutions of either *cis*- or *trans*-$[Rh(en)_2(H_2O)(OH)]^{2+}$ in 1.0 M $NaClO_4$ were adjusted to different pH and photolyzed at 334 nm until no further spectral changes were observed. The *cis*-fraction in the exhaustively photolyzed solutions, ω_{cis}, was calculated for each experiment by the previously published method[7] from a combination of the pH-value and the absorption spectrum of the product solution. In Fig. 2 the experimentally observed *cis*-fractions as a function of pH are compared to that functionality predicted from the quantum yields of Scheme 1, from the molar absorptivities at 334 nm (Table 3), and from the pK_a-values of the complex ions (Table 1). The experimental points for ω_{cis} are seen to agree within experimental uncertainties with the predicted curve. For comparison, the function predicted assuming the photoisomerization quantum yield of *cis*-$[Rh(en)_2(H_2O)(OH)]^{2+}$ to be zero, is also shown in Fig. 2. In accordance with the result mentioned above, it is seen that the *cis*-$[Rh(en)_2(H_2O)(OH)]^{2+}$ ion indeed is photoactive with respect to isomerization.

DISCUSSION

The following discussion will focus mainly on the differences between the photochemical behavior of the bis(ethylenediamine)rhodium(III) complexes and that of the previously investigated[7] tetraamminerhodium(III) complexes. Special emphasis will be placed on the kinetics and the thermodynamics of the excited state rearrangement processes suggested by the theoretical model for the photoisomerization reactions.

In Table 5 the reaction quantum yields for the photoprocesses of the two series of diaquatetra-

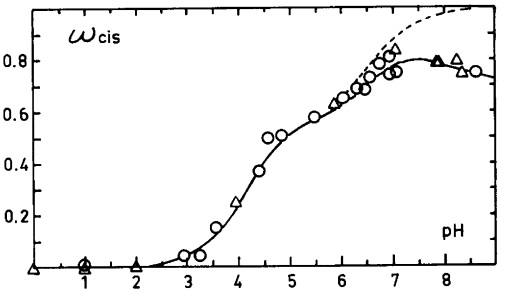

Fig. 2. ω_{cis}, the *cis*-fraction in the photostationary state, after exhaustive photolysis of *cis*-$[Rh(en)_2(H_2O)_2]^{3+}$, Δ, or of *trans*-$[Rh(en)_2(H_2O)_2]^{3+}$, 0, at 334 nm in 1.0 M $(Na,H)ClO_4$ at 25 °C as a function of product solution pH. The full line is calculated from the independently determined parameters: the quantum yields for the photoisomerization processes (Scheme 1), and the molar absorptivities at 334 nm (Table 3), in combination with the pK_a-values of the *cis*- and *trans*-species (Table 1). The broken line is calculated from the same parameters as the full line but assuming that the photoisomerization quantum yield for *cis*-$[Rh(en)_2(H_2O)(OH)]^{2+}$ is zero.

Table 5. Comparison between the photoisomerization quantum yields for bis(ethylenediamine)rhodium(III) and the corresponding tetraamminerhodium(III) complexes in aqueous 1.0 M perchlorate solution at 25 °C.

Photoreaction	Bis(ethylenediamine)[a] Φ in mol. Einstein^{-1}	Tetraammine[b] Φ in mol Einstein^{-1}
cis-$[RhA_4(H_2O)_2]^{3+} \xrightarrow{h\nu}$ *trans*-$[RhA_4(H_2O)_2]^{3+}$	0.27	0.072
cis-$[RhA_4(H_2O)(OH)]^{2+} \xrightarrow{h\nu}$ *trans*-$[RhA_4(H_2O)(OH)]^{2+}$	0.048	[c]
cis-$[RhA_4(OH)_2]^{+} \xrightarrow{h\nu}$ *trans*-$[RhA_4(OH)_2]^{+}$	[c]	[c]
trans-$[RhA_4(H_2O)_2]^{3+} \xrightarrow{h\nu}$ *cis*-$[RhA_4(H_2O)_2]^{3+}$	[c]	0.012
trans-$[RhA_4(H_2O)(OH)]^{2+} \xrightarrow{h\nu}$ *cis*-$[RhA_4(H_2O)(OH)]^{2+}$	0.61	0.59
trans-$[RhA_4(OH)_2]^{+} \xrightarrow{h\nu}$ *cis*-$[RhA_4(OH)_2]^{2+}$	[c]	[c]

[a] $A_4=(en)_2$; present work. [b] $A_4=(NH_3)_4$; from Ref. 7. [c] Photoisomerization not detected.

aminerhodium(III) complexes and their conjugated bases are compared. There is a qualitative difference between the two amine series. The *cis/trans*-$[Rh(NH_3)_4(H_2O)_2]^{3+}$ ions photoisomerize to each other forming a product photostationary state in contrast to the *cis/trans*-$[Rh(en)_2(H_2O)_2]^{3+}$ ions of which only the *cis*-isomer is active with respect to photoisomerization. Notably, the situation for the aquahydroxo species is totally reversed from that for the diaqua species, as only the *trans*-isomer of the $[Rh(NH_3)_4(H_2O)(OH)]^{2+}$ ions photoisomerizes, whereas both *trans*- and *cis*-$[Rh(en)_2(H_2O)(OH)]^{2+}$ are photoactive isomerizing to a common *cis/trans* photostationary state. None of the four dihydroxo complexes show, however, any significant photoactivity. The consequences of the different photochemical properties of the two series of aminerhodium(III) complexes on the photoproduct solution composition are depicted in Fig. 3. The *cis/trans* photostationary state as a function of pH illustrates the behavioral crossover.

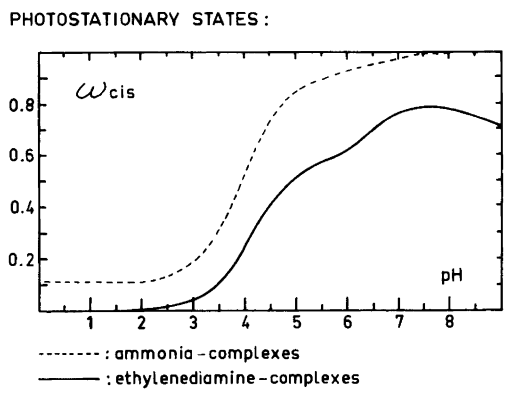

Fig.3. Comparison between ω_{cis}, the *cis*-fraction in the photostationary state, as a function of pH for the tetraamminerhodium(III) (λ_{irr}=350 nm, Ref. 7) and the bis(ethylenediamine)rhodium(III) complexes (λ_{irr}=334 nm, present work) in 1.0 M (Na,H)ClO_4 at 25 °C.

The photoisomerization reactions of dihalotetraminerhodium(III) complexes proceed *via* ligand substitution, *i.e.*[5,20]

$$cis\text{-}[Rh(en)_2Cl_2]^{+} + H_2O \rightarrow trans\text{-}[Rh(en)_2(H_2O)Cl]^{2+} + Cl^{-} \quad (3)$$

with the initial chemical reaction suggested[1-4] to be ligand dissociation for the lowest triplet excited state populated by efficient intersystem crossing from the higher singlet excited state originally generated in the excitation process. Photoisomerization of aquaaminerhodium(III)

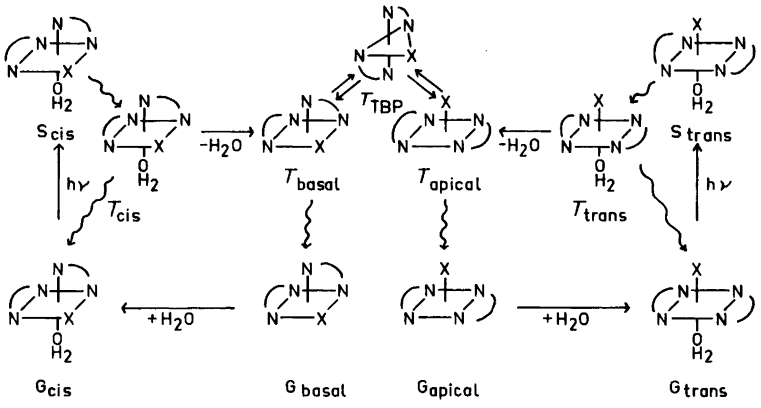

Scheme 2: $\overset{\frown}{N\ N}$ = ethylenediamine; X = H_2O, OH

complexes is analogous to the photoisomerization of the dihalotetraamine complexes initiated by dissociation of a water ligand as recently shown for *cis*-$[Rh(NH_3)_4(H_2O)Cl]^{2+}$ by isotopic labelling.[17] The dissociative mechanism, which now draws support from several different types of experiments,[2,17,21–24] appears to be generally operating for this type of photoreactions of d^6 low spin complexes. The ensuing discussion of the photoisomerization of diaqua- and aquahydroxotetraaminerhodium(III) complexes will be held within the framework outlined by this model.[1–4]

The reaction sequences responsible for photoisomerization (Scheme 2) of *cis*-$[Rh(en)_2(H_2O)_2]^{3+}$ (X=H_2O) and of *cis* and *trans*-$[Rh(en)_2(H_2O)(OH)]^{2+}$ (X=OH) follow the initial excitation of the ground state molecules G_{cis} or G_{trans} to their singlet excited states S_{cis} or S_{trans}, respectively. The intersystem crossing generates the corresponding triplet excited states T_{cis} or T_{trans}, from which deactivation to the parent ground states competes with the dissociation of an H_2O to form the triplet square pyramidal pentacoordinated intermediates T_{basal} or T_{apical}, respectively. The rearrangement between T_{basal} and T_{apical} proceeds *via* the high energy, trigonal bipyramidal intermediate T_{TBP}, also in a triplet state. Deactivation of T_{basal} or T_{apical} leads to the square pyramidal pentacoordinate ground states G_{basal} or G_{apical}, which being coordinately unsaturated react with a solvent molecule giving the photoproducts *cis* or *trans*-$[Rh(en)_2(H_2O)X]^{n+}$, respectively. The energy difference between the *basal* and *apical* square pyramidal triplets is essentially a function of the σ-donor strengths of the five ligator atoms, as the stronger σ-donors have a strong site preference for a basal position.[1–4] Given the σ-donor strength series[25] $\sigma_{OH^-} > \sigma_{saturated\ amine} > \sigma_{H_2O} > \sigma_{Cl^-}$, the photoisomerization of *cis*-$[Rh(en)_2(H_2O)_2]^{3+}$ is a result of the excited state rearrangement

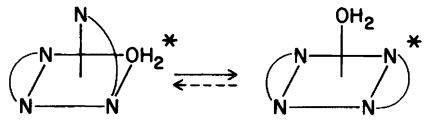

(4)

whereas the photoisomerizations of *cis*- and *trans*-$[Rh(en)_2(H_2O)(OH)]^{2+}$ are the result of the reversible rearrangement

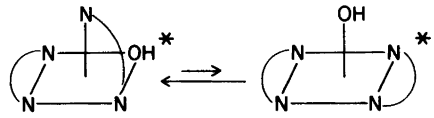

(5)

In this context it is important to note that the excited state lifetimes of these intermediates are in the nsec region and therefore by several orders of magnitude too short-lived to attain excited state acid/base equilibrium with the medium.[7]

The calculations based on the spectroscopic parameters have proved successful in the prediction of the stereochemical consequences of photochemical ligand exchange reaction[2,5–7] including water exchange reactions.[17] They also offer an explanation for the observed differences between the photoisomerization of the tetraam-

Table 6. Energy of the lowest multiplicity allowed ligand field transition ($^1T_{1g} \leftarrow {}^1A_{1g}$, pseudo octahedral symmetry assumed) for *cis*-$[Rh(NH_3)_4(H_2O)_2]^{3+}$ and *cis*-$[Rh(en)_2(H_2O)_2]^{3+}$ and their conjugated bases.

	Energy in kK	
	Bis(ethylenediamine)[a]	Tetraammine[b]
cis-$[RhA_4(H_2O)_2]^{3+}$	31.4	30.7
cis-$[RhA_4(H_2O)(OH)]^{2+}$	31.0	30.4
cis-$[RhA_4(OH)_2]^{+}$	30.4	29.9

[a] $A_4=(en)_2$, present work. [b] $A_4=(NH_3)_4$, Ref. 7.

mine- and bis(ethylenediamine)rhodium(III) complexes. The energies of the $^1T_{1g} \leftarrow {}^1A_{1g}$ transition (pseudo octahedral symmetry assumed, Table 6) indicates that ethylenediamine is a stronger field ligand than ammonia for this class of compounds, and given that the π-bonding properties of the two ligands appear identical,[25] the ethylenediamine ligand must be a significantly stronger σ-donor than ammonia. The more detailed σ-order of the relevant donors is therefore $\sigma_{OH^-} > \sigma_{en} > \sigma_{NH_3} > \sigma_{H_2O}$. Consequently, the energy difference between the *basal* and *apical* isomers of eqn. (4) must be greater than the analogous energy difference for eqn. (6) in which $N=NH_3$:

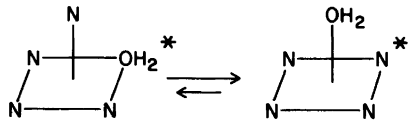

(6)

The small energy difference in eqn. (6) allows the coexistence of both isomers for the aquatetaammine intermediate, whereas the *apical*-aquabis(ethylenediamine) intermediate, is energetically favored over its *basal* counterpart. Another consequence of the σ-donor strength order is that the energy difference between the two isomers of eqn. (7) is greater than the corresponding energy difference of eqn. (5):

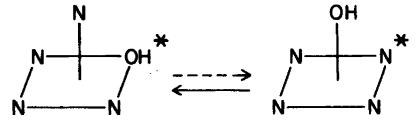

(7)

In this case the *basal*-hydroxotetraammine is energetically favored over the *apical* isomer, whereas the *basal* and the *apical* isomers of the hydroxobis(ethylenediamine) species have comparable energy. These qualitative predictions for the reactions of eqns. (4) – (7), made on the basis of spectroscopic parameters, are in agreement with the observed pattern of photoisomerizations.

Despite the success and the predictive power of the purely spectroscopic model,[1,4] other aspects of the excited state properties and processes have to be taken into account. For example, the arguments presented above do not allow any corrections of the energetics due to the chelate effect present in the ethylenediamine but not in the ammonia complexes. Since the energy difference between products and reactants in the reactions of eqns. (4) – (7) is apparently very small, any such perturbation in these systems might alter the relative energies of the isomers. However, comment on this point must await the results of investigations of complexes with chelating amines having σ-donor properties comparable to the σ-donor properties of ammonia.

The relative rates of deactivation of the *basal* and *apical* triple intermediates may also have some influence upon the product distribution.[2,21] For example, photolysis of *cis*-$[Ir(en)_2Cl_2]^+$ leads to a 10:1 *cis–trans* mixture of the $[Ir(en)_2(H_2O)Cl]^{2+}$ ions significantly different from the 100 % *trans* product of *trans*-$[Ir(en)_2Cl_2]^+$ photolysis.[26] In contrast both *trans*- and *cis*-$[Rh(en)_2Cl_2]^+$ give solely[5] *trans*-$[Rh(en)_2(H_2O)Cl]^{2+}$ as the photoproduct. These differences have been[26] attributed to the larger spin-orbit coupling present in the Ir(III) complexes, making the direct deactivation of $[Ir(en)_2Cl]^{2+*}$ intermediates faster than rearrangement. Thus, the product ratio indicates that the *basal*-$[Ir(en)_2Cl]^{2+*}$ intermediate deactivates about an order of magnitude faster than *basal* to

apical rearrangement. For the Rh(III) analogs, rearrangement is apparently much faster relative to deactivation and the same photoproduct distribution is found for both ions.[24] Consistent with this is the observation that a reexamination of the photoreactions of *cis*- and *trans*-$[Rh(NH_3)_4ClX]^{n+}$ (X=Cl or H_2O) shows that the $[Rh(NH_3)_4Cl]^{2+}$ * intermediate generated from either *cis*-$[Rh(NH_3)_4Cl_2]^+$ or *cis*-$[Rh(NH_3)_4(H_2O)Cl]^{2+}$ undergoes direct deactivation at a rate about one-fifth on the rearrangement rate.[17]

One should keep in mind that not only the relative energies of the *apical* and *basal* excited state intermediate isomers but also the energy barrier for their isomerization are functions of the ligand fields. Thus, it is notable that photoaquation of chloride from *cis*- and *trans*-$[Rh(en)_2(NH_3)Cl]^{2+}$ or photolysis of *cis*- or *trans*-$[Rh(en)_2(NH_3)(H_2O)]^{3+}$ led to little photoisomerization[5,23] at 25 °C, although substantially greater isomerization was noted when *cis*-$[Rh(en)_2(NH_3)(H_2O)]^{3+}$ was photolyzed at 50 °C. The interpretation offered was that the average ligand field of the $[Rh(en)_2(NH_3)]^{3+}$ * intermediate increased the kinetic barrier for isomerization to a point where deactivation is much faster at 25 °C.[23] In this context, it is interesting that the photoisomerization of *cis*-$[Rh(en)_2(H_2O)_2]^{3+}$ goes with a moderately large quantum yield. Although the extent of isomerization relative to deactivation of the *basal*-$[Rh(en)_2(H_2O)]^{3+}$ * excited state intermediate is as yet unknown (this depends on determining the extent of water photoexchange relative to photoisomerization), these results indicate that the apparent similarity of NH_3 and H_2O in their influence on the relative energies of the square pyramidal isomers is not as great in determining the activation barrier for rearrangements.

Acknowledgements. This research was supported by grants from the Danish Natural Science Research Council and by a NATO Research Grant. The authors with to thank Bodil Øby and Jacob Ventegodt for technical assistance, Dr. Karen Kaas for writing the computer program, and Dr. M. P. Hancock for helpful advice. We also thank Johnson Matthey for the loan of the rhodium used in these studies.

REFERENCES

1. Vanquickenborne, L. G. and Ceulemans, A. *Inorg. Chem. 17* (1978) 2730.
2. Skibsted, L. H., Strauss, D. and Ford, P. C. *Inorg. Chem. 18* (1979) 3171.
3. Purcell, K. F., Clark, S. F. and Petersen, J. D. *Inorg. Chem. 19* (1980) 2183.
4. Vanquickenborne, L. G. and Ceulemans, A. *Inorg. Chem. 20* (1981) 110.
5. Petersen, J. D. and Jakse, F. P. *Inorg. Chem. 18* (1979) 1818.
6. Skibsted, L. H. and Ford, P. C. *J. Chem. Soc. Chem. Commun.* (1979) 853.
7. Skibsted, L. H. and Ford, P. C. *Inorg Chem. 19* (1980) 1828.
8. Johnson, S. A. and Basolo, F. *Inorg Chem. 1* (1962) 925.
9. Hancock, M. P. *Acta Chem. Scand. A 33* (1979) 15.
10. Poë, A. J. and Shaw, K. *J. Chem. Soc. A* (1970) 393.
11. Pavelich, M. J. *Inorg Chem. 14* (1975) 982.
12. Burgess, C., Hartley, F. R. and Rogers, D. F. *Inorg Chim. Acta 13* (1975) 35.
13. van Eldik, R., Palmer, D. A. and Harris, G. M. *Inorg Chem. 19* (1980) 3673.
14. Poë, A. J. and Vuik, C. *Can. J. Chem. 53* (1975) 1842.
15. Palmer, D. A., van Eldik, R., Kelm, H. and Harris, G. M. *Inorg. Chem. 19* (1980) 1009.
16. Hancock, M., Nielsen, B. and Springborg, J. *Acta Chem. Scand. A 36* (1982) 313.
17. Mønsted, L. and Skibsted, L. H. *Acta Chem. Scand. A 37* (1983). *In press.*
18. Skibsted, L. H. and Ford, P. C. *Acta Chem. Scand. A 34* (1980) 109.
19. Kaas, K. and Skibsted, L. H. *To be published.*
20. Muir, M. M. and Huang, W.-L. *Inorg Chem. 12* (1973) 1831.
21. Ford, P. C. *Coord. Chem. Rev. 44* (1982) 61.
22. Skibsted, L. H., Weber, W., van Eldik, R., Kelm, H. and Ford, P. C. *Inorg Chem. 22* (1982) 541.
23. Clark, S. F. and Petersen, J. D. *Inorg Chem. 20* (1981) 280.
24. Petersen, J. D. *Inorg. Chem. 20* (1981) 3123.
25. Glerup, J., Mønsted, O. and Schäffer, C. E. *Inorg. Chem. 15* (1976) 1399.
26. Talebinasab-Savari, M. and Ford, P. C. *Inorg. Chem. 19* (1980) 2640.

Received December 16, 1983.

Acta Chemica Scandinavica A 37 (1983) 659–662

Study of Copper(II) Propionate Adducts with Diphenylphosphinoacetylene and Bis(diphenylphosphino)acetylene

MILAN MELNÍK,[a] MARKKU SUNDBERG[b] and ROLF UGGLA[b]

[a] Department of Inorganic Chemistry, Slovak Technical University, 81237 Bratislava, Czechoslovakia and [b] Department of Inorganic Chemistry, University of Helsinki, SF-00100 Helsinki, Finland

Light green compounds of the type $Cu(CH_3CH_2COO)_2 \cdot L$ (L=diphenylphosphinoacetylene or bis(diphenylphosphino)acetylene) have been prepared and for the first time copper has been found to remain in oxidation state +2 with such ligands. The magnetic and spectral behaviour has been investigated. Magnetic susceptibilities of the compounds are interpreted in terms of antiferromagnetically exchange-coupled pairs of copper atoms. The spectral data (IR, UV/VIS and ESR) suggest binuclear structures of the copper(II) acetate monohydrate type, where the phosphine molecules L are in the apical positions interacting with the copper(II) atoms, possibly through acetylenic π-bonding.

The behaviour of bis (diphenylphosphino) acetylene * (dppa) as a ligand has been the subject of a number of studies. Carty and Efraty[1,2] have described the preparation and characterization for compounds of composition $M_2X_4L_2$ (M=Pd(II), Pt(II); X=Cl, Br, I or SCN and L=dppa). On the basis of Raman and IR spectra and molecular weight data they have proposed that the structures are binuclear with bridging dppa. While dppa molecules are bidentate and coordinated only through the two phosphorus atoms, the anion ligands are monodentate. Similar conclusions about the coordination of dppa and also of diphenylphosphinomethylacetylene in compounds of zerovalent and divalent palladium and platinum have been reached by Wheelock *et al.*[3] Likewise Carty and co-workers[4,5] have shown for a series of cyclopentadienyliron carbonyl compounds with dppa that dppa is coordinated through its phosphorus atoms. Also for binuclear carbonyl and cyclopentadienyl nickel compounds[6] and for cobalt carbonyl[7] the same conclusion has been reached. In 1968 Carty and Efraty[8,9] prepared and characterized compounds of the type $(CuX)_2(dppa)_3$ (X=Cl, Br, I, NO_3, NCS, BF_4) and $(AuX)_2(dppa)_n$ (n=1: X=Cl, Br, I, NCS; n=3: X=I, NCS; n=4: X=BF_4, PF_6). Although the preparation was started from the salts of Cu(II) and Au(III), they observed only monovalent copper and monovalent gold compounds. dppa as a ligand rapidly reduces solutions of Cu(II) and Au(III) salts and behaves as a bidentate ligand in which the acetylenic bond is uncoordinated.[9] The ligating properties of diphenylphosphinoacetylene (dpa) have not been studied before.

The present study was undertaken to determine the influence of dppa and dpa on the spectral and magnetic properties of copper(II) propionate and to show how reduction of the central atom can be prevented. For this purpose compounds of the general formula $Cu(CH_3CH_2COO)_2 \cdot L$ (L=dpa or dppa) were prepared and their electronic, infrared and ESR spectra, as well as magnetic behaviour (over the temperature range 93–293 K) were studied.

* Or bis(diphenylphosphino)ethyne; recommended by IUPAC.

0302-4377/83 $2.50

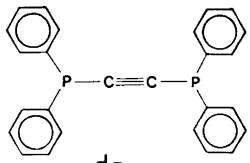

dppa

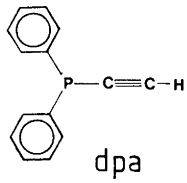

dpa

EXPERIMENTAL

Preparations. The light green $Cu(CH_3CH_2COO)_2$·dpa was prepared by reaction of copper(II) propionate and dpa[10] in equimolar ratios in hot methanol solution. The copper salt (1.5 g) was dissolved in 60 cm^3 of methanol and 1.7 g of dpa was added with stirring. The solution was heated until boiling. After dissolution of dpa the solution was left standing at room temperature. The fine light green microcrystals that formed were filtered off, washed with a small amount of cold methanol and dried at room temperature. Found: C 56.74; H 4.97; Cu 15.55; P 8.34. Calc. for $Cu(CH_3CH_2COO)_2$·dpa C 57.2; H 5.04; Cu 15.56; P 7.83. Crystals of $Cu(CH_3CH_2COO)_2$·dppa were prepared by reaction of copper(II) propionate and dppa[11] in equimolar ratio in hot methanol solution in a similar way as the dpa adduct. Found: C 61.41; H 4.80; Cu 10.44; P 10.18. Calc. for $Cu(CH_3CH_2COO)_2$·dppa: C 63.63; H 5.01; Cu 10.52; P 10.25.

Spectral studies. Infrared spectra (KBr pellets) in the region 300–4000 cm^{-1} were recorded on a Perkin Elmer Grating Infrared Spectrophotometer Model 577. Electronic spectra (Nujol mulls) in the range 10–28 kK were recorded with a Beckman DK-2A Ratio Recording Spectrophotometer and in the region 12.5–50 kK (methanol solutions) on a Perkin Elmer 402 Spectrophotometer. ESR spectra of polycrystalline samples were recorded at room temperature on a Varian Model E4 Spectrometer.

Magnetic measurements. The measurements were carried out over the temperature range 93–293 K using the Gouy method and copper(II) sulfate pentahydrate as calibrant.[12] Diamagnetic corrections were calculated from Pascal's constants.[13] The effective magnetic moments were calculated using the expression $\mu_{eff}=2.83(\chi_M^{corr} T)^{1/2}$. In the calculations the cgs/emu system was used throughout.

RESULTS AND DISCUSSION

Copper(II) compounds with dpa and dppa seem not to have been reported before. Carty and Efraty[9] observed only monovalent compounds despite their use of Cu(II) salts in the preparation. The critical factor seems to be the molar ratio of Cu(II) and dppa. When an equimolar ratio of reaction products is used, or Cu(II) in excess, dppa does not reduce metal atom.[1,2] If dppa is used in excess, however, rapid reduction of metal atoms results.[3,9] It has also been found that the dimeric structure of copper(II) acetate is effective for stabilization of oxidation state of Cu(II).[14] Equimolar amounts of Cu(II) propionate and dppa or dpa were used for the preparation of the title compounds. Copper(II) propionate has a binuclear structure in which the two copper(II) atoms are held together by four triatomic bridges of carboxylic groups.[15] The binuclear structure has been shown to exist also in methanolic solution.[16]

Infrared spectra of the compounds were recorded with a view to examining the bonding between the ligands and the central copper(II)

Table 1. The absorption bands due to stretching vibrations of P–C_6H_5 and C≡C bonds, respectively.

	ν(P–C_6H_5)/cm^{-1}	ν(C≡C)/cm^{-1}
dpa	1090	2032
dppa	1090	–
$Cu(CH_3CH_2COO)_2$·dpa	1092	2024
$Cu(CH_3CH_2COO)_2$·dppa	1093	2025, 2120

atom (Table 1). The absorption band at ≈1090 cm^{-1} has been attributed to the P–C_6H_5 bond of the free ligand,[9] and in both of the present compounds there is an absorption at ≈1090 cm^{-1}. We conclude that the phosphorus atoms are not coordinated to copper atom in the case of either dpa or dppa, since the band is found at a higher wavenumber when the phosphorus atoms are attached to the metal.[9,17] There are no strong absorptions in the region 1160–1250 cm^{-1} due to ν(P=0). Thus the phosphines cannot exist in the corresponding oxidized forms.[18] The absorption due to ν(C≡C) is IR inactive in dppa because of the symmetry, whereas in dpa the same vibration is active. The absorption band at 2032 cm^{-1} has been attributed to this vibration.[19] A weak band is observed in the infrared spectrum of $Cu(CH_3CH_2COO)_2$·dpa at ≈2025 cm^{-1} and thus the ν(C≡C) is shifted to a lower wavenumber relative to the corresponding band of the free dpa. In this same region the infrared spectrum of $Cu(CH_3CH_2COO)_2$·dppa exhibits two weak absorption bands, at 2025 cm^{-1} and 2120 cm^{-1}. These findings seem to us to indicate interaction between copper(II) and the acetylenic bond. The absorption bands at ≈1615 cm^{-1} in $Cu(CH_3CH_2COO)_2$·dpa and ≈1620 cm^{-1} in $Cu(CH_3CH_2COO)_2$·dppa can be assigned to the asymmetric stretching vibration of the carboxyl group. The corresponding symmetric vibration occurs at ≈1390 cm^{-1} in both samples. These stretching frequencies, ν_{as}COO and ν_sCOO, appear at very similar energies to those reported for copper(II) alkanoates,[20] which suggest that both oxygen atoms of the propionate anion are bonded to Cu(II) atoms in a syn-syn configuration.

The electronic spectra of the compounds were measured in Nujol mulls and in methanol solution. The solution as well as solid samples show, for both compounds, a wide asymmetric absorption band with maximum at about 14.5 kK (690 nm) and a shoulder at about 25.6 kK (390 nm). The band at about 14.5 kK is due to *d-d* transitions of the copper(II) atom and the band at about 25.6 kK is considered to be characteristic

Table 2. ESR data for $Cu(CH_3CH_2COO)_2$·dpa and $Cu(CH_3CH_2COO)_2$·dppa.

Compound	$g_\perp$	$g_\parallel$	g_{av}	$\lvert D\rvert$/cm^{-1}
$Cu(CH_3CH_2COO)_2$·dpa	2.08_6	2.34_0	2.17_4	0.330
$Cu(CH_3CH_2COO)_2$·dppa	2.09_1	2.34_2	2.17_8	0.334

Table 3 Magnetic data for $Cu(CH_3CH_2COO)_2$·dpa and $Cu(CH_3CH_2COO)_2$·dppa.

	$Cu(CH_3CH_2COO)_2$·dpa ($-\Delta\cdot10^{-6}$=302.4)		$Cu(CH_3CH_2COO)_2$·dppa ($-\Delta\cdot10^{-6}$=429.5)	
T/K	$\chi_M^{corr}\cdot10^{-6}$	μ_{eff}/B.M.	$\chi_M^{corr}\cdot10^{-6}$	μ_{eff}/B.M.
93	292	0.47	205	0.39
113	327	0.54	245	0.47
133	372	0.63	295	0.56
153	460	0.75	342	0.65
173	530	0.86	371	0.72
193	580	0.95	366	0.75
213	590	1.00	401	0.83
233	585	1.05	414	0.88
253	630	1.13	433	0.93
273	635	1.18	475	1.02
293	637	1.22	489	1.07

of the spin-spin interaction of the bridging system.[21] The band locations are very similar to those of the binuclear copper(II) carboxylates.[22]

The well-resolved ESR spectra obtained for the polycrystalline samples at room temperature are typical of a triplet state in which $|D| \geq h\nu$; that is, resonances were observed at $H_I \approx 300$ G, $H_{II} \approx 4650$ G and $H_{III} \approx 5960$ G. From the shape of the spectra we can assume that the compounds are axially symmetric dimeric or polymeric species. The values obtained for the spin Hamiltonian are given in Table 2. ESR studies of binuclear copper(II) carboxylates have often shown a small but significant fraction of the copper(II) ions to be present in a magnetically dilute form.[23] The spectra of both of the present compounds show a very weak absorption band at about 3220 G, which indicates the presence of this impurity ($g_{iso}=2.11$). The obtained ESR data (Table 2) are comparable with those found for copper(II) compounds with a binuclear structure of copper(II) acetate monohydrate type.[24]

Magnetic susceptibility data of powdered samples are given in Table 3. The magnetic susceptibilities are seen to decrease with decreasing temperature indicating antiferromagnetic interaction between the copper(II) atoms. The fit between the data and the Bleaney-Bowers equation[25] is reasonably good and the $-2J$ values are 287(14) cm^{-1} for $Cu(CH_3CH_2COO)_2 \cdot dppa$ and 282(10) cm^{-1} for $Cu(CH_3CH_2COO)_2 \cdot dpa$.

The experimental data lead us to propose binuclear units whith a square pyramidal stereochemistry around each copper(II) atom. dpa and dppa are semicoordinated to Cu(II) atoms in the apical position, seemingly through acetylenic π-bonding. If we are right, these would be the first copper(II) compounds to display such a bonding. Other studies of the compounds are in progress to verify our conclusion.

Acknowledgement. The authors wish to thank Dr. Matti Karhu for the synthesis of dpa and dppa.

REFERENCES

1. Carty, A. J. and Efraty, A. *Inorg. Nucl. Chem. Lett. 4* (1968) 427.
2. Carty, A. J. and Efraty, A. *Can. J. Chem. 47* (1969) 2573.
3. Wheelock, K. S., Nelson, J. N. and Jonassen, H.B. *Inorg. Chim. Acta 4* (1970) 399.
4. Carty, A. J., Ng, T. W., Carter, W. and Palenik, G. J. *Chem. Commun.* (1969) 1101.
5. Carty, A. J., Efraty, A., Ng, T. W. and Birchell, T. *Inorg. Chem. 9* (1970) 1263.
6. Carty, A. J., Efraty, A. and Ng, T. W. *Can. J. Chem. 47* (1969) 1429.
7. Carty, A. J. and Ng, T. W. *Chem. Commun.* (1970) 149.
8. Carty, A. J. and Efraty, A. *Can. J. Chem. 46* (1968) 1598.
9. Carty, A. J. and Efraty, A. *Inorg. Chem. 8* (1969) 543.
10. Charrier, C. *Theses,* Paris 1964, from Ref. 17.
11. Hartman, H., Beermann, C. and Czempik, H. *Z. Anorg. Allg. Chem. 287* (1956) 261.
12. Figgis, N. and Nyholm, R. S. *J. Chem. Soc.* (1959) 331.
13. Earnshaw, A. *Introduction to Magnetochemistry,* Academic, London 1968, p. 4.
14. Ondrejovič, G., Valigura, D. and Koman, M. *XXII I. C.C.C. Abstracts,* Budapest 1982, Vol. 2, p. 217.
15. Simonov, Yu. A. and Malinovskij, T. I. *Krystallografiya 15* (1970) 370.
16. Melník, M. and Näsänen, R. *Suom. Kemistil. B 42* (1969) 276.
17. Deacon, G. B. and Green, J. H. S. *Chem. Ind. London* (1965) 1031.
18. Bronzan-Planinić, P. and Meider, H. *Polyhedron 2* (1983) 69.
19. Mathis, R., Barthelot, M., Mathis, F. and Charrier, C. *J. Mol. Struct. 1* (1967–68) 481.
20. Melník, M. and Mrozinski, J. *J. Mol. Struct. 35* (1976) 133 and references therein.
21. Dubicki, L. and Martin, R. L. *Inorg. Chem. 5* (1966) 2203.
22. Melník, M. *Coord. Chem. Rev. 36* (1981) 1 and references therein.
23. Lewis, J., Mabbs, E. F., Royston, L. K. and Smail, W. R. *J. Chem. Soc. A* (1969) 291.
24. Van Niekerk, J. N. and Schoening, F. R. L. *Acta Crystallogr. 6* (1953) 227.
25. Bleaney, B. and Bowers, K. D. *Proc. R. Soc. London A 214* (1952) 451.

Received January 21, 1983.

Acta Chemica Scandinavica A 37 (1983) 663–670

Photochemical Water Exchange of Rhodium(III) Complexes. I. Photochemical Water Exchange in Relation to Photoisomerization of *cis*- and *trans*-Tetraammineaquachlororhodium(III) Ions in Aqueous Perchloric Acid

L. MØNSTED and L. H. SKIBSTED

Chemistry Department, Royal Veterinary and Agricultural University, Thorvaldsensvej 40, DK-1871 Copenhagen V, Denmark

The quantum yields for water exchange following ligand field excitation of *cis*- and *trans*-$[Rh(NH_3)_4(H_2O)Cl]^{2+}$ in aqueous acidic 1.0 M perchlorate solution at 25 °C are 0.66±0.02 and 0.39±0.04 mol · einstein^{-1} and with the assumption that photoisomerization is accompanied by water exchange in these complexes, the quantum yields for stereoretentive water exchange are 0.12±0.03 and 0.33±0.04 mol · einstein^{-1}, respectively. Similar competition between stereoretentive and stereomobile photochemical ligand substitution processes was found in the formation of *cis*- and *trans*-$[Rh(NH_3)_4(H_2O)Cl]^{2+}$ from *cis*-$[Rh(NH_3)_4Cl_2]^+$, which proceeds according to:

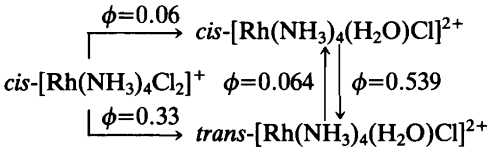

Ligand field (LF) excitation of Rh(III) complexes of the tetraammine series leads to ligand labilization and, in aqueous solution, to photoaquation with relatively high, wavelength-independent quantum yields. Such photolysis reactions are reported typically to lead to only one major product, with other thermal or photochemical reaction paths being negligible at ambient temperature.[1–5]

0302-4377/83 $2.50

Observations on the stereochemical consequences of LF photolysis of these and related hexacoordinated low spin d^6 complexes, have been rationalized on the basis of different but closely related models,[3,6–8] a key feature of which is that ligand dissociation from a hexacoordinated excited state preceeds stereorearrangement.

A key experiment for testing these theoretical models is a determination of the relative extents of photochemical water exchange and photoisomerization of *cis*- and *trans*-$[Rh(NH_3)_4(H_2O)Cl]^{2+}$, in comparison with the stereochemical consequences of photoaquation of chloride in *cis*-$[Rh(NH_3)_4Cl_2]^+$ under identical conditions. As the first part of our investigations of photochemical water exchange in Rh(III) complexes we report here the results of such experiments in aqueous acidic 1.0 M perchlorate solution.

EXPERIMENTAL

Chemicals. *cis*-$[Rh(NH_3)_4Cl_2]Cl.\frac{1}{2}H_2O$,[9] *trans*-$[Rh(NH_3)_4Cl_2]Cl$[10] and *cis*- and *trans*-$[Rh(NH_3)_4(H_2O)Cl]S_2O_6$[3] were prepared by literature methods. Ag(tos), silver *p*-toluenesulfonate, was prepared as described previously.[11] $H_2{}^{18}O$ (I.P.~98 %) was obtained from 'Alfa products'. Other chemicals were of analytical grade.

Preparation of oxygen-18 enriched aquarhodium(III) complexes. 1.0 mmol portions of *cis*-

$[Rh(NH_3)_4Cl_2]Cl.\frac{1}{2}H_2O$ in 1 ml of ^{18}O-enriched water were treated with 1.9 mmol of Ag(tos)/mmol complex at 70 °C for 17 h. The reaction mixture was then frozen and excess $H_2{}^{18}O$ removed by sublimation in vacuum. The remaining solid, which is a mixture of rhodium(III) complexes, AgCl and unreacted Ag(tos), was treated with 0.01 M $HClO_4$, and excess Ag^+ was precipitated by addition of an NaBr solution. AgCl and AgBr were filtered off and the filtrate was applied to a 10 cm × 2 cm column of Sephadex SP−C−25. Elution with 0.25 M $NaClO_4$, pH~2, (~100 ml) until the major band containing *cis*-$[Rh(NH_3)_4(H_2O)Cl]^{2+}$ had moved 3/4 of the column length, was found to separate the *cis*-$[Rh(NH_3)_4(H_2O)Cl]^{2+}$ well from *cis*-$[Rh(NH_3)_4Cl_2]^+$ and *cis*-$[Rh(NH_3)_4(H_2O)_2]^{3+}$. The desired product, *cis*-$[Rh(NH_3)_4(H_2O)Cl]^{2+}$, was then eluted with 1.0 M $NaClO_4$, pH~2. The eluate was diluted with the appropriate amount of 1.0 M $NaClO_4$ and 1.0 M $HClO_4$ to give a final complex concentration between 1 and 4 mM in a 0.50 M $HClO_4$ + 0.50 M $NaClO_4$ reaction medium.

trans-$[Rh(NH_3)_4(H_2O)Cl]^{2+}$ was prepared and purified by a similar procedure starting with *trans*-$[Rh(NH_3)_4Cl_2]Cl$. In this case, however, a reaction time of about 1 week at 70 °C was allowed.

Electronic absorption spectra of eluted fractions were used to identify and check the purity of the complex ions.

Photolysis experiments. The optical train consisted of the light source, an Osram HBO 100/2 high pressure mercury lamp, a light condenser, a heat filter (a 5 cm water-filled cell), a 366 nm interference filter, a precision shutter connected to an electronic timer and lenses focusing the light into the thermostatted photolysis cell. All optical parts were of quartz (Spindler und Hoyer, Göttingen, GFR).

Solutions of ^{18}O-labelled complex ions were kept cold in the dark until a known volume (13 ml in a typical experiment) was transferred to a 5 cm cylindrical spectrophotometer cell. The solutions were allowed 8 min at 25 °C for thermal equilibration in the photolysis cell in the thermostatted cell holder before exposure to light. During the thermal equilibration and irradiation the solutions were stirred magnetically with a teflon-coated magnetic bar. 10 ml aliquots of the photolyzed solution, for which electronic absorption spectra were recorded before and after exposure to light, were quickly frozen in liquid nitrogen and subsequently prepared for mass spectrometric analysis by sublimation in vacuum, as described previously.[11]

The total time elapsed from the preparation of the photolysis solution to freezing was monitored in order to make corrections for thermal exchange reactions.

Photolyses of *cis*-$[Rh(NH_3)_4Cl_2]^+$ were carried out in 2 cm cylindrical cells thermostatted at 25.0 °C. Reactions were interrupted periodically for spectrophotometric measurements and they were continued until no further spectral changes were detectable. Dark reactions were run under identical conditions.

Light intensities, I_o, averaged $5 \cdot 10^{-6}$ einstein min^{-1} as determined by ferrioxalate actinometry[12] over a front window of 2.3 cm^2.

Electronic absorption spectra were recorded on a Cary Varian 219 or on a Zeiss DMR 21 spectrophotometer and *mass spectrometric measurements* were performed as described previously.[11]

Calculations. The results of mass spectrometric measurements, the $^{18}O/^{16}O$ ratios, were expressed as δ-values relative to Vienna Standard Mean Ocean Water and corrected for isotopic fractionation during the sublimation procedure by a previously deduced empirical formula[11] to give the reported values of δ_{corr}.

The reactant and product concentrations in the photolyzed solutions were calculated from the recorded absorption spectra using pure component spectra recorded on the same spectrophotometer under identical conditions. Readings at every 10 nm in the absorbing wavelength region down to ≈ 250 nm were used in these calculations which utilized numerical procedures outlined previously.[13]

The straight line in Fig. 1 of the form $y=\alpha x$ was calculated by orthogonal regression analysis, *i.e.* by minimization of $\Sigma(y_{obs}-\alpha x_{obs})^2/[\sigma^2(y)+\alpha^2\sigma^2(x)]$ where $\sigma^2(y)$ and $\sigma^2(x)$ are the variances upon y and x, respectively.

RESULTS

Two kinds of results were obtained in the present study. Firstly, from the experiments with oxygen-18 enriched complexes the relative extents of photochemical water exchange and photoisomerization of *cis*- and *trans*-$[Rh(NH_3)_4(H_2O)Cl]^{2+}$ were determined. Secondly, the product distribution during photolysis of *cis*-$[Rh(NH_3)_4Cl_2]^+$ was evaluated from a spectral analysis.

cis-*[Rh(NH$_3$)$_4$(H$_2$O)Cl]$^{2+}$*. Upon 366 nm irradiation of aqueous ≈2 mM solutions of oxygen-18 enriched *cis*-$[Rh(NH_3)_4(H_2O)Cl]^{2+}$ in 0.50 M $HClO_4$ plus 0.50 M $NaClO_4$ the absorption spectrum changed and the δ-values increased.

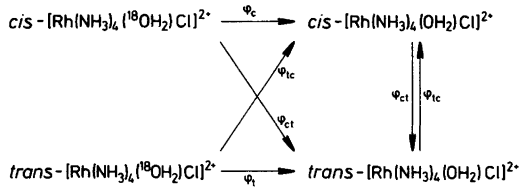

Scheme 1.

The spectral changes agreed with those expected for the photoisomerization reaction,[3,21] and the magnitude of the changes in δ indicated qualitatively a simultaneous water exchange reaction. The rates of these two reactions of enriched *cis*-$[Rh(NH_3)_4(H_2O)Cl]^{2+}$ can both be described by Scheme 1 in which isomerization is the result of a water exchange reaction and by the following rate equations for isomerization and water exchange, respectively,

$$-dc_c/dt = (I_o l/VA)\,(1-10^{-A})(\phi_{ct}\varepsilon_c c_c - \phi_{tc}\varepsilon_t c_t) + k_{ct}c_c - k_{tc}c_t$$

$$-dc_c^*/dt = (I_o l/VA)(1-10^{-A})(\phi_c+\phi_{ct})\varepsilon_c c_c^* + (k_c+k_{ct})c_c^*$$

in which c_c and c_t denote the concentration of *cis*- and *trans*-$[Rh(NH_3)_4(H_2O)Cl]^{2+}$, respectively, and k's are the thermal first-order rate constants. I_o is the intensity of the incident light, V is the volume of the solution under irradiation in a cell with a light path l, and A and ε are the absorbance of the solution and the molar absorption coefficients of the complexes, respectively, at the wavelength of irradiation. Thermal isomerization has not been detected[3] and thermal water exchange has a first-order rate constant $k_c=(1.43\pm0.02)\times10^{-3}$ min^{-1} at 25 °C in 1.0 M aqueous perchlorate solution.[14] Thermal reactions are therefore negligible under the present experimental conditions (*cf.* Table 1), and the coupled first-order differential equations for Scheme 1 can therefore be integrated to give:

$$\ln(c_c^*/c_o^*) = \ln(\delta_\infty-\delta)/(\delta_\infty-\delta_o) = [(1+\phi_c/\phi_{ct})/(1+\rho)]\,\ln[(c_c/c_o)\,(1+\rho)-\rho] \quad (1)$$

with $\rho\equiv\phi_{tc}\varepsilon_t/\phi_{ct}\varepsilon_c$. The experimental results from two series of experiments are presented in Table 1 as the concentrations of *cis*-$[Rh(NH_3)_4(H_2O)Cl]^{2+}$ evaluated from spectral analysis and as δ_{corr}-values. The quantum yield ratio was calculated by linear regression analysis, *cf.* Fig. 1. From the calculated ratio $(1+\phi_c/\phi_{ct})/(1+\rho) = 1.17\pm0.03$, $\phi_{ct}=0.539\pm0.011$ mol einstein^{-1} [21] and $\rho=0.049\pm0.002$ the stereoretentive photochemical water exchange quantum yield ϕ_c is calculated to be 0.12 ± 0.03 mol einstein.$^{-1}$

trans-*[Rh(NH$_3$)$_4$(H$_2$O)Cl]$^{2+}$*. 366 nm irradia-

Table 1. Two series of simultaneous determinations of the degree of photochemical water exchange and of the degree of photoisomerization of *cis*-$[Rh(NH_3)_4(H_2O)Cl]^{2+}$ at 25 °C after irradiation at 366 nm.

t_{irr} min	[*cis*-$Rh(NH_3)_4(H_2O)Cl^{2+}$] mM	δ_{corr} ‰	$\delta_{corr,\infty}$ ‰
Series 1			
0	1.956(18)	−11.36(19)	
1.00	1.853(15)	−10.78(19)	
3.00	1.708(18)	−9.45(15)	2.18(6)
5.00	1.521(17)	−7.50(16)	
7.00	1.383(17)	−6.27(23)	
Series 2			
0	3.23(7)	−11.48(6)	
1.667	2.98(13)	−9.39(11)	
2.00	2.79(10)	−8.26(16)	
2.00	2.90(10)	−8.99(10)	10.91(6)
2.00	2.88(13)	−9.13(19)	
2.00	2.94(10)	−8.89(11)	
2.00	2.86(9)	−8.77(10)	

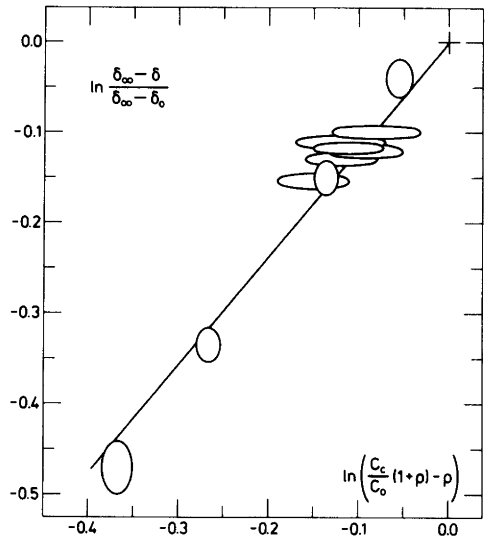

Fig. 1. Determination of the ratio between the water exchange quantum yield and the isomerization quantum yield for *cis*-$[Rh(NH_3)_4(H_2O)Cl]^{2+}$ at 25 °C. λ_{irr}=366 nm. The experimental points are indicated with a range corresponding to $\pm\sigma$ and the full line is calculated by linear regression analysis, *cf.* eqn. (1).

tion of ≈1 mM *trans*-$[Rh(NH_3)_4(H_2O)Cl]^{2+}$ solutions in 0.50 M $NaClO_4$ plus 0.50 M $HClO_4$ at 25 °C results in only small spectral changes. At this irradiation wavelength the absorbance is almost constant during the experiment, and therefore water exchange occurs at a constant rate proportional to the light intensity. The oxygen-18 enriched complex disappears (and δ_{corr} increases) according to a pseudo first-order rate law:

$$d\delta_{corr}/dt \propto -dc_t^*/dt =$$

$$[(\phi_t+\phi_{tc})(I_o/V)(1-10^{-A})(l\cdot\varepsilon_t/A)+k_t]c_t^*=k_{obs}c_t^*$$

Experimental values of δ_{corr} as a function of irradiation time, t, were approximated by a curve calculated from

$$\delta=\delta_o+\delta'\ [\exp(-k_{obs}t)-1]$$

by non-linear regression analysis involving minimization of

$$\Sigma\{\delta_{corr}-\delta\}^2/\sigma^2(\delta_{corr})$$

$\sigma^2(\delta_{corr})$ is the variance of δ_{corr}. Fig. 2 shows the experimental points and the calculated curve. As the thermal reaction time is ≈1 min longer than the time of irradiation, the rate equation is not exact. However, the error introduced hereby is negligible, since k_{obs} has the value of $(3.7\pm0.4)\times10^{-2}$ min^{-1} and k_t has been determined to be $(0.203\pm0.005)\times10^{-2}$ min^{-1} under identical conditions.[14] From these data, the photochemical quantum yield was calculated to be $(\phi_t+\phi_{tc})=0.39\pm0.04$ mol $einstein^{-1}$, which in combination with the quantum yield for *trans* to *cis* isomerization $\phi_{tc}=0.064\pm0.002$,[21] gives $\phi_t=0.33\pm0.04$ mol $einstein^{-1}$.

cis-*[Rh(NH₃)₄Cl₂]*$^+$. Irradiation of an aqueous ~3 mM *cis*-$[Rh(NH_3)_4Cl_2]^+$ solution at 366 nm results in formation of a mixture containing mainly *cis*- and *trans*-$[Rh(NH_3)_4(H_2O)Cl]^{2+}$. Spectra recorded during the photolysis showed isosbestic points at 291 and 268 nm throughout the photolysis, but a numerical analysis revealed

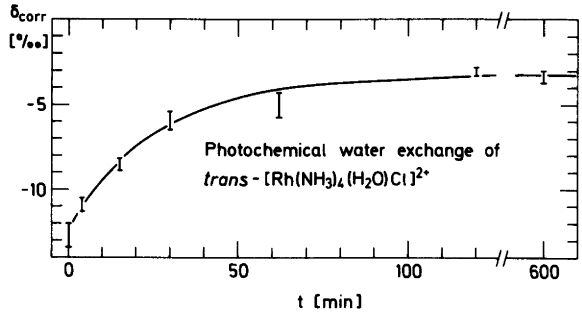

Fig. 2. Photochemical water exchange in *trans*-$[Rh(NH_3)_4(H_2O)Cl]^{2+}$ at 25 °C. λ_{irr}=366 nm. The experimental points are indicated with a range corresponding to $\pm3\sigma$. The solid curve is calculated from the determined parameters.

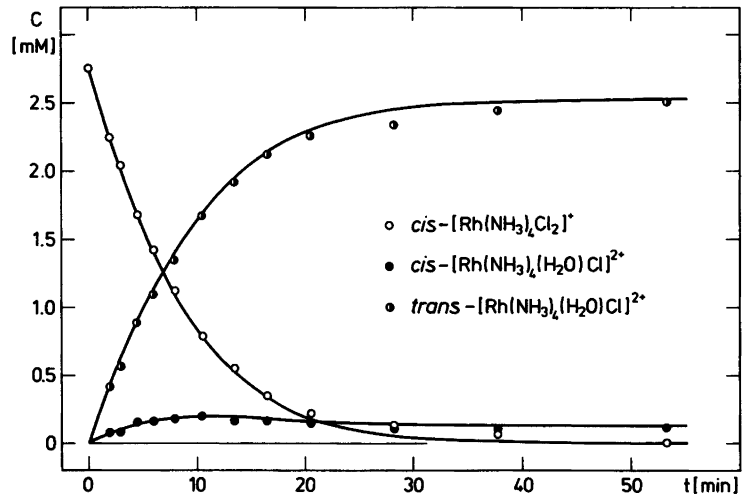

Fig. 3. 366 nm photolysis at 25 °C of 5.52 ml of a 2.75 mM *cis*-$[Rh(NH_3)_4Cl_2]^+$ aqueous solution (0.50 M $HClO_4$+0.50 M $NaClO_4$). The experimental points are calculated from the absorption spectra of the pure components of the reaction mixtures as described in Ref. 13. The solid curves are calculated by numerical integration of the coupled photochemical differential equations using the light intensities, the molar absorption coefficients at the wavelength of irradiation (366 nm), and quantum yields determined by linear regression analysis using data for this experiment as well as for similar experiments [21] starting from the isomeric tetraammineaquachlororhodium(III) species, as described in Ref. 14. The determined quantum yields are given in Table 2. The curve for formation of the triammine species is omitted for the sake of clarity.

that the reaction mixture, in addition to the parent *cis*-$[Rh(NH_3)_4Cl_2]^+$ and the products *cis*- and *trans*-$[Rh(NH_3)_4(H_2O)Cl]^{2+}$, contained small amounts of at least one other component. Fig. 3 shows the result of a spectral analysis using the pure component spectra of *cis*-

Table 2. Ligand photosubstitution quantum yields for some Rh(III) complexes in aqueous solution.[a]

Complex	Products	ϕ[mol einstein^{-1}]	$\varkappa$[b]	Ref.
Water exchange				
$[Rh(NH_3)_5(H_2O)]^{3+}$	$[Rh(NH_3)_5(H_2O)]^{3+}$	0.43(3)		15
trans-$[Rh(NH_3)_4(H_2O)Cl]^{2+}$	*trans*-$[Rh(NH_3)_4(H_2O)Cl]^{2+}$	0.33(4)	0.19(2)	Present work
	cis-$[Rh(NH_3)_4(H_2O)Cl]^{2+}$	0.064(2)		
cis-$[Rh(NH_3)_4(H_2O)Cl]^{2+}$	*cis*-$[Rh(NH_3)_4(H_2O)Cl]^{2+}$	0.12(3)	0.22(3)	Present work
	trans-$[Rh(NH_3)_4(H_2O)Cl]^{2+}$	0.539(11)		
Chloride hydrolysis				
$[Rh(NH_3)_5Cl]^{2+}$	$[Rh(NH_3)_5(H_2O)]^{3+}$	0.18(1)		16
trans-$[Rh(NH_3)_4Cl_2]^+$	*trans*-$[Rh(NH_3)_4(H_2O)Cl]^{2+}$	0.14(1)		1
cis-$[Rh(NH_3)_4Cl_2]^+$	*cis*-$[Rh(NH_3)_4(H_2O)Cl]^{2+}$	0.063(7)	0.19(2)	Present work
	trans-$[Rh(NH_3)_4(H_2O)Cl]^{2+}$	0.328(9)		
	triamminerhodium(III) species	0.013(3)		

[a] Wavelength of irradiation 366 nm except for $[Rh(NH_3)_5(H_2O)]^{3+}$ (313 nm) and *trans*-$[Rh(NH_3)_4Cl_2]^+$ (407 nm). Temperature 25 °C except for $[Rh(NH_3)_5(H_2O)]^{3+}$ (20 °C). [b] $\varkappa$ denotes the ratio of the quantum yield for formation of *cis*-product and that for formation of *trans*-product, *i.e.* $\varkappa=\phi_{tc}/\phi_t$ for *trans*-complexes and ϕ_c/ϕ_{ct} for *cis*-complexes, respectively.

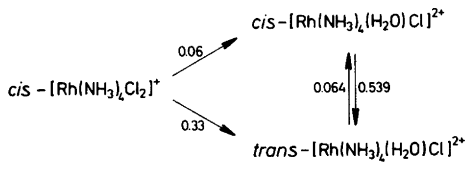

Scheme 2.

$[Rh(NH_3)_4Cl_2]^+$, *cis*- and *trans*-$[Rh(NH_3)_4(H_2O)Cl]]^{2+}$ and a spectrum of the unknown additional component calculated assuming that the end photolyzed solution contained 4 % of the species. The quantum yields calculated from this analysis according to Scheme 2 are given in Table 2. The formation of aquation products by thermal processes could be excluded, since a solution left in the dark during the photolysis showed no spectral changes.

DISCUSSION

LF irradiation of *cis*-$[Rh(NH_3)_4Cl_2]^+$, *trans*-$[Rh(NH_3)_4Cl_2]^+$ and *cis*-$[Rh(NH_3)_4(H_2O)Cl]^{2+}$ in acidic aqueous solution is known to result in formation of the common principal photoproduct *trans*-$[Rh(NH_3)_4(H_2O)Cl]^{2+}$, which has been considered photoinert since only minor spectral changes have been observed after the completion of the primary photoreactions.[1-3] This apparent insensitivity to light does not, however, preclude photoinduced exchange of coordinated water with solvent water molecules, and the present study clearly demonstrates that *trans*-$[Rh(NH_3)_4(H_2O)Cl]^{2+}$ is photoactive with a ligand substitution quantum yield comparable to those for other related rhodium(III) complexes. The photochemical water exchange does, however, result in partial photoisomerization to *cis*-$[Rh(NH_3)_4(H_2O)Cl]^{2+}$, and the water exchange quantum yield is thus the sum of the quantum yield for the stereoretentive and for the stereomobile exchange processes, of which the former is by far the predominant. The sum of the quantum yields for the stereoretentive and the stereomobile water exchange ($\phi_t+\phi_{tc}$) in *trans*-$[Rh(NH_3)_4(H_2O)Cl]^{2+}$ is comparable with the quantum yield for the water exchange in $[Rh(NH_3)_5(H_2O)]^{3+}$ determined previously by Ford and Petersen,[15] as seen from Table 2. In contrast, the total quantum yield ($\phi_c+\phi_{ct}$) for water exchange in *cis*-$[Rh(NH_3)_4(H_2O)Cl]^{2+}$ is significantly higher. The relative magnitude of the water exchange quantum yields for these three aqua-complexes parallel the relative magnitudes of the chloride hydrolysis quantum yields in the corresponding series of chloro-complexes (see Table 2). However, as was recently demonstrated[17] for a series of amminebromorhodium(III) complexes, the reaction quantum yields do not simply reflect the excited state reactivities for this type of compound, since a reaction quantum yield is the ratio between the rate constant for the chemical reaction of the excited state and the sum of the rate constants for all processes which drain the excited state. A combination of the water exchange quantum yields in Table 2 with excited state lifetime and luminiscence quantum yield data permits an evaluation of the factors which control the excited state reactivities for the ammineaquarhodium(III) complexes in question.[21,22]

The observation of both stereoretentive and stereomobile photochemical water exchange in the isomeric $[Rh(NH_3)_4(H_2O)Cl]^{2+}$ species is important from a mechanistic point of view. Theories dealing with the photoisomerization reactions of d^6 complexes assume that ligand dissociation from a hexacoordinate triplet excited state precedes stereorearrangement,[3,6-8] and according to these theories, the product stereochemistries are controlled by the relative energies of the *basal* and the *apical* isomers of the square-pyramidal five-coordinate intermediate, both of which are in a triplet excited state and can isomerize *via* a trigonal bipyramidal intermediate prior to deactivation and trapping by a solvent molecule. According to AOM-calculations[6-8] the stronger σ-donor ligand prefers a *basal* position in the square pyramidal intermediate, which, when the proposed[6,18] series $\sigma_{OH^-}>\sigma_{NH_3}>\sigma_{Cl^-}$ is taken into account, explains the experimental observations of photoisomerization between *cis* and *trans* complexes.[3-5]

This model also provides an explanation for the observed photoisomerization of *cis*-$[Rh(NH_3)_4(H_2O)Cl]^{2+}$ in postulating that photoisomerization is initiated by dissociation of the water ligand. In contrast to this, both empirical and semitheoretical rules[19,20] predict that an equatorial ammonia ligand should be labilized, suggesting that photoisomerization in this type of compound is a purely intramolecular process.

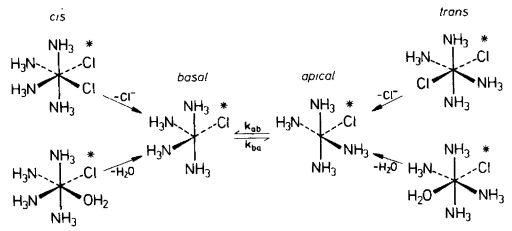

Fig. 4. Excited-state reactions of *cis-* and *trans*-$[Rh(NH_3)_4(H_2O)Cl]^{2+}$ and *cis-* and *trans*-$[Rh(NH_3)_4Cl_2]^+$ within a limiting dissociative model. Excitation and deactivation processes are not shown. *basal*-$[Rh(NH_3)_4Cl]^{2+*}$ is the common intermediate initially formed from *cis*-$[Rh(NH_3)_4(H_2O)Cl]^{2+*}$ and *cis*-$[Rh(NH_3)_4Cl_2]^{+*}$ by ligand dissociation, and, similarly, *apical*-$[Rh(NH_3)_4Cl]^{2+*}$ is the common intermediate formed from *trans*-$[Rh(NH_3)_4(H_2O)Cl]^{2+*}$ and *trans*-$[Rh(NH_3)_4Cl_2]^{+*}$.

The results reported here are very conclusive since water is the labilized ligand and water exchange is thus associated with the photoisomerization process.

A key feature of the dissociative model is that both the isomeric tetraamminedichloro- and tetraammineaquachlororhodium(III) species react *via* a common penta-coordinated excited-state intermediate, $[Rh(NH_3)_4Cl]^{2+*}$, capable of undergoing *basal/apical* rearrangement as depicted in Fig. 4. Fig. 3 shows additional experimental data in support of this hypothesis, since the photolysis of *cis*-$[Rh(NH_3)_4Cl_2]^+$ is seen to result in both stereomobile and stereoretentive chloride substitution. However, the photoreactions of *cis*-$[Rh(NH_3)_4Cl_2]^+$ outlined in Scheme 2 are complicated by significant loss of coordinated ammonia for which a quantum yield of 0.007 mol einstein^{-1} has been reported.[3] This is in contrast to the behaviour of the isomeric tetraammineaquachlororhodium(III) species, for which photochemical ammonia ligand aquation has not been detected.[3,21] The small amounts of uncharacterized reaction products formed in the photolysis of *cis*-$[Rh(NH_3)_4Cl_2]^+$ can thus be accounted for as a mixture of isomeric triammineaquadichloro- and mainly triamminediaquachlororhodium(III) species. From the absorption spectrum of the exhaustively photolyzed solution a triammine isomer mixture can constitute ≈4 % if reasonable molar absorption coefficients for the rhodium(III) species are assumed. The presence of a triammine mixture content leads to a quantum yield for the ammonia loss of 0.013±0.003 mol einstein,$^{-1}$ in good agreement with the previously published value.[3]

The dissociation of chloride from *cis*-$[Rh(NH_3)_4Cl_2]^+$ and of water from *cis*-$[Rh(NH_3)_4(H_2O)Cl]^{2+}$ generates the same intermediate, *basal*-$[Rh(NH_3)_4Cl]^{2+*}$, and the ratio ϕ_c/ϕ_{ct} is consequently expected to be identical for the photoreactions of the two *cis*-tetraammine complexes. The limiting dissociative model for excited-state ligand substitution reactions of aminerhodium(III) complexes has now been tested by a variety of different experiments.[3,17,23,24] The data presented in Table 2, which show that the ϕ_c/ϕ_{ct} ratios are identical within experimental error, provide strong evidence for a common five-coordinated excited-state intermediate in the photoreactions of *cis*-$[Rh(NH_3)_4(H_2O)Cl]^{2+}$ and *cis*-$[Rh(NH_3)_4Cl_2]^+$. This observation provides circumstantial evidence in support of the limiting dissociative model.

The observation that ϕ_{tc}/ϕ_t for the water exchange in *trans*-$[Rh(NH_3)_4(H_2O)Cl]^{2+}$ is identical to ϕ_c/ϕ_{ct} for the two *cis*-tetraammine complexes, could indicate that *basal/apical* excited-state equilibrium is attained prior to deactivation. A distinction between thermodynamic and kinetic control[3,24] of the product stereochemistry cannot, however, be made solely on the basis of the results presented in Table 2, but requires excited-state lifetime data. A more detailed discussion has, therefore, to await such data[22] and the results of a reinvestigation of the photochemistry of *trans*-$[Rh(NH_3)_4Cl_2]^+$, which is now in progress.[21]

Acknowledgements. This research was supported by grants from the Danish Natural Science Research Council and by a grant from the Carlsberg Foundation. The authors wish to thank Bodil Øby for technical assistance and the Geophysical Isotope Laboratory at the University of Copenhagen, in particular Dr. Niels Gundestrup, for carrying out the mass spectrometric analyses. Drs. O. Mønsted and M. P. Hancock are thanked for helpful discussions and we are grateful to Johnson Matthey for a loan of the rhodium used in these studies.

REFERENCES

1. Kutal, C. and Adamson, A. W. *Inorg. Chem. 12* (1973) 1454.
2. Strauss, D. and Ford, P. C. *J. Chem. Soc. Chem. Commun.* (1977) 194.
3. Skibsted, L. H., Strauss, D. and Ford, P. C. *Inorg. Chem. 18* (1979) 3171.
4. Skibsted, L. H. and Ford, P. C. *Inorg. Chem. 19* (1980) 1828.
5. Skibsted, L. H. and Ford, P. C. *J. Chem. Soc. Chem. Commun.* (1979) 853.
6. Vanquickenborne, L. G. and Ceulemans, A. *Inorg. Chem. 17* (1978) 2730.
7. Purcell, K. F., Clark, S. F. and Petersen, J. D. *Inorg. Chem. 19* (1980) 2183.
8. Vanquickenborne, L. G. and Ceulemans, A. *Inorg. Chem. 20* (1981) 110.
9. Hancock, M. P. *Acta Chem. Scand. A 29* (1975) 468.
10. Poë, A. J. and Twigg, M. V. *Can. J. Chem. 50* (1972) 1089.
11. Mønsted, L. and Mønsted, O. *Acta Chem. Scand. A 36* (1980) 259.
12. Hatchard, C. G. and Parker, C. A. *Proc. R. Soc. London A 235* (1956) 518.
13. Mønsted, L. and Mønsted, O. *Acta Chem. Scand. A 32* (1978) 19.
14. Mønsted, L. and Mønsted, O. *Acta Chem. Scand. A. To be published.*
15. Ford, P. C. and Petersen, J. D. *Inorg. Chem. 14* (1975) 1404.
16. Bergkamp, M. A., Watts, R. J. and Ford, P. C. *J. Am. Chem. Soc. 102* (1980) 2627.
17. Sexton, D. A., Skibsted, L. H., Magde, D. and Ford, P. C. *J. Phys. Chem. 86* (1982) 1758.
18. Glerup, J., Mønsted, O. and Schäffer, C. E. *Inorg. Chem. 15* (1976) 1399.
19. Adamson, A. W. *J. Phys. Chem. 71* (1967) 798.
20. Sheridan, P. S. and Adamson, A. W. *J. Am. Chem. Soc. 96* (1974) 3032.
21. Mønsted, L. and Skibsted, L. H. *To be published.*
22. Sexton, D. A., Bergkamp, M. A., Skibsted, L. H., Magde, D. and Ford, P. C. *To be published.*
23. Skibsted, L. H., Weber, W., van Eldik, R., Kelm, H. and Ford, P. C. *Inorg. Chem. 22* (1983) 541.
24. Petersen, J. D. *Inorg. Chem. 20* (1980) 3123.

Received January 14, 1983.

Acta Chemica Scandinavica A 37 (1983) 671–677

3-Chloro-2-methyl-1-propene. Molecular Structure and Conformation in the Gas phase as Determined by Electron Diffraction and Molecular Mechanics Calculation

S.H. SCHEI

Department of Chemistry, University of Trondheim, NLHT Rosenborg, N-7000 Trondheim, Norway

A gas phase electron diffraction study of 3-chloro-2-methyl-1-propene shows that at 20 °C there is 87(7) % of the *gauche* conformer with average torsional angle 115.6 (2.8)° relative to 0° for the *syn* form, which was assumed to be the minor contributing conformer having an r.m.s. torsional amplitude of 12(8)°. The *gauche* structural results in terms of r_a distances and $\angle_\alpha$ angles were found to be; r(C=C)=1.340(6) Å, r(C–CH_2Cl)=1.492(4) Å, r(C–Cl)=1.791(5) Å, $\angle$C=C–CH_2Cl=121.5(1.2)°, ($\angle$C=C–CH_2Cl–$\angle$C=C–CH_3= −0.5°, constraint from molecular mechanics calculation), $\angle$C–C–Cl=112.8(.4)°. Uncertainties are given as 2σ,where σ includes uncertainty due to correlation among observations and parameters used in the data reduction. The molecular mechanics calculations agreed well with the electron diffraction conformational result.

It has been found by both vibrational spectroscopy and electron diffraction (ED) studies, that 2-halosubstitution of 3-chloro-1-propene (hereafter denoted CP) changes the conformational composition considerably from that of CP itself.[1–4]

However, vibrational spectroscopy study of the corresponding methylsubstituted molecule, 3-chloro-2-methyl-1-propene (hereafter denoted CMP) showed that the conformational composition in that case, as for CP, was strongly dominated by the *gauche* form (Fig. 1) and only two conformers were found,[6] in contrast to an earlier vibrational spectroscopy study of CMP[7] which was interpreted as showing three confor-

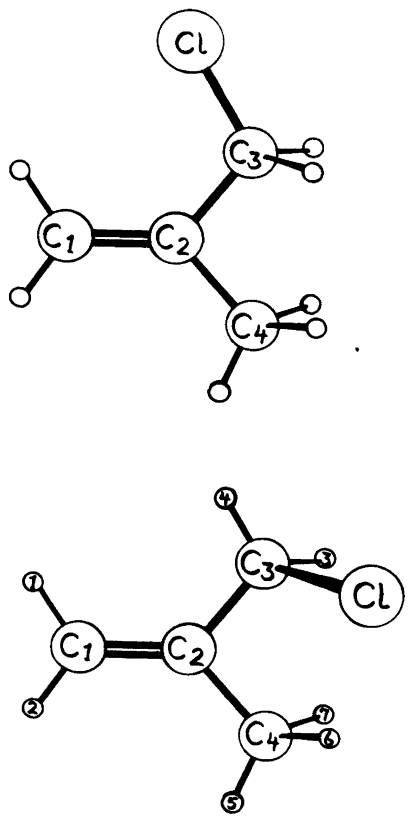

Fig. 1. 3-Chloro-2-methyl-1-propene. *Syn* (upper) and *gauche* (lower) conformers with numbering of the atoms. H-atoms are shown with numbers only.

0302-4377/83 $2.50

mers. The Raman band intensities[6] as a function of temperature in liquid phase gave an energetical preference of 2.5±0.5 kJ mol^{-1} for the *gauche* form, corresponding to about 15 % of the syn conformer at 20 °C. *Syn* was favoured as the second conformer in agreement with the results for other 3-substituted propenes.[5,8–13]

Based on the indications that the second conformer must be *syn*, the ED investigation of CMP was initiated. Contrary to the case of CP, an ED study of CMP will hardly be able to discern between small amounts of *syn* or *anti* (torsional angle 180° relative to *syn*) forms, due to their similar distribution of the C···Cl distances. However, the *gauche* + *syn* presumption should make it possible to obtain both quantitative conformational and structural information about CMP in gas phase.

EXPERIMENTAL AND DATA REDUCTION

A commercial sample of CMP (>97 %) was obtained from Fluka AG. Data were recorded with the Balzers Eldigraph KDG-2[14,15] at a nozzle temperature of 20 °C on Kodak Electron Image plates. The electron wavelength was calibrated against benzene.[16] Optical densities were measured by the Joyce Loebl densitometer. Four plates were selected for analysis from each of the two nozzle-to-plate distances, 50 and 25 cm. The data were reduced in the usual way.[17,18] The least squares refinements were based on one average curve from each camera distance in the form $sI_m(s)$. Fig. 2 shows the composite $sI_m(s)$ curve.

STRUCTURE AND CONFORMATIONAL ANALYSIS

Molecular mechanics calculations. The molecular mechanics (MM) calculations were based on the use of non-bonded potential functions described as Morse curves.[19] The parameters used in these calculations are the same as those used for other chloro-containing molecules.[20,21] The MM calculations were made with complete geometry relaxation, except that the carbon skeleton was restricted to planarity. Well-defined minima were found for *gauche* and *syn* positions, the *gauche* conformer being 2.8 kJ mol^{-1} lower in energy than the *syn* form. The *anti* energy

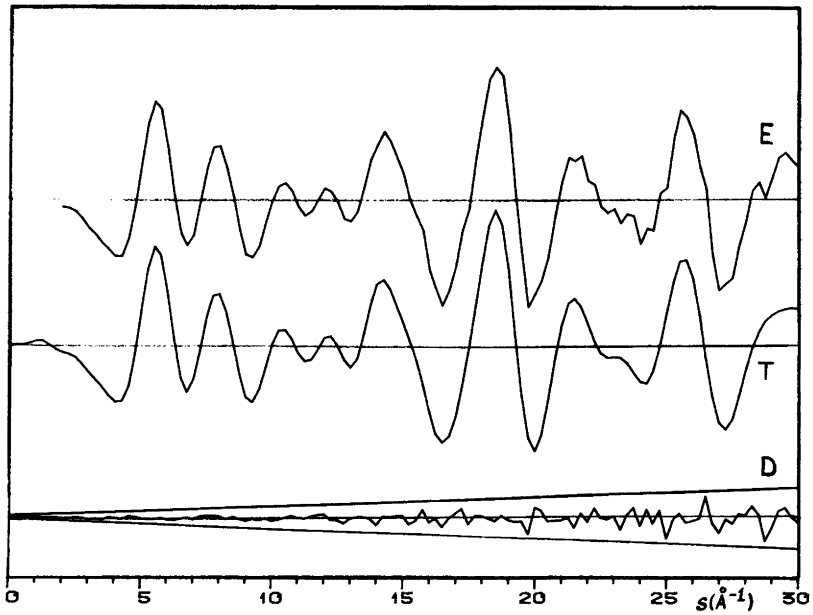

Fig. 2. 3-Chloro-2-methyl-1-propene. Intensity curves in the form sI_m (*s*). Experimental curve (E) is the composite of all plates and distances. Theoretical curve (T) was calculated from parameters in Tables 3 and 4. Difference curve (D) is E−T. All curves are on the same scale. The straight lines show the experimental uncertainties as three times the standard deviation. Δs=0.25 Å^{-1}.

maximum was calculated 15 kJ mol^{-1} above the *gauche* minimum. Results from the calculations are given in Table 1. If the charges on the atoms (Table 1) were neglected, the *syn* minus *gauche* energy difference was reduced to 2.0 kJ mol^{-1}.

The conformational composition resulting from the MM calculations was calculated by inclusion of values for the vibrational and rotational partition functions according to the MM results.[18] Thus, the MM calculations (Table 1) suggest 18 % *syn* conformer at 20 °C.

Vibrational quantities. Normal coordinate calculations based on a valence force field have been made for $CH_2=C(CH_3)-CH_2X$, X=Br, C≡N.[22] A corresponding force field was used for CMP. No refinement of force constants was made. The force constants listed in Table 2 reproduced the *gauche* frequences[6] to an average deviation of 16 cm^{-1}. Root mean square amplitudes of vibration (*l*) are given in Table 3.

Analysis of electron diffraction data. The experimental radial distribution (RD) curve is shown in Fig. 3. The main distances of CMP can be located directly from the figure. It is obvious that the dominating conformer is *gauche*.

A unit weight matrix was used in the least squares refinements. The calculations were made by use of geometry consistent r_a distances.[23]

The *gauche* conformer has symmetry C_1. The lack of symmetry combined with the two C–C distances and the two C=C–C angles of the same magnitude, made geometrical constraints necessary. Studies of other 3-substituted propenes have indicated that relative angle values calculated by the MM method are quite good. Therefore, $\Delta\angle C=C-C = \angle C=C-C_3-\angle C=C-C_4$ was kept at the MM calculated value. $\Delta r(C-C)=r(C_2-C_4)-r(C_2-C_3)$ was estimated to be 0.009 Å from the distances found in propene[24] and CP.[5]

C–C–H angles for the CH_3 and CH_2Cl groups were set equal to the values found in isobutene[25] and CP,[5] respectively. Local C_{3v} and C_s symme-

Table 1. 3-Chloro-2-methyl-1-propene, results obtained from molecular mechanics calculation.[a]

	gauche	*syn*
Energy (kJ mol^{-1})	0.0	2.8
Torsional angle in energy minimum (deg.)	110.0	0.0
Torsional force constant (mdyn Å rad^{-2})	0.09	0.03
Valence angles (deg.)		
∠C=C–C_3	122.5	124.0
∠C=C–C_4	122.0	121.1
∠C–C–Cl	112.5	114.4

[a] The following charges (*q*) were used on the atoms: $q(Cl)=-0.14$, $q(C_{1-2})=-0.01$, $q(C_3)=0.01$, $q(C_4)=-0.02$, $q(H_{1-2})=0.02$, $q(H_{3-4})=0.04$, $q(H_{5-7})=0.02$ in e-units.

Table 2. 3-Chloro-2-methyl-1-propene, the valence force field used in the calculation of vibrational quantities. Force constants are given in mdyn $Å^{-1}$ (stretch) and mdyn Å rad^{-2} (bend, torsion) for *gauche/syn* conformer.

Type	Coordinate	Value
str.	C=C	9.14
	C–C	4.24
	C–Cl	2.66
	=C–H	5.00
	C_3–H	4.82
	C_4–H	4.71
bend	C=C–C_3	0.97/1.83
	C=C–C_4	0.97
	C–C–C	0.73
	C–C–Cl	1.01/1.52
	C=C–H	0.52
	H–C_1–H	0.39
	C–C_3–H	0.76
	H–C_3–H	0.53
	C–C_4–H	0.65
	H–C_4–H	0.54
	Cl–C–H	0.63
tors	C=C	0.49
	C_2–C_3	0.14/0.03
	C_2–C_4	0.08
o.o.p.	$=CH_2$	0.21
	$=CC_2$	0.35
str./str.	C–C/C–C	0.78
	C_3–H/C_3–H	0.08
	C_4–H/C_4–H	0.05
str./bend	C=C/C=C–H	0.40
	C=C/C–C–C	−0.43
	C–C/C–C–C	0.32
	C–C/C–C_3–H	0.36/0.41
	C–C/C–C_4–H	0.35
bend/bend	C–C_3–H/C–C_3–H	−0.16/−0.20
	C–C_4–H/C–C_4–H	−0.01
	Cl–C–H/C–C_3–H	0.07/0.11
	C=C_3–C/C–C–Cl	– /0.52
tors./o.o.p.	C=C/=CC_2	−0.06/–

Table 3. 3-chloro-2-methyl-1-propene. Calculated and refined root mean square amplitudes of vibration (in Å) for bonded distances, C···C, C···Cl and Cl···H distances. Values are given as *gauche/syn*.

No.	Distance	r_a	$l_{calc.}$	$l_{ref.}$[a]	
17	C–H	1.10	0.077		
18	C=C	1.34	0.042		
19	C–C	1.50	0.052		
20	C–Cl	1.79	0.052	0.055(5)	
21	C_1···Cl	3.72/3.03	0.116/0.100	0.117(11)	
22	C_2···Cl	2.73	0.078/0.073	0.063(6)	
23	C_4···Cl	3.29/4.10	0.154/0.073	0.138(15)	
24	C_1···C_3	2.47	0.066	0.066	}
25	C_1···C_4	2.47	0.066	0.066	}(11)
26	C_3···C_4	2.56	0.068	0.068	}
27	Cl···H_3	2.37	0.115		
28	Cl···H_6	2.92/4.37	0.251/0.196		
29	Cl···H_7	3.69/4.48	0.284/0.196		
30	Cl···H_1	3.93/2.57	0.201/0.173		
31	Cl···H_5	4.24/4.87	0.180/0.122		
32	Cl···H_2	4.60/4.10	0.148/0.126		

[a] For type of uncertainty, see text and Ref. 18.

tries were assumed for the CH_3 and CH_2Cl groups.

Since there is only a small amount of the *syn* conformer present, the determination of this amount may be relatively sensitive to the choice of *syn* geometry compared to *gauche* geometry. For similar molecules *syn* minus *gauche* angle values calculated by the MM method seem to reflect trends[26] found by experimental methods. Accordingly, MM calculated differences (*syn* – *gauche*) for both the C=C–C and the C–C–Cl angles were used. It was not possible to release the constraints mentioned earlier. For example, an attempt to refine both ∠C=C–C_3 and ∠C=C–C_4 showed large standard deviation, and the correlation coefficient between those parameters was 0.99. The effect of the constraints was tested by systematic variations of the actual parameters. The constraints in the *gauche* conformer had, within reasonable limits, no influence upon the conformational composition. However, when the *syn* and *gauche* conformers were restricted to have equal geometries, exept for the torsional amplitude $\langle(\Delta\tau_s)^2\rangle^{1/2}$ and the average torsional angle τ_g, then α_s (amount of *syn* conformer) was found to increase 5 %.

In a series of refinements the *syn* conformer was represented by several pseudo-conformers.[18] Then the corresponding *l*-values were calculated without contribution from torsional movement. Refinement of the relative amount of pseudo-conformers gave no change in the total amount of *syn* conformers. The pseudo-conformers were in some refinements kept at distributions corresponding to various potentials. Even this gave only negligible changes in the total α_s.

Different sets of calculated vibrational quantities were used. The best fit between experimental and theoretical data was obtained with a *gauche* torsional force constant f_τ=0.14 mdyn Å rad^{-2}.

As expected, refinements including *anti* instead of *syn* conformer resulted in a nearly equally good fit between theoretical and experimental data. For reasons mentioned earlier, this possibility was disregarded.

Table 4. 3-chloro-2-methyl-1-propene. Final results from the least squares refinements of electron diffraction data at 20 °C. Values are given as *gauche/syn* (r_a in Å, $\angle_\alpha$ in degrees, α and *R*-factor in %).

No.	Parameter	$r_a/\angle_\alpha$
1	r(C=C)	1.340(6)[a]
2	$r(C_2–C_3)$	1.492(4)
3	Δr(C–C)[b]	0.009[c]
4	r(C–Cl)	1.791(5)
5	r(=C–H)	1.098(9)
6	Δr(C–H)[b]	0.009[c]
7	∠C=C–C_3	121.5(12)/123.0[d]
8	$\Delta\angle$C=C–C[b]	−0.5[d]/−2.9[d]
9	∠C–C–Cl	112.8(0.4)/114.7[d]
10	∠C=C–H	119.2(3.9)
11	∠C–C_3–H	112.5[c]
12	∠C–C_4–H	111.0[c]
13	*p*Cl–C–H[e]	120.5[d]
14	τ_g	115.6(2.8)
15	$\langle(\Delta\tau_s)^2\rangle^{1/2}$	12(8)
16	α_g	87(7)
	R^{lc}/R^{sc}[f]	6.7/12.3

[a] For type of error limit, see text and Ref. 18. [b] Defined in text. [c] For choice of value, see text. [d] Value or relative value taken from molecular mechanics calculation. [e] Angle between projections of C–Cl and C_3–H on plane perpendicular to C_2–C_3 bond. [f] lc and sc denotes long and short camera distances, respectively.

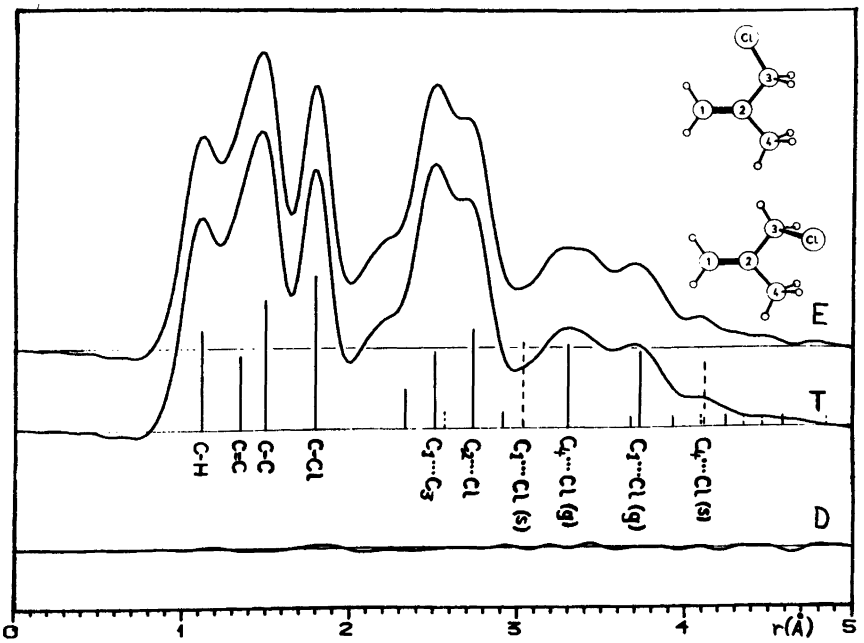

Fig. 3. 3-Chloro-2-methyl-1-propene. Radial distribution curves as Fourier transforms of the intensity curves in Fig. 2, using a modification function $(f_{Cl}(s)\cdot f_C(s))^{-1}$, theoretical data for unobserved area $s < 2.0$ Å^{-1} and damping $B=0.002$ Å^2. The vertical lines show the most important distances, height being proportional to the weight of the distance. The unlabelled lines refer to Cl···H distances. Dotted vertical lines refer to *syn* conformer, but their heights are not scaled to the conformational amount. All curves are on the same scale.

RESULTS AND DISCUSSION

Geometrical, vibrational and conformational results as found from the ED study are given in Tables 3 and 4. The uncertainties are given as 2σ, where σ includes uncertainty due to correlation among observations and uncertainty in the parameters used in the data reduction.[18]

Correlation coefficients for which $|\rho| > 0.5$ are: $\rho(1/7) = -0.56$, $\rho(1/11) = 0.70$, $\rho(2/7) = -0.52$, $\rho(2/15) = 0.52$, $\rho(4/15) = 0.78$, $\rho(5/14) = 0.63$, $\rho(5/15) = 0.99$, $\rho(7/14) = -0.78$, $\rho(7/23) = 0.88$, where parameter numbers are given in Tables 3 and 4.

Figs. 2 and 3 show the theoretically calculated intensity and RD curves, respectively.

87(7) % *gauche* conformer in the gaseous phase indicates no noticable change in conformational composition when passing from liquid[6] (80–85 % depending on the value of the partition functions) to gas. The agreement with the MM calculation (82 %) is better than can generally be expected for this type of molecule. It is interesting to note that the *syn* amount of CMP is not much different from the amount of the most symmetric form in 1-chloro-2-methylpropane (*ca.* 20 %).[27]

The determination of the conformational composition was slightly dependent upon f_τ^g, and introduction of *syn* minus *gauche* angle differences. However, the values chosen for these quantities are reasonable according to existing information on these kinds of molecules.[26] α_g was also slightly influenced by the refinement of a few l_{ij}-values. This dependecy is well covered by the error limit. Further confidence in the result is given by the fact that refined l_{ij}'s show small deviations from calculated values, with one exception. The vibrational amplitude for the distance Cl···C_2 is significantly lower than the calculated value (Table 3). Comparison with similar molecules [18,28–30] shows that the calculated value is quite close to what is normally calculated for a Cl···C distance over one angle.

Table 5. Geometrical parameters of 3-chloro-2-methyl-1-propene compared with related molecules.[a]

Molecule	Ref.	C=C	=C−CH_2Cl	C−Cl	C=C−C_3	C−C−Cl	τ_g
CH_2=C(CH_3)−CH_2Cl(r_a)	This work	1.340	1.492	1.791	121.5	112.8	115.6
CH_2=CH−CH_2Cl(r_a)	5	1.337	1.494	1.792	122.5	110.7	123.5
CH_2=C(CH_2Cl)−CH_2Cl(r_a)	31	1.331	1.502	1.799	121	111.5	115
CH_2=CCl−CH_2Cl(r_a)	2	1.334	1.504	1.776	127.6	110.2	108.9
CH_2−CH_2−CH−CH_2Cl(r_a)	18	–	–	1.798	–	112.6	116.0
CH_3−CH(CH_3)−CH_2Cl(r_g)	27	–	–	1.804	–	112	126
CH_2=C(CH_3)−CH_3(r_g)	25	1.342	–	–	122.0	–	–

[a] Uncertainties are not given, since they are not comparable among the different works.

For chloromethyl-cyclopropane[18] the corresponding $l_{Cl\cdots C}$ was refined close to a value calculated from a related force field. The discrepancy between calculated and refined value in the present case does not seem to have an obvious explanation, but similar differences have also been observed in other molecules.

The f_τ^g which reproduces the *gauche* torsional frequency in gas phase (84 cm^{-1})[6] is 0.08 mdyn Å rad^{-2}, the MM calculation gave 0.09 and the best fit to the ED data was obtained for f_τ^g=0.14 mdyn Å rad^{-2}. The latter gives a torsional frequency of 104 cm^{-1}, close to the observation in liquid phase.[6] The f_τ^g found from ED experiment is 1.5 times larger than f_τ^g calculated by MM, as was the case also for 2,3-dichloro-1-propene and CP. Thus, the relative f_τ^g calculated by MM seems to exhibit some reliability. This is comforting, since the torsional frequencies still are unobserved for many related molecules.

The *gauche* torsional angle is 8° smaller than what was found in CP.[5] The MM calculations suggest a value 6° lower than the ED result, similar to the relative MM and ED results for CP and 2,3-dichloro-1-propene.[20] Thus, the trend in the MM calculations is quite good.

There are very good agreements between C=C−C and C−C−Cl angles as calculated by MM and experimentally found from ED. A difference of 1° is better than one can except from a simple method as MM.

The geometrical parameters for CMP are compared to those of related molecules in Table 5. The results for CMP fit very nicely into the trends established by these molecules.

Acknowledgements. I am particulary grateful to Siv.ing. R. Seip (University of Oslo) for teaching me to operate the ED apparatus. Thanks are also due to Mrs. S. Gundersen (University of Oslo) for technical assistance and to *Norges almenvitenskapelige forskningsråd* for financial support.

REFERENCES

1. Torgrimsen, T. and Klæboe, P. *J. Mol. Struct. 20* (1974) 229.
2. Trongmo, Ø., Shen, Q., Hagen, K. and Seip, R. *J. Mol. Struct. 71* (1981) 185.
3. Schei, S. H. and Klæboe, P. *J. Mol. Struct. 96* (1982) 9.
4. Søvik, O. I., Shen, Q., Schei, S. H., Seip, R., Stølevik, R. and Hagen, K. *J. Mol. Struct. In press.*
5. Schei, S. H., Shen, Q. and Hilderbrandt, R. L. *Preliminary results.*
6. Compton, D. A. C., Hsi, S. C., Mantsch, H. H. and Murphy, W. F. *J. Raman Spectrosc. 13* (1982) 30.
7. Pentin, Yu. A. and Morozov, E. V. *Opt. Spektrosk. 20* (1966) 637.
8. Hirota, E. *J. Mol. Spectrosc. 35* (1970) 9.
9. Schei, S. H. and Shen, Q. *J. Mol. Struct. 81* (1982) 269.
10. Durig, J. R. and Jalilian, M. R. *J. Chem. Phys. 84* (1980) 3543.
11. Niide, Y., Takano, M. and Satoh, T. *J. Mol. Spectrosc. 63* (1976) 108.
12. Van Hemelrijk, D., Van den Enden, L., Geise, H. J., Sellers, H. L. and Schäfer, L. *J. Am. Chem. Soc. 102* (1980) 2189.
13. Kondo, S., Hirota, E. and Morino, Y. *J. Mol. Spectrosc. 28* (1968) 471.

14. Zeil, W., Haase, J. and Wegman, L. *Z. Instrumentenkd. 74* (1966) 84.
15. Bastiansen, O., Graber, R. and Wegman, L. *Balzers High Vacuum Rep. 24* (1969) 1.
16. Tamagawa, K., Iijima, I. and Kimura, M. *J. Mol. Struct. 30* (1976) 243.
17. Andersen, B., Seip, H. M., Strand, T. G. and Stølevik, R. *Acta Chem. Scand. 23* (1969) 3224.
18. Schei, S. H. *Acta Chem. Scand. A 37* (1983) 15.
19. Abraham, R. J. and Stølevik, R. *Chem. Phys. Lett. 58* (1978) 622.
20. Thingstad, Ø, *Thesis,* University of Trondheim, Trondheim 1981.
21. Abraham, R. J. and Stølevik, R. *Chem. Phys. Lett. 77* (1981) 181.
22. Schei, S. H. *Spectrochim. Acta. 39 A* (1983) 327.
23. Kuchitsu, K. and Cyvin, S. J. In Cyvin, S. J., Ed., *Molecular Structures and Vibrations,* Elsevier, Amsterdam 1972, Chapter 2.
24. Tokue, I., Fukuyama, T. and Kuchitsu, K. *J. Mol. Struct. 17* (1973) 207.
25. Tokue, I., Fukuyama, T. and Kuchitsu, K. *J. Mol. Struct. 23* (1974) 33.
26. Schei, S. H. *J. Mol. Struct.* 98 (1983) 141.
27. Pauli, G. H., Momany, F. A. and Bonham, R. A. *J. Am. Chem. Soc. 86* (1964) 1286.
28. Stølevik, R. *Acta Chem. Scand. A 28* (1974) 327.
29. Stølevik, R. *Acta Chem. Scand. A 28* (1974) 445.
30. Grindheim, S. and Stølevik, R. *Acta Chem. Scand. A 30* (1976) 625.
31. Shen, Q. *J. Mol. Struct. 53* (1979) 61.

Received January 6, 1983.

Acta Chemica Scandinavica A 37 (1983) 679–684

Microwave Spectrum, Conformation, Intramolecular Hydrogen Bond and Dipole Moment of 2,3-Butadien-1-ol

ANNE HORN, K.-M. MARSTOKK, HARALD MØLLENDAL * and HANNO PRIEBE

Department of Chemistry, The University of Oslo, P.O. Box 1033, Blindern, Oslo 3, Norway

The microwave spectra of 2,3-butadien-1-ol, $CH_2OHCH=C=CH_2$ and one deuterated species, $CH_2ODCH=C=CH_2$, have been investigated in the 18.0–33.5 GHz region at −10 °C. Only one conformation, the *skew* form, with an intramolecular hydrogen bond formed between the hydroxyl hydrogen atom and the π electrons of the allene group was assigned. The dihedral O–C–C=C angle of the *skew* rotamer is 122(3)° from *syn* (58(3)° from *anti*). (See Fig. 1). Further conformations, if they exist, are at least 4 kJ/mol less stable than *skew*.

The dipole moment is μ_a=1.488(28) D, μ_b=0.8(2) D, μ_c=0.4(2) D, and $\mu_{tot.}$=1.72(12) D. Six vibrationally excited states belonging to two different normal modes were also assigned.

Several conformations are possible for 2,3-butadien-1-ol because the compound has two internal axes of rotation, namely the C–O and C1–C2 axes. Four selected rotamers are shown in Fig. 1. The *anti* form in which the heavy atoms and the hydroxyl group hydrogen atom are coplanar, should be ideal for steric reasons as there are no close contacts between non-bonded atoms in this

* Please address correspondence to this author.

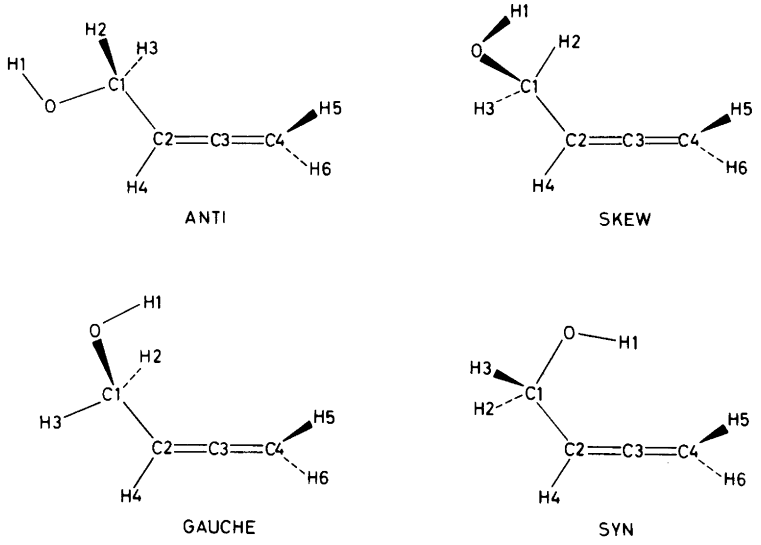

Fig. 1. Four selected conformations of 2,3-butadien-1-ol. In the *skew* form, a 60° rotation, and in the *gauche* form a 120° rotation from *anti* about the C1–C2 bond has been made. Only *skew* was assigned and found to be at least 4 kJ/mol more stable than any other form of the molecule.

0302-4377/83 $2.50

conformation.

The *skew* rotamer has the OCCC dihedral angle twisted 60° from *anti*. The hydroxyl hydrogen atom has been rotated (as compared to *anti*) so that a weak internal hydrogen bond might be formed between this atom and the π electrons of the allene group. In this conformation, the distance between H1 and C2 should be somewhat shorter than the sum of van der Waals radii of carbon and hydrogen. Moreover, the H2 and C3 atoms are brought into close proximity. It is unclear whether this contact would be repulsive or attractive in nature.

In the *gauche* conformation, a further 60° rotation about the C1–C2 bond has been made. The distances between H1 and C2, and between H1 and C3 should both be quite similar and roughly the same as the H1···C2 distance in the *skew* conformation. The O···C3 distance should be about the same as the van der Waals distance. H3 and H4, on the other hand, eclipse each other, and this might perhaps destabilize the *gauche* conformation.

In the *syn* form, the heavy atoms and the hydroxyl group hydrogen atom are again coplanar. The H1···C2 and H1···C3 distances would both be much shorter than the sum of the van der Waals radii of hydrogen and carbon, and the H1···C4 distance somewhat shorter than this sum. The O···C3 distance would also be a bit shorter than the sum of the van der Waals radii.

Some conformational problems related to that of $CH_2OHCH{=}C{=}CH_2$ have already been studied. Allyl alcohol, $CH_2OHCH{=}CH_2$, has a conformation similar to *skew* as its preferred form.[1] CH_2OHCHO,[2] $CH_2OHCOCH_3$,[3] and $CH_2OHCOOH$[4] all have conformations similar to *syn* as their most stable forms. In all these four last-mentioned compounds, intramolecular hydrogen bonding is important for their conformational preferences.

This work was undertaken in order to investigate the conformational preferences of 2,3-butadien-1-ol and the role played by intramolecular hydrogen bonding. It was found that the *skew* form is preferred by the molecule. This conformation is more stable than any other rotamer by at least 4 kJ/mol.

EXPERIMENTAL

$CH_2OHCH{=}C{=}CH_2$ was synthesized as described in Ref. 5 and purified by gas chromatography (Carbowax; 140 °C). The microwave spectrum was studied in the 18.0–38.5 GHz spectral region at a pressure of 1–3 Pa and a

Table 1. Microwave spectrum[a] of the ground vibrational state of $CH_2OHCH{=}C{=}CH_2$.

Transition	Observed frequency[a] (MHz)	Obs.-calc. frequency (MHz)	Centrifugal distortion (MHz)
$3_{0,3}\rightarrow4_{0,4}$	18457.90	0.01	−0.26
$3_{1,2}\rightarrow4_{1,3}$	18547.95	0.05	−0.06
$3_{1,3}\rightarrow4_{1,4}$	18369.92	−0.01	−0.06
$4_{0,4}\rightarrow5_{0,4}$	23071.39	−0.02	−0.51
$4_{1,3}\rightarrow5_{1,4}$	23184.39	−0.11	−0.26
$4_{1,4}\rightarrow5_{1,5}$	22962.04	0.00	−0.26
$5_{0,5}\rightarrow6_{0,6}$	27684.31	0.03	−0.89
$5_{1,4}\rightarrow6_{1,5}$	27820.88	0.04	−0.59
$5_{1,5}\rightarrow6_{1,6}$	27553.87	−0.02	−0.59
$5_{2,3}\rightarrow6_{2,4}$	27692.20	−0.05	0.32
$6_{0,6}\rightarrow7_{0,7}$	32296.42	0.03	−1.41
$6_{1,5}\rightarrow7_{1,6}$	32456.90	0.02	−1.06
$6_{1,6}\rightarrow7_{1,7}$	32145.45	0.00	−1.06
$6_{2,4}\rightarrow7_{2,5}$	32308.67	0.12	0.00
$7_{0,7}\rightarrow8_{0,8}$	36907.56	−0.04	−2.11
$7_{1,7}\rightarrow8_{1,8}$	36736.67	0.02	−1.71
$7_{2,5}\rightarrow8_{2,6}$	36925.22	−0.06	−0.50

[a] ±0.10 MHz.

temperature of about −10 °C. Lower temperatures could not be utilized due to insufficient vapour pressure of the compound. A conventional spectrometer equipped with free-running klystrons was employed.

RESULTS

Microwave spectrum and assignment of the ground vibrational state. The microwave spectrum of 2,3-butadien-1-ol is quite simple and its assignment was readily made. The spectrum consists of lumps of lines of intermediate intensities with nearly constant spacings due to $J \rightarrow J+1$ *a*-type transitions. In the spectral region between the K_{-1}-pile-ups, only very weak lines were seen.

The spectrum * is shown in Table 1. Only low-K_{-1} transitions are included in this table; the high-K_{-1} lines were not sufficiently resolved from each other to allow accurate measurements to be made. This is due to the fact that the assigned *skew* conformation has Ray's asymmetry parameter $\kappa = -0.9938$.[6] *b*- and *c*-type *Q*-branch transitions which might be relatively strong, were searched for but not identified, presumably because of insufficient intensities produced by small dipole moment components along the *b*- and *c*-principal inertial axes. As will be shown below, it was only possible to make rather inaccurate determination of $\mu_b = 0.8(2)$ *D* and $\mu_c = 0.4(2)$ *D*.

Unfortunately, the assigned *a*-type *R*-branch lines do not produce an accurate value for the *A* rotational constant as seen in Table 2. Moreover, it should be pointed out that a large negative correlation of −0.953 exists between *A* and Δ_{JK}. Similar values were found for the vibrationally excited states.

Vibrationally excited states. The ground state lines were accompanied by a rich sattelite spectrum presumably belonging to vibrationally excited states of the molecule. Six vibrationally excited states belonging to two different normal modes were assigned as shown in Table 3.

The most prominent of these excited states has about 60 % of the intensity of the ground state at −10 °C. Relative intensity measurements yielded 90(30) cm^{-1} for this mode which is presumed to be the first excited state of the C1−C2 torsion.

There is an almost constant increase in each of the *B* and *C* rotational constants upon successive excitation of this mode, as can be seen in Table 3. This is typical for a harmonic mode. The increase of *B* is 9.71 MHz, and *C* increases by 4.17 MHz from the ground to the first excited C1−C2 torsional state (Tables 2 and 3). As will be shown below, the OCCC dihedral angle is 58(3)° from *anti*. Increase of this angle in model calculations by 1.5° results in increases of the *B* rotational by 11.70 MHz and of *C* by 5.88 MHz. This is quite similar to the observed values and indicates that the C1−C2 torsion is uncoupled to other vibrational modes.

Furthermore, increase of both *B* and *C* upon excitation presumably means that the conformation approaches the *gauche* and/or *syn* forms. It is

* The microwave spectra of the vibrationally excited states of $CH_2OHCH{=}C{=}CH_2$ as well as of the ground vibrational state of $CH_2ODCH{=}C{=}CH_2$ are available from the authors upon request or from Molecular Spectra Data Center, Bldg. 221, Room B 265, National Bureau of Standards, Washington D.C. 20234, U.S.A., where they have been deposited.

Table 2. Spectroscopic constants[a] for the ground vibrational state of $CH_2OHCH{=}C{=}CH_2$ and $CH_2ODCH{=}C{=}CH_2$.

Species		$CH_2OHCH{=}C{=}CH_2$	$CH_2ODCH{=}C{=}CH_2$
Number of transitions		17	13
Root-mean-square dev. (MHz)		0.059	0.091
A_0	(MHz)	16688(192)	15824(190)
B_0	(MHz)	2329.6451(53)	2293.9667(92)
C_0	(MHz)	2285.1519(55)	2237.8011(91)
Δ_J	(kHz)[b]	1.030(47)	1.217(79)
Δ_{JK}	(kHz)	−25.2(27)	24.6(44)
κ[c]		−0.9938	−0.9917

[a] Uncertainties represent one standard deviation. [b] Further quartic centrifugal distortion constants preset at zero. [c] Ray's asymmetry parameter.[6]

Table 3. Spectroscopic constants[a] for vibrationally excited states of $CH_2OHCH=C=CH_2$.

Vib. state	First ex. C–C torsion	Second ex. C–C torsion	Third ex. C–C torsion	Fourth ex. C–C torsion	Fifth ex. C–C torsion	First ex. bending
No. of lines	15	12	15	9	10	15
R.m.s. (MHz)[d]	0.103	0.081	0.123	0.263	0.256	0.103
A_v (MHz)	18941(307)	17419(309)	16048(250)	16641(140)	19348(1562)	20408(1011)
B_v (MHz)	2339.3639(65)	2349.1666(76)	2359.132(12)	2369.299(29)	2379.618(52)	2326.6963(97)
C_v (MHz)	2289.3236(65)	2293.4351(94)	2297.559(11)	2301.587(35)	2305.651(51)	2285.5097(96)
Δ_J (kHz)[b]	1.441(62)	1.204(99)	1.60(11)	1.99(23)	1.96(43)	1.41(11)
Δ_{JK} (kHz)	−52.2(43)	−19.9(72)	6.5(77)	—[e]	−123(59)	−82.3(89)
κ^c	−0.9939	−0.9926	−0.9910	−0.9905	−00.9913	−0.9955

[a,b,c] Comments as for Table 2. [d] R.m.s. is the root-mean-square deviation. [e] Present at zero.

thus likely that the lowest barrier is found between the observed *skew* and/or the hypothetical *gauche* or *syn* forms. The barrier towards the hypothetical *anti* form is likely to be higher.

The first excited state of what is believed to be the lowest bending mode was also assigned as shown in Table 3. This excited state is roughly 1/3 as intense as the ground vibrational state. Relative intensity measurements yielded 200(30) cm^{-1}.

In addition to these assignments, two or three much weaker satellites were noted, but no definite assignments could be reached.

The assignments made as described above include all the strongest and all lines of intermediate intensities. Presumably, conformations other than *skew* should possess sizable dipole moments. This would lead to easily detectable spectra provided that at least 10 % or so of the total gaseous composition belonged to another form. It is therefore concluded that the identified *skew* conformation make up at least about 90 % of the gas and is at least 4 kJ/mol more stable than any other conformation of the molecule. This estimate is considered to be conservative.

Dipole moment. Stark coefficients of the four transitions shown in Table 4 were used to determine the dipole moment employing the standard procedure.[7] Small formal standard deviations of 0.06 *D* were found for μ_b and 0.07 *D* for μ_c, respectively. However, such small standard deviations for these two dipole moment components are unrealistic in this case, because the *A* rotation constant is poorly determined. The second-order perturbation sums[8] depend strongly on *A* in the case of μ_b and μ_c, and the uncertainties of these two dipole moment components were therefore judiciously increased to 0.2 *D*. It is also presumed that μ_b is in fact less than 0.8 *D*, since no *b*-type lines were found.

The total dipole moment of 1.72(12) *D* is similar to that of allyl alcohol[1] (1.55(4) *D*) as expected.

Deuterated species. The deuterated species, $CH_2ODCH=C=CH_2$, was studied mainly to determine the position of the hydroxyl hydrogen atom. The assignment was straight forward. The spectroscopic constants are shown in Table 2. The correlation coefficient between *A* and Δ_{JK} is −0.858 in this case. Kraitchman's coordinates[9] for the hydroxyl hydrogen atom are found in

Table 4. Stark coefficients[a] and dipole moment[b] of $CH_2OHCH=C=CH_2$.

Transition		$\Delta\nu/E^2$ (MHzV^{-2} cm^{-2})$\times 10^6$ Obs.	Calc.
$4_{1,4}\rightarrow 5_{1,5}$	$\|M\|=1$	2.51(6)	2.31
	$\|M\|=2$	10.1(5)	9.24
$4_{1,3}\rightarrow 5_{1,4}$	$M=0$	−0.392(9)	−0.373
	$\|M\|=1$	−2.70(5)	−2.56
	$\|M\|=2$	−9.7(5)	−9.1
$5_{1,4}\rightarrow 6_{1,5}$	$\|M\|=1$	−0.865(9)	−0.926
	$\|M\|=3$	−5.74(6)	−5.66
	$\|M\|=4$	−10.1(2)	−9.81
$4_{0,4}\rightarrow 5_{0,5}$	$M=0$	−2.72(5)	−2.65

Dipole moment
$\mu_a=1.488(28)$ *D*, $\mu_b=0.8(2)$ *D*[b]
$\mu_c=0.4(2)$ *D*[b] $\mu_{tot}=1.72(12)$ *D*

[a] Uncertainties represent one standard deviation. [b] See text.

Table 5. Plausible structural parameters[a] (bond lengths in *pm*, angles in *degrees*) of $CH_2OHCH=C=CH_2$.

Assumed bond lengths and angles			
C=C	130.9	∠C=C=C	180.0
C−O	141.5	∠C−C−O	112.0
C−C	151.4	∠C−C=C	122.0
O−H	95.0	∠C−O−H	104.0
H_2C−H	109.3	∠H−C=C	121.0
=C−H	108.5	∠C−C−H	109.5

Fitted dihedral angle of *skew* conformation
∠O−C−C=C 122(3) from *syn* (58(3) from *anti*)

Kraitchman's coordinate[b] for hydroxyl hydrogen atom

	|a|	|b|	|c|
Calculated from rotational constants	178.8(75)	120.6(66)	49.1(38)
Calculated from structure	175.2	115.8	58.7

Hydrogen bond parameters			
H1···C2	253	O···C3	346
H1···C3	332		
∠OH1···C2	73	∠OH1···C3	91
∠OH1···C2C3C4[c]	52		

Sum of van der Waals Radii[d]			
H···C[e]	290	O···C[e]	310

Rotational constants (MHz)

	$CH_2OHCH=C=CH_2$			$CH_2ODCH=C=CH_2$		
	Obs.	Calc.	Diff. (%)	Obs.	Calc.	Diff. (%)
A_0 (MHz)[f]	16688	19623	17.6	15824	18445	16.6
B_0 (MHz)	2329.65	2330.08	0.02	2293.97	2295.00	0.04
C_0 (MHz)	2285.15	2289.57	0.19	2237.80	2244.14	0.28

[a] See text. [b] Ref. 9. [c] Angle between O−H bond and C=C=C group. [d] Taken from Ref. 10. [e] van der Waals radius of carbon assumed to be 170 *pm* as in aromatic compounds.[10] [f] Too uncertain to be used for fitting of structure.

Table 5. Rather large uncertainties were obtained for these coordinates. This is caused by the inaccurate *A* rotational constants.

Structure. Only two isotopic species were studied for 2,3-butadien-1-ol and reliable values were only found for the *B* and *C* rotational constants in each case. A complete geometrical structure cannot, therefore, be determined for the *skew* conformation. A selection of structural parameters to be fitted must be made.

The Kraitchman coordinates (Table 5) of the hydroxyl hydrogen atom are so inaccurate that it was not considered worthwhile to fit any of the geometrical parameters of this hydrogen atom. However, these coordinates suffice to show that the *skew* form undoubtedly possesses an intramolecular hydrogen bond.

The rotational constants strongly depend on the OCCC dihedral angle. This angle was fitted in steps of 1° until a satisfactory agreement was found between the observed and calculated *B* and *C* rotational constants. This occurred with a dihedral angle of 122(3)° from *syn* (58(3)° from *anti*). The error limit has been derived taking into account the inherent uncertainties of the assumed structural parameters.

DISCUSSION

The intramolecular hydrogen bond of 2,3-butadien-1-ol is strained and rather weak and similar to that of allyl alcohol.[1] The hydrogen bond is characterized by having a H1···C2 (Fig. 1) non-bonded distance of 253 *pm* which is approximately 40 *pm* shorter than the sum of the van der Waals radii of hydrogen and aromatic carbon as shown in Table 5. The OH1···C2 angle is 73° and the angle between the O–H1 and allene group is 52°. In addition, the non-bonded distance between H2 and C3 is rather short, *viz.* 257 *pm*. It is not obvious if this contact is attractive.

The reasons why 2,3-butadien-1-ol prefers the *skew* conformation can only be hinted at. Hydrogen bonding can perhaps explain why *skew* is more stable than the sterically ideal hypothetical *anti* conformation. Moreover, steric overcrowding might perhaps explain why the *syn* form is not as stable as *skew*. It is more difficult to explain why the *skew* is more stable than the *gauche* form. The hydrogen bonding situation should be fairly similar in these two conformations. *Skew* has the close H2···C3 contact, while H3 and H4 eclipse each other in *gauche*. H2 and C3 might attract each other in *skew*, wheras H3 and H4 might repel each other in *gauche*. This would then result in that the *skew* form is also more stable than the *gauche* conformation by more than 4 kJ/mol.

Acknowledgement. H. P. is grateful to *Norges Teknisk Naturvitenskapelig Forskningsråd* for a scholarship.

REFERENCES

1. Murty, A. N. and Curl, R. F., Jr. *J. Chem. Phys. 46* (1967) 4176.
2. *a.* Marstokk, K.-M. and Møllendal, H. *J. Mol. Struct. 5* (1970) 205; *b. Ibid. 7* (1971) p. 101; *c. Ibid. 16* (1973) p. 259.
3. Kattija-Ari, M. and Harmony, M. D. *Int. J. Quantum Chem. Symp. 14* (1980) 443.
4. *a.* Scharpen, L. H. *Symp. Mol. Struct. Spectrosc., Ohio, Abstr. E4* (1972) 77; *b.* Blom, C. E. and Bauder, A. *Chem. Phys. Lett. 82* (1981) 492; *c.* Hasegawa, H., Ohashi, O. and Yamaguchi, I. *J. Mol. Struct. 82* (1982) 205; *d.* Blom, C. E. and Bauder, A. *J. Am. Chem. Soc. 104* (1982) 2993.
5. Brandsma, L. and Verkruijsse, H. D. *Synthesis of Acetylenes, Allenes and Cumulenes, Studies in Organic Chemistry 8,* Elsevier, Amsterdam, Oxford, New York 1981.
6. Gordy, W. and Cook, R. L. *Microwave Molecular Spectra,* Interscience, John Wiley & Sons, Inc. 1970, p. 163.
7. Marstokk, K.-M. and Møllendal, H. *Acta Chem. Scand. A 36* (1982) 517.
8. Golden, S. and Wilson, E. B. Jr. *J. Chem. Phys. 16* (1948) 669.
9. Kraitchman, J. *Am. J. Phys. 21* (1953) 17.
10. Pauling, L. *The Nature of the Chemical Bond,* 3rd. Ed. Cornell University Press, New York 1960, p. 260.

Received December 15, 1982.

Acta Chemica Scandinavica A 37 (1983) 685–689

The Crystal Structure of Diammine Silver Nitrate, $Ag(NH_3)_2NO_3$, at 223 K

TOSHIO YAMAGUCHI * and OLIVER LINDQVIST

Department of Inorganic Chemistry, Chalmers University of Technology and University of Göteborg, S-412 96 Göteborg, Sweden

The structure of diammine silver nitrate has been determined from diffractometer data collected at 223 K. The space group is *Pnnm* with cell dimensions, $a=8.088(3)$, $b=10.416(5)$, $c=6.261(2)$ Å, [$a=8.122(2)$, $b=10.596(2)$, $c=6.292(2)$ at 294 K] and $Z=4$. The structure has been refined by a block-diagonal least-squares method to R=0.054 based on 338 independent reflections. The diammine silver ions have a complete linear structure with an Ag–N bond length of 2.12(1) Å. The N–O distances in the nitrate group are 1.23(1) Å.

Linear diammine complexes have been of considerable interest in understanding the molecular motions of the NH_3 group in metal ammine complexes.[1,2] Structural investigations of diammine silver complexes reported so far are only $[Ag(NH_3)_2]_2SO_4$,[3] and $Ag(NH_3)_2 \cdot Ag(NO_2)_2$.[4] These investigations confirmed the linear structure of the complex but the Ag–N bond lengths in the two cases are quite different, 1.90 Å and 2.11 Å, respectively. A recent solution X-ray diffraction study[5] has also indicated the presence of the linear $Ag(NH_3)_2^+$ ion in aqueous solution however, with a somewhat longer Ag–N distance (2.22 Å).

The crystal structure of the diammine silver nitrate was first investigated in 1934[6] but the structure determination was not successful. In our attempt to solve the structure from diffractometer data collected at room temperature, it was not possible to locate the nitrate oxygen atoms, which is probably due to a dynamic disorder of the nitrate ion. Hence, intensity data were collected at 223 K, from which the structure could be determined.

EXPERIMENTAL

$Ag(NH_3)_2NO_3$ was crystallized from a concentrated ammoniacal aqueous solution of $AgNO_3$ with the NH_3/Ag mole ratio=2 over KOH pellets in a deccicator. The crystals are not stable but decompose in air with loss of ammonia in a few hours.

Preliminary Weissenberg photographs showed orthorhombic symmetry with systematic absences of reflections: $0kl$, $k+l=2n+1$; $h0l$, $h+l=2n+1$ and hence possible space groups are *Pnnm* and $Pnn2_1$.

It was found that the structure was subjected to a phase transition, cracking the crystals below 220 K. A single crystal was sealed in a 0.2 mm glass capillary and mounted on a syntex $P2_1$ four-circle diffractometer. Three-dimensional X-ray data were collected at 223 K using the Syntex LT1 low temperature equipment. Cell dimensions at both 223 and 294 K were obtained by refinement of setting angles of 15 reflections. Reflections with h, k and $l>0$ were collected and a standard reflection, monitored after every fiftieth reflection, showed that the crystal was stable in the capillary during data collection. Diffracted data were measured in 96 step profiles on each reflection and the Lehmann-Larsen method[7,8] was applied to calculate the net intensities. Reflections with $I>3\sigma(I)$ were considered as significant and corrected for the Lorentz and polarization effects. Corrections for absorption and extinction effects were not made. Experimental details are summarized in Table 1.

* Present address: Department of Electronic Chemistry, Tokyo Institute of Technology, Nagatsuta, Midori-Ku, Yokohama 227, Japan.

0302-4377/83 $2.50

Table 1. Crystal data, the collection and reduction of intensities and the least-squares refinement.

Formula	$Ag(NH_3)_2NO_3$
F.W.	203.9
D_x(g cm^{-3})	2.57
F(000)	392
Crystal habit	Colourless and rectangular
Crystal size (mm)	0.12×0.21×0.28 mm
Radiation	Mo$K\alpha$ (λ=0.71069 Å)
μ(Mo$K\alpha$) (cm^{-1})	36.4
Monochromator	Graphite crystal
Scan. mode	θ–2θ
Maximum 2θ (°)	54
Scan speed (°min^{-1})	Variable, 3.0–20.0
Scan interval, $\Delta 2\theta$ (°)	[(Mo$K\alpha_2$)+1.00]–[(Mo$K\alpha_1$)–1.00]
Reflections recorded	650
Significant reflections	338 ($I/\sigma(I)$>3.0)
Parameters refined	43
$R\equiv\Sigma\|F_o-\|F_c\|\|/\Sigma F_o$	0.054 (R=0.076 including unobserved reflections)

Table 2. Atomic coordinates (×10^4) and anisotropic thermal parameters (×10^4) with *e.s.d.*'s in parentheses. The form of the temperature factors are exp ($h^2\beta_{11}+\cdots+hk\beta_{12}+\cdots$).

Atom	x	y	z	β_{11}	β_{22}	β_{33}	β_{12}	β_{13}	β_{23}
Ag(1)	0	0	0	105(2)	94(1)	217(3)	7(2)	0	0
Ag(2)	0	0	5000	103(2)	125(1)	228(4)	−11(2)	0	0
N(1)	7606(12)	5182(9)	5000	112(17)	163(14)	222(30)	4(24)	0	0
N(2)	6359(11)	6742(9)	0	124(16)	112(9)	261(29)	−29(21)	0	0
N(3)	5753(11)	8410(8)	5000	111(13)	60(7)	290(29)	10(18)	0	0
O(1)	7254(10)	8204(9)	5000	85(11)	153(11)	710(51)	−34(21)	0	0
O(2)	4998(8)	8549(12)	6687(16)	197(16)	363(23)	229(24)	183(24)	95(32)	211(46)

STRUCTURE DETERMINATION AND REFINEMENT

The positions of the silver atoms were deduced from three-dimensional Patterson maps to occupy special positions. All other non-hydrogen atoms were located from difference Fourier syntheses. The positional and isotropic thermal parameters as well as an overall scale factor were refined in the two space groups $Pnn2_1$ and *Pnnm*. The *R*-value was better in the space group *Pnnm* and in addition one of the N–O distances in the nitrate group did not refine well in $Pnn2_1$. Therefore, we concluded the correct space group to be *Pnnm*. Having introduced anisotropic thermal parameters for all atoms, a block-diagonal least-squares[9] refinement gave a final *R*-value of 0.054.

Weights according to $w=1/(12.0+F_o+0.10F_o^2)$ gave an acceptable weight analysis. Scattering factors for neutral atoms were taken from International Tables.[10] The final atomic coordinates and thermal parameters are listed in Table 2. A final difference syntheses showed no anomalies. It was not possible to find the ammonia hydrogen atoms. Disregarding diffraction reasons, it is possible that the ammonia molecule rotates around the Ag–N bond to much lower temperatures.[2] All calculations were carried out on an Hp 2100 computer.[11,12]

DESCRIPTION OF THE STRUCTURE AND DISCUSSION

A stereoscopic view of the unit cell is shown in Fig. 1. Significant interatomic distances and bond angles are given in Table 3. There are two

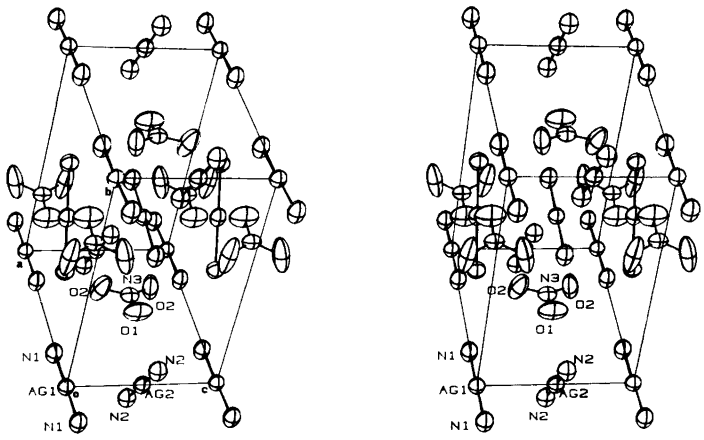

Fig. 1. Stereoscopic view of the $Ag(NH_3)_2NO_3$ structure.

Table 3. Significant interatomic distances (Å) and angles (°) with *e.s.d.*'s in parentheses. The values in brackets are those corrected for thermal motion.[22]

(a) The Ag-coordination	
Ag(1)–N(1)	2.116(10)[2.125(10)]
Ag(2)–N(2)	2.121(10)[2.122(10)]
Ag(2)–O(1^{ii})	2.904(9)
Ag(2)–O(1^{iii})	2.904(9)
N(1)–Ag(1)–N(1^{i})	180
N(2)–Ag(2)–N(2^{i})	180
(b) The nitrate ion	
N(3)–O(1)	1.233(12)
N(3)–O(2)	1.229(10)
O(1)–N(3)–O(2)	120.7(5)
O(1)–N(3)–O(2^{iv})	120.7(5)
O(2)–N(3)–O(2^{iv})	118.6(10)
(c) Possible hydrogen bonds	
N(1)–O(2^{v})	3.13(1)
N(1)–O(2^{vi})	3.13(1)
N(1)–O(1)	3.16(1)
N(2)–O(2^{vii})	3.01(1)
N(2)–O(2^{iv})	3.01(1)
N(2)–O(2^{vi})	3.14(1)
N(2)–O(2^{vii})	3.14(1)

Symmetry codes

(i)	$-x$,	$-y$,	z	(v)	$1/2-x$,	$3/2-y$,	$3/2-z$
(ii)	$1-x$,	$-1+y$,	z	(vi)	$1/2+x$,	$3/2-y$,	$-1/2+z$
(iii)	$-1+x$,	$1-y$,	z	(vii)	x,	y,	$-1+z$
(iv)	x,	y,	$1-z$	(viii)	$1/2+x$,	$3/2-y$,	$1/2-z$

Table 4. Comparison of Ag–N distances (Å) and N–Ag–N angles (°) in some linear and tetrahedral silver(I) complexes in the solid state and in solution.

Compound	*d*(Ag–N)	(N–Ag–N)	Configuration	Ref.
$Ag(NH_3)_2.Ag(NO_2)_2$	2.112(6) 2.117(6)	178.3(3)	Linear	4
$Ag(NH_3)_2NO_3$	2×2.116(10)	180	Linear	This study
	2×2.121(10)	180	Linear	
$[Ag(NH_3)_2]SO_4$	2×1.90	180	Linear	3
$Ag(C_3H_4N_2)_2NO_3$	2.120(8) 2.132(8)	172.0(3)	Linear	14
$Ag(NC_5H_5)_2.H_2O$	2×2.16(2)	172.7(2)	Linear	15
$(CH_3)_4NAg(NCO)_2$	2.015(13) 2.068(12)	177.2(5)	Linear	16
AgNCO	2×2.115(8)	180	Linear	17
$AgNO_3.N_2C_4H_4$	2×2.213(14)	159.2(9)	Bent	19
$Hg(CN)_2.AgNO_3$	2×2.13(4) 2×2.57(6) Ag–O	162(3)	Distorted tetrahedral	18
	2.02(5) 2.18(6) 2.56(5) Ag–O 2.55(6) Ag–O	163(2)	Distorted tetrahedral	
$Ag(NC_5H_5)_2ClO_4$	4×2.322(3)	110.2(2)	Tetrahedral	20
Solution:				
$Ag(NH_3)_2^+$(in H_2O)	2.22(2)		Linear	5
$Ag(NC_5H_5)_4^+$(in NC_5H_5)	2.30(3)		Tetrahedral	21

independent diammine silver ions in the cell. Both are linear and arranged so that they cross each other along the *c* axis.

The nitrate ion is planar and triangular within the standard deviatons, and the N–O distances are in accordance with the literature data. The structural packing of the nitrate ion is ordered but large temperature factors indicate a trace of dynamic motion of the ion also at 223 K. The closest Ag–O distance is 2.90 Å (Table 3).

The hydrogen bonding between the ammonia molecules and the nitrate oxygen atoms is rather weak (Table 3), compared to the normal range of N–H···O distances of 2.78–3.13 Å.[13]

Table 4 gives Ag–N distances in nitrogen coordinated silver compounds in different solids and in solution. The Ag–N bond length in the present compound is in good agreement with those in $Ag(NH_3)_2 \cdot Ag(NO_2)_2$, while the value reported in $[Ag(NH_3)_2]_2SO_4$ is probably too short. In general, the two-fold linear nitrogen coordination at silver is characterized by an Ag–N distance close to 2.12 Å, except the shorter values in cyanato complex found in $(CH_3)_4NAg(NCO)_2$. The N-Ag-N angles are generally close to 180°, except in $Hg(CN)_2 \cdot AgNO_3 \cdot 2H_2O$ and $AgNO_3 \cdot N_2C_4H_4$, in which there are additional short Ag–O contacts (2.55–2.72 Å). In the other structures the Ag–O distances are>2.9 Å.

A previous X-ray investigation of ammoniacal aqueous solution of $AgNO_3$[26] could not definitely prove the linearity of the $Ag(NH_3)_2^+$ ion in aqueous solution. However, it was found that no water molecule coordinated closer than 2.8 Å, indicating that the diamminesilver ion is linear also in aqueous solution. The Ag–N distance found in solution is somewhat longer than those found in the solid state. Bond elongation is normal for solvated complexes compared to the solid state when the ligands are hydrogen bonded to the solvent molecules. The Ag–N bond distance of 2.22 Å obtained in solution may be an upper limit for the Ag–N two-fold coordination

distance.

Tetrahedral N-coordinated Ag^+ ions have recently been studied in silver pyridine compounds both in the solid state and in solution, in which the Ag–N distances were found to be 2.322(3) Å and 2.30(3) Å, respectively.

The silver coordination has also been studied in liquid ammonia by Raman spectroscopic measurements by Gans and Gill[23] and by Lundeen and Tobias.[24] The former authors assign a tetrahedral Ag–N coordination, while the latter ascribe their spectra to a distorted octahedron. In order to clarify the coordination geometry of the silver ion in liquid ammonia, an X-ray investigation on liquid ammonia solution of $AgNO_3$ is planned.

In the case of the aqua silver ion, an X-ray reinvestigation of aqueous $AgClO_4$ solutions showed that four water molecules are bonded to the silver ion.[25] Therefore, silver ammine complex formation can be interpreted in such a way that tetra-aqua Ag^+ ion, $Ag(OH_2)_4^+$, is converted to a stable linear diammine silver ion, $Ag(NH_3)_2^+$, without any additional bonds in aqueous solution. Higher ammine silver ions can be formed at extreme conditions such as in liquid ammonia.

Acknowledgements. The authors thank the late Professor Georg Lundgren for his interest in this work. The financial support by the Swedish Natural Science Research Council (NFR) is gratefully acknowledged.

REFERENCES

1. Maurer, H. M. and Weiss, Al. *J. Chem. Phys. 69* (1978) 4046.
2. Kummer, N., Ragle, J. L., Weiden, N. and Weiss, Al. *Z. Naturforsch. 34a* (1979) 333.
3. Corey, R. B. and Wyckoff, R. W. G. *Z. Kristallogr. 87* (1934) 264.
4. Maurer, H. M. and Weiss, Al. *Z. Kristallogr. 146* (1977) 227.
5. Maeda, M., Maegawa, Y., Yamaguchi, T. and Ohtaki, H. *Bull. Chem. Soc., Jpn. 52* (1979) 2545.
6. Corey, R. B. and Pestrecov, K. *Z. Kristallogr. 89* (1934) 528.
7. Lehmann, M. S. and Larsen, F. K. *Acta Crystallogr. A 30* (1974) 580.
8. Lindqvist, O. and Ljungström, E. *J. Appl. Cryst. 12* (1979) 134.
9. Lindgren, O. *Thesis*, University of Göteborg, Göteborg 1977.
10. *International Tables for X-Ray Crystallography*, Kynoch Press, Birmingham (1974), Vol. 4.
11. Syntex, Report XTL (1973). 10040 Bubb Road, Cupertino, California 95015.
12. Sjölin, L. *Thesis*, University of Göteborg, Göteborg 1979.
13. Khan, A. A. and Baur, W. H. *Acta Crystallogr. B 28* (1972) 683.
14. Antii, C. J. and Lundberg, B. K. S. *Acta Chem. Scand. 25* (1971) 1758.
15. Menchetti, S., Rossi, G. and Tazzoli, V. *Ist. Lombardo (Rend. Sc.) A 104* (1979) 309.
16. Aarflot, K. and Åse, K. *Acta Chem. Scand. A 28* (1974) 137.
17. Britton, D. and Dunitz, J. D. *Acta Crystallogr. 18* (1965) 424.
18. Mahon, C. and Britton, D. *Inorg. Chem. 10* (1971) 586.
19. Vranka, R. G. and Amma, E. L. *Inorg. Chem. 5* (1966) 1020.
20. Nilsson, K. and Oskarsson, Å. *Acta Chem. Scand.* A 36 (1982) 605.
21. Hultén, F., Lindqvist, O. and Yamaguchi, T. *To be published.*
22. Busing, W. R. and Levy, H. A. *Acta Crystallogr. 17* (1964) 142; Busing, W. R. Martin, K. O. and Levy, H. A. *Function and Error Programs.* Report ORNL-TM-306, Oak Ridge National Laboratory, Oak Ridge 1965.
23. Gans, P. and Gill, L. B. *J. Chem. Soc. Dalton Trans.* (1976) 779.
24. Lundeen, J. W. and Tobias, R. S. *J. Chem. Phys. 63* (1975) 924.
25. Yamaguchi, T., Johansson, G. and Holmberg, B. *To be published.*
26. Maeda, M., Maegawa, Y., Yamaguchi, T. and Othaki, H. *Bull. Chem. Soc. Jpn. 52* (1979) 2545.

Received December 27, 1982.

Acta Chemica Scandinavica A 37 (1983) 691–696

Mass Spectrometric Study on Several Metal Dialkyldithiocarbamate Chelates

M.-L. RIEKKOLA

Division of Analytical Chemistry, Department of Chemistry, University of Helsinki, SF-00100 Helsinki 10, Finland

The mass spectra of several metal dialkyldithiocarbamate chelates have been determined with samples introduced by direct inlet probe (ionization energies 23 and 75 eV) and from an interfaced gas chromatograph (23 eV). The general fragmentation pathways are given. The gas phase stability was found to decrease in the metal order Ni>Pd>Cu>Zn>Cd>Pb>Hg>> Se for bis (dithiocarbamates) and Rh>Cr>Co> Fe>>In>As for tris (dithiocarbamates). The effect of the length and shape of the nonfluorinated alkyl group on the gas phase stability is apparent in the ligand order DEDTC> DPDTC>DIBDTC≈DBDTC. Fluorination of diethyldithiocarbamates decreases the gas phase stability. Gas chromatography-mass spectrometry provides an excellent means of verifying that metal chelates elute without decomposition under specified conditions.

Mass spectra have been reported for a number of metal dialkyldithiocarbamate chelates.[1–13] Normally a direct inlet probe has been used for the sample introduction.

As long ago as 1908 Delépine[14] reported that di-isobutyldithiocarbamates of nickel(II) and copper(II) sublime in vacuum and thus are volatile. Since the late seventies the volatility of many metal dialkyldithiocarbamates has been exploited for the development of a method allowing determination of metals by gas chromatography. The compounds have been successfully eluted from both packed[15] and capillary columns.[16,17] It has been noted, too, that fluorination of diethyldithiocarbamates greatly enhances the volatility.[18]

Since 1965 β-diketonate chelates have been found very promising for gas chromatographic determinations, too.[19] A combination gas chromatograph-mass spectrometer (GC–MS) has recently been used to study volatile chromium(III) β-diketonate chelates with geometrical isomers.[20]

The aim of the present work was to study the gas chromatographic behaviour, gas phase stability and influence of the alkyl substituents of several metal dialkyl-substituted (diethyl- (DEDTC), dipropyl- (DPDTC), dibutyl- (DBDTC), di-isobutyl- (DIBDTC) and di (trifluoroethyl)- (FDEDTC)) dithiocarbamate chelates by GC-MS, employing a falling needle injector[21] and short nonpolar glass capillary column in the gas chromatograph. The general fragmentation pathways were compared with those for samples introduced to the MS by direct inlet probe.

EXPERIMENTAL

Materials. The nonfluorinated and fluorinated dialkyldithiocarbamate chelates were prepared and purified according to methods described previously.[16,17,22] The metal chelates investigated are listed in Table 1.

Instrumentation. A glass capillary column coated with OV–101 liquid phase (4 m × 0.30 mm I.D.) was prepared from borosilicate glass (Duran 50), using a slight modification of the method described by Grob and Grob.[23] A Carlo Erba Fractovap Series 2300 gas chromatograph, equipped with a falling needle injector (Chrompack), was connected to a Jeol D 100 mass spectrometer. The capillary column was inter-

0302-4377/83 $2.50

Table 1. Metal *N,N*-dialkyldithiocarbamates studied.

Ligand	Metals
DEDTC	Ni(II), Pd(II), Pt(II), Cu(II), Zn(II), Cd(II), Hg(II), Pb(II), Se(II), Cr(III), Fe(III), Co(III), Rh(III), In(III), As(III)
DPDTC	Ni(II), Pd(II), Cu(II), Zn(II), Cd(II), Hg(II), Pb(II), Se(II), Cr(III), Fe(III), Co(III), Rh(III), In(III), As(III)
DBDTC	Ni(II), Pd(II), Cu(II), Zn(II), Cd(II), Hg(II), Pb(II), Cr(III), Fe(III), Co(III), Rh(III), In(III), As(III)
DIBDTC	Ni(II), Pd(II), Cu(II), Zn(II), Cd(II), Hg(II), Pb(II), Cr(III), Fe(III), Co(III), Rh(III), In(III), As(III)
FDEDTC	Ni(II), Pd(II), Cu(II), Zn(II), Cd(II), Hg(II), Pb(II), Co(III)

faced into the ion source by a Pt/Ir capillary tube (30 cm × 0.30 mm O.D. × 0.15 mm I.D.). A helium separator was not used.

Helium was used as the carrier gas. Samples of the investigated chelates were dissolved in methylene chloride. The injection port and interface temperatures were 250 and 250 °C for metal FDEDTC chelates and 275 and 275 °C, respectively, for DEDTC, DPDTC, DBDTC and DIBDTC chelates. The oven temperatures were 160–200 °C for bis(chelates) and 170–210 °C for tris(chelate) of FDEDTC acid, 200–250 °C for bis(chelates) and 210–260 °C for tris(chelates) of DEDTC acid, and 210–260 °C for bis(chelates) and 220–270 °C for tris(chelates) of DPDTC acid, 230–265 °C for bis(chelates) and 240–275 °C for tris(chelates) of DBDTC acid, and 205–255 °C for bis(chelates) and 215–265 °C for tris(chelates) of DIBDTC acid. Heating rate was 30 °C/min.

The ionization energy of the mass spectrometer was 23 and 75 eV when samples were introduced by direct inlet probe and 23 eV when the gas chromatograph was used. The accelerating voltage was 3 kV and the ion multiplier voltages were 1–1.6 kV. Temperatures of the ion source were within the range 160 °C to 230 °C depending on the volatility of the chelate. The resolution of the instrument was 1200 with a 10 % valley (main slit 250 μm, β-slit 1 mm and collector slit 50 μm).

RESULTS AND DISCUSSION

The molecular ion peaks were detected for almost all dialkyldithiocarbamate chelates introduced by direct insertion probe, but in greatly varying relative abundances. The chelates of the nontransition metals In(III), As(III) and Se(II) were exceptional in displaying no parent molecular ions.

The 10 eV mass spectra of dimethyldithiocarbamates of In(III) and Cr(III) have been reported by Schreiner and Hauser.[4] They found that the parent molecular ion peak of the indium chelate was virtually absent, whereas the molecular ion of the chromium chelate was present with large intensity. It was concluded that the $p\pi$ to $d\pi$ bonding between the sulfur and Cr(III) with t_{2g}^3 subshell leads to stronger metal–sulfur bonds for the chromium chelate. The relatively intense molecular ion peaks found for all chromium chelates in the present study are supportive of their interpretation.

The ions of highest mass number observed by solid probe method for the arsenic(III) chelates were the direct fragments of molecular ions of general formula $(AsL_2)^+$. Similar results have been obtained for As(III) diethyldithiocarbamate[5] and recently for As(III) tetramethylenedithiocarbamate.[10] However, for freshly extracted $As(DEDTC)_3$ the molecular ion peak has been observed.[3] The structure of $As(DEDTC)_3$ is a distorted trigonal antiprism with one of the As–S bonds in each ligand practically covalent and the other one more ionic.[24]

The absence of molecular ions of $Se(DEDTC)_2$ and $Se(DPDTC)_2$ can be attributed to electron impact or thermal or pyrolytic decomposition. $Se(DEDTC)_2$ forms an asymmetric planar chelate, where in both ligands one of the Se–S bonds is much longer than the other leading to probable instability of the compound. It has been inferred that the sulfur to central atom bonding is based mainly on p-orbitals, perhaps with some s-orbital contribution.[25] The structure of $Se(DPDTC)_2$ can be assumed to be similar since the structure of metal dialkyldithiocarbamates is only slightly changed upon the lengthening of the alkyl group.[26] The interpretation of the fragmentation pattern in terms of the solid-state structure, it may be noted, assumes the similarity of the solid- and vapour-state structures.

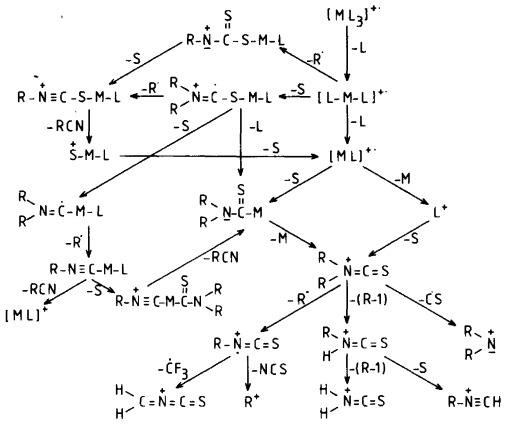

Fig. 1. Proposed general fragmentation pattern for metal dialkyldithiocarbamate chelates (L=ligand and M=metal).

Mass spectra were recorded for all the present metal chelates with sample introduction by direct inlet probe and ionization energies of 23 and 75 eV. Under these conditions no major fragmentation differences were found. Although intensities of the mass spectra recorded by GC–MS were decreased relative to those recorded with direct inlet probe (23 eV), the same fragmentation patterns were observed, with the exception of Se(II), As(III) and Fe(III) dialkyldithiocarbamates. These compounds decomposed in the injector, the capillary column, or the interface, resulting in more than one peak in the total ion chromatogram. Dipropyldithiocarbamate of Se(II) has been found to have two gas chromatographic peaks[17] and di-isobutyldithiocarbamates of Fe(III) and As(III) to decompose during gas chromatographic elution.[27]

The proposed general fragmentation pathways for metal dialkyldithiocarbamates are given in Fig. 1. In addition to the fragment ions of Fig. 1, the following ions may be formed $(R–1)^+$, $(R–2)^+$, CS^+ (*m/e* 44), CS_2^+ (*m/e* 76), $R\overset{+}{N}H{=}CH_2$, $(L–1)^+$. For arsenic and selenium chelates, thiuram disulfide $(L_2)^+$ ions were detected, too. The major peaks are in essential agreement with those reported by Krupčik *et al.* for various nickel(II) and zinc(II) dialkyldithiocarbamates.[9]

The primary fragmentation process for tris-(chelates) is the loss of dithiocarbamate ligand. Ligand-deficient species $(RhL_2)^+$, $(CrL_2)^+$, $(CoL_2)^+$ and $(FeL_2)^+$ appear in quite high abundance, though for Fe(III) chelates only with the solid probe introduction.

The intensities of molecular ions and the ligand loss give information about gas phase stabilities of the chelates. Under the conditions of electron impact fragmentation the order of stability decreases as follows: Ni>Pd>Cu>Zn>Cd>Pb>Hg>> Se for bis(dithiocarbamates) and Rh>Cr>Co>Fe>>In>As for tris(dithiocarbamates). From the stability order it can be concluded that nontransition metals form more labile chelates with dithiocarbamic acids than do transition metals. The mass spectra of Pt(II) were determined only for diethyl derivative. According to these few results, platinum lies between palladium and copper in the stability order.

It has been noted earlier that nickel chelates are more stable than those of zinc.[9] And dimethyl- and diethyldithiocarbamates of rho-

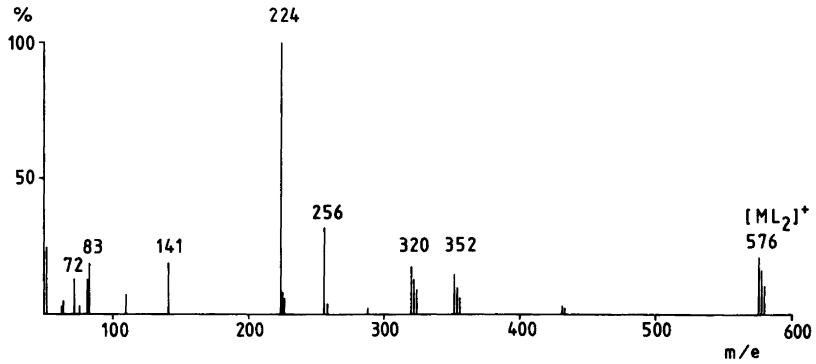

Fig. 2. Mass spectrum of $Zn(FDEDTC)_2$ recorded by GC–MS.

dium and chromium have been found to be more stable than the respective iron and cobalt chelates.[8] These findings are in agreement with the stability order above. $Zn(DEDTC)_2$ has been reported to occur as dimer in the gas phase.[1] In agreement with Krupčik *et al.*[9] no ions appeared in the spectra of zinc chelates at *m/e* ratios higher than the isotopic cluster of molecular ions.

The influence of the alkyl group on the gas phase stability for the nonfluorinated dialkyldithiocarbamates is revealed in the following order: DEDTC>DPDTC>DIBDTC≃DBDTC. Thus the prolongation of the alkyl chain and the increasing molecular weight apparently decrease the stability.

Fluorination of diethyldithiocarbamates does

Table 2. Prominent ions and their relative intensities in the spectra of (a) metal di(trifluoroethyl)-dithiocarbamates and (b) nonfluorinated dialkyldithiocarbamates recorded by GC–MS (23 eV) (L=ligand and M=metal).

(a)

Chelate	$[ML_3]^+$	$[ML_2]^+$	$[ML]^+$	$[L]^+$	$[R_2NCS]^+$	$[RNCS]^+$	$[H_2CNCS]^+$	R^+
Ni $(FDEDTC)_2$	–	28	9	3	100	10	5	19
Pd $(FDEDTC)_2$	–	28	10	4	100	8	7	18
Cu $(FDEDTC)_2$	–	28	15	10	100	6	7	14
Zn $(FDEDTC)_2$	–	21	18	32	100	19	13	19
Cd $(FDEDTC)_2$	–	15	8	72	100	10	11	17
Hg $(FDEDTC)_2$	–	5	–	60	100	7	8	21
Pb $(FDEDTC)_2$	–	2	53	7	100	9	10	14
Co $(FDEDTC)_3$	10	92	9	35	100	8	9	41

(b)

Chelate	$[ML_2]^+$	$[ML]^+$	$[L]^+$	$[R_2NCS]^+$	$[R_2N]^+$	$[RNHCS]^+$	$[H_2NCS]^+$	R^+
Ni $(DEDTC)_2$	100	28	5	100	46[a]	57	29	?
Ni $(DPDTC)_2$	100	27	3	96	47	95	31	61
Ni $(DBDTC)_2$	100	9	6	50	37	61	20	55
Ni $(DIBDTC)_2$	100	4	1	20	17	32	3	70
Pd $(DEDTC)_2$	93	40	3	56	100[a]	79	28	?
Pd $(DPDTC)_2$	89	39	19	42	100	38	22	18
Pd $(DBDTC)_2$	77	32	5	24	69	38	27	100
Pd $(DIBDTC)_2$	100	71	5	25	29	17	5	78
Pt $(DEDTC)_2$	49	13	8	75	81[a]	100	42	?
Cu $(DEDTC)_2$	45	6	6	100	16[a]	56	22	?
Cu $(DPDTC)_2$	34	8	11	75	23	66	34	100
Cu $(DBDTC)_2$	31	4	3	48	9	38	12	100
Cu $(DIBDTC)_2$	36	5	2	30	7	32	3	100
Zn $(DEDTC)_2$	42	15	22	100	28[a]	59	43	?
Zn $(DPDTC)_2$	36	22	24	100	20	61	28	81
Zn $(DBDTC)_2$	28	10	20	80	7	60	25	100
Zn $(DIBDTC)_2$	31	22	11	88	3	25	4	100
Cd $(DEDTC)_2$	28	13	56	100	65[a]	54	60	?
Cd $(DPDTC)_2$	7	7	92	67	50	53	34	100
Cd $(DBDTC)_2$	3	3	97	29	42	32	26	100
Cd $(DIBDTC)_2$	1	2	53	26	7	31	7	100
Hg $(DEDTC)_2$	2	4	100	100	56[a]	43	84	?
Hg $(DPDTC)_2$	1	2	90	70	46	44	38	100
Hg $(DBDTC)_2$	1	1	91	32	40	31	24	100
Hg $(DIBDTC)_2$	1	2	75	28	12	29	8	60

Table 2. Continued.

(b)

Chelate	$[ML_3]^+$	$[ML_2]^+$	$[ML]^+$	$[L]^+$	$[R_2NCS]^+$	$[R_2N]^+$	$[RNHCS]^+$	$[H_2NCS]^+$	R^+
Pb $(DEDTC)_2$	–	15	86	25	100	45[a]	81	56	?
Pb $(DPDTC)_2$	–	3	85	32	82	43	75	46	100
Pb $(DBDTC)_2$	–	3	73	97	29	42	32	26	100
Pb $(DIBDTC)_2$	–	1	70	100	48	41	50	14	90
Cr $(DEDTC)_3$	56	100	7	7	44	50[a]	90	42	?
Cr $(DPDTC)_3$	52	100	6	5	37	18	50	36	71
Cr $(DBDTC)_3$	40	70	6	21	30	10	38	25	100
Cr $(DIBDTC)_3$	41	63	2	29	28	6	32	10	100
Co $(DEDTC)_3$	13	100	17	8	28	24[a]	92	19	?
Co $(DPDTC)_3$	13	100	4	7	14	9	58	17	40
Co $(DBDTC)_3$	6	100	8	5	40	8	85	15	30
Co $(DIBDTC)_3$	9	100	2	5	3	2	6	2	19
Rh $(DEDTC)_3$	64	36	3	14	100	70[a]	93	57	?
Rh $(DPDTC)_3$	56	28	2	9	50	38	30	48	80
Rh $(DBDTC)_3$	42	20	1	7	49	27	18	33	70
In $(DEDTC)_3$	–	40	42	66	100	75[a]	80	51	?
In $(DPDTC)_3$	–	32	47	59	86	51	78	40	100
In $(DBDTC)_3$	–	1	3	100	23	20	41	8	85
In $(DIBDTC)_3$	–	2	3	100	11	11	19	5	82

[a] $[R_2N]^+ + [H_2CNCS]^+$.

not change the fragmentation pattern, in agreement with a recent similar observation for $Ni(FDEDTC)_2$.[12] But whereas the volatility increases markedly,[18] the gas phase stability decreases upon fluorination. $Ni(DEDTC)_2$ has a more prominant molecular ion than $Ni(FDEDTC)_2$ also in the published spectra[11] indicating greater stability for the nonfluorinated compound. The spectra were determined using solid probe and 70 eV ionization energy. The volatility of β-diketonates also increases as the ligands become more extensively fluorinated.[19] But mass spectrometric detection has recently given indication of an inverse relationship between volatility and gas phase stability for some fluorinated Cr(III) β-diketonate chelates.[20]

The intensity of the ions in the high mass region decreases with the lengthening of the alkyl substituent, in agreement with an earlier report.[9] The base peak varies with the alkyl group. The $(R_2NCS)^+$ ion is the most abundant ion for almost all diethyl- and di(trifluoroethyl)dithiocarbamates and it is also quite prominent for other dialkyldithiocarbamates. However, the base peaks for dipropyl-, dibutyl- and di-isobutyldithiocarbamates are very often alkyl ions in the low mass region. Furthermore, there are other prominent peaks for cadmium, lead and mercury chelates corresponding to $(ML)^+$ or $(L)^+$ ions. The electron impact induced loss of $(L–H)^+$ is observed with higher intensity than ion $(L)^+$ for nonfluorinated dialkyldithiocarbamates of Ni(II), Pd(II) and Pt(II). This pattern is also evident in the published spectra of some nickel dithiocarbamate chelates.[9]

Gas chromatography–mass spectrometry provides an excellent means of verifying that metal chelates elute without decomposition under specified conditions. Clearly all the fluorinated metal chelates of Table 1 are successfully eluted by gas chromatography. The use of Fe(III), As(III) and Se(II) chelates is not practical for gas chromatographic separations, and the labile Hg(II) and In(III) dialkyldithiocarbamates require very carefully selected conditions. Selective metal detection may be achieved by combining capillary gas chromatography with mass fragmentography and choosing stable ion fragments which are specific for the metal chelate studied.

Acknowledgements. The author wishes to thank Dr. S. Räisänen for the discussions. A

grant awarded by the Finnish Academy is gratefully acknowledged.

REFERENCES

1. Villa, J. F., Bursey, M. M. and Hatfield, W. E. *Chem. Commun.* (1971) 307.
2. Villa, J. F., Chatfield, D. A., Bursey, M. M. and Hatfield, W. E. *Inorg. Chim. Acta 6* (1972) 332.
3. Wood, B. C. and Skogerboe, R. K. *Appl. Spectrosc. 27* (1973) 10.
4. Hauser, P. J. and Schreiner, A. F. *Inorg. Chim. Acta 9* (1974) 113.
5. Manoussakis, G. E., Micromastoras, E. D. and Tsipis, C. A. *Z. Anorg. Allg. Chem 403* (1974) 87.
6. Fraser, I. W., Garnett, J. L., Gregor, I. K. and Jessop, K. J. *Org. Mass Spectrom. 10* (1975) 69.
7. Tsipis, C. A. and Manoussakis, G. E. *Inorg. Chim. Acta 18* (1976) 35.
8. Given, K. W., Mattson, B. M., Miessler, G. L. and Pignolet, L. H. *J. Inorg. Nucl. Chem. 39* (1977) 1309.
9. Krupčik, J., Leclercq, P. A., Garaj, J. and Masaryk, J. *J. Chromatogr. 171* (1979) 285.
10. Dias, J. R., Zigon, M. and Gomiscek, S. *Org. Mass Spectrom. 16* (1981) 12.
11. Sucre, L. *Detection of Metal Ions by Glass Capillary Gas Chromatographic Separation of Their Volatile Chelates,* Diss., University of California, Davis 1980.
12. Magner, J., Meierer, H. and Neeb, R. *Z. Anal. Chem. 311* (1982) 249.
13. Drasch, G., v. Meyer, L. and Kauert, G. *Z. Anal. Chem. 311* (1982) 571.
14. Delépine, M. *Bull. Soc. Chim. Fr. 4* (1908) 643.
15. Tavlaridis, A. and Neeb, R. *Z. Anal. Chem. 293* (1978) 211.
16. Riekkola, M.-L., Mäkitie, O. and Sundberg, M. *Kem. Kemi 6* (1979) 525.
17. Riekkola, M.-L. *Mikrochim. Acta 1* (1982) 327.
18. Tavlaridis, A. and Neeb, R. *Z. Anal. Chem. 292* (1976) 17.
19. Moshier, R.W. and Sievers, R.E. *Gas Chromatography of Metal Chelates,* Pergamon, Oxford 1965.
20. Sievers, R.E. and Brooks, K.C. *Int. J. Mass Spectrom. Ion Phys. 47* (1983) 527.
21. van der Berg, P. M. J. and Cox, Th. P. H. *Chromatographia 5* (1972) 301.
22. Tavlaridis, A. and Neeb, R. *Z. Anal. Chem. 292* (1978) 135.
23. Grob, K. and Grob, G. *J. Chromatogr. 125* (1976) 471.
24. Colapietro, M., Domenicano, A., Scaramuzza, L. and Vaciago, A. *Chem. Commun.* (1968) 302.
25. Husebye, S. and Holland-Madsen, G. *Acta Chem. Scand. 24* (1970) 2273.
26. Coucouvanis, D. *Prog. Inorg. Chem. 11* (1970) 233; *26* (1979) 301.
27. Riekkola M.-L. *Mikrochim. Acta 2* (1983) 381.

Received February 3, 1983.

Acta Chemica Scandinavica A 37 (1983) 697–702

The Crystal and Molecular Structures of Tetraaquabis(nicotinato *N*-oxide)cobalt(II) and -nickel(II)

HILKKA KNUUTTILA

Department of Chemistry, University of Jyväskylä, SF-40100 Jyväskylä 10, Finland

The crystal and molecular structures of tetraaquabis(nicotinato *N*-oxide)cobalt(II) and -nickel(II), $[M(N\text{-nicO})_2(H_2O)_4]$, M=Co, Ni, have been determined by X-ray techniques. The least squares refinement led to a final *R*-value of 0.049 for the cobalt complex.

Tetraaquabis(nicotinato *N*-oxide)cobalt(II) and -nickel(II) are isomorphous compounds. The crystals are monoclinic. The space group is $P2_1/c$, with $Z=2$ and cell dimensions are $a=8.896(5)$, $b=13.363(9)$, $c=6.719(3)$ Å, $\beta=109.40(4)°$ for the cobalt complex and $a=8.852(9)$, $b=13.277(16)$, $c=6.657(5)$ Å and $\beta=108.79(7)°$ for the nickel complex. Two nicotinato *N*-oxide ligands are coordinated to the central metal atom through one carboxylato oxygen atom, and there are four aqua ligands. The coordination geometry is slightly distorted octahedral.

Several metal complexes with nicotinic acid *N*-oxide (*N*-nicOH) have been synthesized and characterized.[1–11] In particular the kinetic, magnetic and spectral properties of these complexes have been studied. Chloride and perchlorate adducts have been prepared in organic (non-aqueous) media, including ethanol, ethanol–triethylorthoformate and *N,N*-dimethylformamide.[2,3,6–8] Sodium and magnesium compounds have been studied for their therapeutic properties.[9]

Divalent 3*d* metal complexes with nicotinic acid *N*-oxide have been described as hexacoordinated, linear, polynuclear complexes of the type $[M(N\text{-nicO})_2(H_2O)_2]_n \cdot mH_2O$ ($m=2n$ for M=Mn, Fe, Co, Ni, Cu, and $m=3n$ for M=Zn).[4] The authors assume that the nicotinate *N*-oxide groups act as bridging ligands coordinating through N–O oxygen atoms and one COO oxygen atom. Earlier, in a study on the cobalt complex, it was suggested that the nicotinato *N*-oxide ligand is coordinated only through one carboxylic oxygen atom.[1]

Polymeric Cu(II) complexes were the first metal complexes with nicotinic acid *N*-oxide to be subjected to X-ray structure analysis.[10,11,23] In these complexes nicotinate *N*-oxide acts as a bidentate bridging ligand coordinating either through both carboxylato oxygen atoms or through one carboxylato oxygen and the N–O oxygen atom to different copper atoms. Polymerization occurs *via* *N*-oxide groups and the Cu–O bond lengths are quite long (2.426–2.672 Å), indicating a rather weak interaction.

The present structure determination is of the isomorphous Co(II) and Ni(II) complexes with nicotinic acid *N*-oxide and proves the hypothesis of Euler *et al.*[1] about the mode of coordination of the nicotinate *N*-oxide group to the cobalt atom. The structures of isomorphous Co(II) and Ni(II) compounds of picolinic and isonicotinic acid *N*-oxides have been reported earlier.[12–14]

EXPERIMENTAL

Preparation of the complexes. $[Co(N\text{-nicO})_2(H_2O)_4]$ and $[Ni(N\text{-nicO})_2(H_2O)_4]$ crystals were prepared by the procedure used to synthesize metal complexes of pyridine monocarboxylic acid *N*-oxides.[4,15] A slightly modified crystallization was made from dilute solutions. The crystals of the Ni(II) complex were not, however, of satisfactory quality for single crystal X-ray analy-

0302-4377/83 $2.50

Table 1. Crystal and refinement data of $[Co(N\text{-nicO})_2(H_2O)_4]$ and $[Ni(N\text{-nicO})_2(H_2O)_4]$.

	$[Co(C_6H_4NO_3)_2(H_2O)_4]$	$[Ni(C_6H_4NO_3)_2(H_2O)_4]$
F.W.	407.20	406.97
Space group	$P2_1/c$	$P2_1/c$
a (Å)	8.896(5)	8.852(9)
b	13.363(9)	13.277(16)
c	6.719(3)	6.657(5)
β (°)	109.40(4)	108.79(7)
Z	2	2
V (Å^3)	753.4	740.7
μMo$K\alpha$(cm^{-1})	12.51	
Collection mode	$\theta/2\theta$	
Radiation	Mo$K\alpha$	
Scan range	$4°<2\theta<60°$	
Scan rate (°min^{-1})	1.0→15.0	
Refl. meas.	2743	
obs. ($I>3\sigma(I)$)	1591	
$F(000)$	418	
$R(=\Sigma\|\|F_o\|-\|F_c\|\|/\Sigma\|F_o\|)$	0.049	

Table 2. Final positional parameters for $[Co(N\text{-nicO})_2(H_2O)_4]$ including hydrogen atoms and U_{eq} ($\times10^3$) (Å^2) and U_{iso}($\times10^2$) for hydrogen atoms.

Atom	x	y	z	U_{eq}[a]
Co	1.0000	0.0000	1.0000	1.80(1)
O(1)	0.6613(2)	0.9609(1)	0.3359(2)	2.81(7)
O(2)	0.8240(2)	0.1116(1)	−0.0610(2)	2.58(6)
O(3)	0.9752(2)	0.2386(1)	0.1113(2)	2.87(7)
O(4)	0.8810(2)	0.5727(1)	0.2195(2)	3.47(8)
O(5)	0.1173(2)	0.0919(1)	0.8418(3)	3.65(8)
C(1)	0.7449(2)	0.1254(1)	0.4031(3)	2.22(8)
C(2)	0.2869(2)	0.7269(1)	0.1127(3)	2.09(8)
C(3)	0.4412(2)	0.7587(1)	0.2128(3)	2.59(9)
C(4)	0.4401(2)	0.1887(1)	0.2071(3)	2.81(9)
C(5)	0.4767(2)	0.0881(1)	0.2260(3)	7.76(9)
C(6)	0.8492(2)	0.2975(1)	0.4877(3)	2.17(8)
N(1)	0.3730(2)	0.5593(1)	0.1803(3)	2.32(7)
				U_{iso}
H(1)	0.145(3)	0.599(2)	0.037(3)	2.9(6)
H(2)	0.524(3)	0.333(2)	0.273(4)	3.0(6)
H(3)	0.664(2)	0.715(1)	0.369(3)	1.4(5)
H(4)	0.409(3)	0.045(2)	0.185(4)	4.6(8)
H(5)	0.802(4)	0.933(2)	0.190(5)	6.9(10)
H(6)	0.060(3)	0.367(2)	0.264(4)	4.7(8)
H(7)	0.810(4)	0.566(2)	0.109(5)	6.8(9)
H(8)	0.081(4)	0.122(2)	0.275(5)	7.8(10)

[a] $U_{eq}=\frac{1}{3}\sum_i U_{ii}$

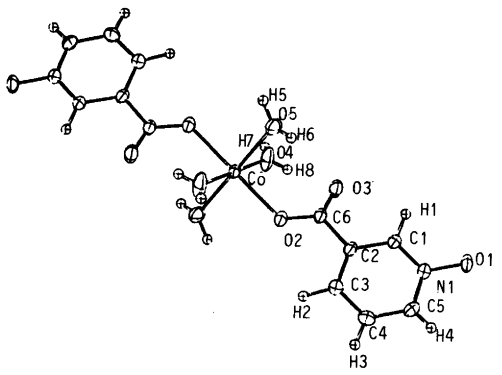

Fig. 1. The labelling and structure of [Co(*N*-nicO)$_2$(H$_2$O)$_4$]. Thermal ellipsoids are drawn to enclose the 50 % probability level.

sis which was, therefore, performed for the Co(II) complex only.

Data collection. The crystal and refinement data are given in Table 1. The crystal and intensity data were measured on a Syntex $P2_1$ four-circle diffractometer using graphite monochromatized Mo$K\alpha$ radiation. The unit cell parameters were calculated by least squares refinement of 15 high order reflections.

The data were corrected for Lorentz and polarization factors. Absorption correction was not made.

Structure determination. The structure of the Co(II) complex was solved by direct methods[16] and Fourier techniques and refined by block diagonal matrix least squares methods with anisotropic temperature factors for all nonhydrogen atoms. All hydrogen atoms were located by difference Fourier syntheses. The final *R*-value was 0.049.

All calculations were carried out with X-Ray System programs[17] on a UNIVAC 1100/60 computer. The scattering factors for Co, C, N and O were those of Cromer and Mann[18] and for hydrogen atoms those reported by Stewart *et al.*[19]

Table 2 presents the final atomic coordinates and the thermal parameters (U_{eq} and U_{iso}) with their standard deviations for the cobalt compound. Lists of structure factors and anisotropic thermal parameters are available from the author upon request.

DESCRIPTION AND DISCUSSION OF THE STRUCTURES

The title compounds tetraaquabis(nicotinato *N*-oxide)cobalt(II) and -nickel(II) are isomorphous complexes based on the crystal data, just as are the cobalt and nickel compounds of picolinic and isonicotinic acid *N*-oxides: diaquabis(picolinato *N*-oxide)cobalt(II) and -nickel(II)[12] and hexaaquacobalt(II) and hexaaquanickel(II) isonicotinate *N*-oxide.[13]

Joined monodentately to the central metal atom are two nicotinato *N*-oxide ligands, through one carboxylato oxygen atom, and four aqua ligands. This is the same kind of coordination mode as the isonicotinato N-oxide ligand has in [Mn(*N*-inico)$_2$(H$_2$O)$_4$].[14] The coordination geometry is slightly flattened octahedral. The labelling and structure of the molecule are given for [Co(*N*-nicO)$_2$(H$_2$O)$_4$] in Fig. 1 and a stereoview of the packing in the unit cell is shown in Fig. 2. Bond distances and angles are presented in Table 3.

The aqua ligands form intramolecular hydrogen bonds with uncoordinated carboxylato oxygen atoms, and hydrogen bonds between the aqua ligands and the *N*-oxide oxygen atoms join complex molecules to each other. The hydrogen bonds are listed in Table 4.

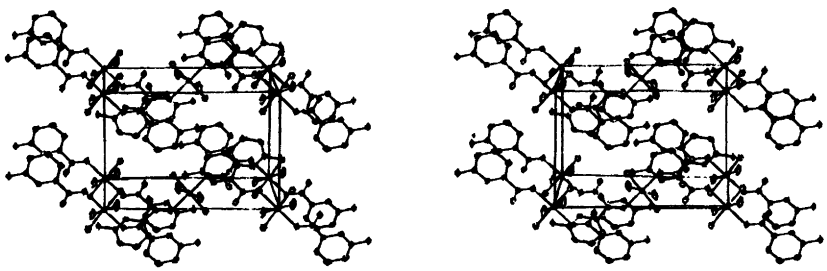

Fig. 2. Stereoview of the packing of [Co(*N*-nicO)$_2$(H$_2$O)$_4$] within the unit cell. Hydrogen atoms have been excluded for clarity.

Table 3. Selected bond distances (Å) and bond angles (°) with their standard deviations for $[Co(N\text{-}nicO)_2(H_2O)_4]$.

Environment of central metal			
Co–O(2)	2.102(1)	O(2)–M–O(4)	88.09(6)
Co–O(4)	2.072(1)	O(2)–M–O(5)	87.06(6)
Co–O(5)	2.113(2)	O(5)–M–O(4)	90.25(6)
		O(4)–M–O(2)	91.91(6)
		O(4)–M–O(5)	89.75(6)
		O(5)–M–O(2)	92.94(6)
Pyridine *N*-oxide group			
N(1)–O(1)	1.347(2)	O(1)–N(1)–C(1)	119.0(1)
N(1)–C(1)	1.344(2)	O(1)–N(1)–C(5)	119.1(1)
N(1)–C(5)	1.331(2)	C(1)–N(1)–C(5)	121.9(2)
C(1)–C(2)	1.384(2)	N(1)–C(1)–C(2)	120.2(1)
C(2)–C(3)	1.379(3)	C(1)–C(2)–C(3)	119.0(2)
C(3)–C(4)	1.379(3)	C(2)–C(3)–C(4)	119.4(2)
C(4)–C(5)	1.381(3)	C(3)–C(4)–C(5)	119.9(2)
Carboxylato group			
C(6)–C(2)	1.508(2)	O(2)–C(6)–O(3)	126.1(2)
C(6)–O(2)	1.260(2)	O(2)–C(6)–C(2)	116.1(1)
C(6)–O(3)	1.249(2)	O(3)–C(6)–C(2)	117.8(1)

Table 4. Hydrogen bonds

Atoms A–H···B	Distances (Å) A–H	H···B	A···B	Angle (°) AHB
O(4)–H(7)···O(1)	0.80(3)	1.91(3)	2.705(2)	172(3)
O(4)–H(8)···O(3)	0.73(3)	1.96(3)	2.624(2)	150(3)
O(5)–H(5)···O(1)	0.88(3)	1.87(4)	2.713(3)	161(3)
O(5)–H(6)···O(3)	0.81(2)	2.01(2)	2.799(2)	163(2)

The coordination of picolinato, nicotinato and isonicotinato *N*-oxide ligands in Co(II) and Ni(II) compounds is presented schematically in Fig. 3. Co–O bond distances are in agreement with the corresponding cobalt(II) bond distances in $[Co(N\text{-}picO)_2(H_2O)_2]$ (2.061(1)–2.148(1)Å) and $[Co(H_2O)_6]$ $(N\text{-}inicO)_2$ (2.052(2)–2.092(2) Å). Both the N–O and C–O bond distances are shortest for $[Co(H_2O)_6]$ $(N\text{-}inicO)_2$. The C–C(ring) distances are similar in three compounds.

The positions of the substituents of pyridine monocarboxylic acid *N*-oxides in the ring appear to play a significant role in the coordination chemistry of the Co(II) and Ni(II) compounds. The substituents, the *N*-oxide and carboxylic groups are in the *ortho*-position in picolinic acid *N*-oxide and a stable 6-membered ring is generated through the *N*-oxide group and one carboxylato oxygen atom when the complex forms.[13] In nicotinic acid *N*-oxide the *N*-oxide group is in *meta*-position to the carboxylic group and does not coordinate to the cobalt and nickel atoms. Coordination occurs only through one carboxylato oxygen atom. In isonicotinic acid *N*-oxide, where the *N*-oxide and carboxylic groups are in *para*-position, neither group is coordinated to the Co(II) or Ni(II) ion,[12] nor to Fe(II),[14] Mg(II) or Zn(II)[20] ion; rather the compounds formed are ionic with hexaaquametal(II) cations and isonico-

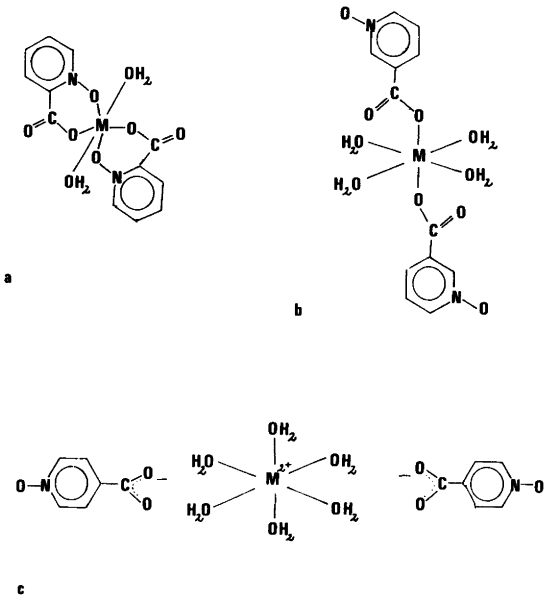

Fig. 3. Cobalt(II) and nickel(II) compounds of pyridine monocarboxylic acid *N*-oxides schematically. (a) $[M(N\text{-picO})_2\ (H_2O)_2]$, M=Co(II), Ni(II);[12] (b) $[M(N\text{-nicO})_2\ (H_2O)_4]$, M=Co(II), Ni(II); (c) $[M(H_2O)_6]\ (N\text{-inicO})_2$, M=Co(II), Ni(II).[13]

tinate *N*-oxide anions. The coordination ability of the *N*-oxide group of pyridine monocarboxylic acid *N*-oxides clearly decreases in the order picolinic acid *N*-oxide > nicotinic and *N*-oxide > isonicotinic acid *N*-oxide in compounds formed in aqueous solutions.[10–14,20–22]

REFERENCES

1. v. Euler, H., Hasselquist, H. and Heidenberger, O. *Ark. Kemi 13* (1959) 583.
2. Muto, Y., Kato, M., Jonassen, H. B. and Ramaswamy, H. N. *Bull. Chem. Soc. Jpn. 40* (1967) 1535.
3. Muto, Y., Kato, M., Jonassen, H. B. and Cusachs, L. C. *Bull. Chem. Soc. Jpn. 42* (1969) 417.
4. Speca, A. N., Gelfand, L. S., Pytlewski, L. L., Owens, C. and Karayannis, N. M. *Inorg. Chem. 15* (1976) 1493.
5. Speca, A. N., Gelfand, L. S., Pytlewski, L. L., Owens, C. and Karayannis, N. M. *J. Inorg. Nucl. Chem. 39* (1977) 537.
6. Gelfand, L. S., Pytlewski, L. L., Cosgrove, D. L., Mikulski, C. M., Speca, A. N. and Karayannis, N. M. *Inorg. Chem. Acta 27* (1978) 297.
7. Gelfand, L. S., Pytlewski, L. L., Mikulski, C. M., Speca, A. N. and Karayannis, N. M. *Inorg. Chim. Acta 33* (1979) 265.
8. Gelfand, L. S., Iaconianni, F. J., Pytlewski, L. L., Speca, A. N., Minulski, C. M. and Karayannis, N. M. *J. Inorg. Nucl. Chem. 42* (1980) 377.
9. Debay, A. G. and Thery, J. L. M. J. *Belg. Pat.* (Sept. 28, 1962).
10. Knuuttila, H. *Inorg. Chim. Acta 50* (1981) 221.
11. Knuuttila, H. *Inorg. Chim. Acta 69* (1983) 173.
12. Knuuttila, P. *Inorg. Chim. Acta 52* (1981) 141.
13. Knuuttila, P. *Acta Chem. Scand. A 36* (1982) 767.
14. Knuuttila, P. *Thesis,* University of Jyväskylä, Jyväskylä 1982.
15. Lever, A. B. P., Lewis, J. and Nyholm, R. S. *J. Chem. Soc.* (1962) 5262.
16. Main, P., Hull, S. E., Lessinger, L., Germain, G., Delercq, J.-P. and Woolfson, M. M. *MULTAN 80. A System for Automatic Solution of Crystal Structure from X-Ray Diffraction Data,* University of York, York 1980.

17. Stewart, J. M. *The X-Ray System, Version of 1976,* Technical Report TR-446, Computer Science Center, University of Maryland, College Park 1976.
18. Cromer, D. T. and Mann, J. B. *Acta Crystallogr. A 24* (1968) 321.
19. Stewart, R. F., Davidson, E. R. and Simpson, W. T. *J. Chem. Phys. 42* (1965) 3175.
20. Knuuttila, P. *Unpublished result.*
21. Knuuttila, H. and Knuuttila, P. *Acta Chem. Scand. A 37* (1983) 227.
22. Knuuttila, H. *Inorg. Chim. Acta 72* (1983) 11.
23. Knuuttila, H., *Thesis*, University of Jyväskylä, Jyväskylä 1983.

Received January 6, 1983.

Acta Chemica Scandinavica A 37 (1983) 703–707

Short Communication

Preparation and Crystal Structure of Copper(II) Chloride Complex with (±)-*trans*-1,2-Cyclohexanediol and Tetrahydrofuran in the Molar Ratio $1:1\frac{1}{2}:\frac{1}{2}$

REIJO SILLANPÄÄ[a] and LASSI HILTUNEN[b]

[a] Department of Chemistry, University of Turku, SF-20500 Turku 50, Finland and [b] Department of Chemistry, Helsinki University of Technology, SF-02150 Espoo 15, Finland

We have prepared coordination compounds of copper(II) chloride that have 1,2-cyclohexanediols as neutral ligands. When trying to prepare compounds that have the formula $CuCl_2 \cdot 2diol$ (diol=(±)-*trans*- or *cis*-1,2-cyclohexanediol), it was found difficult to obtain well-defined compounds in tetrahydrofuran (THF). However, good crystals of $CuCl_2 \cdot 2diol$ compounds can be grown in 1,2-dimethoxyethane (DME), and their molecular and crystal structures have been studied.[1] From the THF solution, however, it is possible to isolate compounds that have the formula $CuCl_2 \cdot 1.5diol \cdot 0.5THF$. In this paper we describe the preparation and the molecular and crystal structure of the complex $CuCl_2 \cdot 1.5$*trans*-chd $\cdot$ 0.5THF.

The compound was prepared by dissolving diol[2] (22.4 mmol) and $CuCl_2$ (11.2 mmol) in 50 ml of THF, and 20 ml of hexane was added. The solution was allowed to stand for two weeks at room temperature in a closed vessel. Green crystals were separated by decantation and washed twice with ethyl ether. The yield was 1.60 g (41.4 %). Analysis for Cu, Cl and diol was performed by standard titrimetric methods. Found: Cu 18.4; Cl 20.8; diol 51.2. Calc. for $Cu_2Cl_4C_{22}H_{44}O_7$: Cu 18.4; Cl 20.6; diol 50.5.

Single-crystal X-ray diffraction measurements were made with SYNTEX $P2_1$ (Fortran version) automatic four-circle diffractometer employing graphite-monochromatized MoK_α radiation. Unit cell parameters were calculated using least squares refinements of 24 reflections. The intensities were recorded using the $\theta/2\theta$ scan technique with varying scan speed (1.5–29.3° min^{-1}) depending on the peak intensity of the reflection. Systematic absences in the reflections showed that the space group is $P2_1/c$.

The crystals of $Cu_2Cl_4C_{22}H_{44}O_7$ are monoclinic with the following cell dimensions: a=8.120(2) Å, b=34.90(2) Å, c=11.132(4) Å, β=105.71(2)°. There are four formula units in the unit cell (D_m=1.50(2) gcm^{-3}, D_c=1.495 gcm^{-3}) and μ(MoK_α) is 17.1 cm^{-1}.

The intensity of one check reflection decreased by 34 %. Correction was applied for crystal decay and Lp, but not for absorption. Out of 5390 independent reflections 2660 intensities having $I>2.0\sigma(I)$ were considered as observed.

The structure was solved with direct methods, which gave positional parameters for Cu and Cl atoms. The atomic scattering factors and anomalous dispersion correction factors for non-hydrogen atoms were taken from *International Tables*.[3] The structure was refined with non-hydrogen and hydrogen atoms having anisotropic and isotropic temperature factors, respectively. As all the C–H hydrogen atoms could not be found in the difference map, their positions were calculated assuming the C–H distances to be 1.0 Å. The coordinates of H(O3) were fixed to those found in the difference map. Omission of 86 poorly agreeing reflections led to final R and R_w values of 0.055 and 0.045, respectively, where $R=\Sigma\Delta/\Sigma F_o$, $R_w=\Sigma\sqrt{w}\Delta/\Sigma\sqrt{w}F_o$, $\Delta=|F_o-F_c|$ and $w=2.916/(\sigma^2(F_o)+0.0003F_o^2)$. Omission of 86 reflections was thought to be reasonable on the basis of the analysis of variances.

All crystallographic computations were performed with program SHELX-76[4] and the figure was drawn with ORTEP-II.[5] The final positional parameters with equivalent temperature factors for non-hydrogen atoms of the complex are given in Table 1.

The temperature factors for the C–H hydrogen atoms refined to the range 0.07(1)–0.19(2) Å^2 and for all O–H hydrogen atoms to 0.06(1) Å^2. The structure factors and anisotropic thermal parameters may be obtained from the authors (R.S.). The labelling of the atoms is indicated in Fig. 1, where an asymmetric unit is depicted.

0302-4377/83 $2.50

Table 1. Fractional atomic coordinates and equivalent isotropic temperature factors ($Å^2$) with their e.s.d.'s for the non-hydrogen atoms of $CuCl_2 \cdot 1.5$*trans*-chd $\cdot$ 0.5THF. The temperature factors are of the form $U_{eq}=(U_{11}+U_{22}+U_{33}+2U_{13}\cos\beta)/3$.

	x	*y*	*z*	U_{eq}
Cu(1)	0.10759(12)	0.38173(3)	0.65858(9)	0.04659(36)
Cu(2)	0.53615(12)	0.36749(3)	0.82631(9)	0.04335(35)
Cl(1)	0.2499(2)	0.4103(1)	0.8404(2)	0.0488(7)
Cl(2)	0.1910(3)	0.4234(1)	0.5357(2)	0.0738(10)
Cl(3)	0.3536(3)	0.3284(1)	0.6939(2)	0.0528(8)
Cl(4)	0.5810(3)	0.3326(1)	0.9967(2)	0.0604(9)
O(1)	−0.0190(7)	0.3473(2)	0.7442(5)	0.0468(21)
O(2)	−0.0609(7)	0.3598(2)	0.5097(5)	0.0547(23)
O(3)	0.5511(6)	0.3992(1)	0.6813(4)	0.0477(20)
O(4)	0.7206(7)	0.4046(2)	0.9125(5)	0.0482(22)
O(5)	0.1716(8)	0.3138(2)	0.9408(5)	0.0567(24)
O(6)	0.0427(8)	0.3813(2)	1.0328(5)	0.0594(25)
O(7)	−0.2523(8)	0.4091(2)	0.3503(6)	0.0867(29)
C(1)	−0.0899(10)	0.3161(2)	0.6634(7)	0.0470(31)
C(2)	−0.1827(10)	0.3334(2)	0.5433(8)	0.0515(32)
C(3)	−0.2523(11)	0.3040(2)	0.4444(7)	0.0559(33)
C(4)	−0.3683(11)	0.2760(3)	0.4926(9)	0.0729(41)
C(5)	−0.2831(11)	0.2601(2)	0.6158(8)	0.0648(38)
C(6)	−0.2044(10)	0.2903(2)	0.7138(7)	0.0491(32)
C(7)	0.6224(10)	0.4363(2)	0.7196(7)	0.0442(30)
C(8)	0.7750(10)	0.4291(2)	0.8266(7)	0.0478(31)
C(9)	0.8570(11)	0.4655(2)	0.8841(8)	0.0599(37)
C(10)	0.9035(13)	0.4898(3)	0.7852(9)	0.0764(42)
C(11)	0.7524(13)	0.4963(3)	0.6715(9)	0.0843(49)
C(12)	0.6688(11)	0.4589(3)	0.6185(8)	0.0635(38)
C(13)	0.1260(12)	0.3142(2)	1.0588(8)	0.0556(36)
C(14)	0.1452(11)	0.3531(3)	1.1150(7)	0.0553(34)
C(15)	0.0957(12)	0.3532(3)	1.2369(8)	0.0694(39)
C(16)	0.1996(13)	0.3243(4)	1.3257(8)	0.0851(49)
C(17)	0.1789(13)	0.2853(3)	1.2696(9)	0.0810(46)
C(18)	0.2237(11)	0.2841(3)	1.1443(8)	0.0615(37)
C(19)	−0.1961(14)	0.4416(4)	0.2984(12)	0.1176(60)
C(20)	−0.3379(15)	0.4588(4)	0.2118(13)	0.1221(66)
C(21)	−0.4736(16)	0.4294(4)	0.1821(11)	0.1058(58)
C(22)	−0.4219(14)	0.4004(4)	0.2846(11)	0.1050(54)

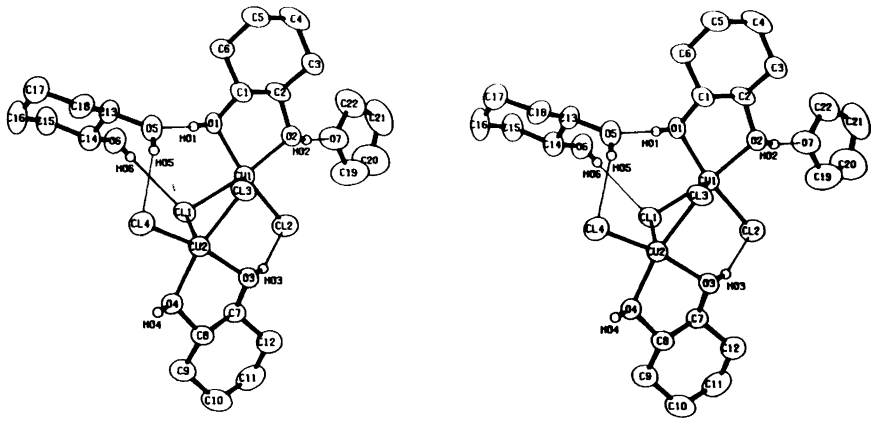

Fig. 1. A stereoscopic view of $[CuCl_2(trans\text{-chd})]_2 \cdot$ (*trans*-chd) $\cdot$ THF showing the atom numbering scheme. Ring hydrogen atoms are not shown.

Table 2. Distances (Å) and bond angles (°) around the copper atoms in the complex.

Cu(1)–Cl(1)	2.272(2)	Cu(2)–Cl(3)	2.247(2)
Cu(1)–Cl(2)	2.225(2)	Cu(2)–Cl(4)	2.199(2)
Cu(1)–Cl(3)	2.680(2)	Cu(2)–Cl(1)	2.804(2)
Cu(1)–O(1)	1.984(6)	Cu(2)–O(3)	1.988(5)
Cu(1)–O(2)	1.995(5)	Cu(2)–O(4)	2.016(5)
Cu(1)···Cu(2)	3.511(1)		
Cl(1)–Cu(1)–Cl(2)	95.4(1)	Cl(3)–Cu(2)–Cl(4)	99.0(1)
Cl(1)–Cu(1)–Cl(3)	89.7(1)	Cl(3)–Cu(2)–Cl(1)	87.2(1)
Cl(1)–Cu(1)–O(1)	92.5(2)	Cl(3)–Cu(2)–O(3)	88.8(2)
Cl(1)–Cu(1)–O(2)	168.0(2)	Cl(3)–Cu(2)–O(4)	167.3(2)
Cl(2)–Cu(1)–Cl(3)	101.9(1)	Cl(4)–Cu(2)–Cl(1)	101.1(1)
Cl(2)–Cu(1)–O(1)	167.1(2)	Cl(4)–Cu(2)–O(3)	167.4(2)
Cl(2)–Cu(1)–O(2)	89.7(2)	Cl(4)–Cu(2)–O(4)	90.9(2)
Cl(3)–Cu(1)–O(1)	88.4(2)	Cl(1)–Cu(2)–O(3)	89.0(2)
Cl(3)–Cu(1)–O(2)	99.9(2)	Cl(1)–Cu(2)–O(4)	98.7(2)
Cl(1)–Cu(1)–O(2)	80.7(2)	O(3)–Cu(2)–O(4)	80.1(2)
Cu(1)–Cl(1)–Cu(2)	86.8(1)	Cu(1)–Cl(3)–Cu(2)	90.4(1)

Table 3. Distances (Å) and bond angles (°) around the oxygen and carbon atoms of the coordinated diol units in the complex.

Diol 1		Diol 2	
C(1)–O(1)	1.429(9)	C(7)–O(3)	1.435(8)
C(2)–O(2)	1.471(9)	C(8)–O(4)	1.439(9)
C(1)–C(2)	1.474(10)	C(7)–C(8)	1.489(10)
C(2)–C(3)	1.500(10)	C(8)–C(9)	1.496(10)
C(3)–C(4)	1.551(12)	C(9)–C(10)	1.516(12)
C(4)–C(5)	1.468(12)	C(10)–C(11)	1.522(12)
C(5)–C(6)	1.526(10)	C(11)–C(12)	1.516(12)
C(6)–C(1)	1.508(10)	C(12)–C(7)	1.504(11)
O(1)–H(O1)	0.72(8)	O(3)–H(O3)	0.93
O(2)–H(O2)	0.91(7)	O(4)–H(O4)	0.77(7)
O(1)···O(2)	2.576(7)	O(3)···O(4)	2.577(7)
O(1)–C(1)–C(2)	106.2(6)	O(3)–C(7)–C(8)	105.5(6)
O(1)–C(1)–C(6)	113.9(6)	O(3)–C(7)–C(12)	114.4(7)
O(2)–C(2)–C(1)	105.8(6)	O(4)–C(8)–C(7)	107.0(6)
O(2)–C(2)–C(3)	112.7(7)	O(4)–C(8)–C(9)	113.7(7)
C(1)–C(2)–C(3)	112.7(7)	C(7)–C(8)–C(9)	112.2(7)
C(2)–C(3)–C(4)	108.7(7)	C(8)–C(9)–C(10)	109.5(7)
C(3)–C(4)–C(5)	112.7(7)	C(9)–C(10)–C(11)	112.6(8)
C(4)–C(5)–C(6)	114.0(7)	C(10)–C(11)–C(12)	111.7(8)
C(5)–C(6)–C(1)	109.2(7)	C(11)–C(12)–C(7)	109.7(8)
C(6)–C(1)–C(2)	111.5(7)	C(12)–C(7)–C(8)	111.3(7)

Table 4. Distances (Å) and bond angles (°) around the oxygen and carbon atoms of the uncoordinated molecules in the complex.

Diol 3			
C(13)–O(5)	1.458(9)	O(5)–C(13)–C(14)	111.4(7)
C(14)–O(6)	1.444(9)	O(5)–C(13)–C(18)	110.3(7)
C(13)–C(14)	1.484(11)	O(6)–C(14)–C(13)	112.2(7)
C(14)–C(15)	1.515(11)	O(6)–C(14)–C(15)	108.6(7)
C(15)–C(16)	1.502(12)	C(13)–C(14)–C(15)	110.9(8)
C(16)–C(17)	1.486(13)	C(14)–C(15)–C(16)	110.5(8)
C(17)–C(18)	1.534(12)	C(15)–C(16)–C(17)	110.9(8)
C(18)–C(13)	1.493(11)	C(16)–C(17)–C(18)	112.3(8)
C(5)–H(O5)	0.81(8)	C(17)–C(18)–C(13)	110.2(8)
O(6)–H(O6)	0.72(8)	C(18)–C(13)–C(14)	113.4(7)
O(5)···O(6)	2.874(9)		
THF			
C(19)–O(7)	1.404(11)	C(19)–O(7)–C(22)	109.9(8)
C(22)–O(7)	1.407(11)	O(7)–C(19)–C(20)	109.2(9)
C(19)–C(20)	1.420(14)	C(19)–C(20)–C(21)	106.0(10)
C(20)–C(21)	1.477(15)	C(20)–C(21)–C(22)	105.2(9)
C(21)–C(22)	1.498(15)	C(21)–C(22)–O(7)	106.5(10)

Table 5. Parameters for possible hydrogen bonds in the complex.[a]

O–H···X	H···X (Å)	O···X (Å)	∠O–H···X (°)
O(1)–H(O1)···O(5)	1.91(8)	2.592(8)	159(8)
O(2)–H(O2)···O(7)	1.75(8)	2.651(9)	170(5)
O(3)–H(O3)···Cl(2)	2.18	3.054(7)	158
O(4)–H(O4)···O(6^{i})	2.00(8)	2.720(8)	157(8)
O(5)–H(O5)···Cl(4)	2.49(8)	3.278(7)	165(7)
O(6)–H(O6)···Cl(1)	2.52(9)	3.224(7)	168(7)

[a] Symmetry code: (i) $1+x,y,z$

The structure consists of chloro-bridged non-centrosymmetric $[CuCl_2(trans\text{-chd})]_2$ dimers to which one diol and one THF molecule are attached by hydrogen bonds. These clusters are held together by one interclustral hydrogen bond and by Van der Waals forces.

The bonding parameters of the Cu atoms are presented in Table 2. The Cu–O and Cu–Cl bond lengths are normal as found in this type of compounds.[1,6] The coordination geometry around the two copper(II) ions is a distorted square base pyramid. The greatest difference in the bonding parameters of the two copper(II) ions is found between the values of the angles Cl(1)–Cu(1)–O(1) and Cl(3)–Cu(2)–O(3), of which the former is 92.5° and the latter 88.8°. The distance Cu···Cu is 3.511(1) Å.

In the coordinated *trans*-chd molecule the torsion angles O(1)-C(1)–C(2)–O(2) and O(3)–C(7)–C(8)–O(4) are 51.4° and −50.3°, respectively, and in the uncoordinated *trans*-chd the torsion angle O(5)–C(13)–C(14)–O(6) is 57.7°. The torsion angle values of 51.4° and −50.3° in the *trans*-chd molecules reveal that the $[CuCl_2(trans\text{-chd})]_2$ dimer contains different *trans*-chd enantiomers.

The bond distances and angles in the organic molecules are presented in Tables 3 and 4. It can be seen from the tables that the coordinated *trans*-chd molecules are more distorted than the uncoordinated ones. The six-membered rings have a *chair* conformation. The hydrogen bonded THF molecule has an *envelope* conformation with C(20) as the "flap" atom. As the torsion

angles of the THF molecule are of the size of 1.2°–17.6°, the ring is flattened from the ideal *envelope* conformation of cyclopentane.[7] However, THF is a flexible molecule with many conformations of nearly equal energy.

There exists an extensive hydrogen bond system which contributes to the stability of the structure in the solid state. The hydrogen bond parameters are given in Table 5.

1. Hiltunen, L., Leskelä, M., Niinistö, L. and Sillanpää, R. *Acta Chem. Scand. A 38* (1984) *To be published.*
2. Roebuck, A. and Adkins, H. *Org. Synth. Coll. Vol. III* (1955) 217.
3. *International Tables for X-Ray Crystallography,* Kynoch Press, Birmingham 1974, Vol. 4.
4. Sheldrick, G. M. *SHELX-76, Program for Crystal Structure Determination,* University of Cambridge, 1976.
5. Johnson, C. K. *ORTEP-II, A Fortran Thermal-ellipsoid Plot Program for Crystal Structure Illustrations. Report ORNL-5138,* Oak Ridge National Laboratory, Tennessee 1976.
6. Antti, B.-M. *Acta Chem. Scand. A 30* (1976) 405.
7. Bucourt, R. In Eliel, E. L. and Allinger, N. L., Eds. *Topics in Stereochemistry,* Wiley, New York 1974, Vol. 8, p. 180.

Received June 28, 1983.

Acta Chemica Scandinavica A 37 (1983) 709–714

The Crystal Structure of (2,2′-Bipyridine)oxoperoxo(pyridine-2-carboxylato)vanadium(V) Hydrate, $[VO(O_2)\,(C_5H_4NCOO)\,(C_{10}H_8N_2)]\cdot H_2O$, at −100 °C

HELGA SZENTIVANYI and ROLF STOMBERG

Department of Inorganic Chemistry, CTH/GU, Chalmers Tekniska Högskola, S-412 96 Göteborg, Sweden

The crystal structure of (2,2′-bipyridine)oxoperoxo(pyridine-2-carboxylato)vanadium(V) hydrate, $[VO(O_2)\,(C_5H_4NCOO)\,(C_{10}H_8N_2)]\cdot H_2O$, has been determined at −100 °C by single-crystal X-ray methods. The compound crystallizes in the monoclinic space group $P2_1/a$ with a=14.276(6) Å, b=10.697(4) Å, c=11.949(4) Å, β=66.51(3)°, and Z=4. Refinement by the least-squares method gave a final R-value of 0.043 for the 1198 observed, independent reflexions.

Vanadium is surrounded by a pentagonal bipyramidal arrangement of ligands, the peroxo group, the nitrogen atom and one carboxylate oxygen atom from pyridine-2-carboxylate and one nitrogen atom from 2,2′-bipyridine forming the pentagonal plane, while the vanadyl oxygen atom and the other nitrogen atom from 2,2′-bipyridine occupy the apical positions. The vanadium atom is displaced 0.27 Å from the pentagonal plane towards the vanadyl oxygen atom. Interatomic distances within the molecule are: $V-O_{peroxo}$ 1.862(5) and 1.887(5) Å, $(O-O)_{peroxo}$ 1.424(7) Å, V=O 1.604(5) Å, $V-O_{equatorial}$ 2.039(5) Å, $V-N_{equatorial}$ (mean) 2.127(6) Å and $V-N_{apical}$ 2.270(6) Å.

The known oxoperoxovanadates(V) can, according to Schwendt *et al.*,[1] be classified as $M^I_n[VO(O_2)_2L]$, $M^I_n[VO(O_2)_2(LL')]$, $M^I_n[VO(O_2)(LL')_2]$ and $M^I_n[VO(O_2)\,(L)\,(LL'L'')]$, where L, LL′, and LL′L″ are mono-, bi- and tridentate ligands, respectively. In connection with our syntheses[2] of $(C_{10}H_{10}N_2)\,[VO(O_2)_2(C_{10}H_8N_2)]_2\cdot 6H_2O$ according to Vuletić *et al.*,[3] a crystalline phase, which proved to be $[VO(O_2)(C_5H_4NCOO)\,(C_{10}H_8N_2)]\cdot H_2O$, was once obtained. Since no pyridine-2-carboxylic acid was added to the reaction mixture, 2,2′-bipyridine, which is quite a stable molecule, had obviously been oxidized to pyridine-2-carboxylic acid by hydrogen peroxide, vanadium(V) probably acting as a catalyst. The compound is obtainable in a more straightforward way as described in the Preparation section. This new compound, abbreviated $[VO(O_2)\,(pic)\,(bipy)]\cdot H_2O$, can be regarded as a special case of $M^I_n[VO(O_2)\,(LL')_2]$ with n=0 and two different bidentate ligands. Its crystal structure is reported in this paper.

EXPERIMENTAL

Preparation 0.62 g (0.0050 mol) pyridine-2-carboxylic acid was dissolved in 10 ml 2–3 % hydrogen peroxide. 0.48 g (0.0025 mol) vanadium pentoxide was added in small portions while the reaction mixture was kept at about 5 °C. To the dark red solution 0.78 g (0.0050 mol) 2,2′-bipyridine, dissolved in 10 ml ethanol, was added. The resulting solution was allowed to crystallize in a refrigerator. Dark red crystals were developed within half an hour.

Data collection. X-Ray reflexion intensities from a crystal of the dimensions 0.09×0.09×0.18 mm were measured at −100 °C with a SYNTEX $P2_1$ automatic four-circle single-crystal X-ray diffractometer using graphite-monochromatized Mo$K\alpha$ radiation. The temperature was kept at −100 °C with a SYNTEX LT1 low-temperature device. The $\theta-2\theta$ scan method was used and the 2θ scan speed was allowed to vary between 2 and

0302-4377/83 $2.50

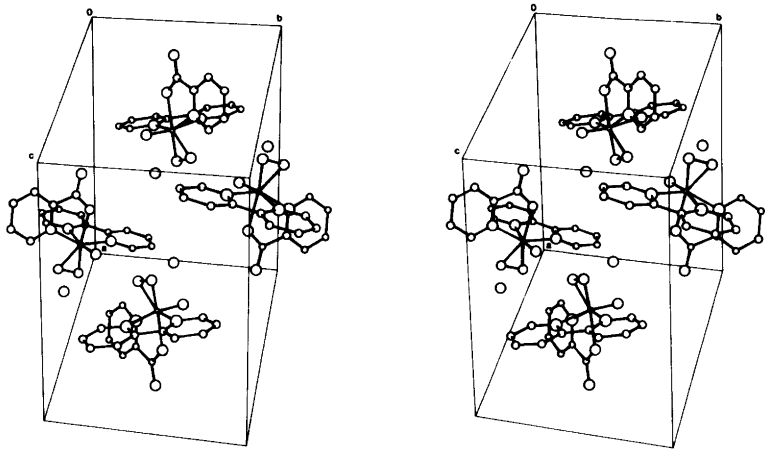

Fig. 1. Stereoscopic drawing of the unit cell of $[VO(O_2)(pic)(bipy)] \cdot H_2O$.

12 °min^{-1} depending on the intensity of the measured reflexion. Data were collected for $2\theta \leq 55°$. A profile analysis based on the Lehmann-Larsen method[4] was applied to the 96-step profile collected for each reflexion. A reflexion measured after each twenty-fourth reflexion showed no significant difference in intensity during the data collection.

Of the 2197 independent reflexions, 1198 with $I_o > 3\sigma(I_o)$ were regarded as being observed and were used in the subsequent calculations. The intensities were corrected for Lorentz and polarization effects but not for absorption.

The unit cell parameters were determined by a least-squares fit of refined diffractometer setting angles for eight reflexions.

CRYSTAL DATA

$C_{16}H_{14}N_3O_6V$; F.W.=395.25

Space group $P2_1/a$ (No. 14; non-standard setting) a=14.276(6) Å, b=10.697(4) Å, c=11.949(4) Å, β=66.51(3)°, Z=4, D_c=1.57 g cm^{-3}, μ(Mo$K\alpha$)=0.67 mm^{-1}.

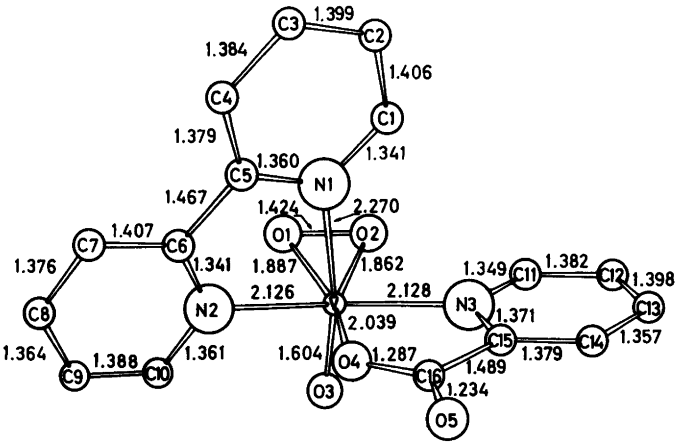

Fig. 2. The molecule $[VO(O_2)(pic)(bipy)]$. The e.s.d.'s are: V–O 0.005, V–N 0.006, O–O 0.007, N–C 0.009 and C–C 0.010–0.012 Å. The average C–H bond distance is 0.97(7) Å.

Table 1. Atomic fractional coordinates for [$VO(O_2)$ (C_5H_4NCOO) ($C_{10}H_8N_2$)] · H_2O. Space group $P2_1/a$. $U_{eq}=\frac{1}{3}\sum_i\sum_j U_{ij}a_i^*a_j^*a_ia_j\cos\alpha_{ij}$.

Atom	x	y	z	$U_{eq}/Å^2$ ($U_{iso}/Å^2$ for H)
V	0.2609(1)	0.4960(1)	0.3078(1)	0.027(1)
O1	0.3988(3)	0.5169(5)	0.2837(4)	0.036(2)
O2	0.3321(4)	0.6048(5)	0.3672(5)	0.040(3)
O3	0.2263(4)	0.3872(5)	0.4086(4)	0.037(2)
O4	0.1483(4)	0.4585(4)	0.2482(5)	0.034(3)
O5	−0.0093(4)	0.4979(5)	0.2620(4)	0.044(2)
O6	0.2247(4)	0.4880(6)	0.6525(5)	0.062(3)
N1	0.3110(4)	0.6122(5)	0.1348(5)	0.030(3)
N2	0.3335(4)	0.3700(5)	0.1610(5)	0.029(3)
N3	0.1446(4)	0.6281(5)	0.4018(5)	0.031(3)
C1	0.2983(6)	0.7358(7)	0.1279(8)	0.041(4)
C2	0.3318(5)	0.7997(7)	0.0159(8)	0.045(4)
C3	0.3775(6)	0.7315(8)	−0.0923(8)	0.050(4)
C4	0.3904(6)	0.6045(8)	−0.0821(7)	0.045(4)
C5	0.3580(5)	0.5461(7)	0.0300(7)	0.032(3)
C6	0.3723(5)	0.4124(6)	0.0458(6)	0.028(3)
C7	0.4231(5)	0.3311(8)	−0.0524(6)	0.037(4)
C8	0.4300(6)	0.2063(8)	−0.0287(7)	0.044(4)
C9	0.3880(6)	0.1636(7)	0.0885(7)	0.040(4)
C10	0.3400(6)	0.2464(6)	0.1837(7)	0.036(4)
C11	0.1462(6)	0.7167(7)	0.4814(7)	0.040(4)
C12	0.0682(6)	0.8019(8)	0.5342(7)	0.043(4)
C13	−0.0161(6)	0.7953(7)	0.5026(8)	0.045(4)
C14	−0.0203(5)	0.7055(7)	0.4244(7)	0.035(4)
C15	0.0594(5)	0.6222(6)	0.3758(6)	0.028(3)
C16	0.0639(5)	0.5200(6)	0.2892(6)	0.029(3)
H1	0.269(5)	0.783(6)	0.216(6)	0.016
H2	0.322(5)	0.901(6)	0.006(6)	0.018
H3	0.401(5)	0.780(7)	−0.185(6)	0.020
H4	0.426(5)	0.564(6)	−0.140(6)	0.018
H7	0.449(5)	0.365(6)	−0.130(6)	0.015
H8	0.466(5)	0.157(6)	−0.098(6)	0.018
H9	0.394(5)	0.077(6)	0.104(6)	0.016
H10	0.309(5)	0.233(6)	0.270(6)	0.015
H11	0.207(5)	0.717(6)	0.490(6)	0.016
H12	0.074(5)	0.867(6)	0.585(6)	0.018
H13	−0.074(5)	0.846(6)	0.544(6)	0.018
H14	−0.071(5)	0.699(6)	0.393(6)	0.014

STRUCTURE DETERMINATION

The positions of the non-hydrogen atoms were obtained from Fourier-maps based on phases determined by the multi-solution programme MULTAN.[5] Block-diagonal and, ultimately, full-matrix least-squares refinement of the positional and anisotropic thermal parameters and a scale factor yielded $R=0.058$ ($R=\Sigma||F_o|-|F_c||/\Sigma|F_o|$). Introduction of hydrogen atoms, except those belonging to the water molecule, reduced R to 0.043. The B_{eq} value of the corresponding carbon atom was used as B_{iso} for the hydrogen atoms. The weighting scheme used was that of Cruickshank:[6] $w=(a+|F_o|+c|F_o|^2+d|F_o|^3)^{-1}$ with $a=50.0$, $c=0.005$, and $d=0.0$. The scattering factors were taken from the *International Tables for X-Ray Crystallography, Vol. IV* (1974).

Table 2. Bond angles in $[VO(O_2)\ (C_5H_4NCOO)\ (C_{10}H_8N_2)] \cdot H_2O$.

	Angle/°
O1–V–O2	44.7(2)
O2–V–N3	79.2(2)
N3–V–O4	76.0(2)
O4–V–N2	77.3(2)
N2–V–O1	79.2(2)
O3–V–N1	166.4(2)
N1–V–N2	73.9(2)
V–O1–O2	66.8(3)
V–O2–O1	68.6(3)
C5–N1–C1	119.1(6)
N1–C1–C2	122.3(7)
C1–C2–C3	118.9(7)
C2–C3–C4	117.4(8)
C3–C4–C5	121.7(8)
C4–C5–N1	120.6(7)
C4–C5–C6	123.8(7)
N1–C5–C6	115.5(6)
C5–C6–N2	116.1(6)
C5–C6–C7	123.1(7)
N2–C6–C7	120.7(6)
C6–C7–C8	118.9(7)
C7–C8–C9	119.9(7)
C8–C9–C10	119.9(7)
C9–C10–N2	120.5(7)
C10–N2–C6	120.0(6)
C15–N3–C11	117.3(6)
N3–C11–C12	123.2(7)
C11–C12–C13	117.9(7)
C12–C13–C14	120.0(7)
C13–C14–C15	119.4(7)
C14–C15–N3	122.2(6)
C14–C15–C16	124.5(6)
N3–C15–C16	113.3(6)
C15–C16–O4	114.4(6)
C15–C16–O5	121.2(6)
O4–C16–O5	124.4(6)

A difference synthesis calculated after the final cycle of refinement showed a maximum electron density of 0.7 e $Å^{-3}$.

Calculations were carried out on an IBM 3033 computer using the crystallographic programmes described in Ref. 7.

Lists of the structure factors and thermal parameters are available form R.S. upon request.

RESULTS AND DISCUSSION

The positional parameters obtained for $[VO(O_2)\ (pic)\ (bipy)] \cdot H_2O$ in the final refinement cycle, as well as U_{eq} (or U_{iso}), are given in Table 1. The content of the unit cell is shown in Fig. 1. Bond distances are given in Fig. 2 and bond angles in Table 2.

The crystals of $[VO(O_2)\ (pic)\ (bipy)] \cdot H_2O$ consist of (2,2′-bipyridine)oxoperoxo(pyridine-2-carboxylato)vanadium(V) molecules and water of crystallization, held together by van der Waals and weak hydrogen bond forces.

The water molecule is hydrogen bonded to one carboxylate oxygen atom, $O5(\bar{x},1-y,1-z)$ with the bond distance 2.832(7) Å.

As shown in Fig. 2, the molecule $[VO(O_2)$-(pic)(bipy)] has a pentagonal bipyramidal arrangement of ligands with normal V=O, $V-O_{peroxo}$, $V-N_{equatorial}$ and $V-N_{apical}$ bond distances (see, *e.g.*, Refs. 8–23 and Table 3). Within the limits of experimental error the atoms defining the equatorial plane all lie in this plane, the maximum deviation being 2.7 σ. The vanadium atom is displaced 0.27 Å from this plane towards the vanadyl oxygen atom. Such a displacement is usually observed for transition metal peroxo compounds. When the apical atoms are different, or one is missing, this displacement is in the range 0.2–0.5 Å, the higher value being observed for pentagonal pyramidal complexes like $[VO(O_2)_2NH_3]^-$ and $[CrO(O_2)_2py]$, while 0.3 Å is commonly encountered in pentagonal bipyramidal compounds (see, *e.g.*, Table 6 in Ref. 10 and Refs. 11, 12 and 20).

The $(O-O)_{peroxo}$ bond length 1.424(7) Å is rather short but is comparable with 1.411(2) Å reported for $NH_4[VO(O_2)\ (H_2O)dipic] \cdot xH_2O$,[11] and 1.419(6) Å for $[Ti(O_2)(C_6H_4NO_2)_2$-$(OPN_3C_6H_{18})]$.[10]

Each pyridine ring in the bipyridine ligand is planar within 1.7σ, and the planes intersect each other at 2.7°. Bond distances and angles within the bipyridine group are in good agreement with data previously reported.[22]

In the pyridine-2-carboxylate ligand the pyridine ring and the carboxylate carbon atom are coplanar within 1.5σ. The dihedral angle between the carboxylate group and the pyridine ring is 4.5°. Bond distances and angles within the pyridine-2-carboxylate ligand show no significant deviations from those previously reported (see Table 4). As is usually observed, one carbon–oxygen bond distance is significantly longer than the other, the corresponding oxygen atom being involved in another bond (to a metal

Table 3. Comparison between distances (Å) found in peroxovanadates (V). $L_{equatorial}$=equatorial ligands other than O_{peroxo}, L_{apical}=apical ligands other than vanadyl oxygen atom.

Compound	V=O	V−O_{peroxo}	$(O-O)_{peroxo}$	V−$L_{equatorial}$	V−L_{apical}	Displacement of V from the pentagonal plane	Ref.
$(NH_4)_4[O(VO(O_2)_2)_2]$	1.601(3) 1.613(3)	1.896(3) 1.884(3) 1.914(3) 1.875(3) 1.895(3) 1.882(3) 1.912(3) 1.878(3)	1.469(4) 1.465(3) 1.474(4) 1.463(4)	2.013(2) 1.994(2)	2.522(3) 2.480(2)	0.45 0.44	10, 31
$NH_4[VO(O_2)_2(NH_3)]$	1.599(3)	1.871(3) 1.872(3)	1.463(4)	2.098(4)	—	0.46	20
$NH_4[VO(O_2)(H_2O)dipic]\cdot xH_2O$	1.579(2)	1.870(2) 1.872(2)	1.441(3)	2.053(2) 2.064(2) 2.088(2)	2.211(2)	0.25	11
$K_3[VO(O_2)_2ox]\cdot H_2O$	1.622(4)	1.934(4) 1.866(4) 1.856(4) 1.911(4)	1.460(6) 1.451(6)	2.060(4)	2.251(4)	0.28	12
$NH_4[VO(O_2)_2bipy]\cdot 4H_2O$	1.619(3)	1.911(3) 1.883(3) 1.909(3) 1.880(3)	1.471(4) 1.465(4)	2.149(4)	2.288(3)	0.32	13
$[VO(O_2)(pic)(bipy)]\cdot H_2O$	1.604(5)	1.887(5) 1.862(5)	1.424(7)	2.126(6) 2.128(6) 2.039(5)	2.270(6)	0.27	This paper
$(Hbipy)[H\{VO(O_2)_2bipy\}_2]\cdot$ $\cdot xH_2O_2\cdot(6-x)H_2O$	1.612(2)	1.869(2) 1.892(2) 1.903(2) 1.995(2)[a]	1.471(3) 1.461(3)	2.154(3)	2.290(2)	0.31	2
$(Hbipy)[VO(O_2)_2bipy]\cdot$ $\cdot(3+x)H_2O_2\cdot(2-x)H_2O$	1.619(3)	1.942(3) 1.862(3) 1.914(3) 1.938(3)	1.473(4) 1.474(4)	2.137(4)	2.284(4)	0.28	30

[a] Attached to a hydrogen atom.

Table 4. Comparison between the carbon–oxygen bond lengths (Å) in the carboxylate group, O(1)–C–O(2), in a number of picolinates ($C_5H_4NCOO^-$=pic). O(2) is coordinated to a metal atom or a hydrogen atom.

Compound	C–O(1)	C–O(2)	Ref.
Hpic	1.214(3)	1.285(3)	24
$Cu(pic)_2 \cdot KSCN$	1.226(9)	1.266(9)	25
$Ni(pic)_2 \cdot 4H_2O$	1.245(8)	1.273(8)	26
$Cu(pic)_2 \cdot 2H_2O$	1.234(2)	1.276(2)	27
$[Fe(pic)_2Cl(H_2O)]$	1.246(3)	1.286(3)	28
$H[MoO(O_2)_2pic] \cdot 2Hpic \cdot H_2O$	1.226(3)	1.295(3)	17
	1.198(3)	1.292(3)	
	1.227(4)	1.252(3)	
$[H_2pic]_4[Mo(CN)_8]$	1.184(8)	1.290(7)	29
	1.200(8)	1.303(7)	
$Ti(O_2)(pic)HMPT$	1.212(4)	1.286(4)	9
$[VO(O_2)(pic)(bipy)] \cdot H_2O$	1.234(8)	1.287(8)	This paper

atom or hydrogen).

Electron density maps based on single crystal data collected for a second crystal, prepared at higher hydrogen peroxide concentration, showed that some of the water of crystallization can be replaced by hydrogen peroxide. This has also been observed for two other products obtained in the system V_2O_5–H_2O_2–bipy–H_2O, and their structures will be published shortly.[2,30]

Acknowledgement. We wish to express our gratitude to Mrs Solveig Olson for technical assistance.

REFERENCES

1. Schwendt, P., Petrović, P. and Úskert, D. *Z. Anorg. Allg. Chem. 466* (1980) 232.
2. Stomberg, R. and Szentivanyi, H. *Acta Chem. Scand. A. In press.*
3. Vuletić, N. and Djordjević, C. *J. Chem. Soc. Dalton Trans.* (1973) 1137.
4. Lehmann, M. S. and Larsen, F. K. *Acta Crystallogr. A 30* (1974) 580.
5. Germain, G., Main, P. and Woolfson, M. M. *Acta Crystallogr. A 27* (1971) 368.
6. Cruickshank, D. W. J. *Crystallographic Computing,* Munksgaard, Copenhagen 1970, p. 195.
7. Lindgren, O. *Thesis,* University of Göteborg and Chalmers University of Technology, Göteborg 1977.
8. Stomberg, R. and Svensson, I.-B. *Acta Chem. Scand. A 31* (1977) 635.
9. Mimoun, H., Postel, M., Casabianca, F., Fisher, J. and Mitschler, A. *Inorg. Chem. 21* (1982) 1303.
10. Svensson, I.-B. and Stomberg, R. *Acta Chem. Scand. 25* (1971) 898.
11. Drew, R. E. and Einstein, F. W. B. *Inorg. Chem. 12* (1973) 829.
12. Begin, D., Einstein, F. W. B. and Field, J. *Inorg. Chem. 14* (1975) 1785.
13. Szentivanyi, H. and Stomberg, R. *Acta Chem. Scand. A 37* (1983) 553
14. Stomberg, R. *Acta Chem. Scand. A 36* (1982) 101.
15. Stomberg, R. *Acta Chem. Scand. A 36* (1982) 423.
16. Stomberg, R. and Ainalem, I.-B. *Acta Chem. Scand. 22* (1968) 1439.
17. Jacobson, S. E., Tang, R. and Mares, F. *Inorg. Chem. 17* (1978) 3055.
18. Trysberg, L. and Stomberg, R. *Acta Chem. Scand. A 35* (1981) 823.
19. Einstein, F. W. B. and Penfold, B. R. *Acta Crystallogr. 17* (1964) 10.
20. Drew, R. E. and Einstein, F. W. B. *Inorg. Chem. 11* (1972) 1079.
21. Giacomelli, A., Floriani, C., Ofir de Souza Duarte, A., Chiesi-Villa, A. and Guastini, C. *Inorg. Chem. 21* (1982) 3310.
22. Edwards, A. J., Slim, D. R., Guerchais, J. E. and Sala-Pala, J., *J. Chem. Soc. Dalton Trans.* (1977) 984.
23. Stomberg, R. *Ark. Kemi 24* (1965) 111.
24. Takusagawa, F. and Shimada, A. *Chem. Lett.* (1973) 1089.
25. Stephens, F. S. *J. Chem. Soc. A* (1970) 2377.
26. Loiseleur, H. *Acta Crystallogr. B 28* (1972) 816.
27. Faure, R., Loiseleur, H. and Thomas-David, G. *Acta Crystallogr. B 29* (1973) 1890.
28. Thundathil, R. V., Holt, E. M., Holt, S. L. and Watson, K. J. *J. Chem. Soc. Dalton Trans.* (1976) 1438.
29. Basson, S. S., Leipoldt, J. G. and van Wyk, A. J. *Acta Crystallogr. B 36* (1980) 2025.
30. Stomberg, R. and Szentivanyi, H. *Acta Chem. Scand. A 38* (1984). *In press.*
31. Stomberg, R., Olson, S. and Svensson, I.-B. *Acta Chem. Scand. To be published.*

Received February 9, 1983.

Acta Chemica Scandinavica A 37 (1983) 715–721

Structure Refinements of $Co_3(PO_4)_2$. A Note on the Reliability of Powder Diffraction Studies

ANDERS G. NORD [a] and THEODOR STEFANIDIS [b]

[a] Section of Mineralogy, Swedish Museum of Natural History, Box 50007, S-104 05 Stockholm 50 and [b] Departments of Structural and Inorganic Chemistry, Arrhenius Laboratory, University of Stockholm, S-106 91 Stockholm, Sweden

The crystal structure of $Co_3(PO_4)_2$ ($P2_1/n$) has been refined by means of the Rietveld full-profile technique, based on powder diffraction data. Photographic X-ray data (Guinier-Hägg) as well as neutron powder diffractometer data have been used. These results and an earlier rigid-group structural refinement with Guinier-Hägg data (Nord, 1974) agree with an X-ray single-crystal study of $Co_3(PO_4)_2$ (Anderson, Kostiner, Miller and Rea, 1975), although individual Co–O and P–O bond distances may deviate by 1–2 σ. The average distances within each polyhedron agree still better. Other examples from the literature are given, and the usefulness of powder diffraction data is discussed.

When X-ray crystallography was in its infancy, powder diffraction data were used for most structure determinations, but since about 1930 single-crystal data have mostly been utilized for this purpose. However, powder diffraction techniques have gained renewed importance, principally owing to the development of the ingenious full-profile refinement technique by Rietveld.[1] This method was first used for neutron diffraction data, but has later been extended to X-ray powder patterns recorded by Guinier-Hägg focusing cameras[2–4] or powder diffractometers.[5,6] Young[7] predicted that papers on X-ray powder diffraction soon may outnumber those on neutron powder diffraction.

At the XII International Congress of Crystallography in Ottawa, 1981, Langford[8] read a review paper on the Rietveld technique, entitled "The renaissance of powder diffraction: from ugly duckling to beautiful swan". It was met with applause but also some criticism. One of the critics started by saying that "he wanted to pour some cold water down the neck of the beautiful swan". The reliability of the profile-fitting technique has also been questioned by Sakata and Cooper[9] and some other authors.

Within a research project on solid solutions, we have frequently based our studies on the $Mg_3(PO_4)_2$ and $Co_3(PO_4)_2$ structures (*e.g.* Refs. 10, 11). X-Ray powder diffraction data were used by Nord[12] to show that $Co_3(PO_4)_2$ is isostructural with magnesium orthophosphate.[13] A detailed structural investigation confirming this fact appeared shortly afterwards.[14] We now report on three Rietveld full-profile refinements of $Co_3(PO_4)_2$, one based on neutron data and two on photographic (Guinier-Hägg) X-ray powder diffraction data. The results of the various refinement techniques are compared, and a brief discussion on the reliability of powder diffraction data and the Rietveld technique is given, together with other examples from the literature.

EXPERIMENTAL

Two samples, *A* and *B* (each~5 g $Co_3(PO_4)_2$), were prepared as earlier described.[12] Accurate X-ray powder diffraction data were obtained with an XDC-700 Guinier-Hägg type focusing camera ($CrK\alpha_1$ radiation, λ=2.28975 Å, r=50.00 mm; KCl internal standard). Copper radiation was not used because of the strong X-ray fluorescence from cobalt. The photographs were evaluated with a computer-controlled film scanner and

0302-4377/83 $2.50

Table 1. Fractional atomic coordinates and isotropic temperature factors (Å^2) for the three profile-refinements of $Co_3(PO_4)_2$. Space group $P2_1/n$ (No. 14, non-standard setting) with general positions 4(*e*): $\pm(x,y,z)$; $\pm(1/2\text{-}x, 1/2\text{+}y, 1/2\text{-}z)$.

Atom	Parameter	Neutron data (study II)	Guinier-Hägg photographic X-ray data Sample *A* (III)	Sample *B* (IV)
Co(1)	*x*	0.609(3)	0.615(1)	0.615(1)
	y	0.137(3)	0.142(1)	0.142(1)
	z	0.076(3)	0.096(1)	0.097(1)
Co(2)	*x*	0	0	0
	y	0	0	0
	z	1/2	1/2	1/2
P	*x*	0.198(1)	0.196(1)	0.205(1)
	y	0.190(1)	0.193(1)	0.192(1)
	z	0.033(2)	0.034(2)	0.037(2)
O(1)	*x*	0.052(1)	0.053(2)	0.048(2)
	y	0.144(1)	0.148(2)	0.145(2)
	z	0.826(2)	0.831(3)	0.838(4)
O(2)	*x*	0.128(1)	0.128(2)	0.121(2)
	y	0.199(1)	0.202(2)	0.199(2)
	z	0.306(2)	0.310(3)	0.306(3)
O(3)	*x*	0.253(1)	0.258(2)	0.257(2)
	y	0.363(1)	0.371(2)	0.370(2)
	z	0.950(1)	0.947(3)	0.954(3)
O(4)	*x*	0.355(1)	0.362(2)	0.367(3)
	y	0.078(1)	0.089(3)	0.085(2)
	z	0.053(2)	0.051(3)	0.050(3)
Co	*B*(Co)	0.8(4)	0.0(2)	−0.6(3)
P	*B*(P)	0.4(2)	−0.4(3)	−1.3(4)
O	*B*(O)	0.1(1)	−0.8(3)	−1.7(3)

associated programs.[15] The transmission intensities were measured up to $\theta \approx 44°$, giving about 2500 recorded intensity values for each photograph after exclusion of three internal standard (KCl) reflections, comprising 74 independent, partly overlapping Bragg reflections. The step length (in θ) is 0.0127°; the peak half-widths are around 0.1° (in θ) so that each reflection peak comprises 12–25 individual intensity values. The background values were subtracted, and the net intensities corrected for polarization and Lorentz effects.[2] Both samples were found to be very pure. Unit cell parameters were refined with the program PIRUM;[16] they are (average of *A* and *B*): $a=7.556(1)$, $b=8.371(2)$, $c=5.064(1)$ Å, $\beta=94.05(1)°$, $V=319.5(1)$ Å^3 ($P2_1/n$ symmetry; $Z=2$). The calculated density is 3.812 g cm^{-3}.

Neutron powder diffraction data were collected with an OPUS-3 diffractometer, equipped with five ^{3}He detectors, at the 2 MW JEEP-2 reactor at Kjeller, Norway. The sample (a mixture of *A* and *B* amounting to about 10 g) was kept in a thin-walled vanadium cylinder. Accurate powder data were collected for $5 \leq \theta \leq 45°$ ($\Delta\theta=0.025°$, $\lambda \approx 1.8820$ Å), with a total scan time of 4 days. The intensity profile contained 144 independent reflections. The graphically determined background was subtracted from the intensity profile to give net intensities.

THE PROFILE REFINEMENTS

The neutron powder diffraction data were processed with Rietveld's full-profile refinement procedure.[1] Some trial refinements were first made to settle the average wavelength, scale factor, zero point, *etc.* In the final stages, the complete structure was refined with 25 parameters: one scale factor, 18 atomic positional parameters, three isotropic temperature factors (for cobalt, phosphorus, and oxygen) and three "profile" parameters. The latter define the almost perfectly symmetric Gaussian shape of the peak profiles. The θ-dependence of H_k, the full width at half maximum of the peak (with maximum at $\theta=\theta_k$), is defined by

$H_k^2 = U \tan^2\theta_k + V \tan\theta_k + W$ (*cf.* Ref. 17).

The scattering amplitudes were taken from the *International Tables for X-Ray Crystallography*.[18] The final R values[1] were $R_I = 0.067$ and $R_p = 0.11$. The atomic parameters are listed in Table 1. Due to the comparatively small scattering amplitude of cobalt, the Co atoms have acquired larger e.s.d. values than the other atoms.

The A and B samples of $Co_3(PO_4)_2$ were then structurally refined with a Guinier-Hägg X-ray version of Rietveld's program, developed by Malmros and Thomas[2] and later modified by Werner *et al.*[3,4] The parameters to be refined were equivalent to those of the neutron diffraction study, with exception of the profile parameters. Sonneveld and Visser[19] found that the modified Lorentzian function (henceforward: *ML*) defining the peak profiles performed better with Guinier data than did either the Gaussian or the Lorentzian function. This was later confirmed for Guinier-Hägg data by Malmros and Thomas.[2] However, an empirical asymmetry parameter P was also introduced,[2] thus increasing the number of parameters by one with respect to the neutron refinement, to 26 instead of 25. The refinements were successfully carried out, arriving at $R_F = 0.090$ (for A) and $R_F = 0.097$ (for B). The atomic parameters are listed in Table 1. The negative "temperature" factors are probably due to absorption effects (*cf.* Refs. 3, 20). The standard deviations of the refined parameters have been obtained by use of all observed intensity values for the peaks (*cf.* Ref. 21). The samples A and B have been checked with a JEOL JSM-35 scanning electron microscope showing that there is no reason to expect preferred orientation effects.

Tables of observed and calculated values of the integrated reflections for the three profile refine-

Table 2. Some crucial data characterizing the five structure refinements of $Co_3(PO_4)_2$.

Study No.	I	II	III	IV	V
Technique	single-crystal refinement	Rietveld refinement ($A+B$)	Rietveld refinement (A)	Rietveld refinement (B)	Rigid-group least-squares refinement
Reference	Anderson *et al.*[14]	This work	This work	This work	Nord[12]
Data	X-ray single-crystal diffractometer	Neutron powder diffractometer	Guinier-Hägg (X-ray)	Guinier-Hägg (X-ray)	Guinier-Hägg (X-ray)
Radiation	Mo$K\alpha$	Neutrons	Cr$K\alpha_1$	Cr$K\alpha_1$	Fe$K\alpha_1$
Wavelength (Å)	0.71069	1.8820	2.28975	2.28975	1.9360
Number of reflections	1032	144	74	74	55
Absorption correction	yes	no (negligible)	no	no	no
Number of refined parameters	59	25	26	26	10
Temperature factors	aniso-tropic	isotropic (three)	isotropic (three)	isotropic (three)	isotropic overall temp. factor (constrained)
R_F	0.039	0.067[a]	0.090	0.097	0.14

[a] Note: R_I is given for refinement (II).

Table 3. Interatomic distances (Å), with observed standard deviations, for the five refinements of $Co_3(PO_4)_2$. D=distance, Δ=the difference (Å) between the value in question and the corresponding value from (I).

	Study I Anderson *et al.*[14] X-ray single-crystal data	Study II This work. Neutron profile refinement		Study III This work. X-ray profile refinement		Study IV This work. X-ray profile refinement		Study V Nord.[12] Rigid-group least-squares refinement (X-ray)	
	D	D	Δ	D	Δ	D	Δ	D	Δ
Co(1)–O(1)	2.229(3)	2.28(2)	0.05	2.19(2)	−0.04	2.23(2)	0.00	2.38(5)	0.15
Co(1)–O(2)	1.978(3)	1.95(2)	−0.03	1.95(1)	−0.03	1.99(1)	0.01	1.94(5)	−0.04
Co(1)–O(3)	2.109(3)	2.12(2)	0.01	2.03(2)	−0.08	2.04(2)	−0.07	2.05(5)	−0.06
Co(1)–O(4)	1.988(3)	1.95(2)	−0.04	1.96(1)	−0.03	1.96(1)	−0.03	2.01(5)	0.02
Co(1)–O(4′)	2.012(3)	1.98(2)	−0.03	2.08(2)	0.07	2.05(2)	0.04	2.02(5)	0.01
Average	2.063	2.056	−0.007	2.042	−0.021	2.054	−0.009	2.080	0.017
Co(2)–O(1) (×2)	2.058(3)	2.06(2)	0.00	2.10(2)	0.04	2.10(2)	0.04	2.02(5)	−0.04
Co(2)–O(2) (×2)	2.144(3)	2.18(2)	0.04	2.19(2)	0.05	2.18(2)	0.04	2.16(5)	0.02
Co(2)–O(3) (×2)	2.174(3)	2.18(2)	0.01	2.12(1)	−0.05	2.14(1)	−0.03	2.21(5)	0.04
Average	2.125	2.140	0.015	2.137	0.012	2.140	0.015	2.130	0.005
P–O(1)	1.526(3)	1.52(1)	−0.01	1.49(2)	−0.04	1.54(2)	0.01	1.53[a]	0.00
P–O(2)	1.533(3)	1.52(1)	−0.01	1.53(2)	0.00	1.53(2)	0.00	1.53[a]	0.00
P–O(3)	1.554(3)	1.58(1)	0.03	1.61(2)	0.06	1.60(2)	0.05	1.53[a]	−0.02
P–O(4)	1.540(3)	1.51(1)	−0.03	1.52(2)	−0.02	1.50(2)	−0.04	1.53[a]	−0.01
Average	1.538	1.533	−0.005	1.537	−0.001	1.542	0.004	1.530[a]	−0.008
O–P–O range (°)	104.6–112.9	104.2–114.6		104.6–117.0		104.7–117.1		109.5[a]	

[a] Constrained value.

ments can be obtained from the authors on request. Illustrations of the crystal structure have been published earlier.[13,14]

DISCUSSION

In addition to the three profile-refinements described above, our comparison will include the earlier mentioned studies by Nord[12] and by Anderson *et al.*[14] The former study was based on Guinier-Hägg photographic data (Fe$K\alpha_1$ radiation), using 55 integrated intensities from well-resolved reflections. The structure was refined utilizing the rigid-group least-squares program system of Scheringer,[22] by which the number of parameters was reduced to 10 by assuming PO_4 to be a rigid, regular tetrahedron. The study by Anderson *et al.*[14] was based on single-crystal diffractometer data (Mo$K\alpha$ radiation). Some crucial data characterizing the five refinements (numbered I–V) are given in Table 2.

In our comparison we will primarily discuss interatomic distances, since these are more relevant and more easily compared than a set of atomic coordinates (see Table 3). All atoms are denoted in accordance with the first study of $Co_3(PO_4)_2$.[12] The bond length values from the single-crystal study[14] (No. I) are regarded as "correct". All distance differences, called Δ, between (I) and refinements (II)–(V) are included in Table 3. We will first compare the average distances within the polyhedra (CoO_5, CoO_6 and PO_4) which build up a three-dimensional framework forming the $Co_3(PO_4)_2$ structure. For refinements (II)–(V) these values agree fairly well with the "correct" values; the differences are in the range 0.001–0.021 Å ($\lesssim 1\sigma$). The O–P–O angles are also fairly similar for all refinements.

Among the individual bond length values, the largest differences (*i.e.*, Δ values) are found in the distorted trigonal bipyramid $Co(1)O_5$. However, Co(1)–O(1) always shows up as the largest bond distance, while the shortest distance is Co(1)–O(2) in all studies except (IV). In study (V), Co(1)–O(1) is considerably longer (2.38 Å) than in the four other refinements. The fairly regular $Co(2)O_6$ octahedron and the almost regular PO_4 tetrahedron exhibit less scattering of bond distance values than the $Co(1)O_5$ group.

In this comparison of structure refinements, the neutron diffraction study (No. II) comes out as the second best. (No. I is naturally the best one). This is partly due to a larger number of observed reflections, but we also attribute the good result of the neutron refinement to a better defined peak-shape function (see below). The Δ differences for (II) are in the range 0.00–0.05 Å for the individual distances. The largest Δ values are registered in the cobalt–oxygen polyhedra [*e.g.* Co(1)–O(1) with Δ=0.05 Å], probably due to the small scattering amplitude of cobalt which reduces the accuracy in the respective positional parameters. The "Guinier-Hägg" X-ray refinements (III and IV) gave somewhat larger Δ values and standard deviations than (II). It is interesting to note, though, that the results of (III) and (IV) closely resemble each other, thus indicating good reproducibility for this method (for instance, compare the Co(1)–O(3) and the P–O(3) D and Δ values in Table 3). Moreover, it should be emphasized that refinements (III) and (IV) certainly do not exaggerate the usefulness of the profile-refinement method; the long wavelength used (Cr$K\alpha_1$) is *not* advantageous since it considerably reduces the number of observed reflections: the 26 parameters were refined on the basis of only 74 reflections. (The use of Cu$K\alpha_1$ radiation usually improves the accuracy, as will be exemplified below). Refinement (V) is the "loser" in Table 3, although it is surprisingly good since only 55 reflections were used and many structural parameters were constrained.

An extensive review of Rietveld refinements with neutron powder diffraction data has been published by Cheetham and Taylor.[23]

In a recent study of forsterite, Mg_2SiO_4, Lager *et al.*[24] have obtained excellent agreement between structural parameters from single-crystal diffractometer data and from a Rietveld refinement based on neutron powder diffraction data (464 reflections, 47 parameters) collected with the high-resolution time-of-flight powder diffractometer at Argonne National Laboratory's ZING-P pulsed neutron source. It thus seems that very good results can be achieved with the Rietveld technique, applied on a simple crystal structure, provided the data are first-class.

Among the critics of the Rietveld technique, Sakata and Cooper[9] claim that the standard deviations of the structural parameters are determined incorrectly and underestimated by a factor of *at least* two. Judging from our results obtained

for $Co_3(PO_4)_2$, this is not true for the neutron diffraction study (No. II). Albinati and Willis,[25] Prince[26] and many others have also shown that the fears of Sakata and Cooper are exaggerated.

As regards the applicability of the Rietveld method on X-ray diffraction data, a cumbersome complication arises because of the difficulty to define the peak profiles accurately.[27] For geometrical reasons this problem is still more complicated with Guinier-Hägg data than for powder diffractometer data, since there are to some extent individual variations of profiles, *i.e.* the peak-shape is not only dependent on tan θ (*cf.* Ref. 28). However, many good results have been obtained with Rietveld refinements based on Guinier-Hägg X-ray data by use of the *ML* peak-shape function. Some examples, all with Cu$K\alpha_1$ data (which is more favourable than Cr$K\alpha_1$) will be quoted.

Malmros and Thomas[2] obtained good agreement between refinements of α-Bi_2O_3 with the Rietveld technique and with X-ray single-crystal data. Further early examples of successful full-profile refinements are the studies of $Mg_3Nb_6O_{11}$[29] and $Zn_2Mg(PO_4)_2$.[30] The structure of $Ni_3(PO_4)_2$ has recently been profile-refined from Guinier-Hägg data.[31] In spite of the disadvantage of a monoclinic angle of 91.12°, which implies severe overlap among reflections like *hkl* and *hkl̄*, all observed individual Ni–O and P–O distances were usually within ±0.02 Å of the "correct" values yielded by an earlier single-crystal study.[32]

To sum up, a structural study based on powder diffraction data is probably always inferior to one utilizing good single-crystal data. However, it is much easier to obtain a powder sample than a single crystal. With powder data, problems like twinning, absorption, or extinction may often be neglected. The Rietveld technique is certainly suitable for refinements of already known and comparatively simple crystal structures. However, the solution of moderately complex crystal structures solely from powder diffraction data is another important advantage of the Rietveld technique.[33–35] Many cation distribution studies have also been performed utilizing X-ray powder data (*cf.* Refs. 10,30,31). We therefore conclude that structural studies based on powder diffraction data may be very fruitful, especially when combined with the Rietveld full-profile refinement technique, and that there is no reason for the "ugly duckling" to hide among the reeds.

Acknowledgements. We are indeed grateful to Professor Arne Magnéli, Professor Peder Kierkegaard and Dr. Per-Erik Werner (all at the Arrhenius Laboratory) for their constructive criticism and valuable comments on the manuscript. We are greatly indebted to Dr. Arne F. Andresen (Kjeller, Norway) for his help during the collection of the neutron diffraction data. This work has received financial support from the Swedish Natural Science Research Council (NFR).

REFERENCES

1. Rietveld, H. M. *J. Appl. Crystallogr. 2* (1969) 65.
2. Malmros, G. and Thomas, J. O. *J. Appl. Crystallogr. 10* (1977) 7.
3. Werner, P. E., Salomé, S., Malmros, G. and Thomas, J. O. *J. Appl. Crystallogr. 12* (1979) 107.
4. Werner, P. E. *Chem. Commun. Univ. Stockholm,* No. *6* (1981).
5. Young, R. A., Mackie, P. E. and von Dreele, R. B. *J. Appl. Crystallogr. 10* (1977) 262.
6. Wiles, D. B. and Young, R. A. *J. Appl. Crystallogr. 14* (1981) 149.
7. Young, R. A. *Natl. Bur. Stand. (U.S.) Spec. Publ. No. 567,* pp. 143–163, Washington (1980).
8. Langford, J. I. *Acta Crystallogr. A 37* (1981) C-2.
9. Sakata, M. and Cooper, M. J. *J. Appl. Crystallogr. 12* (1979) 554.
10. Nord, A. G and Stefanidis, T. *Mater. Res. Bull. 15* (1980) 1183.
11. Nord, A. G. *Acta Chem. Scand. A 36* (1982) 95.
12. Nord, A. G. *Acta Chem. Scand. A 28* (1974) 150.
13. Nord, A. G. and Kierkegaard, P. *Acta Chem. Scand. 22* (1968) 1466.
14. Anderson, J. B., Kostiner, E., Miller, M. C. and Rea, J. R. *J. Solid State Chem. 14* (1975) 372.
15. Johansson, K. E., Palm, T. and Werner, P. E. *J. Phys. E. 13* (1980) 1289.
16. Werner, P. E. *Ark. Kemi 31* (1969) 513.
17. Caglioti, G., Paoletti, A. and Ricci, F. P. *Nucl. Instrum. 3* (1958) 223.
18. *International Tables for X-Ray Crystallography,* Vol. IV, Table 2.6, Kynoch Press, Birmingham 1974.
19. Sonneveld, E. J. and Visser, J. W. *J. Appl. Crystallogr. 8* (1975) 1.

20. Sas, W. H. and de Wolff, P. M. *Acta Crystallogr. 21* (1966) 826.
21. Scott, H. G. *J. Appl. Crystallogr. 16* (1983) 159.
22. Scheringer, C. *Acta Crystallogr. 16* (1963) 546.
23. Cheetham, A. K. and Taylor, J. C. *J. Solid State Chem. 21* (1977) 253.
24. Lager, G. A., Ross, F. K., Rotella, F. J. and Jorgensen, J. D. *J. Appl. Crystallogr. 14* (1981) 137.
25. Albinati, A. and Willis, B. T. M. *J. Appl. Crystallogr. 15* (1982) 361.
26. Prince, E. *J. Appl. Crystallogr. 14* (1981) 157.
27. Young, R. A. and Wiles, D. B. *J. Appl. Crystallogr. 15* (1982) 430.
28. Ersson, N. O. *J. Appl. Crystallogr. 12* (1979) 295.
29. Marinder, B. O. *Chem. Scr. 11* (1977) 97.
30. Nord, A. G. *Mater. Res. Bull. 12* (1977) 563.
31. Nord, A. G. and Stefanidis, T. *Phys. Chem. Minerals 10* (1983) 10.
32. Calvo, C. and Faggiani, R. *Can. J. Chem. 53* (1975) 1516.
33. Waltersson, K., Werner, P. E. and Wilhelmi, K. A. *Cryst. Struct. Commun. 6* (1977) 225.
34. Berg, J. E. and Werner, P. E. *Z. Kristallogr. 145* (1977) 310.
35. Westman, S., Werner, P. E., Schuler, T. and Raldow, W. *Acta Chem. Scand. A 35* (1981) 467.

Received March 4, 1983.

Acta Chemica Scandinavica A 37 (1983) 723–728

Three-coordinated Divalent Tellurium Complexes: The Crystal Structures of Tetraphenylarsonium Diiodophenyltellurate(II) and Tetraphenylarsonium Bromoiodophenyltellurate(II)

SVERRE HAUGE and OLAV VIKANE *

Department of Chemistry, University of Bergen, Realfagbygget, N-5000 Bergen, Norway

Tetraphenylarsonium diiodophenyltellurate(II), $[(C_6H_5)_4As]$ $[C_6H_5TeI_2]$, I, and tetraphenylarsonium bromoiodophenyltellurate(II), $[(C_6H_5)_4As][C_6H_5TeBrI]$, II, form isomorphous monoclinic crystals with space group $P2_1/n$, $Z=4$. The unit cell dimensions for I are: $a=9.9456(11)$, $b=23.1421(22)$, $c=13.5999(17)$ Å, $\beta=108.337(10)°$, and for II: $a=9.8897(10)$, $b=23.1159(34)$, $c=13.4642(16)$ Å, $\beta=108.429(9)°$.

The tellurium atom is three-coordinated, being bonded to a phenyl carbon atom and, in directions nearly normal to the Te–C bond, to two iodine atoms in I, and to one bromine atom and one iodine atom in II. The three-centre systems I–Te–I and I–Te–Br are nearly linear, and the Te–C bond nearly bisects the angle of the three-centre system. The bond lengths and angles involving tellurium are: Te–I=2.9634(13) Å, 2.9456(14) Å, Te–C=2.120(12) Å, I–Te–I=178.03(4)°, I–Te–C=89.0(3)°, 89.4(3)° in I, and Te–I=2.9033(18) Å, Te–Br=2.8676(22) Å, Te–C=2.119(14) Å, I–Te–Br=177.93(6)°, I–Te–C=88.5(4)°, Br–Te–C=89.7(4)° in II.

In a previous paper the crystal structures of tetramethylammonium phenyldithiocyanatotellurate(II) and tetramethylammonium phenyldiselenocyanatotellurate(II) were reported.[1] The present paper reports the crystal structures of tetraphenylarsonium diiodophenyltellurate(II) and tetraphenylarsonium bromoiodophenyltellurate(II). These are so far the only structures of anionic tellurium(II) complexes. In addition to the anionic complexes, divalent tellurium is known to form numerous complexes with ligands as thiourea or substituted thioureas, selenourea or substituted selenoureas, and halides or pseudohalides.[1–10] Tellurium(II) forms square planar or T-shaped complexes. The latter coordination is found when the phenyl group is one of the ligands. The bonding system in the complexes has been assumed to be based on 5*p* orbitals of tellurium.[2] In the square planar complexes the bonding consists of two linear 3c–4e bonding systems at right angle to each other. The T-shaped complexes have one linear 3c–4e system and the phenyl carbon is bonded at right angle to this by a 2c–2e bonding. The 3c–4e bonding system gives weak bonds, and a relative strong bond is followed by a weak bond in *trans* position. The present work is part of an investigation of the relative strength of the *trans* bond lengthening effect to ligands in tellurium(II) complexes.

EXPERIMENTAL

Synthesis and preliminary crystal data for the two present compounds have been reported elsewhere.[11]

Intensity data were collected by use of an Enraf-Nonius CAD-4 computer controlled diffractometer with graphite-monochromatized Mo*Kα* radiation.

The crystals used were coated with epoxy glue. The intensity of two reference reflections of medium intensity, remeasured at intervals of

* Present address: Rogaland Regional College, N-4001 Stavanger, Norway.

0302-4377/83 $2.50

Table 1. Crystal data and refinement characteristics.

	$[(C_6H_5)_4As][C_6H_5TeI_2]$	$[(C_6H_5)_4As][C_6H_5TeBrI]$
a (Å)	9.9456(11)	9.8897(10)
b (Å)	23.1421(22)	23.116(3)
c (Å)	13.5999(17)	13.4642(16)
β (°)	108.337(10)	108.429(9)
V (Å^3)	2971.2	2920.2
M	841.86	794.87
Space group	$P2_1/n$ (No. 14)	$P2_1/n$ (No. 14)
Z	4	4
λMo$K\alpha$ (Å)	0.71073	0.71073
D_x (g cm^{-3})	1.89	1.81
D_{obs} (g cm^{-3})	1.88	1.82
μ (cm^{-1})	43.32	47.79
T (k)	293	293
F(000)	1584	1512
sin θ/λ range	0.578	0.578
Scan mode	ω-2θ	ω-2θ
No. of reflections	4928	4847
No. of reflections with $I>3\delta(I)$	2945	3161
Crystal dimensions (mm^3)	0.14×0.14×0.40	0.13×0.23×0.52
$R(F)$	0.046	0.062
$R_w(F)$	0.044	0.059
No. of parameters refined	157	157
Difference Fourier max. value (e Å^{-3})	1.2	1.2

6000 s of exposure time, decreased by 15 % for I, and 17 % for II during the data collections. The intensity data were scaled in accordance with the variation in the intensities of the reference reflections.

The data were corrected for Lorentz and polarization, absorption and anomalous dispersion effects. The calculated structure factors were based on the scattering factors calculated from numerical Hartree-Fock wave function.[12]

The structures were solved by Patterson and Fourier methods and refined by the full-matrix least-squares method, minimizing the function $\Sigma w(F_o-KF_c)^2$ where K is a scale factor and $w=1/\sigma^2(F_o)$. The refinement was performed with CRYLSQ of X-RAY 76.[13] Hydrogen atoms were not included in the refinements, carbon atoms were included with isotropic thermal parameters and the rest of the atoms with anisotropic parameters. Crystal data and refinement characteristics are given in Table 1. Atomic coordinates are listed in Tables 2 and 3. A list of structure factors and thermal parameters is available from the authors on request.

RESULTS

Bond lengths and angles in tetraphenylarsonium diiodophenyltellurate(II), I, and tetraphenylarsonium bromoidophenyltellurate(II), II, based on the atomic coordinates in Tables 2 and 3, are listed in Tables 4 and 5.

Views of the structures of the anions, as seen normal to the plane through the coordination group, are shown in Fig. 1. A stereoscopic view of the content of the unit cell of the bromoiodophenyltellurate(II) compound is shown in Fig. 2.

In each of the structures the tellurium atom is three-coordinated, being bonded to one phenyl carbon atom and, in directions nearly perpendicular to the Te–C bond, to two iodine atoms in I, and to one iodine and one bromine atom in II, so that each anion shows a T-shaped geometry.

The coordination around the tellurium atom is nearly planar in each structure. The largest deviation from a least-squares plane through Te,

Table 2. Atomic coordinates for tetraphenylarsonium diiodophenyltellurate(II), in fractions of monoclinic cell edges. Origin at a centre of symmetry. Standard deviations from least squares in parantheses.

	x	*y*	*z*
Te	0.19063(9)	0.09031(4)	0.21396(6)
I(1)	0.32344(10)	−0.01858(4)	0.17634(7)
I(2)	0.04904(10)	0.19697(4)	0.24705(7)
As	0.48546(12)	0.30500(5)	0.11500(8)
C(1)	0.0163(12)	0.0417(5)	0.2268(9)
C(2)	0.0214(13)	0.0227(5)	0.3285(9)
C(3)	−0.1016(15)	−0.0063(6)	0.3337(10)
C(4)	−0.2138(14)	−0.0144(6)	0.2535(10)
C(5)	−0.2209(15)	0.0013(6)	0.1534(10)
C(6)	−0.0962(14)	0.0308(5)	0.1401(9)
C(11)	0.4846(11)	0.2274(4)	0.0643(8)
C(12)	0.3574(12)	0.1961(5)	0.0377(8)
C(13)	0.3611(14)	0.1374(6)	0.0079(9)
C(14)	0.4850(15)	0.1135(6)	0.0028(10)
C(15)	0.6121(15)	0.1459(6)	0.0270(10)
C(16)	0.6108(13)	0.2043(5)	0.0626(9)
C(21)	0.6643(11)	0.3363(5)	0.1250(8)
C(22)	0.7754(12)	0.3300(5)	0.2161(8)
C(23)	0.9116(13)	0.3487(5)	0.2201(9)
C(24)	0.9359(13)	0.3733(5)	0.1335(9)
C(25)	0.8224(13)	0.3791(5)	0.0415(9)
C(26)	0.6825(13)	0.3623(5)	0.0353(8)
C(31)	0.3347(12)	0.3486(5)	0.0212(8)
C(32)	0.2714(13)	0.3925(5)	0.0618(9)
C(33)	0.1635(15)	0.4263(6)	−0.0144(11)
C(34)	0.1318(15)	0.4124(6)	−0.1170(11)
C(35)	0.1998(16)	0.3713(7)	−0.1555(11)
C(36)	0.3093(14)	0.3351(6)	−0.0857(10)
C(41)	0.4662(12)	0.3047(5)	0.2507(8)
C(42)	0.4862(14)	0.3568(6)	0.3022(10)
C(43)	0.4699(16)	0.3580(7)	0.4063(11)
C(44)	0.4428(15)	0.3063(7)	0.4446(10)
C(45)	0.4311(17)	0.2545(7)	0.3991(12)
C(46)	0.4433(14)	0.2513(6)	0.2909(10)

Table 3. Atomic coordinates for tetraphenylarsonium bromoiodophenyltellurate(II), in fractions of monoclinic cell edges. Origin at a centre of symmetry. Standard deviations from least squares in parentheses.

	x	*y*	*z*
Te	0.19224(15)	0.08856(6)	0.21498(10)
I	0.32350(16)	0.01847(7)	0.17938(13)
Br	0.05268(17)	0.19239(8)	0.24681(14)
As	0.48855(17)	0.30359(8)	0.11396(14)
C(1)	0.0180(15)	0.0396(7)	0.2268(12)
C(2)	0.0232(16)	0.0204(8)	0.3302(13)
C(3)	−0.0901(17)	−0.0080(9)	0.3422(14)
C(4)	−0.2115(17)	−0.0150(9)	0.2541(15)
C(5)	−0.2206(17)	0.0001(9)	0.1496(15)
C(6)	−0.0940(16)	0.0314(8)	0.1373(14)
C(11)	0.4853(15)	0.2250(7)	0.0655(13)
C(12)	0.3604(15)	0.1954(7)	0.0368(13)
C(13)	0.3629(16)	0.1373(8)	0.0093(14)
C(14)	0.4923(17)	0.1122(9)	0.0023(15)
C(15)	0.6123(17)	0.1450(9)	0.0238(15)
C(16)	0.6098(16)	0.2030(8)	0.0552(14)
C(21)	0.6718(15)	0.3348(7)	0.1259(13)
C(22)	0.7804(16)	0.3266(7)	0.2196(14)
C(23)	0.9283(16)	0.3448(8)	0.2217(15)
C(24)	0.9468(16)	0.3727(8)	0.1359(15)
C(25)	0.8293(16)	0.3803(8)	0.0426(15)
C(26)	0.6871(15)	0.3645(7)	0.0337(14)
C(31)	0.3403(15)	0.3486(7)	0.0189(14)
C(32)	0.2764(16)	0.3924(8)	0.0586(15)
C(33)	0.1614(17)	0.4274(8)	−0.0184(15)
C(34)	0.1318(17)	0.4136(8)	−0.1193(15)
C(35)	0.2003(18)	0.3736(9)	−0.1563(16)
C(36)	0.3183(17)	0.3358(8)	−0.0904(15)
C(41)	0.4666(15)	0.3027(7)	0.2523(12)
C(42)	0.4843(16)	0.3567(8)	0.3004(14)
C(43)	0.4729(18)	0.3625(9)	0.4100(16)
C(44)	0.4429(18)	0.3034(9)	0.4458(16)
C(45)	0.4324(18)	0.2478(9)	0.3936(16)
C(46)	0.4408(16)	0.2458(8)	0.2838(15)

I(1), I(2), and C(1) is 0.021 Å in I, and the largest deviation from the corresponding least-squares plane through Te, Br, I, and C(1) is 0.017 Å in II.

The angles of the tellurium coordination in the two structures, are equal within errors. The three-centre systems I–Te–I and I–Te–Br have a deviation of 2.0° from linearity. The deviation is in such a way that the halogen atoms are approaching the carbon atom. The deviation is probably a result of lone electron pair repulsion on tellurium. Such deviation occurs in all the known structures of divalent three-coordinated tellurium compounds. The angles are found in the range 171.9(5) to 177.22(3)°.[1–9] Within errors, the Te–C bond bisects the angle of the three-centre system. Average value of the Hal–Te–C angles is 89.15°.

The I–Te–I bonding system in I is slightly asymmetric and the mean value of the two Te–I bond lengths, 2.955 Å, is about 0.26 Å longer than the sum of the single bond radii.[14] In II the asymmetry of the I–Te–Br bonding system is more pronounced, the Te–Br and the Te–I bond is, respectively, about 0.36 Å and 0.20 Å

Table 4. Bond lengths (Å) and angles (°) in tetraphenylarsonium diiodophenyltellurate(II). Standard deviations in parentheses.

Te–I(1)	2.9634(13)	I(1)–Te–I(2)	178.03(4)
Te–I(2)	2.9456(14)	I(1)–Te–C(1)	89.0(3)
Te–C(1)	2.120(12)	I(2)–Te–C(1)	89.4(3)
C(1)–C(2)	1.438(18)	Te–C(1)–C(2)	117.4(8)
C(2)–C(3)	1.417(20)	Te–C(1)–C(6)	119.7(10)
C(3)–C(4)	1.305(17)	C(1)–C(2)–C(3)	115.0(10)
C(4)–C(5)	1.389(21)	C(2)–C(3)–C(4)	123.4(14)
C(5)–C(6)	1.475(21)	C(3)–C(4)–C(5)	123.3(15)
C(6)–C(1)	1.369(15)	C(4)–C(5)–C(6)	117.0(11)
		C(5)–C(6)–C(1)	118.1(12)
		C(6)–C(1)–C(2)	122.9(12)
As–C(11)	1.923(11)	C(11)–As–C(21)	106.4(5)
As–C(21)	1.887(11)	C(11)–As–C(31)	109.8(4)
As–C(31)	1.921(10)	C(11)–As–C(41)	110.6(5)
As–C(41)	1.915(12)	C(21)–As–C(31)	111.4(5)
		C(21)–As–C(41)	108.2(5)
		C(31)–As–C(41)	110.4(5)

longer than the sum of the single bond radii.[14] Thus, on substituting iodine for bromine, it is seen that the length of the *trans*-positioned Te–I bond increases by about 0.06 Å. This clearly indicates the more pronounced *trans* bond-lengthening effect of iodine relative to bromine when bonded to divalent tellurium. Similar

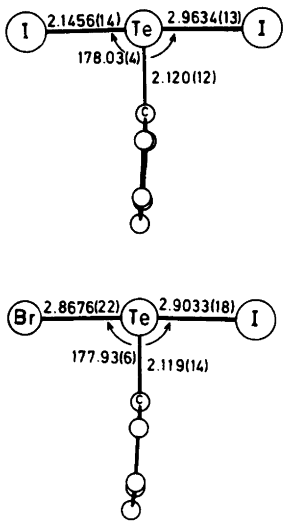

Fig. 1. The diiodophenyltellurate(II) ion, above, and the bromoiodophenyltellurate(II) ion, as seen normal to the plane through the coordination group.

trends in the *trans* bond-lengthening effect of bromine and iodine has previously been found when the ligand in *trans* position to halogen is ethylenethiourea or ethyleneselenourea.[6–8] From the preparation of the present compounds as well as other tellurium(II) complexes, it is known that chlorine, bromine, and iodine displace each other in the order mentioned.[2,3,11,15,16] On regarding tellurium(II) complexes as models for the transition states in nucleophilic displacements at divalent tellurium,[17] it is seen that the nucleophilic reactivity relates to the ability of the nucleophile to engage the tellurium 5*p* orbital in bonding at the expence of the bond at 180°.

The Te–C bond lengths in I and II are equal within errors and they are not significantly different from the Te–C_{sp^2} single covalent bond length, 2.107 Å.[14,18]

Foss[2,3] has stated that the coordination around the tellurium atom in phenyltellurium complexes may be regarded as based on a square-planar arrangement. Approach of the fourth ligand is not observed in the present structures. This is similar to the findings in structures of tetramethylammonium phenyldithiocyanatotellurate(II) and the corresponding selenocyanato compound.[1] The lack of ligand in *trans* position to the Te–C bond can be looked at as indication of the great *trans*-lengthening effect of the phenyl group.

The tellurium atom and the carbon atoms of the phenyltellurium group are nearly co-planar in

Table 5. Bond lengths (Å) and angles (°) in tetraphenylarsonium bromoiodophenyltellurate(II). Standard deviations in parentheses.

Te–I	2.9033(18)	I–Te–Br	177.93(6)
Te–Br	2.8676(22)	I–Te–C(1)	88.5(4)
Te–C(1)	2.119(14)	Br–Te–C(1)	89.7(4)
C(1)–C(2)	1.446(18)	Te–C(1)–C(2)	117.1(9)
C(2)–C(3)	1.351(26)	Te–C(1)–C(6)	117.5(10)
C(3)–C(4)	1.405(20)	C(1)–C(2)–C(3)	119.1(13)
C(4)–C(5)	1.425(27)	C(2)–C(3)–C(4)	118.3(15)
C(5)–C(6)	1.399(26)	C(3)–C(4)–C(5)	125.2(18)
C(6)–C(1)	1.368(19)	C(4)–C(5)–C(6)	115.6(18)
		C(5)–C(6)–C(1)	116.2(19)
		C(6)–C(1)–C(2)	125.2(19)
As–C(11)	1.927(16)	C(11)–As–C(21)	107.4(8)
As–C(21)	1.910(18)	C(11)–As–C(31)	110.9(7)
As–C(31)	1.919(16)	C(11)–As–C(41)	108.7(7)
As–C(41)	1.942(17)	C(21)–As–C(31)	110.8(8)
		C(21)–As–C(41)	108.3(7)
		C(31)–As–C(41)	110.6(8)

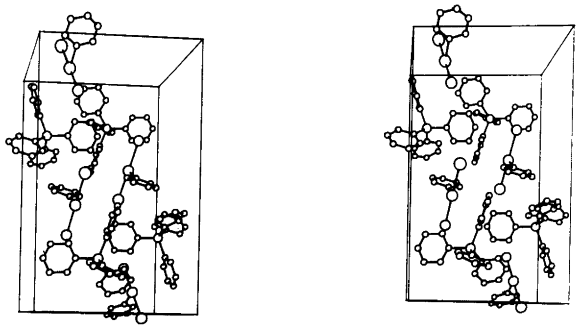

Fig. 2. A stereoscopic view of the content of the unit cell for tetraphenylarsonium bromoiodophenyltellurate(II), as seen along the *a* crystal axis.

each structure, the largest deviation from a least-squares plane being 0.058 Å in I and 0.062 Å in II. The angle between this plane and the least-squares plane through the coordination group is 89.59° in I, and 89.47° in II.

In the tetraphenylarsonium ion the As atom is approximately tetrahedrally surrounded by the four phenyl groups, which are planar within the experimental error. The C–As–C bond angles vary from 106.4(5)° to 111.4(5)° in I, and from 107.4(8)° to 110.9(7)° in II. The average As–C bond length is 1.912 Å in I, and 1.925 Å in II. The C–C bond lengths and the C–C–C bond anles in the four phenyl groups are in the expected range in both structures.[19,20]

REFERENCES

1. Hauge, S. and Vikane, O. *Acta Chem. Scand. A 29* (1975) 755.
2. Foss, O. In Andersen, P., Bastiansen, O. and Furberg, S., Eds., *Selected Topics in Structure Chemistry,* Universitetsforlaget, Oslo 1967, p. 145.
3. Foss, O. *Pure Appl. Chem. 24* (1970) 31.
4. Foss, O. and Marøy, K. *Acta Chem. Scand. 20* (1966) 123.
5. Foss, O. and Husebye, S. *Acta Chem. Scand. 20* (1966) 132.
6. Vikane, O. *Acta Chem. Scand. A 29* (1975) 738.
7. Vikane, O. *Acta Chem. Scand. A 29* (1975) 763.

8. Vikane, O. *Acta Chem. Scand. A 29* (1975) 787.
9. Hauge, S., Johanessen, Ø. and Vikane, O. *Acta Chem. Scand. A 32* (1978) 901.
10. Foss, O. and Hauge, S. *Acta Chem. Scand. 19* (1965) 2395.
11. Klæboe, P., Nielsen, C. J., Suchi, R. and Vikane, O. *Acta Chem. Scand. A 32* (1978) 565.
12. Cromer, D. T. and Mann, J. B. *Acta Crystallogr. A 24* (1968) 321.
13. Stewart, J. M., Ed., *The X-Ray System, Version of 1976,* Technical Report TR-446 of the Computer Science Center, University of Maryland, March 1976.
14. Pauling, L. *The Nature of the Chemical Bond,* 3rd. Ed., Cornell University Press, Ithaca 1960.
15. Foss, O. and Hauge, S. *Acta Chem. Scand. 13* (1959) 2155.
16. Foss, O. and Fossen, S. *Acta Chem. Scand. 15* (1961) 1618.
17. Foss, O. *Acta Chem. Scand. 16* (1962) 779.
18. Bastiansen, O. and Tretteberg, M. *Tetrahedron 17* (1962) 147.
19. Runsink, J., Swen-Walstra, S. and Migchelsen, T. *Acta Crystallogr. B 28* (1972) 1331.
20. Faithful, B. D. and Wallwork, S. C. *Acta Crystallogr. B 28* (1972) 2301.

Received February 7, 1983.

Acta Chemica Scandinavica A 37 (1983) 729–737

Compounds with Intermediate Spin. 7. * Influence of the Substituents on the Magnetic Properties of Tris(dithiocarbamato)iron(III) Compounds

K. STÅHL and I. YMÉN

Inorganic Chemistry, Chemical Center, University of Lund, P.O.Box 740, S-220 07 Lund, Sweden

The influence of inductive and cooperative effects, steric interference and electronic factors on the high spin–low spin equilibrium of solid substituted iron(III)dithiocarbamates [$Fe(S_2CNRR')_3$] has been studied. The discussion is based on pK_a values of the parent secondary amine (RR'NH), magnetic susceptibility measurements, accurate structural parameters and ESCA measurements. The inductive and cooperative effects were found to be of minor importance. The most important factor in determining the spin state is the intramolecular steric interference of the substituents (R and R') acting on the ligand bite angle S–C–S. Increased steric interference increases the low spin contents. No significant shift between different canonical forms could be observed except when the RR'N moiety exhibits aromaticity, making the corresponding $Fe(S_2CNRR')_3$ low spin.

* For part 6 in this series see Ref. 5.

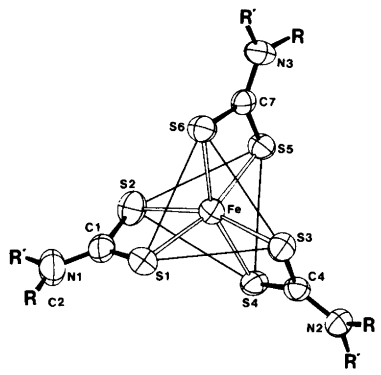

Fig. 1. An $Fe(dtc)_3$ complex viewed along the pseudo threefold axis.

0302-4377/83 $2.50

Substituted iron(III)dithiocarbamates $Fe(dtc)_3$ in the solid state has been subject to numerous structural[1–15] and magnetic[16–19] investigations. All known $Fe(dtc)_3$ structures comprise mononuclear van der Waals packed complexes with pseudosymmetry D_3 (Fig. 1). The magnetic properties can be described as a thermal equilibrium between the low spin (LS) and the high spin (HS) forms, giving effective magnetic moments (μ_{eff}) between ~2 B.M. (low temperature limit, $S=\frac{1}{2}$) and 5.92 B.M. (high temperature

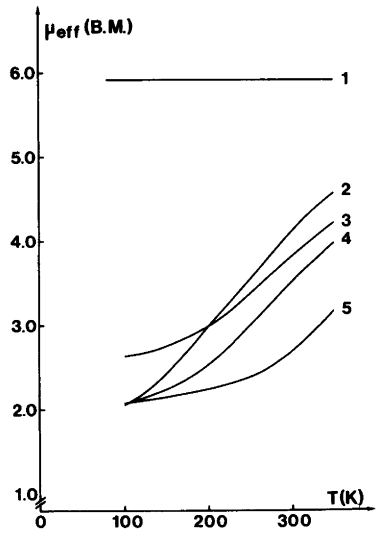

Fig. 2. Effective magnetic moment *vs.* temperature for $Fe(dtc)_3$ compounds with various substituents; 1. Tetramethylene; 2. Dimethyl; 3. Dipropionitrile; 4. Dibenzyl; 5. Diisopropyl.

limit, $S=\frac{5}{2}$) (Fig. 2). At intermediate μ_{eff} the crystal structure observed is the weighted average of the LS and HS forms $(\mu_{eff}^2=x_{HS}(\mu_{eff}^{HS})^2+(1-x_{HS})(\mu_{eff}^{LS})^2$, where x_{HS} is the HS molar ratio).

The magnetic properties in the interval 80–300 K are strongly dependent on the substituents R and R′ and in some cases on solvate molecules in the crystal structure. By varying R and R′ it is possible to obtain compounds exhibiting pure HS behaviour, a more or less complete HS–LS transition or almost pure LS behaviour. There are four main effects through which the substituents may influence the magnetic behaviour.

1. Inductive effects.
2. Cooperative effects.
3. Steric interference on the FeS_6 core.
4. Electronic interactions.

This investigation intends to evaluate the influence of these four factors on the magnetic properties of the various $Fe(dtc)_3$ compounds. The discussion is based on solid state magnetic moments in the interval 80–300 K, accurately determined crystal structures of Fe(III) and some non-Fe dtc compounds, pK_a values of the parent secondary amine RR′NH as a measure of the inductive effects and some ESCA results. The importance of different canonical forms (Fig. 3) will also be discussed. The influence of solvate molecules in the crystal structure on μ_{eff} is discussed elsewhere.[8] This work is part of a series of investigations aiming at correlating the magnetic behaviour of solid iron(III)dithiocarbamates with their structural features.

EXPERIMENTAL

Preparations. Alkali dtcs were prepared by mixing stoichiometric amounts of CS_2, RR′NH and MOH in aqueous solutions according to eqn. (1).

$$M^+ + CS_2 + RR'NH + OH^- + (x-1)H_2O \rightarrow MS_2CNRR' \cdot xH_2O \qquad (1)$$

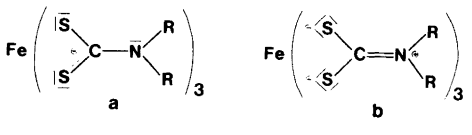

Fig. 3. Proposed canonical forms for $Fe(dtc)_3$.

The compounds were recrystallized from aqueous solutions under reduced pressure.

$Fe(dtc)_3$ were prepared by mixing stoichiometric amounts of CS_2, RR′NH, $FeCl_3$ and NaOH in ethanol solutions and recrystallized from chloroform by slow addition of ethanol.

ESCA measurements. The ESCA measurements were made on the sodium tetramethylene dimethyl, diethyl and diisopropyl dithiocarbamate hydrates using an AEI ES 200 Photoelectron spectrometer. The technique of internal standard established by Larsson, Folkesson and Lykvist[20–22] was used, assuming the Na^+ charge to be exactly +1.0 in all compounds, E_b(Na 1 s)=1071.1 eV is related to $(C_6H_5)_4P^+$ *via* F^- in $(C_6H_5)_4PF$ and NaF. The dimethyldithiocarbamate spectra was recorded at 273 and 103 K, the others at 273 K.

Susceptibility measurements. The magnetic susceptibility (Figs. 2 and 6) was measured on polycrystalline samples with a microcomputer-controlled Cahn RG electrobalance using the Faraday principle.[5,23] To investigate the effects of crystal size and perfection the measurements were repeated after careful grinding of the sample with agate mortar and pestle. The magnetic moments did not show any dependence on the magnetic field strength used (~0.6 and ~0.8 T).

Statistical treatment. Correlations between structural parameters and the magnetic moment have been tested by linear regression (Figs. 7, 9a and b). In Figs. 7 and 9b mean values of the structural parameters have been used. Since it was not possible to give correct relative weights to all observations, due to the different origin of the structural parameters and magnetic moments, equal weights have been used.

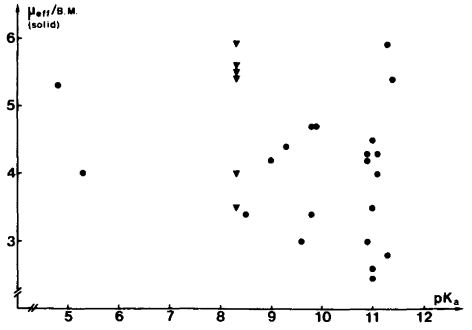

Fig. 4. Effective magnetic moment of some $Fe(dtc)_3$s[1–14,19] *vs.* pK_a of the parent secondary amine.[33,34] The pK_a value for aromatic amines is corrected according to Ref. 25. ▼ indicates tris(morpholinecarbodithiato)iron(III) with various solvate molecules.

INDUCTIVE EFFECTS

It has been proposed that the spin cross-over behaviour of the iron(III)dithiocarbamates is influenced by the inductive effect of the substituents.[24–26] The inductive effect is reflected in the pK_a value of the parent secondary amine, RR'NH. As seen from Fig. 4 there is no correlation between the pKa values and the solid state magnetic moments at room temperature. The lack of influence from the pK_a value on μ_{eff} is especially evident for the morpholinyl substituted $Fe(dtc)_3$ compounds where μ_{eff} varies between 3.0 and 5.92 B.M. depending on which solvent molecule is present in the crystal structure.

COOPERATIVE EFFECTS

Spin transitions in the solid state are often described as a cooperative phenomenon.[27–31] The number of minority spin complexes is increased by nucleation and growth of small minority spin domains. The nucleation and growth is governed by the temperature and the number of nucleation sites. An increased number of nucleation sites will increase the number of minority spin complexes in the beginning of the transition, but will also hinder the domain growth towards the end of the transition. An increased number of nucleation sites can be attained by careful grinding of the compound. The influence of grinding on the μ_{eff} *vs.* T curves seems to be dependent on the

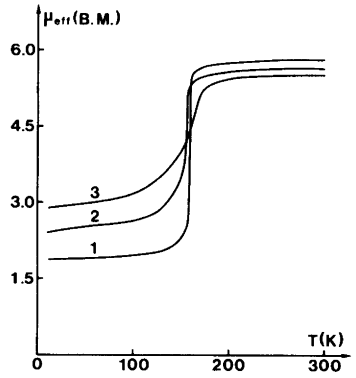

Fig. 5. Effective magnetic moment *vs.* temperature for $[Fe(3\text{–}OCH_3\text{–}SalEen)_2]PF_6$.[28]: 1. Unperturbed microcrystalline solid; 2. Sample ground with mortar and pestle; 3. Sample ground in a ball mill.

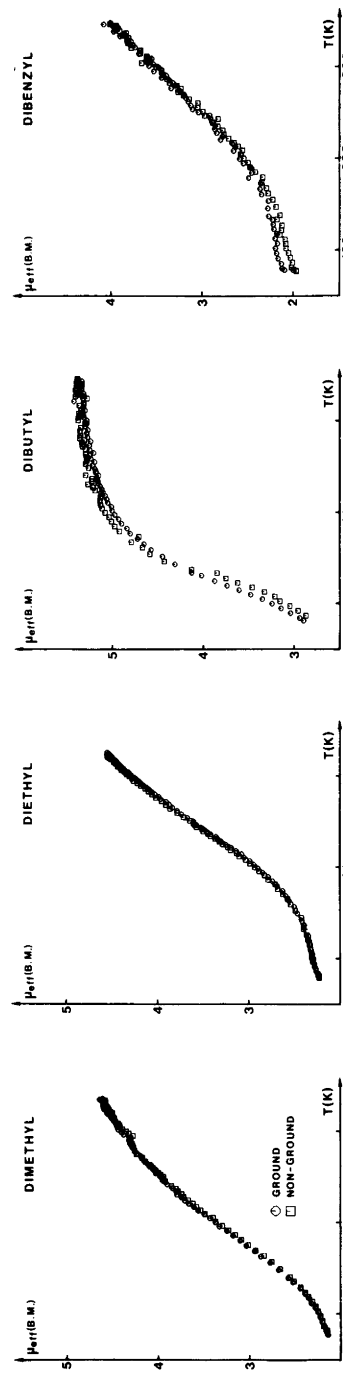

Fig. 6. Effective magnetic moment *vs.* temperature for some ground and non-ground $Fe(dtc)_3$ samples crystallizing without solvate molecules.

nature of the spin transition. The effect is typically dramatic when the unperturbed spin transition is dramatic (*i.e.* almost completed within a few K) (Fig. 5).

In the case of $Fe(dtc)_3$ the spin transitions are always gradual, and in an investigation of the grinding effect on the dimethyl, diethyl, dibutyl and dibenzyl substituted compounds the observed effects were small, (Fig. 6) *i.e.* the cooperative effects on the magnetic behaviour of $Fe(dtc)_3$ are of minor importance.

STERIC INTERFERENCE

For 25 accurately determined $Fe(dtc)_3$ structures[1–14] the linear correlation among 10 mean geometric parameters and μ_{eff} (MY in Fig. 7) has been tested by linear regression. A selection is

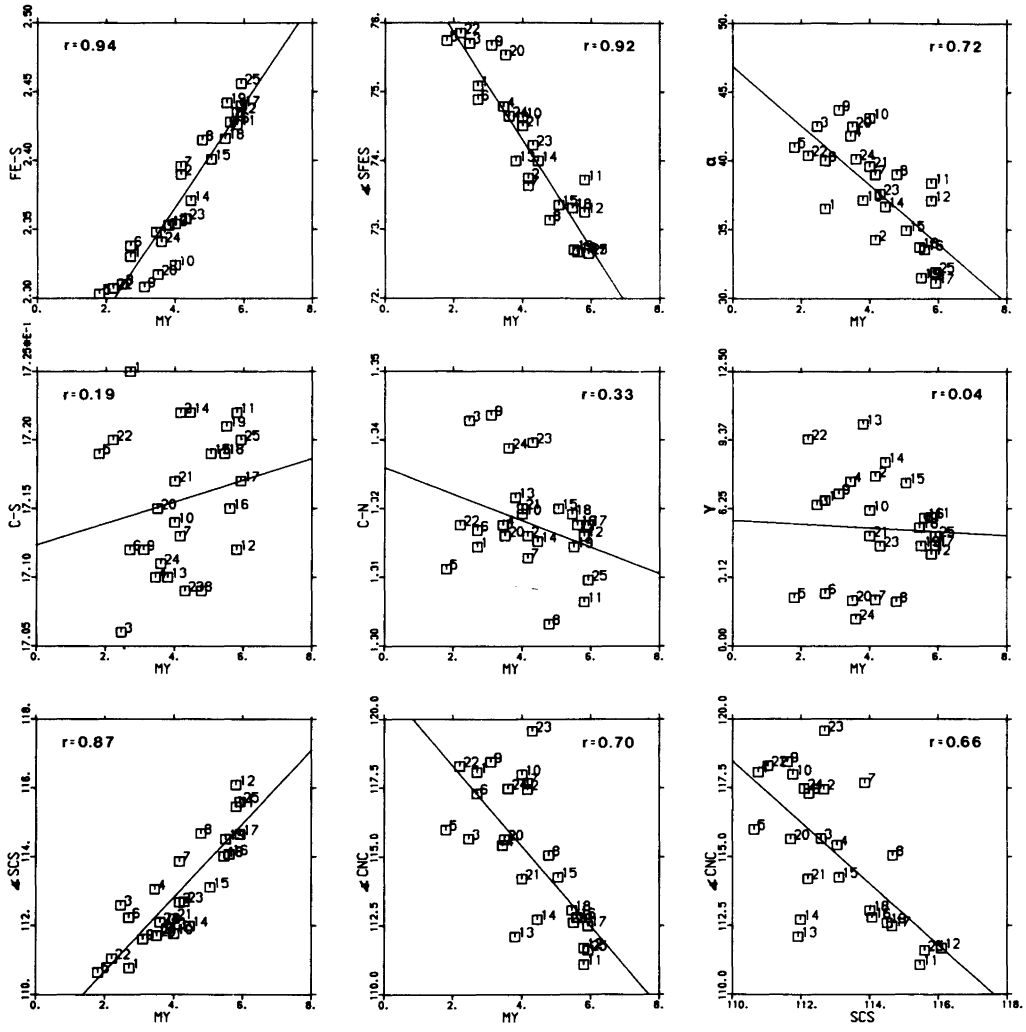

Fig. 7. Correlation between structural parameters and effective magnetic moment (MY) of some substituted $Fe(dtc)_3$s. Data about compounds *1–25* are given in Table 3. α is the trigonal twist angle in the FeS_6 polyhedron and γ is the angle between the normal vectors of the S–C–S and C–N–C planes in the ligands. The probability of 25 randomly distributed observations having a correlation coefficient, $r > 0.505$ is 0.005.

Table 1. S–C–S and C–N–C angles in some substituted dithiocarbamates. n is the number of M–S-bonds per ligand.

Substituents	Cation	S–C–S	C–N–C	$\bar{n}$	Ref.
Diisopropyl	Na^+	118.3(3)	113.8(5)	0	43
$(S_2CN(CH(CH_3)_2)_2$	$NH_2[CH(CH_3)_2]_2^+$	117.7(2)	113.8(2)	0	44
	Li^+	117.5(3)	114.5(5)	0	45
	Zn^{2+}	115.5(1)	114.6(1)	2–3	46
	Cu^{2+}	111.4(2)	115.9(4)	2	47
	Ni^{2+}	109.3(5)	117.3(8)	2	48
Diethyl	Na^+	120.4(4)	114.3(5)	1	49
$S_2CN(C_2H_5)_2$	$NH_2(C_2H_5)_2^+$	120.6(1)	115.2(2)	0	50
	Li^+	119.1(2)	114.4(3)	0	51
	Zn^{2+}	117.7(6)	116.1(8)	2	52
	Cu^{2+}	113.6(5)	117.1(6)	2	53
	Ni^{2+}	110.6(6)	116.9(1.2)	2	54
Dimethyl	Na^+	120.9(1)	114.2(3)	1	55
$S_2CN(CH_3)_2$	$NH_2(CH_3)_2^+$	119.7(1)	114.7(3)	0	56
	Li^+	118.8(1)	115.4(3)	0	57
	Zn^{2+}	118.8(8)	116.9(1.3)	2	58
	Cu^{2+}	113.4(5)	115.3(9)	2	59
	Ni^{2+}	109.9(4)	118.4(5)	2	60
Tetramethylene	Na^+	122.3(1)	110.8(2)	1	61, 62
$S_2CN(CH_2)_4$	$NH_2(CH_2)_4^+$	121.7(1)	110.6(2)	0	63
	Li^+	120.2(1)	110.8(1)	0	64
	Zn^{2+}	119.5(3)	111.7(5)	2–3	65
	Cu^{2+}	115.8(4)	113.5(8)	2	66
	Ni^{2+}	111.4(5)	112.0(7)	2	66

Table 2. Effective charges on the atoms in the four Na^+-dithiocarbamates. Two separate measurements were made for each compound.

	q_S	q_N	q_C
$NaS_2CN(CH_2)_4 \cdot 2H_2O$	−0.46(3)	−0.24(2)	0.05(1)
	−0.46(3)	−0.24(2)	0.05(1)
$NaS_2CN(CH_3)_2 \cdot 2H_2O$	−0.43(3)	−0.21(2)	0.07(1)
	−0.43(3)	−0.21(2)	0.07(1)
$NaS_2CN(C_2H_5)_2 \cdot 3H_2O$	−0.43(3)	−0.21(2)	0.06(1)
	−0.43(3)	−0.21(2)	0.07(1)
$NaS_2CN(CH(CH_3)_2)_2 \cdot 5H_2O$	−0.31(3)	−0.27(2)	0.03(1)
	−0.34(3)	−0.28(2)	0.03(1)

shown in Fig. 7 and Table 3. Since the spin state is dependent on the ligand field strength, a strong correlation is observed between parameters of the FeS_6 core and μ_{eff}.[32] Within the ligands the only parameters significantly correlated to μ_{eff} are the S–C–S and C–N–C angles. Consequently also S–C–S and C–N–C are correlated to each other (Fig. 7). This correlation can be deduced from steric interference within the ligands (Fig. 8). Steric crowding between the substituents is propagated to the S-atoms through a variable number of C–H···S interactions. This steric interference is balanced by an increased repulsion between the S-atoms. A convincing way to

Table 3. The 25 iron(III) dithiocarbamates of Fig. 7.

No.	Substituents	Solvate	Temp. (K)	Ref.
1	Dihydroxyethyl	–	175	1
2	Dihydroxyethyl	–	295	1
3	Dibenzyl	–	175	2
4	Dibenzyl	–	295	2
5	Dimethyl	–	25	3
6	Dimethyl	–	175	4
7	Dimethyl	–	295	4
8	Dimethyl	–	400	3
9	Dipropionitrile	$\frac{1}{2}CHCl_3$	178	5
10	Dipropionitrile	$\frac{1}{2}CHCl_3$	298	5
11	Tetramethylene	$\frac{1}{2}C_6H_6$	175	6
12	Tetramethylene	$\frac{1}{2}C_6H_6$	295	6
13	Morpholinyl	CH_2Cl_2	20	7
14	Morpholinyl	CH_2Cl_2	110	7
15	Morpholinyl	CH_2Cl_2	178	7
16	Morpholinyl	CH_2Cl_2	293	7
17	Morpholinyl	CH_2Cl_2	293	8
18	Morpholinyl	$CHCl_3$	300	9
19	Morpholinyl	H_2O	300	9
20	Morpholinyl	$2C_6H_6$	300	10
21	Morpholinyl	$C_6H_5NO_2$	300	11
22	Diethyl	–	79	12
23	Diethyl	–	297	12
24	Dibutyl	C_6H_6	295	13
25	Tetramethylene	–	295	14

study the variation in steric interference for different substituents is to use space filling precision molecular models (*e.g.* CPK Precision Molecular Models, The Ealing Corporation, Mass).

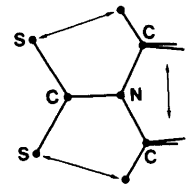

Fig. 8. Steric interference (indicated by arrows) in a dtc ion.

To provide further evidence on the steric interference, some dtc ligands with cations other than Fe(III) were studied (Table 1). For one and the same ligand chelate formation with cations decreases the S–C–S angle and consequently the C–N–C angle increases. As expected, C–N–C in a strained pyrrolidine ring is rather invariant in tetramethylenedithiocarbamate, and the S–C–S to C–N–C correlation increases as the substituents become bulkier, tetramethylene< dimethyl~diethyl<diisopropyl (Table 1). For these four ligand types the shortest intramolecular S···H distances increase in the reverse order from about 2.4 Å for diisopropyl to about 2.9 Å for tetramethylene.

The geometry of the dtc ion in compounds with weakly attached cations (Li, Na, NH_2R_2, Table 1) may be approximated to that in non-bonded dtcs, where S–C–S is solely determined by the steric interference from the substituents. The fact that μ_{eff} of the corresponding $Fe(dtc)_3$ is strongly correlated to S–C–S in the three "non-bonded" ligands (Fig. 9a) gives further evidence of the importance of the steric interaction in determining μ_{eff} in the iron(III)dithiocarbamates. Fig. 9b

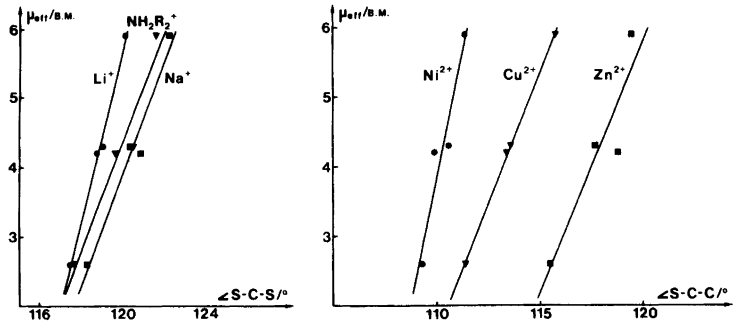

Fig. 9. Effective magnetic moment of some substituted $Fe(dtc)_3$s *vs.* S–C–S angle in the corresponding $M(dtc)_n$. The substituents are from top to bottom tetramethylene, diethyl, dimethyl, diisopropyl. (a) "Non-bonded" ligands, (b) "Bonded" ligands.

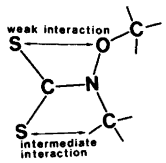

Fig. 10. The weak steric interference in the methylmethoxy substituted dtc giving a high spin $Fe(dtc)_3$.

shows the same general feature as Fig. 9a but does also illustrate the strong cation influence on S–C–S, S–C–S decreases as the cation–ligand bond strength increases.

To conclude, weak steric interference (*e.g.* in tetramethylene dtc) results in ligand bites producing a weak ligand field[32] and Fe(III) remains high spin. When the steric interference is strong (*e.g.* in diisopropyl or other di-sec-alkyl dtcs) the resulting smaller ligand bite produces a strong ligand field and Fe(III) becomes low spin. Finally, when the steric interference is intermediate (*e.g.* in dimethyl-, diethyl- or other di-prim-alkyl dtcs) the ligand bite and ligand field is intermediate and the corresponding iron(III) complex will exhibit spin cross-over behaviour.

This model also explains the high spin behaviour when the substituents are methyl and methoxy groups[25] (Fig. 10).

ELECTRONIC INTERACTIONS

The theory of intramolecular steric interference is not applicable to tris(pyrrolecarbodithiato)iron(III) (Fig. 11*d*). In this compound the S–C–S angles are a bit larger than those expected for a low-spin $Fe(dtc)_3$ compound, the C–N–C angles are confined to ~108° and the S···H distances indicate weak intramolecular S···H interactions.[15] The ligand, however, is somewhat special in having an aromatic pyrrole ring directly bonded to the S_2C-moiety. The aromaticity of the pyrrole ring prevents the lone pair on the N-atom taking part in the S_2C-π-system. As a result the electronic structure is that of Fig. 11*d*, corresponding to canonical form *a* in Fig. 3. From a comparison between different Fe(III)dithio compounds (Fig. 11) it is seen that

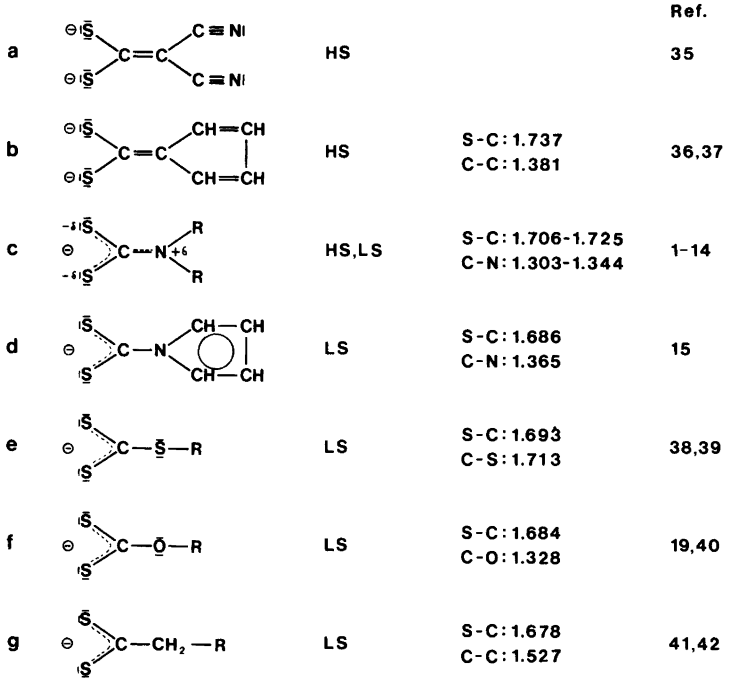

Fig. 11. Dominant canonical forms of various dithio ligands and the spin state of the corresponding $Fe(ligand)_3$. The distances in *b* and *g* are from non-iron compounds.

canonical form *a* in Fig. 3 with low sulfur charges favours the LS state and canoncial form *b* with higher sulfur charges favours the HS state of iron(III). The geometric parameter in common to compounds c–g in Fig. 11, which gives a good correlation to μ_{eff} is the S···S distance. The somewhat larger S–C–S angle in compounds d–g is compensated for by the shorter, partly double bonded S–C bond.

The charge distribution of some sodium-dithiocarbamate hydrates have been studied with ESCA and the results are given in Table 2. The difference in the charge on the S-atoms between the diisopropyl compound, −0.31, and the others −0.43−0.46, is highly significant. The ESCA peaks for the S-atoms were symmetric with half-widths of 2.6 eV for all compounds, indicating equal charges on the two S-atoms in each compound. No significant differences between the 273 and 103 K spectra were observed for the dimethyl compound. The significance in the charge difference was tested by a measurement on a mixed diisopropyl and tetramethylene sample. As expected, the half-widths of the S- and N-atoms increased by approximately 0.15 eV, indicating overlapping peaks. Since the diisopropyldithiocarbamate forms an LS Fe(III) compound and the tetramethylenedithiocarbamate forms HS Fe(III) compounds the ESCA results support the above observation that high sulfur charge favours the HS and low sulfur charge favours the LS state of iron(III) in dithio compounds. The variation in charge on the S atoms might be explained by simple electrostatic arguments. A decrease in S–C–S angle increases the electrostatic repulsion between the two S atoms and thus favours canonical form *a* in Fig. 3.

The S–C and C–N distances are not significantly correlated to μ_{eff} (Fig. 6). The observed scatter in S–C and C–N distances is with a probability of >0.9995 and 0.96, respectively, expected from a random distribution (from χ^2 tests). According to Pauling's equation[39] the difference in S–C distance between the pure canonical forms (*i.e.* with S–C bond order of 1.5 and 1.0) is 0.14 Å, while the largest difference observed is 0.02 Å. It is thus concluded that for $Fe(dtc)_3s$ the variation in the contribution from the two canonical forms is well below 15 %.

An earlier attempt has been made to explain the influence of the substituents on μ_{eff} in solution in terms of intramolecular steric interference.[19] In this earlier explanation the bulkier substituents were expected to increase the C–N–C angle, favouring an sp^2 hybridized nitrogen and thereby canonical form *b* in Fig. 3. Canonical form *b* was therefore postulated to dominate in an LS complex, in contradiction to the results presented above.

Acknowledgements. We are indebted to Drs. Jörgen Albertsson, Åke Oskarsson and Christer Svensson for many stimulating discussions, Dr. Börje Folkesson for measuring the ESCA spectra, Ms. Lena Timby for preparations and drawing of the illustrations and Dr. Inga Elding for the literature data file searches. Financial support from the Royal Physiographic Society in Lund and the Swedish Natural Science Research Council is gratefully acknowledged.

REFERENCES

1. Albertsson, J., Oskarsson, Å. and Nygren, M. *Acta Crystallogr. B 35* (1979) 1473.
2. Albertsson, J., Elding, I. and Oskarsson, Å. *Acta Chem. Scand. A 33* (1979) 703.
3. Albertsson, J., Oskarsson, Å., Ståhl, K., Svensson, C. and Ymén, I. *Acta Crystallogr. B 37* (1981) 50.
4. Albertsson, J. and Oskarsson, Å. *Acta Crystallogr. B 33* (1977) 1871.
5. Albertsson, J., Oskarsson, Å. and Ståhl, K. *Acta Chem. Scand. A 36* (1982) 783.
6. Albertsson, J. and Oskarsson, Å. *Unpublished results.*
7. Ståhl, K. *Acta Crystallogr. B 39* (1983) 612.
8. Ståhl, K. *Inorg. Chim. Acta 75* (1983) 85.
9. Butcher, R. and Sinn, E. *J. Am. Chem. Soc. 98* (1976) 5159.
10. Butcher, R. and Sinn, E. *J. Am. Chem. Soc. 98* (1976) 2440.
11. Cukauskas, E. J., Deaver, B. S. and Sinn, E. *J. Chem. Phys. 67* (1977) 1257.
12. Leipoldt, J. G. and Coppens, P. *Inorg. Chem. 12* (1973) 2269.
13. Mitra, S., Raston, C. and White, A. H. *Aust. J. Chem. 29* (1976) 1899.
14. Mitra, S., Raston, C. and White, A. H. *Aust. J. Chem. 31* (1978) 547.
15. Bereman, R. D., Churchill, M. R. and Nalewajek, D. *Inorg. Chem. 18* (1979) 3112.
16. Cambi, L. and Cagnasso, A. *Atti Accad. Naz. Lincei. 13* (1931) 809; Cambi, L. and Szego, L. *Ber. Dtsch. Chem. Ges. 64* (1931) 2591.
17. White, A. H., Roper, R., Kokot, E., Waterman, H. and Martin, R. L. *Aust. J. Chem. 17* (1964) 294.

18. Ewald, A. H., Martin, R. L., Ross, I. G. and White, A. H. *Proc. R. Soc. London Ser. A 280* (1964) 235.
19. Ewald, A. H., Martin, R. L., Sinn, E. and White, A. H. *Inorg. Chem. 8* (1969) 1837.
20. Folkesson, B. and Larsson, R. *Chem. Scr. 10* (1976) 105.
21. Larsson, R. and Folkesson, B. *Phys. Scr. 16* (1977) 357.
22. Larsson, R. and Folkesson, B. *Chem. Scr. 9* (1976) 148.
23. Blom, B. and Hörlin, T. *Chem. Commun. Univ. Stockholm* (1977) No. 5.
24. Eley, R. R., Myers, R. R. and Duffy, N. V. *Inorg. Chem. 11* (1972) 1128.
25. Zimmerman, J. B., Starinshak, T. W., Uhrich, D. L. and Duffy, N. V. *Inorg. Chem. 16* (1977) 3107.
26. Duffy, N. V. and Uhrich, D. L. *Inorg. Chim. Acta 63* (1982) 5.
27. Haddad, M. S., Lynch, M. W., Federer, W. D. and Hendrickson, D. N. *Inorg. Chem. 20* (1981) 123.
28. Haddad, M. S., Federer, W. D., Lynch, M. W. and Hendrickson, D. N. *Inorg. Chem. 20* (1981) 131.
29. Sorai, M. and Seki, S. *J. Phys. Chem. Solids 35* (1974) 555.
30. Zimmermann, R. and König, E. *J. Phys. Chem. Solids 38* (1977) 779.
31. Gütlich, P., Köppen, H., Link, R. and Steinhäuser, H. G. *J. Chem. Phys. 70* (1979) 3977.
32. Kepert, D. L. *Prog. Inorg. Chem. 23* (1977) 1.
33. Perrin, D. D. *Dissociation Constants of Organic Bases in Aqueous Solutions,* Butterworth, London 1965.
34. Perrin, D. D. *Dissociation Constants of Organic Bases in Aqueous Solutions, Supplement,* Butterworth, London 1972.
35. Fackler, J. P., Jr. and Coucouvanis, D. *J. Am. Chem. Soc. 88* (1966) 3913.
36. Bereman, R. D., Good, M. L., Kalbacher, B. J. and Buttone, J. *Inorg. Chem. 15* (1976) 618.
37. Bereman, R. D. and Nalewajek, D. *Inorg. Chem. 15* (1976) 2981.
38. Ewald, A. H. and Sinn, E. *Aust. J. Chem. 21* (1968) 927.
39. Lewis, D. F., Lippard, S. J. and Zubieta, J. A. *Inorg. Chem. 11* (1972) 823.
40. Hoskins, B. F. and Kelly, B. P. *Chem. Commun.* (1970) 45.
41. Bellitto, C., Flamini, A. and Piovesana, O. *J. Inorg. Nucl. Chem. 41* (1979) 1677.
42. Bellitto, C., Flamini, A., Piovesana, D. and Zanazzi, P. F. *Inorg. Chem. 19* (1980) 3632.
43. Ymén, I. (1983). *Acta Crystallogr. C. 39* (1983) 874.
44. Wahlberg, A. *Acta Crystallogr. B 34* (1978) 3479.
45. Oskarsson, Å. and Ymén, I. *Acta Crystallogr. C. 40* (1984). *In press.*
46. Miyamae, H., Ito, M. and Iwasaki, H. *Acta Crystallogr. B 35* (1979) 1480.
47. Iwasaki, H. and Kobayashi, K. *Acta Crystallogr. B 36* (1980) 1655.
48. Newman, P. W. G. and White, A. H. *J. Chem. Soc. Dalton Trans.* (1972) 2239.
49. Colapietro, M., Domenicano, A. and Vaciago, A. *Chem. Commun.* (1968) 572.
50. Wahlberg, A. *Acta Crystallogr. B 34* (1978) 3822.
51. Ymén, I. *To be published.*
52. Bonamico, M., Mazzone, G., Vaciago, A. and Zambonelli, L. *Acta Crystallogr. 19* (1965) 898.
53. Bonamico, M., Dessy, G., Mugnoli, A., Vaciago, A. and Zambonelli, L. *Acta Crystallogr. 19* (1965) 886.
54. Bonamico, M., Dessy, G., Mariani, C., Vaciago, A. and Zambonelli, L. *Acta Crystallogr. 19* (1965) 619.
55. Oskarsson, Å. and Ymén, I. *Acta Crystallogr. C 39* (1983) 66.
56. Wahlberg, A. *Acta Crystallogr. B 34* (1978) 3392.
57. Ymén, I. *Acta Crystallogr. C. 40* (1984). *In press.*
58. Klug, H. P. *Acta Crystallogr. 21* (1966) 536.
59. Einstein, F. W. B. and Field, J. S. *Acta Crystallogr. B 30* (1974) 2928.
60. Lokaj, J., Garaj, J., Kettmann, V. and Vrábel, V. *Collect. Czech. Chem. Commun. 45* (1980) 2147.
61. Albertsson, J., Oskarsson, Å., Ståhl, K., Svensson, C. and Ymén, I. *Acta Crystallogr. B 36* (1980) 3072.
62. Ymén, I. *Acta Crystallogr. B 38* (1982) 2671.
63. Wahlberg, A. *Acta Crystallogr. B 35* (1979) 485.
64. Ymén, I. *Acta Crystallogr. C 40* (1984). *In press.*
65. Francetič, V. and Leban, I. *Vestn. Slov. Kem. Drus. 26* (1979) 113.
66. Newman, P. W. G., Raston, C. L. and White, A. H. *J. Chem. Soc. Dalton Trans.* (1973) 1332.

Received March 3, 1983.

Acta Chemica Scandinavica A 37 (1983) 739–742

Single-Ion Activities of Sodium Sulfate in Aqueous Solution

TOR HURLEN

Department of Chemistry, University of Oslo, Blindern, Oslo 3, Norway

The single-ion activity coefficients of sodium and sulfate ions in aqueous 0.1–2.0 molal solutions of sodium sulfate at 25 °C have been determined by a liquid-junction approach. The results are compared to previous ones from a double-layer approach. The two approaches mutually agree at low sodium sulfate concentration (<0.2 *m*). The liquid-junction approach gives the most likely results at higher concentration. It gives a linear $\log (f_+^4/f_-)$ *vs.* *m* dependence with positive slope. This is interpreted by a hydration-energy involving treatment of ionic activities.

It has long been known that single-ion activities are indeterminable,[1–3] unless extra thermodynamic means be introduced.[4–9] An interesting approach to such determinations uses double-layer data as extra means.[7,10,11] It directly yields single-ion activity coefficients (γ_i).[10] Another approach draws on estimations of liquid-junction potential differences.[8,12] It primarily yields convenient single-ion activity coefficients (γ_i') defined by eqn. (1)

$$\gamma_i' = \gamma_i r^{-z_i/2} \quad (1)$$

where z_i is the charge number (with sign) of the ion concerned, and r means γ_+/γ_- for potassium chloride in pure, saturated solution of this salt at the temperature concerned.[12] At 25 °C, the value of r appears to be [12,13] close to unity or [14] slightly lower.

The present work aims at testing the above two approaches against each other for sodium sulfate in aqueous solution. Such solutions have already been studied by the double-layer approach.[11] Corresponding studies by the liquid-junction approach are presented below. The present studies especially add to previous ones on aqueous solutions of magnesium and zinc sulfates.[15]

EXPERIMENTAL

The experimental work comprises measurements of the liquid-junction containing equilibrium potential (E') of the Hg/Hg_2SO_4 electrode in aqueous 0.1–2.0 molal Na_2SO_4 solutions against the saturated calomel electrode (sce) under isothermal conditions at 25 °C. The solutions were made from *p.a.* quality salt (Merck) and twice distilled water, and the measurements were performed with equipment and procedures essentially as previously described.[12,15]

TREATMENT

From potential data at 25 °C, the convenient molal activity coefficient (γ_-') of the sulfate ion is obtained by eqn. (2)

$$\gamma_-' = (m^\circ/m) \exp[-(2F/RT)(E' - \Delta\phi - E^\circ + 0.241\ \mathrm{V})] \quad (2)$$

where m/m° is the dimensionless sulfate-ion molality concerned, E° is the molal standard hydrogen-scale potential of the Hg/Hg_2SO_4 electrode, and $\Delta\phi = \phi_t - \phi_r$ is the liquid-junction potential difference between the test solution concerned (ϕ_t) and the saturated KCl solution of the calomel reference electrode (ϕ_r).[12–15] In the present work, 0.612 V is used for E°[15,16] and $\Delta\phi$ is estimated[8] from the Henderson equation[17] with limiting mobility data[18] for the ions.

The convenient molal activity coefficient (γ_+') of the sodium ion is subsequently obtained from γ_-' by eqn. (3)

0302-4377/83 $2.50

Table 1. Potential and activity data for aqueous x m Na_2SO_4 solutions at 25 °C (see text).

Measured		Liquid-junction based			Ref. 18	Double-layer based[11]		
x	E'/mV	$\Delta\phi$/mV	γ'_-	γ'_+	$\gamma_\pm$	γ_+	γ_-	$\Delta\phi$/mV
0.1	419.7	−1.9	0.19	0.67	0.445	0.665	0.199	−1.6
0.2	415.9	−1.8	0.13	0.61	0.365	0.599	0.136	−1.3
0.5	413.3	−1.8	0.065	0.53	0.266	0.500	0.075	0.1
0.7	412.5	−1.9	0.049	0.50	0.233	0.458	0.060	0.8
1.0	412.1	−2.0	0.035	0.48	0.201	0.410	0.048	2.1
1.5	411.8	−2.1	0.024	0.45	0.170			
2.0	411.5	−2.3	0.018	0.44	0.152			

$$\gamma'_+=(\gamma_\pm^3/\gamma'_-)^{1/2} \quad (3)$$

using accepted data[18] for the mean molal ionic activity coefficient ($\gamma_\pm$) of sodium sulfate in aqueous solution.[12,13] These activity coefficients are all bare-ion ones.[19]

RESULTS

The results of the present work are summarized in Table 1. This table also compares the present liquid-junction based data with previous[11] double-layer based ones. The last column of Table 1 gives the values resulting for $\Delta\phi$ from eqn. (2) on accepting the latter activity data, the present potential data (E', $E°$) and $r=1$ [eqn. (1)].

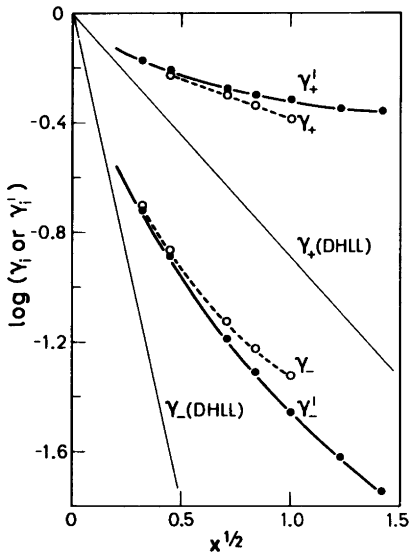

Fig. 1. Log γ_i (double-layer based)[11] and log γ'_i (liquid-junction based) *vs.* $x^{1/2}$ for aqueous x m Na_2SO_4 solutions at 25 °C. Comparison to the Debye-Hückel limiting law (DHLL) for sodium and sulfate ions.

The results of the liquid-junction approach and of the double-layer approach to single-ion activities mutually agree well at the lowest concentrations covered. With increasing salt concentration, however, the two approaches give increasingly differing results. This is illustrated in Figs. 1 and 2.

In Fig. 1, the results of the two approaches are compared both mutually and to the Debye-Hückel limiting law[19] for the ions involved. The logarithm of the activity coefficients is there plotted against the square root of the dimensionless salt molality (x=m/m°). This reveals that the liquid-junction approach shows somewhat larger deviation from the Debye-Hückel limiting law for the sodium ion (and somewhat smaller for the sulfate ion) than does the double-layer approach (assuming r=1).

In Fig. 2, use is made of rational (mol fraction) activity coefficients obtained by eqn. (4)

$$f_i(\text{resp. } f'_i)=[1+(3x/55.51)]\gamma_i\,(\text{resp. } \gamma'_i) \quad (4)$$

where x/55.51 is the mol ratio of Na_2SO_4 to H_2O in solution.[19] The functions $\log(f_+^4/f_-)$ and $\log((f'_+)^4/f'_-)$ from the double-layer and the liquid-junction approach, respectively, are there plotted *vs.* the dimensionless salt molality (x). The former function follows a curve with varying negative slope, whereas the latter function essentially follows a line with positive slope. These

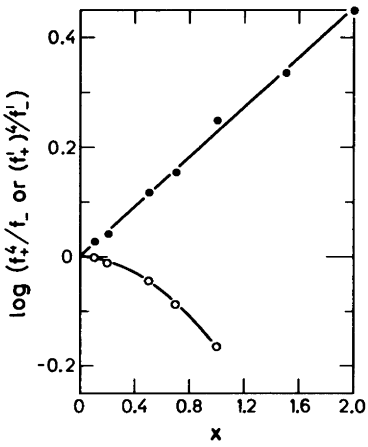

Fig. 2. (○) log (f_+^4/f_-), double-layer based,[11] and (●) log $((f'_+)^4/f'_-)$, liquid-junction based, *vs.* x for aqueous x m Na_2SO_4 solutions at 25 °C.

results are mutually incompatible. With decreasing salt concentration (x→0), both functions approach zero. This agrees with Debye-Hückel values being $f_+^4/f_-=1$ and $(f'_+)^4/f'_-=r^{-3}$, and it supports previous findings[12,13] that r be close to unity.

DISCUSSION

At low salt concentration ($x<0.2$), the present liquid-junction approach and the previous[11] double-layer approach to single-ion activities for sodium sulfate in aqueous solution give essentially coinciding results. This matching is good enough to strongly support[12,13] that r of eqn. (1) be close to unity. With increasing salt concentration, however, the two approaches give increasingly diverging results. It then is a question which one of the two sets of data (Table 1) comes nearest to the truth.

Basically, the double-layer approach[10,11] appears to the author as the better one of the two. However, the data obtained with this approach for sodium sulfate solutions of higher concentration[11] are hard to swallow. This especially applies to the values emerging from these data for $\Delta\phi$ (last column of Table 1) and for f_+^4/f_- (Fig. 2). It seems unreasonable that $\Delta\phi$ should become more and more positive and d log $(f_+^4/f_-)/dx$ more and more negative with increasing sodium sulfate concentration. The results from the liquid-junction approach are in these respects more likely. For $\Delta\phi$, this goes to the heart of the latter approach itself (to the estimate of the sign for $d(\Delta\phi)/dx$). For f_+^4/f_-, some elaboration is needed.

The treatment of ionic activities is often based on an extended Debye-Hückel equation like eqn. (5)

$$\log f_i=-z_i^2A\sqrt{I}/(1+aB\sqrt{I})+b_im \qquad (5)$$

where I is the ionic strength of the solution, A and B are temperature dependent universal constants, a is a salt dependent constant and b_i is a salt and ion dependent constant.[19] For single–salt solutions of sodium sulfate, this yields eqn. (6)

$$\log(f_+^4/f_-)=(4b_+-b_-)m \qquad (6)$$

for the function considered. This prescribes the function to be linear in m (or in $x=m/m°$) as presently obtained with the liquid-junction based data, but not with the double-layer based data (Fig. 2).

From a hydration-energy involving treatment of ionic activities,[20] one easily deduces that eqn. (7)

$$b_i=bz_i^2/r_i \qquad (7)$$

where b is a positive constant and r_i the effective radius of the dissolved i-ion, should apply to the ions of a single-salt solution. For sodium sulfate, this prescribes the sign of d $\log(f_+^4/f_-)/dx$ to be that of $r_+^{-1}-r_-^{-1}$, which most likely is positive. Also this favours the present results from the liquid-junction approach over those from the double-layer approach (see Fig. 2).

A weakness in the present liquid-junction approach is the simplification of directly using concentrations and limiting mobilities in estimating $\Delta\phi$ from the Henderson equation. Even though this practice has been given some justification by considerations of diffusion *contra* conduction in liquid junctions,[8] it still carries uncertainty with it. The double-layer approach avoids this uncertainty, but involves other ones. Here is room for improvement and a need for additional testing methods.

REFERENCES

1. Taylor, P. T. *J. Phys. Chem. 31* (1927) 1478.
2. Gibbs, W. *Collected Works,* Vol. 1, Longmans Green, New York 1928.
3. Guggenheim, E. A. *J. Phys. Chem. 33* (1929) 842.
4. Frank, H. S. *J. Phys. Chem. 67* (1963) 1554.
5. Rabinovich, V. A., Nikerov, A. E. and Rotshtein, V. P. *Electrochim. Acta 12* (1967) 155.
6. Bates, R. G., Staples, B. R. and Robinson, R. A. *Anal. Chem. 42* (1970) 867.
7. Stastny, M. and Strafelda, F. *Collect. Czech. Chem. Commun. 37* (1972) 37.
8. Bagg, J. and Rechnitz, G. A. *Anal. Chem. 45* (1973) 271.
9. Milazzo, G., Bonciocat, N. and Borda, M. *Electrochim. Acta 21* (1976) 349.
10. Daghetti, A. and Trasatti, S. *Can. J. Chem. 59* (1981) 1925.
11. Daghetti, A. and Trasatti, S. *Extended Abstracts, 33rd ISE-meeting,* Lyon 1982, Vol. 1, p. 83.
12. Hurlen, T. *Acta Chem. Scand. A 33* (1979) 631.
13. Hurlen, T. *Acta Chem. Scand. A 33* (1979) 637.
14. Hurlen, T. *Acta Chem. Scand. A 35* (1981) 415 and 457.
15. Hurlen, T. and Breivik, T. R. *Acta Chem. Scand. A 32* (1978) 447.
16. Noer, S. and Grønlund, F. *Ber. Bunsenges. 79* (1975) 517.
17. Vetter, K. J. *Electrochemical Kinetics,* Academic, New York and London 1967, p. 49.
18. Parsons, R. *Handbook of Electrochemical Constants,* Butterworth, London 1959.
19. Robinson, R. A. and Stokes, R. H. *Electrolyte Solutions,* 2nd Ed., revised, Butterworth, London 1970.
20. Hurlen, T. *Acta Chem. Scand. A 35* (1981) 587.

Received February 8, 1983.

Acta Chemica Scandinavica A 37 (1983) 743–753

Hydrophilic Complexes of the Actinides. II. Comparison of TBP, HTTA and HDEHP Liquid–Liquid Distribution Systems

ROBERT LUNDQVIST, JIU-FANG LU * and INGVOR SVANTESSON

Department of Nuclear Chemistry, Chalmers University of Technology, S-412 96 Göteborg, Sweden

The liquid–liquid distribution equilibria of the Am(III), Eu(III), U(IV), Th(IV) and UO_2^{2+} ions with tributyl phosphate (TBP), di-(2-ethylhexyl) phosporic acid (HDEHP) and 2-thenoyltrifluoroaceton (HTTA) have been studied at 25 °C by tracer technique, pH-measurements and optical methods. The ionic strength was maintained constant by adding $NaClO_4$, NaCl or $NaNO_3$, while heptane and toluene were employed as diluents. The distribution equilibrium (extraction) constants are summarized in Tables 1 and 2.

The acidity, the ionic strength and the ligand concentration were in each case varied systematically to ascertain the stoichiometry and kinetics of the extraction reactions. The application and usefulness of the three extraction reagents for their use in actinide complex chemistry studies are discussed in some details.

We have recently focused our interest on actinide complexation with hydrophilic ligands because of its importance for predicting the fate of nuclear waste stored in groundwater environment. Most of our work has been carried out with radioactive tracers using a liquid–liquid distribution system, with the organic phase containing an organophilic extraction reagent and the aqueous phase containing a hydrophilic ligand.

The versatility of the liquid–liquid distribution method for the investigation of metal complexation has led to a vast number of successful studies in the last two or three decades. Some illustrative examples for such applications, reported in the literature, have been examined and compared by Marcus and Kertes, and Beck.[1,2] In order to obtain optimal usefulness of the distribution system, one may have to use different extraction reagents, depending on the metal and hydrophilic ligand, since they will extract with different mechanisms. HTTA (2-thenoyltrifluoroacetone) has been one of the most commonly used extraction reagents for determining stability constants (the "TTA-method"), but HTTA has some drawbacks, particularly at high pH.

The aim of this work is to compare HTTA with two other common extractants TBP (tributyl phosphate) and HDEHP (di-2-ethylhexyl-phosphoric acid). The results will serve as a basis for continued studies of the hydrophilic actinide complexes, and we have chosen to study first some representative metal ions: Eu(III), Th(IV), U(IV), U(VI) and Am(III).

EXPERIMENTAL

Chemicals. All experiments were carried out with *p.a.* quality chemicals when possible. TBP was supplied by Fluka (*puriss p.a.*), HTTA (Merck) was purified by recrystallization. HDEHP was supplied from Farbenfabriken Bayer AG, purified by washings with strong acid, and analyzed by acidic titration. Heptane and toluene served as organic diluent. $NaClO_4$ solutions were prepared from $NaClO_4 \cdot H_2O$ (Fluka) and filtrated through a millipore (pore size 400 nm) disc. The carbonate content was found to be negligible for our purposes.[3]

Radionuclides. ^{22}Na, ^{152}Eu, ^{233}U, and ^{241}Am were purchased from Radiochemical Centre, Amersham, while ^{235}U originated from AB

* Present address: Department of Chemical Engineering, Quinghua University, Beijing, China.

0302-4377/83 $2.50

Atomenergi, Studsvik. ^{234}Th was prepared from natural uranium by extractive separation using the TBP–HCl system. Stock solutions containing about 10^5 Bq/ml of the radionuclides in 0.1 M $HClO_4$ were prepared.

Analysis. The activities of the radionuclides were measured by γ spectrometry or by liquid scintillation. Natural uranium was detected by X-ray fluorescence spectrometry or absorption spectrophotometry (240 and 260 nm for U(VI), 648 nm for U(IV) and 520 nm and 615 nm for U(III)).

Reduction of U(VI). Electrolytic reduction of U(VI) to U(IV) and U(III) was carried out with the use of either a platinum wire or a mercury pool cathode. The anode compartment was separated from the bulk with a dense fritted glass diaphragm as described previously.[4] The current and time necessary for complete reduction were determined by on-line spectrophotometric surveillance of the oxidation state.

Determination of distribution ratios. The distribution experiments were carried out in a closed glass vessel at 25±0.1 °C. 15 ml organic phase, 15 ml aqueous phase and the radioisotope were introduced into the vessel. The system was stirred until equilibrium was attained, which usually took 5–20 min depending on the conditions (extracting agent, pH and reagent concentrations). The HDEHP system is rather slow at high pH and high HDEHP concentration. We found the equilibrium in this type of extraction device to be attained rapidly (*ca.* 5 min) when $[HDEHP]/[H^+] \lesssim 0.5$. Samples of 1 ml volume were withdrawn for radioactivity counting. Due to the extraction of $NaClO_4$ and $HClO_4$ by TBP it was necessary to pre-equilibrate TBP twice with $NaClO_4$ in order to maintain a constant ionic strength of the extraction system. The hydrogen ion concentration was determined (±0.01 pH units) by EMF measurements using a glass–silver–chloride combination electrode (Radiometer, Copenhagen), modified as described earlier.[4] A solution of known acidity served as standard.

RESULTS

TBP. Tributylphosphate belongs to the class of solvating extractants which extract a metal salt into the organic phase by forming an organophilic compound. The extraction equilibria can be written as in eqn. (1),

$$M(H_2O)_p^{m+} + mClO_4^- + n\overline{TBP} \rightleftarrows \overline{M(H_2O)_q(ClO_4)_m(TBP)_n} + (p-q)H_2O \qquad (1)$$

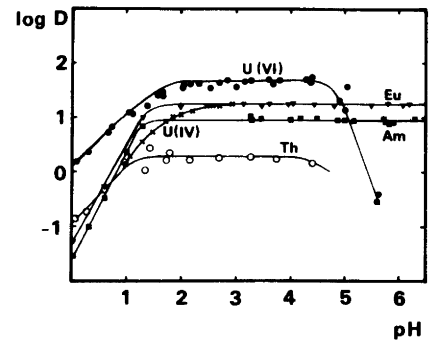

Fig. 1. Extraction of U(VI), U(IV), Th(IV), Am(III) and Eu(III) by tributylphosphate TBP (100 %) from 1 M (Na,H)ClO_4; log D as a function of pH. (●) denotes U(VI), (×) U(IV), (○) Th(IV), (■) Am(III) and (▼) Eu(III). 25 °C.

where m is the charge of the metal cation M^{m+}, p and q stand for the number of solvating water molecules and the bar above the formula indicates the organic phase. Despite the enormous use of TBP in industrial applications, it seems that this reagent has not been used for complex chemistry studies until recently.[3]

The distribution $D=[M(org)]/[M]$ of U(VI), U(IV), Am(III), Eu(III) and Th(IV) between 100 % TBP and 1 M (Na,H)ClO_4 is shown in Fig. 1 as a function of pH. Typically, a plateau is reached at high pH. At lower pH the distribution decreases. The decrease in D starts at about pH 1.5 for Am, Eu and Th while the decrease for U(IV) begins already at pH 3. However, from eqn. (1) one would expect a pH independent

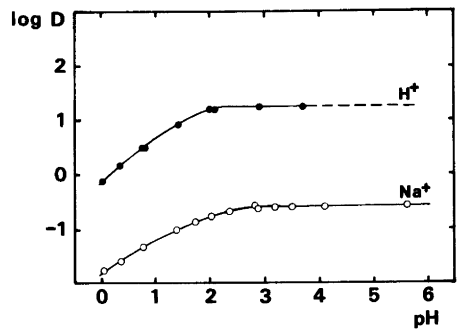

Fig. 2. Distribution, log D, of $HClO_4$ and $NaClO_4$ between 100 % TBP and 1 M (Na,H)ClO_4 at 25 °C as a function of pH. (●) denotes $HClO_4$ and (○) $^{22}NaClO_4$.

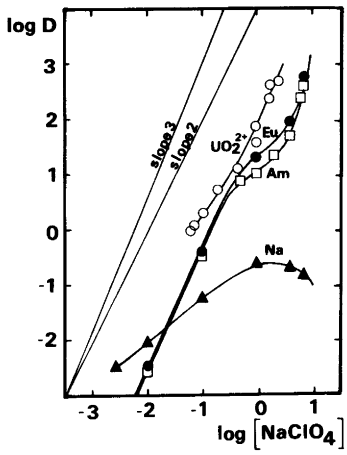

Fig. 3. Influence of the sodium perchlorate concentration on the distribution. Log D, of UO_2^{2+}, Am^{3+}, Eu^{3+} and Na^+ between 100 % TBP and aqueous perchlorate solutions of constant acidity. (○) UO_2^{2+}, pH 2.5, for $NaClO_4$ >1 M pH 3; (□) Am(III), pH 2; (●) Eu(III), pH 2; (▲) Na^+, pH 2.

distribution over the entire acidity range. The observed decrease at lower pH seems mainly (ignoring the influence of the change in the composition of the ionic media) to be due to the competition for "free" TBP caused by the simultaneous extraction of $HClO_4$. $HClO_4$ and

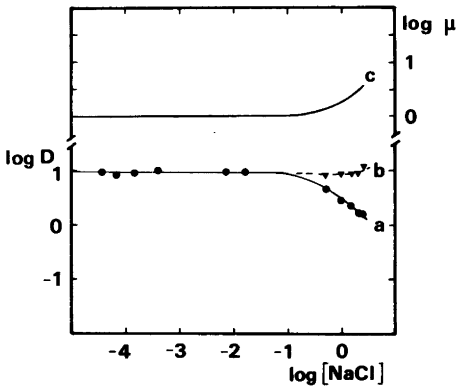

Fig. 4. The effect of ionic strength μ on the distribution, log D, of Am between 100 % TBP and aqueous NaCl. (a) At constant (=1 M) sodium perchlorate concentration, pH 3, 25 °C. (b) The distribution curve corrected for chloride complexation. (c) The ionic strength, μ, of the aqueous phase.

$NaClO_4$ are readily extracted by TBP, see Fig. 2. The distribution constant k_d=[$MClO_4$(org)]/[$MClO_4$] in 1M $NaClO_4$ was derived to 18±2 for $HClO_4$ and 0.3±0.05 for $NaClO_4$. Despite the decrease in the distribution of $HClO_4$ at lower pH, the $HClO_4$ concentration increases in the organic phase since the total $HClO_4$ concentration increases.

At high pH the metal distribution also deviates from the plateau (Fig. 1). This decrease is caused by the onset of hydrolysis of the metal cations [pH≳4.5 for U(VI), pH≳4 for Th(IV), pH≳6.7 for Am(III) and Eu(III)]. Since U(IV) is an acid of considerable strength, it will never reach the plateau corresponding to pH independent distribution coefficients before hydrolysing. Therefore U(IV) will not follow eqn. (1).

Eqn. (1) shows that the influence of the perchlorate ion concentration on the D-value would be proportional to the m:th-power of the perchlorate concentration provided other reactions do not take place, as for example extraction of $NaClO_4$ or $HClO_4$ mentioned above. Fig. 3 shows the influence of the perchlorate concentration on the distribution of Am(III), Eu(III), Na(I) and U(VI). Roughly the slopes of log D *versus* log $NaClO_4$ correspond to the ionic charge m in accordance with eqn. (1).

A more detailed description of the extraction equilibria is difficult, because of *e.g.* the mutual solubility of TBP and the aqueous phase.[5] Hence various values of n have been suggested in the literature (*e.g.* n=5 to 7 for the lanthanides).[6,7] Since precise knowledge of the extraction mechanisms is not needed for our purpose, we have made no attempt to elaborate it. TBP and related metal and acid extraction systems have been extensively treated in several monographies.[1,8–13] Further information on the TBP extraction of U(VI) and U(IV) can be found in Refs. 14–18.

In the use of the TBP distribution system for complexation studies the perchlorate concentration should preferably be held constant in order to simplify the interpretation of the distribution data. However, when studying a weak complexant which requires large additions of ligand, this leads to a noticeable increase in ionic strength. In order to enable us to make corrections for such increases we have made a preliminary study of the influence of the ionic strength on the distribution of Am by adding NaCl at constant 1 M

$NaClO_4$, Fig. 4. The formation of americium chlorides leads to a decrease in the distribution values because the chloride complexes are inextractible as was found from a separate TBP-NaCl experiment in which log $D_{Am} \lesssim -3$ for 0.1–3.5 M NaCl. However, one may compensate for the decrease by correcting for the chloride complexation, the remaining change in the distribution was relatively small; log D_{Am} increases $\lesssim 0.1$ units by an increase in ionic strength from 1 to 3.5 M. The extent of chloride complexation was calculated using stability constants reported in the literature, $\beta_1 = 1.04$, $\beta_2 = 0.43$ (Ref. 21) and we estimate β_3 to 0.1.[19–21]

HTTA. 2-Thenoyltrifluoroacetone belongs to the class of chelate forming agents which form organophilic compounds with metal ions. The distribution coefficient λ_m of the neutral metal chelate is very high for many metals and solvent combinations so λ_m has not always been possible to observe.[1,9–11,22] Straight lines of log D *versus* pH plots are often obtained corresponding to the overall extraction equilibrium shown in eqn. (2) with the extraction constant K_{ex}.

$$M^{m+} + m\,\overline{HTTA} \rightleftarrows \overline{M(TTA)_m} + mH^+ \qquad (2)$$

Fig. 5 shows log D as a function of pH for the distribution of Am^{3+} and Eu^{3+} between an organic phase with heptane or toluene as diluent and a 1 M sodium perchlorate aqueous phase. Fig. 6 shows the log D values of Am^{3+} *versus* the reagent concentration log [HTTA]. The slopes of +3 in both figures are in accordance with eqn. (2), $m=3$. These distribution systems are therefore suitable for studies of hydrophilic complexation of the metal in the aqueous phase. However, a low HTTA concentration will be required for work at high pH to avoid too high log D values.

Furthermore, log D must be appreciably less than log λ_3 if the simple extraction equilibria of eqn. (2) is to be employed. At low HTTA concentration the extraction system seems to be very sensitive to impurities and at pH>4 we also noticed loss of activity to the interface and the walls (poor mass balance). Stirring periods of about 30 min were used in order to establish equilibrium at pH<4. The extraction constants, K_{ex}, obtained are collected in Table 1.

HDEHP. The versatility of di-2-ethylhexylphosphoric acid is due to its capability of forming very extractable selfadduct complexes with metals, of which many have very high distribution values. The extraction will greatly depend upon the choice of organic diluent, because of its influence on the HDEHP activity and aggregation state, and upon the ionic composition of the aqueous phase. Furthermore HDEHP may even extract metal salts at high metal or salt concentra-

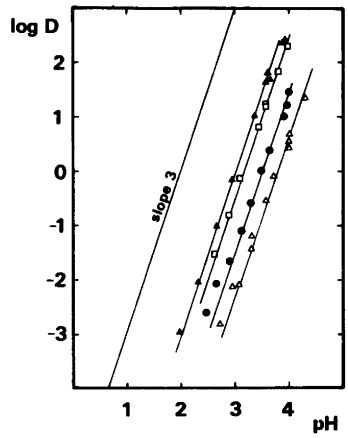

Fig. 5. The pH dependency of the distribution log D of Am and Eu between organic HTTA solutions and 1 M $NaClO_4$ at 25 °C. (●) Am^{3+}; 0.2 M HTTA in n-heptane, (△) Am^{3+}; 0.1M HTTA in n-heptane, (□) Am^{3+}; 0.5 M HTTA in toluene, (▲) Eu^{3+}; 0.5 M HTTA in toluene. (Initial HTTA concentrations).

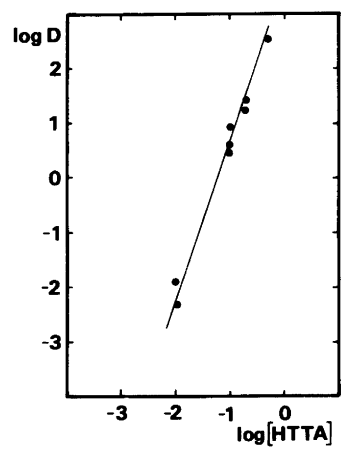

Fig. 6. The relation between the distribution, log D, of Am^{3+} and the initial HTTA concentration in n-heptane. Aqueous phase; 1 M $NaClO_4$, pH 4. 25 °C.

Table 1. Extraction constants K_{ex} for the distribution of Am^{3+} and Eu^{3+} between aqueous $NaClO_4$ and HTTA in various diluents at 25 °C. $K_{ex}[M^{3+}+3HTTA(org) \rightleftarrows M(TTA)_3(org)+3H^+]$. Initial concentration of HTTA was used in the calculations of K_{ex}.

Diluent	log K_{ex} Am	Eu	Conditions M HTTA	M(Na,H)ClO_4	pH	log D range	Ref.
Heptane	−8.40±0.10		0.01−0.5	1	2.5−5	−3−2.5	This work
Toluene	−8.66±0.15		0.5	1	2.3−4	−2−2.4	This work
Toluene		−8.16±0.10	0.5	1	2−4	−3−2.5	This work
Toluene		−8.2[a]	0.2	0.1M(NH_4^+,H^+)CH_2ClCOO^-			13
Benzene		−7.80[b,c]	0.1	0.1	2.5−3.8	−1−1	41
Toluene	−8.6[a]		0.2	0.1M(NH_4^+,H^+)CH_2ClCOO^-			13

[a] Calculated from distribution data, Ref. 40, [b] 25 °C?, [c] ΔH=15.7 kcal/mol, ΔS=16.8 cal/deg mol.

tion by solvation in analogy with neutral organophosphorus compounds like TBP.[1,23] In order to use HDEHP for complex studies it is essential to establish the predominant extraction mechanism of the actual system.

The trivalent metal ions Am^{3+} and Eu^{3+} were found, Fig. 7, to be extracted with a linear relationship to the pH over the entire acidity range investigated. The slope of log *D versus* pH equals +3. The same behaviour was found not only in 1 M $NaClO_4$ but also in 3 and 6 M $NaClO_4$.

Using heptane as diluent it was found that the dependence of log D on the logarithm of HDEHP total concentration was linear with a slope of +2.5, Fig. 8. Fig. 8 also shows that the influence of the HDEHP concentration is independent of the acidity. Assuming that HDEHP predominantly exists as a dimer in heptane under the present conditions (literature data on the dimerization and distribution constants are insufficient but it may be estimated that log $[HDEHP_2]/[HDEHP]^2 \approx 4.5$,[12,13]) one obtains the apparent extraction mechanism, eqn. (3), for Am^{3+} and Eu^{3+}.

$$M^{3+}+2.5\ \overline{(HDEHP)_2} \rightleftarrows \overline{M(DEHP)_3(HDEHP)_2}+3H^+ \quad (3)$$

This behaviour has also been found previously by other investigators from work with heptane and other aliphatic solvents using trace concentrations of trivalent metals.[24–27] The suggested composition of the extracted metal species is derived from the stoichiometry of eqn. (3) only and does not prove the actual structure. The composition could have equally well been written in an alternative way, *i.e.* $MY(HY_2)_2$, where Y=DEHP.

Using aromatic solvents it has been found that the reagent concentration dependency is +3, eqn. (4).[24,27–30] Even in aliphatic solvents a third power reagent concentration dependency has been observed at low HDEHP concentrations ($10^{-4.7}$ to $10^{-3.5}$ M).[29]

$$M^{3+}+3\ \overline{(HDEHP)_2} \rightleftarrows \overline{M(DEHP)_3(HDEHP)_3}+3H^+ \quad (4)$$

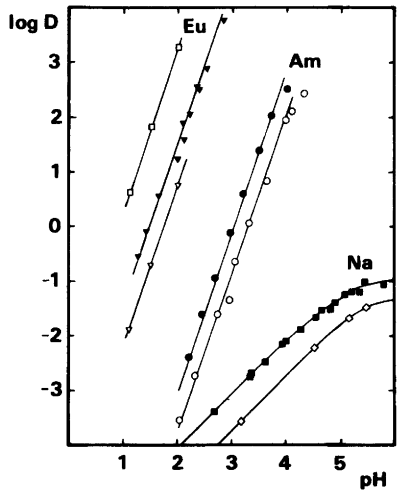

Fig. 7. The distribution, log D, of Am^{3+}, Eu^{3+} and Na^+ between HDEHP in n-heptane and 1 M $NaClO_4$ as a function of pH. 25 °C. (●) Am^{3+} 0.001 M HDEHP; (○) Am^{3+} 0.0005 M HDEPH; (□) Eu^{3+} 0.05 M HDEHP; (▽) Eu^{3+} 0.005 M HDEHP; (▼) Eu^{3+} 0.01 M HDEHP and 6 M $NaClO_4$; (■) Na^+ 0.1 M HDEHP; (◇) Na^+ 0.05 HDEHP.

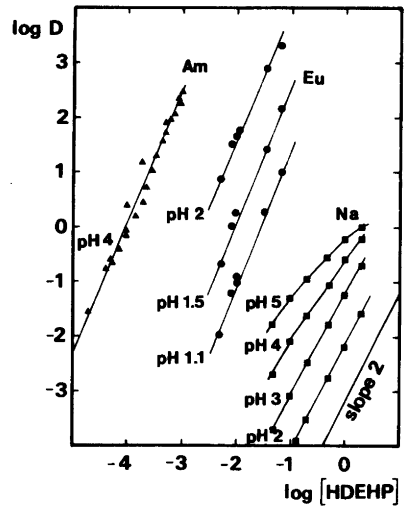

Fig. 8. The HDEHP dependency on the distribution, log D, of Am^{3+}, Eu^{3+} and Na^+. (Initial and total HDEHP concentrations). The aqueous phase is 1 M $NaClO_4$. 25 °C. The slopes of Am^{3+} and Eu^{3+} are 2.5.

The distribution data can be interpreted either in terms of concentration dependencies following eqn. (3) or in terms of activity coefficients of the HDEHP assuming that eqn. (4) represents the ideal behaviour. Authors who prefer to express the extraction mechanism according to eqn. (4) explain the observed slope with a decrease in the activity coefficient of HDEHP. It is believed to be a consequence of the interactions between the HDEHP dimers.[31–33]

The apparent extraction constant K_{ex} for the studied systems of Am and Eu were calculated according to eqn. (3) and these have been collected in Table 2. It should be noted that the initial concentration of the HDEHP dimer has been used in these calculations, although the actual concentration might be somewhat lower due to loss of the reagent to the aqueous phase, and conversion of the reagent into its sodium salt, the latter not only reduces the HDEHP dimer concentration but it also changes the extraction mechanism. However, our choice of HDEHP concentrations and pH were such that the concentration of NaDEHP in the organic phase and of HDEHP in the aqueous phase were negligible.

The extraction of Na^+ was investigated using ^{22}Na, Figs. 7 and 8. We deduced an extraction mechanism according to eqn. (5)

$$Na^+ + 2\,\overline{(HDEHP)_2} \rightleftarrows \overline{NaDEHP(HDEHP)_3} + H^+ \qquad (5)$$

Although this mechanism was previously established, no extraction constants K_{ex} of eqn. (5) were derived for sodium perchlorate solutions.[24,34,35] From the linear relationships of the distribution functions we calculated log $K_{ex} = -3.56 \pm 0.08$ (1 M $NaClO_4$, heptane, Table 2). The extraction mechanism of sodium is, however, changed at high pH because of a gradual, and finally complete, transformation of the extraction reagent in the organic phase into NaDEHP. This was concluded from the stoichiometry of the pH titration and from the existence of plateaues in the relation log $D_{Na} = f(pH)$ at pH≥6 (one plateau for each initial HDEHP concentration). The distribution constant k_d=[NaDEHP(heptane)]/[NaDEHP(1 M $NaClO_4$)]=3.5±0.3 was derived for 25 °C.

Table 2. Apparent extraction constants K_{ex} for the distribution of Am^{3+}, Eu^{3+} and Na^+ between aqueous $NaClO_4$ and HDEHP in various diluents at 25 °C. $K_{ex}(M^{3+}+2.5(HDEHP)_2(org) \rightleftarrows M(DEHP)_3(HDEHP)_2(org)+3H^+)$ and $K_{ex}(Na^++2(HDEHP)_2(org) \rightleftarrows Na(DEHP)(HDEHP)_3(org)+H^+)$. The initial dimer concentration of HDEHP in the organic phase was used in the calculation of K_{ex}.

Diluent	log K_{ex} Am	Eu	Na	M HDEHP (formal conc.)	M(Na,H)ClO_4)	pH	log D range	Ref.
Heptane	−0.85±0.10			$10^{-3.3}-10^{-3}$	1	2−4	−3.5−2.5	This work
Heptane	−0.63[a]			0.02−0.3	1M (Na,H)Cl	0.4−1.7	−1.5−2.2	25
Heptane	0.2[a]			0.02−0.3	0.1M HCl	1	−2.3−1.3	25
Heptane		1.15±0.10		$10^{-3.6}-10^{-1.3}$	1	1.1−3.6	−2−3.3	This work
Heptane		1.08±0.10		10^{-2}	3	1−2.5	−1.5−2.6	This work
Heptane		1.18±0.10		10^{-2}	6	1.3−2.8	−0.6−3.8	This work
Heptane		0.65±0.10		10^{-2}	1M NaCl	1.3−2	−0.8−1.3	This work
Heptane		1.0±0.1		10^{-2}	1M $NaNO_3$	2	1.3	This work
Heptane		1.03[a]		0.02−0.3	1M (Na,H)Cl	0−1	−1−2.5	25
Dodecane		1.4[a]		10^{-3}−0.5	1M (Na,H)Cl	1.28	−3.5−3.4	32
Heptane		1.75[a]		0.02−0.3	0.1M HCl	1	−0.5−2.6	25
Hexane		1.58[a]		0.01−0.1[b]	0.1M HCl	1	−1−1.3	24
Heptane			−3.56±0.08	0.05−1	1	2−3	−4.5− −1.2	This work

[a] Calculated from distribution data. [b] Deviation at higher conc.

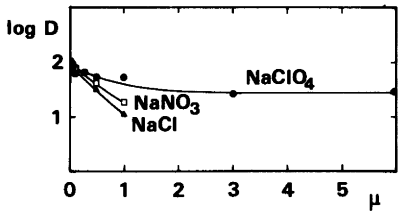

Fig. 9. The influence of the ionic strength μ on the distribution, log D, of Eu^{3+} between 0.01 M HDEHP in n-heptane and an aqueous solution of $NaClO_4$, $NaNO_3$ or NaCl at pH 2 and 25 °C. (●) $NaClO_4$, (▲) NaCl, (□) $NaNO_3$.

Furthermore it was noted that a second organic phase consisting of almost pure heptane forms at pH≳5.8 (if the initial HDEHP concentration was less than 2 M). The volume ratio between the reagent deficient and the reagent rich organic phases increases with diminishing initial HDEHP concentration. This phenomenon leads to the assumption that all NaDEHP is contained in an interfacial film (*i.e.* skin formation) at reagent concentrations below ≈0.1 M.

The influence of the aqueous phase composition was investigated by varying the ionic strength by means of sodium salt additions. Fig. 9 shows the distribution log D of Eu as a function of the NaCl, $NaNO_3$ and $NaClO_4$ salt concentration at pH 2. The $NaClO_4$ was tested up to 6 M, the effect of the increased ionic strength was fairly small, a slow decrease in the distribution values was observed. $NaNO_3$ and NaCl were tested up to 1 M ionic strength and it was found that the decrease in log D was more pronounced. The rate of the decrease followed the order $Cl^- > NO_3^- > ClO_4^-$ which also is the order of complex formation strength between Eu and the anions. Further support for that chloride complexation is stronger than perchlorate complexation was obtained by substituting ClO_4^- with Cl^- at a constant ionic strength of 1 M at pH 2. The D value diminished with increasing chloride concentration.

DISCUSSION

We have made a comparison of the usefulness of the three extractants HTTA, TBP and HDEHP for studying hydrophilic complexation. The conclusions are based on the experience in this study and the results are summarized in Table 3.

Generally, we conclude that TBP is very useful because of its pH independence and its stability, especially when using 100 % reagent. However, it might not be the best choice for studying weak complexes as perchlorate is extracted together with the metal species. Furthermore, the use of TBP at acid conditions is somewhat complicated by the extraction of $HClO_4$. This extraction is not known in great detail although it is believed that perchloric acid is extracted as $HClO_4(TBP)_y$ where $y=3-4$.[6,34]

HDEHP is a very reliable reagent and offers a great freedom in adjusting the distribution level. Very high or low D values can be obtained which makes HDEHP indispensable in studying extremely strong complexants. Its drawbacks are mainly related to slow kinetics under certain conditions and to the strong pH dependency of HDEHP which necessitates careful determination of the influence of the acidity on the complex system. Other disadvantages are the change in extraction mechanism which may occur, depending on the diluent, when increasing the reagent concentration and the conversion of HDEHP into its salt form at high pH which may result in a third phase or skin formation.

HTTA should offer the same advantages as HDEHP but somewhat surprisingly we have not found HTTA to be very easy to work with in contrast to its homologue acetylacetone (HAA) which behaves very regularly. Conflicting observations about the time needed to obtain equilibrium have been made; Edroth, *e.g.*, found no indication of true equilibrium in the HTTA(benzene)–Th(IV),$NaClO_4$ distribution system even after a month, and Kassierer and Kertes found no equilibrium with HTTA-lanthanides even after 6 h if pH<4, whereas the equilibrium was attained rapidly at higher pH.[37,38] In this work we found that at least pseudo-equilibrium is obtained within 30 min if pH<4, but that the reproducibility is poor at pH>4. Despite these contradictory observations about the equilibrium kinetics it seems that our distribution data for HTTA are compatible both with Kassierer and Kertes' results and other values reported in the literature (Table 1).

Unless the kinetics is carefully elucidated, we feel reluctant to recommend the use of HTTA for metal complexation studies, except for analytical

Table 3. Comparison of the usefulness of HTTA, TBP and HDEHP as extraction agents for metal complexation studies.

Reagent class	Reproducibility	Mechanism, complication	Kinetics	Stability of reagent	Suitability for complex studies Weak complexes	Strong complexes	Hydrolysis
HTTA β-diketone	poor mass balance at pH>4	Unpredictable mechanism for some metals.[a]	Sometimes very slow.[e]	light sensitive, decomposition at pH>9.	good	good	poor because nonreproducibility at high pH;[b]
TBP neutral organophosphorous compound	good	Extraction of H^+, Na^+ and NH_4^+ salt.	rapid	stable	poor	good	very good because pH independent extraction mechanism
HDEHP acid organophosphorous compound	good at low pH	Mechanism depends on diluent. Extraction of Na^+ and NH_4^+.	Usually rapid[c]	stable	good	good	poor because nonreproducibility at high pH;[b,d]

[a] *E.g.* UO_2^{2+}, PaO^{2+} and HfO^{2+}, Ref. 39. [b] Very high *D*-values implies use of extremely low reagent concentrations which leads to sensitivity towards impurities *etc.* [c] A detailed kinetic study is given in Ref. 33.[d] Third phase and formation of interface layer (skin). [e] Depending on pH, Refs. 37, 38 and this work.

or separation purposes. Other properties of HTTA which must be considered are its decomposition at pH>9 and its, in comparison with other β-diketones, very stable ketohydrate. In addition β-diketones give unexpected extraction mechanisms with oxycations (*e.g.* UO_2^{2+}, PaO^{2+}, HfO^{2+}).[36]

Acknowledgements. Eng. Theresia Rodinson and Eng. Eva Jomar are thanked for careful experimental assistance. Valuable suggestions and criticism have been given by Prof. Jan Rydberg. Dr. Lu expresses his gratitude for the financial support of the Royal Swedish Academy of Engineering Sciences and Academia Sinica during his two year visit to Sweden. This work was supported by the Swedish Natural Science Research Council which is gratefully acknowledged.

REFERENCES

1. Marcus, Y. and Kertes, A. S. *Ion Exchange and Solvent Extraction of Metal Complexes,* Wiley, London 1969.
2. Beck, M. T. *Chemistry of Complex Equilibria,* Van Nostrand-Reinhold, London 1970.
3. Lundqvist, R. *Acta Chem. Scand. A 36* (1982) 741.
4. Lundqvist, R. *Acta Chem. Scand. A 28* (1974) 243.
5. Leroy, P. *CEA-R 3207, Commissariat a L'Energie Atomique-France,* 1967.
6. Kolarik, Z. *J. Inorg. Nucl. Chem. 36* (1974) 409.
7. Yoshida, H. *J. Inorg. Nucl. Chem. 26* (1964) 619.
8. Ahrland, S., Liljenzin, J. O. and Rydberg, J. *Comprehensive Inorganic Chemistry,* Pergamon, Oxford and New York 1973, Vol. 5, p. 542.
9. Liljenzin, J. O. and Lundqvist, R. *Gmelin Handbuch der Anorganischen Chemie,* 8th Ed., Protactinium, Ergänzungsband 2, Systemnummer 51, Springer, Berlin, 1977, p. 187.
10. Markl, P. *Extraktion und Extraktions-Chromatographie in der Anorganischen Analytik, Metoden der Analyse in der Chemie,* Band 13, Akad.-Verlag., Frankfurt am Main 1972.
11. Sekine, T. and Hasegawa, Y. *Solvent Extraction Chemistry, Fundamentals and Applications,* Dekker, New York 1977.
12. Marcus, Y., Kertes, A. S. and Yanir, E., *Equilibrium Constants of Liquid–Liquid Distribution Reactions. Part 1: Organophosphorous Extractants,* IUPAC Chem. Data Series, No. 3, Butterworth, London 1974.
13. Marcus, Y. *Critical Evaluation of some Equilibrium Constants Involving Organophosphorous Extractants,* IUPAC Chem. Data Series, No. 1, Butterworth, London 1974.
14. Nikolotova, E. I. and Kartachova, N. A. *Handbook of Extraction, Vol. 1., Extraction of Neutral Organic Compounds,* Atomizdat, Moscow 1976.
15. Hesford, E. and McKay, H. A. C. *J. Inorg. Nucl. Chem. 13* (1969) 165.
16. Woodhead, J. L. and McKay, H. A. C. *J. Inorg. Nucl. Chem. 27* (1965) 2747.
17. Marcus, Y. *J. Inorg. Nucl. Chem. 37* (1975) 493.
18. Marcus, Y. and Kolaric, Z. *J. Chem. Eng. Data 18* (1973) 155.
19. Högfeldt, E., Ed., *Stability Constants of Metal-Ion Complexes. Part A: Inorganic Ligands,* IUPAC Chem. Data Series, No. 21, Pergamon, Oxford 1982.
20. Sillén, L. G. and Martell, A. E., Eds., *Stability Constants of Metal Ion Complexes,* Special publications Nos. 17 and 25, The Chemical Society, Burlington House, London 1964 and 1971.
21. Khopkar, P. K. and Narayanankutty, P. *J. Inorg. Nucl. Chem. 33* (1971) 495.
22. Stary, I. and Freiser, H. *Equilibrium Constants of Liquid–Liquid Distribution Reactions. Part IV: Chelating Extractants,* IUPAC Chem. Data Series No 18, Pergamon, Oxford 1978.
23. Lenz, T. G. and Smutz, M. *J. Inorg. Nucl. Chem. 30* (1968) 621.
24. Dubuquoy, C., Guillaumont, R. and Bouissières, G. *Radiochim. Acta 8* (1967) 49.
25. Mason, G. W., Metta, D. N. and Peppard, D. F. *J. Inorg. Nucl. Chem. 38* (1976) 2077.
26. Weaver, B. and Shoun, R. R. *J. Inorg. Nucl. Chem. 33* (1971) 1917.
27. Mason, G. W., Schofer, N. L. and Peppard, D. F. *J. Inorg. Nucl. Chem. 32* (1970) 3911.
28. Peppard, D. F., Mason, G. W., Driscoll, W. J. and Sironen, R. J. *J. Inorg. Nucl. Chem. 7* (1958) 276.
29. Kandil, A. T. and Farah, K. *J. Inorg. Nucl. Chem. 42* (1980) 277.
30. Zikovský, L. *J. Inorg. Nucl. Chem. 35* (1973) 2917.
31. Alstad, J., Augustson, J. H., Danielssen, T. and Farbu, L. *Proc. Int. Solvent Extraction Conf.,* ISEC-77, Lyon 1974, Society of Chemical Industry, London 1974, Vol. 2, p. 1083.

32. Danesi, P. R. and Vandergrift, G. F. *Inorg. Nucl. Chem. Lett. 17* (1981) 109.
33. Danesi, P. R. and Vandergrift, G. F. *J. Phys. Chem. 85* (1981) 3646.
34. McDowell, W. J. and Coleman, C. F. *J. Inorg. Nucl. Chem. 27* (1965) 1117.
35. Lanin, V. P., Smelov, V. S. and Smyk, Z. A. *Sov. Radiochem. 14* (1972) 694.
36. Tebelev, L. G. and Melkaya, R. F. *Sov. Radiochem. 18* (1976) 733.
37. Edroth, B. *Unpublished work.*
38. Kassierer. E. F. and Kertes, A. S. *J. Inorg. Nucl. Chem. 34* (1972) 3221.
39. Lundqvist, R. *Proc. Int. Solvent Extraction Conf. ISEC-80,* Liège, Belgium, Sept. 6–12. Vol. 1, Session 16, Paper 80–51.
40. Magnusson, L. B. and Andersson, M. L. *J. Am. Chem. Soc. 76* (1954) 6207.
41. Kandil, A. T., Aly, H. F., Raieh, M. and Choppin, G. R. *J. Inorg. Nucl. Chem. 37* (1975) 229.

Received February 14, 1983.

Acta Chemica Scandinavica A 37 (1983) 755–764

Microwave Spectrum, Conformational Equilibria, Intramolecular Hydrogen Bonding and Centrifugal Distortion of 3-Phosphinopropionitrile

K.-M. MARSTOKK and HARALD MØLLENDAL

Department of Chemistry, The University of Oslo, P.O.Box 1033, Blindern, Oslo 3, Norway

The microwave spectrum of 3-phosphinopropionitrile, $N{\equiv}CCH_2CH_2PH_2$, has been investigated in the 19.2–36.4 GHz spectral region at about −10 °C. Three conformations, denoted II, IV and V, were assigned. The heavy-atom *gauche* conformation II is stabilized by a weak hydrogen bond formed between one of the phosphino group hydrogen atoms and the π-electrons of the cyano group. No hydrogen bond is possible for the two heavy-atom *anti* conformations IV and V.

II is more stable than V by 0.3(20) kJ/mol. V is more stable than IV by 3(2) kJ/mol. Further rotameric forms are at least 2 kJ/mol less stable than II.

The CCCP dihedral angle is 66(3)° and the CCP angle is 117.0(15)° in II. The CCP angle was determined to be 109.0(15)° in IV, and to be 114.0(15)° in V.

Several vibrationally excited states were assigned for the three rotamers. The C–C torsional frequency of II was determined to be 108(30) cm^{-1} by relative intensity measurements and 107(10) cm^{-1} using the centrifugal distortion constants in a force-field calculation.

In recent years, ethanol derivatives of the form XCH_2CH_2OH, where X=F,[1] Cl,[2a] Br,[2a] OH,[3] NH_2,[4] SH,[5] $HC{=}CH_2$,[6] $C{\equiv}C{-}H$,[7] OCH_3,[8] $NH(CH_3)$[9] and $N(CH_3)_2$,[10] have been studied in the gaseous state by microwave spectroscopy. In each of these cases, the hydrogen-bonded conformation has been found to predominate to such an extent that no further rotamers have been identified by this method. Similar findings have been made for ethylamine derivatives, $XCH_2CH_2NH_2$, with X=F,[11] NH_2,[12] $C{\equiv}N$,[13] and OCH_3.[14]. However, at higher temperatures the heavy-atom *anti* conformation of CH_2ClCH_2OH is present in the gaseous state in considerable amounts as shown by electron diffraction.[2b]

The intramolecular hydrogen bonding ability of the hydroxyl and the amino groups thus seems to be well-documented and relatively strong in these molecules. Few investigations have been made for ethyl thiols of the form XCH_2CH_2SH. The mercapto group is considered to be a considerably poorer proton donor than the hydroxyl and amino groups. The results obtained for CH_2ClCH_2SH,[15] $H_2NCH_2CH_2SH$[15] and $N{\equiv}CCH_2CH_2SH$[16] are in keeping with this view. In the case of CH_2ClCH_2SH,[15] only one heavy-atom *anti* conformation without an internal hydrogen bond was identified. Two conformations were found for $HSCH_2CH_2NH_2$.[15] The one with the highest energy was found to have an intramolecular hydrogen bond with the mercapto group acting as proton donor and the amino group as acceptor. Two rotamers, one with and the other (the heavy-atom *anti* rotamer) without a hydrogen bond were assigned for $N{\equiv}CCH_2CH_2SH$.[16] The hydrogen-bonded conformation was found to be the more stable by 1.3(20)kJ/mol.

No microwave studies have previously been made for ethylphosphines of the type $XCH_2CH_2PH_2$, where X is some proton-accepting group. The phosphino group is presumably even a slightly weaker proton donor than the mercapto group. In order to investigate the

0302-4377/83 $2.50

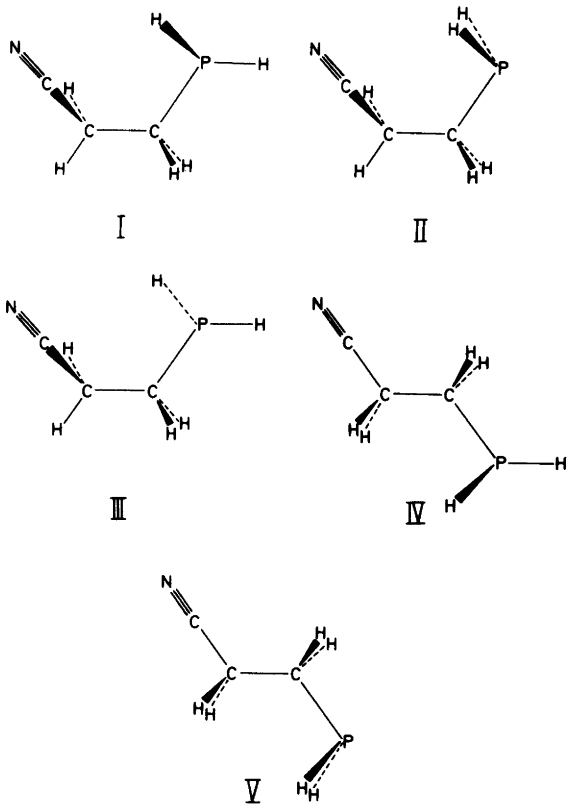

Fig. 1. Possible conformations of $NCCH_2CH_2PH_2$ with all-staggered atomic arrangements. The hydrogen-bonded heavy-atom *gauche* conformation II as well as the two heavy-atom *anti* conformations IV and V were assigned. II is the most stable conformation. It is more stable than V by 0.3(20) kJ/mol. V is more stable than IV by 3(2) kJ/mol.

internal hydrogen bonding ability of the phosphino group, $N{\equiv}CCH_2CH_2PH_2$ was chosen for study.

Five all-staggered conformations are possible for $NCCH_2CH_2PH_2$ as shown in Fig. 1. Weak hydrogen bonds formed between the phosphino group and the π electrons of the cyano group are possible for the heavy-atom *gauche* conformations I and II shown in this figure, while hydrogen bonding is not possible in the three further rotamers III, IV and V. Three rotamers, *viz.* II, IV and V, were found in this work. II is the most stable. It is 0.3(20)kJ/mol more stable than V which again is 3.0(15)kJ/mol more stable than IV. I and III are each less stable than II by at least 2 kJ/mol if they exist at all as stable conformations of $NCCH_2CH_2PH_2$.

EXPERIMENTAL

3-Phosphinopropionitrile was purchased from Aldrich-Europe, Beerse, Belgium, and used as received. Small amounts of CH_3CN, CH_3CH_2CN and $CH_2{=}CHCN$ impurities were noted by their microwave spectra. Spectra were recorded in the 19.2–36.4 GHz region at a pressure of about 0.5 Pa. A few measurements were also made above 36.4 GHz. The cell was cooled to about −10 °C. Lower temperatures could not be employed due to insufficient vapour pressure of $NCCH_2CH_2PH_2$.

The spectrum of 3-phosphinopropionitrile was found to be very dense. Most lines are very weak (peak absorption coefficients being less than roughly $5{\times}10^{-8}$ cm^{-1}). The strongest lines were the *b*-type *Q*-branch ground vibrational state lines of conformation II with *J* between 20 and

Table 1. Microwave spectrum of the ground vibrational state of conformation V of $NCCH_2CH_2PH_2$.

Transition	Observed frequency[a] (MHz)	Obs.-calc. frequency (MHz)	Centrifugal distortion (MHz)
$6_{0,6}\rightarrow 7_{0,7}$	19933.73	−0.09	−0.26
$6_{1,6}\rightarrow 7_{1,7}$	19770.28	0.07	−0.20
$7_{0,7}\rightarrow 8_{0,8}$	22779.72	−0.08	−0.39
$7_{1,6}\rightarrow 8_{1,7}$	22976.01	−0.01	−0.32
$7_{1,7}\rightarrow 8_{1,8}$	22594.11	0.07	−0.32
$8_{0,8}\rightarrow 9_{0,9}$	25624.97	−0.14	−0.55
$8_{1,7}\rightarrow 9_{1,8}$	25847.55	0.16	−0.48
$8_{1,8}\rightarrow 9_{1,9}$	25417.69	0.02	−0.48
$9_{0,9}\rightarrow 10_{0,10}$	28469.70	0.06	−0.76
$9_{1,9}\rightarrow 10_{1,10}$	28241.11	0.03	−0.68
$9_{2,7}\rightarrow 10_{2,8}$	28494.51	−0.03	−0.44
$10_{0,10}\rightarrow 11_{0,11}$	31313.18	−0.15	−1.01
$10_{2,8}\rightarrow 11_{2,9}$	31346.49	0.09	−0.66
$11_{0,11}\rightarrow 12_{0,12}$	34156.22	0.13	−1.31
$11_{1,11}\rightarrow 12_{1,12}$	33887.16	−0.01	−1.22
$11_{2,9}\rightarrow 12_{2,10}$	34198.87	−0.09	−0.93
$11_{2,10}\rightarrow 12_{2,9}$	34175.87	−0.03	−0.93

[a] ±0.10 MHz.

30. The peak absorption coefficients of these transitions were roughly 3×10^{-7} cm^{-1}.

RESULTS

Assignment of conformation V. In our work on $NCCH_2CH_2SH$[16] one heavy-atom *anti* conformation not possessing internal hydrogen bonding, was found to make up a large fraction of the gas. The phosphino group was presumed to be a slightly weaker proton donor than the mercapto group. The existence of heavy-atom *anti* conformations was therefore considered to be quite probable for $NCCH_2CP_2PH_2$. Moreover, in the case of $CH_3CH_2PH_2$[17] a conformation having the phosphino group in a position similar to that of V was found to predominate. Conformation V was therefore assumed to be a likely candidate to search for.

Model calculations of the rotational constants indicated that V should be almost a symmetric top with Ray's asymmetry parameter[18] $\kappa \approx -0.99$. The dipole moment components along the principal inertial axes were predicted to be $\mu_a=3.2$ D, $\mu_b=1.6$ D and $\mu_c=0.0$ D (for symmetry reasons), using, with one exception, the bond moments of Ref. 19. In this reference, no value for the C−P bond moment is given. In our computations this bond moment was arbitrarily assigned a value of 0.0 D, because the electronegativity values of carbon and phosphorous are fairly similar.

A series of relatively strong lines, the *a*-type *R*-branch high-$K_1\neq1$ pile-ups, separated by almost exactly $B+C$ was therefore expected to occur for the heavy-atom *anti* conformation V. This simple series was immediately identified. The K_{-1} pair of lines were then assigned after some searching as were a few other low K_{-1}-transitions. The spectrum is shown in Table 1, which contains 17 well-resolved low K_{-1}-transitions used to derive the spectroscopic constants presented in Table 2. A large correlation matrix element of −0.895 was found to exist between Δ_J and A_0.

The low K_{-1}-transitions were too weak to allow quantitative Stark effect studies to be made both for this conformation as well as for the two further assigned rotamers. Unfortunately, no dipole moments could thus be determined.

The A_0 rotational constant is not accurately determined as can be seen in Table 2. Identification of *b*-type transitions would have produced a much more accurate value for this constant.

Table 2. Spectroscopic constants[a] of the ground vibrational state of conformation V of $NCCH_2CH_2PH_2$.

Root-mean-square (MHz)	0.104
A_0 (MHz)	22607(117)
B_0 (MHz)	1448.0610(67)
C_0 (MHz)	1400.3103(64)
Δ_J (kHz)[b]	0.190(26)
Δ_{JK}(kHz)[b]	−4.0(20)
κ[c]	−0.9955
$I_a+I_b-I_c$ (10^{-20} u m^2)	10.45(12)

[a] Uncertainties represent one standard deviation. [b] Further centrifugal distortion constants kept at zero in the least squares fit. [c] Ray's asymmetry parameter.[18] [d] Conversion factor 505376×10^{-20} u m^2 MHz.

Searches were made for the strongest of the low-J b-type lines, but none were found. The above-mentioned bond moment computations predict that μ_a is roughly twice as large as μ_b. The b-type lines should thus be very weak, and this is assumed to be the reason why they were not identified.

The rotational constants predicted for IV and V were quite similar as were the a-axis dipole moment components for each of these conformations. With no isotopic species studied and no dipole moment determined, there are three reasons why the spectrum of Table 1 is attributed to V and not to IV. Firstly, $I_a+I_b-I_c=10.45(11)\times10^{-20}$ u m^2. This is almost the same as $I_a+I_b-I_c=10.56\times10^{-20}$ u m^2 found for the corresponding conformation of $CH_3CH_2PH_2$.[17] Secondly, the structure calculations described below reproduce the B_0 and C_0 rotational constants satisfactorily. Thirdly, V is more stable than IV by 3.0(15) kJ/mol (see section on energy difference determination). This is close to 2.3(12) kJ/mol found for the corresponding conformational equilibrium of $CH_3CH_2PH_2$.[17]

Vibrationally excited states of V. The ground vibrational state spectrum was accompanied by a relatively strong satellite spectrum presumably belonging to vibrationally excited states of V. These spectral features were similar to those observed for the *anti* II form of $NCCH_2CH_2SH$,[16] as expected. Due to low intensities, only the high-K_{-1} pile-ups were assigned. Four such lumps of lines were identified; three of which presumably belong to successively excited states of the C−C torsional mode. $B+C\approx2853.35(5)$ MHz for the first excited state of the C−C torsional frequency; $B+C\approx2858.22(5)$ MHz for the second; and $B+C\approx2863.18(7)$ MHz for the third vibrationally excited state of this mode. The fact that $B+C$ increases almost linearly upon excitation is typical for a harmonic mode.

The intensity of the first excited state of the C−C torsional frequency is roughly 50 % of that of the ground state at −10 °C as judged by the high-K_{-1} pile-ups. The C−C torsional frequency is then calculated to be *ca.* 130 cm^{-1} which is similar to 121(20) cm^{-1} found for the correspond-

Table 3. Microwave spectrum of the ground vibrational state of conformation IV of $NCCH_2CH_2PH_2$.

Transition	Observed frequency[a] (MHz)	Obs.-calc. frequency (MHz)	Centrifugal distortion (MHz)
$7\rightarrow8^b$	22957.48	–	−0.45
$8\rightarrow9^b$	25827.22	–	−0.64
$9\rightarrow10^b$	28697.12	–	−0.88
$10\rightarrow11^b$	31567.87	–	−1.17
$11\rightarrow12^b$	34436.64	–	−1.53
$12\rightarrow13^b$	37307.69	–	−1.93
$7_{1,6}\rightarrow8_{1,7}$	23152.63	−0.16	−0.45
$8_{1,7}\rightarrow9_{1,8}$	26046.47	0.26	−0.64
$9_{1,8}\rightarrow10_{1,9}$	28939.26	−0.13	−0.88
$10_{1,9}\rightarrow11_{1,10}$	31832.45	0.15	−1.17
$11_{1,10}\rightarrow12_{1,11}$	34724.79	−0.12	−1.52

[a] ±0.15 MHz. [b] Centre frequencies of high-K_{-1}-pile-ups.

ing vibrational mode of $NCCH_2CH_2SH$.[16]

The fourth identified vibrationally excited state was found to have $B+C\approx2852.01(10)$ MHz. Its intensity is roughly 30 % of that of the ground state. This corresponds to a vibrational frequency of *ca.* 200 cm^{-1}. This might be the C–P torsional frequency, or, perhaps, a low-frequency bending mode.

Assignment of conformation IV. The rotational constants predicted for the heavy-atom *anti* conformation IV were quite similar to those predicted for V. The dipole moment components were predicted in the same manner as reported above to be $\mu_a=3.5$ D, $\mu_b=0.8$ D and $\mu_c=0.3$ D, respectively. A series of *a*-type *R*-branch high-K_{-1} pile-ups similar to those found for V was therefore expected to occur for conformation IV and predicted to lie close to the lines identified for the former rotamer.

A series of high-K_{-1} pile-ups with $B+C\approx2869.7$ MHz was noted at the same time as V was assigned. It is most unlikely that this series is a vibrationally excited state of V, because this would have required an enormous – and highly unexpected – vibrational amplitude. Rather, it is assigned as belonging to the heavy-atom *anti* conformation IV (see Fig. 1). The intensity of this series is roughly 50 % of the corresponding series of V described above. The $J_{1,J}\rightarrow J+1_{1,J}$ series falling at higher frequencies than the $K_{-1}\neq1$ pile-ups was identified (Table 3). These transitions are quite weak. Unfortunately, only a few more low-K_{-1} transitions could be tentatively assigned due to the fact that they are weak and fall in regions where overlapping lines often occur. Use of the $K_{-1}\neq1$ pile-up frequencies (Table 3) with the $J_{1,J}\rightarrow J+1_{1,J}$ series was therefore made in order to calculate the spectroscopic constants of conformation IV which appear in Table 4. The A_0 rotational constant is quite inaccurately determined, whereas accurate values were obtained for B_0 and C_0, as can be seen from this table.

Table 4. Spectroscopic constants [a] of the ground vibrational state of conformation IV of $NCCH_2CH_2PH_2$.

Root-mean-square (MHz)	0.187
A_0 (MHz)	23271(1274)
B_0 (MHz)	1459.523(31)
C_0 (MHz)	1410.162(43)
Δ_J (kHz) [b]	0.220(42)
κ [c]	−0.9955

[a,b,c] Comments as for Table 2.

The bond moment calculations described above predict μ_a to be much larger than the two other dipole moment components. No search was made for the *b*- or *c*-type lines, because the *a*-type lines themselves are so weak.

There are two equivalent, mirror image forms of IV. Tunneling resulting in large splittings might thus be expected for the *c*-type transitions. Much smaller splittings might perhaps occur for the *a*- and *b*-type lines. No such splittings were observed for the identified *a*-type transitions. A similar finding was also made for the *a*-type lines of the *gauche* form of $CH_3CH_2PH_2$.[17] (However, some low-*J* *b*-type transitions of $CH_3CH_2PH_2$ were found to be split by a small amount).

The high-K_{-1} pile-ups of one vibrationally excited state were tentatively assigned. $B+C\approx2875.95(15)$ MHz was determined for this mode which is presumed to be the first excited C–C torsional mode for similar reasons as described for the corresponding mode of V.

Assignment of conformation II. After the completion of the assignments of conformations IV and V, it became clear that most of the strongest lines of the spectrum could in no way be ascribed to any one of these two rotamers. The heavy-atom *gauche* conformations I and/or II (see Fig. 1) were therefore suspected of producing these so-far unidentified transitions. Conformation III might also be present, but this rotamer was not assumed to be so energetically favoured as either I or II, because III is not capable of forming weak internal hydrogen bonds.

Moreover, II was assumed to be somewhat more stable than I because it can be produced by a rotation of about 120° from the more stable V conformation, whereas I is similarly formed from the less stable IV. As discussed below, the hydrogen-bonding conditions of II also appear to be a bit more favourable than those of I, and this was another reason why searches were next made for conformation II.

The dipole moment components of II were predicted to be $\mu_a=1.90$, $\mu_b=3.1$ D and $\mu_c=0.3$ D, respectively, using the same procedure as above. In the case of $NCCH_2CH_2SH$,[16] a CCCS dihedral angle of 65(3)° from *syn* was found for

Table 5. Microwave spectrum of the ground vibrational state of conformation II of $NCCH_2CH_2PH_2$.

Transition	Observed frequency[a] (MHz)	Obs.-calc. frequency (MHz)	Centrifugal distortion (MHz)
a-type			
$6_{1,6}\rightarrow 7_{1,7}$	27292.11	0.06	−1.19
$6_{1,5}\rightarrow 7_{1,6}$	29930.67	0.14	−2.75
$7_{1,7}\rightarrow 8_{1,8}$	31119.86	0.09	−1.78
$7_{0,7}\rightarrow 8_{0,8}$	31617.68	0.00	−1.96
$7_{2,6}\rightarrow 8_{2,7}$	32760.28	−0.10	−2.42
$7_{1,6}\rightarrow 8_{1,7}$	34065.30	−0.14	−3.94
$8_{1,8}\rightarrow 9_{1,9}$	34928.96	0.10	−2.50
b-type			
$5_{0,5}\rightarrow 6_{1,6}$	26585.58	0.11	−0.01
$5_{1,5}\rightarrow 6_{0,6}$	20950.73	−0.07	−1.76
$6_{0,6}\rightarrow 7_{1,7}$	29785.47	−0.12	−0.17
$6_{1,6}\rightarrow 7_{0,7}$	25386.31	−0.11	−2.48
$7_{0,7}\rightarrow 8_{1,8}$	33025.50	0.10	−0.49
$8_{0,8}\rightarrow 9_{1,9}$	36336.43	−0.16	−1.03
$8_{1,8}\rightarrow 9_{0,9}$	33918.75	0.12	−4.04
$6_{2,4}\rightarrow 6_{3,3}$	26515.14	0.02	1.13
$8_{2,5}\rightarrow 8_{3,5}$	25089.53	0.01	4.60
$9_{1,9}\rightarrow 9_{2,8}$	25604.78	−0.07	−2.04
$10_{0,10}\rightarrow 10_{1,9}$	27635.03	0.02	−3.59
$10_{2,9}\rightarrow 10_{3,8}$	29852.08	−0.03	1.50
$12_{2,10}\rightarrow 12_{3,9}$	21501.25	0.10	11.66
$13_{0,13}\rightarrow 13_{1,12}$	31209.16	0.08	−22.76
$13_{2,12}\rightarrow 13_{3,11}$	33257.46	−0.02	−2.98
$14_{1,13}\rightarrow 14_{2,12}$	22997.94	−0.09	−27.16
$14_{3,11}\rightarrow 14_{4,10}$	33618.21	0.16	28.52
$15_{2,13}\rightarrow 15_{3,12}$	21166.59	0.14	1.75
$16_{2,13}\rightarrow 16_{3,13}$	21952.00	0.03	−7.85
$17_{1,16}\rightarrow 17_{2,15}$	33032.92	0.17	−61.55
$17_{3,14}\rightarrow 17_{4,13}$	29669.35	−0.18	44.35
$18_{2,16}\rightarrow 18_{3,15}$	25119.16	0.12	−39.71
$19_{2,17}\rightarrow 19_{3,16}$	27509.02	−0.06	−62.05
$19_{3,16}\rightarrow 19_{4,15}$	27876.98	−0.12	38.05
$21_{2,19}\rightarrow 21_{3,18}$	33707.38	−0.10	−115.54
$21_{3,18}\rightarrow 21_{4,17}$	27761.81	0.10	6.22
$23_{3,20}\rightarrow 23_{4,19}$	29868.71	0.05	−57.99
$24_{3,21}\rightarrow 24_{4,20}$	31826.03	−0.08	−102.65
$24_{4,20}\rightarrow 24_{5,19}$	35446.98	−0.10	114.82
$25_{3,22}\rightarrow 25_{4,21}$	34371.28	0.11	−154.30
$25_{4,21}\rightarrow 25_{5,20}$	34503.24	0.05	96.29
$26_{4,22}\rightarrow 26_{5,21}$	34040.82	0.01	63.88
$27_{4,23}\rightarrow 27_{5,22}$	34143.58	−0.08	16.50
$28_{4,24}\rightarrow 28_{5,23}$	34870.36	0.11	−46.31
$29_{4,25}\rightarrow 29_{5,24}$	36253.09	−0.05	−124.31

[a] ±0.10 MHz.

Table 6. Spectroscopic constants[a] of conformation II of $NCCH_2CH_2PH_2$.

Vibrational state	Ground	First ex. C–C-torsion
No. of transitions	66	46
Root-mean-square (MHz)	0.098	0.111
A_v (MHz)	7555.255(11)	7612.678(14)
B_v (MHz)	2257.9275(65)	2250.909(10)
C_v (MHz)	1868.7073(63)	1864.1739(98)
Δ_J (kHz)	1.837(46)	2.051(66)
Δ_{JK} (kHz)	−13.866(63)	−15.783(80)
Δ_K (kHz)	36.0(10)	55.9(11)
δ_J (kHz)	0.5908(14)	0.5829(21)
δ_K (kHz)	2.983(65)	4.47(10)

[a] Comments as for Table 2.

the intramolecularly hydrogen–bonded conformation. The same value was used for the CCCP dihedral angle to predict the rotational constants of this conformation.

The *b*-type *Q*-branch $K_{-1}=2\rightarrow3$ series with *J* between 15 and 20 was first found. The remainder of strong *b*-type *Q*-branch transitions, as well as the weaker *a*- and *b*-type *R*-branch lines with $J<11$ were then readily assigned. No *c*-type lines were seen. A total of about 70 transitions were measured; 42 of which are listed in Table 5.* The spectroscopic constants derived from 66 lines are shown in Table 6. A large number of high-*J*-, *P*- and *R*-branch *b*-type lines occur in the investigated spectral region, but they are so weak that no assignments could be made.

Vibrationally excited state of II. 46 *b*-type transitions of what is presumed to be the first excited state of the C–C torsional mode of II were measured as indicated in Table 6. The changes of the rotational constants upon excitation are similar to what was observed for the corresponding mode of $NCCH_2CH_2SH$.[16]

Relative intensity measurements yielded 105(30) cm^{-1} for this C–C torsional mode, similar to 118(20) cm^{-1} found for the corresponding frequency of $NCCH_2CH_2SH$. A rough diagonal force field (Table 7) was assumed for II in order to calculate the C–C torsional frequency utilizing the quartic centrifugal distortion constants in the manner described previously.[20] A frequency of 107 cm^{-1} was found, as compared to 105(30) cm^{-1} obtained by relative intensity measurements. It is difficult to estimate uncer-

Table 7. Assumed diagonal force field,[a] centrifugal distortion constants and torsional frequency of conformation II of $NCCH_2CH_2PH_2$.

Stretching (10^2 N m^{-1})			
C≡N	17.4	H_2C–CH_2	4.6
C–CN	5.5	C–P	1.7
P–H	3.5	C–H	4.8
Bending (aJ rad^{-2})			
P–C–C	1.0	C–C≡N	0.16
P–C–H	0.76	H–C–H	0.50
C–P–H	0.58	H–C–CN	0.67
H–P–H	0.45	C–C–H	0.61
C–C–C	1.1		
Torsion (aJ rad^{-2})			
C–P	0.25		
C–C	0.346[b]		

Centrifugal distortion constants (kHz)

	Obs.	Calc.
Δ_J	1.837	1.924
Δ_{JK}	−13.86	−12.59
Δ_K	36.0	36.4
δ_J	0.5908	0.5301
δ	2.983	3.149

C–C torsional frequency (cm^{-1})
From force-field calculations 107(10)[b]
Relative intensity 108(30)

[a] See text. [b] Obtained from least-squares fit.

* The complete spectra of the ground and the first excited state of conformation II are available from the authors upon request, or from the Molecular Spectra Data Center, National Bureau of Standards, Bld. 221, Rno. B 265, Washington D.C. 20234, U.S.A., where they have been deposited.

tainty limits for the computed value, but ± 10 cm^{-1} appears to be reasonable. All five quartic centrifugal constants are fairly well reproduced in the computations as can be seen in Table 7.

Further vibrationally excited states were searched for, but not assigned presumably because they are relatively weak and also involve high-J with significant centrifugal distortions.

Searches for further conformations. The assignments made as described above include all the strongest lines of the spectrum. However, there remained a few lines whose intensities at most were approximately 1/3 of the strongest transitions of II. In addition, a rich background of weaker and much weaker lines remained unaccounted for.

The existence of I seemed quite probable, and attempts were now made to find this conformation. Its principal inertial axes dipole moment components were predicted in the same manner as above as μ_a=2.3 D, μ_b=3.1 D and μ_c=0.2 D, respectively. The CCCP dihedral angle was guessed to be close to 65° from *syn* and the CCP angle assumed to be 110° in the predictions of the rotational constants. No *a*- type *R*-branch lines were found, and none of the relatively strong *b*-type *Q*-branch transitions were located, despite quite considerable efforts made to this end.

The unassigned lines need not belong to I. They could belong to unidentified vibrationally excited states of II, − which is considered to be quite probable, at least for many of them − or impurities. Their intensities make it possible to estimate a minimum energy difference between I and any further forms. Since the strongest unidentified lines possess roughly 1/3 of the intensity of the strongest transition of II, conformation II should be at least about $RT \ln 3 \approx 2$ kJ/mol more stable than I, if it is assumed that the dipole moment components are similar, which seems reasonable.

Energy difference between II, IV *and* V. Unfortunately, the dipole moments of the three conformations assigned in this work could not be determined. This precludes the determination of accurate energy differences between them. The calculated dipole moments given above had to be used in order to derive an energy difference.

Because the K_{-1}=1 lines of IV are so weak, the intensities of the K_{-1}-pile-ups of IV were used and compared to the corresponding pile-ups of V. K_{-1}=1 or K_{-1}=0 lines of V were compared to *b*-type *Q*-branch lines of conformation II. Moreover, the statistical weight of II and IV was assumed to be twice that of V.

Conformation II was thus found to be the most stable. It is more stable than V by 0.3 kJ/mol. The error limit is liberally estimated to be ± 2 kJ/mol. V is more stable than IV by 3 kJ/mol with an uncertainty of ± 2 kJ/mol. Any further form of the molecule, such as for example conformation I or III, is less stable than II by at least 2 kJ/mol.

Structure. As only one isotopic species has been studied, no complete structure can be calculated for any one of the three rotamers assigned in this work. Restrictions have to be made. In the cases of IV and V, only the CCP angle was fitted, because the rotational constants strongly depend on this angle and because it is prone to change from one conformation to another as evidenced for $CH_3CH_2PH_2$.[17]

The CCP angles of IV and V were fitted in steps of 0.5° to the *B* and *C* rotational constants. Smaller steps were not considered to be warranted in view of the fact that all further structural parameters were kept fixed at the values shown in Table 8. The fixed structural parameters were selected from recent, accurate studies of related compounds. The C−C≡N angle was assumed to be exactly 180°, although it is realized that small deviations from this have been observed.

Good fits were obtained for both conformations IV and V as indicated in Table 8. The CCP angle was found to be 109.0° in IV and 114.0° in V. Error limits are estimated to be ± 1.5° in both these cases, taking into consideration the inherent uncertainties of the assumed structural parameters. It is reassuring to note that 109.0(15)° found for IV and 114.0(15)° found for V are close to 110.1(2) and 115.2(2)°, respectively, determined for CCP angles of the two corresponding conformations of $CH_3CH_2PH_2$[17] as expected.

The CCP angle as well as the CCCP dihedral angle were fitted to all three rotational constants in steps of 0.5 and 1°, respectively, in the case of conformation II. The CCP angle was found to be 117.0(15)° and the CCCP dihedral angle to be 66(3)°. The fit is again good as can be seen in Table 8. The uncertainty limits were estimated in the same manner as described above.

The mass of the phosphino group hydrogen

Table 8. Plausible molecular structure[a] (bond lengths in pm; angles in degrees) of conformations II, IV and V of $NCCH_2CH_2PH_2$.

Structural parameters kept fixed for II, IV and V			
C–P	188.0	∠CCN	180.00
C≡N	115.7	∠CCC	110.50
C–C	153.0	∠CPH	95.50
C–CN	147.4	∠HPH	93.40
P–H	141.4	∠CCH	109.48
C–H	109.3	∠HCH	109.48
Fitted CCP angle for IV			109.0(15)
Fitted CCP angle for V			114.0(15)
Fitted CCP angle for II			117.0(15)
Fitted CCCP dihedral angle for II from *syn*			66(3)
Rotational constants (MHz)			
Conformation IV			
	Obs.	Calc.	Diff. (%)
A_0	23271(1274)	22912	–
B_0	1459.523(31)	1458.34	0.08
C_0	1410.162(43)	1410.39	0.02
Conformation V			
	Obs.	Calc.	Diff. (%)
A_0	22607(117)	22681	0.32
B_0	1448.0610(67)	1446.48	0.11
C_0	1400.3103(64)	1400.04	0.02
Conformation II			
	Obs.	Calc.	Diff.(%)
A_0	7555.255(11)	7537.47	0.23
B_0	2257.9275(65)	2253.593	0.19
C_0	1868.7073(63)	1870.221	0.08
Hydrogen bond parameters			
$P\cdots C_N$	335	$P\cdots N$	406
$C\cdots H_P$	270	$N\cdots H_P$	305
∠P–H···C	105	∠P–H···N	127
∠C≡N, P–H[b]	14.2		
Sum of van der Waals radii[c]			
C···P	360	H···C[d]	290

[a] See text. [b] Angle between C≡N bond and P–H bond involved in hydrogen bonding. [c] Taken from Ref. 21. [d] van der Waals radius of carbon assumed to be 170 pm as for aromatic carbon atoms.

atoms constitute only about 2 % of the mass of the entire 3-phosphinopropionitrile molecule. Without making isotopic substitutions in the phosphino group, one cannot discriminate between the three heavy-atom *gauche* conformations I, II, and III of Fig. 1 using only the rotational constants. Exploratory fits of the CCP angle and the CCCP dihedral angle were made for I and III. The results were ∠114.5(15)° and ∠CCCP=66(3)° for I, and ∠CCP=114.5(15)° and ∠CCCP=63(3)° for III, respectively. These two fits were insignificantly different from that of II (Table 8). This was, of course, expected.

However, no internal hydrogen bond is possible for conformation III. Moreover, the exploratory fit revealed that the hydrogen bond parameters of I would be less favourable than those of II which appear in Table 8. This is caused by the fact that the CPH and HPH angles both are more than 10° less than the dihedral angle. In addition, the phosphino group seems to prefer the conformation present in II as already noted above. Confusion of conformation II with either I or III is thus considered to be unlikely, although it cannot be completely ruled out.

DISCUSSION

3-Phosphinopropionitrile takes the II conformation as its most stable rotamer. This conformer is presumably stabilized by a weak intramolecular hydrogen bond formed between the phosphino group hydrogen atom and the π-electrons of the cyano group. The hydrogen bond is characterized by having the $H\cdots C_N$ distance about 20 pm shorter than the sum of the van der Waals radii of aromatic carbon and hydrogen,[21] and a $P-H\cdots C_N$ angle of about 105° (Table 8). Any covalent interaction of this bond must thus be marginal. Electrostatic interaction between the P–H and C≡N bonds is, however, favourable as the two bonds are approximately 14° from being parallel. The weak intramolecular hydrogen bond is thus mainly electrostatic in origin.

The fact that the phosphino and cyano groups are capable of interacting in a hydrogen-bonding-like manner parallels the finding made for mercapto and cyano groups as exemplified by $NCCH_2CH_2SH$.[16] The interactions seem to be of similar strengths in both $NCCH_2CH_2PH_2$ and $NCCH_2CH_2SH$. It would be interesting to see if this holds also for other examples.

Finally, ethylphosphines seem to prefer to have the phosphino group in a conformation similar to that of II and V as shown in the case of

$CH_3CH_2PH_2$,[17] as well as for the title compound. Ethyl thiols too, seem to have a similar propensity for forming HSCC *gauche* conformations as already noted.[16] No explanation can be offered for these tendencies, which are not paralleled by alcohols and amines.

REFERENCES

1. Buckton, K. S. and Azrak, R. G. *J. Chem. Phys. 52* (1970) 5652.
2. a. Azrak, R. G. and Wilson, E. B. *J. Chem. Phys. 52* (1970) 5299.b. Almenningen, A., Fernholt, L. and Kveseth, K. *Acta Chem. Scand. A 31* (1977) 297.
3. a. Marstokk, K.-M. and Møllendal, H. *J. Mol. Struct. 22* (1974) 301; b. Walder, E., Bauder, A. and Günthard, H. H. *Chem. Phys. 51* (1980) 223; c. Caminati, W. and Corbelli, G. *J. Mol. Spectrosc. 90* (1981) 572.
4. a. Penn, R. E. and Curl, R. F. *J. Chem. Phys. 55* (1971) 651; b. Penn, R. E. and Olsen, R. J. *J. Mol. Spectrosc. 62* (1976) 423.
5. Sung, E. M. and Harmony, M. D. *J. Am. Chem. Soc. 99* (1977) 5603.
6. Marstokk, K.-M. and Møllendal, H. *Acta Chem. Scand. A 35* (1981) 395.
7. Szalanski, L. B. and Ford, R. G. *J. Mol. Spectrosc. 54* (1975) 148.
8. a. Buckley, P. and Brochu, M. *Can. J. Chem. 50* (1972) 1149; b. Caminati, W. and Wilson, E. B. *J. Mol. Spectrosc. 81* (1980) 356.
9. Penn, R. E. and Buxton, L. W. *J. Mol. Spectrosc. 56* (1975) 229.
10. Penn, R. E. and Birkenmeier, J. A. *J. Mol. Spectrosc. 62* (1976) 416.
11. Marstokk, K.-M. and Møllendal, H. *Acta Chem. Scand. A 34* (1980) 15.
12. Marstokk, K.-M. and Møllendal, H. *J. Mol. Struct. 49* (1978) 221.
13. Braathen, O.-A., Marstokk, K.-M. and Møllendal, H. *Acta Chem. Scand. A 37* (1983) 493.
14. Caminati, W. and Wilson, E. B. *J. Mol. Spectrosc. 81* (1980) 356.
15. Nandi, R. N., Boland, M. F. and Harmony, M. D. *J. Mol. Spectrosc. 92* (1982) 419.
16. Marstokk, K.-M. and Møllendal, H. *Acta Chem. Scand. A 37* (1983) 477.
17. Durig, J. R. and Cox, A. W., Jr. *J. Chem. Phys. 64* (1976) 1930.
18. Gordy, W. and Cook, R. L. *Microwave Molecular Spectra*, Wiley, New York 1970, p. 163.
19. Smyth, C. P. *Dielectric Behavior and Structure*, Mc Graw-Hill, New York 1955, p. 244.
20. Braathen, O.-A., Marstokk, K.-M. and Møllendal, H. *Acta Chem. Scand. A 36* (1982) 173.
21. Pauling, L. *The Nature of the Chemical Bond*, 3rd Ed., Cornell University Press, New York 1960, p. 260.

Received February 21, 1983.

Acta Chemica Scandinavica A 37 (1983) 765–769

Synthesis and X-Ray Crystal Structure of Dichlorobis-(nicotinic acid *N*-oxide)copper(II)

HILKKA KNUUTTILA

Department of Chemistry, University of Jyväskylä, SF-40100 Jyväskylä 10, Finland

A new copper(II) complex of nicotinic acid *N*-oxide (*N*-nicOH), dichlorobis(nicotinic acid *N*-oxide)copper(II), $[CuCl_2(N)\text{-nicOH})_2]$, has been prepared. The crystal and molecular structure has been determined by X-ray techniques and refined to a final *R*-value of 0.050.

The complex forms as one of the synthesis products of $CuCl_2 \cdot 2H_2O$ and nicotinic acid *N*-oxide in ethanolic solution. The space group is $P2_1/c$, with $Z=2$ and cell dimensions are $a=6.019(4)$, $b=13.155(11)$, $c=10.418(8)$ Å and $\beta=115.80(5)°$. Two chloride ligands are joined to the copper(II) ion, along with two nicotinic acid *N*-oxide ligands through the *N*-oxide oxygen atom in a distorted square planar arrangement. The coordination sphere of copper(II) ion is completed by two carboxylic oxygen atoms of adjacent molecules at very long distances [3.082(4)Å].

Several 3*d* metal complexes of nicotinic acid *N*-oxides have been synthesized from aqueous solution and characterized.[1–3] Recently, we determined the structures of two polymeric copper(II)[4,5] and the isomorphous cobalt(II) and nickel(II)[6] complexes of nicotinic acid *N*-oxide by X-ray diffraction analysis.

Metal complexes of monocarboxylic acid *N*-oxides have also been prepared in non-aqueous conditions. The magnetic moment of the complex of copper(II) chloride with pyridine *N*-oxide, tetrachlorobis-μ-(pyridine *N*-oxide)dicopper(II), was observed to be subnormal (0.85 B.M.).[7] In the structure copper(II) ions are bridged by oxygen atoms of the pyridine *N*-oxides.[8] Subnormal magnetic moments were also observed in dimeric complexes of copper(II) halides and substituted pyridine *N*-oxide, including a copper(II) complex of nicotinic acid *N*-oxide.[9] In ethanolic solution, prepared copper(II) halide complexes of pyridine *N*-oxides with an electron-withdrawing substituent such as COOH produce an even larger demagnetization than the parent Cu(II) complex with pyridine *N*-oxide.[10]

Low hydrates of 3*d* metal complexes with nicotinic and isonicotinic acid *N*-oxides have been prepared from *N,N,*-dimethylformamide.[11] Copper(II) chloride [12] and 3*d* metal perchlorate [13] adducts have been synthesized from ethanol–triethylorthoformate solution.

In this paper we present the structure of a new complex of copper(II) chloride and nicotinic acid *N*-oxide prepared from ethanolic solution.

EXPERIMENTAL

Preparation of the complex. Copper(II) chloride dihydrate (0.01 mol) dissolved with ethanol was added to a suspension of nicotinic acid *N*-oxide (0.01 mol) and ethanol. The mixture was refluxed for 2–3 h on a hot-plate. A few drops of 2 M HCl were added to the clear solution, which was then left to stand at room temperature. Two kinds of crystals separated from the solution: as the main product yellow needle-like crystals, too tiny for X-ray structure analysis, and after several months a few green crystals corresponding to the formula $CuCl_2(N\text{-nicOH})_2$, whose structure could be determined.

Data collection and structure determination. The crystal and refinement data are given in Table 1. The crystal and intensity data were measured on a Syntex $P2_1$ four-circle diffracto-

0302-4377/83 $2.50

Table 1. Crystal and refinement data of $[CuCl_2(N\text{-nicOH})_2]$.

F. W.	412.67
Space group	$P2_1/c$
a (Å)	6.019(4)
b	13.155(11)
c	10.418(8)
β (°)	115.80(5)
Z	2
V (Å^3)	742.7
Collection mode	$\theta/2\theta$
Radiation	Mo$K\alpha$ (λ=0.71069 Å)
Scan range	$4°<2\theta<55°$
Scan rate (°min^{-1})	1.0 → 15.0
Refl. meas.	2000
obs. ($I>2.5\sigma(I)$)	1107
$F(000)$	410
$R=(\Sigma\|\|F_o\|-\|F_c\|\|/\Sigma\|F_o\|)$	0.050

meter using graphite monochromatized Mo$K\alpha$ radiation. The unit cell parameters were calculated by least-squares refinement of 15 high order reflections.

Corrections were applied for Lorentz and polarization effects but not for absorption (μ=19.2 cm^{-1}).

The structures were solved by direct methods (positions for copper and chlorine atoms) and Fourier synthesis. Refinement was carried out by block diagonal matrix least-squares calculations with anisotropic temperature factors for all non-hydrogen atoms and isotropic temperature factors for hydrogen atoms located by difference Fourier syntheses. The final R-value with unit weights was 0.050. The final atomic coordinates and the thermal parameters, $U_{eq}[=\frac{1}{3}\times(U_{11}+U_{22}+U_{33})]$, are given in Table 2. Lists of structure factors and anisotropic thermal parameters are available from the author upon request. Programs, computer and sources of scattering factor data are given in Ref. 14.

DISCUSSION

A drawing of the molecular structure is given in Fig. 1 and interatomic distances and angles are given in Table 3. The central copper(II) ion occupying the special position ($\frac{1}{2}$,0,0) of the space group $P2_1/c$ is coordinated to two nicotinic acid N-oxide ligands monodentately through the N-oxide oxygen atom and to two chloride ligands in distorted square planar arrangement. Formally the coordination sphere of Cu(II) ion is completed by two oxygen atoms [O(3)] of the carboxylic groups of adjacent molecules. This Cu(1)–O(3) distance, 3.082(4) Å, is rather long, 0.4 Å greater than the sum of the corresponding

Table 2. Final positional parameters and thermal parameters, $U_{eq}(\times10^3)$ for non-hydrogen atoms and U_{iso} ($\times10^2$) (Å^2) for hydrogen atoms.

Atom	x	y	z	U_{eq}
Cu(1)	0.5000	0.0000	0.0000	31.0(3)
Cl(1)	0.6979(2)	0.0720(1)	0.2153(1)	40.9(6)
O(1)	0.2841(5)	−0.0802(2)	0.0580(3)	41(2)
O(2)	0.9304(6)	−0.2855(2)	0.4053(3)	59(2)
O(3)	0.8281(6)	−0.3086(3)	0.5840(3)	62(2)
C(1)	0.5419(8)	−0.1640(3)	0.2665(4)	35(2)
C(2)	0.6021(7)	−0.1907(3)	0.4042(4)	34(2)
C(3)	0.4662(8)	−0.1507(3)	0.4708(4)	43(3)
C(4)	0.2818(8)	−0.0835(3)	0.3995(5)	44(2)
C(5)	0.2233(8)	−0.0584(3)	0.2612(5)	40(2)
C(6)	0.7986(8)	−0.2680(3)	0.4758(4)	42(2)
N(1)	0.3527(6)	−0.1003(3)	0.1974(3)	35(2)
				U_{iso}
H(1)	0.602(9)	−0.182(4)	0.200(5)	8(2)
H(2)	0.531(8)	−0.164(3)	0.568(4)	5(1)
H(3)	0.186(7)	−0.059(3)	0.441(4)	3(1)
H(4)	0.092(9)	−0.015(4)	0.195(5)	8(2)
H(5)	1.035(10)	−0.336(4)	0.451(5)	9((2)

Table 3. Selected bond distances (Å) and bond angles (°) with their standard deviations for $[CuCl_2(N\text{-nicOH})_2]$.

Environment of copper(II)			
Cu(1)–O(1)	1.962(3)	O(1)–Cu(1)–Cl(1)	86.92(8)
Cu(1)–Cl(1)	2.241(1)	Cl(1)–Cu(1)–O(1)	93.08(8)
Cu(1)–O(3)	3.082(4)	O(3)–Cu(1)–Cl(1)	93.74(6)
		O(3)–Cu(1)–Cl(1)	84.34(12)
Pyridine *N*-oxide group			
		Cu(1)–O(1)–N(1)	120.1(2)
N(1)–O(1)	1.352(4)	O(1)–N(1)–C(1)	119.2(4)
N(1)–C(1)	1.343(5)	O(1)–N(1)–C(5)	118.7(3)
N(1)–C(5)	1.342(7)	C(1)–N(1)–C(5)	122.1(4)
C(1)–C(2)	1.365(6)	N(1)–C(1)–C(2)	119.9(4)
C(2)–C(3)	1.386(7)	C(1)–C(2)–C(3)	119.0(4)
C(3)–C(4)	1.359(6)	C(2)–C(3)–C(4)	119.5(4)
C(4)–C(5)	1.367(7)	C(3)–C(4)–C(5)	120.6(5)
Carboxylic acid group			
C(6)–C(2)	1.490(6)	O(2)–C(6)–O(3)	124.9(4)
C(6)–O(2)	1.315(7)	O(2)–C(6)–C(2)	112.4(4)
C(6)–O(3)	1.190(6)	O(3)–C(6)–C(2)	122.6(5)
O(2)–H(5)	0.92(5)		

van der Waals radii, indicating a very weak interaction.

The angle between the coordination plane of the copper(II) ion and pyridine *N*-oxide group is 81.7°.

In the present complex, nicotinic acid *N*-oxide acts as monodentate ligand coordinating only through *N*-oxide oxygen. The Cu–O(*N*-oxide) bond length, 1.962(3) Å, is in good agreement with reported copper–oxygen(*N*-oxide) distan-

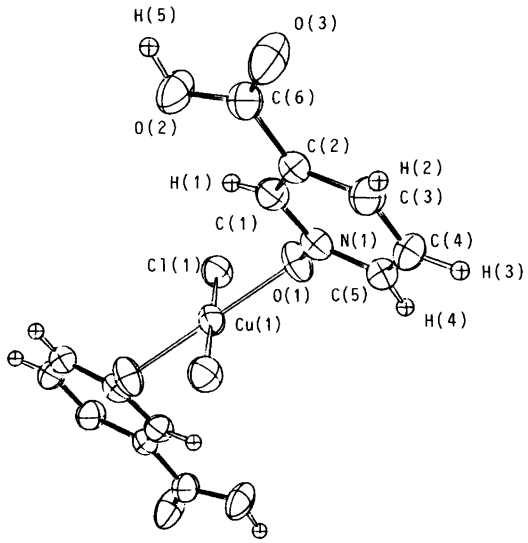

Fig. 1. The labelling and structure of $[CuCl_2(N\text{-nicOH})_2]$. Thermal ellipsoids are drawn to enclose the 50 % probability level.

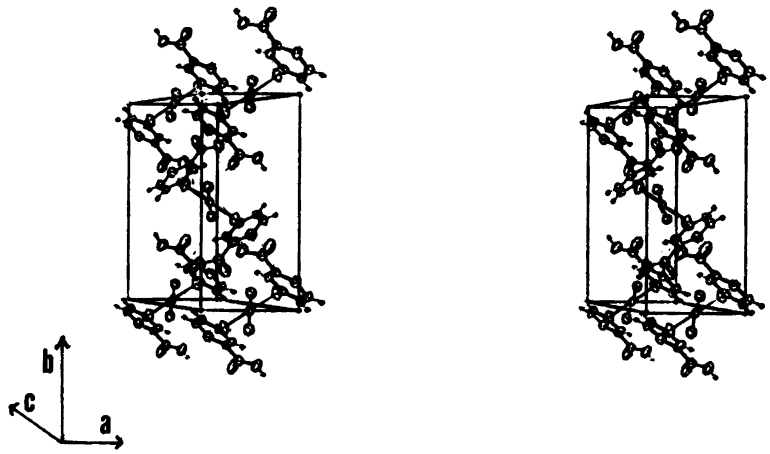

Fig. 2. Stereoview of the packing of $[CuCl_2(N\text{-nicOH})_2]$ within the unit cell.

ces:[15-19,22] 1.97(1) and 1.93(1) Å in dichlorobis(2,6-lutidine *N*-oxide)copper(II), for instance.[15]

In the polymeric copper(II) complexes of nicotinic acid *N*-oxide prepared in aqueous solution, nicotinato *N*-oxide acts as a bidentate ligand coordinating either through both carboxylato oxygen atoms or through one carboxylato oxygen atom and the *N*-oxide oxygen to adjacent copper(II) ions. Polymerization occurs *via* a rather long Cu–O(*N*-oxide) interaction (2.43–2.67 Å).[4,5,23] In the isomorphous cobalt(II) and nickel(II) complexes, tetraaquabis(nicotinato *N*-oxide)cobalt-(II) and -nickel(II), nicotinato *N*-oxide joins monodentately through one carboxylato oxygen atom to the central metal ion.[6]

The Cu–Cl bond distance is 2.241(1) Å. Reported Cu–Cl distances for complexes of pyridine *N*-oxides[15-20] vary widely (2.206–2.955 Å) since the chlorine atom is sometimes coordinated to just one copper and sometimes acts as a bridging atom, in which case one of the Cu–Cl distances may be quite long.

In the carboxylic acid group the C–O distances are C(6)–O(2)(hydroxy) 1.315(7) and C(6)–O(3) 1.190(6) Å and in free nicotinic acid *N*-oxide 1.301(1) and 1.198(1) Å, respectively.[21]

Molecules are held in the crystal lattice by hydrogen bonds between *N*-oxide oxygens and carboxylic OH groups. Distances are O(2)–H(5) 0.915 Å, H(5)...O(1) 1.78(5) Å, O(2)–O(1)* 2.690(4) Å and the angle O(2)–H(5)–O(1) is 171 (5)°. The packing of the molecules is seen in Fig. 2.

*Symmetry operation: $x-1, -y-1/2, z-1/2$.

REFERENCES

1. v. Euler, H., Hasselquist, H. and Heidenberger, O. *Ark. Kemi 13* (1959) 583.
2. Speca, A. N., Gelfand,L. S., Pytlewski, L. L., Owens, C. and Karayannis, N. M. *Inorg. Chem. 15* (1976) 1493.
3. Speca, A. N., Gelfand, L. S., Pytlewski, L. L., Owens, C. and Karayannis, N. M. *J. Inorg. Nucl. Chem. 30* (1977) 537.
4. Knuuttila, H. *Inorg. Chim. Acta 50* (1981) 221.
5. Knuuttila, H. *Inorg. Chim. Acta 69* (1983) 173.
6. Knuuttila, H. *Acta Chem. Scand. A 37* (1983) 697.
7. Quagliano, H. V., Fujita, J., Franz, G., Phillips, D. J., Walmsley, J. A. and Tyree, S. Y. *J. Am. Chem. Soc. 83* (1961) 3770.
8. Schäfer, H. L., Morrow, J. C. and Smith, H. M. *J. Chem. Phys. 42* (1965) 504.
9. Muto, Y., Kato, M., Jonassen, H. B. and Cusachs, L. C. *Bull. Chem. Soc. Jpn. 42* (1969) 417.
10. Muto, Y., Kato, M., Jonassen, H. B. and Ramaswamy, H. N. *Bull. Chem. Soc. Jpn. 40* (1967) 1535.
11. Gelfand, L. S., Pytlewski, L. L., Cosgrove, D. L., Mikulski, C. M., Speca, A. N. and Karayannis, N. M. *Inorg. Chem. Acta 27* (1978) L97.
12. Gelfand, L. S., Pytlewski, L. L., Mikulski, C. M., Speca, A. N. and Karayannis, N. M. *Inorg. Chim. Acta 33* (1979) 265.
13. Gelfand, L. S., Ioconianni, F. J., Pytlewski, L. L., Speca, A. N., Mikulski, C. M. and

Karayannis, N. M. *J. Inorg. Nucl. Chem. 42* (1980) 377.
14. Knuuttila, H. and Knuuttila, P. *Acta Chem. Scand. A 37* (1983) 227.
15. Sager, R. S. and Watson, W. H. *Inorg. Chem. 8* (1969) 308.
16. Sager, R. S. and Watson, W. H. *Inorg. Chem. 7* (1968) 2035.
17. Sager, R. S., Williams, R. J. and Watson, W. H. *Inorg. Chem. 6* (1968) 951.
18. Schäfer, H. L., Morrow, J. C. and Smith, H. M. *J. Chem. Phys. 42* (1965) 504.
19. Sager, R. S., Williams, R. F. and Watson, W. H. *Inorg. Chem. 8* (1969) 694.
20. Williams, R. J., Cromer, D. T. and Watson, W. H. *Acta Crystallogr. B 27* (1972) 1619.
21. Knuuttila, H. and Knuuttila, P. *Unpublished results.*
22. Pavkovic, S. F. and Wille, S. L. *Acta Crystallogr. B 38* (1982) 1605.
23. Knuuttila, H. *Thesis*, University of Jyväskylä, Jyväskylä 1983.

Received February 16, 1983.

Acta Chemica Scandinavica A 37 (1983) 771–776

A Theoretical Investigation of Relative Stabilities and Interconversion Barriers in *gem* Di- and Tetrafluoromethylene Cyclopropane

ANNE SKANCKE and ULF WAHLGREN

Institute of Mathematical and Physical Sciences, P.O.Box 953, N-9001 Tromsø, Norway

Ab initio calculations on the SCF level have been undertaken in order to investigate *gem* di- and tetrafluoromethylene cyclopropane with respect to charge distribution, relative stabilities and interconversion potential barriers to sigmatropic migration. Anticipated geometric trends are reproduced by the calculations, and the relative reactivity characteristics of the different molecules can be interpreted in terms of differences in the charge distributions. For the interconversion reactions, the orbitally allowed transition state for the tetrafluoro substituted species is found to be very high in energy, thus making an orbitally allowed migration unlikely in this case.

Thermodynamic stabilization is normally observed in successive fluorination reactions, for instance eqn. (1).[1]

$$4CH_3F \rightleftharpoons CF_4 + 3CH_4$$
$$\Delta H = -150\ \text{kJ/mol} \qquad (1)$$

In contrast to this, there is an observed kinetic destabilization when fluorine is successively added to a cyclopropane system.[2] Although changes in strain energy of reactants and products seem to explain nicely the thermodynamics of a number of *gem*-difluorocyclopropane reactions,[3] an understanding of the reaction kinetics and mechanisms makes it necessary to study reaction intermediates as well as ground states.

We have in the present work studied some aspects of the reactions (2) and (3).

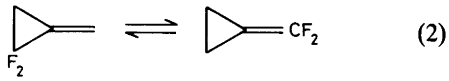

(2)

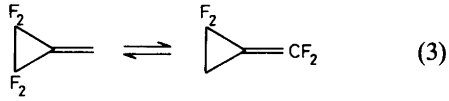

(3)

Ab initio calculations[3] of the reactant and product of eqn. (2) gave as a result a good agreement with the experimental enthalpy difference [H(exp)= −7.9 kJ/mol, E(theor)= −2.6 kJ/mol]. The calculations were carried out with complete geometry optimizations using a 4−21[5] basis set and a final 4−31G basis set at the end point. Our previous experience is that bond length changes are a sensitive measure of the electronic impact of various substituents on the cyclopropane ring.[6–12] Complete geometry optimizations of the reactant of eqn. (3) and the parent methylene cyclopropane are performed on the same level of sophistication as our previously published study of the species in eqn. (2).[3]

We have also carried out calculations of various possible diradical intermediates for reactions (2) and (3). The hydrocarbon analogous rearrangement reaction (4)

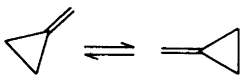

(4)

has been studied theoretically by Hehre *et al.*[13] Since those calculations were carried out at the

0302-4377/83 $2.50

same level of sophistication as ours, they provide an interesting comparison.

The present work includes investigations of the effect of fluorine on the stable species, on the reaction intermediates and various forms of the fluorinated trimethylene methane diradical.

METHODS

The geometry optimizations were carried out at the SCF level using 4−21 basis set[5] using the computer programme TEXAS[14] which calculates the forces on all atoms making possible a simultaneous optimization of all internal coordinates. The gradient method is very convenient for complicated geometry optimizations, and offers a straightforward way to determine molecular structures.

The triplet forms of the diradical were calculated with the Gaussian 76 programme, using an unrestricted Hartree Fock procedure. Standard geometry parameters were employed.

The open shell singlet states deserve some special considerations. For some conformers of the activated states, the two open shells appear in the same symmetry, thus rendering the usual Brillouin theorem (which states that an SCF wave function does not interact with singly excited states) inapplicable. The proper condition is in this case provided by the extended Brillouin theorem,[15] which states that (at self-consistency) the matrix element between the open shell singlet and the difference between the two corresponding closed shell configuration is zero. The matrix element between the open shell wave function and each of the closed shell excitations may, in fact, be quite large, as is the case *e.g.* for some Auger states on water.[16]

Labelling the two open shells a and b, the configuration of interest (only indicating the orbitals a and b) are:

1. $1/\sqrt{2}\,[\{a\bar{b}\}-\{\bar{a}b\}]$
2. $\{a\bar{a}\}$
3. $\{b\bar{b}\}$

It is easily shown that the off diagonal matrix elements between these states are:

$$H_{12}=\sqrt{2}\,F(a^2)_{ab}$$
$$H_{13}=\sqrt{2}\,F(b^2)_{ab}$$
$$H_{23}=K_{ab}$$

where $F(a^2)$ and $F(b^2)$ signify the Fock-operators for the closed shell configurations formed with the canonical orbitals for the open shell state.

All matrix elements needed to calculate proper non-interacting states are thus easily obtained. In the present study the open shell calculations on the open shell singlet states for the difluorinated species were carried out using the restricted OS-SCF method followed by the above described 3×3 CI. The effect of the 3×3 CI was, however, minimal, and no corrections were deemed necessary for the tetra-substituted systems.

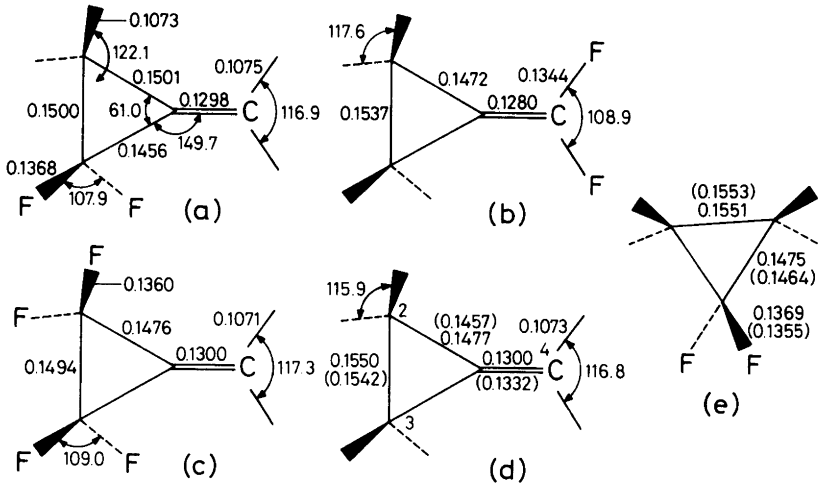

Fig. 1. Results of structure analysis. Distances in nm. See text.

For the latter species, calculations on the singlet form were carried out only on the high symmetry forms. This was decided partly from the results on the difluorinated forms and partly for economic reasons.

RESULTS AND DISCUSSION

(a) *Structure analysis.* We have in a series of articles[6-12] exploited the effect of various substituents upon a cyclopropane ring. For the cases where comparison with experimental structure works was possible, our calculations were generally in good agreement with experiment, *e.g.* for 1,1-difluorocyclopropane, where the main trends of a short C_1-C_2 bond and a long C_2-C_3 bond found in a microwave investigation was reproduced in our calculations. The often reported[17] but perhaps not fully understood shortening of the C–F bond upon successive fluorination was also reproduced in our calculations.

The results of the present calculations are given in Fig. 1, where also our previously reported data for the molecules in reaction (2) and 1,1-difluorocyclopropane[6] are given for comparison.

Experimental values from microwave spectroscopy for methylene cyclopropane and 1,1-difluorocyclopropane are given in parentheses. The agreement is in general satisfactory although for methylene cyclopropane, the calculated differences in bond lengths between the double bond and the C–C bond adjacent to it is somewhat too large.[16] Some of our previous works[7] in this series triggered reinvestigation of microwave work. In these cases, errors had been made in determining the location of the C_1 atom with corresponding errors in the C_1-C_2 and C_1-X distances. The overall size of the molecule had, however, been determined with good precision. In the present case, however, the difference between the calculated and the experimentally determined value of the C_1-C_4 double bond parallels the findings for the double bond in vinylcyclopropane[8] and cyclobutene.[19] The disagreement for methylene cyclopropane seems to reflect a shortcoming in the theoretical work (presumably a basis set deficiency) rather than a misassignment of the experimental spectrum. For the present discussion this is not crucial, since it is the trend in geometry parameters within the series *a–e* that is our prime interest.

Some features may be deduced from Fig. 1:

(1) When *gem*-difluoro or methylene groups are substituents on cyclopropane rings, they have the same ability of shortening the adjacent and lengthening the opposite bond (see *d* and *a*).

(2) When these substituents are simultaneously introduced, they have a nearly additive effect upon ring structure. This is seen in *a* where the C_1-C_2 bond is shortened about twice as much as in *b* and *c*. (The parent cyclopropane has computed C–C bond lengths of 1.5153 Å within the same approximation.) The C_2-C_3 and C_3-C_1 bonds being adjacent to one substituent and opposite to another, have intermediate bond lengths.

A further picture of the electronic distribution of the systems may be achieved by inspection of Table 1 where atomic gross charges are given. Summation of charges of the ring carbons reveals

Table 1. Gross atomic populations, total energies and dipole moments. Basis set 4–31G/ /4–21.[a] Energies in a.u. Dipole moments is debyes.

Gross atom	Molecule a	b	c	d
Cl	6.05	6.13	6.06	6.05
C2	5.26	6.27	5.26	6.31
C3	6.33			
C4	6.34	5.31	6.29	6.38
F	9.41	9.42	9.39	
C1+C2+C3	17.64	18.67	16.58	18.67
E(total)	−352.11522	−352.11622	−549.55566	−154.65886
Dipole	3.3	3.2	4.3	0.3

[a] See Ref. 25 for definition of nomenclature.

that *a* and *c*, both molecules with fluorine on the ring, have considerably less electron density than the hydrocarbon ring. According to Table 1, a whole electron is removed from the ring by introduction of each CF_2 group. The same summation carried out on 1,1-difluorocyclopropane yields a value of 18.25 electrons, but since the calculations on that molecule were carried out using a different basis set, the numbers are not directly comparable.

We believe that this weakening of the ring is essential in explaining the enhanced reaction rates upon successive fluorination. Note that shortened C–C bond distances do not necessarily imply stronger bonds, although this is generally true for open chains.

(b) *Energy considerations.* The total energies given in Table 1 give the energy for the isodesmic reaction

$$2a \rightleftharpoons c+d \qquad \Delta E = +41.72 \text{ kJ/mol}$$

This is a measure of the preference for one or two CF_2 groups in the three-membered ring. This increased strain energy is comparable to the destabilization of 19.2 kJ/mol for monofluorocyclopropane and 41.9 kJ/mol for 1,1-difluorocyclopropane.[3] The latter values were computed by non-geometry optimized 4–31G quality SCF calculations. All these values are consistent with the 19–21 kJ/mol of increased strain energy per fluorine substituent postulated by O'Neal and Benson.[2]

(c) *Reaction intermediates.* Following the calculations by Hehre *et al.*[13] for the corresponding hydrocarbon reaction, we have calculated the stability of a series of possible reaction intermediates. The conformation and spin states of these, along with atomic charges and energy differences compared to corresponding closed rings are shown in Fig. 2.

We have restricted our calculations to diradical intermediates, neglecting possible concerted mechanisms. Because of the size of this problem (46 and 60 electrons for intermediates of *a* and *c* and 24 internal coordinates) we have limited the calculations to standard geometries. For both the di- and tetrasubstituted species the triplet state planar forms are astonishingly low, only about 14.6 kJ/mol above the ring system. This finding is at variance with the results of the hydrocarbon calculation. In the work by Hehre *et al.* the

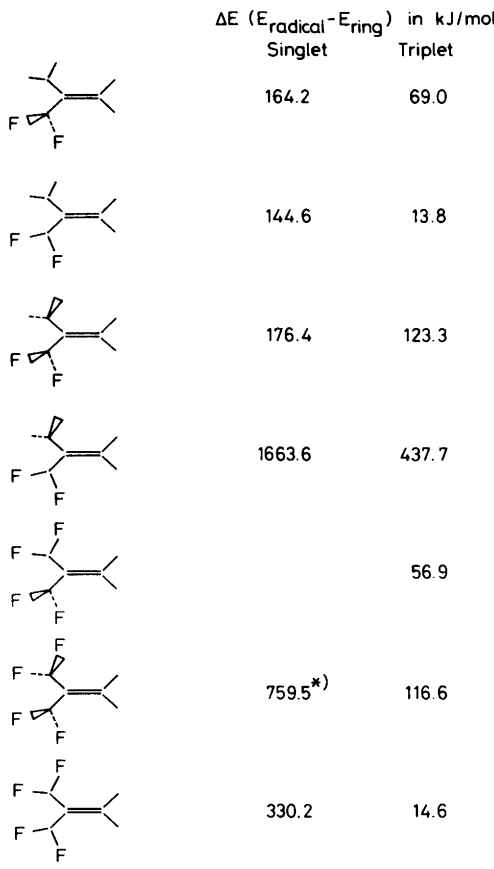

Fig. 2. Energies of various diradical conformers relative to closed ring system. In kJ/mol.

singlet-triplet splitting was found to be only a few kJ/mol and the transition state was found to be a singlet at 186.9 kJ/mol above the ring system. However, a paper by Yarkony and Schaefer on the trimethylene methane diradical predicts the $^3A_2' - {}^1E'$ separation to be 88 kJ/mol on the basis of double zeta quality SCF calculations, and MINDO/2 calculations by Dewar and Wasson[19] predict this energy difference to be about 146 kJ/mol.

As for the singlet forms, we have for the difluorinated species found three close-lying states, the planar form and both forms with orthogonal CF_2 groups, to be of nearly the same energy (144.6, 164.3 and 176.4 kJ/mol above the closed ring form). From an experimental value of

the activation energy[4] of 160±1.6 kJ/mol, it is likely that one of the above-mentioned forms is the reaction intermediate. The level of sophistication of the present calculation and the lack of geometry optimization for the open shell forms makes the proper selection from these forms an uncertain task. It is, however, interesting to note the difference at this point with the above-mentioned results and the results for the hydrocarbon by Hehre. For that higher symmetry species, the energy for the planar form was predicted to be 368 kJ/mol above the ring system. A point of some interest is the small significance of the correction factor for the open shell singlets of a_1 symmetry which were computed to be 22.6 kJ/mol for the perpendicular form of the difluorinated diradical and 0.04 kJ/mol for the planar form. These contributions are included in the energy differences given in Fig. 2.

Inspection of Fig. 2 reveals that the tetrafluorinated species also has low lying triplet states, especially for the planar form, but possesses no low lying singlet states. A kinetic study of the rearrangement reaction (3) gives an energy of activation of 123.7±5 kJ/mol and a relative rate of rearrangement of (3) *vs.* (2) at 150 °C of 7850,[20] whereas at the same temperature the relative rate of reaction (2) *vs.* the hydrocarbon rearrangement is reported to be only 4.4. Although the lower symmetry of the reactant of reaction (2) would lead to a net retardation of (2) compared to (3), this factor could not possibly account for the difference in reaction rates. The experimental kinetic data coupled with the results of the present calculation seem to imply a different reaction mechanism for (3). *A priori* this could be either a concerted type reaction or a "forbidden" crossing to the triplet state. Although we have not attempted to perform calculations of the former, a diradical intermediate does seem to be consistent with both theoretical[13] and experimental[23] findings. The triplet state diradical thus seems to be the most likely candidate to be intermediate of reaction (3). The possibility of a triplet intermediate has been suggested also in an experimental study[23] of analogous systems, although in that case the final products were dimers.

As a final point, we wish to comment on the charge distribution in the open shell forms. This relates to the attention that has been given over the years to the hydrocarbon analogues and which is interestingly summarized in Ref. 20. A key point has been the large positive charge of the central carbon atom which led to its use as a zero point in the definition of the "free valence" concept introduced by Coulson.[24] The numerical value of this was calculated in the previously mentioned paper by Yarkony and Schaefer to be +0.62 el. on the planar form, a value not only reported to be the largest known to a hydrocarbon carbon, but in fact one of the largest encountered on any carbon atom studied by double ζ basis sets. Since it is well known that the carbon in a CF_2 group also bears a highly positive charge (+0.73 el. for 1,1-difluorcyclopropane in Ref. 6) one would assume the fluorinated radicals to be either destabilized or electronically reorganized in order to avoid neighbouring positive charges. From Fig. 2 it is seen that destabilization is clearly not taking place, and a survey of the atomic gross charges for the intermediates gives normal, negative charges ranging from 0.09 el. to 0.20 el. for the central carbon atom for all cases considered.

We wish to stress that we have not tried to determine absolute values of energies with any degree of precision in this work. The present calculations are of a qualitative nature since neither configuration interaction nor geometry optimization have been carried out. However, our prime interest has been to study trends within closely related systems, trends which can withstand a more advanced treatment. An extension of the present work would have to include geometry optimization of the intermediate diradicals, a larger basis set and configuration interaction.

REFERENCES

1. Chambers, R. D. *Fluorine in Organic Chemistry*, Wiley, New York 1973, p. 139.
2. O'Neal, H. E. and Benson, S. W. *J. Phys. Chem. 72* (1968) 1866.
3. Greenberg, A., Liebman, J. F., Dolbier, W. R., Medinger, K. S. and Skancke, A. *Tetrahedron 39* (1983) 1533.
4. Dolbier, W. R., Jr. and Fielder, T. H., Jr. *J. Am. Chem. Soc. 100* (1978) 5577.
5. Pulay, P., Fogarasi, G., Pang, F. and Boggs, J. E. *J. Am. Chem. Soc. 101* (1979) 2550.
6. Skancke, A., Flood, E. and Boggs, J. E. *J. Mol. Struct. 40* (1977) 263.
7. Skancke, A. *J. Mol. Struct. 42* (1977) 235.

8. Skancke, A. and Boggs, J. E. *J. Mol. Struct. 50* (1978) 173.
9. Skancke, A. and Boggs, J. E. *J. Mol. Struct. 51* (1979) 267.
10. Skancke, A. and Boggs, J. E. *Acta Chem. Scand. A 32* (1978) 893.
11. Skancke, A. *Acta Chem. Scand. A 36* (1982) 637.
12. Skancke, A. *Acta Chem. Scand. A 37* (1983) 337.
13. Hehre, W. J., Salem, L. and Wilcott, M. R. *J. Am. Chem. Soc. 96* (1974) 4330.
14. Pulay, P. *Theor. Chim. Acta 50* (1979) 299.
15. Ågren, H., Svensson, S. and Wahlgren, U. *Chem. Phys. Lett. 35* (1975) 336.
16. Levy, B. and Berthier, G. *Int. J. Quantum Chem. 2* (1968) 307. Erratum Ibid *3* (1969) 247.
17. Brockway, L. O. *J. Phys. Chem. 41* (1937) 185; 747.
18. Laurie, V. W., and Stigliani, W. M. *J. Am. Chem. Soc. 92* (1970) 1485.
19. Broch-Mathisen, K. and Skancke, A. *Unpublished data.*
20. Yarkony, D. R. and Schaefer, H. F. *J. Am. Chem. Soc. 96* (1974) 3754.
21. Dewar, M. J. S. and Wasson, J. S. *J. Am. Chem. Soc. 93* (1971) 3081.
22. Dolbier, W. R., Sellers, S. F., Al-Sader, B. H. and Smart, B. E. *J. Am. Chem. Soc. 102* (1980) 5398.
23. Salinaro, R. F., Berson, J. A. *J. Am. Chem. Soc. 101* (1979) 7094.
24. Coulson, C. A. *Valence,* Oxford Univ. Press, 2nd Ed., London, New York 1961, p. 261.
25. Binkley, J. S., Pople, J. A. and Hehre, W. J. *J. Am. Chem. Soc. 102* (1980) 939.

Received February 28, 1983.

Acta Chemica Scandinavica A 37 (1983) 777–785

Coulometric Oxidation of Iodine to Iodine(I)-Bromide with Bromine Generated with Iridium Anode in Hydrogen Bromide Solution

SIGNAR SUNDSTRAND

Department of Inorganic Chemistry, The Royal Institute of Technology, S-100 44 Stockholm, Sweden

Purified iodine has been oxidized to iodine(I)bromide (IBr_2^-) in 4 M HBr medium with constant current coulometry using an iridium anode. With the method described, results may be obtained with an uncertainty not exceeding 0.01 %. In the coulometric titrations the current density was varied between 3 and 40 mA/cm^2, and the sample of iodine between 0.3 and 4 meq. Gran's method was used to evaluate the equivalence points. Their uncertainties were estimated by a method based on the concept of redox buffer capacity. By conventional analysis, using platinum electrodes in hydrogen chloride or hydrogen bromide media, serious errors arise, mainly due to the dissolution of platinum. A convenient method has been developed to prepare pure hydrogen bromide solutions.

In the preceding communication[1] a simple method was reported for the preparation of pure iodine and several test reactions were given to find its trace contamination level.

We intend to use this material primarily for the study of various equilibria but we also desire to explore its suitability as a universal analytical standard because of its uniquely favourable characteristics.

Iodine is a monoisotopic element, non-hygroscopic and perfectly stable in air. Moreover, it may easily take up or donate electrons.

In the present article we studied iodine as a reducing agent by oxidizing it coulometrically. This approach was chosen to avoid the almost insurmountable difficulties to find a chemical oxidant of a purity comparable with our iodine.

Constant current coulometry combined with potentiometric determination of the equivalence point has proved to be quite easy to adapt for (computerized) automatic operation. Hence whatever degree of accuracy is required, the present analysis can be carried out conveniently in any laboratory with readily available instruments.

METHOD OF ANALYSIS

Introduction. In the present work we have been mainly concerned with the problem of oxidizing iodine to the oxidation state one in the ionic medium 4 M HBr.

Several authors have found that iodine is complexed by bromide and Lang[2] established in 1936 that the I(I) cation binds at most two Br^- ions. Forbes and Faull[3] made the first electrometric investigations of this titration method. Bromine as a coulometric intermediate was first systematically studied by Swift[4] and his co-workers.

Evidence will be presented that bromide can be anodically oxidized to tribromide with theoretical current efficiency under the conditions used in this study.

Thus the titration reaction may concisely be expressed as

$$I_2Br^- + Br_3^- \rightarrow 2\,IBr_2^- \qquad (1)$$

The proposed procedure contains the following steps: (1) *in situ* purification (pretreatment) of the ionic medium, (2) the start titration, (3) addition of the accurately weighed iodine sample, (4) the main and (5) the end titration.

0302-4377/83 $2.50

The cell and the emf measurements. The emf measurements were carried out in a cell without liquid junction:

$$- \text{Glass electrode} \mid \text{TS} \mid \text{Ir} + \qquad \text{(I)}$$

The test solution, TS, consisted at the beginning of the experiment of 120 ml 4M HBr plus a small amount of iodine. After a start titration 0.3–4 meq. of iodine were introduced from an alkaline iodine stock solution, and the main titration was undertaken.

The emf of cell (I) can beyond the equivalence point be expressed as

$$E = E_o(\text{I}) + g/2 \lg [Br_3^-]/[Br^-]^3 - g \lg h \qquad (2)$$

In eqn. (2) g denotes $RT\ln 10/F$, $E_o(\text{I})$ represents the sum of the concentration independent terms and h is a symbol for the hydrogen ion concentration.

During the coulometric titration the $[Br_3^-]$ never exceeds 0.5 mM and the changes of h and $[Br^-]$ may be considered as negligible. The volume of the test solution may also be regarded as constant. Eqn. (2) can thus be simplified to

$$E = E_o + g/2 \lg (w - w_o) \qquad (3)$$

where E_o is a conditional constant, w is the amount of electrons withdrawn from the solution (F=96486.7 As mol^{-1} [5,6]), ensuing the pretreatment, and w_o is the intercept on the w-axis in the Gran plot (*cf.* Fig. 1).

The coulometric circuit. We have used the following electrolysis circuit:

$$\begin{array}{l} \text{Ir} \mid \text{TS} \mid \text{Cathode compartment} \\ \llcorner + \text{ Constant current source } - \lrcorner \end{array} \qquad \text{(II)}$$

The cathode compartment was a Wilhelm bridge with the following composition:

$$\mid \text{4M HBr} \mid \text{4M HBr} \mid Hg_2Br_2\,(s) \mid \text{Hg} \qquad \text{(III)}$$

As it is seen, the same ionic medium is used throughout the whole cell.

A simplification arises from the high solubility of iodine in 4M HBr. On the basis of the data gathered by Linke [7], the solubility is probably higher than 80 mM, compared with about 1 mM in water, and most titrations could therefore be done in a homogeneous solution. The concentration level 4M has been chosen as a compromise between our desire to keep the impurity concentration as low as possible but to avoid the risk for coulometric side reactions.

ON THE DETERMINATION OF EQUIVALENCE POINT IN REDOX TITRATIONS

General. We used Gran's method [8] for the localisation of the equivalence point. If the following conditions are fulfilled, a plot of the concentration quotient between the electrode-active species *versus* the amount of reagent added yields a *straight line.*

(1) Redox equilibrium is established.
(2) A single electrode reaction occurs.
(3) Sufficient excess of the reagent must have been introduced that its equilibrium concentration may be set equal to its stoichiometric concentration.

As a consequence of these requirements only data obtained at a *certain distance* from the equivalence point can be approximated by a straight line.

The great advantage of Gran's method is that *unsuspected* systematic errors can be detected as a deviation from the theoretical straight line. The other advantage is that only data on one side of the equivalence point are needed. In our case we have not been able to obtain a straight line on the iodine side due to the sluggish attainment of equilibrium.

Error calculus. Differentiation of eqn. (3) gives

$$dw_o = dw - (w - w_o)\, 2F/RT\, dE \qquad (4)$$

It is to be observed that in this equation E_o is assumed to be an unknown parameter which has to be determined from the same data as w_o. The second term of eqn. (4) for dw_o is proportional to the distance from the equivalence point, so every effort should be made to prepare pure reagents to enable the analyst to carry out reliable measurements with small excesses of the reagent. When the number of measurements is great and the measured quantities are not correlated, the expression for the standard deviation takes the form:

$$\Delta w_o^2 = \Delta w^2 + \{(2F/RT)^2 \Sigma (w_i - w_o)^2\, dE_i^2\}/(N-2) \qquad (5)$$

where N denotes the number of points distinguished by the subscript i. In deriving this equation it was assumed that the same weight is ascribed to each point.

The concept *redox buffer capacity* β is introduced at this stage to make the discussion more general:

$$\beta = \left(\frac{\partial\, [\text{ox}]/c}{\partial\, E}\right)_c = -\left(\frac{\partial\, [\text{red}]/c}{\partial\, E}\right)_c \qquad (6)$$

where the total reagent concentration $C=[ox]+[red]=[Br]_{tot}=[Br^-]+3[Br_3^-]$ is regarded as constant, the derivatives are therefore partial. In our case $[Br_3^-]$ is small compared to $[Br^-]$ and the buffer capacity becomes according to eqns. (2) and (6)

$$\beta=F/RT\,[Br(0)]/[Br]_{tot} \quad (7)$$

This expression can be introduced into the eqns. (4) and (5):

$$\Delta w_o=\{\Delta w^2+(2V[Br]_{tot})^2\,\Sigma(\beta_i dE_i)^2/(N-2)\}^{1/2} \quad (8)$$

Here V is the initial volume of the test solution. Hence the second term of (8) is proportional to the product of the buffer capacity and the precision of the emf measurement, corresponding to the fact that the titration error is proportional to the uncertainty in $[Br_3^-]$, $\Delta[Br_3^-]$, which is obtained when eqn. (6) is integrated. The first term originates from the coulometric equipment.

As we must carry out difference titrations, two error estimates must be made, one for the start and one for the end titration. The two independent errors must be combined to obtain the total error

$$\Delta w_o\,(total)=\{\Delta w_o^2(start)+\Delta w_o^2(end)\}^{1/2} \quad (9)$$

This equation, divided by the amount of the substance titrated, gives the probable relative error.

The definition of the equivalence point and its evaluation. We estimate the two equivalence points corresponding to the start and end titration with linear regression calculation of the two Gran diagrams (*cf.* Fig. 1). In these calculations we only used $E(w)$ data falling within the *same redox buffer capacity range.* A value for w_o which gives no systematic trend in E_o was calculated with a computer in both titrations. The equivalence point is *defined* classically so that it is attained when the amount of reagent equals the amount of substance to be determined multiplied by the stoichiometric factor. Thus it is the point where the amount of electrons withdrawn anodically becomes equal to the amount of iodine introduced.

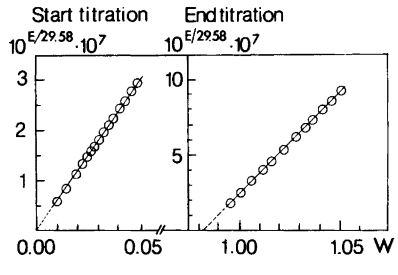

Fig. 1. The graphical estimates of the equivalence points for typical start and end titrations.

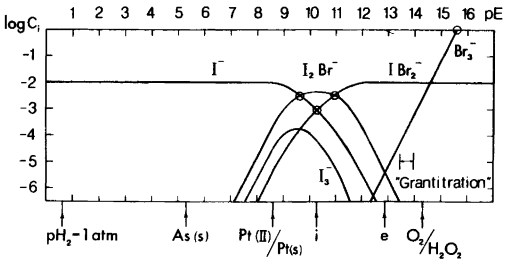

Fig. 2. The logarithmic concentration of the reacting species as a function of the redox potential. "i" is the iodine point (corresponding to an iodine solution in 4M HBr) and "e" the equivalence point. Circles denote experimental data.

The reagent excess, the concentration of tribromide, was measured with emf, and the point of zero excess, equalling the equivalence point, could be calculated by backward extrapolation. This implies the condition that the *electron deficiency* over Br^- and IBr_2^- is zero at the equivalence point.

The electron deficiency η will take the form

$$\eta/2=[Br_3^-]-[I^-]-[I_2Br^-]-[I_2]-2[I_3^-] \quad (10)$$

The point where $\eta=0$ is easily recognized in the distribution diagram (Fig. 2) where it is denoted with "e". The electron deficiency condition establishes a relationship between the titration points and the equilibrium concentrations.

It would have been very difficult to attain the same degree of precision if the analyses were not made as difference titrations which virtually eliminate the systematic errors, including the small emf drifts. A typical titration is illustrated in Table 1. The slight difference between E and E_{calc} (with the given w_o and E_o) demonstrates the precision attainable with coulometric titration.

RESULTS

The final series of titrations are summarized in Table 2. The amount of iodine was varied between 0.3 and 4 meq. Two different iodine preparations were used. With the equipment at

Table 1. A typical end titration involving bromine generation.[a]

Point	Real Time	*w*/mmol electrons withdrawn anodically	*E*/mV	E_{calc}/mV	β/mV^{-1} 10^6	$10^{2E/g}$ 10^{-7}
18	11.12	0.99515	215.05			
18	12.12		214.95	214.95	1.2	1.8481
19	12.18	1.00040	219.19	219.19	1.7	2.5708
20	12.24	1.00496	221.99_5	221.99	2.2	3.1982
21	12.30	1.01091	224.92	224.92	2.7	4.0159
22	12.35	1.01546	226.78	226.78	3.1	4.6416
23	12.41	1.02142	228.86_5	228.87	3.7	5.4595
24	12.47	1.02457	229.85	229.85	4.0	5.8946
25	12.52	1.02773	230.76	230.77	4.3	6.3273
26	12.57	1.03158	231.80	231.80	4.6	6.8608
27	13.03	1.03544	232.75	232.76	5.0	7.3874
28	13.08	1.03999	233.81	233.80	5.4	8.0228
29	13.14	1.04455	234.76_5	234.77	5.8	8.6420
30	13.19	1.04981	235.80	235.80	6.3	9.3670
	13.27		235.78			
	07.29 [b]		235.50 [b]			

[a] The current was maintained at the 5.0019_5 mA level. From eqn. (3) E_{calc} was obtained with w_o=0.98172 mmol and E_o=359.06 mV. The buffer capacity $\beta=F/RT$ [Br(0)]/[Br]$_{tot}$ [b] *Cf.* Fig. 3 illustrating a similar drift.

Table 2. Results. Titration reaction $I_2Br^- + Br_3^- \rightarrow 2IBr_2^-$.

No.	μeq. of iodine introduced	current/mA Titration start- and end	main	yield/%	iodine preparation No.	HBr[a] preparation No.
1	1063	5	20	100.02	1	1
2	980	5	20	100.00	1	1
3	1062	5	20	99.99	1	1
4	311	5	5	100.01	2	1
5	328	10	10	99.99	2	2
6	1178	10	40	99.99	2	2
7	1114	10	40	100.00	2	2
8	4029	10	40	100.00	2	2
9	3934	3	40	100.00	2	2

[a] HBr preparation 1 is prepared from KBr and $HClO_4$, and 2 is commercial HBr purified with Pd(H_2). Note: the amount of iodine is varied by a factor 12, the current density with a factor 8.

our disposal the amount of iodine cannot much exceed 4 meq. Larger samples would require longer electrolysis times and higher currents, while substantially smaller amounts than 0.3 meq. would give larger weighing errors.

It is also shown in Table 2 that two different preparations of the ionic medium, HBr, were used for the analyses. The electrolysis current was made to vary between 5 and 40 mA.

The fact that the results show no systematic variation with current indicates that the current efficiency of tribromide and iodinedibromide

generation exceeds 99.99 %. Another evidence for this statement is given in the experimental part.

Finally we may conclude that the uncertainty of the method described does not exceed 10^{-4}. The standard deviation of the equivalence point determination of the titration illustrated in Table 1 is calculated with eqn. (8) to equal 2×10^{-8} eq. and the total precision can be estimated to 3×10^{-5} according to eqn. (9). Thus the precision in the equivalence point determination is of the same magnitude as the precision of the weighing. Presumably the remaining part of the titration uncertainty is due to systematic errors arising from unidentified side reactions.

EXPERIMENTAL

Titration vessel and electrodes. The titrations have been carried out in a 200 ml vessel provided with six long necks. In contrast to greased surfaces, the teflon coated magnetic stirrer did not react with iodine. Probably its surface contaminants were removed by the pretreatment. The junction between the test solution and the cathode compartment was established with a capillary.

Throughout the titration the test solution was protected from the atmosphere by nitrogen of a slight overpressure provided from a simple manostat. The nitrogen was purified from dust and droplets with a sintered glass filter of porosity G3.

The iridium electrodes were prepared from an iridium foil of 99.9 % purity delivered from the Degussa Company, Germany. The foil was point-welded to a short piece of platinum wire sealed into a soft glass tube provided with a ground joint.

The electrodes were always kept in an oxidizing tribromide/bromide solution, and they were never subjected to ignition, which was found to have a detrimental effect because of the formation of iridium oxide.[9]

The mercury(I)bromide phase in the *cathode compartment, cf.* cell (III), was prepared *in situ* by anodic oxidation from a mercury pool. During the oxidation the pool has to be vigorously agitated, otherwise a tight mercury(I)bromide crust is formed, and gas evolution occurs. This cell could be used as cathode up to at least 40 mA without any hydrogen evolution.

Some $HgBr_4^{2-}$ is formed in the cathode compartment because of the disproportionation of Hg_2Br_2. However, no complication has arisen thereby as the bridge was flushed between the experiments. We had difficulties with commercial Hg_2Br_2, which should be tested before use for Hg(II) content and nitrate.

We decided to use a *glass electrode* as an internal reference in this work in order to avoid liquid junctions. Jena H 268 glass electrodes were employed because of their stability.

The long time stability of the glass electrodes was controlled with the following cell:

$$\text{Glass electrodes} \;\Big|\; \begin{matrix}\text{4 M } H^+,\ \text{40 mM } I_3^- \\ \text{3.76 M } Br^-,\ \text{200 mM } I^-\end{matrix} \;\Big|\; \text{Ir} \qquad \text{(IV)}$$

The emf's of two glass electrodes were measured for ten days. Their difference as well as the emf of cell (IV) was found to change less than 0.15 mV/d which is quite negligible compared to other sources of error.

In this laboratory we have often compared glass and hydrogen electrodes in acid solutions containing up to 5 M HCl or 5 M $HClO_4$.[10] Introducing a correction for the water vapour pressure, the difference between the two electrodes at 1 atm was always found to remain constant within 0.1 mV or better. Hence the glass electrode may be considered to be equivalent with the reversible hydrogen halfcell. The present study indicates that the glass electrode is also useful in 4 M HBr.

Instruments and temperature control. The following equipment was used in the present work: a digital voltmeter, two timers, a constant current source, electrometer amplifiers and a programmable relay scanner. The instruments were controlled by a desktop computer. The instruments used were *calibrated* twice during this work.

The *digital voltmeter* of type HP 2401C from Hewlett-Packard Company was calibrated with a transportable Fluke type 731B DC standard maintained by *Statens Provningsanstalt* (The Swedish Official Standards Laboratory). The voltmeter was set to measure with a precision of 0.01 mV. The noise level amounted however to about 0.03 mV. This could be reduced to 0.01 mV by programming the computer to carry out a smoothing procedure for seven successive emf measurements.

The emf measurements including a glass electrode have been carried out with an Analog Devices *311K electrometer amplifier* assembled in this laboratory. This instrument has been found to have a long time drift smaller than 0.01 mV/week.

To measure the electrolysis time, we used two parallel digital quartz *timers*: type HP 5326B

from the Hewlett-Packard Company and type 5500B from the Ballantine Company. Their quartz frequencies were found to agree within 2×10^{-6}. The timers were triggered by a common signal. The two time period readings always agreed within 0.01 s, corresponding to the time needed to get final relay closures. The *constant current source* was of the type 9770-B from Guildline Instruments Ltd, Canada. The current level fluctuations were kept at about 10^{-5}. To avoid transient signals, the current was passing a dummy resistor of the same magnitude as the electrolysis cell between the titration steps.

The current was determined via the potential drop over a calibrated standard resistor. We had at our disposal a newly calibrated 10Ω resistor (Leeds and Northrup type 4025B). Its uncertainty was 10^{-5} according to the manufacturer. The other resistors used were compared with this standard. The recorded current values are believed to be reliable to within 3×10^{-5}.

The air in the laboratory was controlled and kept constant at 25.0 ± 0.2 °C in the neighbourhood of the instruments. The titrations were carried out in a well guarded silicone oil bath kept at 25.00 ± 0.01 °C.

Procedures. The coulometric titration. Step 1. The experiment commences with a *pretreatment.* The titration vessel is filled with 120 ml of the ionic medium (4M HBr), and a few drops of iodine solution is added. The reducing impurities introduced with the hydrogen bromide, or present on the surfaces of the apparatus, are now assumed to react with the iodine. Next, the excess iodine is completely oxidized to IBr_2^-, then a small excess of bromine is generated (about 10 μeq.). The solution is left overnight, to allow time for sluggish redox reactions to proceed, and the emf is recorded (see Fig. 3).

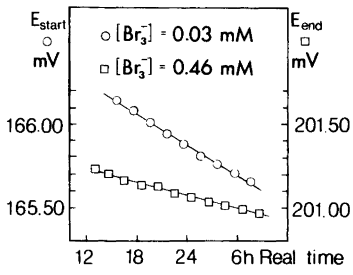

Fig. 3. E, the emf of the cell Glass electrode | TS | Ir+, as a function of time for the starting point (circles) and the last point (squares) of an iodine titration.The slope of the upper line is −0.03 mV/h and that of the lower line −0.015 mV/h. Note the difference in buffer capacity.

Step 2. Overnight some bromine might react, and a coulometric *start titration* must be carried out to get a precise determination of its excess.

By stepwise anodic oxidation about 100 μeq. of bromine are generated, and the emf is measured at each step. The values $10^{2E/g}$ are plotted versus *w* in a Gran diagram (see Fig. 1).

Step 3. At this stage the *iodine sample* is introduced into the test solution. This manipulation takes about 30 s and about 10 ml of nitrogen may be estimated to be displaced from the vessel. With a partial pressure not exceeding 10^{-5} atm, the loss of bromine that might occur is certainly less than 0.01 μeq. which is quite negligible.

Step 4. Now the *main electrolysis* starts. It lasts for one to three hours. During this time the current is controlled about ten times every minute and its mean value is successively calculated and stored in the computer. The current is stopped when a small excess of bromine (about 10 μeq) has been generated, and any iodine that diffused into the Wilhelm bridge is reintroduced by flushing into the vessel.

The stability of the emf at this point is controlled (see Fig. 4). At this stage the buffer capacity of the solution is very small, and the absence of any drift or other irregularities provides a severe test for the precision of our experimental approach.

Step 5. Finally the *end titration* is carried out in order to determine the excess bromine just generated (*cf.* Fig. 1). As far as we could notice, air had no influence on our results and no special care is needed to exclude it. To minimize vapour losses, the vessel is kept closed, and ground glass joints and stoppers are used throughout. To allow for the volume changes during the electrolysis and the flushings, a constant pressure of nitrogen is maintained by a simple manostat.

Further experimental details. In order to obtain results of the highest precision it is necessary to flush the capillary prior both to the start and the end titration in order to reintroduce tribromide. In addition, the volume introduced at the flushing before the end titration must be known,

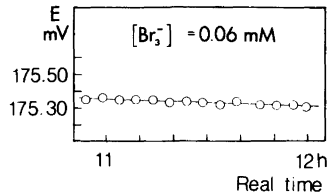

Fig. 4. The drift of *E*, Glass electrode | TS | Ir+, in the immediate vicinity of the equivalence point. The slope of the line is −0.035 mV/h.

and the result corrected for the amount of impurities introduced thereby. A typical correction for a 1 ml flushing was 0.1 μeq. Within the course of a titration some drops unavoidably gather on the walls of the vessel, and they have to be reintroduced into the solution by shaking the vessel prior to the start and end titrations. This step was rather inconvenient but absolutely necessary.

After each passage of current the potential of the anode was measured, but within a few seconds it deviated less than 0.01 mV from that of the indicator electrode. Thus the current yield for bromine generation must be very near to the theoretical value.

Preparation of pure HBr solutions. Two different methods to prepare pure HBr were developed, and the ionic media made from these preparations are denoted as (1) and (2) in Table 2. With commercial products of *pro analysi* quality no reproducible results could be obtained.

Starting from KBr and $HClO_4$. Potassium bromide of *pro analysi* quality was dissolved at 50 °C in doubly distilled water to give an approximately 6 M solution. Solid impurities were removed by filtration. Next concentrated, iron free, perchloric acid and potassium bromide solutions were added alternately in small portions to a beaker equipped with an effective stirrer, and thus microcrystalline $KClO_4(s)$ formed.

The mixture was chilled to 0 °C with ice, and then small portions of the KBr solution was introduced until no more $KClO_4$ precipitated. The mixture was decanted and filtered and the clear solution was distilled twice. At the first distillation the fraction boiling above 110 °C was collected. This fraction was colored by bromine formed at the elevated temperature over the saturated KBr solution resulting from the distillation.

At the second distillation, water and bromine distilled first and the fraction boiling above 120 °C was collected. The main part was azeotropic acid boiling at 126 °C. The distillation was stopped when the temperature above the residual solution reached 160 °C which is far below the boiling point of perchloric acid (200 °C). Some decomposition to bromine was evident at temperatures higher than 126 °C.

This preparation was found by coulometric titration to contain *oxidizing* impurities amounting to as much as 3 μeq./mol of bromide. No traces of perchlorate could be detected with tetraphenyl arsonium chloride reagent. With spectrophotometry (around 250 nm) the iodine content in this preparation could be estimated to about 1 μeq./mol HBr.

The stock solution was only slightly colored and it was kept under nitrogen and protected from light. Still after one year the coloration was only faint.

The components of the solid $KClO_4$ can be recovered (in a less pure state) by suspending the salt in water with ion exchange resin saturated with hydrogen ion and warming.

Starting from commercial HBr. When the starting material is low in bromine the following procedure may be employed. Concentrated azeotropic, 8M, HBr solution is diluted with the same volume of doubly distilled water. A large platinum net, bearing cathodically precipitated palladium saturated with hydrogen, is inserted into the acid, and hydrogen gas is passed through the solution. This procedure gives within a few hours a colorless product.

When the bromine concentration is high, the palladium may be dissolved and the solution becomes red.

The (Pd-free) colorless solution is finally distilled twice. This preparation was found to contain (colorless) *reducing* impurities amounting to as much as 18 μeq./mol HBr. The advantage of this procedure is that no foreign substances are introduced, and any $HAsO_2$ and arsenious bromide complexes get reduced to arsenic metal. The remaining impurity content is however higher than in the acid made from KBr.

Weighing of the samples. As described in a previous communication [1] iodine was dissolved in sodium hydroxide (Merck "Suprapur") to give iodine stock solutions with concentrations ranging from 0.1 to 0.3 M. This sodium hydroxide preparation was found to contain oxidizing impurities up to 15 μeq./mol. In order to minimize the time of contact with stopcock grease, the desired amount of solution was introduced into a weighing burette of conventional design just before weighing. Another burette type constructed to avoid this source of error is illustrated in Fig. 5.

The iodine solution was transferred from the burette into a vial (0.1 mm×10 mm×90 mm) which was introduced into the cell vessel. With this technique we could avoid removing the burette from the thermostated balance room, shorten the total weighing time and thus increase the precision of the weighing. We varied the weighings between 2 and 7 g of solution using a single pan Sartorius balance readable to 0.01 mg. We estimate the precision of the weighing to 0.1 mg, which was quite sufficient for our purposes. We made a correction for the buoyancy of air in the conventional way. The vial was placed in the cell vessel with the help of tweezers, and was then crushed with a glass rod provided with a ground

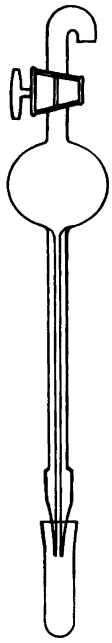

Fig. 5. Weighing burette designed to avoid contact with stopcock grease. The solution is drawn up to the bulb by exhaustion.

glass joint. In order to avoid the formation of a dead space, any remaining large pieces were pulverized at the equivalence point, where the iodine and bromine pressures have their minima. In order to remove impurities, the vials were soaked in a hot strong alkaline solution and then boiled with *aqua regia* before use. This purification was quite necessary to get stable emf readings.

Exploratory experiments in HCl and HBr media. In the initial phase of this investigation, a comprehensive set of iodine oxidations experiments were conducted in hydrogen chloride solutions, where ICl_2^- is formed. This often recommended classical method has proved to provide irregular results (±1 %). Only platinum could be employed as anode material in this medium. The overpotential for the formation of oxygen on iridium was found to be so low that the amount of chlorine generated was far below the theoretical yield. Graphite anodes absorb considerable quantities of halogens which cannot be regained.

In another series of experiments we used platinum electrodes in HBr media. Also in this case we found both positive and negative errors (±0.15 %).

Our test solutions were found to contain an appreciable amount of platinum ions which could be detected by cathodic deposition on a bright platinum foil. Deposition could be observed when platinum had been used as anode in a pure hydrogen bromide solution. An attempt was made to estimate the amount of dissolved platinum with atomic absorption spectroscopy. But as the amounts are close to the detection limits of this method, the results may be regarded as semiquantitative only. We found in three test solutions 0.3, 0.4, and 0.6 μmol of Pt. This was about the magnitude expected on the basis of the spread of the results of the coulometric titrations. The dissolution of traces of platinum was also visible on photomicrographs made prior to and after a bright platinum foil has been used an anode.

Thus dissolution of platinum causes considerable systematic errors also at the low redox potentials (600–850 mV) met in our titrations, a fact that seems not to have been reported earlier.

CONCLUSIONS

Within the frame of the present project the following criteria have proved to be indispensable in order to perform coulometric redox titrations of the highest accuracy.

(1) Use of inert electrode materials like iridium.

(2) Strict difference titration involving *in situ* purification ("pretreatment").

(3) Evaluation of the equivalence point with rigorous error estimate based on reversible potentials transformed to a Gran plot.

(4) Insensitivness to oxygen, like the redox couple IBr_2^-/I_2Br^-.

(5) The redox potentials must throughout the electrolysis lie within the limits set by the decomposition potentials of water *e.g.* by choosing a HBr medium.

Further experiments based on these principles, combined with improved instrumentation, may very likely provide results of substantially lower uncertainty and open the way for the re-evaluation of the Faraday constant.

Acknowledgments. This work has been supported by *Statens Naturvetenskapliga Forskningsråd* (The Swedish Natural Science Research Council). I wish to express my thanks to Dr. Georg Biedermann for much good advice, for stimulating discussions and for his help with various parts of this work. I am also indebted to the Royal Institute of Technology for fellowships. I am most grateful to Professors Ingmar Grenthe and Liberato Ciavatta for valuable comments on the manuscript. Mrs. Hillis Ström prepared the thin glass test tubes and Mr Tage Grimborn suggested the use of the manostat. I owe my thanks to them. I would also like to express my thanks to Mr Bo Surtén who repaired and constructed many parts of our equipment.

REFERENCES

1. Sundstrand, S. *Acta Chem Scand. A 37* (1983) 787
2. Lang, R. *Z. Anal. Chem. 106* (1936) 12.
3. Forbes, G. S. and Faull, J. H. Jr. *J. Am. Chem. Soc. 55* (1933) 1820.
4. Sease, J. W., Nieman, C. and Swift, E. H. *Anal. Chem. 19* (1947) 197. *cf.* Wooster, W. S., Farrington, P. S. and Swift, E. H. *Anal. Chem. 21* (1949) 1457.
5. Craig, D. N., Law, C. A. and Hamer, W. J. *J. Res. Nat. Bur. Stand. (U.S.) 64A* (1960) 127.
6. Bower, V. E. and Davis, R. S. *J. Res. Nat. Bur. Stand. (U.S.) 85* (1980) 175.
7. Linke, W. F. and Seidell, A. *Solubilities of Inorganic and Metal-Organic Compounds,* American Chemical Society, Washington, D.C., 4th Ed. 1958, Vol I, p. 1255.
8. Gran, G. *Analyst 77* (1952) 661; *cf.* also *Thesis,* Royal Inst. of Technology, Stockholm 1981, Sweden.
9. Biedermann, G. and Palombari, R. *Acta Chem. Scand. A 32* (1978) 381 and *private communication.*
10. Biedermann, G., Maggio, V., Romano, V. and Zingales, R. *Acta Chem. Scand. A 35* (1981) 287; *cf.* Pesavento, M. and Biedermann, G. *To be published.*

Received February 28, 1983.

Acta Chemica Scandinavica A 37 (1983) 787–793

Purification of Iodine by Crystallisation from a Hydrogen Polyiodide Solution and Check of its Contamination Level

SIGNAR SUNDSTRAND

Department of Inorganic Chemistry, The Royal Institute of Technology, S-100 44 Stockholm, Sweden

Substantial quantities of iodine may conveniently be purified by saturating a 10 M hydrogen iodide solution with iodine, and precipitating it in microcrystalline form by dilution with water. The non-hygroscopic iodine crystals are filtered, washed and dried at room temperature.

The trace impurity and water contents may reliably be determined by potentiometric, mass spectrometric, radiometric and IR spectrometric methods developed for this purpose. The total amount of foreign substances has always been found to be less than 0.01 %. Alkaline iodine stock solutions may be preserved and sampled without losses for one year or longer.

The several iodine batches prepared are intended to be employed in quantitative analysis and to study the solution chemistry of iodine.

Iodine is known to be an exceptionally rapid oxidizing agent, a fact that results in the introduction of impurities, unless precautions are taken to avoid every contact with reducing substances throughout its preparation and handling.

Classical purification methods involve, for instance, distillation with water vapour and repeated sublimations in a nitrogen stream. In these operations stopcock grease, dust, mineral oil or mercury and other detrimental substances are unavoidable; moreover purification of large amounts of iodine requires some effort. Hence a simpler method of purification was sought for.

For this purpose one may utilize the fact that iodine is highly soluble in concentrated alkali or hydrogen iodide solutions where it forms multiple charged polynuclear ions. When such a solution is diluted with water, iodine crystals precipitate, while the main impurities are unaffected and remain dissolved.

Hydrogen iodide offers, from the preparative point of view, the important advantage that it dissolves more iodine than an equimolar potassium iodide solution, because the H^+ ion is a much less efficient salting out agent than the big alkali cation. To estimate the efficiency of this approach a series of trace analytical methods were developed. The problems arising when iodine solutions have to be prepared, preserved and sampled without losses are also treated in some detail in the present article.

Iodine purification by precipitation upon dilution is a method which was discovered more than a hundred years ago (1865) by Jean Servais Stas[1–3] (*cf.* also Gmelin[4]) who refined it so far that he was able to obtain a fairly correct value for the atomic weight of iodine (126.80). However, Stas employed potassium iodide solutions as solvent, and subjected the precipitated iodine to sublimation, which was believed to result in an improved purification. The present investigation is based on Stas' pioneering research, and the proposed procedure represents an improved version of his method.

METHOD

The present approach is based on the rapid establishment of equilibria of the general type

$$p\,I_2(s)+q\,I^- \rightleftharpoons I_{2p+q}^{q-} \qquad (1)$$

where p and q represent integers greater than unity. According to our preliminary solubility data the predominating iodine bearing species,

0302-4377/83 $2.50

besides I_3^-, is a triply charged anion which may have the composition I_{17}^{3-} at low [3 M Na^+ (ClO_4^- + I^-)], and I_{12}^{3-} at high [10 m Na^+ (ClO_4^- + I^-)] ionic strengths. It is clear from eqn. (1) that the quotient $[I_{2p+q}^{q-}]/[I^-]$ (=the dilution condition) will be constant only if $q=1$. The concentration of polyiodide ions must decrease with $[I^-]^q$ (=the equilibrium condition). Thus iodine crystals will be precipitated when a saturated hydrogen iodide solution is diluted with water ($q=3$). Fortunately the most likely contaminants, chloride and bromide, appear to form only single charged polyhalogenide ions ($q=1$), and they remain in solution.

Before entering the description of the purification procedure in detail, it appears appropriate to summarize the *principles* guiding our choice of experimental conditions.

(a) Only gases and liquids purifiable by distillation are used: hydrogen iodide and water. In the final stage of the preparation oxygen is employed to remove the last traces of HI adhering to the iodine, thereby more iodine is formed.

$$O_2+4H^++4I^-\rightarrow 2H_2O+2I_2 \qquad (2)$$

(b) All steps of the purification are carried out at room temperature. It is therefore easy to protect the iodine solution and the crystals from the laboratory atmosphere with carbon dioxide. This gas is required to prevent decomposition to iodate and iodide.

(c) The degree of supersaturation, when precipitating, is kept at a minimum by vigorous stirring and dropwise addition of water. This was done in order to suppress the amount of mother liquor occluded.

(d) The materials come into contact only with glass and platinum. The solubility of pyrex glass in our acidic solutions must be very low. The crystals are transferred with a platinum spoon.

(e) Several *model experiments* were made with the most likely impurities. In order to check the degree of purification the radioactive tracers $^{36}Cl^-$ and $^{14}CN^-$ were added. (No suitable Br^- isotope is available). These experiments have shown that by a single precipitation 99.8 % of the chloride ions and 98 % of the cyanide ions are removed. It should be recalled that ICI, IBr and ICN cannot be eliminated with sublimation.

(f) Finally it should be pointed out that the iodine in the filtrate may easily be recovered by using, for instance, hydrogen peroxide, oxygen or ozone[5] as oxidizing agent. The advantage of using these oxidants is that no foreign substances are introduced.

PROCEDURE

Purification of 1 kg of iodine with a yield of 60 %.

General. One kg of iodine (8 mol) and 190 ml (373 g) 10 M (fuming) hydrogen iodide solution are mixed in a beaker covered with a watch glass. The dissolution is endothermic, and the beaker should therefore be warmed on a water bath to keep the solution temperature at about 25 °C in order to maintain a high solubility of iodine.

The vapour pressure of hydrogen iodide is considerable at 25 °C and elevated temperatures should be avoided in order to reduce losses. This and the following manipulations should therefore be carried out in a well ventilated hood.

Next, the resulting dense solution, with a metallic lustre, is filtered through a sintered glass filter to remove the floating insoluble material that is usually present in commercial products and any iodine crystals that may remain undissolved.

The precipitation of iodine is carried out in a tall beaker (5 or 10 l). Water is added dropwise from a burette, while the suspension is agitated vigorously. When the starting volume has been increased ten times the additon of water may be stopped. Further dilution brings about only a negligible increase in yield.

The small iodine crystals were gathered in a specially constructed filter funnel illustrated in Fig. 1. With this funnel we could easily wash and dry the iodine crystals in a protective atmosphere of carbon dioxide.

The washing procedure was first monitored by control of the pH of the filtrate, then by estimating the $[I^-]$. When the pH had increased to about 4, the washing continued until addition of Ag^+ to the filtrate yielded a colloidal suspension of AgI(*s*) equal in scattering power to that of an acid saturated iodine solution to which silver ions had been added.

The crystals were finally dried in a desiccator provided with extruded molecular sieves, (the moist crystals contained about 2 weight % water).

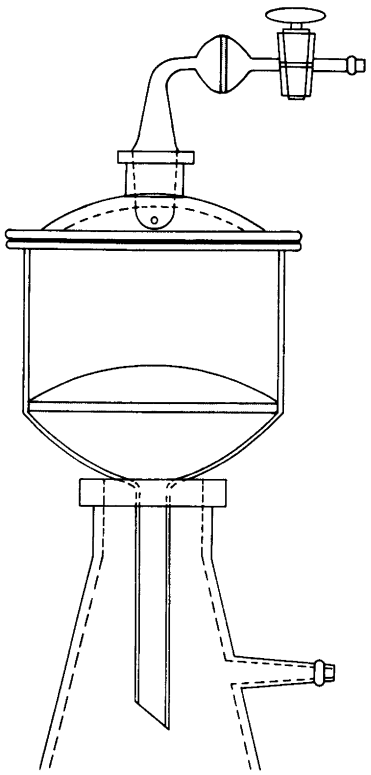

Fig. 1. The edge of a commercial glass filter funnel is bent to a rim, and ground flat to fit the cover of a desiccator. The funnel is used for washing the iodine crystals. The washings are removed by applying a slight underpressure in the filtering flask. CO_2-gas, free from dust, replaces the withdrawn water.

The desiccator was exhausted, and the iodine was left to dry for a few days. It was then filled with oxygen to remove the last traces of HI. Violet iodine vapours became visible at once due to the reaction (2). A new portion of molecular sieves was then introduced to absorb the water formed.

After this step the iodine is ready for use. The yield was generally about 600 g of dry material.

The washings, containing H^+, I^- and I_3^-, were collected for recovery of iodine by oxidation with hydrogen peroxide.

Comments. It would have been preferable to remove the excess water from the crystals by centrifugation. However, the iodine crystals are so soft that they agglomerate. The resulting mass is difficult to remove and, by grinding, new impurities are easily introduced.

We have been using starting materials of *pro analysi* quality. However this procedure has proved to be so efficient that less expensive qualities would have served equally well. As the iodine in the filtrate and the washings are easily recovered, our procedure may be regarded as a fast, convenient and cheap method of purifying iodine.

PREPARATION OF STABLE IODINE STOCK SOLUTIONS

Iodine has a high vapour pressure at room temperature. Hence, some precautions have to be made when the samples are weighed.

This problem has been encountered by several generations of analysts and many proposals have been made to solve it. These are critically surveyed by Kolthoff and Belcher.[6] The problem was recently reconsidered by Bower[7] who suggested the use of a special apparatus. The most common approach is to dissolve iodine in a potassium iodide solution.[6,8,9] This method could not be employed in our case as the iodine stock solutions were used in both oxidation and reduction experiments. We propose a simple approach – dissolution of iodine in alkali and weighing of this solution.

Iodine dissolves readily in a small excess of sodium hydroxide and the disproportionation

$$3\,I_2 + 6\,OH^- \rightarrow IO_3^- + 5\,I^- + 3\,H_2O \qquad (3)$$

is completed within a few hours as can be seen by the discoloration of the solution. Since this reaction is perfectly reversible, we used throughout this project alkaline iodine stocks.

The only disadvantage of the proposed method arises from the need of reacidification to recover I_2. When iodine participates in a classical iodometric reaction, a final readjustment of the pH may also be required to avoid the oxygen error.

Our stock solutions have in each case been found to maintain their iodine content for periods as long as one year, even though samples often were withdrawn.

We have also tried several organic solvents such as carbon tetrachloride, benzene, ethylene glycole and silicone oil to prepare stable iodine solutions. However, all of them were found to contain substantial amounts of redox impurities and had therefore to be discarded.

A convenient method was developed to determine traces of *redox impurities* in alkali hydroxide preparations. The sample was added to an HBr solution with a small but known excess of Br_3^-. The change in Br_3^--excess was determined and taken to equal the amount of redox impurities. The analyses were carried out as described in a following publication[10] dealing with the coulometric oxidation of iodine.

In a typical case the sodium hydroxide originating from the Merck Co ("Suprapur") contained 15 μeq oxidizing impurities per mole. Our own preparations (from sodium) of about the same quality were also tested.

The weighing procedure. The iodine stocks were prepared by determining the weight increase upon introducing as quickly as possible (*e.g.*) 50 milliequivalents (6.35 g) of I_2 into a pyrex flask containing (*e.g.*) 200 ml CO_2- and O_2-free 0.28 M NaOH-solution (about 10 % excess of OH^-). The flask contained a teflon covered magnetic bar and had an ungreased glass stopper. This was replaced with another slightly greased stopper after all the iodine had left the surface. The whole dissolution procedure took about one hour. The complete disproportionation required a few additional hours.

This procedure involves the weighing of objects of several hundreds of grams with a precision of about 0.1 mg. Hence a high quality balance is required, and attention must be paid to ensure that the vessel attains equilibrium with the moisture of the air in the balance room. A thermostated balance room is therefore necessary.

In each case the proper correction for the buoyancy of air was applied.

It should be added that the stopcocks of the weighing burettes used for sampling must fit precisely. Otherwise the slight underpressure which develops by carbon dioxide absorption from the air left in the burette, causes a drift of about 0.05 mg/min because of intrusion of external air.

DETERMINATION OF FOREIGN SUBSTANCES AND IMPURITIES IN THE IODINE PREPARATIONS

General. The several iodine batches prepared are intended for use as standards in quantitative analysis and in redox equilibrium measurements.

To test whether they are suitable for these purposes, we have developed a method to determine trace amounts of hydrogen iodide in the iodine phase. Water was analysed with the IR spectroscopic method developed by Farrow and Hill.[11] A precision of a few parts per 10^5 iodine was obtained in these analyses. A further important task has been to look for *unsuspected* contaminants which might have been introduced in the course of the preparation, or co-precipitated with the iodine. As will be discussed in more detail below, the amount of non-volatile impurities was in each case found to be less than 4 parts per 10^5. One might therefore be inclined to think that the content of foreign non-volatile substances could be reduced by sublimation.

This is indeed a common purification approach. Effective sublimation will require an elevated temperature and a large volume of a streaming gas (or exhaustion). Thereby it is unavoidable to expose the iodine to *uncontrollable* volatile and other impurities.

It seems therefore preferable to analyse iodine for foreign substances and to apply the relevant correction when necessary. A similar approach has proved to be useful for other materials as well, *e.g.* NaI, Fe_2O_3 and sulfur.

The sublimation residue. This test was primarily made to find the amount of dust originating from the incompletely filtered gases and from the air, when the iodine was handled.

Samples of five or ten grams of iodine were weighed into boats made of fused silica. These were then placed in a quartz combustion tube. A narrow zone was heated externally to about 100 °C while a slow stream of purified and filtered nitrogen passed through. A blank experiment was made simultaneously. In the majority of cases a *weight decrease* varying between 0.01 to 0.29 mg was found. The weight of the empty boat (the blank) decreased by 0.05 to 0.34 mg.

To get an estimate of the upper limit for the non-volatile substances, we may consider the experiment with a sample of 5.11 g iodine. A weight increase of 0.14 mg was observed, while the empty boat lost 0.05 mg. Hence we can set the maximum residue to 0.19 mg. The non-volatile residue is thus certainly less than 4 parts per 10^5.

In order to improve the precision of this test, a material with better weight stability than quartz is needed. The commercial quartz boats were found to lose a few parts per 10^6 of their mass in each heating period. This effect might be due to a changed amount of adsorbed gases in the pores.

The mass spectrographic study. A mass spectrograph of the type "Spark Source MS, AEI MS 702" was employed to detect traces of compounds with a mass number exceeding 14. The iodine samples were ground together with graphite in an agate mortar, and small electrodes were made from the mixture.

Only three foreign elements could be discovered: Si, Na and S. An attempt was made to estimate their concentration level, and we obtained the following estimates: (mol ratio $\times 10^4$):

Si=5, Na=0.15, S=0.1.

A considerable part of the iodine sample evaporated between the sweeps, so these figures may be regarded as semiquantitative only. No traces of Cl, Br, Al or Fe were found. We would like to point out that a part of the observed intensity (maybe even the whole) for Si and S might be due to the presence of N_2^+, and O_2^+ in the spectrometer. The starting material (a commercial preparation of *pro analysi* quality) was analysed in the same way; and the following approximate results were obtained: (mol ratio$\times 10^4$):

Si=10, Na=2.5, S=1, Al=5, Fe=0.2.

Thus a considerable purification from all elements except silicon could be achieved in a single precipitation step.

However, we doubt the results for this element because these amounts of silicon dioxide should easily be detected in the evaporation experiments. Perhaps some contamination with SiO_2 occurred when the iodine sample was pulverized in the agate mortar. Alternatively its intensity is overestimated. Wartenberg [12] (*cf.* also [13]) studied this question systematically and found that abrasion from an agate mortar may contaminate the product considerably.

The hydrogen iodide content. Because of our method of preparation it was necessary to determine the amount of occluded hydrogen iodide in the washed, oxidized and dried product.

This was done by measuring the increase of hydrogen ion concentration when the iodine sample was introduced into a (2 M NaCl+1 M NaI) solution containing a small, but exactly known, proton excess.

The sodium iodide was added to dissolve the large amount of iodine (several grams) needed to get a high sensitivity. With the method described one may conveniently determine 0.5 μmol of HI which corresponds to a hydrogen iodide mol fraction of less than 10^{-5}. The hydrogen ion concentration of the NaCl–NaI solution was first adjusted by coulometric reduction of water using a Wilhelm bridge as anode compartment.

About 0.5 mM iodine was added before the coulometric titration in order to remove the redox impurities present.

The hydrogen and triiodide ion concentration were determined after each step of electrolysis by measuring the emf of a glass electrode and a platinum redox electrode *versus* a common external reference electrode.

The emfs of these cells may under the present conditions (25 °C) be expressed by the simple equations:

$$E(\mathrm{GE}) = E_0(\mathrm{GE}) + 59.16 \log h \quad (4)$$

$$E(\mathrm{Pt}) = E_{01}(\mathrm{redox}) + 29.58 \log [I_3^-] - 88.74 \log [I^-] \quad (5)$$

$$\cong E_{02} + 29.58 \log [I_3^-] \quad (6)$$

Here the E_0:s are isothermal constants and h stands for $[H^+]$. As the electrolysis proceeded, the current yield for the reduction of hydrogen ion steadily decreased, while the yield for the triiodide reduction increased.

Beyond 1 mM hydrogen ion concentration no significant further alkalification could be achieved as shown by the constant E(GE) and the successively decreasing E(Pt) values. At this point (pH=3) the electrolysis was interrupted, and air was passed through the test solution. Due to the reaction

$$O_2 + 4H^+ + 6I^- \rightarrow 2\,H_2O + 2\,I_3^- \quad (7)$$

a slow alkalification occurred which was stopped when h had dropped to about 50 μM (pH 4.3). At a lower concentration reversible emf value cannot be obtained in these unbuffered solutions.

In order to calculate the change in hydrogen ion concentration after the additions of iodine E_0(GE) had to be evaluated. This constant was estimated in two ways:

(1) From the set of values of E(GE), E(Pt) and w (mol of electrons introduced at the cathode) a computer made an iteration calculation of the two E_0:s assuming that the *combined* current yield was 100 %.

(2) After the iodine additions a few milliliters of 100 mM HCl were introduced. The emf change of the glass electrode was used to calculate E_0(GE). The two values only differed by a few millivolts.

Approximately one gram portions of the iodine sample were added to the NaCl–NaI solution whose hydrogen ion concentration was about 50 μM. After each addition the emf values were measured. The E(Pt) data thus obtained were used for the control of the computer value of E_{02}.

Also in this case the agreement was good. In a typical experiment 6 g of iodine were found to contain 0.6 μmol of HI, corresponding to a hydrogen iodide mol fraction 1.3×10^{-5}.

This is an estimate only. We ascribed the total E(GE) change (3 mV) caused by the dissolution of iodine to a change in h. The medium is varied by the additions of iodine, and, as about 50 % of the I^- ions are transformed to I_3^-, the activity factor of the hydrogen ions is changed.

For our present purposes this estimate of the hydrogen iodide content was considered satisfactory, but it may be much improved if the medium effects are estimated with the help of model experiments.

Drying of iodine and determination of its final water content. Because iodine is extremely sensitive to redox impurities, we attempted to remove the last traces of water at room temperature instead of melting. The latter procedure would make it necessary to grind the material.

Incomplete removal of water can easily be corrected for.

A series of model experiments were carried out to find the most suitable drying agent. The drying procedure was monitored by using water containing ^3H.[14] Iodine and potassium iodide were dissolved in the smallest possible amount of water.

Iodine was precipitated, washed and dried. In the exploratory experiments the tritium content in the solution corresponded to about 20 MBq/l and in the main series about 600 MBq/l to increase the sensitivity. HI was replaced by KI because of the high vapour pressure of HI.

In each case three samples were prepared as identical as possible to keep the quenching effects (the counting efficiency) on the same level. A non-active iodine blank was used as the reference, the active iodine followed, and another sample with active iodine plus a standard addition of tritiated water was finally counted.

The β counting of the tritium decay was carried out by using a liquid scintillator (ACS) from The Radiochemical Centre, Amersham, GB. A scintillation spectrometer, Packard model 3375, was used for the measurements. This instrument is provided with a special measuring channel for ^3H.

The iodine samples were dissolved in a deoxygenated 0.5 M NaOH solution containing 0.15 M N_2H_4. This solution dissolves iodine rapidly and a colorless solution is formed. Three drying agents were tested: molecular sieves (10 A), sulfuric acid and phosphorus pentoxide. The last two were dispersed in a silica carrier as supplied by the Merck Company. Our results are summarised in Table 1.

Table 1.

Sample No.	Drying agent	Weight % water
1a	Molecular sieves	$0.07_9\pm0.03$
1b[a]	Molecular sieves	$0.08_4\pm0.01$
2a	Molecular sieves	0.073 ± 0.002
3a	Molecular sieves	0.062 ± 0.002
2b	Sulfuric acid	0.016 ± 0.001
3b	Sulfuric acid	0.016 ± 0.001
2c	Phosphorus pentoxide	0.013 ± 0.001
3c	Phosphorus pentoxide	0.037 ± 0.001

[a] Sample 1b was removed after two days from the desiccator and placed into a vessel provided with tritiated water. The analysis was carried out two days later. Sample 1a was analysed at the same time, it had by then been dried for 4 d. The insignificant difference between the two water contents indicates that the hygroscopicity of iodine lies below the detection limit of this method.

In the desiccator provided with P_2O_5 a brown gas with a strong smell had evolved. Iodine probably had reacted with the phosphorus (III) acid impurity usually present in commercial preparations (Ref. 13, p. 353). This drying agent cannot therefore be used.

Some change had also occurred in the desiccator with sulfuric acid. The surface of iodine had formed a compact mass that had to be pulverised with a glass rod. Also in this case we suspect some volatile impurity (*cf.* Ref. 13, p. 352).

However, no change could be detected in the iodine crystals dried over molecular sieves. Although this desiccant seems to react rather slowly, it should be preferred. The drying period must be prolonged and the drying agent preferably renewed after some days.

The procedure finally adopted consisted of drying iodine over molecular sieves that had been heated to 200 °C and allowed to cool under vacuum. The iodine samples were placed in the desiccator, this was exhausted, oxygen was added and finally exhausted a second time as described in the procedure part.

To determine the water content in non-active samples we used the method of Farrow and Hill.[11]

Iodine was dissolved in dried bromine. The IR absorption between 4000–3100 cm^{-1} was measured using Infrasil cells. The water peaks at 3549 and 3647 cm^{-1} were measured. A typical preparation contained 0.014 weight % water in good agreement with the model experiments.

The combined figures for the HI- content and the residual water content indicate that the occluded water contains some hydrogen iodide (approximately 0.7 M). From this we conclude that the iodate content must be negligible.

The efficiency of the purification method. The metal ion impurities were seen from the mass spectrometric study to be reduced considerably with our method. It was also of interest to find the efficiency for the *removal of the negative ion impurities.* Chloride and bromide are common impurities in the commercial hydrogen iodide and iodine preparations, CN^- may be formed when iodine comes into contact with organic substances.

Cl^- and CN^- were used as model ions. Hence, ^{36}Cl and ^{14}CN were used as tracers. Iodine was dissolved and precipitated using radioactive water. KI was employed instead of HI to avoid losses due to volatilization of HCl and HCN. However, the precipitated iodine was washed with non-active water. It was dried in the same manner as described above.

Several independent series of experiments gave the result that the mol fraction of chloride in the iodine phase is about 1000 times lower than in the starting solution, while the cyanide mol fraction is reduced by a factor of 50.

The uncertainty of these conclusions may be estimated by the fact that the total activity (from the iodine and the washings) was found to amount to 106 % of the initial amount of ^{36}Cl activity, and to 95 % of the initial amount of ^{14}CN. The total amounts of tracers used were 300 kBq ^{36}Cl and 150 kBq ^{14}CN. 99.9 % of the total amount of Cl was found in the washings and 98 % of the total CN. The amount of chloride ions in the HI and I_2 preparations were assumed to equal their maximum values according to the specification from the supplier.

Hence we may have little doubt that the decomposition of the multicharged polyiodide complexes by dilution represents a quite efficient way of purifying iodine.

CONCLUSIONS

A single step of slow precipitation from a saturated 10 M hydrogen iodide solution appears to furnish an iodine phase with a contamination level which lies below 0.01 %. A more precise specification is difficult at present because of the uncertainties of trace analytical methods.

Drying with molecular sieves brings the water content down to a few hundredths of a percent within a few days as shown by tritium tracers. The exact value of the water content of a particular iodine sample is easily measured with infrared spectroscopy to within a few parts per 10^5.

Hence this monoisotopic, non-hygroscopic element, which may easily be transformed to a higher or lower oxidation state, may be regarded as an especially valuable analytical standard substance.

Acknowledgements. This work has been supported by *Statens Naturvetenskapliga Forskningsråd* (the Swedish Natural Science Research Council). I wish to express my thanks to Dr. Georg Biedermann for the help with various parts of this work. Mr. Sture Lind modified the filtering funnel for me. I am also indebted to the Royal Institute of Technology for fellowships. I am most grateful to Professor Ingmar Grenthe and Professor Diego Ferri for their valuable comments on the manuscript.

REFERENCES

1. Stas, J. S. *Fortschr. Chem.* (1867) 15 and 159.
2. Gross, G. *J. Am. Chem. Soc. 25* (1903) 987.
3. Vanino, L. *Handbuch der Präparativen Chemie,* Verlag V Ferdinand Enke, Stuttgart 1925, Band 1, p. 59.
4. *Gmelins Handbuch,* 8. Aufl., Syst.-Nr. 8 (Jod), Lief. 2, 1933, p. 56.
5. Biedermann, G. and Ferri, D. *Chem. Scr. 2* (1972) 57.
6. Kolthoff, I. M. and Belcher, R. *Volumetric Analysis III,* Interscience, New York–London 1957, p. 220.
7. Bower, V. E. *NBS Spec. Publ. 343* (1971) 147.
8. Woodward, C. and Redman, H. N. *High Precision Titrimetry, Anal. Sci. Monogr. No. 1, Soc. Anal. Chem.,* London 1973.
9. Analytical Chemists' Committee of Imperial Chemical Industries Limited, *Analyst 75* (1950) 577.
10. Sundstrand, S. *Acta Chem. Scand. A 37* (1983) 777.
11. Farrow, R. N. P. and Hill, A. G. *Analyst 102* (1977) 480.
12. Wartenberg, H. von, Strzelczyk, Br. and Borris, G. *Chem. Fabrik 1* (1928) 617.
13. Lux, H. *Anorganisch Chemische Experimentierkunst,* Auflage 3, Johann Ambrosius Barth, Leipzig 1979, p. 158.
14. Reid, A. F. and Mills, R. *J. Inorg. Nucl. Chem. 26* (1964) 892.

Received February 28, 1983.

Acta Chemica Scandinavica A 37 (1983) 795–801

Coulometric Reduction of Iodine with Copper(I) in Sodium Chloride–Mercuric Chloride Media with Iridium Cathode

SIGNAR SUNDSTRAND

Department of Inorganic Chemistry, The Royal Institute of Technology, S-100 44 Stockholm, Sweden

Purified iodine has been reduced to iodide with copper(I) ions generated by constant current coulometry on an iridium cathode, using the ionic medium 3 M NaCl, 0.3 M $CuCl_2$, 0.05 M $HgCl_2$. This solution disproportionates iodine to $HgICl_3^{2-}$ and ICl_2^-. The redox potential is raised thereby into the vicinity of the half-cell potential of the O_2/H_2O_2 couple (0.7 V).

Gran's method was used to evaluate the potentiometric equivalence point.

The uncertainty of our analysis was found to increase from ±0.03 % to 0.10±0.04 % as the iodine sample was raised from 0.2 to 1.2 mmoles because of the oxygen error. Platinum cathodes gave results, which could not be reproduced.

The present communication represents the third part of a series dealing with the preparation and application of purified iodine. The preceding article[1] summarized our comprehensive oxidation experiments.

For practical and theoretical reasons we turned to the far more difficult problem of reducing iodine to iodide by constant current coulometry. Our main intention has been to provide a method for the standardization of reducing agents.

Moreover one should take advantage of the almost unique property of the element iodine: that it can readily accept as well as donate one electron. Hence its purity can be tested in several ways.

There are three principal *sources of error in iodometry:* oxidation of iodide by oxygen (air) in acid solutions, incomplete attainment of redox equilibrium between iodine and the reagent, and loss of iodine or its reaction products by volatilization. The magnitudes of these errors are difficult to estimate on the basis of the published literature. The present work aims at throwing some light on these questions.

For obvious reasons an *intermediate* reducing agent is required in constant current coulometry. This must be generated *in situ* from the oxidized form of a species, kept at a high and virtually constant concentration in the course of the titration.

A redox intermediate must satisfy three main requirements. It must be generated with a theoretical current efficiency, the intermediate should react rapidly and stoichiometrically, and finally its excess must be determinable, if possible, by potentiometry.

In Swift's laboratory[2] these questions were studied systematically, and it was found that these three conditions are best met by the Cu(II)–Cu(I) couple in a chloride medium. We have corroborated their conclusion. Several other reducing intermediates have been proposed such as Fe^{2+} [3,4,5], Ti(III)[6], the Fe(II)–EDTA-complex[7], and Sn(II)[8,9] but they have proved unsuitable for our purpose. Another advantage of the Cu(II)/Cu(I)-couple is that its $E^{0\prime}$ is as high as 0.51 V in a 3M NaCl-medium[10]. Thus the redox potential can be kept in the vicinity of the potential of the competing couple O_2/H_2O_2 (0.7 V) during the whole titration[11].

METHOD OF ANALYSIS

Procedure. The titration procedure consists of five principal steps: (1) Pretreatment of the ionic medium. (2) Start titration. (3) Main electrolysis, in which an excess of Cu(I) is generated to

0302-4377/83 $2.50

shorten the lifetime of ICl_2^-. (4) Introduction of the iodine sample. (5) End titration.

General. We decided to carry out the coulometric reduction of iodine in a medium consisting of 3 M NaCl, 0.3 M $CuCl_2$ and 0.05 M $HgCl_2$. Under these conditions the concentration changes during a titration may be conveniently visualized with the help of Fig. 1 which shows lines for the copper and iodine bearing species:

$$\lg [Cu(I)]/[Cu(II)] = f(pE) \quad (1)$$

and

$$\lg C_j/a_{I_2}^{1/2} = f(pE) \quad (2)$$

where a_{I_2} denotes the activity of iodine and solid iodine has been taken as reference; C_j stands for $[ICl_2^-]$, $[I^-]$, or $[HgICl_3^{2-}]$. The latter ion, which predominates, represents in the following discussion the sum of *all* the iodide bearing mercury(II) species. The formal potentials needed to construct the redox diagram are denoted by circles. They have been determined from emf measurements, as described in a separate communication[10].

In our solvent *disproportionation* of iodine occurs:

$$I_2Cl^- + HgCl_4^{2-} \rightleftharpoons ICl_2^- + HgICl_3^{2-}; \quad (3)$$

$$\lg K = -2.0 \quad (4)$$

Thereby pE in an iodine solution is increased to the concentration independent value 14.0, denoted by i in the diagram, while in the absence of $HgCl_2$ it is as low as 12.8. Another advantage is that the solubility of iodine is increased to about 4 mM by the addition of 0.05 M mercury(II).

The intermediate Cu(I) was generated from Cu(II), present in a large excess in the solution.

The *titration reaction* can consequently be summarized as:

$$ICl_2^- + HgCl_4^{2-} + 2CuCl_3^{2-} \rightarrow HgICl_3^{2-} + 2CuCl_2 + 5Cl^- \quad (5)$$

The pH was chosen to lie in the vicinity of 3. This represents a compromise between conflicting demands, and is situated near to the maximum pH at which the reaction between IO_3^- and I^- is still sufficiently rapid. Iodate ions are introduced into the solution with the alkaline iodine stock solution[1,12].

The *equivalance point* is denoted by e in Figs. 1 and 2. It is the point with zero electron excess over [Cu(II)] and [I(−I)] and the following equation is valid:

$$[Cu(I)] = 2([ICl_2^-] + [I_2Cl^-] + [I_2] + [I_3^-]) \quad (6)$$

Fig. 2 resembles a conventional pH diagram. It has been constructed because the concentrations of polynuclear species (I_3^-, I_2Cl^- and I_2) cannot be properly illustrated in a relative diagram.

The lines for the three last species in eqn. (6) are omitted from Fig. 1 for the sake of simplicity. They should be represented by two horizontal lines at −1.3 for $[I_2Cl^-]^{1/2}$ respectively −1.6 for $[I_2]^{1/2}$ [13], and the $[I_3^-]^{1/3}$-line with a slope of −1/3 ($pE^0 = 8.8$, estimated with data from[10]).

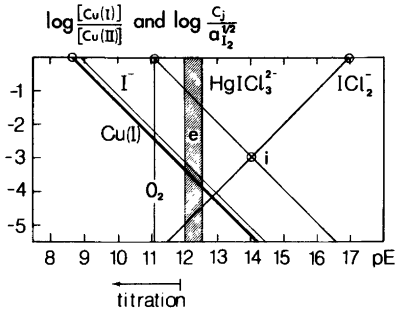

Fig. 1. A simplified redox diagram for copper and iodine in the medium 3M NaCl, 0.3M $CuCl_2$, 0.05M $HgCl_2$. Symbols: "i": pE of an I_2-solution, "e": zone of equivalence points, line "O_2": $pE(O_2/H_2O_2)$ at pH 2.5 and circles: data[10].

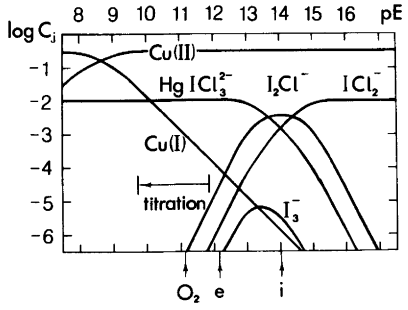

Fig. 2. Logarithmic distribution diagram[10] for the copper- and the iodine bearing species in 3M NaCl medium at the 0.3 M $[Cu]_{tot}$ and the 0.01 M $[I]_{tot}$ levels. Symbols: "i": pE of an I_2 solution, "e": equivalence point, "O_2": $pE(O_2/H_2O_2)$[11,17] at pH 2.5.

The *pE at the equivalance point* varied from 12.0 to 12.5 as the amount of iodine was changed systematically in our titrations. In conventional iodine titration, for instance with thiosulfate, pE at the equivalence point may be estimated to 7.5 (440 mV), which is about 5 pE units (300 mV) lower than our actual values.

Potentiometry. We used a *cell without liquid junction* to measure the Cu(II)/Cu(I) potential in the test solution (TS):

– Glass electrode (GE) | TS | Ir (indicator electrode) + (I)

Here the test solution contains NaCl, $CuCl_2$, $HgCl_2$, HCl, I_2, the Cu(I) generated coulometrically as well as the products of the different redox and complex formation reactions. The emf of this cell at 25 °C can be written as

$$E=E(\mathrm{Ir})-E(\mathrm{GE}) \quad (7)$$

Where

$$E(\mathrm{Ir})=E^{0\prime}[\mathrm{Cu(II)/Cu(I)}]+59.16\lg[\mathrm{Cu(II)}]/[\mathrm{Cu(I)}] \quad (8)$$

$$E(\mathrm{GE})=E^{0\prime}(\mathrm{GE})+59.16\lg h \quad (9)$$

Of these terms the $E^{0\prime}$s represent isothermal constants and $h=[H^+]$.

As the composition of the test solution changed but slightly in the course of a titration, we could neglect the variation of the activity coefficients of the reacting species.

Therefore the emf of cell (I) can be written in the simple form

$$E=E_0+59.16\lg[\mathrm{Cu(II)}]-59.16\lg[\mathrm{Cu(I)}] \quad (10)$$

The [Cu(II)] decreases very little during the start or end titrations, and it may also be regarded as a constant in the first estimate of the equivalence point.

This estimate was then improved by calculating the correct [Cu(II)] in all the measured points.

The evaluation of the equivalence points and the titration error estimates. These calculations were carried out according to the same principles as in the oxidimetric titrations[1]. Titration 6 in Table 1 has a precision of about 2×10^{-5}. Thus the titration error, which is fifty times higher in this case, is certainly not affected to any appreciable extent by the imperfections of the localization of the equivalence point.

EXPERIMENTAL

Techniques. Our choice of experimental conditions has been guided by the desire to minimize the oxygen error. Further we decided for practical reasons to use a technique involving instruments and other equipment readily available in any modern laboratory.

Once the titration had been started, the cell was exposed to the atmosphere no longer than a few minutes altogether. The introduction of redox-active impurities, dust and droplets was avoided by maintaining a slight overpressure of argon. This technique is certainly to be preferred to a continuous stream of gas.

The argon was purified by passing it through a copper column held at 150 °C in order to remove oxygen, and then through a washing bottle containing 3M NaOH. This was saturated with solid Ag_2O in order to oxidize any traces of reducing impurities like CO or H_2. Finally the gas passed through two sintered glass filters of porosity G3.

In *model experiments* this purified gas could be passed through solutions with a low redox buffer capacity[1] ($\beta=20\times10^{-6}$ mV^{-1}) for more than one hour without affecting the redox potential more than 0.01 mV.

For reasons, which we discussed in detail in the previous communication[1], we used the *ampoule technique* to introduce the iodine sample.

Titration procedure. Step 1. Pretreatment in situ purification of the ionic medium to reduce the redox impurity level. Sufficient purified hydrochloric acid was added to completely neutralize the amount of hydroxide ions introduced later with the iodine sample. Immediately before each of the three "Gran titrations" (see below) argon was passed through the solution for about 20 minutes to remove oxygen. About three ml of the ionic medium was transferred by exhaustion up into the capillary of the Wilhelm bridge after the initial treatment with argon. Thereby the capillary could later be flushed with a solution of known composition.

A Gran titration (the very first) was carried out to determine the impurity content of the medium.

After this the solution was left overnight to attain chemical equilibrium and a stable temperature in the cell vessel (*cf.* Fig. 3). In the morning a few drops of iodine solution were added to

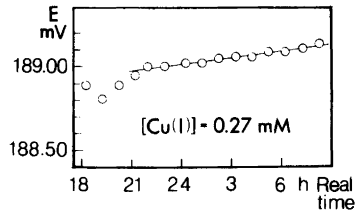

Fig. 3. Drift of the emf of cell (I) preceding a start titration. (The cell was put into the thermostat at 18.00 h). The slope of the line is 0.01_3 mV/h.

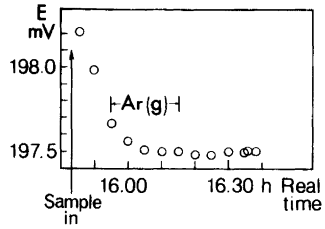

Fig. 4. The emf of cell (I) as a function of time illustrating the rapid attainment of the equilibrium (5), and the purity of our argon. The alkaline iodine sample was introduced at 15.40 h, prior to this instant E was 65.05 mV.

diminish the Cu(I) concentration.

Step 2. Start titration. A Gran titration was now made to determine the excess of Cu(I) and to establish a reference redox potential level defined by eqn. (6).

Step 3. The main electrolysis. An excess of about 0.2 mM Cu(I), compared to the amount of iodine introduced in step 4, was generated to shorten the lifetime of ICl_2^-. This is the lowest concentration providing reversible redox potentials.

Step 4. Iodine sample. During the introduction of the ampoule the neck of the cell was flushed with argon streaming through a glas capillary. No gas was passed through the test solution itself, not to expel any ICl or iodine formed. The establishment of redox equilibrium (5) was controlled (*cf.* Fig. 4), and it was always found to be attained within 15–20 min.

Step 5: End titration. The third Gran titration with stepwise generation of Cu(I) determines the equivalence point. The other details were similar to those described in the previous work.[1]

A complete end titration is shown in Table 2. As is clear from this table a typical end titration lasts for about one hour, while a complete experiment takes from three to five hours. The equilibrium is established within one minute ensuing the pasage of current, and the potentials have always been found to be very stable.

This conclusion is also evident from Figs. 3, 4 and 5. The potentials of the cathode and the indicator electrode did always agree within 0.01 mV. It is also apparent from Table 2 that most of the data and the calculated emf values also agree to within this limit.

Preparation of the ionic medium. For our present purposes only contaminants which may participate in redox reactions have been of interest. Most commercial chemicals, like our starting substance NaCl, contain as the main redox impurities the heavy metal ions Fe^{3+}, Mn^{2+}, VO_2^+, and Cr^{3+}. Fortunately these ions form slightly soluble hydroxides, oxides or other basic salts already in acid solutions. They may therefore be conveniently eliminated by coprecipitation for instance with freshly prepared hydrated silica at about pH 6 (*cf.* Ref. 14). We used instead *in situ* precipitated copper hydroxochloride as the carrier since our medium contained 0.3 M $CuCl_2$. The purified ionic medium has been found, by coulometric titration with Cu(I) ions,

Table 1. Final series of iodometric titrations.

No.	μeq. introduced	Current/mA start- and end-	main titration	Yield / %
1	392	10	10	100.03
2	434	10	51	99.98
3	1069	10	10	99.98
4	2337	10	51	100.05
5	2351	10	10	100.12
6	2356	10	51	100.10[a]

[a] Medium: 3M NaCl + 0.5M $CuCl_2$+0.3 M $HgCl_2$.

Note: The amount of iodine is varied with a factor 6, the current with a factor 5.

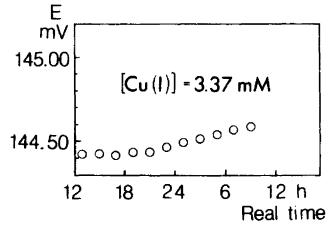

Fig. 5. Stability of the emf of cell (I) after an end titration and the long time drift which is about 0.01_3 mV/h at $t > 20.00$ h.

Table 2. A typical end titration.
Cell: – GE | TS | Ir +

No.	Time/h	w^a/mmol	E/mV	$E_{calc}{}^b$/mV	$\beta/10^6$ mV^{-1}
23	11.28	2.38631	203.08	203.12	22
	11.38		203.08		
24	11.41	2.38803	201.57_5	201.61	23
25	11.44	2.39203	198.38	198.41	27
26	11.46	2.39603	195.55	195.56	30
27	11.49	2.40004	192.99	192.99	32
28	11.53	2.40519	190.03	190.02	37
29	11.55	2.41147	186.82	186.82	42
30	11.58	2.41661	184.46_5	184.46	46
31	12.01	2.42290	181.84_5	181.84	51
32	12.04	2.42804	179.89	179.88	55
33	12.08	2.43432	177.68	177.68	59
34	12.11	2.44060	175.64_5	175.65	64
35	12.14	2.44688	173.76_5	173.76	69
36	12.17	2.45201	172.32	172.32	73
37	12.21	2.45829	170.65	170.66	78
38	12.23	2.46342	169.36_5	169.37	82
39	12.26	2.46969	167.87_5	167.89	86
40	12.30	2.47597	166.47	166.48	92
	14.48		166.46		

[a] w is the amount of electrons introduced at the cathode.[1] [b] According to eqn. (10):
$E_{calc}=11.14+59.16 \lg [(50+2.35789 - w)/(w - 2.35789)]$
Note: $\beta=F/RT$ [Cu(I)]/[Cu]$_{tot}$ is the redox buffer capacity.[1]

to contain about 120 μeqs./l of a reducing agent. This contamination level turned out to decrease rapidly on standing. In one case, studied in detail, it dropped to 10 μeqs./l. The latter figure corresponds to a contamination ratio of 3 parts per 10^6.

This gradual decrease of the concentration of reducing agent (presumably Cu(I)) stopped after three weeks and it is probably due to the oxidation by air which was let in when a sample was withdrawn for analysis. It should be pointed out that in the course of the pretreatment the impurity concentration was reduced still further.

The electrolysis cell. As the electrolysis cell we used a Wilhelm bridge of the general arrangement

(Cathode) Ir | TS | Salt bridge | Anode compartment (II)

The salt bridge had the composition

| Ionic medium | 3M LiCl

and the anode compartment

| saturated LiI | Pt-anode (III)

Lithium chloride and iodide have been preferred because of their high solubilities. The anode was a 2 cm^2 platinum net. During the electrolysis I_3^- is formed:

$$3I^- \rightarrow I_3^- + 2e \qquad (11)$$

This oxidation could be carried out with the theoretical current efficiency up to at least 51 mA. No evidence has been found for oxygen evolution. This current cannot be much exceeded because of the evolution of hydrogen on the cathode. When this occurs, a large difference between the potentials of the cathode and of the indicator electrode remains after the passage of current.

The ampoules and the instruments used were the same as earlier.[1] A new voltmeter, HP 3456A, (Hewlett-Packard) has been employed for the emf measurements and the coulometry. Thereby the accuracy and the precision of emf readings have been greatly enhanced.

EXPLORATORY EXPERIMENTS

In the initial phase of this investigation a great number of exploratory experiments were made which might be of some general interest and will therefore be shortly summarized below.

Comparison of platinum and iridium electrodes. We could not use platinum electrodes in our 3M NaCl medium. From six titrations with platinum electrodes of about 270 mg iodine (2 mmoles) we found the average yield 100.09 ±0.24 %, while six titrations with iridium electrodes with the same amount of iodine and under otherwise identical conditions provided 100.09 ±0.04 %.

Choice of acidity level. It was an inconvenience to work in *acid solutions* (pH 2–3). We found that at pH about 4.5 (acetic acid–acetate buffer) highly stable Cu(II)/Cu(I) potentials can be obtained, however, at this pH the reaction between IO_3^- and I^- (introduced with the iodine stock solution) to iodine was too slow. In our medium this reaction was sufficiently rapid only at pH < 3.

In some experiments we performed the electrolysis in a neutral solution, acidified just prior to the addition of iodine, waited until equilibrium (5) had been established and then realkalified. This was done by introducing a concentrated sodium acetate solution [purified by precipitating $Cu(OH)_2(s)$]. However, this technique did not provide the desired result, probably because of small amounts of redox impurities in the acetate solution.

Choice of intermediate reagent. In a series of preliminary experiments we attempted to find the most suitable intermediate for high precision coulometric reduction of iodine.

We first tried *Sn(II)* which has proved to be a rapid iodometric reagent in volumetric and in potentiometric titrations. Moreover, the Sn(II)/Sn(IV) couple in hydrochloric acid medium has been found (in our laboratory) to furnish reversible potentials, uninfluenced by the choice of the electrode material (Hg or Pt). However, when iodine was introduced, difficulties arose. The redox potential drifted slowly without showing a tendency to attain a stable value. Moreover, different indicator electrodes in the same solution sometimes differed by many millivolts. These complications are probably due to the slow replacement of chloride by iodide in the chloride complexes of tin. Similar troubles were met with in bromide medium.

According to Bock and Greiner[15] the following Sn(IV)/Sn(II) formal potentials are valid in 1M acid medium: 147 mV (HCl), 127 mV (HBr) and −38 mV (HI). This illustrates the higher stabilities of the iodide complexes. We next turned to the *ferrous ion,* but neither the fluoride nor the phosphate complex could be employed, because the rate of iodine reduction was very sluggish, and we could not find any intermediate reagent to catalyze the reaction. The Fe(II)-EDTA complex proposed by Stein[7] could not be utilized because of the high pH (pH 6) required.

Finally, we have taken up the study of *cuprous ion* in chloride medium. Normally when iodide and $CuCl_2$ are mixed in a chloride medium the following reaction occurs:

$$I^- + CuCl_2 + 1\tfrac{1}{2}Cl^- \rightarrow \tfrac{1}{2}I_2Cl^- + CuCl_3^{2-} \qquad (12)$$

But if iodide could be complexed, it would be possible to make this reaction to proceed from right to left.

Furman and Miller[16] found that when Hg(II) is present, the free iodide concentration is diminished so much that iodine can be titrated with reductants whose E^0 values are as high as 0.5–0.6 volt. They also found stable potentials near the equivalence point indicating that the rate of oxidation of complex bound iodide by oxygen is much suppressed. The method presented in this communication is based on this experience.

RESULTS

The final series of analyses are summarized in Table 1. The amount of iodine sample was varied between 400 and 2000 μeqs., and the current between 10 and 51 mA. It is apparent from Table 1 that we got a positive error of as much as 0.1 % at the largest amounts of iodine.

This error is probably caused by the residual oxygen, which has thus proved to be significant, even though the overwhelming part of the iodide ions in our experiments was bound in the form of mercuric complexes (*cf.* Ref. 10). Oxygen is known to act as a very slow oxidizing agent at 25 °C, hence the difference between the three first and the three last experiments is most likely due to the prolonged electrolysis period as well as to the lower redox potentials encountered in titrations 4–6.

CONCLUSIONS

All the problems we met with in this study are presumably due to the residual oxygen remaining after the pretreatment of the test solution.

It is clear from Table 1 that for maximum precision and accuracy small amounts of iodine must be titrated as rapidly as possible without sacrificing the weighing precision, the accuracy of the equivalence point evaluation and the exact determination of the current time integral. The best compromise is probably not far from the conditions chosen in experiments 1 to 3. To raise the precision and accuracy of the coulometric iodine reduction to the vicinity of 0.01 % further efforts are needed to suppress the oxygen error. Preheating the test solution might be one of several possible ways.

Acknowledgements. This work has been supported by *Statens Naturvenskapliga Forskningsråd* (the Swedish Natural Science Research Council). The author is very grateful to Dr Georg Biedermann for advice, and to The Royal Institute of Technology for fellowships. Professors Ingmar Grenthe, Liberato Ciavatta, Diego Ferri and Vincenzo Romano had valuable comments on the manuscript. I would also like to thank Dr Julius Glaser for valuable discussions.

REFERENCES

1. Sundstrand, S., *Acta Chem. Scand. A 37* (1983) 777.
2. Meier, D. J., Myers, R. J. and Swift, E. H. *J. Am. Chem. Soc. 71* (1949) 2340.
3. Marinenko, G. and Taylor, J. K. *J. Res. NBS, 67A,* (1963) 453.
4. Knoeck, J. and Diehl, H. *Talanta 16* (1969) 181.
5. Yoshimori, T., Tanaka, T., Ogawa, M. and Horikoshi, T. *Anal. Chim. Acta 63* (1973) 351.
6. Arthur, P. and Donahue, J. F. *Anal. Chem. 24* (1952) 1612.
7. Stein, H. H. *Diss. Abstr. 16* (1956) 2320.
8. Bard, A. J. and Lingane, J. J. *Anal. Chim. Acta 20* (1959) 463.
9. Takahashi, T. and Sakurai, H. *Rep. Inst. Ind. Science, (University of Tokyo) 13* (1) (1963) 1–37.
10. Biedermann, G. and Sundstrand, S. *Acta Chem. Scand. A 37* (1983) 535.
11. Kern, D. M. H. *J. Am. Chem. Soc. 76* (1954) 420.
12. Sundstrand, S. *Acta Chem. Scand. A 37* (1983) 787.
13. Cason, D. L. and Neumann, H. M. *J. Am. Chem. Soc. 83* (1961) 1823.
14. Ciavatta, L., *Arkiv Kemi 20* (1963) 417.
15. Bock, R. and Greiner, G. *Z. Anorg. Allg. Chemie, 295* (1958) 70.
16. Furman, N. H. and Miller, C. O. *J. Am. Chem. Soc. 59* (1937) 152.
17. Linke, W.F. and Seidell, A. *Solubilities of Inorganic and Metal-Organic Compounds,* American Chemical Society, Washington, D.C. 1965, 4th Ed. Vol II, p. 1231.

Received February 28, 1983.

Acta Chemica Scandinavica A 37 (1983) 803–806

Single-Ion Activities of Lanthanum Chloride in Aqueous Solution

TOR HURLEN

Department of Chemistry, University of Oslo, Blindern, Oslo 3, Norway

Single-Ion activity coefficients of lanthanum and chloride ions in aqueous 0.1–1.4 molal lanthanum chloride solutions at 25 °C have been determined by a liquid-junction approach. For either sort of ion, obedience is found to $\ln f_i = -z_i^2 Ac^{1/3} + (z_i^2/r_i)Bc$, where A and B are constants common to the ions of the salt, c is the salt molarity of the solution and z_i and r_i are the ion charge number and the effective ion radius, respectively. This is interpreted by a combined quasi-lattice and ion-hydration excess energy treatment.

True single-ion activity coefficients (γ_i) are obtainable by a double-layer approach.[1] Convenient single-ion activity coefficients (γ_i'), defined by eqn. (1)

$$\gamma_i' = \gamma_i r^{-z_i/2} \tag{1}$$

where z_i is the ionic charge number (with sign) and r means γ_+/γ_- for potassium chloride in pure saturated solution of this salt, are obtainable by a liquid-junction approach.[2] The two approaches have recently been tested against each other for aqueous solutions of sodium sulfate.[3] This testing is satisfactory at low concentration, favours the liquid-junction approach at higher concentration and shows r to be close to unity at 25 °C.

For aqueous single-salt solutions, rational (mol fraction) activity coefficients are obtained from molal ones by eqn. (2):

$$f_i(\text{or } f_i') = (1 + (\nu x/55.51))\gamma_i(\text{or } \gamma_i') \tag{2}$$

where ν is mol of ions per mol salt and $x/55.51$ is the mol ratio of salt to water in the solution.[4] From studies of alkali-metal halide solutions,[5,6] it appears that such activity coefficients for the ions of single-salt solutions at medium to high concentration are well represented by equations like eqn. (3)

$$\ln[f_i(\text{or} f_i')] = -A_i(c/c^\circ)^{1/3} + B_i(c/c^\circ) \tag{3}$$

where A_i and B_i are salt and ion dependent constants (25 °C, 1 atm) and c/c° is the dimensionless salt molarity of the solution. The two right-hand terms of this equation have been ascribed to quasi-lattice ion–ion interaction and hydration energy loss, respectively.[5,6] In the linear term, m/m° may replace c/c°.

The present work pursues the above description by studies on aqueous solutions of the 3:1 salt lanthanum chloride. Main aims are to test the applicability of eqn.(3) for such solutions and to have more information on the constants A_i and B_i of this equation. By having stable, quite large and spherical ions with little tendency to complex each other or to hydrolyze water,[7] lanthanum chloride is a suitable salt for the present studies.

EXPERIMENTAL

The experimental work comprises measurements of the liquid-junction containing equilibrium potential (E′) of the Ag/AgCl electrode in aqueous 0.1–1.4 molal $LaCl_3$ solutions against the saturated calomel electrode under isothermal conditions at 25 °C. From such data, the convenient molal activity coefficient (γ_-') of the chloride ion is obtained by eqn. (4)

$$\gamma_-' = \frac{m^\circ}{m_-}\exp\left[-\frac{F}{RT}(E' - \Delta\phi - E^\circ + 0.241\text{V})\right] \tag{4}$$

where m_-/m° is the dimensionless chloride ion molality concerned, E° is the standard molal

0302-4377/83 $2.50

hydrogen-scale potential of the Ag/AgCl electrode, and $\Delta\phi=\phi_t-\phi_r$ is the liquid-junction potential difference between the test solution (ϕ_t) and the saturated KCl solution of the calomel reference electrode (ϕ_r), all at 25 °C.[2] In the present work, 0.222 V has been used for $E°$,[8] and $\Delta\phi$ has been estimated from the Henderson equaton[9] with limiting mobility data[8] for the ions.

The convenient molal activity coefficient (γ_+') is obtained from eqn. (5)

$$\gamma_+'=\gamma_\pm^4/(\gamma_-')^3 \qquad (5)$$

using presently determined values for γ_-' and tabulated data[8] for the mean molal ionic activity coefficient ($\gamma_\pm$). These activity coefficients are all stoichiometric bare-ion ones.

The solutions were made from high purity lanthanum chloride (ROC/RIC) and twice distilled water. They were deoxygenated with purified and premoistened nitrogen. The measurements were performed with equipment and procedures essentially as previously described.[2]

RESULTS

The results of the present work are summarized in Table 1, which also gives the previous[8] mean-ion data utilized. The activity data have been transferred to the mol-fraction scale by means of eqn. (2), the molality data to the molarity scale by means of solution density data,[7] and the outcome analyzed for the applicability of eqn. (3). In this analysis,[5] a search is made for a value of A_i which best makes $\ln f_i+A_i(c/c°)^{1/3}$ a linear function of $c/c°$ (with emphasis on the salt molarity range 0.1–1.0). The slope of this function is B_i.

Such testing results are given and illustrated in Figs. 1 and 2. Except for some deviation at high concentration, they essentially show obedience to eqn. (3) with the parameter values:

$$A_+=8.55 \text{ and } B_+=6.43 \qquad (6a)$$
$$A_-=0.95 \text{ and } B_-=0.44 \qquad (6b)$$
$$A_\pm=2.85 \text{ and } B_\pm=1.94 \qquad (6c)$$

for the cation, the anion and the hypothetical mean-ion, respectively, of lanthanum chloride in

Table 1. Data for aqueous lanthanum chloride solutions at 25 °C (see text).

$m/m°$	$c/c°$	$\Delta\phi$/mV	E'/mV	γ_-'	γ_+'	$\gamma_\pm$
0.1	0.0995	0.3	22.8	0.66	0.034	0.314
0.2	0.1985	1.7	8.0	0.62	0.024	0.274
0.3	0.297	2.7	-0.3	0.59	0.023	0.263
0.5	0.493	4.3	-10.2	0.56	0.028	0.266
0.7	0.686	5.5	-17.0	0.55	0.040	0.285
1.0	0.970	6.9	-25.2	0.56	0.078	0.342
1.4	1.339	8.4	-34.6	0.60	0.23	0.470

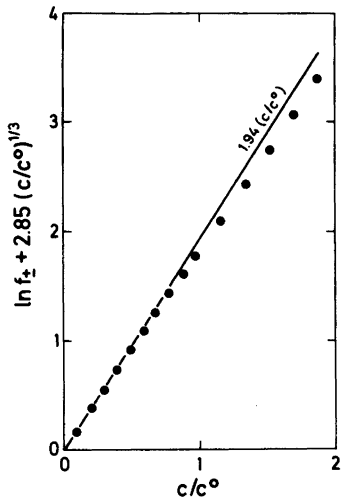

Fig. 1. Tests on the applicability of eqn. (3) to $f_\pm$ (with best fitting value for $A_\pm$).

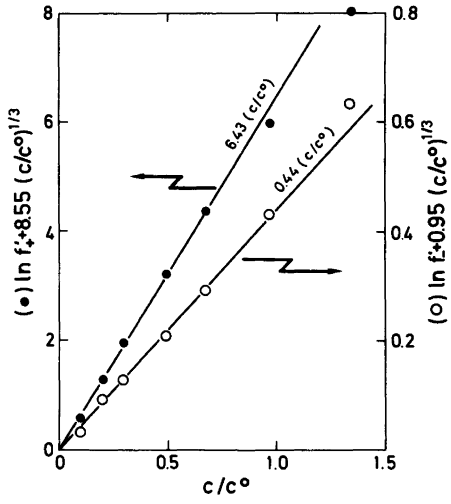

Fig. 2. Tests on the applicability of eqn. (3) to f_+' and f_-' (with best fitting values for A_+ and A_-).

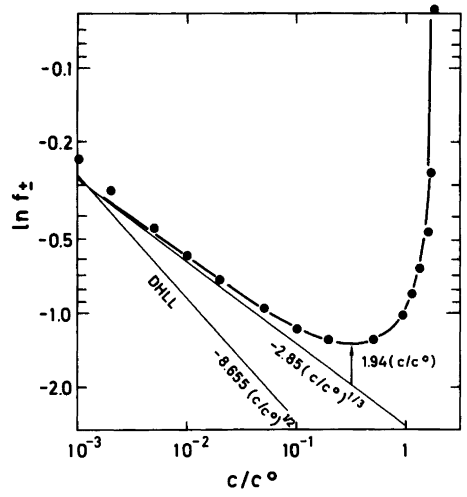

Fig. 3. Log-log plot of $\ln f_{\pm}$ *vs.* c/c° for lanthanum chloride in water at 25 °C. Curve is $-2.85(c/c^{\circ})^{1/3}+1.94(c/c^{\circ})$. DHLL means Debye-Hückel limiting law.

aqueous single-salt solutions at 25 °C. The lines in Fig. 2 should respectively give $\ln f_{+}'=-(3/2)\ln r$ and $\ln f_{-}'=(1/2)\ln r$ at $c/c^{\circ}=0$. That the lines essentially go through origo, supports that r be close to unity.

In Fig. 3, a log-log plot of $\ln f_{\pm}$ (from tabulated data[8]) *vs.* c/c° is given and compared to a curve

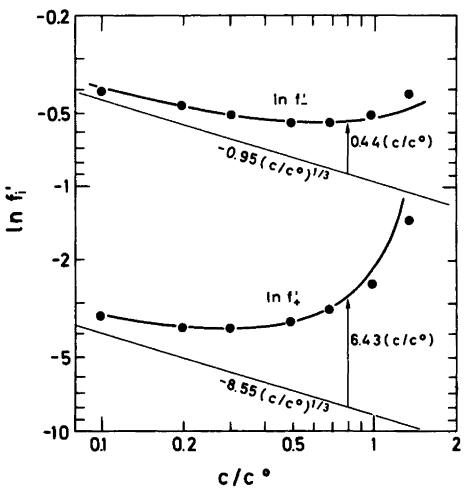

Fig. 4. Log-log plot of $\ln f_i'$ *vs.* c/c° for lanthanum chloride in water at 25 °C. Curves are $-A_i(c/c^{\circ})^{1/3}+B_i(c/c^{\circ})$ with noted values for A_i and B_i.

for the function $-2.85(c/c^{\circ})^{1/3}+1.94(c/c^{\circ})$ over an extended concentration range. The experimental data clearly follow this function well in the molarity range 10^{-2}–1. At higher concentrations, the above noted deviation is seen. At lower concentrations, another deviation appears towards approaching obedience to the Debye-Hückel limiting law (DHLL). In Fig. 4, analogous comparisons are made for the single-ion data over the concentration range covered.

DISCUSSION

Over an extended concentration range, (about 10^{-2}–1 M) the mol-fraction activity coefficients (f_{+}', f_{-}', $f_{\pm}$) of lanthanum chloride in aqueous solution clearly follow eqn. (3) with a negative cube-root term and a positive linear term. This matches what has previously been found for alkali-metal halides,[5,6] and makes this behaviour a more general one for strong electrolytes (ionophores). Since the activity coefficient (by $\mu_i^{ex}=RT\ln f_i$) represents excess energetic interactions over ideal ones ($\mu_i^{ex}=\mu_i-\mu_i^{id}$) for the dissolved ions, the two observed terms may be associated with electrostatic ion-ion interactions and remaining less ideal ion-water interactions by $\mu_i^{ex}=\mu_i^{el}+\mu_i^{re}$ with $\mu_i^{el}=-RTA_i(c/c^{\circ})^{1/3}$ and $\mu_i^{re}=RTB_i\,(c/c^{\circ})$.[6]

A negative cube-root term is expected from quasi-lattice treatment of ion-ion interactions,[10] provided the quasi-lattice type (the quasi-Madelung constant) and the effective dielectric constant be concentration independent. This is qualitatively satisfactory, but gives much room for possible deviations. From lattice energy (or Güntelberg charging) considerations,[6] one furthermore may expect $A_+:A_-:A_{\pm}=z_+^2:z_-^2:|z_+z_-|$ for a single-salt solution. In the present case, this means 9:1:3, which fully agrees with the experimental results [see eqns.(6a)–(6c) above].

A positive linear term is expected from a Born-charging treatment of ion hydration,[6] provided the effective dielectric constant involved (ε) be related to the one for pure water (ε_w) by $\varepsilon_w/\varepsilon=1+\delta c$, where δ is a constant. For single-salt solutions, the static dielectric constant appears to vary somewhat like this up to quite high concentration.[11] Also this is qualitatively satisfactory, but needs more elaboration. The Born-charging treatment furthermore gives $B_+/B_-=$

$(z_+^2/r_+)/(z_-^2/r_-)$, where r_+ and r_- are the effective radii of the dissolved cation and anion, respectively. With the results of eqns.(6a) and (6b), one hence obtains $r_+/r_-=0.62$ for the dissolved ions of lanthanum chloride. The corresponding Pauling radius ratio is 0.635.

The present results and their matching with simple expectations lend confidence to the possibility and profitability of determining single-ion activity data. The work moreover supports the applicability of a combined quasi-lattice and hydration energy treatment of ionic activity coefficients at medium to high electrolyte concentration.

REFERENCES

1. Daghetti, A., and Trasatti, S. *Can. J. Chem. 59* (1981) 1925.
2. Hurlen, T. *Acta Chem. Scand. A 33* (1979) 631.
3. Hurlen, T. *Acta Chem. Scand. A 37* (1983) 739.
4. Robinson, R. A. and Stokes, R. H. *Electrolyte Solutions,* 2nd Ed., revised, Butterworth, London 1970.
5. Hurlen, T. *Acta Chem. Scand. A 34* (1980) 7.
6. Hurlen, T. *Acta Chem. Scand. A 35* (1981) 587.
7. *Gmelin Handbook of Inorganic Chemistry, 8th Ed., Rare Earth Elements (Sc, Y, La-Lu), Part C4b (Chlorides),* Springer, Berlin-Heidelberg-New York 1982, pp. 72–88.
8. Parsons, R. *Handbook of Electrochemical Constants,* Butterworth, London 1959.
9. Vetter, K. J. *Electrochemical Kinetics,* Academic, New York and London 1967, p. 49.
10. Bockris, J. O'M. and Reddy, A. K. N. *Modern Electrochemistry,* Plenum, New York 1970, Vol. 1.
11. Pottel, R. In Franks, F., Ed., *Water,* Plenum, New York and London 1973, Vol. 3, Chapter 8.

Received March 7, 1983.

Acta Chemica Scandinavica A 37 (1983) 807–816

Structure, Thermal Stability and Gas Chromatographic Behavior of Some Dialkyldithiocarbamate Chelates of Palladium(II)

MARJA-LIISA RIEKKOLA,[a] TAPANI PAKKANEN[b] and LAURI NIINISTÖ[c]

Departments of Chemistry, [a] University of Helsinki, SF-00100 Helsinki 10, Finland, [b] University of Joensuu, SF-80101 Joensuu 10, Finland and [c] Helsinki University of Technology, SF-02150 Espoo 15, Finland

Four palladium(II) chelates with the dipropyldithiocarbamate (DPDTC), dibutyldithiocarbamate (DBDTC), di-isobutyldithiocarbamate (DIBDTC), and di(trifluoroethyl)dithiocarbamate (FDEDTC) ligands were crystallized and studied by X-ray diffraction techniques. The compounds form monoclinic crystals, space group is $P2_1/c$. The unit cell constants are a=8.388(1), b=17.992(2), c=14.204(2) Å, β=109.14(1)°; a=8.959(3), b=13.948(5), c=11.072(5) Å, β=113.16(3)°; a=11.890(9), b=13.210(4), c=16.549(9) Å, β=98.36(5)°; and a=8.537(3), b=8.874(3), c=13.119(6) Å, β=101.68(3)° for $Pd(DPDTC)_2$, $Pd(DBDTC)_2$, $Pd(DIBDTC)_2$, and $Pd(FDEDTC)_2$, respectively. The structures were refined to R values 0.033–0.059. In all cases the Pd(II) ion is coordinated by four S-atoms in a planar arrangement.

The infrared absorption frequencies were measured for these chelates as well as for the diethyl derivative (DEDTC) and correlated with the resonance forms and structures. Volatility trends observed in TG and DSC experiments were compared with capillary gas chromatographic behavior. Fluorination markedly increases the volatility and stability against thermal degradation. For the other chelates, no clear trends were observed in the TG/DSC data. The chromatographic elution order (DEDTC<DPDTC≃DIBDTC<DBDTC) indicates the effects of the molecular weight and the shape of the molecule.

Dialkyl-substituted dithiocarbamic acids have proved to be highly versatile chelating agents for the separation of metals as metal chelates by gas chromatography.[1] Their good performance in liquid–liquid extraction and other analytical procedures[2] makes them further attractive for the determination of metals by gas chromatography.

The most important requirements for successful chromatographic elution are volatility and thermal and solvolytic stability. From the available volatility data for metal dithiocarbamate chelates, it is difficult to recognize well-defined trends. No simple correlation has been found between the volatility and structure,[3] even though ligand structure appears to have a significant effect on both the thermal stability and volatility of many other metal chelates.[4–6]

Thus, Moshier and Sievers found that the replacement of hydrogen atoms by fluorine atoms in β-diketones results in a marked increase in the volatility of the metal chelates compared with that of the nonfluorinated analogs.[7] Tavlaridis and Neeb[8] showed recently that fluorination of diethyldithiocarbamate chelates also leads to a large increase in volatility. This increase occurs without change in thermal stability and with a rise in vapor pressure of the order of more than two decades.[9] For the time being di(trifluoroethyl)-dithiocarbamate seems to be one of the most useful ligands for the determination of trace elements as metal chelates by gas chromatography.[10]

In our laboratory (M.-L. R.) palladium chelates have been used as internal standards in gas chromatographic determinations of metals.[11] The purpose of the present work was to study the influence of the ligand structure on the thermal

0302-4377/83 $2.50

properties and gas chromatographic behavior of some palladium dialkyldithiocarbamate chelates having propyl, butyl, isobutyl, and trifluoroethyl as substituents.

EXPERIMENTAL

Preparation of palladium chelates. Bis(dipropyldithiocarbamato)palladium(II) and bis(dibutyldithiocarbamato)palladium(II), [Pd(DPDTC)$_2$ and Pd(DBDTC)$_2$], were prepared as previously described [12] and purified by recrystallization from chloroform–ethanol mixture (1:1, *v*:*v*).

Bis(di-isobutyldithiocarbamato)palladium(II), [Pd(DIBDTC)$_2$] was prepared by a method analogous to that used for Pd(DPDTC)$_2$ and Pd(DBDTC)$_2$. Pd(DIBDTC)$_2$ was recrystallized from acetone and ethanol–chloroform (1:1).

Bis[di(trifluoroethyl)dithiocarbamato]palladium(II), [Pd(FDEDTC)$_2$], was synthesized by mixing aqueous solutions of $PdCl_2$ (Merck) and sodium di(trifluoroethyl)dithiocarbamate.[9] The precipitate was recrystallized from acetone–chloroform (1:10). All palladium chelates formed yellow prismatic crystals.

X-ray crystallography. Data for Pd(DPDTC)$_2$ and Pd(DBDTC)$_2$ were collected at ambient temperature on a Syntex $P2_1$ diffractometer, and for Pd(DIBDTC)$_2$ and Pd(FDEDTC)$_2$ on a Nicolet R3 m diffractometer. Mo$K\alpha$ radiation (λ=0.71069 Å) with graphite monochromator was used. Accurate cell parameters were obtained for the four chelates from 20–24 centered reflections in the range $20° \leq 2\theta \leq 25°$ and are listed, along with other crystallographic data, in Table 1. Intensities were corrected for background, polarization and Lorentz factors. Empirical absorption corrections were made from ψ-scan data. Data collection was conducted according to standard procedures; data relevant to this phase of the work are also presented in Table 1. The structures were solved by the heavy atom method. In Pd(DPDTC)$_2$, Pd(DBDTC)$_2$, and Pd(FDEDTC)$_2$ the palladium atoms were located in special positions and in Pd(DIBDTC)$_2$ in the general positions. All other nonhydrogen atoms were found in successive Fourier maps with atomic scattering factors taken from refer-

Table 1. Crystallographic data.

Compound	Pd(DPDTC)$_2$	Pd(DBDTC)$_2$	Pd(DIBDTC)$_2$	Pd(FDEDTC)$_2$
Formula	$C_{14}H_{28}N_2S_4Pd$	$C_{18}H_{36}N_2S_4Pd$	$C_{18}H_{36}N_2S_4Pd$	$C_{10}H_8F_{12}N_2S_4Pd$
Molecular mass	459.1	515.2	515.2	618.9
Space group	$P2_1/c$	$P2_1/c$	$P2_1/c$	$P2_1/c$
a, Å	8.388(1)	8.959(3)	11.890(9)	8.537(3)
b, Å	17.992(2)	13.948(5)	13.210(4)	8.874(3)
c, Å	14.204(2)	11.072(5)	16.549(9)	13.119(6)
β, deg	109.14(1)	113.16(3)	98.36(5)	101.68(3)
V, Å^3	2025.1(5)	1272.(1)	2572.(3)	973.2(7)
Z	4	2	4	2
μ(Mo$K\alpha$), cm^{-1}	12.9	10.4	10.2	14.7
Density, calc kg dm^{-3}	1.51	1.34	1.33	2.11
Range of transmission	0.894–0.722	0.856–0.798	0.861–0.701	0.499–0.422
Radiation used	Mo$K\alpha$	Mo$K\alpha$	Mo$K\alpha$	Mo$K\alpha$
Scan range, deg of 2θ	2–50	3–45	3–50	5–60
hkl range	−10, 0, 0 10, 22, 16	0, 0, −11 9, 16, 11	0, 0, −20 15, 16, 20	0, 0, −19 13, 13, 19
Scan mode	$\omega/2\theta$	$\omega/2\theta$	$\omega/2\theta$	$\omega/2\theta$
No. of refl. measured	3838	1479	4960	3171
No. of unique data[a]	2356	857	2629	2033
R_1[b]	0.042	0.046	0.059	0.033
R_2[c]	0.046	0.044	0.059	0.034
Goodness of fit[d]	2.03	1.29	1.92	1.11

[a] $|F| > 5\sigma(|F|)$. [b] $R_1 = \Sigma||F_o| - |F_c||/\Sigma|F_o|$. [c] Weight $= 1/(\sigma^2|F| + 0.005\ F^2)$ [d] Goodness of fit $= [\Sigma(|F_o| - |F_c|)^2/(N_{obsd} - N_v)]^{1/2}$

ence 13. The hydrogen atoms were placed in idealized positions and after anisotropic refinements for the nonhydrogen atoms and isotropic refinements for hydrogens the refinements converged at R_1=0.042, 0.046, 0.059, and 0.033, R_2=0.046, 0.044, 0.059 and 0.034, respectively for the four chelates; for definitions see Table 1. All calculations were carried out on a NOVA 3 minicomputer using the SHELXTL program package. The atomic coordinates for the nonhydrogen atoms and U_{eq} values are given in Table 2. Listings of anisotropic temperature factors, observed and calculated structure factors and hydrogen positional parameters are available from the authors (M.-L. R.).

Infrared spectroscopy. The spectra were recorded between 4000 and 200 cm^{-1} on a Perkin-Elmer 577 grating infrared spectrometer using KBr pellets.

Thermal analysis. The TG/DTG data were

Table 2. Atomic coordinates (x10^4) and U_{eq} values (x10^3, Å^2) (a) for $Pd(DPDTC)_2$, (b) for $Pd(DBDTC)_2$, (c) for $Pd(DIBDTC)_2$ and (d) for $Pd(FDEDTC)_2$. Equivalent isotropic U_{eq} defined as one third of the trace of the orthogonalised U_{ij} tensor.

Atom	*x*	*y*	*z*	U_{eq}
$Pd(DPDTC)_2$, molecule *a*				
Pd	5000	0	5000	48(1)
S(1)	7886(3)	220(1)	5634(1)	58(1)
S(2)	5747(3)	−321(1)	6672(1)	56(1)
N	9046(7)	−85(3)	7595(4)	51(3)
C(1)	7754(10)	−66(3)	6770(5)	47(4)
C(2)	8913(10)	−363(4)	8543(5)	56(4)
C(3)	9760(13)	−1137(6)	8831(8)	87(5)
C(4)	8967(16)	−1699(5)	8093(9)	105(6)
C(5)	10722(11)	208(5)	7647(7)	66(4)
C(6)	11043(14)	973(7)	8141(11)	125(7)
C(7)	9788(21)	1489(7)	7962(13)	154(9)
$Pd(DPDTC)_2$, molecule *b*				
Pd)	5000	0	0	50(1)
S(1)	4947(3)	1075(1)	895(2)	59(1)
S(2)	5790(3)	941(1)	−883(2)	58(1)
N	5552(9)	2271(3)	−74(5)	56(3)
C(1)	5429(9)	1552(4)	−34(5)	52(5)
C(2)	5127(11)	2757(4)	653(7)	63(5)
C(3)	3280(11)	2979(5)	314(7)	77(6)
C(4)	2857(15)	3429(6)	1091(9)	89(6)
C(5)	5979(11)	2657(4)	−882(6)	61(5)
C(6)	7831(10)	2877(4)	−570(6)	62(5)
C(7)	8177(12)	3362(5)	−1338(7)	81(6)
$Pd(DBDTC)_2$				
Pd	0	5000	5000	69(1)
S(1)	1964(4)	9090(2)	1588(3)	85(1)
S(2)	−1382(4)	9205(2)	1078(3)	88(1)
N	632(10)	8143(5)	3038(7)	82(4)
C(1)	420(14)	8711(7)	2038(10)	80(6)
C(2)	2247(17)	7770(9)	3847(11)	102(7)
C(3)	2533(19)	6837(10)	3200(18)	125(9)
C(4)	4085(28)	6490(15)	3921(26)	163(13)
C(5)	4630(21)	5709(15)	3109(19)	184(14)
C(6)	−701(15)	7876(7)	3404(19)	94(6)
C(7)	−883(16)	8645(10)	4352(11)	106(7)
C(8)	−2397(19)	8479(10)	4567(13)	145(8)
C(9)	−2630(20)	9199(12)	5499(15)	153(9)

Table 2. Continued.

$Pd(DIBDTC)_2$				
Pd	2464(1)	1426(1)	2340(1)	53(1)
ligand *a*				
S(1)	4121(3)	3141(2)	8186(2)	68(1)
S(2)	3496(3)	2641(2)	6513(2)	68(1)
N	5400(7)	1892(6)	7397(4)	55(1)
C(1)	4494(8)	2472(7)	7366(6)	56(3)
C(2)	5644(10)	1342(8)	6676(6)	82(4)
C(3)	6192(14)	2017(13)	6082(9)	115(8)
C(4)	7247(16)	2437(15)	6436(10)	149(9)
C(5)	6340(14)	1362(13)	5342(7)	149(9)
C(6)	6142(9)	1708(9)	8165(7)	72(5)
C(7)	6006(11)	700(9)	8540(7)	87(5)
C(8)	4826(11)	422(11)	8624(9)	120(8)
C(9)	6759(12)	626(11)	9370(8)	122(8)
ligand *b*				
S(1)	1475(2)	4507(2)	8181(2)	64(1)
S(2)	790(2)	4034(2)	6516(2)	65(1)
N	−460(7)	5273(6)	7342(5)	57(1)
C(1)	467(7)	4669(7)	7348(6)	46(2)
C(2)	−1185(8)	5533(7)	6610(5)	53(3)
C(3)	−1087(10)	6598(8)	6300(6)	72(5)
C(4)	127(12)	6778(12)	6145(10)	174(10)
C(5)	−1901(11)	6810(10)	5561(7)	89(6)
C(6)	−694(9)	5734(8)	8112(6)	67(5)
C(7)	−1182(13)	5074(12)	8685(7)	109(8)
C(8)	−2207(15)	4524(13)	8336(8)	145(9)
C(9)	−1353(13)	5622(12)	9445(7)	135(9)
$Pd(FDEDTC)_2$				
Pd	0	0	0	37(1)
S(1)	2768(1)	192(1)	380(1)	47(1)
S(2)	528(1)	2238(1)	914(1)	48(1)
N	3697(3)	2786(3)	1393(2)	36(1)
F(1)	2366(3)	5217(3)	174(2)	76(1)
F(2)	2603(4)	6703(3)	1472(2)	92(1)
F(3)	4672(3)	5921(3)	935(2)	81(1)
F(4)	5468(4)	383(3)	2568(3)	99(1)
F(5)	6286(4)	2498(4)	3201(2)	102(1)
F(6)	7649(3)	1256(4)	2306(2)	100(1)
C(1)	2492(3)	1865(3)	955(2)	37(1)
C(2)	3351(4)	4213(4)	1852(3)	43(1)
C(3)	3240(4)	5512(4)	1101(3)	53(1)
C(4)	5362(4)	2400(4)	1396(3)	42(1)
C(5)	6178(4)	1632(5)	2379(3)	57(1)

obtained on a Mettler TA 3000 TG 50 thermobalance for samples of *ca.* 10 mg under a nitrogen atmosphere (150 ml/min) at a heating rate of 20 °C/min. DSC curves were recorded on a Mettler TA 3000 DSC 20 system under a dynamic nitrogen atmosphere (150 ml/min) with heating rates of 5 and 10 °C/min. Sample sizes were about 3 mg. High-purity indium (≥99.999 %) was used for calorimetric and temperature calibrations.

Gas chromatography. Carlo Erba Fractovap

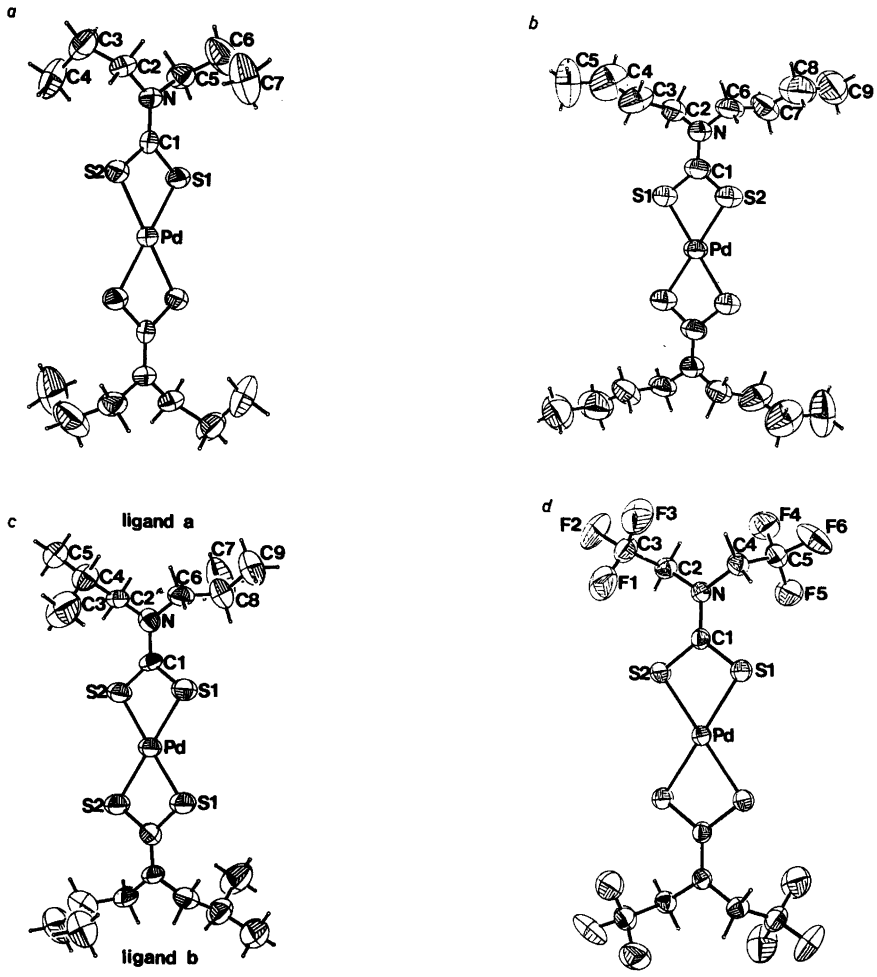

Fig. 1. Perspective drawings (a–d) showing the molecular structures and atomic numbering schemes for $Pd(DPDTC)_2$, $Pd(DBDTC)_2$, $Pd(DIBDTC)_2$, and $Pd(FDEDTC)_2$, respectively. In the case of $Pd(DIBDTC)_2$ the crystallographically independent ligands are distinguished by letters a and b. 50 % thermal ellipsoids are used with the exception of hydrogen atoms which are drawn artificially small.

Series 2150 and 2900 gas chromatographs were employed for splitless injections. On-column injections were performed with Carlo Erba Fractovap Series 4160 with LT programmer. The gas chromatographs were equipped with flame ionization detectors. Fused silica capillary columns with SP-2100 liquid phase (2 m×0.20 mm I.D., Hewlett-Packard) and OV-101 liquid phase (4 m×0.30 mm I.D., Orion Analytica) and glass capillary column coated with OV-101 liquid phase (4 m×0.30 mm I.D., prepared by Dr. S. Räisänen) were used for the results presented. Helium or nitrogen were used as the carrier gas.

RESULTS AND DISCUSSION

X-ray crystallography. The structures and the atomic numbering schemes are shown for the four chelates in Fig. 1. The bond lengths and angles are collected in Tables 3 and 4 along with the data for $Pd(DEDTC)_2$.[14] $Pd(DPDTC)_2$ has two crystallographically distinct molecules, which both have the palladium atom at a center of symmetry. The molecules are designated *a* and *b* in Tables 3 and 4, and have been given the same numbering scheme.

Table 3. Bond distances (Å) for $Pd(DEDTC)_2$, $Pd(DPDTC)_2$, $Pd(DBDTC)_2$, $Pd(DIBDTC)_2$, and for $Pd(FDEDTC)_2$.

Bond	$Pd(DEDTC)_2$[a]	$Pd(DPDTC)_2$ (molecule *a*)	$Pd(DPDTC)_2$ (molecule *b*)	$Pd(DBDTC)_2$	$Pd(DIBDTC)_2$ (ligand *a*)	$Pd(DIBDTC)_2$ (ligand *b*)	$Pd(FDEDTC)_2$
Pd–S(1)	2.317(3)	2.323(2)	2.323(2)	2.316(3)	2.316(3)	2.304(3)	2.320(1)
Pd–S(2)	2.315(3)	2.322(2)	2.329(2)	2.313(4)	2.321(3)	2.323(3)	2.316(1)
S(1)–C(1)	1.73(1)	1.733(8)	1.730(9)	1.727(14)	1.728(10)	1.705(9)	1.703(3)
S(2)–C(1)	1.70(1)	1.706(8)	1.730(8)	1.691(10)	1.719(9)	1.700(10)	1.699(3)
C(1)–N	1.32(1)	1.309(8)	1.306(9)	1.311(13)	1.317(13)	1.357(12)	1.349(4)
N–C(2)	1.49(2)	1.469(10)	1.473(12)	1.452(15)	1.462(13)	1.424(11)	1.457(4)
N–C(4)	1.48(2)	—	—	—	—	—	1.462(4)
N–C(5)	—	1.485(12)	1.486(12)	—	—	—	—
N–C(6)	—	—	—	1.459(17)	1.459(12)	1.481(13)	—

[a] Ref. 14.

Table 4. Bond angles (deg) for $Pd(DEDTC)_2$, $Pd(DPDTC)_2$, $Pd(DBDTC)_2$, $Pd(DIBDTC)_2$, and for $Pd(FDEDTC)_2$.

Angle	$Pd(DEDTC)_2$[a]	$Pd(DPDTC)_2$ (molecule *a*)	$Pd(DPDTC)_2$ (molecule *b*)	$Pd(DBDTC)_2$	$Pd(DIBDTC)_2$ (ligand *a*)	$Pd(DIBDTC)_2$ (ligand *b*)	$Pd(FDEDTC)_2$
S(1)–Pd–S(2)	75.5(1)	75.4(1)	75.5(1)	75.3(1)	75.4(1)	75.3(1)	75.1
Pd–S(1)–C(1)	86.1(4)	86.2(3)	86.8(3)	86.0(3)	86.8(3)	86.5(3)	86.2(1)
Pd–S(2)–C(1)	87.0(4)	86.9(3)	86.6(3)	87.0(5)	86.9(4)	86.0(3)	86.4(1)
S(1)–C(1)–S(2)	111.5(7)	111.4(4)	110.8(4)	111.7(6)	110.7(6)	112.1(5)	112.3(2)
S(1)–C(1)–N	123.1(9)	123.7(7)	124.4(7)	124.1(8)	124.5(7)	123.7(7)	123.8(2)
S(2)–C(1)–N	125.5(9)	124.8(7)	124.8(7)	124.2(10)	124.8(7)	124.1(7)	123.9(2)
C(1)–N–C(2)	120(1)	122.6(7)	121.1(8)	121.2(11)	121.3(8)	122.8(8)	120.1(3)
C(1)–N–C(4)	123(1)	—	—	—	—	—	121.1(3)
C(1)–N–C(5)	—	121.9(7)	122.3(7)	—	—	—	—
C(1)–N–C(6)	—	—	—	121.9(9)	121.7(8)	119.3(8)	—
C(2)–N–C(4)	117(1)	—	—	—	—	—	118.8(2)
C(2)–N–C(5)	—	115.4(5)	116.3(6)	—	—	—	—
C(2)–N–C(6)	—	—	—	116.9(9)	116.7(8)	117.8(8)	—

[a] Ref. 14.

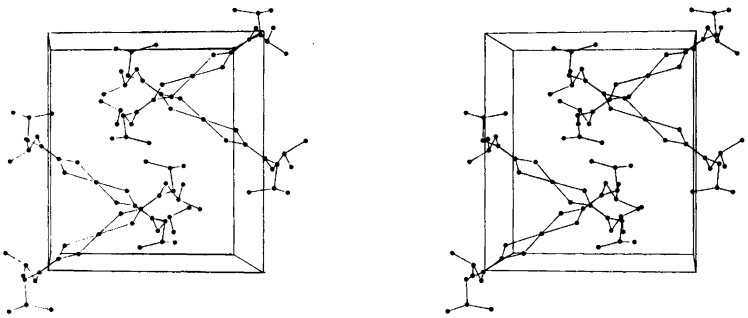

Fig. 2. A stereoview showing the packing of molecules in the unit cell of $Pd(DIBDTC)_2$.

$Pd(DBDTC)_2$ and $Pd(FDEDTC)_2$ have the center of symmetry at the palladium atom while $Pd(DIBDTC)_2$ does not have internal crystallographic symmetry. The di-isobutyldithiocarbamate ligands are chemically equivalent, however, which is indicated by the numbering scheme in Fig. lc.

Intramolecular interactions between hydrogen in the α-carbon of the ligand substituents and sulfur are short (2.547–2.722 Å) in all the present palladium chelates. The corresponding short S···H-contacts have occurred in the structures of nickel(II) di-isopropyl- and di-isobutyldithiocarbamate chelates.[15,16] Judging from intermolecular distances there is no clear evidence for hydrogen bonding in any of the four chelates, the molecules being held together by van der Waals forces. Fig. 2 shows the contents of unit cell and molecular packing for a representative chelate $Pd(DIBDTC)_2$.

When comparing the structural data with those available in the literature[17] it is noted that the ligand structure is only slightly changed upon coordination. The carbon–nitrogen bond C(1)-N has double bond character, typical of metal dialkyldithiocarbamate chelates. Furthermore, the bonds and angles involving the chelating sulfur atoms are not significantly different in any of the chelates and their values are in agreement with the data reported recently by Nikolov.[18]

Infrared spectroscopy. Infrared spectra of metal chelates of dialkyl-substituted dithiocarbamic acids tend to be complicated by the strong coupling of peaks. Three pure uncoupled stretching frequencies, strong and broad $\nu(C{\cdots}N)$, medium strong $\nu(C{\cdots}S)$, and in the far infrared also medium strong $\nu(M-S)$, are characteristic for the spectra. Since they characterize the ligand substitution as well as the central atom the identification of chelates is relatively easy (see Table 5).

Metal dialkyldithiocarbamate chelates have the two resonance forms I and II. Form I reflects

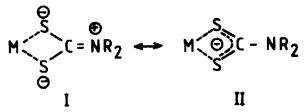

I II

the electron releasing tendency of the R_2N-group. The tendency of the amine group to donate electrons to the sulfur atoms increases their electron donating capacity and their ability

Table 5. Infrared spectral characteristics of some palladium dithiocarbamate chelates.

Metal chelate	$\nu(C{\cdots}N)$ (cm^{-1})	$\nu(C{\cdots}S)$ (cm^{-1})	$\nu(M{-}S)$ (cm^{-1})
$Pd(DEDTC)_2$	1521	990	360
$Pd(DPDTC)_2$	1514	972	355
$Pd(DBDTC)_2$	1510	975	358
$Pd(DIBDTC)_2$	1506	980	362
$Pd(FDEDTC)_2$	1464	990	384

Table 6. TG/DTG data for the palladium chelates.

Metal chelate	Weight loss (%)	Temperature range (°C)	DTG peak temp. (°C)
$Pd(DEDTC)_2$[a]	92	235–440	410
$Pd(DPDTC)_2$[a]	93	240–445	418
$Pd(DBDTC)_2$[a]	93	235–445	420
$Pd(DIBDTC)_2$	96	240–445	418
$Pd(FDEDTC)_2$	100	140–360	270

[a] For these chelates TG data measured with a different apparatus have been reported in Refs. 1 and 12. The present values differ slightly from those reported.

Table 7. DSC data for the palladium chelates with esd's in the parentheses.

Metal chelate	M.p. (°C)	Other peaks (°C)[a]	Heat of fusion (kJ/mol)
$Pd(DEDTC)_2$	243	335,[b] 384[c]	39.03(47)
$Pd(DPDTC)_2$	149	343, 371	30.24(56)
$Pd(DBDTC)_2$	109	345, 362	29.41(31)
$Pd(DIBDTC)_2$	189	330, 388	30.48(25)
$Pd(FDEDTC)_2$	161	240, 303	39.57(44)

[a] All endothermic peaks. [b] Onset temperature. [c] Peak temperature.

to form strong chelates with transition metal ions. Thus the C–N bond has a significant double bond character.

IR data in Table 5 indicate that the significance of resonance form I decreases with the increasing length of the alkyl group as proposed by Kellner.[19] This effect is inferred from the decrease of the stretching frequency $\nu(C\cdots N)$. The effect is very small, the accuracy of the C–N bond lengths, determined by X-ray diffraction, is not sufficient to show the same trend.

The fluorinated chelate has a much lower $C\cdots N$ stretching frequency and somewhat longer C–N bond than in the nonfluorinated chelates. The S–C bond lengths are also slightly shorter, and the $\nu(S\cdots C)$ somewhat higher in the fluorinated compound. These facts indicate that the resonance structure II is favored in $Pd(FDEDTC)_2$.

Thermal analysis. The TG/DTG and DSC data are presented in Tables 6 and 7 which contain for comparison also the values for the diethyldithiocarbamate chelate $Pd(DEDTC)_2$. All chelates first undergo fusion at temperatures ranging from 109 to 243 °C followed by nearly complete volatilization. The fluorinated chelate has clearly

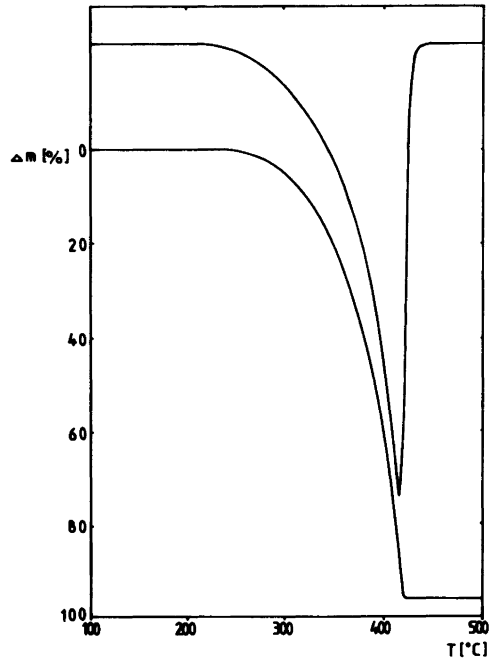

Fig. 3. TG and DTG curves of $Pd(DIBDTC)_2$ in nitrogen atmosphere. Heating rate 20 °C/min.

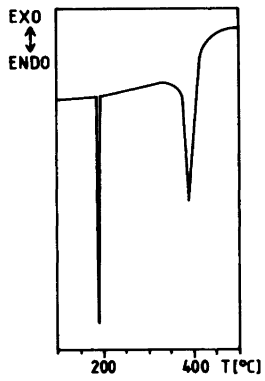

Fig. 4. DSC curve of $Pd(DIBDTC)_2$ in nitrogen atmosphere. Heating rate 5 °C/min.

the highest volatility in spite of its high molecular weight. It also shows no decomposition while for the other compounds the TG data indicate slight degradation of the order of a few percent.

Except for the behavior of the $Pd(FDEDTC)_2$, it is difficult to recognize any other clear trends between the structure and the volatility or the fusion data. The dibutyldithiocarbamate chelate has the lowest melting point and heat of fusion while the diethyl-substituted chelate has by far the highest melting point. On the other hand, there are no significant differences between the volatility of these chelates. It should be noted, however, that the volatilization takes place after complete fusion and experiments performed in vacuum might give different results.

Gas chromatography. The palladium chelates are sufficiently volatile and thermally stable for gas chromatography on short nonpolar capillary columns by using splitless or on-column injections. The influence of fluorination of palladium diethyldithiocarbamate on the volatility is clearly seen in the gas chromatographic characteristics: the fluorinated palladium chelate elutes first and at much lower temperatures than other non-fluorinated ones. Thus fluorine substitution in the ligand results in a marked increase in volatility. The lower column temperatures needed for elution decrease also the possibility of thermal decomposition.

There are problems with splitless injection in the simultaneous separation of the fluorinated and the other palladium chelates studied; the great temperature differences of vaporization cause severe tailing for the nonfluorinated che-

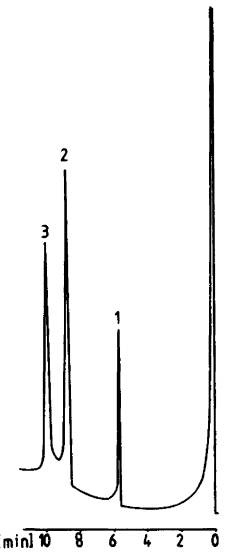

Fig. 5. Gas chromatographic elution of (1) $Pd(FDEDTC)_2$, (2) $Pd(DEDTC)_2$, and (3) $Pd(DIBDTC)_2$ on fused silica OV−101 by using on-column injection. Conditions: det. 300 °C; oven 70 °C (3 min)−150 °C (0 min)−255 °C (1 min)−300 °C (0 min), heating rates 15 °C/min, 25 °C/min, and 25 °C/min, resp; N_2: 7 ml/min and make-up gas 5 ml/min.

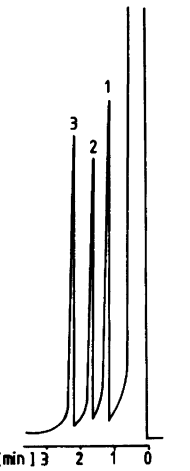

Fig. 6. Separation of (1) $Pd(DEDTC)_2$, (2) $Pd(DPDTC)_2$, and (3) $Pd(DBDTC)_2$ on glass capillary column OV-101 by using splitless injection. Conditions: inj./det. 275 °C; oven 170 °C (0 min) – 270 °C (0 min), heating rate 39 °C/min; He: 8 ml/min.

lates as an indication of adsorption in an injection cavity. With on-column injection the separation succeeds very well (*e.g.* Fig. 5). Splitless injection applied to the separation of the nonfluorinated chelates is successful except for the dipropyl- and di-isobutyldithiocarbamates with the same retention time (Fig. 6). The similar volatility of the dipropyl- and di-isobutyldithiocarbamate chelates has also been observed in the vapor pressure measurements of nickel and copper chelates.[20] Hartmetz *et al.*[21] have compared splitless and on-column injection techniques with fluorinated diethyldithiocarbamates and they have found on-column injection to widen the linearity of calibration curves for some labile metal chelates when using glass capillary columns. For stable metal chelates and with fused silica columns they found only small or no differences.

Volatility trends and molecular properties. Correlation of volatility and molecular structure of metal complexes has been a subject of some studies.[4–6] In the present work a more detailed analysis would be possible in principle. Volatility is a function of intermolecular interactions, in gas chromatographic circumstances vaporization takes place from liquid or solvated state. None of the present structural methods probe directly the complexes in this state. On the other hand it can be assumed that the major interactions operative in liquid state must somehow also show up in the solid state.

For the palladium dialkyldithiocarbamate chelates studied in this work, a correlation between the fluorinated and nonfluorinated compounds and the volatility can be found. The fluorinated chelate is much more volatile than the nonfluorinated derivatives. The principal reason is the fluorination itself, the molecule is surrounded by fluorine atoms, which decrease intermolecular interactions in the same way as in the fluorinated aliphatic hydrocarbons. The secondary effect may be a decrease in the polarization of the S_2CN system due to the electronic effect of the fluorine atoms.

The nonfluorinated chelates have a distinct volatility order. The small variations in the structures of the central $Pd(S_2CN)_2$ fragments do not have any clear trends which could be correlated with volatility. The principal effects are the molecular weight and shape. Increasing molecular weight enhances the polarizability of the molecule and makes it less volatile. These effects taken together qualitatively explain the volatility order: DEDTC<DPDTC≃DIBDTC<DBDTC. The closest intermolecular contacts in solid state are mainly between the ligand terminal groups and the palladium atoms. These interactions are very similar in the nonfluorinated derivatives and cannot be used for the interpretation of the volatility order.

Acknowledgements. The authors wish to thank Prof. R. Neeb for the Na(FDEDTC) sample. The continuous encouragement and interest by Prof. O. Mäkitie is gratefully acknowledged.

REFERENCES

1. Riekkola, M.-L., Mäkitie, O. and Sundberg, M. *Kem. Kemi 6* (1979) 525.
2. Thorn, G. D. and Ludwig, R. A. *The Dithiocarbamates and Related Compounds,* Elsevier, Amsterdam 1962.
3. Hill, J. O. and Magee, R. J. *Rev. Inorg. Chem. 3* (1981) 141.
4. Dilli, S. and Patsalides, E. *Aust. J. Chem. 29* (1976) 2369.
5. Dilli, S. and Robards, K. *Aust. J. Chem. 32* (1979) 277.
6. Dilli, S. and Patsalides, E. *Aust. J. Chem. 34* (1981) 1579.
7. Moshier, R. W. and Sievers, R. E. *Gas Chromatography of Metal Chelates,* Pergamon Press, Oxford 1965.
8. Tavlaridis, A. and Neeb, R. *Z. Anal. Chem. 282* (1976) 17.
9. Tavlaridis, A. and Neeb, R. *Z. Anal. Chem. 292* (1978) 135.
10. Neeb, R. *Pure Appl. Chem. 54* (1982) 847.
11. Riekkola, M.-L., Ritari, M. and Mäkitie, O. in *Euroanalysis-IV Book of Abstracts,* Kivimäki, M. and Niinistö, L., Eds., Association of Finnish Chemical Societies, Helsinki 1981, p. 411.
12. Riekkola, M.-L. *Mikrochim. Acta 1* (1982) 327.
13. *International Tables for X-ray Crystallography,* Kynoch Press, Birmingham 1962, Vol. III.
14. Beurskens, P. T., Cras, J. A., Hummelink, Th.W. and Noordik, J. H. *J. Cryst. Mol. Struct. 1* (1971) 253.
15. Newman, P. W. G. and White, A. H. *J. C. S. Dalton* (1972) 2239.
16. Raston, C. L. and White, A. H. *Aust. J. Chem. 29* (1976) 523.
17. Coucouvanis, D. *Prog. Inorg. Chem. 11* (1970) 233; *26* (1979) 301.
18. Nikolov, G. S. *J. Inorg. Nucl. Chem. 43* (1981) 3131.
19. Kellner, R. *Anal. Chim. Acta 63* (1973) 277.
20. Tavlaridis, A. and Neeb, R. *Z. Anal. Chem. 293* (1978) 211.
21. Hartmetz, G., Scollary, G., Meierer, H., Meyer, A. and Neeb, R. *Z. Anal. Chem. 313* (1982) 309.

Received March 21, 1983.

Acta Chemica Scandinavica A 37 (1983) 817–822

Ab initio SCF Calculations on the Species HO_3, HO_3^+ and HO_3^- and an Estimate of the Stability of HO_3 Relative to OH and Different States of O_2

KIRSTEN BROCH MATHISEN, ODD GROPEN, P. N. SKANCKE and ULF WAHLGREN

Department of Chemistry, Institute of Mathematical and Physical Sciences, University of Tromsø, P.O. Box 953, N-9001 Tromsø, Norway

The geometries of the ions HO_3^+ and HO_3^-, and of the radical HO_3 have been optimized using the gradient technique within the SCF approximation. Calculated energies of different isomers have been compared. For the radical species optimization has been carried through using both medium (double zeta) and large, (10*s*6*p*1*d*/5*s*1*p*)/[5*s*4*p*1*d*/3*s*1*p*], basis sets. The energy of the radical has been compared with calculated energies for the systems $OH(^2\Pi)+O_2(^3\Sigma,^1\Delta,^1\Sigma)$. The large basis set indicates that HO_3 is stable relative to $OH(^2\Pi)+O_2(^1\Delta)$ and to $OH(^2\Pi)+O_2(^1\Sigma)$.

The daytime production of $O_2(^1\Delta_g)$ in the upper atmosphere is based on photodissociation of ozone.[1]

$$O_3+h\nu(\lambda<3102\text{ Å})\rightarrow O_2(^1\Delta_g)+O(^1D) \quad (1)$$

Nighttime production reactions that have been proposed are[2,3]

$$O(^3P)+O(^3P)+M\rightarrow O_2(^1\Delta_g)+M \quad (2)$$

and

$$O(^3P)+HO_2\rightarrow OH+O_2(^1\Delta_g) \quad (3)$$

Attenuation of singlet O_2 is accomplished by radiation and collisional quenching. At altitudes above 80 km the main loss is by

$$O_2(^1\Delta_g)\rightarrow O_2(^3\Sigma_g^-)+h\nu, \quad (4)$$

and below 80 km, where the atmospheric density is higher, the reaction

$$O_2(^1\Delta_g)+M\rightarrow O_2(^3\Sigma_g^-)+M \quad (5)$$

is the prevalent one.[4]

Calculated and observed density profiles for $O_2(^1\Delta_g)$ are in disagreement, especially below 60 km,[4] the calculated concentrations being higher than the observed ones.

It is possible that the radical species HO_3 might be a sink both for $O_2(^1\Delta_g)$ and OH radicals through the reaction

$$O_2(^1\Delta_g)+OH(^2\Pi)\rightarrow HO_3(^2A) \quad (6)$$

where HO_3 either appears as a reaction intermediate or as a stable product.

The possible existence of HO_3 as an intermediate has previously been alluded to.[5] However, SCF calculations with medium-sized basis sets and partial geometry optimizations have led to the conclusion that HO_3 is unstable with respect to $O_2(^3\Sigma_g^-)+OH(^2\Pi)$ by about 15 kcal/mol.[6] Very recently selected forms of the HO_3 species were studied theoretically[7] as an activated complex in a discussion of the mechanism of the reaction

$$H(^2S)+O_3(^1A_1)\rightarrow OH(^2\Pi)+O_2(^3\Sigma_g^-) \quad (7)$$

The related radical CF_3COO has been detected, and ESR data for this species are available.[8] The existence of this radical has led to the suggestion that the reaction

0302-4377/83 $2.50

Table 1. Energies and optimized geometries of different structures of HO_3^+. 4–31G basis. Bond lengths in nm, angles in degrees.

Isomer	R(OH)	$R(O_1O_2)$	$R(O_2O_3)$	$R(O_1O_3)$	∠OOH	∠OOO	α	E(au)	ΔE(kJ/mol)
I_p	0.099	0.150	0.117	—	100.7	112.2	180	−224.1594	0.0
II_p	0.100	0.150	0.117	—	105.5	119.9	0	—	36.8
III_p	0.100	0.151	0.151	0.148	110.5	58.7	66.3	—	146.7
IV_p	0.101	0.146	0.146	0.153	148.2	63.5	0	—	225.7
V_p	0.102	0.129	0.129	—	117.4	125.1	0	—	308.1
VI_p[a]	0.100	0.153	0.117	—	102.4	114.5	90	—	26.8

[a] Does not correspond to a minimum on the energy surface.

Table 2. Energies and optimized geometries of different structures of HO_3^-. 4–31G basis. Bond lengths in nm, angles in degrees. Values in parentheses obtained by augmented basis (diffuse *s*- and *p*-functions).

Isomer	R(OH)	$R(O_1O_2)$	$R(O_2O_3)$	∠OOH	∠OOO	α	E(au)	ΔE(kJ/mol)
I_n	0.096	0.151	0.151	99.8	107.6	180	–	42.6
	(0.096)	(0.150)	(0.150)	(100.6)	(107.5)	(180)	–	(35.1)
II_n	0.097	0.149	0.151	96.8	102.7	0	−224.6360	0.0
	(0.096)	(0.149)	(0.150)	(99.1)	(103.6)	(0)	(−224.6706)	(0.0)
III_n	0.123	0.151	0.151		90.4	0	–	72.3
	(0.124)	(0.151)	(0.151)		(90.4)	(0)	–	(85.7)
IV_n	0.095	0.157	0.157	104.3	119.7	60.6	–	89.0
	(0.095)	(0.156)	(0.156)	(104.4)	(118.6)	(61.0)	–	(77.3)
V_n	0.095	0.157	0.153	112.3	135.5	0	–	111.2
	(0.095)	(0.157)	(0.157)	(112.9)	(134.3)	(0)	–	(100.3)
VI_n[a]	0.096	0.149	0.151	101.5	108.4	90	–	26.3

[a] Does not correspond to a minimum on the energy surface.

$$Me_3CO+O_2 \rightarrow Me_3COOO \quad (8)$$

might take place.[9]

The ion HO_3^+, which is a protonated ozone, has been assumed to be the active species when ozone is used for oxygenation of alkenes in acid medium.[10,11] A complete analysis of the different structural forms of HO_3^+ has been carried through on the SCF level, and with second order Möller-Plesset calculations in selected points.[12]

A very recent experimental study indicates that the ion HO_3^- might be an intermediate in the reaction[13]

$$t\text{-}BuO_2H+O_3 \rightarrow t\text{-}BuO_3H \quad (9)$$

To our knowledge the ion HO_3^- has not been studied by theoretical calculations previously.

The main purpose of the present study is to carry through a complete optimization of the geometries of the different possible forms of the radical HO_3. Furthermore we find it appropriate to reconsider the energy differences between this species in its optimized form and the systems $OH(^2\Pi)+O_2$ ($^3\Sigma_g^-, ^1\Delta_g^+, ^1\Sigma_g^+$). If use of medium and large basis sets indicates moderate energy differences at the SCF level, calculations using methods accounting for electron correlation energies would probably give valuable information on the potential surface for the reaction given by eqn. (6).

In a private communication[14] we have obtained information indicating that concentrations of OH and singlet O_2 in the atmosphere may be too low to make possible a significant production of HO_3. We find it, however, of central interest to study the energetics of the surfaces related to different states of O_2. A more extensive description of HO_3, and the possible reaction channels leading to it will give relevant information on the reaction given by eqn. (7).

We also find it appropriate to discuss the electronic and molecular structures of the ions HO_3^+ and HO_3^- in conjunction with our study of HO_3. The results obtained by Kausch and Schleyer[12] in their structural studies of HO_3^+ are quantitatively confirmed by our calculations. In order to facilitate a comparative discussion of the radical and the ions, we have included our results on HO_3^+.

COMPUTATIONAL METHOD

All calculations in this study were carried out at the RHF–SCF level.

The geometry optimizations of the ions were performed by means of the program TEXAS[15] which uses a force-relaxation method.[16] As this

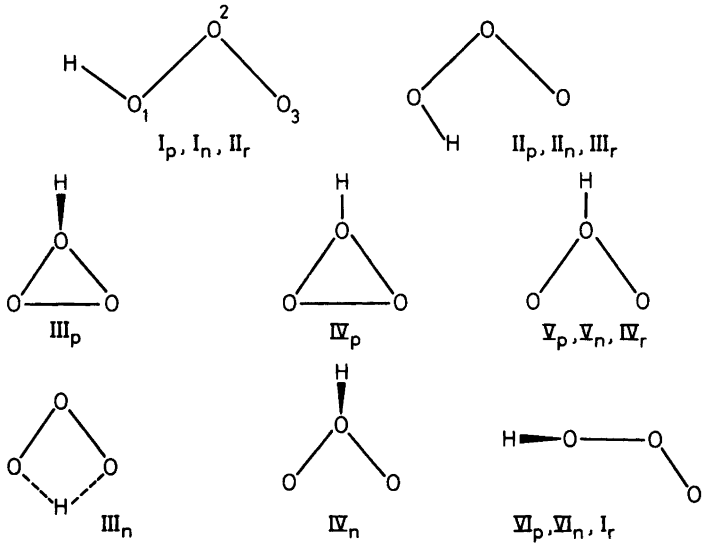

Fig. 1. Different forms of HO_3^+(p), HO_3^-(n) and HO_3(r) discussed in the text and referred to in the tables.

program is designed only for closed shell systems, the optimizations of the radical were undertaken by a special gradient program developed by one of us.[17] The program was based on the closed shell gradient program, MOLFORC.[18] Our program, which can handle one and two open shells, also calculates the energy gradient analytically.

The structures of the ions were optimized using a 4−31G basis set.[19] For some of the conformations this set was augmented by one diffuse *s* and one diffuse *p* orbital (exponent 0.05). The results showing the optimized geometries are displayed in Tables 1 and 2. For labelling of isomers and atoms see Fig. 1.

The basis sets used for the HO_3 radical were the (7*s*3*p*/4*s*)/[4*s*2*p*/2*s*] set[20] for all isomers and the (10*s*6*p*1*d*/5*s*1*p*)/[5*s*4*p*1*d*/3*s*1*p*] set[21,22] for the three isomers found to be the most stable ones using the smaller set. The exponents for the polarization functions were chosen to be 0.95 and 0.80 for the *d*-orbitals on O and the *p*-orbitals on H, respectively. The results of the optimization are given in Table 3.

The energies for the reference systems $OH(^2\Pi)+O_2(^3\Sigma,^1\Delta,^1\Sigma)$ were calculated using the larger basis set. The bond lengths were optimized using a parabola. The results are shown in Table 4.

RESULTS AND DISCUSSION

The global energy minimum was found for the isomers having the H-atom attached to the terminal oxygen atom. This was the case for the ions (structures I_p and I_n) as well as for the radical (structure I_r).

The most stable isomer of HO_3^+ is the *trans*-form (I_p). This is in accordance with results of previous calculations.[12]

The energy difference between the *cis*- and the *trans*-form of HO_3^+ (II_p and I_p) was found to be 37 kJ/mol. Both the forms have a pronounced single-bond double-bond oxygen system. Furthermore, a Mulliken population analysis, shown in Table 5, indicates a net positive charge on the free terminal oxygen atom. This charge distribution favours the *trans*-form.

As revealed by Table 1 there is one closed form (III_p) representing a local minimum on the energy surface. Energetically this form is very high above the global minimum. The closed form (IV_p) which represents the top of the barrier against a conversion from (III_p) to its equivalent

Table 3. Energies and optimized geometries of HO_3. Basis sets (7*s*3*p*/4*s*) and (10*s*6*p*1*d*/5*s*1*p*) (values in parentheses). Bond lengths in nm and angles in degrees.

	R(OH)	*R*(O_1O_2)	*R*(O_2O_3)	∠OOH	∠OOO	α	*E* (au)	Δ*E*(kJ/mol)
I_r	0.097	0.147	0.142	101.7	106.8	91.5	−224.6016	0.0
	(0.095)	(0.138)	(0.128)	(102.9)	(109.5)	(90.1)	−225.0252	(0.0)
II_r	0.097	0.149	0.140	98.8	104.3	180	–	4.6
	(0.095)	(0.140)	(0.127)	(100.4)	(107.3)	(180)	–	(8.4)
III_r	0.097	0.149	0.141	102.4	107.2	0	–	12.1
	(0.095)	(0.140)	(0.127)	(103.2)	(109.8)	(0)	–	(10.9)
IV_r	0.097	0.143	0.143	115.9	128.2	0	–	315.6

Table 4. Energies and optimized bond lengths in nm for $OH(^2\Pi)$ and $O_2(^3\Sigma_g^-, {}^1\Delta_g, {}^1\Sigma_g^+)$. Basis set (10*s*6*p*1*d*/5*s*1*p*). $\Delta E = E(OH+O_2) - E(HO_3)$. $E(HO_3) = -225.0252$ au. Relative energies[a] for different states of O_2.

	R(O–O)	*R*(O–H)	*E*(au)	*ΔE*(kJ/mol)
$O_2(^3\Sigma_g^-)$	0.116		−149.6542	−113.7
$O_2(^1\Delta_g)$	0.116		−149.6073	9.2
$O_2(^1\Sigma_g^+)$	0.116		−149.5608	131.7
$OH(^2\Pi)$		0.096	−75.4143	
Exp.[a]				
$O_2(^3\Sigma_g^-)$				0.0
$O_2(^1\Delta_g)$				94.6
$O_2(^1\Sigma_g^+)$				157.3

[a] Ref. 23.

Table 5. Atomic charges from gross atomic populations for HO_3^+ and HO_3^-. 4–31G basis. For labelling of isomers and atoms see Fig. 1.

		H	O_1	O_2	O_3
HO_3^+	I_p	+0.56	−0.13	+0.16	+0.41
	II_p	+0.53	−0.09	+0.22	+0.34
HO_3^-	I_n	+0.34	−0.55	−0.28	−0.51
	II_n	+0.38	−0.57	−0.26	−0.55

form has an energy indicating a barrier of around 79 kJ/mol.

The open form (V_p) having an oxygen–oxygen link disrupted, is the least stable of the isomers considered. The energy difference of 308 kJ/mol is, however, substantially reduced by inclusion of electron correlation.[12]

For the negative ion HO_3^- the *cis*-form (II_n) was found to be the most stable one. The energy difference between this form and the *trans*-form (I_n) is calculated to be 43 kJ/mol using the 4–31G basis (reduced to 35 kJ/mol in the augmented basis). A Mulliken population analysis, shown in Table 5, gives a charge distribution that indicates a net attraction between the H-atom and the terminal oxygen atom. This change in electrostatic interaction by going from HO_3^+ to HO_3^- may explain the relative *cis-trans* energy differences for these forms.

The two electrons added to HO_3^+ in order to make HO_3^- enter a π-orbital that is antibonding in the O_2–O_3 region. This induces a lengthening of this bond from 0.117 nm in HO_3^+ to 0.151 nm in HO_3^-, thus making the two O–O bond lengths in HO_3^- virtually identical.

We did not succeed in finding any stable closed form (analogous to (III_p) and (IV_p)) for the negative ion. The two additional electrons encountered in going from HO_3^+ enter the 5a″ orbital which is strongly antibonding in the region between the terminal oxygen atoms. As a result the ring is opened and we obtain the two open structures (IV_n) and (V_n), the former being the most stable one.

In order to detect a possible importance of diffuse functions in the basis set for the negative ion, we reoptimized the geometries for this ion using a 4–31 G basis set augmented with diffuse *p*-functions on oxygen and an *s*-function on hydrogen (exponents 0.05). As revealed by Table 2 the diffuse functions did not introduce any significant changes in the geometries, but led to a lowering of the relative energies for all isomers except one (III_n).

A rotation of the H–O bond around the O–O bond did not reveal any local energy minimum. The energy increased monotonically in going from (II_n) to (I_n). See Fig. 1.

The results obtained on the ions would lead us to the preliminary conclusion that in the ground state of the radical HO_3 the hydrogen atom is bonded to a terminal atom in ozone, and that the O_2-O_3 bond is slightly shorter than the O_1-O_2 bond. The results obtained by our calculations confirmed this expectation.

For the radical the global minimum was obtained for a non-planar form (I_r) with torsion angles of 91.5 and 90.2 degrees for the small and the large basis set, respectively. For definition of basis sets and torsion angle, see Table 3. The planar *trans*- and *cis*-forms were found to represent maxima on the potential curve for the rotation of O–H around O–O. The highest energy maximum, the *cis*-barrier [represented by (III_r)], was found to be 12 kJ/mol, indicating an almost free rotation of the O–H group.

Our smaller basis set is of similar quality although not identical to the 4–31G set used by Blint and Newton.[6] They report bond lengths of 0.144 nm and 0.137 nm for O_1-O_2 and O_2-O_3 respectively. Their calculated bond angles deviate from ours by only 1–2 degrees.

All computed bond lengths are somewhat shortened when the large basis set is used, but qualitatively the picture is the same as the one obtained with the smaller basis.

The singly occupied orbital with quasi-π symmetry is mainly localized in the O_2-O_3 region, and is strongly antibinding in this region. For the planar structures the occupation of 3a″ is 0,1, and 2 for HO_3^+, HO_3, and HO_3^-, respectively, and the O_2-O_3 bond length increases along this series.

The calculations did not indicate an energy minimum for any closed form of the radical. We did find a minimum for a planar open form having the hydrogen atom attached to the central oxygen atom. This form (IV_r) has, however, a very high energy 316 kJ above the ground state.

As mentioned in the introduction, the main purpose of the present study is to locate HO_3 energetically relative to the systems $OH+O_2$, HO_2 being in different states. This work also has some relevance for the $H+O_3$ reaction mechanism studied by Schaefer *et al.*[7] Our SCF data presented in Table 4 show clearly that the energy of HO_3 relative to $OH(^2\Pi)$ and excited oxygen molecules is such that the reactions given by eqn. (6) are thermodynamically relevant although they may be less likely for other reasons. On the SCF-level the corresponding reaction involving O_2 in its ground state seems less likely. It is, however, conceivable that CI-effects, which are shown to be important for O_3, may significantly influence these results. Consequently, these reaction systems deserve further studies including parts of the reaction surfaces. Studies along these lines invoking methods for handling electron correlation are in progress.

Acknowledgements. We thank Dr. C. J. Howard, NOAA R443, Boulder, Colorado, for interesting correspondence.

REFERENCES

1. Lissi, E. and Heicklen, J. *J. Photochem. 1* (1972) 39.
2. Bates, D. R. *Physics of the Upper Atmosphere,* Academic, New York 1960.
3. Wood, H. C. *Thesis,* University of Saskatchewan, Canada 1972.
4. Isaksen, I. S. A. *Geophysica Norwegica 30* (1973) No. 2.
5. Fechsenfeld, F. C., Moseman, M. and Ferguson, E. E. *J. Chem. Phys. 55* (1971) 2115.
6. Blint, R. J. and Newton, M. D. *J. Chem. Phys 59* (1973) 6220.
7. Chen, M. M. L., Wetmore, R. W. and Schaefer, H. F., III. *J. Chem. Phys. 74* (1981) 2938.
8. Fessenden, R. W. *J. Chem. Phys. 48* (1968) 3725.
9. Symons, M. C. R. *J. Am. Chem. Soc. 91* (1969) 5924.
10. Olah, G. A., Yoneda, N. and Parker, D. G. *J. Am. Chem. Soc. 98* (1976) 5261.
11. Yoneda, N. and Olah, G. A. *J. Am. Chem. Soc. 99* (1977) 3113.
12. Kausch, M. and Schleyer, P. von R. *J. Comput. Chem. 1* (1980) 94.
13. Nangia, P. A. and Benson, S. W. *J. Am. Chem. Soc. 102* (1980) 3105.
14. Howard, C. J. NOAA R443, Boulder, Colorado. *Private communication.*
15. Pulay, P. *Theor. Chim. Acta 50* (1979) 299.
16. Pulay, P. *Mol. Phys. 17* (1969) 197.
17. Broch Mathisen, K. *Internal Report,* University of Tromsø, Tromsø 1982.
18. Sæbø, S. *Internal Report,* University of Oslo. Oslo 1979.
19. Ditchfield, R., Hehre, W. J. and Pople, J. A. *J. Chem. Phys. 54* (1971) 724.
20. Roos, B. and Siegbahn, P. *Theor. Chim. Acta 17* (1970) 209.
21. Huzinaga, S. *J. Chem. Phys. 42* (1965) 1293.
22. Dunning, T. H. *J. Chem. Phys. 55* (1971) 716.
23. Gilmore, R. F. *J. Quant. Spectrosc. Radiat. Transfer 5* (1965) 369.

Received March 10, 1983.

Acta Chemica Scandinavica A 37 (1983) 823–831

Gas-phase Molecular Structure of Bicyclo[3.3.3]undecane (Manxane) Studied by Electron Diffraction

GRETE GUNDERSEN,[a,*] PETER MURRAY-RUST,[b,*] DAVID W. H. RANKIN,[a,**] RAGNHILD SEIP[c] and C. IAN F. WATT[b,*]

[a] Department of Chemistry, University of Edinburgh, West Mains Road, Edinburgh EH9 3JJ, Scotland, [b] Department of Chemistry, University of Stirling, Stirling, FK9 4LA, Scotland and [c] Department of Chemistry, University of Oslo, Oslo 3, Norway

The electron-diffraction data from the vapour of bicyclo[3.3.3]undecane at 373K are consistent with C_{3h} symmetry of the molecule which exhibits flattening of the skeleton at the bridgeheads and wide carbon valence angles in the bridges. The two types of C–C bonds are not significantly different in length. Some independent and dependent geometrical parameters are (r_a, $\angle_a$ and θ_a): r(C–C) average=154.2(2) pm, $\angle$(C2–C1–C8)=113.5(9)°, $\angle$(C1–C2–C3)=120.3(11)°, $\angle$(C2–C3–C4)=117.7(8)°, θ(C1–C2–C3–C4) =67.4(15)°, θ(C1–C2···C4–C3)=124.4(11)°, θ(C3–C2–C1–C8)=36.1(24)° and θ(C3–C2–C1–C9)=95.4(9)°. The distortion from tetrahedral valence angles is such as to give the shortest H···H interaction between the bridges of 220(4) pm rather than 130 pm, which would result from the tetrahedral model.

Bicyclo[3.3.3]undecane (known as manxane because of similarity between the projection of the proposed structure and the coat of arms of the Isle of Man) was first prepared in 1970,[1,2] and it was said to exist in a molecular conformation with C_{3h} symmetry, as reflected in its high melting point (465K) and its simple infrared spectrum; and as suggested by evaluation of steric interactions in various models.[2]

Manxane and some of its derivatives have been studied by dynamic NMR.[1,3] and most of the properties were rationalized on the basis of a proposed flattening of the bridgehead regions. Molecular mechanics calculations[4] also favoured the C_{3h} model and it was shown that even this conformation was highly strained, in contrast to the flexibility observed for most monocyclic eight-membered rings. The strain is reflected in considerable deviations from the tetrahedral value for the C–C–C angles, with flattening of the bridgehead regions and the angles in the chains approaching 120°. Conversion of a bridgehead to a trigonal center was found to relieve strain and this was related to the enhanced cation and radical reactivity at these sites.[5] Crystal-structure determinations have shown that the two derivatives, 1-azabicyclo [3.3.3]undecane hydrochloride[6] and bicyclo[3.3.3]undecane-1,5-diol,[7] have the expected structural features. However, the heat of formation, calculated from a force field,[8] is not in good agreement with the experimental value.[9]

Manxane itself is not a good subject for crystallographic investigations since it is disordered, sublimes readily, and reacts rapidly with atmospheric oxygen. Hence it was decided to study the molecular structure of manxane by gas-phase electron diffraction: the results are reported in the present paper.

* Present addresses: G. G., Department of Chemistry, University of Oslo, Oslo 3, Norway; P.M-R., Glaxo Group Research Ltd., Greenford Road, Greenford, Middlesex, England; C.I.F.W., Department of Chemistry, University of Manchester, Manchester, M13 9PL, England.

** Author to whom correspondence should be addressed.

0302-4377/83 $2.50

Table 1. Weighing functions, correlation parameters and scale factors.[a]

Camera height	Wave-length	Δs	s_{min}	sw_1	sw_2	s_{max}	Correlation parameter	Scale factor
mm	pm	nm^{-1}						
247.8	5.871	4	40	50	250	292	−0.145	0.700(12)
497.8	5.871	2	20	50	120	148	−0.031	0.732(10)

[a] See Ref. 13 for explanation of the symbols.

EXPERIMENTAL

Manxane was prepared according to literature procedures.[1] The electron-diffraction photographs were taken in Oslo using a Balzers' Eldigraph KDG-2,[10] Kodak Electron Image plates, nozzle-to-plate distances of 497.82 and 247.84 mm, an accelerating voltage of 42 kV, and a nozzle temperature of about 380 K. The electron wavelength was calibrated against diffraction patterns of gaseous benzene and its estimated uncertainty is 0.1 %.

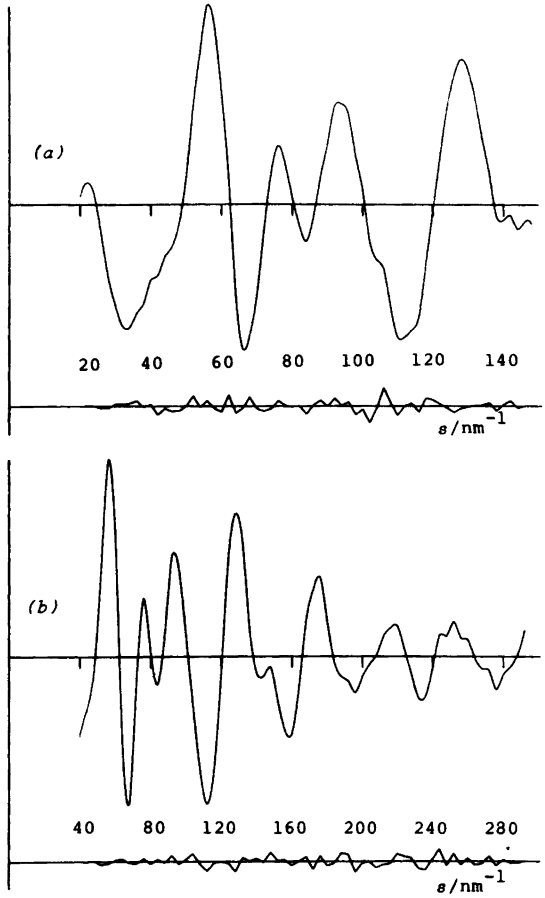

Fig. 1. Experimental molecular scattering intensities for nozzle-to-plate distances of (a) 248 and (b) 498 mm; and the corresponding final weighed difference curves according to the parameter values of Tables 2 and 3.

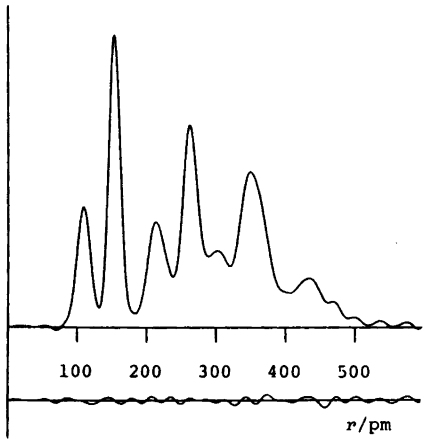

Fig. 2. Experimental radial distribution curve, $P(r)/r$, and difference curve corresponding to the intensities in Fig. 2. Before Fourier inversion the data were multiplied by s. $\exp[-0.000020\ s^2]/(Z_c-f_c)^2$.

The optical densities (D) of three and four plates for the long and short camera distances, respectively, were recorded using the Joyce-Loebl Microdensitometer 6 at the S.E.R.C. Laboratory, Daresbury.[11] The data reduction was carried out by the established programs[12] modified to accomodate sector- and blackness-$[1.+0.03D+0.09D^2+0.03D^3]$ corrections appropriate for data from the Balzers' Eldigraph in Oslo. At the final stage handdrawn background subtractions were replaced by automatic corrections using spline functions. An established least-squares refinement program[13] was used in the structure analysis. The data ranges and the parameters of the off-diagonal weighting functions are given in Table 1 together with the scale factors and the correlations parameters. The complex scattering factors of Schäfer *et al.*[12] were used, and all calculations were carried out on an ICL 2972 computer.

The experimental molecular intensities and the corresponding radial distribution curve are shown in Fig. 1 and 2, respectively.

STRUCTURE ANALYSIS

Preliminary analysis showed that the data could be interpreted in terms of a molecular structure of C_{3h} symmetry with geometrical parameters compatible with those obtained in molecular mechanics calculations,[4] and crystallographic studies of related compounds.[6,7]

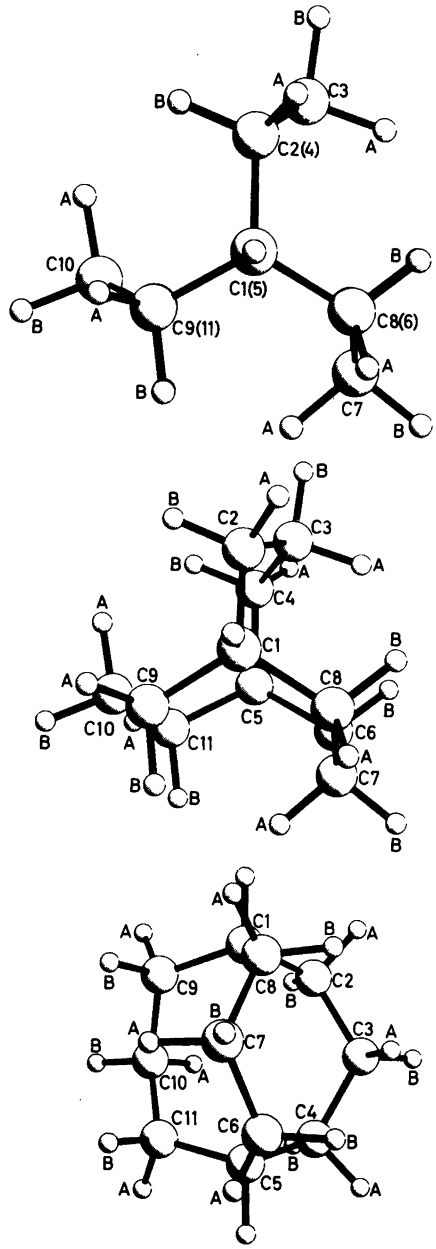

Fig. 3. Three views of the manxane molecule corresponding to the parameter values of Table 2. The numbering of the carbon atoms and the A- and B-labelling of the methylene hydrogen atoms are included. Fig. 3(a) is a projection along the threefold axis through H1, C1, C5 and H5, and Figs. 3(b) and 3(c) are perspective views.

The first two peaks of the radial distribution curve (Fig. 2) represent three types of C–H and two types of C–C bond distances, at 110 and 150 pm, respectively. The next feature, at about 215 pm, contains all one-angle C···H distances. The other types of C···H interactions are found over the whole range of r>260 pm and they are, together with H···H distances, the only contributors to the area beyond 400 pm. However, the main components of the peaks at 260, 300 and 350 pm are C···C distances: three types of one-angle distances at 260 pm; the C3···C8 interactions (see Fig. 3 for numbering of the carbon atoms) at 300 pm and the remaining five types at about 350 pm. The distance distribution is fairly complex and the identification of the C···C distances is obscured by significant contributions from C···H distances in the 260–390 pm region. However, the position of the peak containing the one-angle C···C distances at a large r-value gives direct evidence for the flattening of the bridgehead and widening of ∠(C–C–C) at C2 and C3.

Two perspective views of the manxane molecule and a projection down the C_3 axis are shown in Fig. 3 which also includes the numbering of the atoms. In addition to the C_{3h} molecular symmetry it was assumed that the methylene groups (C–CH_2–C) deviated from local C_{2v} symmetry only by possible differences Δr(C–C) and by a tilt in the CH_2-plane. The tilt parameter (γ) is the angular deviation from co-linearity of the bisectors for ∠(HCH) and ∠(CCC). Inspection of molecular models showed that such tilt could effectively contribute a relief in steric strain: H3A···H8B is lengthened by positive tilt of $C2H_2$ and by negative tilt of $C3H_2$, *i.e.* for γ(C2)>0 and γ(C3)<0°. It was not found worthwhile to distinguish the C–H bond length for the two bridgehead hydrogens from that associated with the eighteen hydrogens of the C–CH_2–C groups. The two *symmetrically* different types of r(C–C) were described by an average, $r(C-C)_{av,}$, and a difference, $\Delta(CC)=r(C2-C3)-r(C1-C2)$. The two types of tilt parameters, γ(C2) and γ(C3), were maintained, but the two types of valence angles, ∠(H–C2–H) and ∠(H–C3–H), were assumed to be of equal magnitude. The molecular geometry was thus described by nine parameters as given in Table 2, which also contains dependent geometrical quantities.

Normal coordinate calculations were carried out to provide a basis for assumptions regarding the magnitudes of the root-mean-square amplitudes of vibration (u-values); and for shrinkage corrections valid for small amplitude molecular vibrations, *i.e.* r_a-refinements. In the r_a-refinements, $r_a=r_\alpha-u^2/r+K$ where K is the calculated perpendicular amplitude correction coefficient; and u is the calculated or refined value in the actual least-squares fitting procedure.

Such calculations of u- and K-values for other cyclic hydrocarbons have been performed using Urey-Bradley force constants taken from force fields for cyclohexane. Two sets of values are currently in use, derived from the force fields

Table 2. Geometrical parameters[a] for manxane, and final least-squares results.[b] See Table 3 for the corresponding interatomic distances and amplitude parameters and Table 4 for elements of the correlation matrix.

Independent parameters (r_a, ∠$_a$, θ_a)		Dependent angles (∠$_a$, θ_a)	
p1, r(C–H)	108.8(2)	∠(C2–C3–C4)	117.7(8)
p2, r (CC_{AV})	153.8(1)	∠(C2–C1–C8)	113.5(9)
p3, Δ(CC)	−0.3(27)	θ(C1–C2···C4–C3)	124.4(11)
p4, ∠(C2–C1–H1)	105.1(11)	θ(C1–C2–C3–C4)	67.4(15)
p5, ∠(C1–C2–C3)	120.3(11)	θ(C3–C2–C1–C8)	36.1(24)
p6, θ(H1–C1–C2–C3)	150.4(8)	θ(C3–C2–C1–C9)	95.4(9)
p7, ∠(H–C–H)	101.6(15)		
p8, γ(C2)	4.8 fixed[c]		
p9, γ(C3)	2.6 fixed[c]		

a See text for model restrictions and explanation of symbols. *b* Ditances (r) in pm and angles in degrees; values in parentheses are least-squares standard deviations, *i.e.* systematic uncertainties are not accounted for. R_G=0.069 [R_D=0.073]. *c* See text.

Table 3. Interatomic distances[a] (r_a) and amplitudes of vibration (u) corresponding to the electron-diffraction structural parameters of Table 2; and u- and K-values calculated from force field A (Table 5) for manxane at 373K.

	Electron diffraction			Force-field calculations[c]	
	r_a/pm	u/pm[b]		u/pm	K/pm
C1–H1	109.7(2)	7.0(3)	*u1*	7.88	1.41
C2–H2A	110.4(2)	7.0		7.94	2.08
C3–H3A	110.3(2)	7.0 } −*u1*		7.93	1.98
C1–C2	154.3(13)	5.2(2)	*u2*	5.37	0.48
C2–C3	154.1(14)	5.2 −*u2*		5.31	0.60
C2···C4	263.3(32)	7.1(7)	*u3*	7.67	0.48
C1···C3	267.0(15)	7.1		7.54	0.31
C2···C8	257.7(15)	7.1 } −*u3*		7.83	0.45
C3···C8	304.9(9)	11.5(6)	*u4*	12.66	0.26
C1···C4	337.5(12)	9.6(12)	*u5*	9.12	0.19
C1···C5	343.0(40)	9.6		9.08	0.11
C3···C7	353.8(11)	12.1 } −u5		11.72	0.22
C2···C7	356.2(5)	9.6		8.72	0.27
C2···C6	367.9(18)	12.1		10.95	0.19
C2···H1	210.7(25)	10.8(4)	*u6*	10.74	0.94
C1···H2A	212.9(12)	10.8		10.70	1.48
C1···H2B	218.0(12)	10.8		10.71	1.47
C3···H2A	212.8(13)	10.8		10.68	1.55
C3···H2B	217.9(14)	10.8 } −*u6*		10.69	1.62
C2···H3A	214.9(9)	10.8		10.68	1.55
C2···H3B	217.7(9)	10.8		10.66	1.45
C3···H1	347.1(17)	12.1 −u5		11.42	0.58
C2···H5	437.7(13)	15.5(12)	*u7*	11.71	0.42
C1···H5	451.7(39)	15.5 −*u7*		11.46	0.34
C1···H3A	287.8(22)	16.5 −*u4*		15.77	0.92
C1···H3B	356.4(12)	11.0 (fixed)		10.95	0.88
C2···H4A	351.3(31)	12.1 −*u5*		10.98	1.16
C2···H4B	292.1(44)	16.5 −*u4*		16.07	1.12
C1···H4A	435.9(13)	15.5 −*u7*		11.53	0.69
C1···H4B	377.3(20)	21.4 −*u5*		18.61	0.59
C3···H8B	285.7(26)	23.1 −*u4*		22.97	0.77
C3···H8A	408.0(11)	19.1(25)	*u8*	15.62	0.75
C3···H9A	421.5(18)	19.1 −*u8*		14.54	0.72
C3···H9B	438.7(11)	20.6 −*u7*		14.28	0.72
C3···H7A	418.5(21)	19.1 −*u8*		15.91	0.62
C3···H7B	441.2(11)	20.6 −*u7*		16.11	0.61
C3···H10A	312.6(25)	23.1 −*u4*		22.38	0.64
C3···H10B	458.0(15)	20.6 −*u7*		14.89	0.60
C2···H8A	340.0(16)	12.1 −*u8*		11.90	1.12
C2···H8B	265.8(19)	16.5 −*u4*		15.93	1.14
C2···H9A	297.7(30)	16.5 −*u4*		14.96	1.09
C2···H9B	350.4(16)	12.1 −*u5*		11.17	1.08
C2···H7A	399.4(14)	19.1 −*u8*		16.08	0.68
C2···H7B	449.5(11)	15.5 −*u7*		12.26	0.69
C2···H10A	269.2(25)	21.4 −*u5*		22.35	0.82
C2···H10B	400.9(13)	19.1 −*u8*		15.96	0.71
C2···H6A	475.7(16)	15.5 −*u7*		12.75	0.60
C2···H6B	378.5(35)	23.1 −*u4*		22.32	0.50
C2···H11A	446.5(10)	20.6 −*u7*		16.67	0.67
C2···H11B	442.0(27)	20.6 −*u7*		16.60	0.62

[a] H···H distances were included in refinements, but are not listed here. [b] Eight groups of independent amplitude variables, *u1* to *u8*; the remainder of the u-values are tied to these as indicated by −*u1* to −*u8*. [c] Based on atomic coordinates corresponding to preliminary geometrical parameters: p_1=110.2, p_2=154.2, p_3=0, p_4=105.6, p_5=120.3, p_6=149.2, p_7=107.5, p_8=p_9=0. (See Table 2 for definitions and results.)

given by, (a): Schachtschneider and Snyder,[15] by (b): Takahasi *et al.*,[16] as for example in electron-diffraction studies of bicyclo[3.1.0]hexane,[17] and bicyclo[3.3.1]nonane,[18] respectively. We carried out calculations for manxane with both sets of force constants using a computer program originally written by R. L. Hilderbrandt.[19] The literature values[16] for set B were scaled, and since several interaction elements of the original force field were omitted, the selected force constants were adjusted to optimize the fit to the observed normal frequencies for cyclohexane before they were transferred to manxane. The two force fields are given in Table 5. Similar values for the calculated amplitude quantities were obtained in both cases. The *u*- and *K*-values corresponding to force field A were chosen for the final structure refinements and they are given for T=373 K in Table 3, omitting the values for the H···H interactions. Complete tables of *u*- and *K*-values for manxane at 0, 273 and 373 K are available upon request.

Optimum values for Δ(CC), $\angle$(H−C−H) and the two tilt parameters were initially determined by refinements in which these parameters were not refined but varied systematically over a range of values. Subsequently they were included with other geometrical parameters in both r_a- and r_α-refinements, although the tilt angles were fixed in the final refinements.

Refinements of *u*-values were included at two levels. Firstly, all amplitudes associated with C···H interactions, except for bond and one-angle distances, were fixed at calculated values, as were those associated with H···H interactions. The remaining amplitudes were refined as independent parameters or in groups in which the amplitudes were tied together by fixed rations as indicated by the magnitudes of the calculated *u*-values. Ultimately, all the amplitudes for the "long" C···H interactions were entered in the refinement scheme, but in this case the refinement diverged unless the two CH_2-tilt parameters were excluded from the refinement.

Table 4. Elements ($\rho_{ij}\times100$) of the least-squares correlation matrix corresponding to parameter values and standard deviations of Tables 2 and 3. Only elements with magnitudes ≥40 are included.

	p1	*p3*	*p4*	*p5*	*p6*	*u1*	*u5*	*u7*	*k1*
p4		−76							
p5		−45	+90						
p6		+82	−87	−64					
p7	+41	+41							+42
u3				−64			−42		
u4		−41	+67	+68	−45		+65		
u5		−56	+91	+86	−74				
u6		−54	+51	+45			+42		
u8								+58	
k1						+70			
k2						+60			

Table 5. Force constants[a] of two approximate Urey-Bradley force fields for manxane, *A* and in parentheses, *B* (see text of article).

K(C−C)	2.23(2.34)	H(CCC)	0.69(0.70)
K(C−H_t)	3.94(4.12)	H(CCH_t)	0.32(0.37)
K(C−H_s)	4.02(4.12)	H(CCH_s)	0.33(0.37)
F(C···C)	0.32(0.20)	H(HCH)	0.52(0.54)
F(C···H)	0.55(0.48)	H_τ	0.078(0.144)
F(H···H)	0.05(0.07)		

[a] In 100 aJ nm^{-2} (K and F) and aJ rad^{-2} (H); 1aJ=1 mdyn Å.

Table 6. Structural parameters for manxane (I) determined by electron diffraction (ED) and molecular mechanics calculations (MM) and for the 1,5-diol (II) and 1-aza (III) derivatives determined by X-ray diffraction (XD).[a].

	I(ED)[b] This work	I(MM) Ref. 4	II(XD)[c] Ref. 7	III(XD)[c] Ref. 6
r(C1–C2)	154.3(26)	154.2	152.9(7)	154.3(6)
r(C2–C3)	154.1(28)	153.5	152.3(8)	151.1(9)[d]
∠(C2–C1–C8)	113.5(18)	115.2	113.8(2)	113.9(6)
∠(C1–C2–C3)	120.3(22)	118.8	118.7(6)	118.1(5)
∠(C2–C3–C4)	117.7(16)	118.3	120.5(5)	119.7(6)
θ(H–C1–C2–C3)	150.1(22)	–	151.5(18)	–
θ(C8–C1–C2–C3)	36.1(48)	–	37.7(8)	39.5(5)
θ(C9–C1–C2–C3)	95.4(18)	–	94.7(8)	96.6(6)
θ(C1–C2–C3–C4)	67.4(30)	–	68.3(8)	67.7(4)
θ(C1–C2···C4–C3)	124.4(22)	–	121.0(–)	–

[a] Distances in pm, angles in degrees. [b] The values in parentheses are 2σ (*cf.* Table 4); the average r(CC) is determined with higher accuracy than the individual bonds, 2σ=0.2 pm; r_a and $\angle_\alpha$ values are given. [c] The values are $\bar{x}=\Sigma x_i/n$, averaged over the C_3- and/or C_h-symmetry equivalent parameters and the uncertainties in parentheses are $[\Sigma(x_i-\bar{x})^2/n\text{-}1]^{\frac{1}{2}}$ as compared to the quoted σ-values for the individual determinations of: II, 0.5–1.0 pm (r), 0.4–0.8° (∠) and 1.0°(θ); III, 0.5 pm (r) and 0.2–0.3° (∠). [d] See text for systematic errors.

In the various refinements the difference in length of the two types of C–C bonds was never significantly different from zero. The angle parameters for the carbon skeletons *p*4, *p*5 and *p*6 (see Table 3) varied in the ranges 104.1(4) to 105.5(13)°, 118.7(4) to 120.6(9)°, and 150.1(9) to 150.7(6)°, respectively. This invariably gave ∠(C1–C2–C3)>∠(C2–C3–C4), although not significantly so in all cases. The r_α-refinements generally gave a smaller ∠(H–C–H) than the corresponding r_a-refinements: 101.0(15) to 102.4(14)° and 102.9(13) to 103.7(13)°, respectively for $\angle_\alpha$ and $\angle_a$. The tilt parameters, γ(C2) and γ(C3), varied in the ranges 2.2(34) to 4.8(18)° and −1.8(24) to 4.8(18)°, respectively.

The possibility that the refined structure could be ambiguous, due to the fairly complex C···C distance overlaps, was considered. Refinements from various starting values for *p*4 to *p*6 (see Table 2) were carried out with special attention to the relative magnitudes on the one-angle C···C distances. However, these refinements ultimately converged to the same minimum, thus indicating that the structural results obtained are unique.

The final results are presented in Tables 2–4. They were obtained in r_α-refinements for which the tilt parameters were fiexed at values γ(C2)=4.8(18) and γ(C3)=2.6(17)°, obtained in a previous r_α-refinements with the amplitude parameters fixed at the calculated values. The *R*-factors for the final results were R_G=0.069 and R_D=0.073, and the corresponding weighted difference molecular intensities and the radial distribution difference curve are shown in Figs. 1 and 2. The fit to the experimental data, as reflected by the difference curves and *R*-factors, is satisfactory considering that the diagrams had low optical density which gave a relatively low signal to noise ratio.

DISCUSSION

The values of the geometrical parameters for the carbon skeleton of manxane are given in Table 6 which also contains corresponding results from the molecular mechanics calculations[4] and from X-ray diffraction studies of two derivatives.[6,7] There is generally a good agreement in the features of the structures.

Compared to tetrahedral arrangements there is flattening of the bridgehead and also a widening of the other chain angles. However, it appears that the MM-results overestimate the flattening somewhat at the expense of the opening of the chain angles, and the ED-results suggest that the central chain angle is smaller than that of C2, contrary to the XD-results. The latter difference could be due to effects from substitution by OH-groups in 1,5-positions and by nitrogen in

the frame at C1. In spite of failed attempts to fit models with reverse relative magnitudes for these angles it should be noted that their determination by electron diffraction is inaccurate: the difference of 2.3° is not significantly different from zero at a 2σ-level, and the analysis is hampered by severe distance overlaps.

It is interesting to note that in the analogous compound with triangularly bridged cyclohexane rings, bicyclo[2.2.2]octane, there are only minor deviations from tetrahedral angles in the carbon skeleton.[20] The flexible cyclooctane has average carbon valence angles of 116.6°,[21] whereas in bicyclo[3.3.1]nonane the bridged cyclooctane ring, which at room temperature exists predominately in the chair, chair conformation with respect to the bridge, has such angles in the range 111.9–113.2°.[18] It has been noted that in molecules with a bridged cyclooctane ring there is an increase in angle strain with the size of the bridge[7] as reflected in the quoted values for bicyclo[3.3.1]nonane, values of 116–117° for a derivative of bicyclo[3.3.2]decane[22] and of 118–120° for bicyclo[3.3.3]undecane derivatives (Table 6). In the bicyclo[3.3.2]decane derivative the eight-membered ring is in a boat, chair conformation with respect to the bridge as is the case of manxane. Steric H···H repulsions between neighbouring bridges are believed to be responsible for the strain in these molecules.[6,7]

Thus in manxane the *endo* hydrogens of C3 are pushed apart from the buttressing intraannular hydrogen atoms of C6 and C8 so as to give the shortest H···H distance between neighbouring bridges of 220(4) pm, rather than about 130 pm which would appear in a model with tetrahedral CCC angles. This repulsion is also seen in the opening of the angles between the C2–C3–C4 and C1–C2–C4–C5 planes to 124.4(22)° from about 96° in the tetrahedral model, as shown in Fig. 3a. The torsional angles about the central C–C bonds are also interesting since staggered conformation is approached with θ(C1–C2–C3–C4)=67.4(30)°, rather than above 90° as in the tetrahedral model. The methylene tilt parameter (Table 3) at C3(C7, C10) is probably not significantly different from zero and it counteracts the lengthening of the H3A···H8B interactions obtained by positive tilt at C2(C4, C8, C6, C9, C11).

The two types of C–C bonds in manxane are not significantly different in length (Table 6). It should be noted that the average value (Table 3) is determined with high accuracy compared with the uncertainty in the determination of the individual bonds, *i.e.* $r_a(C-C)_{average}$ = 154.2(2) pm, including a systematic uncertainty of 0.1 % in the estimated standard deviation.

The length of the C–C bonds in compound III (Table 6) is compatible with the corresponding bonds in manxane (C1–C2/C4–C5) whereas the apparently shorter bonds in compound II may be related to possible substitution effects from the OH-groups in the 1,5 positions. It has been stated that the determined lengths on bonds involving the three central methylene carbon atoms (C3, C7, C10) in III may be systematically too short due to thermal motions.[6]

The average C–C bond length in bicyclo[2.2.2]octane with bridged cyclohexane rings is 154.2(4) pm[20] as compared to a bond length of 153.6(4) pm in cyclohexane.[23] These molecules have similar C–C–C angles. The average C–C bond lengths of cyclooctane,[21] bicyclo[3.3.1]nonane[18] and the present bicyclo[3.3.3]undecane are 154.0, 153.6(1) and 154.2(2) pm, respectively, and it appears that the different steric strain in these molecules is not reflected in significant variations in the C–C bond lengths.

Acknowledgement. We thank the Science and Engineering Research Council (U.K.) for a research grant.

REFERENCES

1. Doyle, M., Parker, W., Gunn, P. A., Martin, J. and MacNicol, D. D. *Tetrahedron Lett.* (1970) 3619.
2. Leonard, N. J. and Coll, J. C. *J. Am. Chem. Soc. 92* (1970) 6685.
3. Coll, J. C., Crist, D. R., Barrio, M.d. C. G. and Leonard, N. J. *J. Am. Chem. Soc. 94* (1972) 7092.
4. a. Chang, L. W. K. *Thesis,* Princeton 1970; b. Engler, E. M. *Thesis,* Princeton 1973; c. Fry, J. L., Engler, E. M. and and Schleyer, P.v.R. *J. Am. Chem. Soc. 95* (1973) 8005.
5. a. Parker, W., Tranter, R. L., Watt, C. I. F., Chang, L. W. K. and Schleyer, P.v. R. *J. Am. Chem. Soc. 96* (1974) 7121; b. Olah, G. A., Liang, G., Schleyer, P.v.R., Parker, W. and Watt, C. I. F. *J. Am. Chem. Soc. 99* (1977) 966.

6. a. Leonard, N. J., Coll, J. C., Wang, A. H.-J., Missavage, R. J. and Paul, I. C. *J. Am. Chem. Soc. 93* (1971) 4628; b. Wang, A. H.-J., Missavage, R. J., Byrn, S. R. and Paul, I. C. *J. Am. Chem. Soc. 94* (1972) 7100.
7. Murray-Rust, P., Murray-Rust, J. and Watt, C. I. F. *Tetrahedron 36* (1980) 2799.
8. Parker, W., Steele, W. V. and Watt, C. I. F. *J. Chem. Thermodyn. 7* (1975) 795.
9. White, D. N. J. and Baill, M. J. *J. Chem. Soc. Perkin Trans. 2* (1977) 1610.
10. Zeil, W., Haase, J. and Wegmann, L. *Z. Instrumentenkd. 74* (1966) 84; b. Bastiansen, O., Graber, R. and Wegmann, L. *Balzers' High Vacuum Report 25* (1969) 1. Balzers A-G für Hochvakuumtechnik und dünne Schichten, 9496 Balzers, Lichtenstein.
11. Cradock, S., Koprowski, J. and Rankin, D. W. H. *J. Mol. Struct. 71* (1981) 113.
12. Huntley, C. M., Laurenson, G. S. and Rankin, D. W. H., *J. Chem. Soc. Dalton Trans.* (1980) 954.
13. Boyd, A. S., Laurenson, G. S. and Rankin, D. W. H. *J. Mol. Struct. 71* (1981) 217.
14. Schäfer, L., Yates, A. C. and Bonham, R. A. *J. Chem. Phys. 55* (1971) 3055.
15. Schachtschneider, J. H. and Snyder, R. G. *Spectrochim. Acta 19* (1963) 117.
16. Takahashi, H., Shimanouchi, T., Fukushima, K. and Miyazawa, T. *J. Mol. Spectrosc. 13* (1964) 43.
17. Mastryukov, V. S., Osina, E. L., Vilkov, L. V. and Hilderbrandt, R. L. *J. Am. Chem. Soc. 99* (1977) 6855.
18. a. Mastryukov, V. S., Osina, E. L., Dorofeeva, O. V., Popik, M. V., Vilkov, L. V. and Belikova, N. A. *J. Mol. Struct. 52* (1979) 211; b. Mastryukov, V. S., Popik, M. V., Dorofeeva, O. V., Golubinskii, A. V., Vilkov, L. V., Belikova, N. A. and Allinger, N. L. *J. Am. Chem. Soc. 103* (1981) 1333; *Tetrahedron Lett. 45* (1979) 4339.
19. Hilderbrandt, R. L. and Wieser, J. D. *J. Chem. Phys. 42* (1966) 4648.
20. Yokozeki, A., Kuchitsu, K. and Morino, Y. *Bull. Chem. Soc. Jpn. 43* (1970) 2017.
21. Almenningen, A., Bastiansen, O. and Jensen, H. *Acta Chem. Scand. 20* (1966) 2689.
22. Murray-Rust, J. and Murray-Rust, P. *Acta Crystallogr. B 31* (1975) 310.
23. Bastiansen, O., Fernholt, L., Seip, H. M., Kambara, H. and Kuchitsu, K. *J. Mol. Struct. 18* (1973) 163.

Received March 9, 1983.

Acta Chemica Scandinavica A 37 (1983) 833–841

The Structure of *cis*-Aquahydroxobis (2-pyridylmethylamine)-chromium(III) Dithionate Studied by X-Ray Diffraction and Spectroscopic Methods

SINE LARSEN, KURT B. NIELSEN and IB TRABJERG

Chemical Laboratory IV, H.C. Ørsted Institute, Universitetsparken 5, DK-2100 København Ø, Denmark

The crystal structure of the title compound has been determined by X-ray diffraction methods. The crystals are monoclinic, space group $P2_1/c$, $Z=4$ with unit cell dimensions a = 10.210 Å, $b=10.680$ Å, $c=16.992$ Å and $\beta=101.25°$. The structure was solved and refined from diffractometer data to a final R-value of 0.046. The complex cation has the pyridine nitrogen atoms in a *trans* configuration and the other ligators in *cis* configurations. The Cr–O(hydroxo) bond is considerably shorter than the Cr–O (water) bond 1.93 Å *vs.* 2.00 Å. The pyridine rings of the ligands are almost perpendicular.

The polarized single crystal spectra recorded with the E-vector in the a–b plane, have the sharpest absorption maxima when E is parallel to the a-axis. Emission and exitation spectra measured on powdered samples show spin-forbidden transitions at 640 and 708 nm. At 1.7 K the observed lifetime was 28μs. The strong-field parameters obtained from the spectra are 10 $Dq=1900$ cm^{-1}, $B=500$ cm^{-1} and $C=3450$ cm.$^{-1}$

A number of different complexes of chromium(III) and cobalt(III) with 2-pyridylmethylamine as ligand have been prepared and characterized by their solution spectra by Kirsten Michelsen.[1–5] If we consider the octahedral complexes with two molecules of 2-pyridylmethylamine as ligands, several isomers are possible due to the difference between the two ligating nitrogen atoms in the bidentate ligand. For the complexes corresponding to a *cis* arrangement of the unidentate ligands three different geometrical isomers may exist. They are named by considering firstly the spatial arrangement of the unidentate ligands, then the arrangement of the pyridine nitrogen atoms and finally the arrangement of the methylamine nitrogen atoms. According to this nomenclature the three geometrical isomers can be classified as a *cis,trans,cis,* a *cis,cis,trans,* and a *cis,cis,cis* isomer. Kirsten Michelsen was able to isolate two series of complexes, called α and β.[2,3] From spectroscopic measurements she concluded that the α-series corresponds to either the *cis, trans,cis* or to the *cis,cis,trans* isomers, and the β-series to the *cis,cis,cis* isomers.

The compound studied in this work is of the α-series assuming equivalence between the hydroxyl group and the water molecule. The structure analysis was undertaken to establish the configuration of the α-series complexes and to obtain information about the overall symmetry and the structure of a *cis*-aqua hydroxo chromium(III) complex since no structural data is available for this particular type of compound. The electronic structure of the complex is elucidated by measurements of crystal spectra in the ligand field range.

EXPERIMENTAL

Chrystallographic examination. A sample of the title compound was kindly provided by Kirsten Michelsen. It crystallizes as bright red plates. Preliminary Weissenberg and precession photographs showed that the crystals are monoclinic, the space group is uniquely determined to be $P2_1/c$ from the systematically absent reflec-

0302-4377/83 $2.50

tions. The density was measured by flotation in a mixture of bromobenzene and 1,2-dibromoethane.

A single crystal with dimensions $0.3\times0.1\times0.03$ mm^3 was chosen for the data collection and for the determination of unit cell parameters on a Picker FACS-1 diffractometer. The measurements were performed at 22 °C using graphite monochromated-Mo$K\alpha$ radiation. The data were obtained by operating the diffractometer in the $\theta-2\theta$ scan mode at a rate of 1°min^{-1} in 2θ. The reflections were collected in the hemisphere ($h\leq0$) which had $2.4° \leq 2\theta \leq 42°$. The symmetrical scan range was increased with 2θ following the expression $\Delta 2\theta_{sc} = 2.4° + 2\times0.346 \tan\theta$. Background counts were made at each end of the scan range for 20 s.

The intensities for 6 standard reflections recorded after every 60 reflections showed that no deterioration or misalignment had occured during the data collection. The data were corrected for Lorentz and polarization effects and the symmetry related reflections were averaged. Of the 1900 independent reflections so obtained 1329 satisfied the inequality $|F|^2 \geq 2\sigma(|F|^2)$, and these were used for the structure solution and refinement.

The following computer programs were employed during the computations: the Vanderbilt system[6] for diffractometer operations, a data reduction program of local origin, ORTEP II[7] for the illustrations, the XRAY[8] system for the crystal structure analysis and Simplex[9] for the weight analysis.

Using the values for the uncharged atoms the scattering factors used in the calculations were taken from Cromer and Mann[10] except for H were the results from Stewart *et al.*[11] were used. The anomalous dispersion corrections added to the scattering factors of chromium and sulfur were calculated by Cromer and Liberman.[12]

Spectroscopic examination. The electronic structure was investigated by recording the single crystal polarized absorption spectra and both emission and excitation spectra of powdered samples.

The largest available crystals with a surface of approximately 0.25×0.5 mm^2 were used for the measurements of the polarized absorption spectra. The crystal surface is parallel to the *a–b* plane elongated along the *b*-axis.

The absorption spectra were recorded at room temperature and at 80K on a 2m Jena Qlspectrograph and a Cary 14 spectrometer. The emission spectra were detected by a Jarrell Ash ½ m Ebert scanning monochromator type JE 82–000 equipped with an EMI S-20 cathode photomultiplier. The excitation for the DC-measurements was made by use of a Varian Lamp type VIX 300 and filtered by a MacPherson 0.3 m scanning monochromator, Model 218.

The lifetime measurements were performed by excitation with a dye laser pumped by an nitrogen laser AVCO 530. A methanol solution 0.01 M in β-methylumbelliferrone and 1.5 M in $HClO_4$ was used as the dye.

DC-signals were amplified by a Keithly nA meter and AC-signals by a Tektronix type 454 oscilloscope with a signal output and a PAR-boxcar integrator, model 160, before they were recorded on a strip-chart recorder.

The spectra obtained from the powdered samples were made by gluing the powder to a copper-plate with Aquadag and mounting the plate in a helium cryostat. The bubbles in the liquid helium were removed by pumping the gasous helium away until the temperature was below the λ-point.

CRYSTAL DATA

cis-Aquahydroxobis(2-pyridylmethylamine)-chromium(III) dithionate. $C_{12}H_{19}N_4O_8S_2Cr$; M = 463.4. Monoclinic $a=10.210(3)$ Å, $b=10.680(4)$ Å, $c=16.992(6)$ Å, $\beta=101.25(2)°$; $V=1817.2$ Å^3; $d_{obs}=1.69$ g/cm^3; $Z=4$; d_{cal} = 1.694 g/cm^3. μ(Mo$K\alpha$)=8.71 cm^{-1}. $F(000)=996$. Systematically absent reflections: $h0l$ when l odd, $0k0$ when k odd; space group $P2_1/c$ (C_{2h}^5 No.14). The plate face is {001}.

DETERMINATION AND REFINEMENT

The positions for the chromium atom and the two sulfur atoms were determined from the Patterson function. The remaining non-hydrogen atoms were located by Fourier syntheses. The structure was refined by the method of least squares minimizing $\Sigma w| |F_o|-|F_c| |^2$. Due to the limited resolution of the diffraction data anisotropic thermal parameters were only introduced if a difference Fourier and Hamilton's R-value test indicated that they provided a better description of the thermal motion. Using this criterium anisotropic temperature factors were gradually introduced to all the heavier atoms. After a unit weighted refinement, a difference Fourier map showed clearly the positions for the hydrogen atoms of the 2-pyridylmethylamine ligands. The hydrogen atoms of the hydroxo group and the water molecule were found in areas with more

Table 1. Final fractional coordinates and equivalent isotropic temperature factors, U_{eq}, in units of $Å^2 \times 10^{-2}$.

Atom	*x*	*y*	*z*	U_{eq} [a]
The cation:				
Cr	0.64812(10)	0.37121(10)	0.24079(6)	2.11(6)
O1	0.5281(4)	0.2397(4)	0.2585(2)	2.4(3)
O2	0.5066(4)	0.4998(4)	0.2426(3)	3.1(3)
N11	0.7310(5)	0.3886(5)	0.3612(3)	2.7(4)
C15	0.6960(9)	0.4738(7)	0.4110(5)	5.3(6)
C14	0.7607(10)	0.4526(8)	0.4894(5)	6.7(7)
C13	0.8616(10)	0.4013(9)	0.5180(4)	6.1(7)
C12	0.8983(8)	0.3145(7)	0.4684(5)	4.4(5)
C11	0.8314(7)	0.3070(6)	0.3898(4)	2.8(5)
C16	0.8587(7)	0.2119(6)	0.3322(4)	3.5(5)
N12	0.7977(5)	0.2407(5)	0.2479(3)	2.5(4)
N21	0.6048(5)	0.3575(5)	0.1173(3)	2.3(4)
C25	0.5043(7)	0.2895(7)	0.0747(5)	3.7(5)
C24	0.4846(8)	0.2811(7)	−0.0075(5)	4.8(6)
C23	0.5652(9)	0.3471(8)	−0.0479(4)	4.6(6)
C22	0.6660(7)	0.4197(6)	−0.0051(4)	3.6(6)
C21	0.6840(7)	0.4229(6)	0.0778(4)	2.7(5)
C26	0.7928(7)	0.4969(6)	0.1267(4)	3.6(5)
N22	0.7765(5)	0.5078(5)	0.2109(3)	2.6(4)
The Dithionate Ion				
S1	0.1727(2)	0.3917(2)	0.29334(11)	2.96(11)
S2	0.1491(2)	0.3146(2)	0.17533(11)	3.03(12)
O11	0.2848(4)	0.4778(4)	0.3016(3)	4.1(3)
O12	0.0494(4)	0.4556(5)	0.2946(3)	5.0(4)
O13	0.1991(5)	0.2867(4)	0.3470(3)	5.6(4)
O21	0.2619(5)	0.2320(5)	0.1807(3)	5.2(4)
O22	0.0250(5)	0.2492(5)	0.1665(3)	5.6(4)
O23	0.1491(6)	0.4169(5)	0.1218(3)	7.0(4)

[a] $U_{eq}=\frac{1}{3}\Sigma_i\Sigma_j U_{ij} a_i^* a_j^* \mathbf{a}_i \cdot \mathbf{a}_j$.

diffuse density. Due to the limited resolution of the diffraction data the contributions from the hydrogen atoms were included but their parameters were not refined. Their positional parameters were fixed at idealized values, the thermal parameters were given the value of the refined isotropic temperature factor of the atom to which it is bonded. The weights [9] used in the final cycles of least squares refinement follow the expression: $w^{-1}=0.32+0.53\sigma^2(F)-0.0036|F|+0.0003F^2$.

In the last cycle of least squares the maximum shift of parameters was 0.24σ and the unit weighted and weighted residual defined as

$$R=\frac{\Sigma||F_o|-|F_c||}{\Sigma|F_o|},\quad R_W=\left\{\frac{\Sigma w(\,|F_o|-|F_c|\,)^2}{\Sigma w|F_o|^2}\right\}^{1/2}$$

had decreased to 0.046 and 0.031, respectively. The goodness of fit, $G=\{\Sigma_w \Delta F^2/(n-m)\}^{1/2}$ where n and m represent the number of reflections and variables is 0.93.

The final parameters are given in Table 1. The parameters in the refinement for the hydrogen atoms, the anisotropic thermal parameters and a list of observed and calculated structure amplitudes may be obtained from the authors.

STRUCTURE

The bond lengths and bond angles for the two ions are given in Table 2 and the stereo chemistry and atomic labelling are illustrated by Figs. 1 and 2. The conformation of the dithionate ion is

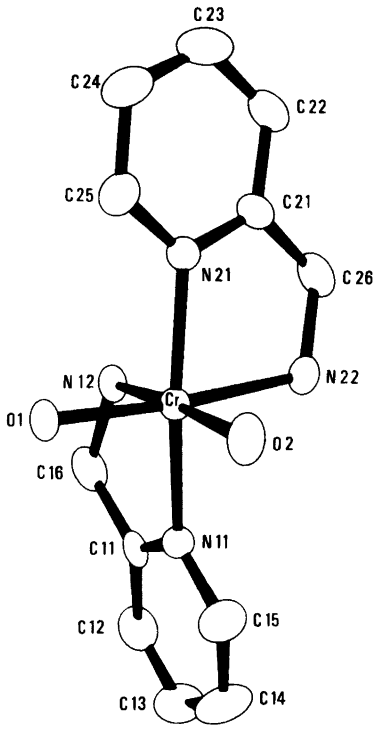

Fig. 1. An ORTEP drawing of *cis*-aquahydroxo-bis-(2-pyridylmethylamine)chromium(III) ion showing the atomic labelling.

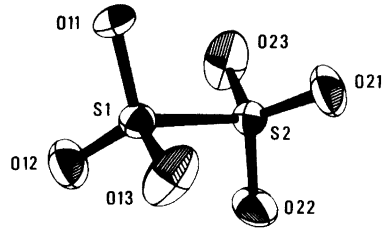

Fig. 2. An ORTEP drawing of the dithionate ion.

approximately staggered, the dihedral angle O13–S1–S2–O23 being –168,8(4)°. The S1–S2 bond length is 2.137 Å and none of the S–O bonds differ significantly from their mean, <S–O>=1.436 Å. All these features are in agreement with those previously obtained in other crystal structure determinations for dithionate containing compounds.[14–19]

The ORTEP drawing of the complex cation shown in Fig. 2 illustrates the spatial arrangement around the chromium atom. The oxygen atoms are *cis*, the pyridine nitrogens are *trans* and the amino nitrogens are *cis*. Thus this compound, which is an example of a type of complexes which Kirsten Michelsen earlier classified as α-isomers, has a *cis,trans,cis* configuration.

As was observed earlier in the structure determination for the di-μ-hydroxobis[bis{ (*S*)–1–(2-pyridyl)ethylamine}] chromium(III) ion[17] there

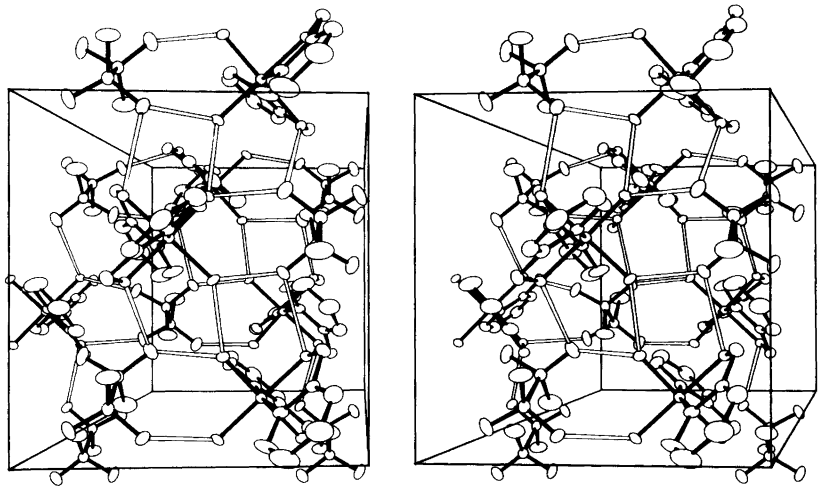

Fig. 3. Stereo pair of the packing viewed along the c^* axis perpendicular to the plate face of the crystals.

Table 2. Bond lengths (Å) and selected bond angles (°) with e.s.d.'s.

Cation					
Cr–O1	1.926(4)	Cr–O2	1.998(5)		
Cr–N11	2.065(5)	Cr–N21	2.063(5)		
Cr–N12	2.054(5)	Cr–N22	2.089(5)		
N11–C11	1.360(9)	N21–C21	1.343(9)		
C11–C12	1.378(10)	C21–C22	1.385(10)		
C12–C13	1.354(12)	C22–C23	1.378(10)		
C13–C14	1.363(13)	C23–C24	1.365(13)		
C14–C15	1.369(11)	C24–C25	1.374(11)		
C15–N11	1.338(10)	C25–N21	1.347(9)		
C11–C16	1.475(10)	C21–C26	1.479(9)		
C16–N12	1.479(9)	C26–N22	1.476(10)		
O1–Cr–O2	90.8(2)	N12–Cr–N22	89.6(2)		
O1–Cr–N11	93.5(2)	O1–Cr–N21	95.2(2)		
O2–Cr–N11	94.6(2)	O2–Cr–N21	93.0(20)		
O1–Cr–N12	89.1(2)	O2–Cr–N22	90.8(2)		
N11–Cr–N12	81.2(2)	N21–Cr–N22	79.8(2)		
C11–N11–C15	119.0(6)	C21–N21–C25	118.8(6)		
N11–C11–C12	120.4(7)	N21–C21–C22	121.5(6)		
N11–C11–C16	115.5(6)	N21–C21–C26	117.2(6)		
C12–C11–C16	124.1(6)	C22–C21–C26	121.4(7)		
C11–C12–C13	119.8(7)	C21–C22–C23	119.2(7)		
C12–C13–C14	119.7(7)	C22–C23–C24	119.2(7)		
C13–C14–C15	119.4(8)	C23–C24–C25	119.6(7)		
C14–C15–N11	121.6(7)	C24–C25–N21	121.8(7)		
C11–C16–C12	113.7(5)	C21–C26–N22	111.9(6)		
C16–N12–Cr	111.5(4)	N26–N22–Cr	112.0(4)		
Anion					
S1–S2	2.137(3)	O11–S1–S2	106.1(2)	O21–S2–S1	103.5(2)
S1–O11	1.454(5)	O12–S1–S2	105.0(2)	O22–S2–S1	102.8(2)
S1–O13	1.436(5)	O13–S1–S2	105.5(2)	O23–S2–S1	106.9(2)
S1–O13	1.437(5)	O11–S1–O12	111.9(3)	O21–S2–O22	112.9(3)
S2–O21	1.439(5)	O11–S1–O13	112.7(3)	O21–S2–O23	114.4(4)
S2–O22	1.430(5)	O12–S1–O13	114.7(3)	O22–S2–O23	114.8(3)
S2–O23	1.422(6)				

Table 3. Hydrogen bond distances in Å. The acceptor hydrogen distances are from 1.60–2.30 Å. ∠A–H–D~140–180°.

Donor	Acceptor	
O1	O21	2.782(6)
O2	O11	2.659(7)
O2	O1[a]	2.586(6)
N12	O22[b]	2.925(8)
N12	O11[c]	3.004(7)
N22	O12[b]	2.925(7)
N22	O21[a]	3.092(7)

[a] $1-x$, $\frac{1}{2}+y$, $\frac{1}{2}-z$. [b] $1+x$, y, z. [c] $1-x$, $y-\frac{1}{2}$, $\frac{1}{2}-z$.

are no differences between the Cr–N(pyridine) and Cr–N(amine) distances. The four independent Cr–N bond lengths are alike and their average value 2.068 Å is in agreement with the Cr–N distances found in related chromium(III) complexes with bidentate ligands.[18–21] The two Cr–O distances are so significantly different that one would expect that the shortest Cr–O1, 1.926(4) Å corresponds to Cr–O(hydroxo) and the longest Cr–O2, 1.998(5) Å to Cr–O(aqua). These values agree well with the bond lengths observed in other chromium(III) hydroxo or aqua complexes.[18–24] Therefore even without any knowledge about the hydrogen positions O1 can

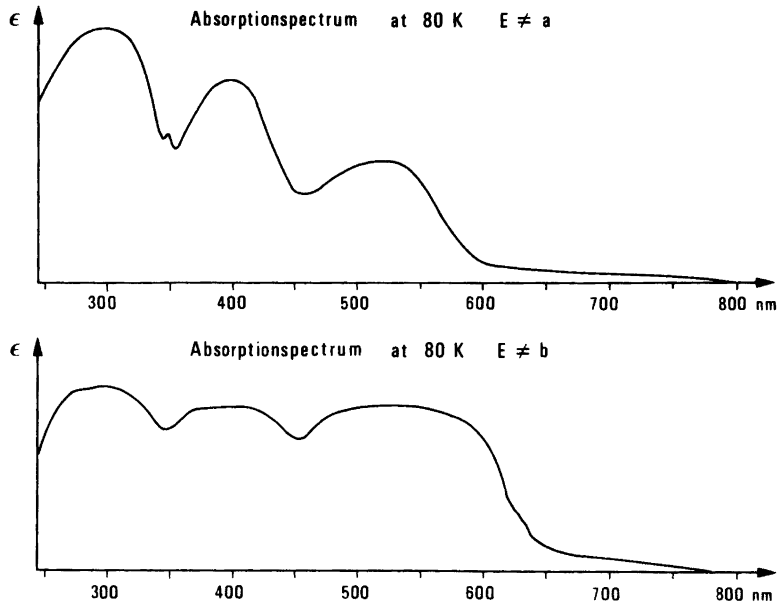

Fig. 4. Polarized absorption spectra at 80 K.

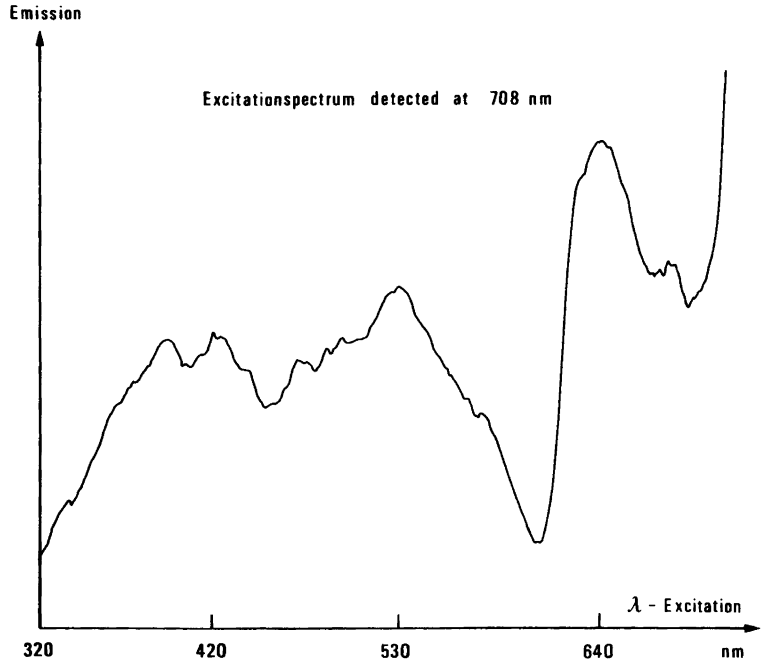

Fig. 5. Uncompensated excitation spectrum recorded at 1.7 K.

be classified as the hydroxo oxygen and O2 as the aqua oxygen.

The calculation of least squares planes showed that the two pyridine rings do not deviate significantly from planarity. The pyridine rings are almost perpendicular. The angle between the

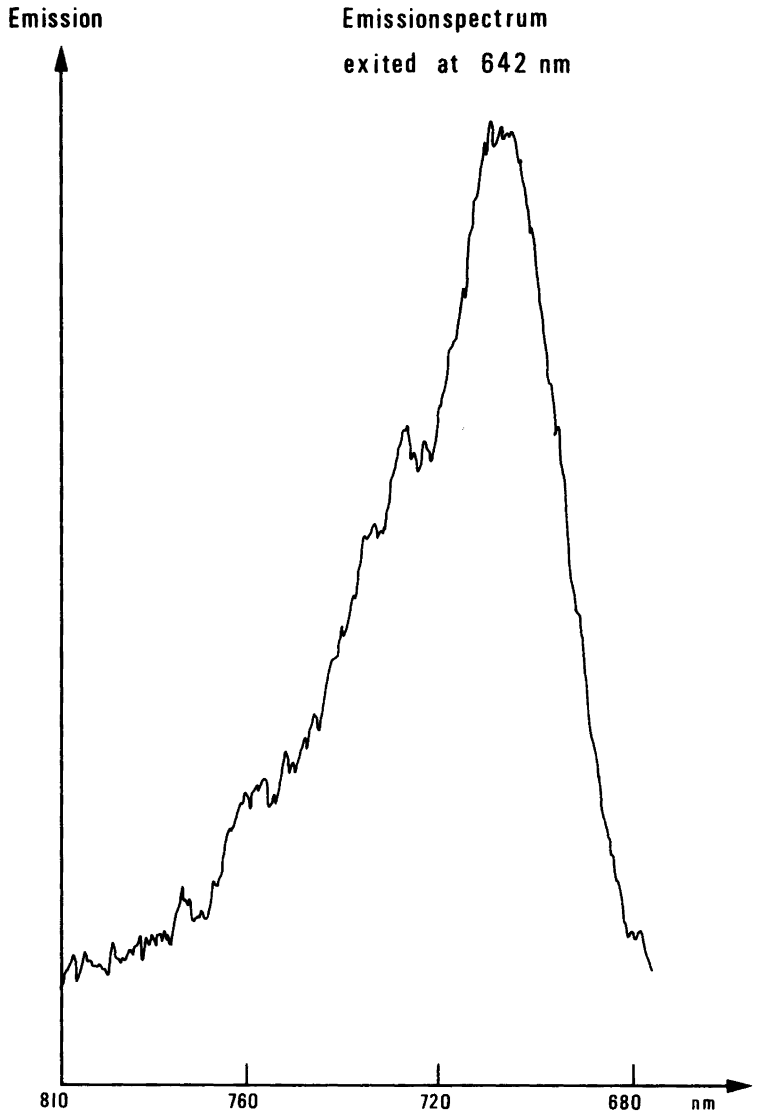

Fig. 6. Emission spectrum recorded at 1.7 K.

least squares planes is 86°.

The two bidentate ligands take opposite conformations, the dihedral angles N11–C11–C16–N12 and N21–C21–C26–N22 are 15.1(9) and –12.7(8)°, respectively, corresponding to a $\delta\lambda$ conformation. The molecular dimensions of the two chelate ligands are internally in good agreement and consistent with the values found in other octahedral complexes with this ligand and the related ligand 2-pyridylethylamine.[18,25–26]

The packing of the crystal illustrated by the stereo pair in Fig. 3 is mainly determined by hydrogen bonding. Table 3 lists the hydrogen bonds, which are formed from all the possible donor hydrogen atoms. The hydrogen bond between the dithionate ion and the complex cation is almost parallel to the *a*-axis resulting in a chain of alternating dithionate and complex ions. The complex ions related by the two-fold screw axis are linked together by a short hydrogen bond

between the water molecule of one molecule to the hydroxo group of the adjacent. This extensive net of hydrogen bonds formed in the directions of the *a* and *b* axis explains why the crystals formed are plates and the plate face is {001}.

ELECTRONIC SPECTRA

Even the largest samples were very small for spectroscopic work, and the absorption spectra could therefore be recorded only with the light propagating along the normal of the plate face. As the molecules are oriented in the crystal with the O1–O2 vector almost parallel to the *b* axis in this plane, crystal spectra could be obtained with the electric polarization vector at all directions within the {001} plane. Several such spectra were recorded at room temperature. By comparing these two and two, it was observed, that the C_{2v} site symmetry with the 2 symmetry axis in the *a*-direction gave the best fit. This is consistent with the symmetry derived from the structure, when only the ligating atoms are assumed.

The absorption spectra recorded at 80 K for the two polarisations parallel to the *a* and *b* axis are shown in Fig. 4. Three broad maxima are seen in both polarizations, but those measured with the polarization parallel to the *b* axis are broader than the similar bands with polarization along the *a* axis. Additionally the maximum with the lowest energy is shifted from 550 to 520 nm going from $E \neq b$ to $E \neq a$. The other peaks are centered around 300 and 400 nm in both polarizations. We assign the peaks at 550 and 520 nm to the $^4A_2 \rightarrow {}^4T_2$ transition (O_h-term symbols), the 520 nm being less broad, as the transition to the $^4A_1$ component in C_{2v} symmetry is forbidden. the tops at 400 nm are assigned to the $^4A_2 \rightarrow {}^4T_1$ transition, and the 300 nm to a charge transfer band.

The emission and excitation spectra were recorded for powdered samples only. An uncompensated excitation spectrum on powder is shown in Fig. 5. Due to the weak emission the spectrum is noisy so that only the gross outlines should be used. Like the absorption spectrum the excitation spectrum contains two broad bands at 400 and 530 nm, providing evidence that the emission stems from the chromium and not from impurities. The excitation spectrum has a maximum at 640 nm which is not observed in the absorption. A peak at 708 nm in the emission spectrum is shown in Fig. 6. The 640 nm top is assigned to the $^4A_2 \rightarrow {}^2T_1$, and that at 708 nm to the $^4A_2 \rightarrow {}^2E$ -spin-forbidden transitions.

From the above assignments, the following ligand field parameters were obtained:

10 Dq=1900 cm^{-1}; B=500 cm^{-1} and C=3450 cm^{-1}.

REFERENCES

1. Michelsen, K. *Acta Chem. Scand. 24* (1970) 2003.
2. Michelsen, K. *Acta Chem. Scand. 26.* (1972) 769.
3. Michelsen, K. *Acta Chem. Scand. 26* (1972) 1517.
4. Michelsen, K. *Acta Chem. Scand. 27* (1973) 1823.
5. Michelsen, K. *Acta Chem. Scand. A 30* (1976) 521.
6. Lehnert, P. G. *J. Appl. Crystallogr. 8* (1975) 568.
7. Johnson, C. K. *ORTEP: A Fortran Ellipsoid Plot Program for Crystal Structure Illustrations,* Report ORNL-3794, Second Rev., Oak Ridge National Laboratory, Oak Ridge 1970.
8. Stewart, J. M. *The X-Ray System, Version of 1972.* Technical Report Tr-192, Computer Science Center, University of Maryland, College Park 1972.
9. Nielsen, K. *Acta Crystallogr. A 31* (1977) 1009.
10. Cromer, D. T. and Mann, J. B. *Acta Crystallogr. A 24* (1968) 321.
11. Stewart, R. F., Davidson, E. R. and Simpson, W. T. *J. Chem. Phys. 42* (1965) 3175.
12. Cromer, D. T. and Liberman, D. *J. Chem. Phys. 53* (1970) 1891.
13. Hamilton, W. C. *Acta Crystallogr. 18* (1965) 502.
14. Kiers, C. T., Piepenbroek, A. and Vos, A. *Acta Crystallogr. B 34* (1978) 888.
15. Harrison, W. D. and Hathaway, B. J. *Acta Crystallogr. B 35* (1979) 2910.
16. Kirfel, A., Will, G. and Weiss, A. *Acta Crystallogr. B 36* (1980) 223.
17. Leskelä, M. and Valkonen, J. *Acta Chem. Scand. A 32* (1978) 805.
18. Larsen, S. and Hansen, B. *Acta Chem. Scand. A 35* (1981) 105.
19. Kaas, K. *Acta Crystallogr. B 35* (1979) 596.
20. Kaas, K. *Acta Crystallogr. B 32* (1976) 2021.
21. Scaringe, R. P., Singh, P., Eckberg, R. P., Hatfield, W. E. and Hodgson, D. J. *Inorg. Chem 14* (1975) 1127.

22. Cline, S. J., Kallesøe, S., Pedersen, E. and Hodgson, P. J. *Inorg. Chem. 18* (1979) 796.
23. Ou, C. C., Borowski, W. J., Petenza, J. A. and Schugar, H. J. *Acta Crystallogr. B 33* (1977) 3246.
24. Kaas, K. *Acta Crystallogr. B 35* (1979) 1603.
25. Bang, E. *Acta Chem. Scand. A 31* (1977) 495.
26. Mikami-Kido, M. and Saito, Y. *Acta Crystallogr. B 38* (1982) 452.

Received February 21, 1983.

Acta Chemica Scandinavica A 37 (1983) 843–851

Some MNDO SCF-MO Computations on Proton-transfer Systems

BO ANHEDE, NILS-ÅKE BERGMAN and LARS MELANDER

Department of Organic Chemistry, University of Göteborg and Chalmers University of Technology, S-412 96 Göteborg, Sweden

The MNDO SCF-MO method has been used in a study of a few potential-energy surfaces for the proton abstraction from carbon acids by anionic bases. The calculated force-constant matrices of the reactant and the transition state have been used for the computation of the semiclassical and tunnelling contributions to the overall primary proton/deuteron isotope effect. The variation in this effect caused by reasonable degrees of energetic unsymmetry in the reaction is similar to that observed experimentally. Both contributions vary and are of comparable importance for not too unsymmetric reactions.

Proton-transfer systems have been studied quantitatively for a long time but there are still aspects of the reaction about which there is no consensus of opinion. The experimentally well-established isotope-effect maximum for energy-balanced reactions [1] may thus be due either mainly to the semiclassical (tunnel-correction-free) isotope effect [2] or mainly to the tunnel effect [3,4] or, finally and perhaps most likely, to finite contributions from both.[5] In simple discussions based on the three-atom model as well as in rather complete computer calculations of isotope effects the crucial force constants in the transition state have originated from pure guesswork or the application of simple rules of thumb. It is obvious that little real progress in this field can be made without better knowledge concerning the shape of the potential-energy surface at the transition state. Such knowledge has to be gained by means of quantum-mechanical computations. The semiempirical methods MINDO/3 and MNDO have already been shown to reproduce kinetic isotope effects satisfactorily for some reactions.[6–9]

In order to obtain full compatibility between model and reality in solution reactions, solvating molecules have certainly to be introduced into proton-transfer models. In this respect the semiempirical methods seem less promising, being unable to reproduce intermolecular nonbonded interactions in a reliable way. This shortcoming and the fundamental fact that the parameters of semiempirical methods like MNDO [10] (Modified Neglect of Diatomic Overlap) are calibrated by means of data for stable molecules tend to discourage their use with transition states. On the other hand, if *ab initio* methods are to be used, reliable results claim also inclusion of configuration interaction, and the computation becomes lengthy and expensive if molecules of the size of interest to the organic chemist are to be handled. In MNDO electron-correlation effects are at least partly taken care of in the calibration procedure, but only for ordinary, stable molecules,[10] and it is likely that such effects manifest themselves differently in transition states with their looser structures. (See, however, Ref. 11.)

In spite of the expected shortcomings of the simpler methods when applied to proton-transfer transition states we decided to make a modest attempt to scan the field by computations according to the ordinary MNDO scheme on reactions between some simple carbon acids and a few simple bases. It is hoped that the results will at least inspire future investigations of the same systems by more reliable methods, because the variety in behavior found already in this limited study seems quite interesting, if real.

METHOD

The calculations were performed according to the semiempirical scheme devised by Dewar and

0302-4377/83 $2.50

Thiel.[10] The actual computer programs used were MNDO by Thiel[12] and a program for calculations of force constants on a MNDO potential surface by W. Thiel, Y. Yamaguchi, G. Ford and S. Olivella, kindly provided by Dr. H. S. Rzepa. (See also Ref. 13).

The latter program was written in FORTRAN for a CDC computer and needed some modifications in order to run on the IBM 3030 N computer at Gothenburg Universities Computing Centre.

For calculations of energy balances the energy of each stable species was computed separately with optimization of all geometric parameters (bond lengths, bond angles and twist angles).

The location of the transition state was determined by the following procedure. The two distances between the proton in flight and its nearest neighbors were assumed to be the major components of the minimum-energy path. When one of these is large compared to its expected value in the transition state it is probably dominating. It is fixed at such a value while all the other geometric parameters are optimized by minimization of the energy. In this way the value of the distance between the proton and its other neighbor is found, and all the structure obtained should not differ too much from one on the minimum-energy path. By observing the variation of the minimized energy and the last-mentioned distance as functions of the predetermined one the approach toward the transition state may be followed. The procedure is then repeated with the roles of the two pertinent distances interchanged. The interrelation between the two distances obtained in this way is best studied in a diagram with the distances as axes. From such a diagram and the energy values for different points in it *approximate* distance values for the transition state may be estimated. Nine pairs of distance values corresponding to a three times three rectangular array around the most likely location of the transition state are then fixed, and the energy is minimized, this time with the *two* distances being held at the predetermined values and optimizing all the other geometric parameters. The resulting nine energy values are then used as input values in a two-dimensional treatment of the type suggested by McIver and Komornicki.[14] The outcome of this is an improved pair of distance values for the transition state, and generally this single improvement afforded values accurate enough for defining the transition state. The final structure of the transition state was obtained by a complete optimization of all variables but the two distances obtained according to the procedure outlined above.

In calculations of kinetic isotope effects the force constant matrices of the transition states and the corresponding reactants were used as input to the BEBOVIB IV program.[15]

The tunnel correction factor Q was computed according to the ordinary Bell formula, for the present purpose written in the form

$$Q = \frac{\frac{1}{2}u_t}{\sin \frac{1}{2}u_t} - \sum_{n=1}^{\infty} (-1)^n \times \left[\exp\left(\frac{u_t - 2n\pi}{u_t}\alpha\right) \Big/ \frac{u_t - 2n\pi}{u_t}\right]$$

where $u_t = h|\nu^{\ddagger}|/kT$ and $\alpha = E/kT$, h and k being Planck's and Boltzmann's constants, respectively, $|\nu^{\ddagger}|$ the absolute value of the imaginary frequency along the reaction co-ordinate, T the absolute temperature, and E the height of the barrier.

RESULTS AND DISCUSSION

Before considering reaction profiles for the proton-transfer systems studied, it is of interest to

Table 1. Calculated and experimental energies for some proton-transfer equilibria in the gas phase.

Equilibrium	Reaction energy/kJ mol^{-1} MNDO[a]	*Ab initio*[b]	Exp. (ΔH)[c]
$HO^- + CH_3CN \rightleftharpoons H_2O + {}^-CH_2CN$	−177.4	−99.7	−78
$HO^- + HC{\equiv}CH \rightleftharpoons H_2O + {}^-C{\equiv}CH$	−34.5	−74.1	−68
$CH_3O^- + CH_3CN \rightleftharpoons CH_3OH + {}^-CH_2CN$	−20.1	−32.1	−29

[a] Present work. [b] Calculated from values (4−31G) in Refs. 18 and 19. [c] From Fig. 3 in Ref. 20.

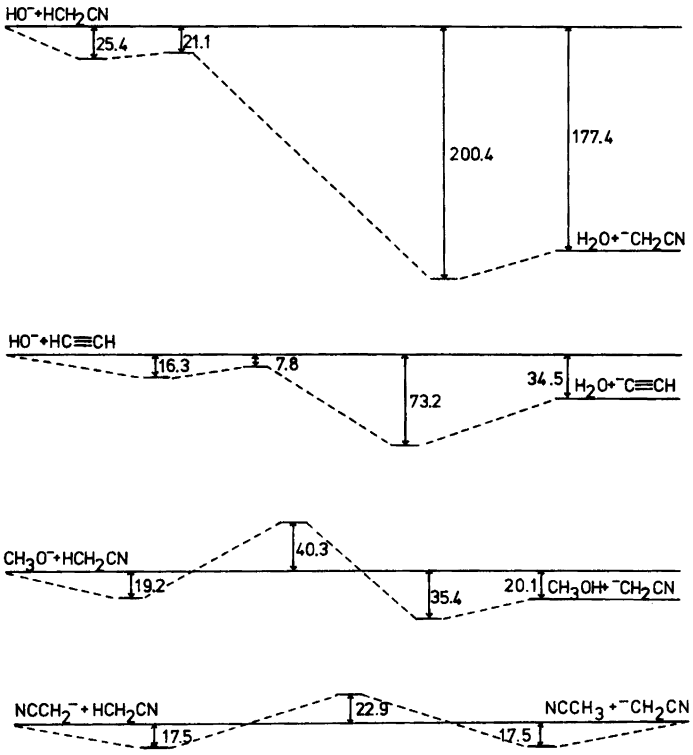

Fig. 1. Energy profiles for some proton-transfer reactions in the gas phase as calculated by the MNDO method. Energies in kJ mol^{-1}.

see if the MNDO method is capable of reproducing the experimental values of the overall energy change in such reactions. We have therefore calculated these energy changes, and the results for three proton-transfer processes can be seen in Table 1 together with the experimental gas-phase data. The results from the present MNDO calculations are in agreement with data published by Dewar *et al.*[10,16]

There are examples in the literature showing that the MNDO method gives rather reliable results for reaction energies.[17] None of these reactions are, however, of the proton-transfer type and it is interesting to note that it seems as if the MNDO method gives reasonable results for the reactions given in Table 1, too. The values calculated by the MNDO method are at least of the same magnitude as the ones calculated by *ab initio* methods at the 4-31G level, also listed in Table 1.

A simplified picture of the energy profiles for the reactions studied so far is presented in Fig. 1.

In all four reactions the reactants form a hydrogen-bonded type of ion–molecule complex* in which the distance between the accepting oxygen/carbon and the proton to be abstracted lies in the range 0.25–0.29 nm. Corresponding complexes are also formed on the product side of the reaction. For the three unsymmetric reactions the carbon–hydrogen distance lies in the range 0.19–0.32 nm. The minima corresponding to the ion-molecule complexes have been found by complete optimization of all variables and thus correspond to true minima. It should be added that in a calculation (unpublished results) on proton-transfer from acetylene to acetylide ion a completely symmetric ion-molecule complex was formed with no barrier for the proton-transfer step.

* This is a common phenomenon in gas-phase reactions and has been noted earlier both in calculations and in gas-phase experiments.

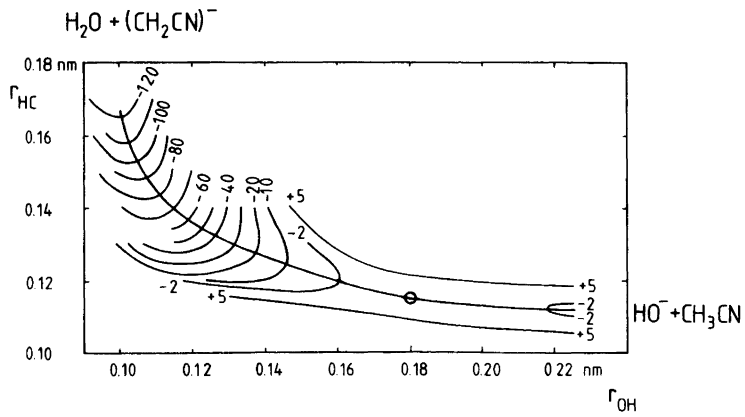

Fig. 2. Potential-energy map for the reaction between acetonitrile and hydroxide ion. Position of the activated complex is denoted by the circle. Energies in kJ mol^{-1} relative to the energy of the activated complex.

In most cases the effort was concentrated upon finding only the stationary points, and thus the horizontal axes in Fig. 1 have no exact physical meaning. Only in the case of the reaction between hydroxide ion and acetonitrile a more thorough mapping of the potential-energy surface was performed, and part of the calculated surface is shown in Fig. 2.

The geometries obtained for the transition states of the four proton-transfer reactions are given in Fig. 3. That these structures correspond to transition states can be seen from Table 2. Only one imaginary frequency of any appreciable size has been found for each transition state. The frequencies corresponding to the three translational and three rotational modes are all rather small and we consider them sufficiently small for the present explorative study. The error in the $3N$-7 real vibrational frequencies should be of little importance.

The calculated geometric data of the neutral reactant molecules are also given in Fig. 3 for comparison. They were obtained by complete optimization of all variables.

Anomalous geometries. As a test of the procedure outlined in the Method section we also tried some odd starting geometries in the optimization.

In one such case the abstracted hydrogen was placed at an 85° angle to the carbon–carbon bond, *1*. The distances between this hydrogen

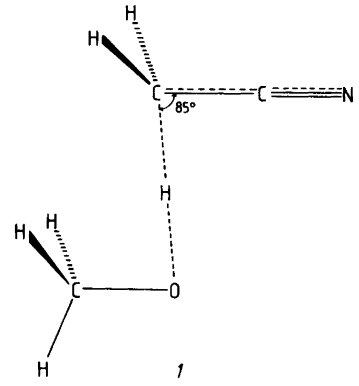

1

Table 2. The imaginary frequency $\nu^{\neq}$ of the decomposition mode and the six spurious frequencies ν corresponding to translation and rotation for each transition state.

Transition state	$\nu^{\neq}/cm^{-1}$	ν/cm^{-1}					
$HO-HCH_2CN$	196.6i	13.1i	1.5i	0.3i	2.0	7.3	16.0
$HO-HCCH$	249.1i	6.3i	3.4i	1.0i	0.9	5.9	94.7
CH_3O-HCH_2CN	1339.1i	54.1i	5.2i	0.0i	0.0i	2.3	15.8
$NCCH_2-H-CH_2CN$	1007.9i	10.9i	0.5i	0.0i	0.0	7.8	14.6

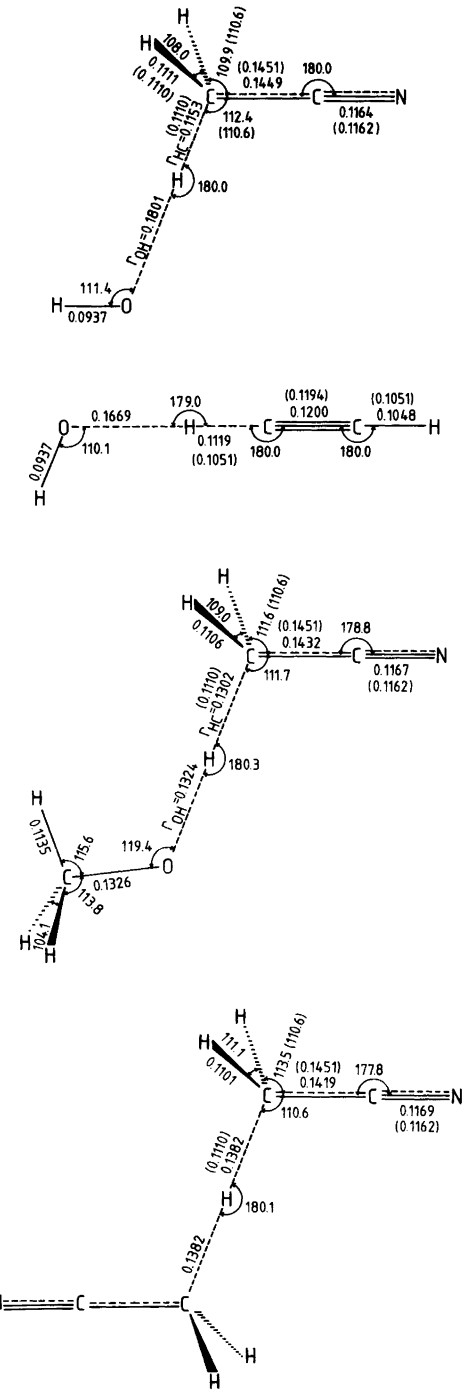

Fig. 3. Optimized transition-state structures. Bond lengths in *nm*. Values in parentheses correspond to reactant values.

and the adjacent carbon and oxygen were kept at the transition state values, while all other parameters were optimized. This procedure led to the same structure and energy as for the corresponding transition state in Fig. 3.

In another trial the optimization was started with the methanol molecule placed at the nitrogen end of the acetonitrile anion, *2*. Initially

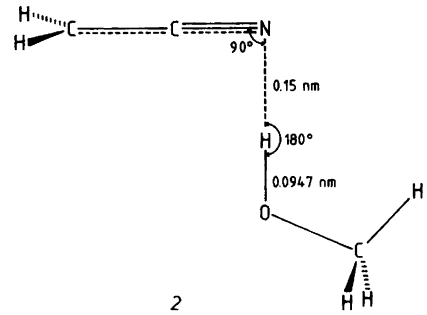

2

the nitrogen–hydrogen distance was set to 0.15 nm. Full optimization resulted in the formation of an ion–molecule complex with an N–H bond length of 0.27 nm and an O–H bond length of 0.095 nm. The O–H bond of this complex is pointing toward the nitrogen atom, and the HNC angle is 151°. This ion–molecule complex is somewhat higher in energy (0.6 kJ/mol) than the one indicated to the right in Fig. 1. In the latter the abstracted proton is at a distance of 0.31 nm from the acetonitrile carbon and the CHO angle is 144.2°.

Force constants, frequencies and isotope effects. A crucial point in calculating properties of potential-energy surfaces is the determination of the curvature at the stationary points of the surface. It has been pointed out, however, that the MNDO method overestimates the frequencies of stretching vibrations by about 10 %.[13] The same is also true for more sophisticated methods as 3–21 G.[21]

In Fig. 4 a histogram is shown of the relative frequency differences for the four stable molecules water, methanol, acetylene and acetonitrile, studied in the present calculations. The number of normal frequencies represented by the four molecules is 28 (degenerate frequencies counted once). It is easily seen that both methods overestimate the frequencies, even if the *ab initio* method seems to give rise to a somewhat smaller spread.

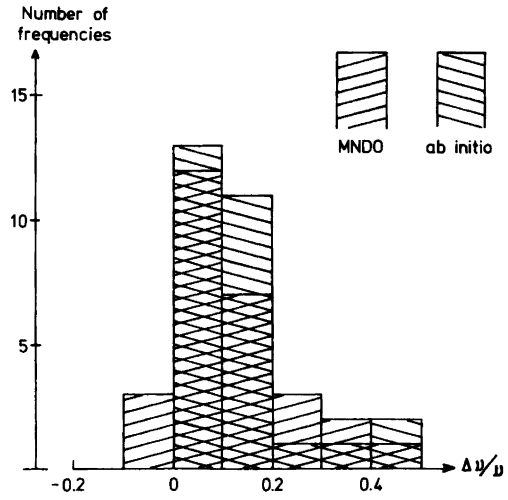

Fig. 4. Histogram showing the relative frequency differences for the four molecules water, methanol, acetylene and acetonitrile. $\Delta\nu/\nu = (\nu_{calc} - \nu_{exp})/\nu_{exp}$. Experimental values from Ref. 22, MNDO values from Ref. 23, *ab initio* data from Ref. 21.

The force-constant matrix obtained originally refers to cartesian co-ordinates but has been transformed into an internal co-ordinate force-constant matrix. The latter force constants are more easily interpreted in terms of changes in bond lengths, bond angles, *etc.* The diagonal ones for reacting bonds in the reactions are given in Table 3.

It is quite remarkable how different in magnitude the force constants of the reacting bonds are. This is in sharp contrast to the results from an electrostatic model for a proton-transfer reaction used by Bell and co-workers.[4] In the case of hydroxide ion and acetonitrile the calculated force constant of the incipient O–H bond in the transition state is even negative.

Although the present computations refer to solvent-free systems, it is very tempting to try to draw conclusions concerning the expected behavior under the more familiar solution conditions. In doing this it is assumed that the vibrational analyses are still valid for (solvated) reactants and transition states in solution. It is further assumed that the barrier height which is needed in tunnel-correction computations is equal to the difference in energy level between the transition state and the reactant molecule-ion complex according to Fig. 1.* This is a very rough way to simulate the effect of the solvation, which causes a drastic change in the relative energy levels and, in particular, lowers the level of the reactants in the cases with oxygen bases. Since the main effect is due to solvation of the reactant base ion (which is non-isotopic in the isotope-effect systems concerned), it may still be hoped that the much weaker solvation effects on the neutral reactant and the large transition-state ion do not completely invalidate the conclusions drawn from these computations on a gas-phase model.

Table 4 shows the semiclassical isotopic rate ratio obtained from the vibrational analyses on

* The barrier height should include the difference in zero-point energy between the transition state and the reactant, which difference is generally larger in the deuteriated system than in the protiated one. This isotopic difference in barrier height has been neglected here, because the weak isotopic dependence of $|\nu^*|$ in the two first reactions in Table 3 indicates a strong dependence of the real frequencies of the transition state, tending to cancel the barrier difference, and an addition of about 4.5 kJ to the deuterium barrier affects only the third decimal in Q_D in the third case and not even that in the fourth case.

Table 3. Stretching force constants (in N cm^{-1}) of reacting bonds in proton-transfer reactions in the gas phase.

$$B^- + H\overset{F_{AH}}{-}A \longrightarrow [B\overset{F_1}{\cdots}H\overset{F_2}{\cdots}A]^{-\ddagger} \longrightarrow B\overset{F_{BH}}{-}H + A^-$$

B^-	H–A	ΔE/kJ mol^{-1}[a]	F_{AH}	F_1	F_2	F_{BH}
HO^-	$H-CH_2CN$	−177.4	6.02	−0.03	4.85	9.26
HO^-	$H-C\equiv CH$	−34.5	7.55	0.01	5.25	9.26
CH_3O^-	$H-CH_2CN$	−20.1	6.02	0.47	2.67	8.99
$NCCH_2^-$	$H-CH_2CN$	0	6.02	1.56	1.56	6.02

[a] Energy change in completed reaction calculated by the MNDO method.

Table 4. Kinetic isotope effects at 25 °C and reaction co-ordinate frequencies for some proton/deuteron-transfer reactions.

Reactants	ΔE^a kJ mol^{-1}	$(k_H/k_D)_s$ [b]	$\lvert\nu_H^{\neq}\rvert$ [c] cm^{-1}	$\lvert\nu_D^{\neq}\rvert$ [c] cm^{-1}	$E^{\neq}$ [d] kJ mol^{-1}	Q_H [e]	Q_D [e]	Q_H/Q_D	k_H/k_D [f]
HO^-+CH_3CN	−177.4	1.69	196.62	191.99	4.3	1.0385	1.0367	1.002	1.7
HO^-+HCCH	−34.5	1.87	249.06	242.91	8.5	1.0628	1.0596	1.003	1.9
$CH_3O^-+CH_3CN$	−20.1	5.77	1339.1	1007.5	59.5	34.03	3.724	9.14	53
$NCCH_2^-+CH_3CN$	0	4.93	1007.9	789.9	40.4	3.703	2.018	1.83	9.0

[a] Energy change in completed reaction calculated by the MNDO method. [b] Semiclassical isotopic rate ratio. [c] Imaginary frequency along the reaction co-ordinate, absolute value. [d] Assumed effective barrier height. [e] Tunnel correction factor. [f] Overall isotopic rate ratio.

Fig. 5. Relative displacements (not mass-weighted, proton case) of the atoms for the decomposition mode of the four transition states.

reactant and transition state assuming the transferred particle to be a proton/deuteron. The strengthening of the isotope effect on approaching an energy-balanced reaction is evident. (The type of base used in the fourth reaction is different from that in the other three, and hence too much attention should not be paid to the fact that the trends discussed in this paragraph do not place the third and fourth reactions exactly in the order expected from their ΔE values.) The decomposition frequencies are also given, and they increase in the same direction. It is also evident that the isotopic difference in these frequencies increases, absolutely as well as relatively, and these facts together with an increase in barrier height make the tunnel-effect contribution to the isotopic rate ratio increase very rapidly and even surpass the semiclassical one. The last column in Table 4 shows the overall isotopic rate ratio. It should be noted that these ratios could be somewhat too large due to the overestimation of the vibrational frequencies by the MNDO method mentioned above.

Fig. 5 shows the decomposition mode of the four transition states.

Conclusions. There are certainly shortcomings in the application of the MNDO method to transition states, and the quantitative significance of the results obtained in the present calculations is, of course, open to discussion. Still it is hoped that the results considered in a more qualitative way may be instructive and more reliable than any results obtained from classical models.

The overall isotope effect varies with the energetic symmetry in the way shown by several experimental systems, and for reasonably symmetric reactions the semiclassical and tunnelling contributions are of comparable importance, at least according to calculations based on current theories. The potential-energy surface seems to behave as assumed by Melander and Saunders in their discussion of the hydrogen transfer as a three-center reaction.[24] Disregarding any entropy contributions, the reaction energies given in Table 4 correspond to an equilibrium constant of 10^{31}, 10^{6}, $10^{3.5}$ and 1 at 25 °C, thus at least in the second and third cases to reasonable degrees of unsymmetry. The fact that the equilibrium points in the direction opposite to that expected for a system in solution does not necessarily mean that the distortion of the potential-energy surface caused by energetic unsymmetry comes out in an unrealistic way. The same principles are probably valid for a distortion in either direction.

Acknowledgements. Our thanks are due to Dr. H. S. Rzepa who kindly provided the program for force-constant calculations. Financial support from the Swedish Natural Science Research Council is gratefully acknowledged.

REFERENCES

1. Melander, L. and Saunders, W. H., Jr. *Reaction Rates of Isotopic Molecules,* Wiley, New York 1980.
2. Melander, L. and Saunders, W. H., Jr. *Reaction Rates of Isotopic Molecules,* Wiley, New York 1980, Sections 2.2.1 and 2.2.2.
3. Bell, R. P. *The Tunnel Effect in Chemistry,* Chapman and Hall, London and New York 1980, Chapter 4.
4. Bell, R. P., Sachs, W. H. and Tranter, R. L. *Trans. Faraday Soc. 67* (1971) 1995.
5. Melander, L. and Saunders, W. H., Jr. *Reaction Rates of Isotopic Molecules,* Wiley, New York 1980, Sections 2.2 and 5.2.
6. Dewar, M. J. S. and Ford, G. P. *J. Am. Chem. Soc. 99* (1977) 8343.
7. Brown, S. B., Dewar, M. J. S., Ford, G. P., Nelson, D. J. and Rzepa, H. S. *J. Am. Chem. Soc. 100* (1978) 7832.
8. Ando, T., Yamataka, H., Yabushita, S., Yamaguchi, K. and Fueno, T. *Bull. Chem. Soc. Jpn. 54* (1981) 3613.
9. Rzepa, H. S. *Chem. Commun.* (1981) 939.
10. Dewar, M. J. S. and Thiel, W. *J. Am. Chem. Soc. 99* (1977) 4899, 4907.
11. Thiel, W. *J. Am. Chem. Soc. 103* (1981) 1413, 1420.
12. Thiel, W. *QCPE 12* (1980) 353.
13. Dewar, M. J. S., Ford, G. P., McKee, M. L., Rzepa, H. S., Thiel, W. and Yamaguchi, Y. M. *J. Mol. Struct. 43* (1978) 135.
14. McIver, J. W., Jr. and Komornicki, A. *J. Am. Chem. Soc. 94* (1972) 2625.
15. Sims, L. *QCPE 12* (1980) 337.
16. Dewar, M. J. S. and Rzepa, H. S. *J. Am. Chem. Soc. 100* (1978) 784.
17. Dewar, M. J. S. and Ford, G. P. *J. Am. Chem. Soc. 101* (1979) 5558.
18. Hopkinson, A. C., Lien, M. H., Yates, K., Mezey, P. G. and Csizmadia, I. G. *J. Chem. Phys. 67* (1977) 517.
19. Pross, A. and Radom, L. *J. Am. Chem. Soc. 100* (1978) 6572.
20. McIver, R. T., Jr. In Ausloos, P., Ed., *Kinetics of Ion-Molecule Reactions,* Plenum, New York 1979, Vol. 40.

21. Pople, J. A., Schlegel, H. B., Krishnan, R., Defrees, D. J., Binkley, J. S., Frisch, M. J., Whiteside, R. A., Hout, R. F. and Hehre, W. J. *Int. J. Quantum Chem.: Quantum Symp. 15* (1981) 269.
22. Shimanouchi, T. *Tables of Molec. Vibr. Freq. 1,* Publ. NSRDS-NBS 39, National Bureau of Standards, Washington DC.
23. Dewar, M. J. S., Ford, G. P., McKee, M. L., Rzepa, H. S., Thiel, W. and Yamaguchi, Y. *Supplementary Publications Scheme,* The British Library Lending Division Sup. PUB. No. Sup. 26079.
24. Melander, L. and Saunders, W. H., Jr. *Reaction Rates of Isotopic Molecules,* Wiley, New York 1980, Section 2.2.2.

Received March 2, 1983.

Acta Chemica Scandinavica A 37 (1983) 853–863

The Molecular Structures of Bicyclo[3.2.0]heptane and Δ^6-Bicyclo[3.2.0]heptene. An Electron-diffraction Study of Gaseous C_7H_{12} and Molecular Mechanics Calculations on C_7H_{12} and C_7H_{10}

ROBERT GLEN,[a,*] GRETE GUNDERSEN,[b,*] PETER MURRAY-RUST,[a,*] and DAVID W. H. RANKIN[b,* *]

[a] Department of Chemistry, University of Stirling, Stirling FK9 4LA, Scotland and [b] Department of Chemistry, University of Edinburgh, West Mains Road, Edinburgh EH9 3JJ, Scotland

The electron-diffraction data of the title compound at room temperature are consistent with molecules predominately in an *endo* (boat) conformation of C_s-symmetry, with flap angles of 65.0(3)° [for C6 (C7)] and 38.8(5)° [for C3] and r_a (C–C) average of 155.0(2) pm. The C–C bonds are shorter in the five-membered ring than in the four-membered ring. This is consistent with results of molecular mechanics calculations (Allinger's MM2) which also show that the bridge bond is the longest bond in the molecule. Significant amounts of a second conformer were not detected, but the co-existence of an *exo* form as indicated by the MM2-results (10 %) cannot be completely ruled out. The data are consistent with a planar four-membered ring and the MM2-results gave only slight puckering (2°) for the *endo* form as compared to 24° for the less favoured *exo* conformer which thus conforms to the trends established by the structure of related compounds.

Concurrent MM2-calculations also favour the *endo* form (99 % at room temperature) of bicyclo[3.2.0]heptene.

Some years ago the crystal structures of two derivatives of bicyclo[3.2.0]heptane were reported.[1] The five-membered rings of the molecules were found to have the *endo* conformation. Considering that the unsubstituted heptene analogue (Δ^6-bicyclo[3.2.0]heptene) was reported to exist in the *exo* form (*i.e.* a chair conformation) in the gas phase, as determined by electron diffraction,[2] it was of interest to make a conformational study of the unsubstituted bicycloheptane. For this molecule a conformational preference of the *endo* (boat) form over the *exo* (chair) form by about 6–10 kJ mol^{-1} (1.4–2.4 kcal mol^{-1}) was indicated by molecular mechanics calculations.[1]

It should be noted that several related bicyclohydrocarbons exist predominately in the *endo* form as summarized elsewhere.[3,4] Also, the result of the electron-diffraction study of bicycloheptene has been seriously questioned, particularly with regard to unreasonable structural features such as C–C–C angles in the five-membered ring of 86.7°, and on grounds of spectroscopic evidence.[5,6] It was said that in the absence of the electron-diffraction results the microwave data would have been interpreted unequivocally in terms of the boat form,[5] and also low frequency infrared and Raman data clearly favoured the boat form as it was concluded that any second conformer is at least 19.5

* Present addresses: R. G., The Wellcome Research Laboratories, Langley Court, Beckenham, Kent, BR3 3BS, England; G. G., Department of Chemistry, University of Oslo, Blindern, Oslo 3, Norway; P. M.-R., Glaxo Group Research Ltd., Greenford Road, Greenford, Middlesex, England.

** Author to whom correspondence should be addressed.

0302-4377/83 $2.50

kJ mol^{-1} [4 kcal mol^{-1}] energetically less favoured.[6]

This paper primarily reports the results of a gas-phase electron-diffraction study of bicyclo[3.2.0]heptane. It was initiated as a natural extension of the structural and conformational study started by molecular mechanics calculations.[1,7] The results of these calculations have to some extent been incorporated in the analysis of the electron-diffraction data, and they are therefore briefly described in the present paper. Pending conclusive experimental clarification on the contrasting structural results for Δ^6-bicyclo[3.2.0]heptene we also present molecular mechanics results for this molecule as obtained in calculations performed concurrently with those for the title compound.[7]

MOLECULAR MECHANICS CALCULATIONS

Several sets of molecular mechanics calculations have been performed,[1,7] but only the results obtained by Allingers MM2 program[8] are quoted in the present paper.

Δ^6-Bicyclo[3.2.0]heptene. It was shown that the *exo* form is less stable by 11.50 kJ mol^{-1} [2.75 kcal mol^{-1}] than the *endo* form, indicating that the gas at room temperature contains 99 % of the *endo* (boat) form. This result is in contrast to the electron-diffraction result and agrees, although not on the magnitude of the energy difference, with the spectroscopic data[5,6] discussed above.

The rotational constants calculated from the atomic coordinates obtained, which are available upon request, are for the *endo* form: A=4429.7,

Table 1. Molecular mechanics results of the *endo* (favoured) and the *exo* forms of bicyclo[3.2.0]heptene and bicyclo[3.2.0]heptane, represented by parameters of models with C_s molecular symmetry. See text for the assumed approximations and actual deviations from C_s-symmetry.

	Bicyclo[3.2.0]heptene		Bicyclo[3.2.0]heptane[b]	
	endo	*exo*	*endo*	*exo*
Geometrical parameters[a]				
C(sp^2)-H	110.2	110.2	—	—
C(sp^3)-H (average)	111.6	111.6	111.6	111.6
C1–C2	153.00	153.04	153.20	153.20
C2–C3	153.65	153.53	153.53	153.58
C1–C5	157.14	157.45	155.42	155.71
C1–C7	151.79	151.66	154.66	154.70
C6–C7	133.91	133.97	154.31	154.55
∠(H–C–H)pent	108.3	108.3	108.2	108.2
∠(H–C–H)but	—	—	112.2	112.2
∠(C6–C7–H17)	133.8	133.8	—	—
∠(C5–C1–H8)	115.7	113.5	114.2	112.6
θ(C4–C5–C1–H8)	131.5	128.9	129.0	126.0
∠(C5–C1–C2)	106.1	106.0	106.2	105.7
α	65.1	63.7	63.2	61.5
β	36.2	−39.2	37.0	−42.0
Dependent angles				
∠(C2–C1–C7)	115.1	116.5	115.7	117.4
∠(C1–C2–C3)	105.0	103.8	104.9	103.9
∠C2–C3–C4)	103.9	104.0	103.4	102.0
Mol fractions (293 K)				
x	0.99	0.01	0.90	0.10

[a] Distances in pm and angles in degrees. See Fig. 2 for numbering of the atoms. The flap angles are: α=180−ϕ(C6–C1···C5–C4) and β=180−ϕ(C3–C2···C4–C5); β is defined positive for the *endo* (boat) form and negative for the *exo*(chair) form. [b] See Fig. 1 for deviations from C_s symmetry and actual parameter values.

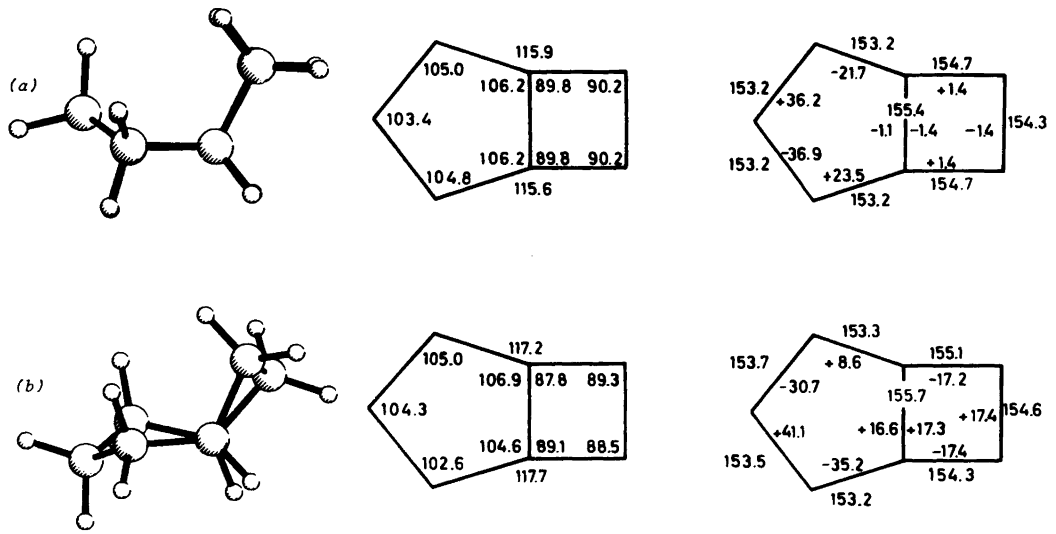

Fig. 1. Results of molecular mechanics calculations for bicyclo[3.2.0]heptane for the *endo* (a) and the *exo* (b) forms: The molecules viewed along the bridge bonds; and calculated valence angles, torsional angles and bond lengths for the carbon skeletons.

B=3088,3 and C=2382.0 MHz; and for the *exo* form: A=4948.8, B=2867.3 and C=2137.3 MHz. Comparisons with the experimental values:[5] A_0=4419.20, B=3080,16 and C_0=2375.33 MHz reveal that the structure calculated for the *endo* form is in remarkably good agreement with the experimental results, the discrepancies corresponding to a scale inconsistency of 0.2−0.3 % in the rotational constants.

The coordinates suggest that C_s molecular symmetry should be adopted for both forms. Assuming C_{2v} local symmetry for the methylene groups, thus disregarding calculated tilts of about 2.5° between the bisectors of the H−C−H and C−C−C angles, and using average values for the H−C−H angles and for the C(sp^3)–H bonds, the coordinates are fairly well represented by the fourteen geometrical parameters of C_s-models given in Table 1.

The approximate structure of the preferred *endo* conformer is not in good agreement with that proposed on the basis of experimental rotational constants alone. This has, for example, α=71.2 and β=22.6°, but the determination was said to be hampered by severe correlation between α and β.[5]

The structural parameters given for the less favoured *exo* form are in poor agreement with those of the *exo* conformer, favoured in the electron-diffraction study, in which both flap angles are rather large, α=76.0 and β= −65.0°.

In conclusion, it appears that the evidence against the structural results of the electron-diffraction study is substantial and they could represent a false minimum in the refinement. In the absence of new experimental results from an electron-diffraction reinvestigation and/or a microwave study using more complete isotopic substitution we believe that the result of the present calculation is the most reliable available for gaseous Δ^6-bicyclo[3.2.0]heptene.

Bicyclo[3.2.0]heptane. The final calculations for this compound [7] also favoured the *endo* (boat) form. The energy difference between the two conformers of 5.5 kJ mol^{-1} [1.3 kcal mol^{-1}] is less than for the corresponding heptene and it suggests that the gas at 293 K contains 10 % of the *exo* (chair) form as a minor conformer.

The calculated structures for the two conformers are depicted in Fig. 1. The corresponding atomic coordinates are available upon request. In contrast to the *exo* form it is seen that the *endo* conformer is close to possessing overall C_s molecular symmetry. For this form the C−C−C−C dihedral angles (θ) of the four-membered ring are in the range 1.1−1.4° and the

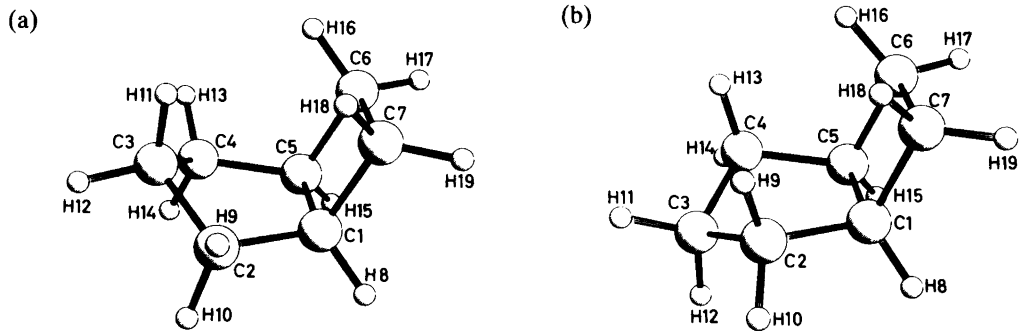

Fig. 2. Molecular models of C_s-symmetry for the *endo* (a) and *exo* (b) conformers of bicyclo[3.2.0]heptane; and numbering of the atoms.

difference between "symmetry related" $\angle$(C−C−C) and θ(C−C−C−C) values of the five-membered ring are slight, compared to substantial differences for the *exo* form which has torsional angles in the four-membered ring of about 17°. However, both forms were approximated to models with C_s symmetry. Additionally, average values were used for the C−H bond lengths and for H−C−H valence angles for the five-membered ring, $\angle(H-C-H)_5$, and of the four-membered ring, $\angle(H-C-H)_4$. Finally local C_{2v} symmetry for the methylene groups was introduced thus neglecting tilts which according to the calculations could be 1−3° in the planes prependicular to the corresponding C−C−C planes. Each of the two C_s-models is then described by thirteen geometrical parameters as defined in Table 1. The parameter values which give the best representation of the calculated atomic coordinates within the constraints described are listed in Table 1. It is seen that the flap angles (α and β) of 63.2 and 37.0° for the *endo* form and 61.5 and −42.0° for the *exo* form are similar to the corresponding angles calculated for the analogous heptene (Table 1).

The values in Table 1 for bicycloheptane reveal that the C−C bonds are longer and the H−C−H angles wider in the four-membered ring than in the five-membered ring. This is consistent with experimental average values for such types of structural parameters as they are said to be 155.5 and 153.4 pm, and 114 and 109.5°, respectively.[9] The longest bond in both forms is that common to the fused rings, r (C1−C5)=155.4−155.7 pm which appears to be in agreement with the situation in bicyclo[2.2.0]hexane which has fused four-membered rings.[10]

The difference of the two forms with respect to the puckering of the four-membered ring is remarkable. The torsional angles given in Fig. 1 correspond to puckering angles (ϕ) of about 2 (*endo*) and 24° (*exo*). The MM2 program is said to give satisfactory reproduction of the puckering for cyclobutane[8]: ϕ is 28.4° as compared to for example 24.1° determined by *ab initio* MO-calculations and 26° given as the most recent experimental value.[11] It has been pointed out that ϕ in bicyclic compounds decreases according to the strain invoked by the fusing ring: ϕ=0° in bicyclo[2.1.0]pentane,[12] and ϕ=11.5° in bicyclo[2.2.0]hexane,[10] whereas it is said that the similarity of the structural parameters of the four-membered rings in *cis* and *trans* bicyclo[4.2.0]octane to those of cyclobutane and its nonfused derivatives, suggest that the strain is accomodated by the more flexible six-membered ring.[13] Thus the flexible *exo* form conforms to the established trend with a ϕ-value intermediate to those encountered for the bicyclic hexane and octane, whereas the favoured *endo* form has an essentially planar four-membered ring with eclipsing neighbouring C−H bonds.

In all the calculations performed[1,7] the *endo* form of bicyclo[3.2.0]heptane has been favoured with an energy preference of 5.5 to 10 kJ mol^{-1} where the lowest energy difference refers to the MM2 calculations. Such calculations have also been used in a conformational study of bicyclo[3.3.1]nonane and they appear to yield conformational compositions which are consistent with results of electron-diffraction studies of the gas at 338 and 673 K.[14]

Table 2. Weighting functions, correlation parameters and scale factors.[a].

Camera height	Wave-length	Δs	s_{min}	sw_1	sw_2	s_{max}	Correlation parameter		Scale factor	
mm	pm	nm^{-1}					*endo*	*exo*	*endo*	*exo*
128.3	5.815	4	60	70	300	324	0.239	0.298	0.734(8)	0.703(17)
286.3	5.788	2	20	50	120	140	0.481	0.486	0.774(10)	0.675(20)

[a] See Ref. 20 for definitions.

ELECTRON DIFFRACTION

Experimental. Bicyclo[3.2.0]heptane was prepared according to literature procedures[15] and the electron-diffraction data were recorded on Kodak Electron Image plates using the Cornell/Edinburgh diffraction apparatus[16,17] with nozzle-to-plate distances of 128 and 286 mm. The sample and nozzle were maintained at room temperature during the exposures. The accelerating voltage was about 44 kV and the electron wavelength was calibrated against diffraction patterns of gaseous benzene[r_a(C–C)=139.7 pm) recorded immediately before and after the sample plates. The optical densities of three and four plates for the short and long camera distances, respectively, were recorded using the Joyce-Loebl Microdensitometer 6 at S.E.R.C. Laboratory, Daresbury.[18]

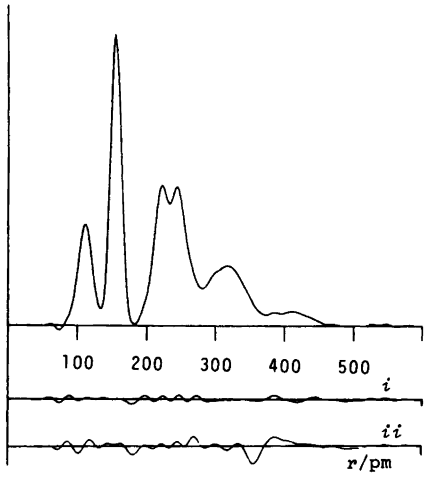

Fig. 3. Experimental molecular scattering intensities for nozzle-to-plate distances of (a) 128 and (b) 286 mm; and the corresponding final weighted difference curves according to the parameter values in Table 4 for the (i) *endo* and (ii) *exo* form of bicyclo[3.2.0]heptane.

Data reduction and analysis procedure. The data reduction was carried out using established programs[17] which at the final stages include an automatic background correction based on spline functions. Least-squares refinement program described previously[19] was used in the structure analysis. The data ranges and the parameters of the off-diagonal weighting functions are presented in Table 2 together with the scale factors and correlation parameters of the final results. The complex scattering factors of Schäfer *et al.*[20] were used and all calculations were carried out on an ICL 2972 computer. The experimental molecular intensities and the corresponding radial distribution curves are shown in Figs. 3 and 4, respectively.

Vibrational amplitude quantities. Root-mean-square amplitudes of vibration and perpendicular amplitude correction coefficients (*u*- and *K*-values) for the two C_s-models of the molecule were calculated using a normal coordinate computer program originally written by R. L. Hilderbrandt[21] and atomic coordinates corresponding to the C_s-structures estimated from the molecular mechanics results (*cf.* Table 1). The calculations were based on the Urey-Bradley force field for hydrocarbons given by Schachtsneider and Snyder.[22] Table 3 lists the force constants and the *u*- and *K*-values associated with the more important interatomic distances. An alternative Urey-Bradley force field discussed in a study of manxane,[23] gave similar results, but the chosen force field (Table 3) is as used in an electron-diffraction investigation of the related bicyclo[3.1.0]hexane.[4] A full list of the calculated *u*- and *K*-values for 293 and 0 K is available upon request.

Structure refinements and results. The initial analysis suggested that an *endo* form of C_s-symmetry could represent the electron-diffraction data of bicyclo[3.2.0]heptane rather well, in contrast to the corresponding *exo* form.

The interpretation of the radial distribution curve (Fig. 4) was fairly straight forward, but as reflected in the distance values given in Table 3,

Table 3. Urey-Bradley force field for bicyclo[3.2.0]heptane and root-mean-square amplitudes of vibration (u) and perpendicular amplitude correction terms (K) calculated for the *endo* and *exo* forms of C_s-symmetry at T=298 K.[a]

K(C–C)	223	F(C···C)	32	H(CCC)	0.69	H(CCH$_t$) 0.32
K(C–H$_t$)	394	F(C···H)	55	H_t	0.078	H(CCH$_s$) 0.33
K(C–H$_s$)	402	F(H···H)	5			H(HCH) 0.52

Atom pair[b]	*endo*			*exo*		
	r	u	K	r	u	K
C–H[c]	111.6	7.94	1.84	111.6	7.93	1.81
C1–C2	153.2	5.27	0.42	153.2	5.28	0.41
C2–C3	153.5	5.23	0.52	153.6	5.23	0.50
C1–C5	155.4	5.41	0.29	155.7	5.43	0.27
C1–C7	154.7	5.28	0.43	154.7	5.26	0.41
C6–C7	154.3	5.23	0.78	154.6	5.23	0.75
C1–H9[c]	219.4	10.50	1.26	219.7	10.49	1.23
C1–H18[c]	223.6	10.45	1.31	223.6	10.44	1.27
C3–H9[c]	219.7	10.49	1.35	220.1	10.49	1.32
C2–H11[c]	220.2	10.48	1.39	220.7	10.47	1.33
C6–H18[c]	223.3	10.44	1.67	223.5	10.44	1.62
C2–H8	225.5	10.20	0.94	224.1	10.26	0.92
C7–H8	222.1	10.42	0.93	224.0	10.36	0.92
C5–H8	225.5	10.48	0.82	223.7	10.57	0.79
C1–C6	218.9	6.34	0.35	219.1	6.32	0.33
C1–C4	246.8	8.08	0.15	246.2	7.99	0.16
C1–C3	243.1	7.08	0.24	241.6	7.21	0.23
C2–C4	240.9	6.92	0.31	238.6	7.03	0.32
C2–C7	260.7	7.38	0.35	263.1	7.31	0.37
C4–C7	324.2	8.79	0.11	325.7	9.49	0.11
C3–C7	313.5	11.23	0.15	363.6	7.76	0.12
C1–H11	288.8	14.46	0.82	340.1	10.33	0.77
C1–H12	339.7	10.45	0.80	282.8	14.65	0.80
C1–H13	337.3	11.15	0.66	301.7	14.39	0.69
C1–H14	304.8	14.71	0.69	338.4	11.13	0.67
C1–H16[c]	296.0	11.42	1.01	296.2	11.37	0.98
C2–H13	337.8	10.15	0.85	279.1	15.13	0.84
C2–H14	286.1	15.01	0.84	337.6	10.09	0.86
C2–H15	332.2	12.33	0.45	328.4	11.88	0.47
C2–H16	360.8	17.62	0.53	363.0	18.39	0.53
C2–H17	422.8	10.78	0.54	423.9	11.03	0.51
C2–H18	347.0	11.82	0.91	349.1	11.78	0.88
C2–H19	268.0	14.99	1.09	271.8	14.81	1.15
C3–H8	341.1	10.39	0.53	305.4	13.25	0.53
C3–H16	306.4	20.46	0.72	386.5	16.19	0.56
C3–H17	420.9	13.10	0.55	457.5	11.08	0.51
C6–H8	295.7	11.29	0.69	295.8	11.35	0.66
C6–H9	377.5	16.00	0.47	337.2	18.80	0.51
C6–H10	412.9	11.77	0.49	422.2	11.80	0.47
C6–H11	302.4	21.89	0.59	446.4	13.22	0.48
C6–H12	422.5	13.28	0.56	426.9	13.37	0.46
C6–H13	278.1	15.45	0.97	267.0	14.78	1.06
C6–H14	355.0	10.71	0.82	335.4	12.37	0.92
H9–H10[c]	180.8	12.94	2.35	180.8	12.94	2.28
H16–H17	185.2	12.68	2.45	185.2	12.67	2.41

[a] Force constants in aJ nm^{-2} (K and F) and in aJ rad^{-2} (H); distances (r) and amplitudes (u and K) in pm. 1 aJ=1 mdyn Å. [b] See Fig. 2 for numbering of the atoms. Most H···H values are omitted. [c] Average values are given for parameters that are symmetrically (by C_s-symmetry) different, but by additional constraints (see text) are assumed to be equal.

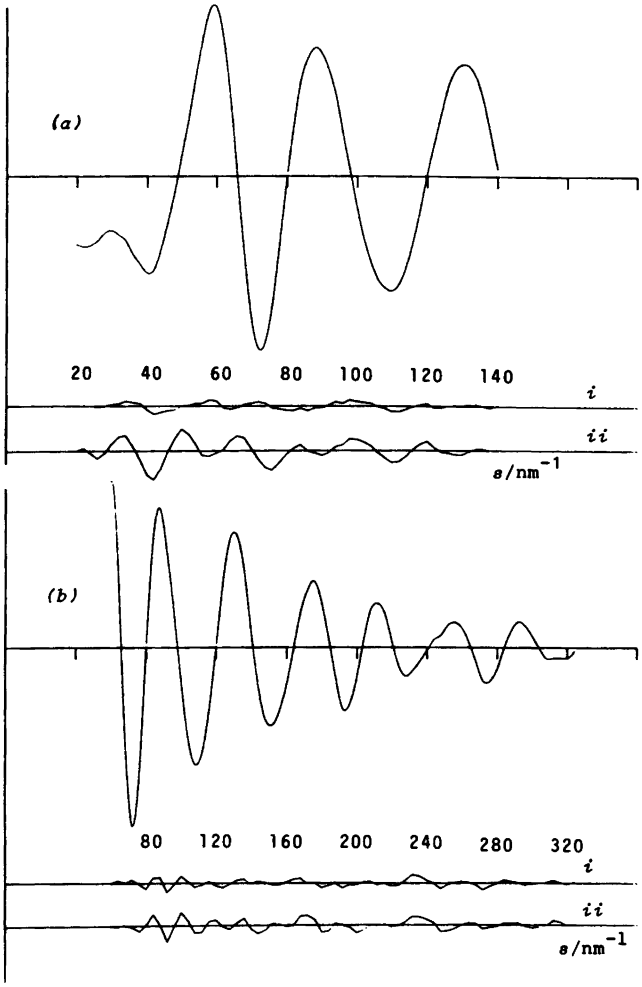

Fig. 4. Experimental radial distribution curve, $P(r)/r$, for bicyclo[3.2.0]heptane and difference curves corresponding to the intensities in Fig 3: (i) *endo* and (ii) *exo* form. Before Fourier inversion the data were multiplied by $s \exp[-0.000015s^2]/(Z_C - f_C)$.[2]

there are severe distance overlaps. The various C–H and C–C bonds account for the peaks at 110 and 154 pm respectively; and one-angle distances are the major contributors to the next peak which has double feature: C···H and C1···C6 (*i.e.* within the four-membered ring) at 220 pm and the remaining one-angle C···C distances at 240–260 pm. The C4···C7 and C3···C7 distances must then be contained in the next feature, but from about 300 pm there are also substantial contributions from C···H distances. The failure of the *exo* form to give a good representation of the data appears to be related to the long C3···C6 (C7) distances at about 360 pm.

Refinements of both forms were carried out and the final molecular models were defined essentially as described in the preceeding section and in Table 1. The two models are thus analogous, but for the sign of the flap angle β. Additional constraints to those previously given concern the relative magnitudes of the C–C bond lengths and the locations of the hydrogen atoms.

Only one C–C bond distance [r(C1–C2)] was kept as an independent parameter and the four

Table 4. Results of structural refinements of C_s-models (see text) for bicyclo[3.2.0]heptane based on electron-diffraction intensities.[a] Elements of the correlation matrices for the variables, *p1* to *p5* and *u1* to *u5*, are given in Table 5.

		endo[R_G=6.75 %]		*exo*[R_G=14.09 %]	
		Distances angles	Amplitudes	Distances angles	Amplitudes
Independent parameters (r_a, $\angle_a$)					
p1	r(C−H)	109.8(2)		108.4(5)	
p2	r(C1−C2)[b]	153.8(1)		153.7(1)	
p3	∠(C5−C1−C2)	106.1(6)		105.8(3)	
p4	α	65.0(3)		69.1(7)	
p5	β	38.8(5)		−40.3(24)	
	∠(H−C−H)pent	110.	fixed	110.0	fixed
	∠(H−C−H)but	114.		114.0	
	∠(C5−C1−H8)	114.2		112.6	
	θ(C4−C5−C1−H8)	129.0		126.0	
Interatomic distances (r_a)[c] and amplitudes (u)					
u1	C−H	111.0(2)	7.9(2)	109.6(5)	7.8(5)
u2	C1−C2[b]	154.0(1)	5.2(1)	154.0(1)	4.9(2)
	C2−C3[b]	154.5(1)		154.4(1)	
	C5−C6[b]	155.4(1)		155.3(1)	
	C1−C5[b]	156.3(1)		156.5(1)	
	C6−C7[b]	155.5(1)		155.6(1)	
	C1···H9	218.8(4)	11.0[u3]	217.7(4)	10.5[u3]
	C1···H18	222.6(2)		221.6(4)	
	C3···H9	219.1(4)		218.2(4)	
	C2···H11	219.7(5)		218.8(4)	
	C6···H18	222.7(2)		221.8(4)	
	C2−H8	225.1(4)		222.4(4)	
	C7−H8	223.6(3)		230.3(8)	
	C5−H8	224.8(2)		222.0(4)	
u3	C1−C6	219.9(1)	6.6(1)	219.9(2)	6.3(3)
u4	C1−C4	247.5(10)	7.5[fixed]	247.1(5)	9.0(9)
	C1−C3	243.5(20)	6.5[fixed]	243.1(19)	7.9[u4]
	C2−C4	241.3(30)	6.3[fixed]	240.1(15)	7.9[u4]
	C2−C7	259.4(4)	6.8[fixed]	253.4(10)	8.2[u4]
u5	C4−C7	323.2(9)	9.2(9)	318.3(9)	8.1[u13]
	C3−C7	308.8(13)	11.7[u5]	354.6(11)	7.8[fixed]
Dependent angles ($\angle_a$, θ_a)					
∠(C1−C2−C3)		104.5(12)		104.3(12)	
∠(C2−C3−C4)		102.9(18)		102.3(9)	
∠(C2−C1−C7)		114.0(2)		110.1(7)	
θ(C5−C1−C2−C3)		23.8(8)		24.8(12)	
θ(C1−C2−C3−C4)		38.4(7)		40.0(21)	
θ(C7−C1−C2−C3)		73.4(10)		120.5(13)	

[a] Distances and amplitudes in pm; angles in degrees. Values in parentheses are least-squares standard deviations which include correlation among the parameters, but not systematic uncertainties. See Fig. 2 for numbering of the atoms and Table 1 for definitions of α and β. Dihedral angles are defined relative to zero for *syn* arrangements and are positive for counter clock-wise rotation. [b] The remaining C−C bond lengths are tied to C1−C2 (r_a) according to the results of molecular mechanics calculations (Table 1). The standard deviation given is thus that of the average and not of the individual C−C bonds. [c] The remaining C···H (see Table 3 for approximate distance distribution and u-values) and H···H distances were included in the refinements but are omitted here.

Table 5. Elements of the correlation matrices (i,j: ρ_{ij} for $|\rho_{ij}|>40$ %) corresponding to the least-squares results given in Table 4 (*p*- and *u*-values) and Table 2 (*k*-values, *i.e.* scale factors).

endo form				*exo* form			
p3, p4:	−45;	*p3, u5*:	−75	*p4, p5*:	42;	*p4, u4*:	62
p4, u5:	44			*p5, u4*:	62		
u2, kl:	69			*u2, kl*:	70		
				u3, u4:	57;	*u3, kl*:	41

remaining types of C−C bonds were given lengths relative to this bond as suggested by the MM2-calculations (Table 1). In the initial refinements, which were carried out prior to the MM2-calculations, it was found that for the *endo* form the best fit was obtained if the C−C bond lengths of the four-membered ring exceeded those of the five-membered ring by about 2 pm whereas for the *exo* form it appeared that the best fit was obtained where all C−C bonds were of equal length. It proved difficult to refine the parameters defining the positions of the hydrogens. With the exceptions of *r*(C−H) they were maintained at fixed values which corresponded to the MM2-results for the H8(15) hydrogens (Table 1). For ∠(H−C−H) 110 and 114° were used respectively for the five- and four-membered ring as refinements had suggested that larger values than those predicted by the MM2-calculations were preferred.

For both models the parameter values deduced from the MM2 results were used as starting values in r_a-refinements in which the vibrational parameters were fixed at the calculated values (Table 3). However, several series of refinements established that the same minima were approached from several sets of starting values for the highly correlated flap angles (α and β). These sets included $\alpha=76$ and $\beta=-65°$ which correspond to the disputed electron-diffraction structure for bicyclo[3.2.0]heptene, and for the *endo* form special attention was given to possible exchange of magnitudes for the C4···C7 and C3···C7 distances. Consecutive r_α-refinements and inclusion of some *u*-values in the refinements resulted in slightly improved fit to the data without significant shifts in the geometrical parameters. The final results for which R_G [19] was 6.75 and 14.09 % [R_D:4.53 and 11.11 %] respectively for the *endo* and *exo* forms are given in Table 4. Errors quoted are standard deviations obtained in the least-squares refinements, *i.e.* they are not augmented to account for systematic uncertainties. Elements of the correlation matrices for the final refinements are given in Table 5. The weighted differences in molecular scattering intensities and the differences between experimental and theoretical radial distributions are included with the corresponding experimental curves in Figs. 3 and 4, respectively.

The possibility that the *exo* form may co-exist with the *endo* form as a minor conformer was considered. However, r_a-refinements for such compositions using the calculated *u*-values did not give improved fit to the data: the obtained R_G factors were: 7.28, 7.32, 7.47, 7.71 and 8.04 % for 100, 95, 90, 85 and 80 % of the *endo* form. It is also seen from Figs. 3 and 4 that the *endo* form represents the data rather well. In particular there are no obvious discrepancies for the 350−360 pm and 300−310 pm regions in which the C3···C6(7) distances for the *exo* and *endo* forms are found.

Possible deviations from C_s-symmetry have not been seriously considered in the present electron-diffraction investigation. In this respect it should be noted that the symmetrical *endo* form represents the data in an acceptable manner, and this may be used as evidence against substantial distortions. Small deviations from C_s symmetry as indicated by the molecular mechanism calculations are judged to be insignificant as far as the electron-diffraction data are concerned, as the complex distance overlaps would obscure attempt to determine the asymmetry parameters. Admitted, the C_s-model may introduce a bias against the *exo* form, which is substantially distorted according to the molecular mechanics results. However, by inspection of the distance distributions of the unsymmetrical form it is clear that the *exo* form could not be present as the major conformer nor in substantial amounts (*i.e.* more than 10 %).

DISCUSSION

Although it may be argued that the molecular mechanics results have been incorporated in the interpretation of the electron-diffraction data, it appears that the two investigations agree that an *endo* form which only shows minor distortions

from C_s-symmetry is the major conformer of bicyclo[3.2.0]heptane at room temperature. The electron-diffraction data do not suggest the co-existence of a second conformer in significant amounts, but in view of the many assumptions and distance overlaps, a contribution of up to 10 % of the *exo* form, as indicated by the molecular mechanics calculations, cannot be completely ruled out. A puckering angle of 16.4° for the four-membered ring in bicyclo[3.2.0]heptane has been predicted from an empirical equation[24] and it is, as discussed previously, remarkable that the preferred form of bicyclo[3.2.0]heptane appears to be only insignificantly puckered. It is possible that substantial puckering would be in conflict with steric interactions between hydrogens across the rings, *i.e.* H11 of C3 and H16(18) of C6(7).

The flap angles obtained, α=65.0(3)° and β=38.8(5)°, are respectively smaller and larger than those obtained for related compounds with fused three- and five-membered rings. For example in bicyclo[3.1.0]hexane[4] α=70.6(11)° and β=25.2(28)° and the latter value is similar to that found for cyclopentene which has β=28.8(25)°.[25] In the present investigation attempts to fit models with smaller β-values failed. The final structure has a bridgehead carbon angle [$\angle$(C2–C1–C7)] of 114.0° compared with for example $\angle$(C2–C1–C6)=113.5(1.1)° in bicyclo[2.2.0]hexane.[10]

In the preliminary analysis it was indicated that the bond lengths in the four-membered ring exceeded those of the five-membered ring by 2 pm, in agreement with the subsequent MM2 calculations and experimental average values.[9] Cyclobutane and cyclopentane have r_g (C–C) values of 155.1(3) [an earlier value is 154.8 pm][26] and 154.6(1) pm,[27] respectively. The average C–C bond length of bicyclo[3.2.0]heptane is 154.9 pm (Table 4) as compared to 155.6 pm for bicyclo[2.2.0]hexane.[10]

The length of the transannular C–C bonds is of particular interest, and it has been stated that the bridgebond *cannot* simply be predicted in terms of a model involving competion from the fused rings, giving a bridgebond of intermediate length. In fact, it appears that the bridgebond is the longest C–C bond in bicyclo[2.2.0]hexane (157.7 pm) and in bicyclo[3.2.0]heptane (156.3 pm) according to an electron-diffraction study[10] and the present MM-calculations. For the former molecule the bridgebond was resolved among three types of C–C bonds. In the present case there are five types of such distances and only 12.5 % of the C–C bond-peak area can be attributed to the transannular bond and any attempt to determine its length based on the electron-diffraction data alone was judged vain. Based primarily on electron-diffraction data very short bridgebonds have been assigned to bicyclo[3.1.0]hexane (145.4 pm)[4] and bicyclo[2.1.0]pentane (143.9 pm).[28] Although agreeing on the average C–C bond length for these compounds a recent *ab initio* Mo-study has questioned the reported relative magnitudes of the C–C bonds for these two copmpounds.[29] The calculated values for the bridgebonds were 150.9 and 152.9 pm for the hexane and pentane, respectively, and for the latter this is in better agreement with structural results obtained from microwave data.[30]

Acknowledgements. We thank the Science and Engineering Research Council (U.K.) for a research grant.

REFERENCES

1. Brown, A., Glen, R., Murray-Rust, P. and Murray-Rust, J. *Chem. Commun.* (1979) 1178.
2. Chiang, J. F. and Bauer, S. H. *J. Am. Chem. Soc. 88* (1966) 420.
3. Legon, A. C. *Chem. Rev. 80* (1980) 231.
4. Mastryukov, V. S., Osina, E. L., Vilkov, L. V. and Hilderbrandt, R. L. *J. Am. Chem. Soc. 99* (1977) 6855.
5. Villarreal, J. R. and Laane, J. *J. Chem. Phys. 68* (1978) 3298.
6. Avirah, T. K., Cook, R. L. and Malloy, T. B., Jr. *J. Chem. Phys. 71* (1979) 3478.
7. Glen, R. *Thesis,* University of Stirling, Stirling 1981.
8. Allinger, N. L. *J. Am. Chem. Soc. 99* (1977) 8127.
9. Baird, N. C. *Tetrahedron 26* (1970) 2185.
10. Andersen, B. and Srinivasan, R. *Acta Chem. Scand. 26* (1972) 3468.
11. Skancke, P., Fogarasi, G. and Boggs, J. E. *J. Mol. Struct. 62* (1980) 259 and references therein.
12. Bohn, R. K. and Tai, Y.-H. *J. Am. Chem. Soc. 92* (1970) 6447.
13. Spelbos, A., Mijlhoff, F. C., Bakkes, Y. H., Bader, R. and Van der Enden, L. *J. Mol. Struct. 38* (1977) 155.

14. Mastryukov, V. S., Popik, M. V., Dorofeeva, O. V., Golubinskii, A. V., Vilkov, L. V., Belikova, N. A. and Allinger, N. L. *J. Am. Chem. Soc. 103* (1981) 1333 and references therein.
15. Blomquist, A. T. and Kwiatek, J. *J. Am. Chem. Soc. 73* (1951) 300.
16. Bauer, S. H. and Kimura, K. *J. Phys. Soc. Jpn. 17* (1962) 300.
17. Huntley, C. M., Laurenson, G. S. and Rankin, D. W. H. *J. Chem. Soc. Dalton Trans.* (1980) 954.
18. Cradock, S., Koprowski, J. and Rankin, D. W. H. *J. Mol. Struct. 77* (1981) 113.
19. Boyd, A. S., Laurenson, G. S. and Rankin, D. W. H. *J. Mol. Struct. 71* (1981) 217.
20. Schäfer, L., Yates, A. C. and Bonham, R. A. *J. Chem. Phys. 55* (1971) 3055.
21. Hilderbrandt, R. L. and Wieser, J. D. *J. Chem. Phys. 42* (1966) 4648.
22. Schachtschneider, J. H. and Snyder, R. G. *Spectrochim. Acta 19* (1963) 113.
23. Gundersen, G., Murray-Rust, P., Rankin, D. W. H., Seip, R. and Watt, C. I. F. *Acta Chem. Scand. A 37* (1983) 823.
24. Mastryukov, V. S. *J. Mol. Struct. 96* (1983) 361.
25. Davis, M. I. and Muecke, T. W. *J. Phys. Chem. 74* (1970) 1104.
26. a. Almenningen, A., Bastiansen, O. and Skancke, P. N. *Acta Chem. Scand. 15* (1961) 711; b. Takabayashi, F., Kambara, H. and Kuchitsu, K. *7th Austin Symposium of Gas Phase Molecular Structure,* Austin, Texas, Paper WA6, March 1, 1978.
27. Adams, W. J., Geise, H. J. and Bartell, L. S. *J. Am. Chem. Soc. 92* (1970) 5013.
28. Bohn, R. K. and Tai, Y.-N. *J. Am. Chem. Soc. 92* (1970) 6447.
29. Skancke, P. N. *J. Mol. Struct. THEOCHEM. 86* (1982) 255.
30. Sudmann, R. D. and Harmony, M. D. *J. Chem. Phys. 56* (1972) 3837.

Received March 15, 1983.

Acta Chemica Scandinavica A 37 (1983) 865–874

The Gas-phase Molecular Structure of Piperidine Studied by Electron Diffraction

GRETE GUNDERSEN * and DAVID W. H. RANKIN **

Department of Chemistry, University of Edinburgh, West Mains Road, Edinburgh EH9 3JJ, Scotland

The electron-diffraction data for piperidine at 293 K are consistent with a chair conformer of the molecule, but they cannot be reconciled with literature values for the rotational constants of a conformer with the iminohydrogen in the axial position. However, the data are consistent with such values for the H-equatorial conformer and the ring geometry obtained by fitting the electron-diffraction intensities and the H(eq) rotational constants simultaneously, is described by (r_a, $\angle_\alpha$, θ_α): r(C–N)=147.2(11) pm, r(C–C)$_{average}$=153.1(6) pm, $\angle$(C–N–C)=109.8(21)°, $\angle$(C–C4–C)=112.8(15)°, $\angle$(N–C–C)=110.5(17)° and $\angle$(C–C3–C)=109.3(17)° giving dihedral angles θ(N–C–C– C)=56.9(4)°, θ(C–C–C–C)=51.9(18)° and θ(C–N–C–C)=63.6(12)°. These findings do not rule out the possibility of the presence of an axial form in minor amounts.

The replacement of a methylene group in cyclohexane by imine is not expected to lead to serious conformational changes of the six-membered ring, and piperidine (pentamethylene imine) is known to exist in a chair conformation.[1] However, the imino hydrogen can occupy either an equatorial or an axial position (see Fig. 1) and a long controversy has been settled in favour of an NH equatorial preference, estimated to be 0.8–2.4 kJ mol^{-1} (0.2–0.5 kcal mol^{-1}) in the vapour state, based on various experimental evidence,[2] while the most recent microwave result gives an energy difference of 3.1 kJ mol^{-1} corresponding to an equatorial-to-axial ratio of 3.5 to 1 at 293 K.[3]

An electron-diffraction study of gaseous piperidine cannot contribute conclusively to the determination of the composition ratio, as the contribution of the imino-hydrogen to the scattered intensity is small. However, the present investigation was initiated in connection with planned studies of *N* substituted piperidines, which called for more detailed structural information about the parent molecule. The molecule is expected to show complex distance overlaps, but it was hoped that when combined with available data from rotational[3] and vibrational[4] spectroscopy the electron-diffraction data would yield unambiguous results for the ring geometry. A similar study has been carried out for the pentamethylene oxide (tetrahydropyrane).[5] The main goal of that investigation was achieved, but model restrictions had to be maintained, even though electron-diffraction and microwave data were combined in the refinement. In the present case an additional problem was encountered since spectroscopic evidence suggests[3] that the ring geometry differs significantly for the H(axial) and H(equatorial) conformers.

EXPERIMENTAL

A commercial sample of piperidine (Fisons Scientific Laboratory) with stated purity of at least 99 % was used in this investigation: its purity was checked by *IR* spectroscopy. The electron-diffraction data were recorded on Kodak Electron Image plates using the Cornell/Edinburgh diffraction apparatus[6,7] with nozzle-to-plate distances of 128.3 and 285.8 mm. The

* Present address: Department of Chemistry, University of Oslo, Oslo 3, Norway.
** Author to whom correspondence should be addressed.

0302-4377/83 $2.50

Table 1. Weighting functions, correlation parameters and scalefactors.[a]

Camera height	Wave-length	Δs	s_{min}	sw_1	sw_2	s_{max}	Cor-relation parameter	Scale factor
mm	pm	nm^{-1}						
128.3	5.848	4	60	70	300	324	0.372	0.668(13)
285.8	5.844	2	20	50	120	140	0.482	0.761(12)

[a] See Ref. 10 for definitions of the symbols. The correlation parameters and scale factors correspond to results IIB of Table 2.

sample and nozzle were kept at room temperature during the exposures, but as the amine evaporated very slowly it was first expanded into a large container and the ambient pressure during the sample run-in was controlled with a needle valve. The accelerating voltage was 42 kV and the electron wavelength was calibrated against diffraction patterns of gaseous benzene [r_a(C–C)=139.70 pm] recorded immediately before and after the sample plates.

The optical densities of three photographic plates for each of the two camera distances were recorded at the S.E.R.C. Laboratory, Daresbury using the Joyce-Loebl Microdensitometer.[8] The data reduction was carried out using established programs[7] which at the final stages include an automatic background correction based on spline functions.[9] A least-squares refinement program described previously was used in the structure analysis.[10] The data ranges and the parameters of the off-diagonal weighting functions are given in Table 1, which also contains the scale factors and the correlation parameters of the final results. The complex scattering factors of Schäfer *et al.*[11] were used and all calculations were carried out on an ICL-2972 computer. The experimental molecular intensities and the corresponding radial distribution curve and shown in Figs. 2 and 3, respectively.

STRUCTURE ANALYSIS

Molecular model. The initial analysis of the electron-diffraction data confirmed that they could be represented by a chair conformation with C_s-symmetry. The two different C–C bonds were at first described by an average distance and a difference parameter, Δ(C–C). However, attempts to assess Δ(C–C) at various stages of the analysis indicate, as in the case of the analogous pentamethylene oxide,[5] that it is not significantly different from zero. Thus for all results quoted it is assumed that r_a(C2–C3)=r_a(C3–C4). Ten parameters were then used to describe the geometry of piperidine and they are defined subsequently with the structural results (Table 2).

The two conformers [H(eq) and H(ax)] were assumed to have equal ring geometries. The N–H(eq) and N–H(ax) bonds lengths were also taken to be equal as were the absolute magnitude of the ∠NH-parameter, which is the angle between the N–H bond and the bisector of ∠(C–N–C). (See Fig. 1.)

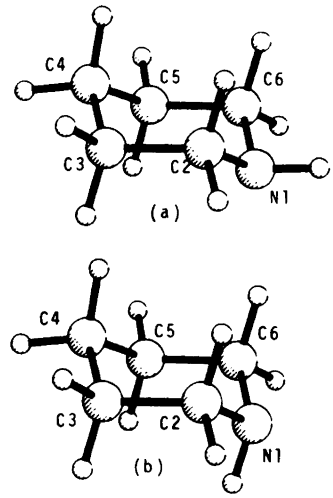

Fig. 1. Views of the equatorial (a) and axial (b) conformation of piperidine, $C_5H_{10}NH$. The numbering of the heavy atoms is given. The methylene hydrogens are numbered according to the corresponding carbon atoms and axial and equatorial positions are identified by A and E, respectively. The imino hydrogen is labelled H(ax) and H(eq) for the H-axial and H-equatorial conformers, respectively.

Table 2. Results from least-squares refinements based on electron-diffraction data alone (I) and combined with experimental values for the rotational constants of the H(eq) conformer(II), assuming the conformational composition ratio [H(ax)/H(eq)] to be 0.30[a].

	IA	IB	IIA	IIB
Geometrical parameters (r_a, $\angle_a$)[b]				
r(N–H)	101.5–	101.5–	101.5–	101.5–
r(C–H)	109.8(3)	109.7(2)	110.5(2)	110.5(2)
r(N–C)	146.9(3)	145.9(4)	147.1(3)	147.2(11)
r(C–C)	153.0(1)	153.3(2)	153.2(2)	153.1(6)
$\angle$(H–C–H)	110.0(10)	109.4(9)	112.1(9)	112.2(9)
$\angle$(C–N–C)	110.7(10)	112.9(32)	111.1(24)	109.8(21)
$\angle$(C–C4–C)	109.6(13)	111.1(53)	111.6(21)	112.8(15)
$\angle$(N–C–C)	110.5(6)	110.5(16)	109.8(18)	110.5(17)
$\angle$(C–C3–C)	111.1(7)	110.3(28)	109.9(18)	109.3(17)
$\angle$(NH)	56.2–	56.2–	56.2–	56.2–
Amplitude parameters[c]				
u1	7.9–	7.7(2)	7.9–	8.0(3)
u2	5.1–	4.4(3)	5.1–	5.1(5)
u3	6.8–	6.8(4)	6.8–	6.7(3)
u4	10.4–	11.0(3)	10.4–	11.0(4)
u5	10.4–	10.4(5)	10.4–	10.6(5)
u6	14.8–	17.8(9)	14.8–	15.7(10)
u7	11.0–	9.4(16)	11.0–	9.4(11)
Dependent angles ($\angle_a$,θ_a)[d]				
$\angle$(C–N–H)	108.4(3)	107.9(8)	108.4(6)	108.7(5)
θ(N–C2–C3–C)	57.2(5)	55.5(12)	56.9(3)	56.9(4)
θ(C–C3–C4–C)	53.2(11)	53.2(38)	53.1(11)	51.9(18)
θ(C–N–C–C)	60.6(16)	60.0(43)	62.7(10)	63.6(12)
θ(C4–C5···C3–C2)	48.4(8)	48.7(22)	48.8(8)	48.0(20)
θ(N–C6···C2–C3)	54.7(13)	54.2(30)	56.8(7)	57.2(16)
Rotational constants ($r_a°$)[e]				
A(ax)	4516(26)	4516(74)	4524.5(14)	4526.2(29)
B(ax)	4465(28)	4460(73)	4450.1(11)	4449.1(13)
C(ax)	2587(5)	2579(5)	2593.2(6)	2593.8(12)
A(eq)	4583(26)	4524(71)	4516.4(2)	4516.4(3)
B(eq)	4382(26)	4431(67)	4436.1(3)	4436.2(3)
C(eq)	2538(5)	2531(5)	2542.5(1)	2542.5(1)
Least-squares agreement factors				
R_G/R_D	7.21/4.61	6.13/5.05	8.75/5.55	8.48/5.56

[a] A and B refer to refinements with the amplitude parameters fixed at the calculated values (Table 4) and refined in groups, respectively. See Tables 4 and 6 for interatomic distances and the correlation matrix for refinements IIB. See Fig. 1 for numbering of the atoms. r- and u-values in pm; $\angle$ and θ in degrees; A to C values, values in MHz; and R-factors in %. The standard deviations in parentheses do not include systematic uncertainties. [b] See text for comments on Δ(CC) and assumed values for r(NH) and $\angle$(NH). The parameters are also labelled *p1* to *p10*. [c] See Table 4 for definitions of u-value groups. [d] The θ(C5···C3) and θ(C6···C2) parameters correspond to the 'flap' angles of planes C3–C4–C5 and C6–N–C2, respectively. [e] See Table 5 for experimental counterparts (r_z), and the text for refinements where the values for the axial conformer are included.

Table 3. Simplified general valence force field for piperidine (Fig. 1).[a]

Diagonal elements				Interaction elements			
k_r	N–H	(1)	6.06	$k_{r,r}$	C–N/C–N	(1)	0.28
	C–H	(10)	4.60		C–N/C–C	(2)	0.28
	C–N	(2)	4.50		C–C/C–C	(3)	0.28
	C–C	(4)	4.10				
$k_\angle$	C–N–H	(2)	0.70	$k_{r,\angle}$	C–N/C–N–C	(2)	0.36
	N–C–H	(4)	0.75		C–N/N–C–C	(2)	0.36
	C–C2–H	(4)	0.83		C–C/N–C–C	(2)	0.36
	C–C3–H, C–C4–H	(12)	0.70		C–C/C–C–C	(4)	0.36
					C–C/C–C4–C	(2)	0.36
	H–C–H	(5)	0.53		C–N/N–C–H	(2)	0.35
	C–N–C	(1)	0.90		C–C/C–C2–H	(4)	0.35
	C–C4–C	(1)	0.80		C–C/C–C3–H, C–C4–H	(12)	0.35
	N–C–C	(2)	0.80				
	C–C–C	(2)	1.00		C–N/C–N–H	(2)	0.35
k_θ	C–C–N–C	(2)	0.17				
	N–C–C–C	(2)	0.15				
	C–C–C–C	(2)	0.17				

[a] Parenthesized values are the number of contributions. The units are $100\times$aJ nm^{-2} (k_r, $k_{r,r}$), aJ rad^{-2} ($k_\angle$, k_θ) and $10\times$aJ rad^{-1}nm^{-1} ($k_{r,\angle}$). 1 aJ$=10^{-18}$ J=1 mdyn Å.

Several constraints were introduced for the methylene groups: (a) all C–H bonds are equal in length; (b) all H–C–H angles are equal; (c) the H–C–H planes are perpendicular to the planes described by the carbon atom and its two adjacent ring atoms; and (d) the bisector of the H–C–H angle and that of the corresponding angle of the ring are colinear.

Calculated vibrational amplitude quantities and conversion terms. Normal coordinate calculations using a computer program originally written by R. L. Hilderbrandt[12] were carried out based on a simplified valence force field similar to one used in a study of pentamethylene oxide.[5] The same force field was used for both conformers and the elements were adjusted to give calculated frequencies in approximate agreement with the observed ones.[4] The final force field is given in Table 3. The two low ν(CH) frequencies at 2803 and 2730 cm^{-1} for the equatorial form were not well reproduced (2866 and 2867 cm^{-1}, respectively). For the frequencies below 1500 cm^{-1} mean deviations of 21 and 19 cm^{-1} were obtained for the equatorial and axial conformers, respectively. The full lists of calculated frequencies and corresponding potential energy distributions and the root-mean-square amplitudes of vibration (u) and perpendicular amplitude correction coefficients (K) calculated for temperatures of 293 and 0 K are available upon request.

The u- and K-values for corresponding distances in the H(eq) and H(ax) conformers are not significantly different. The average values used in the analysis are included in Table 4, with the interatomic distances of the final structure of the molecule.

The vibrational corrections to the rotational constants (δB_{vib}) were calculated and the observed rotational constants[3] were converted to B_z neglecting centrifugal and electronic contributions to the correction (see Table 5). The standard deviations of the B_z-values were taken as 30 % of the calculated δB_{vib} terms.

The structure refinements were based on r_α parameters, but the calculations were always parallelled by computations of r_α°-coordinates from which r_α° rotational constants were computed. The $\angle_\alpha^\circ$ and $\angle_\alpha$ parameters were assumed to be equal, and in the r_α to r_α° conversions which had to be implemented only for bond distances, the a_3 parameter was assumed to be 20 nm^{-1}:

$$r_\alpha - r_\alpha^\circ = \tfrac{3}{2}\, a_3\, (u^2 - u_0^2) - (K - K_0)$$

The u- and K-values are the calculated ones (Table 4) whereas in the conversion

Table 4. Interatomic distances corresponding to refinement IIB of Table 4; vibrational amplitude parameters calculated for T=293 K from the force field of Table 3; and definition of the seven independent u-value groups.[a]

	r_a/pm	K/pm	u/pm	
N–H	103.0–	2.00	7.36	— —
C–H	111.6(2)	1.63	7.90	*u1*
C–N	147.4(11)	0.38	5.07	*u2*
C2–C3	153.3(6)	0.35	5.30	*u2*/0.96
C3–C4	153.6(6)	0.35	5.31	*u2*/0.96
C3···N	246.7(26)	0.18	6.88	*u3*
C2···C6	240.8(22)	0.19	6.86	*u3*/1.00
C3···C5	255.1(20)	0.17	6.93	*u3*/1.00
C2···C4	249.9(27)	0.17	6.80	*u3*/1.00
C4···N	288.5(6)	0.08	7.31	*u3*/0.94
C2···C5	291.3(4)	0.08	7.25	*u3*/0.94
N···H2E	210.8(10)	1.06	10.48	*u4*
C2···H3E	216.3(8)	1.03	10.70	*u4*/1.00
C3···H2E	215.9(6)	1.02	10.50	*u4*/1.00
C3···H4A	215.2(8)	1.02	10.72	*u4*/1.00
C4···H3E	216.3(8)	1.04	10.70	*u4*/1.00
N···H3E	341.5(24)	0.60	10.42	*u5*
C2···H4E	344.6(21)	0.59	10.40	*u5*/1.00
C4···H2E	345.5(22)	0.59	10.31	*u5*/1.00
C2···H6E	336.5(18)	0.61	10.32	*u5*/1.00
C3···H5E	349.0(19)	0.59	10.44	*u5*/1.00
C3···H6A	323.9(19)	0.41	15.02	*u5*/0.75
C2···H5A	333.5(12)	0.42	14.78	*u5*/0.75
N···H4A	332.2(28)	0.41	14.50	*u5*/0.75
N···H3A	271.9(37)	0.65	14.85	*u6*
C2···H4A	276.9(38)	0.61	14.63	*u6*/1.00
C4···H2A	273.1(36)	0.62	14.60	*u6*/1.00
C2···H6A	259.5(32)	0.65	15.00	*u6*/1.00
C3···H5A	284.1(3)	0.62	14.91	*u6*/1.00
C2···H5E	387.3(9)	0.43	11.01	*u7*
C3···H6E	391.7(5)	0.42	10.76	*u7*/1.00
N···H4E	383.9(19)	0.41	11.20	*u7*/1.00
C2···H(eq)	204.3(14)	1.16	10.72	*u4*/1.00
C3···H(eq)	334.7(22)	0.64	10.25	*u5*/1.00
C4···H(eq)	382.3(10)	0.46	10.57	*u7*/1.00
C2···H(ax)	204.3(14)	1.15	10.73	*u4*/1.00
C3···H(ax)	261.3(43)	0.66	15.88	*u6*/1.00
C4···H(ax)	312.9(30)	0.42	16.31	*u5*/0.75

[a] See Fig. 1 for labelling of the atoms. H···H interactions were included in the refinements but are omitted here. See text for averaging of u- and of K-values. The amplitude quantities at T=O K are for the N–H, C–H (average), C–C (average) and N–C bond distances: u_o 7.36, 7.90, 5.30 and 5.03 pm; K_o 1.88, 1.50, 0.26 and 0.28 pm, respectively.

$r_a = r_a - u^2/r + K$

the u-values are as assumed or obtained in the actual refinement.

The radial distribution curve. The interpretation of the radial distribution curve (Fig. 3) reveals that there are severe distance overlaps. The first peak at 110 pm contains ten C–H distances and one N–H distance and the latter cannot be well determined. The peak at 150 pm comprises the C–N and the two types of C–C bond distances. The one-angle N···H and C···H

Table 5. Observed rotational constants (r_o-representations);[3] the vibrational correction terms [δ(vib)] calculated from the force field of Table 3; and the converted rotational constants (r_z-representations) in MHz.

	r_o	δ(vib)	r_z
A(ax)	4494.368(10)	−0.893	4493.48(27)
B(ax)	4395.271(10)	−1.177	4394.09(35)
C(ax)	2535.611(10)	−0.555	2535.06(17)
A(eq)	4517.227(8)	−0.877	4516.35(26)
B(eq)	4437.239(8)	−1.143	4436.10(34)
C(eq)	2542.989(5)	−0.487	2542.50(15)

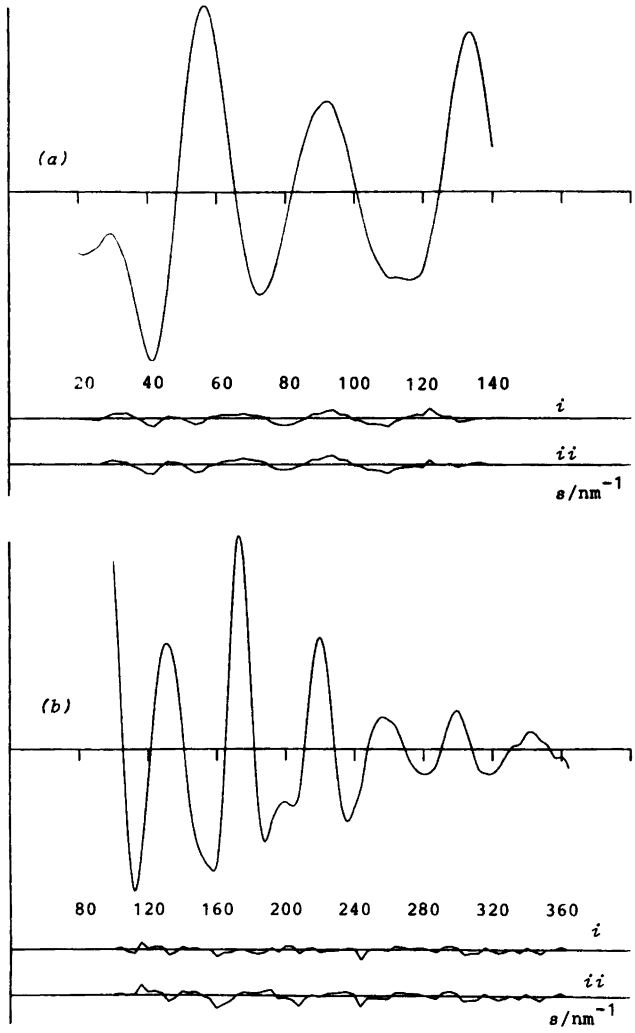

Fig. 2. Experimental molecular scattering intensities for nozzle-to-plate distances of (a) 286 and (b) 128 mm; and the corresponding weighted difference curves according to refinements (i) IB and (ii) IIB of Table 4.

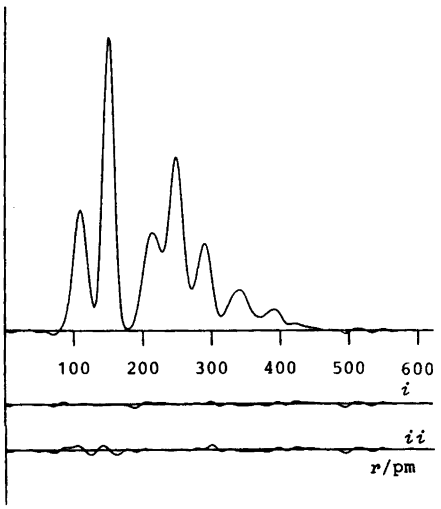

Fig. 3. Experimental radial distribution curve, P(*r*)/*r*, and difference curves corresponding to refinement (i) IB and (ii) IIB of Table 4. Before Fourier inversion the data were multiplied by *s* exp $[-0.000015s^2]/(Z_C-f_C)^2$.

distances are contained in the next feature with a maximum at 215 pm. Again the low contribution from distances involving the imino hydrogen makes it difficult to assess the position of this atom. The major components of the peak at 250 pm are the four types of one-angle C···C/N···C distances, and the three 'long' C···C/N···C distances are unresolved in the next feature at 290 pm. Some 'long' C···H/N···H distances contribute to the latter peaks, but mainly they account for the area beyond 310 pm. With this type of distance overlap great interdependencies of the angular parameters are expected. These are also reflected in high standard deviations and correlation coefficients obtained in the analysis. In the early refinements this appeared to be most severe for the ∠(C−C3−C) and ∠(C−C4−C) parameters which had $\rho=0.92$, but in the final correlation matrix (Table 6) many parameters showed large correlations.

Refinements based on electron-diffraction intensities. As suspected it proved difficult to determine the *r*(N−H) and ∠(N−H) parameters. In most of the refinements they were fixed at assumed values as used in a study of piperazine.[13] r_a(NH)=101.5 pm [r_a=103.0 pm] and ∠NH=56.2° which gives about 108° for ∠(C−N−H). The values are taken from the molecular structures of NH_3[14] and $(CH_3)_2NH$,[15] respectively. Values of r_a=100.6(16) pm and ∠NH=63.4(39)° were obtained in a refinement which had fixed amplitude parameters. Similar values were obtained in a corresponding refinement which included rotational constants (next section). However, in neither case did this lead to significant changes in the least-squares fit or in the values of the remaining geometrical parameters, and all the final results quoted are obtained with the assumptions as described.

Initially several sets of refinements were carried out with the amplitude parameters fixed at the calculated values. Firstly, each of the four skeleton valence angles was varied systematically over the 107−115° range in increments of 1°. The best refined structures in each of these four sets of calculations gave parameters which were used as starting points for full refinements. Secondly, ∠(C−C3−C) and ∠(C−C4−C) were maintained at 108 and 112°, respectively and *vice versa*. The obtained structures were then used as basis for full refinements. All these refinements converted at essentially the same minimum and it appeared that the structure was unambiguously determined.

In the refinements described above the H(ax)/H(eq) conformational composition was fixed at 0.5. For 100 % of the axial conformer convergence problems were encountered and a poorer least-squares fit was obtained than for 100 % (proportion 0) of the equatorial conformer. For 0, 25 and 50 % of the axial conformer present the least-squares fits were similar and there were no significant differences in the structural parameters obtained as the variations in the angular parameters of 1−2.5° were all within 1.5σ. Results obtained for composition 0.30, *i.e.* with 30 % of the axial form as the minor conformer, are presented in Table 2, column IA.

Corresponding refinements which also included all the vibrational parameters except those associated with *r*(N−H) and the H···H interactions were carried out. Altogether seven independent *u*-values were used and the dependent parameters were tied to these by ratios obtained from the relative magnitudes of the calculated values (See Table 4). In subsequent refinements which include microwave data (next section) it proved impossible to obtain reasonable results unless the *u*-values for all the skeletal non-bonded distances were tied together, and

this restriction (Table 4) was used also in the present refinements. The least-squares fits obtained from compositions 1.0 and 0.0 were now comparable, but the obtained *u*-values were in slightly poorer agreement with the calculated values in the former case (100 % axial). Results obtained for a 30:70 mixture of axial and equatorial forms are presented in Table 2, column IB. The weighted difference molecular intensities for the two camera distances and the corresponding difference radial distribution curve are shown in Figs. 2 and 3, respectively.

Combined analysis of electron-diffraction and microwave data. The $r_\alpha°$ rotational constants calculated from structures IA and IB are included in Table 2. Comparisons with the experimental counterparts (r_z-representatives, Table 5) show that all the rotational constants calculated for the axial conformer are too large whereas the equatorial values do not suggest any scale inconsistencies. Considering this problem and the probable [3] difference in the ring geometry for the two forms the rotational constants were at first included in the refinement with an intermediate weight reducing the $\sigma(r_\alpha°)$ values to the 1–6 MHz range. However, it proved impossible to include both sets of values simultaneously: the obtained axial constants were all too large and the equatorial ones too small, and a poor fit to the electron-diffraction data as well as unreasonable structural results were obtained. Only one set of constants was therefore included in the refinement for compositions α=0 (H(eq) only), 1.0 and 0.5, giving two series of refinements for the latter composition.

The *A*(eq) to *C*(eq) values were first fitted to within ±4.5 MHz of the observed counterparts. For α=0 this fit was accompanied by a wide valence angle at N [117.6(7)°]. Reasonable structural results were, however, obtained for α=0.5 with less loss in the fit to the electron-diffraction intensities and an intermediate value of α gave similar results. Results for composition 0.3 obtained with increased weighting of the rotational constants are presented in Table 2 for fixed (IIA) and refined (IIB) amplitude parameters. Weighted molecular intensity and radial distribution differences corresponding to refinement IIB are shown in Figs. 2 and 3, respectively. The interatomic distances and elements of the correlation matrix corresponding to refinement IIB are given in Tables 4 and 6, respectively. The refined vibrational parameters of IIB are in better agreement with the calculated ones than those of refinement IB (Table 2), but both refinements have a high positive correlation in the *p3* and *u2* parameters. The correlation matrix of IB is very similar to that of IIB (Table 6) with respect to the *p6* to *p8* geometrical parameters.

Similar attempts to fit the axial rotational constants showed that this could only be obtained by serious loss in the fit to the electron-diffraction data. Furthermore, the structural results were ambiguous and in all cases they were rather unreasonable. The problems persisted when *r*(NH) and ∠(NH) were adjusted, and when the vibrational parameters were refined. In the latter case the refinements were also hampered by unreasonable *u*-values. Thus it proved impossible to reconcile the electron-diffraction and microwave data for an axial model of piperidine.

DISCUSSION

The clear conclusion of the present investigation is that the gas-phase electron-diffraction data

Table 6. Significant elements of the correlation matrix for geometrical (*p*) and amplitude (*u*) parameters of refinement *IIB* (Table 2). $\rho_{ij}\times100$ for $|\rho_{ij}|>0.4$ are given.

	p3	*p4*	*p5*	*p6*	*p7*	*p8*	*u2*
p4	−99	100					
p6	−68	+68	+48	100			
p7	+50	−50	−42	−97	100		
p8	—	—	−61	−79	+86	100	
p9	—	—	+61	+66	−77	−97	
u2	+95	−94	—	−65	+48	—	100
u3	+49	−51	—	—	—	—	+54
u4	+66	−65	—	−58	+51	—	+68

of piperidine are not compatible with a ring geometry which conforms to the rotational constants assigned[3] to the H(ax) conformer of the molecule. However, the data may be interpreted in terms of structural parameters which are consistent with the rotational constants of the equatorial conformer. Thus if the ring geometry of the axial form is distorted from that of the equatorial conformer (as implied by the microwave data) this shows that the latter form must predominate. However, it does not rule out the possibility that the axial form may co-exist in minor amounts. Simultaneous fitting to the H(eq) rotational constants caused a loss in the agreement to the electron-diffraction intensities which was much worse than of that encountered in an analogous study of pentamethylene oxide.[5] In some cases it appeared that the refinements became more favourable when a proportion of the C2···H(eq) and C3···H(eq) distances was replaced by the shorter C2···H(ax) and C3···H(ax) ones. These effects are marginal, but they may indicate that the axial form is indeed present in the gas at room temperature in agreement with the published energy differences between the two forms.[2,3]

As seen from Table 2, the skeletal valence angles are not consistently determined in the various refinements. Considering the possible presence of a 'distorted' axial form we assume that the results of refinements IIA and B are the best, but not necessarily unambiguous, estimates of the structure for the equatorial form. In all refinements, including IIB which is taken to represent the final results, there are high correlations between the valence angles (Table 6, parameters *p6* to *p9*) and they are determined with low accuracy. This prevents any detailed discussion of their magnitudes, but it is noteworthy that piperazine (HNC_4H_8NH) has $\angle$(C−N−C)=109.0(8)° and $\angle$(N−C−C)=110.4(8)°.[13]

The shape of the ring is probably best visualized using the skeletal torsional angles about the bonds. The magnitudes of the three types of such angles in piperidine (Table 2) are consistently determined in the various refinements: θ(C−C−C−C) is slightly smaller than the torsional angle of 54.9(4)° in cyclohexane[16] whereas θ(C−N−C−C), and to a lesser extent θ(N−C−C−C), are larger than this. The angles obtained are similar to those encountered in the oxide (C_6H_5O) which has, 53.0(10), 56.1(12) and 59.3(10)° for the C−C−C−C, O−C−C−C and C−O−C−C torsional angles, respectively. The reported structure of piperazine[13] has angles of 59.4 and 58.6° for θ(C−N−C−C) and θ(N−C−C−N), respectively.

The determination of r(N−C) is seen to be affected by refinement of the vibrational parameters. In refinement IB a small value was obtained associated with the low *u2* value of 4.4(3) pm, while in refinement IIB it had a high standard deviation, but *u2* was in agreement with the calculated values. The problem is reflected in the high positive correlation coefficient for *p3* and *u2* (Table 6). A value of about 147 pm appears reasonable by comparison with 146.7(4) pm for r_g(N−C) in piperazine.[13] The average C−C bond is also similar in length to comparable bonds in cyclohexane (r_g=153.6(2) pm),[16] piperazine (r_g=154.0(8) pm)[13] and tetrahydropyran (153.1(2) pm).[5]

Thus the ring geometry of piperidine determined in the present study has no unexpected features when compared with related structures. It has been related to the equatorial conformer, but the possible presence of a distorted axial conformer in minor amounts introduces some degree of ambiguity to the determination. The proposed flattening of the axial form as reflected in its rotational constants[3] cannot be studied by gas-phase electron-diffraction. In order to achieve the ultimate goal of the investigation further structural studies are neccessary and an *ab initio* molecular orbital study is forthcoming.

Acknowledgements. We thank the Science and Engineering Research Council for a research grant.

REFERENCES

1. Riddell, F. G. *Quart. Rev. 21* (1967) 364.
2. Blackburne, I. D., Katritzky, A. R. and Taheuchi, Y. *Acc. Chem. Res. 8* (1975) 300 and references therein.
3. Parkin, J. E., Buckley, P. J. and Costain, C. C. *J. Mol. Struct. 89* (1981) 465.
4. Vedal, D., Ellestad, O. H., Klæboe, P. and Hagen, G. *Spectrochim. Acta A 32* (1975) 877.
5. Breed, H. E., Gundersen, G. and Seip, R. *Acta Chem. Scand. A 33* (1979) 225.

6. Bauer, S. H. and Kimura, K. *J. Phys. Soc. Jpn. 17* (1962) 300.
7. Huntley, C. M., Laurenson, G. S. and Rankin, D. W. H. *J. Chem. Soc. Dalton Trans.* (1980) 954.
8. Cradock, S., Koprowski, J. and Rankin, D. W. H. *J. Mol. Struct. 77* (1981) 113.
9. Blair, P. and Rankin, D. W. H. *Unpublished.*
10. Boyd, A. S., Laurenson, G. S. and Rankin, D. W. H. *J. Mol. Struct. 71* (1981) 217.
11. Schäfer, L., Yates, A. C. and Bonham, R. A. *J. Chem. Phys. 55* (1971) 3055.
12. Hilderbrandt, R. L. and Wieser, J. D. *J. Chem. Phys. 42* (1966) 4668.
13. Yokozeki, A. and Kuchitsu, K. *Bull. Chem. Soc. Jpn. 44* (1971) 2352.
14. Kuchitsu, K., Guillory, J. P. and Bartell, L. S. *J. Chem. Phys. 49* (1968) 2488.
15. Wollrab, J. E. and Laurie, V. W. *J. Chem. Phys. 48* (1968) 5058.
16. Bastiansen, O., Fernholt, L., Seip, H M., Kambara, H. and Kuchitsu, K. *J. Mol. Struct 18* (1973) 163.

Received March 10, 1983.

Acta Chemica Scandinavica A 37 (1983) 875–880

Equilibrium and Structural Studies of Silicon(IV) and Aluminium(III) in Aqueous Solution. 8. A Potentiometric Study of Aluminium(III) Salicylates and Aluminium(III) Hydroxo Salicylates in 0.6 M Na(Cl)

LARS-OLOF ÖHMAN and STAFFAN SJÖBERG

Department of Inorganic Chemistry, University of Umeå, S-901 87 Umeå, Sweden

Equilibria between aluminium(III), salicylic acid (2-hydroxy-benzoic acid, H_2L) and OH^- were studied in 0.6 M Na(Cl) medium at 25 °C. The measurements were performed as emf titrations (glass electrode) within the limits $2 \leq -\lg [H^+] \leq 9$; $0.0005 \leq B \leq 0.01$ M; $0.006 \leq C \leq 0.015$ M and $0.6 \leq C/B \leq 30$ (B and C stand for the total concentrations of aluminium(III) and salicylic acid, respectively). All data can be explained with the following species (tentative structures) and corresponding equilibrium constants: AlL^+, $\lg \beta_{-2,1,1} = -3.052 \pm 0.005$; AlL_2^-, $\lg \beta_{-4,1,2} = -8.391 \pm 0.011$; $Al(OH)L_2^{2-}$, $\lg \beta_{-5,1,2} = -15.99 \pm 0.024$ and $Al(OH)_2L_2^{3-}$, $\lg \beta_{-6,1,2} = -25.31 \pm 0.11$. The standard deviations are $3\sigma(\lg \beta_{p,q,r})$. The carboxylic acid dissociation constant $H_2L \Leftrightarrow HL^- + H^+$ was studied in separate titrations and it is found to be $\lg \beta_{-1,0,1} = -2.724 \pm 0.001$. Data were analyzed with the least squares computer program LETAGROPVRID. In some solubility models with kaolinite as solid phase, the strength of complexation is compared to the complex formation in the gallic acid system, reported in earlier papers of this series.

The ability of Si(IV) [1,2] and Al(III) [3–6] to form aqueous complexes with ligand types occurring in natural waters is under extensive study. The most important classes of these ligand types are the high molecular weight organic material called humic and fulvic acids. By different degradation techniques, several types of probable complex formation sites in the humic and fulvic acids have been revealed and one of them, *i.e.* the *o*-diphenolic binding site, has been studied in preceeding papers of this series.[3,5,6] Other often quoted model ligand types for the humic substances are the 2-hydroxybenzoic acid derivatives. The complex formation of the simplest of these derivatives, *i.e.* salicylic acid, to Al^{3+} has, according to Stability Constants,[7,8] been the subject of one earlier investigation.[9] However, as that work is based on a very restricted number of data, especially in neutral and alkaline solutions, we have found it important to perform a careful and unbiased reinvestigation of this system.

EXPERIMENTAL

Chemicals and analysis. Sodium salicylate ($NaC_7H_5O_3$, NaHL) (Merck *p.a.*) was used without further purification after drying. Stock solutions were prepared by dissolving NaHL in water and the HL^- content determined potentiometrically. The titrated amount was in full agreement (within 0.1 %) with that expected from the weighed amount. All other solutions were prepared and analyzed as described elsewhere.[3]

Apparatus. The automatic system for precise emf titrations, the thermostat and the electrodes was described elsewhere.[3] The coulometer was the same as in Part 2 of this series.[1]

0302-4377/83 $2.50

METHOD

The present investigation was carried out as a series of titrations at 25 °C in a constant ionic medium of 0.6 M Na(Cl). In the titrations, the free hydrogen ion concentration, h, was varied either by means of coulometric generated OH^- or by H^+-solution and h was measured with a glass electrode. As the carboxylic pk_a for salicylic acid is too low to permit the customary procedure in calibrating the electrode (*cf.* Ref. 3) the following titration procedure was used: to V_o ml of ≈3 mM HCl in 0.6 M Na(Cl) approximately ten successive coulometric additions with intervening emf recordings were made until the solution was nearly neutralized. Then, V_T ml of HL^-- or Al^{3+}/HL^--solution was added and the titration continued. With this procedure, the electrode calibration can be evaluated as a mean of several measurements within the titration and in our opinion that gives a more accurate calibration than using separate solutions of known H^+ concentration.

The carboxylic acidity constant of salicylic acid was determined in separate titrations within the concentration range 0.002–0.015 M. No attempts were made to evaluate the phenolic acidity constant as this would require the use of a hydrogen electrode.

During the three component titrations, the ratio between the total concentration of aluminium, B, and salicylic acid, C, was held constant. The measurements were performed within the limits $2 \lesssim -\lg h \lesssim 9$; $0.0005 \leq B \leq 0.01$ M and $0.006 \leq C \leq 0.015$ M, covering the C/B ratios: 0.6, 1.5, 5, 7.5, 10, 15 and 30. At $C/B \lesssim 7.5$ the available $-\lg h$ range was restricted to an upper limit due to the formation of a white precipitate. To test reproducibility and reversibility of equilibria, both forward (increasing $-\lg h$) and backward (decreasing $-\lg h$) titrations were performed. To obtain more data points in the most interesting areas some dilution experiments (titrations with pure medium solution) were also performed.

Data treatment. The equilibria which must be considered in the present study can be divided into three groups:

(*i*) the binary salicylic acid equilibrium $H_2L \Leftrightarrow HL^- + H^+$; $\beta_{-1,0,1}$

(*ii*) the hydrolytic equilibria of Al^{3+} $pH^+ + qAl^{3+} \Leftrightarrow H_pAl_q^{p+3q}$; $\beta_{p,q,0}$

(*iii*) three-component equilibria of the general form $pH^+ + qAl^{3+} + r(H_2L) \Leftrightarrow H_pAl_q(H_2L)_r^{p+3q}$; $\beta_{p,q,r}$

In other parts of this series,[4,6] where experiments were also performed in 0.6 M Na(Cl) medium at 25 °C, we have shown that the following main hydrolytic complexes with corresponding equilibrium constants are: $Al(OH)^{2+}$ ($\lg \beta_{-1,1,0} = -5.52$); $Al_3(OH)_4^{5+}$ ($\lg \beta_{-4,3,0} = -13.57$); $Al_{13}O_4(OH)_{24}^{7+}$ ($\lg \beta_{-32,13,0} = -109.2$) and $Al(OH)_4^-$ ($\lg \beta_{-4,1,0} = -23.46$).

In the evaluation of the three-component experimental data, the binary complex models (*i* and *ii*) were considered as known and all effects above this level treated as being caused by ternary species. The mathematical analysis of data was performed with the least squares computer program LETAGROPVRID[10] (version ETITR[11,12]). *pqr*-triplets and corresponding equilibrium constants that "best" fit the experimental data were determined by minimizing the error squares sum $U = \Sigma(H_{calc} - H)^2$. The standard deviations $\sigma(H)$, $\sigma(\beta_{pqr})$ and $3\sigma(\lg \beta_{pqr})$, obtained in the LETAGROP calculations, were defined and calculated according to Sillén.[13,14] The computations were performed on a CD CYBER 730 computer.

DATA, CALCULATIONS AND RESULTS

The data used to evaluate the carboxylic acidity constant of salicylic acid comprises 6 titrations with 129 experimental points. The analysis ended at $\sigma(H) = 0.01$ mM giving $\lg(\beta_{-1,0,1} \pm 3\sigma) = -2.724 \pm 0.001$. Effects due to the formation of dimeric species, reported to occur in solutions of higher H_2L concentrations,[15] were not observed.

The mathematical analysis of the three component data, comprising 15 titrations with 431 experimental points, was started by making a Bjerrum plot $\bar{n}(\lg [L^{2-}])$. The plot is shown in Fig. 1. This figure shows that the data for $\bar{n} \lesssim 2$ obviously could be explained by the formation of AlL^+ and AlL_2^-. For $\bar{n} \gtrsim 2$, however, $\bar{n}$ is dependent of B and C and does not attain any limiting value within the investigated area. This is a clear indication that some ternary hydroxo complex and/or some Al(III) hydrolysis product ($Al(OH)_4^-$) are formed in appreciable amounts.

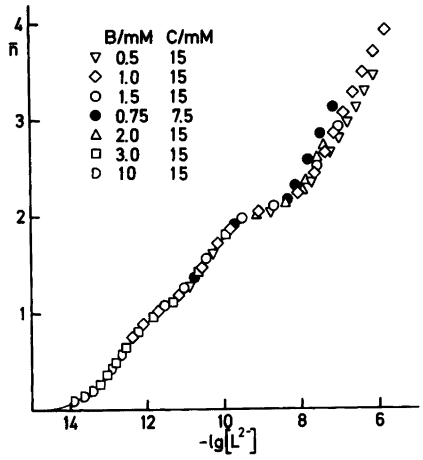

Fig. 1. A part of the experimental data plotted as curves $\bar{n}$(lg [L^{2-}]) for *C/B* ratios 1.5, 5, 7.5, 10, 15 and 30. In the calculation, the value lg $k_2=-13.1$, obtained for the second acidity constant of H_2L by Havelková *et al.*,[9] has been used. The chosen value affects the scale on the x-axis, but not the shape of the $\bar{n}$ curves. Full drawn curve was calculated with lg β_{-211} and lg β_{-412} according to Table 1.

As a consequence, the data was divided into two parts, one with points with $\bar{n} < 2$ and the other with $\bar{n} > 2$. The assumption of two mononuclear complexes at $\bar{n} < 2$ was confirmed when a LETAGROP calculation was performed on these data. The calculation ended at $\sigma(H)=0.04$ mM giving lg $\beta_{-2,1,1}=-3.051\pm0.005$ and lg $\beta_{-4,1,2}=-8.398\pm0.015$ (p,q,r-notations according to iii).

The analysis of data with $\bar{n} > 2$ was performed as a p,q,r-analysis (systematic testing of different p,q,r-complexes) with the simple hypothesis that only one new complex $H_pAl_q(H_2L)_r^{p+3q}$ was present. The criteria for "best fit" was thereby the magnitude of the error squares sum $U=\Sigma(H_{calc}-H)^2$. The result of this analysis is given in Fig. 2 and it is seen that the lowest value of U ($U=0.33$) was obtained for the complex $H_{-5}Al(H_2L)_2^{2-}$ with lg $\beta_{-5,1,2}=-15.99\pm0.04$. The complex AlL_3^{3-}($H_{-6}Al(H_2L)_3^{3-}$), which is the major alkaline species in our earlier investigated Al^{3+}-*o*-diphenolic systems, only gives the second best fit ($U=0.45$; lg $\beta_{-6,1,3}=-16.71\pm0.05$) in this system. A detailed examination of the residuals obtained with either of these two species reveal that the difference between them occurs mainly as a concentration dependence difference at $7\lesssim-\lg h \lesssim 8$ and that the former species ($H_{-5}Al(H_2L)_2^{2-}$) yield a much better fit to the experimental data in this area. It is also found that minor systematic deviations remain for $-\lg h \gtrsim 8$. These effects at high $-\lg h$ could be explained (with either of the complexes above) assuming that a complex $H_{-6}Al(H_2L)_2^{3-}$ was formed. In a final attempt to determine whether

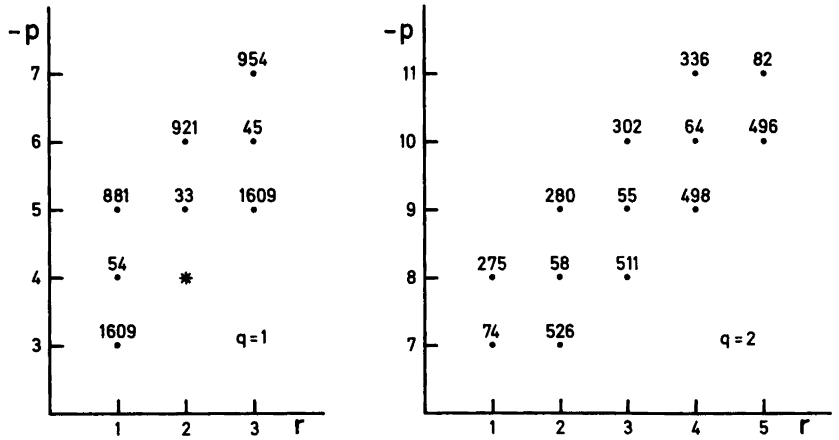

Fig. 2. Result of a *pqr*-analysis for data with $\bar{n} \gtrsim 2$. The figures give the error squares sums $U_H(pr)_q \times 10^2$ assuming one new complex. In the calculations, aluminium hydrolysis and the complexes (−2,1,1) and (−4,1,2) (marked with an asterisk in the left diagram) have been assumed to be known. The calculations are based on 108 experimental points giving $U_H(00)_o=1609 \times 10^{-2}$.

Table 1. Proposed binary and ternary complexes in the three-component system Al^{3+}–OH^-–salicylic acid. The formation constants are related according to the reaction $pH^+ + qAl^{3+} + rH_2L \rightleftarrows H_pAl_q(H_2L)_r^{p+3q}$, where H_2L stands for salicylic acid.

No. of titr./ No. of points	*p q r*	Proposed formula	lg ($\beta_{pqr} \pm 3\sigma$)
6/129	−1 0 1	HL^-	−2.724 ± 0.001
15/431	−2 1 1	AlL^+	−3.052 ± 0.005
	−4 1 2	AlL_2^-	−8.391 ± 0.011
	−5 1 2	$Al(OH)L_2^{2-}$	−15.99 ± 0.024
	−6 1 2	$Al(OH)_2L_2^{3-}$	−25.31 ± 0.11

the dominating species in neutral solutions was $H_{-5}Al(H_2L)_2^{2-}$ or $H_{-6}Al(H_2L)_3^{3-}$, the formation constants for both these species were covaried. It turned out that while the formation constant for (−5,1,2) changed only moderately (a change with 0.09 lg-units) the complex (−6,1,3) was practially eliminated (a change in lg β from −16.71 to −17.52). In an analogous calculation with (−5,1,2) and the third best species, (−4,1,1), the (−4,1,1) species was rejected. Thus, our final proposal for the complexation at $\bar{n} \gtrsim 2$ is given by the species $H_{-5}Al(H_2L)_2^{2-}$ and $H_{-6}Al(H_2L)_2^{3-}$.

The result of the final calculation, performed on the whole data, is given in Table 1. This calculation ended at $\sigma(H)=0.04$ mM indicating a good fit to experimental data.

In order to visualize the amounts of the different species, we have used the computer program SOLGASWATER[16] equipped with plotting procedures, to calculate some distribution diagrams. These are presented in Fig. 3.

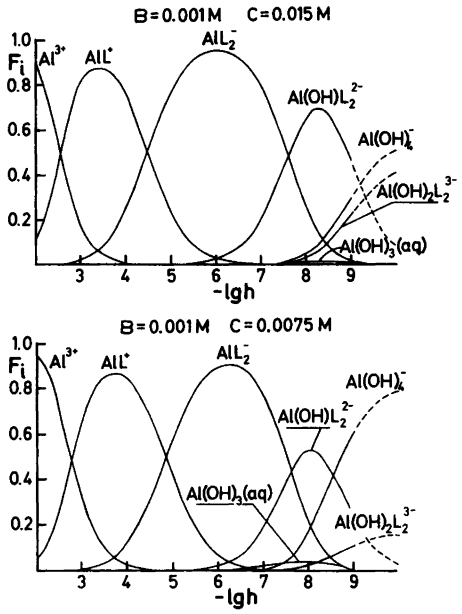

Fig. 3. Distribution diagrams $F_i(\lg h)_{B,C}$-F_i is defined as the ratio between aluminium(III) in a species and total alumimium(III). The calculations have been performed using the computer program SOLGASWATER with constants given in Table 1.

DISCUSSION

The present investigation gives evidence for the formation of four mononuclear aluminium-salicylate complexes. Of these, we believe that the two species occurring at low $-\lg h$ $(-2,1,1)^+$and $(-4,1,2)^-$, are chelates where the carboxylate and the phenolic group in salicylic acid coordinate to Al^{3+} and that these complexes actually could be written AlL^+ and AlL_2^-, respectively. Concerning the two hydrolyzed species, $(-5,1,2)^{2-}$ and $(-6,1,2)^{3-}$, we are of the opinion that these should be written $Al(OH)L_2^{2-}$ and $Al(OH)_2L_2^{3-}$, thus being hydrolysis products of the hexacoordinated species AlL_2^-, *i.e.* $Al(H_2O)_2L_2^-$. The acidity constants of $Al(H_2O)_2L_2^-$, expressed as pk_a-values, are equal to 7.60 and 9.32. Corresponding values for the first acidity constant in the *o*-diphenol systems pyrocatechol[17] and 1,2-dihydroxynaphthalene-4-sulfonate[6] are 8.01 and 8.04, respectively. These values are significantly higher and it seems as if the carboxylate group in the salicylate ion has caused an increase in the acidity of coordinated

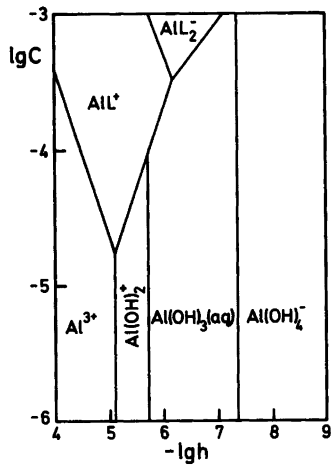

Fig. 4. Diagram showing predominating Al-species. In the calculations kaolinite was equilibrated with solutions of different compositions. The dissolution of kaolinite also yields small amounts of gibbsite, $Al(OH)_3$. Formation constants for kaolinite, amorphous SiO_2 and gibbsite are according to Helgeson.[18]

water molecules. This is probably due to the higher electron demand within a carboxylate group compared with a phenolic oxygen.

When our present results are compared with Havelková's,[9] we find a fair agreement in acidic solution (they reported lg $\beta_{-2,1,1}=-3.1$ and lg $\beta_{-4,1,2}=-8.8$) while, in neutral and alkaline solution, they propose the single complex AlL_3^{3-} with lg $\beta_{-6,1,3}=-18.3$. Probably, their data was too limited to permit a detailed and unbiased analysis in this area.

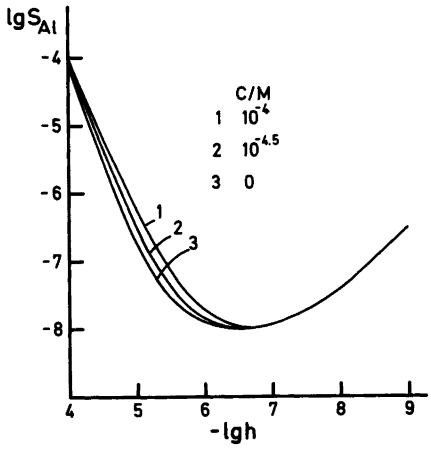

Fig. 5. The solubility of kaolinite, S_{Al}, with $C=0$, 30 and 100 μM, respectively.

In the evaluation of data in alkaline solution, we used an equilibrium constant for the aluminate ion which differs from the literature value by 0.24 logarithmic units. This constant was determined in Part 7[6] of our series. As appreciable amounts of $Al(OH)_4^-$ also form in this system (*cf.* Fig. 3) we found it valuable to covary the formation constants for $Al(OH)_4^-$ and $Al(OH)_2L_2^{3-}$. The constant values did not change significantly (lg $\beta_{-4,1,0}=-23.52\pm0.16$; lg $\beta_{-6,1,2}=-25.24\pm0.23$) but large standard deviations, due to the close connection between the species, were obtained. Thus, a confirmation of the modified stability constant for $Al(OH)_4^-$ was obtained.

The main purpose of our work is to evaluate the complexation ability of different types of ligands towards Si(IV) and Al(III). In an attempt to show the significance of different Al^{3+}-salicylates in a natural water, the clay-mineral kaolinite, $Al_2(OH)_4Si_2O_5$, was equilibrated with solutions of different salicylate contents. In Fig. 4, a predominance area diagram shows that AlL^+ and AlL_2^- both predominate in neutral and slightly acidic solutions. This implies that the solubility of kaolinite increases in the presence of salicylate ions. The magnitude of this increase is shown in Fig. 5 for different values of C. At -lg h 5 and 6

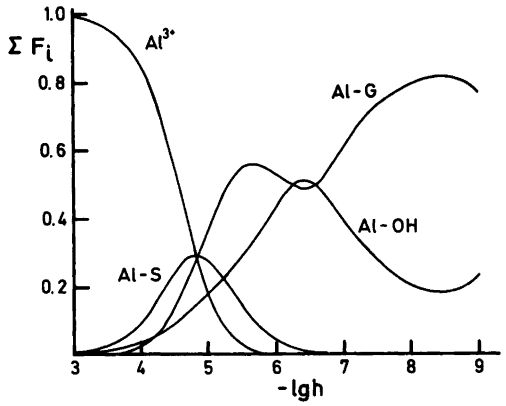

Fig. 6. Diagram showing the sum of distribution coefficients, ΣF_i, for Al-gallates (Al-G), Al-salicylates (Al-S), Al-hydrolysis (Al-OH) as well as $F_{Al^{3+}}$. The total concentration of gallic acid is equal to that for salicylic acid (30 μM) and kaolinite is the stable solid phase. Possible occurrence of mixed Al-S-G complexes have not been taken into consideration as no data for such species are known.

the solubility has increased by factors 1.8 and 1.1, respectively, (C=30 μM), while with $-\lg h \gtrsim 6.5$ there is no increase. In order to compare the stability of the complexes formed in this system with the Al^{3+}–*o*-diphenolic complexes, we performed a model calculation where kaolinite was equilibrated with equal amounts of salicylic acid and gallic acid. The result of this calculation (Fig. 6) is that, except for the most acidic solutions, the Al^{3+}–*o*-diphenolic complexes dominate largely. In fact, in order to obtain equal amounts of Al-gallate and Al-salicylate complexes at $-\lg h$=6, the amount of salicylic acid has to be 8 times larger than the amount of gallic acid. Although actual values of the concentrations of these ligands in natural waters have not been determined, it is most likely that the *o*-diphenols are of at least the same importance as the 2-hydroxy-benzoic acid derivatives in discussing speciation and concentration of dissolved aluminium in a natural water. To compare the phenolic and carboxylate binding sites in a completely fair manner, emf investigations of the systems Al^{3+}–OH^-–1,2-dihydroxybenzene (pyrocatechol) and Al^{3+}–OH^-–benzene-1,2-dicarboxylic acid (phthalic acid) are now in progress.

Acknowledgements. We thank Professor Nils Ingri for much valuable advice, for his great interest, and for all the facilities placed at our disposal. Thanks are also due to Lab.ass. Yvonne Hägglund for valuable help with the experimental part of the potentiometric measurements. The English of the present paper has been corrected by Professor Surendra Saxena. The work forms part of a program financially supported by the Swedish Natural Science Research Council.

REFERENCES

1. Sjöberg, S., Nordin, A. and Ingri, N. *Mar. Chem. 10* (1981) 521.
2. Sjöberg, S., Hägglund, Y., Nordin, A. and Ingri, N. *Mar. Chem. 13*(1983) 35.
3. Öhman, L.-O. and Sjöberg, S. *Acta Chem. Scand. A 35* (1981) 201.
4. Öhman, L.-O. and Forsling, W. *Acta Chem. Scand. A 35* (1981) 795.
5. Öhman, L.-O. and Sjöberg, S. *Acta Chem. Scand. A 36* (1982) 47.
6. Öhman, L.-O., Sjöberg, S. and Ingri, N. *Acta Chem. Scand. A 37* (1983) 561.
7. Sillén, L.G. and Martell, A. E. *Stability Constants of Metal-ion Complexes,* Spec. Publ. 17 and 25, The Chemical Society, London 1964 and 1971.
8. Perrin, D. D. *Stability Constants of Metal-ion Complexes: Part B. Organic Ligands* Pergamon, Oxford 1979.
9. Havelková, L. and Bartušek, M. *Collect Czech. Chem. 34* (1969) 3722.
10. Ingri, N. and Sillén, L. G. *Ark. Kemi 23* (1964) 97.
11. Arnek, R., Sillén, L. G. and Wahlberg, O. *Ark. Kemi 31* (1969) 353.
12. Brauner, P., Sillén, L. G. and Whiteker, R. *Ark. Kemi 31* (1969) 365.
13. Sillén, L. G. *Acta Chem. Scand. 16* (1962) 159.
14. Sillén, L. G. and Warnqvist, B. *Ark. Kemi 31* (1969) 341.
15. Lee, Y.-H. and Lundgren, G. *Coordination Chemistry in Solution. Trans. R. Inst. Technol., (1972)* No. 267.
16. Eriksson, G. *Anal. Chim. Acta 112* (1979) 375.
17. Öhman, L.-O. and Sjöberg, S. *Polyhedron. In press.*
18. Helgeson, H. C. *Am. J. Sci. 266* (1969) 729.

Received March 22, 1983.

Acta Chemica Scandinavica A 37 (1983) 881–890

Metal Ammine Formation in Solution. XXIV. The Copper(II)– and Some Other Metal(II)–Mono- and Diethanolamine Systems

PREDRAG DJURDJEVIC* and JANNIK BJERRUM

Department I, Inorganic Chemistry, H.C. Ørsted Institute, University of Copenhagen, DK-2100 Copenhagen Ø, Denmark

This paper reports a potentiometric and spectrophotometric study of the copper(II)–mono- and diethanolamine systems. Stability constants in these systems and in the zinc(II), cadmium(II) and cobalt(II) systems were determined in 0.5 and 2 M amHClO$_4$ at 25 °C (see Table 3). The amine complex formation was disturbed by hydrolysis in the copper(II) systems, but only to a negligible extent in 2 M amHClO$_4$. The consecutive stability constants in this medium for the copper(II)–monoethanolamine system were found to be: $K_1=10^{4.90}$, $K_2=10^{3.95}$, $K_3=10^{2.85}$, $K_4=10^{1.03}$, and for the copper(II)–diethanolamine system: $K_1=10^{4.74}$, $K_2=10^{3.90}$, $K_3=10^{1.66}$. It was also possible to calculate the acidity constants for the copper(II) complexes from data on media with varying ethanolammonium concentrations in 0.5 M (amH,Na)ClO$_4$. For the acidity constants of the first three Cu(II)–monoethanolamine complexes the values: $K_{1,a}=10^{-6.2}$, $K_{2,a}=10^{-6.8}$ and $K_{3,a}=10^{-7.5}$ were estimated and similar values were obtained for the first two Cu(II)–diethanolamine complexes: $K_{1,a}=10^{-6.2}$, $K_{2,a}=10^{-6.8}$. Polymerization reactions play only a minor role in these systems. It was shown by spectrophotometric measurements that $Cu(mea)_4^{2+}$ is transformed into a penta-amine complex at very high monoethanolamine concentrations. For the diethanolamine complexes it was shown that $Cu(dea)_3^{2+}$ is the dominating complex for [dea]$\gtrsim$1 M and up to the highest attainable amine concentrations.

Copper(II) and other metal(II) complexes of mono-, di- and triethanolamine (in the following abbreviated to mea, dea and tea) have been known since 1932[1] and have been studied in solid state by IR spectroscopic methods.[2–4] The composition and stability of the complexes in solution has been investigated by polarographic,[5–8] potentiometric and spectrophotometric methods.[9–22] These studies have shown that simple monodentate metalamine complex formation is dominant in aqueous ethanolammonium solutions but for copper(II) the solutions are subject to hydrolysis at pH-values higher than 5. The formation of the hydroxo complexes is accompanied to greater or lesser extent by polymerization.[20,21] The tendency of the alcohol groups of the ethanolamines to release protons followed by chelating coordination of the ethoxide groups, is not very pronounced in aqueous solutions.[19]

Comprehensive studies of the copper(II)– and nickel(II)–triethanolamine systems have been made previously,[20,21] and the present paper reports similar studies on copper(II) and some other metal(II)–mono and diethanolamine systems.

EXPERIMENTAL

Reagents and solutions. The metal(II) perchlorate reagents used were all of analytical grade. Monoethanolamine (Fluca, *puriss*) was distilled under atmospheric pressure and the main fraction boiling at 165 °C was used without further purification. Diethanolamine (Fluca, *puriss*) was distilled at ~10 mmHg and the main fraction boiling at 160–163 °C was used without further purification. The various solutions were prepared in volumetric flasks by weighing or pipetting from analyzed stock solutions. 2.50 M stock solutions

* On leave from Department of Chemistry, Svetozar Marković University, Radoja Domanovića 12, 34000 Kragujevac, Yugoslavia.

0302-4377/83 $2.50

Table 1. Selected results of glass electrode measurements on copper(II)-, cobalt(II)-, zinc(II)- and cadmium(II)-monoethanolamine solutions at 25 °C.
pK_{meaH^+}=9.54±0.01 in 0.5 M (meaH, Na)ClO_4, and 9.80±0.01 in 2 M meaHClO_4.

No.	C_{meaH^+}	C_{Cu}	C_{mea}	pH	p[mea]	$\bar{n}_{exp}$	$\bar{n}_{calc.(I)}$	$\bar{n}_{calc.(II)}$
1	2.00	0.04036	0.01546	4.322	5.178	0.384		
2	2.00	0.04036	0.0551	5.446	4.054	1.363		
3	2.00	0.004036	0.00561	5.381	4.119	1.373		
4	2.00	0.004036	0.01356	6.958	2.542	2.651		
5	2.00	0.02018	0.0573	7.049	2.451	2.666		
6	2.00	0.02018	0.0970	8.000	1.500	3.241		
7	0.500	0.02018	0.00767	4.950	4.890	0.380		
8	0.500	0.02018	0.0276	5.896	3.944	1.363	1.424	1.373
9	0.500	0.02018	0.0324	6.082	3.752	1.596	1.626	1.585
10	0.500	0.02018	0.0374	6.291	3.549	1.838	1.823	1.809
11	0.500	0.004036	0.00950	6.654	3.186	2.193	2.146	2.170
12	0.500	0.02018	0.0572	7.240	2.600	2.711	2.798	2.691
13	0.500	0.004036	0.01940	7.665	2.175	3.147	3.220	3.012
		C_{Co}						
14	2.00	0.0344	0.00794	6.441	3.059	0.205		
15	2.00	0.0344	0.01985	6.907	2.593	0.503		
16	2.00	0.0344	0.0397	7.319	2.181	0.963		
17	0.500	0.0344	0.00992	7.071	2.769	0.239		
18	0.500	0.0344	0.01985	7.399	2.441	0.472		
19	0.500	0.0344	0.0397	7.735	2.105	0.926		
		C_{Zn}						
20	2.00	0.01552	0.00397	6.173	3.327	0.226		
21	2.00	0.0621	0.0278	6.410	3.090	0.435		
22	2.00	0.01552	0.00794	6.517	2.983	0.445		
23	0.500	0.01550	0.00397	6.671	3.169	0.213		
24	0.500	0.01550	0.00595	6.843	2.997	0.319		
25	0.500	0.003104	0.00238	6.928	2.912	0.374		
		C_{Cd}						
26	2.00	0.00401	0.001985	6.356	3.144	0.316		
27	2.00	0.00401	0.00397	6.724	2.776	0.572		
28	2.00	0.02004	0.0397	7.408	2.092	1.577		
29	2.00	0.02004	0.0992	8.200	1.300	2.449		

of ethanolammonium perchlorate were prepared by neutralizing 1 l of 5.00 M $HClO_4$ with the amine and diluting to a volume of 2 l. Complete equivalence between amine and perchloric acid was ensured as described previously.[24]

Spectrophotometric measurements (UV and Vis) were made with a Cary 118 spectrophotometer at room temperature (22–23 °C). Cells of path-length 0.1 to 2 cm were used, the reference cells being filled with a corresponding metal(II)-free solution.

pH=$-\log[H^+]$ was determined by glass electrode measurements at 25 °C as described previously.[24]

Estimation of the stability constants. The exponent of the free amine concentration p[am] and ligand number

$$\bar{n}=(C_{am}-[am]+[H^+])/C_{Me}$$

were determined from pH-measurements at constant ethanolammonium ion concentrations in the usual manner.[25] The acidity constants of the ethanolammonium ions pK_{amH^+} were also determined. Part of the data is shown in Tables 1 and 2. All concentrations are in mol/l, and C_X represents the stoichiometric concentrations of the species X. The formation curves for 0.5 M (amH,Na)ClO_4 and 2 M amHClO_4 media are

Table 2. Selected results of glass electrode measurements on copper(II)-, cobalt(II)-, zinc(II)- and cadmium(II)-diethanolamine solutions at 25 °C.
pK_{deaH^+}=8.93±0.01 in 0.5 M (deaH,Na)ClO_4, and 9.33±0.01 in 2 M deaHClO_4.

No.	C_{deaH^+}	C_{Cu}	C_{dea}	pH	p[dea]	$\bar{n}_{exp}$	$\bar{n}_{calc.(I)}$	$\bar{n}_{calc.(II)}$
1	2.00	0.02018	0.00593	3.886	5.144	0.325		
2	2.00	0.01998	0.01304	4.377	4.653	0.654		
3	2.00	0.004036	0.00416	4.706	4.324	1.023		
4	2.00	0.02018	0.0302	5.243	3.787	1.487		
5	2.00	0.004036	0.00630	5.289	3.741	1.519		
6	2.00	0.02015	0.04094	6.223	2.807	1.955		
7	2.00	0.02018	0.05165	6.887	2.143	2.203		
8	2.00	0.02018	0.0838	7.523	1.507	2.611		
9	0.500	0.02018	0.01866	5.294	3.936	0.922	0.913	0.905
10	0.500	0.02076	0.01866	5.266	3.964	0.896	0.881	0.874
11	0.500	0.02077	0.02804	5.640	3.590	1.338	1.305	1.295
12	0.500	0.02075	0.03210	5.803	3.427	1.528	1.482	1.472
13	0.500	0.02044	0.04038	6.245	2.985	1.923	1.931	1.903
14	0.100	0.004036	0.00275	5.672	4.268	0.669	0.691	0.650
15	0.100	0.004036	0.00328	5.880	4.060	0.925	0.969	0.936
16	0.100	0.004036	0.004895	6.062	3.878	1.179	1.233	1.187
17	0.100	0.02053	0.04060	6.656	3.284	1.953	1.940	1.916
		C_{Co}						
18	2.00	0.0344	0.00429	5.828	3.202	0.106		
19	2.00	0.0344	0.0129	6.364	2.666	0.312		
20	2.00	0.0344	0.0429	7.111	1.919	0.895		
21	0.500	0.0344	0.0150	6.686	2.344	0.304		
22	0.500	0.0344	0.0322	7.082	1.948	0.608		
		C_{Zn}						
23	2.00	0.0155	0.00429	5.875	3.155	0.232		
24	2.00	0.0155	0.00858	6.238	2.792	0.453		
25	0.500	0.0155	0.00858	6.728	2.502	0.350		
		C_{Cd}						
26	2.00	0.02004	0.01290	6.351	2.679	0.539		
27	2.00	0.02004	0.0429	7.138	1.892	1.501		
28	2.00	0.02004	0.0858	7.685	1.345	2.027		
29	0.500	0.02004	0.01290	6.833	2.397	0.444		
30	0.500	0.02004	0.0417	7.484	1.746	1.185		
31	0.500	0.02004	0.1250	8.177	1.053	1.821		

shown in Figs. 1 and 2. The formation curves for the nickel(II) systems taken from our previous paper[22] are also plotted. The data and figures show that the formation curves are unchanged for a 5–10-fold variation in the metal(II) concentration within the experimental uncertainty. The formation curves for 0.5 M (amH,Na)ClO_4 medium are also, with the exception of those for copper(II), unaltered by a change in the ethanolammonium ion concentration. From these results it follows that only mononuclear metal-amine complex formation takes place in the solutions. Furthermore, the dependence of the ethanolammonium concentrations show that hydrolysis interferes with metal amine complex formation in the copper(II) solutions. The hydrolysis is negligible in 2 M amHClO_4 and the stability constants in this medium could therefore be calculated in the same way as for the other metal(II) ions. The estimated stability constants are given in Table 3, and the calculated full curves in Figs. 1 and 2 show how well these constants reproduce the experimental data. Stability constants for the metal(II) ethanolammine complexes mentioned

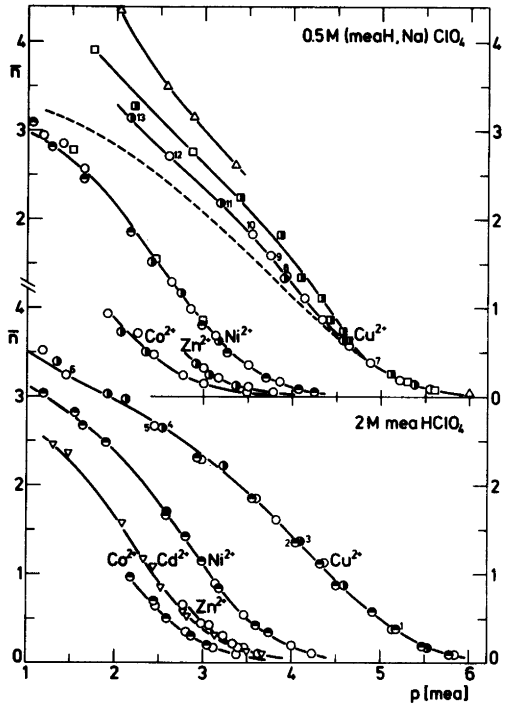

Fig. 1. Formation curves ($\bar{n}$ *versus* p[mea]) at 25 °C for copper(II)–and the other metal(II)–monoethanolamine complexes studied in this paper. For comparison purposes the formation curves for nickel(II) taken from a previous paper[22] are also shown. The different points in 0.50 M meaHClO$_4$ and 2.00 M meaHClO$_4$ at the particular metal concentration are as follows: ◓ (C_{Me}~0.04 M), ○ (C_{Me}~0.02 M), ◑ (C_{Me}~0.004 M) and for cadmium ▽ (C_{Cd}~0.02 M) to distinguish from the zinc points. The points in the 0.50 M (meaH,Na)ClO$_4$ solutions with C_{meaH^+}=0.10 M are denoted: □(C_{Me}~0.02 M), ◨ (C_{Me}~0.004 M) and in the solutions with C_{meaH^+}=0.02 M; △ (C_{Cu}~0.02 M). The solid formation curves are calculated by means of the estimated stability constants. The points numbered 1–13 on the copper curves refer to the solutions described in Table 1. The dotted curve for copper(II) in 0.5 M meaHClO$_4$ is that estimated for the pure copper(II)-amine complex formation in this medium.

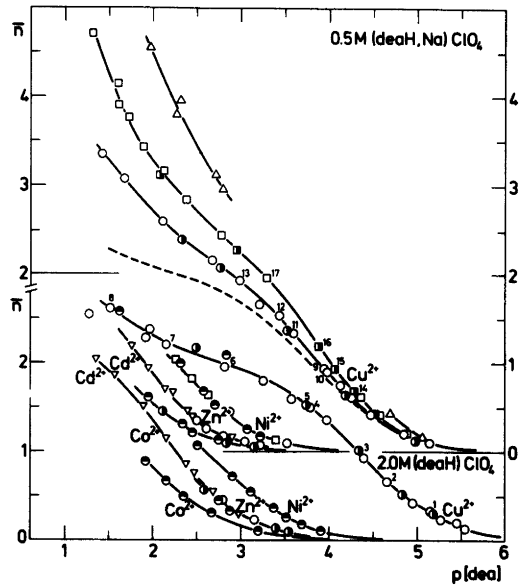

Fig. 2. Formation curves ($\bar{n}$ *versus* p[dea]) at 25 °C for copper(II)– and the other metal(II)–diethanolamine complexes studied in this work. For comparison purposes the formation curves for nickel(II) from a preceding paper[22] are also shown. The plotted points in the figure and all other symbols are the same as those in the legend for Fig. 1. The points numbered 1–17 on the copper curves refer to the solutions described in Table 2.

in Table 3 have also been estimated by other authors[5–8,12–18] and most of these values can be found in Tables of Stability Constants.[23] Some of the data in the literature are not very reliable.

Table 3 shows that pK_{amH^+} and log K_n increases when the salt concentration is changed from 0.5 to 2 M. The influence of the salt concentration increases from the nickel(II) mea to the tea systems,[22] and is higher in the copper(II)- than in the other metal(II) systems. It seems to be a general rule[25] that the consecutive constants in a metal amine complex system change uniformly with the salt medium when hydrolysis is insignificant. It will be seen that the data in Table 3 are reasonably consistent with this rule. In the copper(II) mono- and diethanolamine systems the influence of hydrolysis can be neglected, not only in 2 M amHClO$_4$ but also for the first of the constants in 0.5 amHClO$_4$. The rule can therefore be used to estimate the subsequent constants in 0.5 M amHClO$_4$ (those in brackets). The copper(II) formation curve corrected for hydrolysis is plotted in Figs. 1 and 2.

The hydroxyl groups in the ethanolamines cause a considerable steric effect; the larger values of the ratios between successive stability constants than in the corresponding ammonia systems[22,25] show this directly. The ethanol-

Table 3. Stability constants for ethanolamine and diethanolamine complexes of copper(II) and some other metal(II) ions in 0.5 and 2 M ethanolammonium solutions at 25 °C.

Ethanolamine		Copper(II)			Nickel(II)	
	0.5[a]	2 M[a]	0.5[b]	2 M[c]	0.5[d]	2 M[d]
pK_{meaH}	9.54	9.80	9.60		9.54	9.80
log K_1	4.60	4.90	4.53	4.78	3.12	3.32
log K_2	(3.65)	3.95	(3.75)	4.18	2.56	2.78
log K_3	(2.55)	2.85	–	2.89	1.80	2.00
log K_4	0.75	1.03	–	1.65	(0.32)	(0.40)
	Cobalt(II)		Zinc(II)		Cadmium(II)	
	0.5[a]	2 M[a]	0.5[a]	2 M[a]	0.5	2 M[a]
log K_1	2.23	2.43	2.50	2.70	–	2.65
log K_2	1.56	1.80	2.28	2.48	–	2.17
log K_3	–	–	–	–	–	1.40
Diethanolamine		Copper(II)			Nickel(II)	
	0.5[a]	2 M[a]	0.5[b]		0.5[d]	2 M[d]
pK_{deaH}	8.93	9.32	9.00		8.93	9.32
log K_1	4.20	4.74	4.15		2.60	3.00
log K_2	(3.35)	3.90	–		1.87	2.27
log K_3	(1.11)	1.66	–		–	–
	Cobalt(II)		Zinc(II)		Cadmium(II)	
	0.5[a]	2 M[a]	0.5[a]	2 M[a]	0.5[a]	2 M[a]
log K_1	1.88	2.24	2.13	2.52	2.10	2.47
log K_2	1.19	1.42	(1.40)	1.88	1.71	2.05
log K_3	–	–	–	–	–	0.78

[a] Values determined in this paper for 0.5 M (amH,Na)ClO_4 and 2 M amHClO_4. The uncertainties are of the order ±0.03. [b] Values estimated by Bjerrum and Refn[9] for 0.5 M amHNO_3. [c] Values for 2 M meaHNO_3 estimated in our department in 1968 by Dr. Hans Peter Jensen. [d] Values determined by Bjerrum and Djurdjevic[22] for 0.5 M (amH,Na)ClO_4 and 2 M amHClO_4.

amines coordinate to the metal through the nitrogen atom[26] and it is possible that part of the steric effect is due to a weak chelate coordination of the hydroxyl groups in competition with the solvated water molecules.

Estimation of hydrolysis constants. Confining ourselves to study the hydrolysis reactions at relatively high ethanolammonium ion concentrations it is reasonable to assume that the species $Cuam(OH)^+$, $Cuam_2(OH)^+$ and $Cuam_3(OH)^+$ are the dominating hydrolysis products. Defining the corresponding hydrolysis constants as follows:

$$K_{1,a}=[Cuam(OH)^+][H^+]/[Cuam^{2+}]$$

$$K_{2,a}=[Cuam_2(OH)^+][H^+]/[Cuam_2^{2+}]$$

$$K_{3,a}=[Cuam_3(OH)^+][H^+]/[Cuam_3^{2+}]$$

one can write for the average formation function:

$$\bar{n}=\sum_0^n n[Cuam_n]+2[Cuam(OH)]+3[Cuam_2(OH)]+4[Cuam_3(OH)]/\sum_0^n [Cuam_n]+[Cuam(OH)]+[Cuam_2(OH)]+[Cuam_3(OH)]$$

This expression can be transformed to an equation of the form:

$$a_1K_{1,a}+a_2K_{2,a}+a_3K_{3,a}=b \quad (1)$$

where

$$a_1=\{(2-\bar{n})\beta_1[am]\}/[H^+] \quad (2)$$

$$a_2=\{(3-\bar{n})\beta_2[am]^2\}/[H^+] \quad (3)$$

$$a_3=\{(4-\bar{n})\beta_3[am]^3\}/[H^+] \quad (4)$$

$$b=\bar{n}\sum_0^n \beta_n[mea]^n-\sum_0^n n\beta_n[mea]^n \quad (5)$$

and

$$\beta_n=K_1K_2\ldots K_n$$

This means that the problem of determining the hydrolysis constants is reduced to that of solving a set of linear equations with three unknowns. For the integer n a value of four has to be inserted in eqn. (5) for the monoethanolamine system and three for the diethanolamine system.

In other words the complexes $Cu(mea)_4^{2+}$ and $Cu(dea)_3^{2+}$ have been considered not to contribute to the hydrolysis. A small influence of the Cu(II)-aqua ion has also been neglected. The calculation of the hydrolysis constants in the 0.5 M (amH,Na)ClO_4 medium has been carried out with the estimated stability constants for this medium. The solutions 8–13 (see Table 1) and solutions 10–17 (Table 2) were used for this purpose. The points corresponding to these solutions in Figs. 1 and 2 are marked by figures. The sets of linear equations, eqn. (1), calculated from these data have been solved by the least squares method using a simple computer program. Sets I in Table 4 show the results of this calculation. In another calculation of the hydrolysis constants using a larger computer program the sum of the squares of the differences $\Sigma(\bar{n}_{calc}-\bar{n}_{obs})^2$ was minimized using Gauss-Newton algorithm.[27] For this calculation all data for the 0.5 M $amHClO_4$ media with values of $\bar{n}$ between 0.8 and 3.2 were used, as well as data for $[meaH^+]$=0.1 M in 0.5 M (meaH,Na)ClO_4. Sets II in Table 4 show the results of the calculation. Hydrolysis was so pronounced for $[amH^+]$=0.02 M that the data could not be used in the calculations. The values of $\bar{n}$ which can be calculated using the two sets of hydrolysis constants are compared in the last columns of Tables 1 and 2 with the experimental values. Both sets of constants approach the experimental data about equally well. When solving eqns. (1) it was assumed in the computer program that the uncertainty in b was 10 %. Recalculation with the constants obtained shows that the uncertainty is higher, being on average about 17 %. The uncertainty in the pK-values can be assumed to be of the order ±0.05–0.10.

In the mono- and diethanolamine systems polymerization of the hydrolysis products was found to be negligible in the range of copper concentrations employed. This is different from the behaviour in the triethanolamine system (*cf.* Table 4). In the latter system there is steric hindrance to the uptake of more than one amine ligand, but it is noteworthy that the values of $pK_{1,a}$ for the mono-, di- and triethanolamines are approximately the same. $pK_{2,a}$ for $Cu(mea)_2^{2+}$ and $Cu(dea)_2^{2+}$ are also similar. Table 4 also shows that the acidity of the complexes decreases with the number of coordinated amine molecules: $pK_{1,a}<pK_{2,a}<pK_{3,a}$. There is evidence that the copper(II) aqua-ammine ions are weaker acids than the copper(II) aqua ion.[25,28] The first hydrolysis product of these ions are more or less dimerized.[28] The aqua ion itself has pK_a~8 and log K_{ass}~5.1.[29,30] The fact that the copper(II) ethanolamine ions are more acidic than the copper(II) ammonia ions can be explained by a strong steric influence of the hydroxyl groups of the amino alcohols on the coordinated water molecules.

Table 4. Calculated acidity constants of the copper(II)-ethanolamine complexes in 0.5 M (amH,Na)ClO_4.

	Mea[a]		Dea[a]		Tea[b]
	I	II	I	II	Bjerrum *et al.*[20]
$pK_{1,a}$	6.09	6.40	6.29	6.35	6.41±0.05
$pK_{2,a}$	6.87	6.72	6.75	6.81	
$pK_{3,a}$	7.39	7.77			

[a] the uncertainties in the pK-values are estimated to be of the order ±0.05–0.10. [b] The first hydrolysis product $Cu(tea)(OH)^+$ is dimerized, with log K_{ass}=3.15±0.15.

Spectrophotometric results. Fig. 3 shows

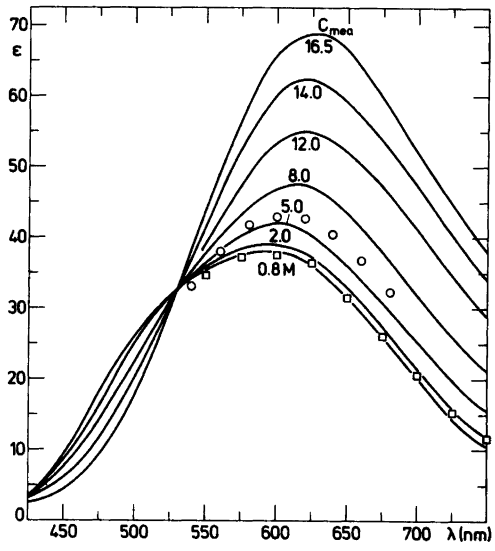

Fig. 3. Spectra (ε,λ) of aqueous copper(II)-monoethanolamine perchlorate solutions with C_{Cu}~0.01 M and C_{mea} varying from 0.8 M up to pure mea (99 %). The nearly constant absorption in the range with C_{mea} between 0.8 and 2 M approaches the spectrum of $Cu(mea)_4^{2+}$. The curves with increasing C_{mea} up to 16.5 M show the formation of $Cu(mea)_5^{2+}$. The □-points indicate the spectrum of a strongly alkaline solution with C_{NaOH}=2.0 M, and C_{mea}=2.0 M. The ○-points show similarly the spectrum of a solution with C_{mea}=8.0 M and C_{NaOH}=2.0 M.

absorption (ε,λ) curves in the visible region for Cu(II)–monoethanolamine solutions with C_{mea} varying from 0.8 M up to the pure amine. The spectrum is nearly unchanged for ethanolamine concentrations between 0.8 and 2 M. In this concentration range formation of the tetrakis(ethanolamine) species is nearly complete. This follows from the value for the fourth consecutive stability constant log $K_4 \sim 0.7$ and the formation curves given in Fig. 1. The solutions used for the spectrophotometric measurements were prepared without ethanolammonium salt, but this has only a slight influence on the spectra when [mea]>~1 M. Between 2 M and up to the pure ethanolamine the spectra are shifted towards the red with an isosbestic point at 530 nm. In the concentration range where the curves pass through the isosbestic point there exists an equilibrium between a tetrakis and a pentakis(ethanolamine) ion as in other copper(II)–amine systems.[28,31] The extent to which the wavelengths at the absorption maxima, assumed to be those of the tetra- and penta-amine ions, agree with those of the analogous copper(II)-ammonia complexes is shown in Table 5. Complexes with aliphatic amines have usually a higher intensity of the ligand field band than those of the corresponding ammonia complexes. It is therefore remarkable that ε_{max} of $Cu(mea)_4^{2+}$ is lower than that of $Cu(NH_3)_4^{2+}$ (see Table 5). The tetrammine copper(II)-ion contains at least one strongly coordinated water molecule.[28,34,35] This water molecule is perpendicular to the plane in the square pyramidal configuration and is responsible for the relatively high intensity of the absorption band.[37,38] It is therefore reasonable to assume that steric strain due to the hydroxyl groups in $Cu(mea)_4^{2+}$ weakens the bonding of the water molecule (as well as of the fifth amine ligand in $Cu(mea)_5^{2+}$), which explains the weak intensity of the absorption bands of these complexes.

Table 5. Comparison of absorption maxima for copper(II)-amine complexes.

Complex	λ(nm)	ε_{max}	
$CuNH_3^{2+}$	745	22	Ref. 33
$Cudea^{2+}$	750	30	estim.
$Cutea^{2+}$	755	32	Ref. 20
$Cu(NH_3)_3^{2+}$	635	41	Refs. 32, 33
$Cu(dea)_3^{2+}$	625	52	[dea]>1M
$Cu(NH_3)_4^{2+}$	590	53	Refs. 32, 33
$Cu(CH_3NH_2)_4^{2+}$	580	85	Ref. 31
$Cu(mea)_4^{2+}$	589	39	[mea]=2 M
$Cu(NH_3)_5^{2+}$	640	83	Refs. 32, 33
$Cu(CH_3NH_2)_5^{2+}$	640	124	Ref. 31
$Cu(mea_5)^{2+}$	630	61	99 % mea

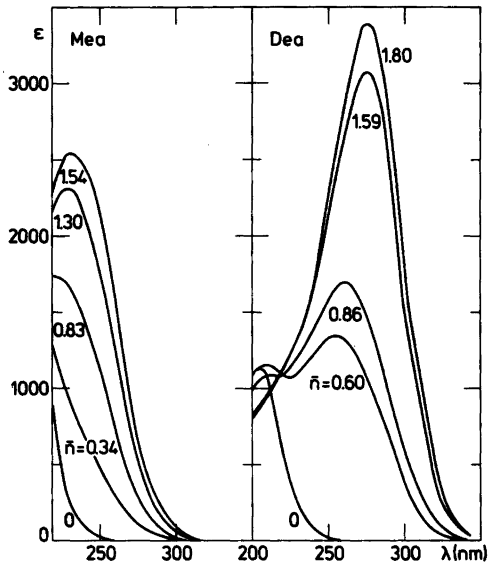

Fig. 4. The UV (ε,λ) spectra of some Cu(II)-mono- and diethanolamine solutions in 2 M am$HClO_4$. The figures on the curves indicate the values of the ligand number $\bar{n}$ of the solutions examined.

The influence of hydroxide ions on the tetra- and penta-amine equilibrium are shown in Fig. 3. As in the ammonia[28] and methylamine[31] systems the penta-amine complex shows some tendency to exchange the fifth amine ligand with a hydroxide ion with formation of $Cuam_4(OH)^+$. In the systems studied until now[28,31] the hydroxotetra-amine ions have a somewhat weaker absorption band which is slightly more shifted towards the red than the corresponding tetrammine ion. However, in our case the results in Fig. 3 are not sufficient to a quantitative treatment.

The UV (ε,λ) absorption spectra of some Cu(II)-mea and Cu(II)-dea solutions with 2 M am$HClO_4$ are shown in Fig. 4. The ligand number varies from 0 to 1.54 in the mea solutions and from 0 to 1.80 in the dea solutions. Since they are electron transfer spectra they have ε_{max}-values of several thousand. As in the analogous Cu(II)-tea system,[20] the absorption band increases in intensity and is shifted towards the visible with increasing ligand number. The UV absorption is practically negligible at wavelengths above ~320 nm in the mea system and ~360 nm in the dea system. It was therefore possible with

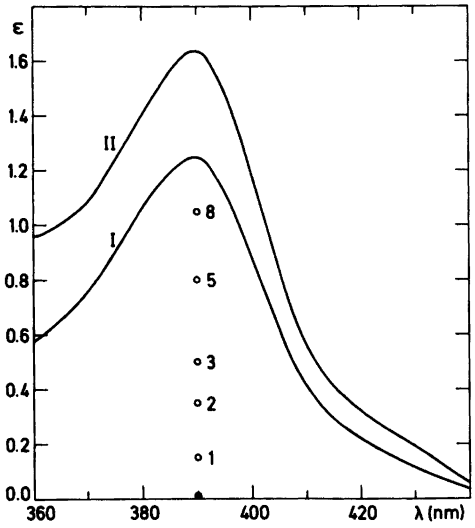

Fig. 5. Formation of a small absorption band at 390 nm in two solutions of the following composition:

	$_{deaHClO_4}$	C_{Cu}	C_{dea}	p[dea]	$\bar{n}$
I	2.00	0.02018	0.00379	5.441	0.200
II	2.00	0.02018	0.00593	5.144	0.325

Curve I and II show the final spectra of the solutions after more than 10 d. The absorption of solution I was followed with time after its preparation.

Time in d	0	1	2	3	5	8
ε_{max} at 490 nm	0.01	0.16	0.35	0.50	0.80	1.05

These data are plotted in the figure.

the Cu(II)–dea system to detect a very weak absorption band at 390 nm. The band is not seen with freshly prepared solutions, but develops during the following days (*cf.* Fig. 5). Similar weak bands in Cu(II)-ammonia solutions at 317 nm[28] and in Cu(II)-methylamine solutions at 328 nm[31] have shown to be caused by the formation of small amounts of di-μ-hydroxo complexes. However, the position of the band at 390 nm and especially the slowness of its formation suggest that other explanations must also be considered. The formation of the band is not accompanied by any change in pH and has therefore no disturbing influence on the calculations we have made for these solutions.

The (ε,λ) spectra of aqueous copper(II)-dea solutions at high amine concentrations are shown in Fig. 6. The only very slight changes in the spectra show that the same complex dominates in the entire range of concentrations from [dea]~1 M and up to the pure amine. The value of the third consecutive stability constant (log K_3~1.11) as well as the formation curves in Fig. 2 show that this complex is the tris(diethanolamine) complex. The observation of the absorption maxima at ~625 nm ($Cu(NH_3)_3^{2+}$ shows λ_{max}~635 nm) supports this assumption (*cf.* Table 5). The values of λ_{max} for the three mono-amine complexes $Cu(NH_3)^{2+}$, $Cudea^{2+}$ and $Cutea^{2+}$ at ~750 nm, are also shown in Table 5 and provide further evidence that λ_{max} is determined mainly by the number of copper-nitrogen bonds in the complex.

As a result of our studies on the copper(II)-ethanolamines it can be concluded that the steric influence of the hydroxyl group in the monoethanolamine is not greater than it is possible for the Cu(II) ion to coordinate the amino groups of four ligands with a considerable strength and even to form a penta-amine complex at very high ethanolamine concentrations. On the other hand, in the copper(II)-diethanolamine system the steric effect of the hydroxyl groups is so great that the Cu(II) ion is unable to coordinate the amino groups of more than three ligands. Finally, in the copper(II) triethanolamine system the steric influence of the ligand is so great that the mono complex shows greater tendency towards uptake of hydroxide ions and deprotonation of the ligand, followed by chelation, than towards binding a second triethanolamine molecule.

Acknowledgements. The authors thank Morten Jannik Bjerrum for carrying out part of the computer calculations, Professor C.K. Jørgensen, Geneva, for fruitful discussions, and Dr. Martin Hancock for correcting the English manuscript.

REFERENCES

1. Hein, F. and Beerstecher W. *Z. Anorg. Allg. Chem. 282* (1955) 93 and references therein.
2. Hughes, M. N. and Rutt, K. J. *J. Chem. Soc. A* (1968) 2788.
3. Cody, J. A., Woodburn, S. J., Blackmore, M. W. and Magee, R. J. *J. Inorg. Nucl. Chem. 32* (1970) 3263.
4. Brannon, D. G., Morrison, R. H., Hall, J. L., Humphrey, G. L. and Zimmerman, D. N. *J. Inorg. Nucl. Chem. 33* (1971) 981.
5. Flannery, R. J., Ke, B., Grieb, M. W. and Trivich, J. *J. Am. Chem. Soc. 77* (1955) 2996.

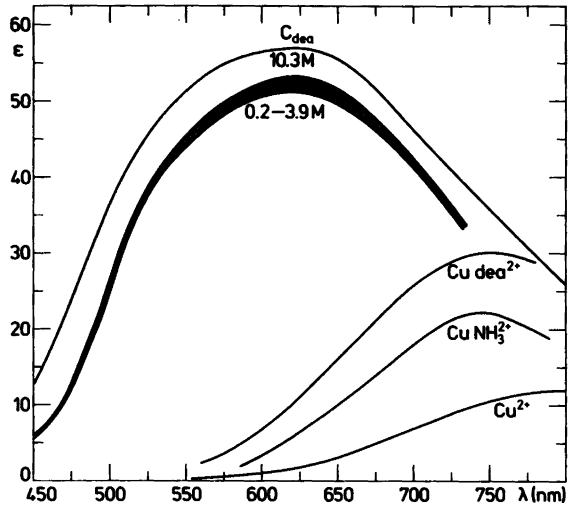

Fig. 6. Spectra (ε,λ) of aqueous copper(II)-diethanolamine solutions at high amine concentrations. Four curves with C_{Cu}~0.01 M and [dea]=0.19, 0.46, 1.44, and 3.85 M are situated close to each other within the hatched area in the figure. In these solutions the dominating complex is $Cu(dea)_3^{2+}$ and further increase of the amine concentration up to 10.3 M (99 % amine) causes only a slight change in the spectra. In the lower part of Fig. 6 the monoamine spectrum of $Cu(dea)^{2+}$ in 2 M deaHClO$_4$ is compared with those of $Cu(NH_3)^{2+}$ in 2 M NH_4NO_3[33] and of $Cu(tea)^{2+}$ in 2 M teaHClO$_4$.[20]

6. Subrahmayna, R. S. *Proc. Indian Acad. Sci. 46* (1957) 377.
7. Migal, P. K. and Pushnyak, A. N. *Russ. J. Inorg. Chem. 4* (1959) 601; Ibid. *5* (1960) 293.
8. Fisher, J. F. and Hall, J. L. *Anal. Chem. 34* (1962) 1094; Ibid. *39* (1967) 1550.
9. Bjerrum, J. and Refn, S. *Proc. 6th Nordiska Kemistmöte,* Lund 1947, p. 227.
10. Bolling, J. M. and Hall, J. L. *J. Am. Chem. Soc. 75* (1953) 3953.
11. Ojima, H. and Sone, K. *Z. Anorg. Allg. Chem. 309* (1961) 110.
12. Gibaud, M. *Compt. Rend. 244* (1957) 1930.
13. Cockerell, L. and Walton, H. F. *J. Phys. Chem. 66* (1962) 75.
14. Mahapatra, S. and Subrahmayna, R. S. *Proc. Indian Acad. Sci. 58* (1963) 161; Ibid. *59* (1964) 299.
15. Douheret, G. *Bull. Soc. Chim. Fr.* (1965) 2915.
16. Sklenskaya, E. V. and Karapet'-yants, M. Kh. *Russ. J. Inorg. Chem. 11* (1966) 1478.
17. Davies, C. W. and Patel, B. N. *J. Chem. Soc. A* (1968) 1824.
18. Gorbachev, S. V., Marchenkova, T. G. and Timofeeva, E. G. *Koord. Khim. 3* (1977) 802.
19. Jensen, H. P. *Acta Chem. Scand. 25* (1971) 1753.
20. Bjerrum, J., Agarwala, B. V. and Refn, S. *Acta Chem. Scand. A 35* (1981) 685.
21. Agarwala, B. V. and Bjerrum, J. *Acta Chem. Scand. A 36* (1982) 459.
22. Bjerrum, J. and Djurdjevic, P. *J. Indian Chem. Soc. 59* (1982) 1229.
23. Sillèn, L. G. and Martell, A. E. *Stability Constants, Chem. Soc. Spec. Publ. 17* (1964) and Suppl. *25* (1970).
24. Ilcheva, L. and Bjerrum, J. *Acta Chem. Scand. A 30* (1976) 343.
25. Bjerrum, J. *Metal Ammine Formation in Aqueous Solution,* P. Haase and Son, Copenhagen 1941, reprinted 1957.
26. Nielsen, K., Grønbæk Hazell, R. and Rasmussen, S. E. *Acta Chem. Scand. 26* (1972) 889.
27. Draper, N. R. and Smith, H. *Applied Regression Analysis,* Wiley-Interscience, New York 1966.
28. Bjerrum, J. and Agarwala, B. V. *Acta Chem. Scand. A 34* (1980) 475.
29. Pedersen, K. *J. Dan. Vidensk. Selsk., Mat-Fys. Medd. 20* (1943) No. 7.
30. Berecki-Biedermann, C. *Arkiv Kemi 9* (1956) 175.

31. Agarwala, B. V., Ilcheva, L. and Bjerrum, J. *Acta Chem. Scand. A 34* (1980) 725.
32. Bjerrum, J. *K. Dan. Vidensk. Selsk., Mat-Fys. Medd. 11* (1932) No. 10.
33. Bjerrum, J., Ballhausen, C. J. and Jörgensen, C. K. *Acta Chem. Scand. 8* (1954) 1275.
34. Schneider, W. and Baccini. P. *Helv. Chim. Acta 52* (1969) 1955.
35. Romano, V. and Bjerrum, J. *Acta Chem. Scand. 24* (1970) 1551.
36. Yamagucki, T. and Ohtaki, H. *Bull. Chem. Soc. Jpn. 52* (1979) 415.
37. Jörgensen, C. K. *Biochemistry of Copper,* Academic, London 1966.
38. Jörgensen, C. K. *Top. Curr. Chem. 56* (1975) 1.

Received March 23, 1983.

Acta Chemica Scandinavica A 37 (1983) 891–895

Benzotriazole Complexes. IV. The Crystal Structure of Bis(benzotriazole)silver(I) Nitrate

INGER SØTOFTE and KURT NIELSEN

Structural Chemistry Group, Chemistry Department B, DTH 301,
The Technical University of Denmark, DK-2800 Lyngby, Denmark

The crystal structure of the title compound, $[Ag(C_6H_5N_3)_2]NO_3$, has been investigated by X-ray diffraction techniques. The crystals are triclinic, space group $P\bar{1}$, with $a=10.048(2)$ Å, $b=10.311(3)$ Å, $c=14.817(1)$ Å, $\alpha=98.44(2)°$, $\beta=107.23(2)°$ and $\gamma=91.15(3)°$. The final R was 0.025. The structure consists of two crystallographically independent $Ag(C_6H_5N_3)_2^+$ ions and two independent NO_3^- ions. Each silver atom is coordinated to two nitrogen atoms, and the average Ag–N distances within the two ions are 2.149(3) Å and 2.196(10) Å. The corresponding N–Ag–N angles are 158.4(1) and 151.3(1)°. The coordination to silver has only a small effect on the geometry of the benzotriazole group. The packing of the structure may be described by layers of $Ag(C_6H_5N_3)_2^+$ ions separated by layers of NO_3^- ions. The shortest Ag–O distances are 2.630(3) Å and 2.679(3) Å. The distances to the next-nearest neighbours of Ag2 are Ag2–N2 of 2.469(3) Å and Ag2–O of 2.752(3) Å. The shortest Ag–Ag distance is 3.763(1) Å, found between Ag atoms related by a center of symmetry.

The present structure analysis is part of an investigation of benzotriazole complexes.[1–3] Benzotriazole is henceforth referred to as BTAH.

EXPERIMENTAL

Colourless crystals of $Ag(BTAH)_2NO_3$ were precipitated by mixing $4 \cdot 10^{-4}$ mol silver nitrate in 5 ml of 7 M ammonia with $3 \cdot 10^{-3}$ mol benzotriazole in 20 ml of 5 M nitric acid. Besides the title compound, triclinic crystals of another compound were precipitated, but since the crystals were of very poor quality, they have not been further investigated. Determination of the possible space groups and the data collection were carried out as described in Ref. 1. The dimensions of the crystal were 0.55×0.20×0.19 mm. The structure was solved by the Patterson technique.[4] The refinement technique and the references to atomic scattering factors are those given in Ref. 1. Crystal data and R-values are listed in Table 1. The final positional parameters with estimated standard deviations are listed in Table 2. The labelling of the atoms in the

Table 1. Crystal data.

M	408.1
μ(Mo$K\alpha$)(cm^{-1})	14.0
Crystal system	triclinic
V(Å^3)	1447.1
a (Å)	10.048(2)
b (Å)	10.311(3)
c (Å)	14.817(1)
α (°)	98.44(2)
β (°)	107.23(2)
γ (°)	91.15(3)
Space group	$P\bar{1}$
D_c (g cm^{-3})	1.87
Z	4
Total number of reflections	5068
Number of independent observations [$I \geq 2\sigma(I)$]	4271
$R=\sum\|\|F_o\|-\|F_c\|\|/\sum\|F_o\|$	0.025
$R_w=\left[\frac{\sum w(\|F_o\|-\|F_c\|)^2}{\sum w\|F_o\|^2}\right]^{\frac{1}{2}}$	0.033

0302-4377/83 $2.50

Table 2. Final atomic coordinates $\times 10^4$. The estimated standard deviations $\times 10^4$ are in parentheses. The values of the silver atoms and the values of the hydrogen atoms are multiplied by 10^5 and 10^3, respectively.

Atom	*x*	*y*	*z*	Atom	*x*	*y*	*z*
N4	5930(3)	9419(3)	2785(2)	N5	424(3)	4276(3)	1636(2)
O1	4995(3)	9998(3)	2274(2)	O4	185(3)	3921(3)	754(2)
O2	6556(3)	8585(3)	2402(2)	O5	1278(3)	5199(3)	2074(2)
O3	6247(3)	9669(3)	3663(2)	O6	−149(3)	3651(3)	2085(2)
Ag1	13858(3)	47018(3)	38178(2)	Ag2	52566(3)	83930(2)	4671(2)
	BTAH 1				BTAH 2		
N1	−1429(4)	7626(3)	3829(3)		4274(3)	1853(3)	3725(2)
N2	−887(3)	6588(3)	3452(2)		3150(3)	2485(3)	3360(2)
N3	149(3)	6277(3)	4145(2)		3003(3)	3350(3)	4056(2)
C4	280(4)	7131(3)	4972(2)		4057(3)	3280(3)	4875(2)
C5	−749(4)	8007(3)	4766(2)		4891(4)	2299(3)	4666(2)
C6	−889(5)	9021(4)	5465(3)		6078(5)	2008(5)	5356(3)
C7	34(5)	9101(4)	6349(3)		6368(5)	2717(6)	6238(3)
C8	1074(6)	8211(5)	6563(3)		5526(5)	3707(5)	6461(3)
C9	1220(5)	7233(4)	5889(3)		4365(5)	4000(4)	5798(3)
H1	−199(5)	793(4)	347(3)		445(4)	130(4)	342(3)
H2	−156(4)	949(4)	531(3)		656(5)	145(5)	524(3)
H3	2(4)	968(4)	682(3)		713(5)	256(4)	668(3)
H4	173(5)	830(5)	718(4)		576(5)	415(4)	704(3)
H5	814(5)	325(4)	397(3)		383(4)	463(4)	591(3)
	BTAH 3				BTAH 4		
N1	2566(3)	5185(3)	497(2)		8307(3)	11377(2)	630(2)
N2	2905(3)	6368(3)	328(2)		7018(3)	10811(2)	353(2)
N3	4265(3)	6574(2)	669(2)		7100(3)	9586(2)	503(2)
C4	4816(3)	5516(3)	1073(2)		8487(3)	9365(3)	884(2)
C5	3714(3)	4613(3)	963(2)		9266(3)	10523(3)	968(2)
C6	3926(5)	3416(4)	1300(3)		10726(3)	10612(4)	1331(2)
C7	5286(5)	3181(4)	1745(3)		11335(3)	9493(4)	1573(3)
C8	6398(4)	4093(4)	1868(3)		10550(4)	8320(4)	1481(3)
C9	6191(4)	5267(3)	1539(2)		9127(4)	8226(3)	1146(3)
H1	175(5)	497(4)	35(3)		846(4)	1224(4)	58(3)
H2	328(4)	285(4)	121(3)		1121(4)	1131(3)	138(2)
H3	541(4)	242(4)	198(3)		1232(4)	957(4)	182(3)
H4	727(4)	392(4)	217(3)		1097(4)	761(4)	163(3)
H5	685(4)	583(3)	162(2)		859(4)	746(4)	105(3)

benzotriazole groups are as in Ref. 1. Lists of thermal parameters as well as lists of observed and calculated structure factors may be obtained from the authors on request.

DESCRIPTION AND DISCUSSION OF THE STRUCTURE

Bond lengths and bond angles with estimated standard deviations are listed in Table 3. The structure consists of two independent $Ag(BTAH)_2^+$ ions and two independent NO_3^- ions. Both silver atoms are coordinated to two N3 atoms. The Ag2–N3 bond lengths are somewhat larger than the Ag1–N3 bond lengths, but all four values fall within the range of values observed in other Ag-complexes.[5–13] The two N–Ag–N angles [158.4, 151.3°] are smaller than the corresponding angles [159–177°] found in the latter compounds.

The distances and angles for the Ag1 and Ag2 contact spheres are shown in Figs. 1 and 2,

Table 3. Bond distances (Å) and bond angles (°) with estimated standard deviations. The figures in parentheses refer to numbers of the BTAH ligands.

Atoms	Distance or angle	Atoms	Distance or angle
Ag1–N3(1)	2.151(3)	Ag2–N3(3)	2.206(3)
Ag1–N3(2)	2.146(3)	Ag2–N3(4)	2.186(3)
N3(1)–Ag1–N3(2)	158.4(1)	N3(3)–Ag2–N3(4)	151.3(3)
N4–O1	1.243(4)	N5–O4	1.253(4)
N4–O2	1.244(4)	N5–O5	1.233(4)
N4–O3	1.229(4)	N5–O6	1.235(4)
O1–N4–O2	119.5(3)	O4–N5–O5	121.0(3)
O1–N4–O3	120.7(3)	O4–N5–O6	119.6(3)
O2–N4–O3	119.8(3)	O5–N5–O6	119.2(3)

Atoms	BTAH 1	BTAH 2	BTAH 3	BTAH 4
N1–N2	1.335(5)	1.328(4)	1.338(4)	1.330(4)
N2–N3	1.309(4)	1.306(4)	1.311(4)	1.314(4)
N3–C4	1.371(4)	1.366(4)	1.369(4)	1.378(4)
C4–C5	1.383(5)	1.384(5)	1.388(5)	1.384(4)
C5–N1	1.347(5)	1.352(4)	1.352(4)	1.353(4)
C5–C6	1.400(6)	1.393(5)	1.396(5)	1.401(4)
C6–C7	1.353(6)	1.346(7)	1.374(6)	1.362(6)
C7–C8	1.401(7)	1.403(8)	1.397(6)	1.397(6)
C8–C9	1.353(6)	1.357(6)	1.367(6)	1.364(5)
C9–C4	1.393(5)	1.400(5)	1.397(4)	1.399(5)
N1–H1	0.76(4)	0.74(4)	0.81(5)	0.92(4)
C6–H2	0.84(4)	0.80(5)	0.83(4)	0.85(4)
C7–H3	0.85(4)	0.88(4)	0.90(5)	0.95(4)
C8–H4	0.94(5)	0.87(5)	0.90(4)	0.87(4)
C9–H5	0.82(5)	0.88(4)	0.83(3)	0.92(4)
C5–N1–N2	112.0(3)	112.4(3)	111.2(3)	111.2(2)
N1–N2–N3	106.7(3)	107.0(3)	107.6(2)	108.2(2)
N2–N3–C4	109.7(3)	109.4(3)	109.2(3)	108.3(2)
N3–C4–C5	107.3(3)	107.9(3)	107.4(2)	107.8(3)
C4–C5–N1	104.3(3)	103.4(3)	104.5(3)	104.5(2)
C4–C5–C6	121.6(3)	121.6(3)	121.8(3)	121.5(3)
C5–C6–C7	116.7(4)	116.9(5)	116.2(4)	116.5(3)
C6–C7–C8	122.0(4)	122.1(4)	122.2(4)	122.0(3)
C7–C8–C9	121.7(4)	121.7(4)	121.6(4)	122.1(4)
C8–C9–C4	117.4(4)	116.8(4)	117.0(3)	116.5(4)
C9–C4–C5	120.7(3)	120.9(3)	121.1(3)	121.4(3)

respectively. In both $Ag(BTAH)_2^+$ ions the two benzotriazole molecules are almost parallel, the angle between the normals of the molecular planes being 5.6 and 10.0° for the Ag1- and Ag2-ions, respectively.

Besides the two nitrogen atoms, there are two nitrate oxygens within the contact sphere of Ag1. The Ag1–O5 and Ag1–O6 distances [2.630(3) and 2.679(3) Å] represent weak interactions between the atoms, and lie within the range of 2.5–2.8 Å found in other compounds.[5,7–15] The shortest Ag1–Ag1 distance is 5.062(1) Å, and is found to Ag1($\bar{x}$, $1-y$, $1-z$).

The contact sphere of Ag2 contains, apart from the N3 atoms from BTAH3 and BTAH4, one N2 atom and one nitrate oxygen. The Ag2–O2 distance [2.752(3) Å] is slightly larger than the largest Ag1–O distance. The N2 atom belongs to the BTAH4 group bonded to the silver atom related to Ag2 by the inversion center at ($\frac{1}{2}$, 1, 0). The Ag2–N2 distance of 2.493(4) Å indicates some interaction between the two atoms. Due to

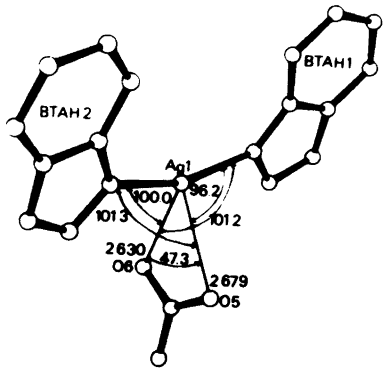

Fig. 1. The coordination around Ag1. The estimated standard deviations for the bond lengths and angles are 0.003 Å and 0.1°, respectively.[16] For Ag–N3 distanes and angles, see Table 3.

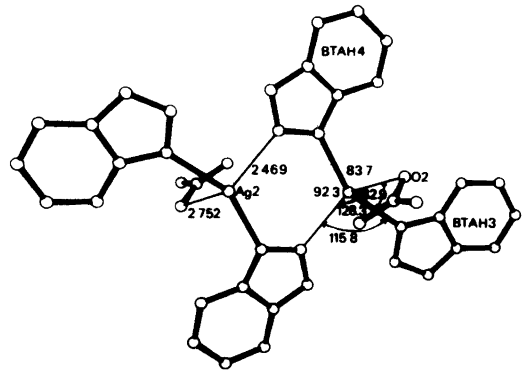

Fig. 2. The coordination around Ag2. The two Ag atoms are related by an inversion center. The estimated standard deviations for the bond lengths and angles are 0.003 Å and 0.1°, respectively. For Ag–N3 distances and angles, see Table 3.

the center of inversion the atoms N2 and N3 and their symmetry related atoms lie in a plane. The Ag2 atoms are 0.34 Å out of plane, and the Ag2–Ag2 separation [3.763(1) Å] is smaller than the separation of 4.251(2) Å found in bis[nitratobis(pentamethylenetetrazole)silver(I)][9] with a similar arrangement around the Ag atoms. In silver nitrate an Ag–Ag distance of 3.22 Å is found.[15]

The BTAH ligands are nearly planar, the deviation of the atoms from the least-squares planes through them being less than 0.02 Å. The sum of the endocyclic angles at C4 and C5 may be compared to idealized values (Ref. 3, Table 6). The idealized values are calculated as average values over triazole rings where the neighbouring atom to nitrogen is either H or C. For the $Ag1(BTAH)_2^+$ ion a comparison shows that the angles in the triazole groups correspond to intermediates between 1- and 1,3-substituted compounds. The triazole groups in the $Ag2(BTAH)_2^+$ ion corresponds more to 1-substituted compounds, which is in agreement with the longer Ag–N bonds found in this ion.

The nitrate ions are nearly planar, the deviations of the atoms from the least-squares planes through them being less than 0.02 Å. The symmetry of the nitrate ion is close to C_{2v} symmetry. Similar results are found in related compounds.

The packing of the structure is shown in Fig. 3. Layers of $Ag2(BTAH)_2^+$ ions ($z\sim0$) and layers of $Ag1(BTAH)_2^+$ ions ($z\sim\frac{1}{2}$) separated by nitrate ions repeat themselves in the direction of the

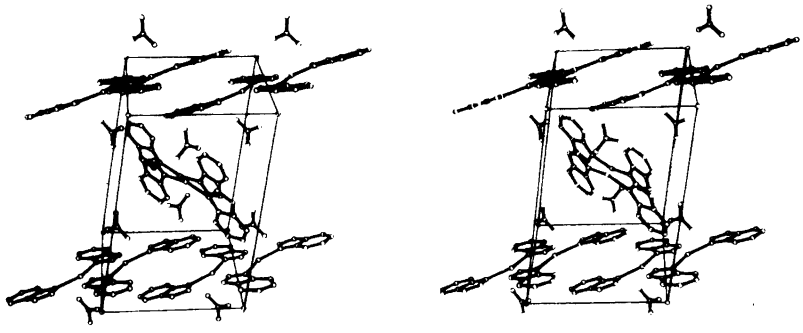

Fig. 3. Stereo view along the a^*-axis of the structure.

c-axis. This arrangement is also found in bis(imidazole)silver(I) nitrate.[7] The angles between the *ab*-plane and the BTAH planes are 76.0, 75.9, 84.4 and 86.6° for the BTAH1, BTAH2, BTAH3, and BTAH4 groups, respectively. For the N4 and N5 nitrate groups the corresponding angles are 89.5 and 80.7°, respectively.

The $Ag(BTAH)_2^+$ layers in the structure are linked *via* hydrogen bonds between nitrate oxygen atoms and N1 atoms. The N–H···O distances are N1(BTAH1)–O2($x-1, y, z$) [2.777(4) Å], N1(BTAH2)–O1($x, y-1, z$) [2.929(5) Å], N1(BTAH3)–O4(x, y, z) [2.851(4) Å], N1(BTAH3)–O5(x, y, z) [2.985(5) Å], and N1(BTAH4)–O6($1+x, 1+y, z$) [2.990(3) Å].

Acknowledgement. This work was supported by a grant from the Danish Natural Science Research Council.

REFERENCES

1. Søtofte, I. and Nielsen, K. *Acta Chem. Scand. A 35* (1981) 733.
2. Søtofte, I. and Nielsen, K. *Acta Chem. Scand. A 35* (1981) 739.
3. Søtofte, I. and Nielsen, K. *Acta Chem. Scand. A 35* (1981) 747.
4. Stewart, J. M., Kundell, F. A. and Baldwin, J. C. *The X-Ray System, Version of 1972,* University of Maryland, College Park, Maryland 1972.
5. Vranka, R. G. and Amma, E. L. *Inorg. Chem. 5* (1966) 1020.
6. Menchetti, S., Rossi, G . and Tazzoli, V. *Rend. Ist. Lomb. Accad. Sci. Lett. A 104* (1970) 309.
7. Antti, C.-J. and Lundberg, B. K. S. *Acta Chem. Scand. 25* (1971) 1758.
8. Acland, C. B. and Freeman, H. C. *Chem. Commun.* (1971) 1016.
9. Bodner, R. L. and Popov, A. I. *Inorg. Chem. 11* (1972) 1410.
10. Cook, D. S. and Turner, M. F. *J. Chem. Soc. Perkin Trans. 2* (1976) 1379.
11. Murthy, R. V. A. and Murthy, B. V. R. *Z. Krist. 144* (1976) 259.
12. Gagnon, C. and Beauchamp, A. L. *Acta Crystallogr. B 33* (1977) 1448.
13. Bang, E. *Acta Chem. Scand. A 32* (1978) 555.
14. Gibbons, C. S. and Trotter, J. *J. Chem. Soc. A* (1971) 2058.
15. Meyer, P., Rimsky, A. and Chevalier, R. *Acta Crystallogr. B 34* (1978) 1457.
16. Johnson, C. K. *ORTEP,* Report ORNL-3794, Oak Ridge National Laboratory, Oak Ridge, 1965.

Received March 25, 1983.